organizers

International Association for Hydro-Environment Engineering and Research

Hostedby Spain Water and IWHR, China

National Technical University of Athens

School of Civil Engineering National Tech. Univ. of Athens

# 7th IAHR EUROPE CONGRESS

## Innovative water management in a changing climate

**SEPTEMBER 7-9, 2022**

**ATHENS, GREECE**
**Divani Caravel Hotel**

Under the Auspices and Support

HELLENIC REPUBLIC
MINISTRYOF
DEVELOPMENTAND INVESTMENTS

HELLENIC REPUBLIC
REGION OF ATTICA

HELLENIC REPUBLIC
Ministry for Climate Crisis and Civil Protection

HELLENIC REPUBLIC
Ministry of Infrastructure and Transport

MINISTRY OF ENVIRONMENT & ENERGY

CITYOF ATHENS

# Abstract Book

www.iahreuropecongress.org

## Keynote Lectures



## RLR Rivers, Lakes and Reservoirs

*RLR Rivers, Lakes and Reservoirs*

*RLR Rivers, Lakes and Reservoirs*



# ECS Estuaries, Coasts and Seas

*ECS Estuaries, Coasts and Seas*

## UHH Urban Hydrology and Hydraulics



## FDCC Floods, Droughts and Climate Change

*FDCC Floods, Droughts and Climate Change*

*FDCC Floods, Droughts and Climate Change*

*FDCC Floods, Droughts and Climate Change*



# TCEM Theoretical, Computational and Experimental Methods

## TCEM Theoretical, Computational and Experimental Methods

### *TCEM Theoretical, Computational and Experimental Methods*



## WREM Water Resources and Energy Management

### WREM Water Resources and Energy Management

### WREM Water Resources and Energy Management



## POSTER PRESENTATIONS

## POSTER PRESENTATIONS

# Water Security Under Climate Change

Jacques GANOULIS[1]

[1]UNESCO Chair/INWEB, Civil Engineering Department, Aristotle University of Thessaloniki, Greece

email: iganouli@civil.auth.gr

ABSTRACT

The relationship between Water and Man is reflected in the way humans use water and apply the water resources management conceptual model. A historical review indicates that the Water-Man relationship has been continuously variable between two opposites: conflict and cooperation. In ancient times, nature and water were considered and respected as divinities. After the second industrial revolution (1870-1970), Man was felt to be able to dominate nature. The construction of the pharaonic Hoover Dam in 1935 is a milestone of the engineering capability to serve human interests by modifying and regulating nature.

Since the late 20th century, the Integrated Water Resources Management (IWRM) is promoted as the state-of-the-art model, integrating not only technical and economic but also environmental and social issues. However, the model implementation in the field is confronted with high environmental externalities, such as diffuse pollution, soil nitrification, especially under climate change, and severe environmental challenges, such as floods and droughts.

In this presentation, we claim that the IWRM model is still anthropocentric and technocratic, and has been unable to achieve water and environmental security up from a certain level. A new eristic-dialectical approach is suggested to complement IWRM by reducing externalities and increasing hydro-resilience. The new model proceeds firstly, by analyzing conflicts between stakeholders' activities and natural laws (Eristic Analysis), and secondly, by unifying opposite objectives through a dialectical approach (Dialectical Resolution). Two case studies from real situations illustrate the suggested eristic-dialectical methodology.

Ref. Jacques Ganoulis (2021). The water–man eristic dialectics for sustainable hydro-governance. Water International, 46:7-8, 1135-1157. https://doi.org/10.1080/02508060.2021.2004003

7th IAHR Europe Congress, September 7th – 9th, 2022, Athens, Greece

# Water governance: Tackling climate crisis challenges

Maria P. Papadopoulou[1]

[1] National Technical University of Athens, Greece
email: mpapadop@mail.ntua.gr

ABSTRACT

Extreme events related to climate change like floods and droughts are expected to further intensify impacts on water resources in the near future posing serious threats to life on earth. The need for urgent solutions is a key to achieve sustainable water resources management on all scales however requires a well-defined water resources legal and regulatory framework and at the same time a sustainable water governance system is critical for the management of water resources.

Water policy defines the rules and instruments with which policy-makers manage conflicting water-uses, control water pollution, and meet environmental water quality standards. A holistic view that included social, economic and environmental sustainability aspects is required to implement practices that will support the legislative aspects of water policy.

On the other hand water governance is a complex process that considers multi-level participation, from public institutions to private sector, civil society and NGOs in co-design decision making process. New approaches and methods of governance should improve the transparancy and accountability in water policy making. Assessment, awareness and accessibility act as critical pilars of a governance system.

Given the vital importance of freshwater, innovative approaches at policy and governance level are needed to tackle climate crisis impacts.

# Research and Innovation Agenda for hydropower as catalyst for the energy transition in Europe

Anton J. SCHLEISS[1], Andrej MISECH[2], Jean-Jacques FRY[3], Mark MORRIS[4]

[1] EPFL-ICOLD, Switzerland
email: anton.schleiss@epfl.ch

[2] EUREC, Belgium
email: misech@eurec.be

[3] EURCOLD, France
email: jean-jacques.fry@wanadoo.fr

[4] SAMUI, France
email: mark.morris@samuifrance.com

ABSTRACT

Hydropower has all the characteristics to serve as a catalyst for a successful energy transition ensuring safe and independent electricity supply in Europe, and worldwide. The Hydropower Europe Forum has been preparing a Research and Innovation Agenda (RIA) and a Strategic Industry Roadmap (SIR) for the hydropower sector. The Research and Innovation Agenda (RIA) provides recommendations on the R&I priorities for hydropower to the EU institutions and national authorities to contribute towards shaping public spending for R&I. The RIA identifies the main challenges for further hydro development, optimised maintenance, environmental and economic performance of existing assets and the related R&I gaps. The suggested research themes and topics in the RIA are offering challenging interdisciplinary R&I opportunities in near future and are asking for a strong involvement of the scientific community being active in the field of hydro-environment research and engineering.

## 1. Hydropower Europe Forum

Hydropower has a long tradition in Europe and contributed significantly to industrial development and welfare in most of the countries in Europe. The ambitious plan for energy transition in Europe seeks to achieve a low-carbon climate-resilient future in a safe and cost-effective way, serving as an example worldwide. The key role of electricity will be strongly reinforced in this energy transition. In many European countries, the phase out of nuclear and coal generation has now started, with a transition to new renewable sources comprising mainly solar and wind for electricity generation. However, solar and wind are variable energy sources and difficult to align with demand. Hydropower already supports integration of solar and wind energy into the supply grid through its flexibility in generation as well as its potential for storage capacity. These services will be in much greater demand in order to achieve the energy transition in Europe and worldwide, ensuring safe and independent electricity supply. Hydropower has all the characteristics to serve as an excellent catalyst for a successful energy transition. There is still a significant untapped potential, which allows hydropower to perform this role. However, this will require a more flexible, efficient, environmentally and socially acceptable approaches to increase hydropower production to complement other renewable energy production.

From November 2018 until February 2022, the Hydropower Europe Forum, supported by a project that has received funding from the European Union's Horizon 2020 research and innovation programme, has been preparing a Research and Innovation Agenda (RIA) for the hydropower sector based on a newly formulated vision for the hydropower development in Europe. The content of the RIA (HPE, 2021) was discussed in several technical fora and transparent public debates through a forum that gathers all relevant stakeholders of the hydropower sector in Europe. Based upon a first enhanced draft, a second wider online consultation process started in August 2020 accompanied by an online event in October 2020 called “Hydropower seeking its role in the clean energy transition.” Some 185 stakeholders actively participated in this second wider online consultation process and feedback was received regarding the priorities of the research themes covering numerous topics and strategic actions. From spring to autumn 2021, the consultation results were discussed in workshops with the Consultation Expert Panel (CEP) with the purpose of establishing final priorities and defining suggested programme timelines, indicative magnitude of funding required as well as expected Technology Readiness Level (TRL) of the research themes. The prioritisation process was finally validated by including the results of a complex system analysis (HPE, 2020) carried out for hydropower in Europe as well as European initiatives regarding the energy transition and the European Green Deal.

## 2. Research and Innovation Agenda (RIA)

The Research and Innovation Agenda (RIA) provides recommendations on the R&I priorities for hydropower to the EU institutions and national authorities to contribute towards shaping public spending for R&I. The RIA identifies the main challenges for further hydro development, optimised maintenance, environmental and economic performance of existing assets and the related R&I gaps. As a result, R&I needs for hydro are listed and clarified, specifying the type of challenge, expected results, R&I activities needed, the relevant stakeholders, and indicative timeframe along with an assessment of the likely funding needed. The RIA is not limited to only technological issues, such as equipment and infrastructure improvement and extension or advanced operation managing systems. It also includes environmental, social and economic issues with a view for sustainable development and to understand how community and the wider public react to hydropower projects and how social acceptance can be enhanced. However, the RIA looks at these issues exclusively through a research and development perspective. The R&I needs have been prioritised according to criteria defined with the support of the Consultation Expert Panel (e.g., consistency with EU policy objectives, maturity of the technology, expected benefits, etc.). The research themes identified are grouped according to the challenges which hydropower in Europe must address, namely:

- Increasing Flexibility
- Optimisation of operations and maintenance
- Resilience of electromechanical equipment
- Resilience of infrastructures and operations
- Developing new emerging concepts
- Environmental-compatible solutions
- Mitigation of the impact of global warming

In total 18 research themes including in total 80 detailed research topics for each of them have been formulated based upon the wide consultation feedback. The RIA is a key contribution to the growing debate on the net zero economy and the European Green Deal and will be highly relevant for discussions on finding the best solutions to provide the new energy system with flexibility ensuring safe and independent supply. They will help European regulators, policymakers, civil society, NGOs, technology developers, planners, utilities and system operators to discuss together and to take balanced decisions on further hydropower development to enable the new energy system to benefit fully from the storage and flexibility potential of this valuable resource. Hydropower provides ancillary and important back-up services which help stabilise the grid for intermittent and non-dispatchable renewable resources such as wind or solar power. Furthermore, hydropower delivers many services beyond just electricity supply, as an important player in both water resources management and water storage. This will be key in the near future due to climate change.

Besides an overview of the current situation of hydropower in Europe and its development potential, the contribution will present in detail the background and challenges of the research themes and the related detailed topics where a strong involvement of the hydro-environment research and engineering community is wished for shaping a successful energy transition in Europe with safe and independent supply.

**Acknowledgements**

The HYDROPOWER EUROPE Forum is supported by a project that has received funding from the European Union's Horizon 2020 research and innovation programme under grant agreement No 826010. Project partners comprise: International Commission on Large Dams (ICOLD), European Association for Storage of Energy (EASE), European Renewable Energies Federation (EREF), Association of European Renewable Energy Research Centres (EUREC), International Hydropower Association (IHA), Samui France SARL (SAMUI), VGB PowerTech e.V. (VGB) and ZABALA Brussels SPRL (ZABALA).

**References**

HPE-Hydropower Europe Forum (2021) Research and Innovation Agenda (RIA). www.hydropower-europe.eu.
HPE-Hydropower Europe Forum (2020) Hydropower in Europe in a complex world - A global system analysis approach. Hydropower Europe Technical Report WP2-DIRp-47, June 2020. www.hydropower-europe.eu

# Hydraulic Engineering in the Era of Extreme-Scale Computing and Data-Driven Modeling

Fotis SOTIROPOULOS[1]

[1]Provost and Senior Vice President for Academic Affairs Virginia Commonwealth University, United States

email: sotiropoulosf@vcu.edu

ABSTRACT

Advances in computational algorithms coupled with exponentially growing computing power and data-driven reduced order modeling pave the way for developing a powerful simulation-based engineering science framework for tackling a broad range of hydraulic engineering flows. Multi-physics large-eddy simulations taking into account complex waterway bathymetry, energetic coherent structures, turbulence/sediment interactions and morphodynamics, free-surface effects and flow structure interaction phenomena are now well within reach and are impacting engineering practice. I review such progress and offer specific examples highlighting the enormous potential of simulation-based engineering science to supplement and dramatically augment the insights that can be gained from physical experiments. I discuss computational challenges but also underscore the enormous opportunities to take advantage of advanced algorithms, powerful supercomputers, and data-driven machine learning to tackle societal challenges in restoration of aquatic environments, sustainable mitigation of the impacts of climate change, and development of efficient and environmentally compatible renewable energy systems.

# Simulation of flow around a wall-mounted semi-ellipsoid – comparison of URANS and DES modelling approaches

Yannick MARSCHALL[1], George CONSTANTINESCU[2], Robert M. BOES[3], David F. VETSCH[4]

[1,3,4] Laboratory of Hydraulics, Hydrology and Glaciology, ETH Zurich, Zurich, Switzerland
email: marschall@vaw.baug.ethz.ch

[2] Department of Civil and Environmental Engineering and IIHR-Hydroscience and Engineering, The University of Iowa, Iowa City, IA, USA

ABSTRACT

In this case study we compare two different numerical approaches, namely URANS (Unsteady Reynolds-Averaged Navier-Stokes) and DES (Detached-Eddy Simulation), to simulate the flow field around a semi-ellipsoid mounted on a flat plate. The considered configuration is in reference to an isolated large boulder in an open stream. The results of the numerical simulations are compared with experimental laboratory data for model validation. We show that the results obtained with DES are in very good agreement with the lab data. By contrast, the more cost-efficient URANS method leads to a different flow pattern in the near-wake region and hence to very poor prediction of the lift and drag forces acting on the semi-ellipsoid.

## 1. Introduction

Numerical simulations using computational fluid dynamics (CFD) become increasingly popular in hydraulic engineering not only for lowland rivers with moderate flow velocity but also for steep rivers with high velocities and small relative submergence of roughness elements (e.g. boulders). Due to the high computational cost of eddy-resolving methods like Large-Eddy Simulations (LES), the use of RANS is still very popular. In most cases, such simulations do not capture with sufficient accuracy the dynamics of the large scale turbulence that plays a major role in predicting flow hydrodynamics, mixing and sediment transport in rivers.

As LES without wall functions is very costly for high Reynolds number flows, we use a hybrid approach (DES) as the method of choice for performing the eddy-resolving simulations. DES is considered a hybrid method between URANS and LES. The turbulence model close to the wall surfaces is equivalent to a RANS model, while it is similar to a LES model in the regions situated away from the wall surfaces (Spalart, 2000). The major benefit of DES compared to well-resolved LES (i.e. no wall functions) is the significantly reduced computational cost.

In steep channels, large boulders contribute to the stability of the riverbed and increase flow resistance (e.g. Bathurst, 1978). Therefore, estimation of the forces acting on the boulders is of great importance to correctly estimate bed stability. In this CFD study, we used a fully submerged, wall-mounted semi-ellipsoid as a first approximation to represent a single large boulder in a river. To assess the predictive capabilities of URANS and DES, we compare the numerical results with the laboratory experiments of Hajimirzaie et al. (2012).

## 2. Method

The 3D numerical simulations were conducted using the commercial CFD software STAR-CCM+ which is based on the finite volume method and is capable of performing turbulent flow simulations using URANS and DES models. Several turbulence models were tested. The k-ω SST for URANS (based on Menter, 1994) and k-ω SST for DES (based on Menter, 2004) were found to perform the best. The present paper reports only results using these two models.

The domain and obstacle sizes and the flow conditions in the numerical model were based on those used in the corresponding experiments. The Reynolds number was 17’800. The water surface was modeled using the rigid lid approach as the submergence of the semi-ellipsoid was high ($d/H$ = 3.9) and the influence of the water surface on the flow around the semi-ellipsoid was expected to be small (Shamloo et al., 2001). A boundary layer velocity profile with low artificial turbulence intensity was specified at the inlet boundary. A zero-gradient pressure boundary condition was applied at the outlet. The wall region was fully resolved with $y^+ \leq 1$ for the first cell normal to the wall. This resulted in a mesh with roughly 6.4M cells. The time step was chosen to be approximately 1/100 of a shedding cycle for URANS and 1/500 for DES, respectively. A further decrease of the time step or increase of the spatial resolution did not result in observable changes of the mean flow field. After an initialization period, the flow parameters were averaged over more than 25 shedding cycles to obtain the mean flow and turbulence statistics.

The results from the numerical simulations were first non-dimensionalized, using the free stream velocity and height of the semi-ellipsoid, and then compared with the results provided by the experimental study. This included contour plots of the mean vorticity in streamwise and transversal direction, streamlines in the centerline cross-section as well as Reynolds stresses. The data provided by the reference experiment is mainly from within the near-wake zone of the semi-ellipsoid and was obtained by PIV measurements.

## 3. Results

The streamlines in Fig. 1 visualize the flow downstream of the semi-ellipsoid and the recirculation zone. For the laboratory experiments and DES, the (non-dimensional) recirculation length was $l_{r,lab} \approx 2.4$ and $l_{r,DES} \approx 2.2$, respectively. For the URANS simulation, the length of the recirculation region almost doubled as $l_{r,URANS} \approx 4.7$. Similarly, the streamwise and transverse vorticity profiles measured in the laboratory experiments and predicted by DES agree well, while those predicted by URANS deviate significantly. The simulation time required for one single timestep was comparable for both URANS and DES (the number of grid cells was similar), nevertheless due to the higher number of timesteps needed to get a statistically steady flow and then to calculate the mean flow, the total simulation time for DES was significantly higher.

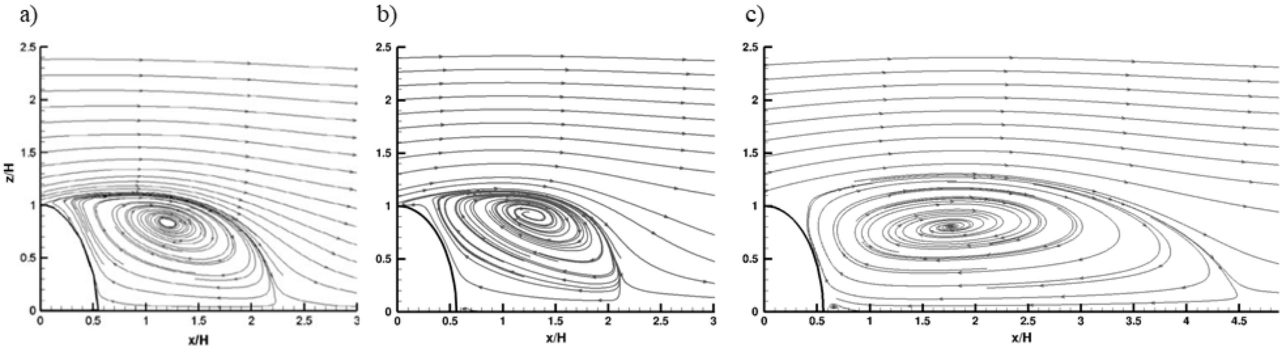


**Fig. 1.** Mean flow streamlines in the longitudinal cross-section along the centre line for a) laboratory experiments (Hajimirzaie et al., 2012), b) DES with the k-ω SST turbulence model and c) URANS simulation with the k-ω SST turbulence model.

## 4. Conclusion

The results show that URANS predicts a mean flow field in the near wake that is quite different from the one observed in the laboratory experiment. In particular, the URANS significantly overestimated the length of the recirculation region downstream of the obstacle. This finding agrees with previous studies, e.g. Nürnberger & Greza (2002), that found URANS is not very accurate for predicting separating flows for obstacles where the position of the separation line is not dictated by the geometry (e.g. by the presence of sharp edges). By contrast, DES performed considerably better and showed good agreement with the experimental data. This study shows that for surface-mounted bodies with a large degree of bluntness eddy-resolving methods are necessary to correctly estimate the flow field in the near-wake zone. The poor prediction of the near-wake flow by URANS also leads to an underprediction of the lift and drag forces acting on the surface-mounted body and thus of the capability of the flow to displace the boulder, which is an important mechanism affecting bed stability.

**Acknowledgements**

The authors thank the Swiss Federal Office for the Environment (FOEN) for their support and funding of the research project leading to the results presented in this report.

**References**

Bathurst JC (1978) Flow resistance of large-scale roughness, Journal of Hydraulic Engineering, 104(12), 1587-1603
Hajimirzaie SM, Wojcik CJ, Buchholz JHJ (2012) The role of shape and relative submergence on the structure of wakes of low-aspect-ratio wall-mounted bodies, Experimental Fluids, 53, 1943-1962
Menter FR (1994), Two-Equation Eddy-Viscosity Turbulence Models for Engineering Applications, AIAA Journal, 32(8), 1598-1605
Menter FR, Kuntz M (2004) Adaptation of Eddy-Viscosity Turbulence Models to Unsteady Separated Flow Behind Vehicles, The Aerodynamics of Heavy Vehicles: Trucks, Busses, and Trains, 339-352
Nürnberger D, Greza H (2002) Numerical Investigation of Unsteady Transitional Flows in Turbomachinery Components Based on a RANS Approach, Flow, Turbulence and Combustion, 69, 331-353
Shamloo H, Rajaratnam N, Katopodis C (2001) Hydraulics of simple habitat structures, Journal of Hydraulic Research, 39:4, 351-366
Spalart P (2000) Trends in turbulence treatments, In Fluids 2000 conference and exhibit, 2306-2314

# 3D numerical modelling of silting processes in a retention basin

Agnes DIERMAIER[1], Ursula STEPHAN[1], Daniel WILDT[2], Michael TRITTHART[2]

[1] Institute for Hydraulic Engineering and Calibration of Hydrometrical Current-Meters, Federal Agency for Water Management, Severingasse 7, 1090 Vienna, Austria
Emails: agnes.diermaier@baw.at, ursula.stephan@baw.at

[2] University of Natural Resources and Life Sciences, Vienna
Department of Water, Atmosphere and Environment, Institute of Hydraulic Engineering and River Research, Muthgasse 107, 1190 Vienna, Austria
Emails: daniel.wildt@boku.ac.at, michael.tritthart@boku.ac.at

ABSTRACT

In the rivers and surface waters of the Weinviertel, Lower Austria, suspended sediment load is aimed to be reduced. Thus, non-controlled, small flood retention basins with permanent open outflow have been investigated whether they can also be used as sediment retention basins. This research focuses on optimizing the sedimentation processes in such a flood retention basin through structural measures. Square basins with four different variants of the position of inlet and outlet were analyzed using the three dimensional numerical hydrodynamic solver RSim-3D. The variant with the highest sedimentation efficiency has the inlet at the southern basin boundary on the west side and the outlet at the eastern basin boundary on the south side.

## 1. Introduction

In recent decades the number of heavy rainfall events has increased in many parts of Europe, such as the Weinviertel region in Lower Austria, albeit with regional differences (Hartmann et al., 2013). Subsequently, topsoil is eroded from intensively used agricultural areas and transported into the river systems. There the material is deposited resulting in a reduced discharge capacity and subsequently reduced flood protection. In addition, ecology and morphology are affected negatively. To retain sediment in predefined and controlled areas, existing flood retention basins are planned to be used.

## 2. Method

Geometrical modifications of the basin were studied for optimizing sedimentation efficiency in a retention basin using the hydrodynamic solver RSim-3D (Tritthart, 2005). The solver uses the Finite Volume Method for the numerical solution of the three-dimensional Navier-Stokes equations. Turbulence is modelled using the standard $k$-$\epsilon$ turbulence model (Launder and Spalding, 1974).

The geometry is based on a operational retention basin in Breitenwaida, Lower Austria. The results are obtained in two steps: (1) solution of steady-state hydrodynamics for a constant inflow of 0.25 m³/s using the RSim-3D solver. (2) Simulation of unsteady sediment transport during a 54 min event with constant inflow concentration of 45 g/l based on the advection-diffusion equation and the steady fluid-velocity field obtained in step (1). Inflow sediment concentration and grain size distribution were determined from water samples in the Weinviertel, representing the typical material of this region.

Various idealizations of the geometry have to be applied for the numerical model to converge within a reasonable simulation time. The final basin geometry has a square shape with an edge length of 12.3 m. Inlet and outlet, respectively, are 0.8 m wide. The simulations are conducted for four different variants (V1, V2, V3 and V4) of inlet and outlet positions (Fig. 1).

## 3. Results

The flow pattern in all four variations shows differing flow paths depending on the position of inlet and outlet. Inlet and outlet position in V2 result in the shortest path through the basin and the respective positions in V3 the longest flow path through the basin (Fig. 1). Since the aim of the investigation was to optimize sediment retention in the basin, V2 was excluded from further sediment simulations due to the short-circuit flow from inlet to outlet.

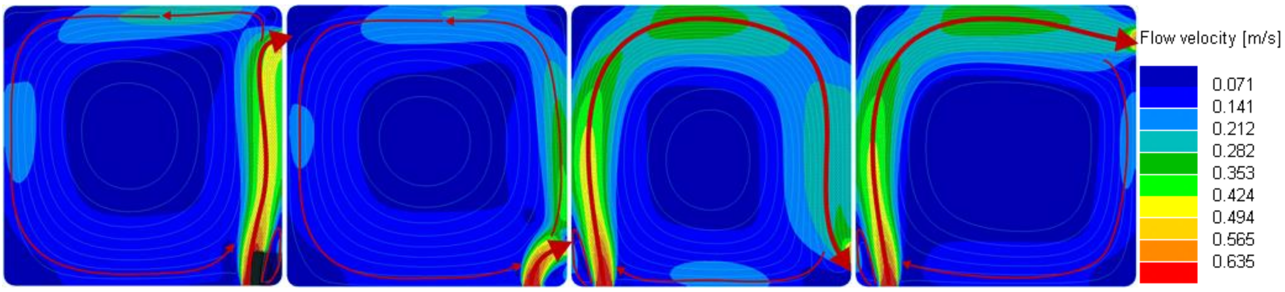


**Fig. 1.** Hydrodynamic results of the four variants: V1, V2, V3, V4 (f.l.t.r.)

The amount of deposited and suspended material in the basin was calculated for the three remaining cases V1, V3 and V4 and is shown in Figure 2. The dashed lines represent the mean sedimentation rates related to the total amount of inflowing sediment after 54 min. V3, which shows the longest flow path through the basin, leads to the highest amount of retained sediment, both deposited and suspended material. V2 and V4 result in almost the same sedimentation rates. It can also be seen that only grain sizes larger than 0.02 mm are deposited and smaller grain sizes will not be retained in the basin. Assuming a certain amount of flocculation of smaller grain sizes, sedimentation rates of these grain sizes might increase.

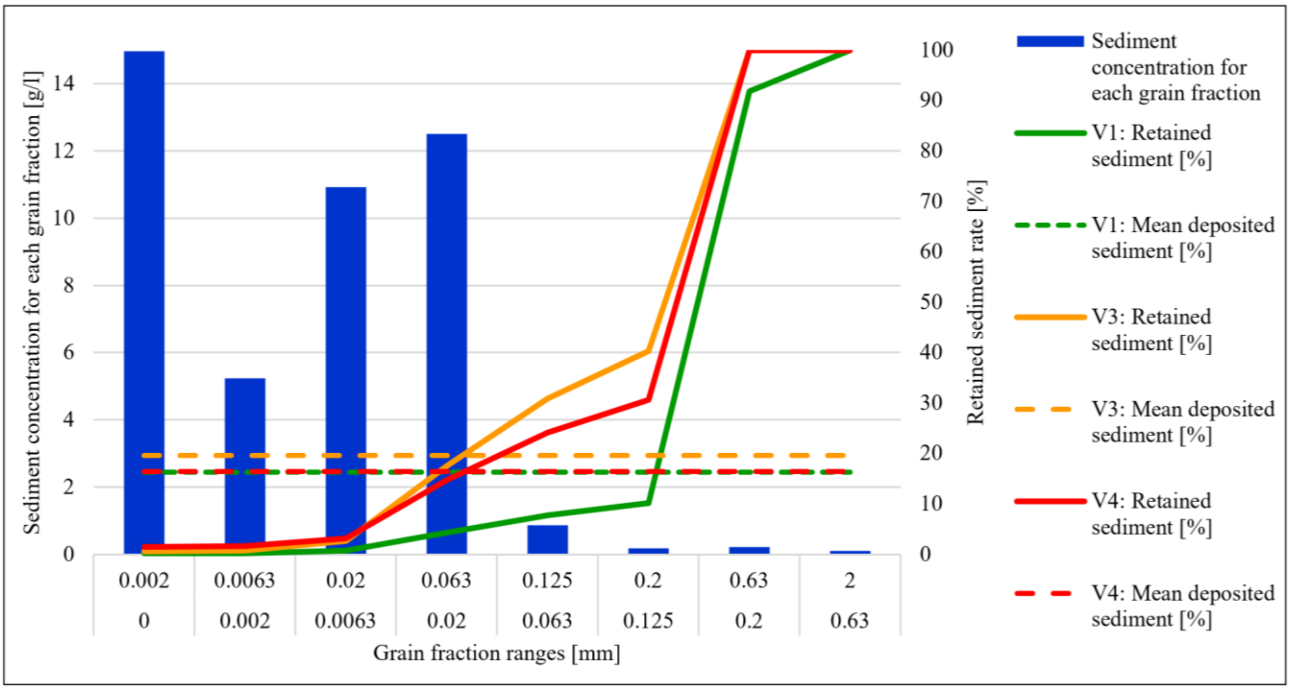


**Fig. 2.** Sediment performance T=54 min

## 4. Conclusion

Generally, the research focused on basins with a permanent outflow and, thus, with a flowing wave retention. The variation study showed that V3 with the longest main flow path through the basin leads to the highest sedimentation rates. For the retention of flood waves with a high amount of suspended load this is an important information. In addition, the study revealed that the lager grain sizes are totally retained in the basin. The findings derived from this study have already been implemented in the retention basin in Breitenwaida by optimizing the inlet and outlet positions.

### References

Hartmann DL, Klein Tank AMG, Rusticucci M, Alexander LV, Brönnimann S, Charabi Y, Dentener FJ, Dlugokencky EJ, Easterling DR, Kaplan A, Soden BJ, Thorne PW, Wild M, Zhai PM (2013) Observations: Atmosphere and Surface. In: TF Stocker, D Qin, G-K Plattner, M Tignor, SK Allen, J Boschung, A Nauels, Y Xia, V Bex, PM Midgley, Climate Change 2013: The Physical Science Basis. Contribution of Working Group I to the Fifth Assessment Report of the Intergovernmental Panel on Climate Change, Cambridge University Press, Cambridge/United Kingdom/New York, 159–254 pp.

Launder B, Spalding D (1974) The numerical computation of turbulent flows. Computer Methods in Applied Mechanics and Engineering 3(2). 269-289 pp. 0045-7825

Tritthart M (2005) Three-Dimensional Numerical Modelling of Turbulent River Flow using Polyhedral Finite Volumes, Wiener Mitteilungen – Wasser, Abwasser, Gewässer No. 193, Vienna University of Technology, Faculty of Civil Engineering, Vienna

# Assessing the impact of human aquatic vegetation removal on water levels by hydraulic analysis

Koen BERENDS[1], Ellis PENNING[2], Carlo RUTJES[2], Rob FRAAIJE

[1] Deltares, The Netherlands
email: Koen.Berends@deltares.nl
email: Ellis.Penning@deltares.nl
[2] Waterschap Aa en Maas, The Netherlands
email: crutjes@aaenmaas.nl
email: rfraaije@aaenmaas.nl

ABSTRACT

In small, shallow lowland streams submerged aquatic vegetation can take up a significant part of the cross-section during the summer season. This vegetation provides important habitat to fauna and plays a role in the natural sediment management of stream basins. However, it also increases the flow resistance, which may lead to flooding of surrounding land. Changes in the hydrologic regime following climate change calls for finding a balance between ecological and societal needs. Key to finding this balance is a good understanding of the relationship between this instream vegetation and water levels. In this study, we analysed hydraulic measurements of a canalized stream in The Netherlands. We estimated the relationship between vegetation and water level set-up using a hydraulic model and a data-driven vegetation model to quantify the impact of removal of vegetation on water levels by mowing. On average, the removal of vegetation is estimated to reduce the water tables by about 20% of the average water depth of 1 meter.

## 1. Introduction

### 1.1. Study Area

Our study area is the upper reach of the small Leijgraaf stream (bottom width 5 m, maximum width 11 m, annual maximum discharge of 2.8 $m^3s^{-1}$, average slope of $3.78 \cdot 10^{-4}$ m/m) located east of ‘s-Hertogenbosch, The Netherlands. This stream is channelized – its main function is irrigation – and there are 13 weirs over 15 km to manage surface- and groundwater levels in the area. Hourly observations of water levels and discharge (through weir formula) are available for multiple years (2003-2020).

### 1.2. Problem and Objective

To prevent damages, the regional water authority regularly removes vegetation by subaqueous mowing. Decisions on when to mow are made using overall multi-year planning schedules that are refined with water level data, weather forecasts and additional visual inspection in the field. However, it is unknown to what extent the visual appearance of vegetation translates to a direct hydraulic effect. In this study, we study the hydraulic effect of vegetation to see whether mowing events can be detected in the hydraulic record as an aid to the visual inspections. To separate other variables that affect water levels, such as discharge and downstream water levels, we use a hydraulic model with a vegetation roughness predictor.

## 2. Method

The relationship between discharge and water level in small stream is often modelled using stage-discharge relationships derived from the Manning-Strickler equations (Perret, 2020). However in a system with weirs the Manning-Stickler equation for uniform flow does not apply and one must use a non-uniform model like the Bélanger equation. Here, we use the SOBEK hydraulic model, but solve it quasi-stationary, meaning that we assume stationary but non-uniform flow. The influence of vegetation is modelled through bed friction using a modified version of Rhee’s law (Rhee, 2008; Errico, 2018):

$$n = \frac{\alpha}{Q} + n_b \tag{1}$$

Where $n$ is Manning coefficient representing total roughness [$sm^{-1/3}$], Q is the discharge [$m^3s^{-1}$], $n_b$ is the bed roughness in absence of vegetation [$sm^{-1/3}$] and α represents vegetation blockage [$m^{-1/9}$]. In Rhee (2008), α is a function of the geometry of the cross-section. Here, we model α as a general lump-term representing the influence of vegetation on roughness. Because aquatic vegetation is generally seasonal, with a single growth season, we model α using a logistic growth model:

$$\alpha = \alpha_m\left(1 + e^{-r(t-t_m)}\right)^{-1} \tag{2}$$

With maximum value $\alpha_m$, growth rate $r$ ($h^{-1}$), time $t$ and time of maximum growth $t_m$. Since this system is actively managed, we do not model a decay term: vegetation is generally removed by mowing, not by natural decay. First, we compute the actual roughness through inverse modelling on a two-day interval. Then, we define a-priori probability distributions for the unknown variables in Equation 1 and 2 [$n_b$, $\alpha_m$, r, $t_m$] and compare that roughness with the one computed from the hydraulic record. Major and lasting deviations from the model are assumed to be caused by human intervention.

## 3. Results

Fig. 1 shows the results for 2015 in one of the sections of the stream between 2 weirs (length 3.0 km). In the left figure, we observe that around day 186 (July 6th) the roughness suddenly decreases and stays low. At these events, we reset the model and started a new period. The result is seen on the right. In total, four potential events were identified. After the first three events, regrowth was detected, while after the fourth and final one, no regrowth was seen. This indicates that either the conditions were no longer favourable to vegetation growth, or the final human intervention removed near everything. We applied this approach on three different sections of the stream over a period of 14 years. In most years, two or three events were identified. The dates of the events were similar between years. The effect on water levels was tested by hydraulic simulation using the roughness before and after the mowing event. On average, the effect was estimated to be about 20 cm, on a typical water depth of 1 m.

## *4.* Discussion and conclusions

We demonstrated an analysis of stream water levels to detect mowing events using a hydraulic model with a simple vegetation roughness predictor. The identified events were consistent between years and sections of the stream. While we are confident that the identified events were caused by human intervention, it is likely that not all mowing events are identified. Cross-checking with a database of planned events (there is no record of actual events) suggest that more events have taken place than are visible in the record. Therefore, we detect only the effective mowing events. Nonetheless, this distinction may help reduce the mowing effort by focussing only on hydraulic effective events and find a balance between ecological and societal needs.

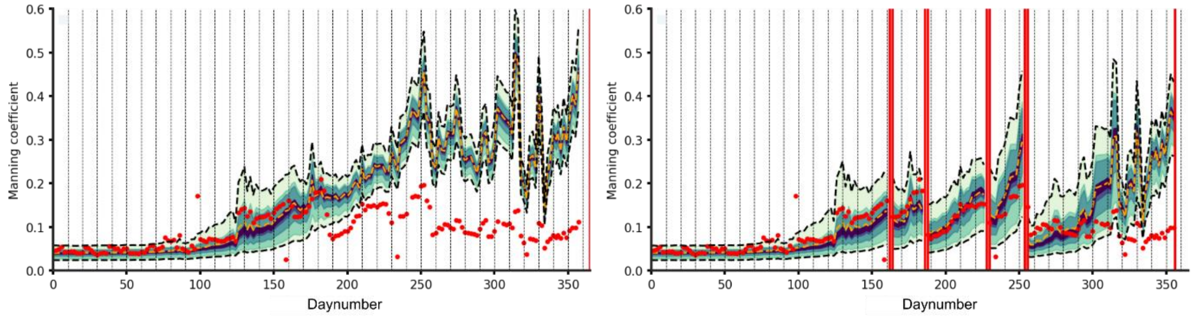


**Fig. 1.** The results for one of the stream sections in 2015. Red dots show measurements, shaded area is the result of the roughness model including model uncertainty. Left: results without mowing events. Rights: periodically reset roughness following identification of four potential mowing events.

**Acknowledgements**

This study took place within the Lumbricus research programme (https://www.programmalumbricus.nl/) and was sponsored by Waterschap Aa en Maas and STOWA.

**References**

Errico, A., Pasquino, V., Maxwald, M., Chirico, G.B., Solari, L., Preti, F. (2018), The effect of flexible vegetation on flow in drainage channels: estimation of roughness coefficients at the real scale. Ecological Engineering 120: 411-421. DOI: 10.1016/j.ecoleng.2018.06.018
Perret, E., Renard, B., Le Coz, J. (2020) A rating curve model accounting for cyclic stage-discharge shifts due to seasonal aquatic vegetation. Water resources research 54 2020WR027745. DOI: 10.1029/2020WR027745
Rhee, D.S., Woo, H., Kwon, B.A., Ahn, H.K. (2008) Hydraulic resistance of some selected vgetation in open channel flows. River. Res. Applic. 24: 673-687. DOI: 10.1002/rra.1143

# Flow Resistance and Energy Dissipation in Brush Fish Pass

Serhat KUCUKALI[1]

[1] Hacettepe University, Civil Engineering Department, Turkey
email: kucukali78@gmail.com

ABSTRACT

In the present paper, the hydraulic characteristics of the brush-type fish pass have been experimentally investigated. The hydraulic test results reveal that the brush fish pass fulfills the requirements of an efficient fishway by providing tranquil flows and sufficient flow depths for different fish species. Flexible hydraulic elements were referred to with three parameters as Cauchy number, the areal density of brush elements, and channel bed slope. The wall friction plays only a minor role in this process. The Darcy-Weisbach friction factor was derived from dimensional analysis and experimental measurements. By using the proposed formula, cross-sectional average velocity and discharge can be estimated for the given channel geometry data. Bed slope appears to be one of the main parameters that control the magnitudes of energy dissipation and turbulent kinetic energy.

## 1. Introduction

In the literature, for fish pass structures, flow resistance formulas developed mainly for rigid obstacles. Baki et al. (2014) observed that flow resistance decreases with increasing relative submergence. In their experiments drag coefficient increases rapidly from 1.2 to 3.0 as the submergence ratio decreases from 1.2 to 0.8. Additionally, Heimler et al. (2008) related the flow resistance with the function of boulder density, boulder configuration, and relative submergence. On the other hand, Cassan et al. (2014) expressed the maximum velocity, which is crucial for fish passability, as a function of rigid obstacle density and bed slope for the subcritical and supercritical regimes. However, the literature lacks flow resistance studies for flexible obstacles in fish pass structures.

## 2. Flow Resistance in Brush Fish Pass: Experimental Investigation

In the present study, a flume with brush-blocks is principally considered as a rough channel with individual distributed macro-roughness elements. Brush blocks affect the flow by forming an obstacle and deflecting flow and by enhancing form drag and skin friction (Meier and Lehmann, 2006). The flow is quasi-uniform in brush fish pass and the Darcy-Weisbach friction factor $f$ is calculated from

$$f = \frac{8S_o R_h g}{U^2} \tag{1}$$

in which $U$ is the cross-sectional-averaged flow velocity, $R_h$ is the hydraulic radius, $g$ is the acceleration due to gravity and $S_o$ is the channel bed slope. For the Darcy-Weisbach friction factor $f$, the effective dimensionless parameters obtained from the dimensional analysis can be listed as:

$$f = fun\left(S_o, A_w, C_y, d/h, BA, Fr, \mathrm{Re}_b\right) \tag{2}$$

where, $S_o$ is the channel bed slope, $A_w$ is the areal density of bristles, slenderness ratio, $s$, which represents the shape of the bristle is included in the Cauchy number $C_y = \frac{\rho U^2}{E} s^3$ (Li et al., 2018; Vettori and Nikora, 2018), in which $E$ is Young's modulus of elasticity of bristle, $d/h$ is the relative submergence of bristles, $BA$ is the brush block arrangement, $Fr$ is the Froude number, $Re_b$ denotes the bristle Reynolds number $\mathrm{Re}_b = \frac{uD_b}{\nu}$.

Systematic experiments were carried out in a 0.40 m wide, 0.5 m deep rectangular flume (bed slope adjustable between 0-12%), with 4 m long Plexiglas sidewalls and PVC bed. Experiments were performed with four different areal bristle densities and three different bed slopes. Derivation of the friction factor also includes the data set from Kassel University hydraulic laboratory that the experiments were conducted in a 2 m wide channel (Hassinger, 2004). 3D flow velocities were collected with the Micro Sontek ADV (16 MHz).

## 3. Results and Discussion

Hydraulic test data reveal that the Darcy–Weisbach friction factor tends to decrease with increases in discharge and Cauchy number, $C_y$, of the bristle. Fig. 3 shows the friction factor $f$ plotted against the Cauchy number $C_y$. The trend is best fitted by the logarithmic function

$$f = -a\ln(C_y) + b \tag{3}$$

Eq. (3) indicates the inverse dependence of the friction factor on the Cauchy number for the proposed fish pass structure and tested flow conditions, and this dependence is in agreement with previous studies for flexible vegetation (Li et al., 2018; Vettori and Nikora, 2018).

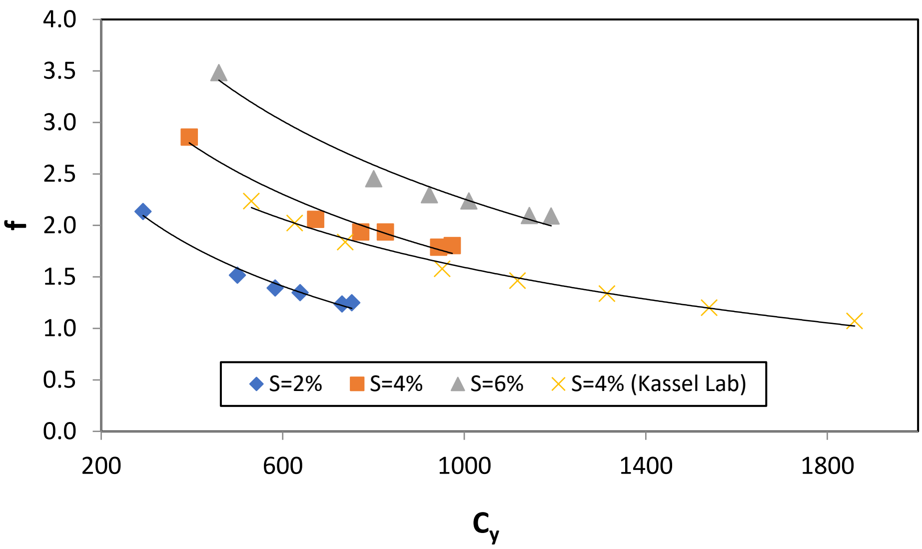


**Fig. 1.** Variation of the Darcy-Weisbach friction factor with the Cauchy number and bed slope for a bristle areal density of.$A_w$=0.011 $m^2/m^2$. Solid lines represent the best-fit curves of Eq. (3).

The bed slope, indirectly the Froude number, controls the turbulent kinetic energy magnitude. With the increase of bed slope from 2% to 6%, the maximum observed turbulent kinetic energy increased approximately by a factor of 4. The spatially averaged TKE is obtained by integrating the local TKE values over the horizontal plane. The spatially-averaged turbulent kinetic seems to be lower (for the same dissipated power) in brush fish than in technical fish passes. Compared to staggered boulders, spatially-averaged TKE in the basin reduced from 0.13 $m^2/s^2$ (Larinier, 2007) to 0.01 $m^2/s^2$ for the same dissipated power of $\Delta P$=270 $W/m^3$. Also, in brush fish pass the maximum TKE is reduced by a factor of 2 with compared the natural like type for the same dissipated power. This can be explained due to the fact that in the brush zone energy dissipation is related to the flow-induced vibrations of the bristles and the main energy dissipation takes place due to the oscillation and bending of bristles rather than by the viscosity of the water in an energy cascade process (Kucukali, 2016).

**Acknowledgments**

This work is supported by the Scientific and Technical Research Council of Turkey under the Scientific and Technological Research Projects Funding Program (3001 TUBITAK) grant with agreement number 315M019.

**References**

Baki, A.B.M., Zhu, D.Z., and Rajaratnam, N. (2014). Mean flow characteristics in a rock-ramp-type fish pass. J. Hydraul. Eng., ASCE, 114 (8), 939–944.
Cassan, L., Tien, T., Courret, D., Laurens, P., and Dartus, D., (2014). Hydraulic resistance of emergent macro roughness at large froude numbers: design of nature-like fishpasses. J. Hydr. Engrg. 140(9), 04014043.
Hassinger, R. (2004). Investigation of the discharge characteristics of the bristle fish pass at the Pfatter in the hydraulic laboratory. Kassel University, Germany (In German).
Heimerl, S., Krueger, F., and Wurster, H., (2008). Dimensioning of fish passage structures with perturbation boulders. Hydrobiologia, 609, 197-204.
Kucukali, S. (2016). Flow and turbulence structure in brush fish pass. Fish Passage Confence 2016, Massacuhtes, USA.
Larinier, M (2007). “Nature-like fish passes.” EIFAC working party - 2nd Meeting on Fish Passage Best Practices, Salzburg, Austria.
Li, Y.H., Xie, L., and Su, T.C. (2018). Resistance of open-channel flow under the effect of bending deformation of submerged flexible vegetation. J. Hydraul. Eng., ASCE, 144(3): 04017072.
Maier, D., and Lehmann, B.(2006). Borstenfischpass – Entwicklung eines Bemessungskonzepts. Wasserwirtschaft 96(10), 16-21.
Vettori, D. and Nikora, V., (2018). Flow-seaweed interactions: a laboratory study using blade models. Environmental Fluid Mechanics, 18, 611-636.

# Permeable Pavements Efficiency Under Clogging and Pollutants Load Removal

Mariana MARCHIONI [1], Maria Gloria DI CHIANO[2] Anita RAIMONDI[3] Claudia DRESTI[4], Umberto SANFILIPPO [5], John SANSALONE[6] & Gianfranco BECCIU[7]

[1, 2, 3, 4, 7] Department of Civil and Environmental Engineering (DICA), Politecnico di Milano (Milan) email: mariana.marchioni@polimi.it

[4] Water Research Institute (IRSA), Consiglio Nazionale delle Ricerche (CNR) (Verbania)

[6]ESSIE University of Florida (UF) (Gainesville)

ABSTRACT

Permeable pavement is used to reduce stormwater volume, peak flow and promote pollutant load removal (Scholz and Grabowiecki, 2007, Brunetti et al., 2016, Marchioni and Becciu, 2014). The volume reduction depends on the base depth, while peak flow and loads removal are dependent on the surface layer, that must present a hydraulic conductivity capable of significantly limiting runoff; while the pore structure acts as a filter retaining particulate matter (PM), deriving from erosive phenomena and anthropogenic activities. The infiltration capacity tends to decrease over time due to the PM accumulation. An adequate maintenance program guarantees that hydraulic conductivity remains above a threshold. The infiltration capacity is a function of the characteristics of the material used in the surface layer, normally permeable concrete (PC), porous asphalt (PA) or interlocking concrete blocks. For this research a series of a rainfall simulation tests were used to analyze the hydrological and load removal response of permeable pavement surface under clogging. Results confirm the permeable efficiency under clogging on stormwater runoff reduction and pollutants removal.

## 1. Methodology

For the tests, 18 PA and PC slabs of 500 × 260 × 50 mm (thickness) and ΦT (total porosity) of 0.15, 0.20 and 0.25 respectively produced in laboratory with a mix design from a previous study (Bonicelli et al. 2015). A rain simulator has been specially designed to perform the tests in laboratory. To simulate clogging phenomena a granular mixture with sand with particle size distribution ranging from 75 to 2,000 μm and a small fraction of *filler* was assembled to simulate dry deposition usually present on urban road pavements (Kim and Sansalone 2008). Tests were carried with rainfall intensity of 50 mm/h, 100 mm/h and 150 mm/h and PM concentrations of 0.5 kg/m$^2$; 1.0 kg/m$^2$ and 1.5 kg/m$^2$ for a total of 285 tests. Further details are reported on Marchioni et al (2021a); Marchioni et al. (2021b); Brugin et al. (2020); Marchioni et al., (2016); Valerio et al., (2016). The filtration mechanisms on porous media were analyzed through a mechanistic model, considering the ratio of the average pore diameter ($d_m$) to pm particle diameter ($d_p$) (McDowell-Boyer. t et al. 1986 (Auset and Keller 2006, McDowell-Boyer et al. 1986). These mechanisms have been identified for PC and PA (Teng and Sansalone 2004, Marchioni et al. 2021a, Marchioni et al. 2021b). In this study $d_p$ was estimated by XRT analysis for PA, a technique widely used for this purpose (Teng and Sansalone 2004, Sansalone et al. 2008, Kuang et al. 2015).

## 2. Results

Figure 1 (a), illustrates runoff coefficient (C) for the 285 tests, obtained as the ratio between the collected runoff volume and the total volume of the simulated storm event. The mean runoff coefficient found was 0.07 with a standard deviation of 0.11, and no surface runoff (C = 0) was observed in 47% of the tests confirming acceptable performance. The hydraulic conductivity of the PA and PC were measured both in initial conditions (before applying loadings) and after carrying out the cycle of tests and proceeding with a deep cleaning using water under pressure. Although a statistically significant decrease in hydraulic conductivity was observed, the efficacy in reducing surface flow was still acceptable. Figure 1 (b), shows PM fate for the rainfall simulation tests where most of the PM (> 85%) remained retained in the surface or inside the porous medium (PA and PC), a percentage less than 15% leached through the porous medium, while less than 2% was washed off by runoff, confirming pollution load removal. For the mechanistic model used, considering an $d_{p,average}$ = 2.52 mm for PA, was estimated a 92% of PM in mass retained by the porous medium where 87% on the surface , forming the *schutzdecke*, and 4% within the core of the specimen. It is also estimated that 8% of PM could leach the porous medium. The results obtained through the model have a percentage difference of 8% compared to the experimental values.

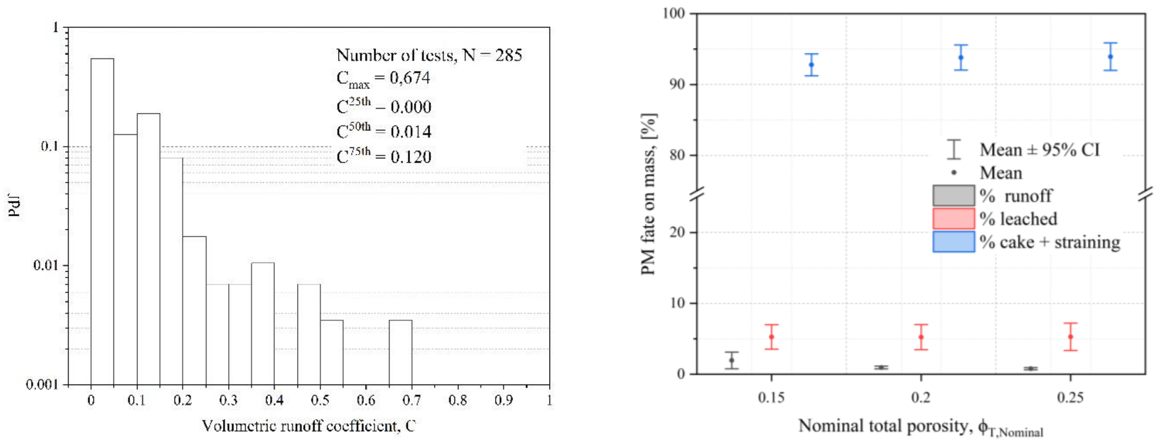


**Fig. 1.** (a) runoff coefficient obtained in the rain simulation tests, (b) PM fate on mass (Marchioni et al., 2021a, Marchioni et al., 2021b).

## 3. Conclusion

Permeable pavement performance for the surfaces considered (PA and PC) showed efficiency in reducing runoff and removing polluting load even under heavy clogging. In conclusion, the study demonstrated the efficiency of permeable pavement for two objectives of stormwater sustainable management, peak flow reduction and load removal.

### References

Adams, B. J., & Papa, F., Urban Stormwater Management Planning with Analytical Probabilistic Models, Wiley: New York, 2000.

Andrés-Valeri, V.C., Marchioni, M., Sañudo-Fontaneda, L. A., Giustozzi, F., & Becciu, G. Laboratory assessment of the infiltration capacity reduction in clogged porous mixture surfaces. Sustainability, 8(8), 751, 2016.

Auset, M. & A. A. Keller. "Pore-scale visualization of colloid straining and filtration in saturated porous media using micromodels." Water resources research 42(12), 2006.

Becciu, G., Raimondi, A., & Dresti, C. Semi-probabilistic design of rainwater tanks: a case study in Northern Italy. Urban Water Journal, 15(3), 192-199, 2018.

Bonicelli, A., Giustozzi, F., & Crispino, M. Experimental study on the effects of fine sand addition on differentially compacted pervious concrete. Construction and Building materials, 91, 102-110, 2015.

Brugin, M., Marchioni, M., Becciu, G., Giustozzi, F., Toraldo, E., & Andrés-Valeri, V.C. Clogging potential evaluation of porous mixture surfaces used in permeable pavement systems. European Journal of Environmental and Civil Engineering, 24(5), 620-630, 2020.

Brunetti, G., Šimůnek, J., & Piro, P. A comprehensive numerical analysis of the hydraulic behavior of a permeable pavement. Journal of Hydrology, 540, 1146-1161, 2016.

Eagleson, P.S. Climate, soil and vegetation: The distribution of annual precipitation derived from observed storm sequences. Water Resources Research, 14(5), pp. 713–721, 1978.

Eagleson, P.S., Dynamics of flood frequency. Water Resources Research, 8(4), pp. 878–898, 1972. https://doi.org/10.1029/WR008i004p00878.

Kim, J.-Y., and J. J. Sansalone. "Event-based size distributions of particulate matter transported during urban rainfall-runoff events." Water Res. 42 (10–11): 2756–2768, 2008.

Kuang, X., G. Ying, V. Ranieri & J. Sansalone. "Examination of Pervious Pavement Pore Parameters with X-Ray Tomography." Journal of Environmental Engineering 141(10): 04015021, 2015.

Marchioni, M., & Becciu, G. Permeable pavement used on sustainable drainage systems (SUDs): a synthetic review of recent literature, 2014.

Marchioni, M., Andrés-Valeri, V.C., Giustozzi, F., & Becciu, G. Laboratory study on the rainfall influence over the sediment transport dynamics on pervious pavements' discharge. Urban Water Syst Floods, 165, 165-76, 2016.

Marchioni, M., Fedele, R., Raimondi, A., Sansalone, J., & Becciu, G. Permeable Asphalt Hydraulic Conductivity and Particulate Matter Separation With XRT,2021a.

Marchioni, M., Raimondi, A., Andrés-Valeri, V.C., Becciu, G., & Sansalone, J. Permeable Pavement Hydraulic Conductivity Indices for Rainfall-Runoff and Particulate Matter Loadings. Journal of Environmental Engineering, 147(12), 04021064, 2021b.

McDowell-Boyer, L.M., J. R. Hunt & N. Sitar. "Particle transport through porous media." Water Resources Research 22(13): 1901-1921, 1986.

Raimondi, A., & Becciu, G. Probabilistic design of multi-use rainwater tanks. Procedia Engineering, 70, 1391-1400, 2014.

Raimondi, A., Marchioni, M., Sanfilippo, U., Stroppa, F. F., & Becciu, G. Probabilistic estimation of runoff from green roofs. International Journal of Computational Methods and Experimental Measurements, 10(1), 13-25, 2022.

Sansalone, J. & G. Ying. "Partitioning and granulometric distribution of metal leachate from urban traffic dry deposition particulate matter subject to acidic rainfall and runoff retention." Water research 42(15): 4146-4162, 2008.

Scholz, M., & Grabowiecki, P. Review of permeable pavement systems. Building and environment, 42(11), 3830-3836, 2007.

Teng, Z., & J. Sansalone. "In situ partial exfiltration of rainfall runoff. II: Particle separation." J. Environ. Eng. 130 (9): 1008–1020. https://doi.org/10.1061/(ASCE)0733-9372(2004)130:9(1008), 2004.

Zhang, S. & Guo, Y., An analytical equation for evaluating the stormwater volume control performance of permeable pavement systems. Journal of Irrigation and Drainage Engineering, 141(4), 2015.

# Hydrodynamics of *Daphnia magna* horizontal migration: phototaxis and predatory cues

Tatiana MÁXIMO[1], Joana Luísa PEREIRA[2], Ana Margarida RICARDO[3], Rui ALEIXO[4], Rui M.L. FERREIRA[5]

[1] Instituto Superior Técnico, Universidade de Lisboa, Portugal
email: tatiana.maximo@tecnico.ulisboa.pt

[2] CESAM, Universidade de Aveiro, Portugal
email: j.pereira@ua.pt

[3,4] Civil Engineering Research and Innovation for Sustainability, IST-ID, Portugal
email: ana.ricardo@tecnico.ulisboa.pt; rui.aleixo@tecnico.ulisboa.pt

5 CERIS, Instituto Superior Técnico, Universidade de Lisboa, Portugal
email: ruimferreira@tecnico.ulisboa.pt

ABSTRACT

Daphnids are amongst the most efficient grazer zooplankters. They serve as representative models in freshwater ecology, e.g. to study zooplankton migration patterns. Horizontal migration of daphnids is not well known, particularly in what concerns the relation with hydrodynamics. Addressing this research gap, we experimentally characterize the horizontal migration of *Daphnia magna* associated to positive phototaxis. A LED light source is installed at the end of the tank opposite to the half-tank where fifty individuals of *D. magna* were initially placed. The study tested two conditions: water with and without fish kairomones. It was observed that the horizontal movement of *D. magna* can be decomposed into advective and diffusive modes. Preliminary results show that horizontal positive phototaxis is reduced in the presence of fish kairomones.

## 1. Introduction

Zooplankton represents a key functional level in freshwater ecosystems, especially in lakes and reservoirs, controlling phytoplankton and transferring carbon and energy to higher food web stages (Pinel-Alloul, 1995). Daphnids are amongst the most efficient grazer zooplankters and hence have been used as representative models in many biological disciplines, including freshwater ecology (Altshuler et al. 2011). For example, they have been extensively used to study zooplankton migration patterns. Migration of zooplankton is driven by abiotic and biotic threats (Rollwagen-Bollens et al., 2020), including by the perception of predatory cues (kairomones), a mechanism that is genetically imprinted. Vertical migration of daphnids, as a behavioral response to light, is relatively well understood and their phototaxis is intertwined with predation risk (Loose, Cartson J. et al., 1993). In the absence of predatory cues, daphnids tend to exhibit positive phototaxis for wavelengths in the visible spectrum, while some variations may occur depending on spectral specificities (e.g. UVR intensity) (Storz, U.C. et al., 1998). However, in shallow lakes, vertical migration is of little relevance, and horizontal migration is likely the prevalent mode of daphnid movement to escape from perceived threats or to respond to light stimuli. Horizontal migration of daphnids is not as well studied as vertical migration and should take into account the hydrodynamics of the fluid environment. Addressing this research gap, we propose to experimentally characterize the horizontal migration of *D. magna* associated to positive phototaxis.

## 2. Experimental methods

The study is conducted under two conditions: water with and without fish kairomones. The experimental set-up comprises a water tank ($40 \times 20 \times 19$ cm$^3$) divided at half-length by a thin opaque vertical barrier. A LED light source is installed at one end of the tank. Fifty individuals of a pre-defined *D. magna* clone are placed in the half-tank opposite to the light source. In the other half there is water with or without fish kairomones. The entire length of the channel is illuminated by red backlight. Particle Image Velocimetry (PIV) tests were carried out to characterize the background velocity, as the removing the vertical gate always produces circulation. The motion of individual daphnids is recorded by a high-speed camera ($1200\times1000$ px$^2$) at 100 fps. The set-up mimics the conditions found in nature when the movement is between the littoral, where macrophyte cover offers protection, and the limnetic area. The experimental procedure entails: selecting the light wavelength, adjusting the power to ensure that the same light intensity for all wavelengths and removing the barrier. The position, velocity and acceleration of the daphnids is obtained with Particle Tracking Velocimetry.

## 3. Results

Fig. 1 shows the background velocity measured with PIV two instants after the gate removal. Two clockwise coherent structures dominate the mixing of the fluids.

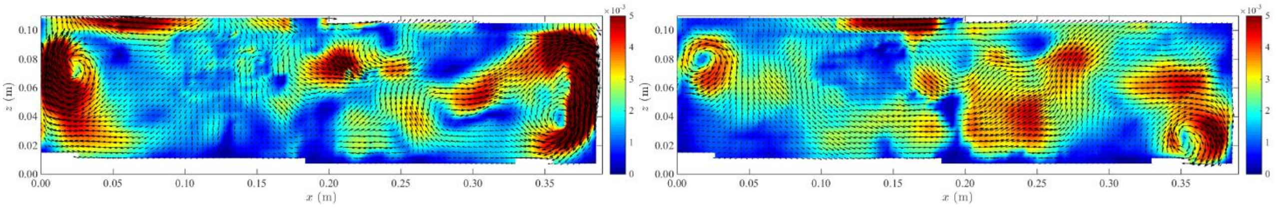


**Fig. 1** - 2D instantaneous velocity maps in a plane perpendicular to the gate at 3s (left) and 145s (right) after the gate removal.

Fig. 2 presents PIV raw images where the seeded fluid is a proxy to the water with fish kairomones. It is observed that after 2.5 minutes the fish kairomones are expected to be felt in the entire channel although full mixing has not been attained.

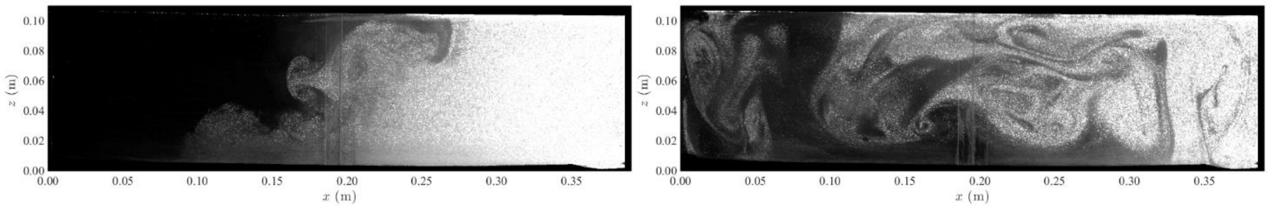


**Fig. 2** - Raw images acquired with a PIV system at 3s (left) and 145s (right) after the gate removal.

The horizontal movement of *D. magna* can be decomposed into an advective and a diffusive mode. Evidence of the influence of fish kairomones is under scrutiny. Preliminary tests (Fig. 3) without and with kairomones showed that the *D. magna* individuals significantly reduce their velocity towards the light source in the presence of fish kairomones, a previously unreported trait of *D. magna* phototaxis.

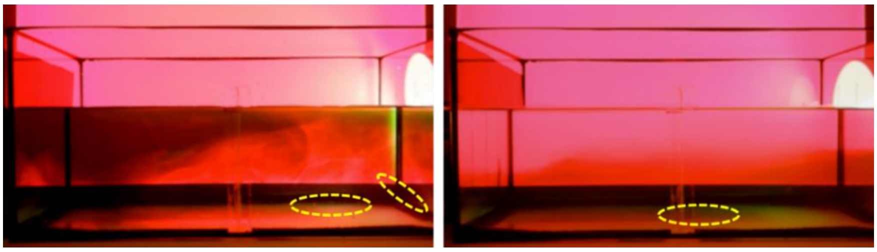

**Fig. 3** – Location of *D. magna* individuals at 66s after the gate removal in the tests without (left) and with (right) kairomones. The yellow ellipses highlight the daphnids' location.

## 4. Conclusion

Light perception promotes the vertical migration of *D. magna*, providing them with the ability to escape visual predators in a circadian cycle. We show that phototaxis also induces horizontal migration. The perception of predatory cues produce a change in the pattern of movement towards the light source, a reduction of the mean velocity *D. magna*. This is a previously unreported finding with major implication in *D. Magna* ethology.

**Acknowledgements**

This work was supported by the project WinTherface (PTDC/CTA-OHR/30561/2017) funded by national funds through FCT. Thanks are due to the financial support to CESAM by FCT/MCTES (UIDP/50017/2020 + UIDB/50017/2020 + LA/P/0094/2020).

**References**

Altshuler I, Demiri B, Xu S, Constantin A, Yan ND, Cristescu ME (2011) An Integrated Multi-Disciplinary Approach for Studying Multiple Stressors in Freshwater Ecosystems: Daphnia as a Model Organism, Integrative and Comparative Biology 51:4, 623–633.
Loose, Carsten J.; von Elert, Eric; Dawidowicz, Piotr (1993) Chemically induced diel vertical migration in Daphnia: a new bioassay for kairomones exuded by fish. Archiv für Hydrobiologie, vol.126 (pg.329-337).
Pinel-Alloul B (1995) Spatial heterogeneity as a multiscale characteristic of zooplankton community, Hydrobiologia 300, 17–42.
Rollwagen-Bollens G, Bollens S, Dexter E, Cordell J (2020) Biotic vs. abiotic forcing on plankton assemblages varies with season and size class in a large temperate estuary, Journal of Plankton Research 42, 221–237.
Storz, U.C.; Paul, R.J. (1998) Phototaxis in water fleas (*Daphnia magna*) is differently influenced by visible and UV light, J Comp Physiol A 183, 709-717.

# Comparative Assessment of Macroinvertebrate Habitat Suitability in Mediterranean (Greek) and Semi-Arid (Moroccan) River Reaches

Christos THEODOROPOULOS[1], Georgios VAGENAS[1,2], Soumia MOUTAOUAKIL[3], Hassan BENAISSA[3,4], Yassine FENDANE[3], Maria STOUMBOUDI[2], Elias DIMITRIOU[2], Mohammed GHAMIZI[3], Anastasios STAMOU[1]

[1] Department of Water Resources and Environmental Engineering, School of Civil Engineering, National Technical University of Athens, Greece (ctheodor@central.ntua.gr)
[2] Institute of Marine Biological Resources and Inland Waters, Hellenic Centre for Marine Research, Greece
[3] Department of Biology, Natural History Museum of Marrakech, University of Cadi Ayyad, Marrakech, Morocco
[4] Institute of Technology of Maritime Fisheries, Al Hoceima, Morocco

ABSTRACT

Ecohydraulic models have long been used to determine environmental flows downstream of dams, but the often lack of local habitat suitability curves (HSCs) prevents their wider implementation. To overcome this, ecohydraulic experts often use HSCs developed in ‘foreign’ river reaches. However, this approach may result in unrealistic ecohydraulic outputs. We developed and compared HSCs for freshwater macroinvertebrates from Greek (Mediterranean climate) and Moroccan (semi-arid climate) river reaches, to (i) either support or discourage the use of ‘foreign’ HSCs in ecohydraulic models, and (ii) provide locally developed HSCs for robust ecohydraulic simulations in Greek and Moroccan river reaches. Macroinvertebrates were influenced by water depth and substrate type in the Moroccan river reaches, and by flow velocity and water depth in the Greek river reaches. Moreover, they had different optimal habitat preferences. Our results discourage the use of ‘foreign’ HSCs in ecohydraulic models, especially in areas of different hydro-climatic properties.

## 1. Introduction

Ecohydraulic models (e.g., those applied to assess environmental flows downstream of dams) require (i) a hydraulic input: flow velocities, water depths and substrate types across the river reach that will be simulated, and (ii) a biological input: habitat suitability curves (HSCs) for aquatic biota, usually fish or benthic macroinvertebrates. If one of these inputs is missing, ecohydraulic simulations cannot be applied. The missing input is usually the biological one, as the development of HSCs in rivers is a costly and time-consuming task (Theodoropoulos et al., 2018). To overcome this frequent lack of HSC data, ecohydraulic experts have often been tempted to use HSCs from other river reaches, potentially with different hydro-climatic properties, and thus different aquatic community structure, often producing unrealistic ecohydraulic outputs (Hudson et al., 2003). Consequently, the development of HSCs for aquatic biota from various river reaches is a crucial step towards applying accurate and ecologically credible ecohydraulic models.

We developed and compared HSCs for freshwater macroinvertebrates from Mediterranean (Greek) and semi-arid (Moroccan) river reaches, to (i) examine potential differences in the habitat preferences of benthic macro-invertebrates from different climatic zones, and (ii) provide a robust biological input for relevant ecohydraulic simulations in Greek and Moroccan river basins, thus overcoming the need to extrapolate HSCs between reaches, which has often led to inaccurate or unrealistic ecohydraulic results.

## 2. Materials and methods

We measured flow velocity (V; m/s), water depth (D; m) and the type of substrate (S; see Theodoropoulos et al., 2018), and collected macroinvertebrates using a rectangular hand-net from (i) 59 unpolluted microhabitats across the upper Oum Er-Rbia River, Morocco (semi-arid climate) and (ii) 380 unpolluted microhabitats from various streams and rivers of similar hydro-climatic properties in Greece (Mediterranean climate). Each microhabitat was 0.25 x 0.25 $m^2$ wide. The resulting datasets included observations of V, D, S and macroinvertebrate taxa, which were converted to a community-based habitat suitability index (K) as follows:

$$\mathbf{K_i = 0.4\,n_i + 0.3\,H_i\ + 0.2\,EPT_i + 0.1\,a_i}$$

where $K_i$ is the habitat suitability of the $i^{th}$ microhabitat, $n_i$, $H_i$, $EPT_i$ and $a_i$ are the macroinvertebrate taxonomic richness (family level), the Shannon’s diversity index, the richness of Ephemeroptera, Plecoptera and Trichoptera and the abundance of the $i^{th}$ microhabitat, respectively. All $K_i$ values were normalized to the 0-1 scale by dividing by the maximum K at each river reach to account for potential spatial and/or temporal autocorrelation. Statistical relationships (p and $R^2$ values) between hydraulic variables (V, D, S) and K were produced, via generalized linear mixed-effects models using the GAMLSS package (Rigby and Stasinopoulos, 2005) in R version 4.0.1. HSCs were similarly developed using generalized additive models.

## 3. Results and discussion

In the Moroccan river reaches (semi-arid climate), water depth and substrate type were the major drivers of macroinvertebrate habitat suitability, being statistically significant and strongly correlated with K ($R^2 > 0.5$). In the Greek river reaches (Mediterranean climate), macroinvertebrate K was significantly influenced by water depth and flow velocity (Table 1), however, correlations were weak to moderate ($0.32 \geq R^2 \geq 0.14$).

**Table 1.** Statistical significance (p) and strength of correlation (pseudo-$R^2$) between hydraulic variables and macroinvertebrate habitat suitability using generalized linear mixed-effects models (**<0.01; *<0.05).

| Hydraulic variables | Habitat suitability \| Greece | | Habitat suitability \| Morocco | |
|---|---|---|---|---|
| | p | $R^2$ | p | $R^2$ |
| Flow velocity (m/s) | 0.046* | 0.14 | 0.248 | 0.64 |
| Water depth (m) | 3.41e-16** | 0.32 | 0.01** | 0.51 |
| Substrate type | 0.15 | 0.13 | 0.001** | 0.81 |

Macroinvertebrates mostly preferred shallow, rocky habitats (large gravel, small, large stones and boulders; optimal D values between 0.1 m and 0.2 m). In the Greek river reaches, macroinvertebrates preferred slow to moderately flowing waters (with wider optimal V range, from 0.4 m/s to 0.9 m/s), in contrast to the Moroccan reaches, where they mostly preferred moderately flowing waters (with narrower optimal V range, from 0.65 m/s to 0.85 m/s). In the Greek river reaches, they had increased tolerance for suboptimal flow velocities: they could largely tolerate V > 0.7 m/s up to 1 m/s and V < 0.4 m/s (K remained > 0.5). In contrast, in the Moroccan reaches, K became unsuitable (< 0.5) in V < 0.6 and V > 0.8 m/s, as well as in D < 0.05 and D > 0.15 m.

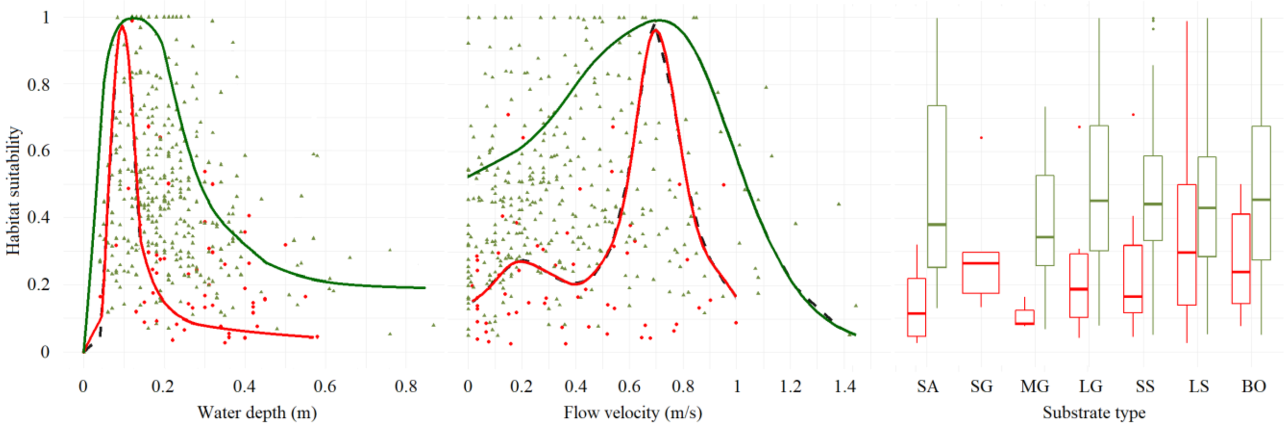


**Figure 1.** Habitat suitability curves for frehswater macroinvertebrates from the Greek (green; n=380) and Moroccan (red, n=59) river reaches. SA: Sand; SG, MG, LG: Small, medium, large gravel; SS, LS: Small, large stones; BO: Boulders

## 4. Conclusion

Macroinvertebrates in Mediterranean and semi-arid river reaches were influenced by different hydraulic drivers (D and S in the Moroccan river reaches; D and V in the Greek river reaches). Moreover, their optimal habitat preferences between the two areas were different. We conclude that the use of macroinvertebrate HSCs in river reaches of different hydro-climatic properties will likely produce unrealistic ecohydraulic outputs, which may further lead to inadequate environmental flow recommendations and thus, inadequate freshwater management strategies.

### References

Hudson HR, Byrom AE, Chadderton WL (2003) A critique of IFIM: instream habitat simulation in the New Zealand context. Science for Conservation, Wellington NZ, 69 pp.
Rigby RA, Stasinopoulos DM (2005) Generalized additive models for location, scale and shape. Journal of the Royal Statistical Society: Series C 54, 507-554.
Theodoropoulos C, Vourka A, Skoulikidis N, Rutschmann P, Stamou A (2018) Evaluating the performance of habitat models for predicting the environmental flow requirements of benthic macroinvertebrates. Journal of Ecohydraulics 3, 30-44.

# Evaluating Hydrological stressors by Monitoring Mussel Behaviours

Ashkan PILBALA[1], Luca TOSATO[2], Vanessa MODESTO[3], Nina BENISTATI[4], Sebastiano PICCOLROAZ[5], Luigi FRACCAROLLO[6], Donatela TERMINI[7], Dario MANCA[8], Tommaso MORAMARCO[9], Nicoletta RICCARDI[10]

[1,2,5,6]University of Trento, Department of Civil, Environmental and Mechanical Engineering, Via Mesiano 77, 38123 Trento, Italy.
email:ashkan.pilbala@unitn.it
email:luca.tosato@unitn.it
email:s.piccolroaz@unitn.it
email:luigi.fraccarollo@unitn.it

[3,8,10]The National Research Council (CNR) - Water Research Institute (IRSA), Largo Tonolli 50, 28922 Verbania, Italy.
email: vane.modesto@gmail.com
email: dario.manca@cnr.it
email: nicoletta.riccardi@irsa.cnr.it
[4,7]University of Palermo, Department of Engineering, Viale delle Scienze, 90128 Palermo, Italy.
email: nina.benistati@libero.it
email: donatella.termini@unipa.it
[9]The National Research Council (CNR) - Research Institute for Geo Hydrological Protection (IRPI), Via Madonna Alta 126, 06128 Perugia, Italy.
email: t.moramarco@irpi.cnr.it

ABSTRACT

Since future climatic scenarios predict an increase in the number and intensity of extreme events, such as droughts and floods, understanding how low and high flow conditions affect aquatic organisms is crucial for the conservation of freshwater biodiversity and ecosystem services. On the other hand, the response of riverine animals to flow intensity and flow conditions can be rapid and unambiguous, i.e., well correlated. In this work, we present an experimental study on the relation between hydrodynamics and biotic communities in fluvial ecosystems and assess the behavior of the animal as a biological early warning system (BEWS) for hydro-morphological change, including sediment transportation.

Freshwater mussels (FM) have been identified as suitable biological indicators to assess environmental stressors to detect disturbances on ecosystems since 1950 (Hiscock, 1950). Kramer et al. (2001) started to use the monitoring of the mussels as a BEWS since 2001, but the suitability of FM for monitoring the impact of hydraulic stressors is still lacking. During the last two decades, these methodologies have been used to measure the presence of pollutants in water bodies. To reach this aim, the Valvometric method has been used, based on the use of Hall sensors (real-time remote monitoring tool) to get the data. The behavioral responses of mussels are characterized by valve opening amplitudes and opening-closure frequencies. We relate these behaviors to hydrological conditions and sediment transport mimicking the onset of floods. The experiments conducted in a laboratory flume (Fig. 1) were carried out by starting with a stage of constant discharge (without sediment transport) followed by an abruptly increased value of discharge, which in most cases is accompanied by sediment transport. Hall sensors and magnets were fixed on the shells of mussels (Fig. 2) and connected to an Arduino system. The opening and closing of the valve were continuously monitored, along with the hydro-morphological conditions. FMs maintained a constant valve gaping frequency that characterizes their normal behavior (feeding and movement). FMs promptly reacted to extreme discharge conditions with sediment transport by increasing valve gaping frequencies, shifting from normal to transition behavior. We checked that a minimum number of animals is necessary to reach some degree of accuracy in the statistical treatment of the data. Most mussels (87 to 97%) reacted promptly to increased discharge with sediment transport, showing a transition from their normal behavior to a significantly higher valve gaping frequency, and the intensity of their reaction significantly increased from the lowest to the highest stress levels. Fig. 3 shows the frequency of mussel gapping during the experiments. We can observe that there is a threshold between the experiments without and with sediment transport on the bed (bedload) which is 0.025 Hz. Therefore, if the responses of mussels

are higher than 0.025 Hz, the condition is with high variation which meant sediment transport has started. In the end, FMs response to hydro-morphological was fast and accurate, showing that they can be used as a reliable BEWS, under general flow conditions.

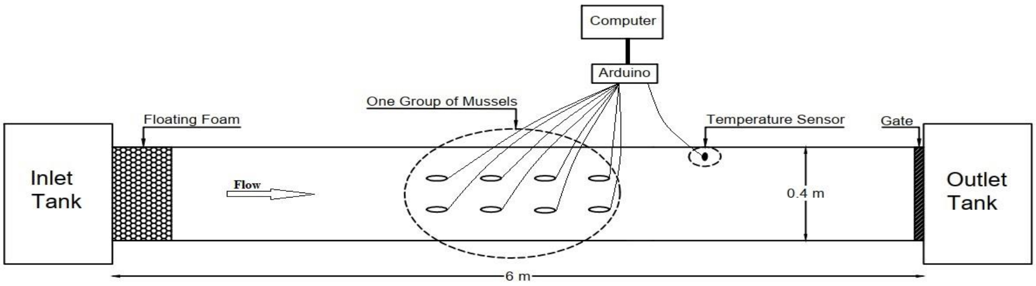


**Fig. 1.** *Plan of experimental flum*

**Fig. 2.** Freshwater Mussels with Hall Sensors

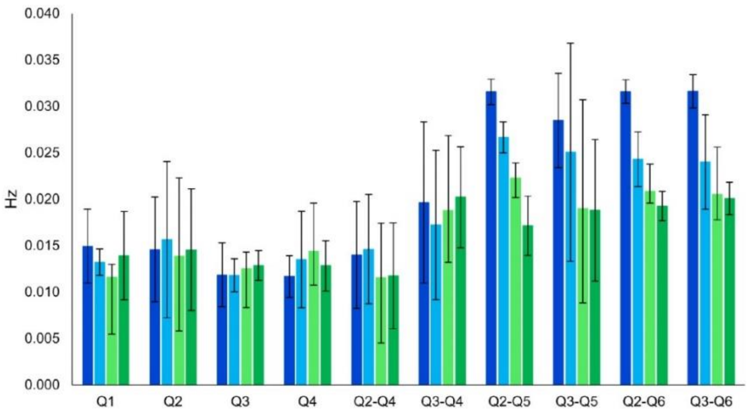


**Fig. 3.** Response of FMs (Frequency) versus different flow conditions: Q1 to Q4 are Constant discharge without sediment transport, Q5 is discharge with low sediment transport, Q6 is discharge with high sediment transport

**Acknowledgments**

This work has been supported by the Italian PRIN 2017 project Enterprising (2017SEB7Z8).

**References**

Hiscock I.D. (1950) Shell Movements of the Freshwater Mussel, *Hyridella australis* Lam. (Lamellibranchiata), Australian Journal of Marine and Freshwater Research 1(2) 259 – 267.

Kramer K. J., Foekema E. M. (2001) The "MUSSELMONITOR” as biological early warning system. Biomonitors and Biomarkers as Indicators of Environmental Change 2, Edited by Butterworth et al. Kluwer Academic/Plenum Publishers, New York, 2000.

# MultiPAC as a tool to validate the success of restoration measures

Stefan HAUN[1], Beatriz NEGREIROS[1], Maximilian KUNZ[1], Sebastian SCHWINDT[1], Alcides AYBAR GALDOS[2], Markus NOACK[2] and Silke WIEPRECHT[1]

[1] Institute for Modelling Hydraulic and Environmental Systems, University of Stuttgart, Stuttgart, Germany
email: stefan.haun@iws.uni-stuttgart.de
[2] Institute of Applied Research, Karlsruhe University of Applied Science, Germany

ABSTRACT

Restoration measures are implemented in many rivers, lakes, and reservoirs worldwide to achieve a good ecological status of these water bodies. As the options for restoration measures are manifold and very site-dependent, associated monitoring is inevitable to conclude on the success of restoration measures. With the here proposed MultiParameter Approach to assess Colmation (MultiPAC), it is possible to obtain in-depth knowledge on the composition and quality of the riverbed. MultiPAC provides information in the form of several measurable physical parameters, which result in a holistic picture of *in-situ* conditions. The approach is applied in this study in a residual river stretch to quantify the short- as well as the long-term impact of different restoration measures. The results show that MultiPAC can quantify changes in substrate conditions, which enables an evaluation of the success of the implemented measures.

## 1. Introduction

Many water bodies are heavily modified and are consequently not in a good ecological state anymore. With the aim to achieve a good ecological status for surface waters, according to the EU Water Framework Directive (2000/60/EC), restoration measures are implemented in many rivers worldwide. The possibilities for restoration measures are manifold, but their success is site-dependent. To validate the success of measures, often only changes in water quality or alterations of habitat conditions are used as a proxy. However, to attain a holistic overview of the habitat conditions of a river stretch, the quality of the substrate is necessary information and of high importance to reveal the ecological evolution of a river stretch. Such quantification is typically based on either expert assessment only or on single parameters. In this study, the novel **MultiP**arameter **A**pproach to assess **C**olmation (MultiPAC) is presented, which enables the quantification of conditions within the interstitial of a river's hyporheic zone. MultiPAC uses multiple physical parameters, which are obtained *in-situ* before and after the implementation of restoration measures (Haun et al., 2022).

## 2. Quantification of morphological conditions and the success of restoration measures

For the quantification of the current morphological conditions of a riverbed and the suitability of different restoration strategies, detailed knowledge of riverbed sediments, their composition, and their properties is indispensable. In this study, a residual river stretch is investigated with MultiPAC (Aybar Galdos et al., 2021). The measurements are conducted before and after the implementation of restoration features.

### *2.1. Study site and implemented measures*

The here considered river stretch of the Inn River is located in Bavaria, Germany. The river is historically characterized by a high summer discharge and low water temperatures in combination with high sediment transport. However, as a direct result of the construction of a diversion weir at Jettenbach, bedload transport is completely interrupted and the discharges have been limited to residual flows. Hence, a supply-limited system is currently in state, resulting in riverbed incision and ecological deficits. To prevent further incision, sills were placed in the river stretch, retaining the bed level, but also initiating the development of an armor layer, and clogging of the hyporheic zone. To promote sediment dynamics, several restoration actions were implemented, such as gravel augmentation and the removal of river bank fixations, which should yield in increased natural or artificial sediment supply. In addition, measures were implemented in March 2020 and in March 2021 to improve habitat conditions in the short-term. The measures involve instream channel reconfiguration of multiple gravel bars (Fig. 1a) and the implementation of a half-moon shaped structure at one of the gravel bars in the channel center (Fig. 1b). The combination of restoration actions intends to stimulate sustainable recovery of dynamic equilibrium conditions in the residual river stretch.

**Fig. 1.** (a) Instream channel reconfiguration and (b) the half-moon shaped structure at the channel centre, to improve habitat conditions as a result of heterogeneous flow and sediment conditions in close vicinity.

### *2.2. MultiParameter Approach to assess Colmation (MultiPAC)*

MultiPAC is used to measure several physical parameters along with expert assessment (mapping of the degree of outer and inner riverbed clogging). The approach consists of measurements of dissolved oxygen content (saturation and concentration) and hydraulic conductivity at several measurement locations and with a high vertical resolution by using a double-packer system called VertiCo (**Verti**cal profiles of hydraulic **C**onductivity and dissolved **O**xygen). The double-packer itself measures depth-dependent slurping rates, which can afterwards be transformed to values of hydraulic conductivity (Seitz, 2020). In addition, the sediment composition and the fine sediment fraction of the interstitial are obtained by freeze-core and shovel sampling. Structure-from-Motion is used to attain the porosity of the freeze-core samples. All these measurement parameters are finally compared with literature values, which serve as a reference to evaluate the condition of the riverbed substrate and to quantify a possible impairment of salmonid reproduction.

## 3. Results and Conclusions

For assessing the changes in riverbed conditions in the residual river stretch, three field measurement campaigns were performed. In a first step, the current status (status quo) was examined, in a second step, the short-term effect of different methods for restructuring gravel bars was investigated, and in a third step, long-term (after one year) changes were monitored. The first investigation (status-quo measurements) shows a high amount of fine sediments in the subsurface and the occurrence of inner- and outer colmation in large parts of the river stretch. In addition, the development of an armor layer is observed in many gravel bars. This also results in low measured dissolved oxygen concentrations and hydraulic conductivity. Hence, the measurements indicate the potential impairment of salmonid spawning grounds for the current state of the river stretch.

The hydraulic conductivity and dissolved oxygen measurements (recorded after the measures were implemented) suggest that restructuring of gravel bars, by breaking up the armor layer and by implementing an island-pool pattern, have a positive effect on the habitat conditions in a short-term. However, the artificial island-pool structures were flattened by only one small summer flood and repetitive measurements showed that the positive effect decreases over time (long-term). Also, the positive effect of the half-moon structure on habitat conditions, given by a loose texture of the substrate and apparent heterogeneous flow pattern right after the measure implementation (short-term), decreases over time (long-term). As a result of high fine sediment transport, small sediment fractions were deposited inside the half-moon structure after the summer flood, and measured oxygen concentration and hydraulic conductivity decreased.

This study proves that MultiPAC enables to quantify the status of the substrate of a riverbed, and can be used to validate the success of restoration measures. By the high vertical resolution of the measurements, even the detection of changes within the hyporheic zone are possible, as well as the quantification of the degree of clogging in different layers of the riverbed.

**Acknowledgments**

The first author received financial support by the Baden-Württemberg Stiftung through the Eliteprogramme for Postdocs.

**References**

Aybar Galdos A, Haun S, Schwindt S, Biserov R, Negreiros B, Kunz M, Markus N (2021) A novel multi-parameter approach to assess the effects of river restoration measures on the sediment matrix, EGU GA 2021, online, 19–30 April 2021, EGU21-6152.
Haun S, Negreiros B, Kunz M, Schwindt S, Aybar Galdos A, Markus N, Wieprecht S (2022) MultiPAC: A novel approach to quantify the clogging degree of a riverbed, EGU GA 2022, Vienna, 3–8 April 2022, EGU22-1318.
Seitz L (2020) Development of new methods to apply a multiparameter approach – a first step towards the determination of colmation, Mitteilungen, Institut für Wasser- und Umweltsystemmodellierung, Universität Stuttgart 276.

# 1D numerical modelling of sedimentation propagation in a narrow reservoir

Sudesh DAHAL[1], Frederic M. EVERS[2], Robert M. BOES[3], David F. VETSCH[4]

[1,2,3,4] Laboratory of Hydraulics, Hydrology and Glaciology; ETH Zürich, Switzerland
[1]email: dahal@vaw.baug.ethz.ch
[2]email: evers@vaw.baug.ethz.ch
[3]email: boes@vaw.baug.ethz.ch
[4]email: vetsch@vaw.baug.ethz.ch

ABSTRACT

Reservoir sedimentation affects the sustainable operation of dam-reservoir systems as it progressively reduces the storage volume and may also impair functionality of dam safety structures such as bottom outlets. The situation is severe because the global annual loss of reservoir volume due to sedimentation is higher than the increase in storage capacity by the construction of new dams. This implies that our reservoirs are not sustainable and further action needs to be taken to ensure sustainable storage to fulfil the demands of a growing population. It requires in-depth investigation of underlying processes involving complex interactions of hydrodynamic and sediment transport phenomena which are not easy to study analytically. In this study, a 1D numerical model is prepared for the case of sedimentation in Solis Reservoir, Switzerland. A set of modelling parameters is obtained that allows to have a fair agreement between model results and the actual sedimentation processes observed in monitoring campaigns. The model can be further used to investigate the effectiveness of different sediment management strategies.

## 1. Introduction

Reservoirs are vital infrastructure worldwide for energy generation and water storage, and the significance increases more as water demand and climate-related stresses increase while the limited feasible storage sites are already exploited to a large extent (Annandale et al., 2016). However, the sustainable operation of reservoirs is threatened by sedimentation which causes a global average storage loss of around 0.5-1% per year while the rate of capacity expansion is much lower (Basson, 2009). Proper understanding of the underlying processes of reservoir sedimentation is thus essential to predict long-term storage availability and to investigate sustainable sediment management measures.

Solis Reservoir in Switzerland (Fig. 1) is selected as a case study site for setting up a 1D numerical model that can be used to analyze different driving processes for reservoir sedimentation. The 61 m high Solis dam was constructed in 1986 which created about 3 km long narrow reservoir of 4.07 $Mm^3$ initial volume. It is fed by the Albula River that drains a watershed of about 900 $km^2$ which includes two more reservoirs in the Julia River tributary. Sediment supply mainly comes from the Albula River, while the sediment from the Julia River is mostly trapped in the upper reservoirs. Due to high rate of sedimentation, the Solis Reservoir lost about 50% of its initial storage volume until 2009 (Auel & Boes, 2011). A Sediment Bypass Tunnel (SBT) was constructed in 2012 that allows for managing sedimentation by diverting high sediment load during flood events (Oertli & Auel, 2015).

## 2. Numerical Modelling

The objective of this study is to develop a 1D numerical model that can simulate the propagation of sedimentation in the Solis Reservoir. BASEMENT is used for the modelling purpose which allows numerical simulation of unsteady flow with multiple-grain sediment transport as bedload and suspended load (Vetsch et al., 2022). The aim is to start the model with the reservoir bathymetry of November 1998 and to simulate the model until November 2001 to compare the simulated bed profile with the measured bed profile (Fig. 1).

The bathymetry data, inflow discharge, and reservoir operating level are obtained from the previous records of the dam operator (ewz). The inflow discharge boundary condition is derived from the data of gauging stations on the Albula and Julia Rivers, and outflows released by the Tiefencastel powerplants located just upstream of the reservoir. The sediment composition is derived from the particle size distribution of bed material samples of Albula River and the reservoir. The suspended sediment inflow is defined in terms of suspended load rating curve of Albula River, which was derived in a previous study (Müller-Hagmann, 2018).

The bedload inflow is computed as transport capacity by using empirical relations. These data are then analyzed to prepare inputs for developing a 1D numerical model using the BASEMENT software.

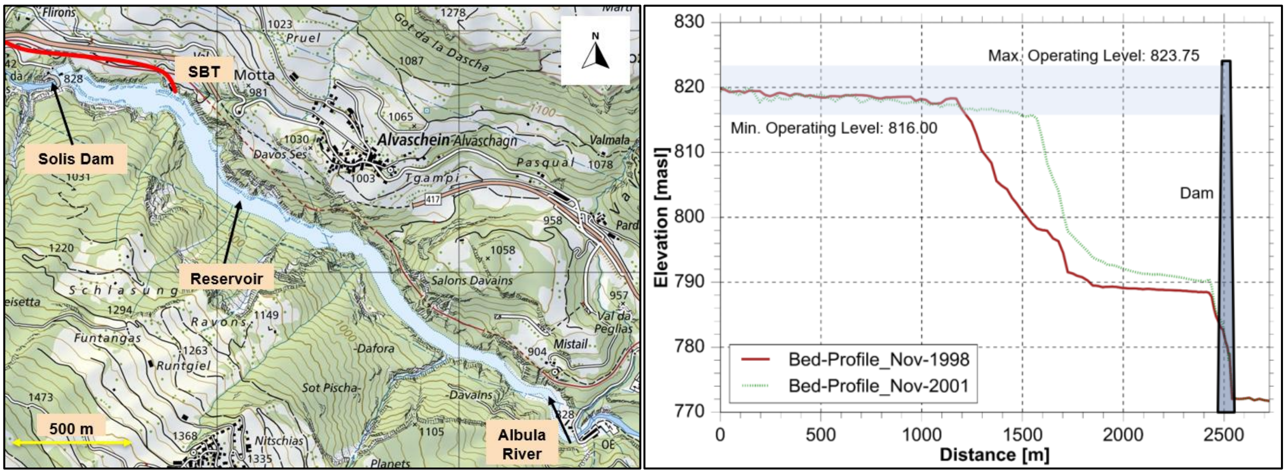


**Fig. 1.** Left: Map of Solis Reservoir (Source: Federal Office of Topography). Right: Longitudinal bed profile of Solis Reservoir showing the sedimentation propagation from November 1998 to November 2001 (Data Source: ewz).

A period of three years from 15th November 1998 to 15th November 2001 is simulated with the model and the resulting reservoir bed profile is compared with the measured bed profile. Different model parameters (Table 1) are calibrated to achieve a simulated bed profile that is similar to the measured bed profile. Furthermore, the effect of varying reservoir level due to hydropower generation on the bed profile is studied.

**Table 1.** Model parameters considered for optimization

| Category | Parameters |
|---|---|
| Roughness | Strickler Coefficient |
| Bed material | No. of sediment fractions |
| Bedload | Transport Capacity formula |
| | Bedload factor |
| | Approach for critical Shields parameter |
| Suspended load | Near bed concentration factor |
| | Approach for sediment exchange with bed |

## 3. Conclusions and outlook

A 1D numerical model is applied for simulating the propagation of sedimentation in a narrow reservoir. The model is calibrated for various hydraulic and sediment transport related parameters such that it allows to have a fair agreement with the actual process of sedimentation. It can be further used to predict the sedimentation for various future scenarios related to flow and sediment variability. This model can also be used to investigate the performance of the SBT in the Solis Reservoir by using the field monitoring data of SBT operations.

**Acknowledgements**

This project has received funding from the Swiss Federal Office of Energy and European Union's Horizon 2020 research and innovation programme under the Marie Sklodowska-Curie (MSC) grant agreement No 847585. The data related to Solis Reservoir were provided by Electric Power Company of Zurich (ewz).

**References**

Annandale GW, Morris GL, Karki P (2016) Extending the life of reservoirs: sustainable sediment management for dams and run-of-river hydropower. The World Bank
Auel C, Boes RM (2011) Sediment bypass tunnel design - review and outlook. Dams and reservoirs under changing challenges, 40312
Basson GR (2009) Management of siltation in existing and new reservoirs. General Report Q. 89. In Proceedings of the 23rd Congress of the International Commission on Large Dams CIGB-ICOLD, May 25–29, 2009, Brasilia, Vol. II
Müller-Hagmann M (2018) Hydroabrasion by high-speed sediment-laden flows in sediment bypass tunnels. VAW-Mitteilung 239 (R. Boes, ed.), Laboratory of Hydraulics, Hydrology and Glaciology (VAW), ETH Zürich, Switzerland
Oertli C, Auel C (2015) Solis sediment bypass tunnel: First operation experiences. In Proc. First International Workshop on Sediment Bypass Tunnels, VAW-Mitteilung 232 (R. Boes, ed.), Laboratory of Hydraulics, Hydrology and Glaciology (VAW), ETH Zürich, Switzerland, pp. 223-233
Vetsch D, Siviglia A, Bürgler M, Caponi F, Ehrbar D, Facchini M, Faeh R, Farshi D, Gerber M, Gerke E, Kammerer S, Koch A, Mueller R, Peter S, Rousselot P, Vanzo D, Veprek R, Volz C, Vonwiller L, Weberndorfer M. (2022) System Manuals of BASEMENT, Version 2.8.2, Laboratory of Hydraulics, Hydrology and Glaciology (VAW). ETH Zürich, Switzerland. Available from http://www.basement.ethz.ch. [Accessed on 14.03.2022]

# Laboratory Design of Representative Real Shallow Basins for Validation of Numerical Models

EL Mehdi CHAGDALI[1], Cédric GOEURY[1], Benjamin DEWALS[2], Sébastien ERPICUM[2], Matthieu SECHER[3], Kamal EL KADI ABDEREZZAK[1]

[1] National Laboratory for Hydraulics and Environment (LNHE), EDF R&D, France
el-mehdi.chagdali@edf.fr
cedric.goeury@edf.fr
kamal.el-kadi-abderezzak@edf.fr

[2] Research Group of Hydraulics in Environmental and Civil Engineering (HECE), University of Liège, Belgium
b.dewals@uliege.be
s.erpicum@uliege.be

[3] EDF Hydro-CIH, France
Matthieu.secher@edf.fr

ABSTRACT

Shallow reservoirs are hydraulic engineering structures widely used for trapping sediments or storing water. Several research works focused on the links between reservoir geometry, boundary conditions and flow patterns but considered simplified configurations. The objective of this study is to complete the existing data by designing a set of new laboratory configurations representative of a range of real cases to get new data for the validation of numerical models and to allow a better understanding of the physics. Two inlet flow configurations are considered with rectangular reservoirs: an open channel (reference case), and a pressurized flow jet; the outlet is a free surface channel for both configurations. A wide range of parameters extracted from real reservoirs are investigated. Parameters with significant impact on the flow pattern are analyzed and retained for the design of laboratory experiences (Reynolds number, Froude number, Friction number…). A numerical pre-simulation is performed with the TELEMAC-3D code to test the hydraulic parameters and establish a preliminary numerical comparison between the reference and jet cases. The 3D results and 2D average results of velocity magnitude extracted from TELAMAC-3D simulations are presented and compared. For the same hydraulic conditions, comparisons between the reference and jet cases show a different flow pattern and distribution.

## 1. Introduction

Shallow reservoirs are hydraulic structures widely used for trapping sediments or storing water. The loss of the effective storage volume due to sedimentation decreases the reservoir functionality for flood control, hydropower generation, irrigation, water supply and reactional activities (Schleiss et al., 2016). The flow pattern and trap efficiency of a shallow reservoir depend on its geometrical shape, hydraulic conditions, boundary conditions (i.e. inlet and outlet), and sediment characteristics (Kantoush, 2008; Camnasio et al., 2013). hydro-morphodynamic numerical models are useful tools for optimizing the design of shallow reservoirs and predicting their performance.

The first experimental studies on shallow reservoirs concerned the effect of a sudden expansion through an inlet free surface channel for a rectangular reservoir. Abbott and Kline (1962) were amongst the firsts to study this subject. The rectangular reservoir was considered with infinite length and results showed the presence of three regions: a first region at the immediate inlet of the reservoir with a three-dimensional stationary recirculation, a two-dimensional stationary region with a point of attachment downstream from the first region, and an unsteady tail region downstream from the second region. For turbulent flow, there was no effect of tested Reynolds number on the length of the three zones. Durst et al. (1974) showed that the flow after a sudden expansion was three-dimensional, while Cherdron et al. (1978) showed that the flow at low Reynolds number was nominally two-dimensional. Durst et al. (1974) and Cherdron et al. (1978) also explained the effect of the Reynolds number on the flow typology. For low Reynolds number, a symmetrical flow was found. For higher Reynolds number, an asymmetry was found that was explained by the small perturbations created at the expansion level. These perturbations are involved in the shear layer created between the main flow and the recirculation in the reservoir corner. As a continuation on the work on sudden expansion through an inlet free surface channel, Mizushima and Shiotani (2001) evaluated the effect of a downstream contraction combined with an upstream expansion at the basin entrance. The inlet and outlet channels were of the same width. Authors found that the addition of the downstream contraction restabilized the symmetric state of the flow.

Kantoush (2008) studied the flow pattern in different shallow rectangular reservoirs with free surface channels at the inlet and outlet. Starting with a reference reservoir, the length was gradually reduced while keeping a fixed width. Conversely, while keeping a fixed length, the width was modified. Different ranges of Reynolds number and Froude number were studied. Dissymmetric flows were observed for some configurations despite of the symmetry of the reservoir. Kantoush (2008) identified four types of flows: symmetrical with two attachment points, asymmetrical with two attachment points, symmetrical with one attachment point, and symmetrical with no reattachment point. Kantoush (2008) also studied gradually expanding reservoirs with one lozenge, one hexagon and one rectangular shape with reduced inlet angles. Dufresne et al. (2010) clarified the transition between symmetric and asymmetric flows in rectangular reservoirs using the shape factor defined as $\mathsf{SF} = L_1/(\Delta B^{0.6} b^{0.4})$, with $L_1$ the reservoir length, $b$ the inlet channel width, and $\Delta B = (B - b)/2$ the width of the sudden expansion with $B$ as the reservoir width. It appears that symmetric flows occur for $\mathsf{SF} < 6.2$ and asymmetric flows take place for $\mathsf{SF} > 6.8$. Camnasio et al. (2013) confirmed experimentally the impact of varying the position of the channel inlet and outlet on the velocity field and sedimentation. Choufi et al. (2014) examined the effect of bottom roughness of a shallow rectangular reservoir with variable geometry and symmetrical inlet and outlet on the flow field. Asymmetric flows could be developed depending on certain edge conditions, resulting from the growth of small perturbations in initial and boundary conditions. Peltier et al. (2014) investigated oscillatory flows of "meandering jet" type in about 50 experiments performed in rectangular reservoirs. The frequency, wavelength and lateral extension of the flow were extracted from Large Scale Particle Image Velocimetry (LSPIV) measurements using a Proper Orthogonal Decomposition (POD). Threshold values on the shape factor and on the Froude number were identified to predict the occurrence of a meandering jet type flow. Relationships were obtained between the characteristics of the meandering jet and friction number $\mathsf{S}$, which was defined by Peltier et al. (2014) as $\mathsf{S} = \lambda \Delta B/(8H)$ with H the water depth and $\lambda$ the friction coefficient.

Some authors were interested on inlet boundary conditions with turbulent circular jet. Stovin and Saul (1994) performed a series of experiments on a rectangular reservoir whose inlet and outlet were circular pipes. Adamsson et al. (2005) performed an experimental study on a large basin (i.e. 13 m long and 9 m wide and 0.8 m high); the inlet was a circular jet with a diameter of 0.23 m and the outlet was a weir. Two large symmetrical recirculations were observed. Dufresne (2008) conducted 55 experiments in a rectangular reservoir with a circular pipe at the inlet and a frontal weir at the outlet. He observed an asymmetrical and stationary flow for low water heights and a symmetrical and stationary flow for higher water heights. A pseudo periodic regime appeared between these two cases. In a broader context than shallow reservoirs, Jirka (2004) showed that jet behavior in ambient water bodies is highly dependent on the initial flow conditions, such as initial volume, momentum and buoyancy fluxes, and discharge angle. Concerning real cases, the analysis of shallow reservoirs managed by EDF Hydro-CIH showed an important difference within their geometries, boundary conditions (e.g. free surface channel, jet, gate, weir) and hydro-morphodynamic conditions (Claude et al., 2019). Table 1 summarizes the characteristics of boundary conditions in reservoirs of interest.

**Table 1.** Boundary conditions characteristics of real cases

| Reservoirs | Inlet boundary | | | Outlet boundary | | |
|---|---|---|---|---|---|---|
| | Type | Number | Position | Type | Number | Position |
| Cheylas | Pressurized jet (plant outtake gallery) | 1 | Inside | Flap gate<br>Pressurized water intake (plant intake gallery) | 3<br>1 | Lateral wall<br>Inside |
| Longefan | Free surface channel | 1 | Corner | Weir | 1 | Corner |
| Cadarache | Radial gates | 2 | Lateral wall | Weir | 1 | Lateral wall |
| La Coche | Pressurized jet (plant outtake gallery + water supply gallery) | 2 | Lateral wall | Pressurized water intake (plant intake gallery) | 1 | Inside |

Existing experimental works depicted above show certain limitations in terms of engineering needs, as they mainly focused on simple rectangular reservoirs with inlet and outlet rectangular free surface boundary channels, generally situated on opposite sides, and in a lesser degree, some experiences with inlet turbulent jet. On the other hand, real reservoirs feature different characteristics of boundary conditions (Table 1). The objective of this study is to design a set of new laboratory configurations representative of a wide range of real cases, complementary to existing studies, which will allow the validation of numerical models, such as the widely used suite of TELEMAC-MASCARET codes (www.opentelemac.org). We are firstly interested in a comparison between two configurations: a “Reference case” with rectangular free surface channels at the inlet and outlet, and a “Jet case” with a free turbulent circular jet at the inlet boundary and free surface rectangular channel at the outlet. Then, an experimental design is set to study, from different geometrical perspectives, the turbulent jet as inlet boundary condition. A wide range of parameters extracted from real reservoirs are investigated (Reynolds number, Froude number, Friction number.). A numerical pre-simulation is performed using the TELEMAC-3D code for the reference and jet cases.

## 2. Choice of parameters and experimental design

The physical model was constructed in the laboratory of Hydraulics in Environmental and Civil Engineering (HECE) group at Liege University (Belgium), based on the facility widely used by Dufresne et al. (2010) and Peltier et al. (2014). The reservoir geometries that will be investigated have to fit in an existing horizontal flume (Fig. 1), $L$ = 10.4 m long, $B$ = 0.985 m wide and $h$ = 0.5 m deep. Considering a safety margin of 5 cm, the maximum water depth is about 0.45 m. The flume bottom and walls are fixed and made of glass. The reservoir width is equal to the flume width and the downstream and upstream extremities are created by solid blocks placed in the flume. The position of these blocks can be modified to change the reservoir length $L_1$. The inlet and outlet are located on opposite sides of the reservoir. The width of outlet boundary is fixed at $b_o$ = 0.08 m for all configurations. Regarding the pump characteristics, the flow rate that can be used is in the range 0.0002 to 0.006 $m^3/s$.

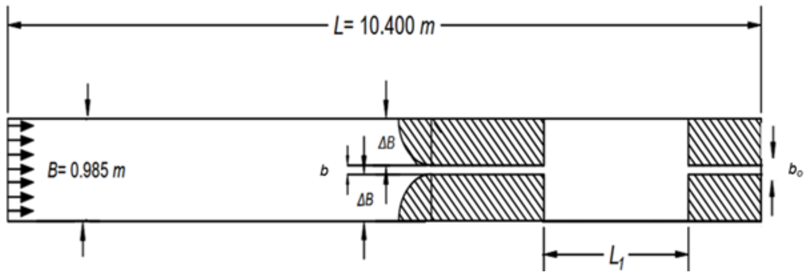


**Fig. 1.** Sketch illustrating the existing experimental flume at HECE laboratory, University of Liège (not to scale).

Following Peltier et al. (2014) the flow is be governed by eight parameters, namely reservoir length $L_1$, reservoir width $B$, inlet channel width or jet diameter $b$, flow depth $H$, mean depth-averaged velocity in the inlet channel $U$, roughness height $k_s$, kinematic viscosity $\nu$, and gravitational acceleration $g$. The velocity is calculated as $U = Q/(bH)$, with $Q$ the inlet flow rate. According to Vaschy Buckingham theorem, six dimensionless parameters can be defined: lateral expansion ratio $B/b$, length-to-width ratio $L/B$, flow depth-to-width ratio (i.e. shallowness parameter) $H/B$, Froude number $\mathsf{F} = U/(gH)^{1/2}$, Reynolds number $\mathsf{R} = 4UH/\nu$, and Friction number $\mathsf{S} = \lambda B/H$. In this later number, the friction coefficient $\lambda$ is a function of the relative roughness $k_s/H$ and Reynolds number $\mathsf{R}$. The friction number is defined differently from Peltier et al. (2014). The width of the sudden expansion $\Delta B$ would not be available for real cases due to asymmetry of their boundary condition positions, the friction number $\mathsf{S}$ is therefore defined in terms of the reservoir width $B$.

Couples of points ($\mathsf{S}$, $\mathsf{F}$) are presented in Fig. 2 for real reservoirs with free surface inlet (Longefan and Cadarache), real reservoirs with inlet pressurized jet (Cheylas and La Coche), laboratory experiments with free surface inlet channel, and laboratory experiments with inlet jet. The Min and Max values correspond to minimum and maximum hydraulic operating values, respectively. For each reservoir $\mathsf{S}$ and $\mathsf{F}$ are calculated using the formulas detailed upper. For real reservoirs, the roughness height $k_s$ is calculated from the median sediment grain size $D_{50}$ and sensitivity analysis is done while taking a minimum value of $k_s = D_{50}$ and maximum value of $k_s = 100D_{50}$; the error bar in the scatter plot displays the confidence interval for the Friction number. The objective is to determine experimental values of $Q$, $b$ and $H$ that will allow reaching minimal and maximal values of Friction and Froude numbers to encompass the couple of points ($\mathsf{S}$, $\mathsf{F}$) in the scatter plot while considering experimental constraints.

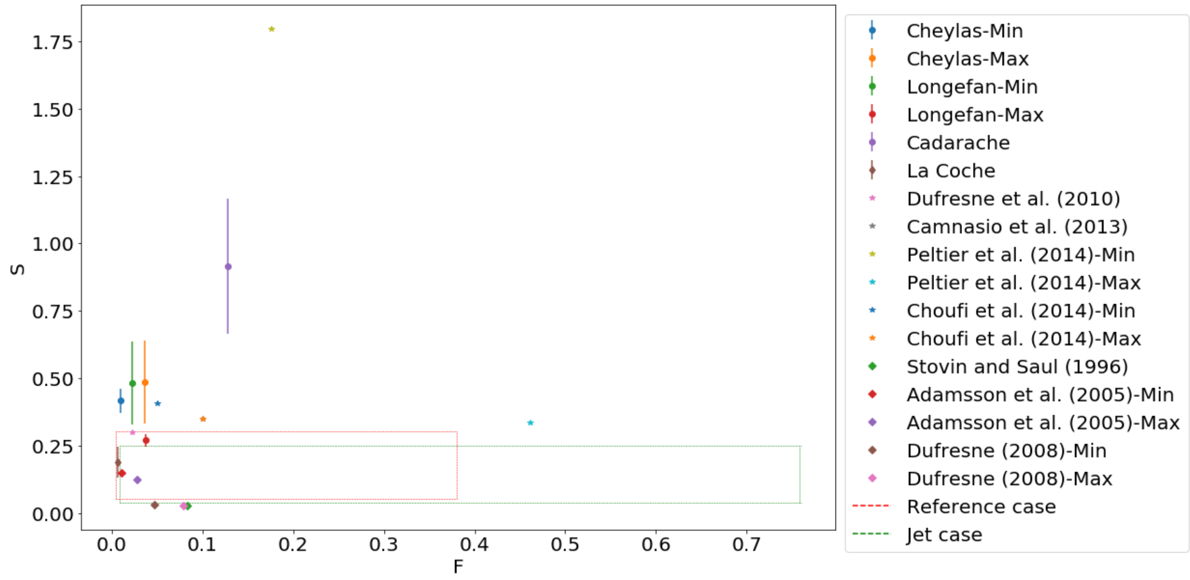


**Fig. 2.** Friction factor S in terms of Froude number F for real reservoirs, laboratory experiments, limits for reference and jet cases.

To allow future comparisons, the same values of $H$ and $Q$ are set for both reference and jet cases, recalling that the flow rate $Q$ is between 0.0002 and 0.006 m$^3$/s and the Froude number F should be set lower than 1 to remain in subcritical flow regime. The tested values for $Q$, $b$ and $H$ for the jet case showed that the constraining limits to encompass a higher number of points is the upper limit of S; the lower limit of S can be obtained for $H = 0.30$ m. Highest values of S could be reached for lowest values of $H$, because of the increase in shallowness parameter and friction coefficient. The lowest value of $H$ is in turn limited by the jet diameter, in order to ensure a desired condition of $H = 2.5b$. Considering the experimental constraints, $b = 0.04$ m is set for jet case, which implies the following lowest flow depth $H = 0.1$ m. Concerning the reference case, the blocks used in Peltier et al.'s (2014) experiments will be reused for operational convenience, which yields inlet channel width of $b = 0.08$ m. Table 2 summarizes the selected parameters retained for the reference and jet cases. Figure 2 shows that experimental jet limits encompass the existing experiences in the literature using jet as inlet boundary condition and La Coche real reservoir. Table 3 summarizes the geometrical parameters retained for this study. For each case, a short reservoir and long reservoir will be studied.

**Table 2.** Selected parameters for reference and jet cases

| | Configuration Number | $b$ (m) | $b_o$ (m) | $H$ (m) | $Q$ (m$^3$/s) | $U$ (m/s) | R | F |
|---|---|---|---|---|---|---|---|---|
| Reference case | 1 | 0.08 | 0.08 | 0.10 | 0.0002 | 0.025 | 1.00 x 10$^4$ | 0.025 |
| | 2 | 0.08 | 0.08 | 0.10 | 0.0030 | 0.375 | 1.50 x 10$^5$ | 0.378 |
| | 3 | 0.08 | 0.08 | 0.30 | 0.0060 | 0.250 | 3.00 x 10$^5$ | 0.146 |
| | 4 | 0.08 | 0.08 | 0.30 | 0.0002 | 0.008 | 1.00 x 10$^4$ | 0.005 |
| Jet case | 5 | 0.04 | 0.08 | 0.10 | 0.0002 | 0.050 | 2.00 x 10$^4$ | 0.050 |
| | 6 | 0.04 | 0.08 | 0.10 | 0.0030 | 0.750 | 3.00 x 10$^5$ | 0.757 |
| | 7 | 0.04 | 0.08 | 0.30 | 0.0060 | 0.500 | 6.00 x 10$^5$ | 0.300 |
| | 8 | 0.04 | 0.08 | 0.30 | 0.0002 | 0.017 | 2.00 x 10$^4$ | 0.010 |

**Table 3.** Geometrical parameters for reference and jet cases

| Case | $L_1$ (m) | $\Delta B$ (m) | $b$ (m) | Shape factor (SF) |
|---|---|---|---|---|
| Reference case | 2.00 | 0.45 | 0.08 | 8.87 (Long reservoir) |
| | 1.05 | 0.45 | 0.08 | 4.65 (Short reservoir) |
| Jet case | 2.00 | 0.47 | 0.04 | 11.4 (Long reservoir) |
| | 1.05 | 0.47 | 0.04 | 5.98 (Short reservoir) |

The purpose of this experimental design is firstly to compare the jet and rectangular cases and then to have a clear description on different configurations of jet behavior that will allow a proper validation of numerical model. The geometrical configurations are detailed in Table 4. For each configuration, four hydraulic conditions will be studied (Table 2). For each case, a short and a long reservoir will be designed (Table 3). The effect of the inlet jet will be compared to the reference case for the four hydraulic conditions set previously. Thereafter, and because of asymmetry of boundary conditions in real cases, different positions of the jet will be tested. For the case of jet at the center position, different exit angles will be studied.

**Table 4.** Geometrical parameters for experimental set-up

| $L_1$ (m) | $\Delta b$ (m) | $b$ (m) | Inlet boundary conditions | Reservoir type | Jet position | Jet angle (°) with respect to $X$ axis at horizontal plan |
|---|---|---|---|---|---|---|
| 2.00 | 0.45 | 0.08 | Rectangular channel | Long reservoir | - | - |
| 1.05 | 0.45 | 0.08 | Rectangular channel | Short reservoir | - | - |
| 2.00 | 0.47 | 0.04 | Jet | Long reservoir | Center | 0 |
| 1.05 | 0.47 | 0.04 | Jet | Short reservoir | Center | 0 |
| 2.00 | - | 0.04 | Jet | Long reservoir | Right side | 0 |
| 1.05 | - | 0.04 | Jet | Short reservoir | Right side | 0 |
| 2.00 | - | 0.04 | Jet | Long reservoir | Left side | 0 |
| 1.05 | - | 0.04 | Jet | Short reservoir | Left side | 0 |
| 2.00 | - | 0.04 | Jet | Long reservoir | Downstream from center | 0 |
| 1.05 | - | 0.04 | Jet | Short reservoir | Downstream from center | 0 |
| 2.00 | - | 0.04 | Jet | Long reservoir | Upstream from center | 0 |
| 1.05 | - | 0.04 | Jet | Short reservoir | Upstream from center | 0 |
| 2.00 | 0.47 | 0.04 | Jet | Long reservoir | Center | 30 |
| 1.05 | 0.47 | 0.04 | Jet | Short reservoir | Center | 30 |
| 2.00 | 0.47 | 0.04 | Jet | Long reservoir | Center | 45 |
| 1.05 | 0.47 | 0.04 | Jet | Short reservoir | Center | 45 |
| 2.00 | 0.47 | 0.04 | Jet | Long reservoir | Center | 60 |
| 1.05 | 0.47 | 0.04 | Jet | Short reservoir | Center | 60 |

## 3. Numerical pre-simulations

The turbulent jet could be divided into three regions: near field, intermediate field, and far field (Fischer et al., 1979). A model with small spatial and short time scales is necessary to accurately describe near-field mixing in the vicinity of the release point (Jirka, 2004). However, in the far field the behavior is dominated by ambient flow conditions that operate on much larger time and space scales. Numerical pre-simulations are performed with TELEMAC-3D numerical code to test hydraulic parameters chosen previously, and to establish a preliminary numerical comparison between reference and jet cases. TELEMAC-3D uses a sigma transformation on the vertical (non-conforming transformation) which facilitates the construction of a 3D mesh. This transformation allows having a structured mesh on the vertical, built as an extrusion of a 2D mesh along the vertical, then divided into layers. Unliked some CFD codes where it is possible to define CAD objects that allow representing the boundary conditions in a faithful way, it is not possible in TELEMAC-3D to represent these boundary conditions accurately. The method used here is the prescription of these conditions on several defined planes. Thus the prescribed flow is transformed into velocity condition on liquid boundary only on the specified planes, while velocities are set to zero otherwise. TELEMAC-3D is applied with non-hydrostatic pressure distribution, k–ε turbulence model in both horizontal and vertical directions, and LIPS (Locally semi-Implicit Predictor-corrector Scheme) for advection of velocity and turbulence. The Strickler formula is used for the friction term; a value of 80 $m^{1/3}\ s^{-1}$ (corresponding to PVC) is retained for the bed and walls, which is equivalent to a roughness height $k_s = 10^{-3}$ mm. The 3D model is composed of seven layers uniformly distributed along the vertical, based on 2D unstructured mesh (0.004 m space step) with a total of 930 000 nodes. Figure 3 shows the 2D unstructured mesh and boundary condition positions for reference and jet cases. For the jet case, the inlet pipe is located horizontally at $x = 0$ and $- 0.02$ m $< y < 0.02$ m and, and vertically between plan 3 located at $z = 0.126$ m and plan 4 located at $z = 0.168$ m ($z = 0$ is set at the reservoir bottom). Configurations 3 and 7 presented in Table 2 are simulated.

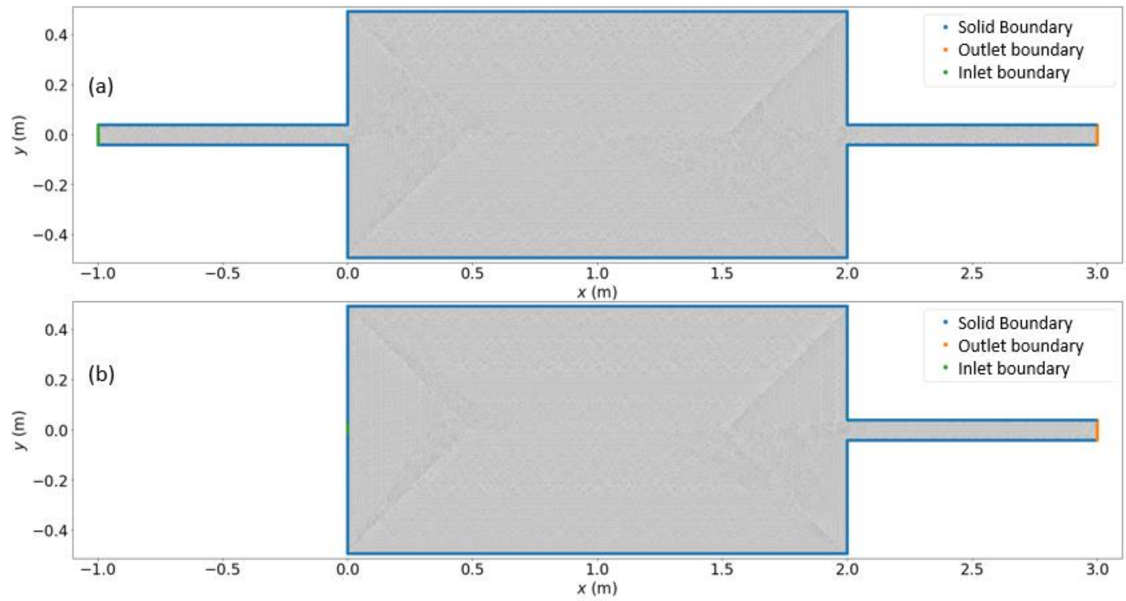


**Fig. 3.** Unstructured 2D mesh and boundary condition positions for (a) reference case, and (b) jet case (2D).

Figure 4 describes the 2D average velocity magnitude and streamlines at different time steps. The 2D average velocity magnitude of TELEMAC-3D simulations is compared for reference and jet cases. A steady state is found for the reference case with symmetrical pattern. The jet case yields an oscillatory flow pattern.

The 3D numerical results are analyzed while comparing velocity magnitude for reference and jet cases at $y$ = 0.0 m. The results show that velocity decreases along the reservoir for both cases (Fig. 5). The jet configuration does not spread along the water depth of the reservoir. The velocity magnitude is higher for jet case compared to reference case and is mainly localized in the jet direction.

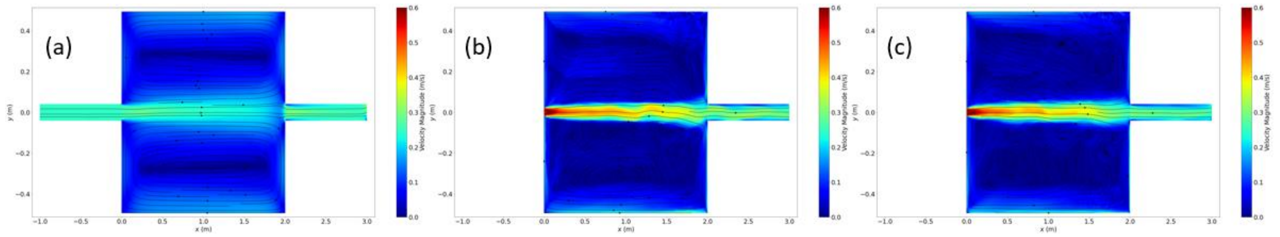


**Fig. 4.** Two-dimensional (2D) average velocity magnitude and streamlines for - (a) Steady state of reference case at t = 800 s, (b) Oscillatory state for jet case at t = 400 s, (c) Oscillatory state for jet case at t = 800 s.

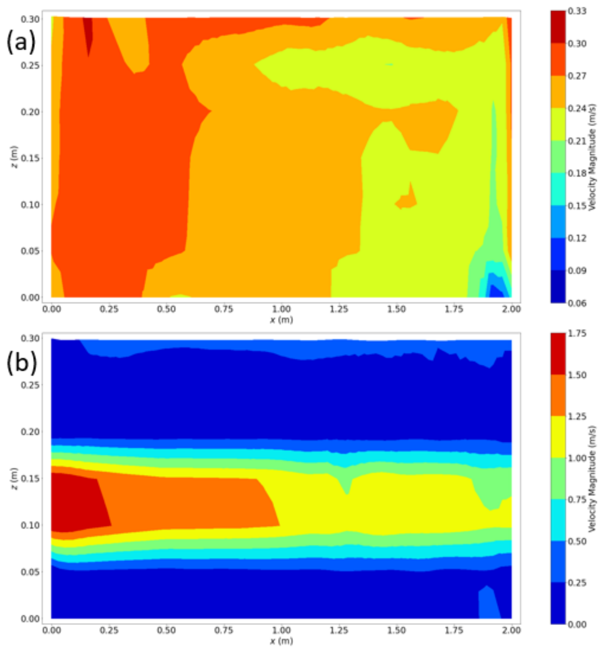


**Fig. 5.** Two-dimensional (2D) velocity magnitude withTELEMAC-3D numerical simulations for – (a) reference case and (b) jet case, at $y$ = 0.0 m. Note that the legend is not uniformized for reference and jet cases because of their different velocity magnitude values.

Figure 6 shows 2D velocity magnitude for reference and jet cases at *x* = 0.1 m (just upstream of the inlet), *x* = 1.0 m (middle) and *x* = 2.0 m (reservoir outlet). The results confirm that the jet does not spread along the flow depth. For the same hydraulic conditions, a different flow pattern and distribution are found depending on the inlet flow configuration.

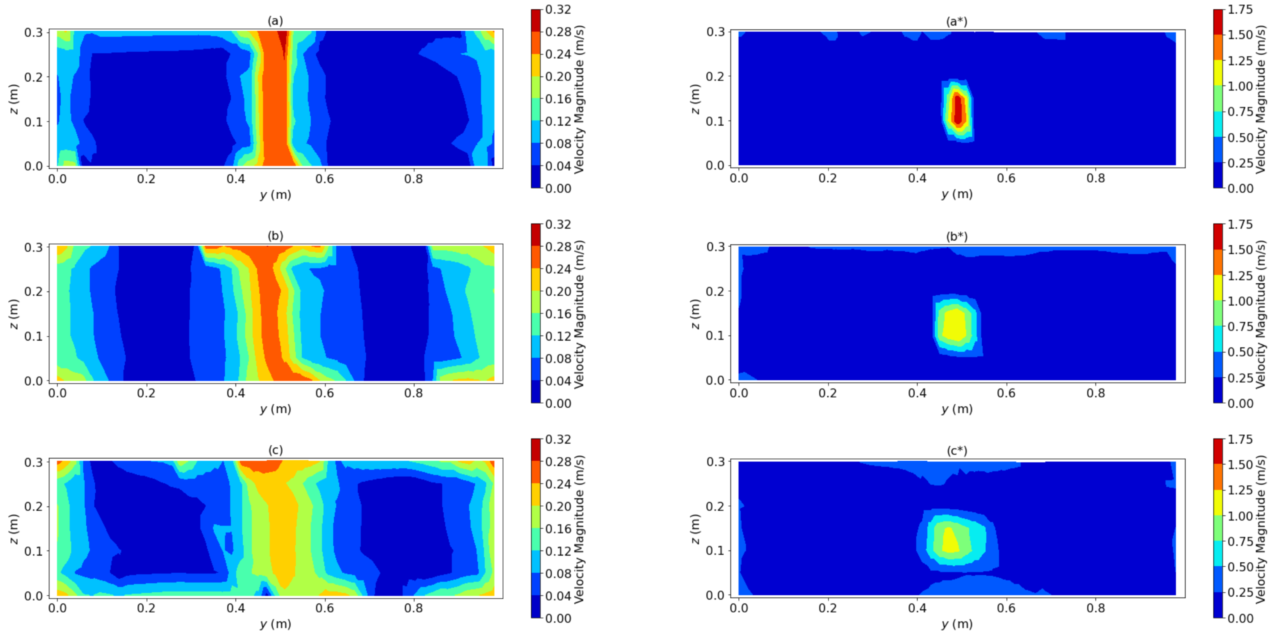


**Fig. 6.** Two-dimensional (2D) velocity magnitude withTELEMAC-3D numerical simulations for reference case (left) and jet case* (right) at (a) and (a*) at x = 0.1 m, (b) and (b*) at x = 1.0 m, (c) and (c*) at x = 2.0 m. Note that legend is not uniformized for reference and jet cases because of their different velocity magnitude values.

## 4. Conclusion

Scaling reals shallow reservoirs according to the Froude number similarity calls for an important geometrical distortion for majority of reservoirs because of the relatively low water depth compared to the horizontal dimensions. Also, real reservoir shapes could not fit into existing laboratory flume because of technical constraints. However, using data from real reservoirs and existing laboratory experiments, the Froude number and the Friction number, which have a significant impact on the flow patterns, have been retained for the design of new laboratory experiences representative of real cases. Two different inlet boundary conditions have been selected for a rectangular reservoir: free surface rectangular inlet channel (reference case) and a turbulent circular inlet jet. The geometrical parameters have been set considering the laboratory experimental constraints, while the hydraulic parameters (flow discharge, water depth) have been set to enhance the maximum and minimum values of Friction number and Froude number considering the experimental limits. Three dimensional (3D) numerical pre-simulations using TELEMAC-3D have been performed, showing the difference of velocity pattern and magnitude between the two cases. A more detailed analysis of turbulent kinetic energy is necessary to understand well the turbulence developed in the jet case.

**Acknowledgements**

This work is partially funded by Association Nationale de Recherche et de la Technologie (ANRT) [CIFRE #2019/1262].

**References**

Abbott D, Kline S (1962) Experimental investigation of subsonic turbulent flow over single and double backward facing steps, Journal of Basic Engineering, 84, 317-325.
Adamsson A, Bergdahl L, Lyngfelt S (2005) Measurement and three-dimensional simulation of flow in a rectangular detention tank, Urban Water Journal, 2(4), 277-287.
Camnasio E, Erpicum S, Orsi E, Pirotton M, Schleiss AJ, Dewals B (2013) Coupling between flow and sediment deposition in rectangular shallow reservoirs, Journal of Hydraulic Research, 51(5), 535-47.
Cherdron W, Durst F, Whitelaw J (1978) Asymmetric flows and instabilities in symmetric ducts with sudden expansions, Journal of Fluid Mechanics, 84,13-31.
Choufi L, Kettab A, Schleiss AJ (2014) Effet de la rugosité du fond d'un réservoir rectangulaire à faible profondeur sur le champ d'écoulement, La Houille Blanche, 83-92.
Claude N, Secher M, Deng J, Valette E, Duclercq M (2019) 2D and 3D numerical modelling of the flow and sediment transport in shallow reservoirs: application to a real case, XXVIth Telemac & Mascaret User Club.
Dufresne M (2008) La modélisation 3D du transport solide dans les bassins en assainissement : du pilote expérimental à l'ouvrage réel (3D modeling of solid transport in waste water basins: from experimental pilot to real reservoir), Doctoral dissertation, Université Louis Pasteur, Strasbourg, France.

Dufresne M, Dewals B, Erpicum S, Archambeau P, Pirotton M (2010) Classification of flow patterns in rectangular shallow reservoirs, Journal of Hydraulic Research, 48(2), 197-204.
Durst F, Melling A, Whitelaw J (1974) Low Reynolds number flow over a plane symmetrical sudden expansion, Journal of Fluid Mechanics, 64, 111.
Fischer H, List J, Koh C, Imberger J, Brooks N (1979) Mixing in inland and coastal waters, Academic Press, 512 pp.
Jirka GH (2004) Integral Model for Turbulent Buoyant Jets in Unbounded Stratified Flows. Part I: Single Round jet, Environmental Fluid Mechanics, 4, 1-56.
Kantoush SA (2008) Experimental study on the influence of the geometry of shallow reservoirs on flow patterns and sedimentation by suspended sediments, Doctoral dissertation, Laboratoire de Constructions Hydrauliques, EPFL, Switzerland.
Mizushima J, Shiotani Y (2001) Transitions and instabilities of flow in a symmetric channel with a suddenly expanded and contracted part, Journal of Fluid Mechanics, 434, 355-369.
Peltier Y, Erpicum S, Archambeau P, Pirotton M, Dewals B (2014) Experimental investigation of meandering jets in shallow reservoirs, Environmental Fluid Mechanics, 14(3), 699-710.
Schleiss AJ, Franca MJ, Juez C, De Cesare G (2016), Reservoir Sedimentation, Journal of Hydraulic Research, 54, 595-614.
Stovin VR, Saul AJ (1994) Sedimentation in Storage Tank Structures, Water Science and Technology, 29, 363-37.

# Preliminary investigation of reservoir sedimentation rates in the Italian Alps with SWAT model

Konstantinos KAFFAS[1], Giuseppe R. PISATURO[1], Vassilios PISINARAS[2], Georg PREMSTALLER[3], Maurizio RIGHETTI[1]

[1] Free University of Bozen-Bolzano, Faculty of Science and Technology, Bolzano, Italy

[2] Hellenic Agricultural Organization-Demeter, Soil and Water Resources Institute, Sindos-Thessaloniki, Greece

[3] Alperia SpA, Department of Engineering & Consulting, Bolzano, Italy

Email: konstantinos.kaffas@unibz.it

ABSTRACT

Reservoir sedimentation is a major issue for dam managers and one of the most characteristic off-site effects of soil erosion combined with the stream sediment processes. In this study, we simulate and analyze the sedimentation rates, due to soil erosion and sediment transport, of the Rio di Pusteria hydropower dam in South Tyrol (Italian Alps). The study period is between two consecutive sediment flushing operations, in June 2014 and May 2019. High-resolution bathymetric analyses before and after the sediment flushings enabled the determination of the aggregated sediment in the reservoir, during this period. The GIS version of the Soil and Water Assessment Tool (ArcSWAT) was used to simulate the hydromorphological processes and calculate the sedimentation rates of the Rio di Pusteria reservoir.

## 1. Study area

The Rio di Pusteria basin is located in north-east South Tyrol (Italy), between 46° 45' 20" N and 46° 57' 39" N latitudes and 11° 36' 48" E and 11° 54' 16" E longitudes. It is a semi-natural basin delimited by two dams, Rio di Pusteria (downstream, outlet) and Kniepass (upstream, inlet), which disconnects the sediment transport upstream from it. Rienz River runs the basin over a course of 16.7 km. The geomorphological setup of the study area is typical Alpine with high altitudes (721-3,235 m), steep slopes (0-85°) and a rapidly changing topography. The land cover mainly comprises coniferous forests (44.4%), Alpine grasslands and pastures (34.4%) and bare rock (6.1%). A detailed description of the study area can be found in Kaffas et al. (2021).

## 2. Data–Methods–Results

A large set of data was used for the purposes of our study, including precipitation and temperature data from three weather stations inside the basin, water discharge data from a hydrometric station slightly upstream of the Rio di Pusteria reservoir, land cover data, 2.5 m resolution DEM, 250 m resolution soil maps. The Kniepass dam discharges were provided by the Azienda Pubbliservizi Brunico (management authority of Kniepass dam), for the entire study period, at a daily time step, while the bathymetric data of the Rio di Pusteria reservoir was provided by Alperia SpA which operates the Rio di Pusteria dam.

### *2.1. Simulation of hydrological and sediment processes with SWAT model*

SWAT is a continuous time, conceptual, deterministic, distributed model that operates on a daily or sub-hourly time step. It has been extensively applied worldwide for a variety of watershed-scale problems. Here, the simulation was conducted at a daily time step from 1 July, 2011 to 26 May, 2019 with a 3-year warm-up period. The SCS-CN method was used for the hydrologic losses, while for soil erosion and stream sediment transport, MUSLE (Williams, 1975) and Yang’s (1996) sand and gravel model were used, respectively. A detailed description of the models used can be found in the SWAT theoretical documentation (Neitsch et al., 2011).

### *2.2. Model calibration based on sediment yield disaggregation*

The reservoir sedimentation rate was retrieved by high resolution (0.25 m, 0.5 m) bathymetric analysis. By comparing the two bathymetries, it was determined that a total of 452,683 t of sediment was trapped in the reservoir during a 5-year period between July 2014 and May 2019. To disaggregate the above value and enrich the calibration dataset, the results of the study of Kaffas et al. (2021) were used, according to which a combined USLE-SDR GIS model was developed to calculate the sediment yield contribution to the Rio di Pusteria reservoir, separately for each year of the aforementioned period. According to the results of the latter study, the measured sediment yield was split into annual values, which were further disaggregated into monthly sediment yields based on the raw results of SWAT. The above enabled the disaggregation of a single 5-year measured sediment yield to monthly sediment yields that can be used for calibrating the model.

The continuous measurement of sediment discharge at highly disaggregated time steps is expensive and labor intensive. Also, single sediment yield values for long time periods >1 year (via satellite imagery, bathymetric analysis, etc.) is very common in literature. This novel and simplified procedure is proposed to tackle this problem and calibrate sediment yields when single-value sediment loads for long periods of time are available.

Stream and sediment discharge were calibrated through 29 hydrological, hydraulic, snow, and sediment parameters: plaps, tlaps, sftmp, smtmp, smfmx, smfmn, timp, CN2, esco, gwqmn, revapmn, gw_revap, ov_n, sol_K, sol_bd, sol_awc, rill_mult, ch_bed_bd, ch_bnk_kd, ch_bnk_d50, usle_K, spexp, ch_bed_d50, ch_bed_kd, ch_bnk_bd, spcon, prf_bsn, ch_erodmo, ch_cov1 (Neitsch et al., 2011), and 4,000 simulations, for a 2-year period from 1 July, 2014 to 31 June, 2016 and yielded a Nash Sutcliffe Efficiency (NSE) of 0.97 and 0.59, respectively. The model was validated from 1 July, 2016 to 26 May, 2019, indicating very satisfactory model performance with NSE values of 0.97 for stream discharge and 0.48 for sediment discharge.

## 3. Comparison between calculation and measurement

The use of the final ranges of the calibrated parameters for the entire period (1 July 2014 – 26 May 2019) resulted in the hydrograph and sediment graph of Figs. 1 and 2. A very low uncertainty (95 Percent Prediction Uncertainty) is observed in stream discharge (NSE=0.96), while the sediment discharge (NSE=0.49) presents an appreciably higher uncertainty but includes the entire measurement. The application resulted to a 5-year calculated sediment yield of 472,680 t which presents a deviation of only -4.2% from the measured value.

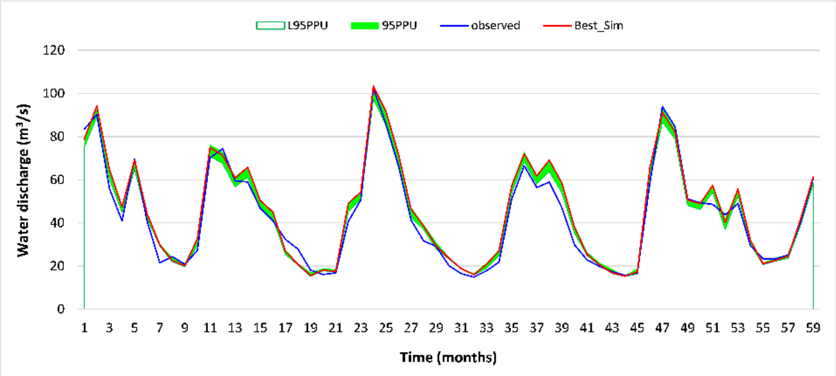


***Fig. 1.*** *Monthly stream discharge at Rio di Pusteria reservoir.*

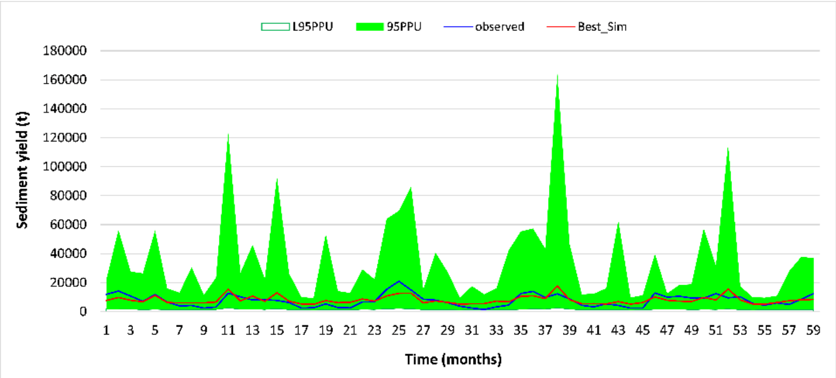


***Fig. 2.*** *Monthly sediment yield at Rio di Pusteria reservoir.*

***References***

*Arnold JG, Srinivasan R, Muttiah RS, Williams JR (1998) Large area hydrologic modeling and assessment part I: model development 1, JAWRA Journal of the American Water Resources Association, 34(1), 73-89*

*Kaffas K, Pisinaras V, Al Sayah MJ, Santopietro S, Righetti M (2021) A USLE-based model with modified LS-factor combined with sediment delivery module for Alpine basins, Catena, 105655*

*Neitsch SL, Arnold JG, Kiniry JR, Williams JR (2011) Soil and Water Assessment Tool Theoretical Documentation - Version 2009, Texas Water Resources Institute, (TR-406)*

*Williams JR (1975) Sediment-Yield Prediction with Universal Soil Loss Equation Using Runoff Energy Factor. In Present and Prospective Technology for Predicting Sediment Yield and Sources, Agricultural Research Service & US Department of Agriculture*

*Soil Conservation Service (SCS) (1972) National Engineering Handbook, Section 4: Hydrology*

*Yang CT (1996) Yang Sediment Transport: Theory and Practice, McGraw-Hill, New York*

# Monte Carlo simulation of sediment-related events in reservoirs as part of a risk-based decision-making tool

Øyvind PEDERSEN[1], Lars JENSSEN[2], Håkon TOFTAKER[3], Hanne NØVIK[4], Eivind SOLVANG[5], Siri STOKSETH[6]

[1]Multiconsult, Norway
email: oyvind.pedersen@multiconsult.no
[2]Norconsult, Norway
email: lars.jenssen@norconsult.com
[3,5] SINTEF, Norway
email: hakon.toftaker@sintef.no
email: eivind.solvang@sintef.no
[4]Sweco, Norway
email: hanne.novik@scatec.com
[6]Statkraft Energi, Norway
email: siri.stokseth@statkraft.com

ABSTRACT

Sedimentation in hydro-power reservoirs can cause adverse outcomes such as damage to components or unexpected downtime. The STRIVAN research project aims to develop a risk-based model to quantify and compare the net present value of mitigation measures. Quantifying risks involves calculating the probability of outcomes as well as the consequence. This work discusses a Monte Carlo simulation approach to estimating probability distributions for outcomes. Monte Carlo simulations combined with a one-dimensional (1D) quasi-unsteady sediment transport model has been implemented in a case study.

## 1. Introduction: The STRIVAN model

The **ST**orage **RI**sk and **V**alue **AN**alysis (STRIVAN) research and development project aims to develop a risk-based decision-making tool for operation, management, and mitigation of sediments in reservoirs. In the STRIVAN model, different alternatives of sediment mitigation measures and timings are assessed in terms of their net present value (NPV) (Nøvik, et al., 2022).

The STRIVAN model follows a modified five-step sequence of risk assessment modelling after Bowels and Schaeffer (2014): 1) initiating events, 2) system responses, 3) outcomes, 4) exposure factors, and 5) consequences. Initiating events are events having an impact on sediment transport into the reservoir, e.g. floods or earthquakes, and the relevant system response is the transport, erosion and deposition of sediments leading to adverse outcomes. The outcomes considered are those that can cause unwanted impacts on technical installations or on operation of assets; for example clogging of intakes or loss of reservoir volume. The exposure can depend on the system state, such as water levels, gate openings *etc*. The economic consequences are considered, such as repair or downtime costs.

## 2. Method: The Monte Carlo simulation approach

A key part of the STRIVAN-model is the determination of probability distributions for outcomes that may cause damage or unexpected downtime. Typically, the probability distribution for initiating events, such as the yearly probability of exceedance for a peak flood or an earthquake of a certain magnitude is available or can be determined by standard methods. For example, peak floods can be determined by flood-frequency analysis. The probability of a sediment related outcome can, however, not be easily deducted from the probability of initiating events. Further, sediment related outcomes of interest, such as depositions in front of an intake, is not the result of a single initiating event, but can be the result of a series of yearly floods, where the sequence of floods matter.

We propose a method of propagating the probability distribution for the initiating event to the outcomes of interest, using a Monte Carlo simulation approach combined with sediment transport modelling. In the context of sediment risks, Monte Carlo simulations can be used by sampling from the given random distributions of initiating events and constructing synthetic time series based on the sampling. The synthetic time series can then be used as input in a model of the relevant system response. To determine the probability distribution of an outcome, the state in which the outcome has occurred must be clearly defined by a threshold. For example, the yearly probability of an outcome can then be estimated by determining in which year the threshold is exceeded for each realization.

## 3. Case-study: Monte Carlo simulation in HEC-RAS sediment transport model

Monte Carlo simulation has been utilized in a case study for sedimentation in the Binga reservoir in the Philippines. Here a quasi-unsteady 1D HEC-RAS model including sediment transport and bed updating was combined with Monte-Carlo simulation of stochastic flood series over a 50-year period. The Monte-Carlo simulations in HEC-RAS were implemented by running a Python script utilizing the HEC-RAS Controller interface. A similar approach has been described in Dyrsaz (2018).

In the HEC-RAS model, bed material compositions were set according to various measurements of grain size distributions. The sediment inflows were calibrated based on historical data, including bathymetries, flow series and reservoir levels from 1960 – 2018. For the Monte Carlo simulations, the HEC-RAS model geometry was based on bathymetric measurements from 2018.

Fifty-year synthetic flood series were generated by drawing peak floods from a Weibull 2-parameter distribution based on historical floods and modifying a template flow series each year. The template was developed based on average flow durations from historical data (Fig. 1).

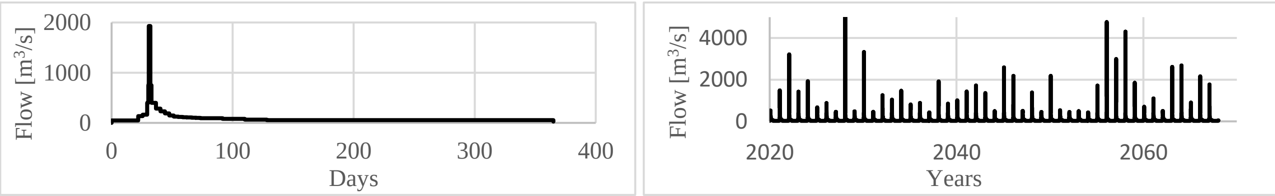


**Fig. 1.** Left: Template flow series for one year, based on average durations. Right: Example of 50-year flow series generated by drawing peak flows from a probability distribution and modifying the template each year.

The Monte Carlo simulations were then used to study different outcomes caused by sediment transport over time. One outcome that was studied was sediments threatening clogging of the intake. The threshold for this outcome was defined as the bed level at the intake reaching the intake sill. For each simulation the year in which this threshold was reached was then recorded, and the corresponding yearly probability and cumulative probability calculated. An example of a simulation, including the corresponding convergence of sample mean and variance is shown in Fig. 2.

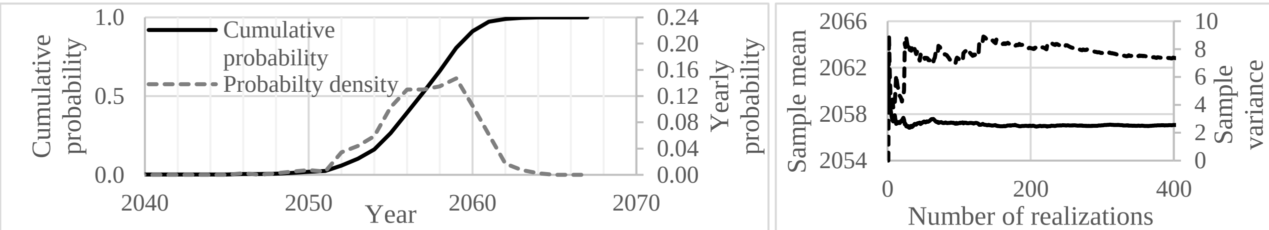


**Fig. 2.** Left: Example of simulated yearly probabilities and cumulative probabilities of exceedance of threshold bed level. Right: Convergence of sample mean (years) and sample variance of the time of threshold exceedance as a function of the number of realizations.

## 4. Discussion

The main advantage of using a Monte Carlo simulation, rather than other modelling approaches - such as a scenario-based approach, is that the outcomes of interest can be expressed in terms of a probability distribution tied to the probabilities of initiating events.

In this study, synthetic series based on peak floods has been studied. The method could plausibly be expanded to include the interaction between several initiating events, such as floods and earthquakes, or including the study of uncertainty in variables such as the sediment inflows or gradations.

**References**

Bowles D, Schaefer M (2014) Probabilistic flood hazard assessment, dam performance PRA and nuclear plant risk, Proceedings of the 9th Nuclear Pant Current Issues Symposium, Charlotte, NC
Dysarz T (2018) Application of Python Scripting Techniques for Control and Automation of HEC-RAS Simulations, Water, 10(1382).
Nøvik H, Stokseth S, Pedersen Ø, Walløe KL, Rüther N, Solvang E, Toftaker, H (2022) Storage and Risk Value Analysis of reservoirs exposed to high sediment load, Hydro 2022 proceedings (preprint)

# Two-dimensional (2D) depth-averaged numerical modeling of a braided river morphodynamics upstream of a dam reservoir

Behnam BALOUCHI[1], Nils RUTHER[2], Ayda MIRZAAHMADI[3], Kordula SCHWARZWÄLDER[4]

[1,2,3,4] Department of Civil and Environmental Engineering, Norwegian Institute of Science and Technology, Norway
email: behnam.balouchi@ntnu.no
email: nils.ruther@ntnu.no
email: aydam@stud.ntnu.no
email: kordula.v.a.schwarzwalder@ntnu.no

ABSTRACT

The river morphology of a braided type river is rather complex. High sediment transport rates and frequently changing discharges are the cause of dynamic planform evolution. The coexistence of alternating bars and the consequent appearing confluences and divergences in interaction with bank erosion have been in the focus of scientific investigations over the last decades. It is still rather challenging to estimate or predict the total sediment transport rate in such type of rivers. The present study attempts to numerically simulate such complex morphodynamics in a braided river reach. A reach of the Devoll River in Albania, located upstream of the Banja dam, is considered. The morphodynamics of this river reach is important as there is an expanding delta upstream of the dam reservoir. The objectives of the two-dimensional (2D) depth-averaged approach of the present study are (i) to show the ability of the HEC-RAS 2D model to simulate the evolution of this braided river, (ii) to evaluate the variation of Braided Index (BI) of chosen reach along the time of input hydrograph, and (iii) to illustrate an applied context to consider future modeling challenges. HEC-RAS 2D uses the shallow water equations solved with an implicit finite volume solver, and the Wu transport formula to solve the sediment transport rate and the corresponding bed changes. The preliminary results are promising to reveal the expected evolution trend of the mentioned braided river.

## 1. Introduction

A braided river is a complex case for morphodynamic simulations due to evolution over time and changes in the hydraulic and morphological parameters (Yassine et al., 2022). A braided river is characterized by alternating bars resulting in a complex system of multiple diverging and converging channel branches which the flow and sediment patterns of them have been investigated separately in the literature (Olsen, 2021). The present study is focusing on a braided river (Devoll River) upstream of the Banja reservoir dam. The Banja reservoir is located on the Devoll River in southeast Albania and has a storage capacity of approximately 400 $Mm^3$. The catchment area of the reservoir has a size of 2900 $km^2$ and is located within a mountainous region with a diversified topography. The Devoll River has its source near the Greek border and has several confluences. Hence, the transport processes of the Devoll River are very important, because they highly impact the sedimentation process within the Banja reservoir. This study aims at investigating this transport process by modeling a braided river reach to quantify the sediment source to the Banja Reservior.

## 2. Methods

In the current study, the topography data used in HEC-RAS model is a digital terrain model (DTM). This DTM was prepared from the ground classified points of the Lidar data taken on February 9th and 10th, 2019. Besides, the grain size distribution curve was measured in the field, describing the bed material by $D_{50}$ of 19 mm. The Manning roughness coefficient checked with the Strickler equation and the reference table as to be 0.025. The equations used in the present 2D depth-averaged numerical modeling are the shallow water equations, and the bed load calculated by the Wu transport equation (Wu et al., 2000). The simulation is run with a roughness coefficient retrieved from substrate measurements at the river bed and floodplain. Validation of results is considered to be done by comparing the plan view or the evolution of river in a frame time of 8 months that there are two google earth images. The 8-months hydrograph obtained using a hydrological model of the catchment, is used as an upstream boundary condition (Fig. 1). It should be noted that the results shown in the next section are the preliminary results which are for the simulation of the first month of hydrograph. The downstream boundary condition is the normal depth with a bed slope of 0.008. The sediment upstream boundary condition is the equilibrium load. This bed slope is computed from a profile of the mainstream of the chosen river reach with a length of approximately 1.5 km. The Braided Index (BI) is calculated as $(\Sigma m + \Sigma l) / \Sigma m$, where $\Sigma m$ is the summation of mainstream length and $\Sigma l$ is the summation of all lateral streams lengths (Kuo et al., 2017).

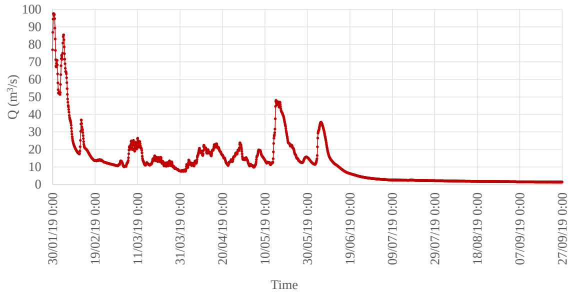


**Fig. 1.** upstream boundary condition hydrograph

## 3. Results

By using the first-month input hydrograph, the preliminary results of 2D depth-averaged numerical modeling are shown in Fig. 2. Figure 2(a) shows the flow simulation of the river reach with the velocity pattern at the beginning of the preliminary simulation hydrograph. In this figure, the maximum velocity zones are visible, especially after the confluence which is shown with a circle in Fig. 2(a). Figure 2(b) shows the bed change at the end of the preliminary simulation hydrograph. According to this figure, it can be seen that there is deposition in the left branch and scouring in the right branch. According to the two mentioned google earth images, it is expected that the right branch morphodynamic is active in comparison with the left branch. Therefore, the evolution trend of the river is observed in this figure by observing the river's intention to be straighter on the right branch. Figure 2(c) shows the variations of bed topography at the start and end of the hydrograph at cross-section A-A. Figure 2(c) shows in analogy to Fig 2(b) the erosion and deposition occurring in the simulation. In addition to the above results, it can be concluded that the braided index (BI) decreased from 2.61 to 1.69 for the specific time frame of the chosen reach of the Devoll River.

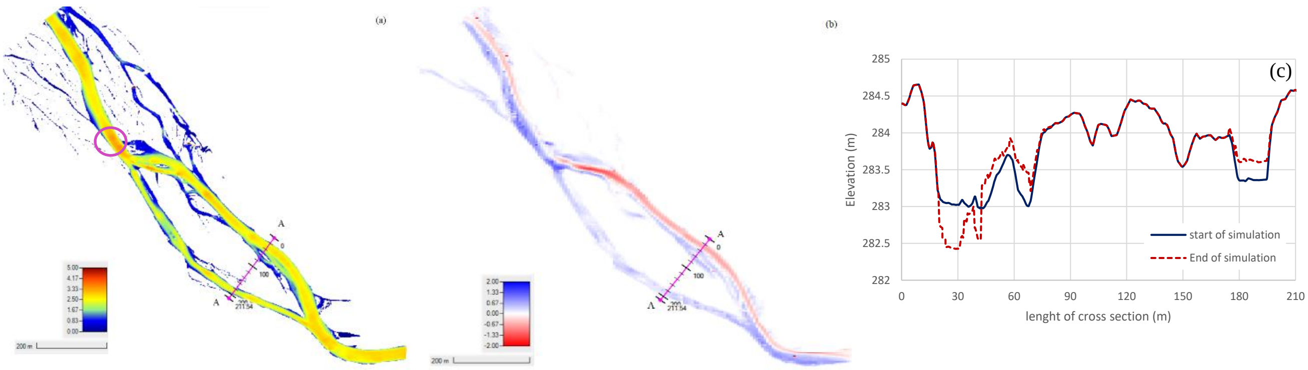


**Fig. 2.** (a) velocity pattern of the river reach at the start of simulation (b) bed change at the end of the simulation, and (c) variation between the bed topography at the start and end of simulation for section A-A.

## 4. Conclusion

These preliminary results are promising and show the applicability of the model for (i) the long-term simulation; and (ii) the investigating the effect of climate change on the sediment transport processes and planform evolution of Devoll River, which is important for the Banja reservoir and the sediment handling plan of the hydropower plant.

**References**

Kuo CW, Chen CF, Chen SC, Yang TC, Chen CW (2017) Channel planform dynamics monitoring and channel stability assessment in two sediment-rich rivers in Taiwan, Water, 9, 84.
Olsen NRB (2021) 3D numerical modelling of braided channel formation, Journal of Geomorphology, 375.
Sanchez A, Gibson S (2020) HEC-RAS Two-Dimensional Sediment Transport User's Manual, CEIWR-HEC, 89 pp.
Yassine R, Cassan L, Roux H, Frysou O, Pérès F (2022) Numerical modelling of the evolution of a river reach with a complex morphology to help define future sustainable restoration decisions, Earth Surf. Dynam. Discuss. [preprint], https://doi.org/10.5194/esurf-2021-91, in review, 2022.
Wu W, Wang SSY, Jia Y (2000) Nonuniform sediment transport in alluvial rivers, Journal of Hydraulic Research, 38(6), 427-434.

# Morphodynamic Modeling of Graded Sediment Transport

Peter Mewis[1]

[1] TU Darmstadt, Germany
email: peter.mewis@tu-darmstadt.de

ABSTRACT

After decades of exploitation many reservoirs reach their design lifespan and suffer from sedimentation. To reduce the risk of high costs and environmental impact it is desirable to model the sediment transfer measures in advance. A specific problem of reservoirs is the wide gradation curve of the accumulated sediments.

In case of graded sediment transport the transport capacity is calculated with a correction factor for the dimensionless Shields stress for each fraction. This factor becomes strongly grain size dependent. Here it is proposed to change the actual shear stresses. The new approach for graded sediment transport is introduced and discussed by modelling the experiment of Günter.

## Introduction

Planning of dams and barrages has to take into account the natural sediment transport of the streams. This transport will increase largely due to climate change. Extreme rainfall events will be more frequent in the future. This unsteady flow will carry a large amount of sediments down the rivers. This may increase the sediment transport volumes by several times.

In reservoirs the transport capacity of the rivers breaks down. The sequence in which the transported sediments accumulate is well known and common to all reservoirs. The sediment trap constructed at the dam root collects very coarse sediments. The finer fractions however move on and cause siltation. Talking about management of reservoirs is thus talking about very different grain sizes and their combined properties at initiation of motion as well as in the case of transport.

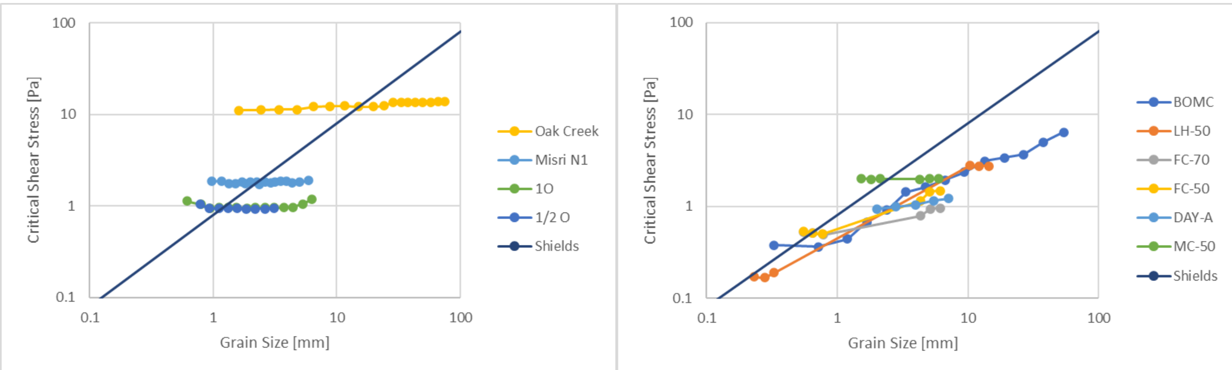


**Fig. 1.** Critical shear stress for initiation of motion of individual size fractions of uni- (left) and bimodal (right diagram) sediment mixtures after Wilcock (1993).

Measurements of the critical shear stress for each fraction in a graded sediment transport case are reproduced from Wilcock (1993) in Fig. 1. Following experiments for unimodal sediments all fractions start to move at the same critical shear stress. For a constant critical Shields value, the values would follow the line in Fig. 1 (left) what is evidently not correct. In the case of wide bimodal sediments shown in Fig. 1 (right) the situation changes. For wide gradation curves the critical shear stress is no longer constant but changes for coarser grains. Following the data of Wilcock (1993) this seems to happen at a distance of a factor of five. Following Patel et al. (2013) this effect is not reproduced by the commonly used formulas, like the approach of Wu et al. (2000).

## Methods

The common approach (DWA, 2020) for graded sediment transport is to apply a "hiding and exposure" correction factor for the critical Shields value of every fraction (Wu et al., 2000):

$$\theta_{c,i}^{m} = \frac{\tau_{c,i}^{m}}{\rho' g d_i} = \xi_i \theta_{c,i} \text{ and after Wu et al. (2000) } \xi_i = \left( \sum_N \frac{p_i \cdot d_i}{d_i + d_j} \Big/ \sum_N \frac{p_j \cdot d_j}{d_i + d_j} \right)^{-0.6} \quad (1)$$

Where $\theta_{c,i}^{m}$ the critical Shields value for fraction $i$ in mixture $m$ [-], $\tau_{c,i}^{m}$ the critical shear stress of fraction $i$ in mixture $m$ [Pa], $d_i$ the grain size, $p_i$ the mass fraction, $\xi_i$ the hiding and exposure factor and $\theta_{c,i}$ the critical Shields value for fraction $i$ [-], $\rho'$ the relative submerged density [-], $g$ the gravity acceleration [m/s²].

Wilcock (1993) proposed to use a constant critical shear stress for all fractions in the case of unimodal mixtures. In case of bimodal mixtures he proposed a correction that depends on $d_i$. Here a similar approach is proposed by taking the sum over all critical shear stresses weighted by their corresponding mass fractions:

$$\tau_{c,i}^{m} = \frac{\Sigma_N(\tau_{c,j} \cdot p_j \cdot w_j)}{\Sigma_N(p_j \cdot w_j)};\ w_j = \begin{cases} 1; for\ i \neq j \\ 2; for\ i = j \end{cases} \quad (2)$$

Instead of changing the dimensionless Shields value $\theta_{c,i}$ here the critical shear stresses are averaged, as it is observed in many experiments. The weighting function $w_i$ is somewhat arbitrarily chosen and should be refined with more experimental data. If it is one, all sieves would have the same critical velocity, what would not lead to bed armoring and makes sense only for unimodal sediment. In general the weighting function $w_j$ should depend on the relative difference of the grain sizes. Here the weighting decreases to zero at a factor of five between grain sizes.

## Results

The three-dimensional morphodynamic-numerical model Bmor3D developed by the author (Mewis, 2016) is run to reproduce the laboratory experiment by Günter (1971) dealing with the effect of bed armoring. The experimental conditions are described in Günter (1971) and DWA M-540 (2021). From Fig. 2 it can be concluded that two fine fractions are washed out with the approach of Wu et al. (2000) while the proposed approach (eq. 2) ensures a better correction of the critical shear stress for the fine fractions.

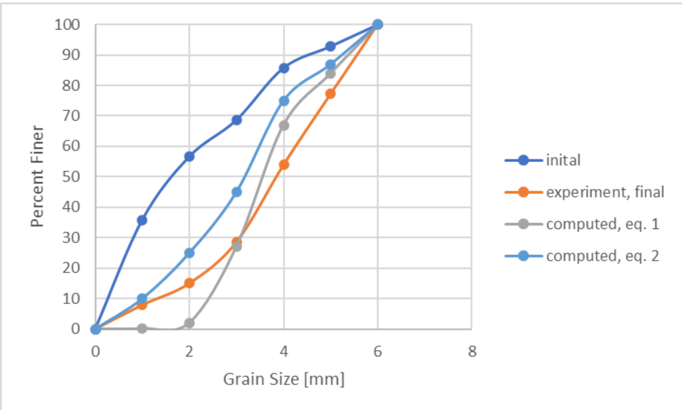


**Fig. 2.** Composition of bed material of the experiment of Günter and computed with eq. 1 (Wu et al. 2001) and eq. 2 (new approach).

## Conclusions

The very wide gradation of the bed material in reservoirs pose a demand for approaches that are able to simulate very wide graded mixtures. The model Bmor3D reproduces the experiment of Günter well with a new approach. This approach must however be developed further and adapted for wider and bimodal sediments.

### References

DWA Merkblatt M-540 (2020) Mehrdimensionale morphodynamisch-numerische Modelle für Fließgewässer. Deutsche Vereinigung für Wasserwirtschaft, Abwasser und Abfall e. V., ISBN 978-3-96862-123-4 (in German).

Günter A. (1971) Die kritische mittlere Sohlenschubspannung bei Geschiebemischungen unter Berücksichtigung der Deckschichtbildung und der turbulenzbedingten Sohlenschubspannungsschwankungen. Dissertation Nr. 4649, Mitteilungen der Versuchsanstalt für Wasserbau, Hydrologie und Glaziologie, No. 3, ETH, Zürich, Switzerland (in German).

Mewis P. (2002) Morphodynamische Modellierung von Flusskurven, Mitteilungen Institut für Wasserbau, TU Darmstadt (in German).

Mewis P. (2016) Formation of river dunes by measurement, linear stability analysis and simulation with Bmor3D, Proceedings of the 13th International Symposium on River Sedimentation, Stuttgart, Germany.

Patel SB, Patel PL, Porey PD (2013) Threshold for initiation of motion of unimodal and bimodal sediments, International Journal of Sediment Research, 28, 24-33.

Wilcock PR (1993) Critical shear stress of natural sediments, Journal of Hydraulic Engineering,119, 4,491-505.

Wu W. M., Wang S. S. Y., and Jia Y. F. (2000) Nonuniform sediment transport in alluvial rivers, Journal of Hydraulic Research,38,6, 427-434.

# A GPU Accelerated Tool for 2D Modelling of hydraulics and Sediment Transport

Danial DEHGHAN SOURAKI[1], Ernest BLADÉ CASTELLET[2], Marcos SANZ-RAMOS[3], David LÓPEZ-GÓMEZ[4]

[1,2,3] Flumen Institute (UPC-CIMNE), Jordi Girona 1-3, B0, 08034 Barcelona
[1]email: danial.dehghan@upc.edu
[2] email: ernest.blade@upc.edu
[3]email: marcos.sanz-ramos@upc.edu
[4] CEDEX. P.º de la Virgen del Puerto, 17, 28005 Madrid
[4]email: david.lopez@cedex.es

ABSTRACT

Iber is a two-dimensional hydraulic model for the simulation of free-surface flow in rivers and estuaries and solves hydrodynamics, turbulence, sediment transport, water quality processes, and habitat. Although Iber profits from some kind of OpenMP parallelization, in cases with a large number of computational elements, Iber will need days for completing the calculations which will make Iber almost unusable in applications where a short computational time is needed like flood warning systems. RIBER is a software that was implemented based on the Iber code such that no substantial modifications were made to the original algorithms. With the help of GPU computing using CUDA, it profits speedups up to almost 15 times faster than Iber. This speed up not only will make RIBER more affordable for flood early warning systems but also doing calibration for different cases using stochastic models is more applicable to it.

## 1. Introduction

First, the study area and governing equations are discussed in a summarized manner. Then a portion of the results was presented. After that, a conclusion is made regarding the presented results.

### *1.1. Study Area*

Ribaroja is a monomythic long and narrow reservoir with a quite regular topology in the Ebro River basin, which encompasses a large portion of the northeastern Iberian Peninsula. The current storage capacity is 210 hm$^3$ with a few weeks of resident time. The Ribaroja reservoir is closed downstream by a gravity dam with a crest of 76 meters above sea level and a base of 16 meters. This is supplemented by considerable discharge input from two tributaries, the Segre and Cinca rivers, which flow from the central Pyrenees and converge around 2 km before the Ebro River confluence at the reservoir's tail.(Bladé Castellet et al., 2019). The present work focuses on the shallow areas at the tail of the reservoir, where the hydrodynamic conditions are similar to those of river flow(Arbat-Bofill et al. 2015).

### *1.2. Governing Equations*

The reader is referred to (Bladé Castellet et al., 2014) for a full discussion and experimental validation of the numerical algorithms used to solve the shallow water equations, which are not included in this study for brevity's sake. The sediment transport module calculates bedload and suspended sediment transfer based on the results of the hydrodynamic and turbulence modules' velocity, depth, and turbulent viscosity fields. There was no consideration of bedload in this study. The movement of suspended sediment was modeled by solving the depth-averaged turbulent convection-diffusion Eq. (1), using the method described in (Cea et al., 2016).

$$\frac{\partial hC}{\partial t} + \frac{\partial h\boldsymbol{U}_x C}{\partial x} + \frac{\partial h\boldsymbol{U}_y C}{\partial y} = \frac{\partial}{\partial x_j}\left(\left(\Gamma + \frac{\boldsymbol{V}_t}{\boldsymbol{S}_{c,t}}\right) h \frac{\partial C}{\partial x_j}\right) + (\mathrm{E} - \mathrm{D}) \qquad (1)$$

Here, C is the depth-averaged concentration of suspended solids; $U_x$ and $U_y$ are the horizontal depth-averaged velocity components; $\nu_t$ is the turbulent viscosity; Γ is the molecular diffusion coefficient for suspended solids; $S_{c,t}$ , is the Schmidt number, which relates the moment turbulent diffusion coefficient with the suspended turbulent diffusion coefficient; D is the deposition rate, and E is the Erosion rate.

In order to address the limitations in terms of efficiency of the Iber model, a new implementation was developed which is called RIBER (Rapid Iber), and is parallelized for GPUs using the Nvidia CUDA (Compute Unified Device Architecture). All the cases were run on a laptop equipped with an AMD RYZEN 9 5900HX processor, 32 GB of RAM, and an NVIDIA RTX 3070 graphic card.

## 2. Results

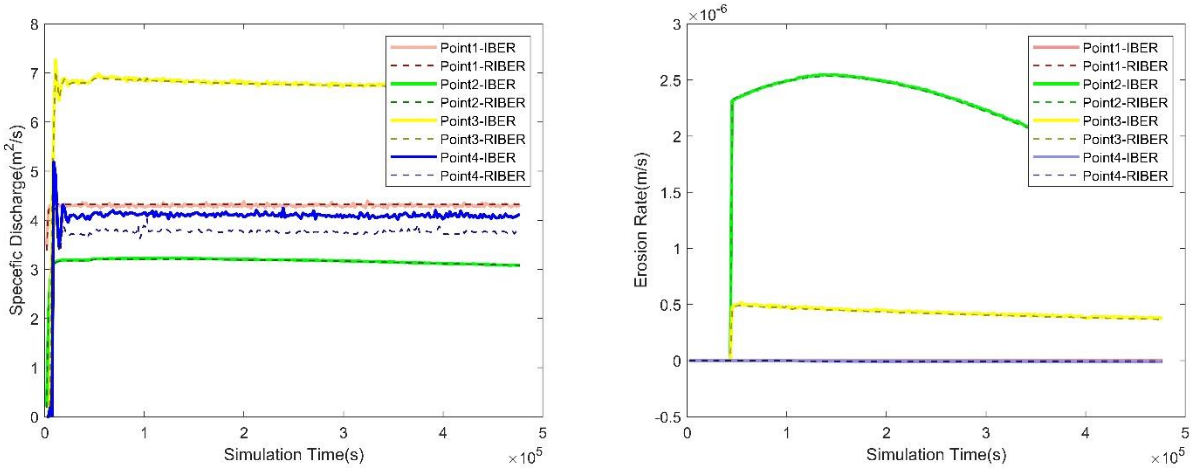


**Fig. 1.** Results of specific discharge (Left) and erosion rate (Right) compared in Iber (serial) with RIBER (parallel) for different points in the reservoir (point1 is the beginning and point 4 is the end of the reservoir).

Both the hydraulic and sediment transport model results of the case can be appreciated in Fig. 1. It shows that in comparison with serial code (constant color lines) the parallel code (dashed color lines) did a good job predicting the results for both models by just some slight differences in the discharge distribution in the outlet of the reservoir (point4), which might be due to the boundary conditions implementation of the outlet. Also in the erosion rate plot (Fig. 1. Right), it can be noticed that in both inlet and outlet (point 1 and point 4) of the reservoir there is no erosion as the results of both models overlap at zero.

## 3. Conclusion

**Table 1.** Computational Time and Speedup

| Software (Serial/Parallel) | Computation Time(s) | Speedup |
|---|---|---|
| Iber (Serial) | 11350 | 1 |
| RIBER(Parallel) | 750 | 15 |

A new parallel implementation of the 2D shallow-water model Iber was presented. The first version of this new implementation, which can be further optimized, named RIBER, takes advantage of different parallelization strategies both on CPUs and GPUs to speed up the computations about 15 times regarding Table 1 while keeping the same accuracy as the original model. The main advantage of 2D models like RIBER is their affordable execution time, which can be an advantage for them to be implemented in flood warning systems. This also will help the model to be calibrated using stochastic models like Monte-Carlo in a considerably shorter time.

**References**

Arbat-Bofill, M., & Sánchez-Juny Ernest Bladé Castellet, M. (2015). Distribución de temperatura y velocidad de embalses : análisis numérico-experimental aplicado a los embalses de Sau (Ter) y Ribarroja (Ebro). http://hdl.handle.net/2117/95799

Bladé Castellet, E., Cea, L., & Corestein, G. (2014). Numerical modelling of river inundations. Ingeniería Del Agua, 18(1), 68. https://doi.org/10.4995/ia.2014.3144

Bladé Castellet, E., Sánchez-Juny, M., Arbat Bofill, M., & Dolz Ripollés, J. (2019). Computational Modeling of Fine Sediment Relocation Within a Dam Reservoir by Means of Artificial Flood Generation in a Reservoir Cascade. Water Resources Research, 55(4), 3156–3170. https://doi.org/10.1029/2018WR024434

Cea, L., Bermúdez, M., Puertas, J., Bladé, E., Corestein, G., Escolano, E., Conde, A., Bockelmann-Evans, B., & Ahmadian, R. (2016). IberWQ: new simulation tool for 2D water quality modelling in rivers and shallow estuaries. Journal of Hydroinformatics, 18(5), 816–830. https://doi.org/10.2166/hydro.2016.235

# On the Vulnerability of Reservoirs to the Combined Effect of Sedimentation and Climate Change: The Contribution of Sediment Management as an Adaptation Strategy

Nikolaos EFTHYMIOU[1], George W. ANNANDALE[2] Pravin KARKI[3]

[1] World Bank, Independent Consultant, Greece
email: nefthymiou@worldbank.org

[2] World Bank, Independent Consultant, USA
email: george@georgewannandale.com

3 Global Lead Hydropower & Dams, World Bank, USA
email: pkarki@worldbank.org

ABSTRACT

The performance of reservoirs, i.e. their capability to provide reliable water services for irrigation, freshwater supply, hydropower production, and flood protection, depends on the variability of the incoming flows and the available storage capacity. Reservoirs have, however, a natural enemy: Sedimentation results in the continuous reduction of their storage capacity through the formation of coarse-grained sediment deltas in the upper reaches and the accumulation of fines in the deeper sections. The combined effect of population growth and reservoir storage loss to sedimentation results in a net reduction of global per capita water storage (Annandale 2013; Annandale et al. 2016). At the same time, a vast body of scientific evidence indicates that anthropogenic climate change disturbs the global historically observed hydrological regime by altering the runoff availability and increasing interannual and seasonal variability (IPCC 2021). Furthermore, the intensification of flood events in combination with dynamic land use changes, deforestation, as well as more frequent and severe wildfires due to temperature increase will also affect surface erosion. Scientific research and experience point towards increased sediment yields and hydrological uncertainty. Increased sediment yield and hydrologic variability induced by climate change will reduce the global reliability of hydropower generation and water supply for domestic, industrial and agricultural use; adding to the crisis of increased water demand due to population growth. Recently evidenced water supply shortages in different cities serve as reminders of the water security issues the global community will face soon.

The important role that reservoir storage plays to ensure the reliability of water supply as hydrologic variability due to climate change increases emphasizes the importance of preserving existing and newly created reservoir storage space through reservoir sedimentation management. Many different reservoir sedimentation management methods have been developed, and successfully applied in the past, including sediment yield reduction by means of watershed conservation, sediment routing and deposit removal (Morris and Fan, 1998). With each method being subject to a set of feasibility constraints, the selection of an optimum sediment management strategy must account for site-specific hydrological conditions, water uses, reservoir geometry and operational characteristics. Climate change characterized by great hydrologic uncertainty adds to the complexity of selecting suitable reservoir sedimentation management strategies, demanding application of robust decision-making procedures.

Recently, the International Hydropower Association (IHA) published the Hydropower Sector Climate Resilience Guide (IHA, 2019), which provides the industry with guidelines to identify, assess and manage climate risks ensuring resilience of the hydropower sector. Building on the IHA guidelines a rapid assessment method, known as the RESservoir CONservation (RESCON) method, has been developed for preliminary screening of state-of-the-art sediment management methods identifying optimal management techniques based on technical and economic feasibility and optimality while concurrently addressing the deep uncertainty associated with climate change.

The associated software (RESCON2) uses readily available data, partially retrieved from global data sets, and is intended for technical and economic analysis during early project development phases. It evaluates the vulnerability of water supply, irrigation and hydropower facilities to reservoir sedimentation and climate change and identifies at pre-feasibility level suitable reservoir sedimentation management approaches that

increase the resilience of water infrastructure. This pre-feasibility climate risk assessment and screening of the state-of-the-art sedimentation management methods shall be followed by detailed numerical studies and techno-economical evaluation during subsequent project development phases.

The analysis comprises:

1. Baseline definition, which evaluates the performance of the facility for the business-as-usual scenario, i.e. historically observed hydrological conditions and currently applied sediment management strategy.
2. Climate stress test, which evaluates the performance of the full ensemble of future hydrological predictions subject to climate change and the current sediment management strategy. This allows a quantification of the vulnerability of the facility in its current state to climate change.
3. Resilience analysis, which evaluates the performance for the ensemble of future hydrological predictions and project configurations differentiated by the applied sediment management strategies. This identifies the relative potential of each sediment management strategy to improve the resilience of the facility.
4. Identification of a project configuration providing robust adaptation to climate change by acknowledging the deep uncertainty of the hydrological predictions due to climate change using the method of minimizing maximum regrets corresponding to each project configuration.

The metric used to characterize the long-term economic performance of a facility for different hydrological scenarios and project configurations is the aggregate Net Present Value (NPV). The latter is calculated by discounting the future stream flows of revenues and costs. Depending on the purposes and water uses of the reservoir, the revenues are related to firm water yield availability and hydropower generation for a given reliability subject to the temporal change in storage due to sedimentation. The economic appraisal also considers water losses and additional costs for implementation of the different sediment management techniques. The calculated regrets correspond to the possible revenue losses or foregone revenues for each hydrological future and project configuration.

It is pointed out that the selected project performance metric characterizes only the economic performance of the facility and does not apply to safety, environmental, social and multi-purpose functions. These aspects shall be further evaluated with additional studies.

The paper showcases the presented analysis in terms of a case study of a hydropower reservoir.

**References**

Annandale GW, Morris GL and Karki P (2016) Extending the Life of Reservoirs, World Bank, Washington DC.
Annandale GW (2013) Quenching the Thirst: Sustainable Water Supply and Climate Change, Create Space Independent Publishing Platform, Charleston SC
International Hydropower Association (2019) Hydropower Sector Climate Resilience Guide, London, United Kingdom, Available from: www.hydropower.org
IPCC (2021) Climate Change 2021: The Physical Science Basis. Contribution of Working Group I to the Sixth Assessment Report of the Intergovernmental Panel on Climate Change, Cambridge University Press, Cambridge, United Kingdom and New York, NY, USA, In press, doi:10.1017/9781009157896.
Morris GL, Fan J (1998) Reservoir Sedimentation Handbook, New York, McGraw-Hill

# NESSIE and LISIE: Innovative underwater dredging robot techniques for reservoir sediment management

Raphaël GAILLARD

WATERTRACKS, France
r.gaillard@watertracks.f

ABSTRACT

This paper presents two innovative cost-effective dredging techniques for managing sediment within the reservoir while respecting the operational rules (dam operation) and environmental constraints downstream of the dam due to the sediment release: NESSIE (New Environmental System for Sediment Innovative Evacuation) and LISIE (LIight Subaquatic Innovative Excavator). Both techniques relay on underwater dredging robots to remove fine sediment materials and dilute them in a controlled, continuous, and measurable way without any water and hydro-power production losses. The dredged sediment is discharged downstream of the dam while strictly complying with dilution criteria specified by the dam operator. Compared to NESSIE, LISIE is suitable for narrow reservoirs and can dredge sediment in the areas near to the dam gates or concrete constructions. Both techniques have proven their high performance in different operations.

## 1. Introduction

Hydraulic dredging, which is the process of excavating deposited sediment from underwater, is a highly specialized technique used to restore the reservoir storage capacity. However, hydraulic dredging is often more expensive than mechanical excavation, and the disposal of dredged material on land or discharging high sediment concentrations associated with dredging slurry directly downstream from the dam can be environmentally unacceptable. Therefore, there is a need to improve this technique while ensuring dam operation (during the dredging operation) and ecological functions of the river system.

## 2. NESSIE and LISIE dredging robots under water

Since 2016, Électricité de France (EDF) was seeking new cost-effective dredging techniques to manage sediment within reservoirs while respecting the operational constraints during operations and reducing the negative environmental impacts of sediment release downstream of the dam. In response to this need, WATERTRACKS has developed an innovative dredging solution for sediment continuity, while promoting the environmental sustainability of the reservoir. The solution is an underwater dredging robot able to self-regulate its production to release sediment downstream of the waterway while strictly complying with dilution criteria specified by EDF. This robot is called NESSIE ® that stands for **N**ew **E**nvironmental **S**ystem for **S**ediment **I**nnovative **E**vacuation. NESSIE is the first ever made underwater low environmental impact dredging robot that is designed to remove fine sediment and dilute them in a controlled continuous and measurable way without any water and hydro-power production losses (Fig. 1). This technique can be applied 24 hr/24 hr, under 1 m to 300 m water depth and is equipped with a cutter for cohesive material; the dredging discharge is 1200 hr/m$^3$. NESSIE has been declared ready to operations by EDF in November 2020, after a first dredging operation of sediment volume of 15 000 m$^3$ up to 60 m depth in Le Sautet dam reservoir.


**Fig. 1.** NESSIE working principle (left) and in field (right).

Subsequently, in 2021 WATERTRACKS has developed LISIE, a complementary dredging robot suitable for confined reservoirs. LISIE stands for **LI**ight **S**ubaquatic **I**nnovative **E**xcavator (Fig. 2). This underwater robot designed as a mini-backhoe excavator is a tool actioner that can fit in narrow and small places compared to NESSIE. LISIE can dredge sediment in the areas near to the dam gates or concrete constructions without any damage for the structures (Fig. 3). The first operation of LISIE was to remove sediment behind entrance grids, reaching them through the tunnel of the Hermillon inlet in Maurienne valley (French Alps).

**Fig. 2.** LISIE robot.

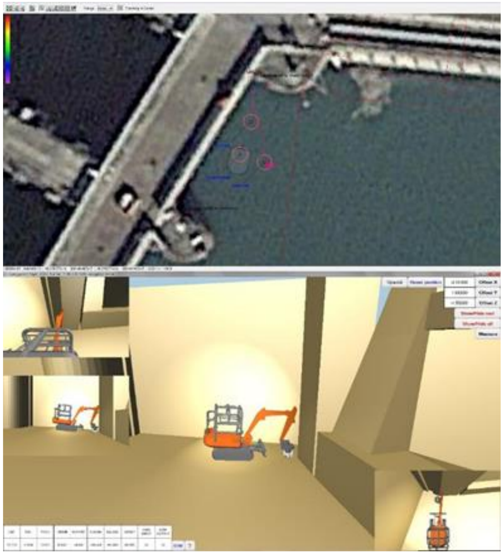

**Fig. 3**. LISIE Monitoring Screens working close to structures

In spring 2022, both NESSIE and LISIE were used together in La Balme de Rencurel dam reservoir (capacity of 60 $Mm^3$), located in the French Alps and used for hydropower production. NESSIE dredged the largest amount of sediment with direct release of suspended load downstream of the dam with strict monitoring of turbidity. LISIE cleaned the inlet grid of the turbine penstock thanks to its innovative air lift tool designed by WATERTRACKS. Despite operational difficulties (e.g., trees, branches, heterogeneous sediment material, leaves and stones) EDF was satisfied by both robots and has extended the duration of the initial contract.

## 3. Conclusions

NESSIE (New Environmental System for Sediment Innovative Evacuation) and LISIE (LIight Subaquatic Innovative Excavator) are innovative underwater dredging robots used for restoring the reservoir capacity reduced by accumulation of sediments. NESSIE and LISIE remove fine sediment and dilute the material before discharging it downstream of the dam, so that respecting the environmental quality of the waterway. During the dredging operation, water is not lost, and hydro-power production is ensured. Both techniques have proven their high performance in different operations for managing.

**Acknowledgements**

The author acknowledges the support of Kamal El kadi Abderrezzak in the preparation of this extended abstract.

# New sediment yield models for mountainous Greek catchments

Sotirios-Theofanis KARALIS[1], Efthymios KARYMBALIS[2], Nikolaos MAMASIS[3]

[1] School of Engineering, Department of Topography & Geoinformatics, University of West Attica, Greece
email: skaralis@uniwa.gr

[2] School of Environment, Geography & Applied Economics, Department of Geography, Harokopio University, Greece
email: karymbalis@hua.gr

[3] School of Civil Engineering, National Technical University, Greece
email: nikos@ntua.gr

ABSTRACT

In this study, we explore the controls over specific suspended sediment yield in 11 stations situated along six major rivers of Western and Northern Greece (Arachthos, Achelooos, Evinos, Aoos, Kalamas and Aliakmon). We investigate the correlations among suspended sediment yield values and 35 characteristics of the corresponding basins. We find the principal controls to be slope and lithology followed by precipitation and runoff. With the use of stepwise multiple regression analysis, we build a model that employs three variables: slope, precipitation and lithology, where the contribution of lithology is an additive term to the slope-precipitation power relationship. The proposed model achieves good statistics ($R^2$ = 0.86).

## 1. Data and Methods

Values of area-specific Suspended Sediment Yield (SSY) for these stations were adopted from Zarris's et al. (2007) reanalysis of existing records and range from 80 to 2150 t km$^{-2}$ y$^{-1}$. These investigators employed the broken rating curve concept, which employs a steeper rating curve for discharges above the bankful discharge. About 35 geomorphic - topographic, morphometric, textural, tectonic, geological-lithological and climatic-hydrological (precipitation-runoff) characteristics, along with land cover variables and RUSLE factors (LS, R, K and C RUSLE), from maps of the European Soil Data Center (Panagos et al., 2015) were extracted for the corresponding basins (Table 1) and correlated with the SSY values.

**Table 1.** Values for SSY and major corresponding characteristics for the studied catchments

| STATION | RIVER | SSY [t km$^{-2}$ y$^{-1}$] | A [km$^2$] | P [mm] | R | SL | LITH [%] | LC [%] | DD [km$^{-1}$] | AL [%] | SHAPE |
|---|---|---|---|---|---|---|---|---|---|---|---|
| Aylaki | Acheloos | 1705 | 1355 | 1314 | 988 | 46.5 | 0.63 | 0.59 | 3.02 | 0.15 | 13.29 |
| Poros Rig. | Evinos | 1447 | 914 | 1198 | 1354 | 44.6 | 0.48 | 0.30 | 3.15 | 0.23 | 11.35 |
| Tsimovo Br. | Arachthos | 1049 | 640 | 1307 | 1207 | 33.5 | 0.84 | 0.38 | 3.63 | 0.01 | 13.10 |
| Gogou Br. | Arachthos | 1592 | 203 | 1753 | 939 | 45.4 | 0.59 | 0.91 | 2.97 | 0.16 | 5.71 |
| Plaka Br. | Arachthos | 1249 | 970 | 1400 | 1256 | 36.8 | 0.71 | 0.51 | 3.46 | 0.01 | 13.10 |
| Soulopoulo | Kalamas | 279 | 660 | 1270 | 1749 | 21.8 | 0.11 | 0.44 | 2.29 | 0.01 | 14.08 |
| Kioteki | Kalamas | 532 | 1481 | 1297 | 1838 | 26.4 | 0.23 | 0.41 | 2.19 | 0.01 | 14.08 |
| Konitsa Br. | Aoos | 2150 | 706 | 1215 | 721 | 40.9 | 0.42 | 0.44 | 2.90 | 0.04 | 8.66 |
| Venetikos | Aliakmon | 81 | 847 | 782 | 682 | 29.9 | 0.13 | 0.42 | 6.46 | 0.01 | 8.66 |
| Siatista | Aliakmon | 233 | 2724 | 687 | 651 | 20.1 | 0.02 | 0.32 | 5.62 | 0.04 | 21.95 |
| Ilarion M. | Aliakmon | 415 | 5005 | 719 | 650 | 19.6 | 0.04 | 0.32 | 6.08 | 0.03 | 24.15 |
| Aylaki | Acheloos | 1705 | 1355 | 1314 | 988 | 46.5 | 0.63 | 0.59 | 3.02 | 0.15 | 13.29 |
| Poros Rig. | Evinos | 1447 | 914 | 1198 | 1354 | 44.6 | 0.48 | 0.30 | 3.15 | 0.23 | 11.35 |
| Tsimovo Br. | Arachthos | 1049 | 640 | 1307 | 1207 | 33.5 | 0.84 | 0.38 | 3.63 | 0.01 | 13.10 |

P is precipitation, R-USLE is in MJ mm ha$^{-1}$ h$^{-1}$ y$^{-1}$, SL is slope in percent, LITH is the fraction of flysch, LC (Land Cover) is the fraction of CORINE code 33 (barren land), DD is Drainage Density, AL (alluvial) is the fraction of CORINE code 333, Shape is Horton's shape factor.

Erodible lithology was represented by the percentage of flysch within the basin, while land cover was represented by the duality barren or not land (CORINE code 33). The principal controls were found to be slope and erodible lithology of the catchments (Fig. 1, left). Mean annual precipitation plays a secondary and somehow ambiguous role as, due to the peculiarities of the small database, it is impossible to discriminate if it affects mainly basins with erodible lithology or basins with large slopes (Fig. 1, right) or both. Land use/cover also has a smaller relevance. Strong correlation was also found with the LS (Length Slope) factor of RUSLE, but with no other RUSLE factor (R or C). Simple and stepwise multiple regression was then used to construct models with the most prevalent factors, using readily accessible and unambiguous characteristics.

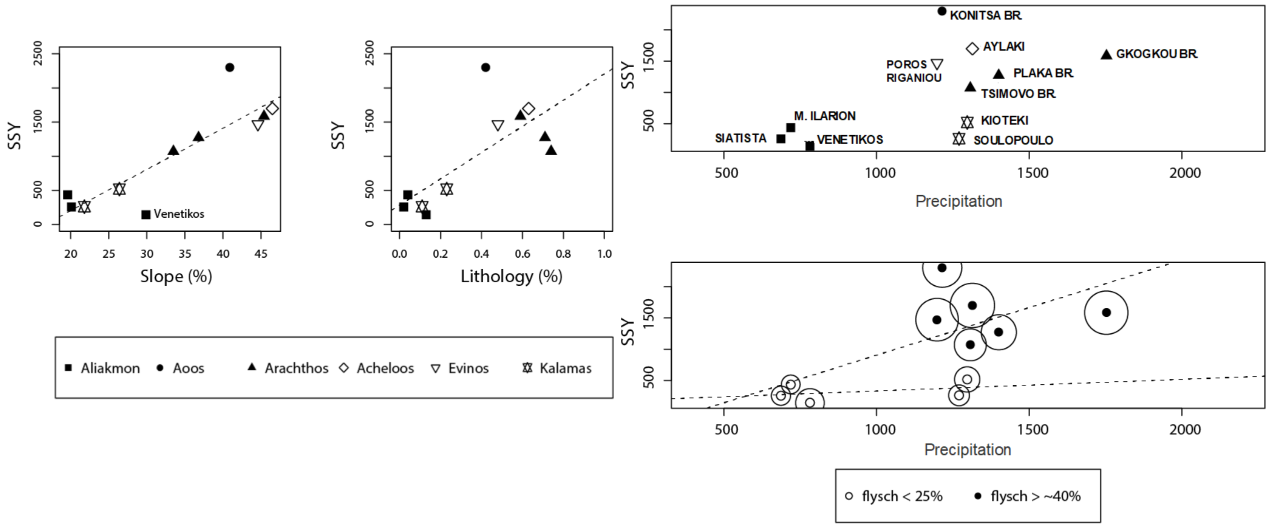


**Fig. 1.** *Scatter diagrams of measured SSY (t km$^{-2}$ y$^{-1}$) with some of the most relevant variables. To the left, morphological slope and erodible lithology, to the right, mean annual Precipitation (mm). Radiuses of circles in the lower left panel represent slope of the catchments.*

## 2. Results

Strong correlations with slope and the LS factor of RUSLE allow for simple regression equations [Eqs. (1)-(2)] with satisfactory statistics. Equation (3) is a power relationship with slope and precipitation and is considered appropriate for basins with resistant lithologies (erodible material less than 25%), while in the final model, Eq. (4), the lithology factor is added as an exponential term to the previous power relationship.

$$SSY = -861.66 + 53.9\ S \quad (1)$$

$$SSY = -875.4 + 309.6\ LS \quad (2)$$

$$SSY = 0.0049\ S^{1.51}\ P^{0.94} \quad (3)$$

$$SSY = 0.0049\ S^{1.51}\ P^{0.94} + 102.87\ e^{1.46L} \quad (4)$$

where *SSY* in t km$^{-2}$ y$^{-1}$ and, *S* – slope [%], *LS* – topographic RUSLE factor [dimensionless], *P* – mean annual precipitation [mm], *L* – fraction of erodible lithology within the catchment. For the equations to be used, slope has to be calculated with Arc-GIS from DEMs with cell size 25 m., since different GIS give different results. As a validation test, Eq. (4) was applied to three basins where SSY was estimated with hydrometric surveys, Acheloos and Agrafiotis rivers in Kremasta reservoir (Zarris et al., 2002) and Charadros river in Marathon reservoir (Xanthakis, 2011). The results were satisfactory ($R^2$ = 0.86). The advantage of the above Eq. (2) is that it can be applied with only the RUSLE2015 maps of the European Soil Data Centre, while Eq. (4) can be used to provide minimum [as Eq. (3)] and maximum sediment yields. It should be noted that results agree to a large extend with the predictions of the BQART model (Syvitski, 2007) and less so with the RUSLE2015 predictions.

***References***

*Panagos P, Borreli P, Poesen J, Ballabio C, Lugato E, Meusburger K, Montanarella L,Alewell C, (2015). The new assessment of soil loss by water erosion in Europe, Environmental Science & Policy, 54: 438-447. DOI:10.1016/j.envsci.2015.08.012.*

*Syvitski J (2007). Geology, Geography, and Humans Battle for Dominance over the delivery of Fluvial Sediment to the Coastal Ocean. The journal of Geology, 2007, 115, 1-19.*

*Zarris D, Lykoudi E, Koutsoyiannis D (2002). Sediment yield estimation from a hydrographic survey: A case study for the Kremasta reservoir basin, Greece, Proc. of the 5th International Conference "Water Resources Management in the Era of Transition". Athens, 4-8 September, pp. 338-345.*

*Zarris D, Lykoudi E, Panagoulia D (2007). Sediment yield estimates in North-western Greece and analyses with hydrologic and geomorphologic factors, Bulletin of the Geological Society of Greece, vol. XXXVII, Proceedings of the 11th International Congress, Athens, May, 2007.*

*Ξανθάκης Μ (2011). Μελέτη της εδαφικής διάβρωσης σε ορεινές λεκάνες απορροής με σύγχρονα τεχνολογικά εργαλεία. PhD thesis, School of Geography, Harokopio University, 288 p.*

# Geospatial assessment on morphodynamic evolution of Adyar River in India

R. RESHMA[1], Soumendra Nath KUIRY[2]

[1] Research scholar, Environmental and Water Resources Engineering Division, Department of Civil Engineering, Indian Institute of Technology Madras, Chennai, India
email: reshmaradhakrishnan094@gmail.com
[2] Associate Professor, Environmental and Water Resources Engineering Division, Department of Civil Engineering, Indian Institute of Technology Madras, Chennai, India
email: snkuiry@civil.iitm.ac.in

ABSTRACT

A river evolves in terms of its geometry, flow direction, and water quality based on various natural and human induced factors such as alluvial depositions, floods and other natural disasters, climate change, construction of hydraulic structures, unplanned urbanization, etc. Water quality restoration, waterbody rejuvenation, and flood damage reduction – all require a primary and precise knowledge of this morphodynamic evolution of the system. Morphodynamic evolution of the Adyar River of Chennai (Tamil Nadu, India) over the past three decades is analyzed in this study with the aid of Google Earth Engine (GEE), freely available Landsat satellite data, and a few assessment indices - Normalized Difference Vegetation Index, Modified Normalized Difference Water Index, and Enhanced Vegetation Index. The spatio-temporal evolution of the river and the corresponding variation in alluvial deposition are extracted. An elevated deposition of sediments is found towards the Adyar estuary, the location where the river joins the Bay of Bengal. Besides, a gradual deviation in the flow path is also observed, though the river center-line alignment is more or less unaltered. The excessive sediment deposition may be due to the haphazard encroachments, urbanization, and industrialization along the floodplains of the Adyar River since the early twentieth century. There is a high requirement for sediment removal and proper maintenance of the river channel to ensure better flow, low sedimentation, and hence reduced damages during future flood events. The morphological pattern evaluated in this study can be used in a long-term morphological numerical model study to regain the health of the Adyar River.

## 1. Introduction

A high degree of unplanned urbanization, human settlements on the floodplains, and natural disasters have altered the course and morphodynamics of many rivers in the world, leading to the destruction of natural biodiversity, frequent floods, and degradation of water quality. Restoration and rejuvenation of polluted rivers are a primary concern for many of the developing nations of the world today. Also, knowledge of annual river planform changes helps in efficient land use allocation and hence in the reduction of flood-induced losses. Satellite data-based morphodynamic assessment using Google Earth Engine (GEE) code editor has gained attention among the research community (Boothroyd et al., 2021a & 2021b; Xu, 2006; Zou et al., 2018). GEE platform enables the analysis to be done without the requirement of high-end processors with large storage capacity. Since the satellite images are freely available in the GEE repository, limitations in high-quality data availability can also be overcome. The objective of this study is to assess the morphological characteristics of the Adyar River, flowing through the Chennai city of Tamil Nadu state in India, in the GEE platform using freely available satellite imagery. The results of this study can be used in the ongoing process of regaining the health of the Adyar River and consequently reducing the damages caused by floods in the future.

## 2. Methodology

Annual image sets for the period of analysis and Region of Interest (ROI) from the Landsat satellite images over the last three decades (January 01, 1990, to January 01, 2021) are separately analyzed for the extraction of the river channel. The cloud masked images are assessed using three indices - Modified Normalized Difference Water Index (MNDWI) (Xu, 2006), Normalized Difference Vegetation Index (NDVI) (Gandhi et al., 2015), and Enhanced Vegetation Index (EVI) (Zou et al., 2018), respectively, to classify water and non-water areas, vegetative cover, and alluvial deposits (Boothroyd et al., 2021a and 2021b). The areas with MNDWI greater than NDVI or EVI and with EVI $< 0.1$ are categorized as water or active channels, while areas with MNDWI $\geq 0.05$ and NDVI $\leq 0.2$, are classified as alluvial deposits. The channel and alluvial deposit layers thus extracted are further enhanced by noise filtering. The planform, the total wetted area, and alluvial deposits are assessed using the GEE geometric tools. The morphodynamic process of erosion and deposition is quantified by the analyzed alluvial depositions and the area of deposits therein.

## 3. Results and Discussion

Mapping and analysis were carried out on a five-year interval, considering a minimum interval for the geomorphological change detection (Boothroyd et al., 2021b). Though the overall centerline and channel position remains more or less unaltered, the river stretch is found to have a gradual shift of its either bank. The shift in flow path may be attributed to the erosion-deposition processes as well as floodplain encroachment. The shift in the flow path can also be attributed to the alluvial deposits along the river as it flows through the city before joining the Bay of Bengal. The annual variation in the wet area and the alluvial deposits are shown in Figs. 1 and 2, respectively. There is a considerable increase in alluvial deposition, which may be one of the causative factors for the observed widening of the river. The deposition is found to be more towards the river mouth, where it joins the Bay of Bengal, which may be due to the deposition of transported sediment from upstream to the low-velocity region of the river mouth. In addition, storm surges bring sediments to the Adyar estuary. This creates an adverse impact during the flood events resulting in a larger overflow in the regions, with an additional tidal effect.

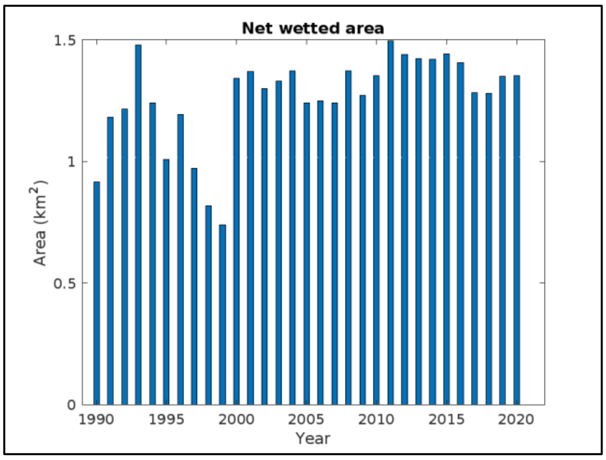


*Fig. 1.* *Net wetted area*

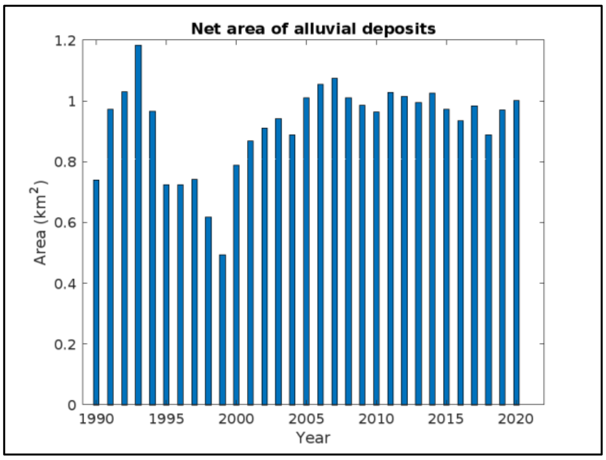


*Fig. 2.* *Area of alluvial deposits along the flow path*

## 4. Conclusions

Though there is a gradual shift in the flow path of the river, the centerline of the river system is overall stable, with a considerable increase in the extent of alluvial deposition along the flow channel, primarily towards the river mouth. Thus, there is a high requirement for sediment removal and proper maintenance of the river channel to ensure better flow, low sedimentation, and hence reduced damages during future flood events. The morphological pattern over three decades evaluated in this study can be used in a long-term morphological numerical model study to regain the health of the Adyar River.

***Acknowledgements***

*We gratefully acknowledge the funding from the Department of Biotechnology (DBT) in India (Computer No. 8981 || BT/IN/Indo-UK/AMR-Env/03/ST/2020-21 || AMRFlows) and the Natural Environment Research Council (NERC) in the UK (NE/T013222/1).*

***References***

*Boothroyd RJ, Nones M, Guerrero M (2021a) Deriving planform morphology and vegetation coverage from remote sensing to support river management applications, Frontiers in Environmental Science, 9, 146*

*Boothroyd RJ, Williams RD, Hoey TB, Barrett B, Prasojo OA (2021b) Applications of Google Earth Engine in fluvial geomorphology for detecting river channel change. Wiley Interdisciplinary Reviews: Water, 8(1), e21496*

*Foga S, Scaramuzza PL, Guo S, Zhu Z, Dilley Jr RD, Beckmann T, ..., Laue B (2017) Cloud detection algorithm comparison and validation for operational Landsat data products, Remote Sensing of Environment, 194, 379-390*

*Gandhi GM, Parthiban S, Thummalu N, Christy A (2015) NDVI: Vegetation change detection using remote sensing and GIS–A case study of Vellore District, Procedia Computer Science, 57, 1199-1210*

*Xu H (2006) Modification of normalized difference water index (NDWI) to enhance open water features in remotely sensed imagery, Int. J. Remote Sens., 27(14), 3025-3033*

*Zou Z, Xiao X, Dong J, Qin Y, Doughty RB, Menarguez MA, ..., Wang J (2018) Divergent trends of open-surface water body area in the contiguous United States from 1984 to 2016, Proceedings of the National Academy of Sciences, 115(15), 3810-3815*

# Preliminary assessment of soil erosion and sediment yield during a catastrophic flash flood event

Konstantinos KAFFAS[1], George PAPAIOANNOU[2], George VARLAS[3], Mario J. Al SAYAH[4], Anastasios PAPADOPOULOS[3], Elias DIMITRIOU[3], Petros KATSAFADOS[5], Maurizio RIGHETTI[1]

[1] Free University of Bozen-Bolzano, Faculty of Science and Technology, Bolzano, Italy

[2] Democritus University of Thrace, Department of Forestry and Management of the Environment and Natural Resources, Orestiada, Greece

[3] Hellenic Centre for Marine Research, Institute of Marine Biological Resources and Inland Waters, Anavyssos, Greece

[4] École des Ponts ParisTech, HM&Co, Champs-sur-Marne, France

[5] Harokopio University of Athens, Department of Geography, Athens, Greece

Email: konstantinos.kaffas@unibz.it

ABSTRACT

In this paper, we model and quantify in forecast mode the soil erosion and sediment yields during one of the most destructive flash floods in recent Greek history. The extreme event known as the flash flood of Mandra occurred in the morning hours of November 15th, 2017, with 300 mm of rainfall falling in approximately 13 hours and an estimated return period between 200 and 500 years (Diakakis et al., 2020). According to the calculations, during the event of Mandra, 2,195 tons and 1,435 tons of sediment were transported to the stream networks of the two under-study torrent basins.

## 1. Study area

The geographic position of the Soures and Agia Aikaterini Torrent basins is in western Attica, located between 38° 3' 14'' N and 38° 7' 19'' N latitudes and 23° 22' 59'' E and 23° 29' 10'' E longitudes. The Soures and Agia Aikaterini basins cover areas of 18.8 km$^2$ and 17.4 km$^2$, with altitudes in the range 122-842 m, and are covered mostly by forests and semi-natural areas while agricultural areas and artificial surfaces cover smaller fractions.

## 2. Methods–Results

Gridded land cover data, 5 m resolution DEM, and 250 m resolution soil maps were used to assess the soil erosion and sediment yields during the flash flood of Mandra based on the runoff forecasts.

### *2.1. Hydrometeorological forecasting*

The Chemical Hydrological Atmospheric Ocean wave System (CHAOS) was selected as a "state-of-the-art" multi-scale forecasting system capable of providing reliable forecasts even for flash flood events (Varlas et al., 2019). Precipitation fields were estimated by means of the meteorological component (WRF-ARW v4.2) of CHAOS. Runoff fields were estimated by the hydrological component (WRF-Hydro v5.1.1) of CHAOS which is a fully distributed hydrological model. Ultimately, 5-min precipitation forecasts and 5-min and 1-hr surface runoff forecasts were produced at a 250 m grid spacing to forecast soil erosion and sediment yields for a 24-hr duration, from 14 to 15 November 2017 at 12:00 UTC, covering the entire period of the flash flood event.

### *2.2. Soil erosion and sediment yield forecasting*

On the basis of the gridded surface runoff forecasts, sediment yields were simulated by means of the Modified Universal Soil Loss Equation (MUSLE) (Williams, 1975).

$$SY = R_f \cdot K \cdot L \cdot S \cdot C \cdot P \cdot F_{CFRG} \tag{1}$$

$$R_f = 11.8 \cdot \left(Q \cdot q_p\right)^{0.56} \tag{2}$$

where $R_f$ – runoff erosivity factor, $K$ – soil erodibility factor [t h MJ$^{-1}$ mm$^{-1}$], $L$ – slope length factor, $S$ – slope steepness factor, $C$ – cover and management factor, $P$ – support practice factor, $F_{CFRG}$ – coarse fragment factor, Q – runoff volume per unit of time [m$^3$], $q_p$ – peak flow rate [m$^3$ s$^{-1}$]. A detailed calculation of the MUSLE factors in Eq. (1) can be found in Kaffas et al. (2021).

Cinnirella et al. (1998) present a variation of MUSLE more relevant to soil erosion:

$$SY = \frac{0.8776}{A_w} \cdot \left(Q \cdot q_p\right)^{0.56} \cdot K \cdot L \cdot S \cdot C \cdot P \cdot F_{CFRG} \quad (3)$$

where $A_w$ – the area [ha]. Soil erosion and sediment yields were calculated at 5 m resolution and an hourly time step, by means of Eqs. (3) and (1), respectively (Figs. 1, 2).

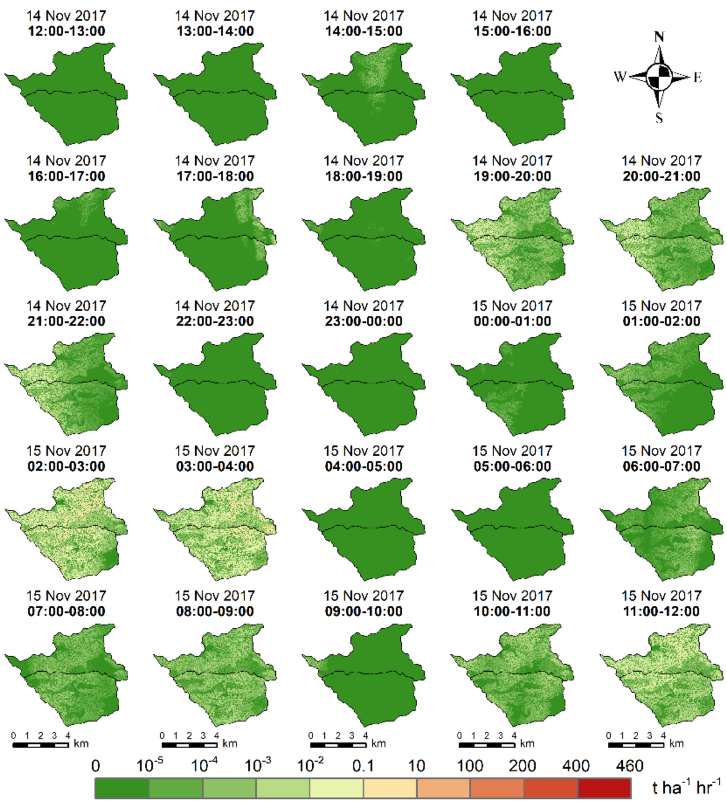


***Fig. 1.*** *Hourly soil erosion forecast for the entire event in Soures and Agia Aikaterini basins.*

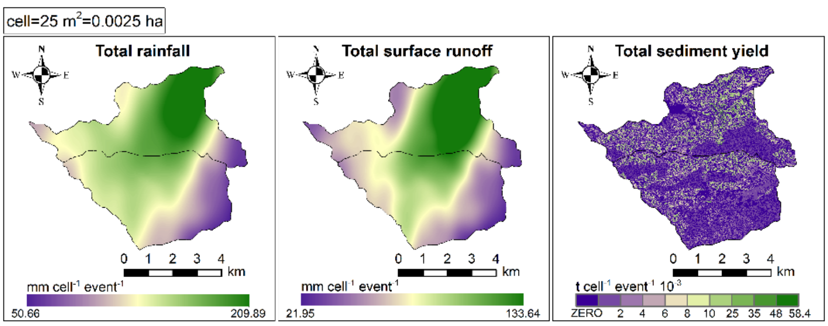


***Fig. 2.*** *Total rainfall, surface runoff and sediment yield in Soures and Agia Aikaterini basins.*

***References***

*Cinnirella S, Iovino F, Porto P, Ferro V (1998) Anti-erosive effectiveness of Eucalyptus coppices through the cover management factor estimate, Hydrological Processes, 12(4)*

*Diakakis M, Boufidis N, Salanova GM, Andreadakis E, Stamos I (2020) A systematic assessment of the effects of extreme flash floods on transportation infrastructure and circulation: The example of the 2017 Mandra flood, International Journal of Disaster Risk Reduction, 47, 101542*

*Kaffas K, Pisinaras V, Al Sayah MJ, Santopietro S, Righetti M (2021) A USLE-based model with modified LS-factor combined with sediment delivery module for Alpine basins, Catena, 105655*

*Varlas G, Anagnostou MN, Spyrou C, Papadopoulos A, Kalogiros J, Mentzafou A, Michaelides S, Baltas E, Karymbalis E, Katsafados P (2019) A multi-platform hydrometeorological analysis of the flash flood event of 15 November 2017 in Attica, Greece, Remote Sensing, 11(1), 45*

*Williams JR (1975) Sediment-Yield Prediction with Universal Soil Loss Equation Using Runoff Energy Factor, In Present and Prospective Technology for Predicting Sediment Yield and Sources. Agricultural Research Service & US Department of Agriculture*

# On how bed load transport may change the equivalent roughness of a flow

Hasan ESLAMI, Hooshyar YOUSEFYANI, Mohsen YAVARY NIA, Alessio RADICE

Politecnico di Milano, Milan, Italy
email: hasan.eslami@polimi.it

ABSTRACT

This study investigates the effect of bed load transport on the equivalent roughness of a flow. To do so, a series of aggradation experiments with supercritical flow are performed in a laboratory channel and corresponding numerical simulations are run. Matching the experimental and numerical profiles, calibrated values are obtained for the Manning coefficient and a bed load factor. The calibrated Manning coefficient is larger than that estimated in preliminary experiments without sediment transport.

## 1. Introduction

Several literature studies have debated on if and how the presence of bed load transport can alter the flow resistance expressed, for example, in terms of a Manning coefficient. Some scholars argued that the flow resistance over a mobile bed with sediment transport is higher than that in clear water flows over a fixed bed (Calomino et al., 2004; Gaudio et al., 2011). Contrarily, others observed the bed load transport reducing the flow resistance. For example, Nikora and Goring (2000) reported that a weak gravel transport as bed load could determine an increase of the streamwise velocity.

The aim of the present study is to contribute to the issue investigating how an equivalent Manning coefficient could best return the bed and water profiles measured during a series of aggradation experiments in supercritical conditions. The experiments have been reproduced in numerical simulations calibrating the Manning coefficient and a bed load factor. It is shown that the calibrated Manning coefficient changed due to the presence of sediment transport in the flow.

## 2. Laboratory facility and measurement methods

The aggradation experiments were conducted at the Mountain Hydraulics Laboratory of the Politecnico di Milano (Lecco campus), using a rectangular flume with a length of 5.2 m, width of 0.3 m, and height of 0.45 m. The flume walls are made of plexiglas to ensure visibility of the ongoing processes. An erodible channel bed is 15 cm thick and is made of Polyvinyl Chloride (PVC) sediment particles with a density of 1,443 kg $m^{-3}$ and a size of 3.8 mm. A sediment feeding system is employed at the upstream end of the channel.

The measurements are taken by image processing, using video shots acquired during the aggradation experiments by several cameras. One of these cameras takes videos of the sediment feeder and the sediment feeding rate is measured by determining the velocity of the fed sediment by Particle Image Velocimetry and converting it into a sediment rate by a transfer function (Radice and Zanchi, 2018). Two cameras take videos of the flume from the side, based on which the bed and water elevation profiles are measured during an experiment (this method was introduced by Radice and Zanchi, 2018, and later amended by Eslami et al., 2021). The bed surface is located at the border between the still sediment and the bed load layer.

The sediment transport capacity $Q_{s0}$ of the flow has been determined in preliminary experiments where the sediment feeding rate was adjusted to induce neither aggradation nor degradation in the channel. The sediment transport capacity has been also computed by imposing a mass balance of sediment during aggradation experiments, returning values generally in agreement with those of the preliminary runs.

## 3. Numerical analysis

The laboratory results of the present experimental campaign have been reproduced using the BASEMENT software developed at the ETH Zürich. Applied boundary conditions were: a constant flow rate and sediment feeding rate at the inlet, and a fixed bed elevation at the outlet. The sediment transport capacity was computed with the Meyer-Peter and Müller equation, but applying a bed load factor ($\alpha_{MPM}$) for a better calibration of the transport formula. The Manning coefficient was also calibrated to obtain profiles of the bed and water elevation matching those measured during the experiments.

## 4. Results and discussion

Table 1 lists the properties of the aggradation experiments. The experiments have been performed changing the run time ($T$), flow rate ($Q$) and sediment feeding rate ($Q_{s,in}$). The ratio of the latter to the initial sediment transport capacity of the channel is a loading ratio ($Lr$). The $Q_{s0}$ is the same for experiments with the same flow rate and is computed as the average of the determinations for each run. The table reports also the calibrated parameters of the numerical models. Figure 1 shows an example of the comparison between experimental and numerical results after calibration.

**Table 1**. Properties of the experimental runs and corresponding numerical simulations

| Experiment | $T$ [s] | $Q$ [m$^3$ s$^{-1}$] | $Q_{s,in}$ [m$^3$ s$^{-1}$] | $Q_{s0}$ [m$^3$ s$^{-1}$] | $Lr$ | Calibrated bed load factor, $\alpha_{MPM}$ | Calibrated Manning coefficient [s m$^{-1/3}$] |
|---|---|---|---|---|---|---|---|
| AE1 | 490 | 0.005 | $1.42\times10^{-4}$ | $8.3\times10^{-5}$ | 1.71 | 1.05 | 0.022 |
| AE2 | 560 | 0.005 | $1.01\times10^{-4}$ | $8.3\times10^{-5}$ | 1.21 | 1.10 | 0.022 |
| AE3 | 340 | 0.005 | $2.43\times10^{-4}$ | $8.3\times10^{-5}$ | 2.92 | 1.20 | 0.020 |
| AE4 | 259 | 0.007 | $2.28\times10^{-4}$ | $1.3\times10^{-4}$ | 1.75 | 1.70 | 0.016 |
| AE5 | 364 | 0.007 | $1.43\times10^{-4}$ | $1.3\times10^{-4}$ | 1.10 | 1.70 | 0.016 |
| AE6 | 233 | 0.007 | $2.55\times10^{-4}$ | $1.3\times10^{-4}$ | 1.96 | 1.75 | 0.017 |

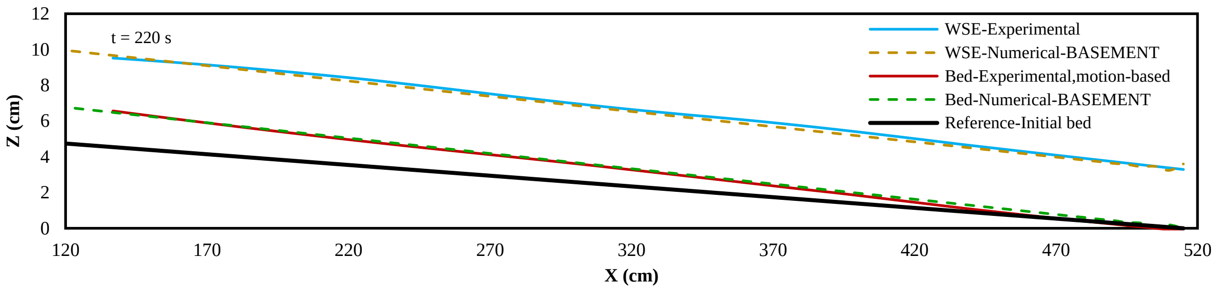


**Fig.1.** Comparison between spatial evolution profiles of bed and water obtained from calibrated numerical model and experimental work at selected time t = 220 s for experiment AE4.

The experiments constitute two homogeneous series with the same $Q$, $Q_{s0}$, and calibrated parameters of the numerical simulations. For $Q$ = 0.005 m$^3$ s$^{-1}$ we have obtained a bed load factor around 1.1 and a Manning coefficient around 0.021 s m$^{-1/3}$, while for the experiments with $Q$ = 0.007 m$^3$ s$^{-1}$ the calibrated bed load factor and Manning coefficient were around 1.7 and around 0.0165 s m$^{-1/3}$, respectively. For comparison, the Manning coefficient of the sediment particles, determined during preliminary runs without sediment transport by Zanchi and Radice (2021), equals 0.015 s m$^{-1/3}$. Zanchi and Radice (2021) derived this coefficient with the clear water flow over a fixed bed and also with the movable bed, but sediment transport was not occurring due to the low water discharge. Thus, in this study with relatively high sediment transport the calibrated values of the Manning coefficient were higher than those estimated for the preliminary runs without sediment transport. Furthermore, by comparing the calibrated Manning coefficient of the experiments with $Q$ = 0.005 m$^3$ s$^{-1}$ and of those with $Q$ = 0.007 m$^3$ s$^{-1}$, one can recognize that the required Manning coefficient for the experiments with higher water discharge is significantly lower than that corresponding to the experiments with lower water discharges. Vice versa, for the experiments with lower water discharge, the calibrated bed load factor is notably lower than that related to the experiments with higher water discharge.

### References

Calomino F, Gaudio R, Miglio A (2004) Effect of bed-load concentration on friction factor in narrow channels, Proc. of River Flow 2004, Naples, Italy, 279–285

Eslami H, Yavary Nia M, Yousefyani H (2021) Experimental and numerical analysis of overloaded channel in supercritical condition, M.Sc. thesis, Politecnico di Milano

Gaudio R, Miglio A, Calomino F (2011) Friction factor and von Kármán's κ in open channels with bed-load, Journal of Hydraulic Research, 49(2), 239–247

Nikora V, Goring D (2000) Flow turbulence over fixed and weakly mobile gravel beds, Journal of Hydraulic Engineering, 126(9), 679–690

Radice A, Zanchi B (2018) Multicamera, multimethod measurements for hydromorphologic laboratory experiments, Geosciences, 8(5), 172

Zanchi B, Radice A (2021) Celerity and height of aggradation fronts in gravel-bed laboratory channel, Journal of Hydraulic Engineering, 147 (10): 4021034

# Relation of the observed water level decrease and morphological changes of the river channel in the middle Danube

Ljubiša MIHAJLOVIĆ[1], Dejana ĐORĐEVIĆ[2], Csaba ABONYI[3], Enikő Anna TAMÁS[4]

[1] Directorate for Inland Waterways, Ministry of Construction, Transport and Infrastructure, Belgrade, Serbia
email: ljmihajlovic@plovput.rs

[2] Faculty of Civil Engineering, University of Belgrade, Belgrade, Serbia
email: dejana@grf.bg.ac.rs

[3] Lower Danube valley Water Authority, Baja, Hungary
email: abonyics@gmail.com

[4] Faculty of Water Sciences, University of Public Service, Baja, Hungary
email: tamas.eniko.anna@uni-nke.hu

ABSTRACT

This work is a continuation of works by Goda et al. (2007) and Tamás et al. (2021) that were prompted by the drying of floodplains and problems in the water supply of irrigation and drainage canal networks in the whole middle Danube region. Previous works focused on hydrology and showed a constant lowering of water levels, which indicated the deepening of the riverbed. In the present study, the relationship between indicators of morphological changes and the decrease in low water levels at Gauging Stations (GS) is sought. At this stage, results confirm a continuous deepening of the riverbed. Despite small correlation coefficient values between low water levels ($Z_{min}$) and percentage increase in the cross-sectional areas in the sand bed part of the investigated reach, the linear decreasing trend in $Z_{min}$ is evident.

## 1. Morphological data

The datasets for this study were provided by the Directorate for Inland Waterways in Serbia and the Lower Danube-valley Water Authority in Hungary. These include cross-sectional data either of the regularly surveyed, inventory cross-sections of the two authorities or at GSs' locations along the 300 km long reach from river km (rkm) 1560 (Dunaföldvár, Hungary) to rkm 1255 (Novi Sad, Serbia). In 60 years, there are seven comparable bathymetric surveys for both countries. The data from older surveys were available only in the paper as either depth maps or cross-sections, so they were digitized. In the case of depth maps, cross-sections were extracted after the digitization of the map. In newer surveys, cross-sections were recorded digitally, using an echo sounder synchronized in operation with an RTK GPS.

After the conformance of the datums in the two countries, the cross-sections were plotted in AutoCAD software. To provide a common ground for comparisons along the investigated reach, a reference water level was adopted. *Étiage Navigable* (EN), defined by the Danube Commission in 2012 for each GS, was increased by 2 m. Such a choice of the reference water level is based on visual observations of each cross-section, and it is justified by the fact that this water level (EN + 2 m) is close to bank full level but remains within the main channel. A cross-sectional area below EN + 2 m was then chosen as a starting point for the analysis of the riverbed incision.

## 2. Results

The evolution of the two chosen cross-sections is presented in Fig.1. The incision may be due to a negative sediment balance caused by river regulation works with cutoffs at the end of the 19th century, extensive dredging in the 20th century and the construction of several Hydro Power Plants in the upstream reaches (Habersack et al. 2019).

Figure 2 shows the percentages of cross-sectional area changes and the correlation between these changes and the minimum water levels at GSs along the Middle Danube River reach. It is readily noticeable that the cross-sectional areas are constantly increasing (Figs. 2a, b). This increase correlates to the decrease in minimum water levels at each GS (Figs. 2c, d). The percentage increase in the cross-sectional area, when compared to the first survey, changes at the rate of 1.6% yearly at the upstream end of the reach to 0.16% yearly at the downstream end (Table 1). The linear decreasing trend in $Z_{min}$ is evident from Figs. 2c, d.

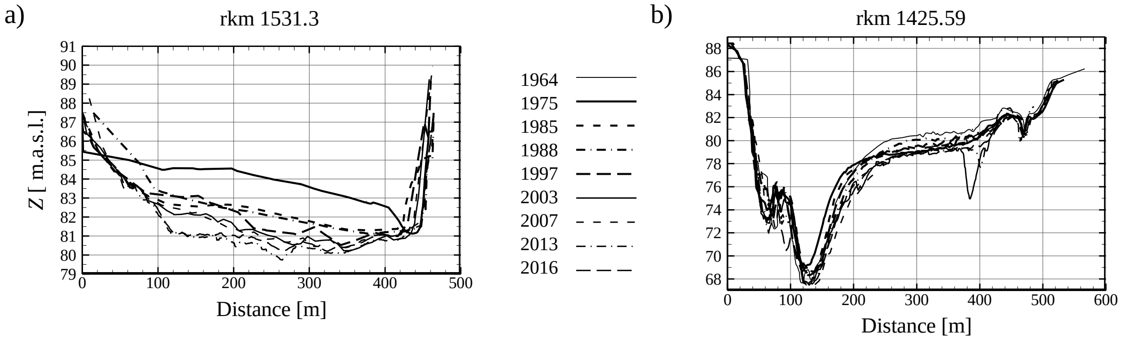


***Fig. 1.*** *Cross-sections evolution at a) GS Paks and b) GS Bezdan; at GS Paks bathymetric data are available from 1975 and for GS Bezdan from 1964.*

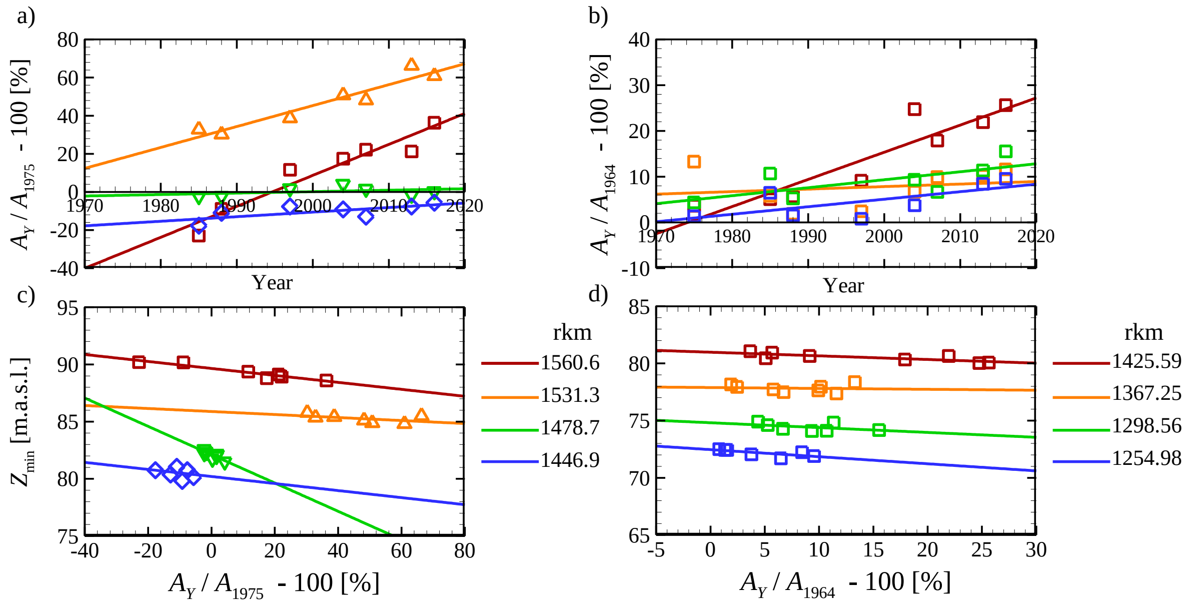


***Fig. 2.*** *Percentages of cross-sectional area changes a) and b) with reference to the initial survey ($A_Y/A_{ref}$ – 100) and the correlation of minimum water levels and percentages of cross-sectional area changes c) and d) at gauging stations in the Middle Danube River reach. $A_Y$ is the cross-sectional area in any year, $A_{1975}$ and $A_{1964}$ are reference cross-sectional areas ($A_{ref}$) for the first survey in Hungary and Serbia, respectively.*

**Table 1.** Rates of increase in the cross-sectional area with reference to the first survey $A_Y / A_{ref} - 100 = a\text{Year} - b$, reference years (ref) are 1975 for GSs in Hungary and 1964 for GSs in Serbia

| Name of GS and river km | *a* | *b* | Name of GS and river km | *a* | *b* |
|---|---|---|---|---|---|
| Dunaföldvár, rkm 1560.60 | 1.62 | 3239.6 | Bezdan, rkm 1425.59 | 0.59 | 1172.1 |
| Paks, rkm 1531.30 | 1.10 | 2149.8 | Bogojevo, rkm 1367.25 | 0.27 | 526.51 |
| Baja, rkm 1478.70 | 0.08 | 152.36 | Bačka Palanka, rkm 1298.56 | 0.17 | 339.07 |
| Mohács, rkm 1446.90 | 0.24 | 489.29 | Novi Sad, rkm 1254.98 | 0.16 | 323.13 |

## 3. Conclusions

With the present study of the morphological changes in the middle Danube, the incision along the entire reach is proven by the increase in cross-section areas. The rate of change of the cross-sectional area decreases going downstream, which corresponds to the findings for the water level decrease in Tamás et al. (2021).

***Acknowledgements***

*The authors wish to thank the Directorate for Inland Waterways in Serbia and the Lower Danube-valley Water Authority in Hungary for the provision of the data.*

***References***

*Goda L, Kalocsa B, Tamás EA (2007) River Bed Erosion On The Hungarian Section Of The Danube, Journal of Environmental Science for Sustainable Society, 1, 47-54*

*Habersack H, Haimann M, Gmeiner P, Baranya S, Holubova K, Vartolomei F (2019) Sediment (dis)balance – A significant river management issue, E-proceedings of the 38th IAHR World Congress.*

*Tamás EA, Đorđević D, Kalocsa B, Vujanović A (2021) Hydrological indicators of the riverbed incision along the free-flowing Danube River reach from Budapest to Slankamen relevant for the lateral connectivity between the river channel and floodplains, Extended Abstracts of the IAD Conference.*

# Modification of sediment transport formulas based on measurements: Application to streams of NE Greece

Loukas AVGERIS[1], Konstantinos KAFFAS[2], Vlassios HRISSANTHOU[3]

[1,3] Department of Civil Engineering, Democritus University of Thrace, Xanthi, Greece
email: lavgeris@civil.duth.gr
email: vhrissan@civil.duth.gr

[2] Faculty of Science and Technology, Free University of Bozen-Bolzano, Bolzano, Italy
email: konstantinos.kaffas@unibz.it

ABSTRACT

Sediment transport and stream discharge are two of the natural procedures which affect the hydromorphological profile of a watercourse. Measurements of water discharge, bed load transport rate and suspended sediment concentration were conducted in Kosynthos River and Kimmeria Torrent in north-eastern Greece. The total sediment concentration was calculated, in both streams, by means of the formulas of Yang, after calibrating the coefficients of the formulas. The comparison between the calculated and measured total sediment concentrations was achieved by means of several statistical criteria. The results indicate that the modified formulas of Yang can be successfully used for the determination of the total sediment concentration in Kosynthos River and Kimmeria Torrent.

## 1. Introduction

Regression analysis has been extensively employed in literature to either derive sediment transport/concentration equations as a function of hydraulic or hydrometeorological parameters or to adjust existing well-known sediment transport models to environments with specific features different from the ones they were created for (Avgeris et al., 2020). Moreover, sediment monitoring stations are very sparse, and hence the bulk of streams worldwide remains ungauged. In addition, the estimation of sediment discharge by conventional measurement methods is expensive and labor intensive, and therefore, alternative, less expensive approaches are sought (Kaffas and Hrissanthou, 2019). The objective of this study is to redetermine the arithmetic coefficients of the total sediment transport rate formulas of Yang based on field data of Kosynthos River (41° 08’ 38.2” N, 24° 53’ 26.9” E) and Kimmeria Torrent (41° 08’ 50.8” N, 24° 56’ 17.5” E). This was achieved by means of multiple regression analysis, and the modified equations provided substantially more accurate calculations of sediment concentration in these streams. The efficiency of the methods was evaluated by comparison between calculated and measured total sediment concentration.

## 2. Materials and methods

A total of 84 datasets of measured stream flow rate, flow depth, bed load transport rate, suspended load transport rate, and median particle diameter was available. The cross-sectional geometry was determined, as well, for every set of measurements. The total measured sediment concentration was derived as a summation of the measured bed load and suspended load transport rates. The total sediment concentration was also calculated by means of four different ways, Yang’s original formulas of 1973 and 1979 for total sediment concentration and two counterparts of those formulas with calibrated coefficients by means of multiple regression based on the field measurements.

In 1973, Yang derived a formula for the total sediment transport in rivers and streams by applying a multiple regression analysis for 463 sets of data in laboratory flumes [Eq. (1)]. In 1979, Yang concluded that the critical unit stream power term in Eq. (1) can be neglected without causing much error when the measured sediment concentration is greater than 20 ppm. The latter Yang formula was developed based on 1259 sets of laboratory and field data [Eq. (2)].

$$\log c_F = 5.435 - 0.286\log\frac{wD_{50}}{v} - 0.457\log\frac{u_*}{w} - \left(1.799 - 0.409\log\frac{wD_{50}}{v} - 0.314\log\frac{u_*}{w}\right)\log\left(\frac{us}{w} - \frac{u_{cr}s}{w}\right) \quad (1)$$

$$\log c_F = 5.165 - 0.153\log\frac{wD_{50}}{v} - 0.297\log\frac{u_*}{w} - \left(1.780 - 0.360\log\frac{wD_{50}}{v} - 0.480\log\frac{u_*}{w}\right)\log\left(\frac{us}{w}\right) \quad (2)$$

where $c_F$ is the total sediment concentration (ppm by weight); $w$ is the terminal fall velocity of the sediment particles [m s$^{-1}$]; $D_{50}$ is the median particle diameter [m]; $v$ is the kinematic viscosity of water [m$^2$ s$^{-1}$]; $s$ is the energy slope; $u$ is the mean flow velocity [m s$^{-1}$]; $u_{cr}$ is the critical mean flow velocity [m s$^{-1}$]; and $u_*$ is the shear velocity [m s$^{-1}$]. The product $u\ s$ is characterized as unit stream power.

On the basis of Kosynthos River data, the arithmetic coefficients of the original formulas of Yang are modified, respectively, as follows:

$$\log c_F = 3.960 - 0.984\log\frac{wD_{50}}{v} - 0.706\log\frac{u_*}{w} - \left(0.471 - 0.224\log\frac{wD_{50}}{v} - 1.292\log\frac{u_*}{w}\right)\log\left(\frac{us}{w} - \frac{u_{cr}s}{w}\right) \quad (3)$$

$$\log c_F = 3.394 - 0.595\log\frac{wD_{50}}{v} - 0.100\log\frac{u_*}{w} - \left(0.953 - 0.517\log\frac{wD_{50}}{v} - 1.955\log\frac{u_*}{w}\right)\log\left(\frac{us}{w}\right) \quad (4)$$

The corresponding modified formulas of Yang for the Kimmeria Torrent data can be seen in Eqs. (5) and (6):

$$\log c_F = 0.892 + 1.064\log\frac{wD_{50}}{v} + 3.004\log\frac{u_*}{w} - \left(0.436 - 0.297\log\frac{wD_{50}}{v} - 1.287\log\frac{u_*}{w}\right)\log\left(\frac{us}{w} - \frac{u_{cr}s}{w}\right) \quad (5)$$

$$\log c_F = 0.179 + 1.551\log\frac{wD_{50}}{v} + 3.830\log\frac{u_*}{w} - \left(1.042 - 0.693\log\frac{wD_{50}}{v} - 2.096\log\frac{u_*}{w}\right)\log\left(\frac{us}{w}\right) \quad (6)$$

In concrete terms, the new arithmetic coefficients of Eqs. (3)–(6) were determined by means of the conventional least squares regression.

## 3. Results and concluding remarks

The comparison between calculated and measured total sediment concentration was made on the basis of the following statistical criteria: Mean Relative Error (MRE), Nash-Sutcliffe Efficiency (NSE) (Nash and Sutcliffe, 1970), linear correlation coefficient r, determination coefficient $R^2$ and discrepancy ratio. In this case, the discrepancy ratio represents the percentage of the calculated total sediment concentration values that lie between the quadruple and the one quarter of the corresponding measured total sediment concentration values. The values of the mentioned statistical criteria are displayed in Tables 1 and 2.

**Table 1.** Statistical criteria of Yang's original and calibrated formulas for Kosynthos River

| | Paired Values | MRE (%) | NSE | r | $R^2$ | Discrepancy Ratio |
|---|---|---|---|---|---|---|
| Original 1973 | 62 | -1226.540 | -83.404 | 0.317 | 0.101 | 0.226 |
| Calibrated 1973 | 62 | -37.293 | 0.521 | 0.766 | 0.587 | 0.968 |
| Original 1979 | 62 | -1577.191 | -66.701 | 0.306 | 0.094 | 0.177 |
| Calibrated 1979 | 62 | -38.302 | 0.522 | 0.776 | 0.602 | 0.887 |

**Table 2.** Statistical criteria of Yang's original and calibrated formulas for Kimmeria Torrent

| | Paired Values | MRE (%) | NSE | r | $R^2$ | Discrepancy Ratio |
|---|---|---|---|---|---|---|
| Original 1973 | 22 | -298.247 | -3.248 | -0.244 | 0.059 | 0.500 |
| Calibrated 1973 | 22 | -14.884 | -0.114 | 0.069 | 0.005 | 0.909 |
| Original 1979 | 22 | -307.673 | -3.247 | -0.239 | 0.057 | 0.636 |
| Calibrated 1979 | 22 | -15.268 | -0.132 | 0.006 | 0.000 | 0.909 |

The statistical criteria of both calibrated Yang's formulas are improved in comparison to those of Yang's original formulas. Specifically, the MRE displays a notable decrease, whilst the NSE –especially for Kosynthos River– is significantly improved. The linear correlation coefficient, r, and the determination coefficient, $R^2$, tend to the optimal values, for Kosynthos River. The calibrated 1973 Yang's formula outperforms the calibrated 1979 Yang's formula for both Kosynthos River and Kimmeria Torrent. Overall, the results can be considered satisfactory for the case of Kosynthos River, while for Kimmeria Torrent more data should be taken into account. On the basis of a sufficient dataset that covers all flow conditions, regression analysis could effectively remedy the lack of sediment data.

***References***

*Avgeris L, Kaffas K, Hrissanthou V (2020) Comparison between Calculation and Measurement of Total Sediment Load: Application to Nestos River, Environmental Sciences Proceedings, 2, 19*
*Kaffas K., Hrissanthou, V (2019) Computation of hourly sediment discharges and annual sediment yields by means of two soil erosion models in a mountainous basin, International Journal of River Basin Management, 17, 63–77*
*Nash JE, Sutcliffe JV (1970) River flow forecasting through conceptual models, part I-A discussion of principles, Journal of Hydrology, 10, 282–290*
*Yang CT (1973) Incipient Motion and Sediment Transport, ASCE Journal of the Hydraulics Division, 99, 1679–1704*
*Yang CT (1979) Unit stream power equations for total load, Journal of Hydrology, 40, 123–138*

# Adaptation of the Engelund-Hansen formula to Nestos River, Greece

Konstantinos VANTAS[1], Konstantinos KAFFAS[2], Epaminondas SIDIROPOULOS[1], Vlassios HRISSANTHOU[3]

[1] Aristotle University of Thessaloniki, Department of Rural and Surveying Engineering, Thessaloniki, Greece

email: kon.vantas@gmail.com

email: nontas@topo.auth.gr

[2] Free University of Bozen-Bolzano, Faculty of Science and Technology, Bolzano, Italy

email: konstantinos.kaffas@unibz.it

[3] Democritus University of Thrace, Department of Civil Engineering, Xanthi, Greece

email: vhrissan@civil.duth.gr

ABSTRACT

Most well-known sediment transport formulas have been derived using specific field or laboratory data, and this hinders their applicability worldwide. Indeed, the success of some of the top-used sediment transport formulas, in certain applications, is comparable only with their failure in others. The adaptation of established formulas to specific data of rivers and streams is a viable solution to this problem, as shown by the authors with respect to the Meyer- Peter and Müller formula (Sidiropoulos et al., 2021). In this study, we modify the widely used Engelund and Hansen (E-H, 1967) sediment transport formula and calibrate it on the basis of measured data from Nestos River in north-eastern Greece.

## 1. Study area

The Greek part of Nestos River basin (Fig. 1, north-eastern Greece) drains an area of approximately 2000 $km^2$ and encompasses the largest cobblestone dam of Greece and the Balkans (Thisavros hydropower dam) with capacity $90 \cdot 10^6$ $m^3$. The greatest part (82%) of the basin is mountainous and is covered mainly by forested and bushy areas. Agricultural and animal farming activities take place near Paranesti, Stavroupoli and Paschalia, the main villages in the area, but in general no intense human activities take place. The mean slope of Nestos River in the basin is 0.35% (Boskidis et al., 2011; Kaffas et al., 2018).

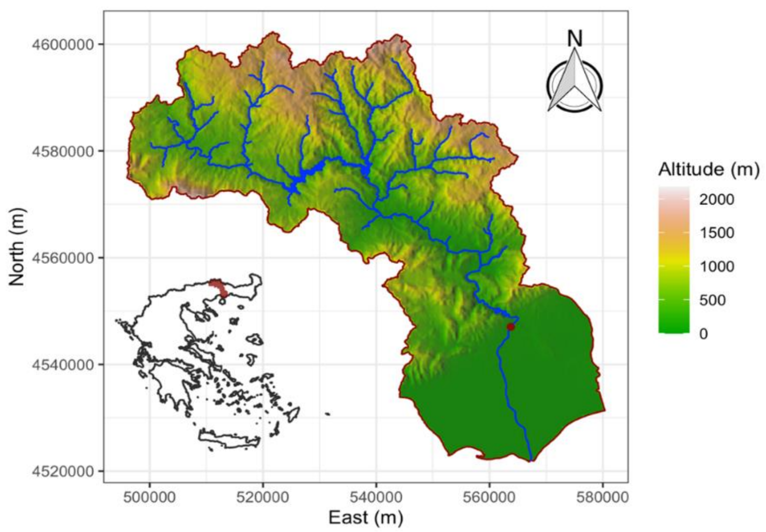


***Fig. 1.*** *Nestos River basin (the red-filled circle marks the location of total load measurements) (Sidiropoulos et al., 2021).*

## 2. Data–Methods–Results

Measurements were conducted at a location between the outlet of Nestos River basin (Toxotes) and the river delta by the Section of Hydraulic Engineering, Department of Civil Engineering, Democritus University of Thrace. A total of 109 datasets of measured streamflow velocity, bed load and suspended load transport rate, median particle diameter, and cross-sectional geometry were used. The total sediment discharge was determined as a sum of the measured bed load and suspended load transport rates.

*2.1. Calculation of total sediment discharge and optimization of E-H formula*

The total sediment discharge was calculated, by means of the Engelund and Hansen (1967) formulas by applying two different forms, the original equations and an optimized one. The measured data consist of: (a) the geometric characteristics of the stream (width, slope); (b) the median diameter of sediment particles; (c) the hydraulic characteristics of the stream (depth, mean flow velocity). In the E-H formulas, the total sediment transport is calculated in terms of unitless values using Eq. (1):

$$f_{EH} \cdot \Phi = \alpha \cdot \theta^{\beta} \tag{1}$$

$$\Phi = \frac{m_F}{\rho_F \sqrt{\rho' \cdot g \cdot d^3}} \tag{2}$$

where $f_{EH}$ – dimensionless friction factor, $\Phi$ – dimensionless total sediment discharge, $\theta$ dimensionless bed shear stress, $\alpha = 0.1$ and $\beta = 5/2$, $m_F$ – total sediment discharge [kg $s^{-1}$ $m^{-1}$], $\rho_F$ – sediment density [kg $m^{-3}$], $\rho'$ – relative submerged specific gravity of sediment (1.65), $g$ – acceleration due to gravity [m $s^{-2}$], $d$ – median particle diameter [m].

Parameters $\alpha$ and $\beta$ in Eq. (1) were obtained by Engelund and Hansen (1967) using a set of data coming from flume experiments.

The dimensionless bed shear stress, $\theta$, is derived as follows:

$$\theta = \frac{\tau_o}{\rho_W \cdot g \cdot \rho' \cdot d} = \frac{h \cdot I}{\rho' \cdot d}, \text{ (as } \tau_o \approx \rho_W \cdot g \cdot h \cdot I) \tag{3}$$

where $\tau_o$ – total bed shear stress [N $m^{-2}$], $h$ – mean flow depth [m], $I$ – bed slope (for uniform flow). In Eq. (3), the flow depth, $h$, replaces the hydraulic radius, when the flow width of the considered cross-section is much greater than $h$.

Finally, the dimensionless friction factor is computed using Eq. (4):

$$f_{EH} = \frac{2 \cdot I}{Fr^2} = \frac{2 \cdot g \cdot h \cdot I}{u_m^2}, \text{ (as } Fr^2 = \frac{u_m^2}{g \cdot h} \text{ for rectangular cross-section)} \tag{4}$$

where $Fr$ – Froude number, $u_m$ – mean flow velocity [m $s^{-1}$].

In this work, $\alpha$ and $\beta$ from Eq. (1) were treated as parameters of adjustment through the minimization of the root mean squared error, between computed and measured values of total sediment discharge, by means of the L-BFGS algorithm (Byrd et al., 1995):

$$\text{RMSE} = \sqrt{\frac{1}{n} \sum_{i=1}^{n} \left( \widehat{m_{F,i}} - m_{F,i} \right)^2} \tag{5}$$

where $n$ – number of data points, $\widehat{m_{F,i}}$ – estimated total sediment discharge by means of the E-H formulas, $m_{F,i}$ – measured total sediment discharge, for $i = 1,2, \dots, n$.

The results indicate that the calculated values from the optimized equation were more accurate by 32%, in terms of the RMSE error metric [0.58 kg $s^{-1}$ $m^{-1}$ to 0.40 kg $s^{-1}$ $m^{-1}$]. The corresponding discrepancy ratios, using as margins the quadruple and the one quarter of the corresponding measured total sediment discharge, are 53% and 67%. The optimal parameters were found to be $\alpha = 0.03$ and $\beta = 1.74$. A source of error lies in the fact that the E-H original formulas were based on experimental data from flumes and not on data from natural streams, as are the data used in this study, hence the need for adjusting the formula. The results are deemed satisfactory and highlight the need for further research regarding optimization techniques for the E-H formula.

***References***

*Boskidis I, Gikas GD, Sylaios G, Tsihrintzis VA (2011) Water quantity and quality assessment of lower Nestos river, Greece, Journal of Environmental Science and Health, Part A, 46(10), 1050-1067*

*Byrd RH, Lu P, Nocedal J, Zhu C (1995) A limited memory algorithm for bound constrained optimization, SIAM Journal on Scientific Computing, 16, 1190-1208*

*Engelund F, Hansen E (1967) A monograph on sediment transport in alluvial streams, Technical University of Denmark, Copenhagen*

*Kaffas K, Hrissanthou V, Sevastas S (2018) Modeling hydromorphological processes in a mountainous basin using a composite mathematical model and ArcSWAT, Catena, 162, 108-129*

*Sidiropoulos E, Vantas K, Hrissanthou V, Papalaskaris T (2021) Extending the Applicability of the Meyer-Peter and Müller Bed Load Transport Formula, Water, 13(20), 2817*

# Sediment yield in the Meuse catchment using a distributed modelling concept

Eva VAN HOFSLOT[1], Hermjan BARNEVELD[1,3], Hélène BOISGONTIER[2], Lieke MELSEN[1]

[1] Wageningen University and Research, Wageningen, The Netherlands
email: eva.vanhofslot@wur.nl
email: hermjan.barneveld@wur.nl
email: lieke.melsen@wur.nl

[2] Deltares, Delft, The Netherlands
email: Helene.Boisgontier@deltares.nl

[3] HKV Consultants, Lelystad, The Netherlands

## 1. Introduction

The annual loads of gravel, sand and silt are important indicators to explain and simulate morphological processes in a river and assess the response to anthropogenic measures and as such crucial for sustainable management of river systems. For the Meuse catchment, the sediment balance is not well known yet. An important question is what the actual loads of alluvial sediment in the river system are. Observed sediment yields are only available for part of the Meuse catchment, requiring an alternative approach to assess erosion, deposition and transport for the complete system: the use of models. However, modelling concepts that are distributed, applicable for short- and long-term simulations, and that distinguish between different types of sediment, are sparse.

WFLOW-SEDIMENT is a new physically based sediment dynamics model, simulating the sediment yield based on the distributed hydrological model WFLOW (Boisgontier and van Gils, 2020). Furthermore, WFLOW-SEDIMENT categorizes the sediment yield into different sediment classes. The model has already been proven useful in similar studies to assess a sediment budget in Europe (Rhine and Seine basins (Boisgontier and van Gils, 2020)) and Japan (Tenryuu basin, Boisgontier and Giri, 2021)). For the Meuse catchment, a calibrated hydrological WFLOW model exists up to the city of Mook in the Netherlands (Fig. 1). The main objective of this study is to construct, calibrate and apply the WFLOW-SEDIMENT model of the Meuse catchment for the last 25 years, and assess the sensitivity of the calculated sediment yield of sub-catchments for parameter settings.

## 2. Study area

The Meuse River is a rain-fed river with a catchment area of around 33,000 km$^2$ in France, Germany, Luxembourg, Belgium and the Netherlands. The catchment can be subdivided into three major geological zones: i) the Lotharingian Meuse, mainly consisting of sedimentary Mesozoic rocks, ii) the Ardennes Meuse, where the river crosses the Paleozoic rock of the Ardennes Massif, and iii) the lower reaches of the Meuse, formed by Cenozoic unconsolidated sedimentary rocks. For the vegetation cover of the catchment upstream of the Belgium/Dutch border, Corine data indicates about 34% to be agricultural land, 20% pasture, 35% forested, and 9% built-up area. In this study, we address the hydrology and sediment yield of the Meuse catchment up to the city of Mook in the Netherlands (Fig. 1).

## 3. Approach

WFLOW-SBM is an open access, physically based, distributed hydrological model. A general advantage of the WFLOW modelling framework is that while calculations are made on a high resolution, computational power is largely reduced by the usage of global parameter approximation (parameter estimations based on transfer functions). Recently, the WFLOW-SEDIMENT module was developed. This module calculates soil erosion, delivery to the stream, and transport and deposition on a catchment scale using the results of the WFLOW-SBM (Boisgontier and van Gils, 2020).

Erosion of sediment in the catchment is governed by rainfall (splash) erosion, overland flow erosion and the sediment transport capacity. For splash erosion, the concepts of EUROSEM (a more physics-based approach using the kinetic energy of the rain drops impacting the soil (Morgan et al., 1998)), or ANSWERS (a more empirical using parameters from the USLE model (Beasley et al., 1991)) can be chosen in WFLOW-SEDIMENT. For overland flow erosion, the concepts of ANSWERS are used, and the overland transport capacity is calculated by the Yalin transport equation which allocates transport capacity to each of the particle classes considered (Foster et al., 1980). The sediment load is calculated on fine temporal and spatial scale (daily, 1x1km grid) for five sediment classes: clay, silt, sand, small and large aggregates.

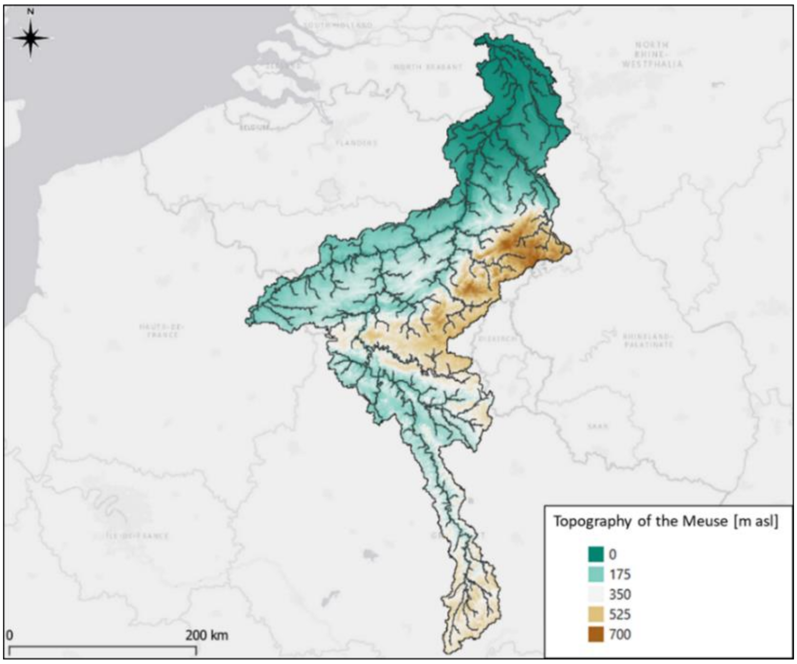


***Fig. 1.*** *Meuse catchment up to the city of Mook in the Netherlands.*

We perform a global sensitivity analysis to identify the governing parameters for calibration. The most sensitive parameters will be calibrated using data sets of observed sediment yield from the tributaries in the Ardennes in Belgium (van Campenhout et al., 2022). The extreme July 2021 flood will serve as a case study, for which gravel transport estimates are available. The performance of the sediment model will also be linked to the performance of the hydrological model. The calibrated model is then applied for the whole Meuse catchment. For the French tributaries, the results are compared to recent estimates of the sediment yield based on USLE. For the Dutch part, no estimates of the sediment yield are available yet. Finally, a local sensitivity analysis at sub-catchment scale is performed to validate the results.

## 4. Results

Preliminary results show that the hydrological model is well calibrated and provides sound input to the sediment module (Boisgontier and van Gils, 2020). WFLOW-SEDIMENT does simulate the sediment yield of the five sediment classes and the first simulations with WFLOW-SEDIMENT provide sediment estimates for the Ardennes which seem in line with observations. Although no observation data are available for France and the Netherlands, the method and model applied provide valuable input to the improvement of the sediment balance for the Meuse River and relative importance of the sub-catchments.

***Acknowledgements***

*This work has been carried out as a MSc-thesis within the framework of a PhD research at Wageningen University & Research as part of the Rivers2Morrow programme (2018-2023). The PhD research is supported by the Dutch Ministry of Infrastructure and Water Management, HKV and Deltares.*

***References***

*Beasley D.B & L.F Huggins. (1991). ANSWERS - Users Manual. Technical report, EPA.*
*Boisgontier, H. & van Gils, J. (2020). Physics-based basin-scale modelling of water quantity and sediment dynamics using WFLOW.*
*Boisgontier, H. & Giri, S. (2021). Evaluation of applicability and environmental analysis models to wide area, Component A: linking catchment erosion with reservoir sedimentation and land-use management. Deltares report 11205910-002-ZWS-0002, p57.*
*Foster, G. R., Lane, L. J., Nowlin, J. D., Laflen, J. M., & Young, R. A. (1980). A model to estimate sediment yield from field-sized areas: development of model.*
*Morgan Q., J.N Smith, R.E Govers, G Poesen, J.W.A Auerswald, K Chisci, G Torri, D Styczen, and M E Folly. (1998). The European soil erosion model (EUROSEM): documentation and user guide. Technical report.*
*Van Campenhout, J., Petit, F., Peeters, A., & Houbrechts, G. (2022). Estimation of the area-specific suspended sediment yield from discrete samples in different regions of Belgium. Journal of Soils and Sediments, 22(2), 704-729.*

# Fine sediment deposition in a restored river reach – case study Alpine Rhine

Benjamin HOHERMUTH[1], Andris WYSS[2], Daniel CONDE[3], Francesco CAPONI[4], Florian HINKELAMMERT-ZENS[5], David F. VETSCH[6]

[1,2,3,4,5,6] Laboratory of Hydraulics, Hydrology and Glaciology, ETH Zurich, Switzerland
email: hohermuth@vaw.baug.ethz.ch (corresponding author)

ABSTRACT

Suspended sediment transport can have significant effects on river morphology and thus needs to be considered in river restoration and flood protection projects. Herein, we present a case study where a 2D depth-averaged numerical model, including a turbulence model and shear stress partitioning was used to simulate suspended sediment deposition in the Alpine Rhine. The calibrated model was used to estimate changes in sediment transport dynamics for a significant river widening which is currently planned as part of a restoration project.

## 1. Introduction

Suspended sediment load often constitutes the main part of the overall sediment load in a river and can have significant effects on river morphology. In the case of the Alpine Rhine, i.e., the part of the Rhine River upstream of Lake Constance, the mean annual suspended sediment load is 1.8 $10^6$ t. The main part of the fine sediment is deposited at the river mouth in Lake Constance. However, part of the suspended load also deposits on the floodplains, requiring frequent removal to maintain flow conveyance. A major river restoration project is currently planned for the Alpine Rhine to improve river ecology and increase flood safety considering an updated hydrology. Therefore, the width of the main channel will be increased from ca. 80 m today to up to 380 m in the future. This will have a significant effect on the remaining floodplains and the implications on suspended sediment transport were studied herein. The main objective was to determine the change of suspended sediment deposition on the floodplains and to check its effect on flood safety.

## 2. Numerical model

The simulations were performed with the BASEMENT software, which is developed by VAW, ETH Zurich and is freely available (https://basement.ethz.ch). Herein, the version 3.2 was used. The main features are described below, for more details see Vetsch et al. (2020) and Vanzo et al. (2021).

The 2D shallow-water equations were extended with a depth-averaged eddy viscosity model to account for the effect of turbulent shear stresses. The kinematic eddy viscosity was computed with a depth-averaged $k$-$\varepsilon$ turbulence model (Cea et al., 2007). A logarithmic flow resistance law was used as closure relation for the shallow-water equations. To account for macro roughness (e.g., riprap bank protection), the total shear stress was partitioned into skin friction and form-induced shear stress based on the user specified equivalent sand roughness values for total ($k_{s,t}$) and grain (i.e., skin) roughness. The effect of vegetation growth was considered based on the approach of Caponi et al. (2021).

The sediment transport model comprises a bed load and a suspended load transport model. The former considers lateral slope effect (Talmon et al. 1995), curvature effect (Engelund, 1974), and gravitational slope collapse (Vetsch et al. 2020). For the present case, the bedload transport equation of Wong and Parker (2006) was applied. As the focus was on suspended load, the bedload models were used with their default coefficients. Suspended sediment transport was modelled with a depth-averaged advection diffusion equation. The turbulence model allowed expressing the mass diffusivity as a function of the turbulent kinematic viscosity through the Schmidt number. Entrainment and deposition were expressed with a source term $S = w(C_e\text{-}C_d)$, with $w$ = settling velocity after Van Rijn (1984), $C_e$ = equilibrium concentration (Van Rijn, 1984), $C_d$ = deposition concentration following the shear stress-based formulation of Xu (1998).

The sediment transport was simulated on a fixed initial bed and without bedload transport of the coarse gravel fraction. The morphology for the widened state was taken from physical model tests and the boundary conditions originated from a gauging station downstream of the model perimeter. The $k_{s,t}$ values were calibrated to match the rating curve of the gauging station. A uniform grain size ($d$) was used in the model with 50 μm $\leq d \leq$ 150 μm determined from volume samples.

### 3. Results and Conclusion

In a preliminary step, the mesh sensitivity was studied, revealing that cell areas of ~2 $m^2$ were needed to adequately resolve the shear zone induced by the inner levees. Then the model was calibrated for the current situation with a compound channel using photographs and satellite imagery of a 10-year flood in 2016. The existing geometry is challenging as it includes inner and outer levees as well as significant roughness variations within a cross-section. Nevertheless, the calibrated model was able to qualitatively reproduce the relevant deposition processes. The simulated deposition heights on the floodplains were in rough agreement with available data. A more detailed calibration was limited by available data quality. A sensitivity analysis revealed that the grain size diameter, the critical dimensionless shear stress for entrainment, and the skin roughness coefficient were the most sensitive parameters controlling the deposition pattern. The Schmidt number was insensitive, indicating that advective processes were dominant for this test case.

The calibrated model predicted a significant increase in suspended sediment deposition for the planned widened state (Fig.1). This was mainly due to the lower flow depths and smaller shear stresses which is consistent with the model formulation. A large part of the depositions occurred on the floodplains as well as in groin fields and local depressions. To conclude, the model was able to realistically reproduce suspended sediment deposition in a complex river geometry with variable roughness. However, some model parameters require calibration and their general validity as well as effects of model limitation are subject to further studies.

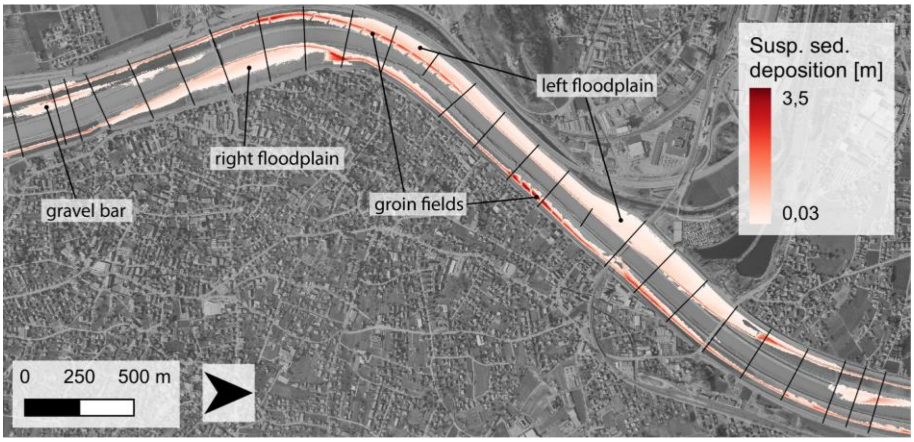


Fig. 1. Suspended sediment deposition after the simulated 2016 flood event (return period ≈ 10 a) for the planned widening. Background: orthoimage of current state (©swisstopo).

The authors thank the International Rhine Regulation (Internationale Rheinregulierung, IRR) for mandating this study to VAW, ETH Zurich and providing data for model calibration.

**References**

Cea L, Puertas J, Vázquez-Cendón ME (2007) Depth Averaged Modelling of Turbulent Shallow Water Flow with Wet-Dry Fronts. Arch. Computat. Methods Eng. 14: 303–341.

Engelund F (1974) Flow and bed topography in channel bends. Journal of the Hydraulics Division ASCE, 100(11): 1631–1648.

Caponi, F., Vetsch, D.F., Siviglia, A. A model study of the combined effect of above and below ground plant traits on the ecomorphodynamics of gravel bars. Sci Rep 10, 17062 (2020). https://doi.org/10.1038/s41598-020-74106-9

Talmon A, Struiksma N, van Mierlo M (1995). Laboratory measurements of the direction of sediment transport on transverse alluvial-bed slopes. J. Hydraul. Res., 33(4): 495–517.

van Rijn LC (1984). Sediment Transport, Part II: Suspended Load Transport. J. Hydraul. Eng., ASCE, 110(11): 1613–1641.

Vanzo D, Peter S, Vonwiller L, Bürgler M, Weberndorfer M, Siviglia A, Conde D, Vetsch DF (2021) BASEMENT v3: A modular freeware for river process modelling over multiple computational backends, Environ. Model. Softw., 143, 105102.

Vetsch D, Siviglia A, Burgler M, Caponi F, Ehrbar D, Facchini M, Faeh R, Farshi D, Gerber M, Gerke E, Kammerer S, Koch A, Mueller R, Peter S, Rousselot P, Vanzo D, Veprek R, Volz C, Vonwiller L, Weberndorfer M (2020) System Manuals of BASEMENT, Version 2.8.1 Laboratory of Hydraulics, Glaciology and Hydrology (VAW). ETH Zurich. http://www.basement.ethz.ch.

Wong M, Parker G (2006) Reanalysis and correction of bed-load relation of Meyer-Peter and Müller using their own database. J. Hydraul. Eng., 132(11): 1159–1168.

Xu Y (1998). Numerical Modeling of Suspended Sediment Transport in Rivers. Mitteilung 98, Institut für Wasserbau, Universität Stuttgart.

# A small investigation of the effects of cylinder diameter on longitudinal dispersion coefficient

Fred SONNENWALD[1], Angus MARSHALL[1], Dzafran BIN RASHIDI[1], Ian GUYMER[1]

[1] The University of Sheffield, United Kingdom
email: f.sonnenwald@sheffield.ac.uk
email: i.guymer@sheffield.ac.uk

ABSTRACT

Measurements of dispersion coefficient within vegetation are essential for evaluating engineered vegetated treatment systems. This study presents a comparison of laboratory measurements of dispersion coefficient from three different cylinder arrays representing vegetation, each with different cylinder diameters.

## 1. Introduction

While many sustainable treatment systems such as ponds and wetlands contain vegetation, the description in literature of the fundamental process of dispersion within vegetation, which is necessary for predicting water quality and hence treatment within these systems (Sonnenwald et al., 2017). Dispersion is the combined effects of turbulent diffusion, differential shear, flow path tortuosity, etc., acting to spread a pollutant. This is typically described by the Advection-Diffusion Equation (ADE), of which the routing solution to the one-dimensional longitudinal ADE is:

$$c(x_2,t) = \int_{-\infty}^{\infty} \frac{c(x_1,\tau)U}{\sqrt{4\pi D_x \bar{t}}} \exp\left[-\frac{U^2(\bar{t}-t+\tau)^2}{4D_x\bar{t}}\right] \mathrm{d}\tau \tag{1}$$

where $c$ is the concentration at $x_1$ and $x_2$ the upstream and downstream measurement locations, $t$ is time, $U$ is velocity, $D_x$ is longitudinal dispersion coefficient, $\bar{t} = (x_2 - x_1)/U$ is travel time, and $\tau$ is a dummy variable of integration (Fischer et al., 1979).

The difficulty in describing dispersion in vegetation is due to the complex variation of vegetation characteristics. Vegetation may be rigid, flexible, submerged, emergent, leafy, woody, etc., all of which determine how it affects flow around it and vice versa (O'Hare, 2015; Nepf 2012). One particular complexity of real vegetation is its variation in stem diameter. Stovin et al., (2022) investigated dispersion in arrays with uniform and varying stem diameter and found no practical difference between the two. This study describes a small investigation into the effects of cylinder diameter on longitudinal dispersion to provide additional confidence in this result.

## 2. Methodology

Sonnenwald et al. (2019) previously presented longitudinal dispersion coefficient in a random array of 8 mm diameter cylinders (solid volume fraction $\phi$ = 0.027). Complementary measurements of dispersion coefficient have been made in a similar 300 mm wide tilting Gunt flume for two additional cylinder configurations, one consisting of 4 mm diameter semi-rigid cylinders ($\phi$ = 0.007) and the second consisting of a 4, 8, 12, 15, and 20 mm cylinder diameter distribution ($\phi$ = 0.046) with a mean of diameter 9.9 mm, as presented in Stovin et al. (2022). These two new vegetation configurations are shown in Fig. 1.

a) 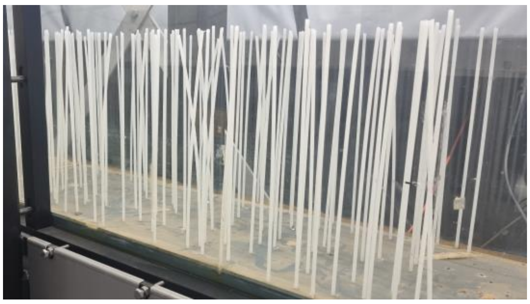 b) 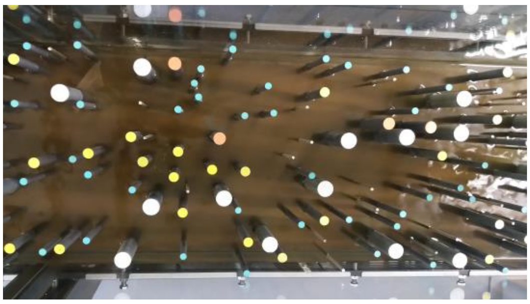

**Fig. 1.** Photographs of the a) semi-rigid 4 mm and b) variable stem diameter cylinder arrays.

Rhodamine WT dye was injected at the flume inlet and measured at multiple downstream locations using Turner Designs Cyclops-7 fluorometers placed at mid-channel width and mid-flow depth. Flow depths were uniform and at least 15 cm. The recorded concentration data were pre-processed with a linear background subtraction and mass-balance was assumed as implied by Eq. (1). Least-squares optimization of Eq. (1) was carried out then to find the longitudinal dispersion coefficient and mean velocity between each pair of adjacent fluorometers. The measurements at each reach and flow rate were then averaged.

## 3. Results

Initial results of this study are presented here. Although the semi-rigid vegetation was expected to bend in the direction of flow, it remained largely stationary with minor oscillations. It is therefore treated as rigid vegetation for convenience. Fig. 2 plots the optimized dispersion coefficients normalized by stem diameter and stem spacing.

Figure 2a shows little variation with velocity $Re_d > 100$, agreeing with Sonnenwald et al. (2019). When normalized by diameter, the 4 and 8 mm vegetation show similar levels of dispersion. The dispersion observed for these two cases is higher than the variable diameter vegetation, which is consistent with the increased variability in longitudinal dispersion observed by Stovin et al. (2022) at $\phi \lesssim 0.04$. Dispersion within the variable diameter vegetation shows remarkably good agreement with the predictor fit by Stovin et al. (2022) to their results.

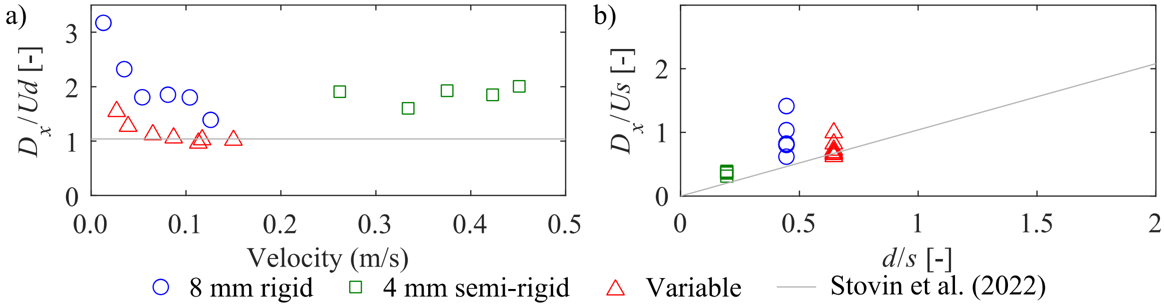


**Fig. 2.** Optimized longitudinal dispersion coefficient Dx a) normalized by stem diameter and b) normalized by mean nearest neighbour stem-spacing $s$, estimated from $\phi$ and $d$ as described by Sonnenwald et al. (2019), compared to the Stovin et al. (2022) prediction of $D_x/Us = 1.04d/s$. Error is of the order of the size of the symbols.

Figure 2b plots dispersion coefficient as a function of $d/s$, another measure of vegetation density similar to solid volume fraction. (As a quick estimate, $d/s \approx 15\phi$.) In this context, the differences due to diameter are broadly smaller than those possible to be due to density, and thus these results provide some evidence in agreement with the conclusions of Stovin et al. (2022).

The authors would like to draw the reader's attention to two additional aspects of Fig. 2b. The use of $d/s$ to represent vegetation density, as suggested by Stovin et al. (2022) and Tanino & Nepf (2008) for longitudinal and transverse dispersion respectively, is a more robust and appropriate scaling than $\phi$ for dispersion within cylinder arrays representing vegetation as it also considers the arrangement of the cylinders. Second, although real vegetation often occurs with densities of $d/s > 2$, the authors are aware of very few experimental results describing longitudinal dispersion coefficient in this region. Further studies within dense vegetation are desirable.

**Acknowledgements**

This work was supported in part by the EPSRC (Grant Nos. EP/K024442/1, EP/K025589/1, and EP/P012027/1). The authors thank Zoe Ball, Ian Bayliss, Leonardo Corredor-Garcia, and Joseph Milner who helped conduct laboratory work.

**References**

Fischer HB, List JE, Koh CR, Imberger J, Brooks NH (1979) Mixing in inland and coastal waters, Amsterdam.
Nepf HM (2012) Flow and transport in regions with aquatic vegetation, Annual review of fluid mechanics, 44, 123-142.
O'Hare MT (2015) Aquatic vegetation–a primer for hydrodynamic specialists, Journal of Hydraulic Research, 53(6), 687-698.
Sonnenwald F, Hart JR, West P, Stovin VR, Guymer I (2017) Transverse and longitudinal mixing in real emergent vegetation at low velocities, Water Resources Research, 53(1), 961-978.
Sonnenwald F, Stovin V, Guymer I (2019) A stem spacing-based non-dimensional model for predicting longitudinal dispersion in low-density emergent vegetation, Acta Geophysica, 67(3), 943-949.
Stovin VR, Sonnenwald F, Golzar M, Guymer I (2022) The impact of cylinder diameter distribution on longitudinal and transverse dispersion within random cylinder arrays, Water Resources Research, e2021WR030396.
Tanino Y, Nepf HM (2008) Lateral dispersion in random cylinder arrays at high Reynolds number, Journal of Fluid Mechanics, 600, 339-371.

# Mass and Momentum Transfer between Interacting Cylinder Wakes via Velocity Statistics

J. Leonardo CORREDOR-GARCIA[1], Virginia STOVIN[1], Ian GUYMER[1]

[1] Department of Civil and Structural Engineering, The University of Sheffield, UK
email: jlcorredorgarcia1@sheffield.ac.uk
email: v.stovin@sheffield.ac.uk
email: i.guymer@sheffield.ac.uk

ABSTRACT

This research presents the results of an experimental study of velocity statistics along the wakes of 2 cylinders in a sparse array, to simulate the stem-scale processes of vegetated flows, and their impact on mass and momentum transfer. The experimental plan was devised to revise the physical assumptions, regarding vegetated flow fields, that underpin current models for vegetated dispersion. Single- and multi-point velocity statistics were measured to study the turbulence structure of the flow and explore the existence and physics of coherent structures, which were found to be the features governing early-stage dispersion. The results of this study show that assumptions of linearity used to model the effects of obstructions on flow fields should be revised. Further, effects such as dissipation, shear and vorticity diffusion should be considered when using empirical assumptions to use Lagrangian-based theories of diffusion from Eulerian results.

## 1. Introduction and Background

The preliminary results presented in Corredor-Garcia et al. (2020) showed how empirical estimations of dispersion, and the lateral extent of secondary wakes can be obtained from Eulerian 2-point statistics, using Taylor's Theory of Diffusion and relevant empirical assumptions (Taylor, 1935a; 1935b). This study expands from this particular case to study the wider implications of using Eulerian Statistics to compute Lagrangian quantities, the analytical limitations and necessary conditions to undertake such transformation (Lumley, 1962; Philip, 1967), and the consequences on the mean velocity field and turbulence structure.

Mass and momentum transfer within cylinder arrays are governed by the interactions between cylinder wakes. This has effects on turbulence through drag, coherence structures, dissipation and vortex diffusion (i.e. transition to three-dimensionality); and on the mean velocity field. Previous studies have evaluated interactions at the near wake level, particularly regarding changes in shedding frequency, flow resistance and vortex size (Sumner, 2010). This paper is the first attempt at extending the study of interactions between array elements at the far wake scale, which are the regions responsible for most of the mass and momentum transfer. Results from this investigation are useful to evaluate current assumptions for vegetated dispersion models, particularly linearity. Further, a detailed analysis of far-wake interactions will provide the necessary physical information to successfully apply Taylor's Theory of Diffusion to develop process-based modes for dispersion.

## 2. Methodology

To characterise the velocity information along representative sections between two cylinders, ADV measurements were obtained along axes within the test section shown in Fig. 1a, located in the central section of a 300 mm wide flume, along the wakes of two adjacent 20 mm-diameter cylinders. Mean velocities, turbulence and single-point correlation functions, $R_{yy}(\tau)$, were measured using a mobile, down-looking probe to avoid interferences with each measurement volume. Two-point correlations, $R_{yy}(\xi)$, were obtained by locating a reference, fixed, side-looking probe at points B0 and A1' (Fig. 1b), to avoid physical interference.

The location of the reference points was defined to focus on the secondary wake, i.e. the onset of vortex shedding. To analyse the behaviour of the wakes, and their interactions at different shedding regimes, two flow rates were tested, defined by the cylinder Reynolds numbers $Re_d = 250$ and $Re_d = 1100$. All points defining the axes in Fig. 1a have a separation of 5 mm.

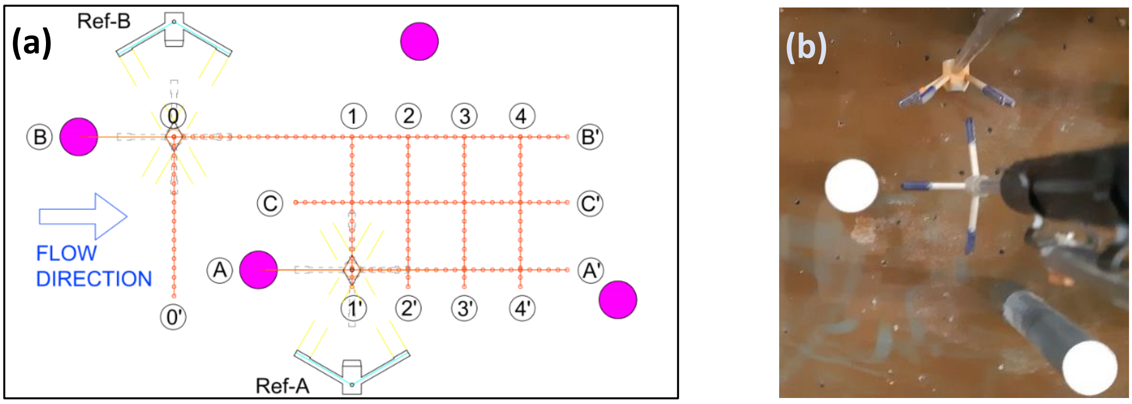


**Fig. 1. (a)** Detailed scheme of the test section, measurement axes and location of reference probes. **(b)** Physical configuration of the ADV probes for simultaneous measurements of velocities.

## 3. Results and Discussion

Mean velocity measurements over the measurement sections show that in random arrays, wakes tend to deform, create preferential pathways and enhance dissipation due to shear. Further, turbulence measurements along the same points indicate that vegetated flows are predominantly heterogeneous, anisotropic and strongly dissipative.

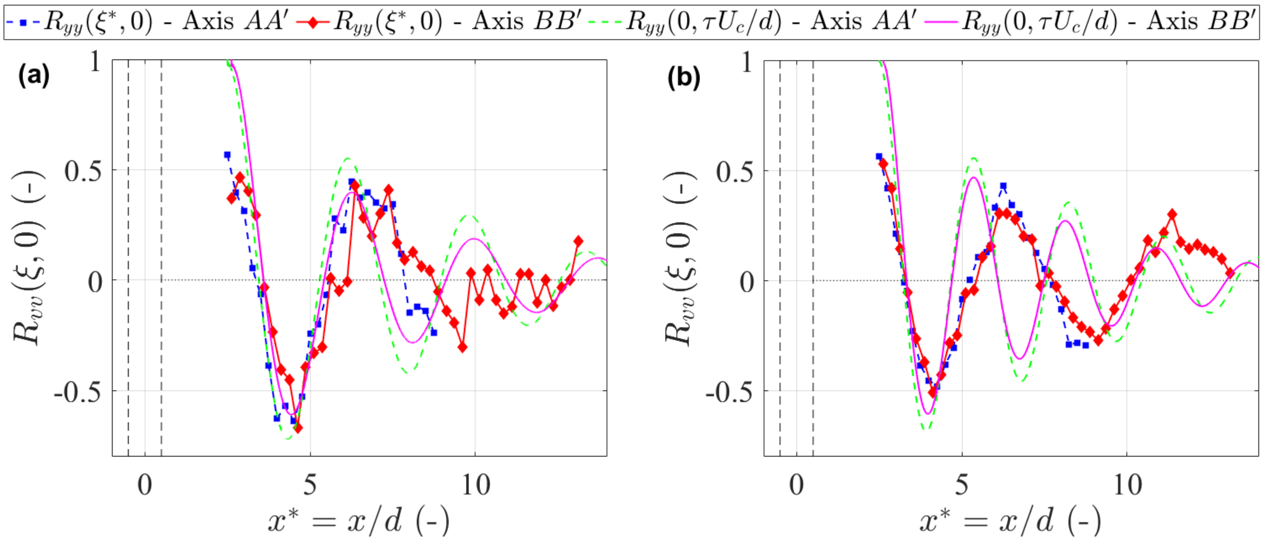


**Fig. 2.** Comparison between time- and space-dependent correlation functions for transverse velocities, **(a)** $Re_d = 250$, **(b)** $Re_d = 1100$.

In early stages of diffusion (time scales shorter than the one needed for particles to move independently of the local turbulence structure), coherent motions from vortex shedding dominate mass transfer along and between secondary wakes, through phenomena such as shear, differential pressures and vorticity dissipation. The latter is evident from the comparison between one- and two-point statistics shown in Fig. 2. The decaying envelope and decrease in the periodicity of $R_{yy}(\xi)$, compared to $R_{yy}(\tau)$, are evidence of these dissipative processes.

Finally, these results show a tendency for vegetated flow fields, and turbulence structures, to be the result of non-linear interactions between the perturbations of vegetation elements. The effects of coherent motions, as illustrated by multi-point correlation functions, are crucial in the understanding of early-stage diffusion, the time scales necessary to achieve Fickian dispersion, and the characteristic length and velocity scales to describe mixing in this regime.

### References

Corredor-Garcia JL, Stovin V, Guymer I, (2020), Preliminary Study on Diffusion of Cylinder Wakes and Their Interactions, Proceedings of the 6th IAHR Europe Congress, 35-36.
Philip JR, (1967), Relation between Eulerian and Lagrangian Statistics, Physics of Fluids, 10, S69-S71.
Lumley JL, (1962), The Mathematical Nature of the Problem of Relating Lagrangian and Eulerian Statistical Functions in Turbulence, in *Mecanique de La Turbulence*, Ed. Du Centre Nat. de la Rech. Sci. Paris, 17-26
Sumner D, (2010) Two circular cylinders in cross-flow: A review, Journal of Fluids and Structures, 26(1), 849-899.
Taylor G, (1935a) Statistical Theory of Turbulence, Proceedings of the Royal Society of London, 151(873), 421-444.
Taylor G, (1935b) Statistical Theory of Turbulence – IV Diffusion in a Turbulent Air Stream, Proceedings of the Royal Society of London, 151(873), 465-478.

# Phosphate adsorption and diffusion model into iron-coated sand grains

Victoria BARCALA[1], Leonard OSTÉ[2], and Thilo BEHRENDS[3]

[1,2] Deltares, The Netherlands
email: victoria.barcalapaolillo@deltares.nl
email: leonard.oste@deltares.nl

[3] Utrecht University, The Netherlands
email: t.behrends@uu.nl

ABSTRACT

Iron-coated sand (ICS) is an iron-based phosphate sorbing material used in filters to remove phosphate from natural and agricultural waters and prevent eutrophication. The objectives of this research were to propose a mathematical and conceptual model for the kinetics of the phosphate diffusion to the inside of the ICS grains. We used columns to calibrate and validate a non-equilibrium adsorption model that fitted the advection-dispersion equation and the mass balance in the solid phase. The interpretation of the model results was supported by scanning electron microscopy images and elemental maps. The adsorption of phosphate by ICS was divided into a fast and a slow process. The fast adsorption described the attraction into the surface of the ICS grains and the slow adsorption described the diffusion of phosphate inside the nanopores of the iron coating. The fast adsorption is in equilibrium, but the slow adsorption is not because it is limited by the phosphorus diffusion inside the iron-coating. Most of the adsorption capacity of the ICS relied on the sorption sites inside the iron-coating, 96.1%. These findings contribute to the design and operation of ICS filters.

## 1. Introduction

Iron-coated sand (ICS) is a by-product of the drinking water industry (Van Beek et al., 2016, 2020). Because ICS is largely available at low costs it has been used as a phosphate sorbing material in full-scale agricultural phosphorus retention measures (Groenenberg et al., 2013; Lambert et al., 2020; Vandermoere et al., 2018). What remains unknown are the adsorption mechanisms, in particular the kinetics of the phosphate diffusion inside the ICS grains (Chardon et al., 2012; Lambert et al., 2020).This study aims to develop a (i) conceptual model of the adsorption mechanisms of phosphorus on ICS; and (ii) a process-based mathematical model to describe the adsorption of phosphorus on ICS.

## 2. Methods

The adsorption column experiment run for 146 days. The inflow water was demineralized water sparkled with 1.60 mg/L ± 0.05 mg/L, and NaCl 0.10 M, giving a 0.10 ionic strength. The pH was 6.80 ± 0.05. The columns were cylinders of 0.308 m height and 0.043 m internal diameter. The reactive core of the columns contained 30 g of ICS and 300 g of quartz sand. The starting porewater velocity was 4.92 cm/h.

We used the column experiments to fit a model of public domain that solves analytically the transport of a solute in a porous media (Simunek et al., 1999; Van Genuchten et al., 2012). The phosphorus adsorption in the columns was modeled using the advection-dispersion transport equation that combines the continuity equation and the equation for the solute flux Eq. (1). There is then a solid fraction of adsorption sites in equilibrium ($f$) and another fraction of sites with non-equilibrium adsorption ($1 - f$). If the system is in equilibrium $f$ is 1 and $s = kc$. If the system is not in equilibrium, the mass balance in the solid phase is included, Eq. (2). When the system is not in equilibrium adsorption does not happen at the same rate in all parts of the porous material either for chemical or physical reasons.

$$\left(1 + \frac{\rho f k}{\theta}\right)\frac{\partial c}{\partial t} = D\frac{\partial^2 c}{\partial x^2} - \frac{v \partial c}{\partial x} - \frac{\rho \alpha}{\theta}(k(1-f)c - s) \tag{1}$$

$$\frac{\partial s}{\partial t} = \alpha(k(1-f)c - s) \tag{2}$$

Where $\rho$ – bulk ICS density [g/L], $\theta$ – porosity, $k$ – equilibrium constant [g/L], c – concentration [mg/L], $t$ – time [h], D – dispersion coefficient [cm$^2$/h], $x$ – longitudinal coordinate [cm], v – pore-water velocity [cm/h], $\alpha$ - mass transfer coefficient [1/h], s – concentration in the solid [mg/g]

The ICS grains were observed before and after adsorption with scanning electron microscopy coupled with energy dispersive x-ray detection (Zeiss EVO 15 SEM, Bruker XFlash EDS)

## 3. Results

Figure 1 shows the equilibrium and non-equilibrium model fitting of the column and the measured data for the first 40 days. The non-equilibrium model adjusted better to the measured values, with a correlation coefficient of 0.988. The phosphorus diffusion inside the ICS grain is shown in Fig.2.

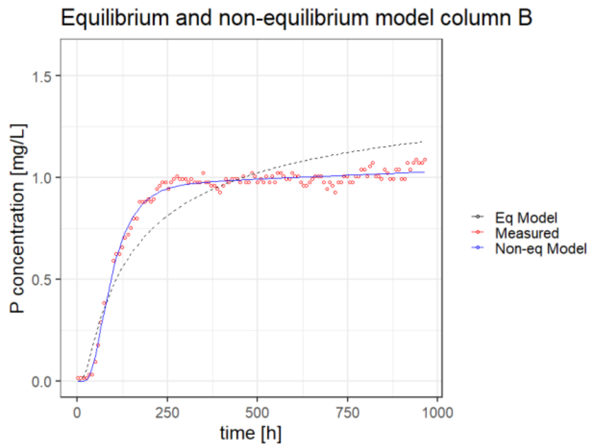


**Fig. 1** Equilibrium and non-equilibrium model fitting.

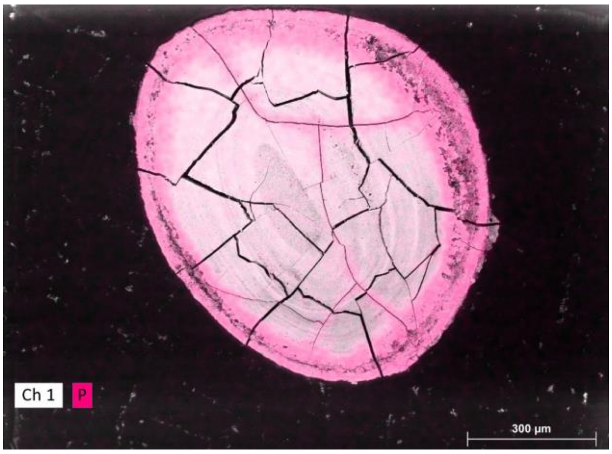


**Fig. 2** Phosphorus diffusion in ICS grain SEM-EDS elemental map

## 4. Conclusions

The adsorption of phosphate by ICS was divided into two processes. A fast equilibrium adsorption where phosphate was attracted by the surface of the ICS grains and a slow adsorption that described the diffusion of phosphate through the nanopores of the coating. Under the flow conditions studied, fast adsorption accounted for just 3.9% of the total adsorption sites. The mass transfer rate of the slows down as the adsorption sites were occupied. The linear distribution coefficient was 3.45 L/g, and the maximum adsorbed concentration in the solid was 5.83 mg/g, for an ICS with 0.127 g/g of iron. These results allow to quantify the long-term efficiency of phosphorus adsorption on ICS filters.

**Acknowledgements**

This study was funded by P-TRAP (EU Grant No. 813438, Marie Skłodowska- Curie Actions). We would like to thank Arcadis and Aquaminerals for the ICS. We would like to acknowledge Rien van Genuchten and Alraune Zech for their support with Stanmod.

**References**

Chardon, W. J., Groenenberg, J. E., Temminghoff, E. J. M., & Koopmans, G. F. (2012). Use of Reactive Materials to Bind Phosphorus. *Journal of Environmental Quality*, *41*(3), 636–646. https://doi.org/10.2134/jeq2011.0055

Groenenberg, J. E., Chardon, W. J., & Koopmans, G. F. (2013). Reducing Phosphorus Loading of Surface Water Using Iron-Coated Sand. *Journal of Environmental Quality*, *42*(1), 250–259. https://doi.org/10.2134/jeq2012.0344

Lambert, N., Van Aken, P., Van den Broeck, R., & Dewil, R. (2020). Adsorption of phosphate on iron-coated sand granules as a robust end-of-pipe purification strategy in the horticulture sector. *Chemosphere*, *267*, 129276. https://doi.org/10.1016/j.chemosphere.2020.129276

Simunek, J., van Genuchten, M. T., Sejna, M., Toride, N., & Leij, F. J. (1999). The STANMOD Computer Software for Evaluating Solute Transport in Porous Media Using Analytical Solutions of Convection-Dispersion Equation. *Agriculture*, *November*, 20.

Van Beek, C. G. E. M., Dusseldorp, J., Joris, K., Huysman, K., Leijssen, H., Schoonenberg Kegel, F., De Vet, W. W. J. M., Van De Wetering, S., & Hofs, B. (2016). Contributions of homogeneous, heterogeneous and biological iron(II) oxidation in aeration and rapid sand filtration (RSF) in field sites. *Journal of Water Supply: Research and Technology - AQUA*, *65*(3), 195–207. https://doi.org/10.2166/aqua.2015.059

Van Beek, C. G. E. M., Hofman-Caris, C. H. M., & Zweere, G. J. (2020). Drinking water treatment and chemical well clogging by iron(II) oxidation and hydrous ferric oxide (HFO) precipitation. *Journal of Water Supply: Research and Technology - AQUA*, *69*(5), 427–437. https://doi.org/10.2166/aqua.2020.140

Van Genuchten, M. ., Simunek, J., Leij, F. J., & Toride, N. (2012). Stanmod: model use, calibration and validation. *American Society of Agricultural and Biological Engineers*, *55*(4), 1353–1366.

Vandermoere, S., Ralaizafisoloarivony, N. A., Van Ranst, E., & De Neve, S. (2018). Reducing phosphorus (P) losses from drained agricultural fields with iron coated sand (- glauconite) filters. *Water Research*, *141*, 329–339. https://doi.org/10.1016/j.watres.2018.05.022

# Quantifying the Spatial Variation in On-/Off-shore Mixing in the Surf Zone

Inez PLUGGE PORTER[1] and Ian GUYMER[1]

[1] The University of Sheffield, United Kingdom
email: ispluggeporter1@sheffield.ac.uk
email: i.guymer@sheffield.ac.uk

ABSTRACT

Solute mixing in the nearshore or surf zone is the result of several combined processes, from fundamental turbulence, through wave hydrodynamics and boundary effects, to the high energy dissipation impact of breaking waves. These processes occur across different spatial and temporal scales and vary spatially. This abstract presents preliminary results from an on-going study to quantify the spatial variation of the on-/off-shore depth averaged mixing coefficient. The programme of work evaluates mixing coefficients by comparing predictions from different numerical models to previously recorded laboratory tracer data. The data consists of multiple constant injections of tracer for orthogonal waves for a range of wave periods and wave heights.

## 1. Introduction

Increasing levels of pollutants are discharged into coastal zones with a detrimental effect on the quality of the coastal environment (Pearson *et al*., 2002). Pollutant loads in the nearshore originate primarily from sewer outfalls and overland surface runoff, containing pathogens, bacteria, heavy metals. Bathing beaches are also polluted by sun creams and skin products. These pollutants pose a risk to public health and coastal biodiversity, causing economic and environmental damage. It has been noted that around 10% of beaches in the UK do not pass the standards of the Bathing Water Directive, often with water samples containing high levels of faecal indicator organisms (Abolfathi and Pearson, 2014). It is critical to understand the spread of these pollutants to regulate and protect the coast and human health.

## 2. Methodology

Experimental studies (see Acknowledgements) were undertaken in the shallow water basin at DHI with dimensions of 18 m x 8 m. An absorbing piston-type wave maker was utilized for generating the waves and the longshore currents were superimposed. Detailed fluorometric measurements were undertaken on the sloping 1:20 plain beach, with an offshore water depth of 0.7 m. Tests were performed with similar offshore wave height (0.12 m) and varying wave periods (1.2~2.9 s) to cover the range of offshore wave steepness between 2~5 %.

## 3. Preliminary Results

Mixing in the nearshore environment has previously been modelled using a mixing coefficient to represent the combined effects of dispersion and diffusion (Pearson *et al*, 2009). Mixing models of particular interest to this study are:

1. Fischer *et al* (1979) gives a constant mixing model, where the mixing coefficient, depth and velocity are assumed spatially uniform across the channel. Winckler *et al*. (2013) have used this to model mixing in coastal waters.
2. Kay (1987) proposed an equation for mixing in a uniformly sloping beach which assumed both velocity and mixing varied with depth and are therefore functions of distance offshore.
3. West *et al.* (2020) developed a finite difference model (FDM) which allowed for the spatial variability of depth, velocity and mixing coefficient in the transverse direction. This FDM has been successfully used to model solute mixing in partially vegetated open channels, but is yet to be applied to coastal waters.

Results presented, Fig. 1, compare the recorded solute concentration distributions obtained from continuous injections, made at 2, 3 & 5 m offshore, for 1.2 s period waves, to the best fit predictions assuming a spatially constant on-offshore mixing coefficient. This results in a mixing coefficient of 0.0112 $m^2/s$.

Allowing a spatial variability in the mixing coefficients and optimizing the fit to data recorded from each individual injection produces significant improvements in the fit to the recorded data. These results are illustrated in Fig. 2 where the optimized transverse mixing coefficients are 0.0227, 0.0159 and 0.00057 $m^2/s$ for injections at 2, 3 and 5 m respectively. This confirms the significant reduction of the mixing coefficient at the furthest offshore location, and the need for a cross-shore spatially variable mixing coefficient. Results comparing the three different mixing models will be presented at the conference.

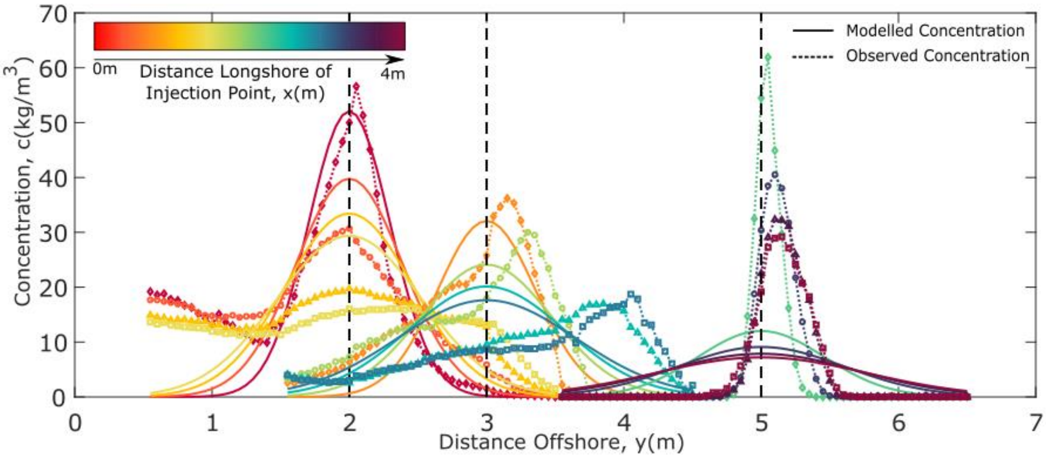


**Fig. 1.** Recorded tracer data for wave period, T, 1.2 s from injections at 2, 3 & 5 m offshore compared to predicted distributions assuming a spatially uniform mixing coefficient

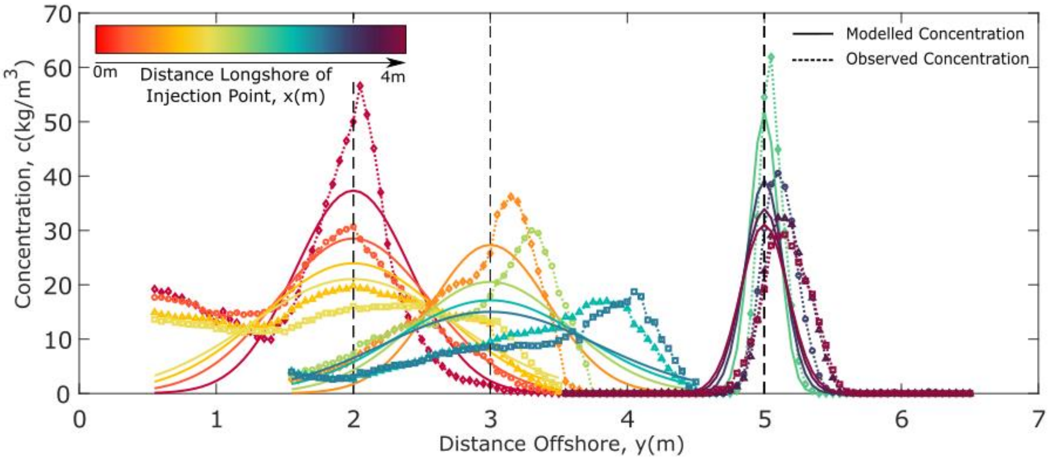


**Fig. 2.** Recorded tracer data for wave period, T, 1.2 s from injections at 2, 3 & 5 m offshore compared to predicted distributions assuming a different mixing coefficient for each injection location.

## 4. Acknowledgements

The laboratory results used in this paper were collected under UK EPSRC grant GR/T24081. The model tests were conducted in the Shallow Water Basin at DHI Water & Environment under contract HRPI-CT-2002-00190 of the European Community – Access to Research Infrastructure action of Improving Human Potential Programme. The support from both EPSRC and the EC is gratefully appreciated.

### References

Abolfathi, S. and Pearson, J. M. (2014) „Solute dispersion in the nearshore due to oblique waves. 34th Conf. on Coastal Engineering, Seoul, Korea, Coastal Engineering Proceedings (34). doi:10.9753/icce.v34.waves.49.

Fischer, H.B., List, J.E., Koh, R.C.Y., Imberger, J. and Brookes, N.H. (1979) Mixing in inland and coastal waters. New York: Academic Press.

Kay, A. (1987) The effect of cross-stream depth variations upon contaminant dispersion in a vertically well-mixed current, *Estuarine, Coastal and Shelf Science*, 24(2), 177–204.

Pearson, J.M., Guymer, I., West, J.R. and Coates, l.E. (2009) "Transverse Solute Mixing in the Surf Zone', ASCE Journal of Waterway, Port, Coastal and Ocean Engineering, 135(4), 127-134.

Pearson, J.M., Guymer, I., West, J.R. and Coates, L., (2002) "Effect of Wave Height on Transverse Solute Mixing", A.S.C.E., Journal of Waterway, Port, Coastal and Ocean Engineering, 128(1), 10-20.

West, P.O., Wallis, S.G., Sonnenwald, F.C., Hart, J.R., Stovin, V.R., & Guymer, I. (2020). "Modelling transverse solute mixing across a vegetation generated shear layer" Journal of Hydraulic Research. doi:10.1080/00221686.2020.1818307

Winckler, P., Liu, P.L-F. and Mei, C.C. (2013) "Advective Diffusion of Contaminants in the Surf Zone" J. Waterway, Port, Coastal, Ocean Eng., 2013, 139(6): 437-454

# Effect of vegetation on Mixing and Dispersion Processes at the apex section of a meander bend

Donatella TERMINI[1], Nina BENISTATI[2]

[1,2] Department of Engineering. University of Palermo (Italy)
email: donatella.termini@unipa.it
email: nina.benistati@unipa.it

ABSTRACT

Aquatic vegetation exerts a strong influence on the fluvial ecosystem. Understanding flow characteristics and turbulent structure in the presence of vegetation is especially important with respect to environmental processes as sediment transport and mixing of transported quantities. In the present paper attention is focused on the kinematic and mixing processes in the presence of flexible submerged vegetation on the bed of a curved channel. In particular, the effect of vegetation on the flux of mass distribution and on the transport process at the apex section of a meandering bend is investigated by comparing the distributions of the dispersion coefficient estimated in vegetated areas and in no-vegetated ones.

## 1. Introduction

On one hand vegetation modifies flow and sediment transport, influencing the evolution of bed morphology; on the other hand these processes affect the distribution of nutrients and oxygen and, thus, water quality conditions. It should be also considered that the alteration of hydrological conditions in fluvial systems determines changes both in river morphology and in riparian or riverbed vegetation. As consequence, the spatial distribution of vegetation can also change in time and in space depending on the combination of many factors, which might affect the settling and growth of the vegetated elements. The major part of studies conducted in this field consider straight flumes with different types of vegetation on the bed. Poggi et al. (2004) investigated flow turbulence structure in the presence of dense, rigid and submerged vegetation and suggested a phenomenological formulation of the mixing length. Tanino and Nepf (2008) analyzed the lateral dispersion processes in the presence of a random array of a rigid and emergent vegetation for different values of vegetation density. Other researchers focused on submerged flexible vegetation (among others Termini, 2015) and verified that the region around the top of the vegetation is the region of highest shear stress and maximum turbulence production. In the present paper attention is focused on the kinematic and mixing processes in the presence of flexible submerged vegetation on the bed of a curved channel. In particular, the effect of vegetation on the flux of mass distribution and on the transport process at the apex section of a meandering bend is investigated.

## 2. Methods

The analysis is performed with the aid of detailed experimental data collected in a laboratory channel. The collected data are processed in order to analyze the distributions of flow velocity components in vegetated and in no-vegetated areas highlighting how vegetation influences the kinematic characteristics of flow and the mixing and dispersion processes also in the no-vegetated areas. Thus, the velocity profiles of the time-averaged flow velocity components in the stream-wise, transversal and vertical directions estimated both inside the vegetated areas and in no-vegetated areas have been analysed and compared. As an example, Figure 1 reports the profiles of the time-averaged flow velocity components in the stream-wise ($\overline{v_l}$), transversal ($\overline{v_t}$) and vertical ($\overline{v_v}$) directions inside the vegetated area (i.e. at a distance of 15 cm from the outer bank of the examined section) and those obtained at the center of the cross-section (i.e. inside the no-vegetated area). To investigate the turbulence flow structure both the temporal and the spatial averaging of the flow quantities have been operated in order to limit the heterogeneity effect. Thus, the normalized dispersion coefficient in the transversal direction, $K_t$, has been determined as $\frac{K_t}{Ud} \approx \left\langle \frac{\sqrt{k'}d}{Ud} \right\rangle = \left\langle \frac{\sqrt{k'}}{U} \right\rangle$, where $U = Q/Bh_o$ ($h_o$=overall-averaged water depth) indicates the mean velocity, $k'$ is the turbulent kinetic energy per unit mass, $d$ is the vegetation stem dimension, the brackets represent the spatial average. Thus, the vertical profiles of the ratio $\frac{\sqrt{k'}}{U}$ and of its longitudinal spatial average $\left\langle \frac{\sqrt{k}}{U} \right\rangle$ at the selected locations inside the vegetated areas and in the no-vegetated areas have been determined and compared. Figure 2, as an example, reports the comparison between the vertical profiles of $\frac{\sqrt{k'}}{U}$ and of the spatial average $\left\langle \frac{\sqrt{k'}}{U} \right\rangle$ obtained at a distance of 15 cm from the outer bank of the considered section (i.e. inside the vegetated area) and those obtained at the center of the cross-section (i.e. inside the no-vegetated area).

## 3. Results and Concluding Remarks

Results essentially confirm that mass exchanges in the presence of vegetation are strongly influenced by the presence of the vegetated stems and by the turbulent structures which form between the vegetated and the no-vegetated areas. The presence of the flexible and dense vegetation determines a reduction of the size of the turbulent structures and limits the transport process not only in the vegetated areas but also in the transition towards the no-vegetated ones.

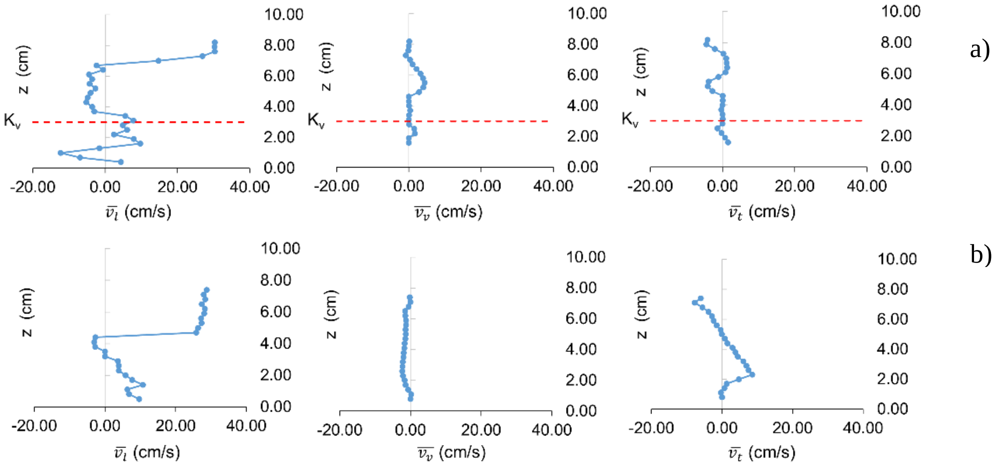


**Fig.1.** Time-averaged flow velocity components with vegetation (a) and without vegetation (b)

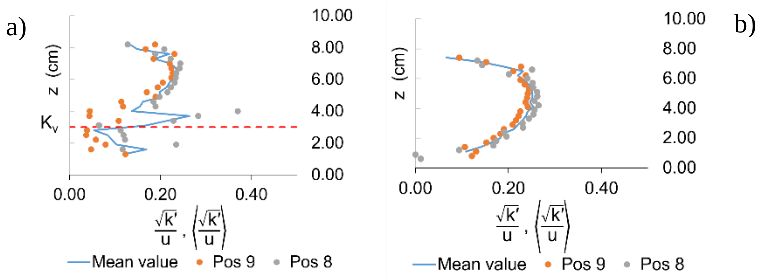


**Fig.2.** $\frac{\sqrt{k'}}{U}$ and $\left\langle \frac{\sqrt{k'}}{U} \right\rangle$ with vegetation (a) and without vegetation (b)

**Acknowledgements**

Part of this work has been supported by PRIN 2017, with the project “(ENTERPRISING)”

**References**

Poggi D., Porporato A., Ridolfi L., Albertson JD., Katul GG., The effect of vegetation density on canopy sub-layer turbulence, Boundary Layer Meteorol. 2004; 111: 565–587.

Tanino Y., Nepf H. Lateral dispersion in random cylinder arrays at high Reynods number. *J of Fluid Mechanics 2008;* 600: 339-371.

Termini D. Experimental analysis of the effect of vegetation on flow and bed shear stress distribution in high-curvature bends. Geomorphology 2016, Volume 274C, 2016.

# Buoyancy-driven exchange flows in inclined ducts: insights from laboratory experiments and mathematical modelling

Adrien LEFAUVE[1], P. F. LINDEN[1]

[1] Department of Applied Mathematics and Theoretical Physics, University of Cambridge, United Kingdom
email: lefauve@damtp.cam.ac.uk

ABSTRACT

## 1. Introduction

**Exchange flows -** Buoyancy-driven exchange flows naturally arise where relatively large bodies of fluid have different densities on either side of a relatively narrow constriction. In a gravitational field, this difference in buoyancy results in a horizontal hydrostatic pressure gradient along the constriction, of opposite sign above and below a 'neutral level'. This pressure gradient drives a counter-flow through the constriction, in which fluid from the negatively buoyant reservoir flows below the neutral level towards the positively buoyant reservoir, and vice versa. Such buoyancy-driven exchange flows result in little to no net volume transport, but crucially, in a net buoyancy transport between the reservoirs which tends to homogenise buoyancy differences in the system. In addition, irreversible mixing often occurs across the interface between the two counter-flowing layers of fluid, creating an intermediate layer of partially mixed fluid.

**Applications** - The net transport and mixing of the active scalar field (e.g. heat, salt or other solutes) and of other potential passive scalar fields having different concentrations in either reservoirs (e.g. pollutants or nutrients) have a wide range of consequences, recognised since the Antiquity. Aristotle offered the first recorded explanation of the movement of salty water within the Mediterranean Sea. Since then, exchange flows through the straits of Gibraltar and the Bosphorus have driven much speculation and research, due to their crucial roles in the water and salt balances of the Mediterranean Sea. More recently, it has been recognised that nutrient transport from the Atlantic partially supported primary production in Mediterranean ecosystems. The quantification, modelling and discussion of the past and current impact of exchange flows in straits, estuaries or between lakes continues to generate a vast literature.

**Broader importance -** More fundamentally, exchange flows are stably stratified shear flows, a canonical class of flows widely used in the mathematical study of stratified turbulence, dating back at least to O. Reynolds and G. I. Taylor. Multi-layered stratified shear flows have complex and still puzzling hydrodynamic stability and turbulent mixing properties. The straightforward and steady forcing of exchange flows make them ideal laboratory stratified shear flows because of the ability to sustain, over long time periods, high levels of turbulent intensity and mixing representative of large-scale natural flows.

## 2. Methodology

**The experiment -** The stratified inclined duct laboratory experiment (Fig. 1) consists of two reservoirs initially filled with aqueous solutions of different densities $\boldsymbol{\rho_0 \pm \Delta\rho/2}$, connected by a long rectangular duct that can be tilted at an angle $\theta$ from the horizontal. At the start of the experiment, the duct is opened, initiating a brief transient gravity current, after which an exchange flow is sustained through the duct for long periods of time, until the accumulation of fluid of a different density from the other reservoir reaches the ends of the duct (typically after several minutes). This exchange flow has at least four qualitatively different flow regimes (laminar, wavy, intermittently turbulent and fully turbulent), based on the experimental input parameters, as first recognised by Macagno & Rouse (1961) and Meyer & Linden (2014). One of the defining features of this flow is that the flow appears to be hydraulically controlled at the ends of the duct, which means that the mean exchange flow speed is bounded. Additional kinetic energy provided by a positive tilt angle $\theta$ must thus be dissipated turbulently inside the duct, causing these transitions to increasingly dissipative flow regimes.

**Objectives -** We will report on a thorough review and exploratory study of these flows by focusing on the behaviour of three key variables:

(i) the qualitative flow regime (laminar, wavy, intermittently or fully turbulent, see Fig. 1);

(ii) the mean buoyancy transport between reservoirs (that we called the net mass flux, $\boldsymbol{Q_m}$);
(iii) the mean thickness $\boldsymbol{\delta}$ of any potential interfacial mixing layer.

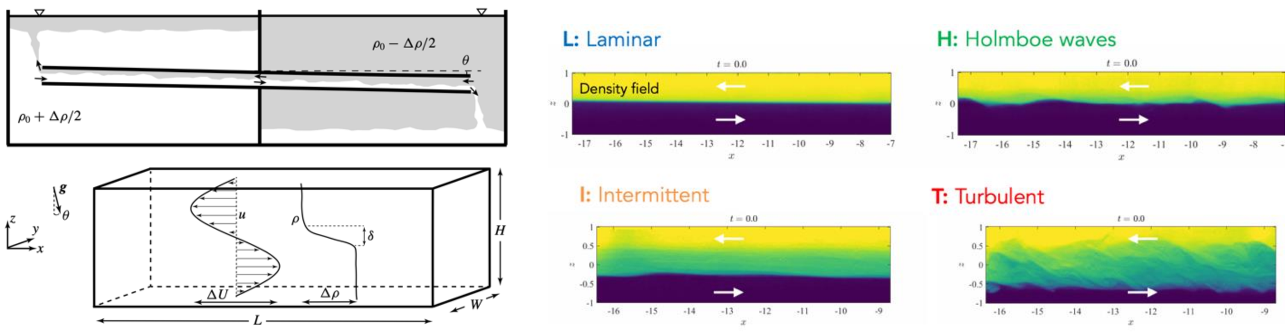


**Fig. 1.** Left: Schematics of the experimental setup (notice the tilt angle $\theta$). Right: Density field visualisations in a sub-section of the duct showing the four qualitatively different flow regimes, exhibiting increasing vertical buoyancy transport and interfacial mixing layer $\boldsymbol{\delta}$.

The above three variables are particularly relevant in applications to predict exchange rates of active or passive scalars (e.g. salt, heat, pollutants, nutrients) between two different fluid bodies (e.g. rooms in a building, seas or lakes on either sides of a strait). However, this study also fits in a larger research effort into the fundamental properties of turbulence in sustained stratified shear flows of geophysical relevance. The above three variables have thus been chosen for their particular ability to be readily captured by simple laboratory techniques while encapsulating several key flow features that are currently the subject of active research, such as: interfacial 'Holmboe' waves, spatio-temporal turbulent intermittency, and layering and mixing.

## 3. Results

Dimensional analysis reveals that the regimes, $Q_m$ and $\delta$ must depend on five non-dimensional independent input parameters: the duct aspect ratios in the longitudinal direction $A=L/H$ and spanwise direction $B=W/H$, the tilt angle $\theta$, the Reynolds number *Re* (based on the initial buoyancy difference driving the flow) and the Prandtl number *Pr* (we consider both salt and temperature stratifications, i.e. $Pr=700$ and $=7$). After reviewing the relevant literature and open questions on the scaling of regimes, mass flux and interfacial thickness with *A*, *B*, $\theta$, *Re*, *Pr*, we present the first extensive, unified set of experimental data (totalling 886 individual experiments and 1545 data points) where we varied systematically all five input parameters and measured all three output variables with the same methodology.

Our results in the ($\theta$, *Re*) plane for five sets of (*A*, *B*, *Pr*) reveal a variety of interesting scaling laws, and a non-trivial dependence of all three variables on all five parameters, in addition to a sixth elusive parameter. We further develop three classes of candidate mathematical models to explain the observed scaling laws: (i) the recent volume-averaged energetics of Lefauve, Partridge & Linden (2019); (ii) two-layer frictional hydraulics; (iii) turbulent mixing models. While our models provide significant qualitative and quantitative descriptions of the experimental results, they also highlight the need for further progress on shear-driven turbulent flows and their interfacial waves, layering, intermittency and mixing properties.

Finally, we will explain how a new generation of high-resolution experimental measurements of the simultaneous three-component velocity and density fields in three-dimensional volumes are now allowing us to gain new quantitative insights into such flows (Lefauve & Linden, 2022a,b).

### References

Macago E. & Rouse H. Interfacial mixing in stratified flow. *J. Engng Mech. Division. Proc. Am. Soc. Civ. Engrs* **87** (EM5), 55–81. (1961)
Meyer C. R. & Linden P. F. Stratified shear flow: experiments in an inclined duct. *J. Fluid Mech.* **753**, 242–253 (2014)
Lefauve A., Partridge, J. L. & Linden P. F. Regime transitions and energetics of sustained stratified shear flows. *J. Fluid Mech.* **875**, 657-698 (2019)
Lefauve A. & Linden P. F. Experimental properties of continuously-forced, shear-driven, stratified turbulence. Part 1. Mean flows, self-organisation, turbulent fractions, *J. Fluid Mech.* **937**, A34 (2022a)
Lefauve A. & Linden P. F. Experimental properties of continuously-forced, shear-driven, stratified turbulence. Part 2. Energetics, anisotropy, parameterisation, *J. Fluid Mech.* **937**, A35 (2022b)

# Idealised modelling of estuarine development affected by human interventions and climate change

Rutger SIEMES[1], Trang Minh DUONG[1], Pim WILLEMSEN[1,2], Bas BORSJE[1], Suzanne HULSCHER[1]

[1] University of Twente, Netherlands; [2] Deltares, Netherlands
email: r.w.a.siemes@utwente.nl

ABSTRACT

Estuaries worldwide are facing the challenge of coping with changing climates. Insufficient supply of sediment to overcome sea-level rise can increase flood risk and saltwater intrusion and drowning of ecosystems. To explore how estuarine eco-morphology is affected by large-scale human interventions and climate change, an idealised eco-morphological model is developed and validated. The model represents the Nieuwe Waterweg estuary in the Rhine-Meuse Delta. Short-term simulations (1 year) are performed after human-induced changes and projected climate changes are implemented in the model.

The model is able to represent annual morphological trends. Results show the sensitivity of the system towards channel depth and the presence and size of wetlands. Simulations will be repeated with projected future climate forcings, enabling assessment of estuarine development after large-scale changes for the present and the future.

## 1. Introduction

Estuarine regions connect our rivers with the ocean, and are important socio-economic zones, being densely populated and hosting many major ports worldwide. They are highly susceptible to changes in climate, from the sea-side (sea level rise, changes in wave climate) and from rivers (changing river discharge and sediment supply). To cope with sea-level rise (SLR), estuaries need sufficient sedimentation (Giosan et al., 2014). Lack hereof can increase flood risk and intrusion of salt water, and can cause drowning of valuable wetland ecosystems. To optimise estuarine functions and prepare for these future threats, improved understanding of estuarine development after potential changes in its climate and/or system configuration is desired. To this end, this study explores the annual behaviour of the 'Nieuwe Waterweg' estuary, in the Rhine-Meuse Delta, after human interventions in the contemporary climate and in projected climate changes.

## 2. Methods

### 2.1. Study area

The Nieuwe Waterweg estuary, the Netherlands (Figure 1), typically has an average discharge of $1600 m^3/s$, with a relatively high discharge in winter and low discharges during summer. The estuary has a mean tidal range of 1.6m and typical average wave heights of 1.1m, which varies over the seasons. It flows out into the wave-dominated coasts of the North-Sea. While historically wetlands were abundantly present, extensive human interventions to this estuary resulted in an embanked and channelized estuarine channel which is annually dredged to maintain its artificial depth, allowing large ships to enter the ports.

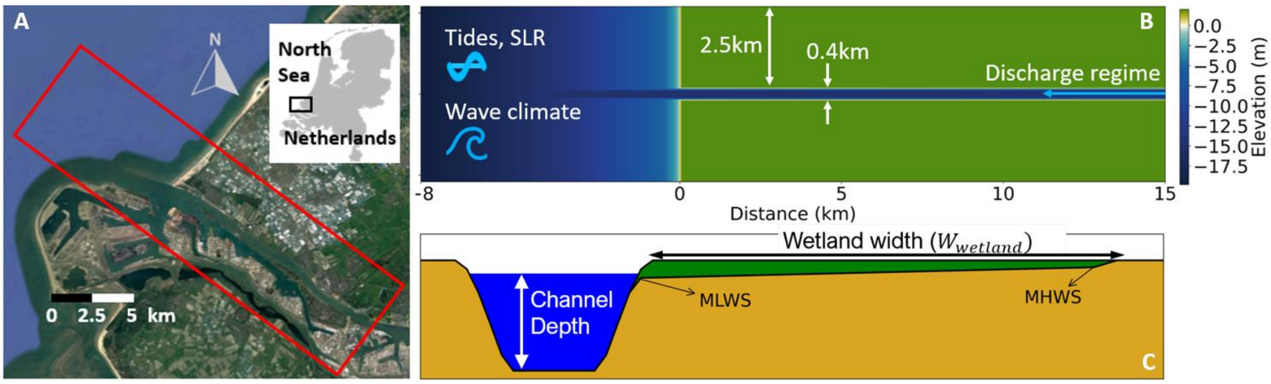


**Fig. 1. A)** Top view of the study area. **B)** The schematised model domain. It is forced by tides and a monthly averaged wave climate on the sea-side side, and by a monthly averaged discharge regime from the river. Future scenarios are implemented by changing system forcings: the wave climate and the discharge regime. **C)** Schematic overview of large-scale interventions implemented within the estuary.

### *2.2. Eco-morphological model setup*

A morphological model is developed in Delft3D-FM (depth-averaged), the successor of Delft3D which is extensively applied for morphological modelling of estuaries. A schematized bathymetry is developed for the contemporary 'Nieuwe waterweg' estuary (Figure 1). The domain is forced by tides, and an annual monthly averaged wave climate from the coast, and by an annual monthly average discharge regime from the river with suspended mud concentrations of 20mg/L. The model representing the contemporary system is validated to gain confidence in its ability to represent the study area.

### *2.3. Scenarios*

Next, simulations are performed after implementation of two large-scale interventions in the system: 1) Wetland restoration, a nature-based solution increasingly recognized for its potential for flood safety, sediment trapping (by vegetation) and additional ecosystem services and; 2) Channel deepening, an intervention often applied to allow larger ships to enter the ports. Wetlands are only implemented along the northern bank of the estuary, due to spatial limitations.

Moreover, using snap-shot simulations, the annual behaviour of the estuary after climate change is assessed. The model is adjusted to represent a future climate, using projected climate changes for the year 2100 (following the 6$^{th}$ IPCC report). System forcings are adjusted for SLR, projected wave climate and discharge regimes. Also, adjustments for the future bathymetry by way of basin infilling are included, (see Duong et al., 2016). Snap-shot simulations are performed with and without human-interventions, in the contemporary and future climate.

## 3. Results & Discussion

The model is validated with observed hydrodynamic timeseries (water levels and waves) and derived average annual morphological trends (Cox et al., 2021) and showed good resemblance. Simulations with the contemporary climate showed that channel deepening increased sedimentation in the estuary. While wetlands showed net accretion in all scenarios, presence of wetlands, and increasing their size, reduced net annual sediment budget in the estuary (Figure 2). These morphological trends were accentuated by the presence of vegetation. Increased channel depth slightly increased wetland accretion.

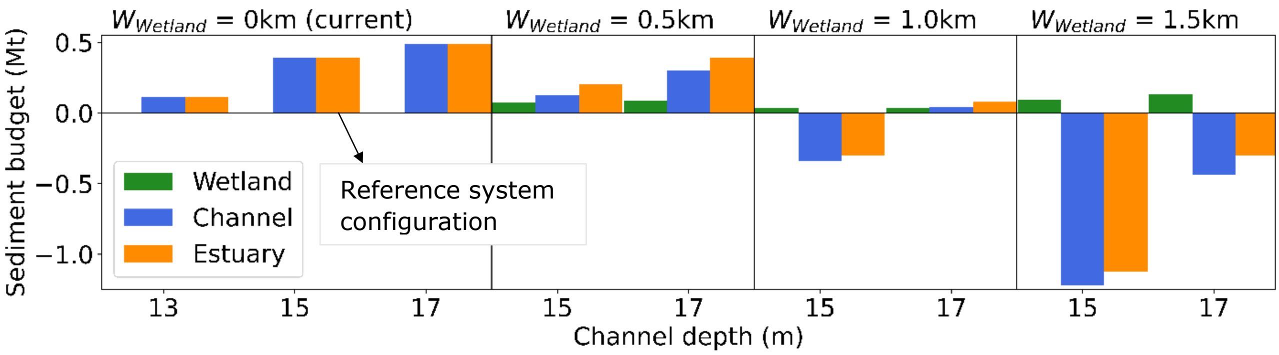


**Fig. 2.** Annual sediment budget for the wetland, channel and the entire estuary (both areas combined), under various configurations of the estuarine system.

Morover, results indicate that lateral location of the wetland substantially affects channel morphology. Strategic placement could aid in steering estuarine morphology. Simulations will be repeated under future forcings, which will give insights in estuarine development under potential climate- and human-induced changes.

**Acknowledgements**

This work is part of the Perspectief Program SALTISolutions, funded by NWO Domain Applied and Engineering Sciences, in collaboration with private and public partners.

**References**

Cox, J. R., Huismans, Y., Knaake, S., Leuven, J., Vellinga, N., van der Vegt, M., Hoitink, A., & Kleinhans, M. (2021). Anthropogenic Effects on the Contemporary Sediment Budget of the Lower Rhine-Meuse Delta Channel Network. *Earth's Future, 9*(7), e2020EF001869.

Duong, T. M., Ranasinghe, R., Walstra, D., & Roelvink, D. (2016). Assessing climate change impacts on the stability of small tidal inlet systems: Why and how? *Earth-science reviews, 154*, 369-380.

Giosan, L., Syvitski, J., Constantinescu, S., & Day, J. (2014). Climate change: Protect the world's deltas. *Nature, 516*(7529), 31-33.

# Non stationary analysis of extreme sea level events in Venice: implications for return levels estimation

Damiano BALDAN[1], Franco CROSATO[1], Elisa CORACI[1], Andrea BONOMETTO[1], Maurizio FERLA[1], Sara MORUCCI[1]

[1] Italian Institute for Environmental Protection and Research, ISPRA, Venice, Italy
email: sara.morucci@isprambiente.it

ABSTRACT

Coastal flooding caused by extreme sea levels is one of the major impacts of climate change. Extreme sea levels are expected to increase in the future due to sea level rise and storm surge intensification. Estimating return levels while assuming stationarity might lead to the underestimation of return levels for the future. Additional uncertainty is related to the choice of the model. In this work, we fit extreme values models to long-term (96 years) sea level record from the city of Venice (NW Adriatic Sea, Italy): a Generalized Extreme Value distribution (GEV), a Generalized Pareto distribution (GP), and a Point Process (PP). We model non-stationarity with a linear dependence of the model's parameters from the mean sea level. Our results show that the inclusion of non-stationarity significantly improves the fit of the GEV and the PP models, but not the GP. The non-stationary PP models the rate of extremes occurrence fairly well. Estimates of the return levels for non-stationary models are generally higher than estimates from stationary models. Thus, projections of return levels in the future might be significantly different from those calculated in the past using stationary models.

## 1. Background

Extreme sea levels can cause the flooding of coastal zones, with significant economic impacts. Probability distribution functions for extreme events have been widely used to derive the design parameters for coastal protection structures under the assumption of stationarity. With climate change, extreme sea levels are expected to increase due to mean sea level rise and storm surges intensification (Lionello et al., 2021). Thus, there is the need for methods that can model non-stationarity explicitly. Several methods were proposed (Coles et al., 2021), but questions remain on the capability of such models to cope with non-stationarity (Razmi et al., 2017; Mudersbach and Jensen, 2010). In this work, we used a long-term (1924 -2019) sea level record from a tide gauge (*Punta della Salute*) located in the city of Venice (NW Adriatic Sea, Italy). The data are expected to be non-stationary due to the combined effects of eustasism and local subsidence. We fit several stationary and non-stationary extremes models and check which model fits the data best. Then, we compare the models estimates for extreme sea levels.

## 2. Methods

We obtained the extremes time series (Fig. 1a) by extracting yearly block maxima (BM) and peaks over threshold (POT). We consider BM and POT as random variables. We fitted BM with a Generalized Extreme Values (GEV) distribution:

$$G(z) = \Pr(BM < z) = \exp\left[-\left\{1 + \xi\left(\frac{z-\mu}{\sigma}\right)\right\}_+^{-1/\xi}\right] \quad (1)$$

Where $a_+ = \max(a, 0)$, $\mu$ is the location parameter, $\sigma$ is the scale parameter (always positive), and $\xi$ is the shape parameter. After selecting a proper threshold u, we fitted POT ($z = y + u$) with a Generalized Pareto (GP) distribution:

$$H(y) = \Pr(POT > u + y \mid POT > u) = 1 - \left[1 + \xi\left(\frac{y}{\sigma}\right)\right]_+^{-1/\xi} \quad (2)$$

The GP distribution uses the same GEV parameters. We also fitted POT with a Point Process (PP), where the process rate $\lambda$ (number of events per unit time) depends on the GEV and GP parameters via:

$$\lambda = \left[1 + \xi\left(\frac{z-\mu}{\sigma}\right)\right]_+^{-1/\xi} \quad (3)$$

We introduced non-stationarity by allowing a linear dependence of the models' parameters (location and scale) from the mean sea level. We fitted three different variants of the models: (a) without covariates, (b) with varying location, (c) with varying location and scale. We tested for the presence of a trend in the BM and POT series with a Mann-Kendal test. We used a maximum likelihood test to check if the inclusion of covariates on location and scale improves the fit significantly. To generate return level plots, we fixed the mean sea level to the value of 2019 (+ 35.5 cm above the historic „1897" local reference calculated as the 1885 - 1909 mean) and calculated the quantiles of the distributions accordingly.

## 3. Results and discussion

The Mann-Kendall test shows that BM have a clear temporal trend ($p < 0.001$), while POT do not ($p > 0.05$). The inclusion of covariates improved the fit (likelihood ratio test) for location and for both location and scale parameters for GEV ($p < 0.001$ and $p = 0.017$, respectively) and PP ($p < 0.001$, and $p = 0.003$), but not for GP. Additionally, including covariates on location and scale in the PP yields good estimates of the rate of the process, as measured by Pearson's correlation ($r = 0.81$ with the inclusion of location, and $r = 0.84$ with the inclusion of location and scale). Models including covariates on the location tend to have an increased return level estimate for smaller return periods, while models with covariates also on the scale tend to estimate higher return levels also for higher return periods (Fig. 1b).

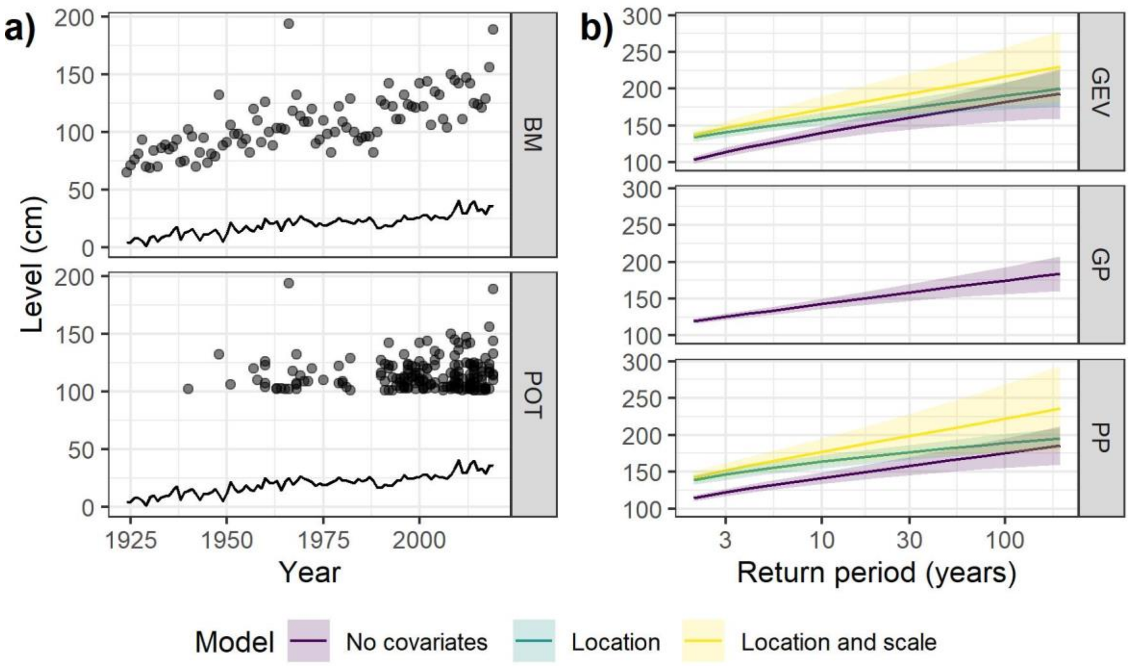


**Fig. 1.** a) data used to fit the parametric models: block maxima (BM), and peaks over threshold (PT). The line represents the mean sea level trend. b) return level plots for the fitted models and their configurations. GEV: Generalized Extreme Value distribution, GP: Generalized Pareto distribution, PP: Point Process. Note: models with varying location and scale for GP were not significant and are not represented.

Our results show that including non-stationary aspects in the modeling of extreme sea levels yields estimates of return levels that might be significantly higher than those estimated from a stationary analyses. The method used to model non-stationary matters, as non-stationariety might be overlooked when using GP models. Additional covariates representing climatic conditions, local morphological changes, and seasonality can be included in the analysis to build solid models for extreme events analysis.

**Acknowledgements**

This work was supported by the EU-INTERREG project ADRIACLIM (grant number IT-HR 10252001)

**References**

Coles S, Bawa J, Trenner L, Dorazio P. (2001) An introduction to statistical modeling of extreme values. London: Springer; 2001
Mudersbach C, Jensen J. (2010) Nonstationary extreme value analysis of annual maximum water levels for designing coastal structures on the German North Sea coastline. Journal of Flood Risk Management. 3(1):52-62.Razmi, A., Golian, S., Zahmatkesh, Z., 2017.
Razmi A, Golian S, Zahmatkesh Z. (2017) Non-stationary frequency analysis of extreme water level: application of annual maximum series and peak-over threshold approaches. Water resources management. 31(7):2065-83.
Lionello P, Barriopedro D, Ferrarin C, Nicholls RJ, Orlić M, Raicich F, Reale M, Umgiesser G, Vousdoukas M, Zanchettin D. (2021) Extreme floods of Venice: characteristics, dynamics, past and future evolution. Natural Hazards and Earth System Sciences. 1;21(8):2705-31.

# An index-based method to assess the resilience of coastal urban areas to climate change-related flooding: The case of Attica, Greece

Charalampos Nikolaos ROUKOUNIS[1], Vassilios A. TSIHRINTZIS[2]

Centre for the Assessment of Natural Hazards and Proactive Planning & Laboratory of Reclamation Works and Water Resources Management, School of Rural and Surveying Engineering, National Technical University of Athens, 9 Heroon Polytechniou Str., 15780, Zographou, Athens, Greece
email: [1]babisrouk@gmail.com; [2]tsihrin@suvey.ntua.gr

ABSTRACT

The aim was to assess the resilience of coastal urban and suburban areas to climate change-related coastal flooding. The analysis of the literature showed that index-based methods in climate change vulnerability and resilience research are effective, providing a solid and user-friendly framework. In this context, a new index of coastal resilience to climate change (Coastal Resilience Index – CResI) is proposed. About 20 different variables are used to create CResI, combining physical, geomorphological and socio-economic characteristics of the study area. Weights and ranks were assigned to the variables, using Multicriteria Decision Analysis (MCDA), and more specifically, the Analytic Hierarchy Process. The proposed framework was applied and validated in the South West waterfront of Athens Metropolitan Area, Greece. The study identified areas of increased vulnerability due to climate change.

## 1. Literature Review

Climate change alongside with rapid population growth and natural and manmade disasters require modern approaches as forward-looking design can have a profound impact on safety and prosperity of individuals and communities as a whole (Rus et al., 2018). The understanding that climate change is a concern of humankind globally has raised the question "who is vulnerable" rather than "what". A literature review was undertaken and a total of 43 articles with applications of different types of coastal vulnerability indicators have been identified (Roukounis and Tsihrintzis, 2022). Some indicators employ only the physical/climatic characteristics of the areas, and others, more complex, take into account both physical and socio-economic factors. In the majority of the literature, the spatial scale is either too broad (national level) or too narrow (specific coastal segments), not taking into consideration crucial characteristics of the coastal urban areas and other relevant coastal infrastructure such as marinas. This study tries to fill this gap with the development of a new Coastal Resilience Index (CResI).

## 2. Methodology and Discussion

The CResI employs 19 variables (geophysical, environmental, topographic, social, economic) which receive scores in the scale 1 (low) to 5 (high vulnerability). Weights and ranks can be assigned to the variables using Multicriteria Decision Analysis (MCDA), by establishing a hierarchical structure and analyzing pairwise comparisons using the Analytic Hierarchy Process (AHP) (Saaty 1987). The AHP is used for addressing complex semi-structured decision-making problems by setting weights to a number of options/scenarios with regard to their importance.

The establishment of the required database is the first step for the development of the CResI, through the compilation of geographic, environmental, topographic, social and economic data. The database can be processed in a GIS environment. CResI is created after combining different approaches of widely used indices (e.g., Gornitz, 1991; Thieler and Hammar-Klose, 1998; Cutter et al., 2003), with later modifications (e.g., Tate et al., 2010; Gaki-Papanastasiou et al., 2010; Karymbalis et al., 2012; Guillard- Gonçalves et al., 2015) as well as more complex indices (e.g., Zanetti et al., 2016; Toimil et al., 2017; Gargiulo et al., 2020). The coastal zone of the present study is located in Attica, Greece, and more specifically it is part of the South West waterfront between the port of Piraeus and the area of Vouliagmeni, with a total length of approximately 70 km. It includes urban, suburban and rural areas, and both natural and artificial coastline. The major part is in the Metropolitan Area of Athens, the financial capital of Greece. It also includes the port of Piraeus, which is one of the most important ports in Europe (Category I) included in the Core Network of the European Union (EU) and in the Motorways of the Sea. The study area also includes smaller touristic ports of high capacity (i.e., Zea Marina, Athens Marina, Flisvos Marina, Alimos Marina, Ag. Kosmas Marina, Vouliagmeni Marina), transport infrastructure (highways, underground and suburban rail, a tramway and bus lines) and other areas of high interest such as the under construction Hellenikon Metropolitan Park.


Figure 1: Area of concern (Source: ESRI, Maxar, GeoEye, Earthstar)

The results show that the majority of the coastal areas have a low resilience score (CResI > 3). More specifically, areas with high population density, as well as areas with land use of significant economic importance are more vulnerable to climate change-related coastal flooding. Also, many important port infrastructures (marinas) are in low-resilience zones. However, high elevation and slope, as well as coastal defense infrastructures decrease the exposure of various areas, such as Mikrolimano and Zea Marina in Piraeus.

**References**

Cutter SL, Boruff BJ, Shirley WL (2003) Social vulnerability to environmental hazards. Soc Sci Q 84(2):242–261. https://doi.org/10.1111/1540-6237.8402002

Gaki-Papanastassiou K, Karymbalis E, Poulos S, Zouva C (2010) Coastal vulnerability assessment to sea-level rise based on geomorphological and oceanographical parameters: the case of Argolikos Gulf. https://www.researchgate.net/publication/235960304

Gargiulo C, Battarra R, Tremiterra MR (2020) Coastal areas and climate change: A decision support tool for implementing adaptation measures. Land Use Policy 91:104413. https://doi.org/10.1016/j.landusepol.2019.104413

Gornitz VM, Daniels RC, White TW, Birdwell KR (1994) The development of a coastal risk assessment database: vulnerability to sea-level rise in the U.S. Southeast. J Coastal Res 12:327–338. http://www.jstor.org/stable/25735608

Guillard-Gonçąlves C, Cutter SL, Emrich CT, Zêzere JL (2015) Application of social vulnerability index (SoVI) and delineation of natural risk zones in Greater Lisbon, Portugal. J Risk Res 18(5):651–674. https://doi.org/10.1080/13669877.2014.910689

Karymbalis E, Chalkias C, Chalkias G, Grigoropoulou E, Manthos G, Ferentinou M (2012) Assessment of the sensitivity of the southern coast of the Gulf of Corinth (Peloponnese, Greece) to sea-level rise. Central Eur J Geosci 4(4):561–577. https://doi.org/10.2478/s13533-012-0101-3

Li K, Li GS (2011) Vulnerability assessment of storm surges in the coastal area of Guangdong Province. Nat Haz Earth Syst Sci 11(7):2003–2010. https://doi.org/10.5194/nhess-11-2003-2011

Roukounis CN, Tsihrintzis VA (2022) Indices of coastal vulnerability to climate change: A review. Review paper accepted for publication in Environmental Processes, Springer

Rus K, Kilar V, Koren D (2018) Resilience assessment of complex urban systems to natural disasters: A new literature review. Int J Disaster Risk Reduct 31:311–330. https://doi.org/10.1016/j.ijdrr.2018.05.015

Saaty RW (1987) The Analytic Hierarchy Process-what it is and how it is used. Math Model 9:161–176. https://doi.org/10.1016/0270-0255(87)90473-8

Thieler ER, Hammar-Klose ES (1999) National Assessment of Coastal Vulnerability to Sea-Level Rise. Open-File Report 0–179, 1. https://pubs.usgs.gov/dds/dds68/reports/gulfrep.pdf (accessed 19/11/2020)

Toimil A, Losada IJ, Díaz-Simal P, Izaguirre C, Camus P (2017) Multi-sectoral, high-resolution assessment of climate change consequences of coastal flooding. Clim Change 145(3–4):431–444. https://doi.org/10.1007/s10584-017-2104-z

Zanetti VB, de Sousa WC Jr, de Freitas DM (2016) A climate change vulnerability index and case study in a Brazilian Coastal City. Sustainability 8(8):1–12 https://doi.org/10.3390/su8080811

# Assessment of Coastal Vulnerability Index with emphasis on the geotechnical variable

Vasileios BOUMPOULIS[1], Nikolaos DEPOUNTIS[1], Theodoros BOUAS[1]

[1] University of Patras, Department of Geology, Laboratory of Engineering Geology, Rio 26504, Greece
vasileios_boumpoulis@upnet.gr and ndepountis@upatras.gr

ABSTRACT

## 1. Introduction

Climate change is expected to increase the frequency and intensity of climate induced extreme events (IPCC, 2021), while the impacts in coastal zones it is considering to be huge, even under small emission scenarios (IPCC, 2022). Moreover, coastal areas are vulnerable and susceptible to coastal hazards and their protection is under a great importance for the ecosystem, the society and the economy. Many methodologies have been developed for analysis incorporating the terms of risk, hazard, vulnerability, and exposure. The most common method to assess vulnerability is the Coastal Vulnerability Index (CVI), which integrates heterogeneous data sources and indicators for the vulnerability classification of the coastal zone.

Two of the most most interfering variables in CVI calculations are the geotechnical variable and the shoreline evolution rate (Boumpoulis et al., 2021). Therefore, one of the main purposes of this study is the assessment of the vulnerability regime in coastal areas using a weighted CVI model with emphasis on the geotechnical variable. In addition, the Multi-Criteria Decision Analysis (MCDA) method of Analytical Hierarchy Process (AHP) is implemented to weight and prioritize criteria and key indicators as it has been proposed by Saaty (1977). As a model area it was selected the Gulf of Patras in Western Greece because of its diachronic erosion problems due to the climate change and most of the data used were collected from the coastal monitoring activities that had been peformed in the frame of TRITON project (Nikolakopoulos et al, 2019).

## 2. Methodology

The selected key parameters of the presented modified (CVI) model are: 1) the use of geotechnical data in order to characterize the coastal formations as geotechnical units, 2) the significant mean wave height with a return period of 10 years, 3) the coastal slope which has been calculated by using a Digital Elevation Model (DEM) (5X5 m), 4) the shoreline evolution (2006-2018) by computing the relevant End Point Rates (EPR), 5) the average tidal range and 6) the Sea Level Rise (SLR). The CVI calculations implemented with the following modifications: 1) use of geotechnical data instead of the geological-geomorphological and 2) use of AHP to weight the CVI parameters.

For the characterization of coastal formations as geotechnical units, a thorough geotechnical program was performed in the research area, including the assessment of soil properties in forty (40) boreholes, laboratory, and in-situ geotechnical tests (SPT and CPT), coastal sediment sampling and engineering-geological mapping.

Influence of each indicator is different in CVI model calculations and due to this, AHP method is applied in the model to weight the parameters for a more robust and reliable results (De Serio et al 2018, Diaz-Cuevas et al 2020). The final weighted CVI equation (Eq. 1) is presented below:

$$\boldsymbol{CVI = W1 * V1 + W2 * V2 + \cdots + Wi * Vi} \quad \mathbf{(1)}$$

where, Wi is the weight value and Vi is the vulnerability score of the i-th parameter. The ranking of CVI values into vulnerability classes was performed by applying the equal interval classification method.

## 3. Results

Based on the results from the geotechnical investigation, the coastal area was classified into 8 zones (geotechnical units) with different mechanical behavior. Consequently, the AHP method was applied to weigh all the CVI parameters (Table 1).

Application of the CVI incorporating geotechnical classification of the coastal formations as well as AHP to weight the CVI parameters, indicates that almost the half of the total shoreline (44.66%) of the study area is under high vulnerability. The rest of the shoreline calculated with 4.07%, 8.49%, 17.65% and 25.12% which represents Very Low, Low, Moderate and Very High vulnerability, respectively (Fig. 1).

***Table 1:*** Weight factor for all the CVI parameters using the AHP methodology

| Variables | Geotechnical characterization | Significant mean height wave | Coastal slope | Shoreline evolution | Average tidal range | Sea Level Rise |
|---|---|---|---|---|---|---|
| **Weight** | 0.35 | 0.12 | 0.20 | 0.21 | 0.04 | 0.07 |

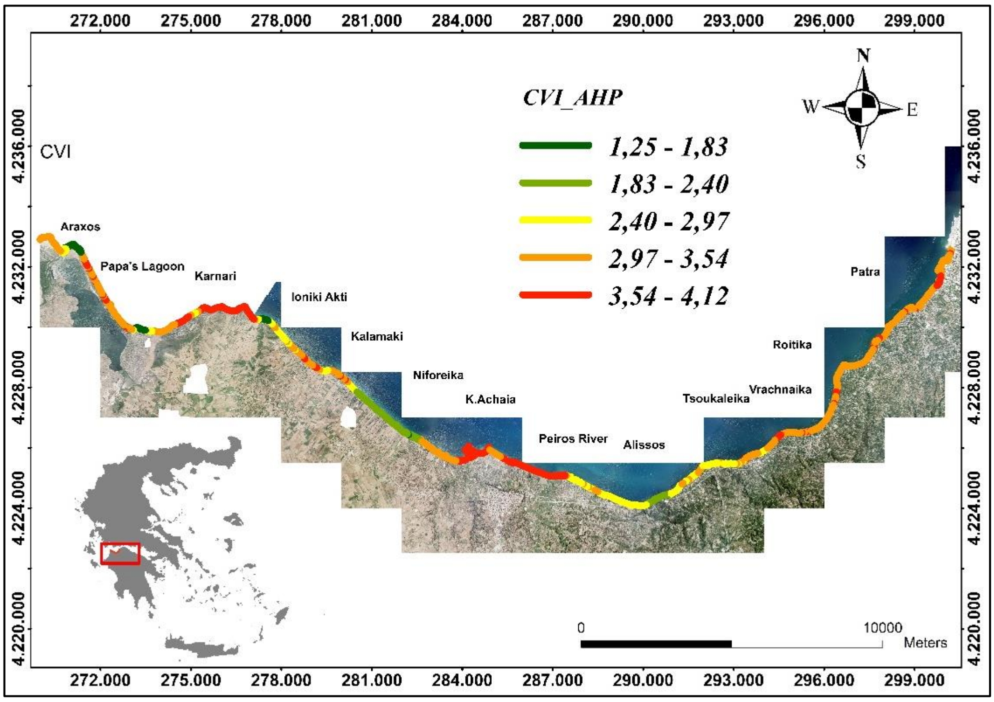


**Fig. 1:** Spatial distribution of CVI values alongside the shoreline of the study area (gulf of Patras)

## 4. Conclusion-Discussion

Among the most common parameters of CVI which are used for vulnerability assessment, many uncertainties and doubts are observed, so that they must be improved to reduce any potential flaws. A first attempt towards the improvement of those uncertainties in CVI calculations is the most precise assessment of the geotechnical variable. By applying the weighted CVI incorporating a more precise geotechnical classification as well as AHP it was found that almost the half of the total shoreline of the study area of the qulf of Patras is under high vulnerability. However, the vulnerability regime could be increased in the future, since no potential future climate projection had been included in the CVI assessment (e.g future SLR until 2100).

**Acknowledgements**

Many of the data used in the current reserch were derived from the TRITON/Greece-Italy/Interreg V/A 2014-2020 co-operation project and authors would like to acknowledge this support.

**References**

Boumboulis V, Apostolopoulos D, Depountis N, Nikolakopoulos K (2021) The Importance of Geotechnical Evaluation and Shoreline Evolution in Coastal Vulnerability Index Calculations, Journal of Marine Science and Engineering 9, 423. https://doi.org/10.3390/jmse9040423

De Serio F, Armenio E, Mossa M, Petrillo A.F (2018) How to define priorities in coastal vulnerability assessment, Geosciences 8, 415. https://doi.org/10.3390/geosciences8110415

Díaz-Cuevas P, Prieto-Campos A, Ojeda-Zújar J (2020) Developing a beach erosion sensitivity indicator using relational spatial databases and Analytic Hierarchy Process, Ocean Coastal Management 189, 105146. https://doi.org/10.1016/j.ocecoaman.2020.105146

IPCC (2021). Climate Change 2021: The Physical Science Basis. Contribution of Working Group I to the Sixth Assessment Report of the Intergovernmental Panel on Climate Change. [Masson-Delmotte, V., P. Zhai, A. Pirani, S. L. Connors, C. Péan, S. Berger, N. Caud, Y. Chen, L. Goldfarb, M. I. Gomis, M. Huang, K. Leitzell, E. Lonnoy, J. B. R.Matthews, T. K. Maycock, T.Waterfield, O. Yelekçi, R. Yu and B. Zhou (eds.)]. Cambridge University Press. In Press.

IPCC, 2022: Climate Change 2022: Impacts, Adaptation, and Vulnerability. Contribution of Working Group II to the Sixth Assessment Report of the Intergovernmental Panel on Climate Change [H.-O. Pörtner, D.C. Roberts, M. Tignor, E.S. Poloczanska, K. Mintenbeck, A. Alegría, M. Craig, S. Langsdorf, S. Löschke, V. Möller, A. Okem, B. Rama (eds.)]. Cambridge University Press. In Press.

Nikolakopoulos K, Konstantinopoulos D, Depountis N, Kavoura K, Sabatakakis N, Fakiris E, Christodoulou D, Papatheodorou G (2019) Coastal monitoring activities in the frame of TRITON project Proc. SPIE 11156, Earth Resources and Environmental Remote Sensing/GIS Applications X, 111560Z. https://doi.org/10.1117/12.2532766.

Saaty T.L (1977) A scaling method for priorities in hierarchical structures. Journal of Mathematical Psychology, *15*, 234–281.

# Development of a Complex Vulnerability Index for Fishing Shelters – The Case of Cyprus

Vasiliki CHALASTANI[1], Andreas PANTELIDIS[1], Christina TSAIMOU[1] and Vasiliki TSOUKALA[1]

[1] Laboratory of Harbour Works, Department of Water Resources and Environmental Engineering, School of Civil Engineering, National Technical University of Athens (NTUA), Zografou 15780, Greece.
email: vanesachala@hotmail.com (for author 1)
email: antreas13athens@hotmail.com (for author 2)
email: ctsaimou@gmail.com (for author 3)
email: tsoukala@mail.ntua.gr (for author 4)

ABSTRACT

Coastal areas are increasingly threatened both by the impacts of climate change as well as human pressures. Seaports lying at the land-sea interface are considered vulnerable infrastructure, affected by sea level rise, storm surges and increased human activities. In this paper, the 16 existing fishing shelters of Cyprus are used as case study to develop a complex vulnerability index to assess and evaluate the current state of the fishing shelters. This vulnerability index includes physical, environmental, socio-economic and infrastructural indicators which describe the structural and operational components of the shelters in a holistic way. These indicators are scored and ranked to describe the degree of vulnerability of each fishing shelter and allow for comparison among shelters. The novelty of this index is that it is informed by on-site visits; questionnaires answered by local fishermen and targeted interviews with representatives of the port authorities. This study highlights the complex interactions between physical and socio-economic conditions in driving vulnerability. The results can assist decision-makers to prioritize interventions and design adaptation pathways that reduce the shelters' vulnerability while increasing their resilience.

## 1. Introduction

Assessing vulnerability of a system via indices, indicators and models has been recognised as an effective first step to design the system's adaptation oprions. The island of Cyprus was selected as case study to examine the vulnerability of the country's fishing shelters. The 16 fishing shelters found along the 320 km of the Cypriot coastline constitute an important asset for, not only the fishing, but also the touristic sector of Cyprus, since they are often used for berthing of touristic vessels too. The assessment of their vulnerability is important improve their resilience, especially under the imminent threats imposed by climate change.

## 2. Methods – Tools

The methodological framework of this study is presented in Fig.1 and comprises 6 steps: i) visits in all 16 shelters to assess their current condition, ii) responses of fishermen to already developed questionnaires regarding the shelter's condition and the fisheries sector in Cyprus, iii) targeted interviews with representatives of the port authorities in Cyprus, namely the Cyprus Port Authority and the Department of Fisheries and Marine Research. These first 3 steps not only constitute the first comprehensive database for the fishing shelters of Cyprus, but their results also feed the subsequent 3 steps namely: iv) the development and scoring of 4 vulnerability sub-indices (physical, environmental, infrastructural, socio-economic), v) the compilation of the 4 sub-indices into a complex vulnerability index (VI) and vi) the ranking of the shelters according to the score of their VI. The variables of the 4 sub-indices are scored for each shelter with a discrete value from 1 to 3 with representing low, medium and high vulnerability (1, 2 and 3 respectively). When available, these scores are based on the quantitative assessment of the variables, otherwise a qualitative scoring is performed. For instance, the distance of all shelters from Natura 2000 sites (variable of the environmental sub-index) is quantified and the distances are ranked in 3 scales, representing a different level of vulnerability. On the other hand, the type of road network (variable of socio-economic sub-index) is qualitatively assessed and scored accordingly. The VI is estimated with Eq. (1) obtained from Kontogianni et al., 2018. However, the novelty of this study lies on the fact that the variables are not scored through literature review but via consideration of the on-site visits, questionnaires and interviews, hence accurately representing the real-time conditions of the examined shelters.

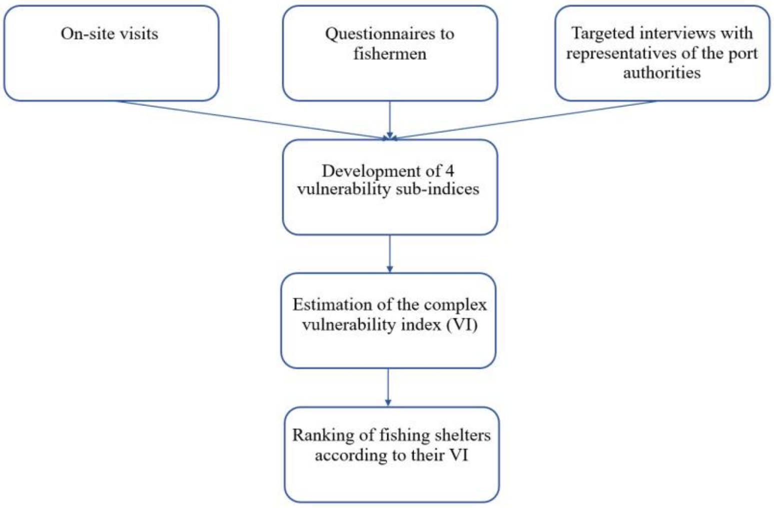


**Fig. 1.** Steps of the proposed methodology for the estimation of the shelters' vulnerability index (VI) and their respective ranking.

$$VI = w_{phys} * norm\left(\sum_{n}^{1} phys\right) + w_{env} * norm\left(\sum_{n}^{1} env\right) + w_{infr} * norm\left(\sum_{n}^{1} infr\right) + w_{soc-ec} * norm\left(\sum_{n}^{1} soc-ec\right) \quad (1)$$

where the norms are the normalized aggregated values for the 4 sub-indices, and the $w_{phys}$, $w_{env}$, $w_{infr}$, $w_{soc\text{-}ec}$ denote the weights for the 4 sub-indices. In this study, the weights are equal for all indices.

## 3. Results – Conclusions

The results of the complex VI indicate that the shelters of the western part of the island are more vulnerable compared to the ones located in the southern and south-eastern part. In particular, the shelters of Ag. Georgios and Pafos (marked as1 and 2 in Fig.2 respectively) are the most vulnerable, with high scores of vulnerability in 3 out of the 4 sub-indices (i.e. all except for the environmental sub-index). The reason for this result is their remote location, high wave heights and lack of repairs. On the other hand, in the southern and south-eastern part, funding was allocated for repairs and improvement of the shelters, thus demonstrating lower vulnerability.


**Fig. 2.** Complex VI for the 16 fishing shelters of Cyprus.

The results of the case study show that the proposed index is capable of not only providing the policy- and decision-makers with information about the overall VI of the shelters, and the factors leading to this VI, but also about the importance of the on-site visits and stakeholders' engagement in the process of vulnerability assessment. Without this components, the assessment lacks real-time information that actually reflect current vulnerability. For this reason, the VI constitutes a powerful tool for the stakeholders in their effort to design adaptation pathways, allocate funds and prioritize interventions.

**References**

Kontogianni A, Damigos D, Kyrtzoglou T, Tourkolias C, Skourtos M (2018) Development of a composite climate change vulnerability index for small craft harbours. Environmental Hazards, 18, 1-18, 10.1080/17477891.2018.1512469

# Advanced Multi-Area Approach for Coastal Vulnerability Assessment

Christina TSAIMOU[1], Georgios KAGKELIS[1], Andreas PAPADIMITRIOU[1], Vasiliki CHALASTANI[1], Panagiotis SARTAMPAKOS[2], Michalis CHONDROS[1], and Vasiliki TSOUKALA[1]

[1] Laboratory of Harbour Works, Department of Water Resources and Environmental Engineering, School of Civil Engineering, National Technical University of Athens (NTUA), Zografou 15780, Greece.
email: ctsaimou@gmail.com (for author 1)
email: giorgos.kagkelis@gmail.com (for author 2)
email: andrewtnt@mail.ntua.gr (for author 3)
email: vanesachala@hotmail.com (for author 4)
email: chondros@hydro.ntua.gr (for author 6)
email: tsoukala@mail.ntua.gr (for author 7)

[2] NIREAS Engineering, 1-3 Skra Str., Athens, 17673, Greece
email: sartabakos@yahoo.gr (for author 5)

ABSTRACT

Integrated Coastal Zone Management (ICZM) policies require a comprehensive evaluation of the complex coastal spatial and temporal characteristics. Stresses induced by natural hazards, human forces and the ever-changing climate are inherently linked with the coastal vulnerability concept that is elaborated through the employment of multi-faceted ICZM practices. Currently, advances in Geographic Information System (GIS) applications enable detailed examination and visualization of the output produced by coastal vulnerability analyses. The present paper pursues to promote advances for assessing coastal vulnerability by investigating segregation of distinct areas identified along a coastal zone into sub-sections and classification of vulnerability parameters aiming at applying a GIS-based multi-area approach. Towards this, the case study of the Coastal Zone of the Municipality of Thivaion, located at the Northeastern Corinthian Gulf of central Greece is examined. This zone encloses six (6) areas of particular interest where vulnerability assessment is prerequisite in terms of a powerful ICZM program. The study allows for robust vulnerability assessments that help decision makers to undertake ICZM actions.

## 1. Introduction

Coastal areas are challenged with maintaining the brittle balance of the interactions arising from natural, environmental and human-induced pressures, as well as the ever-changing climate. Decision-makers pursue to manage these conflicting factors by developing powerful Integrated Coastal Zone Management (ICZM) strategies that are focused on investigating coastal vulnerability and susceptibility to disturbances. In fact, assessing vulnerability of coastal zones is a complex task that requires a multi-dimensional understanding of the dynamic characteristics of coastal systems. Current practices (e.g. Ružić et al., 2019) applied for assessing coastal vulnerability are established upon principal research that encloses the estimation of physical and socio-economic parameters. Given that vulnerability assessment has evolved to a mature science, advances that improve existing methodologies, are a prerequisite to enhance ICZM practices. Therefore, this paper is focused on promoting a flexible multi-area approach that enables a detailed vulnerability assessment for ICZM of coastal zones that consist of various areas of particular interest. The approach includes further segregation of the distinct areas as well as application of various classification techniques of the vulnerability parameters.

## 2. Methodology

To implement a holistic ICZM program for managing various areas that belong to a single authority, the approach presented herein refers to the establishment of a comprehensive vulnerability framework that seeks to examine the multiple stressors influencing each distinct coastal area while investigating their spatial and temporal dependency. Towards this, further segregation of each area is required for a detailed analysis to address the physical (e.g. hydrological and geomorphological features, wave climate and sediment transport), environmental (e.g. distances from critical habitats) and socio-economic (e.g. land use) discrepancies identified along the areas under investigation. Thereafter, estimation of vulnerability parameters is applied individually for all defined sections after gathering all the necessary information through monitoring approaches, field measurements, inventory and existing databases, as well as conducting relative data analyses (e.g. numerical simulations, statistical and Geographic Information System - GIS analyses, etc). To produce an adjustable vulnerability metric system for scoring the estimated parameters while considering the different spatial scales where vulnerability assessment methodologies can be applied, advanced analyses are implemented to investigate values distributions and apply classification techniques incorporated into GIS-based visualization procedures.

## 3. Applications and results

Within the context of the present research, the case study of the coastal zone of the Municipality of Thivaion located at the Northeastern Corinthian Gulf of central Greece was examined. The coastal zone under examination, which consists of separate coastal systems, belongs to a single regional management authority, where development policies are currently promoted in terms of facilitating an effective ICZM. Six (6) distinct areas of particular interest have been identified at the zone under investigation and, consequently, multi-area vulnerability assessment approaches are essential to achieve a holistic ICZM program. These areas are further divided into 25m-length sub-sections for a detailed vulnerability analysis aiming at further investigating the physical, environmental and socio-economic discrepancies identified along the individual coastlines.

Two (2) classification approaches are presented herein to investigate the importance of applying proper scoring scales for a GIS-based visualization of the vulnerability parameters: a) quantile approach where each class includes approximately the same number of estimated values and b) equal interval approach where the range of values for each individual class is the same. Fig. 1 illustrates, indicatively, the vulnerability results for the parameter of significant wave height for Sarantis Beach, which is one of the 6 areas of particular interest of the coastal zone of the Municipality of Thivaion. The outcome indicates that vulnerability assessment results vary depending on the classification method.

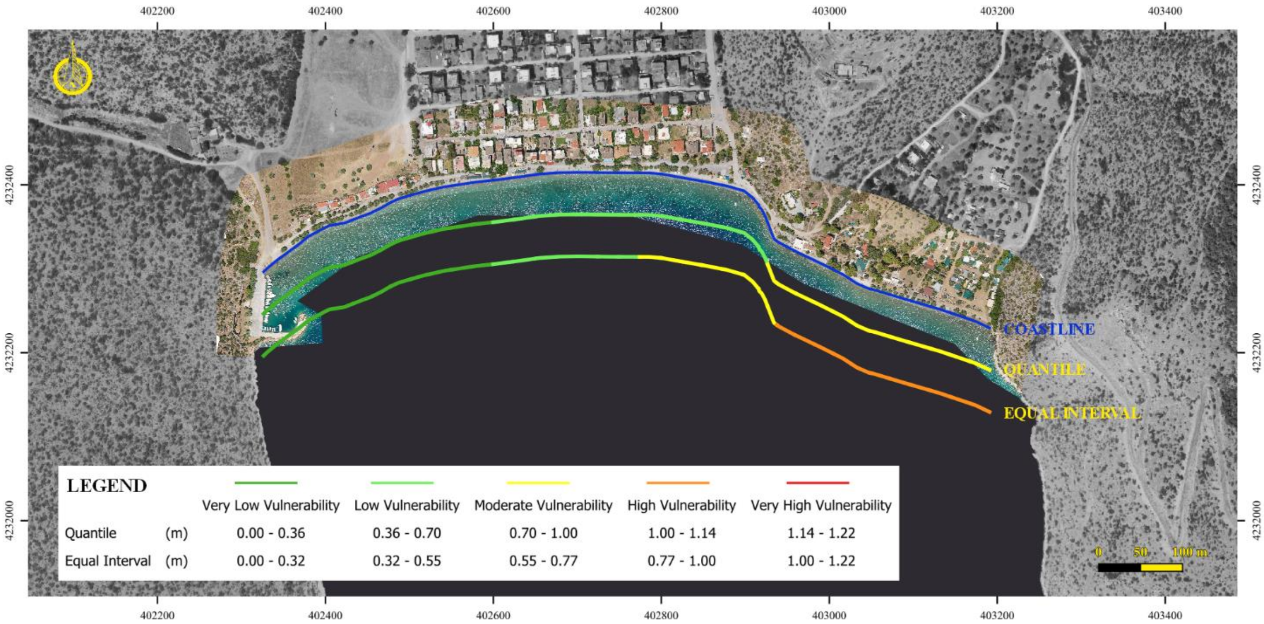


**Fig. 1.** Vulnerability of Saranti Beach in terms of the significant wave height for two classification approaches: a) quantile and b) equal interval.

## 4. Conclusions

The overall investigation highlights the significance of implementing detailed vulnerability assessment approaches for ICZM of multiple distinct areas since the multi-dimensional conflicting stressors affect coastal areas in different ways. Moreover, engaging advanced procedures for classifying and scoring estimated parameters tackles the difficult task of producing a reference system for assessing coastal vulnerability.

**Acknowledgements**

This research was funded by the Municipality of Thivaion within the context of the project "Sustainable Development Plan and Integrated Coastal Zone Management for the Municipality of Thivaion through consideration of coastal vulnerability and potential effects of climate change" (Special Account for Research Funding, National Technical University of Athens - NTUA, No.: 91006700).

**References**

Ružić I, Jovančević SD, Benac C, Krvavica N (2019) Assessment of the Coastal Vulnerability Index in an area of complex geological conditions on the Krk Island, Northeast Adriatic Sea, Geosciences, 9, 219.

# Evaluation of emerging behaviours on anthropogenic shores with a cellular automata model

Manuel TEIXEIRA[1], Erik M. HORSTMAN[1], Kathelijne M. WIJNBERG[1]

[1] University of Twente, The Netherlands
email: m.teixeiramanion@utwente.nl
email: e.m.horstman@utwente.nl
email: k.m.wijnberg@utwente.nl

ABSTRACT

This study aims to develop a model to explore the emerging morphological development of anthropogenic shores. We extended an existing Cellular Automata model for the combined development of Dunes, Beaches and Vegetation (DuBeVeg) by including longshore sediment transport and coastline retreat, sand armouring of the beach, and the formation of beach scarps due to wave action. These processes were combined with aeolian, hydrodynamic, groundwater, and vegetation dynamics that were already represented in the model. The extended model was evaluated for a schematized version of the Sand Motor, a mega-nourishment in front of the Dutch coast. The simulated scale and types of dunes compared well with the real dunes that have developed on the Sand Motor since its construction in 2011. These preliminary results show that the extended model can represent the development of mega-nourishments realistically and can be used to assess the goals of such anthropogenic shores for different configurations and scenarios.

## 1. Introduction

Nature-based solutions have been applied at sandy coastlines for several decades, by continued sand nourishments for maintaining coastal flood protection. This is especially the case in The Netherlands, where it has been national policy to maintain beaches and dunes by regular sand nourishments. Recently, the scale of sand nourishments has been upscaled by several orders of magnitude, significantly modifying the original coastal landscape (i.e. creating Anthropogenic Shores (AS)). Examples of such mega nourishments are the Sand Motor and Hondsbossche Dunes at the Dutch coast. Cellular Automata (CA) models are a promising tool to study the beach-dune morphology that emerges at such mega-nourishments from the combined effects of aeolian processes, hydrodynamics, groundwater dynamics and vegetation dynamics, as well as the biophysical interactions between these processes. However, a realistic representation of the development of mega-nourishments with CA models is not yet available as some relevant physical processes for AS have not been incorporated yet in CA.

## 2. Methodology

The Sand Motor (SM) (de Vriend et al., 2014; Stive et al., 2013) is used as a case study for the extension of the DuBeVeg model to simulate the development of this AS over its first decade after construction. The SM is an example of an AS where the coastal landscape was significantly changed by a one-off local mega-nourishment. The SM is a feeder-type nourishment, forming a temporary coastal feature that will evolve freely and will disappear over time while feeding the adjacent coastline and dunes through natural sand transport processes.

The DuBeVeg model needed adaptation for its application to AS. In previous implementations of DuBeVeg, the beach was considered in an equilibrium state. Therefore, longshore variations of the beach morphology were not considered. However, AS are characterized by a non-equilibrium planform shape and a longshore variability of the morphology. To include this longshore variability and to simulate shoreline retreat of mega-nourishments, the analytical solution of the Pelnard-Considere diffusion equation was integrated in DuBeVeg (Arriaga et al., 2017). This equation imposes shoreline diffusion according to a Gaussian function, following the observed evolution of the shoreline of the SM (Roest et al., 2021). The diffusion rate of the shoreline varies with time depending on the initial shoreline shape and the diffusion coefficient. The diffusion coefficient depends on the local wave climate and the depth of closure, for this model we used the observed diffusion coefficient for the SM of 0.022 $m^2/s$ (Arriaga et al., 2017).

Another process relevant for the development of AS but not yet considered in DuBeVeg is scarp formation of elevated nourishments. Scarps are formed in the cross-shore direction because of the steep slope of the newly created beach profile and the elevated height of the berm. Ongoing wave dynamics erode the seaward side, causing a vertical difference between the eroding shoreface (now at mean sea level) and the high berm. Scarps are observed at the SM during summer conditions, when wave conditions are mild. These scarps are eroded in winter due to increased storm surges (van Bemmelen et al., 2020). Scarp formation was represented in DuBeVeg by lowering the cross-shore profile below surge levels with an equilibrium profile that is less steep than the angle of repose. Then, a vertical scarp results from the connection between the remaining berm and the eroding shoreface. The angle of repose determines the final shape of the scarp.

Lastly, the use of an offshore sand supply for mega-nourishments is relevant for the aeolian dynamics. Coarser shell material in the nourished sand gets exposed when the finer sand is transported away, forming an armoured layer at the surface of the mega-nourishment. This armouring was included in DuBeVeg by reducing the probability of erosion of the area where offshore sand was originally deposited. This effect was applied to the original surface of the nourishment and below. New sand deposits were schematized to have a higher probability of erosion, comparable to the original beach.

## 3. Preliminary results & outlook

The preliminary results show that the processes added to the model, combined with the previously included processes, can produce realistic predictions of the development of the SM. The Gaussian function that is implemented to represent longshore transport successfully represents the retreat of the SM in a 10-year simulation (Fig. 1). The simulated retreat of the shoreline at the center of the mega-nourishment was 360 m, while the observed retreat was 390 m. Dune shapes, dimensions and spacing simulated with the extended DuBeVeg model also agree with the dune formation observed at the SM over the past 10 years. The initial flat surface is transformed into a Nebkha-dune landscape, with simulated embryo dune lengths ranging from 2 to 10 m and heights of up to 1 m (Fig. 2). These results indicate that the extended DuBeVeg model can be used to effectively simulate the morphological development of mega-nourishments. The model can thus be used to assess the realization of the intended goals of mega-nourishments for different configurations and scenarios, e.g. permanent vs. transient nourishments, or different heights and dimensions of the initial nourishment.

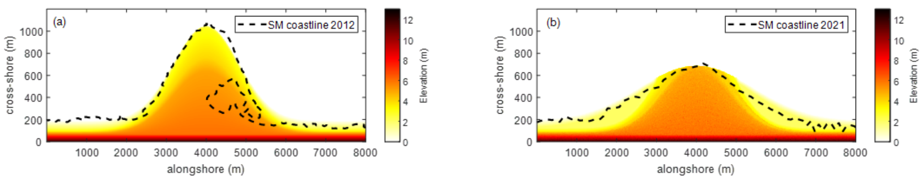


**Fig 1**. (a) Initial topography, (b) final topography after a 10-year simulation.

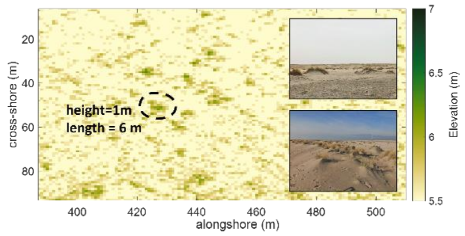


**Fig 2.** Model output of the simulated dune field. Photo inserts show similar dune shapes observed in the field.

**References**

Arriaga J, Rutten J, Ribas F, Falqués A, Ruessink G (2017) Modeling the long-term diffusion and feeding capability of a mega-nourishment. Coastal Engineering, 121, 1–13.
De Vriend H, van Koningsveld M, Aarninkhof SGJ (2014) “Building with nature”: The new Dutch approach to coastal and river works. Proceedings of the Institution of Civil Engineers: Civil Engineering, 167 (1), 18–24.
Galiforni Silva F, Wijnberg, KM, de Groot AV, Hulscher SJMH (2018) The influence of groundwater depth on coastal dune development at sand flats close to inlets. Ocean Dynamics, 68 (7), 885–897.
Keijsers JGS, de Groot AV, Riksen MJPM (2016) Modeling the biogeomorphic evolution of coastal dunes in response to climate change. Journal of Geophysical Research: Earth Surface, 121, 1161–1181.
Roest, B, de Vries, S, & de Schipper, M (2021). Observed Changes of a Mega Feeder Nourishment in a Coastal Cell: Five Years of Sand Engine Morphodynamics. Journal of Marine Science and Engineering. 9,37.
Stive MJF, de Schipper MA, Luijendijk AP, Aarninkhof SGJ, van Gelder-Maas C, van Thiel de Vries JSM, de Vries S, Henriquez M, Marx S, Ranasinghe R (2013) A new alternative to saving our beaches from sea-level rise: The sand engine. Journal of Coastal Research, 29 (5), 1001–1008.
Van Bemmelen CWT, de Schipper MA, Darnall J, Aarninkhof SGJ (2020) Beach scarp dynamics at nourished beaches. Coastal Engineering, 160, 103725.

# Predicting Sediment pickup function using Genetic Programming

Ali Pourzangbar, Maurizio Brocchini

Dipartimento di Ingegneria, Civile, Edile e di Architettura, Università Politecnica delle Marche, Ancona – Italy
email : a.pourzangbar@univpm.it (Ali Pourzangbar)
email : m.brocchini@univpm.it (Maurizio Brocchini)

ABSTRACT

We propose a novel formula to predict the sediment pickup rate over plane beds for both low and high flow conditions. Starting from Van Rijn's (1984) model, improvements are made to resolve two weaknesses, i.e. (1) its low accuracy under high-flow conditions and (2) its prediction of zero pickup for $\theta < \theta_{cr}$, this not matching observations. Our formula, not relying on the shear-excess concept, has been developed by using Genetic Programming (GP) on a wide experimental database built from the published literature. Our formula improves predictions of literature ones.

## 1. Introduction

The sediment pick-up rate, $Pr$, is defined as the sediment particles, in volume or mass, eroded per unit bed area and time (Cheng, 2016) and can be made dimensionless as follows: $\emptyset_{Pr} = Pr/\rho_s((s-1)gd_{50})^{0.5}$, where $s = \rho/\rho_s$ is the fluid to sediment density ratio, $g$ is gravity acceleration and $d_{50}$ is the mean sediment diameter. Because of the complexity of the turbulence structure and fluid-particle interactions involved in the entrainment and deposition processes, a complete theoretical description of the particle pickup process is not yet feasible (Emadzadeh and Cheng, 2016; Van Rijn, 1984). Therefore, experimental research has been exploited by many researchers to predict the pickup rate under different bed and flow conditions such as low-velocity flows ($\bar{u} \leq 1.5m/s$) (Van Rijn, 1984) and high-velocity flows ($\bar{u} > 1.5m/s$) (van Rijn et al., 2019). Many studies, like those proposed by Van Rijn (1984, 2019), represented the pickup rate based on the dimensionless transport-stage parameter $T = \left((\theta - \theta_{cr})\ /\theta_{cr}\right)$, where $\theta_{cr}(= 0.047)$ is the critical Shields parameter. Recent literature suggest some inadequacy of shear-excess-based formulae, which predict zero pickup rate for stresses below the critical one (e.g. Camenen and Larson, 2005; Cheng, 2016). On such grounds some new formulae are being proposed, which do not rely on a critical shear stress.
Among them, of some interest, also because simple to use in depth-averaged solvers, is that by Cheng and Emadzadeh (2016) who proposed a pickup function for the plane bed conditions based on the densimetric Froude number $Fr_* = \bar{u}/\sqrt{(s-1)gd_{50}}$, which is defined based on the depth-averaged velocity $\bar{u}$ and the dimensionless particle diameter $d_*$. Table 1 summarizes some well-known formulae used to predict $\emptyset_{Pr}$ over plane beds.

Table 1. Some formulae for the dimensionless pickup rate

| | | | |
|---|---|---|---|
| Van Rijn (1984) | $\emptyset_{Pr} = 0.00033\ d_*^{0.3}T^{1.5}$ | Eq. 1 | • This formula is empirical and valid for plane beds. No pickup is possible for $\theta \leq \theta_{cr}$ and it is suited to low-flow conditions, with velocities in the range of 0.5-1.5 m/s for various types of sand with $d_{50}$ values in the range of $0.1E-3$ to $1.5E-3m$. |
| Cheng and Emadzadeh (2016) | $\phi_{pr} = 0.0001\ d_*^{2.5}Fr_*\exp(-40/Fr_*)$ | Eq. 2 | • This formula, developed from experimental data collected over a plane channel bed, makes no use of thresholds. |
| Van Rijn (2019) | $\emptyset_{Pr} = 0.00033\ f_D\ d_*^{0.3}T^{1.5}$<br>$f_D = \frac{1}{\theta}\ \ if\ \theta > 1.0$ | Eq. 3 | • This formula is valid for clean, sufficiently dense packed sand without clay and a porosity in the range of $0.4 \pm 0.03$.<br>• $f_D$ is a damping factor that takes all additional effects occurring in the high-velocity range ($\bar{u} > 1.5m/s$) into account. |

## 2. Materials and methods

To get a new formula that does not rely on use of exceedance of a threshold we: 1) start from Van Rijn (2019)'s formula and assume $\theta > \theta_{cr}$, thus removing the threshold at the numerator of the transport-stage parameter, 2) balance this approximation by means of a suitable adaptation of the resulting formula, written in terms of $d_*$ and $\sqrt{\theta/\theta_{cr}^3}$, to a very wide set of experimental data. Such adaptations have been performed by means of the GP approach, while the data have been extracted from some published literature, namely, Van Rijn (1984) and Cheng and Emadzadeh (2016).

## 3. Results

The formulae of Eqs. (4&5) below have been developed for both low and high flow conditions over plane bed using GP:

$$\emptyset_{Pr} = 0.000001102 \ln(d_*) \sqrt{\theta/\theta_{cr}^3}^{\,2} \qquad \text{when } \theta \le 1.0 \qquad (4)$$

$$\emptyset_{Pr} = 0.00035\, d_*^{0.5} \sqrt{\theta/\theta_{cr}^3}^{\,0.75} \qquad \text{when } \theta > 1.0 \qquad (5)$$

Fig. 1 illustrates the performances of the formulae appearing in Table 1 and of our new formula in predicting $\emptyset_{Pr}$. Although Van Rijn's equation performs satisfactorily when $\theta \le 1.0$, it largely overpredicts the pickup rate for the data out of such range (see Fig. 2). Statistical indices, such as Root Mean Square Error (RMSE), Scatter Index (SI) and Correlation Coefficient (CC) have been used to gauge the performances of all models. Such indices show that the newly developed formula provides significantly better predictions than the available ones.

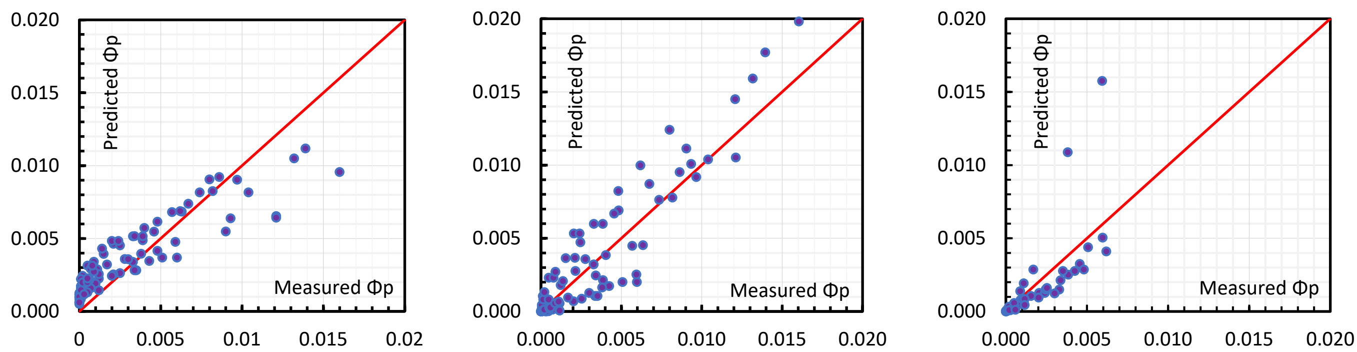


GP; Eq. 4
(CC=0.92, RMSE=0.0018, SI= 54.33%)

Van Rijn (1984); Eq. 1
(CC=0.93, RMSE=0.0017, SI=53.85%)

Cheng and Emadzadeh (2016); Eq. 2
(CC=0.74, RMSE=0.0014, SI=101.21%)

**Fig. 1.** Performances of different equations in predicting the dimensionless pickup rate for low-flow conditions ($\theta \le 1.0$); red solid line is fit line

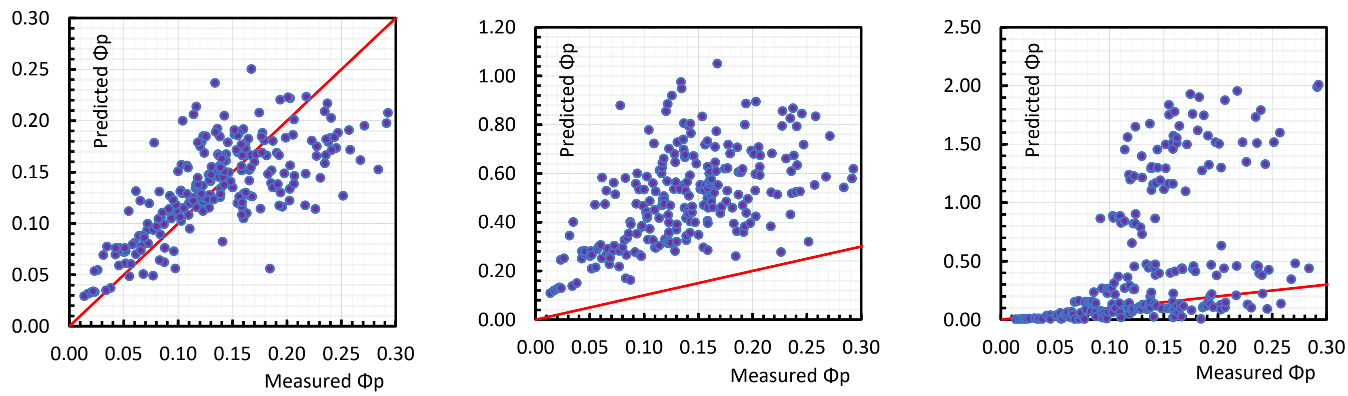


GP; Eq. 5
(CC=0.71, RMSE=0.042, SI= 25.85%)

Van Rijn (2019); Eq. 3
(CC=0.55, RMSE=0.654, SI=475.13%)

Cheng and Emadzadeh (2016); Eq. 2
(CC=0.44, RMSE=1.138, SI=826.28%)

**Fig. 2.** Performances of different equations in predicting the dimensionless pickup rate for high-flow conditions ($\theta > 1.0$); red solid line is fit line

## 4. Summary and conclusions

A new sediment pickup rate formula is proposed that does not rely on the shear-excess concept, this making its use simpler and results closer to observations, particularly for high-flow conditions. Work is underway to extend the range of validity of the proposed formula.

**References**

Camenen, B., Larson, M., 2005. A general formula for non-cohesive bed load sediment transport. Estuar. Coast. Shelf Sci. 63, 249–260.
Cheng, N.-S., 2016. Comparison of Sediment-Pickup Rates over Plane Bed and Dunes. J. Hydraul. Eng. 142, 04016057.
Cheng, N.-S., Emadzadeh, A., 2016. Estimate of Sediment Pickup Rate with the Densimetric Froude Number. J. Hydraul. Eng. 142, 06015024.
Van Rijn, L., 1984. Sediment pick-up functions. J. Hydraul. Eng. 110, 1494–1502.
van Rijn, L.C., Bisschop, R., Rhee, C. van, 2019. Modified Sediment Pick-Up Function. J. Hydraul. Eng. 145, 06018017.

# The Importance of Vertical Structures in Determining the Cross-Shore Flux of Suspended Sediment in the Swash Zone

Joost W.M. KRANENBORG[1], Robert T. MCCALL[2], Ad J.H.M. RENIERS[3], Geert H.P. CAMPMANS[4], Jebbe J. VAN DER WERF[5], Suzanne J.M.H. HULSCHER[6]

[1,4,5,6] University of Twente, the Netherlands
email: j.w.m.kranenborg@utwente.nl
email: g.h.p.campmans@utwente.nl
email: j.j.vanderwerf@utwente.nl

[2,5] Deltares, the Netherlands
email: Robert.mccall@deltares.nl

[3] Delft University of Technology, the Netherlands
A.j.h.m.reniers@tudelft.nl

ABSTRACT

## 1. Introduction

Most studies that use numerical models for wave-resolved morphodynamics in the swash zone, use depth-averaged models. These models typically represent system variables such as flow velocities and sediment concentrations in a depth-averaged or depth-integrated way. Such models then either assume a uniform vertical profile, or some other pre-determined vertical profile shape. Previous research using such models has shown that they can reproduce the depth-averaged hydrodynamics very well. However, in terms of sediment transport and morphodynamics, these models often have difficulty reproducing the sediment transport and morphodynamics (e.g. Mancini et al., 2021; Ruffini et al., 2020).

In order to investigate the importance of the aforementioned vertical structures, we have developed a depth-resolving CFD (computational fluid dynamics) model suitable for modelling sediment transport and morphodynamics in the swash zone. The model uses the Reynolds Averaged Navier-Stokes (RANS) equations and a Volume of Fluid approach and $k-\omega$ turbulence model for hydrodynamics, and includes formulations for bedload, suspended load transport, and bed evolution. More details about the model implementation and validation is presented at the IAHR world conference (Kranenborg et al., 2022).

## 2. Methodology

To investigate the importance of vertical structures, we focus on the suspended sediment flux. The cross-shore flux of suspended sediment $\boldsymbol{F}$ is defined as $\boldsymbol{F} = <\boldsymbol{uc}>$, where $\boldsymbol{u}$ and $\boldsymbol{c}$ are the depth-resolved velocity and sediment concentration, and $<.>$ defines the operation of vertically integrating a quantity over the water column. We can also define an alternative flux approximation $\boldsymbol{F_u}$, which is defined as $\boldsymbol{F_u} = <\boldsymbol{c}>\boldsymbol{U}$, where $\boldsymbol{U}$ is the depth-averaged velocity. In effect, $\boldsymbol{F_u}$ represents the flux that assumes a uniform vertical distribution in the velocity and sediment concentration. We further define the error between the *real* flux and the uniform approximation as $\boldsymbol{e} = \mathbf{abs}(\boldsymbol{F_u} - \boldsymbol{F})$.

We use the RESIST experiments, as specified by van der Zanden et al., (2019), as a scenario for the model. These experiments featured a 1:15 beach consisting of sand with $\boldsymbol{D_{50}} = \mathbf{0.2\ mm}$ and bichromatic waves with a maximum amplitude of $\boldsymbol{H} = \mathbf{0.64\ m}$ and an effective short-wave period of $\boldsymbol{T} = \mathbf{3.7\ s}$. The waves signal was designed in such a way that the signal repeated itself every 29.6 seconds. In the analysis below, we look at the time-averaged quantities over three repetition periods, denoted as $<.>_{\boldsymbol{T}}$.

## 3. Results and outlook

Figure 1 shows the fluxes of suspended sediment as predicted by the model. Panel a) shows that the fluxes, averaged over three repetition periods, presents a large difference in the swash zone. Here, the uniform approximation $F_u$ overpredicts the backwash transport compared with the actual flux $F$. This is also shown in the error $e$ which is large at this position. Panel b) shows that this is at a cross-shore position where a relatively thin sediment layer features very high sediment concentrations. Interestingly, the uniform assumption seems to work well in the breaker zone (around $x = 60 - 65$ m), where clear vertical structures seem present.

The results suggest that depth-averaged models might overpredict sediment transport in the swash due to the vertical dependence of the velocity and sediment concentrations. The overprediction possibly results from the sediment concentration being higher closer to the bed, where the flow velocities are lower due to the bed proximity. At the conference we will present our findings in more detail, elaborating on how these vertical structures in sediment concentration and velocity behave at different stages in the swash.

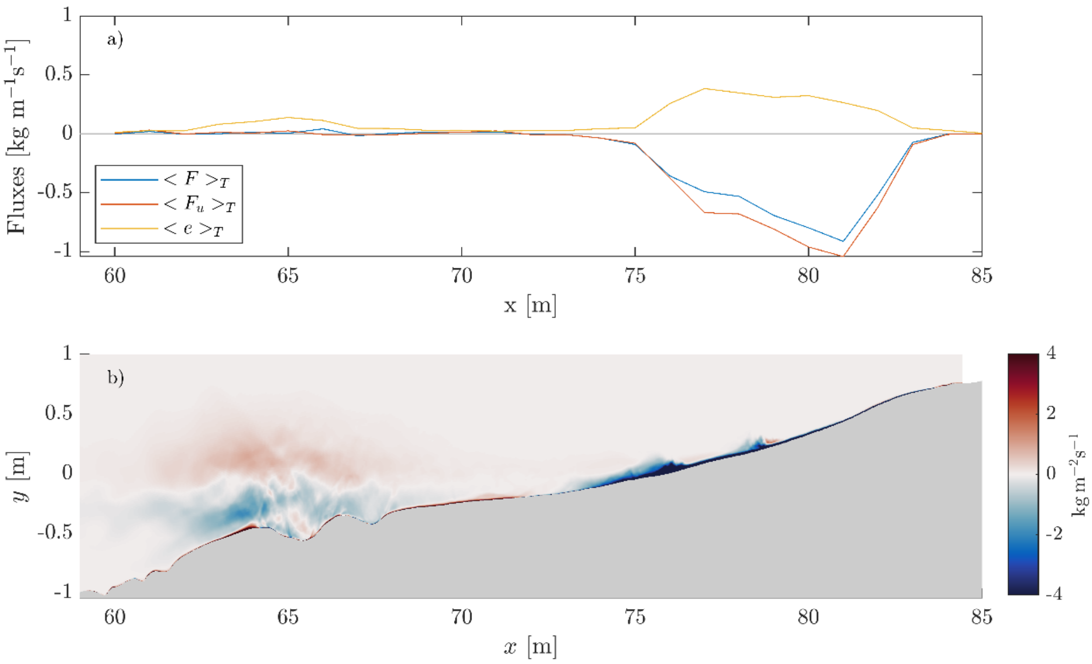


**Fig. 1.** Panel a) shows the time-averaged fluxes $\boldsymbol{F}$, $\boldsymbol{F_u}$ and the error $\boldsymbol{e}$ between them. Note that the definition of $e$ is the time-averaged absolute difference and not merely the difference between $\boldsymbol{F}$ and $\boldsymbol{F_u}$. Panel b) shows the time-averaged cross-shore sediment flux in the model domain.

**Acknowledgements**

This work is part of the research program Shaping The Beach with project number 16130, which is financed by the Netherlands Organisation for Scientific Research (NWO), with in-kind support by Deltares. This work was carried out on the Dutch national e-infrastructure with the support of SURF Cooperative. We also thank Joep van der Zanden for his help with using the RESIST dataset.

**References**

Kranenborg, J. W. M., Campmans, G. H. P., van der Werf, J. J., McCall, R. T., Jacobsen, N. G., Reniers, A. J. H. M., & Hulscher, S. J. M. H. (2022). Depth-resolved modelling of suspended sediment in the surf and swash zones. *IAHR Granada*.

Mancini, G., Briganti, R., McCall, R., Dodd, N., & Zhu, F. (2021). Numerical modelling of intra-wave sediment transport on sandy beaches using a non-hydrostatic, wave-resolving model. *Ocean Dynamics*, *71*(1), 1–20. https://doi.org/10.1007/s10236-020-01416-x

Ruffini, G., Briganti, R., Alsina, J. M., Brocchini, M., Dodd, N., & McCall, R. (2020). Numerical Modeling of Flow and Bed Evolution of Bichromatic Wave Groups on an Intermediate Beach Using Nonhydrostatic XBeach. *Journal of Waterway, Port, Coastal, and Ocean Engineering*, *146*(1), 04019034. https://doi.org/10.1061/(ASCE)WW.1943-5460.0000530

van der Zanden, J., Cáceres, I., Eichentopf, S., Ribberink, J. S., van der Werf, J. J., & Alsina, J. M. (2019). Sand transport processes and bed level changes induced by two alternating laboratory swash events. *Coastal Engineering*, *152*, 103519. https://doi.org/10.1016/j.coastaleng.2019.103519

# Numerical investigation of swash-swash interaction using Nonlinear Shallow Water Equations

Fangfang ZHU[1], Nicholas DODD[2], Riccardo BRIGANTI[3]

[1] University of Nottingham Ningbo China, China
email: Fangfang.zhu@nottingham.edu.cn

[2,3] University of Nottingham, UK
email: nicholas.dodd@nottingham.ac.uk (for Nicholas DODD)
email: riccardo.briganti@nottingham.ac.uk (for Riccardo BRIGANTI)

ABSTRACT

This work presents a numerical investigation of multiple swash events using the Nonlinear Shallow Water Equations (NSWEs) to study the swash-swash interaction processes and their impacts on the beachface evolution. The multiple swash events are generated by identical solitary waves at the seaward boundary separated by various time intervals to achieve different swash-swash interactions. The results show that the weak swash-swash interaction allows the previous swash event to be nearly completed with substantial offshore sediment caused by the backwash flow leading to considerable erosion in the middle swash zone, and deposition in the lower swash zone. While in the strong swash-swash interaction, the incoming flow of subsequent wave interacts with the previous backwash flow, which reduces the offshore sediment transport, resulting in much less erosion in the upper and middle swash zone and less deposition in the lower swash zone.

## 1. Model development

The governing equations are the one-dimensional (1D) NSWEs, the Exner equation, and suspended sediment advection equation in which bed and suspended loads due to bed shear stress are included.

$$\frac{\partial h}{\partial t} + u\frac{\partial h}{\partial x} + h\frac{\partial u}{\partial x} = 0 \tag{1}$$

$$\frac{\partial u}{\partial t} + u\frac{\partial u}{\partial x} + g\frac{\partial h}{\partial x} + g\frac{\partial B}{\partial x} = -\frac{c_d u^2}{h} \tag{2}$$

$$\frac{\partial B}{\partial t} + \frac{3}{1-p}Au^2\frac{\partial u}{\partial x} = \frac{1}{1-p}(w_s c - Mu^2) \tag{3}$$

$$\frac{\partial c}{\partial t} + u\frac{\partial c}{\partial x} = \frac{1}{h}(Mu^2 - w_s c) \tag{4}$$

where $t$ – time [s], $x$ – cross-shore distance [m], $h$ – water depth [m], $u$ – depth-averaged horizontal velocity [m s$^{-1}$], $B$ – bed level [m], $g$ – acceleration due to gravity [m s$^{-2}$], $c_d$ – dimensionless drag coefficient [-], $A$ – bed mobility parameter [s$^2$ m$^{-1}$], $p$ – bed porosity [-], $w_s$ – settling velocity [m s$^{-1}$], $M$ – suspended sediment entrainment parameter [m$^{-1}$ s], $c$ – suspended sediment concentration [m$^3$ m$^{-3}$].

The specified time interval method of characteristics (STI MOC) method is used to solve Eqs. (1)-(4) simultaneously. The reader is referred to Zhu and Dodd (2020) for more information on model development.

## 2. Numerical simulation

We simulate multiple swash events driven by several identical solitary waves of height 0.6 m at the seaward boundary ($\boldsymbol{x} = \mathbf{0}$ m) over an erodible beach of $\boldsymbol{A} = \mathbf{1.7 \times 10^{-3}}$ s$^2$ m$^{-1}$, $\boldsymbol{w_s} = \mathbf{0.0313}$ m s$^{-1}$, and $\boldsymbol{M} = \mathbf{1.9368 \times 10^{-4}}$ m$^{-1}$ s. The dimensionless drag coefficient $\boldsymbol{c_d} = \mathbf{0.01}$. The beach consists of a flat part and a sloping part of slope $\tan \boldsymbol{\alpha} = \mathbf{1/15}$, starting at $\boldsymbol{x} = \mathbf{4}$ m. At $\boldsymbol{t} = \mathbf{0}$ s, water is still of free surface $\boldsymbol{\eta} = \boldsymbol{h} + \boldsymbol{B} = \mathbf{1}$ m.

The time interval $T_I$ between consecutive solitary waves is varied to achieve different swash-swash interactions. Two time interval $T_I$ values between consecutive solitary waves are used: $T_I = 6.39$ s gives strong swash-swash interactions, and $T_I = 28.73$ s gives weak swash-swash interactions, in which there are almost no swash-swash interactions.

The bed changes after two weakly interacting, and two strongly interacting waves are shown in Fig. 1 (also shown are the bed changes after one such wave). The weak interactions allow the backwash bore to develop, which creates the bed-step in the lower swash. Bed-load creates the bed-step, and is responsible for the intense erosion centered at the initial shoreline; suspended load dominates deposition seaward of the bed-step, creates a broader erosive region, also centered at the initial shoreline, and dominates deposition in the upper swash (uprush). In the weak interaction case, the bed change pattern after 2 waves is similar to that after 1 wave but with larger magnitude.

For strong interaction, the absence of intense backwash leads to the absence of intense erosion in the lower swash and of the bed-step. Bed load contributes to a broad region of deposition, while suspended load causes a broad region of erosion in the middle and lower swash zone. Only a narrow deposition region near the shoreline is resulted from suspended load. Note that in this case there is still water covering much of the bed, with much sediment still suspended. After two strongly interacting waves bed change is very similar to that after one.

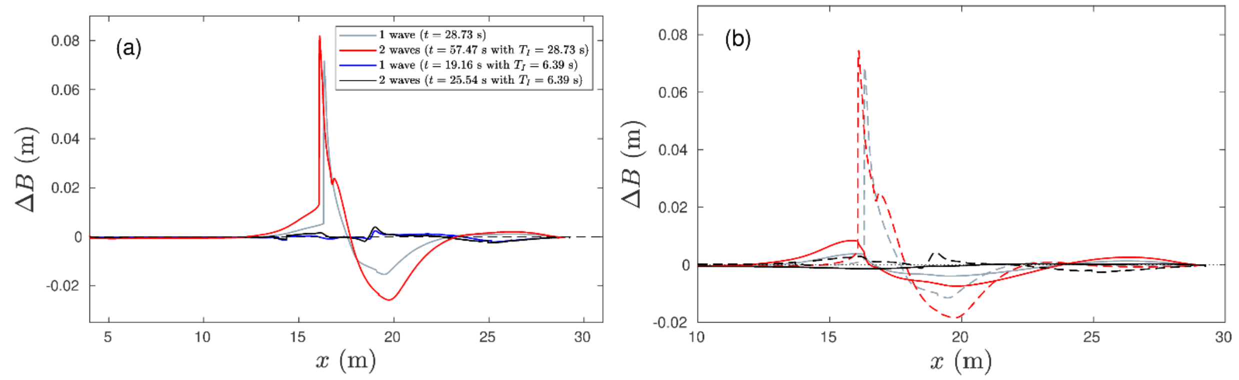


**Fig. 1.** Bed changes after 1 and 2 waves (a), and the contributions by suspended load and bed load (b). In (b), solid line: suspended load, and dashed line: bed load.

The bed changes after 10 waves are shown in Fig. 2(a), along with the contributions of bed- and suspended load (Fig. 2 (b)). Not only is the bed change larger for the weakly interacting event, but it is roughly equally distributed between bed- and suspended load. In contrast, bed-load dominates for the strongly interacting case.

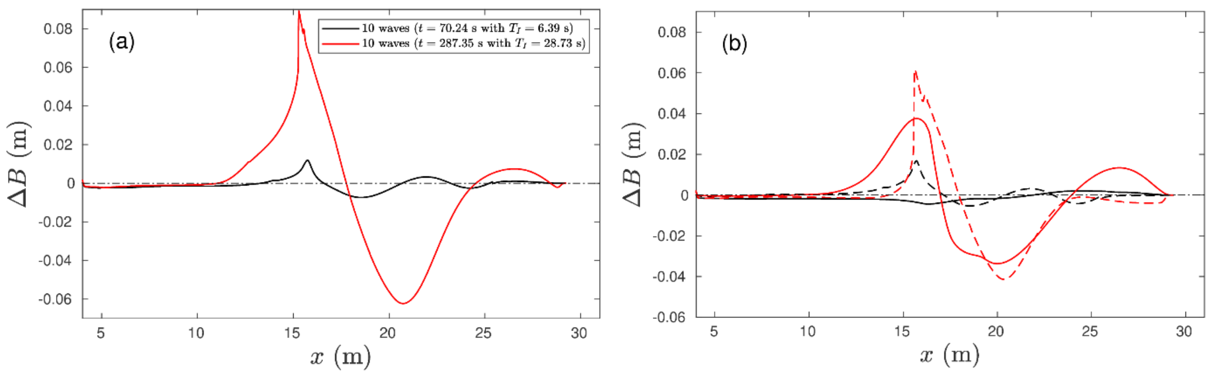


**Fig. 2.** Bed changes after 10 (a), and the contributions by suspended load and bed load (b). In (b), solid line: suspended load, and dashed line: bed load.

## Acknowledgements

This work is supported by Natural Science Foundation of China with the project code 51509135.

**References**

Zhu F, Dodd N. (2020). Swash zone morphodynamic modelling including sediment entrained by bore-generated turbulence. Advances in Water Resources 146, 103756.

# On the simulation of longshore sediment transport in the swash zone in linear wave models

Achilleas G. SAMARAS[1], Theophanis V. KARAMBAS[2]

[1] Department of Civil Engineering, Democritus University of Thrace, PC 67100, Xanthi, Greece
email: achsamar@civil.duth.gr

[2] Department of Civil Engineering, Aristotle University of Thessaloniki, PC 54124, Thessaloniki, Greece
email: karambas@civil.auth.gr

ABSTRACT

## 1. Introduction

Morphodynamic processes are among the most complex ones to accurately simulate in the coastal zone. Their evolution depends on the combined effect of waves and currents, whose interaction becomes increasingly complicated when moving within the breaker zone and towards the swash. Morphological modelling nowadays has to present a wide array of available models that attempt to describe the involved processes at different spatial and temporal scales and at varying levels of detail. The interplay between the reliable representation of the aforementioned processes, the inclusion of the interactions with coastal structures, versatility and computational effort are the factors that eventually define each model's usefulness in coastal engineering research and practice, with these factors weighted accordingly based on each application's objectives.

## 2. The modelling approach of an integrated coastal engineering model

Following a component-based modelling approach, an integrated coastal engineering model would consist by a wave module, a circulation module and a sediment transport / morphology evolution module.

In this context, wave transformation in the nearshore, including the compound wave field near coastal structures, can be simulated satisfactorily by a model based on the hyperbolic-type mild slope equation. Such a model is described in detail by Karambas and Samaras (2017). Linear models like this one, though, are not capable of describing waves in the swash and, thus, could not represent processes that are essential for shoreline evolution. Hence the need for a nonlinear wave-induced circulation model, that would act as the "link" between wave dynamics and morphodynamics modelling. The depth and shortwave-averaged 2D continuity and momentum equations used for simulating nearshore currents in such a model are expressed as:

$$\frac{\partial \zeta}{\partial t}+\frac{\partial (Uh)}{\partial x}+\frac{\partial (Vh)}{\partial y}=0 \tag{1}$$

$$\frac{\partial U}{\partial t}+U\frac{\partial U}{\partial x}+V\frac{\partial U}{\partial y}+g\frac{\partial \zeta}{\partial x}=-\frac{1}{\rho h}\left(\frac{\partial S_{xx}}{\partial x}+\frac{\partial S_{xy}}{\partial y}\right)+\frac{1}{h}\frac{\partial}{\partial x}\left(\nu_h h\frac{\partial U}{\partial x}\right)+\frac{1}{h}\frac{\partial}{\partial y}\left(\nu_h h\frac{\partial U}{\partial y}\right)-\frac{\tau_{bx}}{\rho h} \tag{2}$$

$$\frac{\partial V}{\partial t}+U\frac{\partial V}{\partial x}+V\frac{\partial V}{\partial y}+g\frac{\partial \zeta}{\partial y}=-\frac{1}{\rho h}\left(\frac{\partial S_{xy}}{\partial x}+\frac{\partial S_{yy}}{\partial y}\right)+\frac{1}{h}\frac{\partial}{\partial x}\left(\nu_h h\frac{\partial V}{\partial x}\right)+\frac{1}{h}\frac{\partial}{\partial y}\left(\nu_h h\frac{\partial V}{\partial y}\right)-\frac{\tau_{by}}{\rho h} \tag{3}$$

where $S_{xx}$, $S_{yy}$, $S_{xy}$ – radiation stresses (Copeland, 1985), $h = d + \zeta$ ($d$ – water depth, $\zeta$ – mean water elevation), $U$, $V$ – depth-averaged current velocities, $\nu_h$ – horiz. eddy viscosity coefficient, $\tau_{bx}$, $\tau_{by}$ – bottom shear stresses.

Focusing on the swash zone, it is critical to elaborate on the simulation of longshore sediment transport, as this process dominates local morphodynamics. There, the trajectory of the bore-front for obliquely incident waves follows a parabolic movement, in the direction of the net longshore flow per wave period. The mean longshore transport velocity $U_R$ at the shoreline is determined according to Baba and Camenen (2007) as:

$$U_R=\sqrt{2\,g\,R}\,\sin\Theta \tag{4}$$

where $R = 1.6H_o\xi_o$ – runup height ($H_o$ – deep water wave height, $\xi_o$ – Iribarren number), $\Theta$ – wave direction near the rundown point at depth $d = R/4$. Velocity $U_R$ is presumed constant within the swash zone, the width of which is considered as extending from $d = R/4$ (i.e., the rundown point) to $d = -R$ (i.e. the runup point).

Accordingly, it should also be noted here that in the linear wave model, the water depth within the swash zone is considered to be constant and equal to *R/4*.

The above mentioned velocity is indirectly introduced in the model by multiplying the radiation stresses in the swash zone by a factor $a_s$, based on the rationale that follows. Given that longshore velocity can be expressed analytically by Eq. (5), by assuming a linear variation of $\bar{U}$ the velocity at the shoreline can be approximated by Eq. (6); comparison of Eqs. (4)-(6) shows that the square of the ratio $U_R / \bar{U}_s$ does not deviate significantly from an empirical factor, $a_s$, expressed as in Eq. (7).

$$\bar{U} = 2.7 \frac{\gamma}{2} \sqrt{g d_b} \sin\alpha_b \cos\alpha_b \tag{5}$$

$$\bar{U}_s = 2.7 \gamma \sqrt{g d_b} \sin\alpha_b \cos\alpha_b \frac{d_s}{d_b} \tag{6}$$

$$a_s = 16 \sqrt{\gamma \xi_o^{1.8} \left( H_o / L_o \right)^{0.2}} \tag{7}$$

where $\gamma$ – breaking index, $d_b$, $\alpha_b$ – water depth and incident wave angle at the breaking point, $d_s$ – water depth at the shoreline, $L_o$ – deep water wavelength.

Flooding due to wave setup can be simulated in the wave-induced circulation model using the "dry bed" boundary condition (Militello et al., 2004; details in Karambas and Samaras, 2017 and Samaras and Karambas, 2021). The sediment transport model and the methodology adopted for morphology evolution modelling using this component based approach is described in detail in Karambas and Samaras (2017).

## 3. Validation of the simulation of longshore sediment transport

The aforementioned approach is validated through comparison with the experimental measurements of Wang et al. (2002), who investigated surf-zone currents and suspended sediment concentrations at the USACE's Large-scale Sediment Transport Facility. Experimental setup regarded a spilling and a plunging breaker case. Model results for the longshore sediment flux compare relatively well with measurements (better agreement for the spilling case), especially considering the characteristics of this approach. The model manages to capture the cross-shore distribution of the flux and to identify peaks' locations, although it appears to underestimate values at the peaks and slightly overestimate them along the rest of the profile.

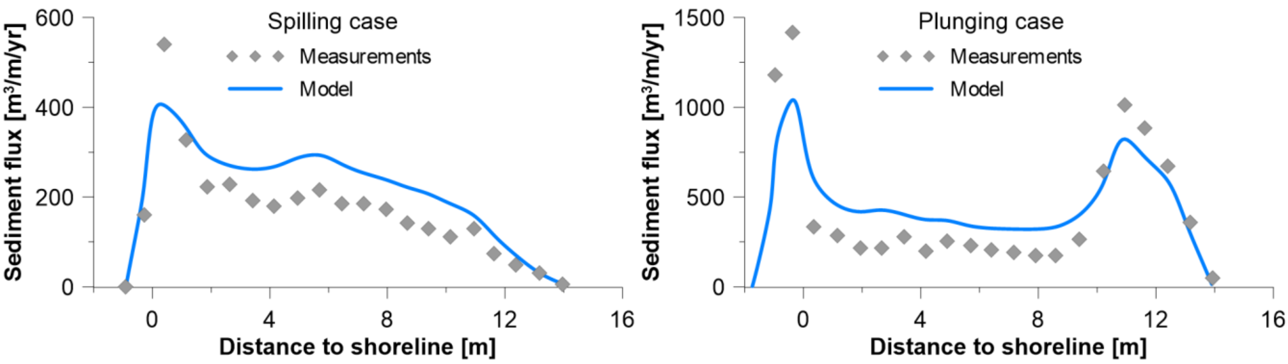


**Fig. 1.** Cross-shore distribution of the longshore sediment flux for the spilling (left) and the plunging (right) breaker cases investigated in the experiments of Wang et al. (2002). Solid lines denote the presented model's results and diamond symbols the measurements.

### References

Baba Y, Camenen B (2007) Importance of the swash longshore sediment transport in morphodynamic models, In: Kraus NC, Rosati JD, eds., Coastal Sediments '07, Louisiana, USA, 2538 pp.
Copeland GJM (1985) Practical radiation stress calculations connected with equations of wave propagation, Coastal Engineering 9, 195-219.
Karambas TV, Samaras AG (2017) An integrated numerical model for the design of coastal protection structures, Journal of Marine Science and Engineering 5, 50.
Militello A, Reed CW, Zundel AK, Kraus NC (2004) Two-dimensional depth-averaged circulation model M2D: version 2.0, USACE ERDC Report 1, Technical Documentation and User's Guide, Washington, DC, USA, 134 pp.
Samaras AG, Karambas TV (2021) Modelling the impact of climate change on coastal flooding: Implications for coastal structures design, Journal of Marine Science and Engineering 9, 1008.
Wang P, Ebersole BA, Smith ER, Johnson BD (2002) Temporal and spatial variations of surf-zone currents and suspended sediment concentration, Coastal Engineering 46, 175-211.

# Erosion modelling in the surf and swash zone: a 3D CFD model vs a 2D Shallow Water Equations Model with a Non-Hydrostatic Pressure Assumption

Ronja EHLERS[1], Weizhi WANG[2], Arun KAMATH[3], Hans BIHS[4]

[1,2,3,4] Norwegian University of Science and Technology, Trondheim, Norway
email[1]: ronja.ehlers@ntnu.no
email[2]: hans.bihs@ntnu.no
email[3]: weizhi.wang@ntnu.no; email[4]: arun.kamath@ntnu.no

ABSTRACT

Coastlines are exposed to external loads from the seaside e.g., due to impact from wind, waves and current. Storm events can result in severe erosion and affect the stability of the slope and coastal structures which eventually provokes a failure scenario and puts coastal structures at risk. The IPCC has identified the following coastal climate impact-drivers that are projected to increase in almost all reference regions: relative sea level, coastal flood and coastal erosion, where the response to ocean warming as a rise in sea level is expected to hold over decades or even centuries (IPCC, 2021). With an increase in wave energy and wave action, coastal zones need to be aware of possible impacts (Griggs & Reguero, 2021; Reguero et al., 2019; Taherkhani et al., 2020). Vertical, impermeable seawalls pose a risk for erosion at the toe of the structure but also in the cross-shore profile of the sediment bed further away from the structure. These highly reflective structures are mainly early approaches built with the purpose of sea defense but are not considered state-of-the art for coastal protection nowadays where more advantageous shapes or partly permeable types are favored. However, the study of the sediment transport processes associated with an artificial reflecting structure such as a seawall in contrast to the natural surf and swash zone can provide insight into the involved mechanisms and dominating factors. Moreover, this study evaluates a Shallow-Water-Equations (SWE) model with a non-hydrostatic pressure assumption for sediment transport modeling at the coastline while comparing it to results from a 3D Computational Fluid Dynamics (CFD) model. The case chosen in this study, a vertical seawall approached by irregular waves with experimental data from Fowler (1992), describes cross-shore sediment transport in a 2D scour scenario. The results are evaluated with focus on the initial and developing interaction between wave, sediment bed and structure, including the breaking point, wave run-up and resulting shear stresses leading to the erosive process.

## 1. Numerical Model

Reliable numerical modelling of the erosion process can assist in the decision process for coastal management measures e.g. choosing locations of erosion protection structures. This study deploys the open-source code REEF3D. Within this framework, the 3D CFD model with free surface tracking and the 2D SWE model with a pressure extension is used. Both models rely on the same algorithm regarding sediment transport while the assumptions for the hydrodynamic model are very different since variables are depth-averaged and breaking waves cannot be directly represented within the SWE model. The intention behind the use of a SWE with a non-hydrostatic pressure profile is the vastly lower computational cost in comparison to the 3D CFD model which enables erosion modelling in a larger space and time scale while compensating the lack of vertical flow resolution to a reasonable degree with the hydrodynamic pressure extension.

The sediment transport algorithm is calculated as a continuum where the bed elevation change is depicted by the Exner equation considering both bed load and suspended load where an equilibrium state results in no bed change. An excess shear stress formulation decides the bed load rate while an advection-diffusion equation governs the suspended load. The exchange between suspended and bed load is governed by an equilibrium concentration at the boundary. For sloping beds or eroded and steepened areas a shear stress reduction simulates the effect of the slope angles on the initiation of motion. An artificial sandslide is triggered for slopes reaching the angle of repose with an adjustment for the downhill / uphill effect regarding the flow direction.

## 2. Setup

The experimental setup by Fowler (1992) consists of a flume with a sediment berm with a slope of 1:15. Fowler (1992) studied setups with different locations of the seawall. The current numerical study includes two cases:

a) Case 01 is the erosion validation case S10, where the seawall reflects the waves from the start of the wave impact. The experimental data includes summarized results in terms of maximum scour depths and corresponding locations of the seawall.

b) Case 02: For the evaluation of the runup and backwash process, a 2nd setup is investigated, without an interference of a reflecting artificial structure, hence including a swash zone.

The results are evaluated regarding the differences and limitations resulting from the two basic numerical approaches used, the sediment transport process, bed shear stress, the wave breaking point, run-up and wave impact.

*2.1. Case 01: Exemplary results for the erosion validation case including a seawall*

Figure 1 and 2 show exemplary results for the erosion validation case S 10 with immediate wave impact on the structure.

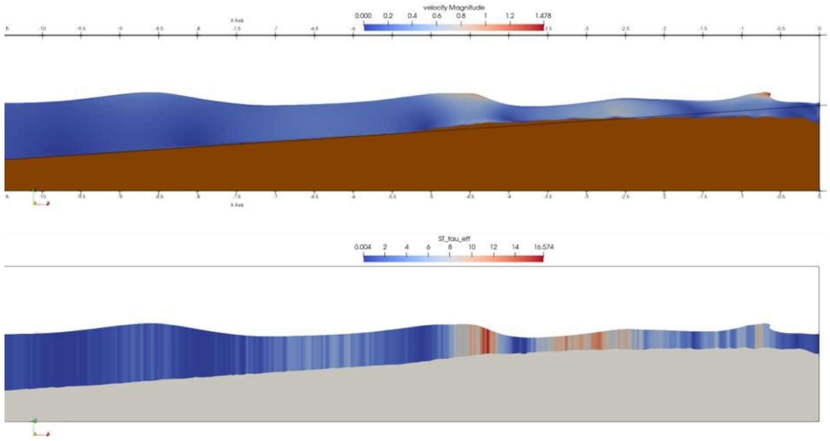

**Fig. 1.** Development of the sediment berm under wave action after t = 300 s with the CFD model. The geometrical setup and wave characteristics are according to the experiment of case S10 in Fowler (1992).

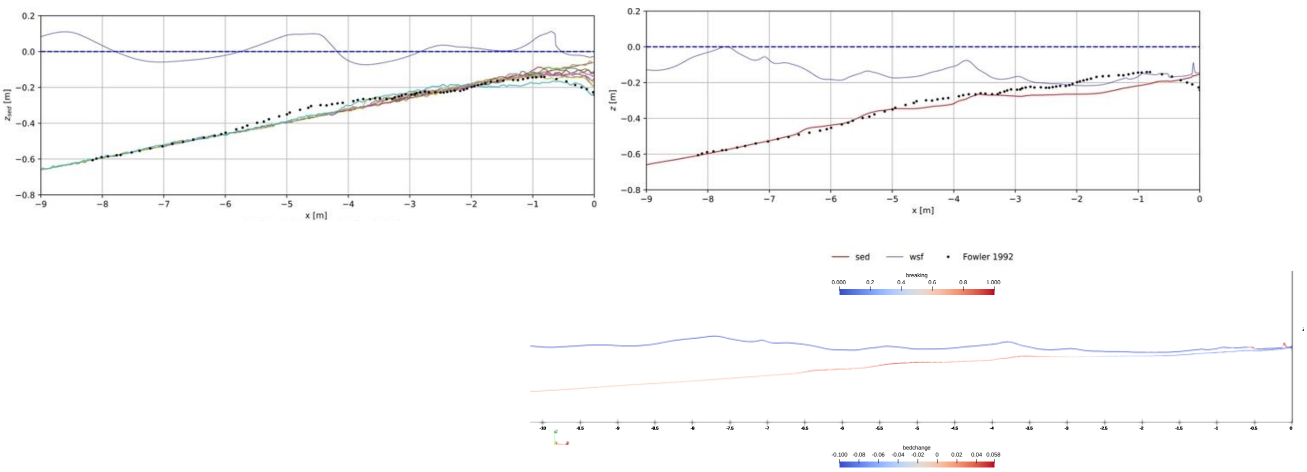


**Fig. 2.** Comparison of the exemplary results for Case 01. The x-axis describes the distance from the seawall. top left: development of the sediment berm with the CFD model; top right: developed sediment berm with SWE; bottom right: SWE model with breaking indication

**References**

Fowler, J. E. (1992). *Scour Problems and Methods for Prediction of Maximum Scour at Vertical Seawalls*. Coastal Engineering Research Center Vicksburg MS.

Griggs, G., & Reguero, B. G. (2021). Coastal Adaptation to Climate Change and Sea-Level Rise. *Water*, *13*(16), 2151. https://doi.org/10.3390/w13162151

IPCC. (2021). Summary for policymakers. In V. Masson-Delmotte, P. Zhai, A. Pirani, S. L. Connors, C. Péan, S. Berger, N. Caud, Y. Chen, L. Goldfarb, M. I. Gomis, M. Huang, K. Leitzell, E. Lonnoy, J. B. R. Matthews, T. K. Maycock, T. Waterfield, Ö. Yelekçi, R. Yu, & B. Zhou (Eds.), *Climate Change 2021: The Physical Science Basis. Contribution of Working Group I to the Sixth Assessment Report of the Intergovernmental Panel on Climate Change*. Cambridge University Press
.

Reguero, B. G., Losada, I. J., & Méndez, F. J. (2019). A recent increase in global wave power as a consequence of oceanic warming. *Nature Communications*, *10*(1), 205. https://doi.org/10.1038/s41467-018-08066-0

Taherkhani, M., Vitousek, S., Barnard, P. L., Frazer, N., Anderson, T. R., & Fletcher, C. H. (2020). Sea-level rise exponentially increases coastal flood frequency. *Scientific Reports*, *10*(1), 6466. https://doi.org/10.1038/s41598-020-62188-4

# Assessment of groundwater availability in the Rhodope aquifer under climate change conditions

Charalampos DOULGERIS, Andreas PANAGOPOULOS, Vassilios PISINARAS

Soil and Water Resources Institute (SWRI), Hellenic Agricultural Organisation, Sindos, 57400, Greece
email: ch.doulgeris@swri.gr

ABSTRACT

In this work, a groundwater assessment of the coastal aquifer of Rhodope-NE Greece is provided under current and future climatic conditions. For this purpose, the FEFLOW software package is used to compile a model based on the regional hydrogeological conceptualisation, calibrate it in steady and transient state modes, and subsequently simulate the groundwater system flow for the period 2002-2019. The calibrated model is used to assess climate change impact on groundwater balance and level fluctuation with bias-corrected climate data for the periods 2031-2050 from RCA4 regional climate model driven by 3 different global circulation models. The results indicate that the fluctuations of precipitation are affecting groundwater recharge and consequently groundwater availability, despite the fact that groundwater recharge contribution to inflows is not high.

## 1. Groundwater model setup

### *1.1. Conceptual model*

The Rhodope aquifer covers an area of approximately 180 km$^2$ and the hydrogeological conditions of the wider area were investigated in the past by several researchers (among others Petalas and Diamantis, 1999; Petalas and Lambrakis, 2006; Petalas et al., 2009; Galazoulas et al. 2015). In general, two main aquifers can be identified. A shallow semi-confined aquifer with an average thickness of 35 m and of limited potential and, an underlain thicker one (50–100 m) which is confined and hosts the regional groundwater reserves. To implement the geometric configuration in the FEFLOW environment, we consider three (3) geological layers and four (4) computational slices. In total, the computational domain area is discretised by a finite element mesh of 2,008 nodes and 2,781 triangular prism elements.

### *1.2. Steady-state model*

Fig. 1 shows the inflows-outflows and other boundary conditions applied in the model domain for the flow problem. Recharge (R=0.753 mm/d) corresponds to 5% of precipitation and together with the lateral inflows of 1 and 10 mm/d from neighbouring geological formations, they constitute the water inflow into the aquifer layers. A constant groundwater pumping of 1,567 m$^3$/d per well from 90 wells in the aquifer represent sufficiently the actual water abstraction in terms of steady-state modelling. The south-west and south east boundaries of the aquifer interact with surface water bodies (sea or lagoon) and thus a constant hydraulic head boundary condition (H=0 m) is assigned.

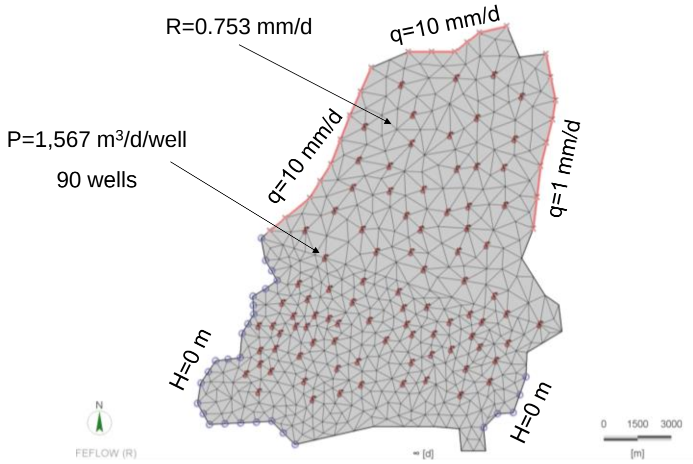


**Fig. 1.** Boundary conditions for the steady-state flow problem in the Rhodope aquifer

To evaluate the model a sloping line comparative graph of simulated vs observed hydraulic heads at control points was constructed (Fig. 2), from where we can conclude that model results are in quite good agreement with field measurements ($R^2$=0.83), and thus a reliable groundwater steady-state flow model for the Rhodope aquifer has been developed.

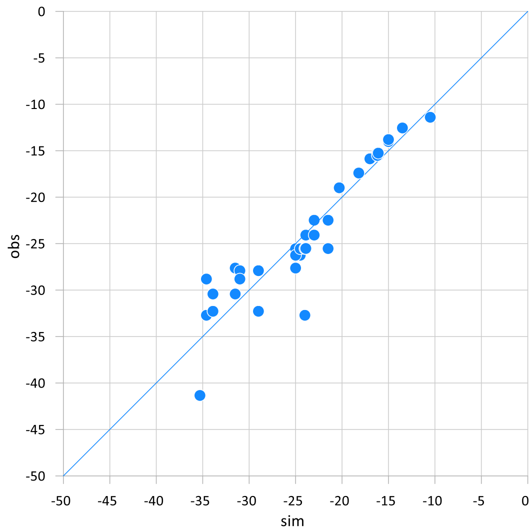


**Fig. 2.** Sloping line comparative graph of simulated vs observed hydraulic heads at control points.

### *1.3. Transient state model*

The calibration period for the transient model was 4 years and the simulated hydraulic head is compared against field observations to estimate the specific storage ($S_s$) coefficient for the lower aquifer layer (confined aquifer). More particularly, two runs of the model performed using uniform value of $S_s$, i.e. one run for $S_s = 10^{-4}$ $m^{-1}$ and another run for $S_s = 5x10^{-4}$ $m^{-1}$. Based on this modelling exercise, we were able to identify the distribution of the specific storage coefficient, while at the same time the model performance was substantially improved.

## 2. Climate change scenarios

In order to assess climate change impact on groundwater balance of Rhodope aquifer, climate data from state-of-the-art Regional Climate Models (RCMs) runs under RCP4.5 emissions scenario were collected and bias-corrected. More in detail, data from RCA4 RCM was used forced by 3 Global Circulation Models (GCMs), which were further corrected using the widely applied linear scaling and distribution mapping methods. The results demonstrate considerable variability in climate change signal depending on the GCM forcing the RCM. Nevertheless, the results demonstrate that the decreased groundwater recharge resulting from the decreased precipitation during drought periods, can affect groundwater availability, thus demonstrating the necessity for the development of climate change adaptation strategies, especially for the agricultural sector which constitutes the dominant groundwater user.

**Acknowledgements**

This research was supported by the MEDSAL Project © (www.medsal.net), which is part of the PRIMA Programme, supported by the European Union's Horizon 2020 Research and Innovation Programme and funded by the Greek national funding agency - GSRT (grant number 2018-7).

**References**

Galazoulas, E.C., Mertzanides, Y.C., Petalas, C. et al. (2015) Large Scale Electrical Resistivity Tomography Survey Correlated to Hydrogeological Data for Mapping Groundwater Salinization: A Case Study from a Multilayered Coastal Aquifer in Rhodope, Northeastern Greece. Environ Process, 2:19–35, https://doi.org/10.1007/s40710-015-0061-y

Petalas, C. and Diamantis, I. (1999) Origin and distribution of saline groundwaters in the Miocene aquifer system in coastal Rhodope area, Thrace, NE Greece. Hydrogeol J, 7:305–316, https://doi.org/10.1007/s100400050204

Petalas, C. and Lambrakis, N. (2006) Simulation of intense salinization phenomena in coastal aquifers—the case of the coastal aquifers of Thrace. J Hydrol, 324:51–64, https://doi.org/10.1016/j.jhydrol.2005.09.031

Petalas, C., Pisinaras, V., Gemitzi, A. Tsihrintzis, V. A., Ouzounis, K. (2009) Current conditions of saltwater intrusion in the coastal Rhodope aquifer system, northeastern Greece. Desalination, 237:22-41, https://doi.org/10.1016/j.desal.2007.12.020

# Local climate change assessment at five pilot sites in the Mediterranean region

Valeria TODARO[1], Daniele SECCI[2], Marco D'ORIA[3], Maria Giovanna TANDA[4], Andrea ZANINI[5], Leonardo AZEVEDO[6], Ahmed GHRABI[7], Jaime GÓMEZ-HERNÁNDEZ[8], Seifeddine JOMAA[9], George P. KARATZAS[10], Ali Kerem SAYSEL[11]

[1,2,3,4,5] University of Parma, Italy, email: valeria.todaro@unipr.it, daniele.secci@unipr.it, marco.doria@unipr.it, mariagiovanna.tanda@unipr.it, andrea.zanini@unipr.it

[6] CERENA/Instituto Superior Técnico, Universidade de Lisboa, Portugal, email: leonardo.azevedo@tecnico.ulisboa.pt

[7] Water Research and Technologies Center, Tunisia, email: a.ghrabi@yahoo.fr

[8] Universitat Politècnica de València, Spain, email: jgomez@upv.es

[9] Helmholtz Centre for Environmental Research (UFZ), Germany, email: seifeddine.jomaa@ufz.de

[10] Technical University of Crete, Greece, email: karatzas@mred.tuc.gr

[11] Boğaziçi University, Turkey, email: ali.saysel@boun.edu.tr

ABSTRACT

The objective of this study is to provide an overview of local climate change over the Mediterranean (MED) area under the scope of the InTheMED project, EU funded in the framework of the PRIMA programme. Future precipitation and temperature projections are assessed until the end of this century for five different pilot sites, located in the MED region. To this end, the outputs of 17 Regional Climate Models under the RCP4.5 and RCP8.5 scenarios are used. For each pilot site, the raw climate model data were downscaled at each monitoring station location and bias-corrected on the basis of observations recorded in a 30-year historical period. The changes in the annual precipitation are heterogeneous across the five pilot sites: a negligible variation is expected for some areas and a decrease of up to 30% for others. On the contrary, a significant increase in temperature is expected for all sites, confirming the ongoing warming in the MED region.

## 1. Introduction

InTheMED aims to implement innovative management tools and remediation strategies for inland and coastal aquifers in the MED basin with the aim to mitigate anthropogenic and climate change impacts. The analyses are performed considering five pilot sites, located between the two shores of the MED: Requena-Utiel (Spain), Tympaky (Greece), Castro Verde (Portugal), Konya (Turkey) and Grombalia (Tunisia). The present study provides future projections of precipitation and temperature in the five study areas under different scenarios. In particular, we made use of climate model data given by Regional Climate Models (RCMs) developed in the context of the EURO-CORDEX project (Jacob et al., 2014). Two scenarios, the so-called Representative Concentration Pathways (RCPs), adopted by the IPCC for the Fifth Assessment Report (AR5) were considered. In order to assess the uncertainty of the predictions, we adopted a multi-model approach in which different RCMs, which have a grid resolution of about 12.5 km, are downscaled from different General Circulation Models (GCMs, with a scale of hundreds of kms) to form a large ensemble of simulations. In the following sections, we describe the available historical and climate model data, the methods used to manage the historical series and perform the local downscaling and bias correction of climate models. Then, we present the main results and conclusions.

## 2. Data and methods

The analysis is performed considering an ensemble of 17 climate models, which are a combination of different GCMs and RCMs, and the RCP4.5 and RCP8.5 scenarios. The climate model data need to be downscaled and bias-corrected on the basis of precipitation and temperature data recorded in a historical period in order to well represent the climate variability at the local scale; we made use of the data recorded in the 30-year historical period 1976-2005. The number of available rain and temperature gauges considered for each pilot site is reported in Table 1. Since a continuous set of observations is needed to perform the bias correction, the gaps in the observations were filled following the FAO method (D'Oria et al., 2017): the missing data are replaced using linear relationships between the data in the stations to be filled and the best correlated neighboring station that presents contemporary records.

**Table 1.** Number of precipitation and temperature gauging stations for each pilot site.

| | Requena-Utiel (Spain) | Tympaki (Greece) | Castro Verde (Portugal) | Konya (Turkey) | Grombalia (Tunisia) |
|---|---|---|---|---|---|
| Precipitation station | 8 | 2 | 60 | 18 | 6 |
| Temperature station | 1 | 2 | 4 | 18 | 1 |

Then, to obtain the climate model data at the gauging station location, we adopted an inverse distance interpolation method considering the nine RCM cells closest to the specific station. Finally, the climate model data have been bias-corrected using the Distribution Mapping method (D'Oria et al., 2017) so that their cumulative distribution functions, at monthly scale, agree with the ones of the observed data in the historical period. The same correction is then applied for the future projections.

## 3. Results

The results indicate different precipitation changes in the future for the five sites. According to the annual mean, negligible or no variations are detected for some areas (Spain, Turkey, Tunisia), while moderate decreases are expected for Tympaky (Greece) and Castro Verde (Portugal). However, the inter-model variability often exceeds the mean variation in the projection period, denoting a large uncertainty in the future estimation of the precipitation. The analysis of the annual mean temperature denotes progressive warming in all the analyzed MED pilot sites. For the sake of brevity, Figure 1 reports the annual precipitation and the annual mean temperature for the Tympaky gauging station. A decrease in annual precipitation is expected in the future, more evident under the RCP8.5 scenario; the variability between the RCMs remains high. For the temperature, an evident increasing trend is shown for both scenarios. According to the median values, an increase in the mean temperature of about 1.5 °C is expected over the century under the RCP4.5 and of about 5 °C under the RCP8.5.

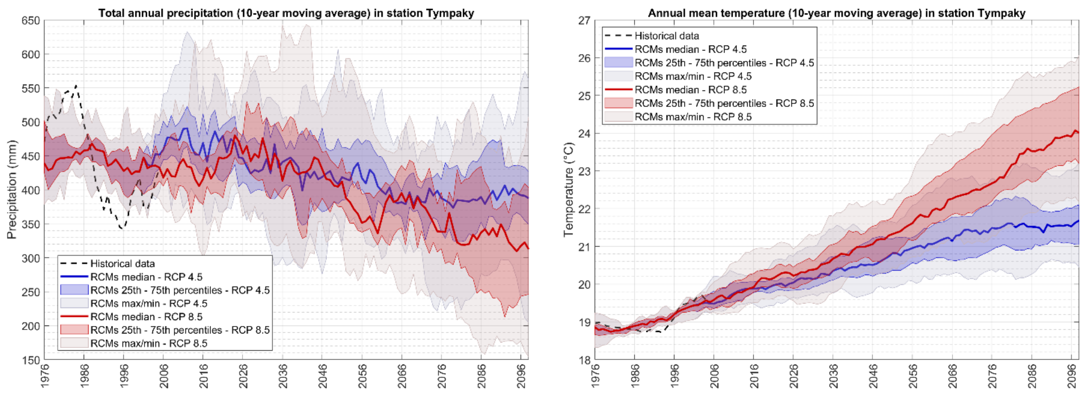


**Fig. 1.** Total annual precipitation (left) and annual mean temperature (right) in terms of 10-year moving average observed and simulated by the 17 RCMs under the RCP 4.5 and RCP 8.5 scenarios for the station Tympaky (Greece).

## 4. Conclusion

In this study, we assessed the local climate change at five pilot sites in the MED region by means of precipitation and temperature projection until 2100. Regarding the annual precipitation, no systematic changes are expected in the future, but decreases are detected for some of the investigated pilot sites. On the contrary, all RCMs agree on the progressive increase in the annual mean temperature for all the case studies, especially for scenario RCP8.5. Further analysis will concern the computation of drought indices for some pilot sites with the aim to evaluate the impact of climate change on droughts and then water resources.

**Acknowledgements**

This research is supported by the PRIMA programme under grant agreement No1923, project InTheMED. The PRIMA programme is supported by the European Union.

**References**

D'Oria M, Ferraresi M, Tanda MG (2017) Historical trends and high-resolution future climate projections in northern Tuscany (Italy). Journal of Hydrology, vol. 555, p. 708-723

Jacob D, et al. (2014) EURO-CORDEX: New high resolution climate change projections for European impact research. Regional Environmental Change 14 (2), 563–578

# Application of a Fuzzy Inference System in Decision Making for Water Resources Management

Ioanna V. ANYFANTI[1], George P. KARATZAS[1], Emmanouil VAROUCHAKIS[2], Paraskevas DIAKOPARASKEVAS[1]

[1] Technical University of Crete, School of Chemical and Environmental Engineering, Chania, Greece
email: ianyfanti1@isc.tuc.gr

email: karatzas@mred.tuc.gr

email: pdiakoparaskevas@isc.tuc.gr

[2] Technical University of Crete, School of Mineral Resources Engineering, Chania, Greece
email: varuhaki@mred.tuc.gr

ABSTRACT

The Mediterranean region has come up against the impacts of climate change during the last decades: increase of mean temperature and decrease of precipitation. In combination with the tendency of urbanization and augmentation in the needs of agri-food products, it causes direct and indirect increase in the water demand. Also, the anthropogenic pressure on surface water and groundwater sources has been intensified, as well. In many cases, beside the overexploitation, the coastal aquifers face the saltwater intrusion problem, which could limit even more the groundwater resources Limited sources and augmented needs lead to competitiveness among the different water uses and the related stakeholders, respectively. At this point, conflicting issues could be mediated by using decision support systems by enabling the assessment of different alternative solutions based on mutually agreed, predetermined criteria, thus leading to transparency and rationalism in the decision – making process. The current work discusses the development of an innovative tool for decision aiding, considering social, economic, and environmental criteria using a Fuzzy Inference System (FIS). The system is being developed based on the Tympaki coastal aquifer study site, in Crete, Greece. Each one of the considered criteria is separately approached with the suitable method: a cost – benefit analysis is elaborated for the social and economic criteria and the multi-objective optimization technique is applied for the maximization of the well pumping rates subjected to a specified value for the hydraulic head level at the observation locations to mitigate saltwater intrusion, which is considered as the environmental criterion. An issue of great importance that is raised is the heterogeneity that characterizes the criteria and the FIS is considered as a possible way to combine them in the same scale of measurement.

## 1. Methods, Tools and Results

For the description of the current situation, different simulation approaches were used for the different criteria. In addition, climate change RCPs scenarios and the corresponding Shares Socioeconomic Pathways (SSPs) were explored. The socio-economic situation was evaluated using the Cost – Benefit Analysis coupled with Bayesian Decision Analysis. The WEAP model and a statistical model were used to provide the projections of scenarios on socio-economic factors. The FEFLOW groundwater simulation model was used for the environmental criterion. The model was used within the simulation – optimization procedure, where a piece-wise linear optimization technique was used to maximize the pumping rates of the wells in the area, subjected to the hydraulic head level at the observation wells aiming at the mitigation of saltwater intrusion.

### *1.1. The socio-economic analysis*

The socio-economic assessment analysis was used to evaluate two possible policies/actions: a) $A_0$: use only groundwater and b) $A_1$: Use surface water and implement aquifer recharge. If the probability of an action is known, the procedure continues with the Cost – Benefit Analysis; otherwise, the Bayesian Risk Analysis is used. Expected loss functions are expressed for the possible decisions and state of the goal function is provided. The optimal decision, in the Cost – Benefit Analysis is the action with the minimum expected value of the loss function, while in Bayesian Risk Analysis is the action with the minimum risk. Equation (1) shows which action is riskier. If R is positive, then the decision $A_1$ is riskier than the decision $A_0$ and thus, we need to redesign the mitigation measure. On the other hand, for negative values of R, we estimate the volume of ground water needed to cover the water demands. In the Tympaki basin, for up to 15 over-pumping violations using scaled cost effects, action $A_1$ is more affordable compared to action $A_0$, involving aquifer recharge of 0.9 $Mm^3$ (18%) plus 2 $Mm^3$ (40%) from the reservoir to cover the needs, 1.1 $Mm^3$ (22%) groundwater and 1 $Mm^3$ (20%) wastewater treatment plant effluent for irrigation. For more violations the financial and environmental costs of the mitigation measure: aquifer recharge and surface water use are lower compared to groundwater use only.

$$R=R(A_1)-R(A_0) \tag{1}$$

### *1.2. The optimal pumping schemes*

The simulation – optimization procedure consists of 3 components/sub-routines: a) the groundwater modelling, b) the construction of a response matrix based on iterative simulation runs of the groundwater model, and c) the optimization of the pumping rates by using the response matrix. For the groundwater modelling, discretization of the unconfined aquifer was applied using a triangular finite element mesh. There are 2 layers and each one of them has 7670 elements and 3 slices with 3959 nodes for each slice. The depth of the model comprises 130 m deep from the sea level for the unconfined aquifer. The pumping rates $Q_i$ were imported in FEFLOW with daily time-step and with the values being different for the wet and dry season. For the construction of the response matrix, at first place, the model was run for daily pumping rates equal to 0. The results for the hydraulic head, $H_O$, in the 11 observation wells (nodes) were collected and the model was run again for 20 times, equal to the number of the pumping wells in the area. For each run, the pumping rate of a different pumping well was disturbed as $dQ_i$ and the corresponding results, $H_j$, were obtained. The response matrix A was created as shown in Eq. (2) and was used for the linear optimization problems as in Eq. (3),(4),(5).

$$A = \begin{matrix} \frac{\partial H_1}{\partial Q_1} & \cdots & \frac{\partial H_1}{\partial Q_{20}} \\ \vdots & \ddots & \vdots \\ \frac{\partial H_{11}}{\partial Q_1} & \cdots & \frac{\partial H_{11}}{\partial Q_{20}} \end{matrix} \tag{2}$$

$$\max \sum_{i=1}^{20} q_i \tag{3}$$

Subjected to:

$$h_j \geq h_{ref} \text{, for } j = 1, \ldots, 11 \text{, where } h_j = H_o + A * (Q - Q_o) \tag{4}$$

$$\text{and } 0 \leq q_i \leq UB_i, for\ i = 1, \ldots, 20 \tag{5}$$

The same procedure is repeated until two consecutive optimum solutions converge to the same values. The simulation – optimization process has been implemented for the same ten-year period, 4/2010 – 3/2020, and for four different values of the hydraulic head constraint, $h_{ref}$. The amount of groundwater savings was 35000 $m^3$/year for $h_{ref}$ = 6.5m. For, $h_{ref}$ = 6.25m the situation remained invariable, while for $h_{ref}$ = 6.75m and $h_{ref}$ = 7m an optimal solution could not be achieved.

## 2. Discussion

The results of these analyses, as well as the input data will be used to train the FIS for different simulation periods, climatic scenarios and for all the different criteria to enable decision making for a wide spectrum of possible conditions and adaptation scenarios. With the development of the FIS, all the criteria can be fuzzified through a membership function and assigned with values between 0 and 1. Then, they will be overlayed and defuzzified, giving a single output for grading the different alternatives. In this way, it is expected that the evaluation of the different criteria in each alternative is standardized in the same scale and that the FIS acts as an easy-to-handle tool.

**Acknowledgements**

This work was developed under the scope of the InTheMED project. InTheMED is part of the PRIMA programme supported by the European Union's Horizon 2020 research and innovation programme under grant agreement No 1923.

**References**

Karterakis, S. M., Karatzas, G. P., Nikolos, I. K., & Papadopoulou, M. P. (2007). Application of linear programming and differential evolutionary optimization methodologies for the solution of coastal subsurface water management problems subject to environmental criteria. *Journal of Hydrology*, *342*(3–4), 270–282.
Varouchakis, E.A., Palogos, I., Karatzas, G.P., 2016. Application of Bayesian and cost benefit risk analysis in water resources management. J. Hydrol. 534, 390-396. DOI:http://dx.doi.org/10.1016/j.jhydrol.2016.01.007

# Innovative and accessible tool to support groundwater management in the Requena-Utiel and Cabrillas-Malacara aquifers in Spain

Vanessa A. GODOY[1], Janire URIBE-ASARTA[1], J.Jaime GÓMEZ-HERNÁNDEZ[1]

[1] Universitat Politècnica de València, Spain
vaalde1@upvnet.upv.es
j.uribeasarta@gmail.com
jaime@dihma.upv.es

ABSTRACT

Random Forest, a machine learning algorithm, is used to construct a surrogate model of groundwater flow for the Requena-Utiel and Cabrillas-Malacara aquifers, in Spain. The objective is to provide an innovative, quick, open, and minimally accurate tool that allows managers and stakeholders to assess the impact of groundwater use and climate changes in the aquifers. The surrogate model has proven its versatility, ease of deployment, and high performance with very accurate approximations. In addition, it is a fast and easy-to-use method.

## 1. Introduction

Sustainability of stressed aquifers requires the definition of management rules, which need good aquifer knowledge and stakeholder participation. Numerical models are tools frequently employed to understand the behavior of the aquifer and to support its management. Although many simplifications are made during the conception of a numerical model, its development and use are neither simple nor fast, making its use not accessible for stakeholders without technical knowledge in hydrogeology. Surrogate models are easy-to-use tools able to provide quick and precise answers to aquifer users at all technical levels. These models are built with artificial intelligence methods from several training cases considering possible ranges of variations in the inputs or outputs in the aquifer. Highly specialized knowledge is required at the building stage, however, once the model is built, it can be easily deployed on a webpage to replace the original numerical model. In this work, we use the artificial intelligence method Random Forest (Breiman, 2001) to build a surrogate model of the groundwater flow of the Requena-Utiel and Cabrillas-Malacara aquifers, in Spain, which were declared as in quantitative unsustainable condition by the Jucar River Basin Authority. The aim is to provide an innovative and accessible tool to support stakeholders and managers to assess the impact of possible changes in water extraction from existing wells and the impact of rainfall variations on the piezometric levels.

## 2. Description of the surrogate model

The surrogate model was built in six steps: First, the groundwater flow of the study area was numerically modeled and calibrated using MODFLOW 2005 (Harbaugh, A.W., 2005) and FloPy (Bakker et al., 2016). The modeling was done using all available information from 1940 to 2016, with a monthly discretization. The aquifer was modeled as heterogeneous (by zones) for hydraulic conductivity and storativity, with three layers discretized into a regular mesh of square cells of 500 m x 500 m, obtaining a total of 37,719 cells arranged in 127 columns, 99 rows, and 3 layers. Several recharge zones, aquifer-rivers interaction, irrigation return flows, and pumping wells were also considered. Second, a training data set was created by generating 100 combinations of pumping rates and recharges. The recharge rate was assumed to take values in the range given by an oscillation of 40% above or below the average of the last ten years. Pumping extractions were considered to take values in the range given by one half to twice the average of the last ten years. For each combination, a numerical model was run and the results of the hydraulic heads at 100 selected locations were saved monthly from 2022 to 2051. At the end of this step, we had a training dataset with 36,000 elements, four predictor variables (month, year, multiplicative factor of recharge, and multiplicative factor of pumping rate), and 100 target variables (hydraulic head at specified locations). Third, the processed data were shuffled and separated into 2 subsets to evaluate the model's performance: 90% for training, and 10% for testing. Fourth, the dataset was trained (by feeding it with the 90% subset) and the Random Forest regression was implemented in Python by using the sci-kit-learn library (Pedregosa et al., 2011). For the sake of comparison, two other machine learning methods were also implemented and evaluated: AdaBoost (Freund & Schapire, 1997) and XGBoost (Chen & Guestrin, 2016). Fifth, predictions were done at each specified location, and the results were interpolated over the whole study area. And sixth, the surrogate model was deployed via Flask on Heroku.

## 3. Results

The performance of the surrogate model was obtained by evaluating the regression score and the mean square error for the testing subset data. The time needed to obtain a response when using the numerical or the surrogate models was also computed. Results shown that Random Forest, AdaBoost, and XGBoost performed similarly and presented high accuracy of the models against the training data. Random Forest, the method chosen to build the deployed surrogate model, not only presented high accuracy, but also the computational time was reduced by 557 times when compared to the time required by MODFLOW. Figure 1 shows a screenshot of the test version of the webpage (in Spanish) that could be used by the stakeholders to assess the impact of changes in pumping rates and rainfall on the piezometric levels.

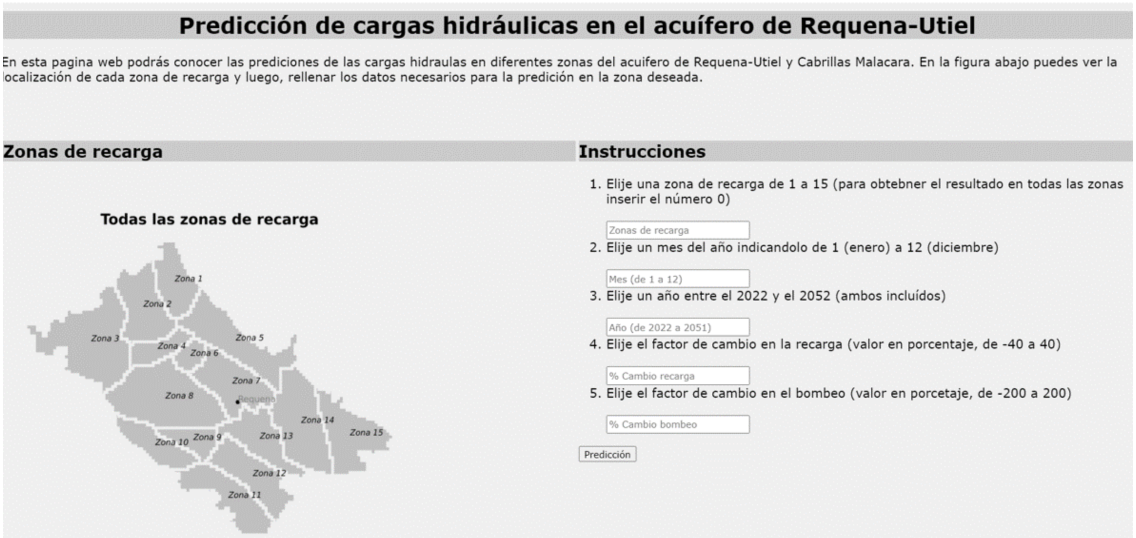


**Fig. 1 Screenshot of the test version of the webpage (in Spanish) to predict piezometric levels.**

## 4. Final comments

The different surrogate models resulted in very similar and precise approximations in the ranges of inputs and outputs for which training data were generated. A test version of the webpage was built, which could be used by the different groundwater users to predict piezometric levels and assess the aquifer response. It was concluded that surrogate models are innovative, accessible, and powerful tools to support aquifer management.

**Acknowledgments**

Research financed by the InTheMED project, which is part of the PRIMA Programme supported by the European Union's Horizon 2020 Research and Innovation Programme under Grant Agreement No 1923.

**References**

Harbaugh, A.W. (2005). MODFLOW-2005, the U.S. Geological Survey modular ground-water model -- the Ground-Water Flow Process: U.S. Geological Survey Techniques and Methods

Bakker, M., Post, V., Langevin, C. D., Hughes, J. D., White, J. T., Starn, J. J. and Fienen, M. N. (2016). Scripting MODFLOW Model Development Using Python and FloPy: Groundwater, v. 54, p. 733–739, doi:10.1111/gwat.12413. 6-A16.

Pedregosa, F., Varoquaux, G., Gramfort, A., Michel, V., Thirion, B., Grisel, O., ... & Duchesnay, E. (2011). Scikit-learn: Machine learning in Python. the Journal of machine Learning research, 12, 2825-2830.

Freund, Y., & Schapire, R. E. (1997). A decision-theoretic generalization of on-line learning and an application to boosting. Journal of computer and system sciences, 55(1), 119-139

Chen, T., & Guestrin, C. (2016, August). Xgboost: A scalable tree boosting system. In Proceedings of the 22nd acm sigkdd international conference on knowledge discovery and data mining (pp. 785-794), https://doi.org/10.1145/2939672.2939785

# Blending geostatistics and geophysics to develop the hydrogeological structure of a coastal aquifer system

Emmanouil A. VAROUCHAKIS[1], Leonardo AZEVEDO[2], João L. PEREIRA[2], George P. KARATZAS, Seifeddine JOMAA

[1]School of Mineral Resources Engineering, Technical University of Crete, Chania, Greece

[2]CERENA, Instituto Superior Técnico, Universidade de Lisboa, Portugal

[3]School of Environmental Engineering, Technical University of Crete, Chania, Greece

[4]Department of Aquatic Ecosystem Analysis and Management, Helmholtz Centre for Environment Research - UFZ, Magdeburg, Germany
email: evarouchakis@isc.tuc.gr

ABSTRACT

Geostatistics and geophysics can be successfully combined in interpreting the hydrogeological characteristics of an aquifer system. This work aims at the development of a set of plausible 3D geological models combining 1D and 2D geophysical profiles, spatial data analytics and geostatistical simulation techniques. The resulting set of models represents possible scenarios of the structure of the coastal aquifer system under investigation. and identify regions associated with higher uncertainty.

## 1. Method

Groundwater resources in Mediterranean coastal aquifers are under threat from salt water intrusion and climate change. This situation is deteriorated by the absence of sustainable groundwater resources management plans. Management and monitoring of groundwater systems requires interpretation of hydrogeology. This work employs the development of a 3D geological model from geophysical data (Fig. 1) using geostatistical and simulation techniques such as 3D Kriging and Sequential Gaussian Simulation (SGS) to provide the structure of a coastal aquifer system. A geophysical survey provided cross sections profiles in the study area that were inverted to hydraulic conductivity and electrical conductivity information. Therefore, the inverted geophysical data were used to estimate the spatial distribution of the hydraulic conductivity and electrical conductivity in the study area.

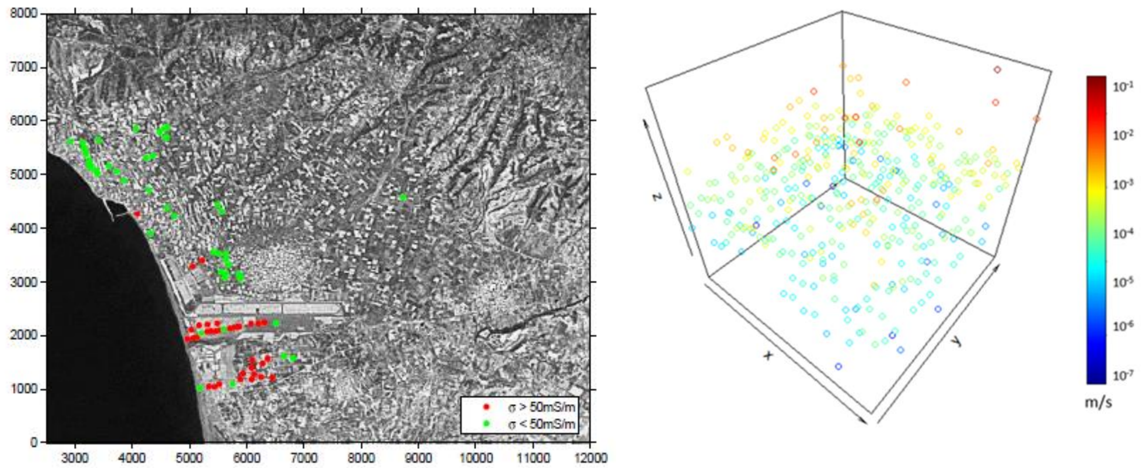


Fig. 1 a) Location map of geophysical measurements b) Inverted hydraulic conductivity data in 3D

The modified Box–Cox technique was applied to transform the data close to normal distribution to allow the application of the SGS method. The sequential Gaussian simulation (SGS) is a stochastic approach for producing equiprobable realizations (maps) of spatial distribution of a variable on a grid by means of kriging methodology. Variogram analysis was employed to investigate the spatial dependence of the monitoring data, while the simulation analysis provided the spatial distribution of hydraulic conductivity considering the bounds of estimations uncertainty.

The SGS algorithm steps are outlined below as follows:
(1) Examine if the original data follow normal distribution and apply transformation.
(2) A node at a specific location is randomly selected that has not been yet simulated.
(3) Apply 3D kriging estimation at the location and calculate the corresponding kriging variance.
(4) Draw a random value from the normal distribution, which corresponds to the simulated value.
(5) The newly simulated value is added in the dataset and the process moves to another location.
(6) Repeat the procedure above until there are no locations left.
(7) If needed, back transformation to the original data scale applies to all values.

## 2. Results

The proposed methodology exploited the spatial information from the geophysical survey on hydraulic conductivity values, to provide its spatial distribution in three dimensions inside the convex hull of the measurements (Fig. 2).

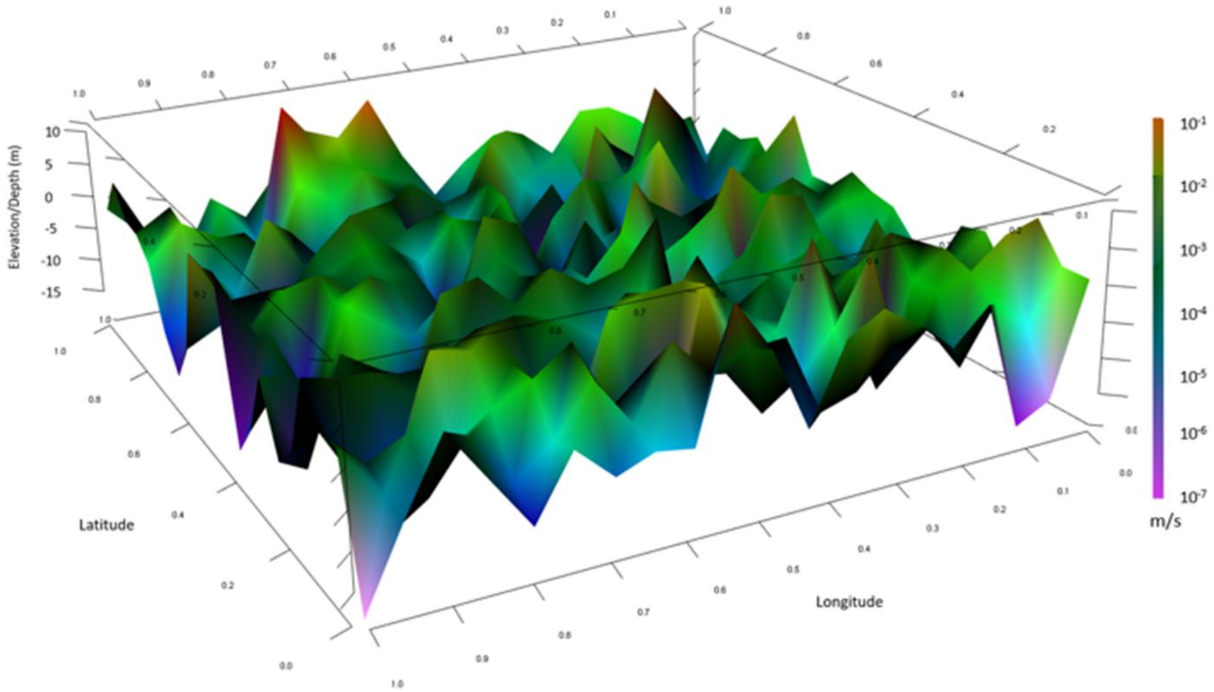


Fig. 2 Hydraulic conductivity spatial distribution in 3D

The resulting model will help to identify primary gaps in existing knowledge about the groundwater system and to optimize the groundwater monitoring network. A similar approach will be followed for the spatial analysis of the electrical conductivity data. A comparison with a numerical groundwater flow model will identify similarities and differences and it will be used to develop a typical hydrogeological model, which will aid the management and monitoring of the area's groundwater resources. This work will help the development of a reliable groundwater flow model to investigate future groundwater level fluctuations at the study area under climate change scenarios.

**Acknowledgements**
The project is funded by the General Secretariat for Research and Technology of the Ministry of Development and Investments under the PRIMA Programme (Sustain-COAST). PRIMA is an Art.185 initiative supported and co-funded under Horizon 2020, the European Union's Programme for Research and Innovation This work was also funded under the scope of the InTheMED project. InTheMED is part of the PRIMA programme supported by the European Union's Horizon 2020 research and innovation programme under grant agreement No 1923.

**References**
Pipatpan, S., and N. Blindow, 2005. Geophysical saltwater-intrusion mapping in Timbaki/Crete. Report within MEDIS: "Towards sustainable water use on Mediterranean islands: addressing conflicting demands and varying hydrological, social and economical conditions"; 114.
Varouchakis, E.A., 2021. Median Polish Kriging and Sequential Gaussian Simulation for the Spatial Analysis of Source Rock Data. Journal of Marine Science and Engineering 9(7), 717.

# Combined measurement techniques for the monitoring of hydrologic processes in the unsaturated zone

Efthymios Chrysanthopoulos[1], Christos Pouliaris[1], Ioannis Tsirogiannis[2], Petros Kofakis[3], Andreas Kallioras[1]

[1] Department of Mining and Metallurgical Engineering, Laboratory of Engineering Geology & Hydrogeology, National Technical University of Athens, Greece
email: echrysanthopoulos@metal.ntua.gr
email: pouliaris@metal.ntua.gr
email: kallioras@metal.ntua.gr
[2] Department of Agriculture, University of Ioannina, Greece
email: itsirog@uoi.gr
[3] Department of Agribusiness and Supply Chain Management, AUA, Greece
email: kofakis@gmail.com

## 1. Introduction

Soil moisture is a hydrologic parameter of paramount importance in agricultural studies, as most services in agricultural ecosystems, such as water storage, food and fiber supply, water and climate regulation, are associated with its spatial and temporal variability (Novick et al., 2022). In order to describe the state of water in the soil two types of variables are required; volume of water and water potential.

This study involves the development of an integrated monitoring programme of the above parameters, by utilizing an experimental agricultural farm of the Department of Agriculture of the University of Ioannina, in Western Greece (Arta). The various monitoring activities include: (i) vertical and spatial distribution of the volume and energy of water through the unsaturated zone; (ii) the continuous monitoring of groundwater level fluctuations; (iii) the design and development of a wireless network with several end-nodes within the field, that will facilitate the transmission of generated data from the sensors to a gateway which will act as a bridge between the monitoring infrastructure and the remote server. The communication protocol is LoRaWAN providing long-range, low-power consumption, low data rate and secure data transmission.

## 2. Monitoring of soil water content

### *2.1. TDR sensors*

Conventional sensors for point measurements of soil moisture are installed in several locations within the field in order to provide wide distribution of soil water content in the upper decimeters of unsaturated zone, which is the soil water zone. However, unsaturated zone consists of several sub-zones, each of them hosting various hydrological processes and contributing to the water balance. Complex processes, such as downward movement of groundwater, return flow to the atmosphere via evaporation and plant root uptake (Kallioras et al., 2016), cannot be monitored with conventional sensors, which have predominantly been made to observe a particular process. Custom made time domain reflectometry (TDR) probes are installed at desired depths across the unsaturated zone, offering continuous monitoring of soil water content.

### *2.2. Tensiometers*

In contrast to the soil volumetric water content, soil water potential -which is the sum of matric forces (adhesive and cohesive) and others (osmotic, gravitational and pressure)- is hardly measured in situ. This lack of observations and measurements incorporates large uncertainties into hydrological models, while most of them are based on pedotransfer functions (PTFs) to predict the parameters of water retention curve models, which relates matric potential ($\Psi_s$) to the volumetric soil moisture content ($\theta$), using empirical equations directed by a limited set of soil properties.

The reasons why $\Psi_s$ is rarely measured systematically may be due the fact that no single instrument can capture the entire range of it and existing sensing systems have a lot of limitations. For the research activities of this study, conventional tensiometers will be used for measuring matric potential up to -90 kPa, which in combination with continuous measurements of $\theta$, will grant a details about soil structure and hydrological processes.

*2.3. Pressure plate apparatus*

Apart from in situ measuring of matric potential ($\Psi_s$), the pressure plate apparatus method will be used to relate soil moisture tension and the moisture content of soils. Due to the range measurement limitations of in situ techniques, implementing the pressure plate apparatus method is going to facilitate the determination of moisture – retention on large number of samples within the field. Furthermore, the compatibility of the different methods can be demonstrated.

## 3. Monitoring of soil solution

*3.1. Sampling lysimeters (porous suction cups)*

Additionally with modern and conventional sensing technologies for soil water content monitoring, soil solution sampling and analysis is being performed using porous suction cups installed on multi-level basis. Their use in different studies to collect soil water for analytical purposes is wide. In addition, campaign-wise undisturbed soil core sampling will be performed, in order obtain porewater quality profiles along the unsaturated zone after the application of tailored water extraction techniques.

## 4. Data transmission facilities

According to the architecture of LoRaWAN network, the variety of sensors which are used in the experimental field for monitoring soil water content, groundwater level fluctuations and a climate station, are considered to be end nodes. End nodes or end devices send LoRa modulated wireless messages to the gateways. A gateway, an antenna which receives broadcasts from end devices and send data back to end devices, is installed in the vicinity of the field. The installed gateway is joined to a LoRaWAN Network Server, using a backhaul 4GLTE. The Network Server manages the gateway, the end-nodes and the applications in the entire network. In that way all the data monitored in the field are stored in a server, which facilitates their manipulation and the correlation between them.

Some of the benefits of using LoRaWAN are the significant low power for the operation of the entire network, the long range of signal transmission and reception compared to technologies like WiFi, Bluetooth or ZigBee and the low cost of end nodes with the use of open-source software. In view of these assets LoRaWAN is well suited for sensors which operate in low power mode.

In general, the application of wireless sensor networks for monitoring the majority of hydrological processes in the area of a field offers significant benefits, such as the deep understanding of dynamic processes, which could drive to the improvement of knowledge about the physical system. Also, the implementation of a wireless sensor network allows multi-parametric environmental monitoring and the storage of the data on a remote server, granting the opportunity even for real-time calculations, feeding hydrological models.

**Acknowledgements**

This research has been co-financed by the European Union and Greek national funds through the Operational Program Competitiveness, Entrepreneurship and Innovation, under the call SUPPORT OF REGIONAL EXCELLENCE (project code MIS: 5047059).

**References**

Novick K, Ficklin D, Baldocchi D, Davis K, Ghezzehei T, Konings A, MacBean N, Raoult N, Scott R, Shi Y, Sulman B, Wood J (2022) Confronting the water potential information gap, Nature Geoscience, 15, 158-164

Kallioras A, Khan A, Piepenbrink M, Pfletschinger H, Koniger F, Dietrich P, Schuth C (2016) Time-domain reflectometry probing systems for the monitoring of hydrological processes in the unsaturated zone, Hydrogeology Journal, 24, 1297-1309

# Living-lab on improving groundwater governance in the Requena-Utiel aquifer

Vanessa A. GODOY[1], Danielle SECCI[1,2], Janire URIBE-ASARTA[1], J.Jaime GÓMEZ-HERNÁNDEZ[1], Esther LÓPEZ-PÉREZ[1], Marta GARCÍA-MOLLÁ[1], Carles SANCHIS-IBOR[1], Elena LÓPEZ-GUNN[1], Adrià RUBIO-MARTIN[1], Sergio SEGURA-CALERO[1], Manuel PULIDO-VELAZQUEZ[1]

[1] Universitat Politècnica de València, Spain
vaalde1@upvnet.upv.es, j.uribeasarta@gmail.com, jaime@dihma.upv.es
estloppe@upvnet.upv.es, mgarmo@esp.upv.es, csanchis@hma.upv.es
elopezgunn@icatalist.eu, adrumar@cam.upv.es, serseca@upvnet.upv.es
mapuve@hma.upv.es

[2] Università degli Studi di Parma, Italy
daniele.secci@unipr.it

ABSTRACT

The European research projects InTheMED and eGROUNDWATER share the aim of promoting innovative and sustainable management of the Mediterranean aquifers. One of the ways to achieve this objective is the creation of dynamic spaces in which all interested actors can cooperate, experiment and evaluate innovative ideas, different scenarios and new technologies on real cases of interest. In this regard, a living lab on improving groundwater governance, coordinated by the eGROUNDWATER team with the participation of the InTheMED team, was organized including all stakeholders who play a significant role in the management of the Requena-Utiel aquifer, which is a shared pilot site of the two projects. The aim of the living lab was to identify, together with stakeholders, problems and mitigation measures, and to evaluate possible strategies to satisfy the individual needs according to a sustainable use of the groundwater resources.

## 1. Introduction

The management of aquifers all around the world is a challenging task that cannot be achieved without inclusive participation. The projects InTheMED and eGROUNDWATER are part of the PRIMA Programme and, among other things, have the complementary mission of implementing innovative, sustainable, and participatory management tools for Mediterranean aquifers to mitigate anthropogenic and climate-change threats. To do this successfully, the creation of new long-lasting spaces of social learning among different interdependent stakeholders, NGOs, and scientific researchers is crucial. A first step towards a participatory aquifer management has been taken in Requena, Spain, where a living-lab on improving groundwater governance took place on the 4th of March 2022 with the participation of 28 people related to groundwater use, protection, and research including environmental technicians, individual users, irrigation community representatives, researchers, Requena and Utiel City Hall personnel and an ONG member. The main objective of the living lab was to arrive at a diagnosis of the problem of groundwater unsustainability and perform a brainstorming exercise about possible measures, technological needs, and tool design. In this work, we share our experience on conducting such living-lab and explore its strengths and weaknesses regarding the mitigation of anthropogenic and climate-change threats.

## 2. The living lab

Based on the information obtained during the year 2021 after some interviews with the stakeholders, the living-lab was organized in three sessions as follows:

In the first session, a successful case of irrigation advisory service in groundwater management in La Mancha Oriental aquifer, about 50 km far from Requena, was presented. It was shown that the adequate management of groundwater resources can reverse the bad quantitative condition of an aquifer, provides considerable savings to the farmer, and stabilizes or even recovers piezometric levels. At the end, such presentation caused an interesting discussion about groundwater distribution and availability and aquifer recovering after management strategies.

In the second session, the main objective was to identify the problems in groundwater management and distribution. The participants were divided in two groups for a balanced participation of stakeholders and each participant, individually, was invited to write on post-it notes the main problems related to the use and management of the groundwater in Requena-Utiel; these notes were placed on a large whiteboard for conceptual mapping (Figure 1a). Next, the main problems identified by all the participants were voted in a qualitative manner through a Likert scale, from very important to irrelevant for the management of groundwater. Finally, the two groups were put together to discuss the issues identified (Figure 1b). In this session, the problems mentioned by stakeholders were, among others, lack of (reliable) information about the aquifer, lack of studies of the aquifer and its piezometric condition, lack of control, risks related to groundwater quality in the future, slowness of the public administration, illegal wells, growing demand for water, production focused on quantity and not quality, the groundwater distribution is unfair (they think they could be allowed to use much more water than they are), and the complexity of the technical documents reporting the aquifer state.

In the third session, the groups continued their discussion from the second session by brainstorming about possible measures to achieve a good condition of the aquifer, technological needs, and tool design. This session followed the same method as in the second session, but now the stakeholders wrote on post-it notes the solutions or measures to deal with the problems related to the use and management of groundwater in the Requena-Utiel aquifer. Finally, measures were voted in a double Likert scale, in terms of effectiveness (from very effective to counterproductive) and acceptability (from very acceptable to non-acceptable). At the end of the third session, the two groups were put together to discuss the measures identified. Stakeholders were very optimistic about the use of tools based on Information and Communication Technologies (ICTs) to help manage the aquifer, such as web pages or mobile applications. They also mentioned the importance of remote sensing in the correct management of irrigated areas and stressed the value of the detailed study of the aquifer, with modern tools. They demanded more control of the private wells by the Jucar River Basin Authority. And finally, they cited the need for more didactic and summarized technical reports and presentations, since they are very interested in understanding more about the real state of the aquifer

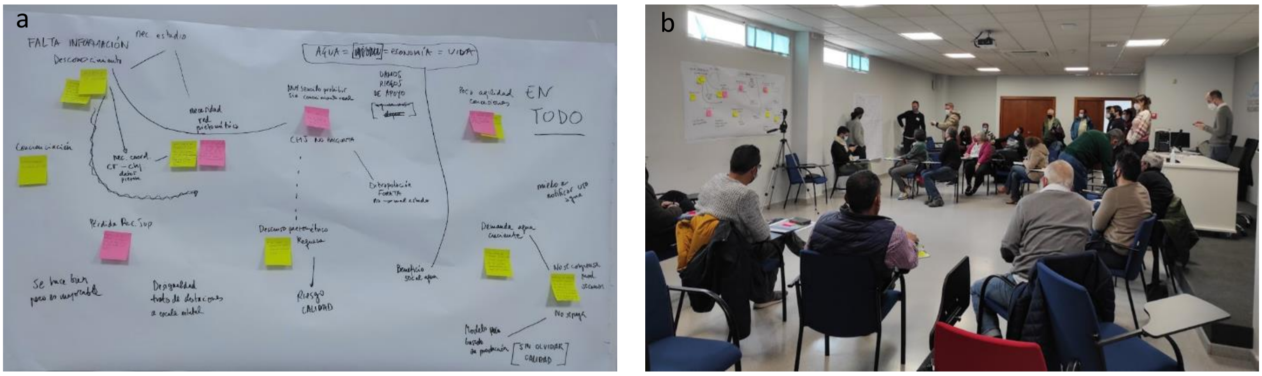


**Fig. 1. a: Problems in the groundwater management and distribution identified by the participants. b: The two groups of participants sharing the results of the second session.**

## 3. Final comments

Although many participants agree that it is necessary to create more participatory spaces, study the aquifer more in detail, know its capacity, use ICT-based tools, and disseminate the information in a clear and simple way, there was no consensus on the bad quantitative condition of the aquifer. On the one hand, the main strength of the participatory workshop was the intense participation of stakeholders and their willingness to collaborate with the management of the aquifer. On the other hand, the contradictory speeches about the condition of the aquifer showed that the main weakness of this process was the lack of prior and reliable knowledge about the aquifer, due to the complexity of the reports on aquifer state.

**Acknowledgements**

Research financed by the InTheMED project, which is part of the PRIMA Programme supported by the European Union's Horizon 2020 Research and Innovation Programme (GA n. 1923). It has also received funding from the eGROUNDWATER project (GA n. 1921), part of the PRIMA programme supported by the European Union's Horizon 2020 research and innovation programme.

**Reference**

Vennix, J. 1996. Group Model Building: Facilitating Team Learning Using System Dynamics, Wiley.

# Regional-Scale Modeling of Surface-Subsurface Flow: The Konya Closed Basin Case Study

Onur Cem YOLOĞLU[1], Nadim K COPTY[2], Mehmet Can TUNCA[3], Irem DALOĞLU[4], Ali Kerem SAYSEL[5]

[1,2,3,4,5] Boğaziçi University, Turkey, email: onur.yologlu@boun.edu.tr, ncopty@boun.edu.tr, mehmetcantunca@gmail.com, irem.daloglu@boun.edu.tr, ali.saysel@boun.edu.tr

ABSTRACT

Basin-scale hydrological modeling is an essential tool for the management of water resources, particularly in arid and semi-arid regions. The development of such models is particularly challenging for large watersheds where the definition of the system parameters is associated with high levels of uncertainty. To address these challenges, we describe a geostatistical approach utilized to define the input parameters. The approach combines direct measurements as well as soft data to improve the reliability of the defined parameters. The focus is on the Konya Closed Basin case study, one of 5 case studies examined in the IntheMed project supported by the PRIMA programme.

## 1. Introduction

The Konya Closed Basin is one of the primary agricultural regions of Turkey. The basin, characterized by a semi-arid climate, is located in central Anatolia, covering an area of about 60,000 km$^2$ with no major flows into or out of the basin (Fig. 1). Agricultural is mostly concentration in the central part of the basin as shown in the 2018 Corine land cover map (Fig. 2). Because of the mismatch between precipitation, mostly in the wet season, and agricultural water needs which are concentrated in the dry season, the basin relies heavily on groundwater resources for irrigation (Ozbahce and Tari 2010, Bozdağ, 2015). As a result of the unsustainable exploitation of groundwater resources, the Konya plain aquifer system has experienced a drastic decline in groundwater levels in recent years (Yilmaz et al., 2021). The problem is exacerbated by the large number of unregulated wells, estimated to be as much as 100,000 wells.

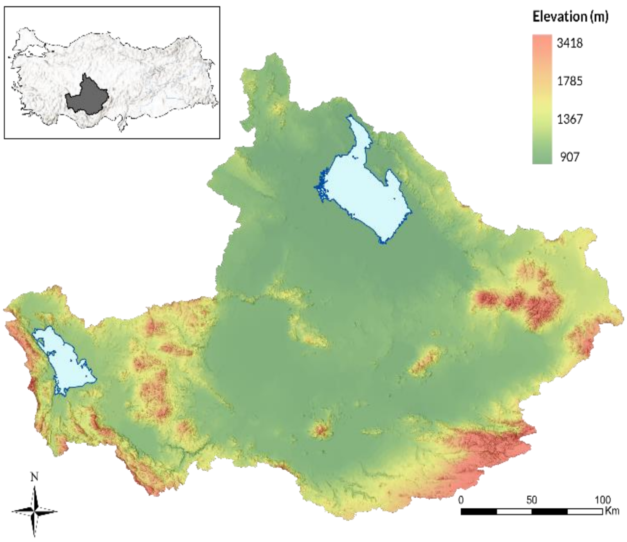


**Fig. 1.** Topographic map of the Konya Closed Basin.

## 2. Modeling Approach

To help manage this vital resource, a surface/subsurface flow model was developed. Covering the entire basin, the model is based the HYDRUS unsaturated flow package (Seo et al., 2006; Twarakawi et al., 2008) coupled to MODFLOW computer program (Harbaugh et al., 2000), thus allowing for the simulation of vertical water flow through the vadose zone and horizontal flow in the underlying aquifer system. The specific processes accounted for in the model include evapotranspiration, infiltration, irrigation, and groundwater extraction for agricultural, domestic and industrial use. The purpose of the model is to reproduce the observed historical water level data and estimate the net recharge in the basin.

Given the vastness of the region being modeled, the unavoidable coarseness and simplifications of such large regional models, and the limited availability of detailed hydrogeological data, the model is associated with a relatively high level of uncertainty. To improve the reliability of the model, direct measurements, as well as soft data collected at different scales, are incorporated into the model. Specifically, the model combines point groundwater level data, meteorological data and pumping test data, geologic data, land cover data (Corine), surface topography, and water content (GRACE) satellite data. To account for the uncertainty in the definition of the input parameters, geostatistical techniques are used to define key parameters such as the hydraulic conductivity, precipitation, aquifer thickness, ground elevation, and groundwater extraction. Historical groundwater level data were used as the main calibration parameter.

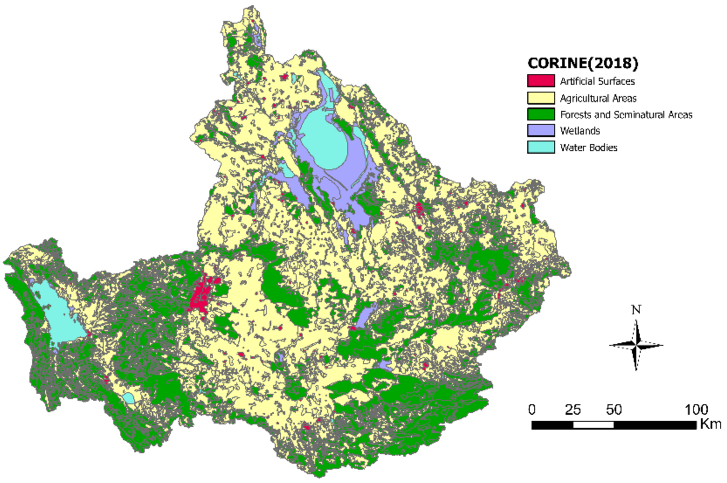


**Fig. 2.** Dominance of Agriculture in the Konya Closed Basin (map based on Corine Land Cover data).

## 3. Overview of Findings

Results show that the model was able to reproduce the observed groundwater level trends of the past two decades. Recharge areas are primarily located in the higher elevation regions of the basin with water flowing towards the central portions of the plain where intensive irrigation is located. The modeling results underscore the impacts of the expansion of irrigated lands and the switch towards more water-demanding crops on the basin's overall water deficits. As part of the efforts to move towards more sustainable use of the groundwater resources in the basin, there is a need to switch back to rain fed crops in the dryer portions of the basin. The model is used to predict the basin-wide long term water budget under various scenarios. The paper also highlights the challenges of modeling groundwater flow at the basin scale and discusses possible approaches to address these difficulties.

**Acknowledgement**

This research is part of the InTheMED project which is supported by the PRIMA programme under grant agreement No1923.

**References**

Bozdag A (2015) Combining AHP with GIS for assessment of irrigation water quality in Çumra irrigation district (Konya), Central Anatolia, Turkey, Environmental Earth Sciences 73 (12), 8217-8236

Harbaugh AW, Banta ER, Hill MC, McDonald MG (2000) MODFLOW-2000, the U.S. Geological Survey modular ground-water model user guide to modularization concepts and the ground-water flow process. Denver, CO, Reston, VA: U.S. Geological Survey

Özbahçe A, Tarı AF (2010) Effects of different emitter space and water stress on yield and quality of processing tomato under semi-arid climate conditions, Agric Water Manage 97, 1405–1410

Seo HS, Šimůnek J, Poeter EP (2007) Documentation of the HYDRUS Package for MODFLOW-2000, the U.S. Geological Survey Modular Ground-Water Model, GWMI 2007-01, Int. Ground Water Modeling Center, Colorado School of Mines, Golden, CO, 96 pp.

Twarakavi NKC, Šimůnek J, Seo HS (2008) Evaluating interactions between groundwater and vadose zone using HYDRUS-based flow package for MODFLOW, Vadose Zone Journal, 7(2), 757-768

Yılmaz G, Çolak MA, Özgencil IK, Metin M, Korkmaz M, Ertuğrul S, Soyluer M, Bucak T, Tavşanoğlu ÜN, Özkan K, Akyürek Z, Beklioğlu M, Jeppesen E (2021) Decadal changes in size, salinity, waterbirds, and fish in lakes of the Konya Closed Basin, Turkey, associated with climate change and increasing water abstraction for agriculture, Inland Waters 11(4), 538-555

# Numerical Modelling of Heaving Wave Energy Converter Arrays for Coastal Protection

Eva LOUKOGEORGAKI[1], Theofanis KARAMBAS[2]

[1] Department of Civil Engineering, Aristotle University of Thessaloniki, PC 54124, Thessaloniki, Greece
email: eloukog@civil.auth.gr

[2] Department of Civil Engineering, Aristotle University of Thessaloniki, PC 54124, Thessaloniki, Greece
email: karambas@civil.auth.gr

ABSTRACT

In the present work, the deployment of Wave Energy Converter (WEC) arrays for coastal protection against erosion is numerically investigated. Heaving cylindrical WECs are chosen to be installed offshore a coast and their effects on coastal hydro-morphodynamics are assessed. The simulation of the wave propagation, the breaking wave induced currents, the sediment transport and the bed morphology evolution is based on a numerical Boussinesq-type coastal hydro-morphodynamic model, which is appropriately extended to include the nonlinear wave-heaving cylinders interaction and the wave transformation induced by the WEC array. The results demonstrate the effectiveness of the WEC array to mitigate coastal erosion and flooding.

## 1. Introduction

Recent technological advances seek for the efficient exploitation of the vast wave energy towards reduction of greenhouse gas emissions and mitigation of climate change effects. For absorbing an adequate amount of power, Wave Energy Converters (WECs), such as heaving cylinders, have to be deployed in the form of multi-body arrays. The presence of WEC arrays combined with their energy absorption ability have a direct impact on the surrounding wave field and lead to reduced energy transmission in their leeward side. Exploiting this feature, WEC arrays could be deployed at near-shore locations as multiple-purpose systems, which mitigate coastal erosion and flooding simultaneously with electricity production. In order to illustrate this potential, advanced hydro-morphodynamic models including nonlinear wave-WECs interactions have to be utilized. Motivated by this, in the present paper a Boussinesq-type numerical model for assessing hydro-morphodynamic effects of heaving WEC arrays is developed and applied at a coastal area in Greece.

## 2. Numerical modeling

The present model is based on an existing fully hydro-morphodynamic two-dimensional horizontal (2DH) Boussinesq-type numerical model (Tsiaras et al., 2020), describing the processes of nonlinear wave propagation, sediment transport and morphological changes, and being suitable for the design of structures for coastal protection against erosion. The wave-cylinders interaction is introduced in that model by solving simultaneously an elliptic equation that determines the pressure exerted by the fluid on the floating bodies, according to Karambas and Loukogeorgaki (2022). The heave motion for the partially immersed floating cylinders under the action of waves is obtained by solving numerically the equation of motion based on Newton's law. Accordingly, both near and far-field hydrodynamics are simulated, including wave-floating bodies interaction, near shore wave propagation, breaking wave induced currents and morphology evolution.

## 3. Results and discussion

The model is applied to predict the morphological changes in Podamos beach (Chalki island, Greece) induced by the deployment of a WEC array consisting of seven heaving cylinders (Fig. 1). The diameter of each cylinder is 20 m, the draft is 3 m and the water depth is 8 m. The distance between the bodies is 50 m. The dimensions of the devices and the array's layout characteristics have been defined from preliminary runs in the frequency domain by applying a Boundary Integral Equation Method model, so that the deployed array leads to an ~25-30% wave height reduction at its leeward side for a wave period $T$=6.0 s. In Fig. 1, the effect of the WEC array on the wave propagation is shown, illustrating the reduction of the incident (to the beach) wave energy. In Fig. 2, the cross-shore morphology evolution is shown, without and with the presence of the WEC array. The wave conditions are: wave height in the absence of the WEC array, $H$=3.5 m, wave height in the presence of the WEC array, $H_{WEC}$=2.45 m (i.e., 30% reduction due to WEC array), and period $T$=6.0 s.

The characteristic mean grain size is $d_{50}$=0.2 mm. Coastal erosion and flooding is mitigated, despite the moderate reduction of the wave height. This is an expected impact, having in mind that sediment transport rates depend upon a power of the wave height (i.e., ~$H^{2.5}$). Consequently, even a relatively small reduction of the wave height could result to significant morphological changes.

## 4. Conclusions

A WEC array can be combined with the need of coastal protection. By installing this multi-body system in the proximity of a coast, mitigation of coastal erosion and flooding can be achieved together with the exploitation of wave energy. The present wave-heaving cylinders interaction and coastal hydro-morphodynamic numerical model can be used for the design of the above multi-purpose system.

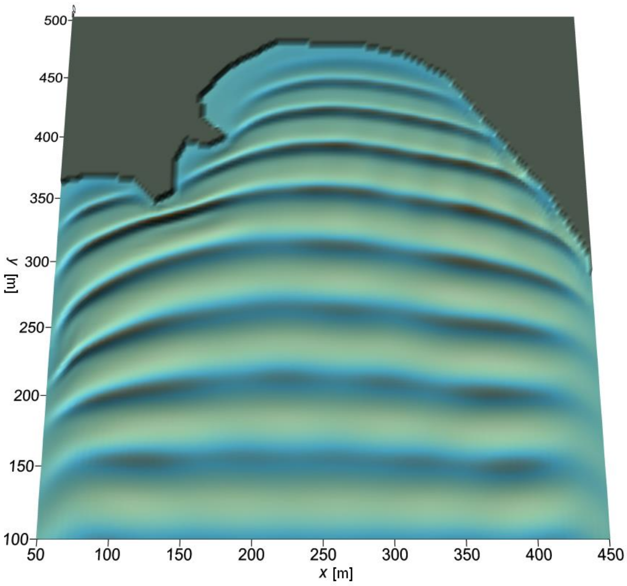


**Fig. 1.** Snapshot of the computed free surface elevation at Podamos beach (Chalki island, Greece) without (left) and with (right) the presence of the WEC array.

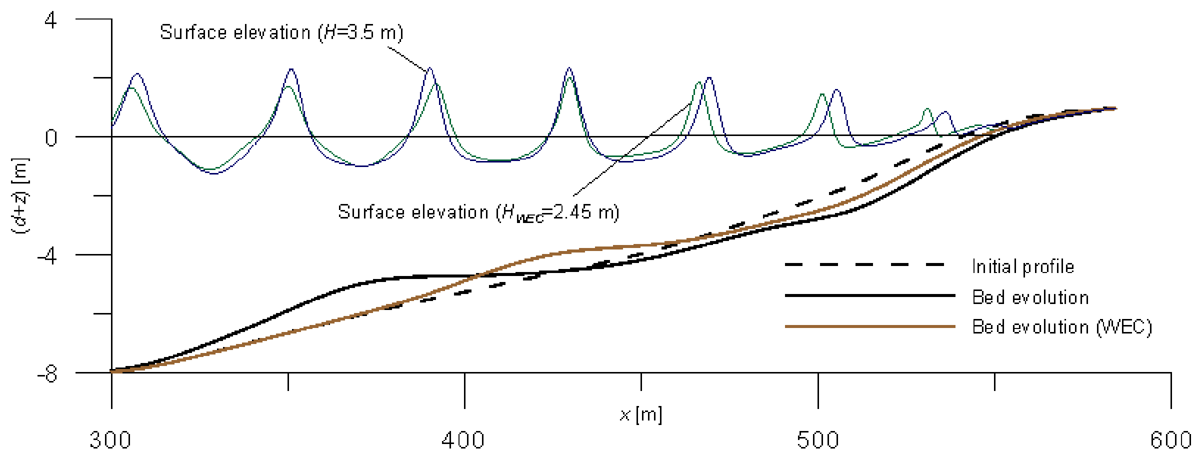


**Fig. 2.** Instantaneous surface elevation and cross-section morphology evolution at Podamos beach (Chalki island, Greece). Wave conditions: $H$=3.5 m, $H_{WEC}$=2.45 m (30% reduction of $H$), $T$=6.0 s, $d_{50}$=0.2 mm.

### References

Karambas Th, Loukogeorgaki E (2022) A Boussinesq-type model for nonlinear wave-heaving cylinder interaction, Energies, 15(2), paper no. 469; https://doi.org/10.3390/en15020469.
Tsiaras A-Ch, Karambas Th, Koutsouvela D (2020) Design of detached emerged and submerged breakwaters for coastal protection: Development and application of an advanced numerical model, Journal of Waterway, Port, Coastal and Ocean Engineering, 146(4), paper no. 04020012; https://doi.org/10.1061/(ASCE)WW.1943-5460.0000566.

# Powering offshore aquaculture through ocean renewable energy technologies

Daniel CLEMENTE[1,2], Paulo ROSA-SANTOS[1,2], Tiago FERRADOSA[1,2], Francisco TAVEIRA-PINTO[1,2]

[1] Interdisciplinary Centre of Marine and Environmental Research (CIIMAR)
[2] Faculty of Engineering of the University of Porto (FEUP)
email: up201009043@edu.fe.up.pt
email: pjrsantos@fe.up.pt
email: tferradosa@fe.up.pt
email: fpinto@fe.up.pt

ABSTRACT

This paper addresses potential technological solutions, based on ocean energy sources, towards meeting energy demand from offshore aquaculture buoys and systems. An overview on both research fields is provided, followed by estimates of power supply and demand from three wave energy technologies and six aquaculture case studies, respectively. A comparison is then established between the two sets for a pilot zone on the Portuguese coastline. It is concluded that only one solution – the Wave Dragon – could fully cover all case study energy demands, while the OCECO 4 and the Wavestar options cover four out of the six scenarios.

## 1. Introduction

Current challenges such as consumption increase, fishing quotas and stock rupture have led to mounting pressure on the fishing industry. To compensate for it, aquaculture has seen an expansion surge over the past few decades, given its potential as an alternative and more sustainable source of highly nutritious (*e.g.*, protein), low impact food, among other uses. Although about 50% of this demand is already met by aquaculture, growth issues have arisen. Some regard the incrementing demand for energy supply, given the needs of equipment (*e.g.*, water temperature, salinity, *pH*, concentration of nutrients, feeders and biosensors) for optimized production, while others are related to space management, as coastline competition with other activities is mounting (Ocean Energy Systems, 2022). This has promoted interest in shifting aquaculture activities towards offshore areas, which offers new opportunities to be exploited.

Ocean energy sources (OES) are an encompassing field of research with numerous contributors, from tidal to wave energy. They can demonstrate greater energy density than even solar or wind energy and are less susceptible to resource intermittency. An abundant and renewable, yet untapped resource is available for harvesting: 151 300 TWh/yr (Taveira-Pinto *et al*., 2015). However, challenges such as technological convergence, harshness of the ocean environment, energy output regularity and high levelized costs of energy hinder further advancements, namely in terms of commercial deployment (Clemente *et al*., 2021). A viable technological demonstration is pivotal towards the development of OES.

On one hand, aquaculture is being “forced” into offshore areas. It is also requiring cumulative energy demand for monitoring and feeding equipment, which should not be reliant upon diesel fuel. On the other hand, OES need a “winning concept” capable of supplying renewable energy reliably, consistently and safely. There are further opportunities in terms of cost savings through onsite supply, lower risk of fuel spills, potential integration with other uses (*e.g.*, hydrogen, batteries or desalination) and technological scalability. Therefore, combining both sectors seems sensible, so long as certain premises are ensured. For instance, offshore conditions shouldn’t be too calm or hazardous, so that ocean energy technologies can operate efficiently without risking the safety of both aquaculture and OES systems (Ocean Energy Systems, 2022). The former is particularly difficult, as it extends to an OES device’s mode of operation, power matrix and efficiency, since there are hundreds of competing concepts around the world.

This paper addresses the specific challenge of energy supply and demand through OES-based systems. The goal is to compare them in terms of performance and limitations towards supplying aquaculture systems. To that end, three wave energy converters (WECs) – Wave Dragon, OCECO 4 and Wavestar – were selected. The comparison was established by estimating the annual energy generation (AEP) in an offshore pilot zone on the Portuguese coastline: São Pedro de Moel (Giannini *et al*., 2020). The AEP was matched against the demands from six aquaculture case studies from (Ocean Energy Systems, 2022).

## 2. Methods, results and conclusions

### 2.1. Power output and demand estimate and comparison

A recent report provides an encompassing summary of energy needs for several offshore aquaculture case studies (Ocean Energy Systems, 2022). It considers the variable requirements of different species (*e.g.*, fish, mollusks, seaweed or crustaceans) and operation site, including lighting, pumping, feeding, transport, crew/worker quarters, aeration and desalination. Six of the reference case studies were selected: four related to finfish salmon farming in Australia, Chile, Norway and Scotland; one finfish seabass farming from Singapore; and one shellfish oyster from the USA. The AEPs were extrapolated from daily energy requirements (365 days per year was assumed), to which adds the corresponding aquaculture production.

The AEP for each of the three WECs was calculated by multiplying the corresponding power matrices by the respective resource matrix of the São Pedro de Moel pilot zone (36 m water depth), which can be consulted in (Giannini *et al*., 2020). The power matrices for the OCECO 4 - Portuguese kinetic wave energy device - and Wave Dragon - applied in the aforementioned report - were obtained from literature references (Castro-Santos *et al*., 2018; Giannini *et al*., 2020), while that of the Wavestar - previously tested in a Portuguese pilot zone - can be consulted in the project's website (Wavestar, 2021).

The comparison is summarized below, in Table 1. It is perceivable that the Wave Dragon would be capable of supplying any of the aquaculture case studies should any of them be implanted within the São Pedro de Moel pilot zone, with an estimated AEP of 7.84 GWh/yr. This is in agreement with the outcomes of the offshore aquaculture report, where the Wave Dragon is successfully applied to a seaweed farm in Wales. As for the OCECO 4 and the Wavestar, the AEP are considerably lower: 1.10 GWh/yr and 0.78 GWh/yr. Even so, they are capable of supplying all aquaculture case studies apart from the 10 000 tonnes salmon farm and the 170 tonnes of seabass. It is worth noting that these values regard a single unit of each WEC. For a complete demand coverage, five units of the OCECO 4 and seven to eight of the Wavestar would be required.

**Table 1.** AEP estimates and energy supply versus demand for the São Pedro de Moel pilot zone.

| | Case studies | | | | | | | | | |
|---|---|---|---|---|---|---|---|---|---|---|
| Power needs (GWh/yr) | Salmon | 10k ton/yr | 0.27k ton/yr | 3.12k ton/yr | 1k ton/yr | Seabass | 0.17k ton/yr | Oyster | 0.17k ton/yr | AEP (GWh/yr) |
| | | 5.48 | 0.14 | 0.26 | 0.26 | | 3.44 | | 0.37 | |
| Supply *versus* Demand | OCECO 4 | X | √ | √ | √ | | X | | √ | **1.10** |
| | Wave Dragon | √ | √ | √ | √ | | √ | | √ | **7.84** |
| | Wavestar | X | √ | √ | √ | | X | | √ | **0.78** |

### 2.2. Complementary concluding remarks

The energy potential for the three WECs is perceivable from Table 1. Nevertheless, other considerations are required (Ocean Energy Systems, 2022). For starters, the Wavestar has an additional limitation, as it is not conceived to operate in storm conditions (above 3 m, for this concept). Secondly, the São Pedro de Moel is merely representative of the energy potential, as it would be required to conduct a feasibility study on implementing offshore aquaculture in this region. Thirdly, apart from renewable energy supply, devices such as these three WECs can absorb/mitigate incoming wave energy, so that a shielded region is created behind the wave farm, where the aquaculture cages, buoys and auxiliary systems can be deployed. Fourthly, it will be pertinent to ensure that the power output is provided on a regular basis, which may imply storage systems. Lastly, cost savings can be achieved through co-location or hybridization (*e.g.*, a WEC aquaculture buoy).

**Acknowledgements**

The authors acknowledge funding in the form of a PhD scholarship grant by the FCT, co-financed by the EU's ESF through the North Portugal Regional Operational Programme (NORTE2020), with reference 2020.05280.BD. This work was also funded by the project OCEAN3R (NORTE-01-0145-FEDER-000064), supported by NORTE2020, under the PORTUGAL 2020 Partnership Agreement and through the European Regional Development Fund (ERDF)

**References**

Castro-Santos, L., Silva, D., Bento, A.R., Salvação, N., Guedes Soares, C., 2018. Economic Feasibility of Wave Energy Farms in Portugal. Energies 11, 16. https://doi.org/10.3390/en11113149
Clemente, D., Rosa-Santos, P., Taveira-Pinto, F., 2021. On the potential synergies and applications of wave energy converters: A review. Renew. Sustain. Energy Rev. 135, 17. https://doi.org/10.1016/j.rser.2020.110162
Giannini, G., Rosa-Santos, P., Ramos, V., Taveira-Pinto, F., 2020. On the Development of an Offshore Version of the CECO Wave Energy Converter. Energies 13, 25. https://doi.org/10.3390/en13051036
Ocean Energy Systems, 2022. Offshore Aquaculture: a Market for Ocean Renewable Energy. OES, Europe.
Taveira-Pinto, F., Iglesias, G., Rosa-Santos, P., Deng, Z.D., 2015. Preface to Special Topic: Marine Renewable Energy. J. Renew. Sustain. Energy 7, 061601. https://doi.org/10.1063/1.4939086
Wavestar, 2021. Projects | Wavestar [WWW Document]. URL http://wavestarenergy.com/projects (accessed 4.29.22).

# Extending the application of offshore wind monopiles to intermediate water depths

João CHAMBEL[1,], Arunjyoti SARKAR[2], Mohd ISHTIYAK[2], Tiago FAZERES-FERRADOSA[1], Paulo ROSA-SANTOS[1], Francisco TAVEIRA-PINTO[1]

[1] Interdisciplinary Centre of Marine and Environmental Research and Faculty of Engineering of University of Porto, Porto, Portugal.
email: up201304674@edu.fe.up.pt
email: tferradosa@fe.up.pt
email: fpinto@fe.up.pt
email: pjrsantos@fe.up.pt
[2] Indian Institute of Technology Kharagpur, Kharagpur, India
email: arun@naval.iitkgp.ac.in
email: : mdishtiyakmalik@gmail.com

ABSTRACT

As the offshore wind sector sets new goals concerning the installed capacity in Europe, it becomes evident the need to implement offshore wind farms in ambitious locations with large wind energy potential. Often, such locations are characterized by larger water depths and longer distances to shore. While offshore wind floating foundations are yet to reach a mature state of development, the standard monopile foundations, which are the most commonly used, struggle to be applicable for water depths above 30 m (Fazeres-Ferradosa *et al.*, 2019). Additionally, floating solutions are typically suitable for water depths above 60 m or more (Ishtiyak *et al.*, 2021). A key problem of using bottom fixed foundations, as monopiles, jackets, gravity-based foundations and others is that for water depths between 30 to 50 m, they tend to become rather massive in dimensions and footprint. This not only increases the foundation's costs, but it also raises challenges in the construction, transport and installation. Recently, the Bottom Supported Tension Leg Tower (BSTLT) with inclined tethers for offshore wind turbines has been developed and validated (Sarkar and Gudmestad, 2017; Ishtiyak *et al.*, 2021). This concept enables the application of monopile foundations in water depths up to 50 m, without the need to significantly increase its diameter. Hence, the BSTLT provides an interesting alternative for intermediate water depths. This study briefly looks into the bending moment of the BSTLT concept in comparison with the standard monopile case. Preliminary results show that from the BSTLT generally performs efficiently for water depths of 50 m and has potential to extend the standard monopile foundation to transitional/intermediate water depths.

## 1. BSTLT concept and analysis

The BSTLT concept consists in a standard monopile, which then has a transition piece that connects to the tower (superstructure) that supports the wind turbine, coupled with hinge and 4 pre-tensioned tethers (4.5 MN) that provide additional stability to the system (Fig. 1). These tethers and hinge enable the use of monopiles with standard diameters in deeper waters, as it provides further resistance to the bending moment at the seabed level. The details of the concept are available in Ishtiyak *et al.* (2021). Sarkar and Gudmestad (2017) proposed the link between the tethers and the monopile to be made through 4 horizontal arms, orthogonal to the monopile and the transition piece. In the present case, these are not used, and the tethers are directly linked to the monopile in an obliquus direction 45º (horizontal plane) and with a base that is 60 m distanced to the monopile. This optimized configuration resulted from the parametric and geometric study performed in Ishtiyak *et al.* (2021). For comparison between the monopile and the monopile with BSTLT the same diameter (6.0 m) and thickness (60 mm) and length (50 m) has been used. Both cases include a 3 bladed configuration, mass of rotor and nacelle, 110 t and 240 t respectively and a tower of 6.0 m at bottom, 4.75 m at top and a length between the transition piece and the top of 89 m. Hub height was considered to 99 m above mean seal level. A 50 m water depth was applied. The material considered was steel with $\rho$ = 7850 kg/m3, E = 210 GPa, $\mu$ = 0.3. The analysis considers a 5 MW reference turbine of NREL. The remaining configuration details and bending moment calculations and analysis followed the approaches already established in Sarkar and Gudmestad (2017) and Ishtiyak *et al.* (2021).

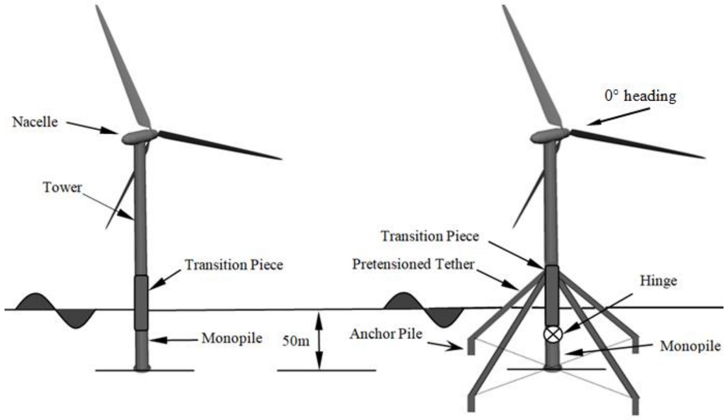


**Figure 1.** Conventional monopile supported OWT (left), monopile with BSTLT (right).

## 2. Results and conclusions

The means and the standard deviations of the bending moment at the monopile base for different environmental states (Table 7) are compared in Fig. 2 for both structures. The results show that the bending moment and its variation at the monopile base with BSTLT reduces considerably as the hinge is lowered. Large values of bending moment in the standard monopile case, observed in some of the highest environmental states, can be attributed to the dynamic amplification caused by the closeness of the fundamental natural period of the structure to the zero up-crossing periods (Tz). It can also be noticed that the performance of BSTLT with hinge at 20 m below MSL is similar to the standard monopile case as far as the individual environmental states is concerned. However, as the hinge is lowered, the BSTLT can outperform the standard monopile.

**Table 1.** Environmental conditions considered for bending moment calculation.

| Environmental state | Wind speed (m/s) | Tz (s) | Hs (m) |
|---|---|---|---|
| 16 | 18 | 5.0 | 3.0 |
| 17 | 20 | 5.0 | 2.5 |
| 18 | 20 | 5.0 | 3.0 |
| 19 | 22 | 5.0 | 3.0 |
| 20 | 22 | 6.0 | 4.0 |
| 21 | 24 | 5.0 | 3.5 |
| 22 | 24 | 6.0 | 4.0 |

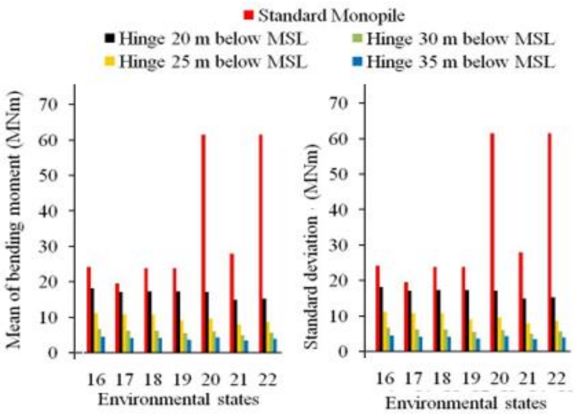


**Fig. 2**. Environmental conditions considered for bending moment calculation.

**Acknowledgements**

This work is supported by the project POCI-01-0145-FEDER-032170 (ORACLE project), funded by the European Fund for Regional Development (FEDER), through the COMPETE2020, the Programa Operacional Competitividade e Internacionalização (POCI) and FCT/MCTES through national funds (PIDDAC). This work is also funded by exclusively national funds through FCT - Portuguese Foundation for Science and Technology under the project POSEIDON, Reference PTDC-ECI-EGC-5177-2020. T. Fazeres-Ferradosa has been supported by the program of Stimulus of Scientific Employment Individual Support (2020.02393.CEECIND) from FCT - Portuguese Foundation for Science and Technology. João Chambel is supported by FCT – Portuguese Foundation for Science and Technology – through the Ph.D. scholarship 2021.07393.BD.

**References**

Fazeres-Ferradosa, T., Taveira-Pinto, F., Rosa-Santos, P., Chambel, J. (2019). A review of reliability analysis of offshore scour protections. Proceedings of the Institution of Civil Engineers: Maritime Engineering, 172 (3), pp. 104-117. DOI: 10.1680/jmaen.2019.11
Miner, A. (1945). Cumulative damage in fatigue. Journal of Applied Mechanics. 12, pp. 159–164.
Ishtiyak, M., Sarkar, A., Fazeres-Ferradosa, T., Rosa-Santos, P., Taveira-Pinto, F. (2021). Bottom-supported tension leg towers with inclined tethers for offshore wind turbines. Proceedings of the Institution of Civil Engineers: Maritime Engineering, 174 (4), pp. 124-133. DOI: 10.1680/jmaen.2021.001
Sarkar, A., Gudmestad, O.T. (2017) Bottom supported tension leg tower for offshore wind turbines. Proceedings of the International Conference on Offshore Mechanics and Arctic Engineering - OMAE, 10. DOI: 10.1115/OMAE2017-61009

# The impact of the SWAN model calibration on the energy production of wave energy converter systems

Ajab Gul MAJIDI[1,2], Victor Ramos[1,2], Paulo Rosa Santos[1,2], Luciana das Neves[1,2], Francisco Taveira-Pinto[1,2]

[1] Department of Civil Engineering, Faculty of Engineering of the University of Porto (FEUP), Rua Dr. Roberto Frias, S/N, 4200-465 Porto, Portugal.

[2] Interdisciplinary Centre of Marine and Environmental Research of the University of Porto (CIIMAR), Avenida General Norton de Matos, S/N, 4450-208 Matosinhos, Portugal.

email: ajabgulmajidi@gmail.com
email: jvrc@fe.up.pt
email: pjrsantos@fe.up.pt
email: lpneves@fe.up.pt
email: fpinto@fe.up.pt

ABSTRACT

The application of wave models to create the wave resource matrix is typically required for the accurate estimation of the extractable wave energy by different wave energy converters (WECs). However, the accuracy of these predictions is highly dependent on the wave model calibration. The goal of this research work is to evaluate the impact on the electricity production of SWAN calibration and how this model may be improved by modifying it considering site measurements. The evaluation is based on the expected energy production for OEBuoy point absorber WEC in different locations along the Atlantic coast of the Iberian Peninsula. The model has been adjusted using the newly developed ST6 physical settings package. The results demonstrate a significant level of uncertainty in the quantity of energy output projected using various wind scaling factors within HWANG, FAN, and ECMWF wind drag formulas. In comparison to the SWAN default parameters, the calibrated model adjusted the mean energy output value of all 10 sites by 11.2 %.

## 1. Model description

The wind scaling factor and wind drag formulas (Hwang, 2011; Fan et al., 2012; ECMWF, 2016) are the most sensitive and affecting factors in the calibration of the ST6 source term package, according to Amarouche et al. (2019). SWAN default, ST6 default, HWANG wind drag formula with 32 and 35, FAN wind drag formula with 28, 32, and 35, and ECMWF wind drag formula with 32 and 35 wind scaling factors were compared in this study. The unstructured grid was created with the SMS/ADCIRC program and features a space-varying grid size of 0.002º (Fig. 1a). The bathymetry used was obtained from the General Bathymetric Chart of the Oceans (IHO, 1984) with a spatial resolution of 0.0036º (Fig. 1b). ERA5 wind reanalysis with 1-hour temporal and 0.25º spatial resolution is used to force the model (Hersbach et al., 2018). The boundary conditions are derived from ERA5 wave hindcast reanalysis with 1-hour temporal and 1-degree spatial resolution (Hersbach et al., 2018). The results are calibrated against the measurements of B6 and validated against the remaining 9 in-situ measurements. Table 1 provides information about the considered buoys.

**Table 1.** Buoy ID, location, water depth, and the number of data records available in 2010 for all the considered buoys in the study.

| Buoy ID | ID code | Lon (º) | Lat (º) | Depth (m) | Data No |
|---|---|---|---|---|---|
| B1 | 6200084 | -9.3675 | 41.9665 | 292.5 | 4996 |
| B2 | 6200192 | -9.64 | 39.51 | 1547.1 | 2629 |
| B3 | 6200199 | -9.21 | 39.56 | 65.4 | 2214 |
| B4 | 2136 | -3.04 | 43.64 | 827.0 | 8513 |
| B5 | 2242 | -6.18 | 43.75 | 748.0 | 6020 |
| B6 | 2248 | -9.43 | 42.12 | 691.3 | 4996 |
| B7 | 2246 | -9.21 | 43.5 | 424.8 | 8726 |
| B8 | 2244 | -7.68 | 44.12 | 1650.0 | 1160 |
| B9 | 2342 | -6.96 | 36.49 | 467.0 | 6863 |
| B10 | Leixões Buoy | -8.983 | 41.3167 | 84.8 | 2524 |

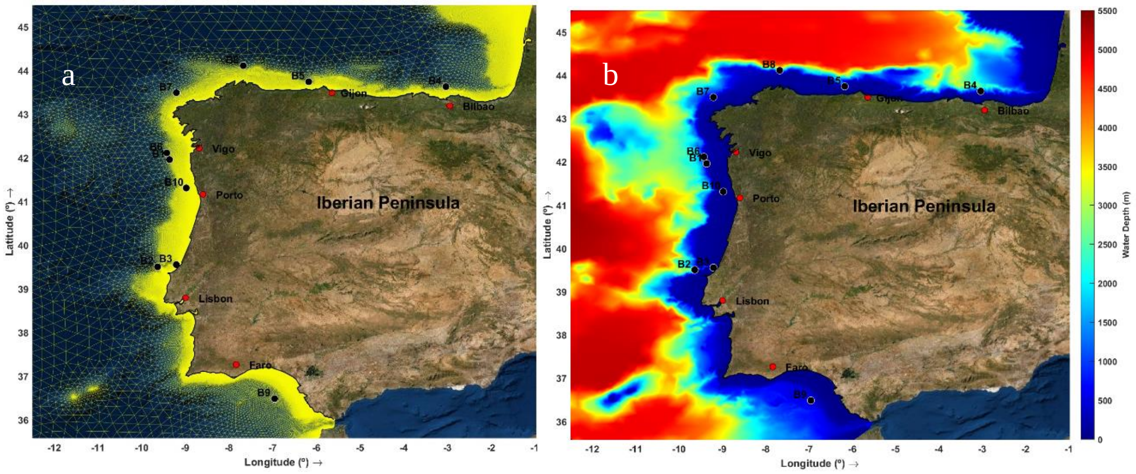


**Fig. 1.** The defined unstructured mesh grid system (a), bathymetry (b), and buoy locations (black dots) for the study area.

## 2. Results

The energy output differences in percentage (model estimation *versus* real wave data) for all 10 sites evaluated, as well as 9 possible SWAN modifications for OEBuoy are computed and the results are provided in Table 2. The mean values in Table 2 were calculated using the mean energy output of the model and the real data from all ten locations. In comparison to the SWAN default parameters, the calibrated model corrected the mean energy output value of all 10 sites by 11.2%.

**Table 2.** The OEBuoy energy production difference in percentage against the temporally matched real measurements with different time durations for 10 distinct locations in the study area and 9 different SWAN settings.

| Buoy ID | T (YEAR) | ECMWF32 | ECMWF35 | FAN28 | FAN32 | FAN35 | HWANG32 | HWANG35 | ST6-DEF | SWAN-DEF |
|---|---|---|---|---|---|---|---|---|---|---|
| B1 | 0.57 | -12.88 | -7.96 | -20.36 | -14.54 | -9.96 | -9.84 | -3.67 | -9.73 | -10.96 |
| B2 | 0.30 | -5.58 | 5.82 | -21.12 | -8.41 | 0.39 | 0.52 | 14.30 | 0.60 | -4.54 |
| B3 | 0.25 | 3.91 | 13.95 | -10.62 | 0.16 | 9.69 | 10.01 | 22.01 | 10.78 | 4.39 |
| B4 | 0.97 | -13.31 | -7.06 | -21.61 | -15.18 | -9.60 | -9.18 | -1.88 | -9.39 | -10.13 |
| B5 | 0.69 | -7.91 | 0.61 | -17.72 | -10.06 | -3.10 | -2.63 | 7.17 | -2.68 | -7.61 |
| B6 | 0.57 | -13.46 | -8.06 | -20.51 | -14.83 | -10.30 | -9.97 | -3.16 | -9.95 | -11.16 |
| B7 | 1.00 | -10.83 | -4.33 | -21.15 | -13.82 | -6.63 | -6.35 | 0.84 | -6.54 | -11.12 |
| B8 | 0.13 | 5.98 | 14.15 | -4.60 | 3.33 | 11.79 | 11.62 | 20.66 | 11.94 | 8.04 |
| B9 | 0.78 | -17.34 | -9.06 | -29.35 | -21.01 | -12.44 | -12.04 | -1.90 | -11.78 | -13.08 |
| B10 | 0.29 | -2.22 | 4.85 | -13.25 | -4.66 | 1.89 | 1.58 | 12.33 | 2.39 | -0.98 |
| Mean | 0.56 | -10.16 | -3.24 | -19.96 | -12.54 | -6.04 | -5.77 | 2.49 | -5.74 | -8.73 |

**Acknowledgments**

The authors acknowledge European Centre for Medium-Range Weather Forecasts (ECMWF) for supplying wind data, Copernicus Marine Environment Monitoring Service (CMEMS) for providing wave observations, and GEBCO for providing bathymetry data. The authors acknowledge funding in the form of a PhD scholarship grant by the FCT, co-financed by the EU's ESF through the NORTE 2020 program (Ref: 2021.04847.BD). This research was also funded by the project PORTOS – Ports Towards Energy Self-Sufficiency (Ref: EAPA_784/2018) and co-financed by the Interreg Atlantic Area Program and by the OCEANERA-NET COFUND project WEC4Ports – A Hybrid Wave Energy Converter for Ports (Ref: OCEANERA/0004/2019), under the frame of FCT. Victor Ramos has been supported by the program of Stimulus of Scientific Employment Individual Support (CEECIND/03665/2018) from the FCT.

**References**

Amarouche, Khalid, Adem Akpınar, Nour El Islam Bachari, Recep Emre Çakmak, and Fouzia Houma. 2019. "Evaluation of a High-Resolution Wave Hindcast Model SWAN for the West Mediterranean Basin." *Applied Ocean Research* 84 (March): 225–41. https://doi.org/10.1016/J.APOR.2019.01.014.

ECMWF, IFS Documentation CY43R1 - Part VII: ECMWF Wave Model, 2016. https://doi.org/10.21957/18mel2ooj.

Fan, Yalin, Shian Jiann Lin, Isaac M. Held, Zhitao Yu, and Hendrik L. Tolman. 2012. "Global Ocean Surface Wave Simulation Using a Coupled Atmosphere–Wave Model." *Journal of Climate* 25 (18): 6233–52. https://doi.org/10.1175/JCLI-D-11-00621.1.

Hersbach, H., Bell, B., Berrisford, P., Biavati, G., Horányi, A., Muñoz Sabater, J., Nicolas, J., Peubey, C., Radu, R., Rozum, I., Schepers, D., Simmons, A., Soci, C., Dee, D., Thépaut, J-N. (2018): ERA5 hourly data on single levels from 1979 to present. Copernicus Climate Change Service (C3S) Climate Data Store (CDS). https://doi.org/10.24381/cds.adbb2d47.

Hwang, Paul A. 2011. "A Note on the Ocean Surface Roughness Spectrum." *Journal of Atmospheric and Oceanic Technology* 28 (3): 436–43. https://doi.org/10.1175/2010JTECHO812.1.

International Hydrographic Organization. 1984. General bathymetric chart of the oceans (GEBCO): Ottawa, Canada: Canadian Hydrographic Service.

# Numerical assessment of alternative geometries of a shoreline wave energy converter

Theofano KOUTROUVELI[1], Luciana DAS NEVES[2], Paulo ROSA SANTOS[3], Francisco TAVEIRA-PINTO[4], Tomás CALHEIROS CABRAL[5]

[1,2] IMDC nv – International Marine and Dredging Consultants, Belgium
theofano.koutrouveli@imdc.be
luciana.das.neves@imdc.be

[2,3,4,5] FEUP – Faculty of Engineering of the University of Porto, Portugal
pjrsantos@fe.up.pt
fpinto@fe.up.pt
tcabral@fe.up.pt

ABSTRACT

Wave energy conversion (WEC) technologies have been extensively studied in the past decades. However, further research on the hybridization of different WEC concepts to operate more efficiently under various metocean conditions still needs to be done. Within the OCEANERA-NET project WEC4PORTS, a novel shoreline hybrid WEC (h-WEC) combining two well-known wave energy conversion principles, an oscillating water column (OWC) and a multi-reservoir (4 reservoirs in the present configuration) overtopping device (OTD), is being optimized for installation in multi-purpose breakwaters. This paper focuses on the three-dimensional numerical model developed with OpenFoam for comparing five alternative configurations of the h-WEC, by studying their hydrodynamic efficiency under different sea-states of the northern Atlantic coast of Portugal near the northern outer rubble-mound breakwater of the port of Leixões – the research prototype.

## 1. Model set-up

Wave propagation over the h-WEC device is studied numerically with the OpenFoam 6 software using a two-phase flow approach and the Volume of Fluid (VOF) method. The combined water/air flow is governed by the incompressible three-dimensional Reynolds Averaged Navier-Stokes equations (interFoam) and a Shear-Stress Transport (SST) k-ω model for turbulence closure. The numerical domain with a length of 382m, a width of 26m and a total height of 34m (including the air phase), consists of a wave flume and the Breakwater-integrated h-WEC. Five alternative geometries of the h-WEC are considered, a reference one and four alternatives, which differ from the Reference geometry either in the configuration of the oscillating water column inlet or in the number of oscillating water columns. All tested geometries share the same OTD device geometry with 4 reservoirs (Fig. 1). The numerical grid is, in all configurations, a non-uniform parametric one with hexahedral/split-hexahedral elements and consists of around 7 million cells. Refinement procedures are applied close to the areas of interest, i.e. the OTD reservoirs, the OWC, the free-surface area and the breakwater.

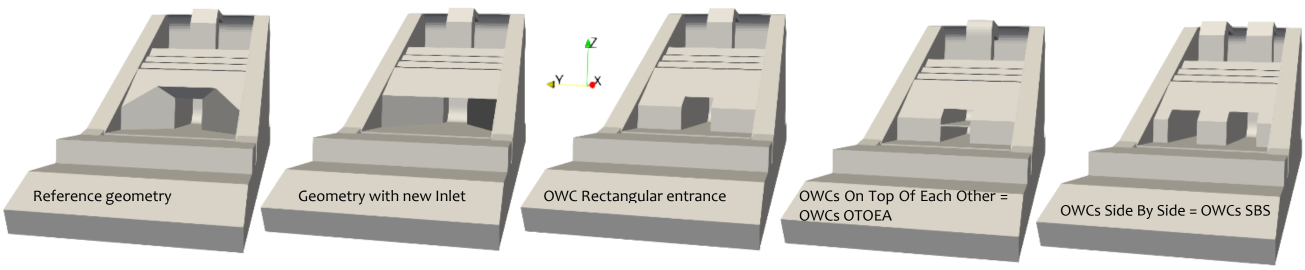


**Fig. 1.** Different geometries simulated.

## 2. Results

All five geometries are tested under a regular wave, having a 1m wave height and 10s wave period, which are characteristic of a frequent sea-state along the coast of Leixões. Said wave is generated by a velocity boundary condition at the left boundary of the model domain, including active absorption, and corresponds to Case A simulations in Table 1. Selected geometries, following resulted from simulations within Case A are, in addition, tested under wave periods of 8s and 12s (Case B and C in Table 1), covering the expected range of natural frequencies of the OWC devices.

**Table 1.** Overview of the different wave periods and corresponding geometries simulated.

| Case | *T* (s) | *H* (m) | Still Water level (mZHL) = MSL at Leixões prototype breakwater | Geometries tested |
|---|---|---|---|---|
| A | 10 | | | Reference geometry, Geometry with new Inlet, OWC Rectangular entrance, OWCs OTOEA, OWCs SBS |
| B | 8 | 1 | +1.67 | Reference geometry, Geometry with new Inlet, OWCs OTOEA |
| C | 12 | | | Reference geometry, Geometry with new Inlet, OWCs OTOEA |

The evaluation of the efficiency is based on: the free surface elevation inside the OWC chamber (amplification coefficient), wave overtopping discharges over the multiple reservoirs of the OTD device, and the pneumatic and the hydraulic efficiencies. Since all geometries share a similar OTD device, it is expected that the OWC component will play a more significant role in the evaluation of the h-WEC.. The time-series of the wave amplification coefficient in the OWC devices for all different geometries and Cases is shown in Fig. 2, while in Table 2 the hydraulic and pneumatic efficiencies are presented. From the results on the wave amplification, it is demonstrated that for all Cases the most efficient geometry is the one with the two OWCs OTOEA, while the second most efficient geometry is the Reference geometry. The results presented in Table 2 show that the Reference geometry has a more consistent performance regarding the pneumatic efficiency within the Cases, while the differences in hydraulic efficiencies within the different geometries of the same Case are not very pronounced. In general it is confirmed that the optimum Breakwater-integrated h-WEC is one that must consider the performances of the OWC and OTD devices concurrently.

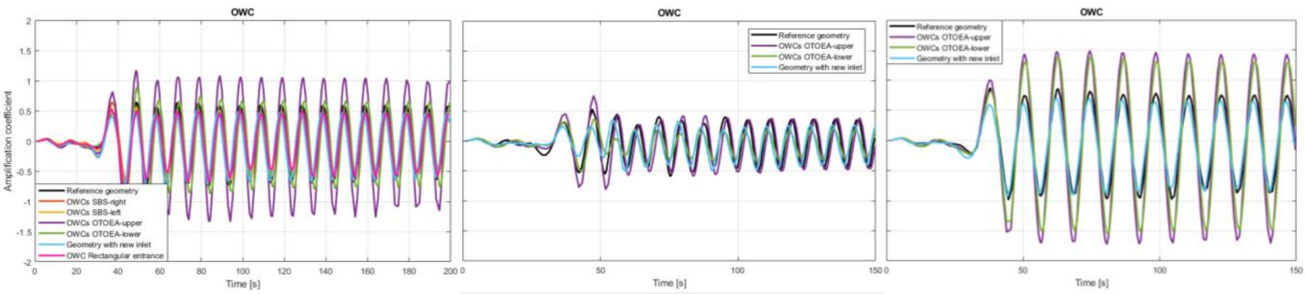


**Fig. 2.** Comparison of the wave amplification coefficient in the OWCs for all geometries and for Cases A, B and C (from left to right).

**Table 2.** Pneumatic and hydraulic efficiencies of the OWC and OTD components for all Cases simulated.

| Geometry | Case A | | Case B | | Case C | |
|---|---|---|---|---|---|---|
| | $\eta_{pne}$ (%) | $\eta_{Hyd}$ (%) | $\eta_{pne}$ (%) | $\eta_{Hyd}$ (%) | $\eta_{pne}$ (%) | $\eta_{Hyd}$ (%) |
| Reference geometry | 41.0 | 19.3 | 32.4 | 36.6 | 46.0 | 17.2 |
| Geometry with new Inlet | 13.7 | 21.4 | 7.5 | 46.1 | 16.9 | 17.8 |
| OWC Rectangular entrance | 55.2 | 22.9 | - | - | - | - |
| OWCs SBS Right/Left | 55.9/54.0 | 20.6 | -/- | - | -/- | - |
| OWCs OTOEA Upper/Lower | 67.5/18.4 | 22.8 | 9.9/1.7 | 33 | 69.3/53.0 | 17.3 |

**Acknowledgements**

The authors wish to acknowledge Nicolás Diego Badano for the support in setting up the OpenFoam numerical models. The authors are also very thankful to WEC4PORTS partners, INEGI and Eire Composites, for their insightful contribute to the present research. Furthermore, the authors are also thankful to SE@PORTS partners, INEGI, IHCantabria, PLOCAN and Fórum Oceano.

**Funding**

This work is being funded by the OCEANERA-NET Second Joint Call 2019 project WEC4PORTS—a hybrid Wave Energy Converter for PORTS (proposal ID 5111), with the references HBC.2019.2443, under the frame of the Belgian Agentschap Innoveren en Ondernemen (VLAIO).

# Submerged bar in a 2-D representation by coupling spectral wave and coastal hydrodynamics models

Anastasia K. FRAGKOU[1], Christopher OLD[2], Vengatesan VENUGOPAL[3], Athanasios ANGELOUDIS[4]

[1,2,3,4] School of Engineering, University of Edinburgh, Edinburgh, UK
email: A.Fragkou@ed.ac.uk

ABSTRACT

A multi-scale parallelised coupled model is developed to investigate wave-current interactions at regional scales. The coupled framework consists of the spectral wave model Simulating WAves Nearshore (SWAN) and the coastal hydrodynamics shallow-water equation model Thetis. The coupling process is facilitated by the Basic Model Interface (BMI). In this study, we assess the model's ability to accurately capture wave-current interactions in a 2-D configuration through the simulation of Dingemans (1987) experimental setup on the behaviour of waves acting upon a submerged bar. The coupled model accurately captures the significant wave heights and the current velocities showcasing a similar level of efficiency as another coupled wave and 3-D current model presented by Roland et al. (2012).

## 1. Introduction

The phenomenon of wave-current interactions is crucial at coastal areas, as surface gravity waves and currents are often encountered simultaneously affecting each other. The accurate representation of such interactions is motivated by a plethora of applications and phenomena, including the evolution of coastal morphology due to sediment transport, their impact in marine energy projects, scouring around offshore structures and the design of offshore and coastal infrastructures. The multi-scale parallelised coupled model of the spectral wave model SWAN (Booij, et al., 1999) with the shallow-water equation model Thetis (Kärnä, et al., 2018) aspires to accurately capture wave-current interactions. The novelty of this coupled model lies in the employment of a semi-implicit numerical scheme and a Discontinuous Galerkin discretisation for the shallow water equation component (Kärnä, 2020), which induces considerably less computational cost than the explicit schemes utilized in other existing coupled models. Additionally, it is the first of such models available in Python, a high-level programming language among the 5 most popular ones in recent years. Its performance in a 2-D situation is examined with a submerged breakwater setup.

## 2. Methodology

The coupled model consists of the parallel structured SWAN model and the unstructured 2-D configuration of the shallow-water equations model Thetis. It is facilitated by the Basic Model Interface (BMI; Hutton, et al., 2020) framework, which contains a set of standard functions used to couple physical process models. SWAN and Thetis have been refactored to fit into the provided BMI libraries, in Fortran for SWAN and in Python for Thetis. Due to the different programming languages utilized by the models, SWAN is wrapped into a Python package for invocation by Python exploiting its BMI version, a Fortran-C interoperability layer, and Cython.

The two models run iteratively and exchange information at prescribed time-intervals. SWAN provides the necessary parameters for the calculation of wave effects on currents, performed by Thetis. These are the significant wave height, $H_s$; the mean wave direction, $\theta_m$; the wavelength, $\lambda$; and the percentage of wave breaking, $Q_b$. In turn, Thetis returns the water elevation, $\eta$; and current velocity vector, $\boldsymbol{u}$.

The model is validated using the experiment of Dingemans (1987) which consists of a semi-cylindrical submerged bar with the bathymetry ranging from 0.10 m to 0.40 m in a flume 30 m long and 26.4m wide (Fig. 2). The waves are generated at the left boundary following a JONSWAP spectrum with significant wave height $H_s = 0.10$ m and peak period $T_p = 1.25$ sec with direction towards the right. The numerical domain consists of two domains (Fig. 1): (a) an outer domain with dimensions 30 m x 70 m; and (b) a nested domain with the same length and 50 m width. The purpose of the outer domain is to generate the appropriate wave boundary conditions for the top and bottom boundaries for domain $D_2$. In Thetis, no-slip boundary conditions are applied.

The mesh utilized in SWAN is a rectilinear structured grid of spacing $dx = 0.40$ m, which is also the mesh element length $\wedge h$ resolution for the unstructured grid employed by Thetis. The timesteps of SWAN and

Thetis coincide with the coupling timestep $\Delta t_{\text{coupl}} = 10$ sec. The effects of bed friction have been considered with the default values of the Madsen formulation in SWAN and the Manning formulation with a constant manning coefficient $n_M = 0.03$ for Thetis. Depth-induced wave-breaking is also accounted for with the default rate of dissipation $\alpha_{BJ} = 1$ and breaker index $\gamma = 0.73$, whereas wind input and wetting and drying have been neglected.

Roland et al. (2012) also employed this case to validate their coupled model, which consists of a 3-D current model with a spectral wave model. They utilized an unstructured grid with horizontal resolution 0.20 m near the breakwater and vertical mesh resolution 0.05 m, while the coupling timestep is equal to 0.5 sec.

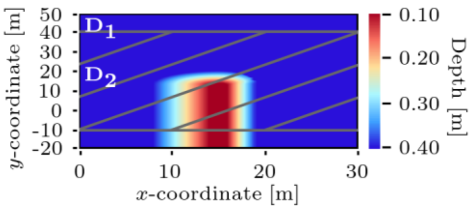


**Fig. 1.** Numerical domain for the Dingemans (1987) experiment

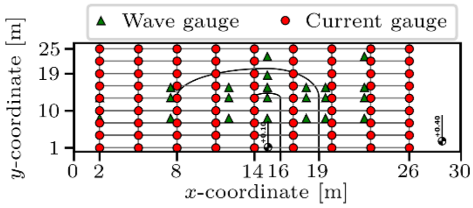


**Fig. 2.** Location of wave and current gauges in Dingemans (1987) experimental setup

## 3. Results and Discussion

Compared to the coupled model of Roland et al. (2012), our model captures better the significant wave height (Fig. 3). The model's predictions exhibit a correlation $r = 0.69$ against the observed experimental data and mean absolute (m.a.) error of 0.9 mm, while Roland et al. (2012) $r = 0.59$ with a similar m.a. error. Dingemans (1987) recorded current velocities at half depth, whose $u$-component (Fig. 4) is more accurately predicted by Roland et al. (2012) with $r = 0.81$ and r.m.s. error 0.002 m s$^{-1}$ in comparison to our model's correlation $r = 0.65$ with r.m.s. error 0.004 m s$^{-1}$. This increase in accuracy does not transfer in the $v$-component of the current velocities (Fig. 5) with both models showcasing a correlation $r = 0.70$ and r.m.s. error 0.001 m s$^{-1}$.

The discrepancy in $u$ velocity predictions between the two coupled models lies presumably in the 3-dimensionality of the Roland et al. (2012) hydrodynamic model in correlation with the velocities' nature; Roland et al. (2012) simulated surface velocities while our model is limited to depth-averaged ones. Furthermore, the violation of one of the shallow-water equation assumptions in our coupled model may also contribute to this behaviour, as the mesh is of the same or smaller order compared to the water depth. This is justified here as the primary application of the model is to function at larger regional scales.

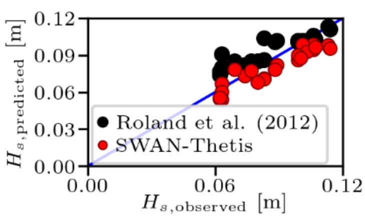


**Fig. 3.** Predicted $H_s$ from Roland et al. (2012) and the model compared against derived experimental values

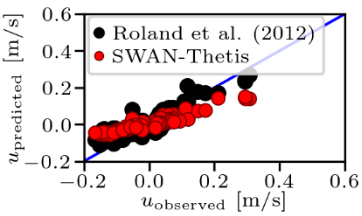


**Fig. 4.** Predicted $u$ current velocity from Roland et al. (2012) and the model compared to recorded measured ones

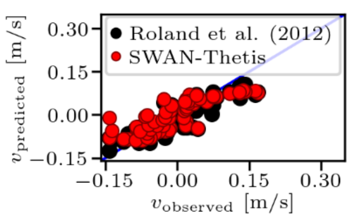


**Fig. 5.** Predicted $v$ current velocity from Roland et al. (2012) and the model compared to recorded measured ones

### References

Booij, N., Ris, R. & Holthuijsen, L., 1999. A third-generation wave model for coastal regions: 1. Model description and validation. *Journal of geophysical research: Oceans*, 104(C4), pp. 7649-7666.

Dingemans, M., 1987. Verification of numerical wave propagation models with laboratory measurements: HISWA verification in the directional wave basin. *h0228.*

Hutton, E. W., Piper, M. D. & Tucker, G. E., 2020. The Basic Model Interface 2.0: A standard interface for coupling numerical models in the geosciences. *Journal of Open Source Software*, 5(51), p. 2317.

Kärnä, T., 2020. Discontinuous Galerkin discretization for two-equation turbulence closure model. *Ocean Modelling*, Volume 150, p. 101619.

Kärnä, T. et al., 2018. Thetis coastal ocean model: discontinuous Galerkin discretization for the three-dimensional hydrostatic equations. *Geoscientific Model Development*, 11(11), pp. 4359-4382.

Madsen, O. S., Poon, Y.-K. & Graber, H. C., 1989. Spectral wave attenuation by bottom friction: Theory. In: *Coastal engineering 1988.* s.l.:s.n., pp. 492-504.

Roland, A. et al., 2012. A fully coupled 3D wave-current interaction model on unstructured grids. *Journal of Geophysical Research: Oceans*, 117(C11).

# A Wavelet-based analysis of solitary wave forces at submerged rectangular barriers

Domenico Davide MERINGOLO[1], Federico CASELLA[1], Francesco ARISTODEMO[1]

[1] Dipartimento di Ingegneria Civile, Università della Calabria, via Pietro Bucci 1 – cubo 42B
email: davide.d86@gmail.com; federico.casella@unical.it; francesco.aristodemo@unical.it

ABSTRACT

A time-frequency modeling of the wave loads induced by non-stationary oscillatory signals such as solitary waves on a submerged rigid rectangular breakwater was performed. To this purpose, small-scale laboratory tests were undertaken in a wave channel, adopting 12 pressure sensors along the external contour of the barrier to deduce the hydrodynamic loads. The raw experimental data were filtered through the Wavelet analysis, selecting a Mexican hat Wavelet. A sensitivity analysis of the resulting drag, inertia and lift coefficients deduced from the empirical calibration of the widespread Morison's formula was finally carried out.

## 1. Introduction

Low-crested breakwaters have been adopted to protect the coasts in order to prevent erosion and inundation processes as well as to provide safe navigation under the wave action. The increase in the construction of these structures is mainly due to their low environmental impact. Regarding the category of submerged rigid breakwaters and solitary waves as wave forcing, past studies mainly focused on wave transmission, reflection and dissipation processes. Moreover, the near flow field characterized by the occurrence of breaking phenomena and the characteristics of vortexes at the external contour of the barrier were also investigated (e.g., Huang and Dong, 2001). Few works analyzed the solitary wave-induced forces. A first research was carried out by Huang and Dong (2001), who studied a dike with a relative height of the breakwater, $a/d$ = 0.5, where $a$ is the height of the breakwater and $d$ is the water depth. Some cases with variable wave non-linearity $A/d$, where $A$ is the wave amplitude, were analyzed. Huang and Dong (2001) examined only horizontal loads, showing a prevalence of positive peaks with respect to negative ones, and a negligible role of shear stresses in reproducing the in-line forces. The study by Liu (2004) linked to thin barriers underlined the appearing of a linear trend for the maximum horizontal loads as a function of $A/d$. However, these studies were limited to a small range of $A/d$, focusing on the horizontal forces alone. For a submerged barrier with $a/d$ = 0.5, Tripepi et al. (2020) have analyzed the characteristics of both horizontal and vertical loads, evidencing that the latter plays an important role for the potential sliding of the barrier. Owing to the weak deformation of the shape of the solitary wave at the barrier for the considered $a/d$, the Authors have applied semi-empirical formulas to reproduce the time variation of the forces. However, the adopted equations, such as the classical Morison scheme, have the limit of determining the hydrodynamic loads for non-breaking conditions. Indeed, the mentioned equations can be used for underwater structures which do not influence the free surface (e.g., Aristodemo et al., 2022). The work by Tripepi et al. (2020) has been here extended, involving a rectangular-type barrier and three relative heights ($a/d$ = 0.5, 0.7 and 0.9). By the experimental viewpoint, the tests were carried out in the wave flume of GMI Laboratory at UNICAL. The loads were deduced from a series of pressure sensors placed at the external surface of the rectangular barrier. The wave characteristics and the horizontal movement of the wavemaker were recorded by wave probes and an ultrasonic sensor, respectively.

## 2. Laboratory tests

The laboratory tests were undertaken in the wave flume (41 m length, 1 m width and 1.2 m depth) of the GMI Laboratory at UNICAL. The wave channel was given by a piston-type paddle. The longitudinal profile of the apparatus to perform the experiments is shown in Fig. 1a. The barrier was placed at a distance of 9.08 m from the paddle, with $a$ = 0.127 m and $b$ = 0.254 m. The loads were deduced from sensors placed at the external surface of the barrier. Due to the dimensions of the transducers and to avoid a too large breakwater, the transducers at the beaten and lee sides were slightly staggered, with reference to the centerline of the channel. A similar arrangement was also used in a previous experiment with a horizontal cylinder (Tripepi et al., 2020).

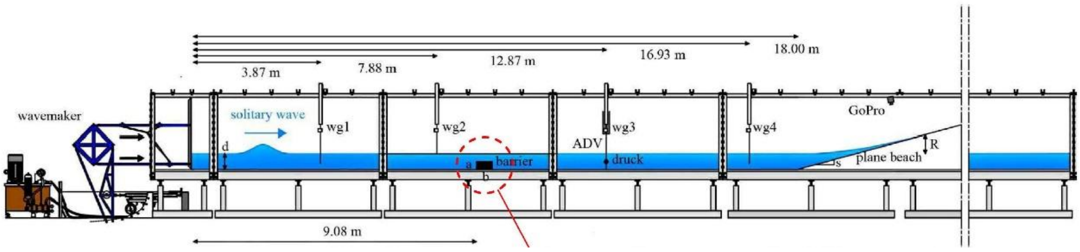


**Fig. 1.** Longitudinal profile of the experimental apparatus.

Here, the horizontal, $F_H$, and vertical, $F_V$, loads were deduced as:

$$\begin{cases} F_H(t) = a_1[\Delta p_1(t) + \Delta p_2(t) + \Delta p_3(t)] - \Delta p_7(t) - \Delta p_8(t) - \Delta p_9(t) \\ F_V(t) = a_2[\Delta p_1(t) + \Delta p_9(t)] - a_3[\Delta p_4(t) + \Delta p_5(t) + \Delta p_6(t)] \end{cases}$$

being $a_1$, $a_2$ and $a_3$ the influence areas. They are equal to $a/4$, $a$ and $a/2$, respectively. To deduce the vertical forces acting at the bottom of the barrier, the lack of pressure sensors in this part led to consider a trapezoidal pressure distribution. This methodology was usually taken into account for stability aims of breakwaters. The surface elevations were deduced from two wave gauges (wg1 and wg2), located before and after the barrier. These tools were mounted at a distance of 7.88 m and of 12.87 m from the paddle, respectively. The sampling frequency of the transducers and the gauges was 100 Hz, while the displacement of the paddle was verified using an ultrasonic sensor located behind it, with a frequency of 50 Hz. By imposing various displacements to the paddle, 33 tests were undertaken. Three water depths, $d_1$, $d_2$ and $d_3$, respectively equal to 0.254 m, 0.181 m and 0.141 m, were used. The relative height of the breakwater $a/d$ was 0.5, 0.7 and 0.9, respectively. For test with $A$ = 0.072 m and $d$ = 0.254 m, Fig. 2 highlights the raw and filtered time series of $F_H$ and $F_V$, and the related Wavelet coefficients for the filtered signals. It is noted that the raw data are quite noise due to various disturbances (Fig. 2a), and the application of a high-pass filtering leads to a smoother resulting force profile (Fig. 2b). The obtained positive and negative Wavelet coefficients are in phase (i.e., positive coefficients) or out of phase (i.e., negative coefficients), with reference to the original mother signal of the Wavelet. In other words, positive values occur when the force signal is in phase with the corresponding shape of the Wavelet. Regarding the force features, $F_H$ is larger than $F_V$ and it appears before. This characteristic was observed for all cases (e.g., Tripepi et al., 2020).

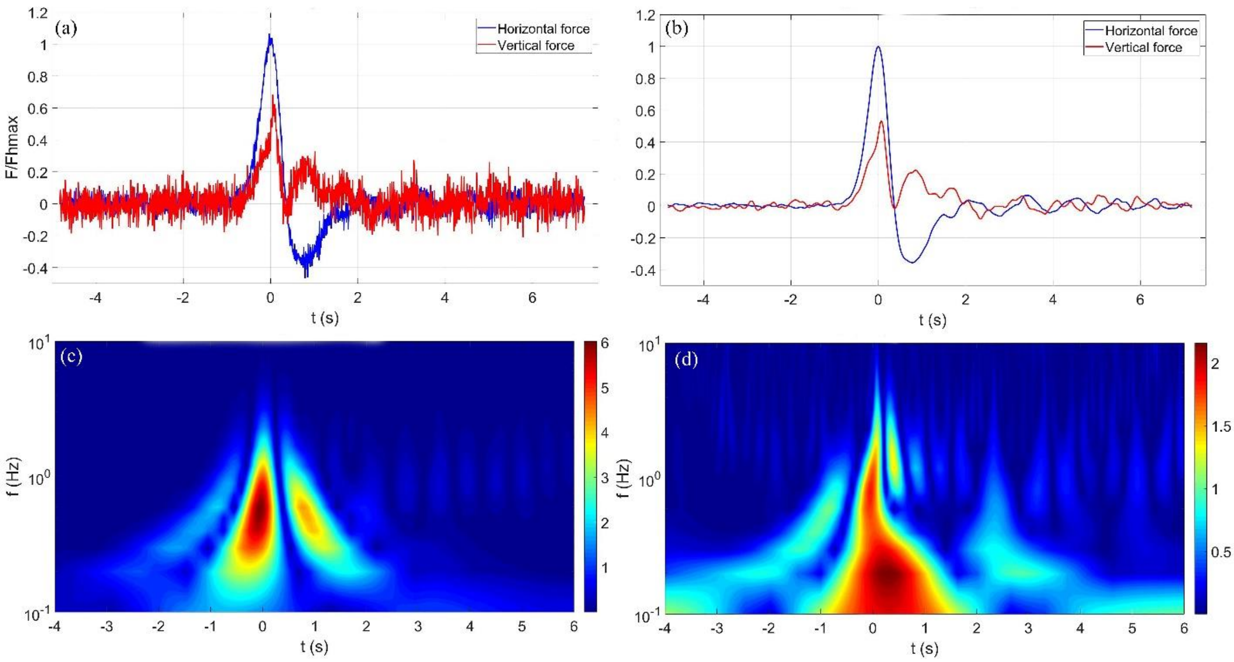


**Fig. 2.** (a) Time series of raw horizontal and vertical loads; (b) Time series of filtered horizontal and vertical wave loads; (c) Wavelet coefficients of filtered horizontal load; (d) Wavelet coefficients of filtered vertical load (test with $A$ = 0.072 m and $d$ = 0.254 m).

**References**

Huang, C.-J., Dong, C.-M. (2001). On the interaction of a solitary wave and a submerged dike. Coast. Eng. 43, 265-286.
Lin, P. (2004). A numerical study of solitary wave interaction with rectangular obstacles. Coast. Eng. 51, 35-51.
Tripepi, G., Aristodemo, F., Meringolo, D.D., Gurnari, L., Filianoti, P. (2020). Hydrodynamic forces induced by a solitary wave interacting with a submerged square barrier: Physical tests and δ-LES-SPH simulations. Coast. Eng. 158, 103690, 1-17.

# Perched beach nourishment against coastal erosion and flooding: Experimental and numerical simulation

Dimitrios SPYROU[1], Theofanis KARAMBAS[2]

[1]Department of Civil Engineering, Aristotle University of Thessaloniki, PC 54124, Thessaloniki, Greece
email: dispyrou@civil.auth.gr

[2] Department of Civil Engineering, Aristotle University of Thessaloniki, PC 54124, Thessaloniki, Greece
email: karambas@civil.auth.gr

ABSTRACT

A extensive two-dimensional laboratory investigation was performed, in order to study the cross-shore profile evolution of a perched beach, after the application of beach nourishment method. The presence of the geotextile artificial reef leads to wave reflection and additional dissipation of the wave energy and obstruct the sand from drifting seawards Also an advanced Boussinesq type nonlinear wave model has been developed in order to simulate cross-shore hydro-morphodynamic processes. The comparison between experimental and numerical beach profile indicates good agreement.

## 1. Introduction

Beach nourishment combined with a submerged structure is a very common method against beach erosion and flooding. The response of the cross-shore hydro-morhodynamics depends on the interaction between the waves, the submerged reef, and the characteristics of the artificial beach. The reef dissipates and reflects the wave energy and obstruct the sand from drifting seawards (Gonzalez et al., 1999, Musumeci et al., 2012).

## 2. Experimental methodology

The experiment has been conducted (in a 1:20 scale) in the Laboratory of the Department of Hydraulics and Environmental Engineering, Aristotle University of Thessaloniki, Greece. A sandy beach was formed in a 14.05 m long wave flume. The flume was 0.40 m. wide. The slope of the surf-zone was set equal to 1:10. The water level was 0.28 m. A submerged structure, made of geotextile material, was placed one meter (towards the shore) from the point where bed slope (1:10) begins. The freeboard was 9 cm. A well sorted fine natural sand of $d_{50}$=0.2 mm is used in the experiments. Four wave periods was selected, T = 1.00 sec, T = 1.25 sec, T = 1.54 sec, T = 2.00 sec. The wave height was constant and equal to 0.1 m (H = 0.1 m) and 0.04 m (H=0.04 m). The beach fill slope was 1:2 and 1:4 respectively. The berm height of the beach fill was B=0.05m.

## 3. Numerical model

Cross-shore morphology evolution of a nourishment project is simulated by an improved version of the Boussinesq nonlinear wave model described in Spyrou and Karambas (2021). The hydrodynamic model (wave and undertow model) provides to the sediment transport model all the required information (wave height, bottom velocity, wave energy dissipation, mean sea level). The bed load transport (including sheet flow sediment transport rate and suspended load over ripples) is estimated with a quasi-steady, semi-empirical formulation, developed by Camenen, and Larson ( 2007) for an oscillatory flow combined with a superimposed current. Phase-lag effects in the sheet flow layer were included through a coefficient proposed by Camenen and Larson (2007). In order to incorporate the suspended sediment transport rate, the depth-integrated transport equation for suspended sediment is solved (Kobayashi and Tega, 2002, Spyrou and Karambas, 2021).

## 4. Experimental and numerical results - Conclusions

Figures 1 and 2 show the instantaneous surface elevation, the initial profile, the final profile at the end of the experimental process, and the results from the mathematical model. The presence of the geotextile artificial reef leads to wave reflection and additional dissipation of the wave energy, mitigating the erosive wave conditions.

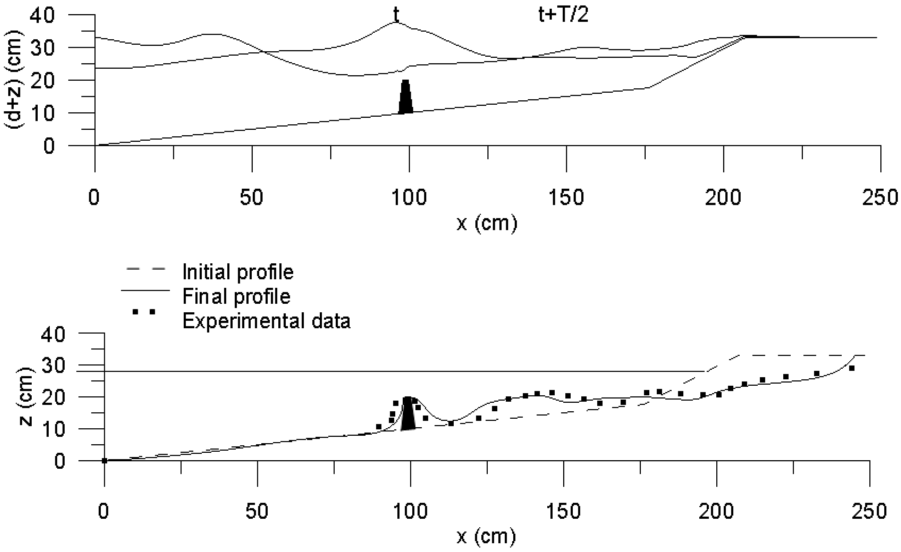


**Fig. 1.** Instantaneous surface elevation, cross-section morphology evolution. H = 0,10 m T=1.54 sec, slope=1/2.

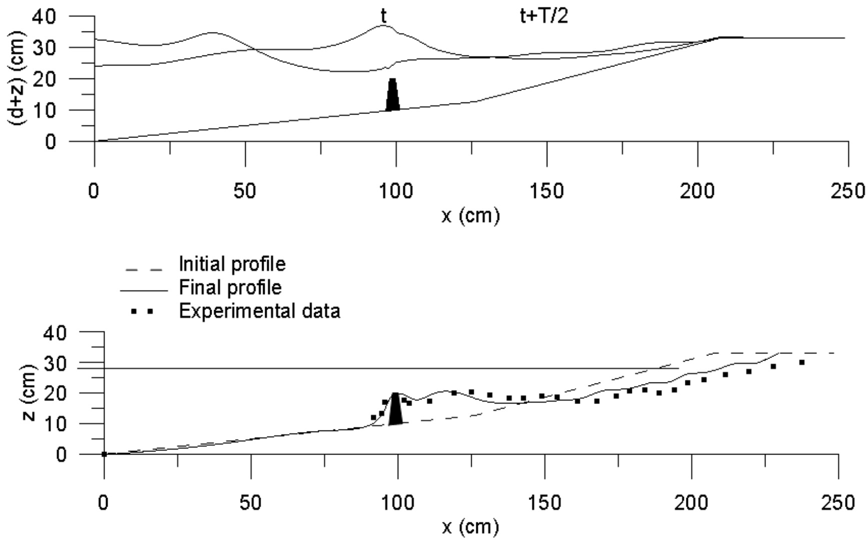


**Fig. 2.** Instantaneous surface elevation, cross-section morphology evolution. H = 0,10 m T=1.54 sec, slope=1/4.

Together with beach face erosion a bar begins to form near the shore and then it moves seawards as the experiment evolves. It ends up in a position in contact with the submerged breakwater. The submerged structure is an obstacle to further movement of the sand. The sand is not carried seawards, but remains trapped between the constructed layout and the shoreline. Also, in comparison with the previous experiments, under the same conditions but without submerged structure (Spyrou and Karambas, 2021), the coastline recession and coastal flooding is decreased. Consequently the method can be considered as an improvement of the beach nourishment method and can used against beach erosion and flooding. Finally, the cross-shore profile resulting from the numerical application is very well related to the experimental one.

**References**

Camenen, B., Larson, M. (2007), A unified sediment transport formulation for coastal inlet application, Technical report ERDC/CHL CR-07-1, US Army Engineer Research and Development Center, Vicksburg, MS.

Gonzalez, M, Medina, R., Losada, M.A. (1999), Equilibrium beach profile model for perched beaches, Coastal Engineering, 36(4), 343-357.

Kobayashi N. and Y. Tega (2002), Sand Suspension and Transport on Equilibrium Beach, Journal of Waterway, Port, Coastal, and Ocean Engineering 128 (6).

Musumeci R. E., L. Cavallaro and E. Foti (2012), Performance of perched beach nourishments, Coastal Engineering Proceedings 1(33), DOI:10.9753/icce.v33.sediment.112.

Spyrou D., Th. Karambas (2021), Experimental and Numerical Simulation of Cross-Shore Morphological Processes in a Nourished Beach. Journal of Coastal Research 1 September 2021; 37 (5): 1012–1024. doi: https://doi.org/10.2112/JCOASTRES-D-20-00098.1

# Hydrodynamic evaluation of Naissaar Harbour with a phase-resolved coastal wave model

Weizhi WANG[1], Rain MÄNNIKUS[2], Tarmo SOOMERE[3], Hans BIHS[4]

[1,4] Norwegian University of Science and Technology, Norway
email: weizhi.wang@ntnu.no (for author 1)
email: hans.bihs@ntnu.no (for author 4)

[2,3] Tallinn University of Technology
email: rain.mannikus@gmail.com (for author 2)
email: soomere@cs.ioc.ee (for author 3)

ABSTRACT

Nonlinear wave transformations take place due to the effects of bathymetry and coastline geometry. Several nonlinear transformations cannot be represented correctly in a phase-averaged model, a phase-resolved modeling strategy is often required. Shallow water equation-based phase-resolving models are computationally efficient, but their accuracy is limited by water depth conditions. In this article, a full nonlinear potential flow (FNPF) model REEF3D::FNPF is used for the phase-resolving wave modelling near the Naissaar harbor. The accuracy of the FNPF model is not limited by the water depth and thus can model both the short wind-generated waves and the long waves under extreme events related to climate change. The holistic understanding of the hydrodynamic environment provides vital information for future investigations into the large-scale cross-shore and longshore sediment transport and morphology evolution in that region.

## 1. Introduction

The Naissaar harbor is in the Gulf of Finland, near Tallin in Estonia. The narrow profile of the Gulf of Finland allows long fetch and thus the development of wind waves in the east-west direction. Recently, an improved and upgraded harbor at Naissaar is planned, where the hydrodynamic environment near the harbor, including the wave conditions and their impact on the sediments, needs to be investigated. The area of interest is seen in Fig.1 (a), the dimension is 4 km in the east-west direction and 3 km in the north-south direction. The maximum water depth within the domain of interest is 36.5 m. The input irregular wave has a significant wave height of 1.42 m and a peak period of 10 s. The JONSWAP spectrum and Mitsuyasu direction spreading function are used for the short-crested sea.

## 2. Numerical model

### 2.1. Governing equation

The governing equation of the fully nonlinear potential flow model REEF3D::FNPF (Bihs et al., 2020) is the Laplace equation:

$$\nabla^2\phi = 0 \tag{1}$$

Together with the fully nonlinear boundary conditions, the velocity potential $\phi$ can be solved.

### 2.2. Breaking wave algorithm

The breaking wave algorithm consists of the breaking detection algorithm and the energy dissipation algorithm. The shallow water phase velocity-based detection method and the wave steepness-based detection methods are both used. Once breaking waves are detected, the corresponding energy dissipation can be determined using the filtering algorithm or the artificial viscosity method.

### 2.3. Coastline algorithm

The coastline algorithm follows the procedure proposed by Wang et al. (2022). The wetting and drying cells around the coastline can be detected based on the local water depth. Thereafter, the signed distance level-set function is used to determine the coastline position and calculate distances away from the coastline. Two-cell wide coastal relaxation zones are then arranged along the coastlines to avoid numerical instability at the infinitesimal water depth.

## 3. Results

The numerically reconstructed bathymetry in REEF3D::FNPF is shown in Fig.1(b).

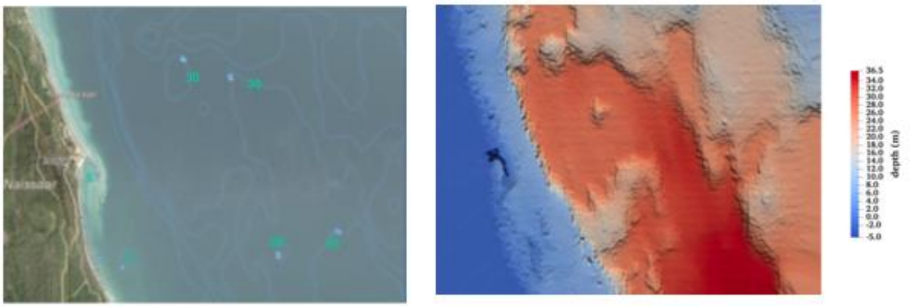

(a) (b)

**Fig. 1.** The sea floor bathymetry of the area of interest. (a) bathymetry map; (b) reconstructed bathymetry in the numerical wave tank.

Three wave gauges are arranged from offshore to inside the harbor, as seen in Fig. 2(a). The numerically simulated wave surface elevation is shown in Fig.2(b).

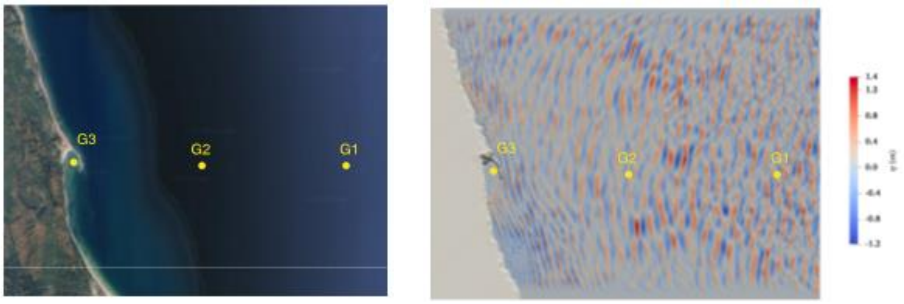


(a) (b)

**Fig. 2.** (a)wave gauge locations; (b) free surface elevation simulated in REEF3D::FNPF at t=5120 s.

The evolution of the wave spectra is shown in Fig.3. Wave shoaling and breaking take place at G2 due to the submerged reef seen in Fig.1 (b). The wave energy is significantly reduced inside the harbor due to the protection of the breakwater. However, significant low-frequency waves remain, presenting potential challenges for the moored vessels.

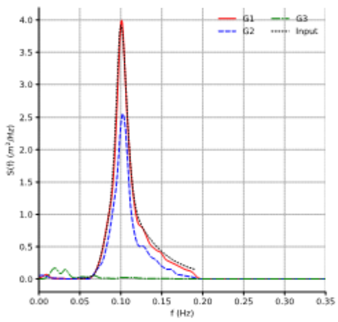


**Fig. 3.** Wave spectra at three wave gauges. The solid line, dashed line and the dash-dotted line represent the wave spectra at wave gauges 1,2 and 3. The dotted line represents the input wave spectrum.

**Acknowledgements**

The authors thank the financial and technical support from the EEA project EMP480 - solutions to current and future problems on natural and constructed shorelines, eastern Baltic Sea. We are also grateful for the bathymetry data provided by Rain Mannikus.

**References**

Bihs, H., Wang, W., Pákozdi, C. and Kamath, A. (2020). REEF3D::FNPF—A flexible fully nonlinear potential flow solver. Journal of Offshore Mechanics and Arctic Engineering, 142(4), 041902.

Wang, W., Pákozdi, C., Kamath, A., Fouques, S. and Bihs, H. (2022). A flexible fully nonlinear potential flow model for wave propagation over the complex topography of the Norwegian coast. Applied Ocean Research, 122, 103103.

# Wave Run-Up and Overtopping Quantification at Different Coastal Structures

R.D. Mateus[1], R.F. Carvalho[1], R. Lemos[2], C.J.E.M. Fortes[2]

[1]University of Coimbra, MARE, Department of Civil Engineering, Coimbra, Portugal
email: rafael_271996@hotmail.com, email: ritalmfc@dec.uc.pt
[2]National Laboratory of Civil Engineering, Lisboa, Portugal
email: rlemos@lnec.pt;email: jfortes@lnec.pt

ABSTRACT

With the sea level rise and all the processes associated with wave action, it is expected that the existing formulas for wave run-up and wave overtopping evaluation will be misfits, justifying further studies. In this work different methodologies to quantify wave run-up and overtopping will be evaluated by comparing the results obtained with traditional experimental tests made in a physical scale model, which consists of a sloped structure facing the direction of different irregular incident wave and tide level conditions. The first methodology is based on physical scale model films acquisition and an algorithm made in Matlab® consisting in digital images processing and analysis. The second methodology is based on numerical simulations using OpenFOAM®. Both methodologies show usefulness.

## 1. Introduction

The sea level rise due to climate changes and the consequent different conditions nearshore in the vicinity of coastal structures, will have an impact on those structures since extreme events become more frequent and more energetic. So, the knowledge of wave transformation close to coastal structures in those conditions become crucial for understanding physical processes (wave run-up and overtopping, in special) and to finally get a better design of those structures. Physical scale models and traditional experimental measurements have been crucial. However, they are expensive from the point of view of installed equipment and timely consumption of human resources. Digital methods and numerical methods can be an alternative. In this work, we will use digital images analysis using Matlab® to estimate wave parameters as well as numerical models based on the deterministic description of the hydrodynamics using advanced numerical models within OpenFOAM®. Both results (digital and numerical methods) are compared with measurements of free surface elevation acquired in the physical scale model with traditional methods.

## 2. Experimental Method

The physical model was built in the experimental facilities of the Department of Hydraulics and Environment (DHA) of LNEC, in the irregular wave channel of the Maritime Hydraulics Pavilion (COI1). The channel is 49.6 m long, 0.8 m wide and 1.0 m high and equipped with an irregular wave generator. The model, presented in Fig. 1a), is a real case and was built and explored according to Froude's law of similarity at a geometric scale of 1/90, to guarantee that the defined test conditions could be reproduced in the irregular wave channel with the available resources. This choice of scale implies that the time and volume scales were approximately 1:9.49 and 1:729000, respectively. A sloped structure 2.5:1 with height of 21.5 cm was implemented on the highest part of the bottom. Several equipment was installed in the flume, such as resistive probes measuring free-surface elevation along the channel and devices to measure the overtopping volume. We tested different water level with irregular wave train characterized by different combinations of the wave peak period and significant wave height.

## 3. Digital Analysis

Several films were performed under different light conditions to stablish the best conditions for the digital image processing and analysis procedure. Image analysis was carried out using different software: i) Free video to jpg converter to create a sequential of capture frames; ii) Matlab®, in which a set of scripts was created to automatically detect water height in several mark locations (Fig 1b1), where edge detection and distance between points from the edge has to be process in order to evaluate water height (Fig 1b2) and volume over the structure and define run-up and overtopping using different numerical techniques such as interpolation.

## 4. Numerical Model

OpenFOAM® is a widely used open source C++ toolbox, which includes different solvers, tools and libraries. It includes the solver interFoam and several boundary conditions, specially designed for coastal processes. InterFoam solver consists in solving Navier-Stokes equations / Reynolds-Averaged Navier-Stokes (RANS) equations governing the motion of the 3D incompressible and isothermal flows in which the free surface is described using a Volume-Of-Fluid method (VOF). Simulations require a detailed 3D model of the geometry that was constructed by coordinates to define the bottom and the structure using Salome to represent it through a stl ("stereolithography") file, to be used in OpenFOAM® snappyHexMesh tool to build a mesh in a parallelepiped cutted by the stl (Fig 1). Following guidelines of having 7 to 10 cells across the wave height and 100 cells along the wavelength (Carvalho et al., 2021), values of dx = dy = dz = 0.1 m were reached. Refinements parameters near the paddleboards, the sloped structure and the lateral walls were defined in snappyHexMesh Dictionary, using 2 levels for every surface-based refinement and 3 cells between levels. Data displacement from the paddle board generating a JONSWAP spectrum was extracted to define wave paddle boundary condition.

## 5. Results and Conclusions

Digital images taken from the physical model were processed to evaluate the water height at six different pre-defined "windows" using MATLAB scripts, which detect edges, define 2 points at the edges and calculate distance between them (Fig 1b1 and b2). Fig 1b3 shows the sequence of water depth in the selected six "windows". 100 frames from a video were tested and similarities between the results of the program and the ones from the probes of the canal can be noticed. The image quality still causes few data errors, which can be improved by new tests with different lighting conditions. Fig. 1c shows preliminary simulations with OpenFOAM®. Boundary condition to generate waves according the physical models should be improved.

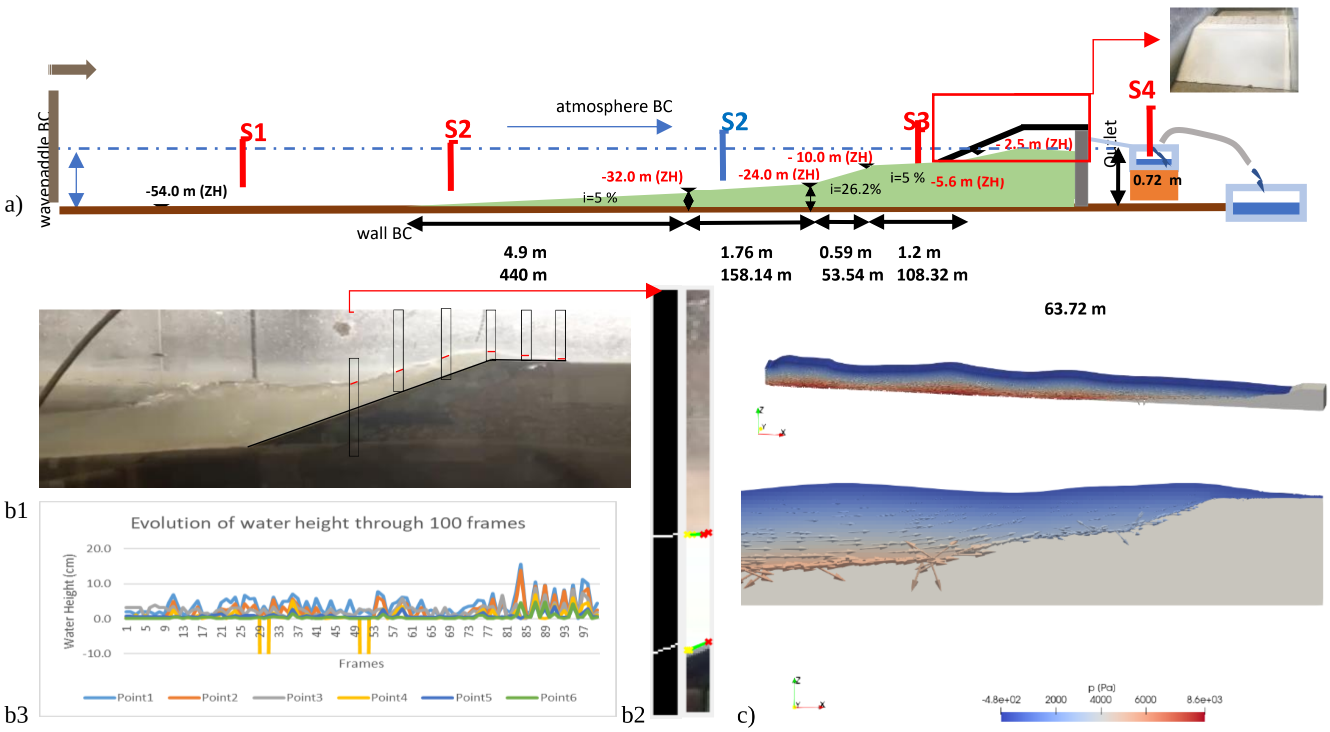


**Fig. 1.** Physical scale model: a) Bottom profile of the flume with the structure schema; b) images of the structure and run-up definition c) CFD preliminary simulations: 8s perspective and 9.5 s side view.

**Acknowledgements**

FCT (Portuguese Foundation for Science and Technology) through the Project UID/MAR/04292/2020, financed by MEC (Portuguese Ministry of Education and Science) and FSE (European Social Fund), under the programs POPH/QREN (Human Potential Operational Programme from National Strategic Reference Framework) and POCH (Human Capital Operational Programme) from Portugal2020. The authors also acknowledge the Laboratory for Advanced Computing at University of Coimbra for providing HPC, computing.

**References**

Carvalho, R.F., Santos, J.A., Barajas O. G., Beg, Md. N. A., Lopes, P.M., Fortes, C.J.E.M., Lara, J. L.. Experimental and Numerical Simulations of Oblique Extreme Wave Conditions in Front of a Breakwater's Trunk and Round Head. JICZM - J. of Integrated Coastal Zone Management, Vol. 21(2) 73-85, 2021, ISSN 1646-8872, DOI 10.5894/rgcin294.

# Numerical simulations of wave breaking over coastal vegetation as a beach protection solution

Iason CHALMOUKIS[1], Georgios LEFTHERIOTIS[1], Athanassios DIMAS[1]

[1] Department of Civil Engineering, University of Patras, Greece
email: ichalmoukis@upatras.gr)
email: gleytheriot@upatras.gr
email: adimas@upatras.gr

ABSTRACT

The objective of this work is to present an advanced, hydrodynamic numerical model specifically targeting the improvement of coastal vegetation for beach protection. Coastal vegetation (CV) is an effective and low-cost coastal protection method that also mitigates the impacts of climatic variability, while maintaining biodiversity. The model is based on the formulation of three-dimensional, large-eddy simulations. The combined water and air flow is modelled following the porous media approach to study the CV flow resistance. The effectiveness of CV is based on the comparison of wave and current results for beaches with and without CV.

## 1. Introduction

Coastal erosion and flooding are expected to intensify in the future because of the increasing frequency of extreme meteorological events, together with their potential to damage littoral infrastructures, touristic beaches and coastal ecosystems. Coastal management principles favor environment-friendly methods for beach protection in contrast to the "hard" works of the past (breakwaters, revetments, etc.). Nature-based solutions (NBS) like coastal vegetation (CV) have received significant attention in the previous decade. Several numerical experiments have been performed to study vegetation effects on wave propagation. However, most of the numerical models are based on the shallow water two-dimensional (2D) vertical-averaged equations (Maza et al. 2015) that do not resolve the depth-varying flow dynamics. One of the first approaches for wave damping over vegetation areas was presented in Dalrymple et al. (1984) where different values of a drag coefficient were used to take into account the plant motion. The model of Darlymple et al. (1984) was extended in Mendez & Losada (2004) in order to compute wave height transformation over a CV field with adequate accuracy. Yang et al. (2018) studied numerically the effect of CV on wave propagation using a drag coefficient computed by the Morison equation, with the fully nonlinear Boussinesq equations, which also do not resolve the depth-varying flow dynamics. They concluded that the CV can effectively cause wave attenuation, depending on wave and vegetation characteristics. From previous studies, it is clear that the effect of CV on wave attenuation has not been extensively analyzed taking into account the three-dimensional (3D) flow dynamics and especially along the water depth. In the present research work, the study focuses on typical storm waves while the complete 3D flow field is resolved.

## 2. Numerical implementation

The combined water and air flow is modelled as one-fluid flow governed by the 3D incompressible Navier-Stokes equations, appropriate to model flow in porous media (Liu et al., 1999):

$$\frac{\partial u_i}{\partial x_i} = 0 \tag{1}$$

$$\frac{1+c_A}{n}\frac{\partial u_i}{\partial t} + \frac{1}{n^2}\frac{\partial}{\partial x_j}\left(u_i u_j\right) = -\frac{1}{\rho}\frac{\partial p}{\partial x_i} + \frac{\delta_{i3}}{\mathrm{Fr}^2} - \frac{\partial \tau_{ij}}{\partial x_j} + \frac{1}{\mathrm{Re}}\frac{1}{n}\frac{1}{\rho}\frac{\partial}{\partial x_j}\left(\mu\left(\frac{\partial u_i}{\partial x_j} + \frac{\partial u_j}{\partial x_i}\right)\right) - \frac{\left(1-n^2\right)}{n^3}\frac{\nu}{D_g^2}\frac{20}{\mathrm{Re}}u_i - 1.1\left(1+\frac{7.5}{\mathrm{KC}}\right)\frac{1-n}{n^3}\frac{1}{D_g}u_i\sqrt{u_i u_i} + f_i \tag{2}$$

where $x_i$ are the Cartesian coordinates, $t$ is the time, $u_i$ are the resolved velocity components, $c_A$ is the added mass coefficient, $n$ is the effective porosity, $p$ is the pressure, i.e., the sum of dynamic and hydrostatic pressure, $\rho$ is the normalized (by its water value) fluid density, $\delta_{ij}$ is the Kronecker's delta function, Fr is the Froude number, $\tau_{ij}$ are the SGS stresses related to the LES formulation, Re is the Reynolds number, $\mu$ and $v$ are the normalized (by their water values) fluid dynamic viscosity and kinematic viscosity, respectively, $D_g$ is the mean grain diameter of the porous media, and KC is the local Keulegan-Carpenter number. The external forcing term, $f_i$, is associated with the implementation of the Immersed Boundary method for the imposition of flow boundary conditions on the seabed. The sea surface evolution is tracked by the level-set method, and the porous media approach is used to model the CV flow resistance. The computational cost for performing these large-scale simulations is extremely high. Thus, High Performance Computing (HPC) methods are used in this work. Incident waves of certain height and period are generated by a numerical piston-type wavemaker at the offshore side of the computational domain (Fig. 1).

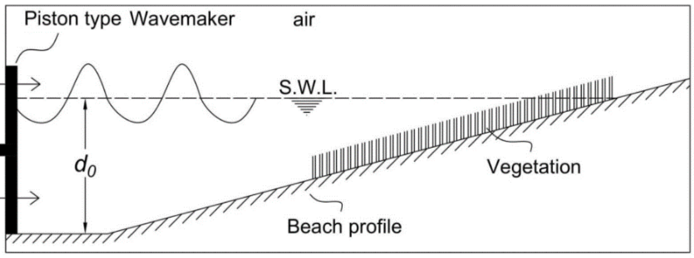


**Fig. 1.** Sketch of the configuration of the numerical domain with a coastal vegetation zone.

## 3. Results

Numerical simulations of wave propagation and breaking over a beach of constant slope tan$\beta$ = 1/15 have been performed, with and without the presence of CV. The Reynolds number based on the water depth at the wavemaker is equal to $Re_d = 1.3\times10^6$. The characteristics of the incident waves correspond to laboratory scale dimensional values of $H$ = 0.18 m for the incident wave height and $T_s$ = 1.676 s for the wave period. The water depth at the wavemaker in dimensional units is equal to $d$ = 0.60 m. The vegetation field (Fig. 2b) starts at depth of 0.45 m, its length is equal to two wavelengths, and its equivalent porosity is $n_{eq}$ = 0.82. The envelope of the free-surface elevation during two waves is presented in Fig. 2 after ten waves, over a beach without and with CV. Wave breaking occurs at $x_1/d_0 \approx 20$ and at $x_1/d_0 \approx 17$ for the case without CV and with CV, respectively. The presence of the CV reduces the wave height by about 13%.

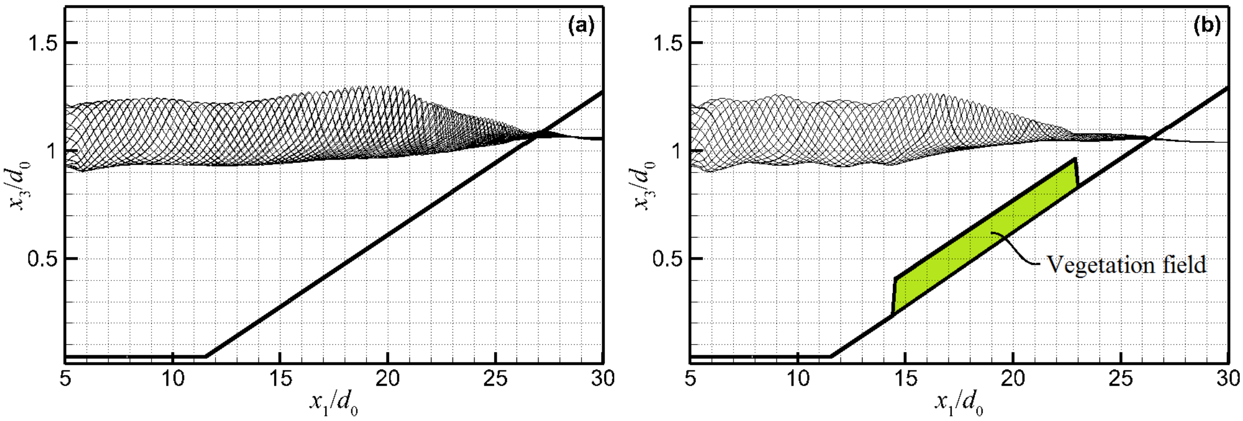


**Fig. 2.** Envelope of the free surface elevation of waves breaking over a beach of constant slope 1/15 without (a) and with CV (b).

**Acknowledgements**

This work was supported by computational time granted from the Greek Research & Technology Network (GRNET) in the National HPC facility – ARIS – under project ID CoastHPC.

**References**

Dalrymple RA, Kirby JT, Hwang PA (1984) Wave diffraction due to areas of energy dissipation, Journal of Waterway Port Coastal and Ocean Engineering, 110, 67-79.
Liu PLF, Pengzhi L, Chang K, Sakakiyama T (1999) Numerical modeling of wave interaction with porous structures, Journal of Waterway Port Coastal and Ocean Engineering, 125(6), 322-330.
Maza M, Lara J, Losada I (2015) Tsunami wave interaction with mangrove forests: A 3-D numerical approach, Coastal Engineering, 98, 33-54.
Mendez F, Losada I (2004) An empirical model to estimate the propagation of random breaking and nonbreaking waves over vegetation fields, Coastal Engineering, 51, 103-118.
Yang Z, Tang J, Shen Y (2018) Numerical study for vegetation effects on coastal wave propagation by using nonlinear Boussinesq model, Applied Ocean Research, 70, 32-40.

# Monitoring and Modelling of Coastal Change on a Dissipative Beach on the Southwest Coast of Ireland

Stephen NASH[1,2,3], Siegmund NUYTS[1,2,3], Andi EGON[1,2,3,4], Sheena FENNELL[1,2], Eugene FARRELL[2,3,5]

[1] College of Science & Engineering, National University of Ireland Galway, Ireland
[2] Ryan Institute, National University of Ireland Galway, Ireland
[3] MaREI Research Centre, National University if Ireland Galway, Ireland
[4] Oceanography, Bandung Institute of Technology (ITB), Indonesia
[5] School of Geography, Archaeology, and Irish Studies, National University of Ireland Galway, Ireland
email: stephen,nash@nuigalway.ie

ABSTRACT

A combined monitoring and modelling approach is used to investigate coastal change on a dissipative beach in Brandon Bay, Ireland. Time-lapse cameras were deployed and assessed for their suitability for detection of shoreline edge and wave run-up. Surveyed beach profiles were used to assess changes in beach elevation from December to February 2022 and a coupled wave-morphology model was developed using SWAN and XBeach to simulate the observed changes.

## 1. Introduction

There is an urgent need to understand the linkages between coastal shoreline changes and their drivers so that we can better protect coastal communities. The generic controls that influence all coasts include, but are not limited to, wave-wind action, storm surge, tides, and sediment budgets (Devoy 2015). The magnitude of their respective roles cannot be assessed without the relevant long-term monitoring data on the drivers and responses (O' Connor et al., 2011). Conventional terrestrial and water surveys are not repeated frequently enough for this purpose (Guisado-Pintado and Jackson, 2020) but autonomous monitoring systems and coupled ocean-coastal zone models can provide the long time periods and high temporal resolutions needed. Here, we assess a low-cost, autonomous shoreline monitoring system deployed on a dissipative beach in Brandon Bay, southwest Ireland (Fig. 1), using off-the-shelf time-lapse cameras, and a coupled wave-morphology modelling system developed to simulate changes in beach elevation due to storm events.

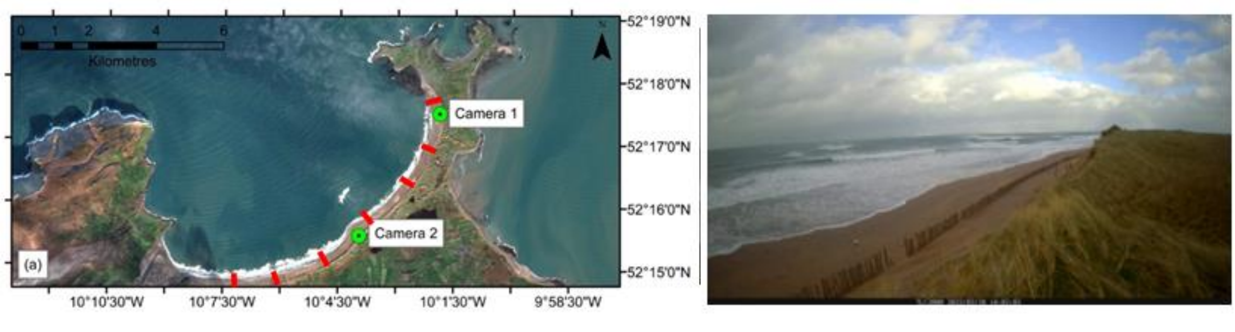


Fig. 1. Brandon Bay study area showing camera locations and survey profile transects (left) and sample image from camera 2 (right).

## 2. Methodolog

Two Brinno TLC2000 time-lapse cameras were installed on the beach (Fig. 1.) at elevations of 11 m and 14 m ITM, respectively, and covering alongshore lengths of 200 m and 250 m. The cameras were calibrated using the chessboard approach of Zhang (1998) and the images (Fig. 1) were geo-rectified using ten ground control points at each site. Shoreline edge detection was conducted by detecting the difference between red and blue colour channels (as per Harley et al. (2019)) of time exposure (Timex) images created by taking the average of a number of images taken at regular intervals over a 10-minute period. The accuracy of the approach was assessed for images taken at 1s, 2s, 5s, 10s, 20s and 30s. Wave runup was determined from Timestack images created by layering together a series of photos taken at timed intervals to generate a single image. Image georectification, and subsequent analyses, was done using MATLAB, with modified versions of the scripts provided by the Coastal Imaging Network (Bruder and Brodie, 2020).

A nested wave model was developed using SWAN comprising (1) a regional northeast Atlantic model with a uniform spatial resolution of 0.5° and time step of 10 minutes and (2) a local Brandon bay model with a uniform spatial resolution of 0.01° and time step of 5 minutes. Wave data from the local model was then used to drive a coastal morphology model developed using XBeach at a spatial resolution of 5 m and time step of 1 minute. The SWAN models were validated against measured wave data for both domains. Wave and beach conditions from December to February 2022 were modelled and compared with surveyed beach profiles measured at seven different transects along the beach (Fig. 1) in December and February 2022.

## 3. Results

Shoreline edges and wave run-up were successfully detected using the images from the timelapse cameras (Fig. 2). Cloud cover and spray affected the quality of the image analyses and required some manual checking of the processed images. Stage of tide also affected edge detection with pooling of water on the beach as the tide receded towards low tide confusing the algorithm, and the water edge being out of the cameras view on spring high tides. As expected, the detected shoreline edge was sensitive to the time interval of the images used to create the Timex image but even the 30 second interval edges were close to that of the 1-second interval (Fig. 2), which is currently used as the standard in Timex image analysis.

The beach profile surveys showed noticeable erosion of the beach in the three month period from December to February with reductions in elevation of up to 0.5 m (Fig. 2). In February, three storms occurred in succession and the effects of each separate storm were noticeable. In general, the model was capable of predicting the observed trends in the measured changes in beach elevation (see example in Fig. 2) but requires further calibration to improve its accuracy.

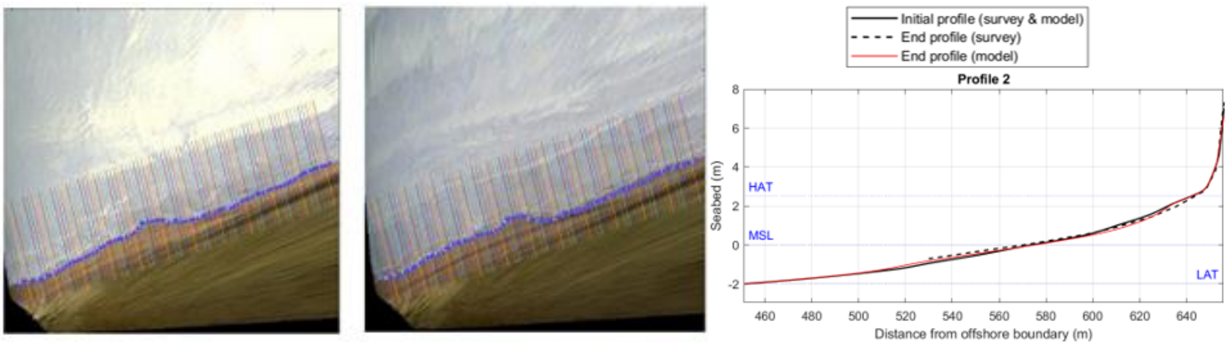


Fig. 2. Shorelines using 1s (left) and 30s (centre) Timex images, and measured and modelled beach profiles at northern-most transect.

## 4. Conclusion

Shoreline edge and wave-run-up were successfully detected using Timex and Timestack images, respectively. It was found that the temporal resolution of Timex images can be increased from 1 second to 5 seconds with negligible loss in accuracy. This small change has significant benefits for camera battery and memory. The XBeach results are promising, thus-far, and once fully calibrated the model will be used to study the effects of storms of different directions and intensities, successive storm events, and future climate impacts.

**Acknowledgements**

This research was supported by funding from Geological Survey Ireland through the Geological Survey Ireland Geoscience Research Programme (Grant no. 2020-SC-013) and Science Foundation Ireland (SFI) through the MaREI Research Centre for Energy, Climate and Marine (Grant no. 12/R.C./2302). The authors would also like to acknowledge the Irish Centre for High-End Computing (ICHEC) for providing high-performance computer support for model simulation.

**References**

Bruder BL, Brodie KL (2020). CIRN Quantitative Coastal imaging toolbox. SoftwareX, 12 (2020), Article 100582.
Devoy RJN (2015). The Development and Management of the Dingle Bay Spit-Barriers of Southwest Ireland. In Coastal Spits, Cooper JAG, Jackson DW (eds). Springer: Dordrecht.
Guisado-Pintado and Jackson, (2020). Monitoring cross-shore intertidal beach dynamics using oblique time-lapse photography. Journal of Coastal Research SI 95, 1106-1110.
O'Connor MC, Cooper JAG, Jackson DWT (2011). Decadal Behavior of Tidal Inlet–Associated Beach Systems, Northwest Ireland, in Relation to Climate Forcing. Journal of Sedimentary Research, 81,38-51.

# On the mechanism of enhancing renewal time through differential tidal forcing in coastal lagoons

Androniki I. KARTSAKALI[1], Nikolaos Th. FOURNIOTIS[2], Georgios M. HORSCH[1]

[1]Department of Civil Engineering, University of Patras, Patras, Greece
email: akartsakali@upnet.gr
email: ghorsch@upatras.gr

[2]Department of Civil Engineering, University of the Peloponnese, Patras, Greece
email: nfou@uop.gr

ABSTRACT

The mechanism of creating flow-through-like conditions induced by differential tidal forcing at the two inlets of coastal lagoons is examined by using particle tracking. Both particles released at one location over a period of time, and particles spread over space and released at a single time instant are used. The numerical simulations, performed using MIKE 21 Flow Model FM (HD, PT), reveal some features of this complicated flow.

## 1. Introduction

Hydraulic exchange between a lagoon and the adjacent sea, has long been recognized as a key parameter affecting the water quality in the lagoon, including anoxic episodes and dystrophic crises. If regulated, it could be used as a management tool, although it is far from obvious how the exchange can be enhanced, as attested from documented instances where the addition, for example, of a new tidal inlet has had minimal influence in preventing dystrophic crises (e.g., Cladas et al., 2016). The problem is further complicated because the increase of the exchange flow is bound to influence the circulation in the lagoon, thus affecting its ecological balance.

## 2. The problem defined

Fourniotis et al. (2021), prompted by studies showing widely varying renewal times of lagoons of similar dimensions and having at least two tidal inlets, examined a method of enhancing the renewal time of such lagoons. The method consists of artificially reducing the tidal range in one of the inlets, thus creating differential tidal forcing. (That study, as well as the present deals with the result of differential forcing and not with how it may be achieved). They showed, by numerical simulation, using MIKE 3 Flow Model FM (HD, TR), of tidally induced hydraulic exchange of the Papas Lagoon, in Western Greece, that the method considerably enhances renewal time. For this method to become practical, the dependence of the enhancement of renewal time on the problem parameters (geometry of the lagoon, distance between the tidal inlets, difference in tidal range etc.) must first be clarified. This is in addition to the need to examine the concomitant alteration induced in the lagoon's circulation, which might influence its overall ecological function. Detailed examination of above-described mechanism is initiated herein.

In order to make the discussion general, we apply our numerical experiments in an idealized geometry, to rid them from specific bathymetric or coastline details. The geometry, shown in Fig 1, consists of a lagoon (green in Fig. 1) 1 km wide, 5 km long and 2 m deep, connected by two inlets with a northern sea (red/orange, in Fig. 1) and a western sea (blue/purple, in Fig. 1) respectively. The seas are 40 m at the outer, deepest end and slope up, to 2 m at the end close to the lagoon. The inlets are 260 m long, 50 m wide and 1 m deep. The tide is applied at the outer part of the northern and western seas. To examine the differences induced by the differential forcing, we examine scenario 1, in which the tidal range is 40 cm and 20 cm, at the northern and western seas respectively, and compare it with scenario 0, in which the tidal range is 40 cm in both seas.

## 3. Results

The difference, in terms of the exchange flow, between the two scenarios, can be seen in Fig. 2, where we note that the cumulative volume which exits from the western inlet (the one with the lower tidal range) oscillates around zero for scenario 0, and increases continuously (albeit not monotonically) for scenario 1. The opposite happens in the northern inlet (not shown here). This implies the establishment of an effectively flow-through regime in scenario 1, and some of the overall features of this flow, have been revealed by Fourniotis et al

(2021) by examining the diffusion properties of the flow. Obviously, however, the flow-through nature of this oscillating flow is intermittent, due to tidal forcing, and to explore its details, particle-tracking numerical experiments are being performed. An instance of such an experiment is shown in Fig. 1. The experiment consists of releasing particles at the end each of the inlets, right at their respective entrance into the lagoon, first at the northern inlet (left panel) and then at the western inlet (right panel), and observing their paths. Specifically, the particles are released in equally spaced time intervals of the third simulated tidal cycle (i.e. at the end of warm-up), ten within each tidal period.

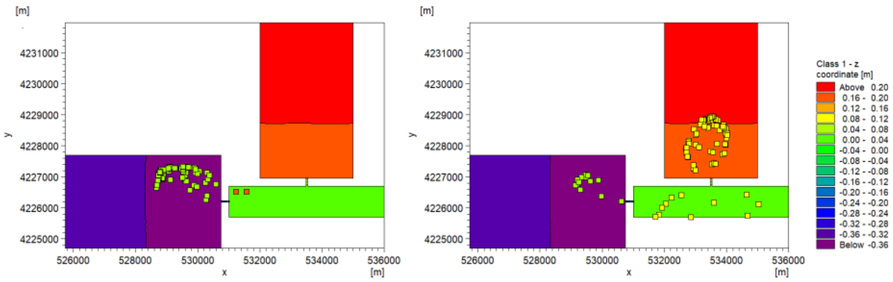


**Fig. 1.**Idealized geometry of a lagoon (green, lower right) connected to the adjacent seas (in the north and in the west) with tidal inlets. With yellow squares are marked the positions, at the end of 30 days, of particles released at the northern inlet (right panel) and the western inlet (left panel). The colours indicate the elevation of the free surface. Forcing is provided by the tides in the two adjacent seas (see text).

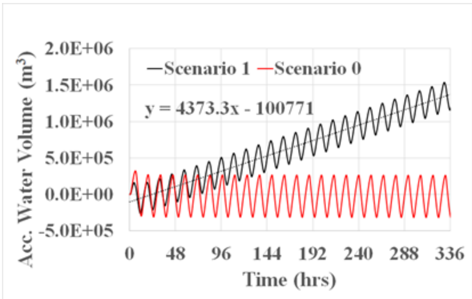


**Fig. 2.**Accumulated volume of water exiting from the western inlet as a function of time. With red curve corresponding to scenario 0 and with black corresponding to scenario 1.

From Fig. 1, we observe that while all of the particles (except two) released at the western inlet (left panel) end up, at the end of a 30 day simulation, in the western sea, whereas a fraction of those released at the northern inlet (right panel) end up at the western sea, another fraction circulate within the lagoon, and the last fraction exits in the northern sea. This is a clear manifestation of complicated nature of the flow-through-like circulation. In this experiment, the particles are released in a single location over a period of a tidal cycle. In other complementary experiments, particles are spread throughout the lagoon, at one initial instant and observed thereafter. Based on the results of these simulations, several features of the differentially forced tidal flow within the lagoon, have been recorded.

## 4. Conclusions

The mechanism of enhancing renewal time in coastal lagoons having at least two inlets, through differential tidal forcing, is explored by performing particle-tracking numerical experiment in a lagoon of idealized geometry. This method, which can be viewed as complementary to studying the diffusion of mumerical tracers, reveals many details of the complicated periodically forced flow.

**Acknowledgements**

We would like to express our gratitude to the Danish Hydraulic Institute (DHI) for making available to A.K. the 2021 version of MIKE 21 Flow Model FM (HD and PT).

**References**

Cladas Y, Papantoniou G, Bekiari V, Fragkopoulou N (2016) Dystrophic crisis event in Papas Lagoon, Araxos Cape, Western Greece in the summer 2012. Mediterr. Mar. Sci. 17,32-38. doi:10.12681/mms.1409
DHI (2022) MIKE 21 FLOW MODEL FM, Hydrodynamic Module, User Guide, DHI Software, 170p.
DHI (2021) MIKE 21 FLOW MODEL FM, Particle Tracking Module, User Guide, DHI Software, 64p.
Fourniotis NTh, Leftheriotis GA, Horsch, GM (2021) Towards enhancing tidally-induced water renewal in coastal lagoons, Environmental Fluid Mechanics, 21: 343-360, doi.org/10.1007/s10652-020-09776-0

# Accelerating coastal bed evolution predictions utilizing Numerical Modelling and Artificial Neural Networks

Andreas PAPADIMITRIOU[1,2], Michalis CHONDROS[1,2], Anastasios METALLINOS[1,2], Vasiliki TSOUKALA[2]

[1] Scientia Maris, Agias Paraskevis 117, Chalandri 15234, Greece
email: andrewtnt@mail.ntua.gr (for author 1)
email: michondros@scientiamaris.com (for author 2)
email: ametallinos@scientiamaris.com (for author 3)

[2] Laboratory of Harbour Works, Department of Water Resources and Environmental Engineering, School of Civil Engineering, National Technical University of Athens (NTUA), Zografou 15780, Greece.
email: tsoukala@mail.ntua.gr (for author 4)

ABSTRACT

Process-based models have been employed extensively in the last decades for the prediction of coastal bed evolution in the medium term (1-5 years), under the combined action of waves and currents, due to their ability to resolve the dominant coastal processes. Despite their widespread application, they are associated with a high demand in computational resources, rendering the annual prediction of the coastal bed evolution a tedious task. To combat this, various accelaration techniques such as wave input reduction or elimination of lowly-energetic sea-states have been implemented in many practical applications. The purpose of this research is to further expand on the concept of accelerating morpholgical simulations by developing a methodology centered around employing an Artificial Neural Network (ANN), tasked with eliminating wave records unable to initiate sediment motion and hence further reduce computational times. The ANN has been trained on a 2DH idealized plane sloping beach with a robust dataset produced by simulations of three sophisticated numerical models. The proposed methodology has been implemented for a real field case in the coastal area of Rethymno, Greece and the obtained results were deemed very satisfactory by maintaining a balance between accuracy of results and computational efficiency, having strong implications for practical coastal engineering purposes.

## 1. Introduction

Numerical modelling of the coastal bed evolution in the medium term has been at the forefront of research efforts for the past decades. While process-based models are capable of resolving the dominant coastal processes, they are associated with staggering computational burden rendering morphological modelling simulations a tedious task. On this subject various acceleration techniques such as wave input reduction (Papadimitriou et al., 2020), model reduction and behavior-oriented modelling have been employed. Often due to the sheer amount of input forcing conditions arbitrary thresholds are applied to eliminate lowly-energetic wave conditions considered unable to initiate sediment motion. However, these criteria are arbitrarily defined and do not consider the full set of wave characteristics (i.e., height, period and incident angle) and the geomorphological and sediment characteristics of the study area (i.e., the seabed slope, the bottom roughness and the mean sediment diameter), leading to erroneous conclusions. The scope of this paper is to provide a novel methodology to systematically dispose sea-states considered unable to initiate sediment motion by concerting numerical modelling and Artificial Intelligence techniques. The obtained results have strong implications for further accelerating morphological modelling simulations while maintaining the accuracy and reliability of the results which is extremely valuable for real-life engineering applications.

## 2. Methodology and application

For coasts subject to forcing due to the combined action of waves and currents the criterion of incipient sediment motion orders that the maximum value of the Shields parameter, $\theta_{max}$, over a wave cycle is higher than the critical Shields parameter, $\theta_{cr}$. It follows that the total bed shear stress depends on the near-bed wave orbital velocity amplitude, current speed magnitude and bottom friction coefficient whereas the critical Shields parameter depends on the sediment characteristics. Taking the above into consideration a methodology has been realized for the accurate and systematic elimination of lowly-energetic offshore sea-states utilizing an Artificial Neural Network (ANN).

For the training of the ANN a 2DH configuration of an idealized plane sloping beach was setup. A combination of numerical models, consisting of a hyperbolic mild slope (HMS) wave model, a hydrodyamic model (HYD) based on the shallow water equations and a sediment transport & morphology model (SDT), are tasked with performing separate simulations considering the following input parameters (IP); offshore wave characteristics ($H_s$, $T_p$, incident wave angle), Nikuradse bottom friction coefficient ($k_s$), bed slope ($m$) and mean sediment diameter ($d_{50}$). The output parameters (OP) of the numerical modelling chain are the maximum value of $\theta_{max}$ in the surf zone and the corresponding value of $\theta_{cr}$. Utilizing a "Saltelli" sampling scheme a total of 14336 combinations of the input parameters were obtained which were then reduced to 500 utilizing a Fuzzy C-Means clustering algorithm. The combination of IPs and the corresponding 500 OPs were ultimately used as a "training dataset" for a multilayer feed forward ANN with 2 Hidden Layers. After the training procedure the neural network is tasked with providing prediction of the $\theta_{max}$ and $\theta_{cr}$ for any given values of offshore sea-state characteristics, bed slope, mean sediment diameter and bottom friction coefficient.

The methodology developed herein was then implemented for a real-field case of a coastal area in the vicinity of Rethymno Port, Greece and the general steps undertaken will be presented briefly below. A dataset of offshore sea-state characteristics is obtained and representative values of the beach slope, $d_{50}$ and $k_s$ are provided. Then for each record the ANN provides unique values of $\theta_{max}$ and $\theta_{cr}$. Any record with $\theta_{cr} < \theta_{max}$ is disposed from the dataset. Effectively by eliminating the lowly energetic sea-states the total length of the dataset is reduced and one can perform process-based model simulations for a fraction of the total simulation time associated with the full dataset. Finally, in the reduced dataset we implemented the Annual Equivalent wave heights method of wave schematization to obtain a reduced set of representative wave conditions which will be used to force the process-based modelling chain of the HMS, HYD and SDT models. Rate of bed level change results are then compared to a "benchmark" simulation containing a robust wave climate of 68 sea-states and model evaluation is carried out calculating the Root Mean Square Error (RMSE) and visual inspection of the results. For a more comprehensive evaluation, comparison of results obtained by applying an "arbitrary threshold", eliminating significant wave heights < 0.5m, a value typical for engineering applications, was undertaken. For the case in question, the results obtained by implementing the proposed methodology were deemed very satisfactory, as shown in Fig. 1c, compared to the "benchmark" simulation results (Fig. 1a) while reducing computational model run-time significantly. Conversely, implementation of an arbitrary threshold, lead to significantly worse results as can be deduced by visually inspecting the results (Fig. 1b), while also increasing RMSE by an order of magnitude (RMSE=1.30E-8) compared to the one obtained by implementing the proposed methodology (RMSE=2.04E-9).

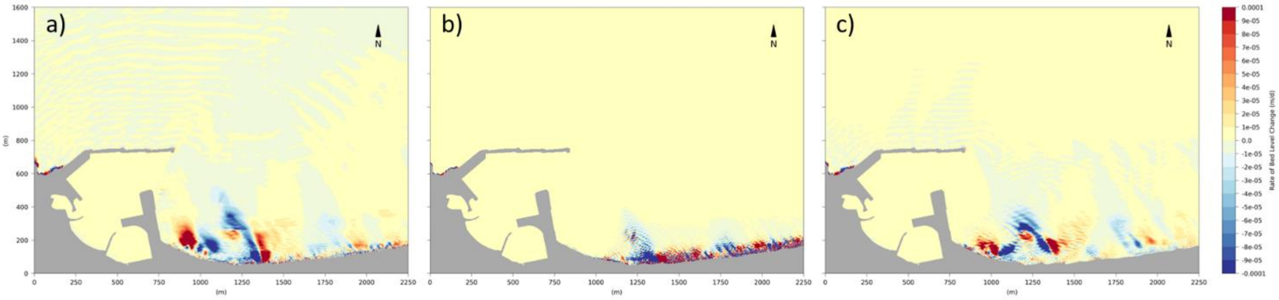


**Fig. 1.** Rate of bed level change results of: a) "Benchmark" with 68 sea-states, b) Annual equivalent wave heights with "Arbitrary threshold" eliminating $H_s$ < 0.5 m and c) Annual equivalent wave heights with the proposed methodology by implementing Artificial Neural Network

## 3. Conclusions

The development of a novel methodology concerting numerical modelling simulations and Artificial Intelligence within this research is considered a valuable asset for coastal engineers desiring to obtain accurate predictions of coastal bed evolution while simultaneously reducing the computational effort.

**Acknowledgements**

This research has been co-financed by the European Regional Development Fund of the European Union and Greek national funds through the Operational Program Competitiveness, Entrepreneurship and Innovation, under the call RESEARCH – CREATE – INNOVATE (project code: T2EDK- 03811).

**References**

Papadimitriou A, Panagopoulos L, Chondros M, Tsoukala V (2020) A Wave Input-Reduction Method Incorporating Initiation of Sediment Motion, Journal of Marine Science and Engineering 8(8):597.

# Performance evaluation of the K-Means clustering algorithm for the prediction of annual bed morphological evolution

Andreas PAPADIMITRIOU[1] and Vasiliki TSOUKALA[1]

[1] Laboratory of Harbour Works, Department of Water Resources and Environmental Engineering, School of Civil Engineering, National Technical University of Athens (NTUA), Zografou 15780, Greece.
email: andrewtnt@mail.ntua.gr (for author 1)
email: tsoukala@mail.ntua.gr (for author 2)

ABSTRACT

The morphological coastal bed evolution is of high interest to engineers, scientists and the public due to the vast number of activities concentrated near the shoreline. Traditionally, process-based models have been employed to predict bed level changes in time scales of 1-5 years, however they are associated with prohibitive computational restrictions. To reduce the computational burden, wave Input Reduction methods, aiming to reduce the forcing input and accelerate morphological simulations have been developed. The present paper aims at evaluating the K-Means algorithm as an alternative approach to select wave representatives for morphological simulations. Several alternative configurations were tested in order to enhance and coerce the algorithm to “smartly” select the representative waves. The examined configurations were implemented in the coastal area of Rethymno, Greece for an annual dataset of sea-state wave characteristics and the results were deemed very satisfactory compared to those obtained by the full wave climate, rendering the use of K-Means algorithm a valuable tool for coastal engineers and scientists.

## 1. Introduction

Process-based models have been employed in the past decades for the purpose of predicting annual coastal bed evolution under the combined action of waves and currents due to their ability to resolve most of the dominant nearshore processes driving sediment transport. However, these models are associated with high demand of computational resources rendering the medium term (1-5 years) prediction of coastal bed evolution a tedious task. Consequently, various acceleration techniques have been employed by coastal modelers, with the most notorious being wave Input Reduction (IR) methods, aiming to reduce the forcing input of process-based models by selecting a set of representative wave conditions able to reproduce the changes induced by the full wave climate. Essentially, binning IR methods divide the bivariate wave height and mean wave direction climate in bins containing an equal fraction of a proxy quantity driving longshore sediment transport (such as wave energy flux) and then obtaining a representative for each bin (Benedet et al., 2016). The aim of this research is to examine whether the K-Means clustering algorithms can provide a viable alternative to Binning IR for the purpose of predicting coastal bed evolution at an annual scale, reducing both computational times while also maintain accurate results.

## 2. Methodology

The widely-used K-Means (KM) clustering algorithm will be utilized in the framework of this research and various alternative configurations will be examined aimed at coercing the algorithm at smartly “selecting” centroids in order to incorporate longshore sediment transport gradients which are responsible for the medium term coastal bed evolution. At total, six different configurations were tested with the main distinct characteristics showcased in Table 1. In general, the tests examined herein focus mainly on the cluster centroid initialization method by concerting Binning IR methods with the KM algorithm, swapping of clustering variables to longshore transport quantities ($S$, $E_{fl}$, $MWD$) and application of filtering methodologies to eliminate lowly-energetic sea-states. It should be noted that the number of representatives was kept constant at 12 throughout all the alternative configurations and the sequencing of wave conditions was random for the first test KM-01 while for the subsequent tests the set of centroids with the most similar ordering to the KM-01 test was obtained by implementing the optimization “Kuhn-Munkres” algorithm to systematically reduce the effect of sequencing on the results. An efficient parabolic mild slope wave model was an integral part of tests KM-04 through KM-06 model and was implemented to obtain nearshore wave characteristics.

**Table 1: Overview of the alternative KM algorithm configurations**

| Test | Input Variables | Cluster Initialization Method | Applied weights |
|---|---|---|---|
| KM-01 | $H_{mo}, T_p, MWD$ | K-Means++ | - |
| KM-02 | $H_{mo}, T_p, MWD$ | Energy Flux method centroids | - |
| KM-03 | $H_{mo}, T_p, MWD$ | K-Means++ | Energy flux of individual wave records |
| KM-04 | $S, E_{fl}, MWD$ | K-Means++ | - |
| KM-05 | $H_{mo}, T_p, MWD$ | Pick-up rate method centroids | - |
| KM-06 | $S, E_{fl}, MWD$ with elimination of non-breaking sea-states | K-Means++ | - |

## 3. Applications and results

The alternative configurations were implemented for the coastal area near the Port of Rethymno in Crete, Greece. Offshore sea-state wave characteristics were obtained from the Copernicus database for the year 2012, containing a total of 8762 records. For the morphological modeling simulations, the process-based model MIKE21 CM FM was implemented. The simulations were performed through the “Morphodynamic” approach, i.e. online coupling & constant feedback interaction between the wave, hydrodynamic and sediment transport models. The obtained representatives by implementing all the KM tests are shown in Fig.1. It can be deduced that between the examined alternative configurations of the algorithm significantly different clusters (shown with different colors in Fig. 1) and representative wave conditions are distinguished.

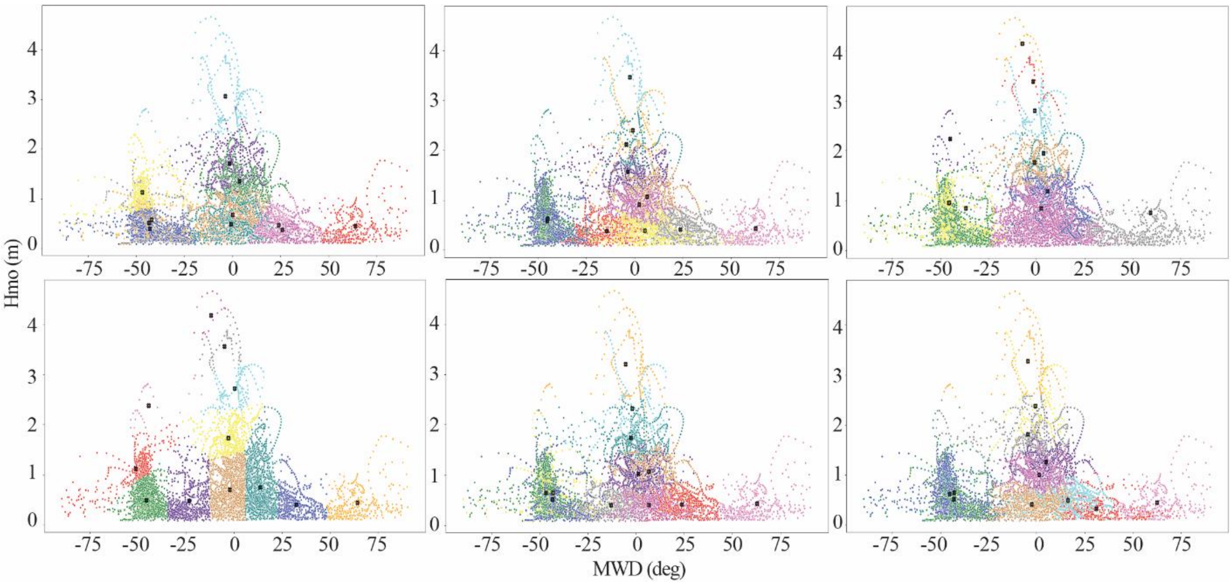


**Fig. 1.** Obtained clusters and representative wave conditions by implementing the KM-tests alternative configurations: KM-01, KM-02, KM-03 (top), KM-04, KM-05, KM-06 (bottom)

Model results were systematically evaluated for each test by comparing the obtained results with a “brute force” benchmark simulation containing the full wave climate and calculating the Brier Skill Score (BSS). All tests were ultimately found to give “Excellent” results (BSS > 0.5) with the model run-time reduction varying between 25-50%.

## 4. Conclusions

The overall investigation highlights the capability of utilizing the K-Means clustering algorithm as an alternative to binning wave Input Reduction methods, effectively reducing computational times while also maintaining the accuracy of the process-based model results.

### References

Benedet, L., Dobrochinsky, P., Walstra D., Klein A., Renniers A. (2016) A morphological modeling study to compare different methods of waveclimate schematization and evaluate strategies to reduce erosion losses from a beach nourishment project, Coastal Engineering, 4, 115-120.

# SINERGEA - Real-time forecasting system for managing floods, bathing water quality and wastewater energy consumption

Luís M DAVID[1], Anabela OLIVEIRA[2], Marta RODRIGUES[3], André B FORTUNATO[4], João ROGEIRO[5], João BARREIRO[6], Filipa FERREIRA[7], José S. MATOS[8], Flávio SANTOS[9], Ramiro NEVES[10], António MARTINS[11]; Osvaldo SILVA[12]; Alexandre ATAÍDE[13]; Nuno SILVA[14], Joaquim FREIRE[15], Alexandra CRAVO[16], António SOARES[17], Hugo RODRIGUES[18], Paulo B AZEVEDO[19]

[1,2,3,4,5] Laboratório Nacional de Engenharia Civil, Portugal, ldavid@lnec.pt
[6,7,8] CERIS, Instituto Superior Técnico da Universidade de Lisboa, Portugal, joao.barreiro@tecnico.ulisboa.pt
[9,10] MARETEC, Instituto Superior Técnico da Universidade de Lisboa, Portugal, flavio.t.santos@tecnico.ulisboa.pt
[11,12,13,14,15] Águas do Algarve S.A., Portugal, antonio.m.martins@adp.pt
[16] CIMA, Universidade do Algarve, Portugal, acravo@ualg.pt
[17,18] Siemens, S.A., Portugal, antoniom.soares@siemens.com
[19] Município de Albufeira, Portugal, paulo.azevedo@cm-albufeira.pt

ABSTRACT

## 1. Introduction

Coastal cities face growing challenges from flooding, sea water quality and energy sustainability, which increasingly require an intelligent, real-time management. Urban drainage infrastructures often require pumping stations (PS) in low-lying areas, which transport to the wastewater treatment plant (WWTP) all waters likely to pollute downstream beaches, including rainfall-derived infiltration inflows and stormwater from small rain events. During the bathing season, decentralized management measures, including nature-based solutions, can be used to retain stormwater and promote its transport to the WWTP after the rainy event. However, the growth in pumped and treated flows increases energy consumption. In addition, real-time tools are required to support the assessment and prediction of the quality of bathing waters, to assess the possible need to prohibit beach water usage. During heavy rainfall events, decentralized management systems can also contribute to mitigate downstream flooding. Nevertheless, this requires the operation of the entire system to be different from that used to protect bathing water.

## 2. The SINERGEA IT infrastructure

Within the SINERGEA Project, an intelligent platform was developed and is being demonstrated to support the management of flooding emergencies and bathing water contamination, and the efficient use of energy consumed by sanitation infrastructures. This system integrates real-time information provided by different entities, including monitoring networks, infrastructure operation data and a forecasting framework. The forecasting system includes several models covering all relevant water compartments: atmospheric, rivers and streams, urban stormwater and wastewater infrastructure, and receiving coastal water bodies.

The SINERGEA system uses the XHQ platform (eXtended HeadQuarters), which is an Enterprise Operations Intelligence software developed by Siemens. It aggregates, integrates, analyses and displays information from various sources, including personalized products in real time, based on the available information. The intelligent forecasting system that simulates in real time the water quantity and quality and energy consumption is based on LNEC's generic forecast framework WIFF (Fortunato et al., 2017).

Figure 1 shows the input and output variables between the models used for modelling and forecasting discharges in coastal waters. The meteorological modelling uses the WRF model, applied with a 1 km grid resolution for the case study region (Albufeira, south coast of Portugal). Urban drainage modelling uses the MOHID Land model (www.mohid.com) loosely coupled with the SWMM model (US EPA). A deterministic model of energy consumption in pumping and treatment plants was developed and data-driven approaches that suit the objectives of the case study and the monitored data will be investigated. The modelling of hydrodynamics and water quality in the receiving body is performed with the SCHISM modelling system (ccrm.vims.edu/schismweb) in 3D mode, taking into account the interactions between baroclinic flow and short-period waves, and simulating hydrodynamics and faecal contamination (Rodrigues et al., 2011). The intelligent system uses a database of indicators for flooding, bathing water and energy issues, based on a wide combination of scenarios and management alternatives.

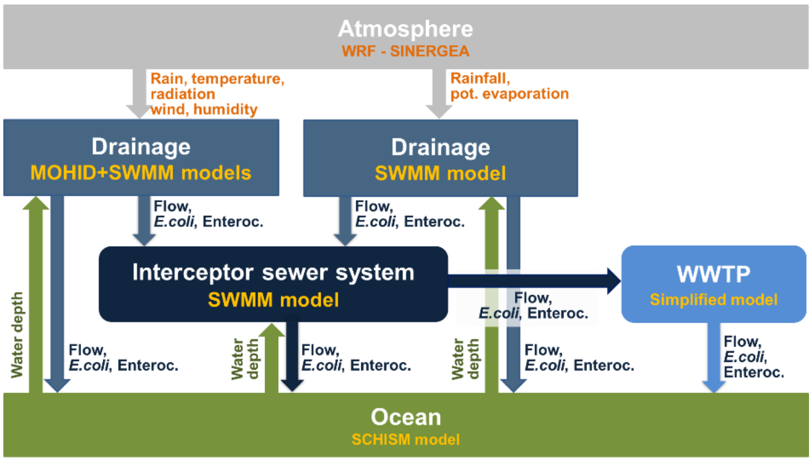


**Fig. 1.** Input and output variables between models for modelling and predicting the quality of water discharged into the receiving water body.

## 3. Case study results

The SINERGEA system is being demonstrated on the city of Albufeira, Portugal, and its coastal neighbourhood. The stream and the separate sewer networks are managed by the municipality, the interceptor sewer system and the WWTP are managed by a wastewater utility, and the coastal bathing water by the National Water Authority. The interceptor sewer system has 10 pumping stations and serves various coastal urban-tourist developments. Figure 2 illustrates some results.

**Flooding**

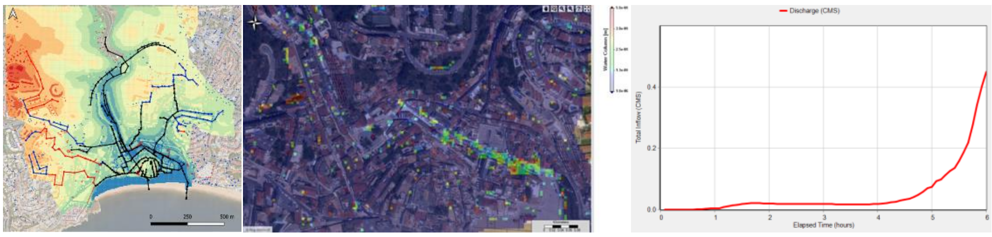

1D/2D model domain and infrastructures (left); Ex. of results for water depth (middle) and outlet discharge.

**Bathing water quality**

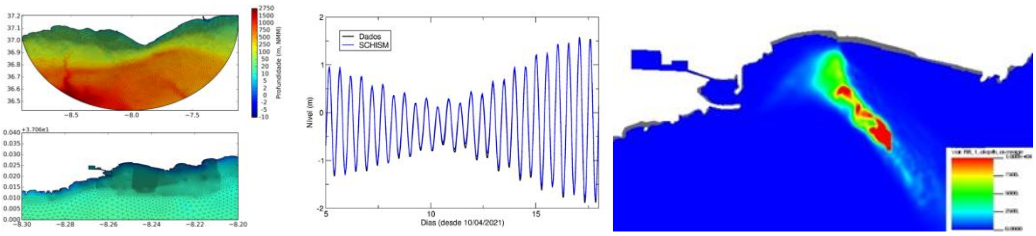

Coastal zone model: horizontal grid and bathymetry, water levels validation, and example of an emergency scenario.

**Energy and sanitary sewer overflows**

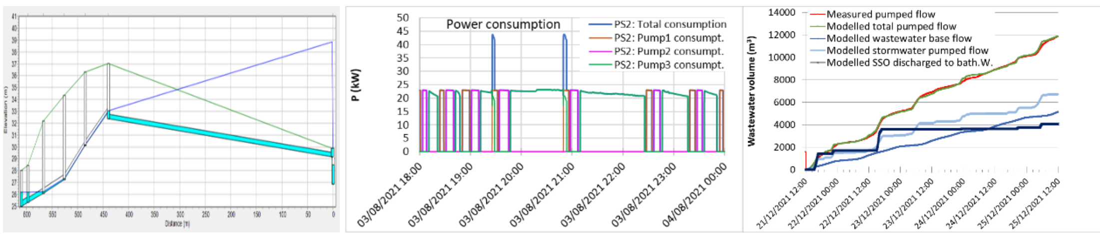


Examples of modelled energy line, power consumption, and calibration of pumped and SSO flows at a pumping stat.

**Fig. 2.** Case study models and results for the three components studied: flooding, bathing water quality and energy.

**Acknowledgements**

This work was co-funded by the European Regional Development Fund (FEDER), under programs POR Lisboa2020 and CrescAlgarve2020, through Project SINERGEA (ANI 33595).

**References**

Fortunato AB et al. (2017). Operational forecast framework applied to extreme sea levels at regional and local scales. J. Operational Oceanography 10:1.
Rodrigues M et al. (2011). Modeling fecal contamination in the Aljezur coastal stream (Portugal). Ocean Dynamics, 61(6), 841-856.

# Acoustic Rainfall Sensing in Urban Environment Using Machine Learning

Mohammed I.I. ALKHATIB[1], Amin TALEI[2], Tak Kwin CHANG[3], Andreas A. HERMAWAN[4], Valentijn PAUWELS[5]

[1,2,3,4] Discipline of Civil Engineering, School of Engineering, Monash University Malaysia, Malaysia
email: mohammed.alkhatib@monash.edu
email: amin.talei@monash.edu
email: chang.takkwin@monash.edu
email: andreas.aditya1@monash.edu

[5] Department of Civil Engineering, Monash University, Clayton, Victoria, Australia
email: valentijn.pauwels@monash.edu

ABSTRACT

This study proposes a novel acoustic rainfall sensing approach based on the machine learning technique, Gaussian Process Regression (GPR). Rainfall audio data is collected for 15 rainfall events from five different spots in an urban environment in Subang Jaya, Selangor, Malaysia. These spots are close to a weather station recording the rainfall data with 1-min resolution. In total, 40 acoustic features were extracted from the rainfall audio data, of which 7 were selected through cross-correlation analysis and visualization methods. Using the 7 selected acoustic features as inputs, the calibrated GPR model estimated rainfall with $R^2$=0.784, RMSE=0.270 (mm/min), and MAE=0.191 (mm/min). It was concluded that the proposed model could potentially be utilized for rainfall crowdsourcing through citizens' science.

## 1. Background

Rainfall data is one of the essential inputs for hydrological modelling and prediction. The high spatial and temporal resolution of rainfall data can enhance the accuracy and predictive capabilities of any flood forecasting and warning system, especially in urban areas with fast runoff response (Emmanuel et al., 2012). Despite having rain gauges, radars and satellite images for rainfall estimation, alternative rainfall sensing approaches are still needed to complement the conventional methods. However, most of the studies on acoustic rainfall sensing are sensor-based, which naturally makes them point measurement tools. This study aims to develop an acoustic rainfall sensing tool using machine learning techniques and recorded rain audio as inputs. This proposed model can potentially be utilized in citizen science applications.

## 2. Methodology

### *2.1. Study site and data used*

This study is conducted at the Monash University Malaysia campus and surrounding, located in Subang Jaya, Selangor, Malaysia. Five Zoom H2n field sound recorders were used to record rainfall sound in an uncompressed WAV format at a sampling frequency of 44.1 kHz at 16-bit depths. All sound recorders are within a 200-m perimeter of a weather station (Watchdog spectrum 2000 brand) that collects 1-minute rainfall data with a minimum detection value of 0.2 mm. The five audio data collection points represent typical urban environments with diverse human activities. 15 rainfall events with 1-min resolution (rainfall and its audio data) were collected from Sep-2020 to May-2021 (4239 data points). The data was then split into training, validation, and testing datasets (60%, 20%, 20%).

### *2.2. Acoustic features extraction and shortlisting*

Forty acoustic features of time, frequency, and cepstral domains were extracted from the recorded rainfall audio data and analyzed to shortlist those best correlated with rainfall data. A cross-correlation analysis and several visualization methods were used in the feature selection process.

### *2.3. Acoustic rainfall sensing model*

Different combinations of selected acoustic features were used as inputs to develop a Gaussian Process Regression (GPR) model (Rasmussen and Williams, 2006). GPR belongs to the nonparametric kernel-based probabilistic models. The model assumes that the training dataset follows a gaussian prior probability and then infers the corresponding posterior probability using a Bayes theorem. Coefficient of Determination ($R^2$), Root Mean Squared Error (RMSE) and Mean Absolute Error (MAE) were used to assess the model performance.

## 3. Results and discussion

Cross-correlation analysis and visualization methods such as generating Mel spectrograms (frequency vs. time) and spectrums (frequency bs. Sound energy) were used to select the suitable acoustic features. Figure 1 shows a sample spectrum for 2 mm/min rainfall intensity recorded at the five stations (points A-E). It was observed that the acoustic features at each collection point are different. The feature selection analysis of this study found that a combination of acoustic features Spectral Roll-off (SRO) and Mel Frequency Cepstral Coefficients (MFCCs) 1, 2, 4, 8, 10, and 13 are the best-performing ones for rainfall estimation in the GPR model.

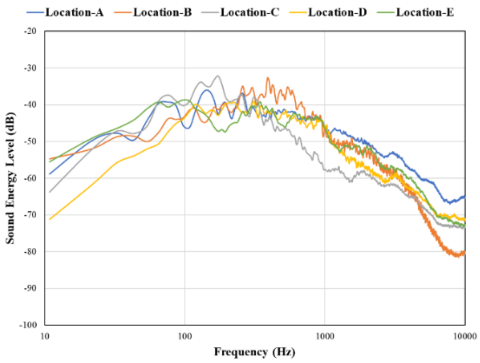


**Fig. 1.** Sample spectrums of rainfall sound, recorded in five locations (A-E), at rainfall intensity of 2 mm/min.

An exponential squared kernel was used in the GPR model, and the model parameters σ and β were set at -0.1461 and 0.2301, respectively. The performance of the GPR model in rainfall estimation is presented in Table 1. To visualize the model performance, Fig. 2 illustrates the observed vs. simulated rainfall data for the testing dataset, where the resolution of the rainfall data is converted to a more practical unit of mm per 5-min. As it can be seen, the GPR model successfully simulates rainfall data for both low and high intensities. In conclusion, the proposed acoustic rainfall sensing model can estimate rainfall with reasonably high accuracy and could potentially be used for crowdsourcing rainfall data.

**Table 1.** The GPR model performance in rainfall estimation at training, validation, and testing stages.

| Dataset | $R^2$ | RMSE (mm/min) | MAE (mm/min) |
|---|---|---|---|
| Training (60% of data) | 0.836 | 0.233 | 0.164 |
| Validation (20% of data) | 0.757 | 0.278 | 0.201 |
| Testing (20% of data) | 0.784 | 0.270 | 0.191 |

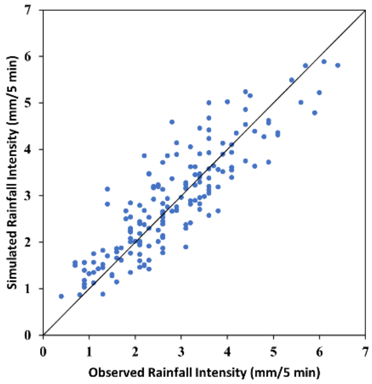


**Fig. 2.** Scatter plot of observed vs. simulated rainfall data by GPR model for the testing dataset.

**Acknowledgements**

This project was funded by a grant (FRGS/1/2021/TK0/MUSM/02/6) from the Ministry of Higher Education, Malaysia.

**References**

Rajurkar, M.P., Kothyari, U.C., Chaube, U.C. (2002) Artificial neural networks for daily rainfall-runoff modelling, Hydrological Sciences Journal, 47, 865–877.
Rasmussen, C.Edward., Williams, C.K.I. (2006) Gaussian processes for machine learning, MIT Press.

# Spatiotemporal variation of precipitation and temperature in Iran at the past five decade

Mohsen MAGHREBI[1], Sadegh PARTANI[2], Farshid BOSTANMANESHRAD[3]
[1] Graduate School of Environmental Engineering, College of Engineering, University of Tehran, Tehran, Iran
Email: Moghrebi@ut.ac.ir
[2] Faculty of Engineering, University of Bojnord, Bojnord, Iran
Email: S_partani@ub.ac.ir
[3] Regional Water Company of Tehran, Iran
Email: Radfarshid20@yahoo.com

ABSTRACT

Temperature and precipitation are important indicators of the hydrological cycle that affect different aspects of human life. This paper aims to present and analyze the spatiotemporal variation and change point detection of precipitation and monthly air temperature (average, minimum and maximum) for a duration of 1964 to 2014 in the major urban area across Iran using Theil-Sen and Mann-Kendall trend analysis. This research output showed that highest range of rainfall changes occurred at stations adjacent to the Caspian Sea (Rasht and Gorgan synoptic stations) in the north and the Persian Gulf border (Bushehr synoptic station) at the south of the country. Winter, spring and autumn precipitation decreased by 92%, 73%, and 46% of whole stations, respectively. Application of Theil-Sen estimator also showed that, minimum and maximum temperature has been increased and the central area of Iran has the highest rate of temperature rise. Also, the average temperature trend showed that autumn average temperature decreased while the temperature increased in other seasons. Also, Mashhad, Zahedan, Tabriz, Khorramabad and Shiraz stations, record continuously increasing trend of temperature in all months. This study sheds light on the challenges of accessing surface water resources in arid and semi-arid environments due to natural and anthropogenic driven factor.

## 1. Introduction

New research on climate parameters clearly shows that, there is obvious evidence of climate change pattern at global or regional scale (Maghrebi et al., 2020). Besides, this change may affect agriculture or economical activities and create social, economic or ecological side effect (Ghafarian et al., 2018). Therefore, temporal and spatial variations of precipitation and temperature are important from both the scientific and executive aspects point of view. Several studies have addressed the importance of climate parameter change detection and trends in Iran since the last century, but all of them have a spatial and temporal limitation. For example, Raziei et al. (2005) used 36 years of yearly precipitation from 79 climatological stations in arid and semi-arid regions of Iran. This research output shows that the precipitation trend has spatial character and decreased in the southeast corner of Iranian territory (Raziei et al., 2005). The most important goal of this research is to detect the trends of annual, seasonal and monthly precipitation and temperature (maximum, minimum, average) over Iran between 1964 and 2014, which is a longthy historical data available in the study area using the Mann–Kendall and Theil-Sen estimator. The innovations of this research include a) this research cover the whole Iranian territory b) duration of investigation cover the maximum common same period c) monthly, seasonal and yearly trend have been analyzed.

## 2. Methodology

In this study, the Mann-Kendall (MK) test was employed for the detection of trends in data sets. In this regard, the null and alternative hypothesizes were that the data was a set of m independent variables and a sample that followed a monotonic trend, respectively. This test is calculated as Eq. (1).

$$S=\sum_{k=1}^{m-1}\sum_{j=k+1}^{m}\operatorname{sgn}\left(x_j-x_k\right)\quad \text{where}\quad \operatorname{sgn}(x)=\begin{cases}1 & \text{if}\quad x>0\\ 0 & \text{if}\quad x=0\\ -1 & \text{if}\quad x<0\end{cases}\qquad (1)$$

Where m is the number of data points and also the mean and variance of S are zero and unit, respectively. For m > 10, S statistic is transformed to the standard normal variable Z by Eq. (2) (Tabari and Talaee, 2011)

$$Z = \begin{cases} \frac{S-1}{\sigma} & \text{if} \quad S > 0 \\ 0 & \text{if} \quad S = 0 \\ \frac{S+1}{\sigma} & \text{if} \quad S < 0 \end{cases} \tag{2}$$

Where σ is the standard deviation of S. In Eq. (2), positive and negative values show an increasing and decreasing trends in the used data set, respectively.

## 3. Rustles and Discussion

Precipitation magnitude and variation show a strong spatial and temporal character. Maximum precipitation occurs at the north stations (along the Caspian Sea with a decreasing trend from west to east) and minimum precipitation occurs in the central part of Iran. Maximum annual precipitation occurs in Rasht station (West Caspian Sea) in 1972 (1967.6 mm) and minimum precipitation records occur in the Yazd station in 2010 (9.3 mm). The maximum annual rainfall in central and eastern Iran has never been more than 250 mm (one-third of the world's average precipitation (Aradpour et al., 2021). Moreover, maximum precipitation variation occurs beside the Caspian Sea in the north and Persian Gulf in the south. Synoptic stations of Rasht, Gorgan, Yasuj and Bushehr show the large range of changes in average annual rainfall over the past five decades. 18 stations average annual precipitations are higher than average annual precipitation. Average annual precipitation in Iran over the past five decades was 254.37 mm with maximum 346.2 (in 1982) and minimum 157.8 (in 2010). max29.9 % of annual precipitation fall in autumn, 18.5% in spring, 6.4% in summer and respectively 45.2% in winter. Seasonal precipitation falls in range of autumn (23.67-118.94 mm), spring (14.42-86.9 mm), summer (4.49-30.23 mm) and winter (63.57-180.39 mm). Most of the winter rainfall is in the western, eastern and central stations also summer rainfall mostly occur in the north, northeast and the southeast stations in the study area.

## 4. Conclusion

The monthly, seasonal and annual trends of Temperature (maximum, minimum, average) and precipitation were analyzed by the Mann–Kendall test and Sen's slope estimator. The results of this study revealed that, Average annual rainfall in Iran was 254.37 mm with maximum 346.2 (in 1982) and minimum 157.8 (in 2010). Also, 29.9 % of annual precipitation fall in autumn, 18.5% in spring, 6.4% in summer and respectively 45.2% in winter over the past five decades. Seasonal precipitation is in the autumn (between 23.67-118.94 mm), spring (between 14.42-86.9 mm), summer (between of4.49-30.23) and winter (between 63.57-180.39 mm). Theil-Sen estimator on seasonal precipitation demonstrates that spring and winter have a negative trend while autumn and summer shows an increasing trend over the Iranian territory. Spatial seasonal Theil-Sen estimator also shows that Isfahan (1.13mm/year) and Ilam (2.79 mm/year) station has increased trend in winter while other stations shows a strong decreasing trend. The winter precipitation series also showed a negative trend at approximately 92% of the stations. Ilam, Zahedan, Isfahan, Tehran, Ghazvin and Zangan stations show an increasing trend in spring season while other stations show a decreasing trend. The winter temperature series showed an increasing trend at about 81% of the stations. In spring most of the stations showed the increasing trend. The autumn temperature series revealed an increasing trend approximately 46% of the stations. Monthly Theil-Sen estimator application shows that Mashhad, Zahedan, Tabriz, Khoramabad and Shiraz record continuously increasing trend in all months. Also the monthly increasing pattern mainly focused on the central part of Iran.

## 5. References

ARADPOUR, S., NOORI, R., VESALI NASEH, M. R., HOSSEINZADEH, M., SAFAVI, S., GHAHRAMAN-ROZEGAR, F. & MAGHREBI, M. 2021. Alarming carcinogenic and non-carcinogenic risk of heavy metals in Sabalan dam reservoir, Northwest of Iran. Environmental Pollutants and Bioavailability, 33, 278-291.

GHAFARIAN, P., PEGAHFAR, N. & OWLAD, E. 2018. Multiscale analysis of lake-effect snow over the southwest coast of the Caspian Sea (31 January–5 February 2014). Weather, 73, 9-14.

MAGHREBI, M., NOORI, R., BHATTARAI, R., MUNDHER YASEEN, Z., TANG, Q., AL-ANSARI, N., DANANDEH MEHR, A., KARBASSI, A., OMIDVAR, J. & FARNOUSH, H. 2020. Iran's Agriculture in the Anthropocene. Earth's Future, 8, e2020EF001547.

RAZIEI, T., ARASTEH, P. D. & SAGHAFIAN, B. Annual rainfall trend in arid and semi-arid regions of Iran. ICID 21st European regional conference, 2005. 15-19.

TABARI, H. & TALAEE, P. H. 2011b. Temporal variability of precipitation over Iran: 1966–2005. Journal of Hydrology, 396, 313-320.

# The hydrologic performance of green roofs in urban environment: a state-of-the-art analysis of select literature.

Erica ORSI[1], Gaetano CRISPINO[1], Corrado GISONNI[1]

[1] Department of Engineering, Università degli Studi della Campania Luigi Vanvitelli, Aversa, Italy
email: erica.orsi@unicampania.it
email: gaetano.crispino@unicampania.it
email: corrado.gisonni@unicampania.it

ABSTRACT

In the last years green roofs are being used as a control measure for urban stormwater management as they retain, detain and slowly release rainwater. Green roofs present many economic, social and environmental benefits. The research focuses on the main outcomes highlighted by selected literature studies on the hydraulic performance of green roofs. The hydraulic efficiency has been specifically assessed through the definition of two parameters of great interest to design the tailwater drainage system: the peak reduction and the volume reduction indexes.

## 1. Introduction

The world has observed a rapid urbanization over the past decades, with the increase of the construction to accommodate the shift in population from rural to urban areas. This results in several environmental issues on a global scale, such as urban floods and Urban Heat Island (UHI) effects. Moreover, the growing urbanization influences the natural water cycle: the impermeable surfaces augment and, consequently, there is an increase of the surface runoff and a reduction in infiltration. Climate change further aggravates these problems by increasing both the frequency and intensity of climatic extremes. These critical issues can be partially solved by installing Green Roofs. A Green Roof (GR) installation consists in the introduction of plants and soil on the building rooftop. GRs can be used as control measure for urban stormwater management as they retain rainwater, promote evapotranspiration (ET), and delay peak flows. Rainwater landing on GRs enters a complex hydrological system. The system retains water in vegetation, substrate and layered materials, thus providing runoff retention capacity for stormwater management. In addition, water leaving the GR systems through ET contributes to a cooling effect, the mitigation of UHI effect and the indoor thermal environment isolation. Other significant GRs benefits include the improvement of the water runoff quality by the filtration of pollutants and heavy metals out of rainwater and the reduction in air pollution and greenhouse gas emissions thanks to the ability of the vegetation to filter the air. Nowadays, the scientific and technical literature studies on the hydrologic behavior of GRs can be considered as quite exhaustive. However, some gaps have to be still filled to define the main hydraulic performance parameters of GRs and to characterize them by adopting standard commercial numerical models as Storm Water Management Model (SWMM), Hydrus-1D and Soil Water Atmosphere and Plant (SWAP). In this regard, this research aims to resume the main outcomes highlighted by selected literature studies in the range of the assessment of the hydraulic performance of extensive GRs.

## 2. Hydraulic benefits of green roofs

The hydraulic efficiency of extensive GRs can be evaluated by quantifying the reduction of volume and peak outflows. The reduction of the peak outflows from the catchment equipped with one or more GRs is typically compared with the conventional roof scenario (GR is not installed). The Peak flow Reduction *PR* is usually defined as:

$$PR\ [\%] = 100 \times (Q_{0max} - Q_{GRmax}) / Q_{0max} \qquad (1)$$

where $Q_{0max}$ and $Q_{GRmax}$ are the outflow peaks in the conventional roof and GR implementation scenarios, respectively. In general, literature simulations results reveal that the *PR* is not influenced by climatic conditions, but it is mainly affected by rainfall-event characteristics and GR retention capacity.

The Volume Reduction *VR* is influenced by many factors, e.g., the initial water content, the slope of the roof, the vegetation, the growth media, the meteorological conditions and the precipitation. *VR* can be computed as:

$$VR\ [\%] = 100 \times (V_0 - V_{GR}) / V_0 \tag{2}$$

where $V_0$ and $V_{GR}$ are the outflow volumes of the reference conventional roof and GR implementation, respectively. So far, not many studies have investigated how *PR* and *VR* of GRs vary by changing boundary conditions. A summary of the main outcomes derived by these investigations is shown in Table 1 and Fig.1.

**Table 1.** Details of literature studies on the peak and volume reduction efficiency of GRs.

| Authors | Site | Max. Rainfall Depth [mm] | Substrate Depth [mm] | *PR* [%] | *VR* [%] | Numerical Model |
|---|---|---|---|---|---|---|
| Stovin et al. (2012) | Sheffield (UK) | 99.6 | 80.0 | 60.0 | 30.0 | - |
| Masseroni and Cislaghi (2016) | Seveso Basin (Italy) | - | 192.0 | 58.0 | 35.0 | SWMM |
| Fassman-Beck et al (2018) | Auckland (Australia) | - | 50.0-150 | 73.0-89.0 | - | - |
| Palla et al. (2018) | Genoa (Italy) | 462.8 | 120.0 | 30.0 | 30.0 | SWMM |
| Palla and Gnecco (2020) | Bergamo (Italy)<br>Genoa (Italy)<br>Castelbuono (Italy) | 96.4<br>462.8<br>91.8 | 120.0<br>120.0<br>120.0 | 60.0 | 40.0<br>30.0<br>52.0 | SWMM |
| Mrowiec et al. (2021) | Częstochowa (Poland) | 70.7 | 50.0-70.0 | 60.0 | 35.9 | SWMM |

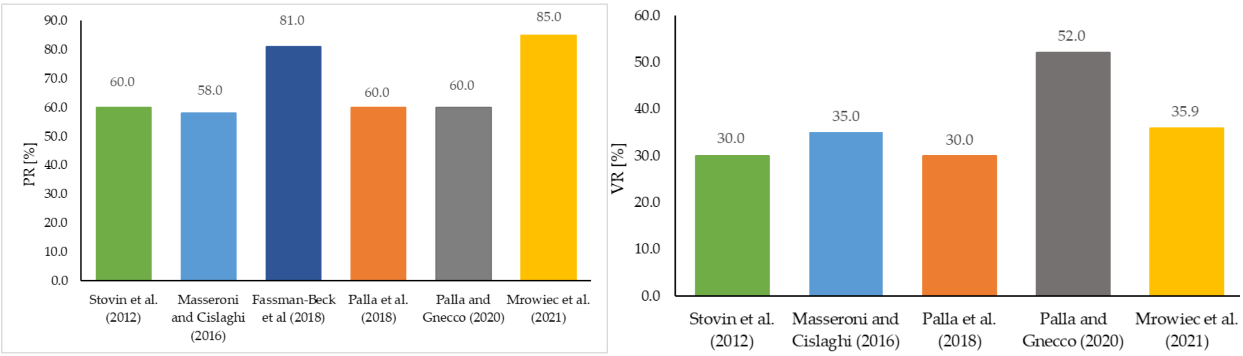


**Fig. 1**. Peak and volume reductions reported in literature studies.

## 3. Conclusions

This paper pays attention on the evaluation of the role of greenery systems in reducing stormwater runoff, through the volume and the peak reduction. As shown, the quantification of the hydraulic efficiency parameters of GRs in the selected literature is quite heterogeneous and a guideline for estimating preliminary values of flow and volume reductions of GRs is still far to be achieved. It is a challenge to predict the hydraulic performance, as the system hydraulic behavior is affected by the specific type and location of GR location. For this, a numerical investigation to assess the variation of the hydraulic parameters of GR efficiency by considering an urban block retrofitted with GRs, in Naples (Italy), is ongoing. The simulation is being implemented by SWMM and the methodological approach of Palla et al. (2018) is applied to estimate the actual ET. Preliminary results confirm the positive impact of GRs in the stormwater management

### References

Fassman-Beck E, Voyde E, Simcock R, Hong YS (2013) 4 living roofs in 3 locations: does configuration affect runoff mitigation? Journal of Hydrology, 490, 11–20

Masseroni D, Cislaghi A (2016) Green roof benefits for reducing flood risk at the catchment scale, Environmental Earth Sciences, 75(7), 1-11

Mrowiec M, Ociepa E, Deska I (2021) Role of extensive green roofs in water management in urban drainage systems, International Journal of Conservation Science, 12, 701-712.

Palla A, Gnecco I, La Barbera P (2018) Assessing the Hydrologic Performance of a Green Roof Retrofitting Scenario for a Small Urban Catchment, Water,10, 1052.

Palla A, Gnecco I (2020) A continuous simulation approach to quantify the climate condition effect on the hydrologic performance of green roofs. Urban Water Journal, 17:7, 609-618

Stovin V, Vesuviano G, Kasmin H (2012) The hydrological performance of a green roof test bed under UK climatic conditions, Journal of Hydrology,414, 148–161

# Predicting mixing in benched surcharged manholes

Fred SONNENWALD[1], Angus C. L. WONG[1], Ian GUYMER[1]

[1] The University of Sheffield, United Kingdom
email: f.sonnenwald@sheffield.ac.uk
email: i.guymer@sheffield.ac.uk

ABSTRACT

Surcharged manholes in combined sewer networks experience a range of complex mixing conditions that hydraulic modelling packages do not consider. This paper investigates the mixing response of a benched surcharged manhole.

## 1. Introduction

In combined sewer networks, rainfall enters the network causing both manholes to become surcharged and combined sewer overflows to occur. Thus, water quality modelling within sewer networks is of interest to help ensure receiving waters are not adversely affected. To predict water quality, both the hydraulics and the mixing processes that affect the spread (dispersion) of pollutants are important. Mixing within pipes is well understood (e.g., Taylor, 1954). However, while manholes are a common element of sewer networks, mixing within them is less well understood due to their complex geometries.

Mixing within unbenched manholes can be described as either "below-threshold" or "above-threshold", depending on surcharge water depth in relation to threshold depth, both relative to the inlet pipe soffit (Sonnenwald et al., 2021). In the below-threshold condition, mixing resembles a continuously stirred tank reactor, i.e., well-mixed (Levenspiel, 1972). In the above-threshold condition, flow short-circuits and comparatively very little mixing occurs. The threshold depth is a function of inlet pipe and manhole diameters.

Most manholes built today are benched (WRC, 2012), but there is less literature addressing mixing in benched manholes. The results of Saiyudthong (2004) suggest that mixing within benched manholes is similar to an above-threshold unbenched manhole. Despite this and other research, modelling packages such as InfoWorks ICM persist in assuming instantaneous complete mixing within all manholes at all times (Innovyze Inc., 2019).

Mixing within manholes can be best described using Residence Time Distributions (RTDs). The RTD $E$, when convolved with an upstream concentration profile ($u$), predicts a downstream concentration profile ($y$):

$$y(t) = \int_{-\infty}^{\infty} E(\tau)u(t-\tau)\mathrm{d}\tau \tag{1}$$

where $t$ is time and $\tau$ is a dummy variable for integration. An RTD can be obtained from experimental results using deconvolution (Guymer and Stovin, 2011) and can be predicted in unbenched manholes using a compartmental mixing model (Sonnenwald et al., 2021). The Cumulative Residence Time Distribution (CRTD, $F$), the cumulative sum of the RTD, can be interpreted to infer the underlying flow conditions (Levenspiel, 1972). Note that the instantaneously well-mixed RTD can be expressed as $E_{WM} = \exp(-tQ/V)$, where $Q$ is flow rate $V$ is manhole volume, and $tQ/V$ is dimensionless time.

As there are few studies describing mixing within benched manholes, this study aims to record solute transport traces in a laboratory-scale surcharged benched manhole and reveal the underlying CRTD. This will be used to inform on how to best represent mixing within benched manholes.

## 2. Methodology

A 216 mm straight-through circular manhole with aligned 24 mm diameter inlet and outlet pipes was fitted with 1:12 slope full pipe-depth benching (Fig. 1). Fluorescent Rhodamine WT dye was injected upstream of the inlet pipe and dye concentrations recorded at 50 Hz using two Turner Designs Cyclops-7 fluorometers, fitted to the pipes 600 mm either side of the manhole centre. Over 60 solute traces were collected with surcharges ranging from 12 to 234 mm and flow rates ranging from 0.088 to 0.370 L/s. The data were pre-processed with a linear background subtraction and the start and ends of the trace being determined by 1% of peak concentration. Mass-balance was assumed as implied by Eq. (1). Maximum Entropy Deconvolution, in which the entropy (amount of information) in the RTD is maximized subject to the constraint that the RTD satisfy Eq. (1), was used to obtain the RTD and CRTD (Sonnenwald et al., 2015; Guymer et al., 2020).

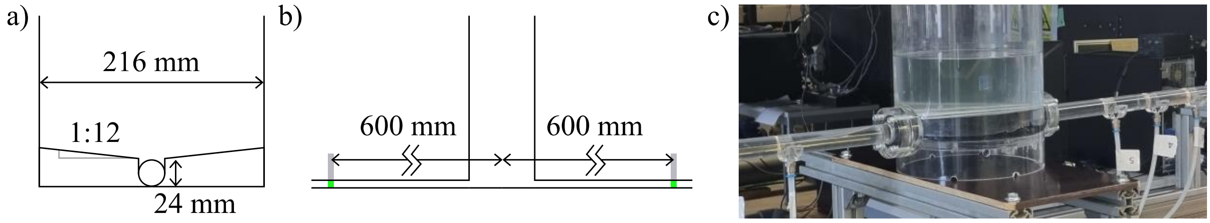


**Fig. 1.** Model manhole a) end-view showing benching, b) side-view showing fluorometer placement, c) photograph

## 3. Results

Initial results of this study are presented here. Example low- and high-surcharge deconvolved CRTDs for a benched manhole are plotted in Figs. 2a and 2b respectively, compared to the theoretical well-mixed CRTD, plotted in Fig. 2c. The observed mixing behaviour clearly varies from the well-mixed assumption employed by hydraulics modelling packages, and these results suggest those packages are vastly over-estimating mixing.

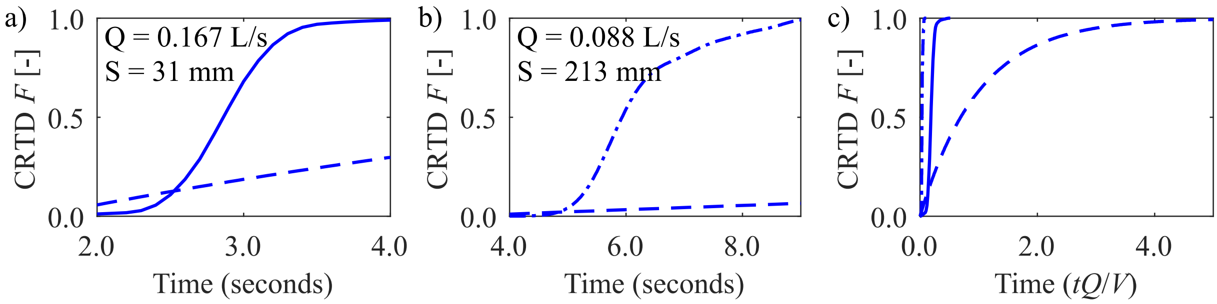


**Fig. 2.** Cumulative Residence Time Distributions, illustrating mixing, for a) an experimental low-surcharge benched manhole (solid line), b) an experimental high-surcharge benched manhole (dash-dot line), and c) the assumed well-mixed response of hydraulic water-quality modelling packages (dashed line).

Figure 2a, the low-surcharge CRTD, appears to be a cumulative Gaussian distribution, suggesting that in certain conditions the Advection-Diffusion Equation (ADE) could represent mixing within a benched manhole. Considering the half-circular section of a dry weather flow channel, this is reasonable. As surcharge increases this assumption, is less valid.

The first part of the high-surcharge CRTD (Fig. 2b) appears to be close to cumulative Gaussian in shape. This suggests that most of the flow still follows the dry weather flow channel. The longer tail indicates upwards exchange into the surcharge volume, which acts as a dead zone and increases mixing. This complex behaviour cannot be described by a simple mixing model, neither an ADE-based approach nor well-mixed CRTD.

Further investigation of mixing in surcharged benched manholes is ongoing and a comparison of these results with the compartmental mixing model developed by Sonnenwald et al. (2021) will be presented.

**Acknowledgements**

This work was supported in part by the EPSRC (Grant No. EP/P012027/1). The authors thank to Joseph Milner for his assistance in the laboratory.

**References**

Guymer I, Stovin VR (2011) One-dimensional mixing model for surcharged manholes, Journal of Hydraulic Engineering, 137(10), 1160-1172.

Guymer I, Stovin V, O'Brien R, Dennis P, Saiyudthong C, Lau STD, Sonnenwald, F (2020) University of Sheffield experimental manhole traces and CRTDs, Sheffield.

Innovyze Inc. (2019) InfoWorks ICM 10.5 Manual, Portland, "Network Model".

Levenspiel O (1972) Chemical reaction engineering, New York, 257 pp.

Saiyudthong C (2004) Effect of changes in pipe direction across surcharged manholes on dispersion and head loss, PhD Thesis, University of Sheffield.

Sonnenwald F, Stovin V, Guymer I (2015) Deconvolving smooth residence time distributions from raw solute transport data, Journal of Hydrologic Engineering, 20(11), 04015022.

Sonnenwald F, Mark O, Stovin V, Guymer I (2021) Predicting manhole mixing using a compartmental model, Journal of Hydraulic Engineering, 147(12), 04021046.

Taylor GI (1954) The dispersion of matter in turbulent flow through a pipe, Proceedings of the Royal Society of London Series A. Mathematical and Physical Sciences, 223(1155), 446-468.

WRC (2012) Sewers for adoption, Swindon.

# Influence of storm drain inlet locations on urban pluvial flooding hazard at local scale

Giuseppe T. ARONICA[1], Joao P. LEITAO[2], Angela CANDELA[3]

[1] Department of Engineering, University of Messina, Messina, Italy
email: giuseppetito.aronica@unime.it

[2] Eawag, Swiss Federal Institute of Aquatic Science and Technology, Dübendorf, Switzerland
email: joaopaulo.leitao@eawag.ch

[3] Department of Engineering, University of Palermo, Palermo, Italy
email: angela.candela@unipa.it

ABSTRACT

## 1. Introduction

The assessment of the impact of surface drainage conditions and the related effect on urban flooding is the general aim of the present research study. The main objective is to analyze the surface drainage efficiency by evaluating the influence of storm drain inlet location on pluvial flooding. This study focuses on the impact of surface drainage system, in terms of positioning, typology and size of inlets, on pluvial flood hazard.

## 2. Methods

In this study the FLURB-2D propagation model has been used (Palla et al., 2018). It is a two-dimensional inertial model based on the Saint Venant equations and it was, originally, developed with a different purpose. The model was worked out to simulate alluvial plains flow propagation when topography is uneven (Aronica et al., 1998) and it was, first, applied to urban areas by Aronica and Lanza (2005). Details about the hydrodynamic model are reported in Aronica et al. (1998), Aronica and Lanza (2005) and Palla et al. (2018). Inlets in the study area have a different hydraulic behavior as a function of flow depth value: they are comparable to weirs for flow depth lower than 0.12 m and to orifices for flow depths greater than 0.12 m. Four different hypothetical scenarios for the location of the drain inlets were considered (Table 1). Drain inlets located: at street intersections ("St. crossings"); at the middle of the street ("Middle"); along the lower elevation side of the street ("Ledge"); and along the higher elevation side of the street ("Hedge"). The hydraulic capacity of an individual drain inlet was kept constant for the different scenarios depending only on the local water stage. This results in different total hydraulic drainage capacity.

**Table 1.** Description of the drain inlet scenarios

| Scenario | Number of drain inlets | Description |
|---|---|---|
| *St. crossings* | 26* | Drain inlets are located only at street crossings. |
| *Middle* | 147 | Drain inlets are located in the center line of the streets spaced 25 m. |
| *Ledge* | 146 | Drain inlets are located along the lower elevation side of the streets spaced 25 m. |
| *Hedge* | 147 | Drain inlets are located along the higher elevation side of the streets spaced 25 m. |

* This scenario represents a substantially smaller drain inlet hydraulic capacity when compared to the three other scenarios.

## 3. Case study

The methodological approach presented in this study is applied in a real study area in the town of Messina (Italy). Ganzirri lake is situated within the area of Messina city, and it is located, approximately, 13 km north-east of the city center (Figure 1). The area around the lake is, entirely, densely urbanized, with streets and blocks with limited pervious parts. The drainage system is mainly separated from the sewer system and there is no stormwater drainage system. Starting from the morphology of the study area, a mesh has been defined in order to cover the entire surface drainage network, and the internal nodes were made to coincide with the drain inlets. The mesh area is about 0.47 km$^2$, it is discretized as 42,520 triangular elements and 24,792 nodes. Geometric features (x, y, z coordinates) of nodes have been derived from a DEM, with 0.5 m resolution obtained from a drone survey carried out in 2019.


**Fig. 1.** Overview of the study area, Ganzirri village, in the town of Messina, Italy (from Google Maps).

Street network of the area is covered by the mesh and each triangular element is considered impervious (paved or asphalted) while buildings are represented as voids in the mesh. Each inlet has a contributing area (totally paved) which is not, directly, connected to a single inlet as it results from the flow hydrodynamics in the domain. FLURB-2D simulates overland pluvial flow propagation, and the interactions with the subsurface drainage network are not simulated. The analysis is carried out by using as input synthetic hyetographs derived from the analysis of rainfall data. A network of inlets is considered, distributed in the study area. Direct rainfall distributed over the meshed area represents model boundary conditions in terms of inflow and the inlet stage-discharge relationship for the outflow.

## 4. Results

The results show that the location of the drain inlets have implications on the maximum water depth across the simulation domain (Fig. 2). This indicates that, as expected, when using detailed elevation data to set up two-dimensional flood models, the impact of the location of the drain inlets starts to become visible and needs to be taken into account.

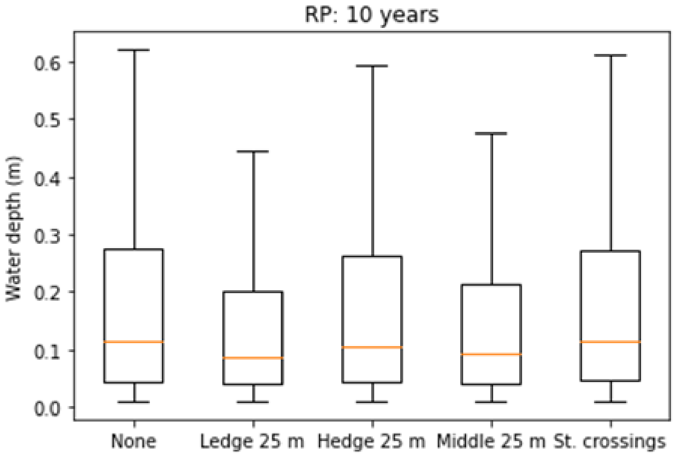


**Fig. 2.** Distribution of the maximum water depth across the whole simulation domain, for a rainfall event with a return period of 10 years.

## 5. Conclusions

These preliminary results indicate that more refined analyses need to be conducted to fully understand (i) the requirements in terms of the drain inlet representation details to accurately simulate urban flood simulations and ultimately (ii) to assess the real impact of drain inlet location on pluvial flooding and inform decision makers to improve the hydraulic performance of the drainage systems.

### References

Aronica G.T., Nasello C., Tucciarelli T. (1998) A 2D multilevel model for flood propagation in flood affected areas, Journal of Water Resources Planning and Management (ASCE), 124(4), 210-217

Aronica G.T., Lanza L. (2005) Drainage efficiency in urban environment, Hydrological Processes, 19(5), 1105-1119

Palla A., Colli M., Candela A., Aronica G.T., Lanza L.G. (2018) Pluvial flooding in urban areas: the role of drainage inlets efficiency, Journal of Flood Risk Management, 11, 663-676

# Optimizing clarification utilizing a coupled computational fluid dynamics and machine learning (CFD-ML) tool: "DeepXtorm"

Haochen Li [1], John J. SANSALONE [2]

[1] Engineering School of Sustainable Infrastructure and Environment, University of Tennessee, United States
email: hli111@utk.edu

[2] Engineering School of Sustainable Infrastructure and Environment, University of Florida, United States
email: jsansal@ufl.edu

ABSTRACT

DeepXtorm combines computational fluid dynamics (CFD) and machine learning (ML) as a modeling platform (CFD-ML) developed from physical model data and CFD simulations over a wide range of urban drainage clarifier configurations, loadings, hydrodynamics and particulate matter (PM) granulometry. A novel augmentation of CFD with ML models is developed and trained to create surrogate clarification models. For a clarifier, this CFD-ML platform facilitates (1) analysis, (2) design optimization, and (3) optimization of clarifier retrofits to minimize cost for a required level of clarification. Results with CFD-ML benchmarking indicate that: (a) historical models based on residence time (RT) are not accurate or generalizable for clarifier PM separation, (b) RT models are agnostic to geometrics, hydrodynamics and PM granulometry; and do not reproduce PM separation, (c) trained ML models provide high predictive capability (± 15%) for PM separation. Dynamic similitude analysis indicates that clarification is primarily a function of the Hazen number and clarifier horizontal to vertical aspect ratio. With a common presumptive guidance of 80% for PM separation, a Pareto frontier analysis with the CFD-ML model generates significant economic benefit for planning/design/retrofits. CFD-ML demonstrate that enlarging clarifier dimensions (increasing RT) to address impaired behavior can result in exponential cost increases, irrespective of infrastructure adjacency conflicts.

## 1. Introduction

Urban drainage generated from storm events transports chemical, pathogens, and PM constituents to receiving waters; impacting aqueous chemistry acutely and chronically with consequences to public health. For a half-century, clarification systems, specifically urban drainage clarifiers have been a common unit operation (UO) with unit process (UP) functionality deployed in built environs for hydraulic/volumetric management and clarification. Urban drainage clarification basins in the United States (US), now exceeds 10 million. These basins intercept approximately 25% of the runoff in the USA with potential significant benefit to the urban water cycle and built environs. Despite basin ubiquity, fundamental PM and PM-associated chemical transport and fate processes are poorly understood. This knowledge gap is a result of the complexity of nonlinear interaction and multiphase coupling of turbulence, partitioning and heterodisperse PM. Currently, design and regulatory guidance of clarifiers employs presumptive criteria based on mean residence time (RT), driven by basin volume and mean flow metrics. Decades of such design and practices have led to an impairment designation for most clarification basins. More importantly, basins do not meet intended functionality, with effluent discharges of PM, chemicals and pathogens harmful to humans and the urban water cycle. In most cases, geometric expansion of basins, tanks or tunnels is not viable due to infrastructure constraints; an even greater constraint in the built environs of Europe. There is a critical need to supplant existing tools with higher-fidelity physics-based simulation tools to inform (1) design/regulatory guidance, (2) basin functionality, and (3) intra-basin retrofits, such as with internal baffles to train clarifier hydrodynamics.

## 2. Methodology

Figure 1 summarizes the CFD-ML model methodology with the ML models illustrated (ANN: artificial neural network, RF: random forest, DT: decision tree and SR: symbolic regression). The databases are generated from CFD simulations (HiPerGator at University of Florida) for a 160,000 combinations of geometric configurations, PM granulometry, loading conditions and physical model data as shown in (a). Data structure layouts for the ML model development with dimensionless basin quantities are illustrated in (b) and the ML models illustrated in (c) through (e). The deployment of the ML surrogate model is illustrated in (f). Details of the CFD development and ML models are provided by Li and Sansalone 2022a, Li and Sansalone 2022b.

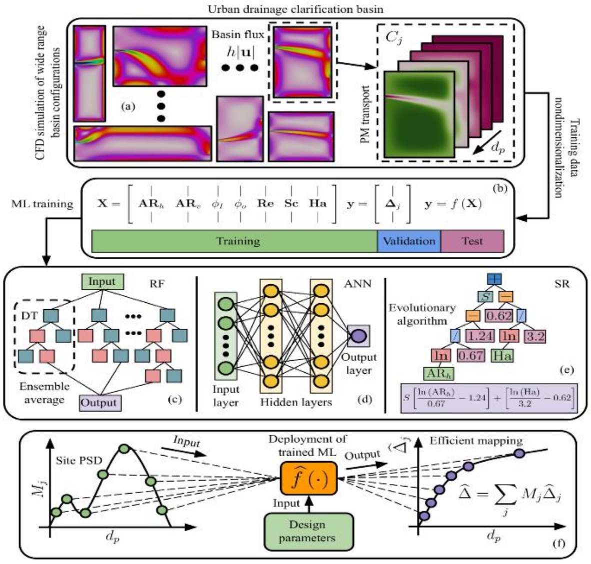


Figure 1. Illustration of the flowpath of the CFD-ML modeling methodology

## 3. Results

Figure 2 illustrates the results of the CFD-ML tool, DeepXtorm for a rectangular basin (6:1 length to width) with a depth of 3 m and 1.4 hectares of surface area at normal pool elevation. The basin receives direct wet weather flows from a 50 hectare urban drainage area. Three results are illustrated in Figure 2. The Heinemarm (1981) result is an historical embodiment of PM clarification based on RT where Harper and Baker (2003) represents current presumptive guidance for PM and nutrient clarification. The Optimized result is based on CFD-ML and this result was benchmarked with monitoring data and clarifier retrofit/land costs (FDOT, 2016). At the Florida requirement of 80% load removal by this clarifier there is a 15.8 million USD reduction in land and construction costs through CFD-ML optimization to retrofit the clarifier as compared to RT requirements.

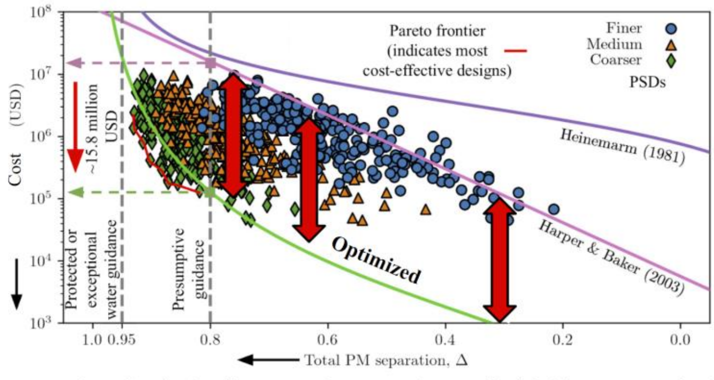


Figure 2. CFD-ML optimized clarifier, Pareto frontier and conventional RT method cost curves

## 4. Conclusions

DeepXtorm is a CFD-ML modeling platform for urban drainage clarifiers that facilitates (a) analysis of an existing system, (b) optimization of a proposed design, or (c) retrofit optimization of an impaired clarifier to upgrade performance. Model viability is based on 160,000 CFD simulations facilitated by high performance computing and then coupled in DeepXtorm with ML algorithms to optimize clarifier geometrics (or retrofits) to achieve a required level of performance, for example 80% PM or nutrient clarification. Results, benchmarked with monitoring and cost data for a full-scale operational clarifier, demonstrate that optimization provides cost reduction of at least 10X compared to presumptive guidance based on RT requirements.

### References

Li H., Sansalone J. (2022a) A CFD-ML augmented alternative to residence time for clarification basin scaling and design, Water Research, 209, 117965.

Li H., Sansalone J. (2022b) Interrogating common clarification models for unit operation systems with dynamic similitude, Water Research, 215, 118265.

FDOT, Florida Department of Transportation, (2016). Performance of the FAA pond at Naples Municipal Airport. Technical Report. URL: https://www.florida-aviation-database.com/library/filedownload.aspx?guid=680 1edf132e-6c5c-4774-9045-faccb850e305.

# Common malfunctions in urban drainage and their impact on surface flooding based on an integrated 1D/2D hydraulic model

Fabian FUNKE[1], Stefan REINSTALLER[2], Manfred KLEIDORFER[1]

[1] *Department of Infrastructure, Unit of Environmental Engineering, University of Innsbruck, Austria*
email: fabian.funke@uibk.ac.at
email: manfred.kleidorfer@uibk.ac.at
[2] Graz *University of Technology, Institute of urban water management and landscape engineering, 8010 Graz, Austria*
email: stefan.reinstaller@tugraz.at

ABSTRACT

## 1. Introduction

Urban drainage infrastructures are exposed to a variety of external influencing factors that can negatively affect hydraulic performance and increase the risk of flooding. This includes changing precipitation characteristics due to climate change (Hosseinzadehtalaei et al., 2020), an increase in impermeable surfaces due to advancing urbanization (Tscheikner-Gratl et al., 2019) but also other failures and malfunctions (Mugume et al. 2015) in the technical grey and green infrastructure. With an increasing share of sustainable urban drainage systems (SUDS) and uncertainties regarding responsibility, care and maintenance of these facilities (Lashford et al., 2019), as well as progressive aging of conventional sewers that are inspected and maintained too infrequently, an increase in malfunctions can be assumed. In this work, we are investigating common malfunctions in urban drainage systems using a 1D/2D urban flood model of a small Austrian municipality (10,000 inhabitants). The goal is to quantify the impact of failures and malfunctions in both grey and blue-green infrastructures on flooding areas for different rainfall events and compare them to other possible scenarios like climate change.

## 2. Method

The case study of this work is the small city Feldbach (Austria) with a studied catchment area of 1.3 km$^2$. The study site could be described as an urban catchment with a small city center in the north and a semi-urban boundary area in the south. The area is bordered in the north by the river Raab (Figure 1). In terms of flood modeling, several processes must be considered: i) the impact of the hillside catchment with intense agriculture use in the boundary areas; ii) two small creeks from south to north; and iii) high water levels in river Raab can influence the drainage system in the city center.

An integrated 1D/2D urban flood model with the commercial software PCSWMM2D was created to predict the water depth and the flow velocity in flooding areas of the study site (Abdelrahman et al. 2018). The model is based on a three-layer approach, that combines each relevant hydrologic and hydraulic process in a parallel integrated way. This includes the: i) hydrological model, which calculates runoff as input for the 1D and 2D hydraulic model layers, including the low impact development (LID) approach from the Storm Water Management Model SWMM5.1; ii) flow transport processes on the surface (2D); and iii) flow transport process in the sewer system (1D).

In total 10 different scenarios were designed for the urban case study: i) the base scenario which represents the current state of the study area; ii) two reference scenarios with climate change and wet preconditions; and iii) the malfunction scenarios with seven single malfunction scenarios and one worst case which is all of the single scenarios combined (Table 1). Each scenario was run with design rainfall events with a Euler II distribution and an interval length of 1 hour as well as return periods between 1 and 100 years. The severity of the reference and malfunction scenarios in comparison to the base case is assessed by 3 different objective values: i) the total flooded area with water depths > 10cm; ii) the number of buildings affected by flooding; and iii) the total combined sewer overflow emissions released into the neighboring stream.

## 3. Results and discussion

So far, the methodology has been tested in a much smaller virtual urban case study (Funke et al., 2022) and is now being transferred to the Feldbach real-world case study. The first results in the small virtual case study show a clear difference between the analyzed scenarios. The highest flooding values result from the reference

scenarios climate change and wet preconditions, followed by malfunctions in the technical grey infrastructure. Malfunctions in SUDS show the smallest increase in flooding values, which is partly due to their relatively small share of the total area. All scenarios are highly dependent on the rainfall event characteristics, with no differences in the flooding values compared to the base case for low return periods and rising differences for medium to high return periods. We expect similar results in the real-world case study with probably slight changes between the different scenarios. Based on the results, we will be able to give recommendations to municipalities and cities on how to deal with common malfunction to limit and prevent urban flooding.

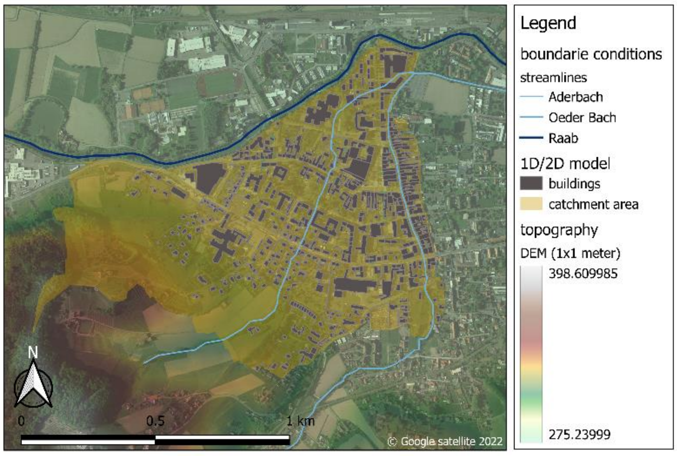


**Fig. 1.** Overview map of the urban study site Feldbach in Austria, including the relevant streams (Raab, Aderbach and Oeder Bach) and the DEM used for the integrated 1D/2D model (resolution 1x1 meter).

**Table 1.** Type, name and description of the reference and malfunction scenarios analyzed in the urban case study

| Scenario type | Scenario name | Description |
|---|---|---|
| Reference Scenarios | Climate Change | Increased rainfall depth of the design rainfall event |
| | Wet Precondition | 6-hour continuous rain before a design rainfall event |
| Malfunctions in technical grey infrastructures | River flood | CSO blockage due to river flood |
| | Blocked Inlets | Blocked street inlets due to leaves, rubbish or snow |
| | Overflow basin sedimentation | Deposits in overflow basin due to previous events or lack of maintenance |
| | Conduit blockage | Conduit blockage due to drought, root intrusion or lack of maintenance |
| Malfunctions in SUDS and green infrastructures | Green roof substrate erosion | Erosion of green roof substrate due to storms, lack of maintenance or drought |
| | Permeable pavement clogging | Clogging of permeable pavements due to sediment accumulation |
| | Swale erosion and sedimentation | The storage volume of the swale is reduced by erosion of embankments and deposition of foreign material |
| | Worst case | All 7 single malfunctions in technical grey and green infrastructure combined |

**References**

Abdelrahman, Y. T., El Moustafa, A. M., & Elfawy, M. (2018). Simulating flood urban drainage networks through 1D/2D model analysis. Journal of Water Management Modeling, 2018, 1–7. https://doi.org/10.14796/JWMM.C454

Funke, F., Reinstaller, S., Muschalla, D. & Kleidorfer, M. (2022): Impact of model structure on analysing malfunctions in urban drainage systems. Proceedings of: Urban Drainage Modelling Conference 2022, 10.01.2022, Costa Mesa (California). https://udm2022.org/published-abstracts/

Hosseinzadehtalaei, P., Tabari, H., & Willems, P. (2020). Climate change impact on short-duration extreme precipitation and intensity–duration–frequency curves over Europe. Journal of Hydrology, 590(March), 125249. https://doi.org/10.1016/j.jhydrol.2020.125249

Lashford, C., Rubinato, M., Cai, Y., Hou, J., Abolfathi, S., Coupe, S., Charlesworth, S., & Tait, S. (2019). SuDS & sponge cities: A comparative analysis of the implementation of pluvial flood management in the UK and China. Sustainability (Switzerland), 11(1), 1–14. https://doi.org/10.3390/su11010213

Mugume, S. N., Gomez, D. E., Fu, G., Farmani, R., & Butler, D. (2015). A global analysis approach for investigating structural resilience in urban drainage systems. Water Research, 81, 15–26. https://doi.org/10.1016/j.watres.2015.05.030

Tscheikner-Gratl, F., Caradot, N., Cherqui, F., Leitão, J. P., Ahmadi, M., Langeveld, J. G., Le Gat, Y., Scholten, L., Roghani, B., Rodríguez, J. P., Lepot, M., Stegeman, B., Heinrichsen, A., Kropp, I., Kerres, K., Almeida, M. do C., Bach, P. M., Moy de Vitry, M., Sá Marques, A., … Clemens, F. (2019). Sewer asset management–state of the art and research needs. Urban Water Journal, 16(9), 662–675. https://doi.org/10.1080/1573062X.2020.1713382

# Environmental assessment of a new Green Wall system: experimental results on runoff reduction and nutrients leaching

Stefania Anna PALERMO[1], Michele TURCO[1], Anna Chiara BRUSCO[1], Behrouz PIROUZ[1], Patrizia PIRO[1]

[1] Department of Civil Engineering, University of Calabria, 87036 Rende (CS), Italy
email: stefania.palermo@unical.it

ABSTRACT

Green Walls represent a sustainable solution to mitigate the impacts due to climate changes and urbanization. While these systems have been widely investigated in different fields of sciences, studies on the potential of green wall systems to manage urban stormwater are still limited. Thus, this study presents experimental findings on runoff reduction and nutrients leaching from a new green wall system.

## 1. Introduction

Nature-Based Solutions (NBS) are sustainable systems to manage stormwater in urban areas. Their principal purpose is to reproduce natural processes to filter, infiltrate, evaporate, store, and detain runoff near its source (Kozak et al., 2020). The most common benefits of NBS are urban flooding risk mitigation, urban heat island effects reduction, water quality restoration, air quality improvement, enhancement of biodiversity and many others (Emilsson and Ode Sang, 2017; Kabisch et al., 2016; Raimondi and Becciu, 2021).

Green Wall (GW) is one of the most popular NBS; generally, these systems are classified, based on the functional elements, into Green Facades (direct or indirect) and Living Walls (continuous or modular). More detail about GW types and components can be found in Manso and Castro-Gomes (2015) and Palermo and Turco (2020).

GWs have been already investigated in different fields of sciences: several studies have analyzed their use as greywater treatment systems (Addo-Bankas et al., 2021; Boano et al., 2021), and other studies have focused on thermal or energy issues (Andric et al., 2020; Daemei et al., 2021; Kenai et al., 2021; Koch et al., 2020), and lastly on their efficiency to improve the air in urban cities (Paull et al., 2021; Ysebaert et al., 2021). While studies on the potential of GW to manage, stormwater are still limited. Thus, this study aims to present some experiments conducted in the "Urban Hydraulic and Hydrology Laboratory" (LIU) of the Department of Civil Engineering (University of Calabria) regarding the efficiency of an innovative green wall system to retain runoff. Moreover, the nutrient leaching concerning the nitrogen cycle and phosphorus was also evaluated.

## 2. Materials and methods

The GW system, developed and tested in the LIU, consists of a panel of 100 cm x 100 cm with two boxes for vegetation growth. Each box has a height of 16 cm, length of 100 cm and width of 14.5 cm and presents the same stratigraphy consisting of: (i) a surface layer vegetated with plants; (ii) a soil substrate (70% Irish Peat and 30% Perlite) with a depth of 12 cm; (iii) a filter layer (geotextile with high permeability) to prevent fine soil particles moving into the underlying layer; (iv) a drainage layer in clay pebbles with a depth of around 2 cm.

The hydrological response of the GW was assessed by developing an experimental system to reproduce a series of rainfall-runoff tests in a controlled environment. Several rainfall events were replicated using a rainfall simulator consisting of ten sprinklers which delivered the water pumped from a storage tank. Constant rainfall intensities were distributed on the top of the green wall panel, and a tipping bucket device measured the outflow rate with a resolution of 0.2 mm.

To analyze the system's hydrological efficiency, the Runoff Coefficient (RC) was estimated on an event scale as the percentage difference between discharged volume and rain volume.

To assess the nutrient leaching behaviour of the new GW system, the outflow from each rainfall event was sampled. The concentrations of $NO_3^- - N$, $NO_2^- - N$, $NH_4^+ - N$, and $PO_4^{3-} - P$ in the samples were determined by UV-VIS spectrophotometry.

## 3. Results and discussion

The results in terms of Runoff Coefficient (RC) and nutrients concentrations ($NO_3^- - N$, $NO_2^- - N$, $NH_4^+ - N$, $PO_4^{3-} - P$ ) for three selected rainfall events are reported in Table 1.

**Table 1.** Characteristics of the rainfall events (Antecedent Dry Weather Period - ADWP, rainfall duration - D; rainfall intensity – i), Runoff Coefficient -RC; Concentrations of $NO_3^- - N$, $NO_2^- - N$, $NH_4^+ - N$, $PO_4^{3-} - P$, resulting from the laboratory tests on the green wall panel. The concentration is expressed as mean value ± relative error.

| Test | Rainfall Characteristics | | | RC (%) | Concentration (mg/L) | | | |
|---|---|---|---|---|---|---|---|---|
| | ADWP (hh:mm) | D (min) | i (mm/h) | | $NO_3^- - N$ | $NO_2^- - N$ | $NH_4^+ - N$ | $PO_4^{3-} - P$ |
| 1 | 95:20 | 20 | 98.13 | 31.82% | 2.53±0.17 | 0.01±0.36 | 3.89±0.01 | 2.36±0.05 |
| 2 | 06:01 | 10 | 165.52 | 31.92% | 3.58±0.10 | 0.02±0.25 | 3.21±0.05 | 2.00±0.04 |
| 3 | 72:08 | 10 | 189.14 | 44.40% | 3.05±0.13 | 0.01±0.69 | 2.14±0.03 | 1.59±0.04 |

The results in terms of Runoff Coefficient (RC) display the good hydrological efficiency of the new green wall in reducing runoff under different precipitations.
The average value of the concentration of $NO_3^- - N$ and $NH_4^+ - N$ in each outflow sample ranges from 2.5 to 3.6 and from 2.1 to 3.9, respectively; while the concentration of $NO_2^- - N$ is very low, with average values less than 0.02. The concentration of $PO_4^{3-} - P$ ranges from 1.6 to 2.4, considering the mean value. In addition, nutrients concentrations in outflow samples collected at different time intervals of the same rainfall event were also evaluated. This last analysis showed a decrease in $NO_3^- - N$ concentration and an increase in $NH_4^+ - N$ concentration during the outflow.

The findings show how rainfall features affect nutrient leaching behaviour and runoff reduction efficiency. In conclusion, given the excellent rainwater retention capacity and the low nutrient concentrations in the outflow, the new green wall system is a promising sustainable strategy for urban stormwater management.

**Acknowledgements**

The green wall panel was developed during the Project "Innovative Building Envelope through Smart Technology (I-Best)" founded by National Operational Project for E&C 2014-2020 ERDF – I AXIS - Action 1.1.3. CUP B28I17000290008.
The author S.A.P is a researcher funded by REACT EU National Operational Project for Research and Innovation 2014-2020. IV AXIS. Action IV.4, Action IV.6. CUP: H25F21001230004. ID: 1062_R18_GREEN.

**References**

Addo-Bankas, O., Zhao, Y., Vymazal, J., Yuan, Y., Fu, J., & Wei, T. (2021) Green walls: A form of constructed wetland in green buildings, Ecological Engineering, 169, 106321.
Andric, I., Kamal, A., & Al-Ghamdi, S. G. (2020) Efficiency of green roofs and green walls as climate change mitigation measures in extremely hot and dry climate: Case study of Qatar, Energy Reports, 6, 2476-2489.
Boano, F., Costamagna, E., Caruso, A., Fiore, S., Chiappero, M., Galvão, A., ... & Masi, F, (2021). Evaluation of the influence of filter medium composition on treatment performances in an open-air green wall fed with greywater, Journal of Environmental Management, 300, 113646.
Daemei, A. B., Shafiee, E., Chitgar, A. A., & Asadi, S. (2021), Investigating the thermal performance of green wall: Experimental nalysis, deep learning model, and simulation studies in a humid climate, Building and Environment, 205, 108201.
Emilsson, T., & Ode Sang, Å. (2017), Impacts of climate change on urban areas and nature-based solutions for adaptation. In Nature-based solutions to climate change adaptation in urban areas (pp. 15-27), Springer, Cham.
Kabisch, N., Frantzeskaki, N., Pauleit, S., Naumann, S., Davis, M., Artmann, M., ... & Bonn, A. (2016), Nature-based solutions to climate change mitigation and adaptation in urban areas: perspectives on indicators, knowledge gaps, barriers, and opportunities for action, Ecology and Society, 21(2).
Kenai, M. A., Libessart, L., Lassue, S., & Defer, D. (2021), Impact of green walls occultation on energy balance: Development of a TRNSYS model on a brick masonry house, Journal of Building Engineering, 44, 102634.
Koch, K., Ysebaert, T., Denys, S., & Samson, R. (2020), Urban heat stress mitigation potential of green walls: A review, Urban Forestry & Urban Greening, 55, 126843.
Kozak, D., Henderson, H., de Castro Mazarro, A., Rotbart, D., & Aradas, R. (2020), Blue-green infrastructure (BGI) in dense urban watersheds. The case of the Medrano stream basin (MSB) in Buenos Aires, Sustainability, 12(6), 2163.
Manso, M., & Castro-Gomes, J. (2015), Green wall systems: A review of their characteristics, Renewable and sustainable energy reviews, 41, 863-871.
Palermo, S. A., & Turco, M. (2020), Green Wall systems: where do we stand?, In IOP Conference Series: Earth and Environmental Science (Vol. 410, No. 1, p. 012013). IOP Publishing.
Raimondi, A., & Becciu, G. (2021), Performance of green roofs for rainwater control, Water Resources Management, 35(1), 99-111.
Paull, N. J., Krix, D., Irga, P. J., & Torpy, F. R. (2021), Green wall plant tolerance to ambient urban air pollution, Urban Forestry & Urban Greening, 63, 127201.
Ysebaert, T., Koch, K., Samson, R., & Denys, S. (2021), Green walls for mitigating urban particulate matter pollution—A review, Urban Forestry & Urban Greening, 59, 127014.

# Development of a warning system for the risk of flooding associated with the urban drainage network

Antonio LASTRA[1], Alejandro PINILLA[1]

[1] Canal de Isabel II, Madrid, Spain
email: alastra@canal.madrid
email: apinilla@canal.madrid

ABSTRACT

The aim of this project is developing a system to identify and quantify flood risks caused by overflows of the urban drainage network in order to obtain a tool for decision-making in prioritizing technical improvement measures and for planning new infrastructure. Currently, 136 municipalities of Madrid region have been individually characterized.

This assessment is carried out through the results of overflow hydraulic models in the urban drainage network, which are the input for a 2D hydraulic model to simulate the geographical distribution of floods for 10-year return period rainfall.

## 1. Introduction

The objective of this study is the development of a system for the identification and quantification of the risk of floods associated with the Urban Drainage network in urban and peri-urban areas of Madrid region, and with this to be able to have a tool to help prioritize and plan new infrastructures to be carried out in the Urban Drainage network. The impact of the study is in 136 municipalities of the Community of Madrid, in which Canal de Isabel II manages the urban drainage network.

## 2. Methodology

For this, risk is defined as the probability of damage to people, goods or services as a result of a flood, according to the following Eq. (1):

$$\boldsymbol{R = H \cdot E \cdot V} \tag{1}$$

where H – Hazard, E – Exposure, V – Vulnerability

Taking this into account, the hazard has been calculated as the potential for flooding caused by overflows produced in the urban drainage network due to a type of rain in Madrid region over a period of 10 years. Finally, the overflows in the wells of the sewer network are obtained from the analysis of a hydraulic model in one dimension for each municipality studied. On the other hand, these results are applied as boundary conditions in the 2D hydraulic model, from which different magnitudes of flooding are obtained, such as the residence time of the water flooding, velocity of flow and the map of water depths.

For the exposure and vulnerability associated with overflow floods in the urban drainage network (when is required by high rainfalls), the people and goods exposed to the flood and the conditions that make them more vulnerable to damage are considered. Different factors are taken into account, such as: population density, economic activity, the intensity of road traffic, considering the dimension, the type of road and the number of bus lines that circulate on each road. Place of special interest are also considered, such as hospitals, health centers, residences, social services or shopping centers, among others, and finally the environment, such as the possible effect of floods on reservoirs or natural parks.

## 3. Results

The municipal risk results obtained in this study by applying the criteria of hazard, exposure and vulnerability are maps in GIS format, in which it can be observed for each element of the area studied in each municipality, the height and velocity of the water, the time of the flood and whether or not it is a safe zone. Additionally, a global flood risk result is obtained for each municipality, characterized on a scale from insignificant to very serious.

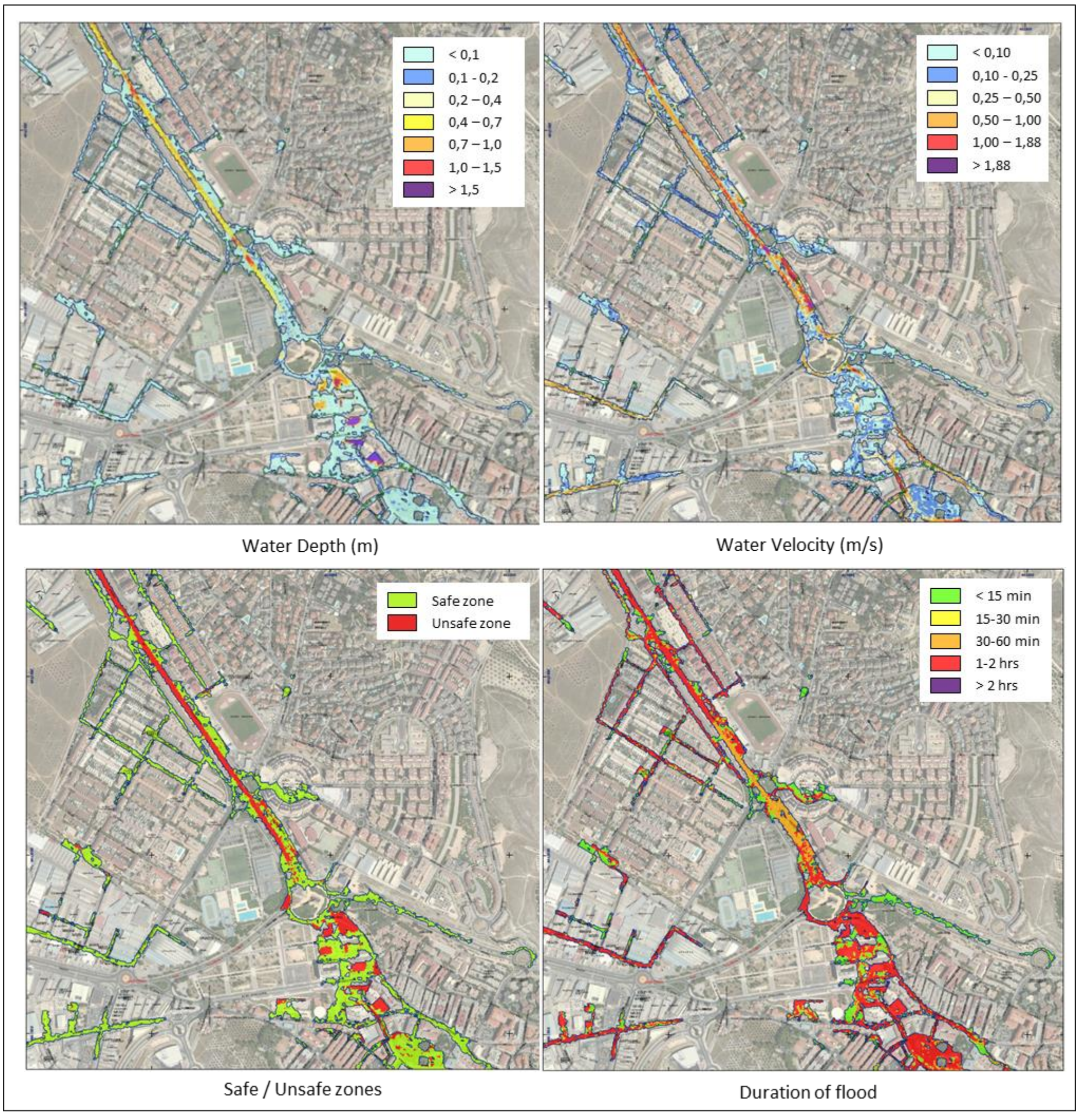


**Fig. 1.** Water Depth, Water Velocity, Safe or Unsafe Zones and Duration of flood: Four hazard maps produced for one municipality under study in Madrid region

## 4. Conclusions

Results are given for a 3 m2 elements in terms of water level, velocity, flooding duration and whether it is a safe area or not. Risk level is then assessed as the likelihood of damage to people, goods, or services as a consequence of a flood. Future work will apply this methodology to real-time meteorological data from radars to establish an early-warning system.

**References**

Hammond M J, Chen A S, Djordjević S, Butler D and Mark O. (2015). Urban flood impact assessment: A state-of-the-art review. Urban Water Journal, 12(1): 14-29.

Rezende O M, Miranda F. M. and Haddad A. N. (2019). A Framework to Evaluate Urban Flood Resilience of Design Alternatives for Flood Defence Considering Future Adverse Scenarios. Water, 11(7): 1485

Wang Y, Chen A. S., Fu G., Djordjević S., Zhang C. and Savić D. (2018). An integrated framework for high-resolution urban flood modelling considering multiple information sources and urban features. Environmental Modelling & Software, 107: 85-95.

# Modelling the integrated drainage network to support the management of the hydraulic risk: a case study in Northern Italy

Giovanna GROSSI[1], Arianna DADA[1], Davide SAVIOLA[1], Paolo LEONI[1]

[1] Università degli Studi di Brescia, Italy
email: giovanna.grossi@unibs.it

ABSTRACT

According to a very recent report of the European Environment Agency (EEA, 2020), urban adaptation to climate change requires special attention to extreme weather events and particularly heavy storms, as they are expected to cause the most pronounced impacts in European cities. In agreement with this direction, some Italian regions are setting regulations to limit surface runoff production in urban areas. Most of them include measures to ensure compliance with the principle of the 'hydraulic' and 'hydrological' invariance for the urban area, meaning that runoff volumes generated by an intense meteoric event must remain unchanged or at least must be limited. In some cases, municipalities are even requested to prepare the Hydraulic Risk Management Plan, as a response to the need of a more effective stormwater management. The planning activity requires a modelling framework accounting for both the open channel network (mainly addressing irrigation demand) and the sewer pipe network. Preliminary results are presented here for Brescia, a town located in Northern Italy, at the foothills of the Alps. Potential flood risk is linked to the dense historical irrigation and drainage channels network that cross the urban area from north to south and the old city centre.

## 1. Methodology

According to a recent regulation approved by Regione Lombardia (BURL, 2019), some Italian municipalities are requested to prepare a Hydraulic Risk Management Plan. A modelling framework was set to account for both the surface drainage network and the sewer pipe network operating in the Municipality of Brescia (Lombardia, Northern Italy) through separate hydraulic models. In the urban area, the flood risk lies separately in the two networks, and also in the dense traditional irrigation and drainage channel network that crosses the town from north to south and collects many combined sewer overflows (Fig. 1). Most critical areas are those hosting the post-war urban development, where the waterways have been modified or covered in the last decades, disregarding their fundamental role during heavy storms. Some other critical areas, deserving special attention, are modelled in more detail, such as some urban areas at the bottom of some side slopes.

Data for the construction and calibration of the models are kindly provided by A2A Ciclo Idrico, the company that manages water services in Brescia, and by the Municipality of Brescia. So far, some of the many steps needed have been taken to assess the hydraulic vulnerability of the town by applying SWMM model (Rossman, 2015) for the minor hydrographic network and InfoWorks model (InfoWorks ICM 10.5.3) for the sewer pipe network. For the modelling activities the geometric data (diameters, shapes, materials, lenghts etc.) of both the main trunks of the sewer system and of the minor hydrologic system were available. This geometric information is being constantly updated and integrated through on-site verification and measurements, gradually increasing the detail level of the models. Besides, critical overflows are assessed through field observation and past event simulations.

Both scale event analysis and continuous simulation are carried out to test the resilience of the drainage system, also with respect to future climatic conditions. In fact, design event simulation can support sizing and testing of single devices during heavy storms, while continuous simulation shows the performance of the system not only during one event but also when a sequence of events occurs, as well as during interstorm periods. Future climatic conditions are accounted for both at the event scale and in continuous simulation by applying climate scenarios built based on regional climate model outputs.

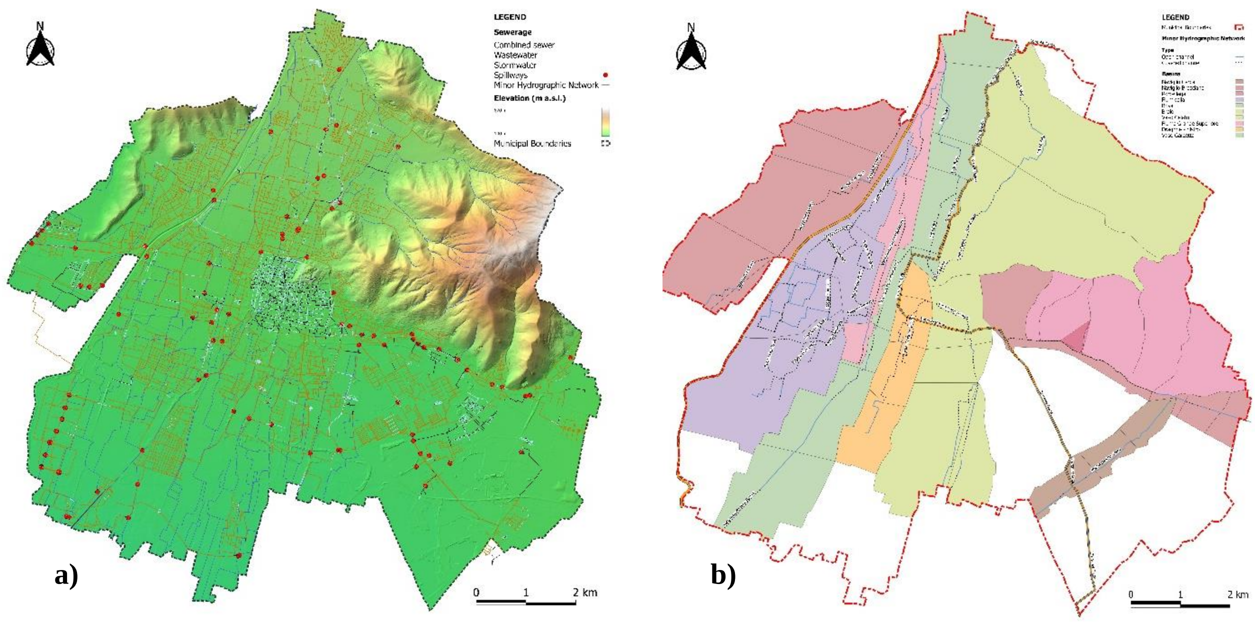


**Fig. 1.** a) Brescia Digital Elevation Model 5x5 m cell resolution with sewerage system and minor hydrographic network. b) Minor hydrographic network basins.

## 2. Results

Preliminary results of the hydraulic simulation of the complex system show some critical issues mainly related to the urbanization of the last decades and the many connections between the surface network and the pipe network. Uncontrolled soil sealing is the main problem responsible of the increased hydraulic risk affecting the town and making it more and more vulnerable to climate change. Critical combined sewer overflows are mainly related to a large upstream drained area and increased imperviousness.

Besides, in the part of the town hosting most industrial activities, a combined used of NBS (Natural based Solution) and real time control of water volumes stored in the pipes is expected to be effective. On the other hand, stormwater management in the old town centre can benefit only from reduced inflow from upstream areas and desealing is planned in some other areas. Taking advantage of the modelling framework, the efficiency of potential structural and non–structural measures under current and future climate are being tested.

## 3. Future work

The building of the modelling framework is still in progress and it is expected to be continuously updated as field survey data become available. A progressive validation of the models is essential to build an effective tool for the development of the Hydraulic Risk Management Plan, as requested by local rules in Lombardy Region. Further scenarios, including different solutions and future climate conditions, might also be applied to increase the reliability of the performance testing of the whole drainage system.

### References

Berteni F, Dada A, Saviola D, Leoni P, Baiguera M, Zampori B, Montagnoli T, Lazzaroni G, Ribolla G, Grossi G (2021) Integrated urban drainage system modelling to support the development of the Hydraulic Risk Management Plan for Brescia (Northern Italy), 15th International conference on Urban Drainage, Melbourne 2021.

BURL - Bollettino Ufficiale Regione Lombardia (2019) Regolamento Regionale 19 aprile 2019, n. 8: "Disposizioni sull'applicazione dei principi di invarianza idraulica ed idrologica. Modifiche al regolamento regionale 23 novembre 2017, n. 7", 17, suppl. del 24 Aprile 2019.

European Environment Agency (EEA). The European Environment—State and Outlook 2020: Knowledge for Transition to a Sustainable Europe; European Environment Agency: København, Denmark, 2019.

InfoWorks ICM 10.5.3 [Computer software]. (2020), Portland, Oregon, Innovyze (https://www.innovyze.com/en-us).

Rossman L.A., Storm Water Management Model User's Manual, SWMM Version 5.1. Water Supply and Water Resources Division, National Risk Management Research Laboratory, Cincinnati, OH, USA, U.S. Environmental Protection Agency, 2015.

# Indirect impacts: a weak point in the flood risk chain addressed by a graph approach

Marcello AROSIO[1], Luigi CESARINI[1], Chiara ARRIGHI[2], Mario MARTINA[1]

[1] Scuola Universitaria Superiore IUSS Pavia, Palazzo del Broletto - Piazza della Vittoria 15, 27100 Pavia (Italy);
[2] Department of Civil and Environmental Engineering, University of Florence, Via S. Marta 3, 50139, Firenze (Italy)
email: marcello.arosio@iusspavia.it – luigi.cesarini@iusspavia.it - mario.martina@iusspavia.it - chiara.arrighi@unifi.it

ABSTRACT

Models for the flood assessment of direct losses are the most widely used, while the application of models for indirect impacts and cascading effects are much less frequent. This work presents a method based on a graph approach that explores some of the indirect flood impacts to help filling existing knowledge gaps. The approach has been applied in two urban case studies: flood in Mexico City and Monza city. Finally, it summarizes how the graph perspective allows to analyze the system properties and propagate the cascading impacts.

## 1. Introduction

Floods have become one of the costliest natural hazards. Combining the flood hazard component with exposure and vulnerability data and models enables the computation of flood risk. Methodologies for risk assessment may differ according to the typology of losses considered, which can be divided into direct and indirect, and tangible and intangible. Models for the assessment of direct loss are the most widely used, while the application of models for indirect impacts and cascading effects is much less frequent (Sieg *et al.*, 2019).

Some authors attribute the direct damages to the affected area, instead the loss of connectivity within the broader economic network are usually referred to as indirect effects. Examples of analysis of indirect impacts beyond conceptual frameworks are related to infrastructures, e.g., traffic disruption due to flooded roads or malfunctioning of water supply systems if lifting stations are flooded (Arrighi *et al.*, 2017), which extend to areas much wider than flooded area. The classification between tangible and intangible is more straightforward, the first are damages that can be priced, e.g., replacement of road pavement, instead the second are damages for which no market prices exist, e.g., discomfort due to lack of freshwater (Arrighi *et al.*, 2020).

## 2. Methods

The methodology adopts a systemic structure which allows to describe the entire system properties by a graph. Formally, a graph G consists of a finite set of elements V(G) called vertices (or nodes), and a set E(G) of pairs of elements of V(G) called edges (or links). Depending on the specific context of the analysis, the categories (i.e., taxonomy, e.g., public office, education, leisure) of the most relevant nodes exposed to the hazard are selected. Those nodes are relevant in the systems for the function they assume. Each node can provide or receive service to or from others (links). Links can be of different types according to the nature of the connection: physical, geographical, cyber, or logical (Rinaldi, et al., 2001). In more practical terms, the mathematical graph G, built from a list of nodes V and E can be obtained using the igraph package for network analysis R (http://igraph.org/r/). The full library of functions adopted is provided by Nepusz and Csard (2020). For an in-depth description of the model, please refer to Arosio *et al.*, (2020).

The approach has been applied in two urban case studies: (i) pluvial flood in Mexico City, a very complex and extremely dense city with almost ten million of inhabitant (Arosio *et al.*, 2020); and (ii) both pluvial and river flood in Monza city (Italy), and with more than 100 thousand habitants (Arosio, *et al.*, 2021).

## 3. Results

The graph methodology promotes a paradigm shift from a reductionist to a holistic risk approach by considering the exposed assets as unique system of elements. The system perspective allows to: 1) analyze the system properties; 2) propagate the impacts and built risk curves for direct and indirect impact; 3) consider number of services lost; and 4) represent the definition's resilience characteristics.

The application to Mexico City highlighted the central node of the graph (i.e., hospital), which has the capability of influencing many other nodes due to its role of hub (i.e., it has the highest hub value). Furthermore, the application to Monza shows a good correspondence between the authority values of the nodes and the distance from the city center: nodes closer to the center have higher values of authorities (Fig. 1).

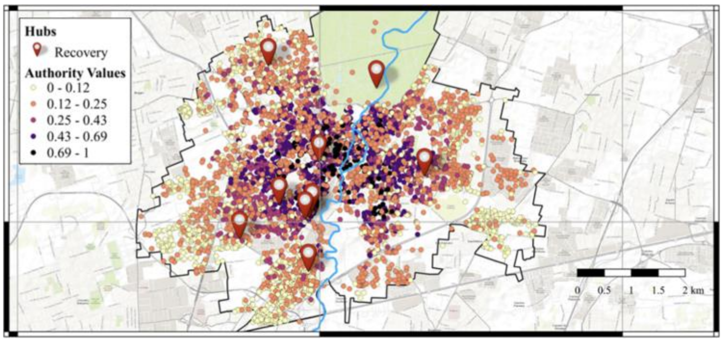


**Fig. 1.** Map of the authority values in Monza city (Arosio, et al., 2021).

Both case studies show how the impacts are propagated thorough the system, from the buildings in the flooded area to the elements outside of it that are impacted by the loss of services (e.g., social, and economic) coming from the flooded providers. The risk curves built for the case of Monza show that the total risk (i.e., direct plus indirect nodes) is much higher than only considering the direct impacts. Finally, the integration of redundant services and the provider capacity, adopted for the case of Monza, simulates an adaptable system that responds dynamically to an external perturbation. These two aspects fully reflect resilience definition (adopted by United National General Assembly) and provide a unique quantitative metric for the flood resilience of Monza.

## 4. Conclusion

The main limitations of the proposed approach to fill the gap of the assessment of indirect impacts are, firstly, the amount of geospatial data required to set up the graph (e.g., information on the relations between elements) and the overall extension of the graph, i.e., where to stop in the geographical propagation of indirect effect. The difficulties in identifying the boundaries in indirect impact assessment are however common also to the modelling approaches adopted for infrastructures (Arrighi, *et al.*, 2020). Secondly, graph-based indirect impacts are not easily comparable to standard direct monetary impacts, widely adopted for prioritization of risk mitigation measures, nevertheless they provide a social measure of lost services which fully complement direct damages. Finally, more elaborated curves should describe how the direct impact could trigger the cascade propagation, while, at the moment, only binary vulnerability functions have been adopted.

**Acknowledgements**

The authors would like to acknowledge the Lombardy Region in Italy for funding the IUSS Data Center project by means this research was performed.

**References**

Arosio, M. *et al.* (2020) “Indirect impact assessment of pluvial flooding in urban areas using a graph-based approach: The Mexico city case study,” *Water (Switzerland)*, 12(6). doi:10.3390/w12061753.
Arosio, M., Cesarini, L. and Martina, M.L.V. (2021) “Assessment of the disaster resilience of complex systems: The case of the flood resilience of a densely populated city,” *Water (Switzerland)*, 13(20). doi:10.3390/w13202830.
Arosio, M., Martina, M.L.V. and Figueiredo, R. (2020) “The whole is greater than the sum of its parts: A holistic graph-based assessment approach for natural hazard risk of complex systems,” *Natural Hazards and Earth System Sciences*, 20(2), pp. 521–547. doi:10.5194/nhess-20-521-2020.
Arrighi, C. *et al.* (2017) “Flood impacts on a water distribution network,” *Natural Hazards and Earth System Sciences*, 17(12), pp. 2109–2123. doi:10.5194/nhess-17-2109-2017.
Arrighi, C., Pregnolato, M. and Castelli, F. (2020) “Indirect flood impacts and cascade risk across interdependent linear infrastructures,” *Natural Hazards and Earth System Sciences*, (November), pp. 1–18. doi:10.5194/nhess-2020-371.
Merz, B., Kreibich, H., Schwarze, R., and Thieken, A. (2010) “Assessment of economic flood damage,” *Natural Hazards and Earth System Sciences*, 10(8), pp. 1697–1724. doi:10.5194/nhess-10-1697-2010.
Nepusz, T. and Csard, G. (2020) *Package “igraph” - Network Analysis and Visualization*. Available at: https://cran.r-project.org/web/packages/igraph/igraph.pdf.
Rinaldi, S.M., Peerenboom, J.P. and Kelly, T.K. (2001) “Identifying, understanding, and analyzing critical infrastructure interdependencies,” *IEEE Control Systems Magazine*, 21(6), pp. 11–25. doi:10.1109/37.969131.
Sieg, T. *et al.* (2019) “Integrated assessment of short-term direct and indirect economic flood impacts including uncertainty quantification,” *PLoS ONE*, 14(4), pp. 1–21. doi:10.1371/journal.pone.0212932.

# A weak point at the geomatics/hydraulics interface: Creating a river model geometry between conflicting needs of a large domain and a high resolution

Rocco BONORA, Alessandro CARETTO, Thomas CANNELLA,
Gloria FACCENDA, Sonia INVERNIZZI, Damodar MAGGETTI, Alessio RADICE

Politecnico di Milano, Milan, Italy
email: alessio.radice@polimi.it

ABSTRACT

Within the flood risk modelling chain, a weak point exists at the interface between geomatics and hydraulics, because the (sometimes rich) data available on geoportals are typically inadequate as geometry inputs for river hydrodynamic models. Producing good-quality geometric data can be very time consuming, particularly if the domain under investigation is large. The manuscript presents strategies used in an ongoing project on inundation modelling in a densely urbanized area.

## 1. Introduction

A hydrodynamic flood model requires data for (i) hydrological/hydraulic quantities such as flood hydrographs and rating curves, (ii) geometric data for the river and surrounding areas, (iii) soil cover data to estimate suitable roughness values, (iv) data on singularities such as hydraulic and interfering structures. This extended abstract relates to creating a suitable river geometry file for two-dimensional hydrodynamic simulations.

The production of a geometry input may require compromising between the wishes to model a large system and of maintaining a high resolution. The size of a domain under investigation is dictated by the river length, while the detail needed in the geometric description relates to the river width. In this sense, the area northern to Milan is quite unfavourable: even though, on the one hand, most rivers are not very long, their width is, on the other hand, very small (in some cases, few metres), thus requiring a high detail. Furthermore, territorial information is nowadays more and more furnished by agencies and used by modelling codes in the form of gridded data (Digital Terrain Models, DTM) that are easily displayed as raster layers in Geographic Information Systems (GIS) but do not enable space-variable resolution to be used.

The extended abstract presents the strategies used in a project, promoted by the River Basin District Authority of the Po river, that is presently under conduction within the update of the Flood Risk Management Plan. Within the entire basin of the Po, the manuscript considers the Area with Potential Significant Flood Risk (APSFR) called “Milano nord”, that comprehends a large territory around the city of Milan. The APSFR includes ten water courses, for a total length of about 250 km and with average width of around 10 m, flowing in a densely urbanized area with a major presence of hydraulic and transportation structures. Issues considered in the manuscript are: (i) interpolating data for ground-surveyed cross sections to produce a DTM of the river bed to be integrated with that of the surroundings; (ii) manually correcting the stationing of cross sections to fix errors induced by approximate conversions between reference systems; (iii) fictitiously widening channel banks in case of narrow protection structures, possibly creating new sections to handle transitions.

## 2. Methods and example

As other studies in the literature (e.g., Caviedes-Voullième et al., 2014; Falcão et al., 2016; Schäppi et al., 2010), we developed a section interpolator to create a river bed bathymetry. The interpolator requires, as an input, (i) cross section data in terms of station-elevation profiles, (ii) the x-y coordinates of the left and right section extreme points, and (iii) x-y coordinates of a polyline for the main channel axis; this polyline needs to be carefully drawn following a DTM. The section profiles are linearly interpolated. To georeference the interpolated sections, two steps are implemented: first, interpolated sections (with a spacing that typically needs to be as large as few times the section width) are placed perpendicularly to the channel axis; in a nested round of interpolation (with a spacing that needs to be close to the desired resolution for the final DTM) the sections are placed varying linearly their inclination in the xy plane between those of two sections interpolated in the first round. In both rounds, the partition of an interpolated cross section to be placed to the left and right of the axis polyline is determined interpolating linearly the partition for two bounding surveyed sections.

Figure 1 depicts a problem one may encounter; the final reach of the Pudiga river is used as an example. The DTM was provided by the Ministero dell'Ambiente e della Tutela del Territorio e del Mare (the Italian Ministry of the environment) in 2008 using the reference system ETRS_1989_LAEA. The cross sections were surveyed around 2002 using the ED1950_UTM32N spatial reference. After projecting both data into the WGS1984_ UTM32N system, elevation profiles can be extracted from the DTM at the section locations and compared to the surveyed section profiles. Shifts of up to some metres can be spotted (panel (e)), most likely due to an insufficient precision of the reference system conversion. If one does not account for that, errors will be present in the final merged DTM to be used in the hydro-dynamic simulations (panel (c)). These errors can be even larger than the river width in case the cross sections are narrow (the Pudiga section in Figure 1 is less than 6 m wide and results shifted by more than 8 m). By contrast, imposing a section shift solves the problem (see the final DTM in panel (d)) but requires manually editing the section stationing data, with some degree of subjectivity and, however, taking an extremely long time in case many sections are to be considered.

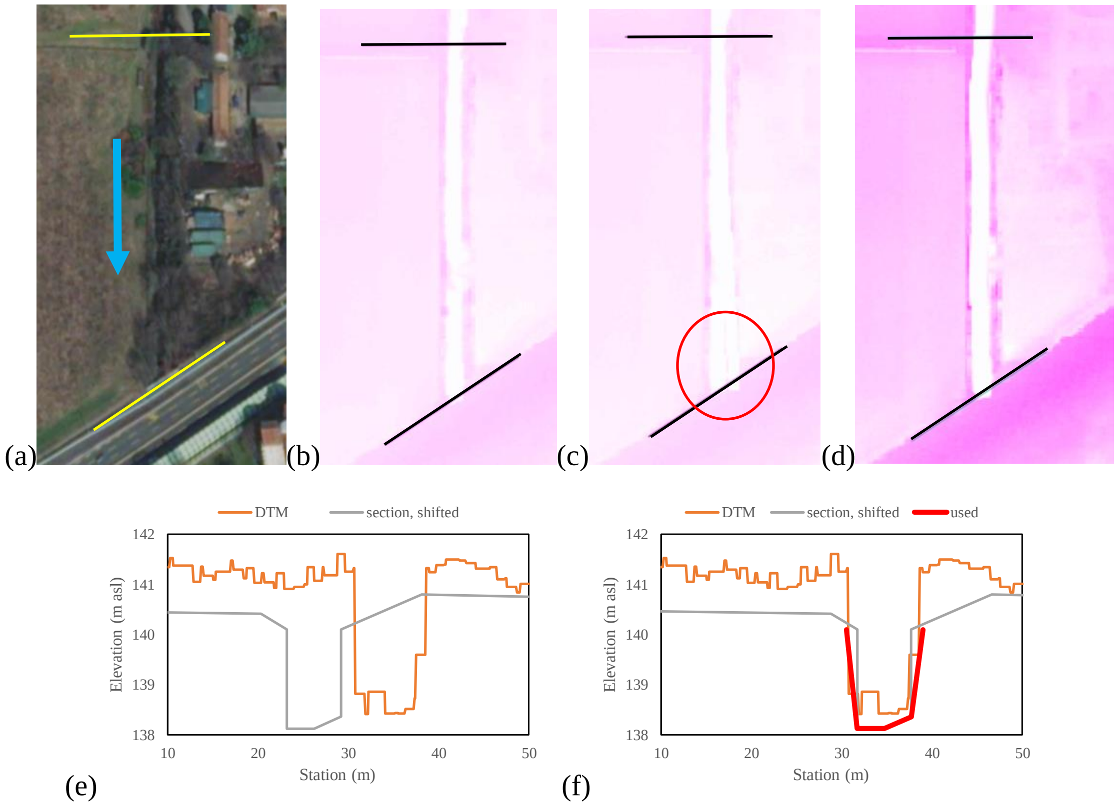


**Fig. 1.** (a) aerial photo; (b) the available DTM; (c) the mosaic between the original DTM and the interpolated section bathymetry not accounting for the shift, yielding a duplicated channel; (d) the mosaic accounting for the shift; (e) the comparison between an elevation profile extracted from the original DTM and the downstream surveyed section; (e) the used shifted portion of the section returning (c).

Finally, in some cases a water-containing bank is a thin wall misrepresented in gridded data. Even if a cross section correctly includes the edge of the wall and the point cloud interpolating the sections represents it well, the thin structure will be filtered out gridding the data. The structure can be fictitiously widened so that it can be preserved after data gridding; furthermore, additional sections may be used to represent the start and end of the thin wall. The same may need to be done for secondary walls, distant from the main channel. This is also a work that, albeit conceptually simple, requires huge effort to be done within an entire modelling domain.

**Acknowledgements**

The present work has been financially supported by the Autorità di Bacino Distrettuale del Fiume Po, under a contract on methods for updating flood hazard maps within the basin ("Metodologie per l'aggiornamento delle mappe di pericolosità idraulica relativamente al secondo piano operative annuale – Idraulica di superficie").

**References**

Caviedes-Voullième D., Morales-Hernández M., López-Marijuan I, García-Navarro P (2014) Reconstruction of 2D river beds by appropriate interpolation of 1D cross-sectional information for flood simulation, Environmental Modelling & Software, 61, 206-228.
Falcão AP, Matias M Caviedes-Voullième P, Pestana R, Gonalves AB, Heleno S (2016) Methodology to combine topography and bathymetry data sets for hydrodynamic simulations: Case of the Tagus river, Journal of Surveying Engineering, 142, 5016005.
Schäppi B., Perona P., Schneider P., Burlando P (2010) Integrating river cross section measurements with digital terrain models for improved flow modelling applications, Computers & Geosciences, 36, 707-716.

# Flume validation of hydraulic resistance models for arboreal vegetation

Lisdey Verónica HERRERA GÓMEZ[1], Giovanni RAVAZZANI[2], Marco MANCINI[3], Michele FERRI[4]

[1,2,3] Politecnico di Milano, Department of Civil and Environmental Engineering, Italy
email: lisdeyveronica.herrera@polimi.it
email: giovanni.ravazzani@polimi.it
email: marco.mancini@polimi.it

[4] Eastern Alps District Authority, Italy
email: michele.ferri@distrettoalpiorientali.it

ABSTRACT

Hydraulic resistance due to vegetation is a fundamental aspect of river engineering and management. As it is well known, vegetation obstructs the streamflow area, reducing the velocity and thus increasing water levels and the risk of flooding. Although many efforts have been made to estimate vegetation resistance, few studies are devoted to validating and comparing the literature models. In this research, laboratory tests were carried out to validate the roughness coefficients given by literature equations for two arboreal species present along the banks and floodplains of the Piave River in Italy. The material and dimensions of vegetation on a laboratory scale were defined from the mechanical properties of these species. The results highlight the performance of the models and suggest the ones that best represent the experimental measurements.

## 1. Introduction

Roughness induced by vegetation can be assessed using qualitative approaches, based on descriptions or photos comparison, or quantitative approaches. While the first ones are very subjective and can be used as an initial estimation of the roughness, quantitative approaches are based on theoretical or empirical equations obtained from flume experiments or computational modeling.

In the literature, vegetation roughness is evaluated according to the type of vegetation, rigid or flexible, and the flow conditions, submerged or emergent. In particular, this contribution aims to validate and compare 12 literature models that estimate roughness due to arboreal vegetation for submerged and emergent conditions. The models examined include traditional approaches such as that of Petryk & Bosmajian (1975) and more recent ones such as the models proposed by Huthoff et al. (2007), Baptist et al. (2007), and Luhar & Nepf (2012), among others.

## 2. Methodology

### *2.1. Vegetation model*

During the water-vegetation interaction, the plant offers a hydrodynamic resistance that depends on the drag coefficient and the cross-section of the plant (geometric properties) and tends to bend if the flexural rigidity (mechanical property) of the stem is smaller than the force exerted by the current. In this study, the Buckingham Pi theorem was applied to identify the function that defines the problem and thus ensure that laboratory vegetation had a dynamic behaviour equivalent to real trees. The function obtained has already been defined in the literature by the theory of elastic-static models. Therefore, using the elasticity modules determined experimentally for several samples of Robinia and Sambucus species, it was possible to select the material and dimensions to represent the vegetation in the laboratory. Thereby, Robinia and Sambucus were simulated by Ayous and Balsa dowels of 8mm and 4mm diameter, respectively.

### *2.2. Experimental setup*

The experiments were carried out at Laboratory Fantoli of Politecnico di Milano in a horizontal flume of 30 m length, 1 m width, and 0.60 m depth. The flume bed was covered by dowels inserted into boards of 1 m x 0.5 m for a total distance of 5 m. Vegetation was assembled in staggered and linear configurations. A current meter and a meter stick were employed to measure velocities and flow depths upstream, downstream, and within vegetation sections. The tests included different degrees of submergence, densities and discharges ranging from 40 l $s^{-1}$ to 100 l $s^{-1}$. Table 1 shows the characteristics of the analysed tests groups.

**Table 1.** Experimental groups

| Group | Configuration | Density (%) | Number of tests |
|---|---|---|---|
| 1 | ϕ = 8mm, Staggered | 1.74 | 8 |
| 2 | ϕ = 4mm, Staggered | 0.44 | 6 |
| 3 | ϕ = 8mm, Linear | 0.87 | 8 |
| 4 | ϕ = 4mm, Linear | 0.22 | 6 |

## 3. Results and discussion

The roughness coefficients calculated from the literature models were plotted against the Strickler coefficients (Ks) measured during the tests (Fig. 1). The results indicate a better performance of the models when the vegetation density is high, but when it is sparse, the accuracy decreases. For instance, the relative error for group 1 ranged from 5 % to 10 %, while for group 4 it was between 13 and 22 %. Figure 1 only shows the models that best fit the experimental measurements; it can be observed that the methods proposed by Huthoff et al. (2007), Kowobari et al. (1972), Luhar & Nepf (2012), and Baptist et al. (2007) have the most reliable prediction of the roughness coefficient in the analyzed cases. One can conclude that although recent approaches seem to give the best roughness estimation coefficients, the classic ones are still valid.

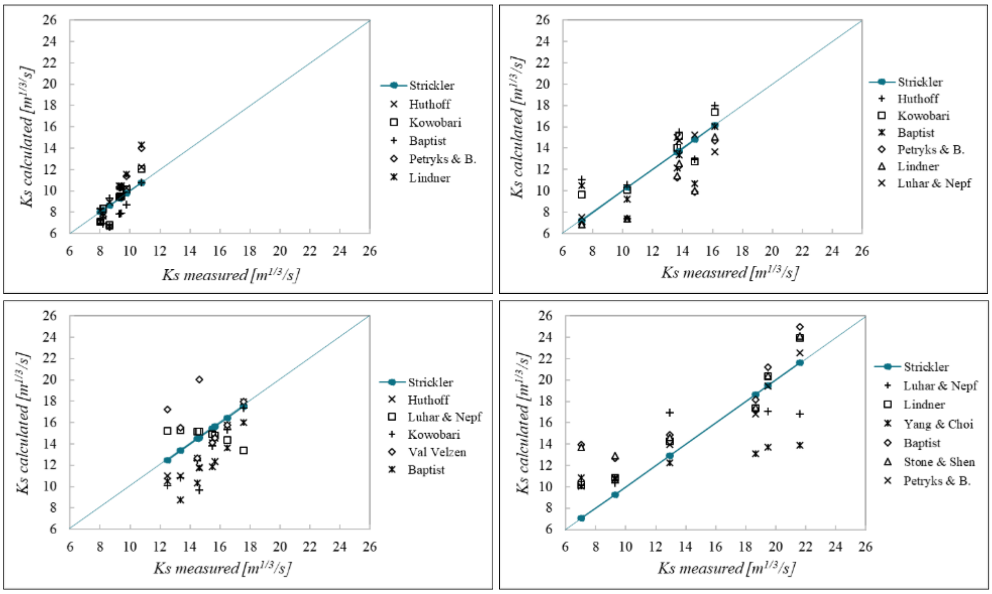


**Fig. 1.** Comparison of measured and calculated Strickler coefficient (Ks) of group 1 (top left), group 2 (top right), group 3 (bottom left) and group 4 (bottom right)

Additionally, the vegetation model based on the mechanical properties of real trees allowed us to identify an oscillation phenomenon during the experiments. These oscillations were mainly observed for the 4 mm dowels and caused an additional energy dissipation that might explain the higher errors obtained for these test groups. Currently, an analysis is being carried out to study this phenomenon and its influence on the roughness coefficient.

**Acknowledgements**

This work was supported by the project "CONVENZIONE OPERATIVA ai sensi degli artt. 6 e 7 del protocollo di collaborazione tra l'Autorità di Bacino delle Alpi Orientali, il Politecnico di Milano - DICA e la Fondazione Politecnico di Milano".

**References**

Baptist MJ, Babovic V, Rodríguez Uthurburu J, Keijzer M, Uittenboogaard RE, Mynett A, Verwey A (2007) On inducing equations for vegetation resistance, Journal of Hydraulic Research, 45, 435-450.
Huthoff F, Augustijn DCM, Hulscher SJMH (2007) Analytical solution of the depth-averaged flow velocity in case of submerged rigid cylindrical vegetation, Water Resources Research, 43, W06413.
Kowobari TS, Rice CE, Garton JE (1972) Effect of roughness elements on hydraulic resistance for overlandflow, Transactions of the ASAE:979–984.
Luhar M, Nepf HM (2012) From the blade scale to the reach scale: A characterization of aquatic vegetative drag, Advances in Water Resources, 51, 305-316.
Petryk S, Bosmajian G (1975) Analysis of flow through vegetation, Journal of Hydraulic Division, 101, 871-884.

# An Integrative Approach to Hydrological and Hydrodynamic Modelling of Flood Events

Antonia DALLMEIER[1], Markus REISENBÜCHLER[1], Wolfram MAUSER[2], Michaela CERNY[2]

[1] Chair of Hydraulic and Water Resources Engineering, Technical University Munich, Germany
email: antonia.dallmeier@tum.de
email: markus.reisenbüchler@tum.de
[2] Department of Geography, Ludwig-Maximilians-Universität Munich, Germany
email: w.mauser@lmu.de
email: m.cerny@lmu.de

ABSTRACT

In this study, the quality of flood routing of a hydrological model using empirical formulas and a numerical hydraulic model is compared. The results are presented graphically and evaluated using goodness-of-fit-criteria. The knowledge gained allows to improve the flood routing of the hydrological model.

## 1. Introduction

As a result of climate change, heavy precipitation and flood events will most likely increase in intensity and frequency. This affects not only large watersheds and main watercourses, but also small rivers or even takes place outside of water bodies (e.g. urban flash floods) (IPCC 2022). In order to predict the impact of natural hazards, to develop water management plans or to design river engineering applications, information about the discharge is needed. Hydrological models can overcome this data gap by modelling discharge data at any point of interest. The flood routing in hydrological models such as PROMET (Mauser and Bach 2009) is calculated using empirical formulas like the Manning-Strickler formula. Accordingly, flow processes within the catchment area, such as retention, flow regulation through structures or meandering of the watercourse, can only be represented in a simplified way (Mauser and Bach 2009). Thus, the resulting shape of the hydrograph, the runoff volume and the wave propagation time are prone to errors for detailed investigations. This limits the use of hydrological models as a reliable, fast and efficient tool for flood prediction to some extent. The aim of this study is to demonstrate a concept to overcome the limitation of flood routing in hydrological modelling by the outcome of hydraulic modelling.

## 2. Methods

The flood routing of the hydrological model PROMET is compared to the flood routing of a calibrated hydraulic model covering the area of the river Schmutter, a tributary of the Danube, between the gauging stations Fischach (inlet) and Achsheim (outlet) on the basis of one flood event. In PROMET, lateral as well as routed discharges of a typical and frequently occurring flood event (27.05.2007 - 02.06.2007, HQ5) are calculated using a spatial resolution of 250x250 m. The hydraulic simulations are performed on a calibrated model using HYDRO_AS-2D software (Nujic 2002). The routed discharges calculated by the hydrological model at the upstream gauging station as well as the lateral discharges within the domain are added as boundary conditions. After a first analysis of the hydraulic simulations, it appears that areas are already flooded during low flood events and thus the water is retained in the flood plains. In order to represent this process in the hydrological model, a storage model is integrated in PROMET. Again, the flood event is simulated in the adapted PROMET and the results are used as boundary conditions for the hydraulic simulations. Subsequently, the routed discharges of the hydrological model and of the hydraulic simulations are plotted and evaluated against measured data using the goodness-of-fit (GoF)-criteria RMSE and NSE (Moriasi et al. 2007).

## 3. Results and Discussion

In Fig. 1, the inflow hydrograph (a) as well as the resulting hydrographs at the model outlet (b) are shown. The routed discharge of the hydrological model without storage is strongly overestimated and hardly reproduces the characteristic shape of the flood wave, despite the fact that at the inlet the hydrograph of the hydrologic model represents the measured data quite good. In combination with the GoF-criteria in Table 1, a significant improvement of the discharge hydrograph can already be seen by extending the hydrological model with a simple storage model. Thus, the peak discharge as well as discharge volume can be predicted more accurately.

However, the shape of the hydrograph and the wave propagation time still show differences. Since the shape of the wave, peak discharge and wave propagation time are better represented by the flood routing of the hydraulic model, further knowledge about these processes can be obtained from the hydraulic model allowing us to improve the storage model as well as other modelling parameters in the future. For example, the hydraulic model can be used to establish a relationship between the flooded area and the stored volume in the inundation areas leading to a dynamic storage model. Based on these findings, characteristics of the model domain can be incorporated into the hydrological model and thus the flood routing of the hydrological model can be further improved within another feedback loop.

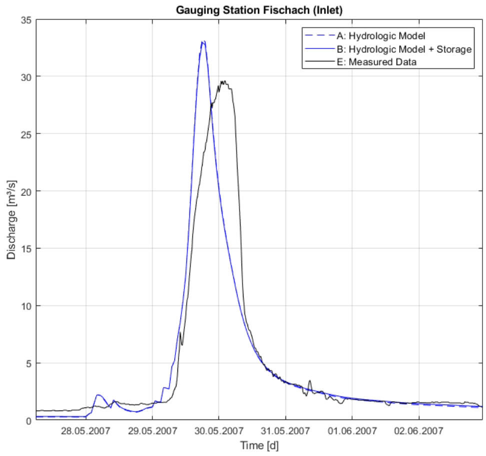


a)

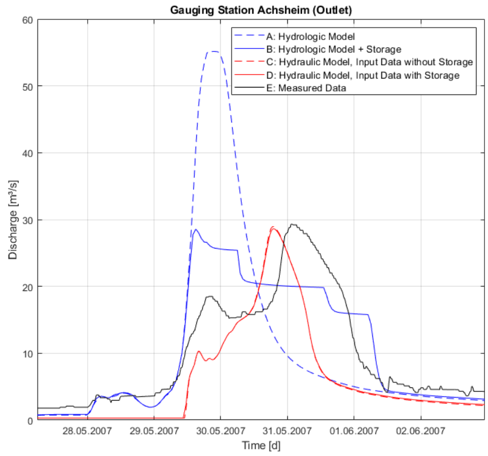


b)

**Fig. 1.** a) Input hydrographs at the inlet (Fischach); b) hydrographs of the routed discharge at the outlet (Achsheim) of the hydrological model without (A) and with (B) storage model, the hydraulic simulation using the input data of the hydrological model without (C) and with (D) storage model as well as the measured hydrograph (E)

**Table 1.** GoF-criteria RMSE and NSE for the routed discharges at the outlet (Achsheim) in terms of the measured hydrograph.

| | Hydrological Model | Hydrological Model + Storage | Hydraulic Model | Hydraulic Model + Storage |
|---|---|---|---|---|
| RMSE [m³/s] | 13.15 | 4.77 | 6.35 | 6.27 |
| NSE [-] | -1.58 | 0.66 | 0.4 | 0.41 |

## 4. Conclusion

This study shows a comparison of the flood routing of a hydrological and a hydraulic model and how both models can benefit from each other. Due to the physically based formulas of 2D channel hydraulics, i.e. shallow-water-equations, flood routing of a hydrological model can benefit from the insights of hydraulics. Information about flow processes within the catchment cannot be obtained only from measured hydrographs at gauging stations. The findings of hydraulic simulations can be used to improve the flood routing of a hydrological model. An advanced hydrological model could serve as a reliable and fast flood forecasting in the future, since the computation time of the hydraulic model is more than 100 times larger than the hydrological model. In this specific case, the hydrological simulation took 1 minute while the hydraulic simulation took 48 hours on a standard personal computer using 6 CPUs. This makes hydrological modelling preferable as forecasting tool.

**Acknowledgements**

This study has received funding from the Bavarian Ministry for the Environment and Consumer Protection under the research project “VieWBay – Virtueller Wasserraum Bayern”.

**References**

Intergovernmental Panel on Climate Change IPCC (2022) Climate Change 2022: Impacts, Adaptation and Vulnerability – Summary for Policymakers, pp. 11-15

Mauser W, Bach H (2009) PROMET – Large scale distributed hydrological modelling to study the impact of climate change on the water flows of mountain watersheds, Journal of Hydrology, 376, 362-377.

Nujic M. (2002). Hydro_As-2d - Ein zweidimensionales Strömungsmodell für die wasserwirtschaftliche Praxis, Benutzerhandbuch (User Manual).

Moriasi D N, Arnold J G, Van Liew M W, Bingner R L, Harmel R D, Veith T L (2007) Model evaluation guidelines for systematic quantification of accuracy in watershed simulations, Transactions of the American Society of Agricultural and Biological Engineers, 50 (3), 885-900.

# A Simple and Efficient Approach for Automatic Calibration of 2D-Hydraulic Models

Leon Frederik DE VOS[1], Markus REISENBÜCHLER[1], Nils RÜTHER[1]

[1] Chair of Hydraulic and Water Resources Engineering, Technical University Munich, Germany
email: frederik.de-vos@tum.de
email: markus.reisenbuechler@tum.de
email: nils.ruether@tum.de

ABSTRACT

This study presents a simple yet efficient approach to automatically calibrate hydraulic models with few iterations. The method is explained and its results are shown on a test region of the river Salzach, Germany. The results are evaluated with statistical interpretation and presented graphically.

## 1. Introduction

2D-hydraulic models are widely used in an integrative flood risk modelling chain. However, the quality of the modelling results is strongly dependent on the calibration of the numerical hydraulic models. The calibrated parameter is usually an empirical friction coefficient, as it cannot directly be determined by satellite imagery or on-site measurement, being a clear weakness of such models. Conventional calibration requires the user to give an educated guess for the friction coefficients, run the model with a reference event, compare the modelling results with observed data from the reference event and adapt the friction coefficients. This iterative and thus time-consuming process is then repeated until the modelling results are in (subjective) satisfying accordance with the reference data. Subjectivity, therefore, always influences the calibration process, regardless of the user's experience (Cunge 2003).

Automatic calibration could therefore fasten the calibration process and remove the user's subjectivity to some extent. Recent research presents methods using heuristic algorithms with varying mathematical complexity, that can be limited by needing a large number of iterations, when applied to more complex 2D-hydraulic models (Dung et al, 2011, Lin et al. 2017). This study presents an automatic calibration method, that aims to find a stable calibrated solution within few iterations while applying basic mathematics.

## 2. Methods

The proposed automatic calibration method is an iterative process: The initial hydraulic model starts with the same roughness coefficient at all nodes, respectively elements, of the riverbed grid mesh. After one model run, the observed maximum water level is interpolated onto the grid nodes and converted to the water depth $h^i_{o,int}$ at every node $i$. The following equations then calculate the new friction coefficient at each node:

$$\epsilon^i_j = \frac{h^i_{o,int} - h^i_j}{h^i_{o,int}} \tag{1}$$

$$n^i_{j+1} = n^i_j \cdot \frac{2}{1+e^{-2\epsilon^i_j}} \tag{2}$$

where $h^i_j$ – simulated water depth at node $i$ in simulation $j$, $\epsilon^i_j$ – relative deviation between simulation and observation, and $n^i_{j+1}$ – friction coefficient for the next simulation $j$+1. The next simulation is started with the newly calculated friction coefficients. This process is then iterated until a user stop criteria is reached (e.g. a certain number of iterations). Note that the friction of the floodplain next to the riverbed is not changed, but a priori determined according to the land use.

The developed automatic calibration tool is tested on a 12 km section of the river Salzach (Germany). The model is automatically calibrated using observed maximum water levels every 200 m along the river during the 2013 flood event (~HQ100). The hydraulic simulations are conducted with the open-source software openTELEMAC-MASCARET (EDF, 2021) using the Manning friction model. For this study, the calibration is started with three different initial Manning conditions – smooth case: 1/50, medium case: 1/35, rough case:

1/15 [s/m$^{1/3}$] – to investigate the convergence of the calibration process. The calibration results are assessed with the goodness-of-fit-criteria RMSE and NSE.

## 3. Results and Discussion

Fig. 1a) shows the evolution of the RMSE for the three initial Manning conditions during the calibration iterations. Table 1 shows the initial and optimal RMSE and NSE for each initial condition. The smooth case reaches the best calibration fit, even though the medium case fits best initially. However, also the rough case can significantly improve during calibration; this shows that the calibration result is not entirely independent of the initial condition, yet can still reach satisfactory results independent of the initial condition. The biggest advantage in already having a good initial condition is that less calibration iterations are necessary until the calibrated solution converges (e.g. medium case for j=4, whereas rough case for j=10).

Fig. 1b) depicts the relative difference between the observed and the simulated water depths along the river Salzach from upstream (x=0 km) to downstream (x=12 km) in flow direction. All deviations are less than 5 % for x<7 km with the rough case slightly overpredicting and the other cases underpredicting the observed water depths; the rough case actually presents the best results in this area. For x>8 km, all cases start to overpredict the water depth. This might be due to a 180° turn followed by a 90° turn with change in curvature of the Salzach, unprecise measurement data or the influence of the downstream boundary condition and must be further investigated.

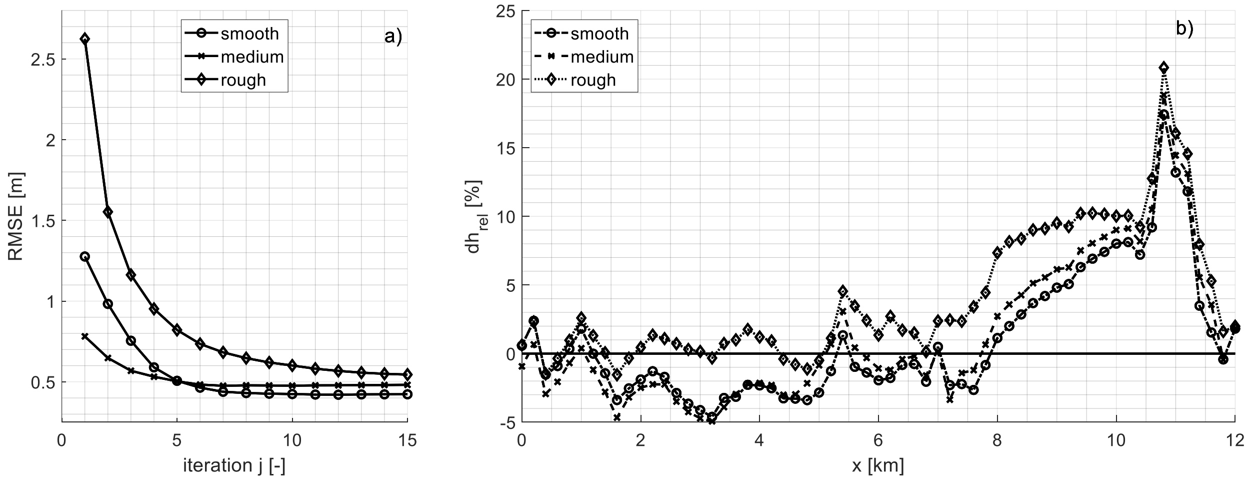


**Fig. 1.** a) Evolution of the RMSE for three initial Manning conditions during the calibration iterations; b) Relative difference between the observed and the simulated water depths along the river for the simulation with the lowest RMSE for three initial Manning conditions.

**Table 1.** The initial and optimal RMSE- and NSE-values for three initial Manning conditions. Additionally, the iteration after which the RMSE only still improves by less than 10 % is given.

| Initial Manning conditions | $RMSE_{init}$ [m] | $RMSE_{opt}$ [m] | No. of iterations with RMSE>RMSEopt ·1.1 [-] | $NSE_{init}$ [-] | $NSE_{opt}$ [-] |
|---|---|---|---|---|---|
| Smooth | 1.28 | 0.42 | 5 | -0.17 | 0.87 |
| Medium | 0.78 | 0.48 | 4 | 0.56 | 0.84 |
| Rough | 2.62 | 0.54 | 10 | -3.93 | 0.79 |

## 4. Conclusion

This study presents a simple yet efficient method for automatic calibration of 2D-hydraulic models. We could show that the automatic calibration can give good results regardless of the initial condition. The results of the calibration for this specific test case converge after 5-10 iterations. However, the origin of the differences at the downstream boundaries have to be further studied, as well as the influence of the floodplains. Future improvement of the calibration method can look into how to reach a converged solution faster by refining the calculation of new friction coefficients and how to further limit the influence of the initial friction coefficients.

### References

Cunge JA (2003) Of data and models, Journal of Hydroinformatics, 5 (2), 75–98.
Dung NV, Merz B, Bárdossy A, Thang TD, Apel H (2011) Multi-objective automatic calibration of hydrodynamic models utilizing inundation maps and gauge data, Hydrology and Earth System Sciences, 15 (4), 1339–1354.
Electricité de France (EDF) (2021), TELEMAC-2D User Manual. Version v8p3.
Lin FR, Wu NJ, Tu CH, Tsay TK (2017) Automatic Calibration of an Unsteady River Flow Model by Using Dynamically Dimensioned Search Algorithm, Mathematical Problems in Engineering.

# Comparing Direct 2D and 1D-2D Coupled Hydraulic Modelling Approaches for Flood Hazard Quantification

Kutay YILMAZ[1], Yunus ORUÇ[2], Çağla Irmak ÜNAL[3]

[1]ALTER International Engineering and Consultancy Inc, Turkey
[1]email: ktyylmz@gmail.com

[2]email: yns.orucc@gmail.com
[3]email: irmakunal13@gmail.com

ABSTRACT

Flood disasters are considered catastrophic events that can affect human life along with their economic and environmental effects. In recent years, the frequency of flooding has been increasing with the effect of climate change. Various software and methods are used in the studies carried out to determine the precautions to be taken for a probable flood and to reduce the potential hazard. Available software programs offer 1D, 2D, and 1D/2D coupled solutions to identify probable inundation areas and corresponding flood hazards. In this study, a study area from northern Turkey was selected in order to apply both direct 2D and 1D/2D combined hydraulic modelling approaches with HEC-RAS, and their effects on hazard quantification were evaluated. The results show that the flood inundation area resulting from the 1D/2D coupled model is wider than the direct 2D solution.

## 1. Introduction

Floods are a major concern in recent years due to their increasing occurrence worldwide. Hydrodynamic modelling is an important part of determining probable hazards. Hydrodynamic models are often implemented either by considering direct 2D modeling or 1D/2D coupled modeling approaches. In this study, Yağlıdere Stream which is located in Giresun Province of the East Blacksea region of Turkey selected. Moreover, direct 2D and 1D/2D coupled modelling approaches were implemented. Inundation areas for each approach were exported to the GIS environment and compared. It was determined that there exist differences in the inundation area of each approach. 1D/2D coupled model resulted in a wider inundation area. However, there is not much difference in the hazard classes. Within the scope of this study, the variation of direct 2D and 1D/2D coupled modeling approaches on flood propagation and the hazard was investigated.

## 2. Hydraulic Modeling

Both 2D and 1D/2D coupled hydraulic models of the Yağlıdere Stream are implemented by using HEC-RAS which is widely used in modeling open channel and surface flows and identifying flood inundation areas. Surface roughness is an important parameter of hydrodynamic modelling and its determination requires special attention. In this study, surface roughness is determined by examining land use data by considering CORINE 2018 and corresponding surface roughness values proposed by the study of Papaioannou (2018). All the parameters such as DEM resolution, mesh size, and surface roughness values are kept constant and determined for each model. The hydraulic variables, the inflow hydrograph, and the normal depth are used as boundary conditions in the hydraulic models. Both models are analyzed with HEC-RAS to obtain spatially varied water depth and velocity data which are used to determine spatially varied hazard maps.

## 3. Hazard Quantification

Flood hazard quantification is often determined by taking into account the water depth and velocity obtained from the analysis of the hydraulic model. There are different methods for quantifying flood hazards. In this study, hazard quantification is implemented by considering the threshold values and methods determined by the study of Smith et al. (2014) as given in Table. 1.

**Table 1.** Thresholds and Hazard Classes by Smith et al. (2014)

| Hazard Class | Explanation | V*D | Depth (D) (m) | Velocity (V) (m/s) |
|---|---|---|---|---|
| H1 | Generally safe for buildings, vehicles, and people | ≤0.3 | 0.3 | 2 |
| H2 | Dangerous for small vehicles | ≤0.6 | 0.5 | 2 |
| H3 | Dangerous for vehicles, children, the elderly | ≤0.6 | 1.2 | 2 |
| H4 | Dangerous for vehicles and people | ≤1 | 2 | 2 |
| H5 | Dangerous to vehicles and people, possible structural damage to buildings | ≤4 | 4 | 4 |
| H6 | Dangerous for vehicles and people, risk of collapse for buildings | ≥4 | - | - |

After having implemented the hydraulic models, a script is inserted into the software to construct hazard classes.

## 4. Results and Discussion

The results from the analyses of the two models suggested that flood inundation areas and corresponding hazards would differ depending on the modeling approach. The total inundated area is 0.308 $km^2$ for the 1D/2D coupled model whereas it is 0.321 $km^2$ for the 2D model. The difference is not significant but the 1D/2D model resulted in a larger inundated area with voids. However, the direct 2D model inundated a narrower area without voids. 1D/2D model predicts a more precise solution. Moreover, hazard quantification was made for each model and results were presented in Fig. 1.

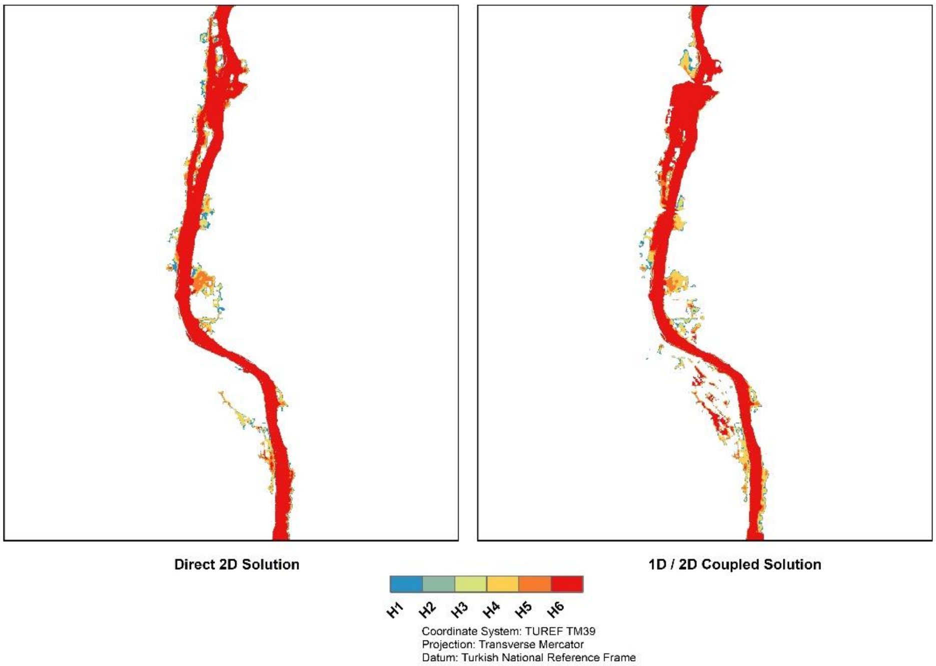


**Fig. 2.** Spatially varied hazard for 2D and 1D/2D coupled models.

As it can be seen from Fig. 2, hazard classes are similar for both models. Anthi-Eirini et al. (2017) suggested a 1D/2D coupled modeling approach for more sensitive results. It was concluded that the 1D/2D coupled modeling approach yields more detailed results than the direct 2D modeling by examining the analyses of the models.

### References

Anthi-Eirini K. Vozinaki, Giasemi G. Morianou, Dimitrios D. Alexakis & Ioannis K. Tsanis (2017) Comparing 1D and combined 1D/2D hydraulic simulations using high-resolution topographic data: a case study of the Koiliaris basin, Greece, Hydrological Sciences Journal, 62:4, 642-656

Papaioannou, G.; Efstratiadis, A.; Vasiliades, L.; Loukas, A.; Papalexiou, S.M.; Koukouvinos, A.; Tsoukalas, I.; Kossieris, P. (2018) An Operational Method for Flood Directive Implementation in Ungauged Urban Areas. Hydrology, 5, 24.

Smith, G. P., Davey, E. K., & Cox, R. (2014). Flood Hazard.

# Comparison of one- and two-dimensional models for possible flood prediction of the Kimmeria watershed

Sofia LALIKIDOU[1], Apostolos VASILEIOU[2], Panagiotis ANGELIDIS[3], Eirini EFRAIMIDOY[4], Christos AKRATOS[5], Michail SPILIOTIS[6], Fotios MARIS[7], Ioannis DOKAS[8]

[1,2,3,4,5,6,7,8]Democritus University of Thrace, Department of Civil Engineering, Greece
emails: slalikid@civil.duth.gr[1], apovassi@gmail.com[2], pangelid@civil.duth.gr[3], eirhnhefr@gmail.com[4], cakratos@civil.duth.gr[5], mspiliot@civil.duth.gr[6], fmaris@civil.duth.gr[7], idokas@civil.duth.gr[8]

ABSTRACT

Climate change has contributed to the increase of extreme weather events worldwide. The dominant scientific opinion on climate variability is that it will increase the frequency of heavy rainstorms, causing high devastation risk from floods for many communities (Karl et al., 2009). Therefore, only an effective flood hazard management framework can reduce an upcoming flood hazard increase. The most modern management techniques include hydro-informatic applications, such as flood forecast modeling (Golian et al., 2010), flood hazard, and flood risk mapping in order to achieve an accurate assessment of the flood zones and vulnerable areas. The aim of this paper is to compare and contrast two hydraulic models (1D and 2D) to determine which one is more suitable for flood mapping. The chosen study area is the catchment of Kimmeria. Kimmeria stream (Kydoneas) contributes to Kosynthos river in the plain section while it springs from the mountainous region of Xanthi, Greece. The total area of the watershed is 35.5 km$^2$ while the total stream length is 6.5 km.

## 1. Methods and Materials

The methodology followed in this paper concerns two basic sections, the hydrologic modelling and the hydraulic modelling.

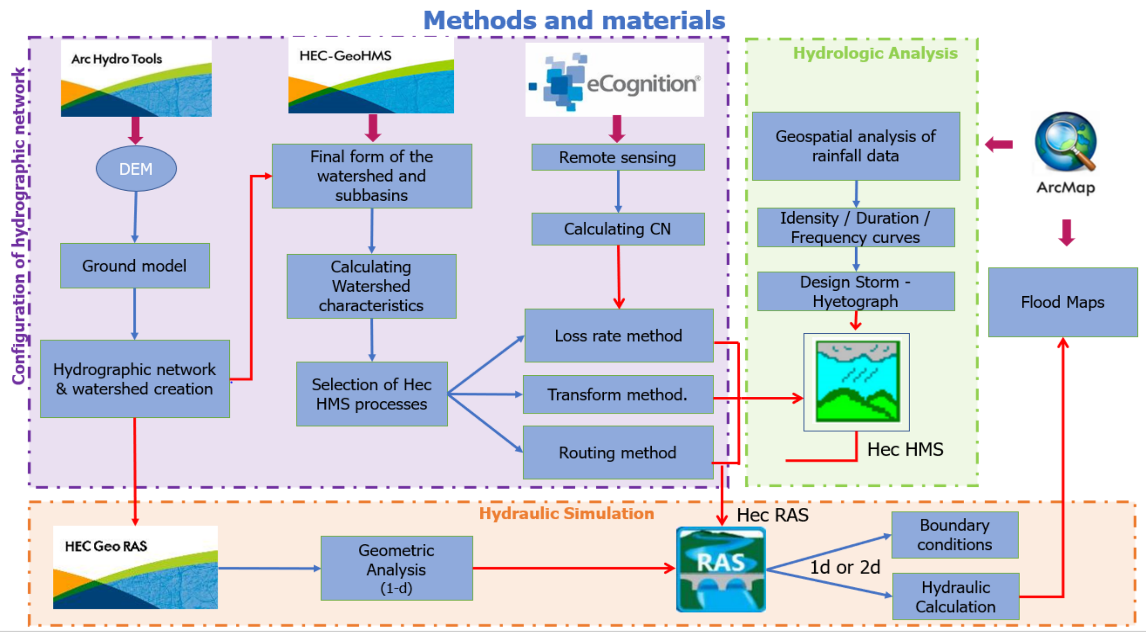


**Fig. 1.** Chart flow of creating a flood map

The rainfall-runoff modelling was realised with the HEC-HMS 3.5 software, which has been developed by the US Army Corps of Engineers (USACE) Hydrologic Engineering Center (HEC). It aims to simulate the precipitation runoff processes of watershed systems and includes different components, such as runoff volume, baseflow, and channel flow (USACE, 2010).

The hydrologic modelling of the basin regards the construction of the unit hydrographs. In order to achieve the latter, several hydrologic multi-analysis pre-processing and main processing operations upon the DEM were required, using the ARC Hydro 2.0 and the geospatial extension HEC-GeoHMS 10.2 in ArcGIS 10.2 environment. The chosen method for the watershed losses is a USDA Natural Resources Conservation Service development, the runoff Curve Number (CN) (Fig.1). From the hydraulic simulation, hydrographs of return period T = 50, 100 and 500 years were obtained, with peak flow of 172.9 $m^3/s$, 216.4 $m^3/s$ and 330.5 $m^3/s$, respectively. Hec Ras software was selected for the hydraulic simulation. For the 1D model the use of the extension of HEC-GeoRAS 10.2 river geographic analyses took place in the ArcGIS 10.2 environment. The analysis included the construction of various thematic lines such as the main flow lines, the flowpath lines, the riverbank lines and the cross sections. At the exact points of the different thematic lines, a digital topographic map of the area was used as a background. For the two-dimensional solution, a grid (20 m x 20 m) with an average cell size of 404.34 $m^2$ was created, while the number of total cells was 24,033. The equation to solve the 2D model was the equation of wave diffusion. Finally, in both cases, the hydraulic modeling was performed for instationary flow conditions using the hydrographs produced in the previous step.

## 2. Results and discussion

From the analysis of the results, the following table (Tab. 1) resulted where the most significant differences of the models are displayed.

**Table 1.** Comparison of 1D and 2D flow models (*the flooded area in the 1D model remains the same for all the return periods due to limitations of the model)

| | 1D T=50 years | 1D T=100 years | 1D T=500 years | 2D T=100 years | 2D T=100 years | 2D T=500 years |
|---|---|---|---|---|---|---|
| Max water height | 5.69 m | 7.15 m | 9.23 m | 6.71 m | 8.27 m | 10.12 m |
| Flooded area | 12.9 $km^2$ (*) | 12.9 $km^2$ (*) | 12.9 $km^2$ (*) | 11.02 $km^2$ | 12.03 $km^2$ | 12.57 $km^2$ |
| Max channel velocity | 8.17 m/s | 8.61 m/s | 9.88 m/s | 7.52 m/s | 7.93 m/s | 9.01 m/s |
| Average Overflow velocity | 5.57 m/s | 6.11 m/s | 8.53 m/s | 6.24 m/s | 6.86 m/s | 8.69 m/s |

Based on all the comparisons made, it is obvious that the two-dimensional model is more suitable for flood mapping for the study area. The results provided by the 2D model were more detailed and therefore more accurate in the overflow areas in comparison with historical flood events. The values obtained for the maximum water height and the flooded area were more conservative in two-dimensional analysis than those obtained during the one-dimensional analysis. The identified differences are due to the larger number of computational points of the two-dimensional model, which allows more detailed results to be extracted. In general, the 2D Diffusion Wave equations allow the software to run faster and have greater stability properties. Finally, it is worth to be mentioned that the reliability of the results of the two-dimensional model is inextricably linked to the analysis of the digital terrain model. Indicatively, it is reported that with the use of a digital terrain model of 5 m resolution, the obtained results for the study area are considered unreliable. The choice of using one or two-dimensional hydraulic model depends on the topographic data as well as the available work time. Also, 2D models should be used when flow patterns are complex and 1D model assumptions are significantly violated. 2D models generally provide more accurate representations of flow distribution, velocity distribution, water surface elevation, backwater, velocity magnitude, velocity direction, flow depth, and shear stress.

**Acknowledgements**

We acknowledge support of this work by the project "Risk and Resilience Assessment Center –Prefecture of East Macedonia and Thrace -Greece." (MIS 5047293) which is implemented under the Action "Reinforcement of the Research and Innovation Infrastructure", funded by the Operational Programme "Competitiveness, Entrepreneurship and Innovation" (NSRF 2014-2020) and co-financed by Greece and the European Union (European Regional Development Fund).

Co-financed by Greece and the European Union

**References**

Golian S, Saghafian B, Maknoon R (2010) Derivation of Probabilistic Thresholds of Spatially Distributed Rainfall for Flood Forecasting, Water Resource Management, volume 24, pp. 3547-3559, doi: 10.1007/s11269-010-9619-7.

Karl TR, Melillo JM, Peterson TC (Eds) (2009). Global climate change impacts in the United States. New York: Cambridge University Press.

USACE, (2010). U.S. Army Corps of Engineers, Hydrologic Engineering Center, HEC-HMS. Available online at: http://www.hec.usace.army.mil/software/hec-hms/

# Identification of the weak points in the application of a methodology for the design of Flood Early Warning Systems in Climate Change Conditions – The case of the town of Mandra, Attica, Greece

Anastasios STAMOU[1], George MITSOPOULOS[1], Evangelos BALTAS[1]

[1] Department of Water Resources and Environmental Engineering, School of Civil Engineering, NTUA
email: stamou@mail.ntua.gr
email: baltas@mail.ntua.gr
email: gmitsop@central.ntua.gr

ABSTRACT

An 8-step methodology for the design of a Flood Early Warning System (EWS) under Climate Change conditions is briefly described. The methodology is applied in the town of Mandra in Attica, Greece, which in November 2017 experienced a disastrous flash flood. The methodology is based on research on scientific papers on existing EWS, calculations performed with a detailed flood prediction model and a questionnaire survey conducted in October and November 2018. In this design procedure the following weak points were identified: (1) the lack of experience on EWSs in Greece, (2) the lack of Monitoring Networks in many Greek towns, and (3) the lack of data for the calibration and verification of flood prediction models.

## 1. Introduction

Early Warning Systems (EWS) are tools to mitigate flood risk whose key elements are flood risk knowledge; monitoring, forecasting, and warning services; dissemination and communication of warnings; and flood preparedness and response. In Greece there are no EWS, while worldwide there are many EWS of various types and complexity. In the present work, a methodology for the design of EWS is briefly presented that was developed based mainly on the literature on EWS; this methodology is applied in the town of Mandra in Attica, Greece, which in November 2017 experienced a disastrous flash flood, to identify its main weak points.

## 2. The methodology

The main steps of the design methodology are the following:

Step 1. Collection and processing of the required data that usually include (D1) topographical, geological, hydrogeological, geotechnical and land uses, (D2) hydrometeorological, flood incidences, information from Flood Risk management plans, (D3) environmental and ecological, (D4) hydraulic works, mainly flood protection, (D5) infrastructure works and (D6) other data, such as social, flood vulnerability, and economic.

Step 2. Design of the Monitoring Network (MN), whose main components are: (1) sensors for precipitation and hydrodynamic characteristics (MN-SEN), (2) radars (MN-RAD) and (3) satellites (MN-SAT). The MN-SEN are typically used for the calibration of MN-RAD, the correction of predictions made by the MN-SAT and the calibration of the Flood Prediction Model (FPM). The design of the MN includes: (1) the utilisation of existing MN, (2) the optimal design of the network, and (3) the determination of the characteristics of the sensors and the collection and transmission of data to the Flood Forecasting Centre (FFC).

Step 3. Building and calibration of the FPM. The main actions of step 3 include the following: (1) the definition of the calculation domains and the boundaries of the hydrologic and the hydrodynamic model, (2) the selection and the building of the hydrologic and the hydrodynamic model using the data of step 1, e.g., DEM and DSM, (3) the calibration of the hydrologic and the hydrodynamic model using the data of step 1 to determine the values of the Curve Numbers and the friction (Manning) coefficients, respectively, and (4) the optimization of the FPM. When building the hydrologic model, the effects of CC can be taken into account as follows: (1) choice of the appropriate Representative Concentration Scenario (usually the RCP8.5), (2) extraction of the Boundary Conditions (BCs) from a Global Climate Model (such as the ICHEC-EC-EARTH), (3) use of these BCs in a Regional Climate Model (such as KNMI-RACMO22E from the Database Eurocordex), (4) estimation of the future (under CC) precipitation and (5) its use as input in the hydrologic model. Alternatively, a simpler approach can be applied by considering “what-if” scenarios.

Step 4. Application of the FPM to determine the areas of high flood risk following a typical procedure, such as the one applied in the Flood Risk Management Plans. Such a procedure typically involves the definition of calculation scenarios, e.g., for T=50, 100 and 1000 years, and the calculation of flood (1) hazard, (2) vulnerability and (3) risk for all scenarios.

Step 5. Calculation of the main warning characteristics. These characteristics depend on the type of the warning services offered that are (T1) threshold-based, (T2) flood forecasting via simple simulation tools and models, (T3) vigilance mapping Internet service, and (T4) flood inundation using integrated hydrologic-hydrodynamic models. The main warning characteristics are generally: (1) Flash Flood Guidance (for T3), (2) water elevation – discharge curves (for T1), (3) level-to-level correlations (for T2), (4) time-of-travel relationships (for T2), (5) flood arrival times (for T2) and (6) extent of flood inundation areas (for T4).

Step 6. Design of the FFC that include (1) the operating systems and hardware (workstations), (2) the application programs (software) needed to collect, analyse, integrate, display data and disseminate products, (3) the redundancy and backup programs of hardware and (4) the maintenance programs of hardware and software.

Step 7. Determination of the Warning (dissemination & communication) methods.

Step 8. Preparation of the Flood Preparedness & Response plan.

## 3. Results and discussion

The methodology was applied in the town of Mandra and the main design aspects of the proposed EWS are summarized in Mitsopoulos et al. (2022a). The main weak points that were identified were the following:

1. There are no EWS in Greece; thus, the experience of their design, including the methods for flood warning (steps 6 and 7), preparedness and response (step 8) is very limited. In Mandra, a preliminary questionnaire survey was performed that identified the main characteristics of these methods (Mitsopoulos et al., 2022a).
2. The lack of information on EWS combined with the lack of operating MN in many Greek towns make the design and implementation of a EWS a very difficult task. In Greece, only flood forecast simulations that are performed at national level using Numerical Weather Prediction models by the Hellenic National Meteorological Service (HNMS) can be used in the design of EWS.
3. A reliable FPM needs to be calibrated and verified using field data. Such data are collected by MN or are contained in the Hellenic Flood Risk Management Plans. Data from these plans are produced at relatively small scales (1: 25000) and thus they are very rarely useful in the calibration and verification of FPM due to the very local scale of the flood incidents. In Mandra, field measurements of the flood of 2017, which include maximum water levels and their arrival times and flood inundation extend, were available and used in the calibration of the FPM (Mitsopoulos et al., 2022b) and its optimization (Mitsopoulos et al., 2022c).

## 4. Conclusions

In the application of the proposed design procedure in the town of Mandra the following weak points were identified: the lack of experience on EWS, the lack of MN, and the lack of appropriate data for the calibration and the verification of the FPM.

**Acknowledgements**

The present work was performed within the framework of the project "National Network on Climate Change and its Impacts (NNCCI)" of the General Secretariat of Research and Technology under Grant "2018ΣΕ01300001".

**References**

Mitsopoulos G, Bloutsos A, Panagiotatou E, Baltas E, and Stamou A (2022a) Design Aspects of an Early Warning System for Flash Floods: The Case of the Town of Mandra in Attica, Greece, Proceedings of the 39th IAHR World Congress 19-24 June 2022, Granada, Spain.

Mitsopoulos G, Diakakis M, Panagiotatou E, Sant V, Bloutsos A, Lekkas E, Baltas E, Stamou AI, (2022b) How would an extreme flood have behaved if flood protection works were built?" the case of the disastrous flash flood of November 2017 in Mandra Attica Greece, Urban Water Journal, 1–11. https://doi.org/10.1080/1573062x.2022.2103002.

Mitsopoulos G, Panagiotatou E, Sant V, Baltas E, Diakakis M, Lekkas E, Stamou A (2022c) Optimizing the Performance of Coupled 1D/2D Hydrodynamic Models for Early Warning of Flash Floods, Water, 14(15), 2356. https://doi.org/10.3390/w14152356.

# Evaluation of Monthly Precipitation and Temperature Trends in the U.S.

Ramesh S. V. TEEGAVARAPU

[1] Florida Atlantic University, Boca Raton, Florida, 33431, USA
email: rteegava@fau.edu

ABSTRACT

Trends in annual extremes of monthly precipitation totals and minimum and maximum temperatures at over 1200 locations in the U.S. are evaluated. Monthly data of these climatic variables obtained from the United States Historical Climatology Network (USHCN) for the period 1910-2019 are used for this analysis. The trends are evaluated using nonparametric Spearman's rank correlation and Mann-Kendall tests. Trends in specific months for temperature and precipitation are also assessed. Results indicating statistically significant increasing trends for precipitation are mainly noted for sites in the northeastern U.S. Decreasing as well as increasing trends are noted for annual extremes of maximum temperature with spatially uniform increasing trends evident for minimum temperature. Discrepancies from the two nonparametric tests are noted in the number of sites with statistically significant trends when two nonparametric tests are used.

## 1. Variations and Trends in Climatic Variables

Trends and variations in extremes of essential climatic variables have been evaluated in several past studies (Teegavarapu, 2013, 2018) to understand the influences of climate change and variability on these variables. Nonparametric statistical tests such as Spearman's rank correlation (SRC) and Mann-Kendall (M.K.) test (McCuen,2016). The presence of autocorrelation or persistence in any time series is known to have an influence on the trends. Therefore, variants of M.K. tests that consider persistence are also used to evaluate the trends. Results related to these tests are not presented in this paper.

### *1.1 Precipitation and Temperature Extremes*

Monthly temperature and precipitation data at 1218 sites in the conterminous U.S. obtained from the United States Historical Climatology Network (USHCN) is used in this study for analysis of spatially varying trends. Trends in minimum and maximum temperature and precipitation totals are evaluated using nonparametric Spearman's rank correlation tests. Trends in annual extremes of monthly precipitation totals using the S.R. test are shown in Fig. 1. The eighteen regions referred to as hydrologic units defined by the United States Geological Survey (USGS) are also shown in Fig. 1. Approximately 16% of sites located in the north and northeastern region show increasing trends, while the rest of the sites show no statistically significant trends. Decreasing trends are noted in the western region of the U.S.

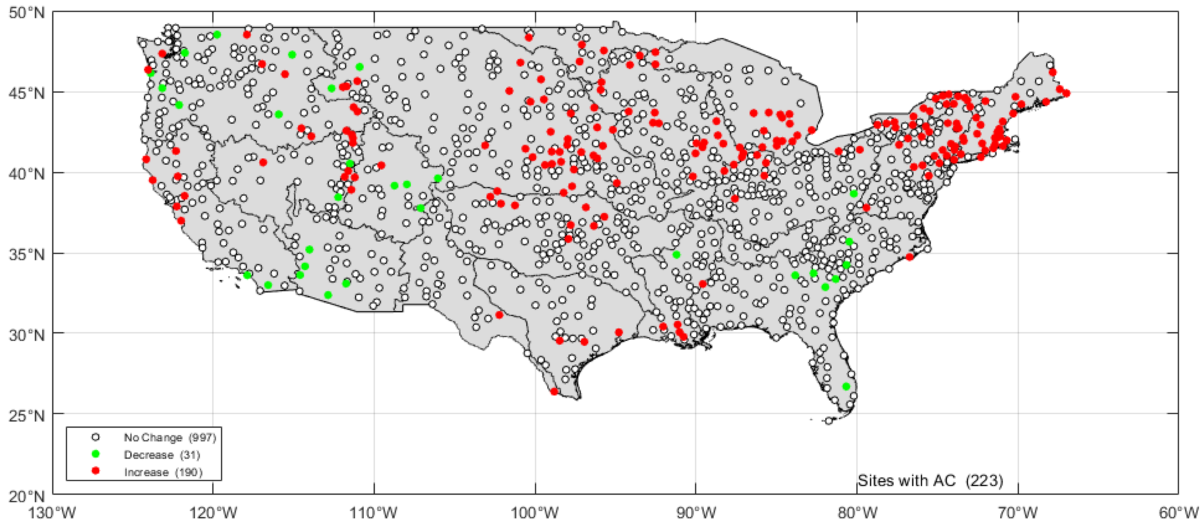


**Fig. 1.** Trends in annual extremes of monthly precipitation totals in the U.S.

Trends in annual extremes of monthly maximum and minimum temperatures are assessed using SR tests and they are shown in Fig. 2 and Fig. 3 respectively. Increasing trends are noted in maximum temperature in mostly southern and south-eastern and Midwest and northwestern parts of the U.S. with decreasing trends identified in the central region.

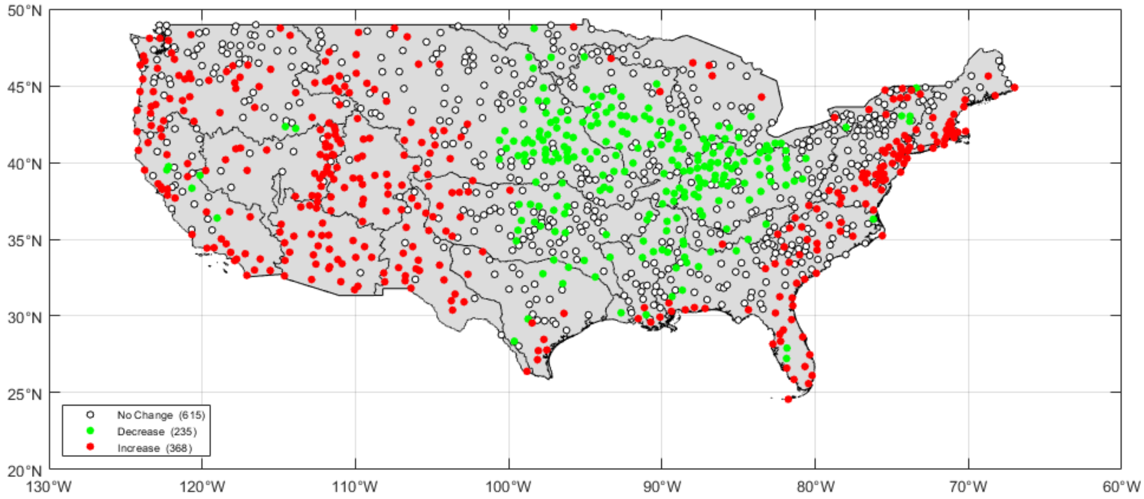


**Fig. 2.** Trends in annual extremes of monthly maximum temperature in the U.S.

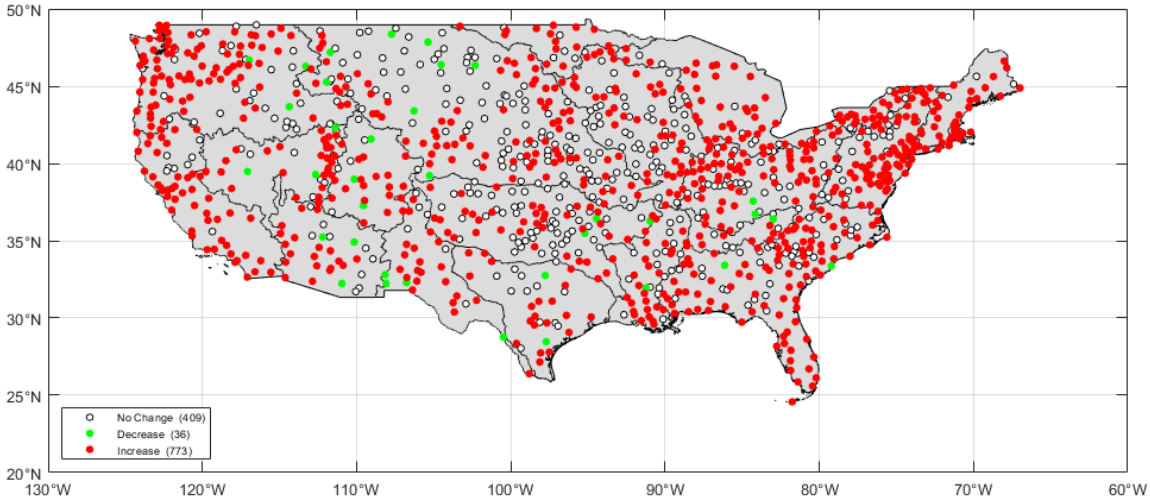


**Fig. 3.** Trends in annual extremes of monthly minimum temperature in the U.S.

## 2. Conclusions

Trends in annual extremes of temperature and precipitation at a coarse temporal scale (i.e., month) at more than 1200 sites in the U.S. are evaluated. Two nonparametric tests are used to evaluate trends in these climatic variables. Preliminary results from the trend analyses reported in this w work suggest spatially varying trends that non-uniform for precipitation and uniform of minimum temperature are noted. Further studies are being conducted to understand the variations in extremes at finer temporal scales, associations between temperature and precipitation and changes linked to climate variability.

**Acknowledgements**

Data is obtained through U.S. Historical Climatology Network databased hosted by National Oceanic and Atmospheric Administration (NOAA), USA.

**References**

McCuen RH, Modeling Hydrologic Change: Statistical Methods, CRC Press, Boca Raton, 448 pp.
Teegavarapu RSV (2013) Floods in Changing Climate: Extreme Precipitation, Cambridge University Press, Cambridge, 286 pp.
Teegavarapu RSV (2018) Trends and Changes in Hydroclimatic Variables: Links to Climate Variability and Change, Elsevier 421 pp.

# A parsimonious approach for regional design rainfall estimation: the case study of Athens

Theano ILIOPOULOU[1], Demetris KOUTSOYIANNIS[1]

[1] Department of Water Resources and Environmental Engineering, School of Civil Engineering, National Technical University of Athens, Heroon Polytechneiou 5, GR-157 80 Zografou, Greece
email: tiliopoulou@hydro.ntua.gr, dk@itia.ntua.gr

ABSTRACT

Design rainfall estimation at the regional scale is the cornerstone of hydrological design against flooding, particularly essential for ungauged areas. We devise a parsimonious and flexible methodology for regional estimation of rainfall extremes for time scales of minutes up to a few days and any return period, i.e. producing the ombrian curves. Estimation of the distribution parameters is performed by an advanced regional pooling approach employing knowable (K-) moments that allow reliable high-order moment estimation and handling of space dependence; which is non-negligible in homogenous regions. The regionalization approach is based on elevation, which is often sufficient to explain the rainfall variability within a generally homogenous climatic region. The methodology is effectively applied in the Attica region, comprising Athens and its surrounding basins.

## 1. Introduction and Methodology

Design rainfall for engineering applications is conveniently obtained from ombrian (from the Greek word 'όμβρος' meaning rainfall) curves, i.e. mathematical relationships linking rainfall intensity to timescale and return period, usually known as 'intensity-duration-frequency' curves. Koutsoyiannis (2021) recently developed a framework for integrating typical ombrian curves to stochastic models of the multi-scale rainfall intensity. The framework can be applied at any time scale, arbitrarily large, yet for large time scales the mathematics are more involved, while these scales are less relevant to flood analyses. Here, we apply the framework only for small time scales to produce the ombrian curves for the Attica region.

Under some simplifying assumptions (Koutsoyiannis, 2021), the rainfall intensity $x$ for small timescales $k$ (of the order of minutes to a few days) and return period $T$ is given by the following relationships; the first (Equation (1)) valid for return period estimated from series of rainfall exceedances and the second (Equation (2)) from series of annual maxima (where $\Delta$ = 1 year):

$$x = \lambda \frac{(T/\beta)^{\xi} - 1}{(1 + k/\alpha)^{\eta}}, \qquad \xi > 0 \tag{1}$$

$$x = \lambda \frac{(-(\beta/\Delta)\ln(1 - \Delta/T))^{-\xi} - 1}{(1 + k/\alpha)^{\eta}}, \qquad \xi > 0 \tag{2}$$

where $\lambda$ an intensity scale parameter in units of $x$ (e.g., mm/h), $\beta$ a timescale parameter in units of the return period (e.g., years), $\alpha$ a timescale parameter in units of timescale (e.g., h) with $\alpha \geq 0$, $\eta$ a dimensionless parameter with $0 < \eta < 1$, and $\xi > 0$ the tail index of the process.

The parameter estimation is based on a two-step procedure. The timescale parameters are estimated following the Koutsoyiannis et al. (1998) procedure, whereas the distribution parameters are estimated by a novel regional pooling approach. Two groups of stations were identified: (a) group A comprising 9 stations with lower on average annual maxima at the daily scale which are generally located at elevation <160 m and (b) group B comprising 5 stations with higher on average annual maxima at the daily scale which are generally located at elevation >160 m. After standardization of the stations' 24 h annual maxima by their group mean, the parameters of the pooled maxima distribution are estimated using only the first set of non-central K-moments (Koutsoyiannis, 2019) that is not impacted by the effect of space dependence, unlike higher moments (Koutsoyiannis, 2021, Iliopoulou et al. 2022). For the given stations that exhibit significant spatial correlation this correspond to the first16 non-central K-moments.

To regionalize the scale parameter $\lambda$ to any region of interest, e.g. a sub-basin within the studied area, the following relationship is applied:

$$\lambda = f_A\, \lambda_A + f_B\, \lambda_B \tag{3}$$

where $f_A$ the ratio of the area's extent that lies at elevation < 160 m to the total extent and $f_B$ the ratio of the area's extent that lies at elevation ≥ 160 m to the total extent, and $\lambda_A, \lambda_B$ the scale parameters of the two groups.

## 2. Results and Discussion

The parameter estimates are shown in Table 1 for both elevation groups, while an example of the fitting of the model to two stations representative of groups A and B respectively, is shown in Figure 1. It is seen that the empirical distribution functions are generally in good agreement with the theoretical ones.

**Table 1.** Ombrian parameters $\alpha, \eta, \xi, \lambda$ and $\beta$ for Equations (1)-(2).

| Parameters | $\alpha$ (h) | $\eta$ (-) | $\xi$ (-) | $\lambda$ (mm/h) | $\beta$ (years) |
|---|---|---|---|---|---|
| Elevation group A | 0.1 | 0.73 | 0.07 | 445 | 0.07 |
| Elevation group B | 0.1 | 0.73 | 0.07 | 579 | 0.07 |

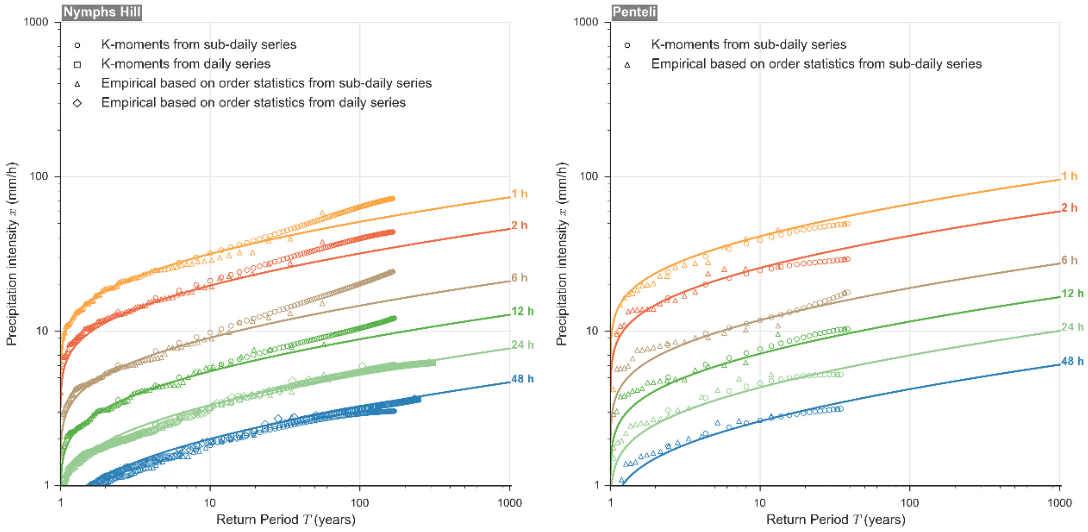


**Fig. 1.** Theoretical and empirical distributions of annual maximum intensities at 1 h to 48 h scales (depending on the available samples) from the daily and sub-daily stations at (a) Nymphs Hill (group A) and (b) the sub-daily station at Penteli (group B). The empirical intensities plotted based on order statistics are also shown for validation.

The ombrian curves for any region within the given area are derived based on the four common parameters and the regionally varying parameter which is obtained as a result of the region's elevation distribution (Equation (3)). In this way the framework is parsimonious and easy to apply at the basin scale, without the need for further spatial interpolation. Its merits are further discussed in the context of a new regional flood hazard assessment framework for the Attica region.

**Acknowledgements**

This work is performed within the frame of the research project "Risk Assessment for Earthquakes, Fire and Flood in the Attica Region" conducted by/in collaboration with the BEYOND research center of the National Observatory of Athens.

**References**

Koutsoyiannis D. (2021). Stochastics of Hydroclimatic Extremes - A Cool Look at Risk, ISBN: 978-618-85370-0-2, 333 pages, Kallipos Open Academic Editions, Athens. Available online: https://repository.kallipos.gr/handle/11419/6522 (accessed on 01/04/2021).

Koutsoyiannis, D. (2019). Knowable moments for high-order stochastic characterization and modelling of hydrological processes. *Hydrological sciences journal*, 64(1), 19-33. https://doi.org/10.1080/02626667.2018.1556794

Iliopoulou, T., Malamos, N., & Koutsoyiannis, D. (2022). Regional ombrian curves: design rainfall estimation for a spatially diverse rainfall regime. *Hydrology*, *9*, 67. https://doi.org/10.3390/hydrology9050067

Koutsoyiannis, D., Kozonis, D., & Manetas, A. (1998). A mathematical framework for studying rainfall intensity-duration-frequency relationships. *Journal of hydrology*, 206(1-2), 118-135. https://doi.org/10.1016/S0022-1694(98)00097-3

# Climate Change indicators: the evolution of the snow cover in Lombardy over the last 15 years

Hamzah FAQUSEH[1], Roberto RANZI[2], Giovanna GROSSI[3]

[1] University School for Advanced Studies - IUSS Pavia, University of Brescia, Italy
email: hamzah.faquseh@unibs.it

[2,3] University of Brescia
email: roberto.ranzi@unibs.it
email: giovanna.grossi@unibs.it

ABSTRACT

This study is focusing on analyzing the variability of the Snow Water Equivalent (SWE) in space and time in seven mountain basins located in Lombardy (northern Italy) during the period 2006-2020. Based on data provided by the regional environment protection agency, monthly trends and interannual variation are analyzed, even if on a relatively short time. The estimation of snowpack water content (Snow Water Equivalent - SWE) on a regional scale indicates some changes in the total quantity of solid-state water stored in the snow on a monthly basis. A shift of the snow cumulation and melting times through the years can be considered an important climate change indicator, showing the alterations in the common season patterns, and providing important indications for the efficient management of water resources.

## 1. Introduction

Climate change significantly impacts on the availability of water resources, included the water stored in the snowpack. The SWE is of considerable importance in the hydrological balance, as it represents a water reserve that has a gradual release capacity and a factor to be monitored in the hydrogeological control and alert chain. Lombardy is the fourth-largest Italian administrative region, sited in the northwest of the country, distributed in twelve provinces and it is also the most populated one, with a total of 10.060.574 people living there. The surface is about 23.8623 Km$^2$, and it mostly consists of mountains (40,5%) and plains (47,1%), with the remaining portion being hills (12,4%). The river basins located in Lombardy and considered for the SWE estimation in this study are: Adda, Serio, Brembo, Chiese, Mera, Mincio, Oglio.

## 2. Methodology

The estimate of SWE carried out by the regional environmental protection agency (ARPA Lombardia) for each water basin is calculated through a simplified approach, which accounts for the melting and deposit of snow, with output measurements occurring every week, on a grid of 100x100 meters (Bellingeri et al., 2006). Melted snow is estimated using a “degree-day” simplified melting model, based on the mean air temperature, the snow melting threshold temperature and the degree-day factor (DDF). The use of satellite sensors is important for evaluating the SWE depletion curves, the chosen sensor has to meet the specific needs that the monitored areas require, such as the spatial and spectral resolution, the extent of the observed areas and the satellite passage frequency (Ranzi et al., 1999). ARPA Lombardia uses images generated by MODIS sensors, which have a coarser resolution (500 m) compared to LANDSAT (30 m). MODIS images represent though a better choice in case of clouded sky, because the missing data can be reconstructed by comparing the data of the previous day with the one of the following one, experiencing relatively low data loss. ARPA Lombardia exploits an unsupervised algorithm with a clustering process defined by the operator and divided in three classes: snow pixels, no-snow pixels, and no-data pixel. Every no-data pixel can then be converted either into a snow pixel or a no-snow pixel through specific linear unmixing algorithms, based on the probability for a no-data pixel to be more similar to either one of the remaining classes (Ciraolo et al., 2007). These data are used as layer masks to exclude from the SWE maps each pixel associated with a no-snow class, producing snow cover extent maps. Snow cover extent maps are then combined with the digital elevation model of the area (DEM), to create snow depletion curves describing the extension of the snow cover area in each altitudinal zone. ARPA Lombardia verified variations both in the precipitation volume, which decreased over the observed years, and in its different seasonal distribution over the years, and an increasing variation trend of average monthly surface temperature presents clear similarities with the global warming of the Earth's surface, being recognizable even at local scale. Using SWE curves it is possible to identify the growing trend at the beginning of the snow season, when the snow begins to fall, usually between November and December, then deposits and finally stratifies itself over the ground, and the decreasing trend of the melt season, when the increase in temperature and the lack of new snow provide lower availability of snow water equivalent. Usually, the beginning of the melt season occurs in the second half of March. SWE value gradually increases and eventually reaches its maximum in the first weeks of March, only to enter the melt season and decrease for the rest of the reference year. Mean snow cover depth was calculated for every value registered in each water basin, dividing the SWE measurements, expressed in millions of $m^3$, by the surface of the respective water basin, obtained by their shapefile.

## 3. Results and discussion

The years with the highest contribution in terms of snow water equivalent are 2009 and 2014, while 2007 had the lowest contribution in terms of snow water equivalent. The highest snow water equivalent, in terms of millimeters, can be found in the Adda Prelacuale water basin, followed by Mera, Adda Totale (which is lower than its parts because in this case it is the result of an overall mean between the three values) and Oglio, in both 2014 and 2007. The decreasing trend shown in December gives a precious piece of information: the amount of snow water equivalent contribution in December is decreasing as the years pass, meaning that a shifting of the beginning of the snow season might be taking place, delaying it increasingly later in the year. Italy is facing a severe drought at the beginning of this year (2022) and besides Lombardy, as the decreasing trend of SWE shows. The differences in current water storage compared to the average of the period 2006-2020 is shown in the following Table 1.

**Table 1.** Lombardy – Situation of water storage as of 13/3/2022 and comparison with the reference period 2006-2020.

| Water reserves | December 2021 | | March 2022 (a) | | Average period 2006-2020 (b) | | Minimum period 2006-2020 (c) | |
|---|---|---|---|---|---|---|---|---|
| | Millions m3 | Change from 12/19 | Millions m3 | Change from 6/3 | Millions m3 | Difference (a-b) (%) | Millions m3 | Difference (a-c) (%) |
| Snowpack (SWE) | 586.2 | +15.8% | 803.8 | -2.5% | 2,536.4 | -68.3% | 925.0 | -13.1% |
| Reservoirs (**) | 497.4 | -6.4% | 193.0 | -7.6% | 313.9 | -38.5% | 182.9 | +5.5% |
| Lakes | 609.9 | -4.2% | 534.5 | -3.0% | 739.6 | -27.7% | 387.6 | +37.9% |
| Total | 1,693.4 | +1.1% | 1,531.2 | -3.3% | 3,589.8 | -57.3% | 1495.5 | +2.3% |

**: the quantities relating to the reservoirs refer to the sum of the basins of the Maggiore, Como, Idro and Iseo lakes

## 4. Conclusions

These data of the SWE evolution over the observed years provide useful indications for the sustainable management of water resources, even if a more robust analysis will be possible in future years.

**Acknowledgements**

This research activity is being carried out at University of Brescia in the framework of the national PhD program on Sustainable Development and Climate Change (XXXVII cycle) coordinated by the University School for Advanced Studies Pavia (IUSS).

**References**

Bellingeri, D., Peretti, G., Serra, R., Zini, E. (2006) Stima della disponibilità idrica sotto forma di neve nei bacini idrografici alpini lombardi mediante integrazione di dati satellitari modis e misure nivometriche a terra.
Ranzi, R., Grossi, G. and Bacchi, B. (1999) 'Ten years of monitoring areal snowpack in the Southern Alps using NOAA-AVHRR imagery, ground measurements and hydrological data', Hydrological Processes. John Wiley & Sons Ltd, 13, pp. 2079–2095.
Ciraolo, G., La Loggia, G. (2007) 'Water resources assessment and management under water scarcity scenarios. Centro Studi Idraulica Urbana, pp. 49–68.

# Cross-interactions of ecological and hydrological droughts in the central Spanish Pyrenees

Sergio M. VICENTE-SERRANO[1], Javier ZABALZA[1], Iván NOGUERA[1], Dhais PEÑA-ANGULO[1], Carmelo JUEZ[1], Conor MURPHY[2], Fernando DOMÍNGUEZ-CASTRO[3,4], Lars EKLUNDH[5], Hongxiao JIN[5], Tobias CONRADT[6], Jorge LORENZO-LACRUZ[7], Ahmed EL KENAWY[8]

1Instituto Pirenaico de Ecología, Consejo Superior de Investigaciones Científicas (IPE–CSIC), Zaragoza, Spain,
2Irish Climate Analysis and Research UnitS (ICARUS), Department of Geography, Maynooth University, Maynooth, Ireland,
3Aragonese Agency for Research and Development Researcher (ARAID),
4Department of Geography, University of Zaragoza, Zaragoza, Spain
5 Department of Physical Geography and Ecosystem Science, Lund University, Lund, Sweden
6Potsdam Institute for Climate Impact Research, Potsdam, Germany
7Department of Human Sciences, Area of Physical Geography, University of La Rioja, Logroño, Spain
8Department of Geography, Mansoura University, Mansoura, Egypt

svicen@ipe.csic.es

ABSTRACT

Drought is one of the most import natural hazards affecting Spain since it causes several environmental and socioeconomic negative impacts. The assessment of drought impacts is complex given the few available data and the several cross interactions among the different hydrological and ecological systems that drive the partition between blue and green water. Soil hydrology processes are also important and land cover changes can be determinant to understand the evolution of hydrological droughts in the last decades.

The Spanish central Pyrenees is a key region for the generation of water resources, which are mostly used in the lowlands. Thus, the water resources stored and generated in the mountainous areas of the Pyrenees are essential to maintain irrigated agriculture downstream. In the last decades land use has dramatically transformed in the central Pyrenees as consequence of human depopulation and the abandonment of mountain agriculture and livestock. This has caused natural revegetation that has altered the landscape with important morphodynamic and hydrological consequences. Land transformation has altered Pyreneean hydrology, and caused an important decrease of water resources as consequence of enhanced plant transpiration. In addition, there is important sensitivity of natural ecosystems to drought in the region.

There is limited knowledge of the cross interactions between hydrological and ecological systems during drought periods, a key issue to understand the partition between green and blue water during periods of water scarcity. For this reason, in this study we have modelled water cycle and ecological processes in a representative basin located in the Spanish central Pyrenees. The objective was to determine how meteorological droughts affect differently hydrological systems and ecosystems in order to determine interactions that may drive differential ecological and hydrological drought impacts.

## 1. Methods and results

We have used the RHESSys hydro-ecological model, which is designed to simulate integrated water, carbon and nutrient cycling and transport over complex terrain at small to medium scales, to model eco-hydrological processes in the Upper Aragón catchment located in the central Spanish Pyrenees from 1970 to 2018. The basin covers an area of 2181 $km^2$. The average annual precipitation is 1303 mm, although it can reach 1500 mm in the most elevated sites and falls below 800 mm in the Inner Depression. Precipitation is mostly recorded between October and May with a summer dry season characterized by isolated rainstorm events caused by convective processes. The Yesa reservoir, with a capacity of 446.8 $hm^3$, is an important water management infrastructure because it supplies water for irrigation to the Bardenas region (81,000 ha) located 80 km to the south of the basin.

Simulated processes include vertical fluxes of humidity (interception, transpiration, evapotranspiration and groundwater recharge), and lateral fluxes between spatial units. From the digital elevation model of the study area at a resolution of 100 m of cell size, the basin is subdivided in a hierarchical organization of landscape units, which enables different processes to be modeled at various scales, and enables the basic modeling units to be of arbitrary shape rather than strictly grid based. The spatial levels define a hierarchy comprising progressively finer units. Each spatial level is associated with different processes modeled by the RHESSys and at a particular scale. At the finest scale patches are typically defined by areas in the order of $m^2$, while basins ($km^2$) define the largest scale. The modeling units are defined by the user prior to running the model, with partitioning tailored to take advantage of the patterns of variability within the landscape. This procedure permits efficient parameterization and reduces the error associated with landscape partitioning.

A Monte-Carlo simulation by running the model iteratively using different values of each parameter to be calibrated was used to find optimum sets of the following four parameters: i) depletion of hydraulic conductivity with depth (m); ii) hydraulic conductivity in saturated soils (K); iii) infiltration through macropores (gw1); and iv) lateral ater fluxes from hillslopes to the main channel (gw2). The period 1996–2006 was used to calibrate the model, whereas the period 1975–1995 was used for validation, founding very good statistics in the process of validation.

RHESSys simulated different key variables in the basin including streamflow, soil moisture, leaf area, net primary production, etc. Figure 1 shows the monthly 1970-2018 evolution of these variables in the basin and it also compares the relationship between observed and modelled monthly streamflow.


**Fig. 1.** Observed (red) and modelled streamflow (blue) and modelled eco-hydrological variables in the Aragon

Hydrological and ecological variables were strongly affected by meteorological droughts. Nevertheless, the impact of droughts strongly diverged among the different analysed systems. The results show that in drought periods hydrological variables show stronger response and more acute deficits in comparison to ecological variables, which are characterized by less interannual variability. This suggests that in periods of water deficits, water supply for plant physiological processes is an important driver that explains the propagation of droughts throughout the hydrological cycle. Thus, plant coverage interacts with meteorological droughts to cause more severe hydrological droughts downstream. This issue suggests the large importance of land cover changes in mountain Mediterranean areas and the possibility of developing land management practices to improve the availability of water resources during dry periods.

**Acknowledgements**

This work was supported by projects CGL2017-82216-R, PCI2019-103631, and PID2019-108589RA-I00 financed by the Spanish Commission of Science and Technology and FEDER; CROSSDRO project financed by AXIS (Assessment of Cross(X)-sectoral climate Impacts and pathways for Sustainable transformation), JPI-Climate co-funded call of the European Commission, SustES - Adaptation strategies for sustainable ecosystem services and CSIC Interdisciplinary Thematic Platform (PTI) clima y servicios climáticos. (PTI-CSC).

# A new hybrid fuzzy probabilistic approach for the analysis and classification of meteorological and hydrological drought

Christopher PAPADOPOULOS[1], Mike SPILIOTIS[1], Panagiotis ANGELIDIS[1], Basil PAPADOPOULOS[1]

[1]Department of Civil Engineering, Democritus University of Thrace, Greece
email: cpapadp@civil.duth.gr
email: mspiliot@civil.duth.gr
email: pangelid@civil.duth.gr
email: papadob@civil.duth.gr

ABSTRACT

A hybrid fuzzy frequency factor-based methodology is used in order to improve the coupling between the observed and theoretical probabilities in meteorological and hydrological drought analysis. Thus, the frequency factor $K_T$ is related to the historical samples of rainfall and streamflow, correspondingly, through fuzzy linear regression based on Tanaka's model and a modified fuzzy linear regression model. Simultaneously, a fuzzy estimation of the mean value and the standard deviation is achieved. Hence, the crisp thresholds of the pre-defined drought categories are fuzzified based on the produced fuzzy linear relations. The classification of meteorological and hydrological drought is achieved by comparing the crisp data with the fuzzified drought thresholds using a fuzzy measure. The proposed methodology has been applied in the cases of southern Crete, Greece, and the transboundary Evros (Meric or Maritsa) River by covering the case of meteorological and hydrological drought, respectively.

## 1. Fundamentals and methodology

Meteorological and hydrological drought analysis is performed based on probability analysis. The probability analysis has the advantage that the empirical probability function can be used, and hence several hypothesis tests can be implemented. In practice, we use a theoretical probability function that matches the sample. A popular method of analysis is the frequency factor method in which each examined hydrological variable is linearly related to the frequency factor $K_T$. Based on the empirical probabilities, $K_T$-values are calculated in the assumption of the normal (N), lognormal (LN), Pearson III (P III), and the log Pearson III (LP III) distribution.

Then, the fuzzy linear regression of Tanaka (1987) is performed between the $K_T$ (cause) and the observations (causality) (Eq. (1)) in order to improve the coupling between the observed and theoretical probabilities (Spiliotis et al., 2018). From a mathematical point of view, Tanaka's model concludes in a linear programming problem where the objective function minimizes the total spread of the produced fuzzy band which includes all observed data. The decision variables of the linear programming problem are the regression coefficients considered symmetric triangular fuzzy numbers (STFN) whose central values and the semi-widths are estimated. The coefficients of fuzzy regression are identical to the mean value and standard deviation when the frequency factor method is used. Hence a hybrid model is structured where the parameters are fuzzy numbers. Instead of statistical measures, the suitability of Tanaka's model is checked through the value of the objective function which minimizes the total fuzziness. A lower value of the objective function means higher suitability of the fuzzy regression model. In addition, other measures of suitability are used which generally take into account the distance of the fuzzy estimates from the observations, and the mean value and standard deviation of the samples (Papadopoulos et al., 2019, Papadopoulos, 2022). Furthermore, another objective function is used which takes into account both the distance between the observations and the fuzzy estimates and the total fuzzy spreads. It is proved that the objective function of the modified fuzzy regression model includes the objective function of the Tanaka's model (Papadopoulos et al., 2019). In this article the case of log-Pearson III distribution is presented (Eq. 1).

The drought thresholds are discrete values of the random variable $Z$ inserted in the calculation of $K_T$. Thus, based on the produced fuzzy relations, each drought threshold $k$ ($thr,k$) can be calculated as a fuzzy magnitude (STFN) of the examined hydrological variable. To classify drought each observation is compared with each fuzzified drought threshold using the fuzzy measure $G_{k,j}$ (Eq. (2)) which denotes the degree to which an observation is greater than the examined fuzzified drought threshold. Measure $G_{k,j}$ is based on the fuzzy measure of risk proposed by Ganoulis (2004).

$$y_{T,j} \subseteq \tilde{y}_{T,j} = \tilde{\lambda} + \tilde{\zeta} \cdot K_{T,j} \tag{1}$$

Where $y_{T,j}$ is the observation of the examined hydrological variable regarding the hydrological year $j$, $\tilde{y}_{T,j}$ is its fuzzy estimation, $\tilde{\lambda}$ and $\tilde{\zeta}$ are the mean value and standard deviation of the log-transformed data.

$$G_{k,j} = \int_{\tilde{y}_{thr,k} \le y_j} \mu_{thr,k}(y)\, d(y) \Big/ \int_{-\infty}^{+\infty} \mu_{thr,k}(y)\, d(y) \tag{2}$$

The nominator of Eq. (2) denotes the area included between the membership function of each examined fuzzified drought threshold and the observation (the hatched area of Fig. 2b), while the denominator denotes the entire area included by the membership function of the examined fuzzy threshold of drought.

## 2. Implementation and discussion

Drought analysis and classification were performed based on the annual cumulative rainfall recorded from the meteorological station of Gortyna in southern Crete, Greece, and the annual cumulative streamflow of the transboundary Evros (Meric or Maritsa) River measured at Pythio's bridge, Greece. According to the results, the historical samples were best described by the LP III distribution (Fig. 1). However, the N and P III distributions described the historical sample of annual rainfall also well, while the LN distribution fit also the streamflow data well. Most hydrological years are characterized as mild drought years or non-drought years for both samples. The fuzziness of drought thresholds increases for significant drought years (Fig. 2) because the $K_T$-value, in terms of absolute value, increases. Last, both of the fuzzy linear regression models produced similar results. However, based on the suitability measures the modified fuzzy linear regression model produced marginally better results.

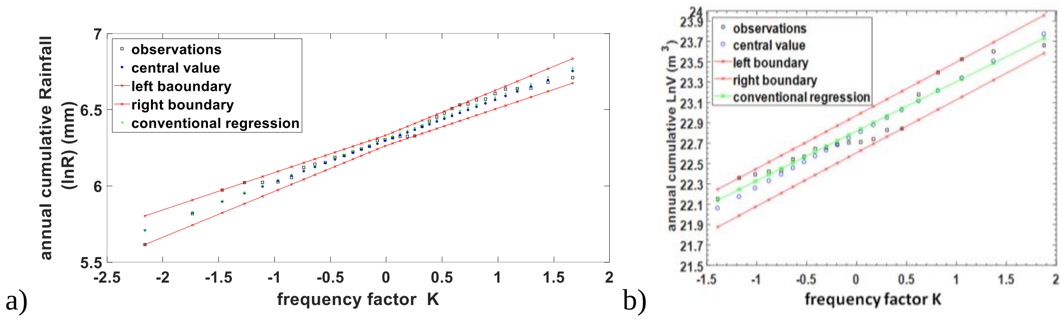


**Fig. 1.** Fuzzy linear regression a) between $y_{T,j}=lnR_{T,j}-K_{T,j}$ based on Tanaka's model in the assumption of LP III distribution, b) between $y_{T,j}=lnV_{T,j}-K_{T,j}$ based on the modified fuzzy linear regression model in the assumption of LP III distribution.

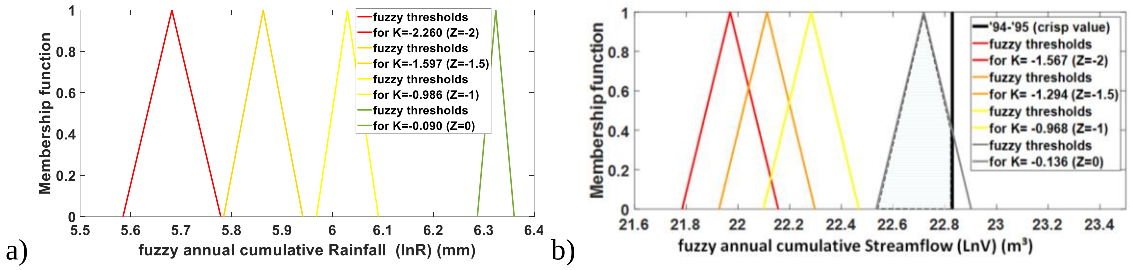


**Fig. 2.** a) Comparison between an observation and a fuzzified drought threshold, b) fuzzified thresholds of meteorological drought (LP III).

### References

Tanaka H, (1987) Fuzzy data analysis by possibilistic linear models, Fuzzy Sets and Systems, 24(3), 363-375.

Papadopoulos C, Spiliotis M, Angelidis P, Papadopoulos B, (2019) A hybrid fuzzy frequency factor based methodology for analyzing the hydrological drought, Desalination and Water Treatment, 167, 385-397.

Papadopoulos C. Fuzzy hybrid models for the analysis and assessment of hydrological extreme events. PhD Dissertation, Democritus University of Thrace, Department of Civil Engineering, Greece, 2022 (in Greek).

Spiliotis M, Angelidis P, Papadopoulos B, (2018) A Hybrid Fuzzy Regression−Based Methodology for Normal Distribution (Case Study: Cumulative Annual Precipitation), In 14th IFIP International Conference on Artificial Intelligence Applications and Innovations (AIAI), Rhodes, Greece, May 2018, Springer International Publishing, IFIP AICT-519, 2018, 568-579 pp.

Ganoulis J, (2004). Integrated Risk Analysis for Sustainable Water Resources Management, In Comparative Risk Assessment and Environmental Decision Making, Kluwer Academic, 38, 275-286 pp.

# Flood modelling and mapping based on a spatial distributed roughness coefficient estimation framework

George Papaioannou [1], Vassiliki Markogianni [2], Athanasios Loukas [3] and Elias Dimitriou [2]

[1] Department of Forestry and Management of the Environment and Natural Resources, Democritus University of Thrace, 68200 Orestiada, Greece;

[2] Institute of Marine Biological Resources and Inland Waters, Hellenic Centre for Marine Research, 19013 Anavyssos, Greece;

[3] School of Rural and Surveying Engineering, Aristotle University of Thessaloniki, 54124 Thessaloniki, Greece;

Email: gpapaio@fmenr.duth.gr

ABSTRACT

In this paper, the usage of an objective framework for the generation of spatial distributed Manning's n roughness coefficient maps and their impact on river flood modeling are examined. The methodology was implemented for a specific part of the ungauged Xerias stream, Greece and later applied for the entire Xerias stream that outflow to the sea. The analysis is based on the extreme flash flood event occurred on 9 October 2006, with 232 mm of rainfall falling in, approximately, 12 hours. The proposed methodology can be valuable technique for flood inundation modelling in other streams with similar river-bed and hydrological conditions.

## 1. Study area

The geographic location of Xerias watershed is in Thessaly region, located between latitude 39°20'0" to 39°28'41" N and longitude 22°49'22" to 23°03'15" E. Xerias upper watershed is about 71 km$^2$, while the total watershed is approximately 120 km$^2$. Elevation ranges from 0 to 1600 m and the mean annual precipitation is about 700 mm. Forested and semi-natural areas cover most of the watershed area. The lowest part of Xerias stream passes through the suburban and urban areas of Volos city. The length of the test site for the development of the roughness estimation methodology is about 2.2 km and the length of the remaining reach to the sea is approximately 6 km. During the flash flood event of October 2006 several infrastructures were damaged and a part of the city was flooded.

## 2. Methods–Results

Several methodological approaches have been followed for the river flood modeling application: 1) fieldwork for data collection with Unmanned Aerial Vehicle (UAV) and grid sampling, 2) grain size classification based on local entropy values, 3) twofold validation of the grain size classification methodology, 4) generation of the spatial distributed roughness coefficient maps, 5) evaluation of selected roughness coefficient values based on flood extent data, 6) application of the methodology for the entire stream reach, 7) validation of the flooded area based on non-conventional flood data.

### *2.1. Field work*

The field work involves the topographical survey using UAV and the grid sampling. The UAV images were used to generate a high-resolution Digital Terrain Model (DTM) through photogrammetric analysis. The river-bed materials were collected by using sampling frames of 1m$^2$, applying the typical grid sampling method. All perpendicular axes of the bed materials were measured using a digital caliper. The values of the measured axis of all materials (11 sample grids) were used to estimate the grain size-frequency distributions and the estimation of the typical predefined diameters such as $D_{50}$, $D_{65}$, $D_{84}$ and $D_{94}$.

### *2.2. Grain size classification using UAV images*

Initially the orthophoto mosaic derived from the field survey was converted from RGB (Red, Green, Blue) to HSV (Hue, Saturation, Value), HLS (Hue, Lightness, Saturation), and Intensity bands. Then, various pixel-based image analysis methods were explored for substrate classification included several supervised and unsupervised classification methods. In particular, the Maximum Likelihood Classifier (MLC), K-Means and the ISODATA algorithms were examined to recognize the dominant existing sediment classes of the orthophoto mosaic, spatially clipped at main river-bed's boundaries. Subsequently, Object-Based Image

Analysis (OBIA) techniques were tested for river-bed segmentation. Finally, the image texture measure of entropy has been proven the most sufficient -among other object features- to map surface grain size in bed rivers. Thus, in this study, the band of entropy was reclassified to interpret the grain size classes along the Xerias stream. The proposed methodology was validated twice; initially by using 240 random points equally distributed across the sampling grids and checking their correct or not classification and then by comparing the estimated area percentage of the field measurements with the generated surface grain size classified map. Results showed that the proposed method can be implemented for semi-automated mapping of at least smaller grain size (sand-mud, cobble, gravel) with an error of ±35% (first validation) and ±48% (second validation) at a spatial resolution of 1.3 cm.

### *2.3. Roughness coefficient estimation*

Since the typical estimation of roughness coefficient based on literature review and photographs can be subjective, grid sampling method and several empirical formulas were used to estimate Manning's n roughness coefficient. Details on the selected empirical formulas can be found in previous work (Papaioannou et. al., 2017). Therefore, river-bed grain size frequency results combined with the empirical formulas provided a range of river-bed roughness coefficient values. The classification of the floodplain areas was based on detailed land cover data. Classified river bed and the land cover data combined with the estimated roughness coefficient values were used to generate the spatial distributed roughness coefficient maps. Four different roughness coefficient scenarios were generated to select the one with the highest accuracy for the flood inundation modelling of the entire stream.

### *2.4. Hydraulic-Hydrodynamic modeling configuration*

HEC-RAS v.6.1 hydraulic-hydrodynamic model was used for the flood inundation modelling of Xerias stream reach of 2.2 km and the remaining reach length of 6 km that crosses Volos city. Several hydraulic modelling approaches (1D, 2D, 1D/2D) were tested and the prevailed one was used for river flood modeling of the entire stream. Many model parameters and other configurations were determined based on the HEC-RAS user manual (Brunner and CEIWR-HEC, 2021). The high-resolution UAV-DTM was used for the river and riverine geometry determination. The inflow hydrograph used in this analysis was based on the Clark Instantaneous Unit Hydrograph methodology. Further details on the flood-hydrograph can be found on the work of Papaioannou and associates (Papaioannou et al., 2016). All bridges within the study area were configured as structure type bridges. The evaluation of the results of the upper part (2.2 km) of Xerias stream were based on contingency tables and the following two skill scores:

$$F1 = \frac{A}{A+B+C} \qquad (1) \qquad\qquad F2 = \frac{A-B}{A+B+C} \qquad (2)$$

A is the correctly predicted flooded area (hits), B is the flooded area false prediction (false alarms), C is the flooded area that is not predicted by the model (misses). Several conventional and non-conventional data retrieved from previous work of the authors (Papaioannou et. al., 2019) were used for the validation of the flooded areas within the city of Volos which concerns the river flood modelling of the entire Xerias stream.

### *2.5. Hydraulic-Hydrodynamic modelling application-results*

According to the initial analysis of river flood modeling at the upper part of Xerias stream, the two-dimensional (2D) model provided the best results compared with the results of the other modeling approaches. The second best results have been acquired for the coupled (1D/2D) modelling approach. The highest estimated roughness coefficient values provided the optimum results based on the F1 and F2 scores. Results derived from the river flood modeling of the entire stream reach are in a good agreement with the conventional and non-conventional flood-related data. The proposed framework provides a methodological approach that reduces the uncertainty involved in Manning's n roughness coefficient determination.

**References**

Papaioannou, G., Varlas, G., Terti, G., Papadopoulos, A., Loukas, A., Panagopoulos, Y., & Dimitriou, E. (2019). Flood Inundation Mapping at Ungauged Basins Using Coupled Hydrometeorological–Hydraulic Modelling: The Catastrophic Case of the 2006 Flash Flood in Volos City, Greece. Water, 11(11), 2328. MDPI AG. Retrieved from http://dx.doi.org/10.3390/w11112328

Papaioannou, G.; Vasiliades, L.; Loukas, A.; Aronica, G.T. Probabilistic Flood Inundation Mapping at Ungauged Streams Due to Roughness Coefficient Uncertainty in Hydraulic Modelling. Advances in Geosciences 2017, 44, 23–34, Retrieved from https://doi.org/10.5194/adgeo-44-23-2017

Papaioannou, G.; Loukas, A.; Vasiliades, L.; Aronica, G.T. Flood Inundation Mapping Sensitivity to Riverine Spatial Resolution and Modelling Approach. *Natural Hazards* **2016**, *83*, 117–132, doi:10.1007/s11069-016-2382-1.

Brunner, G.W.; CEIWR-HEC *HEC-RAS River Analysis System: User's Manual Version 6.0*; Davis, CA, 2021;

# Extreme discharge analysis of the largest river in South-eastern Europe

Igor Leščešen[1], Biljana BASARIN[1] Manfred MUDELSEE[2,3]

[1] Department of Geography, Tourism and Hotel Management, Faculty of Sciences, University of Novi Sad, Trg Dositeja Obradovića 3, Novi Sad, Serbia
email: igorlescsen@yahoo.com; biljana.basarin@dgt.uns.ac.rs

[2]Climate Risk Analysis, Kreuzstrasse 27, 37581 Bad Gandersheim, Germany
[3]Advanced Climate Risk Education gUG, Kreuzstrasse 27, 37581 Bad Gandersheim, Germany
email: mudelsee@climate-risk-analysis.com

ABSTRACT

With a length of 945 kilometres and a total area of roughly 97,000 km$^2$, the Sava has the second-largest sub-basin of the Danube and within Southeastern Europe, the Sava is the longest river with the largest river basin. The Sava River basin spreads across parts of Slovenia, Croatia, Bosnia and Herzegovina and as well Serbia.

In this study the daily discharge values for the 1961-2020 period for six stations located on the Sava River were used. The sixty-year time span provides reliable results taking into account that the average record length recommended by the WMO is 30 years. For the extraction of high discharge values, the peaks-over-threshold (POT) method was applied with the threshold levels set at the 90th percentile. A minimum time span of 15 days between two consecutive peaks was applied to achieve independence between two successive events (Mallakpour and Villarini 2015, Mudelsee 2020). For the inspection of time-dependent flood occurrence rates and assessment of significant changes, a kernel estimation was applied with confidence bands. A Gaussian kernel function, K, was applied to weight observed flood dates, $T(i)$, $i$ = 1,…, $N$ (number of floods), and estimate the occurrence rate, λ, at time t as:

$$\lambda_{(t)} = \sum_i K\left(\left(t - T_{(i)}\right)/h\right). \tag{1}$$

Cross-validation was used to selection the bandwidth ($h$ = 10 years). Confidence bands (90%) around $\lambda(t)$ were determined using a bootstrap resampling technique. This procedure was repeated 2,000 times, and a 90$^{th}$ percentile-$t$ confidence band calculated. Additionally, a trend analysis was performed in the study. Many authors have highlighted the necessity of using a dependable nonparametric stationary test for trend detection (Cassalho et al. 2018). Among many available tests, the Mann-Kendall (MK) test (Kendall, 1975) is the most frequently used for the detection of trends in hydrological and climatological time series (Leščešen et al. 2022). In this study, the MK test was applied at a significance level of 0.05.

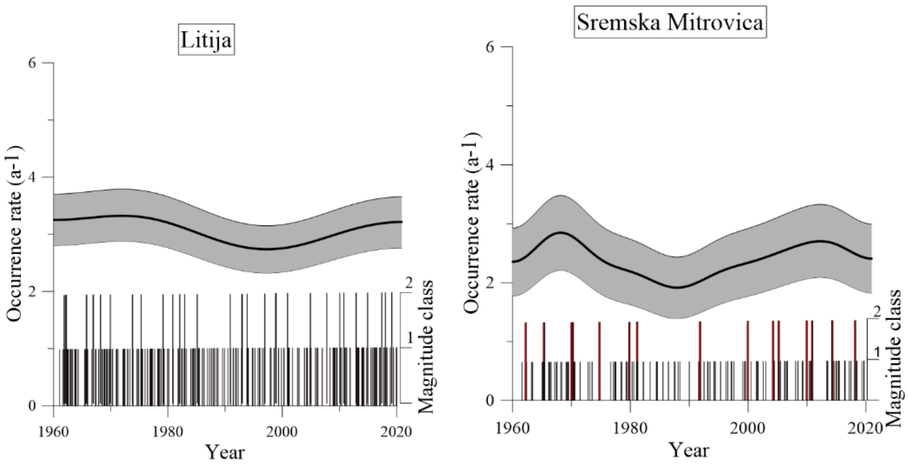


**Fig. 1.** Occurrence rates (solid lines) of Sava River floods at three representative stations (Litija and Sremska Mitrovica) for flood magnitude 1 with bootstrap 90% confidence band (shaded). Kernel estimation using bandwidth of 10 years is applied to the flood dates. For more details on the statistical methodology, see Mudelsee (2020).

Figure 1 shows estimated occurrence rates of Sava River floods at Litija and Sremska Mitrovica stations.For both stations, we found a clear decrease in the occurrence of magnitude 2 events by the end of the 1990s, which was followed by an increase for both magnitudes 1 and magnitude 2 events. The difference in occurrence rate between stations is likely due to the orographic and climatic differences between them. Litija is located in a predominantly mountainous part of the basin and thus under the influence of an Alpine pluvial-nival regime, while Sremska Mitrovica is located in the Pannonian basin with moderate continental climate and under the influence of the Pannonian pluvial-nival regime.

The results of the trend analysis are presented in Table 1. Negative discharge trends in the upper and middle parts of the basin can be contributed to the decreased amount of snowmelt over the Dinaric mountains that represent the main water input from the right-side tributaries of the Sava River. This has a significant influence on the regime of the Sava River downstream of Zagreb station (Čanjevac et al., 2018).

**Table 1.** Results of the trend analysis for six selected gauging stations in the Sava River basin.

| Station | Linear trend equation | Mann-Kendall test results | |
|---|---|---|---|
| | | Trend | Significance |
| Litija | y = -0.0028x + 731.49 | 0.000 | 0.962 |
| Šentjakob | y = 0.2255x + 429.5 | 0.269 | 0.149 |
| Čatež | y = 0.0802x + 1235 | 0.017 | 0.881 |
| Zagreb | y = 0.6904x + 1207.1 | 0.471 | 0.155 |
| Županja | y = -0.1785x + 3825.9 | 0.000 | 0.800 |
| Sremska Mitrovica | y = -0.1785x + 3825.9 | 0.000 | 0.800 |

These negative trends can likely be attributed to regional warming as well as to the low-frequency oceanic processes which further can cause the decline in precipitation and increasing evaporation in the basin. Presented results are in agreement with the results of other authors (Blöschl et al., 2019; Leščešen et al., 2022).

**Acknowledgements**

This research was supported by ExtremeClimTwin project, which has received funding from the European Union's Horizon 2020 research and innovation programme under grant agreement No 952384.

**References**

Blöschl, G., Hall, J., Viglione, A., Perdigão, R.A.P., Parajka, J., Merz, B., Lun, D., Arheimer, B., Aronica, G.T., Bilibashi, A., Boháč, M., Bonacci, O., Borga, M., Čanjevac, I., Castellarin, A., Chirico, G.B., Claps, P., Frolova, N., Ganora, D., Gorbachova, L., Gül, A., Hannaford, J., Harrigan, S., Kireeva, M., Kiss, A., Kjeldsen, T.R., Kohnová, S., Koskela, J.J., Ledvinka, O., Macdonald, N., Mavrova-Guirguinova, M., Mediero, L., Merz, R., Molnar, P., Montanari, A., Murphy, C., Osuch, M., Ovcharuk, V., Radevski, I., Salinas, J.L., Sauquet, E., Šraj, M., Szolgay, J., Volpi, E., Wilson, D., Zaimi, K., Živković, N. (2019). Changing climate both increases and decreases European river floods. Nature 573, 108–111. https://doi.org/10.1038/s41586-019-1495-6

Čanjevac, I., Orešić, D. (2018) Changes in discharge regime of rivers in Croatia, Acta geographica Slovenica, 58-2, 2018, 7–18, DOI: https://doi.org/10.3986/AGS.2004

Cassalho, F., Beskow, S., de Mello, C.R. (2018). At-Site Flood Frequency Analysis Coupled with Multiparameter Probability Distributions. Water Resour Manage 32, 285–300 https://doi.org/10.1007/s11269-017-1810-7

Kendall M.G. (1975) Multivariate analysis. London: Griffin.

Leščešen, I., Šraj, M., Pantelić, M., Dolinaj, D. (2022) Assessing the impact of climate on annual and seasonal discharges at the Sremska Mitrovica station on the Sava River, Serbia, Water Supply 22 (1): 195–207. https://doi.org/10.2166/ws.2021.277

Mallakpour, I., Villarini, G., 2015. The changing nature of flooding across the central United States. Nature Climate Change 5, 250–254. doi:10.1038/nclimate2516.

Mudelsee M. (2020) Statistical Analysis of Climate Extremes. Cambridge, UK: Cambridge Univ. Press.

# Impact of climate change on the hydraulic risk downstream the Eugui Dam (northern Spain) quantifying flood losses

Marco LOMPI[1,2], Luis MEDIERO[2], Enrica CAPORALI[2]

[1] Department of Civil and Environmental Engineering, University of Florence, Firenze, Italy email:
marco.lompi@unifi.it
enrica.caporali@unifi.it
[2] Department of Civil Engineering: Hydraulics, Energy and Environment, Universidad Politécnica de Madrid (UPM), 28040, Madrid, Spain email:
luis.mediero@upm.es

ABSTRACT

Floods are expected to increase in frequency and magnitude on average in Europe (Alfieri et al., 2015). Therefore, hydrological dam safety may also decrease in the future, as floods are the main hydrological load in dams. In a previous study, the impact of climate change on expected maxima reservoir water levels was quantified at the Eugui Dam (Spain). However, this study focuses on the impact of climate change on the outflow discharges at the Eugui Dam (Spain), also quantifying the expected changes in direct flood losses in buildings in the Metropolitan Area of Pamplona located downstream of the dam.

## 1. Data and Case Study

The case study is the River Arga that crosses the city of Pamplona in Northern Spain with a catchment area of about 510 km$^2$. The Eugui Dam is upstream Pamplona with a catchment area of about 69 km$^2$ (Figure 1).

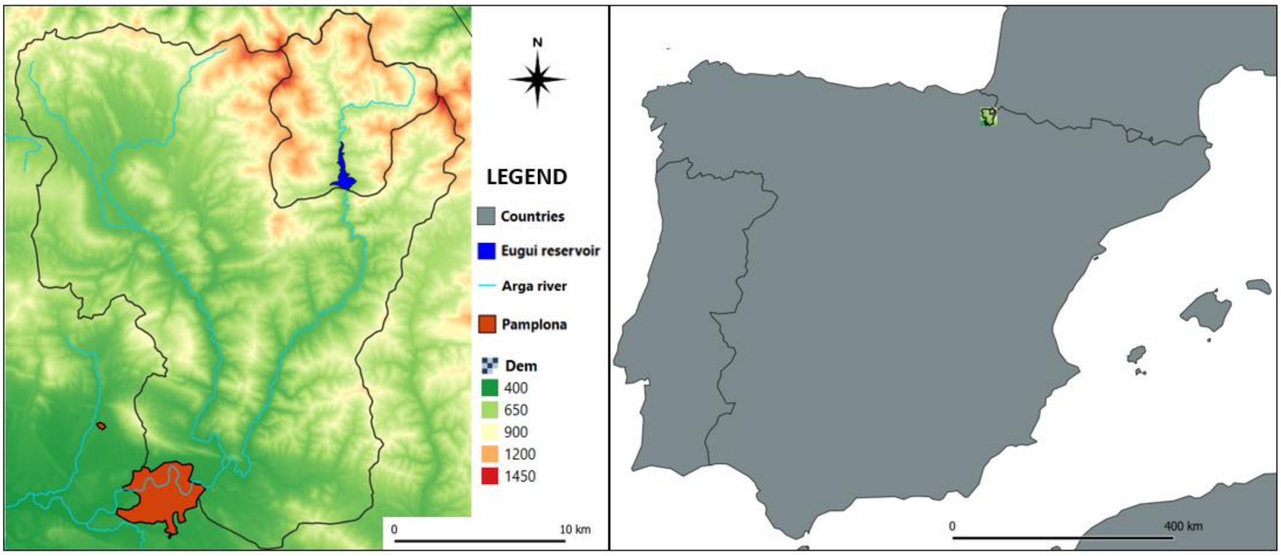


**Fig. 1.** a) River Arga catchment upstream to the city of Pamplona in Northern Spain and Eugui reservoir in its river catchment. b) Location of the River Arga catchment in Spain.

Rainfall, temperature and streamflow data in the period with observations (13 years) were used for the calibration of the hydrological model (see next section). Climate projections of rainfall and temperature are supplied by 12 climate models (Garijo and Mediero, 2019) in two emission scenario (RCP 4.5 and RCP 8.5) and three time windows (2011-2040, 2041-2070, and 2071-2100).

## 2. Methodology

The methodology is divided into six parts: i) estimates of expected inflow hydrographs in the Eugui Reservoir in the future; ii) assessment of the impact of climate change on expected initial reservoir water levels at the beginning of flood events in the future; iii) stochastic procedure to combine the probabilities of inflow hydrographs and initial reservoir water levels in the future, simulating flood routing in the Eugui Reservoir;

iv) assessment of the uncertainty sources in the procedure; v) two-dimensional (2D) hydrodynamic modelling of fluvial floods generated by the River Arga in Pamplona; and vi) assessment of flood damages in Pamplona.

Expected changes in flood quantiles for the River Arga in Pamplona were obtained in Lompi et al. (2021), using climate projections as input data of the RIBS event-based and fully-distributed hydrological model (Garrote and Bras 1995a). Daily reservoir water levels expected in the future are obtained combining the HBV continuous hydrological model, to simulate future daily inflow discharges in the Eugui Dam, with a reservoir operation model, to obtain daily outflow discharges and reservoir water levels. The HBV model (Bergstrom 1992) and the reservoir operation model are calibrated with 13 years of observations. The minimum number of simulations required to reach a given threshold (Th) in the model error is obtained. Th is measured with two objective functions: (i) Reff for HBV, that measures the model efficiency (Th>0.85, as a perfect calibration corresponds to a Reff value equal to one), and (ii) Root Mean Squared Error (RMSE) for the reservoir operation model (Th<1.5 m, as a perfect calibration corresponds to an RMSE value equal to zero).

The stochastic procedure generates 10.000 random initial reservoir water levels and inflow hydrographs with a 15-minute time step for each scenario. Flood routing in the reservoir is simulated using the Volumetric Evaluation Method (VEM), obtaining 10.000 maxima reservoir water levels and outflow discharges. Delta changes of maximum outflow discharge quantiles are considered as the ratio between the outflow peak discharges in the future and in the control period for a given return period. Delta changes greater than one will point to an increase in expected outflow discharges in the future. Uncertainty in estimates of rainfall delta changes, inflow hydrographs supplied by the RIBS model, and reservoir water levels, associated to HBV model biases, are considered. The uncertainty chain assessment provides the median values of the future outflow discharges with its confidence interval represented by six percentiles (5th-95th, 10th-90th, and 32th-68th).

The median values of expected maxima outflow discharges released by the dam in the future are summed to the expected natural contribution of the part of the River Arga catchment located downstream the dam, which is obtained with the RIBS model, for all the scenarios. Moreover, flood waves that travel from the dam to the city of Pamplona are routed with the Muskingum model. Water depths in the Pamplona Metropolitan Area are simulated with the 2D IBER hydrodynamic model (Bladé et al., 2014), that uses the inflow hydrographs by the Ulzama and Arga rivers upstream Pamplona. Finally, direct flood losses in buildings in Pamplona are estimated by using the SaferPlaces Platform (Mediero et al., 2022).

## 3. Results and discussion

The results show an increase in the expected maxima outflow discharges released by the dam in the future due to the lamination of more increase inflow event in the future. Particularly, delta changes of maxima reservoir water levels are greater than one for all the return periods in the RCP 8.5, considering the ensemble of all the climate models, pointing to a decrease in the hydrological dam safety. Therefore, the results highlight an increase of the hydraulic risk in the future in the RCP 8.5, especially at the end of the century. These results are mainly driven by an increase in the overtopping probabilities for such a scenario, where seven of the 12 climate models have an overtopping return period below 1000 years.

**Acknowledgements**

The authors acknowledge funding from the project PID2019-107027RB-I00 'SAFERDAMS: Assessment of the impact of climate change on hydrological dam safety' of the Spanish Ministry of Science and Innovation (PID2019-107027RB-I00 / AEI / 10.13039/501100011033).

**References**

Alfieri L, Burek P, Feyen L, Forzieri G (2015). Global warming increases the frequency of river floods in Europe, Hydrology and Earth System Sciences, 19, 2247–2260.
Bergström S. (1992) The HBV-Model — Its Structure and Applications. SMHI Reports RH No. 4, Norrköping.
Bladé E, Cea L, Corestein G, Escolano E, Puertas J, Vázquez-Cendón E, Dolz J, Coll A, (2014). Iber: herramienta de simulación numérica del flujo en ríos. Revista Internacional de Métodos Numéricos para Cálculo y Diseño en Ingeniería, 30, 1, 1-10
Garijo C, Mediero L (2019). Influence of climate change on flood magnitude and seasonality in the Arga River catchment in Spain, Acta Geophys, 66, 769–790.
Garrote L, Bras RL (1995a). A distributed model for real time forecasting using digital elevation models, Journal of Hydrology. 167 (1–4), pp. 279–306.
Lompi M, Mediero L, Caporali E. (2021) Future Flood Hazard Assessment for the City of Pamplona (Spain) Using an Ensemble of Climate Change Projections, Water, 13, 792.
Mediero L, Soriano E, Oria P, Bagli S, Castellarin A, Garrote L, Mazzoli P, Mysiak J, Pasetti S, Persiano S, Santillán D, Schröter K (2022). Pluvial flooding: High-resolution stochastic hazard mapping in urban areas by using fast-processing DEM-based algorithms, Journal of Hydrology, 608.

# Developing an adaptive strategy for urban flood risk management using a participatory exploratory modelling approach

Virginia Rosa COLETTA[1], Alessandro PAGANO[2], Irene PLUCHINOTTA[3], Nici ZIMMERMANN[4], Umberto FRATINO[5], Raffaele GIORDANO[6]

[1,5] DICATECh, Politecnico di Bari, Bari, Italy
email: virginiarosa.coletta@poliba.it
email: umberto.fratino@poliba.it

[2,6] IRSA-CNR, Bari, Italy
email: alessandro.pagano@ba.irsa.cnr.it
email: raffaele.giordano@cnr.it

[3,4] IEDE, The Bartlett, University College London, London, United Kingdom
email: i.pluchinotta@ucl.ac.uk
email: n.zimmermann@ucl.ac.uk

ABSTRACT

Urban areas are experiencing an increasing level of flood risk mainly due to climatological and socio-economic factors. Novel approaches for supporting decision-makers in exploring different urban future configurations and developing adaptive strategy for urban flood risk management are therefore needed. A multi-step methodology based on participatory exploratory modelling approach, and in particular System Dynamics modelling approach, is used for this purpose. Reference is made to the Thamesmead case study (London), within the CUSSH[1] and CAMELLIA[2] urban regeneration projects.

## 1. Introduction

Over the past century, traditional flood risk models extensively have taken into account uncertainty (i.e., in model inputs, model parameters and model structure) using probability distributions and resulting in a distribution of outputs around some "best-guess". Decision-makers were claiming that the future can be predicted thanks to the trust placed in the ability of traditional approaches to hypothesize future events (Maier et al., 2016). Indeed, assuming that the future is fairly closely related to the past is the basis of classical statistics and probability analysis. This assumption works when the evolution is slow, system elements are not too tightly connected and there are not too many Black Swans, i.e. events that lie outside the realm of regular expectations, carry extreme impacts and are explainable only after the fact (Taleb, 2007). Besides, these approaches focus exclusively on the phenomena, whereas the characteristics of the affected system – e.g., vulnerability, capacity to react, etc. – are almost neglected. Climate changes are already affecting the forecasting reliability. Moreover, assuming that flood risk assessment claims for assessing the urban system characteristics as well, the rapid unforeseeable changes we are witnessing – e.g., migration flows, land use changes – cannot be ignored.
Within this context, starting from the results of traditional flood risk models, the intent of this research is to use an exploratory modelling approach, such as System Dynamics (SD) modelling approach, to evaluate how the system would behave under different assumptions enabling the development of adaptive strategies for urban flood risk management (Kwakkel and Pruyt, 2015).
To increase the potential of the exploratory modelling, the research activity uses a participatory approach, integrating both scientific and stakeholder knowledge to further understand the uncertainty and complexity of how different factors interact and act on the urban system under flood risk (e.g., Moallemi and Malekpour, 2018). Specific reference is made to the one of the case studies of the urban regeneration projects CUSSH and

[1] https://www.ucl.ac.uk/complex-urban-systems/
[2] https://www.ucl.ac.uk/complex-urban-systems/

CAMELLIA, namely Thamesmead (London), a former inhospitable marshland vulnerable to different types of flooding mechanisms.

## 2. Methodology

The work intents to develop an approach for: i) exploring different flood management scenarios; ii) identify appropriate strategies to improve system resilience to flooding, using Nature Based Solutions (NBS) or hybrid solutions (e.g., a combination of green, blue, and grey infrastructures); iii) identify co-benefits, i.e., environmental, social, and economic benefits that could be produced through the implementation of NBS or hybrid solutions; iv) support the adoption of an adaptive approach to risk management, taking into account the possible evolutionary paths of the investigated system. To this end, a multi-step modelling methodology is implemented. It includes both a qualitative and quantitative phase using the participatory SD modelling approach, i.e., a computer-aided approach for strategy and policy design (Pagano et al., 2019).

In the qualitative modelling phase available information (reports, exiting models, etc.) and the local stakeholder knowledge (collected via semi-structured interviews and workshops) on flood risk and past flooding events in the study area are integrated to build a Causal Loop Diagram (CLD) that relates the problem of flooding with the main urban dynamics of the area. It is a qualitative SD model, i.e., a map of system feedback structure useful for understanding the interactive relationships between different components within (and outside) a system (Coletta et al., 2021). Then, Behaviour Over Time (BOT) graphs of some key system variables under three different conditions (desired future, most likely future, feared future) are drawn by stakeholders and hypotheses on both urban dynamics and policies implementation in the case of flooding are formulated integrating the CLD narrative with BOT graphs. Starting from the developed CLD, the quantitative modelling phase concerns the creation of a quantitative SD model, namely Stock and Flow model, related to the urban flood risk analysis and the definition of flood mitigation/prevention measures. To choose the flood adaptation strategy for the urban system, the model is integrated with the Dynamic Adaptive Policy Pathways (DAPP) approach, which enables the development of a series of actions over time (pathways) and is based on the idea of making decisions as conditions change, before severe damage occurs, and as existing policies and decisions prove no longer fit for purpose (Hallegatte, 2009). This integration enables to i) identify, for each possible configuration of the urban system (scenario), the actions that can address its vulnerabilities; ii) identify for each action the Adaptation Tipping Point (ATP), i.e., the condition in which it fails; iii) subsequently choose the most convenient sequence of actions (pathway) for the system.

## 3. First results and next steps

The first part of the methodology has already been carried out, while the second part is being completed.

From the application of the qualitative SD approach, it was possible to create a CLD on flood risk that i) incorporates the complexity of how the three components of risk (i.e., hazard, exposure, and vulnerability) interact in the urban system and ii) integrates the hydrological sub-system with other sub-systems (such as the social, economic, and environmental). In addition, a set of flood risk prevention/mitigation measures, useful in the near future for the implementation of the DAPP approach, was obtained.

Currently, the construction of the quantitative SD model is being completed; then the DAPP approach will be implemented with the help of stakeholders to identify the flood adaptation strategy for the study area.

**Acknowledgements**

The work described in this paper is part of the PhD research of the corresponding author and it fits into the ongoing activities of the CUSSH and CAMELLIA projects.

**References**

Coletta VR, Pagano A, Pluchinotta I, Fratino U, Scrieciu A, Nanu F, Giordano R (2021) Causal Loop Diagrams for supporting Nature Based Solutions participatory design and performance assessment, Journal of environmental management, 280, 111668

Hallegatte S (2009) Strategies to Adapt to an Uncertain Climate Change, Global Environmental Change, 19 (2): 240–247

Kwakkel JH, Pruyt E (2015) Using System Dynamics for Grand Challenges: The ESDMA Approach, Systems Research and Behavioral Science, 32, 358–375

Maier HR, Guillaume JHA, Van Delden H, Riddell GA, Haasnoot M, Kwakkel JH (2016) An uncertain future, deep uncertainty, scenarios, robustness and adaptation: How do they fit together?, Environmental Modelling & Software, 81,154-164

Moallemi EA, Malekpour S (2018) A participatory exploratory modelling approach for long-term planning in energy transition, Energy Research & Social Science, 35, 205–216

Pagano A, Pluchinotta I, Pengal P, Cokan B, Giordano R (2019) Engaging stakeholders in the assessment of NBS effectiveness in flood risk reduction: A participatory System Dynamics Model for benefits and co-benefits evaluation, Science of the Total Environment, 690, 543–555

# A decision support tool for emergency operations on drinking water supply systems

Alessandro PAGANO[1], Elena CARCANO[1], Raffaele GIORDANO[1], Ivan PORTOGHESE[1], Emanuela CAMPIONE[2], Valeria PALMIERI[2], Andrea DURO[2]

[1] Istituto di Ricerca sulle Acque - CNR, Italy
email: alessandro.pagano@ba.irsa.cnr.it

[2] Dipartimento Nazionale della Protezione Civile, Italy
andrea.duro@protezionecivile.it

ABSTRACT

There is an increasing concern -worldwide- on the impacts that extreme events may have on Water Supply Systems (WSS). The need to guarantee the safe provisioning of water for basic health and hygiene needs, even during emergency conditions, is a key concern for decision makers and first responders. In this framework, the present work aims to collect and structure information related to real events, along with information derived from both the scientific and the grey literature, to develop a Decision Support System (DSS) for the selection of the most suitable emergency management measures for drinking water supply systems. The DSS, therefore, significantly relies on 'expert' knowledge, which is being elicited from several Italian water utilities (WUs) through semi-structured interviews and is based on the use of Multi-Criteria Decision Analysis (MCDA) tools. It is meant to be used both by emergency managers for a first screening of potential measures to implement and by the Water Utilities to support the risk-mitigation-planning activities.

## 1. Methodology

Several semi-structured interviews are thus being carried out with Italian water utilities (WUs) who have experience in emergency management, in order to identify (and weigh) the most important criteria affecting the decision process. The interviews are mainly based on a fixed structure that can be adapted to the specificities of each case being analyzed, but generally aim to collect the following information: i) a simple characterization of the event under analysis, including the type of hazard and its key characteristics (e.g., magnitude, duration, main impacts on the population and on the built environment/other infrastructures); ii) characterization of the main impacts of the event on the WSS and on the levels of service; iii) site description; iv) overview of the infrastructural systems (main features and state); v) description of the measure(s) adopted to deal with the emergency, and of the criteria and sub-criteria that influenced the decision process. With specific reference to the items i) and ii), the weight given to criteria and sub-criteria is significantly case-specific. For this reason, properly characterizing the specific 'emergency type' under investigation is crucial, and fundamental also to deriving general and replicable guidelines. Regarding the item v), the information provided by the WUs are then integrated with recent scientific evidence on the topic, such as Mazumder et al. (2018), Salehi et al. (20918), Ghandi and Roozbahani (2020). The following Table 1 provides a summary of the main criteria and sub-criteria that are considered in the decision process, which is based on a AHP (Analytical Hierarchical Process) model. Full details on the model are included into Pagano et al. (2021).

For the purpose of the present work, a common classification of the emergency types has also been proposed, starting from a work by Bross and Krause (2021), but also considering the evidence from the interviews. The main elements that are being considered in the present work for characterizing an emergency type are: i) the water quality; ii) the water quantity (availability) in the short, medium and long term; iii) the level of functioning of the existing infrastructural system; iv) the functioning of tanks/reservoirs; v) the state of other infrastructures (mainly power supply and transport). The characterization of general 'emergency types' should help avoid any specific reference to the hazard, rather focusing on its impacts on the WSS and on the level of service.

**Table 1.** List of the main criteria and sub-criteria

| Criteria | Subcriteria |
|---|---|
| Technical performances | Durability and long-lasting performances, Flexibility of use, Improvement of water quantity, Protection of water quality, Structural improvement, Time for implementation |
| Economic viability | Initial cost, operation and maintenance costs, Opportunity cost |
| Environmental sustainability | Need for natural resources, Environmental impacts |
| Social acceptability | Disruption time, Need for excavation, Perceived community benefits, Perceived effectiveness, Perceived health benefits, Potential impacts on the surrounding areas |
| Local conditions | Effectiveness with structural damages, Diameter reduction, Interaction with other infrastructures, Need for preliminary operations, Need for specific information, Need for specific materials/skills/resources, Previous experience, Suitability for complex sites |

## 2. Main findings

First, it should be remarked that all the WUs specified the need for effective emergency planning as a prerequisite for successful emergency management. To this end, the role of Water Safety Plans and the definition of internal risk management plans/procedures is crucial. Previous experiences with extreme events suggested that emergency measures (e.g., the use of water tanks or bottled waters) should be limited as much as possible and used for a very limited time span, because of the higher social and economic costs they have. The repair/rehabilitation of existing infrastructures, along with the use of alternative/temporary water sources is generally preferrable. Clearly, this is an option only if the existing infrastructure has not been extensively damaged by the event and the use of mobile tanks depends on the accessibility of the sites in the aftermath of the event. Depending on the emergency type, the role of some management/operational measures might become highly useful. For example, in case of drought (which can be to some extent predicted), several WUs were able to limit losses and to improve the WSS performance, e.g., including pressure regulating devices or enhancing the districtualization of the infrastructure, improving leak detection activities as well as maintenance, increasing awareness of users. Such measures may not be sufficient to deal with severe emergency conditions but can help improve the global resilience of the system in the long term. Some side impacts should also be carefully considered, such as the potential negative effect of frequent and significant pressure regulation on the state of old pipes and joints, and the potential contamination of water as a consequence of low pressure in the system. It should also be remarked that the previous experience with other events/measures as well as the personal knowledge or the immediate availability of materials and devices are often crucial determinants in the decision-making process. From the organizational point of view, some good practices are related to the definition of alliances and agreements for mutual support among neighboring WUs, the activation of agreements with local authorities, the digitalization of network information and models, the allocation of staff and resources for emergency operation. This holds true also with respect to external services (such as mobile water tanks) that should be established well before the occurrence of extreme events.

## 3. Conclusions

All the information collected and used in the present work aims at providing decision-makers with a MCDA tool that can be used for a preliminary screening among multiple emergency management measures for water supply. Ongoing (and future) activities aim to further extend this research to a wider base of WUs in Italy and beyond in order to build reliable tools and guidelines for supporting structured and replicable decisions.

**Acknowledgements**
The present work has been carried out within a Research Agreement between the National Department of Civil Protection and IRSA-CNR (DPC Prot. U. n. 2031 15/01/2019 and PRE/0049513 18/09/2020). The authors would like to thank all Water Utilities and experts involved in the activities.

**References**
Bross L, Krause S (2021). Will there be enough water? A system dynamics model to investigate the effective use of limited resources for emergency water supply, Systems, 9(2), pp. 1-23.
Ghandi M, Roozbahani A (2020) Risk management of drinking water supply in critical conditions using fuzzy PROMETHEE V Technique, Water Resources Management, 34, pp. 595–615
Mazumder RK, Salman AM, Li Y, Yu X (2018) Performance evaluation of water distribution systems and asset management, Journal of Infrastructural Systems, 24:03118001
Pagano A, Giordano R, Vurro M (2021). A decision support system based on AHP for ranking strategies to Manage Emergencies on Drinking water Supply Systems, Water Resources Management, 35, pp. 613-628.
Salehi S, Jalili Ghazizadeh M, Tabesh M (2018) A comprehensive criteria-based multi-attribute decision-making model for rehabilitation of water distribution systems, Structural and Infrastructural Engineering, 14, pp.743–765.

# New perspectives on droughts under a changing climate: nature- based solutions

Harm DUEL[1], Judith TER MAAT[2], Reinaldo PENAILILLO[3], Ellis PENNING[4]

[1,2,3,4,] DELTARES, the Netherlands
email: harm.duel@deltares.nl
email: judith.termaat@deltares.nl
email: reinaldo.penailillo@deltares.nl
email: ellis.penning@deltares.nl

ABSTRACT

In recent years, countries around the world have been hit hard by drought events that affect ecosystem health, biodiversity, food supplies, agricultural incomes, employment, drinking water supplies and energy production. As the risk of drought is increasing due to ongoing climate change the High-level Experts and Leaders Panel (HELP) on Water and Disasters has drafted a report as guidance for designing strategies and implementing actions to increase resilience against drought events. The guidelines are based on best practices and lessons learned from over 25 case studies across the world. Nature-based solutions and respecting ecological limits are key components for building resilience. To underpin these key principles, STARS4Water project is increasing the understanding of water resources availability under changing climate and the effectiveness of nature-based solutions to reduce drought risks and impacts on ecosystems, society and economic sectors.

## 1. Introduction

According to different estimates at global level, at least 1.5 billion people have been directly affected by drought this century, and the economic cost over that period has been estimated at $124 billion. However, the real cost is likely to be many times higher because such estimates do not include much of the impact in developing countries (UNDRR, 2021). Drought is also having a destabilizing effect on human livelihoods, triggering widespread emigration in some regions. In a recent survey by the UN's International Organization for Migration (IOM), drought was cited by 21% of the respondents as a very important reason to leave, and by an additional 18% as part of the reason to leave (IOM and UNCCD, 2019).

Within Disaster Risk Reduction (DRR) and water-related climate risks, much attention is paid to floods and storm surges. However, droughts are among the most far-reaching yet most impactful natural hazards to both nature and humanity. There is an urgent need for being better prepared for future drought events and the international community is asking for guidance to design climate-resilient drought management strategies.

## 2. Approach

Over recent years, several international organizations have published reports drawing attention to droughts and proposing new approaches to drought risk management (e.g., WMO & GWP, 2014; UNESCO, 2016; UNCCD, 2017, Browder et al., 2021). Together with international experts within the HELP community, we have reviewed these approaches on how response planning and measures in relation to climate change are addressed. We also have reviewed over 25 case studies from different climatic regions and socio-economic conditions over the world to identify best practices and lessons learned. Key findings have been translated into guiding principles for operationalizing climate resilient, integrated drought risk management and planning.

## 3. Results and Discussion

We have distinguished 12 guiding principles for building resilience against drought events due to changing climate (Figure 1). Nature-based solutions (NbS) and respecting ecological limits are key for increasing resilience to drought events, and it is identified as one of the principles. Freshwater is a finite and vulnerable resource, essential to sustain life, the environment and economic development. Availability of water resources is highly depending on the hydrological processes within a watershed. In return, the hydrological processes are interlinked with the natural carrying capacity of ecosystems to regulate, retain, conserve and recharge water to rivers, lakes and ground water aquifers. Therefore, it is essential to maintain natural water flows and water-related ecosystems under different climate-hydrological conditions. NbS are crucial to restore and manage the natural carrying capacity of watersheds and to increase the resilience against drought events. Restoring the hydrography as a fundamental way of thinking can underlie many choices for NbS, including the combination of NbS for both droughts and floods. For effective implementation of NbS a good system understanding at a landscape scale as well as assessments based on monitoring and data analysis are valuable sources of information.

| | | |
|---|---|---|
| HELP core principles | Principle 1: | Respect environmental limits for land and water use |
| | Principle 2: | Increase the resilience of the whole of society, including its vulnerable communities, to droughts and water scarcity |
| HELP principles on modes of thinking | Principle 3: | Think in terms of integrated systems |
| | Principle 4: | Think and plan in cyclic terms |
| | Principle 5: | Plan from the bottom-up and co-design measures with affected communities |
| | Principle 6: | Embrace proactiveness and learn to deal with uncertainties |
| HELP principles on planning aspects | Principle 7: | Work in coordination with international agreements and conventions |
| | Principle 8: | Consider drought risk management as an issue without borders |
| | Principle 9: | Mitigate the impact of drought and water scarcity on ecosystems and biodiversity |
| | Principle 10: | Invest in nature-based and hybrid infrastructure |
| | Principle 11: | Tap into public-private finance and expand the role of drought-risk insurance |
| | Principle 12: | Strengthen monitoring and evaluation |

**Fig. 1.** The HELP principles for drought risk management (Duel et al., 2022).

By putting these principles in practice together when developing Drought Risk Management Plans significant progress to certain levels can be made in all regions and countries experiencing droughts, depending on the specific context. Outlining at an earlier stage the key interdependencies underlying the current risks and drought-related resilience, increases the chances of avoiding systemic changes and implementing effective solutions, including NbS.

**Acknowledgements**

This abstract was based on the HELP report on guiding principles for drought risk management. The report was prepared through a joint collaborative action by international experts on the responsibility of the High-level Experts and Leaders Panel on Water and Disasters (HELP). This action was led by the Ministry of Infrastructure and Water Management of the Netherlands and coordinated by Deltares and AGWA. The STARS4Water project is funded under the Horizon Europe research programme (call CL6-2021-CLIMATE-01-01: Improved understanding, observation and monitoring of water resources) and will start in October 2022. The project is executed by a consortium of European research institutes and river basin organizations and is coordinated by Deltares.

**References**

Browder, Greg, Ana Nunez Sanchez, Brenden Jongman, Nathan Engle, Eelco Van Beek, Melissa Castera Errea, and Stephen Hodgson. 2021. An EPIC Response: Innovative Governance for Flood and Drought Risk Management—Executive Summary. World Bank, Washington, DC

Duel, Harm, Henk Wolters, Ingrid Timboe, Judith ter Maat and John Matthews, 2022. HELP Guiding Principles for Drought Risk Management under a Changing Climate. Catalysing actions for enhancing climate resilience. HELP report (www.wateranddisaster.org).

IOM (International Organization for Migration) and UNCCD (United Nations Convention to Combat Deser tification), 2019. Addressing the Land Degradation – Migration Nexus: The Role of the United Nations Convention to Combat Desertification. Geneva. Available at https://www.unccleam.org/sites/default/ files/inventory/iom_unccd_desertification_2019_final. pdf.

UNCDD, 2017. Towards national drought policies in Latin America and the Caribbean Region, White Paper. Bonn, Germany, April 2018. Lead authors Tsegai, D. (UNCCD), R. Stefanski (WMO) and P. Meijas Moreno (FAO).

UNDRR United Nations Office for Disaster Risk Reduction, 2021. Policy brief Disaster risk reduction and climate change

WMO, GWP, 2014. National Drought Management Policy Guidelines: A Template for Action. https://www. droughtmanagement.info/find/guidelines-tools/guidelines/

UNESCO, 2016. Drought risk management: A strategic approach. Published by UNESCO, Paris on behalf of WWF. Contributing authors: Sayers, P.B., Li Yuanyuan, Moncrieff, C, Li Jianqiang, Tickner, D., Xu Xiangyu, Speed, R., Li Aihua, Lei Gang, Qiu Bing, Wei Yu and Pegram G.

# Approaching the valuation of costs and benefits of Nature-based Solutions on climate adaptation against drought

Carlos BENITEZ[1], Guido SCHMIDT[2], Thomas Dworak[3]

[1] EMGRISA, Spain
email: cbenitez@emgrisa.es

[2,3] Fresh Thoughts Consulting GmbH
email: guido.schmidt@ fresh-thoughts.eu
email: thomas.dworak@fresh-thoughts.eu

ABSTRACT

In response to the widespread social concern about the increasingly intense, frequent, and spatially widespread risks of drought, recent years have brought forth multiple studies aimed at identifying, systematizing and characterizing measures and actions to cope with droughts: from conceptual models to strategic proposals, policy reviews, compilations of evidence and a variety of analytical tools. Something similar happens with the Nature Based Solutions [NBS]. Following the European ambition of innovating with nature to achieve more sustainable and resilient societies, they are presented as a promising answer to the environmental and social stress caused by global change: climate adaptation, gaining security in the supply of water services, protecting against floods, and halting the loss of biodiversity and valuable ecosystems. There is a broad consensus that NBS can be a cornerstone for channeling public and private investment in the hydrological cycle towards the transition to a climate-neutral and sustainable economy, but progress needs to be made in understanding and quantifying both the costs involved and the multiple benefits derived.

The research is framed within a technical assistance contract with the European Commission and is part of a comprehensive work package to provide technical support to the newly established Expert Group on Water Scarcity and Droughts.

## 1. Introduction

The design of adaptation measures must be based on their capacity to address climate risks and increase the resilience of society and ecosystems, which are intrinsically linked. From this perspective, NBS seem particularly suited to jointly dealing with some of the foreseeable impacts of increasing climate hazard such as the consequences of extreme events on population and economic activity, favoring the progressive acclimatization of ecosystems to the new and changing conditions.

As in any other Programme of action, determining the costs and benefits of the technical alternatives is essential to select the most appropriate set of measures for the natural conditions and social context, and to establish an adjusted financing model. However, this assessment is particularly complex in the case of NBS. For example, compared to the relative simplicity of calibrating the cost of building a new reservoir and allocating the regulated volumes to various objectives (flood safeguard and water available for specific users and the environment), there is the complexity of approximating the benefits and distributing the costs of a package of NBS with similar expected contribution in terms of water availability / flood protection.

## 2. Objectives

The stated objectives of the assignment are:

a) The assessment of the impact of adaptation measures/actions on the viability of economic activities and their potential effects along the value chain.

b) An overview of climate adaptation measures/actions addressing drought, their immediate costs and benefits and the future ones under increasing risk of droughts.

c) A summary of which measures/actions will be beneficial for (nearly) all fresh water using sectors by decreasing their vulnerability to droughts.

Different climate scenarios and timeframes (such as 2030, 2050, 2100) should be presented.

## 3. Approach

The methodological approach starts with the compilation and systematization of the measures proposed so far to promote adaptation to climate change ─both NBS and other types─, together with a review of the various systems for classifying and characterising adaptation measures/actions. This task involves the assimilation, integration or unbundling of measures/actions as presented in previous references.

In addition to the review of background documents, a specific assessment has been performed to get insight on the level of implementation of adaptation measures across Europe. This exercise is part of a broader research effort to achieve a better understanding of national drought policies covering all EU Member States. A team of international expert assessors have completed an assessment template after analysing available water and climate adaptation planning documents and conducting interviews with drought-responsible managers and stakeholders.

The final step is the building of a catalogue of adaptation measures, classified under a common structure for their description to facilitate their comparison and integration in national or regional strategies, as well as the assessment of their costs and effectiveness, thus ensuring that the objectives are met.

## 4. Expected results and initial discussion

The characterization model of the measures is not closed at the time of writing this communication but will include at least the following elements: name; basic description, classification under different systems; potential contribution to mitigate other climate risks; drivers, pressures, impacts addressed; economic sector(s) benefited; ecosystem services benefited; expected changes in land use and the landscape; success and limiting factors; costs (investment, operation & maintenance); expected benefits (direct, indirect); pre-evaluation of effects on EU environmental objectives (as set forth in the EU Taxonomy for sustainable activities); timeframe and scenarios.

As already stated, approaching costs and benefits is probably the most critical and complex aspect of the characterization. Once the catalogue has been initially populated with costs data from background documents, different strategies will be used for completing data gaps including further literature and web research on specific measures/actions, deeper analysis of water planning documents and interviews with experts / practitioners. The assessment of benefits may be even more challenging. The Project PESETA by the Joint Research Centre has already developed an assessment framework by using the LISFLOOD hydrological and water use model to simulate the annual minimum river flow as drought hazard indicator, whilst the Water Exploitation Index Plus (WEI+) is used as an indicator for water scarcity. Considering that the main effect of drought mitigation measures must be the reduction of the imbalance between water resources and demands ─under normal conditions and during drought episodes─, the benefits derived from the measures/actions must be linked to the magnitude of this reduction and the damaged avoided for the water users and the environment.

**Acknowledgements**

Dagmar BEHRENDT KALJARIKOVA (European Commission - Directorate General for Environment) and Willem-Jan GOOSSEN (Directorate-General for Climate Action) for leading and advice. Edi Interviews and Jan Cools (Intersus Sustainability Services) for helping to integrate the consideration of the multi-benefit nature of NBS.

**References**

Brill G, Shiao T, Kammeyer C, Diringer S, Vigerstol K, Ofosu-Amaah N Matosich M, Müller-Zantop C, Larson W, Dekker T (2021) Benefit Accounting of Nature-Based Solutions for Watersheds: Guide, United Nations CEO Water Mandate and Pacific Institute. Oakland, California, 111 pp
European Commission Directorate-General for Regional and Urban policy (2015) Guide to Cost-Benefit Analysis of Investment Projects 364 pp
Feyen L., Ciscar J.C., Gosling S., Ibarreta D., Soria A. (editors) (2020) Climate change impacts and adaptation in Europe. JRC PESETA IV final report, 71 pp
Somarakis G., Stagakis S., Chrysoulakis N. (Eds.) (2019) ThinkNature - Nature-Based Solutions Handbook. ThinkNature project funded by the EU Horizon 2020 research and innovation programme under grant agreement No. 730338
Benitez C., Wolters H., Martí B. and Mora B. (2018) EU Water and Marine Measures Data base. Deliverable to Task B2 of the BLUE2 project "Study on EU integrated policy assessment for the freshwater and marine environment, on the economic benefits of EU water policy and on the costs of its non- implementation". Directorate-General for Environment of the European Commission, 112 pp
Strosser P, Delacámara G, Hanus A, Williams H, Jaritt N (2015) A guide to support the selection, design and implementation of Natural Water Retention Measures in Europe - Capturing the multiple benefits of nature-based solutions, Directorate-General for Environment of the European Commission, 98 pp

# Insights into siting of sand dams in the Angolan drylands

Luigi PIEMONTESE[1], Natalia LIMONES[2], Giulio CASTELLI[3], Marcus WIJNEN[4], Aleix SERRAT-CAPDEVILA[5], Elena BRESCI[6], Alice GRAZIO[7], Irina Liudmila MIGUEL[8], Marco Paulo CARLOS[9], Pietra CHAVES[10]

[1,3,6] Università degli Studi
di Firenze, Florence, Italy
email: luigi.piemontese@unifi.it
email: giulio.castelli@unifi.it
email: elena.bresci@unifi.it
[2] University of Seville, Spain
email: natalialr@us.es
[4,8,9,10] Independent Consultant
email: mwijnen@verizon.net
email: ilfmiranda@hotmail.com
email: marco.paulo.carlos@gmail.com
email: chavespietra@gmail.com
[5] The World Bank, Angola
email: aserratcapdevila@worldbank.org
[7]COSPE onlus, Florence Italy
email: alice.grazio@cospe.org

ABSTRACT

The provinces of the South of Angola are suffering a severe drought from the weak rainy season in 2012/2013 until now. Intermittent rains during this period brought some relief but were not enough to instigate a recovery. Some areas in southern Angola, as well as other parts of southern Africa, recorded the driest season in 35 years in 2015/2016, a peak of severity linked to the El Niño effect.

Angola tackles drought under a crisis management approach (Serrat-Capdevila et al., 2022). These methods do not solve the long-term problems, but they have traditionally avoided the worst social impacts by diminishing the pressing emergencies. Consequently, there is an evident need to move from crisis management to risk management and resilience building, especially in the rural areas of the southern provinces. Previous work has mapped and characterized the drought vulnerabilities of communities in the Center and South of Angola, learning about their access to safe water, and exploring sustainable rural water supply options to improve drought resilience (Limones et al., 2020; Serrat-Capdevila et al., 2022). Depending on resource availability, topography, soils and geology, different options for water supply and storage infrastructure can be considered for further analysis across the most vulnerable areas identified. In case surface water or shallow or intermediate groundwater is not available in sufficient quantities, the use of Nature-based solutions for managed aquifer recharge should be considered. In the drylands of the southern Benguela and Namibe provinces, for example, where bedrock is close to the surface and significant amounts of sandy sediment are available, the potential for constructing sand dams needs to be explored. Sand dams are barriers built along ephemeral streams that create small reservoirs filled in trapped sand, which in turn stores water in the pores (Lasage et al., 2015).

Although some colonial structures are serving as such, sand dams projects have not been documented in Angolan drylands (Ritchie et al., 2021; Serrat-Capdevila et al., 2022). Transferring water harvesting solutions like sand dams, widespread in other dry regions like the Horn of Africa and some parts of India, for example, to other areas of the world, could help creating additional reliable water resources and water points along ephemeral streams and expanding communities' water and food security.

However, finding an adequate location for the dam, both from the water harvesting point of view and from the community engagement point of view, is essential to guarantee usefulness, effectiveness and sustainability of the technology. Local communities' habits, perceptions and knowledge must be included in the siting phase to avoid misplacement or conflicts.

## 1. Objectives and approach

This work draws on mixed-methods for sand dams technology siting, connecting the conventional top-down geographic and bio-physical analysis with bottom-up participatory research and field validation. The analysis focuses on and discusses about several aspects:

- The study defined some landscape, hydrological and geomorphological principles to follow for water resources development in arid and semi-arid lands of the region by compiling the necessary baseline information for informed decision making: a comprehensive medium to high resolution data of climate, terrain, geology, geomorphology, soil composition, NDVI and socioeconomic features was put together. Obviously, the selection of the geospatial information to compile depends on the method implemented to support decision and, at the same time, the method is conditioned by data quality and availability. The state of the art and the general situation regarding wadi water resources assessments and modelling was assessed through a scientific literature review and an evaluation of previous similar efforts. The authors developed a straightforward GIS methodology -based on multicriteria analysis and overlay of the available raster and vector thematic maps- for water resources assessment and development of wadis, which yielded a preliminary set of potentially suitable points or river sections with capacity for the construction of small-scale managed aquifer recharge at the community level.
- This process was followed by field inspection for calibration of the model. It involved the selection of 18 random analysis points from the preliminary set of suitable locations. One of the purposes of the field assessment was to check whether the dimensions of the selected stream order correspond to stream dimensions and hydrological conditions which are feasible for the construction of small to medium size sand dams. Field inspection was also essential to verify the morphological parameters and geometric features of the selected site, particularly regarding stream bed width, valley width, including terraces if they exist, banks height and presence and condition of basement outcrops in them, dam section profile, and stream slope, in order to assess the magnitude of the reservoir created. The field analysis provided invaluable inputs to adjust the GIS model and to judge how far such a desk analysis can reach in terms of capturing the site-scale requirements. Consequently, the authors reflect on limitations, challenges and opportunities, developing a reference methodology for field validation of sand dam sites, and guiding on how the preliminary geographic and bio-physical GIS model should be taken with caution and systematically incorporate feedback from the field.
- In this same vein, siting must be guided by constant consultations with local residents about the infrastructure best suited to their needs, possible alternatives and the planning and governance arrangements necessary to ensure sustainable functionality. This work discusses about the timing and context in which such debates are adequate, and proposes a systematic qualitative approach that has been tested in several communities of Benguela and Namibe, based on a developed semi-structured interview questionnaire for key informants and focus group discussions, ensuring inclusive representation. This part of the analysis brings crucial knowledge on water availability, wadi water use and needs based on participants perception that cannot be obtained otherwise, and reveals a set of main themes and issues related to water security in the area. Based on the community-specific water-related problems, the authors identified the main socio-economic conditions to account for during the siting on a sand dam, which also feed, calibrate and enhance the GIS suitability model. The authors drew on the Benguela and Namibe case to propose a generic approach to larger-scale participatory siting beyond the study area.

By advancing in these topics, this work is supporting the Government of Angola and donors in their efforts to develop a program of interventions to enhance water security in the South of Angola.

**Acknowledgements**
The work was developed within the context of these two projects:

- “TransAgua: valorização das boas práticas dos pastores transumantes em gestão dos recursos hídricos e adaptação às mudanças climáticas”, funded within the FRESAN Program, by the Istituto Camões – Instituto da Cooperação e da Língua.
- The “Drought Resilience in the South of Angola Project” by the World Bank Water Global Practice and the Korean Green Growth Trust-fund, aimed at prioritizing water resources mobilization responses to the drought in the south of Angola.

**References**

Lasage, R., Aerts, J.C.J.H., Verburg, P.H., Sileshi, A.S. (2015) The role of small scale sand dams in securing water supply under climate change in Ethiopia. Mitig Adapt Strateg Glob Change 20, 317–339.
Limones, Marzo-Artigas, Wijnen, Serrat-Capdevila (2020) Evaluating drought risk in data-scarce contexts. The case of southern Angola, Journal of Water and Climate Change, 11 (S1).
Ritchie, H., Eisma, J.A., Parker, A. (2021) Sand Dams as a Potential Solution to Rural Water Security in Drylands: Existing Research and Future Opportunities. Front. Water 3.
Serrat-Capdevila, A., Limones, N., Marzo-Artigas, J., Marcus, W., & Petrucci, B. (2022) Water Security and Drought Resilience in the South of Angola. World Bank Publications.

# Determining Nature-based Solutions and Key Performance Indicators to address Water – Ecosystem – Food Nexus Challenges in Pinios River Basin, Greece

Dimitrios MALAMATARIS[1], Konstantinos BABAKOS[2], Anna CHATZI[3], Andreas PANAGOPOULOS[4], Evangelos HATZIGIANNAKIS[5], Vassilios PISINARAS[6]

[1,2,3,4,5,6] Soil and Water Resources Institute, Hellenic Agricultural Organization "DEMETER", Sindos, 57400, Greece
email: d.malamataris@swri.gr
email: k.babakos@swri.gr
email: a.chatzi@swri.gr
email: a.panagopoulos@swri.gr
email: e.hatzigiannakis@swri.gr
email: v.pisinaras@swri.gr

ABSTRACT

Limited water availability along with the increasing pressures on protected natural ecosystems, and the increasing agricultural productivity cost in most of the Mediterranean area, dictate addressing the main needs and challenges within the framework of the Water - Ecosystem - Food (WEF) Nexus. The concept of Nature-based Solutions (NBS) could manage Nexus challenges, providing new approaches to ecological and social adaptation. Impacts of NBS interventions need to be measured and assessed following a concrete impact evaluation framework. In this study, the main Nexus challenges of two water-stressed agricultural sub-basins, namely Agia and Pinios River Delta, in Central Greece, were identified in the framework of the PRIMA LENSES project and used as pilot areas. The most appropriate NBSs to increase the socio-environmental resilience of the pilot areas were also determined and presented along with the relevant indicators which could be utilized for measurement of their efficiency.

## 1. Introduction

Agia watershed which is the core of the Pinios Hydrologic Observatory (PHO) and Pinios River Delta (PRD) are situated in Pinios River Basin that constitutes the most productive agricultural plain of Greece. Agriculture accounts for more than 90% of total water consumption, while the unsustainable approaches of natural resources management have resulted in significant groundwater heads decline and seasonal, at least, failure to preserve ecological flow at rivers, posing a significant threat to environmental sustainability and food security (Pisinaras et al., 2018). The importance of developing NBS was recently recognized, considering their contribution to both environmental and socio-economic resilience. Effectiveness of NBSs in terms of associated improvements could be measured using appropriately derived Key Performance Indicators (KPIs).

## 2. Materials and Methods

### *2.1. Challenges identification*

The key needs and challenges faced across the PHO and PRD were identified and framed through personal interviews that were carried out with stakeholders, representing all the different institutional levels and Nexus sectors, i.e. water, ecosystem and food.

### *2.2. Nature-based Solutions determination*

The most appropriate NBSs for the pilot areas were determined and proposed based on the classification scheme developed in the framework of the EU funded ThinkNature project (Somarakis et al., 2019), which constitutes a state-of-the-art guide of NBSs, which provides, amongst others, an extensive list of efficient solutions of different primary objectives or functions and levels of ecosystem intervention.

### *2.3. Key Performance Indicators selection*

Aiming at assessing the performance of different types of NBSs in terms of supporting the delivery of ecosystem services and increasing the resilience of the pilot areas against Nexus challenges, KPIs derived from the relevant EC Handbook for practitioners (Dumitru & Wendling, 2021) were selected.

## 3. Results and Discussion

The main challenges identified in the pilot areas relate to the over-exploitation of surface and groundwater resources, and the low implementation of environmental-friendly agroecological practices. The most appropriate NBSs were selected for both pilot areas to optimize the WEF Nexus, contributing to more than one Nexus components and related challenges. NBSs were selected with the aim to improve water resources management and increase soil organic matter along with the enhancement of soil hydraulic properties. The most suitable KPIs for each different NBS were selected, as illustrated in Figures 1 & 2.

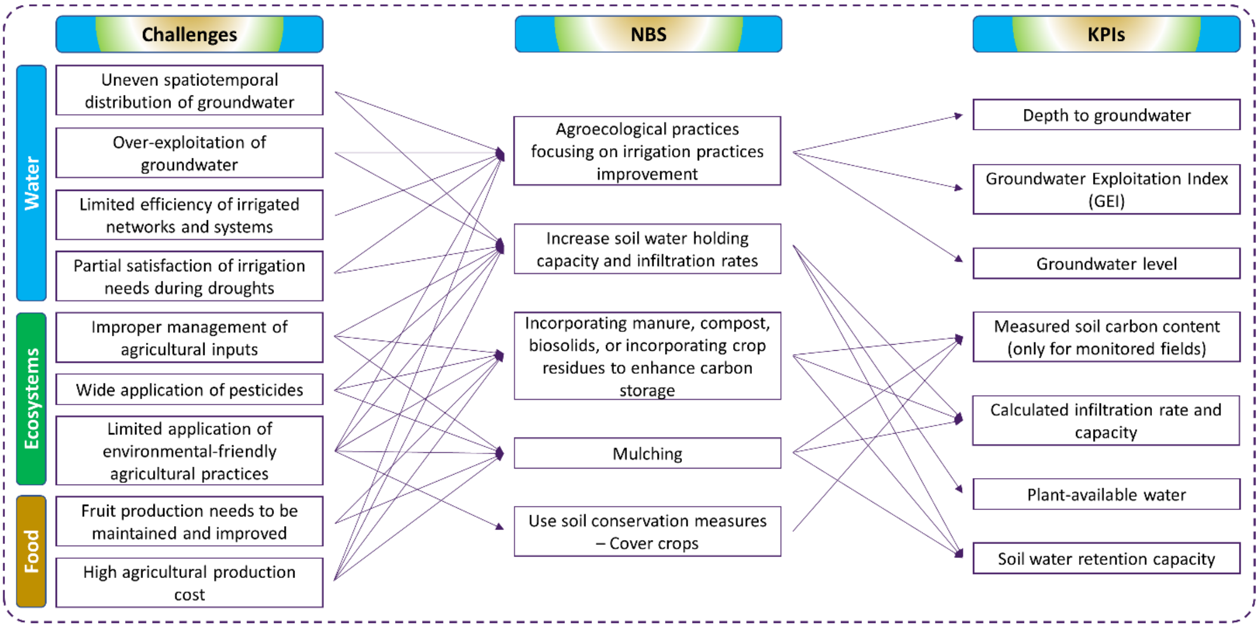


**Fig. 1.** Nexus challenges – NBS – KPIs interrelation in Agia watershed.

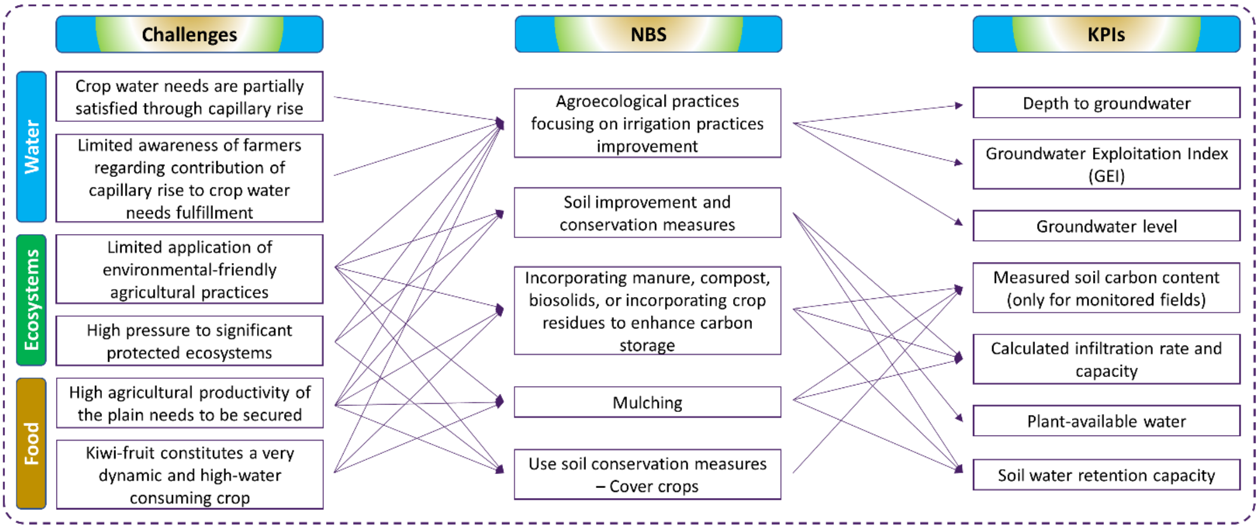


**Fig. 2.** Nexus challenges – NBS – KPIs interrelation in Pinios River Delta.

### Acknowledgements

This paper was realized in the framework of the PRIMA programme supported by the European Union. GA nº [2041] [LENSES – Learning and action alliances for Nexus environments in an uncertain future] [Call 2020 Section 1 Nexus IA].

### References

Dumitru A, Wendling L (2021). Evaluating the impact of nature-based solutions: Appendix of methods. European Commission.
Pisinaras V, Panagopoulos A, Herrmann F, Bogena HR, Doulgeris C, Ilias A, Tziritis E, Wendland F (2018) Hydrologic and geochemical research at Pinios Hydrologic Observatory: Initial results. Vadose zone journal, 17(1), 1-16.
Somarakis G, Stagakis S, Chrysoulakis N (Eds.) (2019) Thinknature Nature-Based Solutions Handbook. ThinkNature project.

# Traditional stone weirs: a green infrastructure to tackle water scarcity in small arid islands

Thanos GIANNAKAKIS[1], Nicholas M. GEORGIADIS[2], Kaloust PARAGKAMIAN[3], Ioannis NIKOLOUDAKIS[4], Nicos KARAMANES[5] Fanourios-Nikolaos SAKELLARAKIS [6]

[1] WWF Greece, Irakleio, Greece
t.giannakakis@wwf.gr

[2,6] Mediterranean Institute for Nature and Anthropos, Athens, Greece
nicosg@med-ina.org
fanikos@med-ina.org

[3,4] Hellenic Institute of Speleological Research, Irakleio, Greece
k.paragamian@gmail.com
inikoloudakis@gmail.com

[5] Paros Water Supply and Sewerage Company, Paros, Greece
nkaramanes@deya-parou.gr

## ABSTRACT

Water has always been in demand on small islands. Traditionally, island communities have used a variety of approaches to address their water shortage like small reservoirs, wells, cisterns, etc. Among the various technics, the construction of stone weirs along the riverbeds of seasonal streams were of common practice. A number of small weirs were constructed in 1300 meters of Kavouropotamos stream (Paros Island), based on existing knowledge and experience from Naxos and Kythera islands. These green infrastructures increase water percolation and enrich the aquifer and at the same time provide water for the adjacent farmlands, while also help maintain water during the dry summer period, thus creating small biodiversity oases for flora and fauna. The significance of stone weirs for biodiversity and the aquifers will be shown through a monitoring process.

## 1. Introduction

Mediterranean Basin has been pointed out as one of the climate change hotspots, and impacts are expected to be more severe than many other areas of the world (IPPC 2013). Especially islands are among the most vulnerable places while human activities and especially tourism put extra pressure on environmental assets. Specifically, water has always been in high demand, however now, water scarcity emerges as one of the most challenging topics in the area (EEA 2015). Besides humans, water shortage can also have a high toll on biodiversity, while the fact that Mediterranean islands are hotspots of global biodiversity creates also a big challenge for any conservation strategy (Vogiatzakis et al. 2016).

To address water shortage, people used to build small stone weirs along the riverbeds of seasonal streams. These “deseis” or “anavathmoi” (some of the Greek names for the weirs) were small traditional infrastructures, constructed and maintained by farmers. This technique has been gradually abandoned, however since they were applied again in Naxos (early 1990s) and in Kythera (2020), their significance has once again come up in the discussion.

The purpose of the project is to document the impact of weirs to both water scarcity and biodiversity, by constructing a number of them to a seasonal stream in Paros Island and monitoring the changes in water retention, vegetation, and species diversity.

## 2. Planning and construction phase

Kavouropotamos stream (i.e. the stream of the crabs) in Paros Island was selected for the construction of the weirs based on the following criteria: seasonality of water flow, geological data, ground inclination, proximity to existing roads, adjacent agricultural land, ability to cooperate with local citizen groups, and ability to secure data collection for the monitoring of the project.

**Fig.1.** One of the 34 weirs constructed in Kavouropotamos stream.

Initially, the specific locations of the weirs were selected and a technical study was prepared and promoted to the relevant authorities in order to acquire all necessary permits. Following, three local stone masons along with their crews were selected based on their fine ability to use traditional techniques in their stone work. On early June 2022, a ten-day construction phase was started, at the beginning of which a four-day workshop was organised. During the workshop 16 people from all over Greece were trained on stone construction by the masons and the relevant engineers and architects of the project team. In total, 34 weirs were built on a total length of 1300 meters of the stream. For the construction local materials were used while the height of the weirs never exceeded 0,5m.

## 3. Monitoring and expected results

Previous small-scale projects on the islands of Naxos and Kythera have shown significant results however, in both cases, outcomes were not monitored nor documented in a scientific way. In Paros Island, a pre and post construction monitoring system was designed, emphasizing on the impact of the stone weirs on i) the ecosystems and biodiversity of the area (flora and fauna diversity and abundance), and ii) aquifer's water level.

In regards to the biotic parameters, three field visits have already been made (Oct 2021, April & June 2022), focusing on qualitative and quantitative information for flora species and habitat types, bats, herpetofauna, and invertebrates (both terrestrial and freshwater). Information acquired from this first monitoring stage will be compared with the data collected during the three post construction field visits (Oct 2022, April & June 2023). A significant population increase of the freshwater crab *Potamon hippocrate* which is almost extinct in the area and the preservation of the Balkan Water Frog *Pelophylax kurtmuelleri* will be considered a success if achieved.

Changes in aquifer level are measured in a borehole at the boundaries of the Kavouropotamos watershed by the Water Supply and Sewerage Company of Paros. Water level measurements are also taken monthly from a private well located in close proximity to Kavouropotamos stream.

Systematically documenting the benefits of the weirs' construction in Paros Island will allow for a successful scaling up since the local and regional communities and authorities will understand the services that they provide and their importance to wildlife.

**Acknowledgements**

The authors would like to acknowledge the contribution of the Paros Water Supply and Sewerage Company, the Municipality of Paros, the interdisciplinary research collaborative "Boulouki", Paros Festival, Mr Spyros Mitrogiannis from the local NGO Archilochos, the herpetologist Vasia Spaneli, and Elena Symeonidou from the Paros Park.

**References**

EEA (2015). The European environment — state and outlook 2015: synthesis report, European Environment Agency, Copenhagen.
IPCC (2013). Climate Change 2013: The Physical Science Basis. Contribution of Working Group I to the Fifth Assessment Report of the Intergovernmental Panel on Climate Change, edited by T.F. Stocker, D. Qin, G.-K. Plattner, M. Tignor, S.K. Allen, J. Boschung, A. Nauels, Y. Xia, V. Bex and P.M. Midgley, Intergovernmental Panel on Climate Change, Cambridge University Press, Cambridge, United Kingdom and New York, NY, USA.
Vogiatzakis IN, Mannion AM, Sarris D (2016) Mediterranean island biodiversity and climate change: the last 10,000 years and the future. Biodivers Conserv, 25, 2597–2627

# Smart Blue Green roofs of Amsterdam: how drought-proof are they?

Leon KAPETAS[1], Marc van GEMERT[2], Friso KLAPWIJK[3], Kasper SPAAN[4]

[1] Urban Innovative Actions, Belgium
[2] City of Amsterdam, Netherlands
[3] Metropolder, Netherlands
[4] Waternet, Netherlands

Email[1]: leonkapetas@gmail.com
Email[2]: m.van.gemert@amsterdam.nl
Email[3]: friso@metropolder.com
Email[4]: Kasper.Spaan@waternet.nl

ABSTRACT

In recent years, cities have been exploring and experimenting with a diversity of Nature-based Solutions to address a series of climate/weather related challenges. Underutilized roofs spaces have offered a good opportunity for greening with good examples from across the world. One of the most distinguished roof technologies have been smart Blue-Green roofs which make a significant contribution to flood management, heat mitigation and urban biodiversity. Amsterdam has recently completed the RESILIO program, with more than 10,000 square meters of such roofs developed in social housing and private buildings. This project funded by Urban Innovative Actions (the innovation arm of the European Regional Development Fund) demonstrated the climate co-benefits of the approach through extensive experimental monitoring work. The next step in the process is to make these innovative roofs standard practice; for this, decision makers will need to be sure of the roof's ability to withstand droughts in the new contexts of implementation. This is critical for upscaling further within the city and for transferr ing the approach to other European cities.

## 1. Introduction

Several cities around the world are experiencing the impacts of climate change, including flash floods, higher temperatures, and an increasing drought frequency. Nature-based urban adaptation approaches have been proposed as effective adaptation measures (European Commission, 2021), yet they require extensive testing and evaluation before they can be up-scaled within a city or transferred to other cities. In this context, Amsterdam is experimenting with smart Blue-Green Roofs (BGRs), i.e. explores ways to maximize the adaptation potential of otherwise underutilized roof spaces.

## 2. Approach

While BGRs have been recently implemented in the Netherlands, the approach followed in the RESILIO project goes a (significant) step further: the smart grid of roofs enables real time data exchange for dynamic water level control across multiple roofs. The blue layer underlying a roof can be controlled when to retain and when to release water ahead of a rainfall event. In forecasted large events, roofs will empty to increase storage capacity and reduce pressure to the sewer system. However, during smaller events, certain roofs can hold water which will be taken up later by the roof green just above through a capillary system. This is the first intercommunicating adaptive water management system of such type worldwide. Figure 1 shows schematically how a smart BG roof is designed.

Beyond flood control and greening, BGRs offer thermal insulation to the building, thus contributing to the mitigation of the urban heat island effect (up to three degrees of temperature reduction), but are also designed for the delivery of ecological and amenity benefits.

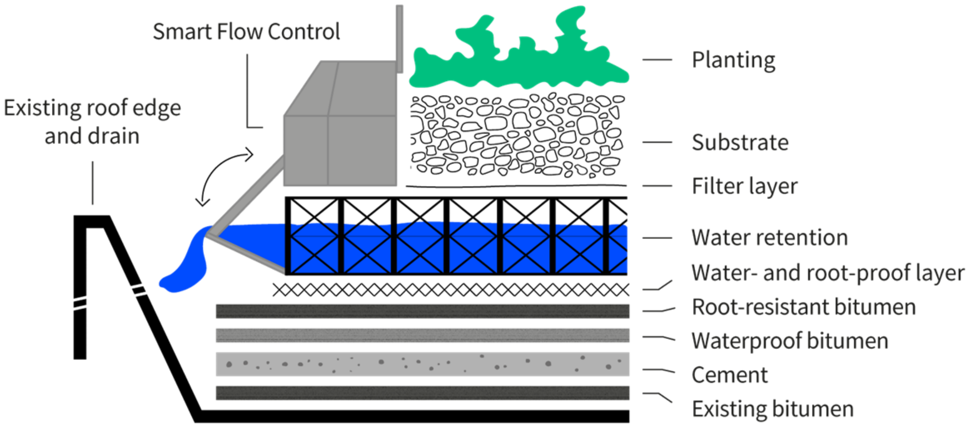


**Fig 1.** Conceptual cross-section of a smart Blue Green roof (“RESILIO project,” 2022)

## 3. Results and Discussion

While BGRs contribute to climate resilience of cities and buildings, the limits of their own resilience need to be explored. How well can they provide their services during droughts? How to best manage them when droughts are predicted? What greening options are most suitable to withstand droughts and how well do BGRs perform in other climatic zones? This are critical questions to answer before upscaling and transferring the technology. First results indicate that the intermittency of rainfall events as well as their intensity will largely dictate how full/empty roofs are found. By extension, this will dictate the type of vegetation cover selection, along with maintenance considerations. Figure 2 shows alternative vegetation options – choices that will depend on cost, water saving concerns and landscaping aspirations. Careful co-design with the user community, hydrology and ecology experts, and maintenance teams is recommended.


Fig 2. Example cross sections showing the different layers of three types of green roofs – different water demands in each case (source: Eva Drukker, Wageningen University & Research) (City of Amsterdam, Waternet, MetroPolder et al., 2022)

**Acknowledgements**

The authors wish to thank the Urban Innovative Actions for co-funding this project under the Theme on Climate Adaptation (2019-2022).

**References**

City of Amsterdam, Waternet, MetroPolder, Company, Rooftop Revolution, Amsterdam University of Applied Sciences, (AUAS), Vrije Universiteit Amsterdam (VU), Stadgenoot, de Alliantie and Lieven, de Key., 2022. RESILIO Final report: a roof journey. Amsterdam.
European Commission, 2021. Evaluating the Impact of Nature-based Solutions: Appendix of Methods. Luxenburg.
RESILIO project [WWW Document], 2022. URL https://resilio.amsterdam/en/smart-blue-green-roofs/

# Advanced numerical modelling of large debris impact on piers during extreme flood events

Denis ISTRATI[1], Anis HASANPOUR[2]

[1,2] University of Nevada, Reno, United States
email: distrati@unr.edu
email: hasanpour@nevada.unr.edu

ABSTRACT

Given the exposure of riverine bridges to more intense and frequent flooding events and the observed large floating debris (e.g. vehicles) in recent floods, this study presents a numerical investigation of the debris-flow-structure interaction and associated loads. A multi-physics sophisticated modeling approach is used, in which a dam break-induced flow is simulated via particles, the debris and bridge via continuum elements, and the interaction of the different domains via penalty-based contacts. The preliminary results reveal that the large debris exerts on piers impulsive loads that are 6 to 10 times larger than the fluid forces, which highlights the need to (i) consider such scenarios in the design and risk assessment of riverine bridges, and (ii) develop appropriate mitigation strategies in order to improve the resilience of transportation networks.

## 1. Introduction

Bridges play a critical role in the economic prosperity of communities as components of transportation networks. However, oftentimes they are exposed to water hazards and extreme flooding events that jeopardize their integrity. For example, the failure of the Spencer Creek Dam in Nebraska in 2019 after heavy rains, generated extreme flows downstream that led to the washout of several riverine bridges due to large hydraulic loads. In addition to the fluid loads, past studies demonstrated that bridges are exposed to debris loads from accumulated logs (Parola et al, 2020), increasing further their vulnerability. Moreover, recent work in other relevant fields, e.g. tsunami inundation, demonstrated the critical effect of large floating debris, such as, containers, for coastal bridges (Istrati et al., 2020). Given the fact that in recent floods in Germany many vehicles and other large objects were seen floating and taken away by the extreme flows, which could indicate a potential impact on downstream structures, the objective of this study is to conduct a preliminary assessment of large debris effects on riverine bridges exposed to extreme flood events via advanced numerical modeling.

## 2. Multi-physics Numerical Model

Investigating numerically the effects of large debris on structures particularly during dam break-induced extreme flows is quite challenging due to (i) the transient flow and formation of a turbulent bore right after the dam, (ii) the nonlinear debris-fluid interaction with large displacements during the floating phase, (iii) the complex contact between the debris, the flow and the bridge, and (iv) the dynamic response of the structure. To overcome these challenges the authors used a multi-physics modeling approach, in which the fluid is simulated via the Smoothed Particle Hydrodynamics Method (SPH), while the debris, the bridge and the channel are simulated via the Finite Element Method (FEM), as shown in Fig. 1.

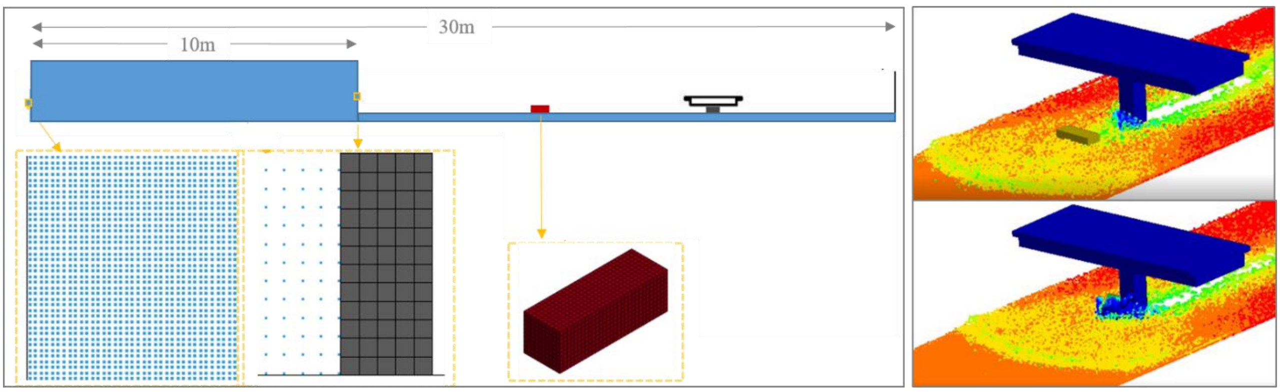


**Fig. 1.** Sketch of numerical flume and SPH-FEM parts (left) and selected snapshots of the debris impact process on the bridge pier (right)

The fact that both the fluid and the structural parts are represented via Lagrangian methods enables the simulation of the interaction of the different parts via penalty-based nodes-to-surface contacts (fluid-to-solid) and surface-to-surface contacts (solid-to-solid). More information about the modeling approach can be found in Hasanpour et al. (2021). This approach is first validated against the experimental data of Shafiei (2016), which simulated the three-dimensional impact of a disc and a container on a square prism 0.3m wide and 0.6m tall, corresponding approximately to a 1:20$^{th}$ scale of real-life dimensions. In those experiments the extreme flow was generated via a dam break mechanism, i.e. sudden opening of a reservoir gate. Furthermore, the flume was 14m long, 1.2m wide and 0.8m deep and the reservoir was 11m x 7.3 x 0.6m, and the authors investigated only dry conditions (water depth d=0 at bridge location), which means that the debris was resting on the ground before the opening of the gate. Following the successful validation of the SPH-FEM approach, the numerical tank was increased in length in order to increase the volume of water in the reservoir and enable the investigation of wet conditions (d>0) without the boundary conditions at the outlet to affect the results. In this new parametric investigation, the disc debris was replaced by a simplified rectangular box with scaled-down dimensions (length, width, height) and weight of a vehicle, while the structure was a box-girder bridge superstructure (1.2m x 0.5m x 0.1m) supported on a square pier 0.2m wide with a variable height in order to compare different scenarios. The reservoir level was between 0.4m and 0.6m, which at full-scale corresponded to the upper limit of a 'small dam' according to the classification of the US Army Corps of Engineers (USACE, 1979). The final numerical model had a 1cm particle and mesh size and had 3.7million elements.

## 3. Results and Discussion

Figure 2 presents numerically predicted time histories of the debris displacement and velocity, and, the total forces on the pier. These preliminary results give an insight into the debris movement and debris-flow-pier interaction. For example, it can be observed that in the case of no initial water at the pier location (d=0), the flood-borne debris accelerates faster and reaches larger impact velocities than the cases with an initial water depth (d>0), making the former a more critical scenario for the safety of the bridge. Moreover, in the latter cases the debris seems to slow down before the impact on the pier, which could be potentially attributed to the larger amount of water that is 'trapped' between the debris and the pier and the reflection of this water on the pier. Irrespective of the flow conditions, the most important finding of the study is that the large debris generates impulsive impact loads on piers that are about 6 to 10 times larger than the fluid forces. Interestingly, for the cases with an initial flow height (d>0), multiple impulsive peaks can occur since the debris tends to remain in front of the pier for a longer duration, however, further investigation is required in order to decipher this complex phenomenon preferably with numerical models at full-scale. Last but not least, the study proves the feasibility of assessing the debris risk for bridges via a coupled SPH-FEM modeling approach.

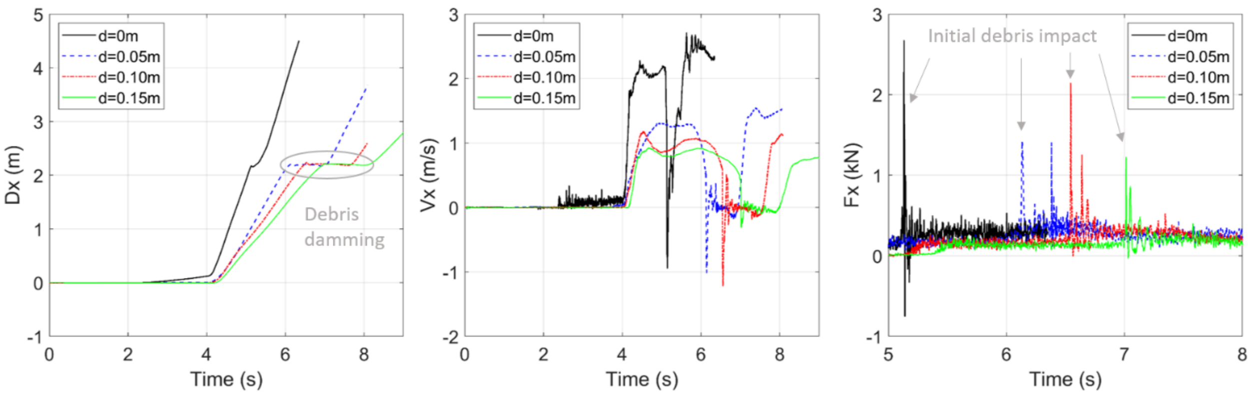


**Fig. 2.** Time histories of the debris horizontal displacement and velocity, and the total forces on the bridge pier

**Acknowledgements**

The authors acknowledge the Engineering Computing Team at the University of Nevada, Reno for providing computational support and resources that have contributed to the research results reported within this paper.

**References**

Hasanpour A, Istrati D, Buckle IG (2021) Coupled SPH–FEM Modeling of Tsunami-Borne Large Debris Flow and Impact on Coastal Structures. Journal of Marine Science and Engineering, 9(10), 1068.
Istrati D, Hasanpour A, Buckle IG (2020) Numerical investigation of tsunami-borne debris damming loads on a coastal bridge", 17th World Conf Earthq Eng, Sept. 27 – Oct. 2, 2021, Sendai, Japan
Parola AC, Apelt CJ, Jempson MA (2000) Debris forces on highway bridges (No. 445). Transportation Research Board.
Shafiei A (2016). Tsunami Inland Structures Interaction and Impact of Floating Debris, Doctoral dissertation, University of Auckland
USACE (1979). Recommended guidelines for safety inspection of dams, ER 1110-2-106 26, Sept 1979

# An Integrated Hydrologic/Hydraulic Analysis of the Medicane "Ianos" Flood Event in Kalentzis River Basin, Greece

Lampros VASILIADES[1], Evangelia FARSIROTOU[2], Aris PSILOVIKOS[3]

[1] Department of Civil Engineering, University of Thessaly, Pedion Areos, 38334 Volos, Greece
email: lvassil@civ.uth.gr

[2,3] Department of Ichthyology & Aquatic Environment, University of Thessaly, Fytoko Str., 38446 Volos, Greece
email: efars@uth.gr
email: psiloviko@uth.gr

ABSTRACT

The flood event that occurred on September 18th 2020 in Kalentzis river basin due to the Medicane "Ianos", is reproduced using an integrated hydrologic/hydraulic modelling framework to simulate the flood hydrograph and the flood extent in the greater area of Karditsa city. Extreme rainfall amounts observed in the mountainous and lowland areas, with estimated return periods of 1000 and 200 years, respectively, for rain duration of 24 hours, are used to estimate areal precipitation at 15-min time interval at subwatershed level. Using the HEC-HMS software and the Natural Resources Conservation Service (NRCS), Unit Hydrograph procedure simulated flood hydrographs, at important tributaries junctions, which were then applied in HEC-RAS 2D model for flood routing and estimation of flood attributes (i.e., water depths and flow velocities), as well as mapping of inundated areas.

## 1. Introduction

Mediterranean Hurricanes or "Medicanes", also known as tropical-like cyclones (TLCs), are extreme cyclonic windstorms morphologically and physically similar to tropical cyclones occurring in the Mediterranean Sea. Medicanes pose serious threats to human life and infrastructure, such as heavy rainfall and flooding, intense wind, lightning, tornadoes, high waves and storm surge (Romero & Emanuel, 2013). On September 17-20 2020 Medicane "Ianos" impacted Greece and had caused significant wind damage, and precipitation related impacts that resulted in four fatalities and extended infrastructure damages and landslides in the Ionian Islands and in Central Greece (Lagouvardos et al., 2021). The objective of this study is to model and reconstruct the flood event caused by Medicane "Ianos" in Kalentzis River basin (with total basin area of 654 km$^2$), using a CN-based unit hydrograph rainfall-runoff model and a 2D hydraulic/hydrodynamic model for flood routing and hazard mapping.

## 2. Methodology and Results

A combined hydrological and hydraulic–hydrodynamic modelling approach is applied for flood inundation modelling and mapping at Kalentzis ungauged watershed. Figure 1 shows the study area with the important tributaries (Gavras, Karampalis, Kalentzis and Lipsimos rivers) with the selected discretization modelling scheme that includes 16 subwatersheds, six reaches and seven junctions. Rainfall data of five meteorological stations in the wider area at 15-min intervals are used to represent the spatiotemporal rainfall distribution of "Ianos" event and to estimate areal rainfall at subwatershed level. The hydrological approach is based on semi-distributed modelling (at sub-watershed scale) of the rainfall-runoff process using the HEC-HMS software and the SCS-CN method for extracting the excess from the gross rainfall, and the unit hydrograph theory, for propagating the surface runoff to the subbasin outlets (further details of the methodology could be found in Papaioannou et al. 2018). Finally, the hydrographs derived from the hydrological model were used as inputs in the 2D HEC-RAS hydrodynamic model for flood inundation modelling and mapping. The DEM provided by the Greek National Cadaster and Mapping Agency S.A. (NCMA) with a resolution of 5.0 m was used and mapping results and all examined reaches were modelled with flexible mesh sizes (ranging from 9.10 – 900 m$^2$), roughness coefficient values based on CORINE land cover data (Büttner et al., 2017) and a computation interval of 2.0 s.

Conventional and non-conventional flood data and impact records of the extreme flash-flood event that occurred on September 18th 2020 were used for the comparison of the simulated flood extent of the "Ianos" Medicane in the greater area of Karditsa city. Figure 2 illustrates the maximum water depths and velocities and the estimated flood extent resulting from the rainfall-runoff and the hydrodynamic flood routing modelling processes. It is interesting to note that the simulated flood extent of Fig. 2 (estimated about 236 $km^2$) is in close agreement with the observed flooded area estimated from Sentinel images by the Copernicus Emergency Management Service (EMSR465: Floods in Thessaly Region, Greece). Hence, the modelling procedure of this study could be expanded in a methodological framework to support flood hazard mitigation policies in the study area.

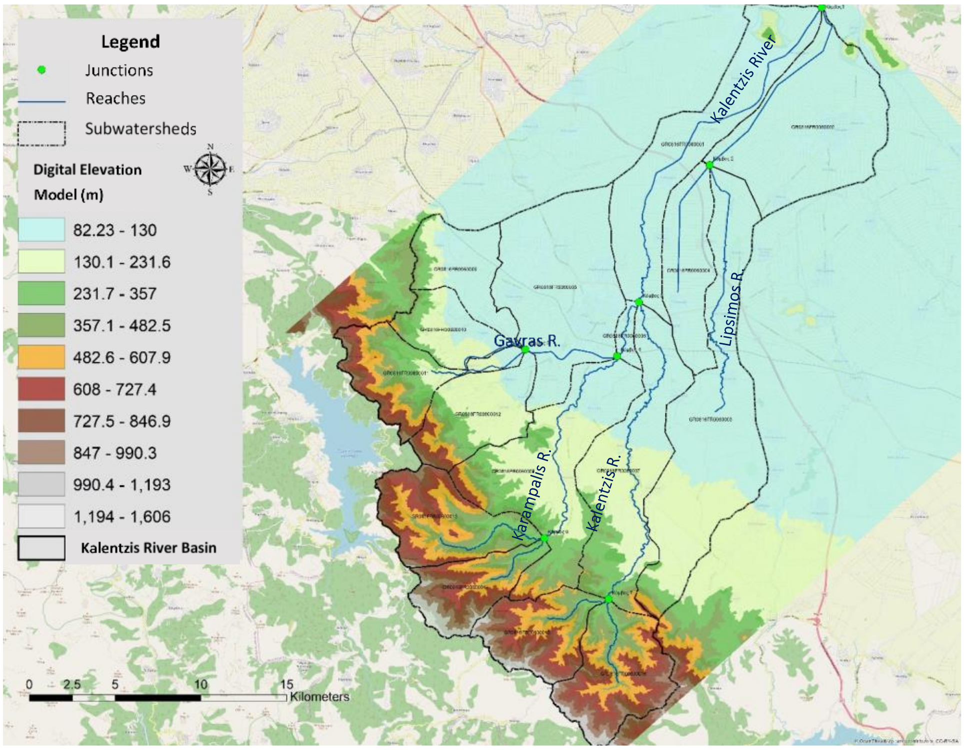


**Fig. 1.** Kalentzis River basin with employed modelling components (selected sub-watersheds, stream reaches, junctions for flood inundation modelling and mapping).

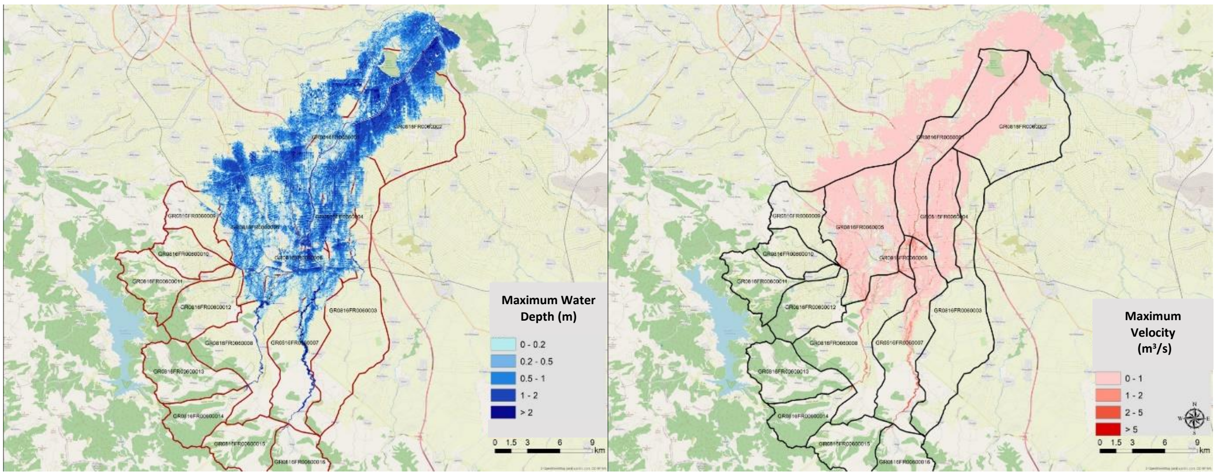


**Fig. 2.** Simulated flood extent and maximum water depths and velocities in Kalentzis River basin.

## References

Büttner G, Kosztra B, Soukup T, Sousa A, Langanke T (2017) CLC2018 Technical Guidelines. Final Service Contract No 3436/R0-Copernicus/EEA 56665.
Lagouvardos K, Karagiannidis A, Dafis S, Kalimeris A, Kotroni V (2021) Ianos – A hurricane in the Mediterranean, Bull. Amer. Meteor. Soc., https://doi.org/10.1175/BAMS-D-20-0274.1 .
Papaioannou G, Efstratiadis A, Vasiliades L, Loukas A, Papalexiou SM, Koukouvinos A, Tsoukalas I, Kossieris P (2018). An operational method for Flood Directive implementation in ungauged urban areas, Hydrology, 5(2), 24, https://doi.org/10.3390/hydrology5020024 .
Romero R, Emanuel K (2013) Medicane risk in a changing climate, J. Geophys. Res. Atmos., 118, 5992-6001, doi:10.1002/jgrd.50475.
Vasiliades L, Farsirotou E, Psilovikos A (2021) Technical Report for the Flooding Phenomenon in the area of Karditsa on the 18th of September 2020. Deliverables I – II & Appendices I – IV. Fire Department of Karditsa, Greece, March 2021.

# 3D flood flow predictions in large-scale rivers using data-driven physics-informed machine learning algorithms

Zexia ZHANG[1], Fotis SOTIROPOULOS[2], Ali KHOSRONEJAD[3]

[1,3] Civil Engineering Department, Stony Brook University, USA
[2] Mechanical and Nuclear Engineering, Virginia Commonwealth University, USA
email: zexia.zhang@stonybrook.edu
email: sotiropoulosf@vcu.edu
email: ali.khosronejad@stonybrook.edu

ABSTRACT

To overcome the high computational cost of high-fidelity models, we developed autoencoder convolutional neural networks (CNNs) algorithms to reconstruct the first- and second-order statistics of turbulent flood flow in large-scale rivers. The training dataset for construction of the CNN models is obtained from large-eddy simulation (LES) results of the flood flow in a large-scale meandering river with several piers foundations. The developed CNNs are validated using separately done LESs of meandering rivers with different piers foundation configurations. The results show good agreement between the LES and CNNs predictions while the CNNs are several orders of magnitude computationally more efficient than LES.

## 1. Introduction

Extreme flood flows could excessively erode the foundation of infrastrustures installed in the tream and cause disastrous hazards. The turbulence statistics such as time-averaged velocity and Reynolds stresses are crucial in the analysis of flood flow dynamics and sediment transport (Khosronejad et al., 2020). However, obtaining the high-fidelity flow field data of the turbulence statistics using numerical simulations is computationally expensive due to the large computational domain size and long sampling time. Therefore, in this study, we examined the potential of the convolutional neural network (CNN) in the reconstruction of the turbulence statistics from instantaneous flow field data. The results show the CNN predictions have a good agreement with the large eddy simulation (LES) results while the computational cost of the CNN model was only a small fraction of the LES.

## 2. Methodology

### 2.1. Study cases

To examine the performance of autoencoder CNNs in predicting turbulence statistics of flood flow, turbulent flow past wall-mounted bridge piers in three test cases are considered, as shown in Fig. 1. The rivers are 2110 m (River 1) and 2740 m (River 2) in length, 100 m in width, and 3.3 m in depth. Virtual cylindrical bridge piers are 2 m in diameter and installed 25 m apart (River 1) and 33 m apart (River 2) at the apex of the river bends. Flows are from left to right. Turbulent flow field data are calculated using the in-house LES code (Khosronejad and Sotiropoulos, 2020).

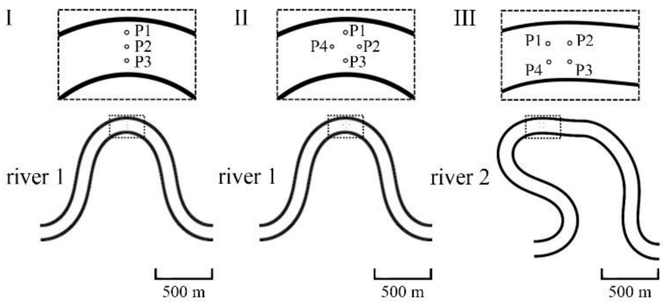


**Fig. 1.** Schematic of planforms of the virtual meandering rivers used for the training and validation of CNNs. Case I is the training case. Case II and III are validation cases.

### 2.2. Convolutional neural networks model

The autoencoder CNN model composed of six convolutional layers was used to reconstruct the test cases' 3D flood flow turbulence statistics. The inputs include snapshots of the velocity components in the instantaneous flow field generated by LES. The output is the time-averaged flow field, which includes time-averaged velocity, Reynolds stresses, and turbulent kinetic energy. The CNN is trained using ten instantaneous flow fields of test case I at different time steps, and using 2000 epochs to converge. Then the trained model is validated using cases II and III.

## 3. Results and discussion

The error between CNN predictions and LES results of test cases II and III are assessed using the mean absolute error (MAE) and the mean absolute relative error (MARE). Table 1 shows the two statistical error indices of the first- and second-order statistic results. $\bar{u}$, $\bar{v}$, and $\bar{w}$ are time-averaged velocity components in streamwise, spanwise, and vertical directions, respectively. $U_b$ is the bulk velocity of the flood flow. *tke* is the turbulent kinetic energy. The MAEs indicate that the CNN predictions have high accuracy in all the statistical properties, although the MARE of $\bar{w}$ / $U_b$ is relatively large because the vertical component has an infinitesimal absolute value. The *tke* contours and profiles shown in Fig. 2 indicate that the CNN has a better performance on captureing the wake structures than the Reynolds-averaged Navier-Stokes (RANS) model.

**Table 1.** Statistical error indices for the turbulence statistics in the validation cases river 1 and 2.

| River 1 | MAE | MARE | River 2 | MAE | MARE |
|---|---|---|---|---|---|
| $\bar{u}$ / $U_b$ | 0.019 | 0.047 | $\bar{u}$ / $U_b$ | 0.019 | 0.2851 |
| $\bar{v}$ / $U_b$ | 0.026 | 0.247 | $\bar{v}$ / $U_b$ | 0.027 | 0.3623 |
| $\bar{w}$ / $U_b$ | 0.004 | 72.277 | $\bar{w}$ / $U_b$ | 0.004 | 41.956 |
| *tke* / $U_b^2$ | $4.03\times10^{-4}$ | 0.0867 | *tke* / $U_b^2$ | $6.80\times10^{-4}$ | 0.1486 |

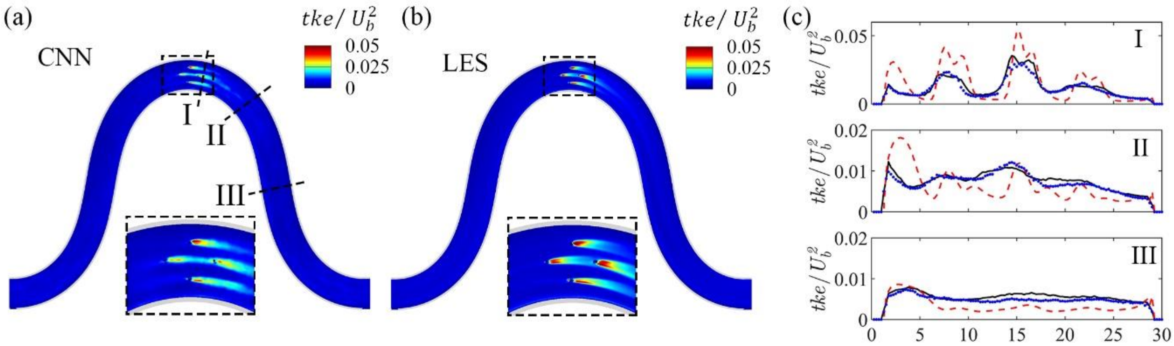


**Fig. 2.** CNN and LES computed *tke* result of validation case II. (a) and (b) shows the contours of CNN predicted and LES calculated *tke* normalized with the square of bulk velicity at the free surface from the top view. (c) shows the profiles of CNN predicted (blue dots), LES calculated (black solid line), and RANS computation (red dashd line) normalized *tke* along the three spanwise lines of I, II, and III in (a).

In addition, the computational cost of the CNN approach for generating the turbulence statistics was 0.5 CPU hours. Including the 150 CPU hours of calculating the instantaneous flow fields as the inputs, the total cost of the CNN approach is still one order of magnitude smaller than that of LES, i.e., ~2500 CPU hours.

## 4. Conclusions

An autoencoder CNN algorithm is developed to predict the first- and second-order turbulence statistics of flood flow in large meandering rivers. The results show a good agreement with the LES results, while the computational cost is only a small fraction of LES.

**Acknowledgments**

This work was supported by the National Science Foundation (grants EAR-0120914 and EAR-1823530). The computational resources were provided by the Civil Engineering Department, Stony Brook Research Computing and Cyberinfrastructure, and the Institute for Advanced Computational Science at Stony Brook University.

**References**

Khosronejad A, Flora K, Zhang Z, Kang S (2020) Large-eddy simulation of flash flood propagation and sediment transport in a dry-bed desert stream. International Journal of Sediment Research, 35(6), 576-586.
Khosronejad A, Sotiropoulos F (2020) A short note on the simulation of turbulent stratified flow and mobile bed interaction using the continuum coupled flow and morphodynamics model. Environmental Fluid Mechanics, 20(6), 1511-1525.
Zhang Z, Flora K, Kang S, Limaye AB, Khosronejad A (2022) Data-driven prediction of turbulent flow statistics past bridge piers in large-scale rivers using convolutional neural networks. Water Resources Research, e2021WR030163.

# Microscopic simulation of human response dynamics during a flood-induced evacuation from a football stadium

Mohammad SHIRVANI[1], Georges KESSERWANI[2]

[1, 2] Department of Civil and Structural Engineering, University of Sheffield, UK
email: mshirvani1@sheffield.ac.uk
email: g.kesserwani@sheffield.ac.uk

ABSTRACT

Agent-Based Modelling (ABM) is an increasingly used approach for characterisation of human behaviour in evacuation simulation modelling. ABM-based evacuation models used in flood emergency are developed mostly for vehicular scenarios at regional scale. Only a few models exist for simulating evacuations of on-foot pedestrians responding to floods in small and congested urban areas. These models do not include the heterogeneity and variability of individuals' behaviour influenced by their dynamic interactions with the floodwater properties. The flood-pedestrian simulator is an evacuation modelling framework which was developed to simulate the two-way interactions across and between local floodwater flow and heterogeneous pedestrian movements. It enables microscopic analysis of flood-risk to evacuating people at an individual level in both space and time. This article represents the application of the simulator for a real-world case study of a mass evacuation from a football stadium in response to a flood emergency.

## 1. Overview of flood-pedestrian simulator

The present simulator integrates a hydrodynamic model into a pedestrian model in a single agent-based modelling environment, called FLAMEGPU, where both the models are spatially and temporally synchronised and run simultaneously (Shirvani et al., 2021a). The selected hydrodynamic model is formulated based on the mathematical description of water flows using the solution of Shallow Water Equations (SWE) on a numerical grid. The pedestrian model on FLAME GPU is programmed based on the formulation of a social force model for people's dynamics including their movement patterns and their interaction with each other and their surrounding environment. The dynamic interactions between the flood and pedestrians have been formulated based on a number of behavioural rules driving the mobility states and way-finding decisions of individuals in and around the floodwaters as well as the local changes in the floodwater properties as a result of pedestrians' crowding. The simulator incorporates a high level of heterogeneity in population characterisation and realistic behavioural rules extracted from a large number of stochastic datasets, such as (i) age, gender, body height and mass distribution of a subject population; (ii) age- and gender-related variable moving speeds of individuals in both dry and flooded zones based on real-world datasets and experimental information; and (iii) autonomous decision making of individuals in choosing one of multiple emergency exit destinations influenced based on their personal perception of the risk from the floodwater or by the most popular destination selected by others (Shirvani et al., 2021b).

## 2. Hillsborough stadium case study

The case study consists of a site including an area of 16,384 $m^2$ that is adjacent to the eastern side of the Hillsborough football stadium in Sheffield which is framed with a dark red square in Fig. 1. The stadium main entrances (yellow line, Fig. 1) are opened to a T-junction that constitutes the walkable area including the main roads, main stadium's entrances, and pedestrian pathways to usual destinations to the south, east and north that are shown with the green lines.

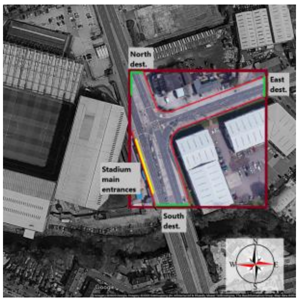


**Fig 1.** The study site (red square) including the walkable area (red area within the red square) with different destinations located in the south, east and north sides of the walkable area (green lines) and the stadium's main entrances (yellow line), © Google.

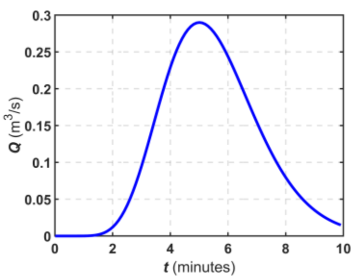


**Fig. 2.** Inflow hydrograph used to generate the floodwater propagation occurring from the north-east side of the site.

### 2.1. Scenario description and simulation configuration

The evacuation scenario consist of the site hit by a flood during a football match where 4,080 spectators are caught unaware of the rainfall accumulation around the stadium. The floodwater accumulates from the north and east sides to move downhill towards the main entrance of the stadium. The flooding flow was generated by formulating an inflow hydrograph based on the November 2019's rainfall volume accumulation of 1,045.3 $m^3$ and a 0.0638 m rainfall over the entire 16,384 $m^2$ site (Fig. 2). Once the floodwater has reached the stadium's main entrances people start to evacuate the stadium immediately. A dispatch measure was considered to control the influx rate of evacuees entering the walkable area during the flooding. Three thresholds of floodwater depth to the body height were selected at which point pedestrians divert their moving direction to a safer destination. This was done to account for the uncertainty associated with individuals' different risk perception, where 20 %, 30 % and 40 % thresholds represent people with high-risk, medium-risk and low-risk perception, respectively.

### 2.2. Results and discussion

A series of 20 simulation runs was performed for each of the 20 %, 30 % and 40 % threshold. Outputs averaged from each series of simulation included spatial information of pedestrians and their stability state as they evacuated. Considering the stochastic uncertainties associated with the motion of the pedestrians, the plausibility of the averaged outputs from the 20 runs was evaluated by considering the maximum Margin of Error (MOE) in the simulation outputs as outlined in Table 1. It can be seen that the maximum MOE increases as the risk perception level decreases, suggesting a notable increase in the uncertainty as the risk perception component is incorporated into the modelling of pedestrian behaviour.

**Table1.** Maximum margin of error (MOE) for the average number of pedestrian agents with different stability states that are extracted from the recorded outputs throughout the simulations for each 20 %, 30 % and 40 % threshold.

| Stability states | Maximum *MOE* | | |
|---|---|---|---|
| | 20 % threshold | 30 % threshold | 40 % threshold |
| Toppling-only | ± 2 | ± 5 | ± 13 |
| Toppling-and-sliding | ± 1 | ± 4 | ± 7 |

Figure 3 shows the two-dimensional spatial distribution of the evacuating pedestrians over the flood map based on the UK Environment Agency's Hazard Rating (HR) at 25 min when pedestrian presence in the walkable area seemed to be at its highest. The pedestrians are represented by dots with different colours representing their stability state based on the predictions made with the 20 %, 30 % and 40 % thresholds.

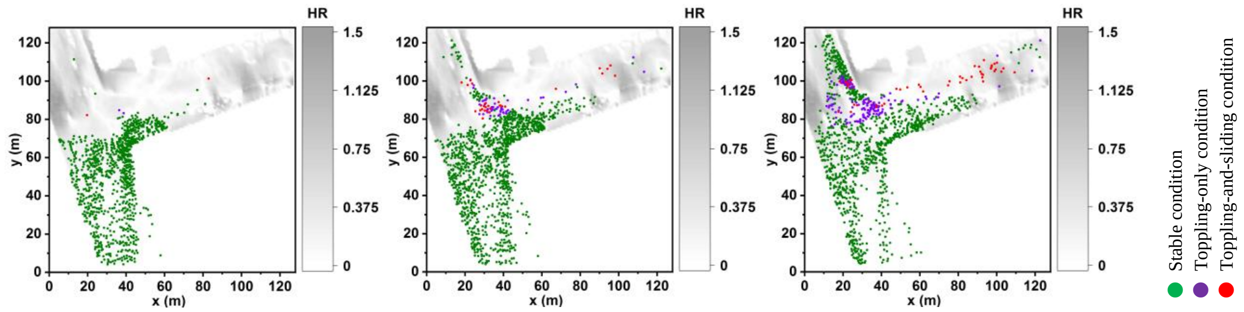


**(a)** 20 % threshold **(b)** 30 % threshold **(c)** 40 % threshold

**Fig. 3.** The spatial distribution of pedestrians over the walkable area at 22 min simulation time under the predicted stability states (coloured dots) along with the HR flood map (grey shade).

The analysis in Fig. 3 suggests that pedestrians that avoid entering a floodwater depth beyond 30 % of their body height are most likely to select the south destination, where their condition remains stable to keep evacuating with minimum risk of immobilisation. Those with a tendency to enter deeper floodwaters would go to the east or north destinations, towards which the majority would still be able to evacuate. Overall, the predictions produced by the simulator seem useful in planning evacuation in outdoor spaces where the pedestrians' choices could be influenced by their autonomous decision making on the safest destination.

**Acknowledgements**
This work is part of the SEAMLESS-WAVE project (visit https://www.seamlesswave.com for more information).

**References**

Shirvani, M., Kesserwani, G., Richmond, P. (2021a) Agent-based simulator of dynamic flood-people interactions, Journal of Flood Risk Management, 14(2), e12695.
Shirvani, M., Kesserwani, G. (2021b) Flood–pedestrian simulator for modelling human response dynamics during flood-induced evacuation: Hillsborough stadium case study, Natural Hazards and Earth System Sciences, 21(10), 3175-3198.

# Bayesian coupling of hydrological models for simulation of extreme flood events

Evangelos ROZOS[1], Panayiotis DIMITRIADIS[2]

[1] Institute for Environmental Research & Sustainable Development, National Observatory of Athens, 15236 Athens Greece
email: erozos@noa.gr

[2] Department of Water Resources and Environmental Engineering, School of Civil Engineering, National Technical University of Athens, 15780 Athens, Greece
email: pandim@itia.ntua.gr

ABSTRACT

In this study, we are suggesting a simple methodology based on Bayesian inference to couple either the results of a single hydrological model with various objective functions or the results of multiple hydrological models in order to improve the reliability of the prediction of alarming events. The methodology was tested in a case study with data of limited length, and the results were encouraging.

## 1. Introduction

The technological advances in computer science have allowed hydrologists to explore new paths to improve the performance of their models. For example, various researchers have combined machine learning methods with standard models to achieve more accurate simulations of river flows (e.g., Noymanee and Theeramunkong, 2019; Senent-Aparicio et al., 2019; Yang et al., 2020, Rozos et al., 2021, etc.). These approaches have been proven valuable in cases where the observation time series has a significant length to include a sufficient number and variety of response patterns of the system. Unfortunately, this is not the typical case. For example, suppose a case study in which a hydrological model is employed by a flood-warning system. If machine learning is used to improve the performance, but the streamflow is observed for, say, less than a year, then the machine learning could deteriorate the performance due to a potential overfitting effect. In this study, we are suggesting an alternative methodology to improve the performance of a hydrological model being intended for flood-warning systems. We employ two objective functions for the model calibration, and then we employ a Bayesian coupling of the two simulations obtained by the independently calibrated models.

## 2. Materials and methods

In this study, we have used LRHM (Rozos, 2020), a conceptual hydrological model that employs two simple model-building blocks (direct runoff and soil moisture model) that are linearly combined to simulate the observed runoff (an idea related to the genetic programming model building; see Herath et al., 2021). LRHM was trained independently with two objective functions, the Nash–Sutcliffe efficiency, and the maximum absolute error between simulated and observed time series. The first objective function results in a more balanced fit, whereas the latter gives more emphasis on the deviations of high flows. In order to estimate the probability of exceeding the alarm threshold $\theta$ at time step $t$, Bayesian inference is used:

$$\mathrm{P}(q_t > \theta \mid \mathrm{QNSE}_t > \theta) = \mathrm{P}(\mathrm{QNSE} > \theta \mid q > \theta) \times \mathrm{P}(q > \theta) \,/\, \mathrm{P}(\mathrm{QNSE} > \theta) \quad (1)$$

$$\mathrm{P}(q_t > \theta \mid \mathrm{QMAX}_t > \theta) = \mathrm{P}(\mathrm{QMAX} > \theta \mid q > \theta) \times \mathrm{P}(q > \theta) \,/\, \mathrm{P}(\mathrm{QMAX} > \theta) \quad (2)$$

where $q_t$ is the observed discharge at time step $t$, $\mathrm{QNSE}_t$ and $\mathrm{QMAX}_t$ are the simulated flows at time step $t$ with the model calibrated with the NSE objective function and the model calibrated with the maximum absolute error objective function respectively, $\mathrm{P}(q>\theta)$ is the frequency the observed discharge exceeds $\theta$ in the calibration period, $\mathrm{P}(\mathrm{QNSE}>\theta)$ and $\mathrm{P}(\mathrm{QMAX}>\theta)$ are the frequencies the simulations of the two models exceed $\theta$ in the calibration period, $\mathrm{P}(\mathrm{QNSE}>\theta \mid q>\theta)$ and $\mathrm{P}(\mathrm{QMAX}>\theta \mid q>\theta)$ are the frequencies the two models correctly simulated an exceedance of $\theta$ in the calibration period whenever the observed discharge exceeded $\theta$, and is the alarm threshold (usually the discharge capacity of a cross-section).

Then, the following decision table can be used to estimate the probability of an event given an alarm signal:

**Table 1.** Event probability given an alarming signal.

| Condition | Probability |
|---|---|
| $QNSE_t > \theta \wedge QMAX_t > \theta$ | max( $P(q_t > \theta \mid QNSE_t > \theta)$, $P(q_t > \theta \mid QMAX_t > \theta)$ ) |
| $QNSE_t > \theta$ | $P(q_t > \theta \mid QNSE_t > \theta)$ |
| $QMAX_t > \theta$ | $P(q_t > \theta \mid QMAX_t > \theta)$ |

## 3. Case study

The Morland water basin is 10 km² located within the Eden Demonstration Test Catchment (DTC) in North West England. Rainfall data are collected at 15-minute intervals from two automatic weather stations located in the upper part of the catchment (Owen et al., 2012) and extend from 27 October 2012 to 20 January 2013. Only 60% of the available data was used for the calibration of the models and the estimation of the frequencies used in the Bayesian inference. The remaining 40% was used for validation. The following figures display the results of the simulations of LRHM with the two objective functions.

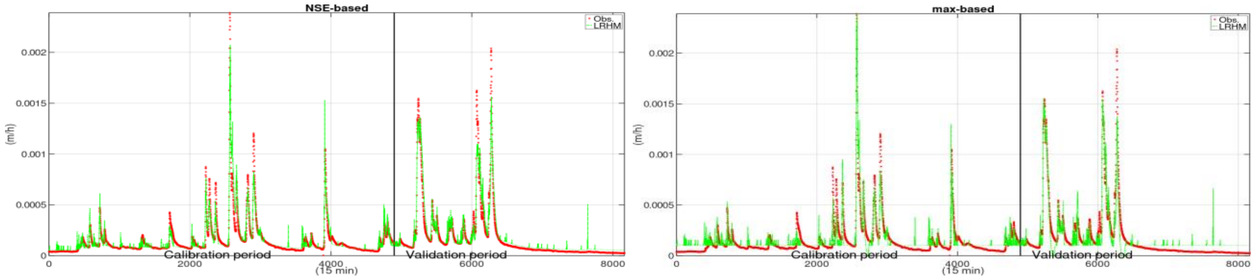


**Fig. 1.** Simulation of Morland River discharge with LRHM calibrated with NSE and max-absolute-error objective functions.

According to Table 1, the conditional probabilities obtained from the calibration period, with $\theta$=0.0015, are the following. The probability that the true discharge exceeds $\theta$ given that only LRHM with the NSE objective function exceeds $\theta$ is 1×1/2=50%. The probability that the true discharge exceeds $\theta$ given that only LRHM with the max absolute error objective function exceeds $\theta$ is 1×1/1=100%.

Regarding the 3 events of the true discharge exceeding $\theta$ in the validation period (Figure 1), the Bayesian coupling gives the following. The first two events were predicted by the LRHM with the max absolute error, of which the confidence is 100%. The last event was predicted by the LRHM with NSE objective function, of which the confidence is 50%. It is encouraging that all events in the validation period were detected.

## 4. Conclusions

In this study, an example of Bayesian coupling of hydrological models (same model with different objective functions, but in general could be different models) for early warning systems was demonstrated. This approach appears to be advantageous over data-driven alternatives (e.g., machine learning approaches) in cases with a limited amount of data. A disadvantage of the suggested approach is the rough estimation of the uncertainty. This can be improved by increasing the number of the coupled models.

**Acknowledgements**

This research was funded by the Internal Grant/Award of National Observatory of Athens "Low computational burden flood modelling in small to medium-sized water basins in Greece".

**References**

Noymanee J, Theeramunkong T (2019) Flood Forecasting with Machine Learning Technique on Hydrological Modeling. Procedia Comput. Sci., 156, 377–386.
Owen GJ, Perks MT, Benskin CMH, Wilkinson ME, Jonczyk J, Quinn PF (2012) Monitoring agricultural diffuse pollution through a dense monitoring network in the River Eden Demonstration Test Catchment, Cumbria, UK. Area, 44(4), 443-453.
Rozos E, Dimitriadis P, Bellos V (2021) Machine Learning in Assessing the Performance of Hydrological Models. Hydrology;9(1):5.
Rozos E (2020) A methodology for simple and fast streamflow modelling. Hydrol. Sci. J., 65, 1084–1095.
Herath HMVV, Chadalawada J, Babovic V (2021) Genetic programming for hydrological applications: To model or forecast that is the question. J. Hydroinform., 23, 740–763.
Senent-Aparicio J, Jimeno-Sáez P, Bueno-Crespo A, Pérez-Sánchez J, Pulido-Velázquez, D (2019) Coupling machine-learning techniques with SWAT model for instantaneous peak flow prediction. Biosyst. Eng., 177, 67–77.
Yang S, Yang D, Chen J, Santisirisomboon J, Lu W, Zhao B (2020) A physical process and machine learning combined hydrological model for daily streamflow simulations of large watersheds with limited observation data. J. Hydrol., 590, 125206.

# Mathematical Modelling of Nature-Based Solutions for flood risk reduction under Climate Change conditions

Elpida PANAGIOTATOU[1], Anastasios STAMOU[2]

[1,2] Department of Water Resources and Environmental Engineering, School of Civil Engineering,
National Technical University of Athens, Greece
email: epanagiotatou@mail.ntua.gr[1]
email: stamou@mail.ntua.gr[2]

ABSTRACT

We present a methodology for the mathematical modeling of Nature-Based Solutions (NBS) in a catchment area in order to determine the reduction of the flood risk. The methodology is based on a literature survey that we performed to identify the main NBS that are being applied worldwide and the implemented hydrologic and hydrodynamic models that are usually 1D/2D. We describe briefly the 12 steps of the methodology. Two of the most important steps are (1) the effect of the Climate Change impacts via climate models or by simply considering what-if scenarios and (2) the simulation of NBS using well-known 1D/2D models after performing the required modifications in the geometrical characteristics, the distribution of Manning coefficients and the equations of hydraulic structures, such as weirs, based on computations using 3D hydrodynamic models.

## 1. Introduction

The Directive 2007/60/EC of the European Parliament and of the Council (Directive, 2007) includes recommendations for: (1) better integration of the effects of Climate Change (CC) in the management of Flood Risk (FR) reduction; and (2) promotion of NBS, even as additional measures combined with gray infrastructure (dams, embankments and paved open pipelines). NBS are nature-inspired interventions that not only reduce FR, but address contemporary societal challenges (e.g., extensive urbanization) in a cost-effective way, providing multiple benefits to human well-being and biodiversity (Debele et al., 2019). The main NBS that have been applied extensively worldwide to reduce FR are restoration of rivers and their floodplains and removal of embankments (NBS1), planting of trees (NBS2), floodplains or storage areas in the floodplain (NBS3) and wooden leaky barriers or engineered logjams in rivers and/or floodplains (NBS4). NBS enhance the physical capacity of a river basin to manage heavy rainfall (1) by increasing the flood flow area, thus reducing flow velocities (NBS1, NBS3 and NBS4), (2) creating storage spaces (NBS1 and NBS3), (3) increasing the hydraulic roughness thus resulting in the deceleration of the flow (NBS1, NBS2 and NBS4) and by increasing flow depths (NBS2 and NBS4), and (4) by increasing infiltration and evapotranspiration (NBS2). In this work, we present a methodology for the mathematical modelling of Nature-Based Solutions (NBS) in a catchment area in order to determine the reduction of the flood risk.

## 2. Materials and Methods – Literature survey

The methodology is based on a literature survey that we performed to identify the main NBS that are being applied worldwide (see Introduction) and the implemented hydrologic and hydrodynamic models. Usually, these models for NBS1, NBS2 and NBS3 are hydrologic, hydrodynamic (1D, 2D or 1D/2D) or integrated hydrologic-hydrodynamic. To simulate floodplain restoration, we can simply extend the river cross sections of the hydrodynamic models. We can simulate planting of the riparian zone and the river bottom by increasing the values of Manning's roughness coefficients in the hydrodynamic model; moreover, to investigate the effect of evapotranspiration, we can implement an integrated hydrologic-hydrodynamic model. Storage areas are often simulated with hydrodynamic models by extending the river sections and calculate their outflow discharge by weir equations and stage-discharge relationships. The simulation of NBS4 is much more complicated than the other NBS; typically, it is performed via hydrodynamic models by (1) increasing the roughness coefficients, (2) reducing the flow surface, e.g., by raising the bottom elevation, (3) combining (1) and (2), (4) using1D equations of hydraulic structures, (5) increasing roughness coefficients and adding a drag force term in the equation of momentum, and (6) using 3D models.

## 3. Presentation of the methodology and discussion

The proposed methodology is shown in Figure 1; it consists of 12 steps that are performed in 6 stages: (I) initial work (Step 1), (II) building, calibration and validation of the integrated hydrologic-1D/2D hydrodynamic model (Steps 2 to 7), (III) determination of the effect of CC impacts (Step 8), (IV) formulation of NBS combinations - scenarios (Step 9), (V) modification - extension of the integrated (hydrologic-hydrodynamic) model to simulate the NBS (Step 10), (VI) application of the model, performance of calculations of the integrated model to estimate of flood hazard, vulnerability and risk for all the NBS scenarios - selection of the optimal scenario that minimizes flood risk (Steps 11 and 12). We started applying the methodology in the Rapentosa River Basin that contains the "Coastal – Lowland Area of Marathon-Nea Makri"; this area that is coded as GR06RAK0007 within the implementation of the Directive 2007/60/EC on the assessment and management of flood risks in Greece, was identified as one of the 9 Areas of Potential Significant Flood Risk (APSFR) in Attica. We collected the main input data, including the Digital Elevation Model (DEM) and selected the hydrologic and the hydrodynamic models that are HEC-HMS (HEC, 2000) and 1D/2D HEC-RAS (Brunner, 2016), respectively.

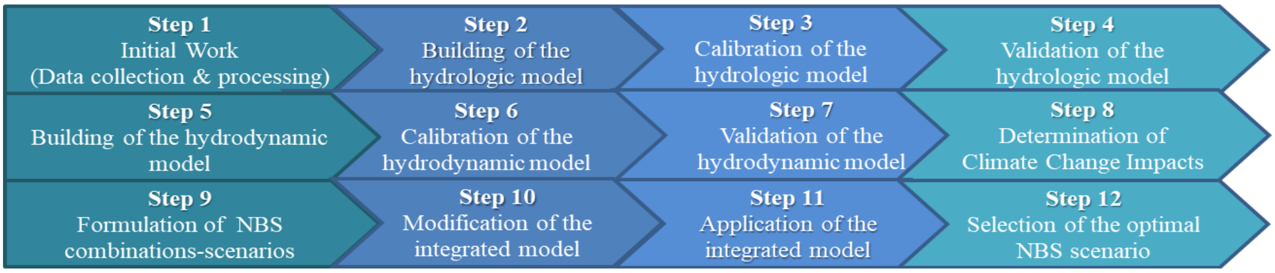


**Fig. 1.** Schematic representation of the proposed methodology for the integrated mathematical modelling of NBS for Flood Risk Reduction.

Two of the most important steps of the proposed methodology are 8 and 10. In order to determine the CC impacts, we combine the regionally downscaled climate projections from the EURO-CORDEX project (Jacob et al., 2014) with HEC-HMS as follows (see also Spyrou et al., 2021): Firstly, we select the Representative Concentration Scenario RCP8.5 that is the input to the General Circulation Model (GCM) ICHEC-EC-EARTH. Secondly, we define the boundary conditions of the Cordex Regional Climate Model (RCM) KNMI-RACMO22E (KNMI, 2017) using the results of the GCM. Thirdly, we provide the RCM calculations as input to the HEC-HMS. Alternatively, a simpler approach is to use what-if scenarios. At Step 10, we modify-adjust the 1D/2D HEC-RAS (a) to simulate NBS1, NBS2 and NBS3 by altering the geometry (including the DEM) and the roughness values of the computational domain, (b) to simulate NBS4 using the HEC-RAS weir equations with coefficients that are adjusted to match the results of 3D calculations with the model FLOW3D (Flow Science Inc, 2014) for various combinations of NBS4 geometrical characteristics.

## 4. Conclusions

A 12-step methodology is presented based on a literature survey for the integrated (hydrologic-hydrodynamic) mathematical modelling of NBS in a catchment area in order to determine the reduction of the flood risk. Two of the most important steps of the methodology deal with the determination of the CC impacts and the modification-adjustment of the integrated model, mainly the hydrodynamic, to simulate the NBS.

### References

Brunner G (2016) HEC-RAS River Analysis System Hydraulic Reference Manual Version 5.0, USACE CEC: DAVIS, CA, USA

Debele SE, Bogdanowicz E and Strupczewski WG (2017) The impact of seasonal flood peak dependence on annual maxima design quantiles, Hydrological Sciences Journal, 62, 1603–1617

Directive 2007/60/EC of the European Parliament and of the Council of 23 October 2007 on the assessment and management of flood risks (OJ L 288, 6.11.2007)

Flow Science Inc (2014) FLOW-3D User's Manual

Jacob D, Petersen J, Eggert B, Alias A, Christensen OB, Bouwer LM, Braun A, Colette A, Déqué M, Georgievski G et al (2014) EURO-CORDEX: New high-resolution climate change projections for European impact research, Regional Environment Change, 14, 563–578

KNMI (2017) cordex EUR-11 KNMI RACMO22E, World Data Center for Climate (WDCC) at DKRZ

Spyrou C, Loupis M, Charizopoulos N, Apostolidou I, Mentzafou A, Varlas G, Papadopoulos A, Dimitriou E, Panga D, Gkeka L, Bowyer P, Pfeifer S, Debele SE and Kumar P (2021) Evaluating nature-based solution for flood reduction in Spercheios River Basin under current and future climate conditions, Sustainability, 13, 3885

U.S. Army Corps of Engineers, Hydrologic Engineering Center (2000) HEC-HMS Hydrologic Modeling System, Technical Reference Manual, CPD-74B, Hydrologic Engineering Center, Davis, CA

# Mathematical models of erosive flash floods, huaycos and lahars

Andrew J. HOGG[1], Mark J. WOODHOUSE[2], Jake LANGHAM[1] and Jeremy C. PHILLIPS[2]

[1] School of Mathematics, University of Bristol, UK
email: a.j.hogg@bristol.ac.uk (Author 1), j.langham@bristol.ac.uk (Author 3)

[2] School of Earth Science, University of Bristol, UK
email: mark.woodhouse@bristol.ac.uk (Author 2), j.c.phillips@bristol.ac.uk (Author 4)

ABSTRACT

## 1. Introduction

Huaycos - flash floods in the Peruvian Andes - and lahars – volcanic debris flows - are potent natural hazards that threaten regularly lives and livelihoods. They comprise debris-laden fluid that flows rapidly down steep slopes, bulking up considerably through erosion of the underlying bed as they progress. Owing to their rapid onset and the significant threat that they pose to communities and infrastructures, it is important to predict their motion to assess quantitatively some of the impacts that they may cause. This paper presents a new mathematical model of the physical processes that govern the motion and a new, free-to-use implementation of a numerical algorithm to integrate them, which may be used to predict the flows quantitatively.

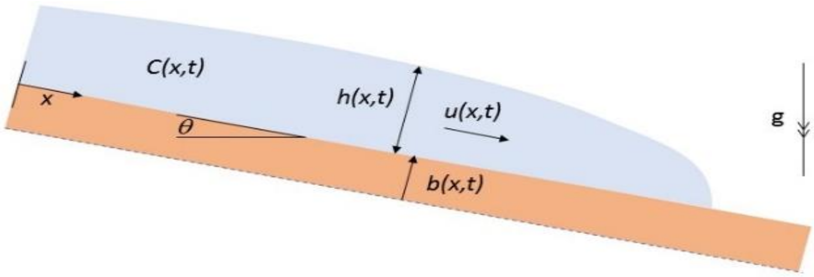


**Fig. 1**. Flow configuration for a model of a debris-laden flow down an inclined boundary, here shown on a constant incline and as a function of one spatial variable. Dependent variables are flow depth, h(x,t), flow velocity, u(x,t), concentration of particles, C(x,t) and bed elevation, b(x,t). Motion is driven by gravitational acceleration, g.

## 2. Methods

The mathematical model utilizes the relative shallowness of the flow (the flow depth is much less than the streamwise extent), which implies that the motion is predominantly parallel to the underlying slope and the pressure (or 'normal' stress) is hydrostatic. Figure 1 depicts a flow down a constant incline and defines the depth-averaged dependent variables; more generally the inclination spatially varies, and the dependent variable are functions of time, *t* and the two spatial coordinates parallel to the boundary, but for brevity here, we suppose that there is variation with only one spatial dimension. Conservation of fluid mass is given by

$$\frac{\partial}{\partial t}\big(h(1-C)\big)+\frac{\partial}{\partial x}\big(hu(1-C)\big)=-(1-C_b)\frac{\partial b}{\partial t}, \tag{1}$$

where $C_b$ denotes the volumetric concentration of solids in the bed. This equation relates the rate of change of fluid volume with the divergence of the fluid flux and the addition of fluid from the saturated bed. Likewise, conservation of mass in the solid phase

$$\frac{\partial}{\partial t}(hC)+\frac{\partial}{\partial x}(huC)=-C_b\frac{\partial b}{\partial t}. \tag{2}$$

Here we have assumed that two phases move with the same depth-averaged velocity, *u(x,t)*. Bed erosion, *E*, and deposition, *D*, balance the rate of change of the bed elevation and are given by

$$C_b\frac{\partial b}{\partial t}=D-E. \tag{3}$$

Finally, relating the density, ρ, to the concentration, *C*, and densities of the solid and fluid phases, $\rho_s$ and $\rho_f$, respectively, $\rho=\rho_f(1-C)+\rho_s C$, we may form the depth-averaged expression for the streamwise balance of the momentum of the entire mixture. This eliminates the need to model explicitly the inter-phase forces. The driving force is downslope gravitational acceleration, which is primarily balanced by the resistance at the base of the flow. Additionally, the expression for the rate of change of the momentum features the divergence of the momentum flux, the streamwise pressure gradient and the potential drag arising from the acceleration of entrained bed material.

$$\frac{\partial}{\partial t}(\rho u h)+\frac{\partial}{\partial x}\left(\rho u^2 h+\tfrac{1}{2}g\cos\theta\rho h^2\right)=\rho h g\sin\theta-\tau_b-\rho_b u_b\frac{\partial b}{\partial t}, \tag{4}$$

where $u_b$ and $\rho_b$ are the basal streamwise velocity and density, respectively.
There are two key changes that must be made to the governing system of equations before they can be used for predictions. First as posed in (1)-(4), the system is mathematically ill-posed. This technical result has a crucial consequence: it is not possible to compute grid-resolved solutions. Instead, we reinstate a small, neglected term, the streamwise variation of stress, which is sufficient to regularise the system (see Langham *et al.* 2022). Additionally, we compute solutions on measured topography. For example, we have conducted drone surveys of catchments in Chosica, Peru and used photogrammetry to construct a high-resolution digital elevation model (DEM). Therefore, it is convenient to compute in a rotated and projected coordinate system - Earth-centred coordinates - which enable the measured DEM to be used directly without further manipulation.

### 3. Results

Our model is integrated using efficient modern numerical algorithms, driven by source conditions such as a prescribed hydrograph upstream in the catchment, or an instantaneous release of material The model is available to use free of charge, at www.laharflow.bristol.ac.uk, with computations made using servers in Bristol. Figure 2 shows a computed result that simulates a huyaco event at La Libertad de Chosica, Peru. Note that the DEM has street-scale features and that the flow is directed by this topography. The flow reached quite high flow depths (~3m) and flow speeds (~10 $ms^{-1}$). It was also highly erosive, picking up deposited material and tearing up the unpaved street. These predictions are consistent with observations of the 2016 event and evidence the plausibility of our modelling framework and computations. Other examples in different international settings and at much larger scales will be reported, along with their use in hazard assessment.

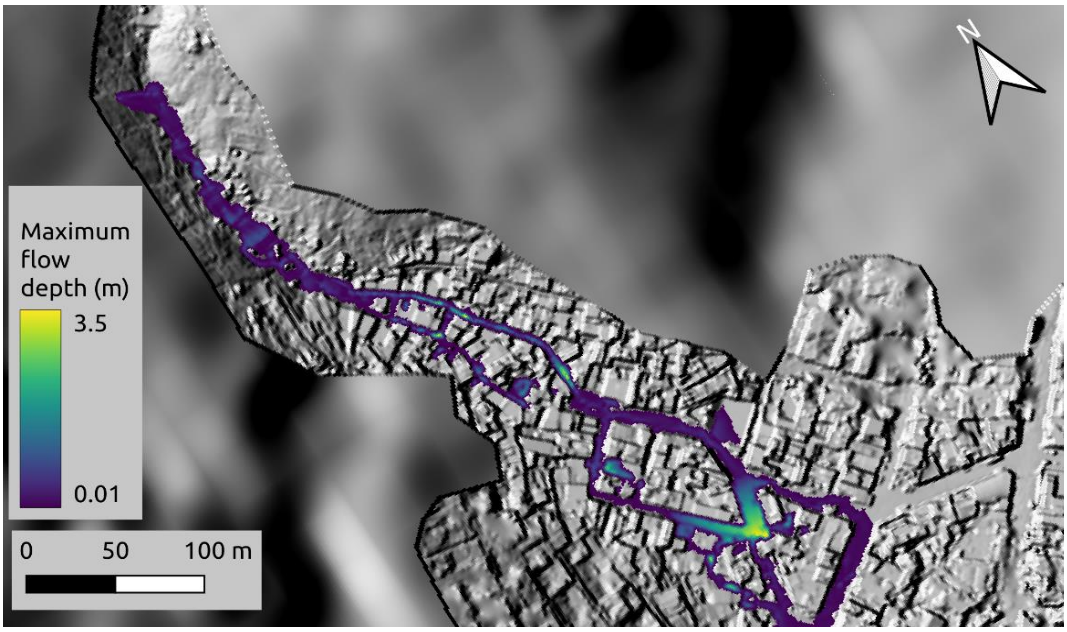


Fig. 2. Plan view of maximum flow depth during a huayco event simulated at La Libertad de Chosica, Peru. The source hydrograph is specified at the northerly end of the quebarda, and the flow downstream is predicted by the model. The DEM is depicted in grey, showing the resolution of street-scale features that guide the flow.

**Acknowledgements**

The authors acknowledge financial support from NERC UK (NE/S00274X/1, NE/J019984/1) and Global Challenges Research Fund, University of Bristol

References

Langham, J, Woodhouse MJ, Hogg AJ, Phillips JC 2021 Linear stability of shallow morphodynamic flows, *J. Fluid Mech.*, 916, A31, doi:10.1017/jfm.2021.235.

# Sensitivity of a coupled 1D/2D model in input parameter variation exploiting Sentinel-1-derived flood map

Ioanna ZOTOU[1]*, Kleanthis KARAMVASIS[2], Vassilia KARATHANASSI[2], Vassilios A. TSIHRINTZIS[1]

[1] Centre for the Assessment of Natural Hazards and Proactive Planning & Laboratory of Reclamation Works and Water Resources Management, School of Rural, Surveying and Geoinformatics Engineering, National Technical University of Athens, 9 Heroon Polytechniou St., Zographou, 157 80 Athens, Greece
*email: iwannazwtou@central.ntua.gr; tsihrin@central.ntua.gr

[2] Remote Sensing Laboratory, School of Rural, Surveying and Geoinformatics Engineering, National Technical University of Athens, 9 Heroon Polytechniou St., Zographou 157 80, Athens, Greece
email: karamvasis_k@hotmail.com; karathan@survey.ntua.gr

ABSTRACT

## 1. Introduction

Hydrodynamic models are valuable tools in the direction of flood forecasting and mitigation of the subsequent damages. Various kinds of satellite data have been widely exploited to assist flood models in different ways over the last decades. The present work seeks to investigate the sensitivity of an integrated 1D/2D hydraulic model, in the variation of roughness coefficient and upstream inflow. For the generation of the upstream inflow, a hydrologic simulation of the contributing watershed combined with a Monte-Carlo uncertainty analysis was performed. The influence of roughness coefficient changes in model results was tested by examining separately the main channel and the 2D area. In order to quantify model performance, simulation results were compared against a satellite data-derived inundation boundary. In the latter case, an automatic flood delineation approach (FLOMPY), which exploits multi-temporal Sentinel-1 radar data has also been employed. The presented methodology was applied in a flood event which took place in early February 2015, in Spercheios River, Central Greece.

## 2. Materials and methods

The separate parts of the methodology adopted in the current study are briefly described in the following subsections.

### *2.1. Hydrologic and hydraulic modeling*

To model the response of Spercheios River in the examined storm event, a coupled approach consisting of a HEC-HMS hydrologic and a HEC-RAS hydraulic model was adopted. In absence of runoff data, the hydrologic model was employed in order to generate the upstream inflow for use in the hydraulic model. It encompassed three hydrologic regions, i.e., upper Spercheios watershed, Gorgopotamos watershed and Asopos watershed, each draining the upstream area of the respective upper boundary of HEC-RAS model. To address the uncertainty introduced in the hydraulic simulation due to the un-calibrated response of HEC-HMS model, a Monte Carlo uncertainty analysis was also encompassed. Five indicative hydrographs, as generated from the abovementioned analysis, were exploited as input for the hydraulic model. For the simulation of the generated runoff through the HEC-RAS hydraulic model, an integrated 1D/2D approach was considered, with the 1D part incorporating the main channel, and the 2D, respectively, the overbank flow. For the determination of roughness coefficients in the 2D areas, appropriate Manning $n$ value ranges were established per land use category based on the literature. For the 1D river, the coefficient value ranges were formulated after a segmentation of the entire river length into three categories, i.e., lower, middle and upper river reaches, and assuming that resistance to flow increases as we move towards the upper reaches of the river.

### *2.2. Sensitivity analysis and quantification of model performance*

With respect to the roughness coefficient, the sensitivity analysis was implemented separately for the 1D river and the individual land uses of the 2D area. Six land use categories were considered in the analysis due to their largest contribution to the total model surface area and their proximity to the main channel. These were the "Paved roads and driveways", "Construction sites", "Cultivated Crops", "Emergent Herbaceous Wetlands", "Pasture/ grasslands" and "Mixed forests". From each established value range per land use or river reach category, five indicative values, i.e., the minimum, maximum, mean and the 25% and 75% of the value range, were tested. Each time the influence of a specific parameter, i.e., roughness coefficient of the main channel or of a given land use, was tested, and all other parameters remained constant. To examine the effect of upstream inflow variation in the simulation results, five indicative inflow hydrographs, as generated from the Monte Carlo analysis, were examined. The results consisted of the inundation extent on the 3rd of February 2015, at 04:31 a.m. UTC (time of flood image acquisition), for each of the totally forty simulated scenarios. For each of them, the flooded area was compared against that derived through the FLOMPY algorithm (Karamvasis and Karathanassi, 2021) and the model performance was quantified according to the coincidence between the model and the FLOMPY-derived flood extent.

## 3. Results and discussion

The results showed that the greatest influence on the simulation results is exerted by the variation in the inflow discharge, leading to a change in the derived flooded area from 11 $km^2$ to 20 $km^2$ depending on the simulated scenario. This also translates into a 5.5% variation in model performance, giving greater coincidence with the satellite data-derived flood map, for the middle-upper upstream inflow scenarios. With respect to the roughness coefficient, it was found that model results are primarily affected by the coefficient variation in the main channel and to a slightly smaller extent by the 2D area. This seems reasonable since flow conditions in the main channel dictate whether water will overtop the channel banks and spill into the overbank area. Regarding the 2D area, the coefficient value for the "cultivated crops" was almost entirely responsible for the changes in model response, which can be explained by the particularly wide area this land use occupies. The rest of land uses exerted a negligible or no impact at all due to the limited surface area they cover or because they were not subjected to flood at any of the examined scenarios. It was also concluded that, for the main channel, higher coefficient values give a better model response, whereas for the "cultivated crops", a higher performance of the model occurs for roughness coefficients around the lower-middle areas of the established value range. Fig. 1 illustrates the variation in the model-predicted inundation area as well as in the coincidence with the FLOMPY result, relative to the change in roughness coefficient value for the six land uses considered (Fig. 1a-f) and the main channel (Fig. 1g). Overall, satellite data-derived flood mapping proved to be advantageous in supporting modeling procedure, serving as a reference base for detecting changes in model performance. It also shows potential for use for calibration/validation purposes provided, however, that particular caution is being taken regarding the uncertainty accompanying satellite products and the selected flood mapping methodologies themselves.

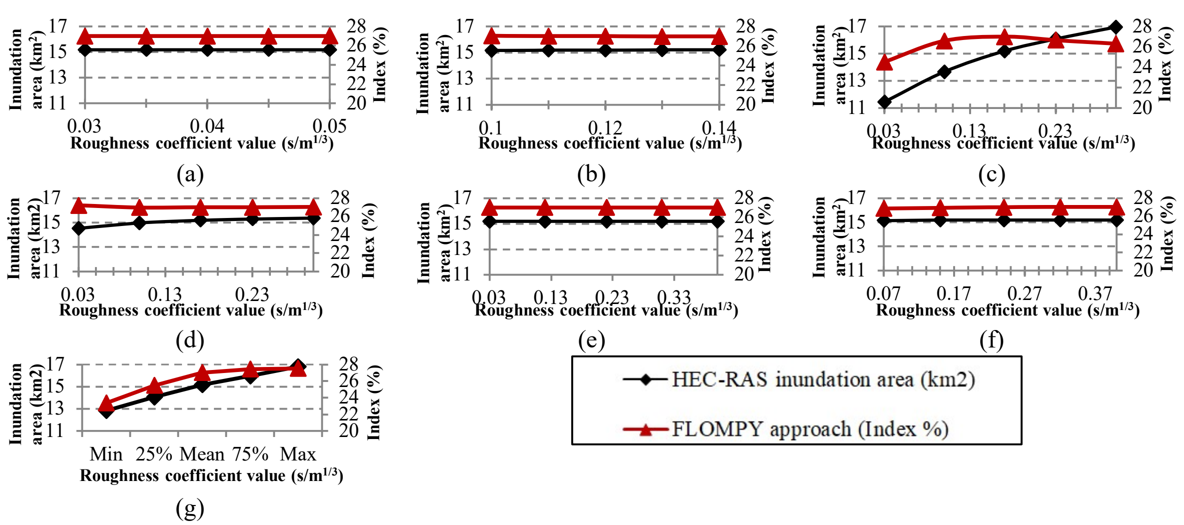


**Fig. 1.** Inundation area predicted by the model and index value (%) as a function of variation in roughness coefficient value in the: (a) Paved roads and driveways"; (b) "Construction sites"; (c) "Cultivated Crops"; (d) "Emergent Herbaceous Wetlands"; (e) "Pasture/ grasslands"; (f) "Mixed forests" and (g) main channel

### References

Karamvasis K, Karathanassi V (2021) FLOMPY: An Open-Source Toolbox for Floodwater Mapping Using Sentinel-1 Intensity Time Series, Water, 13(21), 2943. https://doi.org/10.3390/w13212943

# Semi-distributed rainfall-runoff modelling using landscape classification

Ino PAPAGEORGAKI[1], Ioannis NALBANTIS[1]

[1] School of Rural and Surveying and Geoinformatics Engineering, National Technical University of Athens, Greece
email: ino@central.ntua.gr
email: nalbant@central.ntua.gr

ABSTRACT

Within the approach of semi-distributed rainfall-runoff modelling we adopt the concept of landscape classification into hydrological landscape classes, which later form the spatial units for semi-distributed modeling. For runoff production, we apply the FLEX–Topo model by Savenije (2010). The proposed methodology is applied to a Greek basin with encouraging results. Landscape classification is performed using orthophotos and a neural network as the classifier, while four classes are identified based on five geomorphological criteria, which are calculated from ground elevation information.

## 1. Introduction

In the past, rainfall-runoff modeling has evolved from simple to more detailed structures that represent physical processes almost at the micro scale. This led to complicated distributed models with the adverse effect of increased predictive uncertainty. On the other hand, lumped models may fail to represent processes in the studied drainage basin due to their simplicity. In between the two approaches lies semi-distributed modeling which seeks the optimal level of complexity to achieve predictive accuracy. Runoff prediction in ungauged basins requires the transfer of hydrological information in space, which is greatly facilitated by using physically observable quantities, such as geomorphological characteristics. These allow the landscape classification for the identification of areas that are distinct with respect to the predominant runoff generating mechanisms. The proposed methodology can assist modeling of flood phenomena which are progressively more frequent worldwide, causing heavy damages inflicted on human societies and the environment.

## 2. Materials and methods

### *2.1. Landscape classification*

The principles of the methodology described by Gharari et al. (2011) are adopted and the surface of the studied drainage basin is classified using five criteria: the Height Above the Nearest Drainage (HAND, (Saleska, 2011), ground slope, aspect, and the distance from the nearest drain or branch of the hydrographic network, considered along the flow direction path. For the computation of HAND and distance the hydrographic network of the basin is constructed following the methodology proposed by Papageorgaki and Nalbantis (2018). For this, the Critical Support Area (CSA) for stream initiation is extracted from maps for three periods for wetness conditions: wet, dry and intermediate. In this study the latter is kept as representative of average hydrological conditions. Orthophotos are used to visually classify selected points or benchmarks within the basin in four classes. These are later introduced into an Artificial Neural Network (ANN) with one hidden layer to classify all cells of the basin (Ehsani 2007). The ANN is trained using 70% of benchmarks, while the remaining 30% is devoted to testing and validation. The four landscape classes are: bare soil areas (class 1), forested hillslopes (class 2), cultivated hillslopes (class 3) and riparian areas (class 4). These classes are related to the classification by Winter (2001) and Scherrer and Naef (2003), who also linked them to four dominant runoff mechanisms (Freer et al. 2002).

### *2.2. The FLEX-Topo model*

FLEX-Topo model is a topography-driven conceptual modelling approach (Savenije, 2010) based on a conceptual representation of the dominant hydrological processes in hydrological landscapes. The main idea is that model structure is dependent on a limited number of landscape classes derived from topographic information. These classes are represented by lumped conceptual sub-models running in parallel, which leads to a semi-distributed model. Thus, maximum simplicity is achieved while maintaining efficiency. The model is calibrated and validated based on daily discharge data at the basin outlet. It is noted that snow accumulation and melt is considered by dividing the basin area into eight elevation zones.

### *2.3. Study basin and data*

The proposed methodology is applied to a river basin located in the western part of continental Greece. This is the Evinos river basin at the Poros Reganiou hydrometric station with an upstream basin area of 882 $km^2$, mean elevation of 979 m above the mean sea level, and steep slopes (Fig. 1). Its average annual streamflow is 694 $hm^3$ (Mamassis and Nalbantis, 1995). Data cover the period from 1977–78 to 1985–86. Six precipitation gauging stations are used while air temperature measurements from two meteorological stations are obtained. For landscape characteristics, the European Digital Elevation Model (Copernicus, EU-DEM version 1.1) with spatial resolution of 25 m is used.

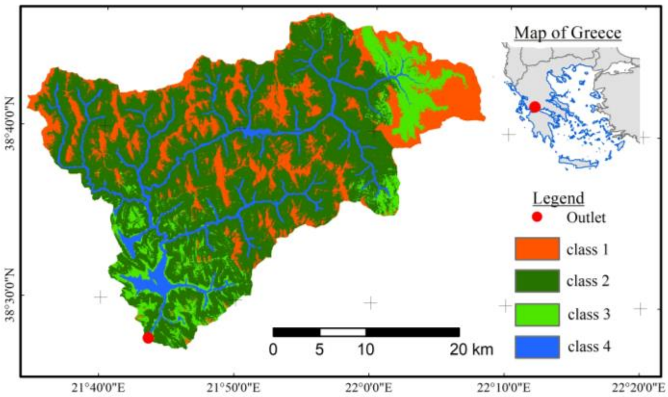


**Fig. 1.** Spatial distribution of four landscape classes of Evinos river basin, in western continental Greece.

## 3. Results

Vegetation cover was also tested as an additional criterion in classification. Furthermore, classifications were performed, with numerous combinations of criteria and number of classes. The classification of Fig. 1 was retained as its percentage of successful classification in validation confusion matrix is greater than 84%. The percentage of basin area was 19.5%, 61.6% 10.6% and 8.3% for class 1, class 2, class 3 and class 4, respectively. Model calibration for the five-year period 1977-78 to 1981-82 gave a Nash Sutcliff Efficiency (NSE) of 0.69, while for validation on the remaining four-year period NSE was found 0.63.

## 4. Concluding remarks

Landscape classification is considered as a promising tool for constructing rainfall runoff models that enable runoff predictions in ungauged basins. This proved to be the case with the test basin used in this study. Tests with three and four classes and various combinations of morphometric characteristics revealed that additional information regarding vegetation was necessary for achieving a successful classification in validation stage.. Moreover, all the employed morphometric characteristics were found to be necessary to achieve a successful classification. The prediction accuracy for runoff, although fair, needs some improvement, e.g., through better consideration of the spatial variation of input data.

**References**

Ehsani AH (2007) Artificial Neural Networks: Application in morphometric and landscape features analysis, KTH, Royal Institute of Technology, Stockholm, pp. 53

Freer J, McDonnell J, Beven K, Burns D, Hooper R, Aulenbach B, Kendall C, Peters N (2002) Understanding the spatial and temporal dynamic contributions of subsurface storm runoff at the hillslope scale, Water Resources Research, 38(12), 5-1–5-16

Gharari S, Hrachowitz M, Fenicia F, Savenije HHG (2011) Hydrological landscape classification: investigating the performance of HAND based landscape classifications in a central European meso-scale catchment, Hydrology and Earth System Sciences, 15(11), 3275-3291

Mamassis N, Nalbantis I (1995) Study of hydrological balances, Evaluation and management of water resources of Sterea Hellas, project report 20, National Technical University of Athens, pp. 118

Papageorgaki I, Nalbantis I (2018) On spatio-temporal modelling of stream network initiation, Environmental Processes, 5(1), 239-257

Saleska S (2011) Height Above the Nearest Drainage, a hydrologically relevant new terrain model. Journal of Hydrology doi: 10.1016/j.jhydrol.2011.03.051

Savenije HHG (2010) Topography driven conceptual modeling (FLEXTopo), Hydrology and Earth System Sciences, 14, 2681–2692

Scherrer S, Naef F (2003) A decision scheme to indicate dominant hydrological flow processes on temperate grassland, Hydrological Processes, 17, 391–401

Winter TC (2001) The concept of hydrologic landscapes, Journal of American Water Resources Association, 37(2), 335–349

# LIFE BAETULO Project: an example of Climate Change adaptation to cope with flash floods in urban areas based on a multi-risk Early Warning System

Beniamino RUSSO[1, 2], Montse MARTINEZ[1], Andrea PAINDELLI[1]

[1]AQUATEC Proyectos para el Sector del Agua, Spain

brusso@aquatec.es

mmartinez@aquatec.es

a.paindelli@aquatec.es

[2]Technical College of La Almunia (EUPLA, University of Zaragoza), Spain

ABSTRACT

Launched on July 2020 with a duration of 2,5 years and funded by the European Union, LIFE BAETULO project (LIFE19 CCA/ES/001180) (www.life-baetulo.eu) aims to provide a climate change adaptation tool to the city of Badalona (Spain) in the form of Integrated Early Warning System (IEWS) to cope with local major climate hazards. This project, coordinated by AQUATEC (Agbar group), is helping reduce exposure, vulnerability and finally the risk for citizens and city assets. Conceptualized as a web-platform, it connects a wide range of sensors located across the whole urban area (water level meters in drainage system, rain gauges, meteorological stations, combined sewer overflow sensors, etc.) as well as specific models such as meteorological forecasting and urban flood models. The secondary goal of the project is being a reliable reference for technology replicability, offering a clear example of direct and indirect climate related impacts reduction measured by the project KPIs (Key Performance Indicators). This abstract intends to provide a quick overview of the IEWS architecture and main results obtained so far, with specific details regarding the climate hazards of flash floods and Combined Sewer Overflows, which are the most damaging and incisive climate change threats currently affecting Badalona due to its geographic and urban characteristics.

## 1. Introduction

As stated by the European Environmental Agency (EEA, 2021), the frequency and magnitude of extreme weather events is expected to increase in the coming decades, resulting in recurring economic losses which poses constant challenges to urban life. The Intergovernmental Panel on Climate Change (IPCC) with its last publication (IPCC, 2022) updated the definition of resilience as the capacity of the urban system to cope with hazardous events, responding or reorganizing in a way that maintain the essential function and the capacity for adaptation, learning and transformation. With respect to Spain, the Spanish National Meteorological Agency (AEMET) has been collecting, through its “Open Data Climate” repository, a large amount of data regarding last 40 years of meteorological events and impacts and concluding that at least 32 million Spanish citizens have been suffering directly or indirectly from climate related consequences (AEMET, 2019). AEMET report outcomes are in line with Mediterranean climate trends with expanding semi-arid climates and longer summers, more frequent heat waves and tropical nights with an expected impactful increment of rainfall intensity for shorter durations (EEA, 2021). In geographical conditions such as that of Badalona, characterized by the connection between upper hilly catchments with intensive urbanized sea level catchments, led to recurring flooding events during the recent years, with non-negligible damages to underground transportations and city assets. (ElPeriodico, 2011) (LaVanguardia, 2019) (LaSexta, 2020). Within the BINGO Project (Van Alphen, et al., 2021) a wide set of adaptation alternatives were proposed: infrastructure actions such as green, gray and blue solutions, soft actions aimed to improve the management of the existing systems, and governance solutions which together with the legal/policy actions act directly on human behavior (EEA, 2021). Extensive economic evaluations led to the adoption of a soft measure, embodied by an Integrated Early Warning System (LIFE BAETULO solution) as the most cost-effective measure.

## 2. The BAETULO Platform and the Pluvial Flood threat

The system is forecasting and monitoring climate hazard episodes combining specific tools such as meteorological forecasting and urban flood models as well as a comprehensive number of sensors located across the whole urban area (water level meter in drainage system, rain gauges, meteorological stations, combined sewer overflows (CSO) sensors, etc.). The combination between the various data sources allows estimating the corresponding risks and leading to the activation of the climate related emergency protocols. Such activations are supervised by a person in charge of the platform operations, ensuring coordination before, during and after every episode.

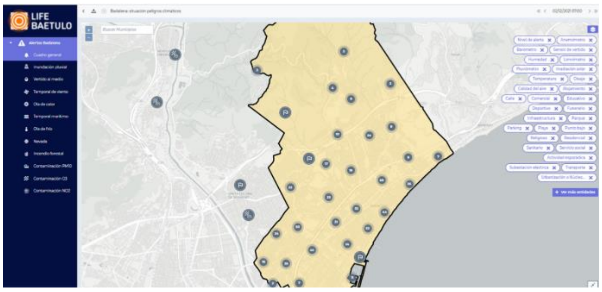


| Hazard | Variables | Elements | Thresholds | Activation rules |
|---|---|---|---|---|
| Urban floods | Nowcasting 2h rainfall intensity (Hyds)<br>Nowcasting 2h collected rainfall (Hyds)<br>Rainfall intesity forecast (SMC)<br>Collected rainfall forecast (SMC)<br>Collected rainfall (Rain gauges)<br>Water depth in street (Water depth camera)<br>Water depth in drainage system (digital water meter)<br>SMP warning for rainfall intensity forecast (SMC)<br>SMP warning for collected rainfall forecast (SMC)<br>SMP warning for rainfall intensity (SMC)<br>SMP warning for collected rainfall (SMC) | Municipality | Pre-Warning | [SMC Warning rainfall intensity (Barcelonès)>= Level 3] Or<br>[SMC Warning collected rainfall (Barcelonès)>= Level 3] Or<br>[Collected rainfall 1h SMC forecast for Badalona >=40mm (T2)] Or<br>[Collected rainfall 1h ECMWF forecast) >= 40 mm (T2)] Or<br>[Collected rainfall 24h ECMWF forecast) >= 100 mm (T10, Manual Software)] |
| | | | Warning | [SMC Warning rainfall intensity (Barcelonès)>= Level 4] Or<br>[SMC Warning collected rainfall (Barcelonès)>= Level 4] Or<br>[Collected rainfall SMC >= Level 4] Or<br>[Rainfall intensity SMC >= Level 4] Or<br>[30 minute rainfall accumulation Radar >= 30 mm, from T2)] Or<br>[Rain gauges (4)>= 30mm/30min from T2)] Or<br>[Water level meter (20) > XX mm] (unique for every sensor) Or<br>(water depth in conduits below 50cm from the top) |
| | | | Emergency | [Rain gauges (4)>= 45 mm/30 min (T10)] Or<br>[Observed water detpth in streets > 15cm)] Or<br>[Water level meter (20) > XX mm] (nique for every sensor) |

**Fig. 1.** At left: Screenshot of the BAETULO platform with all the climate hazards listed on the left part and the vulnerable elements georeferenced in the map. At right: thresholds and activation rules for the pluvial flood hazard.

The hazards thresholds were defined in function of official protocols and previous investigations, such as the exhaustive flood risk assessment conducted for Badalona in the context of BINGO project (Martínez-Gomariz, et al., 2020), where a wide set of 1D-2D modeling were performed, combining surface runoff and underground drainage system modeling and identifying those critical branches characterized by pressure flows and spills for moderate rainfall events. The urban area was divided into three risk categories: low, medium and high, depending on the resulting matrix combination between hazard and vulnerability. Hazard is defined by the combination between surface water depth and velocity while the vulnerability is a combination of various factors such as population age and density and location of vulnerable elements (hospital, schools, open areas etc.). Risk maps were calculated for various rainfall intensity and return periods, considering climate change trends for a wide range of projections. Such maps will be implemented within the BAETULO platform, to appear depending on the rainfall forecast and for being used as support for pre, during and post event operation. Rainfall forecasting, both in terms of cumulated and intensity, are provided by the "Catalan Weather System" (SMC) and the European Centre for Medium-Range Weather Forecasts (ECMWF) while rainfall observations come from the network of rain gauges within the municipality and in the surroundings. The status of the drainage system is constantly monitored by water meters located across the whole drainage system while some of them are specific to detect shorelines CSOs. Up to date, the Platform is in its testing year, but local Stakeholders have already shown great interest not just for a mere climate risk management but also to simplify infrastructure operation and maintenance. Future developments will see the creation of a tailored mobile app, to be used as Citizen's primary communication channel. The BAETULO project lays the basis for a potential replicability virtually anywhere there is enough knowledge of the urban complex, together with a forecasting and monitoring infrastructure to offer an exhaustive overview of the urban area to protect.

**References**

AEMET, 2019. Informe sobre el estado del clima de España 2019. http://www.aemet.es/.
BINGO, 2017. s.l.:http://www.projectbingo.eu/research-sites/badalona.
EEA, 2021. Europe's changing climate hazards — an index-based interactive EEA report. HTML - TH-AL-21-015-EN-Q- ISBN 978-92-9480-407-5 ISSN 1977-8449, p. doi: 10.2800/458052.
ElPeriodico, 2011. El temporal corta la L-9 y L-10 del metro y afecta a las rondas. Volumen https://www.elperiodico.com/es/barcelona/20110429/temporal-corta-l-9-l-987769.
IPCC, 2022. AR6 WG1-WG2. s.l.:https://www.ipcc.ch/assessment-report/ar6/.
LaSexta, 2020. Inundaciones, caída de árboles y cortes en las líneas de tren: las imágenes de la DANA en Cataluña. Volumen https://www.lasexta.com/noticias/sociedad/inundaciones-caida-de-arboles-y-cortes-en-las-lineas-de-tren-las-imagenes-de-la-dana-en-cataluna_202009075f55feb47fc2c100015f55a0.html.
LaVanguardia, 2019. Calles inundadas y estaciones de metro cerradas: las incidencias por el temporal en Barcelona. Volumen https://www.lavanguardia.com/local/barcelona/20191204/472058751703/calles-inundadas-estaciones-metro-cerradas-incidencias-temporal-barcelona.html.
Martínez-Gomariz, E. y otros, 2020. Socio-Economic Potential Impacts Due to Urban Pluvial Floods in Badalona (Spain) in a Context of Climate Change. Water, p. DOI: 10.3390/w11122658.
Van Alphen, H.-J.y otros, 2021. Selecting and analysing climate change adaptation measures at six research sites across Europe. Nat. Hazards Earth Syst. Sci., pp. DOI: 10.5194/nhess-21-2145-2021.

# Hyperparameter tuning in a machine learning prediction model for surface water quality using high-frequency input data

Elisa CORAGGIO[1], Theo TRYFONAS[1], Claire GRONOW[1], Dawei HAN[1]

[1] Department of Civil Engineering, University of Bristol, United Kingdom
email: elisa.coraggio@bristol.ac.uk

email: theo.tryfonas@bristol.ac.uk

email: claire.gronow@bristol.ac.uk

email: d.han@bristol.ac.uk

ABSTRACT

A good understanding of water quality is fundamental for managing water resources in future scenarios that include water scarcity and climate change. Despite the advancement in technologies and high-frequency datasets for water quality in surface water becoming widely available, there is still insufficient knowledge on how to build effective prediction models using such datasets.

This study proposes a technique for finding the suitable input features (including data frequency) needed to build a robust water quality prediction model that is able to predict the surface water body's behaviour in the future.

## 1. Introduction

Looking at recent extreme weather events the World is already experiencing the importance of accurate predictions and early warning systems. When it comes to water quality, prediction tools are not always available and often rely on historical low-frequency datasets or relatively small training and validation datasets that fail to accurately capture changes in water quality (Chen et al., 2020).

With new technology developed in the areas of smart cities and wireless sensors networks, water quality monitoring has the potential of becoming more and more a data-rich science.

Having the possibility of recording high frequency data does not mean automatically being able to obtain a better performance when building a water quality prediction model. Often, data collected with a very high frequency may convey redundant information. Therefore, according to the timeframe that the model aims to predict, the model's performance should be evaluated using a different selection of input features (including data frequency).

The aim of this work is to provide guidance on how to select the input data frequency based on how far in the future the water quality prediction model aims at predicting the water body's behaviour.

Furthermore, it investigates the problem related to how many timesteps in the past should be included in the model to optimise its performance.

## 2. Materials and method

For the purpose of this work, a high frequency water quality dataset collected between 2018 and 2020 in Bristol Floating Harbour has been used (Coraggio et al., 2022). The dataset contains data with a 5 minutes frequency for the following water quality parameters: temperature, dissolved oxygen (DO), fluorescent dissolved organic matter (fDOM), turbidity and conductivity.

The dataset has been split into training, validation and testing dataset respectively in the percentage of 60%, 20% and 20%.

The main focus of this work is on selecting input features and tuning the model parameters for the water quality prediction. The prediction models are based on linear regression, used as benchmark model, and random forest regression. Random forest regression has been already successfully applied for surface water quality predictions in literature with monthly data (Chen et al., 2020; F. Wang et al., 2021; S. Wang et al., 2022).

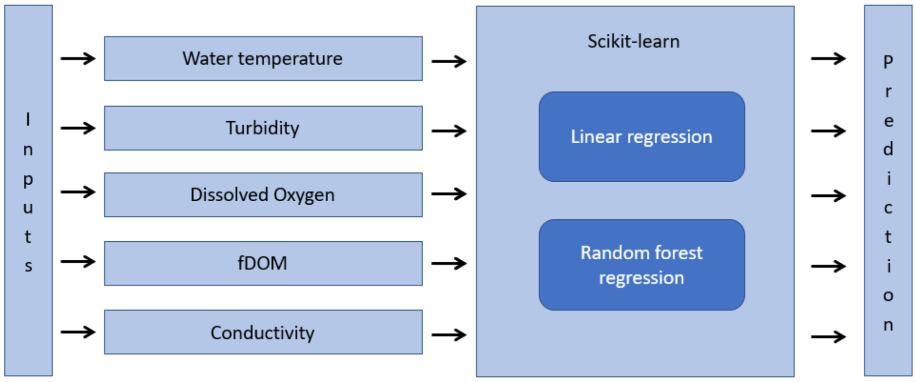


**Figure 1** Methodology framework

In this study, the hyperparameter tuning task is set by defining a matrix containing defined lags and input frequencies. The selection of these parameters is based on physical knowledge of the water quality changes in surface water and the trial-and-error exploration.

Once the optimum lag for a specific frequency is identified, the model parameters are evaluated in order to find the optimum input frequency for the prediction model.

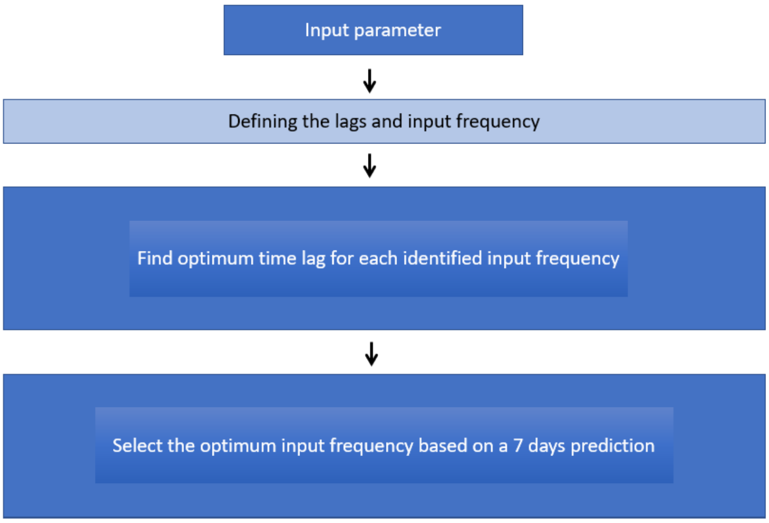


**Figure 2** Process for hyperparameters tuning

**Acknowledgements**

This work is funded as part of the Water Informatics Science and Engineering Centre for Doctoral Training (WISE CDT) under a grant from the Engineering and Physical Sciences Research Council (EPSRC), grant number EP/L016214/1. This work was supported in part by the Engineering and Physical Sciences Research Council's (ESPRC) 'UK Collaboratorium for Research in Infrastructure & Cities (UKCRIC): Urban Observatories' grant (ref. EP/P016782/1).

**References**

Chen, K., Chen, H., Zhou, C., Huang, Y., Qi, X., Shen, R., Liu, F., Zuo, M., Zou, X., Wang, J., Zhang, Y., Chen, D., Chen, X., Deng, Y., & Ren, H. (2020). Comparative analysis of surface water quality prediction performance and identification of key water parameters using different machine learning models based on big data. *Water Research*, *171*, 115454. https://doi.org/10.1016/J.WATRES.2019.115454

Coraggio, E., Han, D., Gronow, C., & Tryfonas, T. (2022). Water Quality Sampling Frequency Analysis of Surface Freshwater: A Case Study on Bristol Floating Harbour. *Frontiers in Sustainable Cities*, *3*, 159. https://doi.org/10.3389/FRSC.2021.791595/BIBTEX

Wang, F., Wang, Y., Zhang, K., Hu, M., Weng, Q., & Zhang, H. (2021). Spatial heterogeneity modeling of water quality based on random forest regression and model interpretation. *Environmental Research*, *202*, 111660. https://doi.org/10.1016/J.ENVRES.2021.111660

Wang, S., Peng, H., & Liang, S. (2022). Prediction of estuarine water quality using interpretable machine learning approach. *Journal of Hydrology*, *605*, 127320. https://doi.org/10.1016/J.JHYDROL.2021.127320

# Slide Model-Invariant Prediction of Landslide-Tsunamis Using Machine Learning

David JENKINS[1], Valentin HELLER[2], Archontis GIANNAKIDIS[1]

[1] Department of Physics and Mathematics, School of Science & Technology, Nottingham Trent University, Nottingham NG11 8NS, UK
email: david.jenkins@ntu.ac.uk
email: archontis.giannakidis@ntu.ac.uk

[2] Environmental Fluid Mechanics and Geoprocesses Research Group, Faculty of Engineering, University of Nottingham, Nottingham NG7 2RD, UK
email: valentin.heller@nottingham.ac.uk

ABSTRACT

Landslides impacting a body of water can generate large landslide-tsunamis. Therefore, producing reliable and fast methods of predicting such waves is vital. No single empirical equation exists for universally predicting the landslide-tsunami characteristics involving both granular and block slide models. To fill this gap, we created a machine learning model using the Gradient Boosting method to predict the relative maximum tsunami amplitude $a_M/h$ and height $H_M/h$ for both slide types, where $h$ is the still water depth. Our model produced an $R^2$ score of 0.919 for $a_M/h$ and 0.937 for $H_M/h$. Our method has shown promise and opens us possibilities to employing machine learning in real-world landslide-tsunami predictions.

## 1. Introduction

When a subaerial landslide impacts a body of water, a landslide-tsunami is generated. To better understand and analyse landslide-tsunamis, laboratory experiments have often been conducted (Fig. 1a) to model these events. This has resulted in a wide range of empirical equations that predict the maximum landslide-tsunami amplitude $a_M$ [m] and height $H_M$ [m] as a function of the slide parameters, such as the slide mass $m_s$ [kg], volume $\cancel{V}_s$ [m$^3$], thickness $s$ [m], impact velocity $V_s$ [m s$^{-1}$], the slope angle $\alpha$ [°], and the water depth $h$ [m] (Fig. 1b). There are, however, significant discrepancies in the prediction of $a_M$ and $H_M$ by employing empirical equations across different studies. It would be of great practical utility to have a single method that can predict landslide-tsunami characteristics irrespective of the experimental conditions and parameter values. Machine learning (ML) is a rapidly growing branch of artificial intelligence for predicting outcomes via learning from experience. While ML techniques have been used in the past to predict results of such laboratory experiments (Meng et al., 2020), endeavours to analyse results across different studies are limited. The main goal of the present work is to produce a single ML model that can accurately predict characteristics of waves created in laboratory experiments that simulate granular (Heller and Hager, 2010) and block (Heller and Spinneken, 2013) landslides.

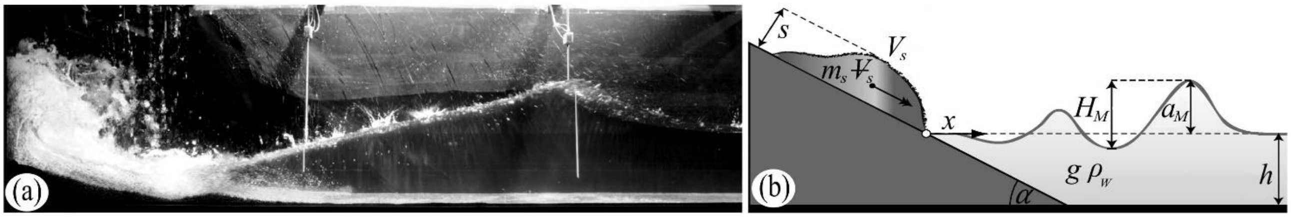


**Fig. 1.** (a) Picture of a landslide-tsunami in a flume and (b) definition sketch with slide and wave parameters (after Heller and Hager, 2010).

## 2. Materials and Methods

The datasets from Heller and Hager (2010) and Heller and Spinneken (2013) were obtained under very similar experimental conditions, apart from the slide model; the former used granular and the latter block slides. The experiments mimicked tsunami generation into a flume of water by the impact of landslides. The generated waves were measured using wave gauges along the flume. The dimensionless parameters, used in the literature to derive the empirical equations for predicting $a_M$ and $H_M$, served as the input features for the ML models. Concretely, these inputs were the landslide Froude number $\mathsf{F} = V_s/(gh)^{1/2}$, relative slide thickness $S = s/h$, relative slide mass $M = m_s/(\rho_W bh^2)$, and the relative grain diameter $D_g = d_g/h$ where $g$ [m s$^{-2}$] – gravitational acceleration, $\rho_W$ [kg m$^{-3}$] – water density, $b$ [m] – slide width, and $d_g$ [m] – average grain diameter (Heller and Hager, 2010). Our supervised ML regression method of choice was Gradient Boosting (Friedman, 2001). It is a technique which relies on using multiple separate weaker decision trees and improving on the performance iteratively. It is routinely used by winners of ML competitions. Data was split into two subsets, a training set (n = 294), used to develop and optimise the models, and a testing set (n = 61), used to evaluate the model on unseen examples. The testing set was comprised of 60% granular slides and 40% block slides examples. To align with the existing empirical equations, the ML models predict the relative maximum wave amplitude $a_M/h$ and height $H_M/h$ rather than $a_M$ and $H_M$.

## 3. Results and Discussion

After conducting the usual ML process of optimisation and hyperparameter tuning, our model achieved an $R^2$ score of 0.919 for $a_M/h$ and 0.937 for $H_M/h$ on the testing set. The performance as measured by $R^2$ scores is superior to the empirical equations for the separate slide types. For $a_M/h$, empirical equations produced scores of $R^2 = 0.88$ for granular slides and $R^2 = 0.85$ for block slides, and for $H_M/h$, $R^2 = 0.82$ and $R^2 = 0.89$. The features that proved to be the most informative in our ML model (as measured by Mean Decrease in Impurity) were, in descending order, $M$, $S$, F, and $D_g$. The observed values from the experiments have been plotted against the predicted values from the empirical equations and the ML models for both $a_M/h$ (Fig. 2a) and $H_M/h$ (Fig. 2b), allowing for a direct comparison of all examples in the testing set. As made evident by Fig. 2, the universal ML models performed consistently well across the full range of predictions, even slightly outperforming the individual empirical equations in the higher prediction value range.

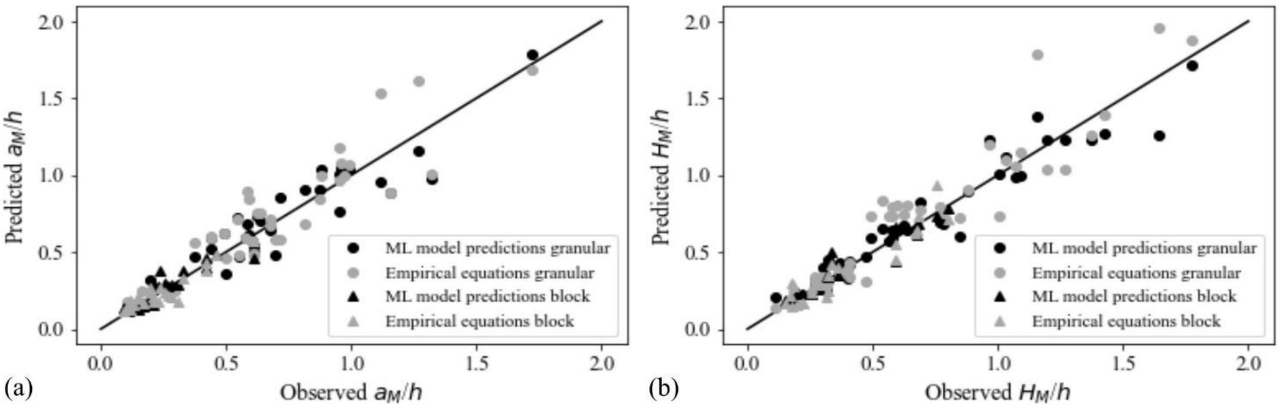


**Fig. 2.** Comparison of the proposed universal Gradient Boosting model and the separate empirical equations from Heller and Hager (2010) and Heller and Spinneken (2013) for (a) relative maximum wave amplitude $a_M/h$ and (b) relative maximum wave height $H_M/h$.

## 4. Conclusions

Predicting $a_M$ and $H_M$ of landslide-tsunamis remains an important element in hazard assessment of these natural phenomena. In this study, we built a single ML model using Gradient Boosting that can accurately predict characteristics of waves created in laboratory experiments that simulated granular and block landslides. The strong performance in predicting both $a_M/h$ and $H_M/h$ with significant $R^2$ scores of 0.919 and 0.937, respectively, displays the potential success of ML to build a universal model for predictions involving more than one set of conditions. In the future, we will also incorporate data from experiments with different water body geometries, such as a basin. Applying these models to predict features of real-world landslide-tsunamis and tuning to ensure upscaling preserves performance will also be addressed in future work.

**Acknowledgements**

The PhD study of DJ is funded by the Department of Physics and Mathematics, School of Science and Technology, Nottingham Trent University.

**References**

Friedman JH (2001) Greedy function approximation: A gradient boosting machine, Annals of Statistics, 29, 1189-1232
Heller V, Hager WH (2010) Impulse product parameter in landslide generated impulse waves, Journal of Waterway, Port, Coastal, and Ocean Engineering, 136(3), 145-155
Heller, V, Spinneken J (2013) Improved landslide-tsunami prediction: Effects of block model parameters and slide model, Journal of Geophysical Research: Oceans, 118(3), 1489-1507
Meng Z, Hu Y, Ancey C (2020) Using a data driven approach to predict waves generated by gravity driven mass flows, Water, 12, 600

# Impact of climate change on floods and hydrological dam safety with a stochastic rainfall generator and a rainfall-runoff model

Enrique SORIANO[1], Andrea PETROSELLI[2], Davide Luciano DE LUCA[3], Ciro APOLLONIO[4], Salvatore GRIMALDI[5], Luis MEDIERO[1]

[1] Department of Civil Engineering: Hydraulics, Energy and Environment, Universidad Politécnica de Madrid, 28040, Madrid, Spain
e.soriano@upm.es
luis.mediero@upm.es

[2] Department of Economics, Engineering, Society and Business (DEIM), Tuscia University, 01100, Viterbo (VT), Italy
petro@unitus.it

[3,] Department of Informatics, Modelling, Electronics and System Engineering, University of Calabria, 87036 Arcavaccata di Rende (CS), Italy
davide.del,uca@unicat.it

[4] Department of Agriculture and Forest Sciencies (DAFNE), Tuscia University, 01100, Viterbo, (VT), Italy
ciro.apollonio@unitus.it

[5] Department for innovation in biological, agro-food and forest systems (DIBAF), Tuscia University, 01100, Viterbo (VT), Italy
salvatore.grimaldi@unitus.it

ABSTRACT

Design floods are usually estimated with statistical analyses of observed data. However, time series of observations are usually short. Moreover, dams require assessment of design floods for high return periods, which estimates have high uncertainties. In addition, climate change is expected to increase the frequency and magnitude of floods in the future. A stochastic methodology to assess hydrological dam safety considering climate change is presented. The methodology is applied to the Eugui Dam (Spain). The stochastic model STORAGE is used to simulate time series of precipitation. Precipitation projections supplied by 12 climate models in three periods and two emission scenarios are used to consider climate change in the STORAGE model. Precipitation time series generated stochastically by STORAGE are transformed into runoff time series by using the continuous COSMO4SUB hydrological model. It provides continuous runoff time series as output from which annual maximum inflow hydrographs to the Eugui reservoir can be extracted. The Volume Evaluation Method is applied to simulate the operation of spillway gates, obtaining maximum reservoir water levels and outflow hydrographs. Therefore, the methodology proposed allows practitioners and dam owners to check hydrological dam safety requirements detailed in the regulations, accounting for climate change.

## 1. Introduction

A good characterization of flood hydrographs is crucial for dam design and management. Design hydrographs are usually obtained with hydro-meteorological analyses based on observed precipitation data and rainfall-runoff models. However, observations of precipitation are usually daily, though sub-daily data is required to characterize catchment response, in particular for small basins. Stochastic rainfall generators can overcome such a drawback, benefiting from their low complexity and fast computation times. In addition, stochastic rainfall generators allow the generation of long rainfall time series that can be useful to reduce the uncertainty in flood estimates for high return periods. For example, dam spillways are designed with return periods of 500-10 000 years in Spain. Furthermore, it is expected that climate change will increase flood magnitude and frequency in the future. Recent studies indicate that climate change has modified the magnitude and timing of floods in Europe in last decades. The number of floods exceeding given severity and magnitude thresholds increased in the period 1985-2009. Furthermore, climate projections point to an increase in floods in some areas (IPCC, 2007). Global circulation models (GCMs) have been developed to simulate how climate change will affect global atmospheric behavior. GCMs usually have a spatial resolution of about 100-250 km. Regional climate models (RCMs), with a spatial resolution of 25-50 km, are used to obtain more detailed results.

In Spain, there are two sources of climate change projections: the data provided by the *Agencia Estatal de Meteorología* (AEMET) and the projections provided by the Coordinated Regional Climate Downscaling Experiment (CORDEX). Garijo et al. (2018) found that the CORDEX precipitation projections performed better for studies focused on extreme events than the AEMET projections. Therefore, climate change projections provided by CORDEX will be used in this study.

This study aims to assess how climate change will affect hydrological dam safety at the Eugui Dam (Spain) that has a gated spillway. The paper is organized as follows. First, a description of the study area, followed by a description of the data and models used. Subsequently, the methodology used is described. The results of the maximum reservoir water levels in flood events obtained with the previous procedure will be commented. Finally, conclusions will be presented.

## 2. Materials and Methods

The Eugui Dam selected for the study is located in the region of Navarre in northern Spain. The dam is on the River Arga that belongs to the Ebro River Basin Authority. The draining catchment area to the Eugui Reservoir is 69 km$^2$. The observed flow data required for model calibration were obtained from a 15-min gauging station located at the dam that provides reservoir water levels and outflow releases from the dam. Therefore, inflow discharges can be obtained by applying mass conservation. Three models are used in this study. The STORAGE stochastic rainfall generation model (De Luca et. al., 2021) is based on the Neymann-Scott Rectangular Pulse Model. This model allows to simulate rainfall at different sub-daily scales, thus obtaining more accuracy when generating flood hydrographs. The COSMO4SUB model is used for runoff generation. It generates continuous runoff time series as output data from which annual maximum hydrographs are extracted. Finally, the Volumetric Evaluation Method (VEM) (Girón 1988) is used to simulate the optimal operation of the spillway gates in flood events.

## 3. Results

Reservoir outflow quantiles for a set of return periods are calculated by fitting a GEV distribution function to the VEM outputs, in order to obtain the expected changes driven by climate change in the future compared with the control period. The results show that the median values of outflow quantiles are expected to be lower in both future scenarios than in the control period. The change magnitude is reduced for high return periods (500-5000 years). High return periods have been considered, as they are required for spillway design and safety assessment.

## 4. Conclusions

At the Eugui dam, future outflows are expected to be equal or lower than in the current situation represented by the control period. The reservoir water levels are also expected to be lower than in the current situation, though the dam crest elevation will be exceeded when it is assumed that the reservoir is full at the beginning of the flood event. In addition, this is a restrictive condition, and the results can also point to the need to leave greater surcharges when floods are expected, quantifying their magnitude.

**Acknowledgements**

This research has been supported by the project 'SAFERDAMS: Assessment of the impact of climate change on hydrological dam safety' (PID2019-107027RB-I00 / AEI / 10.13039/501100011033) and the grant for pre-doctoral contracts to train PhD students PRE2020-091861 both funded by the Spanish Ministry of Science and Innovation. The international collaboration with the Tuscia University for the realization of this research has been supported by the 'Programa Propio UPM 2021' funded by the Universidad Politécnica de Madrid with the collaboration of Santander bank.

**References**

De Luca D.L., Petroselli A. (2021). STORAGE (STOchastic RAinfall GEnerator): a user-friendly software for generating long and high-resolution rainfall time series. Hydrology 2021, 8, 76.
Garijo C, Mediero L, Garrote L (2018) Usefulness of AEMET generated climate projections for climate change impact studies on floods at national-scale (Spain). Ingeniería del agua 22(3):153–166
Girón, F.; Yagüe, J.; Martínez, R. Flood routing in reservoirs base on hydrological forecasting. In Proceedings of the Trans Twentieth International Congress on Large Dams, Beijing, China, 2000; Rapports on Question 79, Response 25 (Q79-R25); International Commission on Large Dams: Paris, France, 2000; Volume 4, pp. 403–417
Grimaldi S., Nardi F., Piscopia R., Petroselli A., Apollonio C. (2021). Continuous hydrologic modelling for design simulation in small and ungauged basins: a step forward and some tests for its practical use. Journal of Hydrology 595, 125664.

# Theoretical Hydrodynamic Formulation for Wave Interactions with Permeable Cylindrical Elements

Dimitrios KONISPOLIATIS[1], Ioannis CHATJIGEORGIOU[1]

[1] Laboratory for Floating Structures and Mooring Systems, Division of Marine Structures, School of Naval Architecture and Marine Engineering, National Technical University of Athens, Greece
email: dkonisp@naval.ntua.gr; chatzi@naval.ntua.gr

ABSTRACT

A theoretical hydrodynamic formulation is presented for wave interactions on structures composed by permeable and impermeable surfaces. The idea conceived, is based on the capability of permeable bodies to dissipate the wave energy and to minimize the environmental impact, developing wave attenuation and protection. In this study the diffraction problem of water waves by a permeable vertical, sea bottom seated, cylindrical body is formulated within the framework of the linear potential theory. The results revealed that porosity plays a key role in reducing/controlling the exciting wave loads, hence porous barriers can be set up to protect a marine structure against the wave attack.

## 1. Introduction

In the recent decades, much effort has been made on wave interaction with submerged, bottom mounted surface piercing, marine structures. Such structure formation is encountered in piles of floating islands, quay piles, connecting bridge columns and columns of very large floating structures, i.e., floating airports. However, these structures are often struggled to commercialize due to harsh environment conditions at the locations of installation and the severe exciting wave loads. Therefore, research has been focused on marine structures with permeable portion since they can reduce the influence of the wave interaction through the pores of the body surface when compared to impermeable bodies. Permeable bodies constitute an important class of numerous works in the literature. To raise some of them as examples, Wang and Ren (1994) examined a concentric surface-piercing two-cylinder system, in which the exterior cylinder is permeable and the interior body is assumed impermeable, whereas Teng et al. (2001) studied the diffraction problem of a cylindrical body with upper porous outer wall and inner solid column. Williams et al. (2000) investigated water wave interactions with a floating porous cylinder embodying a permeable side surface and impermeable top and bottom. Other similar studies on permeable structures are those from Bao et al. (2009) and Sankar and Bora (2019; 2020).

## 2. Theoretical formulation

A permeable system of two co-axes, vertical, sea bottom seated, and surface piercing cylindrical bodies is considered. The exterior cylinder is assumed permeable and thin of thickness, with radius $a$, while the interior cylinder is impermeable, with a radius $b$. The system, which is bottom fixed, is surrounded by a fluid of finite depth $d$ (see Fig. 1). The fluid domain is divided into two regions, i.e., region $I$ ($r \geq a; 0 \leq z \leq d$) and region $II$ ($b \leq r \leq a; 0 \leq z \leq d$), and it is assumed incompressible, inviscid and its motion irrotational. A cylindrical coordinate system $(r, \theta, z)$ is considered on the seabed, and its origin is located at the center of the impermeable cylinder. The flow is governed by the diffraction velocity potential $\varphi_D^k,\ k = I, II$. It holds that $\varphi_D^I = \varphi_0^I + \varphi_7^I$, where $\varphi_0^I$ is the velocity potential of the incident harmonic waves and $\varphi_7^I$ the scattered potential around the system. The complex velocity potentials $\varphi_D^k,\ k = I, II$ have to fulfill the Laplace equation in the entire fluid domain and the proper boundary conditions on the free water surface and the seabed. Also, $\varphi_7^I$ must satisfy an appropriate radiation condition at infinity. Furthermore, the following equation on the mean body's impermeable and permeable surfaces should be also satisfied.

$$\frac{\partial \varphi_7^{II}}{\partial r} = ikG(\varphi_7^{II} - \varphi_7^{I}), \text{on } r = a; \quad \frac{\partial \varphi_7^{II}}{\partial r} = 0, \text{on } r = b \tag{1}$$

In Eq. (1) $k$ denotes the wave number and $G$ stands for a dimensionless permeable coefficient (Konispoliatis et al., 2022). Applying the method of separation of variables in the Laplace equation the velocity potential can be expressed as a superposition of eigenfunction solutions satisfying the corresponding boundary conditions at the surface boundaries of the body (Konispoliatis et al., 2022).

## 3. Numerical results

This subsection is dedicated to the presentation of the horizontal exciting forces on the system's impermeable wetted surface (i.e., inner cylindrical body). Here, the inner radius equals to $b = a/2$ and the water depth $d = 4b$. Several real and complex dimensionless porous coefficients are examined, i.e., $G = 0.5, 1, 2.5, 5$ and $G = 0.5 + i,\ 1 + i, 2.5 + i, 5 + i$. Also, the case without the presence of the permeable sidewall is considered. It should be noted that for $G = 0$ the sidewall is assumed impermeable (i.e., no water is getting inside or outside the surface), whereas as $G$ increases, more water is allowed through the pores of the side surface, until $G \gg 0$, in which the surface is, literally, completely permeable to fluid (i.e., no presence of the surface). The presented numerical results are normalized by the factor $2\rho g d b(H/2)$, where $\rho$ is the water density and $g$ is the gravity acceleration.

It can be seen from the Fig. 2a, b that as the porous coefficient decreases the horizontal exciting forces on the impermeable cylindrical body also decrease, since the permeable surface dissipates the wave energy, concluding that the presence of the permeable surface can reduce the wave loads on the body. As far as the effect of the real and complex porous coefficient on the exciting forces is concerned, it can be seen that the imaginary part of $G$ causes a decrease of the values of the horizontal forces. Physically, the real and imaginary part of the porous coefficient represent the drag term and the inertia term (Teng et al., 2001).

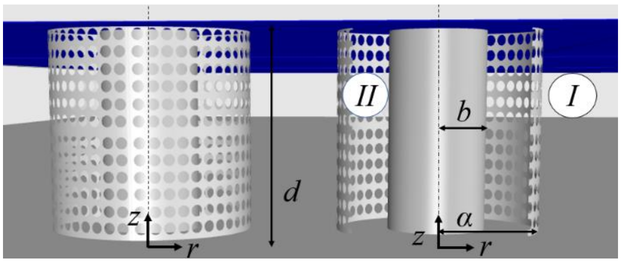


**Fig. 1.** 3-D representation of the examined permeable cylindrical system

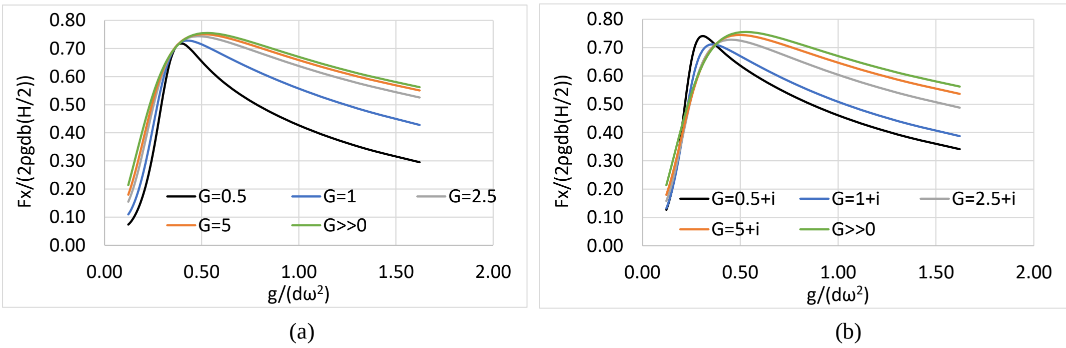


**Fig. 2.** Dimensionless horizontal exciting forces for various examined $G$ values. The results are also compared with the case of a fully permeable side wall, i.e., $G$ >>0: (a) Real values of $G$; (b) Complex values of $G$

**Acknowledgements**

This research has been financed by Greek national funds through the Operational Program "Competitiveness, Entrepreneurship & Innovation" of the National Strategic Reference Framework (NSRF) – Research Funding Program: "MATISSE: Study of the appropriateness and the adequacy of modern materials for offshore fish cage – numerical and experimental investigation in realistic loading conditions".

**References**

Bao W, Kinoshita T, Zhao F (2009) Wave forces acting on a semisubmerged porous circular cylinder, Proceedings of the Institution of Mechanical Engineers, Part M: Journal of Engineering for the Maritime Environment, 223 (3), 349–360
Konispoliatis DN, Chatjigeorgiou IK, Mavrakos SA (2022) Hydrodynamics of a moored permeable vertical cylindrical body, Journal of Marine Science and Engineering, 10 (3), 403
Sankar A, Bora SN (2019) Hydrodynamic forces due to water wave interaction with a bottom-mounted surface-piercing compound porous cylinder, Ocean Engineering, 171, 59–70
Sankar A, Bora SN (2020) Hydrodynamic coefficients for a floating semi-porous compound cylinder in finite ocean depth, Marine Systems and Ocean Technology, 15, 270–285
Teng B, Zhao M, Li Y (2001) Wave diffraction from a cylinder with porous upper wall and an inner column, Acta Oceanologica Sinica, 23, 6
Wang KH, Ren R (1994) Wave interaction with a concentric porous cylindrical system, Ocean Engineering, 21 (4), 343–360
Williams AN, Li W, Wang KH (2000) Water wave interaction with floating porous cylinder, Ocean Engineering, 27, 1–28

# Assessing the spatial impact of the skewness-ratio originating from the time irreversibility and long-range dependence of streamflow in flood inundation mapping

Panayiotis DIMITRIADIS[1], Theano ILIOPOULOU[1], Demetris KOUTSOYIANNIS[1]

[1]Department of Water Resources and Environmental Engineering, Greece
email: pandim@itia.ntua.gr; tiliopoulou@hydro.ntua.gr; dk@itia.ntua.gr

ABSTRACT

The skewness-ratio (i.e., standardized skewness of the differenced process) is shown to have a high impact to the average (over all inundated cells) of flood-related variables, such as depth and velocity, when is originated from a streamflow process exhibiting time-irreversibility (i.e., its joint distribution changes after reflection of time about the origin) and/or long-range dependence (i.e., power-law asymptotic decay of its autocorrelation function). A simple way to quantify time-irreversibility is through the skewness coefficient of the differenced process, while the long-range dependence behaviour can be identified through the climacogram estimator (i.e., adapted for bias variance of the averaged process vs. scale). In this work, the spatial distribution of the skewness-ratio is assessed and quantified through a real case scenario of flood mapping. It is found and discussed that depending on the distance from the river, different degrees of skewness-ratios may exist and have an impact on the temporal distribution of the flood-momentum and the increase of flood-risk.

**Keywords**: stochastics, flood, streamflow, dependence, irreversibility

## 1. Introduction, Methods and Application

The long-range dependence (also known as long-term persistence or the Hurst phenomenon; Hurst, 1951) is related to the asymptotic power-law behaviour at large scales of the autocorrelation function of a stochastic process. It is shown that it can be efficiently simulated through the explicit preservation of the climacogram (i.e., adapted for bias variance of the averaged process at the scale domain; which is preferred to the more traditional autocovariance and power-spectrum at the lag and frequency domains, respectively; Dimitriadis and Koutsoyiannis, 2015) along with the probability distribution function of the process expressed through any number of its marginal moments (Koutsoyiannis and Dimitriadis, 2021). Interestingly, most of the key hydrological-cycle processes are shown to exhibit the long-range dependence behaviour (Dimitriadis et al., 2021).

The time-irreversibility is a model attribute of a stochastic process related to its distribution in time, which is shown to be efficiently simulated through the preservation of the skewness coefficient of the differenced process (Koutsoyiannis, 2019). Although for most of the key hydrological-cycle processes, time-irreversibility can be assumed negligible at fine scales (and is often apparent in high-resolution timeseries), for the streamflow process its impact can last even for several days (Vavoulogiannis et al., 2021).

Both the long-range dependence and the time-irreversibility can highly increase the variability of the streamflow process, and therefore, to any related processes such as the ones involved in flood inundation mapping (e.g., flood depth and water velocity). In this work, the impact of time-irreversibility and long-range dependence is assessed through the spatial distribution of the skewness-ratio (i.e., standardized skewness of the differenced process) of the depth and velocity through a Monte-Carlo application of flood mapping at the Peneios river in Greece (Fig. 1).

## 2. Results and Discussion

To test the impact of both behaviours (i.e., time-irreversibility and long-range dependence) in the flood mapping, a Monte-Carlo experiment is performed at the area of interest (Fig. 1). Particularly, 100 synthetic streamflow timeseries are generated by preserving the important stochastic properties of a daily recorded timeseries of more than 10 years of length at an upstream station at the area of interest. For the simulation of the streamflow, the Asymmetric Moving Average (AMA) scheme (Koutsoyiannis, 2020) is employed, where the observed skewness coefficient of the timeseries and the differenced timeseries is estimated as 3.9 and 1.3, respectively, the Hurst parameter (indicative of the strength of the long-range dependence) is estimated as $H = 0.8$, and the Pareto-Burr-Feller probability distribution is used (for definition see Dimitriadis et al., 2021).

For the flood inundation, the dynamic-wave scheme of the HEC-RAS 2D model is applied with a rectangular grid of 50×50 m$^2$ pixel area (www.hec.usace.army.mil/software/hec-ras/). It is found that the skewness-ratio of both the flood depth and the water velocity are affected by the explicit preservation of time-irreversibility and long-range dependence, but at a different degree dependent on the distance from the river, which carries the longitudinal momentum of the flood, and therefore, it is expected to have an impact on flood-risk.

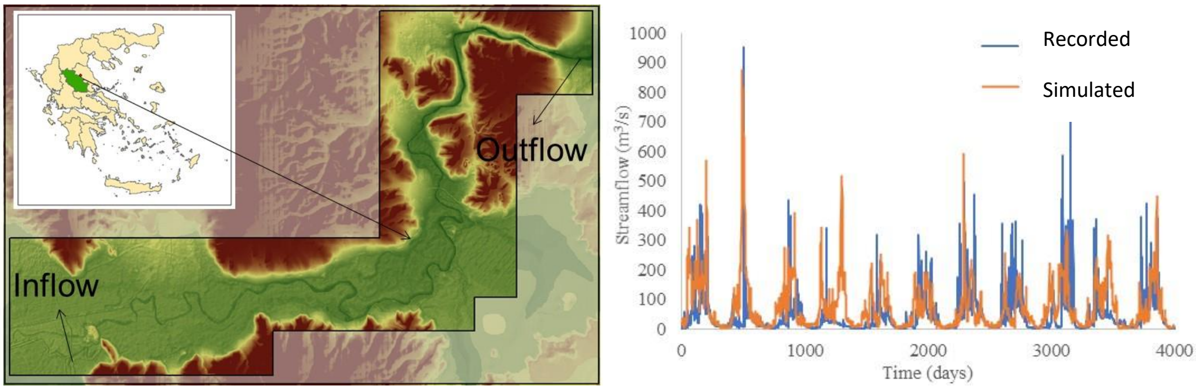


**Fig. 1.** The area of interest at the Peneios river in the Thessaly plain (Greece) [left]; A recorded timeseries at the upstream station (inflow) and a simulated one preserving time-irreversibility and long-range dependence.

**Acknowledgements**

This research is partly carried out / funded in the context of the project “Development of Stochastic Methods for Extremes (ASMA): identification and simulation of dependence structures of extreme hydrological events” (MIS 5049175) under the call for proposals “Researchers’ support with an emphasis on young researchers—2nd Cycle”. The project is co-financed by Greece and the European Union (European Social Fund; ESF) by the Operational Programme Human Resources Development, Education, and Lifelong Learning 2014–2020.

Ευρωπαϊκή Ένωση
Ευρωπαϊκό Κοινωνικό Ταμείο

Επιχειρησιακό Πρόγραμμα
Ανάπτυξη Ανθρώπινου Δυναμικού, Εκπαίδευση και Διά Βίου Μάθηση
Ειδική Υπηρεσία Διαχείρισης
Με τη συγχρηματοδότηση της Ελλάδας και της Ευρωπαϊκής Ένωσης

ΕΣΠΑ 2014-2020
ανάπτυξη - εργασία - αλληλεγγύη

**References**

Dimitriadis P, Koutsoyiannis D (2015) Climacogram versus autocovariance and power spectrum in stochastic modelling for Markovian and Hurst–Kolmogorov processes, Stoch. Environ. Res. Risk Assess., 29, 1649–1669.

Dimitriadis P, Koutsoyiannis D, Iliopoulou T, Papanicolaou P (2021) A global-scale investigation of stochastic similarities in marginal distribution and dependence structure of key hydrological-cycle processes, Hydrology, 8 (2), 59.

Hurst HE (1951) Long-Term Storage Capacity of Reservoirs, Trans. Am. Soc. Civ. Eng., 116, 770–799.

Koutsoyiannis D., Time’s arrow in stochastic characterization and simulation of atmospheric and hydrological processes, Hydrological Sciences Journal, 64 (9), 1013–1037, doi:10.1080/02626667.2019.1600700, 2019.

Koutsoyiannis D (2020) Simple stochastic simulation of time irreversible and reversible processes, Hydrological Sciences Journal, 65 (4), 536–551.

Koutsoyiannis D, Dimitriadis P (2021) Towards generic simulation for demanding stochastic processes, Sci, 3, 34.

Vavoulogiannis S, Iliopoulou T, Dimitriadis P, Koutsoyiannis D. (2021) Multiscale temporal irreversibility of streamflow and its stochastic modelling, Hydrology, 8 (2), 63.

# Reconstructing a flood event: collecting field data and numerical modeling

Vasilis BELLOS[1], Ioannis KOURTIS[2], Eirini RAPTAKI[3], Spyridon HANDRINOS[4], Ioannis SIBETHEROS[5], Vassilios A. TSIHRINTZIS[6]

[1] Democritus University of Thrace, Greece
email: vbellos@env.duth.gr

[2,3,6] National Technical University of Athens
email: johnkourtis90@hotmail.com; eirinirap26@gmail.com; tsihrin@survey.ntua.gr

[4,5] University of West Attica
email: cw6661@uniwa.gr; sibetheros@uniwa.gr

ABSTRACT

Herein, a reconstruction of the flash flood of Mandra (Greece, 2017) is presented, based on field data collection and the use of two different numerical models. Specifically, we developed a field dataset of post-flood mud footprints on buildings and used it to calibrate the hydrodynamic HEC-RAS software; then, the hydrodynamic MIKE FLOOD software was run, using the same input parameter values as in the calibrated HEC-RAS model (informed modeling).

## 1. Introduction

On 15th of November 2017, a severe flood hit the town of Mandra which is located about 20 km north-west of the center of Athens, Greece. The socio-economic consequences were huge, while 24 casualties were reported. Since then, there have been several attempts to model this event, e.g., Diakakis et al. (2019) and Bellos et al. (2020). In this work, we perform a posterior simulation of the event at three steps: a) collecting field data of post-event mud footprints on buildings; b) simulating the event applying the HEC-RAS software and using the collected field data for calibration and validation of the required input parameters; c) running the MIKE-FLOOD software using the above calibrated values.

## 2. Post-event analysis

A few days after the flood event, maximum water depth data were collected in the field, using as a proxy the mud footprints observed on the walls of the inundated houses and buildings. Specifically, the research team collected 44 maximum water depths distributed in the city, which are depicted in Figure 1.

For the numerical modeling, HEC-RAS was used first within the urban area, and specifically the 2D diffusion wave model, which is a simpler model of the 2D Shallow Water Equations. The input was an ensemble of 100 hydrographs, produced by Bellos et al. (2020) based on a Monte Carlo approach, which enter the city from the upstream Agia Aikaterini catchment. In order to represent the buildings within the city, a local increase of Manning coefficient was employed. The required input parameters of the model were calibrated via a grid-search algorithm against the collected field data, as described by Handrinos et al. (2021). As far as the Confidence Interval (*CI*) of the input flood hydrograph is concerned, the calibrated value was $CI$=30%, whereas for the Manning coefficient $n$ of the city roads, the calibrated value was $n=0.06$ s/m$^{1/3}$.

Subsequently, we transferred the HEC-RAS calibrated input parameter values to MIKE FLOOD, which also solves the 2D diffusion wave equations, but using a different numerical method. The MIKE FLOOD configuration (computational area, boundary conditions, bathymetry, boundaries of buildings) was the same as in HEC-RAS, except for the way used to represent buildings (free-slip boundary condition). The comparison between the observed data, the numerical results derived by the calibrated HEC-RAS model and the corresponding results derived by the informed MIKE FLOOD model is depicted in Figure 2. The Root Mean Square Error (RMSE) metric for HEC-RAS was 0.73 m while the corresponding for MIKE was 1.63 m.


**Fig. 1.** Computational domain of Mandra town and location of the observation points

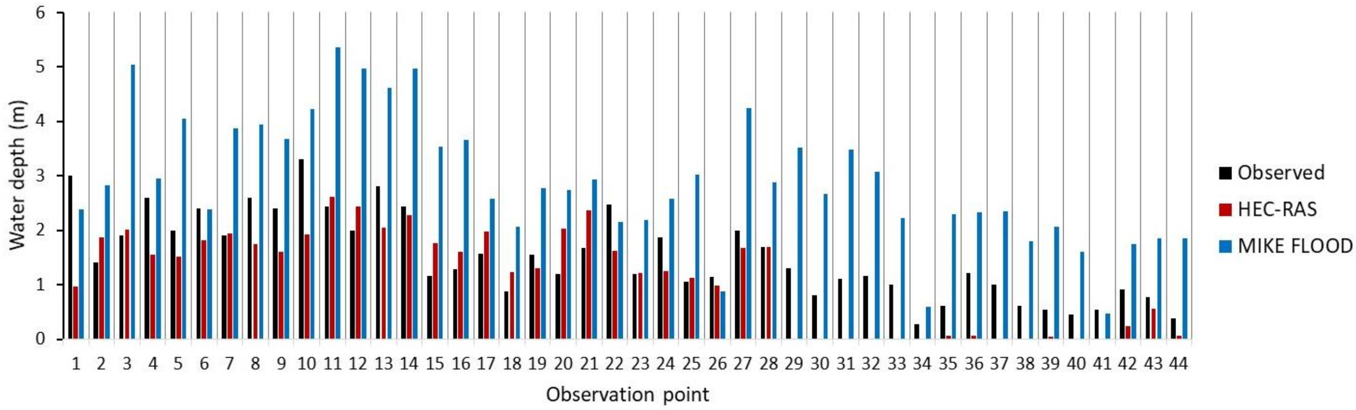


**Fig. 1.** Comparison between observed data, HEC-RAS results (calibrated) and MIKE FLOOD results (informed)

## 3. Discussion and concluding remarks

In this work, a three-step reconstruction of a flood event is presented, which includes maximum flood depth field data collection, calibration of the required input parameters of a numerical model against the observed field data, and transfer of the calibrated input parameters to another numerical model. In general, there is an area of the city where both models failed to reproduce the flood sufficiently, either overestimating or underestimating the maximum observed flood depths (gauges 29-41), which is probably due to each model's structure and the simplifying assumption regarding the validity of the diffusion wave model. For the remaining observation points, the calibrated HEC-RAS seems to capture the flood characteristics reasonably well. On the other hand, the indirectly calibrated MIKE FLOOD seems to overestimate flood depths in a systematic way. The latter observation does not indicate that one software is better than the other, but that every software has its dynamics and the transferability of the parameter values cannot be performed in blind trust, while a direct calibration of a model's input parameters is preferable.

**Acknowledgements**: Thanks are expressed to DHI (Greece) for providing free access to the MIKE FLOOD software.

**References**

Bellos V, Papageorgaki I, Kourtis I, Vangelis H, Kalogiros I, Tsakiris G (2020) Reconstruction of a flash flood event using a 2D hydrodynamic model under spatial and temporal variability of storm, Natural Hazards, 101(3), 711-726.

Diakakis M, Andreadakis E, Nikolopoulos EI, Spyrou NI, Gogou ME, Deligiannakis G, Katsetsiadou NK, Antoniadis Z, Melaki M, Georgakopoulos A, Tsaprouni K, Lekkas E (2019) An integrated approach of ground and aerial observations in flash flood disaster investigations. The case of the 2017 Mandra flash flood in Greece, International Journal of Disaster Risk Reduction, 33, 290–309.

Handrinos S, Bellos V, Sibetheros I (2021) Simulation of an urban flash flood: the 2017 flood event in Mandra, Attica. Proceedings of 17th International Conference on Environmental Science and Technology, Athens, Greece.

# Effects of nonlinearity on crest dimensions of extreme waves in random seas

George SPILIOTOPOULOS[1], Vanessa KATSARDI[1]

[1] Department of Civil Engineering, University of Thessaly, Greece
email: gspiliotop@uth.gr
email: vkatsardi@uth.gr

ABSTRACT

This work highlights the effects of nonlinearity on extreme events rising during directional focused and random wave simulations in finite water depths. Large waves are formed through a series of linear and nonlinear focused and random simulations. The effect of water depth and directionality is considered by applying different directional spreadings relating to a range of short crested to long crested sea states. The sea-state becomes more long-crested during the formulation of the extreme events in both focused and random nonlinear simulations, while being highly dependent on the directionality of the wavefield.

## 1. Introduction

The determination of the largest crest elevations of the design wave is paramount for the determination of any over-topping and the calculation of the wave loads acting on marine and coastal structures. The affected area hit by an extreme event, associated with the crest width, can have a large effect on the stability and resilience of the structure. Adcock et al. (2015) have worked on simulated nonlinear random deep-water directional waves measuring the changes of the crest width during the formulation of large waves compared to linear theory, using the weakly nonlinear Schrödinger equation. They have shown that even where there is only a marginal change in the maximum surface elevation, there is an increase in the crest width and the large waves tend to move to the front of the wave packet, extending the crest width but also the duration of the extreme events compared to the ones predicted by linear theory; the so-called "walls of water".

This study focuses on the large events' wave-front of the wave crest and highlights the necessity to incorporate physics beyond linear theory in relation to the crest width. Firstly, it seeks to confirm the deep-water findings of Adcock et al. considering a fully nonlinear model incorporating a broad-banded energy distribution in the various frequencies. The main purpose of this work though, is to investigate whether these findings in deep-water are also relevant to large waves propagating in finite water, for a series of short-crested to long-crested directional focused and random wavefields.

## 2. Wave Modelling

### *2.1. HOS-Ocean*

HOS-Ocean (Ducrozet et al., 2016) is an open-source fully nonlinear model that can simulate the evolution of a fully nonlinear wavefield, incorporating the wave energy spread both in the various frequencies and the various directions without any narrow-banded assumptions. It is based on the High-Order Spectral method, presented in the original work of West et al. (1989) and Dommermuth and Yue (1989).

### *2.2. Initial Conditions*

The initial conditions for all simulations involved a JONSWAP amplitude spectrum with a peak period of $T_p$ = 10s, a peak enhancement factor of $\gamma = 2.5$ and a linear amplitude sum of the frequency components equal to $A = \Sigma_{ai}$ = 9.5m for focused wave events and A = 25m for the random. The Mitsuyasu (1975) spreading parameters used for comparison are s = 7, s = 45 and s = 150. The simulations were first conducted for infinite water depth conditions and then for finite water depth (15m), keeping every other parameter the same.

### *2.3. Measuring crest width*

In order to measure an effective crest width, a minimum of 30% of the $\eta_{max}$ of each linear case is considered, so as to measure the portion of the crest that is exceeding this height. By measuring crest width above a certain threshold, ensures that the measurement accurately represents the effect of the large wave, while considering the heights that hold more significance for an event labeled as extreme.

## 3. Results

### 3.1. Deep Water

Overall, the results in deep water are relatively consistent with the findings of Adcock et al. (2015), showing significant increases in crest width while maintaining a small but significant increase in crest height. Particularly in less directional cases, where the crest width increase is close to 40%, the change in shape of the highest crest is evident; the crest has a slight bend around the direction of propagation while having a slimmer profile creating a so-called "wall of water".

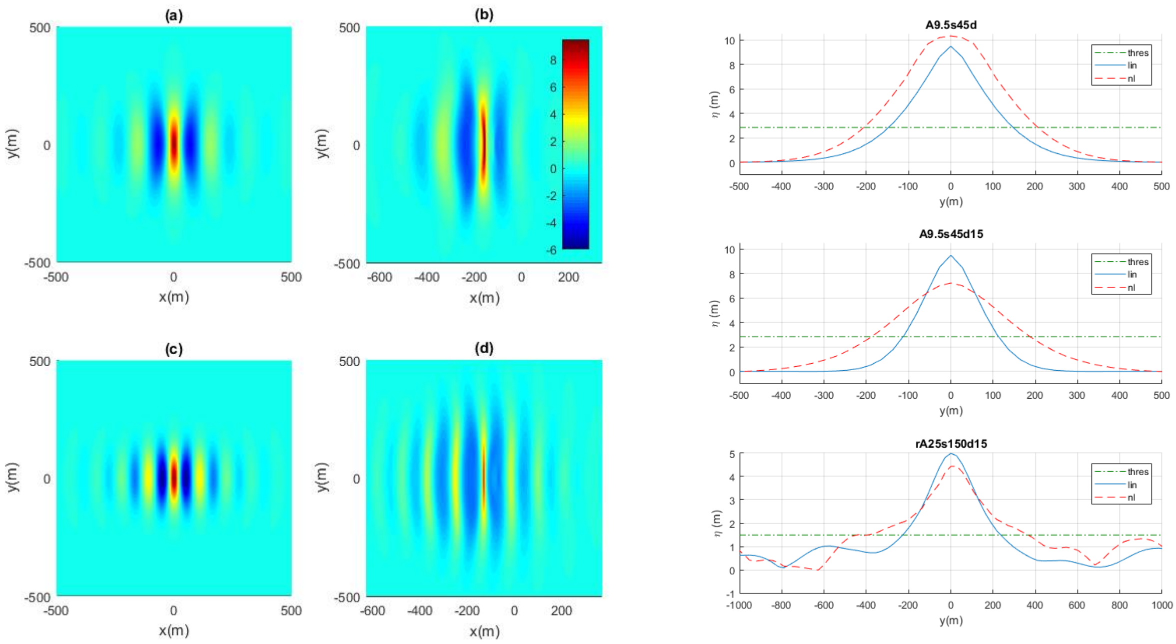


**Fig. 1.** Left: Contour plots for long-crested focused events for (a,c) linear case, (b,d) nonlinear case in (a,b) deep, (c,d) intermediate water, Right: Comparisons between linear and nonlinear crest width

### 3.2. Intermediate Water

In intermediate water, the results show a significant difference in the trend shown in deep water. Crest height is significantly reduced, particularly in the less directional cases but the energy is spread much more widely along the perpendicular direction to propagation (y). This causes a large increase in crest width, with the disturbance in the wavefield during the extreme events being almost double as wide during nonlinear propagation.

## 4. Conclusions

In all simulations, focused and random, a clear trend of increased crest width during nonlinear formation of large wave events is evident, both in deep and intermediate water. While confirming the results of Adcock et al. (2015) in deep water, this work makes the case for the formation of similar "walls of water" in intermediate depth. Despite reduction in crest height compared to linear, nonlinear results show a much wider energy spread along the perpendicular direction to propagation, particularly in less directional wavefields. This has the effect of significantly wider distance over the 30% of the linear $\eta_{max}$ threshold, despite the reduction in crest height.

**References**

Adcock, TAA, Taylor, PH, and Draper, S, (2015). Nonlinear dynamics of wave-groups in random seas: unexpected walls of water in the open ocean. Proceedings of the Royal Society A, 471(20150660).

Dommermuth, D, and Yue, D, (1987). A high-order spectral method for the study of nonlinear gravity waves. Journal of Fluid Mechanics, 184, pp. 267–288.

Ducrozet, G, Bonnefoy, F, Le Touzé, D, and Ferrant, P, (2016). HOS-ocean: Open-source solver for nonlinear waves in open ocean based on High-Order Spectral method. Computer Physics Communications, 203, pp. 245–254.

Mitsuyasu, H, (1975). Observations of directional spectrum of ocean waves using a cloverleaf buoy. Journal of Physical Oceanography, 16, pp. 750–760.

West, B, Brueckner, K, Janda, R, Milder, M, and Milton, R, 1987. A new numerical method for surface hydrodynamics. Journal of Geophysical Research, 92, pp. 11803–11824.

# Point-to-pixel comparison of a satellite and a gauge -based Intensity-Duration-Frequency (IDF) curve: The case of Karditsa, Greece

Ioannis M. KOURTIS[1], Vasilis BELLOS[2], Ioanna ZOTOU[1], Harris VANGELIS[1], Vassilios A. TSIHRINTZIS[1]

[1]National Technical University of Athens, Greece

[2]Democritus University of Thrace, Greece

email: gkourtis@mail.ntua.gr; vbellos@env.duth.gr; iwanna_zwtou@hotmail.com; harrivag@mail.ntua.gr; tsihrin@otenet.gr

ABSTRACT

In the present work, Intensity-Duration-Frequency (IDF) curves are developed based on a global precipitation dataset, namely the satellite dataset of the National Oceanic and Atmospheric Administration (NOAA) called Climate Prediction Center Morphing (CMORPH) product. IDF curves were developed using the Generalized Extreme Value Distribution (GEV). Parameters of the distribution were estimated employing the L-Moments method, for time scales ranging from 30 min to 48 h and for return periods of 2, 5, 10, 25, 50, 100, 500, 1,000 and 10,000 years. Furthermore, the satellite-based IDF curves were compared, a "point-to-pixel" analysis, with the rain gauge-based IDF curves recently developed by the Greek Flood Risk Management Plan for Thessaly River Basin District. The results revealed a variability ranging from about -15 % to about 60 %, depending on the duration and the return period examined. Overall, as the return period increases the percent difference decreases.

## 1. Introduction

Development of Intensity-Duration-Frequency (IDF) curves is based on frequency analysis of past records of rainfall Annual Maxima Series (AMS) and/or Peak over Threshold (POT) series. However, in many regions around the world, especially in developing countries, long rainfall datasets are not available because of limitation in spatial coverage, short rainfall records and low data quality. Researchers have investigated the use of alternative rainfall measurement methods for developing IDF curves, such as radar and satellite (e.g., Marra et al., 2017; Bertini et al., 2020). However, there are still limitations related to these approaches. In relation to the aforementioned issues, the main goals of the present work were to: (i) develop IDF curves utilizing a satellite derived global dataset; and (ii) compare the satellite-based IDF curves with the rain gauge-based IDF curves recently reported by the Greek Flood Risk Management Plan for Thessaly River Basin District (RBD; 2017).

## 2. Materials and Methods

The IDF curve for the Karditsa station (lat.: 39.37, long.: 21.93, altitude: 103 m a.m.s.l.), recently developed by the Greek Flood Risk Management Plan for the Thessaly RBD (2017), is given by Eq. (1).

$$i = \frac{42.103(T^{0.18} - 0.466)}{(1+\dfrac{t}{0.754})^{0.691}} \quad (1)$$

where: $i$ is the rainfall intensity (mm/h), $T$ is the return period (years), and $t$ is storm duration (h).

During the last years, a wide variety of satellite precipitation products have been developed (e.g., GPCP, CMAP, TRMM, CPC, PERSIANN, CMORPH, GPM, MSWEP), with temporal resolution ranging from 30 min to monthly and spatial resolution ranging from 0.1° to 2.5°. For more information and an inter-comparison of the various products the interesting reader is referred to Sun et al. (2017). In the present work, we utilized the CMORPH dataset (Joyce et al., 2004), as it has the highest spatial (i.e., 8 km x 8km) and temporal resolution (i.e., 30 min) and the longest record (1998-2019). Data was downloaded from the data server of the Climate Prediction Center (CPC) of the National Oceanic and Atmospheric Administration (NOAA; ftp://ftp.cpc.ncep.noaa.gov/precip/global_CMORPH/). A MATLAB code was written in order to extract the needed information (i.e., precipitation data for the pixel of Karditsa station). Finally, the Generalized Extreme Value (GEV) distribution was used for modeling AMS, with parameters being computed using the L-Moments method, for rainfall duration of 30 min, 1 h, 2 h, 3h, 6 h, 12 h, 24 h and 48 h and return periods of 2, 5, 10, 25, 50, 100, 500, 1,000 and 10,000 years. All computations were undertaken utilizing the Hydrognomon software.

## 3. Results and concluding remarks

Eq. (2) presents the IDF curve, developed based on the CMORPH global dataset. The IDF curve has been developed for the pixel representing Karditsa station. The distance between the cell center and the rain gauge is about 500 m.

$$i = \frac{68.733(T^{0.15} - 0.450)}{(1 + \frac{t}{0.996})^{0.836}} \quad (2)$$

where: $i$ is the rainfall intensity (mm/h), $T$ is the return period (years), and $t$ is storm duration (h).

The change factor of rainfall intensities, Eq. (2) to Eq. (1), ranges from 0.78 to 1.63. Fig. 1 presents the change factor between the satellite-derived and the rain gauge-derived IDF curves for different durations and return periods. It can be observed, that as the return period increases the change factor (i.e., difference) between the satellite-derived and the rain gauge derived intensities decreases. Overall, the change factor in precipitation intensities ranges according to the return period and the duration examined. However, it must be noted that the reported change factor is affected by the use of a "point-to-pixel" analysis. Due to the nature of such an analysis there is an anticipated difference between the two estimates (point vs areal).

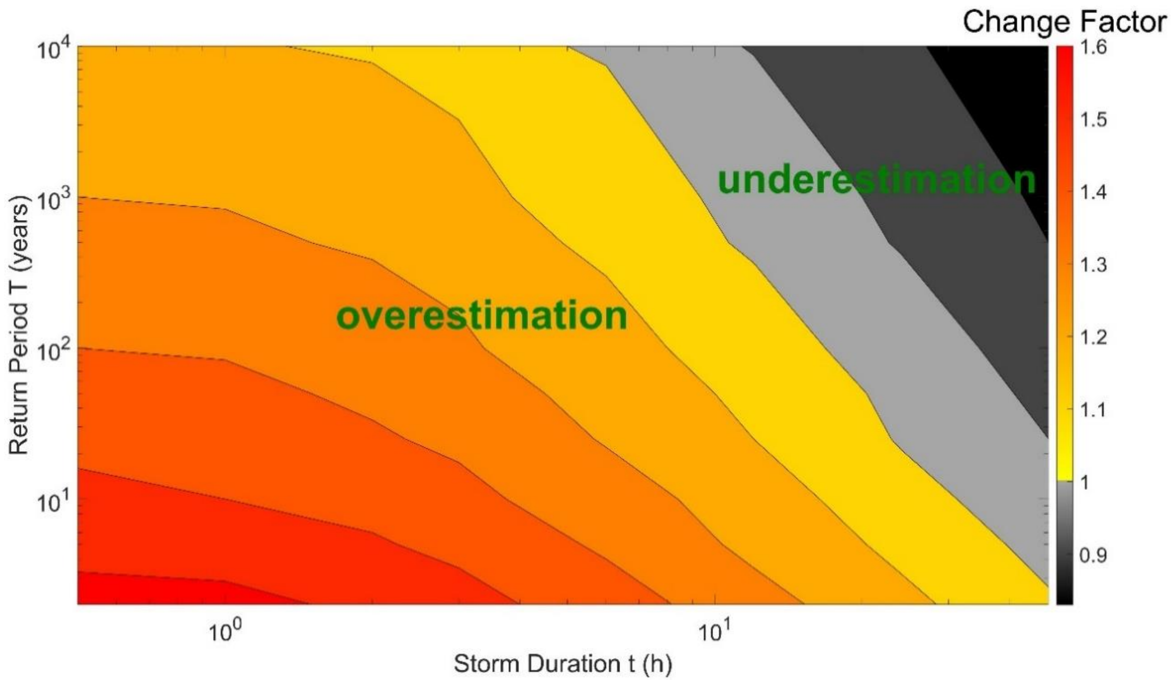


**Fig. 1.** Change factor between rainfall intensities for the satellite-derived and the rain gauge-derived IDF curves

Development of IDF curves is essential for planning of long-term management and adaptations in water related sectors. Overall, the comparison between the satellite-derived and the rain gauge derived IDF curves demonstrates the potential of using satellite-derived rainfall information for ungauged and/or poorly gauged basins. However, standardized guidelines for development of IDF curves employing satellite, radar and re-analysis precipitation data do not exist.

**References**

Bertini C, Buonora L, Ridolfi E, Russo F, Napolitano F (2020) On the use of satellite rainfall data to design a dam in an ungauged site, Water, 12(11), 3028

Flood Risk Management Plan for Attica River Basin District (EL06) (2017) IDF Curves (In Greek). (https://floods.ypeka.gr/egyFloods/gr08/report/GR08_P02_T1.pdf)

Joyce RJ, Janowiak JE, Arkin PA, Xie P (2004) CMORPH: A method that produces global precipitation estimates from passive microwave and infrared data at high spatial and temporal resolution, Journal of Hydrometeorology, 5(3), 487-503

Marra F, Morin E, Peleg N, Mei Y, Anagnostou EN (2017) Intensity–duration–frequency curves from remote sensing rainfall estimates: comparing satellite and weather radar over the eastern Mediterranean, Hydrology and Earth System Sciences, 21(5), 2389-2404

Sun Q, Miao C, Duan Q, Ashouri H, Sorooshian S, Hsu KL (2018) A review of global precipitation data sets: data sources, estimation, and intercomparisons, Reviews of Geophysics, 56(1), 79-107

# Improving flooding hazard numerical models through satellite observations

Kevis MBONYINSHUTI[1], Vito BACCHI[1], Boris BASIC[1], Sébastien BOYAVAL[2], Cédric GOEURY[1]

[1] National Laboratory of Hydraulic Environment, EDF R&D

email : kevis.mbonyinshuti@edf.fr
email: vito.bacchi@edf.fr
email: boris.basic@edf.fr
email: cedric.goeury@edf.fr

[2] The Saint-Venant Hydraulics Laboratory, France
email: sebastien.boyaval@enpc.fr

ABSTRACT

## 1. Context and objectives

Various tools are now available to confidently extract information about the dynamics of large water masses from satellite observations. We consider how to use them to improve the numerical prediction of floods by hydraulic models based on the 2D SWE, like TELEMAC- (www.opentelemac.org).

A number of studies have already tried to improve the calibration of the 2D SWE (i.e. the friction) for flood prediction. However, the procedure still needs qualifying on considering the various possibilities to use i.e. postprocess the data (Hostache et al., 2018).

In this contribution, we propose a procedure to post-process and next assimilate Sentinel-I SAR data into TELEMAC-2D. To start with, we evaluate the numerical prediction of a flood event of 3 days by TELEMAC-2D in comparison with the data post-processed following our proposed procedure. The numerical results show that our post-process data correlate well with numerical predictions obtained from pure in-situ data. So they could be further used to guide future predictions, after hybrid calibration with data collected in-situ and remotely.

## 2. Materials and methods

### *2.1. Case study*

The study area is in the center-east part of France, on the northern-east side of Lyon Metropolitan city, within the 20 300 km² of the Rhone at Lyon catchment area. We were provided with a TELEMAC-2D model of the area composed of 117 682 nodes and 233 906 meshes. It was built accordingly to obtain maximum precision in the Rhone riverbed and near road embankments for an optimum operation of the hydraulic gates. Thus, the different levels of mesh refinement are 25m long and 15m wide structured mesh in the riverbed and 10m to 50m mesh for the other areas. The model was calibrated on the flooding event of February 16th, 1990 using a detailed flood map of the event, flood lines and Cusset hydroelectric power plant operation details.

In-situ observation data of the current study domain originate from hydrometric stations located at the upstream and downstream of the domain. The latter are accessible through a National portal (https://www.hydro.eaufrance.fr/). Inflow discharge as well as water level since November 2014 are recorded by the stations.

Regarding satellite data, SAR has been chosen as the main source of information, its weather-independence and day-and-night capabilities provides tremendous advantages for monitoring flooding events. Sentinel-1 SAR products presents high temporal and spatial quality, while they are accessible through ESA Sentinel Hub (https://scihub.copernicus.eu/dhus/).

Remaining data include a 5m Digital Elevation Model (DEM) of the area, from French National Institute of Geographic and Forest Information open database (https://www.ign.fr/). The DEM is important for the retrieving of flood water depth maps, while it it has a 20 cm elevation accuracy. A 2018 Copernicus Mission's

Corine Land Cover grid of 100m resolution is used to extract the land characteristics. These characteristics are integrated in the model as suitable friction coefficients.

### *2.2. Methodology*

Flood extent mapping is a required step in accessing flood water depth maps. Using Sentinel-1 amplitude images, a flood extent map is retrieved after radiometric and geometric corrections. Two methods have been compared, namely the adaptive threshold method of Martinis et al (2015) and the Random-Forest classification method.

Flood extent maps provide flood boundaries information. Hence, flood water stages at the land-water interface as well as flood depth across the floodplain can be derived for a given event owing to an overlay operation with a high-resolution DEM, followed by a water surface elevation interpolation across the floodplain. After confronting processed data with hydrometric stations and numerical model results, remotely sensed datasets are used to recalibrate model roughness coefficients through 2D hydrodynamic calculations (Goeury et al, 2022).

## 3. Preliminary Results

Figure 1 presents flood extent extraction limitation using a single threshold technique owing to sensors difficulties in detecting flooded urbans areas due to double bounce backscatters.

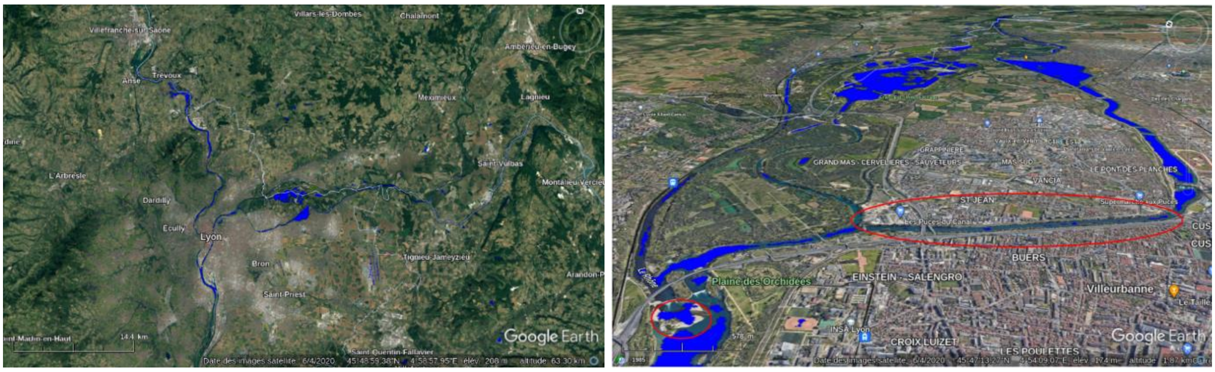


**Fig. 1.** Flood extent extraction from SAR Sentinel-1-A band-C image acquired on January 26th 2018, polarisation VV (Mbonyinshuti Kevis).

**Acknowledgements**

This study results from Kevis MBONYINSHUTI research internship at EDF LNHE, fully funded by EDF R&D. The authors wish to acknowledge Pierre-Louis Frison from LASTIG – Gustave Eiffel University, France, for his help and expertise in SAR data usage throughout the project.

**References**

Goeury, C., Audouin, Y., & Zaoui, F. (2022). Interoperability and computational framework for simulating open channel hydraulics: application to sensitivity analysis and calibration of Gironde Estuary model. Environmental Modelling & Software, 148, 105243.
Hostache, R.; Chini, M.; Giustarini, L.; Neal, J.; Kavetski, D.; Wood, M.; Corato, G.; Pelich, R.-M. & Matgen, P. Near-Real-Time Assimilation of SAR-Derived Flood Maps for Improving Flood Forecasts Water Resources Research, 2018, 54, 5516-5535.
Martinis, S., Kersten, J., & Twele, A. (2015). A fully automated TerraSAR-X based flood service. *ISPRS Journal of Photogrammetry and Remote Sensing*, *104*, 203-212.
Nguyen, T. H., Delmotte, A., Fatras, C., Kettig, P., Piacentini, A., & Ricci, S. (2021). Validation and improvement of data assimilation for flood hydrodynamic modelling using sar imagery data. arXiv preprint arXiv:2109.07470.
Schumann, G., Bates, P. D., Horritt, M. S., Matgen, P., & Pappenberger, F. (2009). Progress in integration of remote sensing–derived flood extent and stage data and hydraulic models. Reviews of Geophysics, 47(4).

# Principal Component Analysis in development of empirical scour formulae

Antonija HARASTI[1], Gordon GILJA[2], Nikola ADŽAGA[3], Kristina Ana ŠKREB[4]

[1,2,3,4] Faculty of Civil Engineering, University of Zagreb, Croatia
email: antonija.harasti@grad.unizg.hr (for author 1)
email: gordon.gilja@grad.unizg.hr (for author 2)
email: nikola.adzaga@grad.unizg.hr (for author 3)
email: kristina.ana.skreb@grad.unizg.hr (for author 4)

ABSTRACT

There are still unexplored phenomena that affect scour depth. On a group of bridge piers protected with riprap sloping structure, appearance of intensified downstream scour hole has been noticed. Considering that the geometry of riprap sloping structure affects the downstream scour hole, new parameters have to be included in the empirical formulae. Since employing new parameters may lead to inaccurate scour estimation because their dependence on other parameters is unknown, a Principal Component Analysis (PCA) is performed in this work to select the most important parameters in the scour process before introducing new parameters. The aim of this work is to test the contribution of the new parameters to the total variance of the scour depth.

## 1. Introduction

Scour is a complex phenomenon due to many independent processes that affect scour depth – complexity of the channel geometry, 3D flow pattern associated with vortex system, riverbed particle size distribution depending on of specific sediment transport mode (live-bed or clear-water), uncertainty due to the duration or sequence of multiple flood events, etc (Kuspilić and Gilja, 2018), (Gilja et al., 2019). Since many parameters are involved in the stochastic scour process, the parameters that most affect scour depth must be selected to obtain simplicity of the empirical formulae (Cikojević et al., 2019), (Harasti et al., 2021). An effective method for this purpose is principal component analysis (PCA analysis). It reduces the number of parameters and retains only those that contribute most to the variance, while maintaining sufficient accuracy of the scour depth. Previously, PCA analysis was used to test the contribution of new parameters for different granulometric classes before proposing new scour formulae (Annad et al., 2021). Furthermore, PCA analysis eliminated unnecessary parameters before grouping similar observations with hierarchical clustering to develop new scour depth formulae (Oğuz and Bor, 2021).

## 2. Results

Data uses in this paper were overtaken from USGS public database (Benedict and Caldwell, 2014). The data were filtered to include only the following ranges (Table 1) with 144 samples left.

**Table 1.** Formatting rules

| Description | Symbol | Min | Max | 1 | 2 | 3 |
|---|---|---|---|---|---|---|
| Pier-scour depth [m] | $d_s$ | 2 | 10.4 | - | - | - |
| Pier width normal to flow [m] | $b_e$ | 0.6 | 28.7 | - | - | - |
| Pier width [m] | b | 0.5 | 19.5 | - | - | - |
| Pier length [m] | l | 2.4 | 38.1 | - | - | - |
| Recurrence interval [year] | RI | 2 | 500 | - | - | - |
| Median particle diameter [mm] | $D_{50}$ | 0.008 | 31.2 | - | - | - |
| Approach velocity [m/s] | $v_0$ | 0.2 | 3.9 | - | - | - |
| Approach depth [m] | $y_0$ | 2 | 22.5 | - | - | - |
| Angle of flow attack [°] | θ | 0 | 46 | - | - | - |
| Pier type | type | - | - | single | no information | group |
| Pier nose shape | shape | - | - | round | square | sharp |

PCA analysis shows that 46 % of the variation in the dataset can be explained by two principal components. Geometric variables have the greatest impact on the first component (F1): scour depth $d_s$, pier width b, pier length l and pier width normal to flow $b_e$ with a contribution of 30 %. The second component (F2) is dominated by hydraulic parameters (approach water velocity $v_0$ and water depth $y_0$) and angle of flow attack θ with 16 % of data variability (Fig. 1).

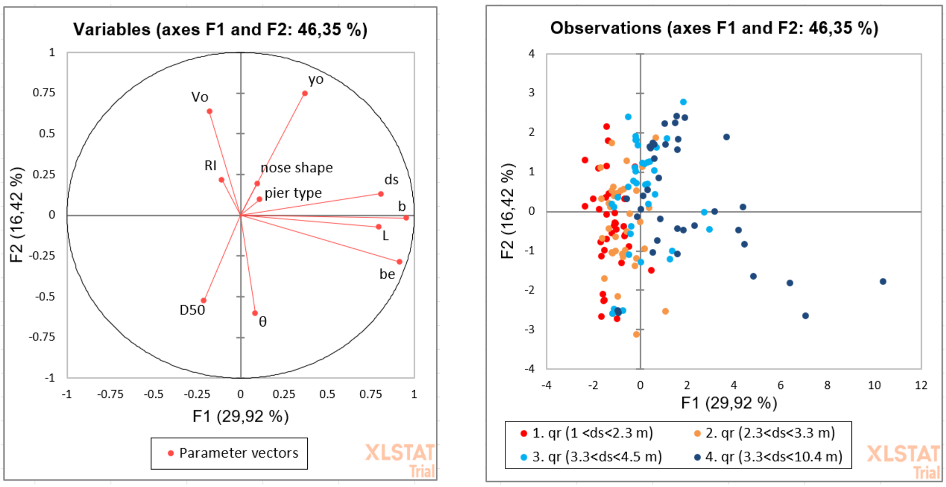


**Fig. 1.** Loading plot (left); PCA score plot (right)

Parameter vectors closer to the center of the coordinate system of loading plot vary more such as: recurrence interval RI, pier type, and pier nose shape. When two vectors are positioned in the opposite quadrants, they usually have a negative covariance, which means that $d_s$ increases with increasing $y_0$ and with decreasing $D_{50}$. When the vectors meet at an angle of 90 degrees, they are probably not correlated which is evident in the case of $d_s$ in relation to the θ and $v_0$. If we exclude RI, pier type, and pier nose shape from the analysis, the first three components (with the same variables $d_s$, b, l, $b_e$, $y_0$, $v_0$) explain 75 % of the variability in the dataset. The PCA score plot shows all samples with their contribution to the first and second principal components. Data were divided into quartiles according to scour depth. Clustering of certain data could be noticed. All quartiles are vertically aligned in order from the 1st to the 4th quartile, indicating that greater scour depths have a greater impact on the first component. The 4th quartile data are farthest from the center of the coordinate system which means that greater scour depths do not vary in relation to smaller scour depths.

## 3. Conclusion

PCA analysis proved to be a useful tool for estimating the contribution of each variable, especially for complex natural phenomena such as scour with a large number of configuring variables. Based on the PCA results, clustering of certain data has been noticed. Therefore, when new parameters are implemented in the scour formulae, it is recommended to analyze the interdependence of the parameters with regression models, as this exceeds possibilities of PCA analysis. The contribution of this work represents the basis for the future development of a new empirical formula with new parameters that affects the scour depth (Gilja et al., 2020).

**Acknowledgements**

This work has been supported in part by Croatian Science Foundation under the project R3PEAT (UIP-2019-04-4046).

**References**

Annad M, Lefkir A, Mammar-kouadri M, Bettahar I (2021) Development of a local scour prediction model clustered by soil class. Water Practice and Technology, 16, 1159-1172, doi:10.2166/wpt.2021.065
Benedict ST, Caldwell AW (2014) A pier-scour database: 2,427 field and laboratory measurements of pier scour; Reston, Virginia, 32 pp, URL: https://pubs.usgs.gov/ds/0845/
Cikojević A, Gilja G, Kuspilić N (2019) Sensitivity analysis of empirical equations applicable on bridge piers in sand-bed rivers. Proceedings of 16th International Symposium on Water Management and Hydraulic Engineering, Skopje, N. Macedonia, 100-109
Gilja G, Marić M, Kuspilić N (2019) Calculation of local scour at bridges over large Croatian rivers. Proceedings of EGU General Assembly, Vienna, Austria
Gilja G, Cikojević A, Potočki K, Varga M, Adžaga N (2020) Remote Real-time Riprap Protection Erosion AssessmenT on large rivers. Proceedings of EGU General Assembly, Vienna, Austria
Harasti A, Gilja G, Potočki K, Lacko M (2021) Scour at Bridge Piers Protected by the Riprap Sloping Structure: A Review. Water, 13, 3606, doi:10.3390/w13243606.
Kuspilić N, Gilja G (2018) Influence of watercourse flow on bridge safety. Proceedings of Electronic collection of papers of the Faculty of Civil Engineering, 26-41
Oğuz K, Bor A (2021) Prediction of Local Scour around Bridge Piers Using Hierarchical Clustering and Adaptive Genetic Programming. Applied Artificial Intelligence, 1-26, doi:10.1080/08839514.2021.2001734.

# The implicit information nature of hydrological uncertainty: estimating and detangling components of uncertainty

Evangelos FINDANIS[1], Athanasios LOUKAS[1]

[1] Department of Rural and Surveying Engineering, Faculty of Engineering, Aristotle University of Thessaloniki, Greece
email: findanis@topo.auth.gr; agloukas@topo.auth.gr

ABSTRACT

In the present paper, concepts of the Theory of Information, developed by Claude Shannon (Shannon, 1948), are applied to estimate and detangle components of hydrological uncertainty. The difference between the information contained in observed and simulated time series of runoff is considered as the total hydrological uncertainty because uncertainty is the gap between available and required knowledge. This approach is more intuitive than the traditional treatment of uncertainty as confidence intervals. Moreover, a theoretical framework is developed, in which the components of total uncertainty are explicitly defined and a novel method of splitting epistemic uncertainty into structural and parametric is being applied. In the benchmark article titled “Twenty-three unsolved problems in hydrology (UPH) – A community perspective” (Blöschl et al., 2019), it is noted that disentangling and reducing the model uncertainty into its components is considered one of the unsolved problems in hydrology and a challenge of modern hydrology.

## 1. Introduction

The present paper is based on the Theory of Information, developed by Claude Shannon (Shannon, 1948). According to this paper, any time series X contains information estimated by Shannon’s definition of entropy:

$$H(X) = -\sum_{i=1}^{N} p(x_i)\log_2 p(x_i) \tag{1}$$

where H(X) denotes the information of X and $x_i$ denotes a discrete value of X ($1 \le i \le N$). When the logarithm of Eq. (1) has a base equal to 2, the unit of measurement of information is the bit. Similarly, a pair of time series X and Y contain information denoted as H(X,Y), which is calculated by the following equation:

$$H(X,Y) = -\sum_{i=1}^{N}\sum_{j=1}^{M} p(x_i, y_j)\log_2 p(x_i, y_j) \tag{2}$$

The mutual information between time series X and Y is denoted by I(X,Y) and is given by the equation:

$$I(X,Y) = H(X) + H(Y) - H(X,Y) \tag{3}$$

## 2. Application of Information Theory to hydrological simulation

According to Gong et al. (2013), the various types of hydrological uncertainty can be treated as the difference between the informational content of the time series $\{\mathbf{X}\}_{obs}$, $\mathbf{Q}_{obs}$, and $\mathbf{Q}_{sim}$. Let $\{\mathbf{X}\}_{obs}$ denote the set of the observed time series used as inputs of the model, $\mathbf{Q}_{obs}$ the time series of observed runoff, and $\mathbf{Q}_{sim}$ the time series of the simulated runoff. Thus, we define:

1. the required information $H(\mathbf{Q}_{obs})$ for the simulation as the informational quantity needed to be inputted into the model, to obtain a perfect simulation of the time series of observed runoff $\mathbf{Q}_{obs}$.

2. the available information of the given data set as the informational content of set $\{\mathbf{X}\}_{obs}$ which can be associated with the time series $\mathbf{Q}_{obs}$ and, by extension, can be exploited by the hydrological model. The available information of a data set $\{\{\mathbf{X}\}_{obs};\mathbf{Q}_{obs}\}$ is equal to $I(\{\mathbf{X}\}_{obs};\mathbf{Q}_{obs})$.

3. the explained information by the model as part of required information that can be reproduced from the simulation. This quantity is equal to the mutual information of time series $\mathbf{Q}_{obs}$ and $\mathbf{Q}_{sim}$, i.e., $I(\mathbf{Q}_{obs};\mathbf{Q}_{sim})$.

4. the aleatory uncertainty of the given data set as the deficit of available information which forces the hydrological simulation to be unperfect. Therefore, aleatory uncertainty is defined as the difference between required and available information.

5. the epistemic uncertainty of a model as the information loss, which occurs while conducting the simulation, due to the imperfect structure of the model and the parametric uncertainty. Thus, epistemic uncertainty is the difference between available and explained information.

Let $\Phi$ and $\Psi$ denote the aleatory and epistemic uncertainty respectively. Based on the above definitions, it can be written that:

$$\Phi = \mathrm{H}(\mathbf{Q}_{\mathrm{obs}}) - \mathrm{I}(\{\mathbf{X}\}_{\mathrm{obs}};\mathbf{Q}_{\mathrm{obs}}) = \mathrm{H}(\mathbf{Q}_{\mathrm{obs}} \,|\, \{\mathbf{X}\}_{\mathrm{obs}}) \tag{4}$$

$$\Psi = \mathrm{I}(\{\mathbf{X}\}_{\mathrm{obs}};\mathbf{Q}_{\mathrm{obs}}) - \mathrm{I}(\mathbf{Q}_{\mathrm{sim}},\mathbf{Q}_{\mathrm{obs}}) \tag{5}$$

## 3. Decoupling epistemic uncertainty into structural and parametric uncertainty

The epistemic uncertainty depends on the structure of the model and its selected parameters. Therefore, we embrace the following axiomatic relationship,

$$\Psi = \Delta + \Theta \tag{6}$$

where $\Delta$ and $\Theta$ denote the structural and parametric uncertainty, respectively. The parametric uncertainty is a function of model parameters $\boldsymbol{\theta}$, i.e., $\Theta=\Theta(\boldsymbol{\theta})$, whereas $\Delta$ is independent of $\boldsymbol{\theta}$. We define the structural uncertainty of a model, as the global minimum of function $\Psi(\boldsymbol{\theta})$. It holds,

$$\Delta = \Psi(\boldsymbol{\theta}_0) \tag{7}$$

where $\boldsymbol{\theta}_0$ is the set of parameters which minimizes the function $\Psi$, namely

$$\left.\frac{d\Psi}{d\boldsymbol{\theta}}\right|_{\boldsymbol{\theta}=\boldsymbol{\theta}_0} = 0 \tag{8}$$

Thus, the structural uncertainty $\Delta$ is treated as the minimum value of epistemic uncertainty found in the entire domain of $\boldsymbol{\theta}$, and the parametric uncertainty $\Theta$ as the fluctuation of epistemic uncertainty from its minimum omnipresent value. After implementing Eqs. (7) and (8) to calculate structural uncertainty, Eq. (6) for $\Theta$ is solved to estimate the parametric uncertainty corresponding to a given parameter set $\boldsymbol{\theta}_1$. Therefore,

$$\Theta(\boldsymbol{\theta}_1) = \Psi(\boldsymbol{\theta}_1) - \Psi(\boldsymbol{\theta}_0) \tag{9}$$

## 4. A proposed framework for determining uncertainty components

The steps of the proposed framework to calculate the aleatory, epistemic, parametric, and structural uncertainties are presented below:

1. Select the appropriate hydrological model for the simulation.
2. Pinpoint the observed input data $\{\mathbf{X}\}_{obs}$ and the observed time-series of runoff $\mathbf{Q}_{obs}$.
3. Calibrate the hydrological model. Let it assumed that the best set of parameters is equal to $\boldsymbol{\theta}_1$.
4. Perform the simulation to produce time series $\mathbf{Q}_{sim}$
5. Implement Shannon's definition to estimate the marginal entropies $\mathrm{H}(\mathbf{Q}_{obs})$, $\mathrm{H}(\mathbf{Q}_{sim})$ and the joint entropies $\mathrm{H}(\mathbf{Q}_{obs}, \mathbf{Q}_{sim})$, $\mathrm{H}(\{\mathbf{X}\}_{obs},\mathbf{Q}_{obs})$ and $\mathrm{H}(\{\mathbf{X}\}_{obs})$.
6. The information required to acquire an accurate simulation of $\mathbf{Q}_{obs}$ equals to $\mathrm{H}(\mathbf{Q}_{obs})$.
7. The aleatory uncertainty of observed data is estimated by Eq. (4).
8. The available information $\mathrm{I}(\{\mathbf{X}\}_{obs};\mathbf{Q}_{obs})$ contained in the data, which can be exploited by the hydrological model, is equal to $\mathrm{H}(\{\mathbf{X}\}_{obs})\text{-}\Phi$.
9. The explained information by the model is equal to $\mathrm{I}(\mathbf{Q}_{obs},\mathbf{Q}_{sim})$ and it is calculated via Eq. (3).
10. Use Eq. (5) to estimate the epistemic uncertainty $\Psi$ of the calibrated model. This value of $\Psi$ is denoted by $\Psi(\boldsymbol{\theta}_1)$ because it corresponds to the parametric set $\boldsymbol{\theta}_1$.
11. Recalibrate the model using the criterion min($\Psi$) to determine the parametric set $\boldsymbol{\theta}_0$, for which the parametric uncertainty is zero. This process requires looping through steps 4, 5, 9 and 10. The minimum value of $\Psi$ is, by definition, the structural uncertainty of the model.
12. Use Eq. (9) to estimate the parametric uncertainty of the model for $\boldsymbol{\theta}=\boldsymbol{\theta}_1$.

The above framework has been applied to specific cases and models.

**References**

Blöschl G. et al (2019), Twenty-three unsolved problems in hydrology (UPH) – A community perspective, Hydrol. Sci. J., 64 (10), 1141–1158.

Gong, W., H. V. Gupta, D. Yang, K. Sricharan, and A. O. Hero III (2013), Estimating epistemic and aleatory uncertainties during hydrologic modeling: An information theoretic approach, Water Resour. Res., 49, 2253–2273.

Shannon, C.E. (1948), A Mathematical Theory of Communication. Bell System Technical Journal, 27: 379-423.

# The Effect of Vegetation on High-Fidelity Modeling of Natural Rivers

Kevin FLORA[1], Ali KHOSRONEJAD[1]

[1] Department of Civil Engineering, Stony Brook University, NY, USA
email: kevin.flora@stonybrook.edu
email: ali.khosronejad@stonybrook.edu

ABSTRACT

High-fidelity numerical modeling of natural rivers can provide valuable insight for many engineering purposes; however, the many complexities in the riverine environment require simplifying assumptions to facilitate the numerical simulations. Our study explores how complex vegetation along the banks can impact the hydrodynamic results in rivers using large eddy simulations (LESs) by incorporating trees into the model using two approaches: (1) discrete modelling of individual tree-like structures and (2) extraction of momentum from tree regions using a vegetation model. The results from both approaches demonstrated that trees redistributed the flow within the river. The unit flow rate was significantly reduced along the banks and increased in the center of the river when compared to simulations which omitted bankline trees. Likewise, the bed shear stress was redistributed in the simulations with trees which can impact morphological predictions such as bank erosion and sediment transport potential in rivers. In addition, both vegetation approaches showed reductions in TKE within the tree regions but increases in TKE immediately adjacent to the banks due to shear layers. The two vegetation approaches did differ, however, with respect to near-bank turbulent structures.

## 1. Methodology

To explore the effect of bank-lined trees, a case study for a long reach of a large natural river was simulated at flood stage using LES for three scenarios: (1) baseline case without trees, (2) using discrete tree-like structures, and (3) using a vegetation (canopy) model.

### *1.1. Case Study*

The American River is a large meandering river located in Northern California. A 1150 m long reach of the main channel of the river was studied which was lined on both banks with mature trees. The channel bed was comprised of sand, gravel and cobbles and displayed noticeable bedforms, scour holes and gravel bars. Using a flood discharge of 3330 $m^3/s$, the mean depth in the river was 12.2 m with a mean velocity of 2.24 m/s.

### *1.2 Numerical Model*

The LESs were computed using our in-house code, VFS-Geophysics, which employs the Curvilinear Immersed Boundary Method (CURVIB) for effectively discretizing the riverine geometry and bridge substructure elements using unstructured surfaces for the complex boundaries within the structured flow domain (Khosronejad et al., 2020). A sloping rigid lid approximation was used for the water surface and a fully developed, turbulent inflow was applied at the upstream boundary. For each simulation, 24.3 million computational grid nodes spaced uniformly in all directions at 0.6 m were used (Flora, et al., 2021, Flora and Khosronejad, 2021).

### *1.3 Vegetation Modeling*

Two different strategies were used to incorporate the trees along the riverbanks into the numerical models. These two approaches were compared to a baseline LES case which did not account for vegetation.

For the first approach, 1900 tree-like structures representing the size and shape of the trunk and lower canopy branches for the trees along our study site were placed along the banks of the river using unstructured mesh elements and are resolved using the CURVIB method. The size and orientation of each tree-like structure was randomly varied to provide a more natural layout as observed in nature. The spatial placement of the trees was determined from aerial imagery and led to variation in inundation for the structures due to the varied topography along the banks (Fig. 1a).

A second tree modeling approach incorporated a "vegetation model" into the code which acted as a momentum sink in regions that were delineated as tree regions. This approach applied a drag force term to the momentum equation as defined by Shaw & Schumman (1992) as

$$F_i = -\rho C_d A_f \left(u_j u_j\right)^{1/2} u_i \delta(x_k - X_k) \quad (1)$$

where $\rho$ is the density of the water, $C_d$ is the drag coefficient and $A_f$ is the projected area of the vegetation per unit volume which varied with tree height (Fig. 1b). The Dirac delta, $\delta$, distinguishes computational nodes $x_k$ where the force is applied that are inside the vegetated region, $X_k$, from those outside of the vegetated area.

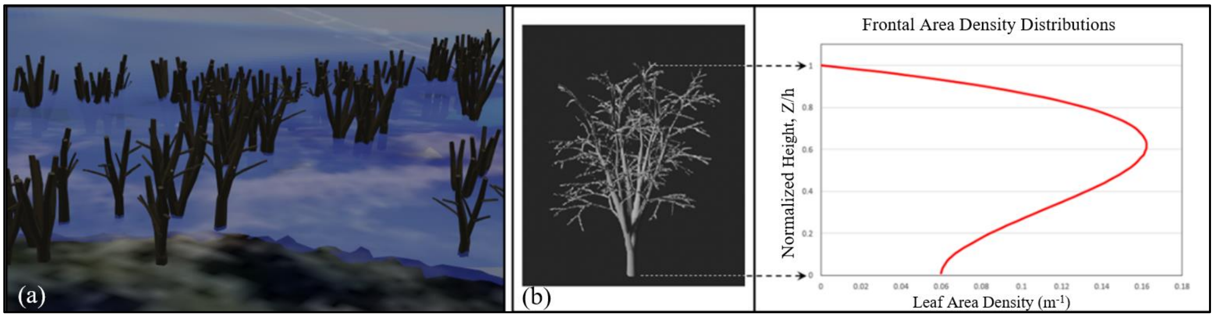


Fig. 1. (a) Example of partially inundated tree-like structures along the bank of the river. (b) . Frontal area density distributions used in the Vegetation Model showing the variation in frontal area density ($A_f$) normalized by tree height (h) for a typical tree.

## 2. Results

Comparing the LES results revealed a hydrodynamic redistribution of flow in both approaches which included the bankline trees as seen in Fig. 2a-c. The vegetation strongly reduced the velocity magnitude near the banks and increased the flow velocities near the center of the channel by about 10 to15 percent. A similar effect on bed shear stress was also observed. A significant difference in the two vegetation modeling approaches is that the tree resolving approach increases vorticity and TKE along the banks due to shedding from the tree-like structures (Fig. 2e); whereas, the vegetation model dampens out the vorticity near the banks (Fig. 2f).

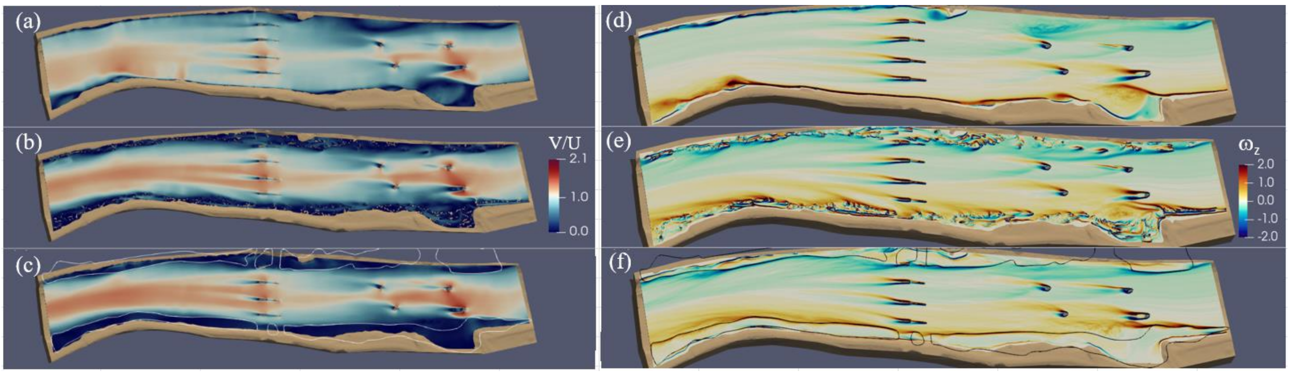


**Fig. 2**. Contours of the time-averaged velocity magnitude (V) at the water surface normalized with the mean-flow velocity (U=2.24 m/s) for the cases (a) without trees, (b) resolved trees and (c) the vegetation model with vegetated regions outlined in white. Contours of the normalized time-averaged out-of-plane vorticity ($\omega_z$) near the water surface for (d) the case with no vegetation, (e) the case with resolved trees and (f) the case with vegetation model. The black line represents the vegetated regions. Flow is from right to left.

## 3. Conclusion

Vegetation is a common feature occurring in riverine environments which should be accounted for in high-fidelity numerical models. The two vegetation approaches used in this study show possible strategies for incorporating bankline trees which have practical implications for assessing the hydrodynamic, morphological and environmental conditions occurring during the flood event in the river.

### References

Flora, K., Khosronejad, A. (2021). On the Impact of Bed-Bathymetry Resolution and Bank Vegetation on the Flood Flow Field of the American River, California: Insights Gained Using Data-Driven Large-Eddy Simulation, Journal of Irrigation and Drainage Engineering, 147:9.
Flora, K., Santoni, C.,Khosronejad, A. (2021), Effect of bank vegetation on the hydrodynamics of the American River under flood conditions: a numerical study, Journal of Hydraulic Engineering, 1992:1-14.
Khosronejad, A, Flora, K., Kang, S. (2020). Effect of Inlet Turbulent Boundary Conditions on ScourPredictions of Coupled LES and Morphodynamics in aField-Scale River: Bankfull Flow Conditions. Journal of Hydraulic Engineering, 146:3.
Shaw, R. H. & Schumann, U. (1992). Large-eddy simulation of turbulent flow above and within a forest, Boundary-Layer Meteorology, 61:47–64.

# A multi-hazard WebGIS platform to share coastal observatories data and model predictions

Anabela OLIVEIRA[1], Miguel ROCHA[1], Gonçalo JESUS[1], André B. FORTUNATO[1], Alphonse NAHON[1], João ROGEIRO[1], Paula FREIRE[1],

[1] Hydraulics and Environment Department, National Laboratory for Civil Engineering, Lisbon, Portugal
email: aoliveira@lnec.pt
email: morocha@lnec.pt
email: gjesus@lnec.pt
email: afortunato@lnec.pt
email: anahon@lnec.pt
email: jrogeiro@lnec.pt
email: pfreire@lnec.pt

ABSTRACT

The adequate emergency and risk management of flood and erosion in coastal areas requires a combination of comprehensive monitoring networks, accurate prediction tools and information platforms that can convey data and predictions in a timely and user-friendly way. Herein, we present a novel web GIS platform for coastal flood and erosion management targeted at areas subject to the combined action of waves, surges and tides. Information for each coastal region is organized through a coastal observatory concept, and the information is tailored to the specific characteristics of each observatory. Many data types were implemented, including historical and real-time sensor data and processed remote sensing information obtained from local cameras or satellites. Predictions are based on a chain of high-resolution models that operate from the ocean to the coast, simulating wave and current hydrodynamics and their interactions, as well as morphodynamics, based on models FES2014, WW3, SCHISM and XBEACH. The WebGIS platform provides both spatial and temporal information aiming at characterizing hazard, vulnerability and risk. The platform is demonstrated through the application to a complex observatory in the central West Portuguese coast, Cova Gala, to address both flooding and erosion concerns.

## 1. Introduction

Coastal erosion and flooding are among the major hazards in areas exposed to energetic wave conditions, storm surges and high spring tides. The consequences of hazardous events depend on the characteristics of the coast, requiring detailed monitoring and forecast tools for an adequate prediction of events (Freire et al., 2020). Web platforms, integrating GIS capacities and tailored to the needs of end users, are becoming a valuable asset in coastal management (Khalid and Ferreira, 2020; Rocha et al., 2021). Herein, we present and apply a WebGIS platform that integrates the multiple dimensions of risk assessment, from vulnerability to hazard, from regional to local scales, and provides a one-stop-shop access to historical and real-time data as well as models predictions. The present deployment of the WebGIS platform includes a coastal observatory located in the west coast of Portugal. At Cova Gala, flooding due to wave overtopping and/or dune erosion is the major concern and a very complete observatory was built, including real-time sensor data, satellite processed images and a complex prediction modeling system.

## 2. The MOSAIC WebGIS platform and its components

The MOSAIC WebGIS platform is a generic tool to support flood risk assessment (Rocha et al., 2021), developed with Django, a Python-based free and open-source web framework, focused on modularity and reusability. It includes a frontend and a backend, with a shared repository for data upload, storage and sharing. A complex data model ensures the integration of multiple sources of information, either from models, sensors or remote sensing (Fig 1).

Coastal predictions are provided through the OPENCoastS service (Oliveira et al., 2021) and its underlying Water Information Forecast Framework (WIFF, Fortunato et al., 2017). WIFF provides a fully flexible customization for the integration of new models through the concept of building blocks required to assemble custom forecast systems. A model workflow was implemented in WIFF comprising regional waves using WW3, global tidal levels using FES2014, both forcing SCHISM simulations (Fig. 2), which in turn force a local deployment of XBeach. Data sources include historical, targeted field campaign and real-time data and remote sensing images from Sentinel 2, processed to determine the water/land interface.

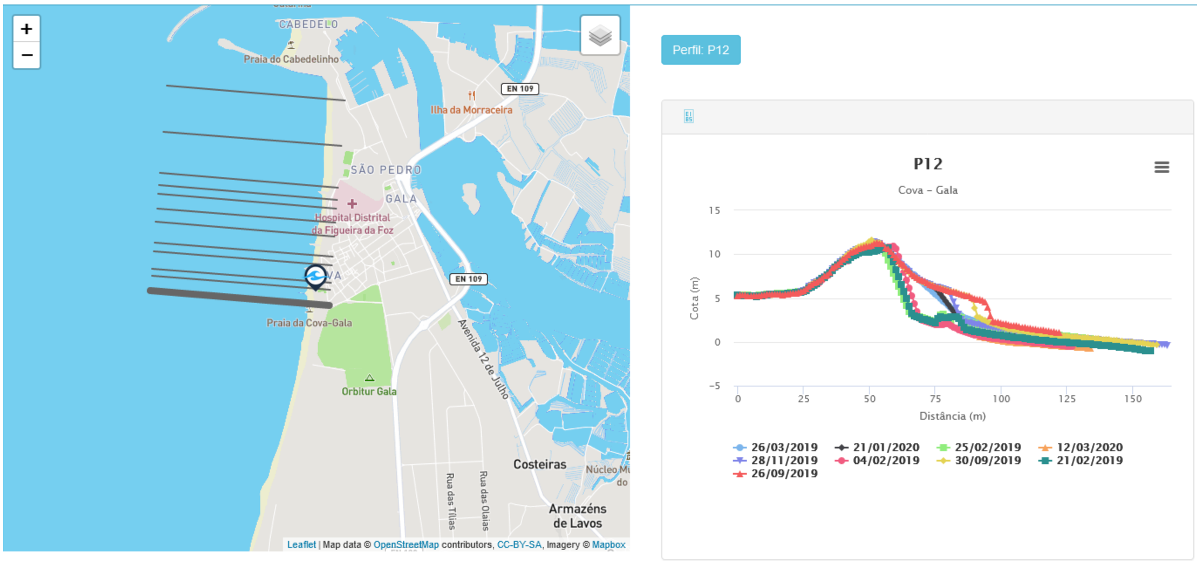


**Fig. 1.** Field campaigns: beach profiles over 1 year

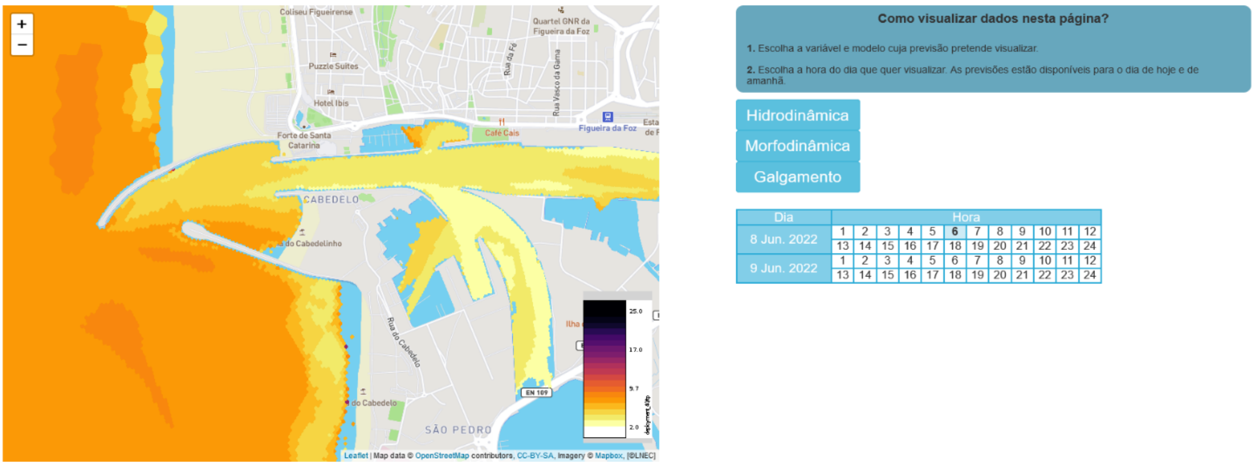


**Fig. 2.** Cova Gala: SCHISM hydrodynamic model predictions - water levels.

## 3. Conclusions

A WebGIS platform for coastal flood and erosion risk management is presented and illustrated in a complex coastal observatory, aiming at supporting emergency actions. The next steps will entail integrating data into the forecasting procedure through assimilation techniques. Morphodynamic predictions are being integrated in WIFF, but accuracy issues require the definition of an intelligent procedure for bathymetry update.

**Acknowledgements**

This paper is part of the work of project MOSAIC.pt (PTDC/CTA-AMB/28909/2017), funded by the Fundação para a Ciência e a Tecnologia (FCT).The OPENCoastS service is offered through the H2020 project EGI-ACE (grant agreement No. 101017567).

**References**

Freire, P.; Oliveira, F.S.B.F.; Oliveira, J.N.C. (2020). Coastal Flooding Process: Comparing Different Coastal Typologies Response to Extreme Hydrodynamic Conditions. J. Coast. Res. 95, 797–802.

Fortunato, A.B.; Oliveira, A.; Rogeiro, J.; Costa, R.T.; Gomes, J.L.; Li, K.; Jesus, G.; Freire, P.; Rilo, A.; Mendes, A.; et al. (2017). Operational forecast framework applied to extreme sea levels at regional and local scales. J. Oper. Oceanogr. 2017, 10, 1–15.

Khalid, A.; Ferreira, C.M. (2020). Advancing real-time flood prediction in large estuaries: iFLOOD a fully coupled surge-wave automated web-based guidance system. Environ. Model. Softw. 2020, 131.

Oliveira, A.; Fortunato, A.B.; Rogeiro, J.; Teixeira, J.; Azevedo, A.; Lavaud, L.; Bertin, X.; Gomes, J.; et al. (2020). OPENCoastS: An open-access service for the automatic generation of coastal forecast systems. Environ. Model. Softw. 2020, 124, 104585.

Rocha, M.; Oliveira, A.; Freire, P.; Fortunato, A.B.; Nahon, A.; Barros, J.L.; Azevedo, A.; Oliveira, F.S.B.F.; Rogeiro, J.; Jesus, G.; Martins, R.J.; Santos, P.P.; Tavares, A.O.; et al. (2021). Multi-Hazard WebGIS Platform for Coastal Regions. Appl. Sci. 11, 5253.

# Drought identification using the DrinC model based on gauge and satellite meteorological data

Andreas V. TSIHRINTZIS[1], Harris VANGELIS[1], Ioannis KOURTIS[1], Dimitris TIGKAS[1]

[1]National Technical University of Athens, Greece

email: tsihrin@gmail.gr; tsihrin@otenet.gr; harrivag@mail.ntua.gr; gkourtis@mail.ntua.gr; ditigas@mail.ntua.gr

ABSTRACT

Drought analysis in Kythira Island, Greece, is performed in this paper. The analysis is based on four drought indices: SPI, RDI, aSPI and eRDI. Drought assessment was achieved through the DrinC model, which was also used for the calculation of PET, utilised by RDI and eRDI, and $P_e$ which is used by aSPI. A meteorological station dataset (HNMS) and a satellite dataset (DEAR-Clima) were exploited. A general agreement among the values of the four indices for the two datasets is detected, which is also confirmed by the Nash–Sutcliffe coefficient. The known extreme drought event of 1990 is detected by all the indices.

## 1. Introduction

Drought identification is considered valuable for determining the impacts of drought on various sectors (economy, environment, society, etc.) and designing the preparedness plans to manage the anticipated drought impacts (Rossi et al. 1992). Furthermore, drought monitoring is considered essential for establishing early warning systems and adopting the appropriate measures to mitigate the anticipated damages (Wilhite 2009; Bordi and Sutera 2007). In this paper, four drought indices were used to assess drought in a Mediterranean context, exploiting two different datasets and utilising the DrinC model.

## 2. Materials and Methods

Drought identification was performed for the Greek island of Kythira. The island is lying opposite the south-eastern tip of the Peloponnese peninsula (36°15′27″N, 22°59′51″E). Although the island is located between the mainland of Greece and the island of Crete, it is part of the regional unit of Attica. The climate of Kythira is typical Mediterranean and according to the dataset obtained from the Hellenic National Meteorological Service (HNMS) for the period 1955-2011, the mean annual temperature is about +18° C, while the mean annual rainfall depth is approximately 540 mm.

Four drought indices were calculated for the specific drought analysis. The first two, are the widely used Standardised Precipitation Index (SPI) proposed by McKee et al. (1993) and Reconnaissance Drought Index (RDI) developed by Tsakiris and Vangelis (2005). The last two, namely the Agricultural Standardised Precipitation Index (aSPI) developed by Tigkas et al. (2019) and the Effective Reconnaissance Drought Index (eRDI) proposed by Tigkas et al. (2017), are modifications of the former two indices aiming at improving the ability to assess agricultural drought. The main advantage of the four indices is their limited data requirements. The DrinC model (Tigkas et al. 2015) was used to assess and monitor drought based on the available data. Apart from the calculation of drought indices based on the appropriate probability distribution, the estimation of potential evapotranspiration (PET) utilised by RDI and eRDI, as well as the estimation of effective precipitation ($P_e$) utilised by aSPI, were also performed through the model.

Two datasets were utilised for the analysis. The first dataset was obtained by the HNMS, while the latter was datamined from the platform Data Extraction Application for Regional Climate (DEAR-Clima). A 6-month timescale was selected for the calculation of the indices (in monthly calculation step), which is considered suitable for assessing water deficits in various systems, including also proper reference periods coinciding with the development stages of major crops in the region. Finally, the Nash–Sutcliffe efficiency coefficient (NSE) was used to correlate the output of the indices based on the two datasets.

## 3. Results and concluding remarks

A correlation between the rainfall depths of the two datasets was performed resulting in high correlation (NSE=0.85) and detecting a slight underestimation of rainfall depths by the satellite dataset. Indicatively, the values of the standardised RDI (RDIst) and the aSPI for the 6-month timescale, calculated based on each dataset (HNMS and DEAR-Clima) are presented in Figs. 1 and 2, respectively.

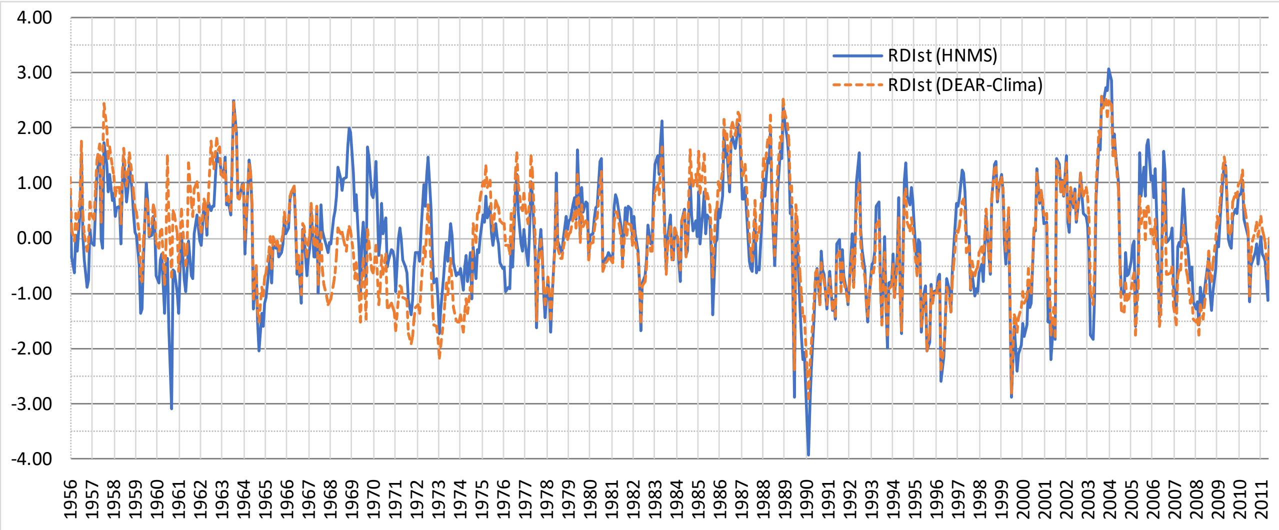


**Fig. 1.** The standardised RDI (RDIst) for each dataset

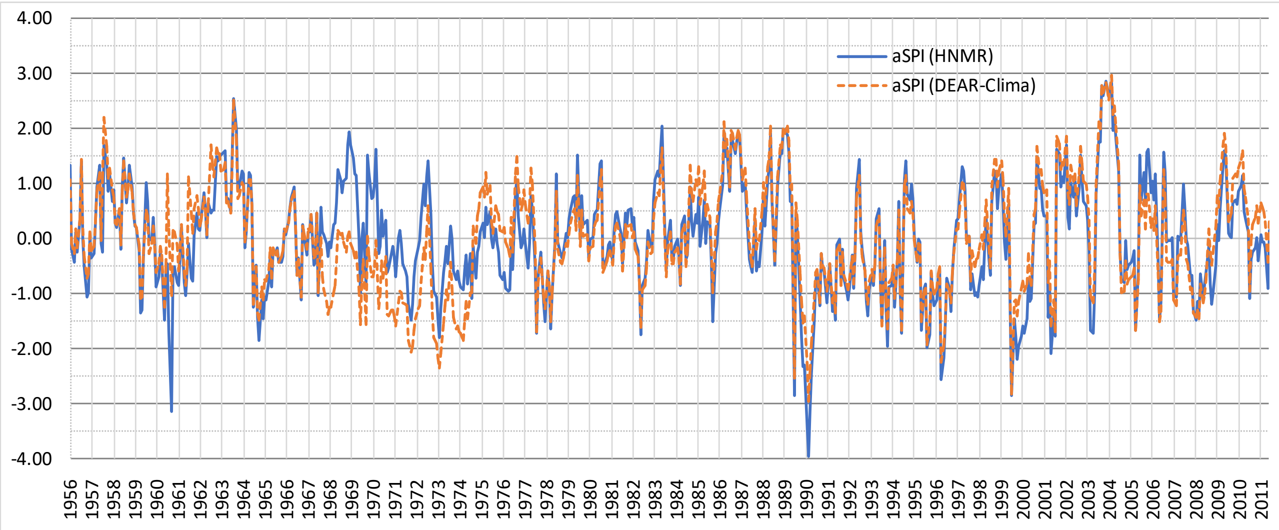


Fig. 2. The aSPI for each dataset

As can be detected in the above Figures, there are no significant differences in the values of each index using the two datasets, except for the period 1968-1976. This is also evident by the NSE coefficients which range from 0.60 to 0.75. There is also a general agreement between the drought events identified by the four utilised indices. Finally, all the examined indices capture sufficiently the known extreme drought event of 1990 which occurred in the Greek territory.

**References**

Bordi I, Sutera A (2007) Drought monitoring and forecasting at large scale. In: Rossi G. et al. (eds.), Methods and tools for drought analysis and management, Springer, pp 3–27.
McKee TB, Doeskin NJ, Kleist J (1993) The relationship of drought frequency and duration to time scales. In: proceedings of the 8th conference on applied climatology, Anaheim, CA, Jan. 17–23, 1993, American Meteorological Society, Boston, pp 179–184.
Rossi G, Benedini M, Tsakiris G, Giakoumakis S (1992) On regional drought estimation and analysis. Water Resources Management, 6, 249–277, doi:10.1007/BF00872280.
Tigkas D, Vangelis H, Tsakiris G (2015) DrinC: a software for drought analysis based on drought indices. Earth Science Informatics, 8(3), 697–709, doi:10.1007/s12145-014-0178-y.
Tigkas D, Vangelis H, Tsakiris G (2017) An enhanced effective reconnaissance drought index for the characterisation of agricultural drought. Environmental Processes, 4(suppl 1), 137-148, doi:10.1007/s40710-017-0219-x.
Tigkas D, Vangelis H, Tsakiris G (2019) Drought characterisation based on an agriculture-oriented standardised precipitation index. Theoretical and applied climatology, 135, 1435-1447, doi:10.1007/s00704-018-2451-3.
Tsakiris G, Vangelis H (2005) Establishing a drought index incorporating evapotranspiration. European Water, 9(10), 3–11.
Wilhite DA (2009) Drought monitoring as a component of drought preparedness planning. In: A. Iglesias et al. (eds.), Coping with drought risk in agriculture and water supply systems, Spinger Science & Business Media B.V., pp 3–19.

# Flood mitigation through the combination of barrage management and polder operation

M. Sc. Sarah DICKEL[1], Univ.-Prof. Dr.-Ing. Stephan THEOBALD[2]

[1,2] Department of Hydraulic Engineering and Water Resources Management, University of Kassel, Kassel, Germany
email: s.dickel@uni-kassel.de; s.theobald@uni-kassel.de

ABSTRACT

The flooding and damage caused by large floods, such as the events of 2002 and 2013, demonstrate the vulnerability of settlement structures along large rivers. The 2013 flood represented an event of above $HQ_{100}$ at the Danube in Passau and downstream due to the influence of the Inn River and had record water levels with catastrophic effects in part (Bayerisches Landesamt für Umwelt, 2014). As a result, the 2013 flood caused damage of around 190 million euros in the city of Passau alone (Wittmann et al., 2015). Due to the existing development of large rivers with barrages, the question arises whether a flood reduction can be achieved by an adapted operation of the barrages – here, the interaction with the operation of polders is also of particular interest (Dickel and Theobald, 2022).

## 1. Method to study the interaction of barrage management and polders

The investigation of the more than 200 km long section of the River Inn in Bavaria is carried out on the basis of a self-developed model system, in which a one-dimensional hydrodynamic-numerical model is coupled with control elements for the representation of the operation of hydraulic structures and the interaction with the flow behavior of the river (Theobald, 2008; Theobald et al., 2022). For a development of practice-relevant control specifications – both for the so-called barrage management and the polder operation – a consideration of operationally available data is essential, as well as extensive analyses and sensitivity investigations. Eight of the 15 barrages on the Inn River integrated in the model (Fig. 1, red) are considered in barrage management, three of which are located upstream of the confluence with the Salzach River (circled in orange) and five on the lower Inn River (circled in green). The exemplarily investigated polder (yellow) is located in the direct operational area of the barrage management. The controlling strategies consider different reference gauges at the Inn and Salzach rivers (cf. Fig. 1).

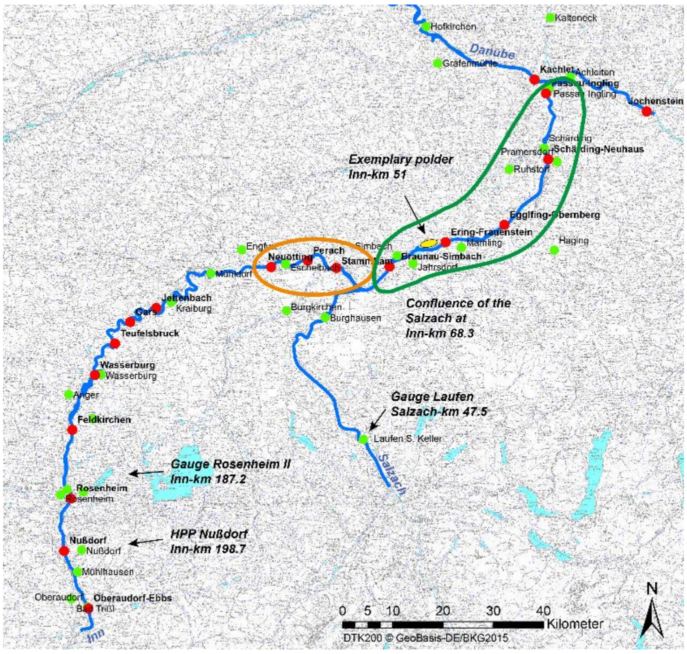


**Fig. 1.** Modeled area of the Inn River in Bavaria with barrages (red dots) considered in barrage management, divided into barrages upstream of Salzach (orange) and downstream (green) as well as gauges (green dots) and location of exemplary polder (yellow)

In barrage management, the headwater at the barrage is lowered so that the volume thus made available in the reservoir can be used to retain volume and reduce the flood peak by increasing the headwater. The control specifications include flood forecasts and discharge measurements (Nußdorf hydropower plant and Laufen gauge) for the lowering, while the time-sensitive increasement is carried out entirely on the basis of measurements related to the reference gauges Rosenheim II (Inn) and Laufen (Salzach). The increasement starts as soon as a subsiding of the flood is registered at the respective reference gauge. In addition to overlapping effects of Inn and Salzach, maximum water level, width of crests and onset times of flood peaks are taken into account. The measurement-based filling process of the polder is carried out analogously.

## 2. Flood peak reduction through combined operation of barrage management and polder

Combined operation of barrage management and polder (Fig. 2, squares) results in a largely additive superposition of the individual effects (Fig. 2, crosses and circles) at gauge Passau Ingling, as can be seen, for example, in the 2013 flood. The absolute discharge reductions of the combined operation, which are between 4 and 12 % (ΔQ = 190 to 507 m³/s), arise from a volume retention in the area of the flood peak of 11.5 to 20 million m³ for barrage management depending on maximum discharge and of 13.4 million m³ through the operation of the polder. Also with regard to the water level reductions, the combined operation shows an almost additive overlapping of the individual effects, so that the reductions of combined operation are between 17 and 36 cm at the gauge Passau on the Danube and of 23 to 68 cm at the gauge Schärding on the Inn. This corresponds to a significant reduction at the neuralgic locations, which are affected by flooding and damage even during smaller floods. Here every reduced decimeter of the maximum water level is essential in general.

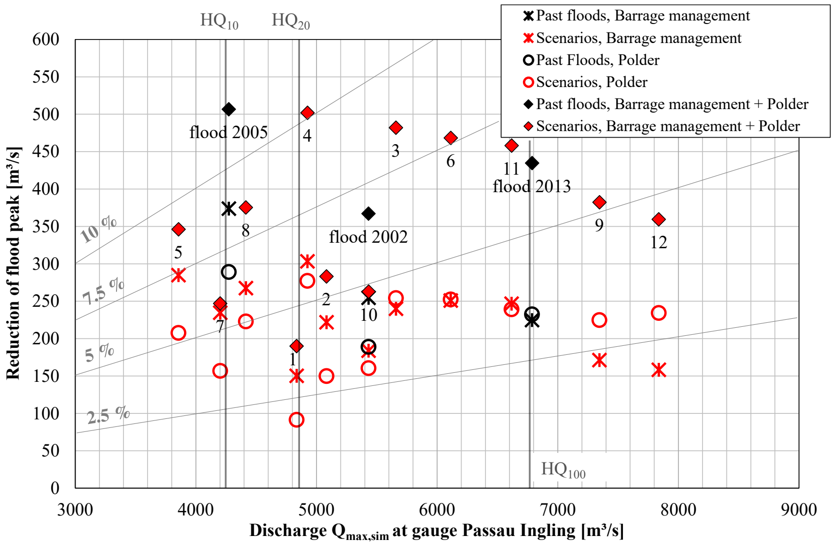


**Fig. 2.** Absolute peak reduction trough sole barrage management, sole polder operation and their combination at gauge Passau Ingling

The experiences with regard to large floods of the past decades clearly show the necessity of an integral investigation of different flood protection measures. In the overall context of flood protection or retention, the investigated barrage management represents an additive component to polders, for example. The high reductions determined clearly show the synergy effects of combined operation and their interaction. Considering the aspects mentioned above and detailed investigations, the applied method is transferable to other river systems.

**Acknowledgements**

Special thanks are due to the staff of the Bavarian State Office for the Environment, the Technical University of Munich, the Technical University of Vienna and the participating German and Austrian state and specialist authorities for their excellent cooperation within the framework of the project “Retentionspotentialstudie Inn”. Thanks also go to the contact persons at VERBUND AG.

**References**

Bayerisches Landesamt für Umwelt (2014) Junihochwasser 2013: Wasserwirtschaftlicher Bericht, Augsburg
Dickel S, Theobald S (2022) Staustufenmanagement als Teil des Hochwassermanagements – Modellierung des bayerischen Inns, Wasserwirtschaft 112(4/2022)
Theobald S (2008) Simulationswerkzeuge zum automatisierten Betrieb von Staustufen, Wasserwirtschaft 98(6/2008), 10–12
Theobald U, Dettmann S, Theobald S (2022) Automatisierter Staustufenbetrieb auf Basis lokaler Wasserhaushaltsregelungen, Wasserwirtschaft 112(4/2022)
Wittmann S, Jurisch M, Krcmar H (2015) Managing Network Based Governance Structures in Disasters: The Case of the Passau Flood in 2013, Journal of Homeland Security and Emergency Management 12(3)

# LES investigation on entrainment in intrusive gravity currents interacting with internal solitary waves

Luisa OTTOLENGHI[1], Claudia ADDUCE[2], Giovanni LA FORGIA[3]

[1] High Council for Public Works, Ministry of Infrastructure and Transport, Rome, Italy
email: luisa.ottolenghi@uniroma3.it

[2] Department of Engineering, Roma Tre University, Rome, Italy and Institute of Marine Sciences, National Research Council, Rome, Italy
email: claudia.adduce@uniroma3.it

[3] Department of Civil and Mechanical Engineering, University of Cassino and Southern Lazio, Cassino, Italy
email: giovanni.laforgia@unicas.it

ABSTRACT

We investigate by three-dimensional large eddy simulations (LESs) the generation of internal solitary waves (ISWs) by intrusive gravity currents (IGCs), and their subsequent interaction. The numerical domain was set in order to release a uniform fluid in a three-layer stratified ambient, triggering pycnoclines displacements. The intrusion, indeed, induces the generation of a train of ISWs that propagates downstream. During the simulations, each ISW is completely reflected by the vertical wall placed at the end of the domain. This allowed us to study the interaction between the IGC and the reflected, upstream-propagating ISWs. By adopting different initial settings, we analyze the influence of the ambient stratification on entrainment of ambient water into the intermediate layer and on the induced mixing.

## 1. Introduction

Internal solitary waves propagate in stratified environments in presence of thin layers characterized by strong, vertical density gradients between the surrounding waters. The interaction between tidal currents and the seabed topography, as well as surface and submerged plumes represent the main hydrodynamic processes that can lead to ISWs generation. In particular, intrusive plumes are density driven currents propagating into an intermediate layer of the stratified receiving ambient. Real field observations and experimental studied showed that train of ISWs are progressively released downstream of the plume if: (i) the density of the intrusive current is different from the depth-averaged densities of the ambient, (ii) the intrusion propagates in subcritical regimes, (iii) the current thickness is larger than the intermediate layer. Each internal wave moves with an approximately constant velocity, while the intrusion gradually slows-down due to turbulent dissipation. ISWs are observed to separate from the current behind. In small-scale basins (e.g. lakes or sea locks), in presence of continental or near-shore slopes the ISWs partially break and part of their energy can be reflected (e.g. Toberman et al 2017). Under this condition, the reflected ISWs frontally interact with the shore-ward incoming intrusion. Main dynamics driving the process have been recently studied by laboratory (La Forgia et al., 2020) and numerical experiments (Ottolenghi et al., 2020). The present work aims at estimating how the interaction between ISWs and IGSs may contribute to modify the stratified environment, in terms of entrainment and mixing processes.

## 2. Numerical setting

Present LESs are performed by using the numerical model of Armenio and Sarkar (2002), based on the filtered, Boussinesq approximated, Navier–Stokes equations (more details about the numerical approach can be found in Ottolenghi et al., 2020). We set the numerical domain $L$=2.16 m long, $H$=0.2 m high, and $W$=0.2 m wide, with 1024, 256 and 64 cells along $x$ (streamwise), $y$ (vertical), and $z$ (spanwise) directions, respectively (Fig. 1a). A vertical discontinuity is located at the distance $x_0$=0.1 m from the left wall of the domain in order to set different density distributions within the lock and the ambient fluid regions. The lock is composed by uniform fluid of the density $\rho_1$=1020 kg m$^{-3}$, while the ambient fluid is characterized by a three-layer stratification. The lower layer has a density $\rho_2 > \rho_1$, the intermediate layer has a density equal to the lock one, $\rho_1$, and the upper layer has a density $\rho_0 < \rho_1$. In the present work, we take advantage of the database generated in Ottolenghi et al. 2020 to investigate how the interaction between IGCs and ISWs affects entrainment and mixing processes. We performed a series of 14 LESs by varying the upper layer depth $H_1$ (from 0.03 to 0.05 m), the intermediate layer thickness $h_2$ (from 0.005 to 0.015 m) and the upper and lower layer densities ($\rho_0$=1000-1010 kg m$^{-3}$, $\rho_2$=1030-1040 kg m$^{-3}$). This allowed us to investigate different stratification conditions. For each case, we estimate the entrainment of ambient waters into the intermediate layer and the mixing in terms of change of background potential energy, as in La Forgia et al. (2021).

## 3. Results and discussion

The simulation begins as the uniform fluid into the lock interacts with the stratified ambient: an intrusion develops, intruding the intermediate layer. At a later stage, an ISW generates downstream the nose of the current and gradually separates from the intrusion due to its higher celerity (Fig. 1b). The ISW reaches the end of the domain, where it is completely reflected. Then it flows backward towards the source of buoyancy. The reflected ISW then collides with the IGC: the wave is compressed in the upper layer modifying its original configuration, while the intrusion is pushed at lower depths. As the head region of the intrusion overtakes the wave trough, the two phenomena can be distinguished again: the current loses energy and decelerates, while the wave continues flowing leftward (Ottolenghi et al, 2020).

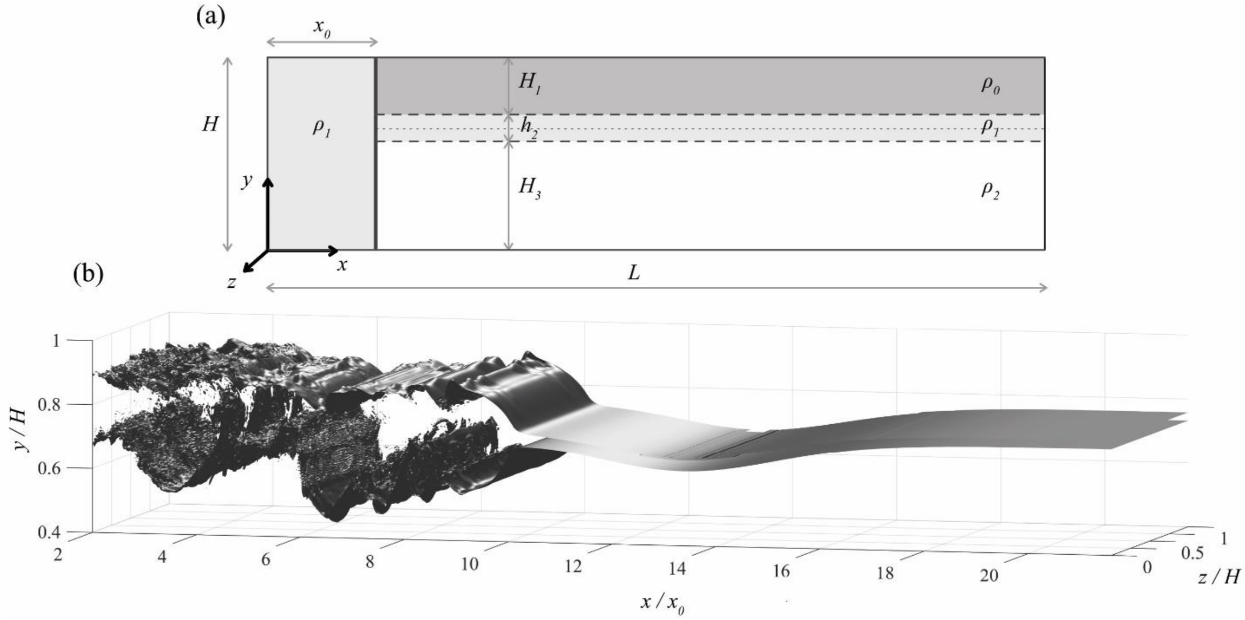


**Fig. 1.** (a) Sketch of the initial numerical setting; (b) Iso-density surfaces at $t$=14.3 s, associated to $\rho^*$= 0.1 (upper) and $\rho^*$= 0.9 (lower), being $\rho^* = (\rho - \rho_0)\,(\rho_2 - \rho_0)^{-1}$. Initial setting parameters: $h_2$=0.005 m, $H_1$=0.0525 m, $H_3$= 0.1425 m, $\rho_0$=1000 kg m$^{-3}$, and $\rho_2$=1040 kg m$^{-3}$.

During each simulation, entrainment of fresher water from the upper layer and saltier fluid from the lower one induced a relatively large increase of the intermediate layer thickness. Our results suggest that, during IGC propagation, turbulent, shear instabilities developing at the intrusion edges represent the hydrodynamic process able to affect fluids entrainment the most. Although during the current-wave engage the intermediate layer thickness remains approximately constant, we observed a relatively large increase of mixing. Furthermore, this evidence appeared more pronounced for larger undisturbed intermediate layer thickness. While the intrusion is responsible of fluid entrainment, which causes a significant increase of the intermediate layer thickness, the current-wave interaction represents a physical process able to amplify mixing of the entrained water masses.

**Acknowledgements**

This research was funded by the Italian Ministry of Education, University and Research (MIUR) through the Departments of Excellence 2018–2022 Program.

**References**

Armenio V., Sarkar S. (2002) An investigation of stably stratified turbulent channel flow using large-eddy simulation. Journal of Fluid Mechanics. 459, 1–42.
Toberman, M., Inall, M., Boyd, T., Dumount, E. & Griffiths, C. (2017) Nonlinear internal waves and plumes generated in response to sea-loch outflow, AUV, and time-lapse photography observations. J. Geophys. Res. Ocean 122, 5522–5544.
La Forgia G., Ottolenghi L., Adduce C., Falcini F. (2020) Intrusions and solitons: propagation and collision dynamics, Physics of Fluids, 32, 076605.
Ottolenghi L., Adduce C., Roman F., La Forgia G. (2020) Large eddy simulations of solitons colliding with intrusions, Physics of Fluids, 32, 096606.
La Forgia, G., Cavaliere, D., Adduce, C., & Falcini, F. (2021) Mixing efficiency for breaking internal solitary waves, Journal of Geophysical Research: Oceans, 126, e2021JC017275.

# Terminal height predictions of inclined plane negatively buoyant jets

Aristeidis BLOUTSOS[1], Ilias PAPAKONSTANTIS[2], Thanasis MANTSIS[3], Panayotis YANNOPOULOS[4], George CHRISTODOULOU[5]

[2,3,5] School of Civil Engineering, National Technical University of Athens, Greece
email: ipapak@mail.ntua.gr (for author 2), thanos_axl@hotmail.com (for author 3), christod@hydro.ntua.gr (for author 5)

[1,4] Department of Civil Engineering, University of Patras, Greece
email: arblouts@upatras.gr (for author 1), yannopp@upatras.gr (for author 4)

ABSTRACT

## 1. Introduction

The disposal of dense effluents such as the desalination brine in coastal waters, leads to the formation of turbulent negatively buoyant jets. Inclined discharges are commonly employed to increase the entrainment and thus the final dilution. Several experimental studies have been presented for inclined round dense jets, e.g. Papakonstantis et al. (2011a,b), Lai and Lee (2012), Oliver et al. (2013a), but less experimental data exist for inclined plane dense jets, e.g. Voustrou (2014), Voustrou et al. (2015), Papakonstantis and Mylonakou (2021).

Integral models were specifically developed for inclined round dense jets, which take into account either the reduced entrainment (e.g. Papanicolaou et al., 2008; Lai and Lee, 2012) or reduced buoyancy flux (Oliver et al., 2013b) in the rising branch, or explicitly model the loss of mass from the concave side of the jet through the escaping mass approach (EMA) (Yannopoulos and Bloutsos, 2012; Bloutsos and Yannopoulos, 2020). However, integral modeling of plane dense jets has not been attempted so far. In this work, two different integral models, EMA and GM2D, are used to predict the terminal height of the upper boundary of plane dense jets discharged at several angles between 15º and 90º. The predictions are compared to relevant experimental data reported by Voustrou (2014) and Papakonstantis and Mylonakou (2021).

## 2. Description and application of the models

EMA is a second order approach model based on the integral form of equations of continuity, momentum, and tracer mass conservation, considering also escape of masses (Yannopoulos and Bloutsos, 2012). These equations are written in a curvilinear cylindrical coordinate system (Bloutsos and Yannopoulos, 2018). Their integration on a transverse cross-section is made by using Gaussian profiles for the variation of velocities and concentrations. The escaped mass concentration is estimated as a portion $\Lambda$ of the centerline concentration. A sensitivity analysis for $\Lambda$ ranging from 0.02 to 0.40 showed insignificant effect on the terminal height. All cases examined herein, with inclinations in the range $15° \leq \theta_0 \leq 75°$, were calculated using $\Lambda$=0.04. The closure of the system of equations is made by assuming linear spreading rates for the mean axial velocities and mean concentrations; the boundary conditions and other useful details of the model are given by Yannopoulos and Bloutsos (2012). The solution of integral equations is obtained by the 4th-order Runge-Kutta algorithm, which is incorporated in the Fortran Power Station code of EMA.

The GM2D model is based on the volume, momentum and buoyancy conservation in an inclined turbulent buoyant jet discharged from a thin slot. Gaussian distributions for both the velocity and the apparent acceleration of gravity are applied. The model follows the formulation presented by Papanicolaou et al. (2008) for round negatively buoyant jets and it consists of six nonlinear differential equations for the variation of the local flow parameters i.e. the volume flux, the momentum flux, the inclination angle, the buoyancy flux (being constant along the trajectory) and the coordinates $x$, $z$ along the jet centerline. A formula used for estimating the local entrainment coefficient in round buoyant jets (Fischer et al., 1979; Papanicolaou et al., 2008) was properly adjusted for the plane jet (Kotsovinos and List, 1977; Ramaprian and Chandrasekhara, 1983). The equations are solved using a Runge-Kutta routine in MatLab software (Mantsis, 2020), assuming as initial conditions the source flow parameters at a distance equal to $5.2w$ (Jirka, 2006), where $w$ is the discharge slot width. The terminal height of the upper jet boundary was obtained by adding to the maximum centerline height (calculated by the model) the concentration jet width $\lambda b$; $b$ being the velocity jet width and $\lambda$ the ratio of concentration and velocity jet width considered equal to 1.3 (Jirka, 2006). It is noted that for angles $\theta_o \geq 60°$, a constant value of $b$ was considered equal to $0.30l_M$, where $l_M$ is a length scale defined as $l_M = wF_o^{4/3}$ ($F_o$ being the initial densimetric Froude number).

## 3. Comparison with experimental data

Figure 1 shows the EMA and GM2D model predictions for the normalized terminal height, $Z_f/l_M$, in comparison to the experimental data of Papakonstantis and Mylonakou (2021) and Voustrou (2014), with respect to the discharge angle, $\theta_0$. Both models predict satisfactorily the qualitative variation of $Z_f/l_M$ with $\theta_0$; the quantitative agreement is good for small angles (up to about 30°), but the models overestimate the height for $\theta_0 \geq 45°$. The GM2D prediction is also very good for $\theta_0 = 90°$, where $Z_f/l_M$ suddenly decreases due to the high interaction between the upward and the downward flow.

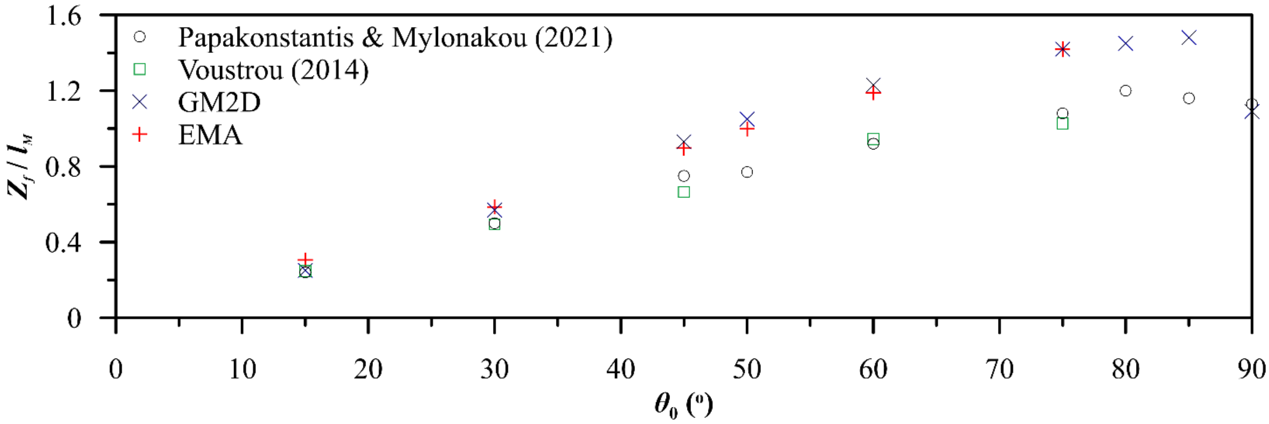


**Fig. 1.** Comparison between model predictions and experimental data for the terminal height of upper jet boundary.

## 4. Conclusions

Both EMA and GM2D models' predictions, regarding the terminal height of upper boundary of a negatively plane buoyant jet, are practically comparable. They predict well the cases for inclination angles less than 45°, while overestimate it for greater angles except 90°, where the GM2D model prediction is very good.

### References

Bloutsos AA, Yannopoulos PC (2018) Curvilinear coordinate system for mathematical analysis of inclined buoyant jets using the integral method, Math. Probl. Eng., 2018.
Bloutsos AA, Yannopoulos PC (2020) Revisiting Mean Flow and Mixing Properties of Negatively Round Buoyant Jets Using the Escaping Mass Approach (EMA), Fluids, 5(3), 131.
Fischer HB, List EJ, Koh RCY, Imberger J, Brooks NH (1979) Mixing in inland and coastal waters. Academic Press
Jirka GH (2006). Integral Model for Turbulent Buoyant Jets in Unbounded Stratified Flows Part 2: Plane Jet Dynamics Resulting from Multiport Diffuser Jets. Environ. Fluid Mech., 6, 43-100.
Kotsovinos NE, List JE (1977) Plane turbulent buoyant jets. Part 1. Integral properties. Journal of Fluid Mechanics, 81, 35-44
Lai CCK, Lee JHW (2012) Mixing of inclined dense jets in stationary ambient. J. Hydro Environ. Res., 6, 9–28
Mantsis T. (2020). Modelling of inclined turbulent negatively buoyant jets. Diploma Thesis, NTUA (in Greek)
Oliver CJ, Davidson MJ, Nokes RI (2013a) Removing the boundary influence on negatively buoyant jets. Environ. Fluid Mech., 13, 625–648
Oliver CJ, Davidson MJ, Nokes RI (2013b) Predicting the near-field mixing of desalination discharges in a stationary environment", Desalination, 309, 148-155.
Papakonstantis IG, Christodoulou GC, Papanicolaou PN (2011a) Inclined negatively buoyant jets 1: Geometrical characteristics, J. Hydraul. Res., 49, 3–12.
Papakonstantis IG, Christodoulou GC, Papanicolaou PN (2011b) Inclined negatively buoyant jets 2: Concentration measurements. J. Hydraul. Res., 49, 13–22.
Papakonstantis IG, Mylonakou EL (2021) Flow Visualization Experiments of Inclined Slot Jets with Negative Buoyancy, Environmental Processes, 8, 1549–1565.
Papanicolaou PN, Papakonstantis IG, Christodoulou GC (2008) On the entrainment coefficient in negatively buoyant jets, J. Fluid Mech., 614, 447–470.
Ramaprian BR, Chandrasekhara MS (1983) Study of vertical plane turbulent jets and plumes, IIHR Rep. No 257, Iowa Institute of Hydraulic Research.
Voustrou M.K. (2014) Experimental study of negatively inclined plane turbulent buoyant jets. MSc Thesis (in Greek)
Voustrou MK, Yannopoulos PC, Christodoulou GC (2015). Experiments on plane negatively buoyant jets. E-proceedings of 36th IAHR world congress, 28 June – 3 July 2015, The Hague, The Netherlands
Yannopoulos PC, Bloutsos AA (2012). Escaping mass approach for inclined plane and round buoyant jets. J. Fluid Mech., 695, 81–111.

# Numerical study of turbulence characteristics of bidirectional flow through a trapezoidal channel

Katrin KAUR[1], Daniela MALCANGIO[2], Janek LAANEARU[3],

[1,3] Department of Civil Engineering and Architecture, Tallinn University of Technology, Ehitajate tee 5, 19086 Tallinn, Estonia
email: katrin.kaur@taltech.ee
email: janek.laanearu@taltech.ee

[2] Department of Civil, Environmental, Land, Building Engineering and Chemistry (DICATECh), Polytechnic University of Bari, Via Edoardo Orabona 4, 70125 Bari, Italy
email: daniela.malcangio@poliba.it

ABSTRACT

The dynamics of stratified exchange flow due to saltwater intrusion into ambient freshwater in a submerged and obstructed channel is modelled using the computational fluid dynamics approach. The numerical experiments are designed to aid the interpretation of density interface-generated turbulence characteristics. The computational domain of the numerical study is a full-scale representation of the experimental apparatus of a trapezoidal stratified flow flume in the Coriolis Rotating Platform at LEGI, Grenoble.

## 1. Validation data

Large-scale laboratory experiments were conducted at the Coriolis Rotating Platform at the Laboratoire des Écoulements Géophysiques et Industriels (LEGI) in Grenoble. This facility consisted of a 13 m diameter and 1.2 m deep circular tank containing a 6.5 m long trapezoidal flume crossed by a stratified flow (De Falco et al., 2021). In the experiments, the velocity field was captured with the Particle Image Velocimetry (PIV) and Acoustic Doppler Velocimetry (ADV) techniques, and the density field was captured using the Laser Induced Fluorescence (LIF) approach and micro-conductivity probes. The experiments were conducted at different freshwater inflow rates while keeping the saltwater flow constant. The experimental measurements focused on obtaining high-resolution velocity and density field data in different vertical planes that span the width of the channel.

## 2. Numerical modelling

The 3D numerical modelling of buoyancy-driven flow has clearly demonstrated that the hydraulically-driven internal flow is modified by the interfacial friction and the eddy-diffusivity dependent mixing (Laanearu et al., 2021). To investigate the turbulence characteristics of the internal-flow interface in more detail, advanced Computational Fluid Dynamics (CFD) simulations, applying a multiphase flow solver accounting for miscibility between the water phases, are undertaken.

The study is conducted using OpenFOAM, an open source CFD software (OpenCFD Ltd.). The CFD solver applied, is for modelling multiple incompressible fluids, two of which are immiscible, using the Volume of Fluid (VOF) method (Hirt & Nichols, 1981) phase-fraction based interface capturing. In the VOF-based method, a transport equation is solved for the fraction of the cell occupied by the liquid phase, i.e., the phase fraction indicator function. The effect of salt and freshwater diffusion on the bidirectional flow dynamics is investigated by adjusting the diffusion coefficient of the miscible phases.

The solver of the OpenFOAM software is coupled with different turbulence models to achieve the best agreement with experimental results. The Reynolds-Averaged Navier-Stokes (RANS) approach, which requires a solution to the Reynolds stress term, is one of the most widely used methods for turbulent flows. Several different turbulence models are available to model the Reynolds stress term. Two-equation models that simulate the eddy viscosity via turbulent kinetic energy production and dissipation, are commonly used.

### *2.1. Computational domain and boundary conditions*

The computational domain is created as a 3-dimensional full-scale representation of the trapezoidal channel of the experiments, complete with a basin containing saltwater inflow and a basin with freshwater inflow (Fig.

1). The domain is discretized using a dominantly hexahedral computational grid, and the appropriate element size distribution is determined on the basis of a sensitivity study. The walls of the computational domain are considered hydraulically smooth and a no-slip boundary condition is applied. The upper boundary represents a free surface under atmospheric boundary conditions.

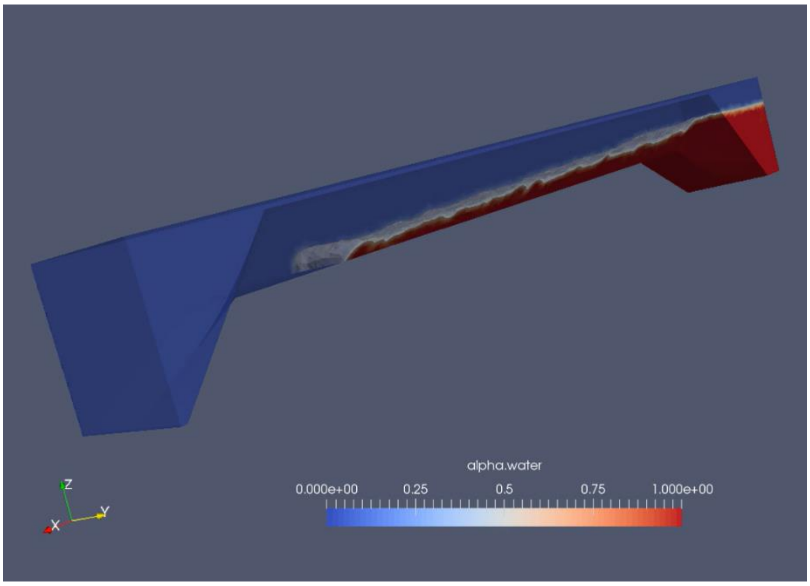


**Fig. 1.** CFD simulation of stratified flow in the trapezoidal channel: saltwater (red) intrusion into ambient freshwater (blue).

### *2.2. Numerical experiments*

Two widely used turbulence models are applied and the simulated profiles compared with the experimentally obtained ones. In the standard *k*- $\varepsilon$ model, the eddy viscosity is determined from a single turbulence length scale, so the calculated turbulent diffusion is that which occurs only at the specified scale, whereas in reality all scales of motion will contribute to the turbulent diffusion. The RNG approach, which is a mathematical technique that can be used to derive a turbulence model similar to the *k*- $\varepsilon$ (Yakhot et al., 1992), results in a modified form of the $\varepsilon$ equation which attempts to account for the different scales of motion through changes to the production term and improves the accuracy for rapidly strained flows. The effect of swirl on turbulence is also included in the RNG model, which improves the accuracy of swirling flows. In addition, the RNG theory provides an analytical formula for turbulent Prandtl numbers.

Comparison is also made for simulated flow fields under conditions of varying diffusivity between the miscible phases of salt and freshwater. Three different values of the diffusivity constant are tested. It is noted that the rate of diffusion is also controlled by the share rate between the phases. The saltwater intruding into stationary freshwater layer produces relatively more diffusion in the numerical simulations than in the experiments. Whereas the modelling of the bidirectional flow of fresh and saltwater produces more similar behavior to the experiments.

**Acknowledgements**

This research has received funding from the European Union's Horizon 2020 research and innovation program under Grant Agreement No. 654110, HYDRALAB+, and from the Estonian Research Council under grant PRG1487. The authors acknowledge the respective contributions of all participants of HYDRALAB+ grant 654110.

**References**

De Falco MC, Adduce C, Cuthbertson A, Negretti ME, Laanearu J, Malcangio D, Sommeria J (2021) Experimental study of uni- and bi-directional exchange flows in a large-scale rotating trapezoidal channel, Physics of Fluids, 33, 036602

Laanearu J, Kaur K, Malcangio D, Cuthbertson A, Adduce C, De Falco MC, Negretti E, Sommeria J (2021). Numerical modelling of the bottom gravity current in an obstructed channel with trapezoidal cross-section, 6th IAHR Europe Congress Warsaw Poland 2020, Polish Academy of Sciences, 247−248

Hirt CW, Nichols BD (1981) Volume of fluid (VOF) method for the dynamics of free boundaries, Journal of Computational Physics, 39(1), 201-225

Yakhot V, Orszag SA, Thangam S, Gatski TB, Speziale CG (1992) Development of turbulence models for shear flows by a double expansion technique, Physics of Fluids A, 4(7), 1510-1520

# The surface pattern of unconfined, hyperpycnal river plume plunging

H. Shi[1], M. E. Negretti[2], J. Chauchat[2], K. Blanckaert[3], U. Lemmin[1], D. A. Barry[1]

[1]Ecological Engineering Laboratory (ECOL), Environmental Engineering Institute (IIE), Faculty of Architecture, Civil and Environmental Engineering (ENAC), École Polytechnique Fédérale de Lausanne (EPFL), Lausanne, Switzerland
[2]Université Grenoble Alpes, CNRS, Grenoble INP, LEGI UMR 5519, Grenoble, France
[3]Research Unit Hydraulic Engineering, Institute of Hydraulic Engineering and Water Resources Management, Technische Universität Wien, Vienna, Austria
haoran.shi@epfl.ch; maria-eletta.negretti@legi.cnrs.fr; julien.chauchat@univ-grenoble-alpes.fr; koen.blanckaert@tuwien.ac.at; ulrich.lemmin@epfl.ch; andrew.barry@epfl.ch;

ABSTRACT

Negatively buoyant river inflow into lakes and oceans often develops a three-dimensional plunging hyperpycnal current field. Recent field observations of the Rhône River plume in Lake Geneva show that the unconfined hyperpycnal river inflow spreads laterally, forming a triangular shaped pattern at the water surface before plunging. In order to improve the understanding of such an unconfined plunging process, a laboratory and a numerical study was performed. Experiments were conducted using salinity to control the density difference. A Computational Fluid Dynamics (CFD) model based on the Boussinesq assumption and Large Eddy Simulation was calibrated with the experimental results. It was found that as the hyperpycnal river inflow moves straight out into the ambient, it also sinks laterally on both sides forming a lock-exchange type secondary current, i.e., as it diverges on the both sides near the bottom, it converges towards the centreline near the water surface. As a result, a near-surface triangular pattern forms. The vertex of the surface triangle is defined as the ultimate plunge point and indicates the longitudinal distance $x_{up}$ that the hyperpycnal current moves before it totally plunges. It was demonstrated that the ultimate plunge point advances offshore when the initial densimetric Froude number increases. Numerical model results and field observations of the Rhône River plume agreed reasonably well with respect to the estimated location of the ultimate plunge point.

## 1. Methods

### *1.1. Experimental setup*

Experiments were conducted in the Coriolis Platform at LEGI (Université Grenoble Alpes, CNRS, Grenoble, France), which consists of a 13-m diameter by 1.2-m deep circular tank. A 4-m long, 2-m wide ($B_0$) horizontal inlet channel connects to a 4.75-m long by 8-m wide flat plate with an 8° slope. This geometry mimics the morphology at the Rhône River mouth with a scale of 1:60. The tank was filled with water (density $\rho_0$). Saline water with density $\rho_a$ was then fed into the inlet channel with constant discharge with bulk mean velocity $U_0$ and water depth $H_0 = 0.08$ m. For flow visualization, fluorescent dye (Rhodamine 6G) was added to the inflow. During the flow visualization, the light sheet of a 25-W Yag laser (wavelength of $\lambda = 532$ nm) was set horizontally at 4 cm below the surface and images were captured with GoPro and Nikon D5 cameras.

### *1.2. Numerical model*

A numerical model was developed based on the open-source CFD package OpenFOAM using a transient solver *BoussinesqPimpleFoam* based on Boussinesq assumption and Large Eddy Simulation. The model was calibrated with the experimental results.

### *1.3. Field observations*

A thermal camera, installed by ECOL on a nearby mountain, provided remote images of the Rhône River mouth area. The location of the ultimate plunge point under different inlet conditions was determined from these images. The river inflow is colder than the ambient water and has higher suspended density concentration, thus, higher density. Discharge, temperature and suspended sediment concentration of the river inflow and temperature of the ambient lake water were obtained from local hydrological stations.

## 2. Results

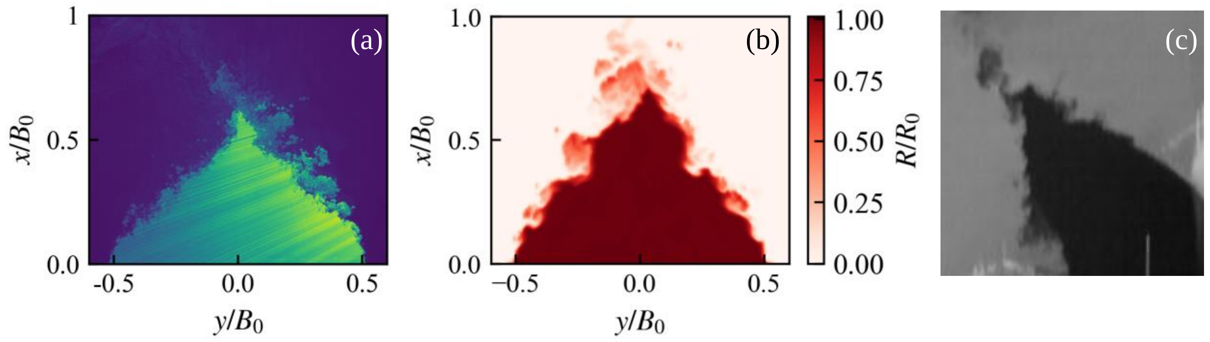


**Fig. 1.** (a) Dye-visualized image taken during the experiment; (b) Modelled density distribution near the water surface ($R$ denotes the relative density difference and $R_0$ denotes its initial value at the river mouth); (c) A thermal image taken at the Rhône River mouth on 25 July 2019 at 3 am (local time). All images refer to an inlet condition with the initial densimetric Froude number $Fr_{d\text{-}0} = 3$.

Figure 1a shows a dye-visualized image taken during the experiments with the initial densimetric Froude number $Fr_{d\text{-}0}$ equal to 3, the initial densimetric Froude number follows,

$$Fr_{d-0} = \frac{U_0}{\sqrt{gH_0(\rho_a - \rho_0)/\rho_0}} \tag{1}$$

where $g$ denotes the gravity acceleration. For comparison, Fig. 1b presents the surface density distribution in the corresponding numerical case. Figure 1c illustrates the thermal image taken at the Rhône River mouth when $Fr_{d\text{-}0} = 3$. Similar to the experimental and numerical model results, a triangular shape is also evident in the field. This triangular shape arises from the superposition of the longitudinal offshore transport of the hyperpycnal current and lateral lock-exchange type flow as reported by Hogg et al. (2013). The longitudinal distance of the ultimate plunge point (the vertex of the surface triangle) obtained from the experimental, numerical model results and field observations are compared in Fig. 2, showing that with increasing $Fr_{d\text{-}0}$, the longitudinal distance of the ultimate plunge point from the river mouth ($x_{up}$) increases. Numerical model and experimental results can be fitted by an exponential formula (dashed line in Fig. 2): $x_{up}/B_0 = 0.5(Fr_{d\text{-}0} - 1)^{0.6}$. The formula slightly underestimates $x_{up}$ observed in the field. This may due to the fact that the bottom topography of the sloping bed in front of the river mouth is much more complicated than the smooth sloping bottom used in the experiments and the numerical model. Moreover, the density difference between the Rhône River mouth and the ambient Lake Geneva water not only results from the temperature difference, but also from the suspended sediment load. Large-size suspended sediments may rapidly deposit, reducing the excess density of the hyperpycnal current that may cause the ultimate plunge point to move offshore. This unique combination of laboratory experiments, numerical modelling and field observations has contributed towards the understanding of the plunging dynamics of unconfined hyperpycnal river plumes and the quantification of the plunge point location.

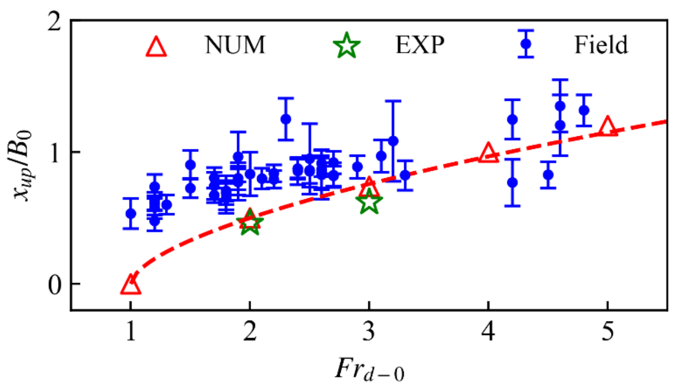


**Fig. 2.** The relationship between the longitudinal distance of the ultimate plunge point from the river mouth and the initial densimetric Froude number. The dashed line represents the empirical formula Eq. 1.

**References**

Hogg, C. A. R., Marti, C. L., Huppert, H. E., & Imberger, J. (2013). Mixing of an interflow into the ambient water of Lake Iseo. Limnology and Oceanography, 58(2), 579–592.

# Vegetation effects on natural convection in sloping waterbodies due to solar radiation

Vassilios Papaioannou[1], Panagiotis Prinos[1]

[1]Hydraulics Laboratory, Dept. of Civil Engineering, Aristotle University Of Thessaloniki Greece

email: vaspapa@civil.auth.gr

email: prinosp@civil.auth.gr

ABSTRACT

In this work the vegetation effects on natural convection, due to incoming solar radiation, in sloping waterbodies is investigated numerically. The vegetation is present in the sloping part of the waterbody which consists of a sloping region (with slope equal to 0.1) and a deep region with a horizontal bottom. Numerical simulations, using the Volume Averaged Navier Stokes (VANS) equations together with the Volume Averaged Energy (VAE) equation, for Grasshof and Prandtl numbers equal to $2 \cdot 10^6$ and 7 respectively, are performed. The results indicate significant vegetation effects on the exchange flow and the large scale circulation which are the result of a different generation mechanism of natural convection. The intensity of the horizontal exchange for the non-vegetated lake is greater than that for the vegetated one while the circulation is clockwise for the non-vegetated case and anticlockwise for the vegetated one. Numerical results (temperature, velocities, streamlines and discharge) are compared qualitatively with results of Mao et al. (2009).

## 1. Introduction

Thermally driven flows (also called natural convection) have significant effects on horizontal transport of nutrients, pollutants, or chemical substances in the littoral regions of waterbodies (lakes, reservoirs, wetlands), especially in the absence of wind or other momentum sources (James et al., 2001). When the waterbody has a uniform slope with increasing water depth in the offshore direction, the daytime heating, due to solar radiation, results in a faster heating of the shallow (nearshore) region than that of the deep (offshore) which generates a horizontal temperature gradient that drives a nearshore-offshore exchange flow (Zhang et al., 2009). With the presence of vegetation (floating/emergent), usually in shallow waters, and the respective shading, the heating of the waterbody in the vegetated region is blocked ( totally or partially) and the generated horizontal convective currents are due to the differential heating of the free surface. The temperature differences between the vegetated regions and open water can be up to 2$^{o}$C, which is sufficient to produce evident temperature gradients and establish a near-surface flow from the illuminated to the shaded regions (Lightbody et al., 2008). This phenomenon has been investigated by Zhang et al. (2009), Tsakiri et al. (2016) and Papaioannou et al. (2021) for a waterbody with horizontal bottom. For a sloping water body, Lin et al. (2015) investigated the role of emergent vegetation on periodically thermal-driven flow over a sloping bottom and derived asymptotic horizontal velocity and exchange flow rates in good agreement with previous studies, however, for very small slopes due to asymptotic solutions used.

In this study, for investigating the vegetation effects on natural convection in sloping waterbodies the VANS and VAE equations are solved numerically which account for the vegetation resistance to flow through additional resistance terms based on the porosity and permeability of the vegetation. The latter (either floating or emergent) is supposed to block all the incoming radiation in the sloping region. In addition, the case with no vegetation is considered for which a scaling analysis and numerical results are available (Mao et al., 2009) for a non-vegetated triangular waterbody.

## 2. Model Formulation

The sloping waterbody consists of a vegetated region with bed slope equal to 0.1 and a non-vegetated region with horizontal bed. Although a much more complex bathymetry may exist in field conditions, the present model aims to capture the basic flow mechanisms induced by the depth variation from the nearshore to the offshore.

The Volume Averaged Navier Stokes (VANS) equations, for two-dimensional, unsteady, incompressible flow together with the Volume Averaged Energy (VAE) equation are solved. The Boussinesq approximation is also used, which treats the density as a constant due to small temperature difference.

The effect of vegetation on the motion of the convective currents is accounted through additional resistance term in the momentum equations. The source term, due to vegetation, is based on the porous media flow theory (Losada et al., 2016). The radiation model considered in this work, is based on Beer's Law and is introduced to the VAE equation through an additional source term $S_r$ $\left(=\frac{I_o}{\rho_o C_P} n e^{-n(h-y)}\right.$, where $\rho_o$= fluid density, $I_0$ = radiation intensity at the water surface, $C_P$ =specific heat of water at the reference temperature, and n = attenuation coefficient, h=water depth). The source term represents the absorption of radiation by the fluid and is added only in the open region of the tank. In the floating/emergent vegetated region, it is assumed that the water does not absorb any radiation.

## 3. Analysis of the results

The large scale circulation, developed in the sloping water body, for quasi-steady conditions is shown in figure 1 for all cases. The streamlines ψ, made dimensionless with $\rho_o kh$ (k=thermal diffusivity) are shown at a time t, made dimensionless with $h^2/k$, for which quasi steady conditions have been established. In the two cases with vegetation the circulation is anticlockwise due to the differential heating between the “hot” free surface of the deep region with the horizontal bottom and the “cold” free surface of the sloping region. The extent of the circulation region in the case of emergent vegetation in the sloping region is much less due to the resistance exerted to the flow by the emergent vegetation. In the case with no vegetation (classical natural convection due to solar radiation) the opposite circulation occurs since the shallow, sloping region is heated faster that the deep region. Detailed results will be presented during the congress.

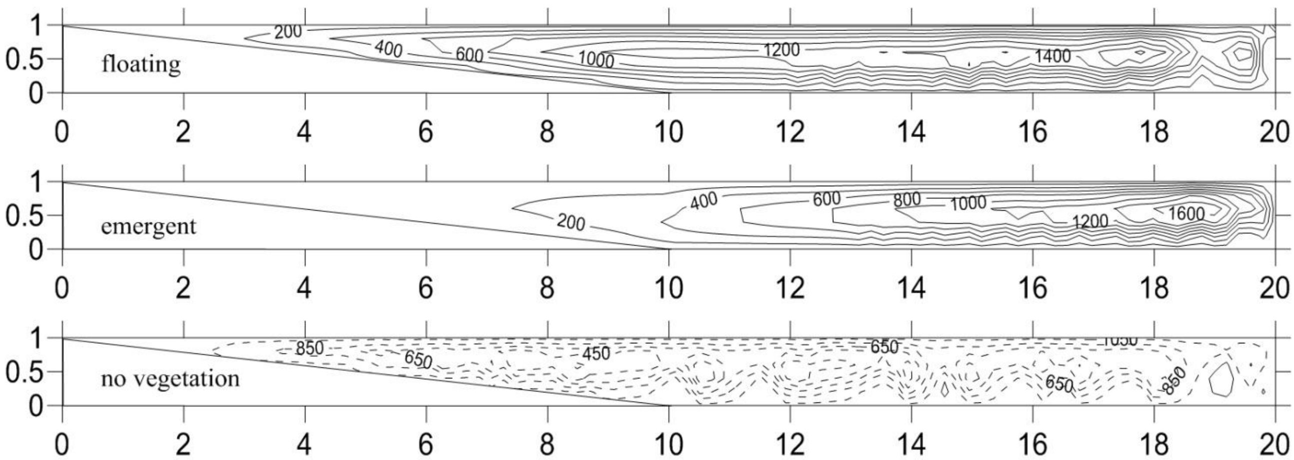


**Fig. 1.** Streamlines ($\psi/\rho_o kh$) at $t/(h^2/k)$ = 0.1428 (Pr=7 and Gr=$2\cdot10^6$). Dotted lines indicate clockwise circulation.

**References**

James WF, Barko J (2001) Estimation of phosphorous exchange between littoral and pelagic zoned during nighttime convective circulation. Limnology and Oceanography 36(1):179–187

Lightbody A, Avener M, Nepf H (2008) Observations of short-circuiting flow paths within a free-surface wetland in Augusta, Georgia. Limnology and Oceanography 53(3):1040–1053

Lin Y, Wu C (2015) Effects of a sharp change of emergent vegetation distributions on thermally driven flow over a slope. Environmental Fluid Mechanics, 15, 771-791

Losada JI, Lara LJ and Manuel del Jesus (2016) Modeling the Interaction of Water Waves with Porous Coastal Structures. Journal of Waterway, Port, Coastal, and Ocean Engineering, 03116003, 142.

Mao Y, Lei C, Patterson JC (2009) Unsteady natural convection in a triangular enclosure induced by absorption of radiation – a revisit by improved scaling analysis. J. Fluid Mech., vol. 622, pp. 75–102.

Papaioannou V, Prinos P (2021) A Macroscopic Approach for Simulating Horizontal Convection in a Vegetated Pond. Environ. Process. 8, 199–218.

Tsakiri M, Prinos P (2016) Microscopic numerical simulation of convective currents in aquatic Canopies. Procedia Engineering 162, 611 – 618, Elsevier. 7

Zhang X, Nepf HM (2009) Thermally driven exchange flow between open water and an aquatic canopy. J Fluid Mech 632:227–243.

# Gravity currents flowing over roughness elements

Maria Rita MAGGI[1], Claudia ADDUCE[1,2], Maria Eletta NEGRETTI[3]

[1] Department of Engineering, Roma Tre University, Italy
email: mariarita.maggi@uniroma3.it

[2] Institute of Marine Sciences, National Research Council
email: claudia.adduce@uniroma3.it

[3] Univ. Grenoble Alpes, CNRS, Grenoble INP, LEGI, 38000, France
email: eletta.negretti@legi.cnrs.fr

ABSTRACT

Lock-exchange gravity currents experiments are performed to characterize the influence of bottom roughness elements on the dense flow through Particle Image Velocimetry. The main parameter varied is the relative height of the roughness elements, realized with square bricks, to the gravity current depth. The analysis performed of the instantaneous velocity fields highlights how the drag force induced by the roughness changes significantly the current dynamics. The front velocity and the inner streamwise velocity are reduced as the height of the bottom roughness increases. Furthermore, recirculation areas developing among the background elements are observed during the current propagation.

## 1. Introduction

Gravity currents are flows driven by buoyancy differences between two fluids, which can be caused by gradients in salinity or temperature. Those flows are observed in many geophysical flows (Simpson 1997) including oceanic overflows such as the Mediterranean Outflow or the North Atlantic overflows from the Norwegian–Iceland–Greenland Sea among others.

In the past, several studies on gravity currents propagating over smooth bed have been developed (Inghilesi et al., 2018; Zordan et al., 2018), but these currents often develop over complex boundaries. The propagation of dense bottom gravity currents is strongly controlled by topographic features (Negretti et al., 2017; De Falco et al., 2021) and the understanding of the mechanism involved in such flows is of crucial importance for a proper modeling. The roughness effect on gravity currents dynamics is a challenging task and there is still a lack of knowledge mainly due to the large variability of the roughness characteristics that makes the analysis of the currents dynamics complex (Jiang et al., 2018).

In this study, we show how the roughness height affects the inner velocity of gravity currents by means of Particle Image Velocimetry (PIV). A description of the experimental setup and the measurements details are provided below with a focus on the front propagation and on the description of the inner velocity features.

## 2. Experimental details and results

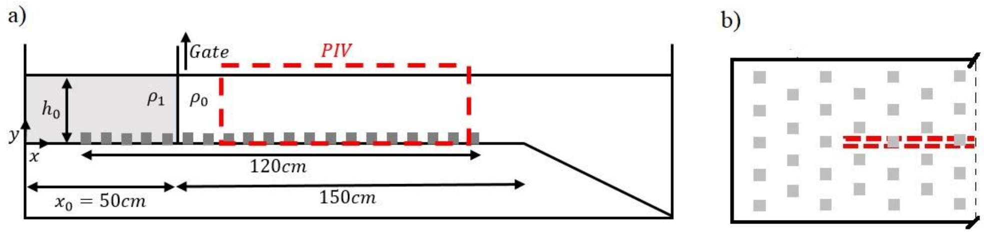


**Fig. 1.** a) Schematic side-view and b) plan view of the tank used to perform laboratory experiments. The area investigated by PIV is reproduced in red.

The laboratory experiments are performed at the LEGI facilities in 6m long Perspex tank, with horizontal bed and rectangular cross section of 25x30 $cm^2$. Squared bricks, located with a constant spacing, are used to make the bottom roughness. The channel is divided in two portions through a removable gate placed at $x_0$=50m from the left wall of the channel. The whole tank is filled up to the same water depth $h_0$=10cm. A sketch of the experimental apparatus is shown in Fig.1. Several experiments, with a constant reduced gravity

$g'=g\Delta\rho/\rho_0$=5cms$^{-2}$ are performed by varying the roughness elements dimension. Three series of test were performed by varying the height of the roughness elements: $h_e$ = 0.64cm in test E1, $h_e$ = 1.60cm in test E2 and $h_e$ = 2.56cm in test E3, additionally a reference test E0 with smooth bed condition is performed. The instantaneous velocity field was measured by PIV whose acquisition is captured over a window with a size of 64.7 × 11.3cm, at 51.3cm after the location of the gate removal ($x_0$). The images are captured with a CCD camera at a frame rate of 21.5Hz. The velocity fields are carry out using a cross-correlation PIV algorithm with the software package DaVis (LaVision).

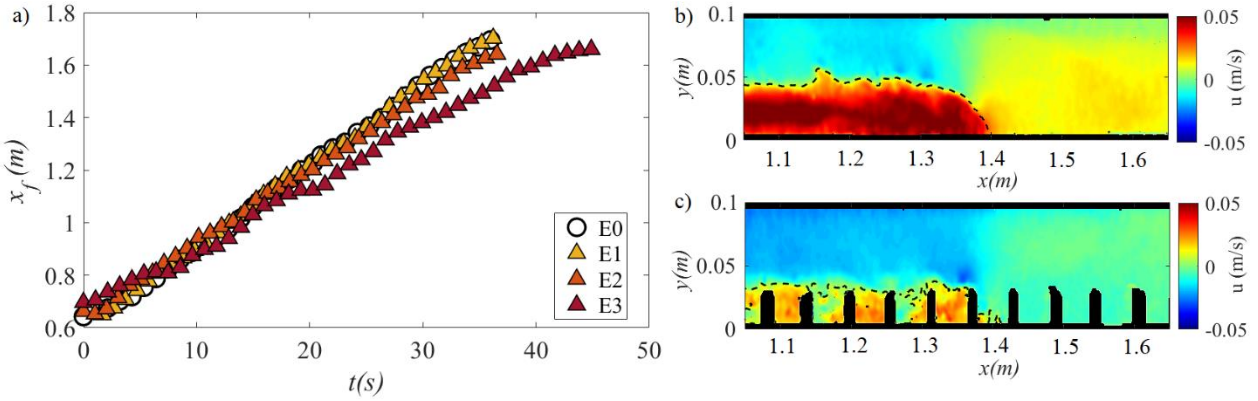


**Fig. 2.** a) Front position $x_f$ as function of time $t$ for all the experiments performed. Streamwise velocity field, $u$, after the current has travelled the distance x=1.4m, respectively for E0 (b) and E3 (c) run.

The front characteristics are analyzed in order to have a global picture of the current dynamics (Fig.2a). We define the experimental front position, as the point where the spatial derivative of the longitudinal velocity $u$ in the streamwise direction $\partial u/\partial x$ is maximum. The E0 and the E1 runs show exactly the same behavior until the end of the window of analysis, therefore it is pointed out that the advancement of the front is not affected by a small roughness. By increasing the height of the bottom roughness (E2 and E3 runs), a slight transition of regime is observed, underlined by the different inclinations of the curves $x_f$–$t$. The greater the height of the bottom roughness, the greater the deceleration of the advancing dense flow.

To better understand how the flow structure is modified by the presence of the bed roughness, the streamwise velocity field, $u$, for E0 and E3 runs is reproduced in Fig.2b-c. The black dashed line represents the boundary between current and ambient fluid; it is calculated by considering the condition $u\approx 0$ for the upper limit and $\partial v/\partial x\approx 0$ for the frontal limit. In the E0 run (smooth bed) the core of the current is characterized by high $u$ values, while at the interface lower values of $u$ can be observed. A different behavior occurs in case of a rough bottom. The roughness introduces significant complexity on the current dynamics; the streamwise velocity $u$ decreases, due to the drag force introduced by the roughness, and the front of the current loses definition. Moreover, recirculation patterns are observed between the roughness elements, in this case the velocity field exhibits a spatial variability characterized by the alternation of zones with higher and lower velocity.

**References**

Simpson JE (1997) Gravity Currents: In the Environment and the Laboratory. Cambridge University Press, Cambridge.
Inghilesi R, Adduce C, Lombardi V, Roman F, Armenio V (2018) Axisymmetric three-dimensional gravity currents generated by lock exchange, J. Fluid Mech, 19, 4041-4053.
Zordan J, Schleiss A, Franca M (2018) Structure of a dense release produced by varying initial conditions, Environ, Fluid Mech., 1–19.
Negretti ME, Flor JB, Hopfinger EJ (2017) Development of gravity currents on rapidly changing slopes, J. Fluid Mech. 833, 70–97.
De Falco MC, Adduce C, Maggi MR (2021) Gravity currents interacting with a bottom triangular obstacle and implications on entrainment, Advances in Water Resources, 103967.
Jiang Y, Liu X (2018) Experimental and numerical investigation of density current over macro-roughness, Environmental Fluid Mechanics 18(1), 97–543 116.

# Gravity currents flowing down a non-uniform slope

Maria Rita MAGGI[1], Claudia ADDUCE[1,2], Maria Eletta NEGRETTI[3]

[1] Department of Engineering, Roma Tre University, Italy
email: mariarita.maggi@uniroma3.it

[2] Institute of Marine Sciences, National Research Council
email: claudia.adduce@uniroma3.it

[3] Univ. Grenoble Alpes, CNRS, Grenoble INP, LEGI, 38000, France
email: eletta.negretti@legi.cnrs.fr

ABSTRACT

Gravity currents experiments flowing onto non-uniform sloping boundaries are performed to characterize the dynamics of the dense flow through the Particle Image Velocimetry and the Planar Laser Induced Fluorescence in order to measure velocities and the density fields. The main parameters explored are the inflow rate and the buoyancy of the inflow. The analysis performed highlights two different types of shear instabilities at the interface between the dense flow and the ambient fluid: the Holmboe instability, downstream the slope and in the initial part of the slope characterized by a slight angle variation; the Kelvin–Helmholtz instability on the steepest part of the slope.

## 1. Introduction

Gravity currents are flows driven by buoyancy differences between two fluids that may be attributed to a number of factors including gradients in salinity or temperature. These phenomena widely occur in the environment as oceanic overflows, sea breeze fronts, avalanches, submarine landslides (Simpson 1997).

Most of the previous studies dealing with gravity currents consider those flows developing over horizontal or constant small sloping boundaries; currents are generated by lock exchange, finite volume releases or constant supply conditions (Cenedese et al., 2010; Martin et al., 2019). In nature, slope changes are frequent and generally accompanied by local small-scale mixing that affects the behavior on larger scales (Turner 1973; Baines 2008).

In this study, we explore the properties and the behavior of two-dimensional gravity currents flowing onto a non-uniform slope by means of Particle Image Velocimetry (PIV) and the Planar Laser Induced Fluorescence (PLIF). A description of the experimental setup and the measurements details are provided below; the discussion focuses on the shear flow instabilities.

## 2. Experimental details and results

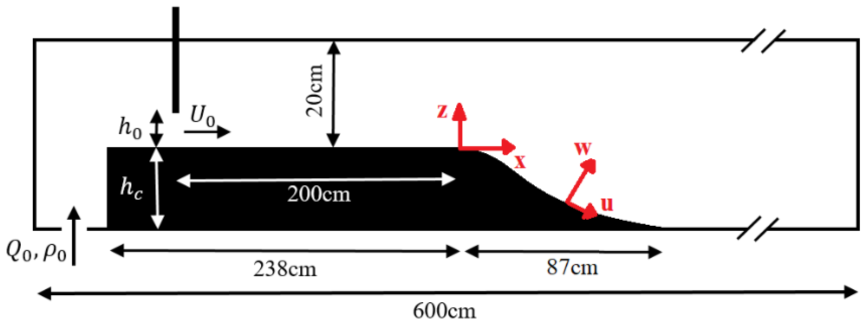


**Fig. 1.** Schematic side-view of the tank used to perform laboratory experiments.

The laboratory experiments are performed at the LEGI facilities in 6m long Perspex tank. The first portion of the channel is elevated by $h_c$=28cm, and is horizontal of total length of L=200cm and width b=25cm. A the end of the horizontal portion a curved slope with a hyperbolic tangent profile and total length of 87cm is placed. A sketch of the experimental apparatus is shown in Fig.1. The buoyancy driven flow has been generated using saline solutions injected in the left side at the bottom of the channel with constant flow rate Q through a pump.

Once the pump is switched on, the outlet in the right side of the tank is opened in order to enable the flow to evacuate to prevent a return flow and ensuring a constant total water depth. The volumetric inflow rate Q (per unit width) at the top of the slope and the reduced gravity g′ of the inflow are the two parameters varied. The instantaneous velocity field is determined using the PIV whose acquisition is captured over a window with a size of 100 × 100cm which allows to frame all the slope. The images are captured with a CCD camera (FlowMaster3, 14bit, 1200x1600pixels) at a frame rate of 23.23Hz. The velocity fields are obtained using a cross-correlation PIV algorithm with the software package DaVis (LaVision). For dye visualizations Rhodamine 6G was added to the salt water of the gravity current in order to estimate the density profiles and some averaged values of the density field. When gate is removed, dense water starts to flow, firstly along the horizontal section then over the hyperbolic tangent slope. For each experiment, all values have been averaged in time by taking into account only the steady layer flow (after the current head has passed).

Figure2 shows the interface variation along time for a given position. As example we discuss a single experiments with Q=807cm$^3$s$^{-1}$ and g'=5cms$^{-2}$; the results obtained in the other experiments are similar. In Fig.2a the dye interface indicates the occurrence of Holmboe instability (HI) upstream the slope. The HI is expected to occur when the velocity shear layer thickness is larger than the thickness of the density interface (Fernando 1991; De Falco et al., 2021). The HI is characterized as two sets of waves with one layer cusping into the upper layer and the other into the lower layer, and propagating in opposite direction. When the slope angle increases, the flow strongly accelerates and Kelvin–Helmholtz instabilities develop (Fig.2b).

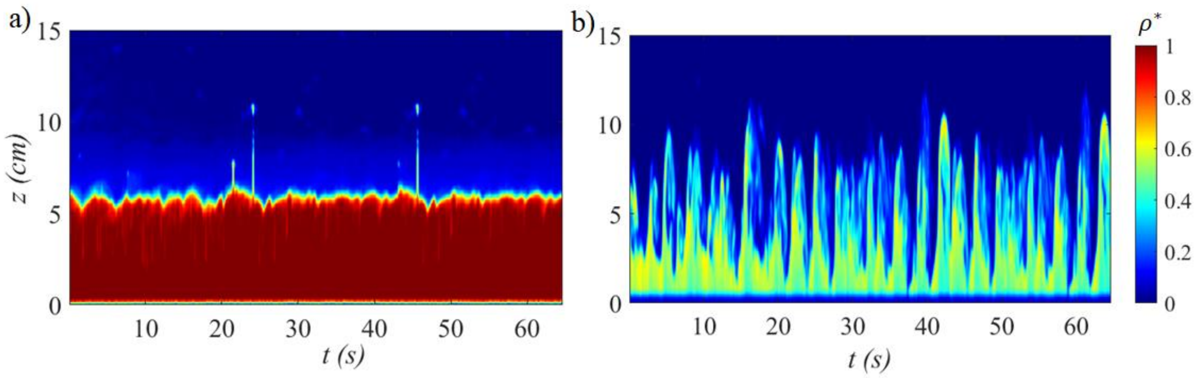


**Fig. 2.** Dye visualization of the instantaneous gravity flow with insets showing time sequence of the density interface fluctuations 5cm upstream of the beginning of the slope a) and in the middle of the slope b).

**References**

Simpson JE (1997) Gravity Currents: In the Environment and the Laboratory. Cambridge University Press, Cambridge.
Cenedese C, and Adduce C (2010) A new parameterization for entrainment in overflows, J. Phys. Oceanogr. 40(8), 1835-1850.
Martin A, Negretti ME, and Hopfinger EJ (2019) Development of gravity currents on slopes under different interfacial instability conditions, J. Fluid Mech. 880, 180-208.
Turner JS (1973) Buoyancy Effects in Fluids. Cambridge University Press, Cambridge, 367 pp.
Baines PG (2008) Mixing in downslope flows in the ocean-plumes versus gravity currents, Atmosphere-Ocean 46:4, 405-419.
Fernando HJS (1991) Turbulent mixing in stratified fluids, Fluid Mech. 23, 455-93.
De Falco MC, Adduce C, Cuthbertson A, Negretti ME, Laanearu J, Malcangio D, & Sommeria J (2021) Experimental study of uni- and bi-directional exchange flows in a large-scale rotating trapezoidal channel. Physics of Fluids, 33(3), 036602.

# The motion of gravity currents that simultaneously flow on and drain from a step

Andrew J. HOGG[1] and Edward W.G. SKEVINGTON[2]

[1] School of Mathematics, University of Bristol, UK
email: a.j.hogg@bristol.ac.uk

[2] Energy and Environment Institute, University of Hull, UK
email: e.w.skevington@hull.ac.uk

ABSTRACT

## 1. Introduction

Releases of dense fluid propagate as gravity currents over horizontal surfaces driven by buoyancy associated with their excess density relative to the surroundings. They may surmount distant barriers. This study investigates the potential confinement of gravity currents theoretically in the situation where the initial motion occurs within a topographic depression, from which the fluid climbs a step and flows away over a horizontal surface while simultaneously draining back into the depression (see fig. 1). At very large-scales, this configuration is of relevance to volcanic surges that are initially confined within a crater, while at more moderate scales, it is of relevance to the topographic confinement of dense pollutants within water courses.

## 2. Methods

We investigate the two-dimensional interaction between a flowing, dense fluid and the confining stepped topography, focusing on situations in which the motion is independent of the spanwise coordinate. The flow is due to the density difference between the released fluid of density $\rho+\Delta\rho$ and the surrounding environmental fluid of density $\rho$, which together produce the reduced gravity $g'=\rho g/(\rho+\Delta\rho)$ where $g$ is the gravitational acceleration. The mathematical model evaluates the unsteady evolution of the depth of the dense fluid, $h(x,t)$, and its velocity $u(x,t)$, where $x$ is the streamwise coordinate. The dense fluid is instantaneously released from a reservoir of length $l_0$ and depth $h_0$ and flows towards at barrier at some distance $L$ downstream of the release. The topography varies smoothly and is specified through an elevation $b(x)$, which connects the horizontal

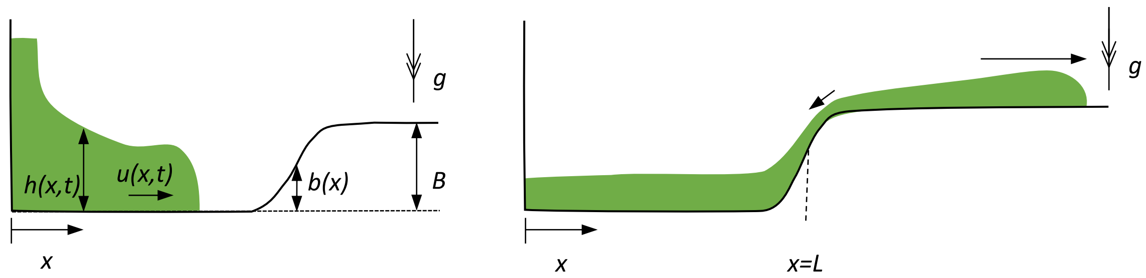


domain within the depression to the horizontal domain on top of the step, which is of height $B$ (see fig 1).

**Fig. 1**. Schematic of the flow configuration: (a) the current approaching the step; and (b) the current flowing along and draining from the step.

Since the motion is assumed shallow and the velocity field predominantly parallel to the underlying bed, the pressure is hydrostatic to leading order. The governing equations are the inviscid, nonlinear shallow water equations, given by

$$\frac{\partial h}{\partial t}+\frac{\partial}{\partial x}(uh)=0 \quad \text{and} \quad \frac{\partial u}{\partial t}+u\frac{\partial u}{\partial x}+g'\frac{\partial h}{\partial x}=0, \tag{1}$$

which respectively represent mass conservation and the balance of momentum. At the front of the flow ($x=x_f(t)$), dense fluid displaces and uplifts the less dense environment, and the motion is no longer hydrostatic. Instead we impose a dynamic condition, termed the Froude number condition, which is given by

$$u(x_f(t),t)=\frac{\mathrm{d}x_f}{\mathrm{d}t}=Fr\sqrt{g'h(x_f(t),t)}\,. \tag{3}$$

The Froude number, $Fr$, is a function of the density ratio and the depth of the current relative to the environment. When the environment is deep, the Froude number becomes constant and this is the regime that we investigate by imposing $Fr$ is constant (greater than unity) determined through theoretical considerations (Benjamin, 1968, Ungarish & Hogg, 2018) or empirically from experiments (Huppert & Simpson, 1980). The other boundary condition is that the back wall of the depression is impermeable, $u(0,t)=0$, and the fluid is initiated from lock-release conditions: $h(x,0)=h_0$ for $0<x<l_0$, $h(x,0)=0$ for $x>l_0$ and $u(x,0)=0$.

We numerically integrate the system (1)-(3) numerically to determine the volume of fluid per unit width, $V_1$, within the topographic depression $0<x<L$, and the volume, $V_2$ on the step, given by

$$V_1 = \int_0^L h \, \mathrm{d}x, \qquad V_2 = h_0 l_0 - V_1. \tag{4}$$

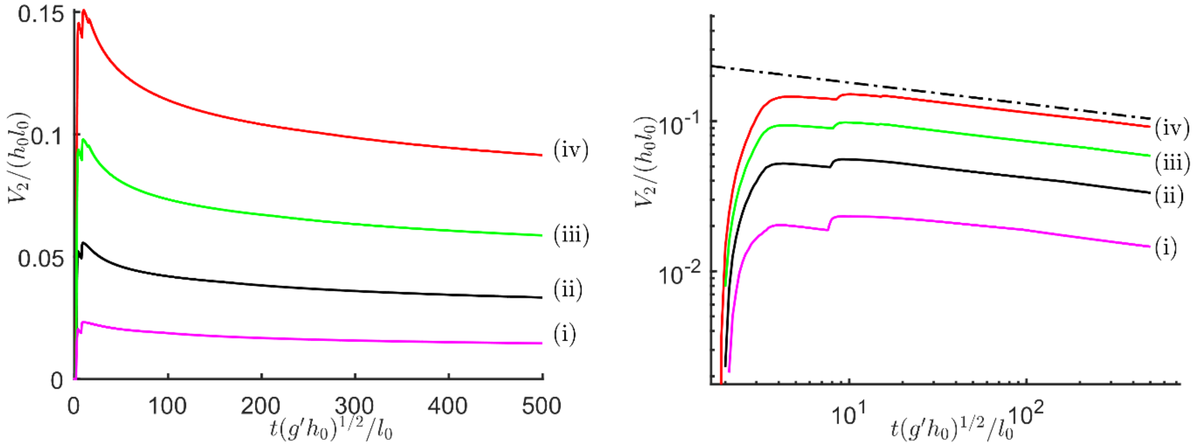


**Fig 2**. The volume of fluid per unit width, $V_2$, on the upper portion of the step as a function of dimensionless time on (a) linear and (b) logarithmic scales when $Fr$=1.2 and $L/l_0$=2. The topography is given by $b(x)=B/2(1+tanh\ (10(x-2))$ with step amplitude: (i) $B$=0.9; (ii) 0.8; (iii) 0.7; and (iv) 0.6. The dashed line shows $V_2 \sim t^{-0.142}$; this exponent is determined by the similarity solution of the second kind.

## 3. Results

Provided the height of the step, $B$, is less than a critical value, the gravity current is able to overtop it and propagate away from the depression. This leads to the volume, $V_2(t)$, initially increasing in time (Fig 2a). There are oscillations in $V_2(t)$ because fluid sloshes between the step and the backwall, leading to a series of overtopping events. At much later times, the volume $V_2(t)$ declines, entering a regime in which it decreases as a power law of the time; it is found numerically that the exponent of this decay is a universal value (Fig 2b). Thus ultimately, and perhaps surprisingly, all of the dense fluid returns to the depression.

The simultaneous draining from and propagation along the step may be investigated theoretically. We show that the dynamics enter a self-similar mode of spreading in which the volume that has escaped from the depression declines in proportion to $t^{-\gamma}$. This is a self-similarity of the second kind (Barenblatt, 1996); the anomalous exponent, $\gamma$, may not be determined by dimensional reasoning alone, but rather emerges by numerically integrating the governing equations in which it appears as an eigenvalue. Its value is shown to be a function of the frontal Froude number and the self-similar spreading and draining correspond very closely to the direct integration of the shallow water equations from lock-release conditions.

The flow dynamics are more complicated when the excess density is due to the suspension of particles which settle out of the flow and are deposited on the underlying boundary. In this scenario we demonstrate that the volume of particles transported out of the depression to settle on the step is a non-vanishing function of the settling velocity; unlike their compositional counterparts, particle-driven currents climb the step and lose their excess density through settling, before draining returns the fluid to the depression. We also report comparison between our theoretical model and laboratory experiments to validate our predictions for the particle transport and current velocity on the step.

**References**

Barenblatt GI (1996) Scaling, self-similarity and intermediate asymptotics, Cambridge Univ. Press 386 pp.
Benjamin TB, (1968) Gravity currents and related phenomena, Journal of Fluid Mechanics, 31, 209–248.
Huppert HE, Simpson JE, (1980) The slumping of gravity currents, Journal of Fluid Mechanics, 99, 785–799.
Ungarish M, & Hogg AJ, (2018) Models of internal jumps and the fronts of gravity currents: unifying two-layer theories and deriving new results, Journal of Fluid Mechanics, 846, 654–685.

# Numerical experiments of asymmetric gravity currents collision with LES

Angelos KOKKINOS[1], Panagiotis PRINOS[1]

[1] Hydraulics Laboratory, Department of Civil Engineering, Aristotle University of Thessaloniki, Thessaloniki, Greece
email: angeloks@civil.auth.gr

email: prinosp@civil.auth.gr

ABSTRACT

This work presents LES results of two colliding gravity currents in the framework of a lock-release set-up. Gravity currents collision is important in many physical conditions and especially in atmospheric flows such as sea breezes, thunderstorm outflows, katabatic flows, etc. A partial-depth set-up is used a better simulation of the collision in the deep air column of the atmosphere. The numerical model solves the filtered Navier-Stokes equations in conjunction with a transport equation for the concentration assuming Boussinesq approximation for density. The focus is on the examination of the dynamical features and mixing during collision of gravity currents with varying densities and/or heights. The ratio of the reduced gravities ($r_g$) of the two currents varies from 0.25 to 1.0 and the ratio of the lock heights ($r_D$) varies from 0.25 to 2.5. It is found that the maximum height of the displaced fluid is not affected by the ratios $r_g$ and $r_D$. The maximum vertical velocity is detected at the time of collision while intense mixing is detected during collision mainly on the less dense vertically displaced fluid.

## Introduction

Gravity currents are buoyancy driven flows in which hydrostatic pressure gradients due to concentration or temperature variation produce a primarily horizontal motion. These currents occur in a wide range of physical conditions such as sea breezes, avalanches, sandstorms, or oceanic fronts in water masses resulting from temperature or salinity differences. Gravity current collision is an important interaction between opposing gravity currents which has received attention in atmospheric studies due to the detected relation with the triggering of mesoscale convection (Intrieri et al., 1990). In recent years lock-exchange experiments have carried out to give physical insights into the dynamics of collision (Okon et al., 2021;van der Wiel et al., 2017; Zhong et al., 2018). This study presents a new set of numerical results of colliding gravity currents using Large-Eddy simulation (LES). It has been shown that LES can describe accurately most of the features of gravity currents (Ooi et al., 2009). The asymmetric collision of two counter-flowing gravity currents is investigated, i.e gravity currents with different densities and/or different initial lock height.

## Setup and numerical model

The lock-exchange configuration is composed of two locks at the left and right corners of a horizontal tank. At t=0 the locks are released, and the dense fluids start moving one towards the other. The heights of the locks are $D_1$ and $D_2$. The length of the locks is always equal to $D_1$. The size of the tank is L x H x W, where $L=10D_1$ is the length and $H=2D_1$ is the tank height. From dimensional analysis for any quantity A, it is $A=f(r_g, r_D, Gr_D)$, where $r_g=(\rho_2-\rho_0)/(\rho_1-\rho_0)$, $r_D=D_2/D_1$ and $Gr_D$ is the Grashof number ($=u_bD_1/\nu^2$). The buoyancy velocity is $u_b=(g_1'D_1)^{1/2}$ and the reduced gravity of the denser fluid is $g_1'=g(\rho_1-\rho_0)/\rho_0$. In the simulations $r_g$ varies from 0.25 to 1.0, $r_D$ varies from 0.25 to 2.5 while Grashof number is equal to $5\cdot10^8$.

The numerical model solves the three-dimensional filtered incompressible Navier-Stokes equations. Boussinesq gravity currents are considered, density is related to concentration and an extra transport equation for the concentration is considered. The unresolved scales of motion are taken into account through a dynamic Smagorinsky SGS model. SGS diffusivity is calculated explicitly considering a constant turbulent Schmidt number, $\Gamma_{SGS}=\nu_{SGS}/Sc_t$, where $Sc_t=0.85$. The simulations are performed with a finite volume method using the open source OpenFOAM code. For the temporal and spatial discretization, 2nd order schemes are used. The space is discretized using a uniform mesh $0.01D_1$ along all directions. Special care is given in the vertical direction near the bottom so that the boundary layer is resolved. No slip condition is chosen for the bottom wall where boundary layer is developed, while slip condition is employed at the left, right and top walls. Periodic condition is imposed in the spanwise direction to avoid the influence of the lateral walls.

## Results

After the release of the dense fluids from the locks, gravity currents start moving one towards the other with no interaction. Soon after the lock release the currents move with constant front velocity (slumping phase). Figure 1 presents the concentration for three characteristic times slightly before, during and after the collision for the case with $r_g$=0.5 and $r_D$=1.0. During the slumping phase the left, denser fluid moves faster with $U_{f,1}/U_{f,2}$=1.45 setting the place of collision at x=11.5$D_1$. As the currents converge, they interact with reduced velocities. Despite that, the denser fluid front velocity remains higher than the less dense one just before the collision and equal to $U_{f,1}/U_{f,2}$=4. From the velocity vectors, Fig. 1a, it seems that intense vertical velocity is developed pushing the ambient fluid upwards. In the asymmetric collision the currents collide at an angle in contrast to the symmetric case ($r_g$=1.0). At that time the maximum vertical velocity appears equal to $v/U_{f,1}\approx 2.0$. Maximum vertical displacement is equal to approximately 1.45$D_1$ for all the simulations indicating no trend of vertical displacement with the examined parameters. In asymmetric collision the denser current intrudes underneath the less dense current pushing it up (Fig. 1b) in contrast to the symmetric collision. The less dense fluid overrides the denser fluid moving upwards while maintaining a non-zero horizontal velocity. During collision there is intense mixing which takes places mainly on the deflected less dense fluid while a bore of the denser fluid is created moving in the same direction as before collision. The bore is moving with considerably lower velocity and height than those of the initial gravity current (Fig. 1c). Detailed results for all the $r_g$ and $r_d$ will be presented at the congress.

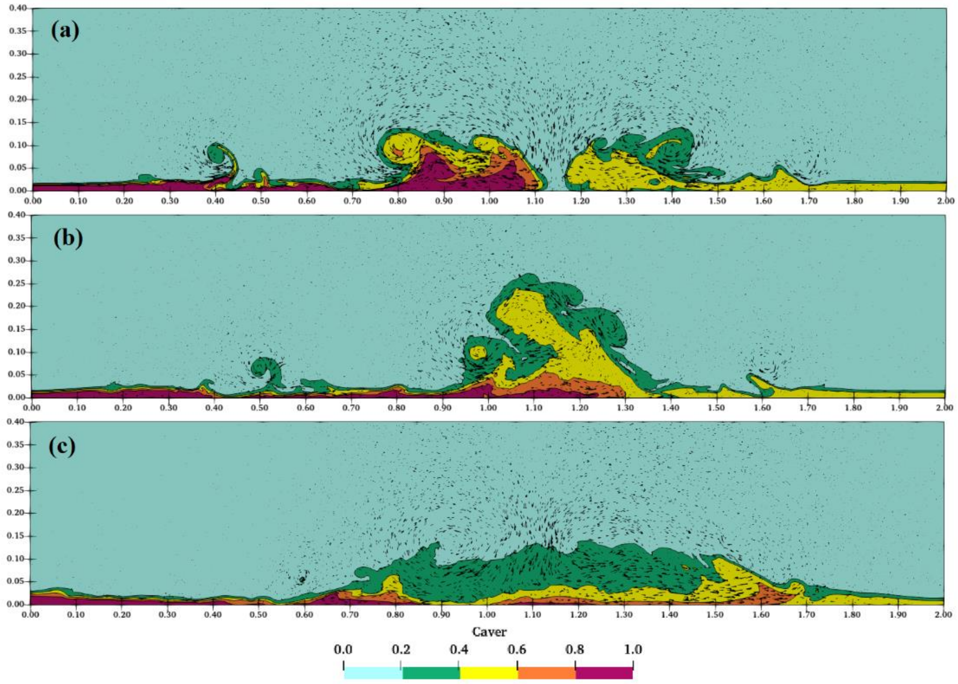


**Fig. 1**. Spanwise averaged concentration contours and velocity vectors slightly before (a), during (b), and after (c) the collision for the case with $r_g$=0.5 and $r_D$=1.0

**Acknowledgements**

The simulations were performed using the Aristotle University of Thessaloniki (AUTh) High Performance Computing Infrastructure and Resources.

**References**

Intrieri J M, Bedard A J, & Hardesty R M, (1990) Details of colliding thunderstorm outflows as observed by Doppler lidar, Journal of the Atmospheric Sciences, 47(9).
Okon SU, Zhong Q, & He Z, (2021) Experimental study on the vertical motion of colliding gravity currents, Physics of Fluids, 33(1), 016601,
Ooi SK, Constantinescu G, & Weber L, (2009) Numerical simulations of lock-exchange compositional gravity current, Journal of Fluid Mechanics, 635, 361–388.
van der Wiel K, Gille ST, Llewellyn Smith SG, Linden PF, & Cenedese C, (2017) Characteristics of colliding sea breeze gravity current fronts: a laboratory study Quarterly Journal of the Royal Meteorological Society, 143(704), 1434–1441.
Zhong Q, Hussain F, & Fernando HJS, (2018) Quantification of turbulent mixing in colliding gravity currents Journal of Fluid Mechanics, 851, 125–147.

# Experimental Study of Multiple Turbidity Currents and Their Deposits in Response to a Simultaneous Slope Break and Loss of Confinement

Jonathan WILKIN[1], Alan CUTHBERTSON[2], Sue DAWSON[3], Nadia PENNA[4], Uisdean NICHOLSON[5], Dorrik STOW[6], Karl STEPHEN[7]

[1,2] School of Science and Engineering (Civil Engineering), University of Dundee, UK
email: j.z.wilkin@dundee.ac.uk, a.j.s.cuthbertson@dundee.ac.uk

[3] School of Social Sciences (Geography), University of Dundee, UK
email: s.dawson@dundee.ac.uk

[4] Dipartimento di Ingegneria Civile, Università della Calabria, Italy
email: nadia.penna@unical.it

[5-7] Institute of GeoEnergy Engineering, Heriot Watt University, UK
email: u.nicholson@hw.ac.uk, d.stow@hw.ac.uk, k.d.stephen@hw.ac.uk

ABSTRACT

Results are presented from a series of scaled parametric experiments that explore the response of supercritical turbidity currents and their evolving deposits within a morphological transition zone between a confined, sloping channel and an unconfined, horizontal basin, resulting from a simultaneous break in slope and loss of confinement. Of particular interest is the effect that antecedent turbidity currents and their deposits have on the subsequent current flow dynamics and the evolution of the channel and basin depositional features. The experimental set-up is designed to permit multiple turbidity currents to be simulated sequentially to reproduce layered deposits in the confined lower slope, the channel-lobe transition zone, and the proximal lobe conditions generated in the unconfined basin, as analogous to deep-water, base of slope sedimentary environments.

## 1. Introduction

Submarine turbidity currents play a crucial role in the transport of the Earth's sediment budget by transferring vast quantities of sediments from continental shelves to deep oceanic basins, often via steep canyons on the continental slope. The morphological transition between the slope and basin floor is often characterised by a break in slope and/or loss of confinement at the channel termination that can cause the current flows to switch from net-bypassing to net-depositional behaviour. The study focuses on the flow dynamics of turbidity currents in the lower slope of a confined channel and a horizontal unconfined basin following a simultaneous slope break and loss of confinement (SB-LOC), as representative of a channel-lobe transition zone (CLTZ). We investigate the effect that existing sedimentary deposits from antecedent turbidity currents have on the dynamics of subsequent currents and the resulting combined deposits, with the aim of yielding new data and understanding on how sequential turbidity currents generate multilayer deposits, as well as identifying key parametric controls on bed erosion, sedimentary bypass, and net deposition processes.

The experiments are conducted in a custom-built channel-basin facility at the University of Dundee (Figure 1A). Each experimental run consists of three sequential turbidity currents that are scaled on non-dimensional parameters for the flow properties (densimetric Froude and Reynolds numbers) and sedimentary conditions (Shields and Rouse numbers) (e.g. de Leeuw et al., 2016). The parametric variations between different runs are initiated by changing the volume flux and volumetric sediment concentration at the channel inlet, along with the channel slope angle. The evolving turbidity current structure before and after the SB-LOC (Figure 1B) is measured by ultrasonic velocity profilers (UVPs) over the duration of the current (~45s), while the resulting deposit structure and thickness in the channel and basin (Figure 1C) are obtained via direct measurements and high-resolution photogrammetry techniques, respectively.

## 2. Results

Figure 2A shows the spatial evolution of the time-averaged velocity profiles for a turbidity current upstream and downstream of the SB-LOC location. The reduction in layer thickness at UVP2 illustrates the collapsing and radially-expanding current after the SB-LOC, while the significant velocity reduction at UVP3 and UVP4 shows the inhibiting effect of the existing basin deposit from previous currents on the downstream propagation of the subsequent event. Figure 2B also indicates a substantial increase in the channel deposit thickness over sequential turbidity current events, with a stepped bed profile forming close to the channel inlet.

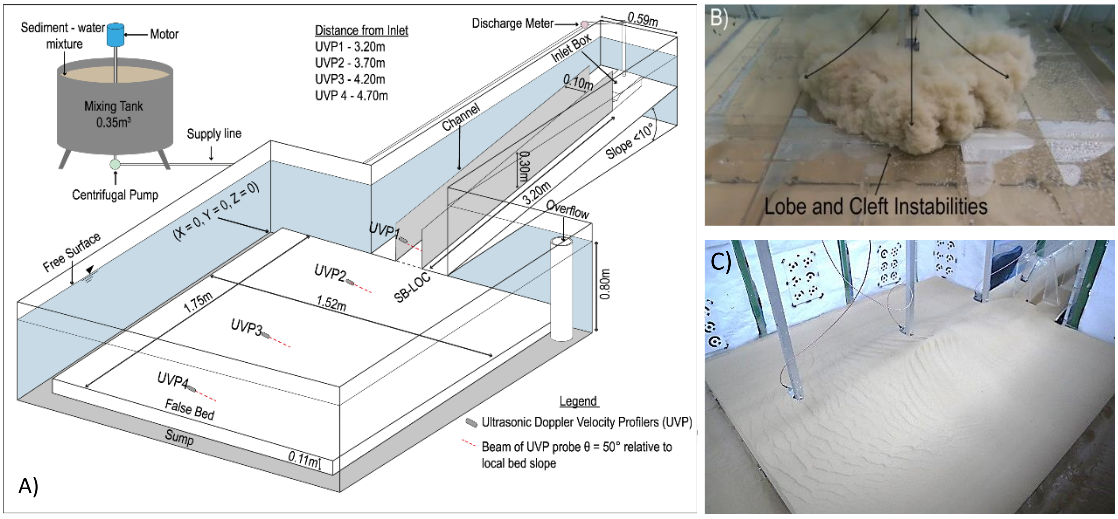

**Fig. 1.** (A) Schematic representation of the channel-basin experimental set-up, (B) image showing radial expansion of turbidity current into unconfined basin (following SB-LOC), (C) sedimentary basin deposit following three sequential turbidity currents.

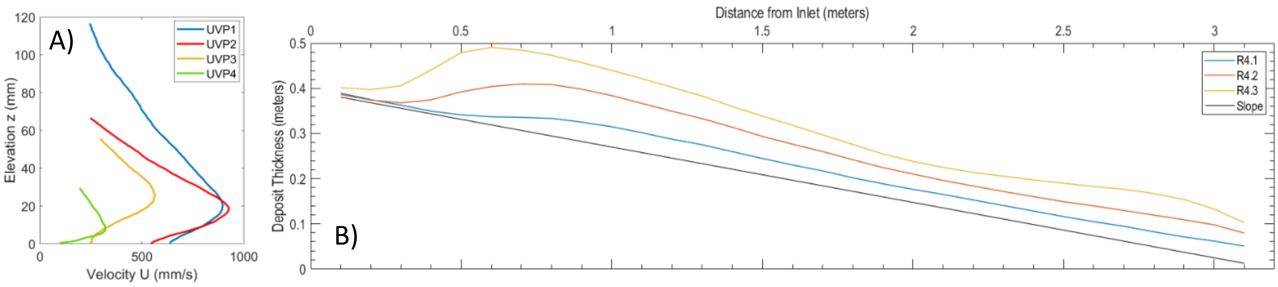

**Fig. 2.** (A) Time-averaged streamwise velocity profiles for turbidity current in confined channel (UVP1&2) and in basin (UVP3&4), (B) development of the along-channel deposit thickness over three sequential turbidity currents.

Figure 3 shows the resulting evolution of the planform deposit structure and overall thickness over sequential turbidity current events (Figure 3A-C), as well as the change in deposit thickness between individual events (Figure 3D,E). Overall, these deposits are shown to be largely symmetrical, with the initial formation of flanking levees, a sediment bypass region, and a lobal deposit downstream of the SB-LOC (Figure 3A). Over subsequent turbidity current events, however, the bypass region diminishes (Figure 3B,C) and the lobe develops and (to some extent) migrates towards the SB-LOC. This creates a partial blockage of the expanding flow in subsequent events, resulting in the lateral spread and bifurcation in the evolving deposits (Figure 3E).

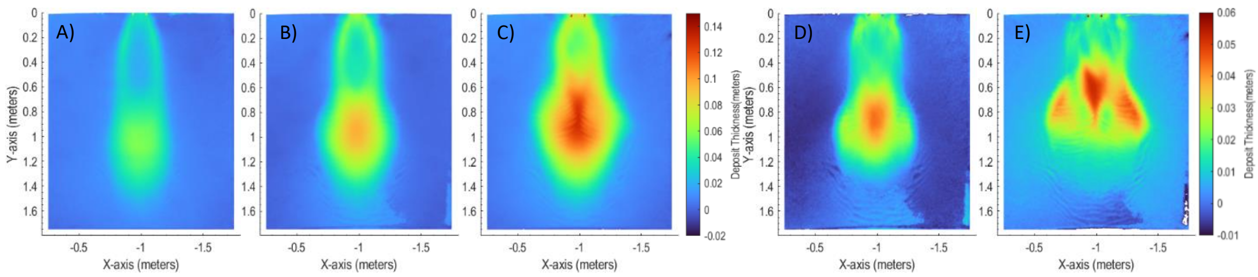

**Fig. 3.** (A)-(C) Planform deposit structure and thickness $z$ in the unconfined basin following sequential turbidity currents, (D)-(E) planform changes in deposit thickness $\Delta z$ between 1st – 2nd and 2nd – 3rd turbidity current events, respectively.

**Acknowledgements**

The work in this paper is undertaken as part of the Natural Environment Research Council (NERC) Centre for Doctoral Training (CDT) in Oil & Gas under its “Extending the Life of Mature Basins” research theme.

References

de Leeuw J, Eggenhuisen JT, Cartigny MJB (2016) Morphodynamics of submarine channel inception revealed by new experimental approach, Nature Communications, 7, 10886.

# Atmosphere – Ocean interaction in the Agulhas Current Region

Jacopo BUSATTO[1], Claudia ADDUCE[2], Chunxue YANG[3]

[1,2] Department of Engineering, Roma Tre University, Italy
email: jacopo.busatto@uniroma3.it,
claudia.adduce@uniroma3.it

[1,2,3] Institute of Marine Sciences, National Research Council
email: chunxue.yang@artov.ismar.cnr.it

ABSTRACT

Internal ocean processes, dynamically induced, cause high sea surface temperature gradients and surface heat fluxes. The correlation and the covariance between temperature and heat fluxes can be used to distinguish sources of variability allowing to define an ocean and an atmosphere driven regime. Here we introduce this method using observational data with different resolutions to distinguish different regimes of variability and to investigate spatial resolution effects. We focused over the Agulhas Current region and the Eastern South Atlantic, where waters flowing following the African coastlines in the Indian Ocean generate turbulence. Such mesoscale activity can lead to the detection of the ocean-driven regime. The increase of resolution gives a better representation of the cross-covariance patterns, indicating an improvement on the detection of eddies.

## 1. Introduction

Water flowing southward from the Indian Ocean along the Agulhas Current (De Ruijter, 2008, Lutjeharms, 2006), that is the Western Boundary Current of the Indian Basin, interact with the bathymetry (Speich et al., 2006) and cold waters of the Antarctic Circumpolar Current (ACC), once it reaches the Agulhas Bank, and generate turbulence that spreads into the Southern Atlantic bringing warm and salty waters (Agulhas Leakage, Beal et al. 2006). Reached the Southern tip of Africa, it retroflects Eastward (Lutjeharms et al., 2001) following the Subtropical Front along the ACC. Sea Surface Temperature (SST) is linked to the surface heat fluxes (SHF). Atmospheric variables, affect oceanic properties that respond with longer time scales (Hasselmann, 1976). However, in region where temperature gradients and heat fluxes are stronger (i.e., in Western Boundary Current regions), variation on those quantities are due to ocean dynamics (Bishop et al., 2017; Bellucci et al., 2021). Theoretical models (Bishop, 2017) suggest that SST - SHF covariance can be used to detect the sources of the variation on these two elements, distinguishing an ocean driven regime and an atmosphere driven regime. In this study, using observational data with different spatial resolution, we highlight spatial resolution impact on the ability of reconstructing those signals over the Agulhas region. Since this is a mesoscale active region (Lutjeharms, 1989, Sandalyuk et al., 2021), this methodology is effective to investigate the heat exchange processes due by oceanic dynamics. Observations are obtained from J-OFURO3 (Tomida et al. 2019) and OAFlux (Yu et al., 2008) dataset. The increase in ocean resolution leads to a better representation of cross-correlation and cross-covariance forms, indicating an improvement in the ability of detecting eddies and turbulence effects.

## 2. Results

Monthly data have been treated before any calculation: seasonal variability and interannual trends had to be removed to isolate the intrinsic ocean atmosphere signal. Once that is performed, lead-lag cross covariance is obtained. For the SST-SHF covariance, in the ocean driven regime, a symmetric pattern, in dependence of the lag value, is expected. For the atmosphere driven regime, SST-SHF covariance should show an antisymmetric pattern (Bishop et al., 2017). In figure 1 covariance patterns are shown. Rows consist of the covariance obtained for lag equal to -1, 0 and 1 respectively. Positive lag means SST leads over SHF. Darker shades of green over the Agulhas Retroflection regions can be noticed. Following lag variations, the dark green area is wider when lag is zero (central row), due to the symmetric pattern expected from the theory. In the open ocean areas (Atlantic and Indian Ocean in the figure) green shaded and blue shaded areas, for negative and positive lag respectively, can be recognized, expressing the antisymmetric expected pattern for an atmosphere driver regime.

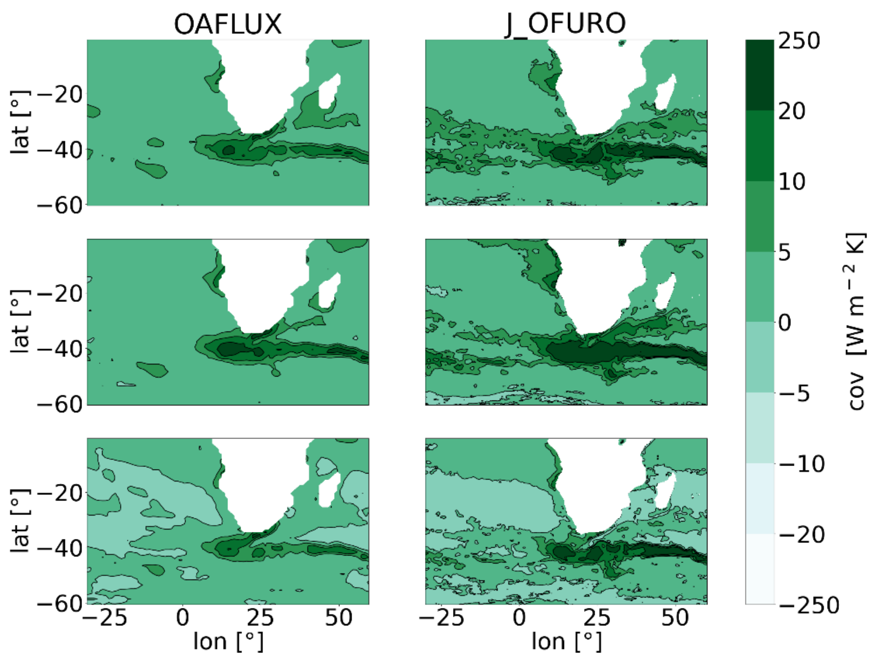


**Fig. 1.** SST-SHF covariance patterns for observational data. Rows indicate lag configuration, -1, 0, 1 respectively. Negative lag means SST leads over SHF.

## 3. Discussion

Heat fluxes and temperature correlation is investigated in the Agulhas Current region. As shown in the previous section, lower horizontal resolution data have lower covariance values, symptoms of a worse ability of eddy and small scales detection. In the open ocean areas, such as the Southern Atlantic the antysimmetric patterns can be found, without any particular difference between the two observational datasets. In those area, the atmosphere causes variation in the ocean temperature in wider length scales, allowing low resolution sampling to detect the leading processes. Where smaller scales become relevant, i.e., Western Boundary Current regions or eddy-active areas, variation in the ocean temperature can modify surface heat fluxes in the atmosphere.

**References**

Beal LM, Chereskin TK., Lenn YD, & Elipot S (2006) The Sources and Mixing Characteristics of the Agulhas Current, Journal of Physical Oceanography, 36(11), 2060-2074.
Bellucci A, Athanasiadis P, Scoccimarro E. (2021) Air-Sea interaction over the Gulf Stream in an ensemble of HighResMIP present climate simulations, Clim Dyn 56, 2093–2111.
Bishop SP, Small RJ, Bryan FO, & Tomas RA (2017) Scale Dependence of Midlatitude Air–Sea Interaction, Journal of Climate, 30(20), 8207-8221. Retrieved Aug 20, 2021.
De Ruijter WPM (2008) The Agulhas Current, Eos Trans. AGU, 89(10), 98– 98.
Hasselmann K (1976) Stochastic climate models. Part I, theory, Tellus 28:473–485.
Lutjeharms JRE, Ansorge IJ (2001) The Agulhas Return Current, Journal of Marine Systems, Volume 30, Issues 1–2.
Lutjeharms JRE (1989) The Role of Mesoscale Turbulence in the Agulhas Current System,Elsevier Oceanography Series, Elsevier, Volume 50, Pages 357-372.
Lutjeharms JRE (2006) The Agulhas Current, Springer.
Sandalyuk NV & Belonenko TV (2021) Three-dimensional structure of the mesoscale eddies in the Agulhas Current region from hydrological and altimetry data, Russian Journal of Earth Sciences, 21(4).
Speich S, Lutjeharms JRE, Penven P, and Blanke B (2006) Role of bathymetry in Agulhas Current configuration and behaviour, Geophys. Res. Lett., 33, L23611
Tomita H, Hihara T, Kako S, Kubota M, Kutsuwada K (2019) J Oceanography, 75,171–194.
Yu L, Jin X, Weller R (2008) Multidecade Global Flux Datasets from the Objectively Analyzed Air-sea Fluxes (OAFlux) Project: Latent and Sensible Heat Fluxes, Ocean Evaporation, and Related Surface Meteorological Variables. OAFlux Project Tech. Rep. OA-2008-01.

# Hydraulic modelling of interfacial processes for two-layer maximal exchange

Janek LAANEARU[1], Alan CUTHBERTSON[2]

[1] School of Engineering (Civil Engineering and Architecture), Tallinn University of Technology, Estonia
email: janek.laanearu@taltech.ee

[2] School of Science and Engineering (Civil Engineering), University of Dundee, UK
email: a.j.s.cuthbertson@dundee.ac.uk

ABSTRACT

The paper deals with the hydraulic modelling of two-layer maximal exchange; where two control sections are required for the stratified, bi-directional flow to be fully controlled. A novel mass flux transfer model is considered in the two-layer hydraulic exchange that includes a solution for the reversed-flow conditions of the two-layer system. This stratified-flow effect is associated with an internally-generated net-exchange barotropic flow components, which may be associated with the interfacial mixing processes. Similar recirculation-type effect in the stratified flow is present in salt-wedge estuaries. Predictions from the hydraulic model incorporating mass flux transfer between the counterflowing layers is compared to experimental data of exchange flows with and without net-barotropic forcing.

## 1. Introduction

Stratified-flow dynamics in estuaries and sea straits, connecting water masses of different origin and properties, can be driven by variable internal forcing conditions due to topography and external forcing under different hydrodynamic and atmospheric conditions (e.g. river flows, tides, wind stresses). Internal-flow dynamics are dependent on interfacial mixing and turbulence due to friction at the channel boundary. A salt-wedge estuary, for example, may include exchange flow through a freshwater river channel outflow in the upper layer experiencing entrainment of denser, counter-flowing marine waters of different density in the lower layer (Arita and Jirka, 1987).

Despite internal-flow hydraulics being of considerable importance to a wide range of environmental fluid flows in estuaries, the internal-flow hydraulics for more complex topographies has typically found less attention. An aim of the present study is to demonstrate how non-rectangular cross-section channels shapes, that have variable constriction topographies, can be analyzed by adopting the hydraulic functions of two-layer flow (Dalziel, 1991). The present study focuses specifically on channel cases with quadratic-shape cross sections, introduced for the two-layer hydraulic exchange in Laanearu and Davies (2007). This model is an extension of the two-layer hydraulic model study by Dalziel (1992), who introduced a functional approach defining real-valued roots of the internal-flow head function; a prerequisite for the two-layer hydraulic exchange flow to be realizable. The internal-flow head function for a rectangular channel cross-section had been introduced by Armi (1986). However, previous experimental studies (e.g. Zhu and Lawrence, 2000) of two-layer exchange flows through geometrically-determined opening have been developed to make use of internal-flow hydraulic theory and also consider internal energy losses. The presence of external forcing in the two-layer hydraulic exchange is also accounted for by imposing a net-exchange barotropic flow component either in the upper fresh or lower saline fluid layer. Furthermore, the hydraulic modelling of two-layer system is also modified by parameters to deal with boundary and interfacial friction and entrainment effects between layers, all of which are needed to account for turbulent stresses and buoyancy fluxes, respectively, within the internal flows.

## 2. Internal-flow hydraulics of two-layer maximal exchange

According to Laanearu and Davies (2007), the internal-flow head for buoyancy-driven flow through the quadratic-type channel can be defined as the following function:

$$H = \left(\frac{\xi\, h(x)^{(\xi-1)}}{w(x)}\right)^2 K\left(\left(\frac{1}{h_2(x)^{\xi}}\right)^2 - \frac{q^2}{\left(h(x)^{\xi}-h_2(x)^{\xi}\right)^2}\right) + h_2(x) + h_s(x) \tag{1}$$

where $h(x) = h_1(x) + h_2(x)$ is the cross-sectional maximum of two-layer fluid height (i.e. water depth at its deepest point), with $h_1$ and $h_2$ being the upper and lower-layer fluid heights, $w(x)$ is the cross-sectional maximum of two-layer fluid width (i.e. water-surface width), and $\xi$ is a channel shape factor that represents the inverse ratio of the cross-sectional flow area of a specific channel geometry to the equivalent rectangular cross-sectional area having identical $w(x)$ at the surface and $h(x)$ at the axis of cross-sectional symmetry. For instance, if $\xi = 1.0$, the channel has a rectangular cross section (Armi, 1986), while $\xi = 3/2$ and $\xi = 2.0$ correspond to parabolic and triangular cross section, respectively, (Dalziel, 1992). The lower-layer volume-flux parameter $K = Q_2{}^2/(2\,g')$, the upper and lower layer flow rates ratio squared $q^2 = Q_1{}^2/\,Q_2{}^2$ are defined by the volumetric fluxes $Q_1(x)$ and $Q_2(x)$ in the upper and lower layers, respectively. For the case of non-mixing flow, the hydraulic model parameters $K$ and $q^2$ are constants at any along-channel location $x$.

## 3. Internal-flow head loss and interfacial displacement of two-layer exchange

The two-layer hydraulic modelling can be used to investigate the "mixing" characteristics of the internal-flow dynamics of the stratified bi-directional flow that is generated in a channel with a sill obstruction. Thus, the critical flow at the sill crest, corresponding to a control section $\boldsymbol{sill}$ ($\boldsymbol{s}$), and the critical flow at the end of the channel within the denser-fluid reservoir, corresponding to the second control section $\boldsymbol{exit}$ ($\boldsymbol{e}$), are both present for maximal exchange. In the hydraulic modelling theoretical solutions, presented above, the "globally" determine parameter squared ratio $\boldsymbol{q^2 = Q_1{}^2/\,Q_2{}^2}$ of the source fresh water and salt water volume fluxes squared across the sill is considered to be constant along the channel in the non-mixing case, i.e. $\boldsymbol{q^2 = q_e{}^2 = q_s{}^2}$ . However, if the interface displacement (e.g. due to interfacial processes) between the superimposed layers of stratified flow occurs, the key non-dimensional parameter can be introduced in the internal-flow hydraulic model, which is defined as

$$M = \Delta Q_2/Q_{2e} \tag{2}$$

where per definition, the interfacial-displacement parameter $M > 0$. Thus the loss of volumetric flow rate in the lower layer $\Delta Q_2 = Q_{2e} - Q_{2s} > 0$ corresponds to "entrainment" of the saline water layer between channel two control sections $exit$ and $sill$, and the increase of volumetric flow rate in the upper layer $\Delta Q_1 = Q_{1s} - Q_{1e} < 0$ corresponds to "detrainment" of the fresh water layer between channel two control sections $sill$ and $exit$. In the case of interfacial "mixing" process ($M > 0$), the ratio of source fresh and saline volume fluxes in the internal-flow hydraulic model formulae at the channel control section $exit$ is

$$q_e = q + M \tag{3}$$

and at the control section $sill$ is

$$q_s = q/(1 - M) \tag{4}$$

## 4. Concluding remarks

It should be underlined here that the introduction of the interfacial "mixing" parameter $M$ in the two-layer hydraulic model for the maximal exchange without the net-exchange barotropic flow component ($q = 1.0$) actually involves the net-exchange barotropic flow component in the upper layer, i.e. generally $q > 1$ due to the interface displacement. It should be mentioned here that the maximal exchange of the two-layer "mixing" flow corresponds to the comparatively small changes in the upper- and lower-layer volumetric flow rates between the channel control sections $exit$ and $sill$. The two-layer maximal exchange "mixing" effect can be expressed with the difference of magnitude for the flow-rates ratio parameters at two controls, i.e. $q_e - q_s$ . However, in the case of more intensive interfacial mixing, the two control sections $exit$ and $sill$, may be dynamically decoupled by the internal-flow hydraulic jump, and the two-layer hydraulic exchange should be classified as the sub-maximal in nature (De Falco et al, 2021).

**References**

Arita M, Jirka GH (1987) Two-layer model of saline wedge. I: Entrainment and interfacial friction, J Hyd Eng 113(10): 1229–1248.
Armi L (1986) The hydraulics of two flowing layers with different densities, J Fluid Mech, 163, 27–58.
Dalziel SB (1991) Two-layer hydraulics: A functional approach. J Fluid Mech, 223, 135–163.
Dalziel SB (1992) Maximal exchange in channels with nonrectangular cross sections, J Phys Oceanogr, 22, 1188–1207.
De Falco MC, Adduce C, Cuthbertson A, Negretti ME, Laanearu J, Malcangio D, Sommeria J (2021) Experimental study of uni- and bi-directional exchange flows in a large scale rotating trapezoidal channel, Phys Fluids, 33(3), 036602.
Laanearu J, Davies P (2007) Hydraulic control of two-layer flow in "quadratic"-type channels, J Hydraul Res, 45(1), 3−12.
Laanearu J, Cuthbertson A (2022) Hydraulics of stratified sill flows within varying channel geometries: investigating energy loss and mixing of two-layer maximal exchange. Environ Fluid Mech (in review).
Zhu DZ, Lawrence DA (2000) Hydraulics of exchange flows. J Hydraul Eng 126(12), 921–928.

# Numerical simulations of density-driven exchange flows generated across a submerged trapezoidal sill-channel

Manel GRIFOLL[1], Alan CUTHBERTSON[2], Jarle BERNTSEN[3], Maria Chiara DE FALCO[4], Claudia ADDUCE[4]

[1] Universitat Politècncia de Catalunya (UPC – BarcelonaTech), Barcelona, Spain
email: manel.grifoll@upc.edu

[2] University of Dundee, Dundee, Scotland, UK
email: a.j.s.cuthbertson@dundee.ac.uk

[3] University of Bergen, Bergen, Norway
email: jarle.berntsen@uib.no

[4] Università Roma Tre, Roma, Italy
email: claudia.adduce@uniroma3.it

ABSTRACT

This study presents the results of laboratory-scale numerical simulations of density-driven exchange flows generated across a submerged trapezoidal sill-channel obstruction under both non-rotating and rotating frames of reference using the Bergen Ocean Model (BOM), a three-dimensional general ocean circulation model. The results from the numerical simulations aim to simulate the large-scale experimental data obtained in the LEGI Coriolis rotating platform in Grenoble, which velocity and density fields where measured through image velocimetry (PIV) measurements and micro-conductivity density probe data from the equivalent laboratory experiments. The BOM simulations reproduce the main dynamic properties of the large-scale exchange flows through the trapezoidal channel, with the lower layer saline intrusion flux shown to reduce (i.e. due to partial blockage) as the upper freshwater flow is increased. The effect of increasing the Coriolis parameter on the exchange flow dynamics and the cross-channel flow structure is also considered.

## 1. Introduction

Restricted exchange flows occur in many natural aquatic environments (e.g. estuaries, sea straits, fjords, ocean basins) when horizontal density and/or pressure gradients are generated between adjacent, connected water masses due to variations in salinity and temperature (i.e. baroclinic forcing) or tides, freshwater inflows, and wind-driven currents (i.e. barotropic forcing), respectively. The hydraulic control, lateral distribution and mixing of the exchange flows generated also depends on topographical constraints (e.g. seafloor bathymetry, channel shape and roughness), and Coriolis forces due to the Earth's rotation when the channel is relatively wide in comparison to the Rossby radius of deformation. A recent experimental study by De Falco et al. (2021), investigated experimentally the dynamics of uni- and bi-directional exchange flows in a large-scale rotating trapezoidal sill-channel. Within these experiments, they highlighted the significant influence of net-barotropic forcing, coupled with Coriolis effects, on lateral distribution and relative magnitude of the counter-flowing water masses. In this context, the current study presents some preliminary results from numerical simulations that aim to investigate the complex dynamics of bi-directional exchange flows within the trapezoidal channel including interfacial mixing characteristics, secondary flow structures and the eventual exchange blockage.

## 2. Numerical model and experimental set-up

The Bergen Ocean model (BOM) (Berntsen, 2000) is a terrain-following ı-coordinate numerical simulation tool for ocean modelling, discretized on a staggered C-grid. A fully non-hydrostatic version of BOM is applied in laboratory scale studies including numerical simulation of flow of dense water in a V-shaped laboratory scale canyon (Berntsen et al. 2016) and the simulation of exchange flows in a submerged sill obstruction under both non-rotating and rotating frame of references (Cuthbertson et al., 2021). In the current study, the channel and sill geometry under investigation are the same configuration as considered previously in the experimental study by De Falco et al. (2021), where a submerged trapezoidal-shaped sill-channel restricts the bi-directional exchange flow generated between freshwater A and saline water B basins (see Figure 1a). The numerical mesh consists in 0.1 m horizontal grid size in both along and across the channel and 161 equidistant $\sigma$-layers in the vertical. This results in 20 grid cells across the channel width to facilitate accurate representation of secondary circulations generated across the sill. In addition, 177 grid cells are implemented along the channel length to ensure an appropriate flow development region in both basins. The grid resolution is much higher vertically than horizontally in order to represent the sharp interface between the dense and fresh water layers. The key dimensions of the sill-channel configuration in the equivalent BOM model domain are crest height h = 0.5 m; sill length L = 6.5 m; trapezoidal cross-sectional slope 45º; and channel-sill width at bottom B = 1.0 m.

Following the laboratory experiment configuration, the BOM model domain is initially filled with freshwater of density $\rho_1 = 1000$ kg.m$^{-3}$, with no residual flow in the domain. Within the non-rotating BOM simulations, the model parameters are set equivalent to experiment B1O conditions [see Table 1 in De Falco (2021)]. The volume flux ratio $Q^*$ of the freshwater $Q_1$ and saline water $Q_2$ inflows into the model domain is kept constant at $Q^* = 0.0$ (i.e. $Q_1 = 0.0$ l.s$^{-1}$; $Q_2 = 4.4$ l.s$^{-1}$) over the first 1500 s before being gradually ramped up (i.e. through incremental increases in $Q_1$ values) to a maximum value of $Q^* = 1.8$ over run duration of 2000 s. Then, with a subsequent ramp, the simulations finishes at $Q^* = 4.5$ (2500 s). Within all numerical experiments $Q_2$ was kept constant (i.e. $Q_2 = 4.4$ l.s$^{-1}$) to match the experimental set-up. Within all BOM simulations, the baroclinic time step is set to 0.025 s to ensure model stability.

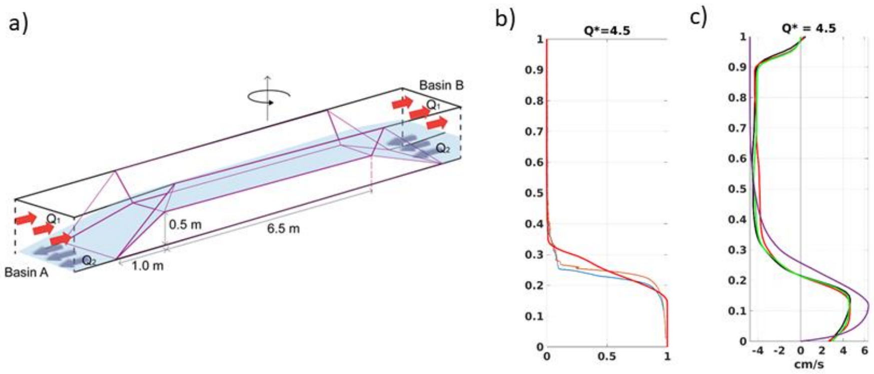


**Fig. 1.** a) Schematic representation of the trapezoidal channel including the saline and freshwater flow [adapted from De Falco et al. (2021)]. The angle of the trapezoidal sill-channel is 45º and the bottom with is 1.0 m. b) normalized density profiles for different sections at $Q^*$=4.5 (BOM simulations in red). c) along-channel velocity profiles at $Q^*$=4.5 for BOM simulation (purple) and 3 centreline PIV measurements.

## 3. Initial BOM simulations and experimental results comparison

Initial experiments were conducted to measure the bi-directional stratified flow dynamics generated across the submerged sill-channel where Earth rotation effects were not considered (i.e. Coriolis parameter f = 0). Laboratory experimental measurements were targeted at obtaining high-resolution density and velocity fields at different transverse sections across the channel width. Two-dimensional Particle Image Velocimeter (2D PIV) was used to obtain measurements of the velocity field in vertical (XZ) planes along this central region of the trapezoidal channel. Vertical profiles of the density field were obtained using micro conductivity probes. A complete set of the instrumentation and measurements can be found at De Falco et al. (2021). Figure 1b and 1c show the normalized density and along-channel velocity profiles, respectively, at $Q^* = 4.5$ for the BOM simulations and 3 centreline PIV measurements. The density and velocity profiles modelled by BOM exhibited qualitatively similar trends with the experimental measurements, but also demonstrated lower gradients in the interfacial region of the bi-directional flow, indicating more intense mixing than suggested by the experimental measurements. However, overall the implemented model provides an excellent tool to explore the exchange flow dynamics and secondary (i.e. cross-channel) circulations under a wide range of parametric conditions. In future BOM simulations, it is planned to increase $Q^*$ values further to higher values to investigate the blockage mechanisms of the saline intrusion flux. Furthermore, additional BOM simulations in a rotating frame of reference will be conducted over a range of different Coriolis f values that match the rotating experimental runs considered in the laboratory studies of De Falco et al. (2021) (i.e. f = 0.06 and f = 0.01).

**References**

Berntsen J (2000) USERS GUIDE for a modesplit σ-coordinate numerical ocean model. Technical Report 135, Dept. of Applied Mathematics, University of Bergen, Johs. Bruns gt.12, N-5008 Bergen, Norway. 48p
Berntsen J, Darelius E, Avlesen H (2016) Gravity currents down canyons: effects of rotation, Ocean Dyn 66, 1353–1378
Cuthbertson A, Berntsen J, Laanearu J, Asplin M (2021) Rotational effects on exchange flows across a submerged sill, Environ Fluid Mech, 21, 405 – 432.
De Falco MC, Adduce C, Cuthbertson A, Negretti ME, Laanearu J, Malcangio D, Sommeria J (2021) Experimental study of uni and bi-directional exchange flows in a large scale rotating trapezoidal channel, Phys Fluids, 33, 036602.

# Experiments on macroplastic storage in rivers with spur dikes

Łukasz PRZYBOROWSKI[1], Jarosław BIEGOWSKI[2], Zuzanna CUBAN[2], Anna ŁOBODA[1], Małgorzata ROBAKIEWICZ[2]

[1] Institute of Geophysics Polish Academy of Sciences, Poland
email: lprzyborowski@igf.edu.pl
email: aloboda@igf.edu.pl
[2] Institute of Hydro-Engineering Polish Academy of Sciences
email: jarbieg@ibwpan.gda.pl
email: marob@ibwpan.gda.pl
email: zuzannacuban@ibwpan.gda.pl

ABSTRACT

A physical model in the concrete open channel will be prepared to investigate macroplastic river transport processes in the presence of spur dikes and vegetation. The goal is to assess the number of uniform floating plastic litter caught in created obstacles. We assumed that plastic particles transported downstream channel will get captured into concavities between spur dikes on both sides of the channel. Additionally, the number of captured pieces will vary between the scenarios, including elongating one spur and adding artificial vegetation between spurs. The quantity and paths of plastic debris, as well as the flow field, will be analysed by photogrammetric methods and acoustic Doppler velocimetry, respectively.

## 1. Introduction

The production of plastics increases every year - in Europe, it increased by about 100 million tons between 2008 and 2018 (Plastics Europe, 2019). International and local-scale initiatives were recently undertaken to tackle plastic pollution in water environments, while researchers started collecting data about the amount and type of plastics found and transported in water bodies (e.g., Van Emmeric et al., 2020; Al-Zawaidah et al., 2021). Windsor et al. (2019) pointed out the need to investigate how macroplastics, i.e., pieces > 0.5 cm, are accumulated in rivers, which can be considered as plastic reservoirs in upcoming decades (Van Emmerick et al., 2022). The macroplastic can be deposited, i.e., on the riverbanks, stopped by the infrastructure or entangled within riparian vegetation, especially in low-velocity areas (Cesarini et al., 2022). That type of plastic is also harmful to the environment, as it can degrade into microplastics, be digested, or entangle the animals and affect water infrastructure by clogging it (Van Emmeric et al., 2020).

Floating litter can be captured along the river in concavity zones (Tominaga et al., 2020). Artificial constructions, such as spur dikes, can create zones where plastics are prone to get stuck and vegetation can also catch the litter (Cesarini et al., 2022). Based on the available knowledge and existing laboratory infrastructure, laboratory experiments to track macroplastic in the presence of spur dikes with and without the presence of vegetation are proposed.

## 2. Experimental setup

The experiments will be performed in the spring of 2022 in the open-air hydraulic laboratory of the Institute of Hydro-Engineering, Polish Academy of Sciences, in the concrete channel (length 60 m; width 5 m, slopes 1:2) with a system of 5 pairs of spurs (length 1.2 m, height 0.4 m, width 0.5 m at the bottom and 0.1 m at the top). Polypropylene square plates with a side of a few centimetres will be used as the litter, to be recognized by the house-made particle tracking velocimetry (PTV) software (Cuban, 2021), which will provide information on the behaviour of plastic particles in the presence of regular spurs. Flexible artificial plants will be arranged inside one of the concavities between the spurs, to replicate aquatic vegetation growing in rivers. The plastics will be dropped into the flowing water upstream of the obstacles along the middle of a cross-section. A high-resolution camera situated above the channel will record the paths of the particles. Acoustic Doppler velocimetry will be used to measure the velocity field in the reach. Due to the need of estimating water velocity at the surface level, sawdust or crushed leaves will be tossed into the flowing water to facilitate the use of large-scale particle image velocimetry like free-to-use software FUDAA-LSPIV (Le Coz et al., 2014).

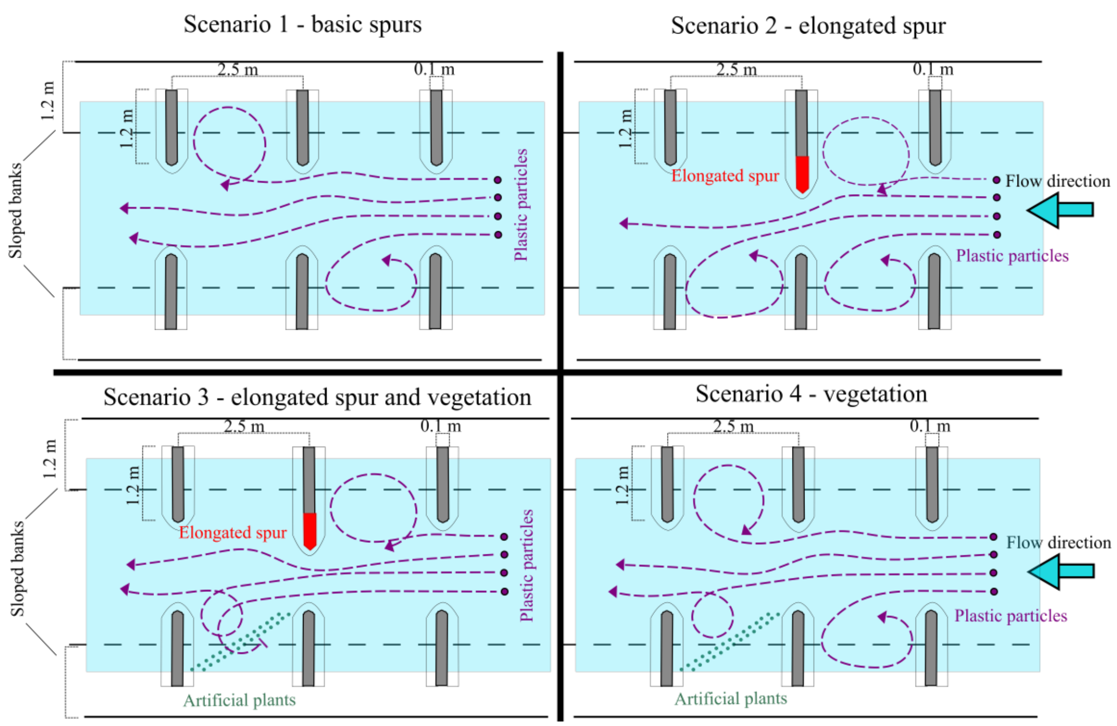


**Fig. 1.** Top view of the proposed experimental setup – 4 scenarios to be tested within the channel reach with the emerged spur dikes.

Four basic scenarios, each at three flow conditions will be conducted to test how each solution is likely to capture plastic particles (Fig. 1). We expect that the scenario with both vegetation and elongated spur present, should alter the stream path the most. That way, the particles are expected to fall into the opposite area where they should entangle within plants' stems, preventing them from flowing further downstream the channel. The paths of particles between the scenarios will be analysed using PTV and compared to the measured velocity field.

## 3. Summary

Though many inventions, monitoring actions and initiatives have been undertaken recently to get rid of the plastic in the environment, there is still a lack of experimental research investigating macroplastic transport processes. Therefore, this measurement campaign aims at providing more understanding of this phenomenon, especially when the previous experiments conducted in this laboratory showed plastic tiles being temporally caught within concavities. A new setup with the proposed alterations is specifically designed to calculate the probability of spur dikes catching plastic garbage and to describe its behaviour in such specific conditions. The introduction of additional elements in form of vegetation, which is known to effectively catch plastic litter (Cesarini et al., 2022), together with the longer spur, should enhance the capture process. Although the factors like variability in plastic density, shape and wind exposure will not be investigated in the presented case, the obtained knowledge can be still used to modify existing river structures or help in plastic cleaning activities.

**Acknowledgements**

The work of ŁP, AŁ, JB, ZC and MR was supported by a subsidy from the Polish Ministry of Education and Science.

References

Al-Zawaidah H, Ravazzolo D, Friedrich H (2021) Macroplastics in rivers: present knowledge, issues and challenges, Environmental Science: Processes & Impacts, 23(4), 535-552
Cesarini G, Scalici M (2022) Riparian vegetation as a trap for plastic litter, Environmental Pollution, 292, 118410
Cuban Z (2021) Investigation of ice and sediment transport in a canal with spur buildings, Master Thesis, Gdańsk University of Technology
Plastics – the facts 2018 An analysis of European plastics production, demand and waste data, PlasticsEurope, 2018
Le Coz J, Jodeau M, Hauet A, Marchand B, Le Boursicaud R (2014) Image-based velocity and discharge measurements in field and laboratory river engineering studies using the free FUDAA-LSPIV software, Proceedings of the international conference on fluvial hydraulics, River Flow, 3(9), 2014-05 pp.
Tominaga A, Tang Z, Zhou T (2020) Capture method of floating garbage by using riverside concavity zone, River Flow 2020, 2154-2162 pp.
van Emmerik T, Schwarz A (2020) Plastic debris in rivers, WIREs, Water, 7, 1–24
van Emmerik T, Mellink Y, Hauk R, Waldschläger K, Schreyers L (2022) Rivers as Plastic Reservoirs, Frontiers in Water, 212
Windsor FM, Durance I, Horton AA, Thompson RC, Tyler CR, Ormerod SJ (2019) A catchment-scale perspective of plastic pollution Global Change Biology, 25(4), 1207-1221

# Investigation of plastic presence in the river sediment of the Arno River (Italy)

Mirco MANCINI[1], Daniele MARTUSCELLI[2], Lorenzo INNOCENTI[3], Simona FRANCALANCI[4], Maurizio BECUCCI[5] and Luca SOLARI[6]

[1,2,3,4,6]Department of Civil and Environmental Engineering, University of Florence, Florence, Italy,
[5]Department of Chemistry "Ugo Schiff", University of Florence, Sesto Fiorentino, Italy
email: mirco.mancini@unifi.it (for author 1)
email: daniele.martuscelli@unifi.it (for author 2)
email: lo.innocenti@unifi.it (for author 3)
email: simona.francalanci@unifi.it (for author 4)
email: maurizio.becucci@unifi.it (for author 5)
email: luca.solari@unifi.it (for author 6)

ABSTRACT

The need of studying how plastics affect water ecosystems, such as rivers, lakes, and oceans, has been emerged in last years. Despite this, there is a lack of knowledge, mainly due to the poor data availability, which does not allow to understand the dynamics and the accumulation of plastic waste in rivers. Recent studies observed that only a small fraction (≈ 3%) of the total plastic waste generated within the river basin is discharged into the ocean, so the large part of the plastic waste remains entrapped within the river system. Once plastics entered the river corridors, their dynamics is strongly affected by the flow regime and by the channel boundaries, e.g. the river morphology or the presence of in-channel structures. In this work, the focus is on the analysis of micro- and macro-plastics (< 5 and> 5 mm, respectively) trapped into river sediment. The major aim of the study is the investigation of plastics accumulated in river sediments along the Arno River (Italy).The sampling campaign was designed to study the influence of the flow regime on the plastic distribution.

## 1. Introduction

Plastics are ubiquitous in human society due to the many properties of plastic polymers, and plastic pollution growth in years becoming dangerous for earth ecosystems, particularly for water ecosystems. For this reason, an increasingly large part of the human society is now committed to combating plastic pollution and finding effective solutions for removing micro- and macro-plastics from the natural environments (Waters et al., 2016). Water ecosystems represent the main mean of transportation for plastic items as they might easily enter into open waters (Gonzalez-Fernandez and Hanke, 2017), i.e. rivers and lakes, through many source points, e.g. the urban runoff, and the outflow of the wastewater treatment plant (Becucci et al, 2022). Once plastics entered open waters, they started to be transported downstream depending on their settling velocity (Francalanci et al., 2021). From the moment they begin their residence in rivers, a complex dynamic is set in motion whereby this plastic waste may be transported to seas or oceans, or, more likely, remain within river corridors (van Emmerik et al., 2019, Tasseron et al., 2020). During their residence time in rivers, plastic polymers may change their properties (e.g. density) due to the physical and biological processes they undergo, and, consequently, also their dynamic changes in time.

In the present work, the focus is on the plastics trapped in bed sediments along the Arno River corridor in Italy. This is an ongoing study, designed to provide the quantification and the characterization of plastics along the river. A series of sample locations were identified on the river bars; the collected samples are analyzed, provided plastics is separated from sediment and plastic polymers are identified and characterized (size, shape, density ..). In addition, the study will provide a first relationship between the river flow regime and the distribution of plastics into the river corridor.

## 2. Methodology

The analysis is conducted by collecting samples from emerged river bars along the Arno River (see Fig. 1). These locations were identified by considering the three main urban areas that develop close to the river, i.e. the Valdarno urban in the upper part of the river catchment, the urban area of the city of Florence in the lowland part of the river catchment, and the urban area of the city of Pisa close to the river mouth. A total number of 12 samples sites have been identified, for each of them few sampling points are considered.


**Fig. 1.** Sampling sites along the Arno River.

For each sample, extraction of plastics was performed by the density separation method. The samples were homogenized, and then only 300 g of sediments was considered for the test. The tests were performed into a 1000 mL glass beaker considering 600 mL of saturated $CaCl_2$ solution characterized by a density of 1.41 g/cm$^3$.Samples were allowed to settle for 24 h, then 40 mL of the supernatant was collected for the following step, i.e., the digestion of biological organic content performed with using 40 mL of $H_2O_2$ at 30% by weight. This sample was kept in motion for 24 h by means of a vibrating plate to facilitate the oxidation process. The solid matrix was then transferred to 20÷25 μm porosity paper filters by Whatman and filtered through vacuum filtration system. Lastly, the filters were placed inside a clean, covered aluminum Petri capsule and dried in an oven at 105 °C for 1 hour. The paper filters containing the digested materials were observed at first by visual inspection in order to identify the presence of plastic fragments and then by Raman spectroscopy to be individually characterized terms of dimensions, shape, and plastic polymer.

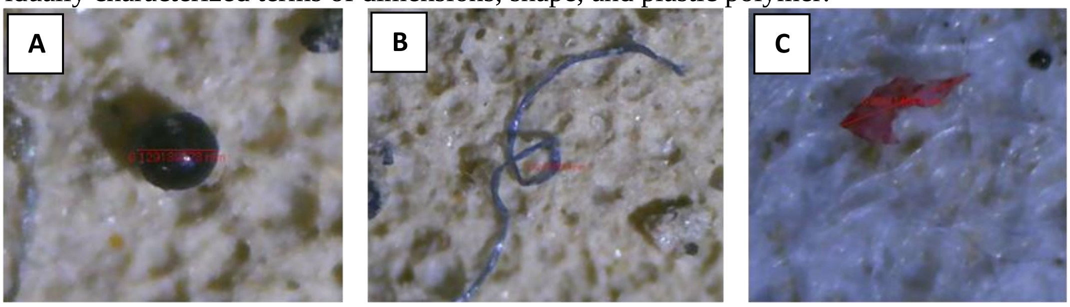


**Fig. 2.**Visual observation of candidate microplastic particles: (A) sphere, (B) fiber, and (C) fragment

## 3. Conclusion

The abstract presents a methodology for investigating the presence of plastics in river sediments. A series of samples have been collected along the Arno River (Italy) with the aim of provide a first quantification and characterization of plastic polymers deposited on river bars., The present analysis will be useful for investigating the role of floods in the distribution of plastics along the river corridor.

### References

Becucci, M., Mancini M., Campo R., Paris E., (2022) Microplastics in the Florence wastewater treatment plant studied by a continuous sampling method and Raman spectroscopy: A preliminary investigation, Sci. Total Environ., 2022, 808, 152025.
Francalanci, S., Paris, E, Solari, L (2021) On the prediction of settling velocity for plastic particles of different shapes, J.Environmental Pollution, 2021, 290, 118068.
González-Fernández D and Hanke G(2017) Toward a Harmonized Approach for Monitoring of RiverineFloating Macro Litter Inputs to theMarine Environment.Front. Mar. Sci. 4:86.doi: 10.3389/fmars.2017.00086.
Tasseron, P., Zinsmeister, H., Rambonnet, L., Hiemstra, A.F., Siepman, D., and van Emmerik, T. (2020). “Plastic Hotspot Mapping in Urban Water Systems.” Geosciences (Switzerland) 10(9): 1–11.
van Emmerik, T., Loozen, M., Van Oeveren, K., Buschman, F., and Prinsen, G. (2019). “Riverine Plastic Emission from Jakarta into the Ocean.” Environmental Research Letters 14(8).
Waters CN, Zalasiewicz J, Summerhayes C, Barnosky AD, Poirier C, Gałuszka A, et al. 2016. The Anthropocene is functionally and stratigraphically distinct from the Holocene. Science, 351(6269):aad2622. doi:10.1126/science.aad2622.

# Presence of microplastics in two karst springs for drinking water in Slovenia

Lara VALENTIĆ[1], Oliver BAJT[2], Tanja Pipan[1,3]

[1] ZRC SAZU Karst Research Institute, SI-1000 Ljubljana, Slovenia
email: lara.valentic@zrc-sazu.si
email: tanja.pipan@zrc-sazu.si

[2] National Institute of Biology, Marine Biology Station, SI-6330 Piran, Slovenia
email: oliver.bajt@nib.si

[3] UNESCO Chair on Karst Education, University of Nova Gorica, SI-5271 Vipava, Slovenia
email: tanja.pipan@zrc-sazu.si

ABSTRACT

Studies of microplastic (MP) pollution are becoming interesting topic for research, but the research of MP in karst environment is still in its infancy. This study was done on two karst springs in Slovenia (Malni and Rižana), that are the most important sources of drinking water for local inhabitants. The results showed that 17% of particles in Malni are plastic, while for Rižana the result is 5.4%. The most common polymers found were different resins, rubber and copolymers.

## 1. Introduction

Karst surface covers about 15% of the global land surface and more than a fifth in Europe alone (Goldscheider et al. 2020). In many regions karst aquifers often represent the only exploitable water reserves and are therefore invaluable sources for human health, food security, and the economic sector (Ravbar et al. 2015). Recently, there have been some studies of MP pollution in karst environment (Valentić, 2018; Panno et al., 2019; Balestra and Bellopede, 2022). According to those few existing preliminary studies, the karst underground environment contains predominately MP fibres, with study of Valentić (2018) indicating a correlation between the low density of MP and rapid transport of such particles through the karst aquifer. Figure 1 represents some possible MP transport routes in karst environment.

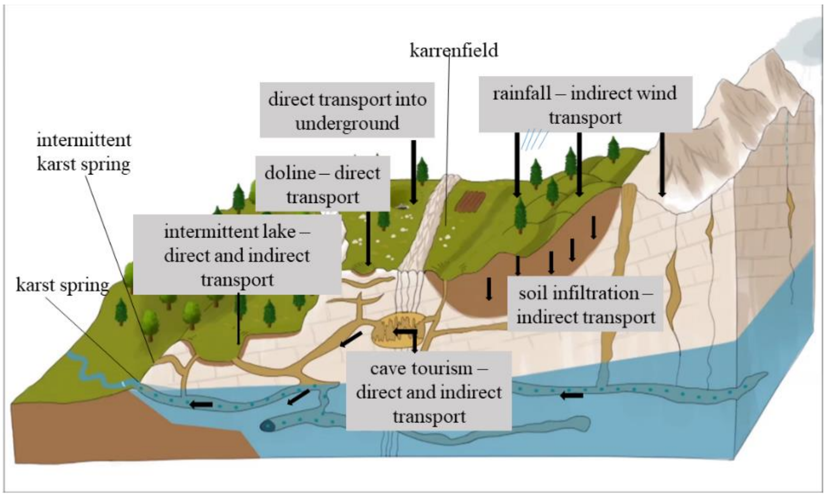


**Fig. 1**: Schematic MP transport routes (grey boxes) in the karst underground and karst aquifer. All of the MP is transported through the aquifer and ends in karst springs (Source: Ravbar 2007, with modifications).

## 2. Study area and results

The study was conducted on two karst springs in Slovenia – spring Malni and spring Rižana. Both springs are regionally extremely important sources of drinking water – they are the only springs that present water supply for the entire year. There are some other smaller springs, but they are either too torrential in nature or biochemically unsuitable for use.

Sampling of Malni was continuous, on a weekly basis, from October 2020 to May 2021, while sampling of spring Rižana was done approximately once a month, from the end of November 2020 to June 2021. Rižana is (compared to Malni) much more torrential spring – the flow can easily differ 20x times or more between low levels and high levels of water, therefore making it challenging for sampling on a weekly basis.

Results from Malni show, that the quantity of MP particles is the highest during the first rain event after longer period of drought. This is similar to the behavior of other, water soluble pollutants, like concentrations of nitrates and phosphates (Ravbar et al. 2015). Spring Rižana does not show any clear trends of MP quantity. Majority of measured particles consist of fibres (65% in Malni and 86% in Rižana), varying in length, but are mostly 5 – 20 µm in diameter. The confirmed plastic polymers from both springs are represented in Fig. 2. Determined MP particles represent 17% of all particles for Malni and 5.4% for Rižana spring.

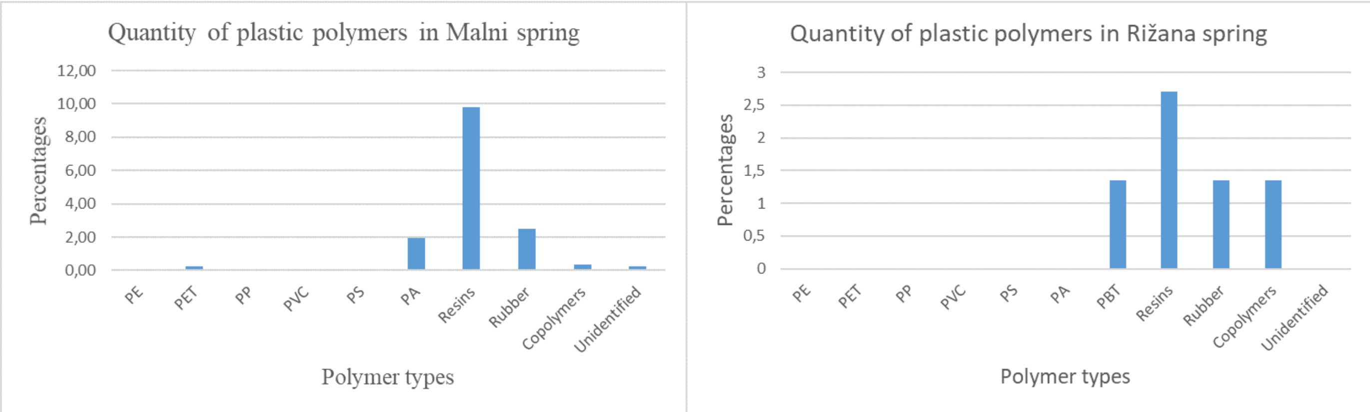


**Fig. 2**: Confirmed MP polymers in all samples, from both springs. PE = polyethylene, PET = polyethylene terephthalate, PP = polypropylene, PVC = polyvinylchloride, PS = polystyrene, PA = polyamide, PBT = polybutylene terephthalate. Resins, rubber and copolymers include a wide variety of polymers, while unidentified are those spectra that could potentially be plastic, but we were unable to find a spectrum in polymer library to determine it.

As we can see from Fig. 2, the most commonly found plastic polymers are different resins (like polyacrylamide, urea formaldehyde etc.) and rubber (like chloroprene). Rižana spring samples also contained different copolymers. This indicates, that MP pollution comes from sources that contain a lot of complex materials, but we were unable to determine the exact source. Since majority of MP particles found are fibers, we expect that the fibers of different polymers are either coated with plastic polymer or the polymer itself was already produced in the fiber shape. We suspect that Malni spring samples contain more MP compared to Rižana due to more densely populated catchment area and easier access to frequent sampling.

## 3. Conclusions

Results from springs show that MP is indeed present in karst sources of drinking water. It follows same pattern as other water soluble pollutants (the highest concentration is after longer period of drought), which will simplify monitoring of MP pollution in the future. We were unable to determine exact sources of pollution, but the confirmed particles are mostly different resins, rubbers and copolymers.

**Acknowledgements**

Authors acknowledge funding from the program Karst Research P6-0119 and Young Researcher programme 6316-21/2017-66 (for LV), both funded from the Slovenian Research Agency, and the project RI-SI-LifeWatch (Development of Research Infrastructure for International Competitiveness of the Slovenian RRI Space). The operation is co-financed by the Republic of Slovenia, Ministry of Education, Science and Sport and the European Union from the European Regional Development Fund.

**References**

Balestra V, Bellopede R (2022) Microplastic pollution in show cave sediments: First evidence and detection technique. Environmental pollution 292, 118261.
Goldscheider N, Chen Z, Auler AS, Bakalowicz M, Broda S, Drew D, Hartmann J, Jiang G, Moosdorf N, Stevanovic Z, Veni G (2020) Global distribution of carbonate rocks and karst water resources. Hydrogeology Journal 28, 1661–1677.
Panno SV, Kelly WR, Scott J, Zheng W, McNeish RE, Holm N, Hoellein TJ, Baranski EL (2019) Microplastic contamination in karst groundwater systems. Ground Water 57 (2), 189–196.
Ravbar N, Kogovšek J and Pipan T (2015) Environmental value and vulnerability of karst resources. In: Zupan Hajna N, Ravbar N, Rubinić J and Petrič M (Eds.): LIFE and water on Karst, Monitoring of transboundary water resources of Northern Istria. Ljubljana, Založba ZRC, pp. 23 – 35.
Ravbar N (2007) The protection of karst waters. A comprehensive Slovene approach to vulnerability and contaminant risk mapping. ZRC Publishing, ZRC SAZU Ljubljana, pp. 256, Ljubljana.
Valentić L (2018) Analysis of microplastics in selected surface and underground karst waters. Master's thesis, University of Nova Gorica, Faculty of Environmental Sciences.

# Using Drum Screen Units to Stop Transported Macroplastics in Rivers

Yannic FUCHS, Susanne SCHERBAUM, Arnd HARTLIEB, Peter RUTSCHMANN

Chair and Laboratory for Hydraulic and Water Resources Engineering, TUM, Germany
email: yannic.fuchs@tum.de

ABSTRACT

This study investigates a novel river cleaning system, removing macroplastics from running waters. The cleaning method uses drum screen units to pass transported plastic particles towards the riverbank. A series of experiments in a physical test stand of a single drum screen analyses the flow depth distribution of representative macroplastic particles and the interaction of the particles with the horizontal bar rake system of the drum screen.

## 1. Introduction

Plastic waste in rivers does not only cause widespread harmful effects on the inland aquatic ecosystem (Azevedo-Santos et al., 2021), but it also impedes the functionality of infrastructure installed in watercourses (Honingh et al., 2020). Macroplastics (>25 mm) form the highest fraction of the total plastic yield by mass (Moore et al., 2011). The highest riverine plastic emissions to the oceans occur in Southeast Asia (Meijer et al., 2021). Therefore, cleaning concepts for plastic-polluted rivers demand to focus on transported macroplastic particles and flow characteristics in Southeast Asian rivers. The investigated concept stops floating and suspended debris by horizontal, drum-shaped bar rakes that pass the intercepted particles towards the riverbank through a self-cleaning mechanism of rotating drums. An experimental series of 1035 test runs studied the potential of a single drum screen to stop macroplastics. The experiments are conducted on nature scale to reproduce the vertical flow depth distribution of the plastic particles and their interaction with the horizontal bar rakes without scale effects. (i) We assume a strong dependence of the flow depth distribution on material-specific properties and different stopping behavior at the drum screen for different plastic types and size classes. (ii) Finally, we expect a rising stopping ratio by higher blocking ratios of the drum screen.

A)

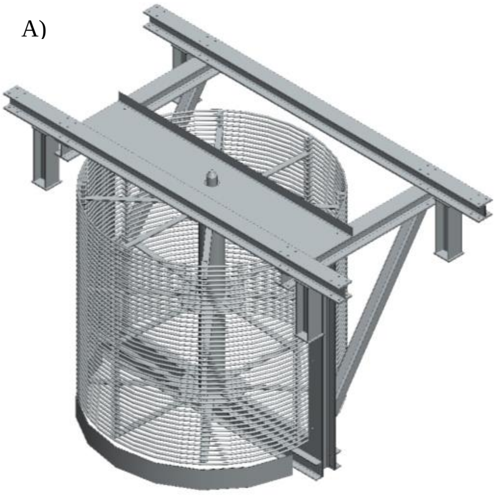

## 2. Material and Methods

The test channel was 250.00 m long, 2.48 m wide, and 2.00 m high. Figure 1A shows the technical sketch of the tested drum screen unit with a height of 2 m and a diameter of 2 m. Figure 1B illustrates the test stand with all control and measurement devices. Plastic particles in watercourses exhibit wide heterogeneity in composition and transport-relevant physical properties. Therefore, we tested the six polymer types EPS, LDPE, HDPE, PS, PET, and PVC. All polymer types were investigated as commonly used base bodies and as square fragments with edge lengths of 25 mm, 50 mm, and 100 mm. During the test runs, we varied decisive flow characteristics as the approach flow depth from 1.2 m to 1.8 m and the approach flow velocity from 0.2 m/s to 1.0 m/s. Changes in the bar spacing from 15 mm to 25 mm and

B)

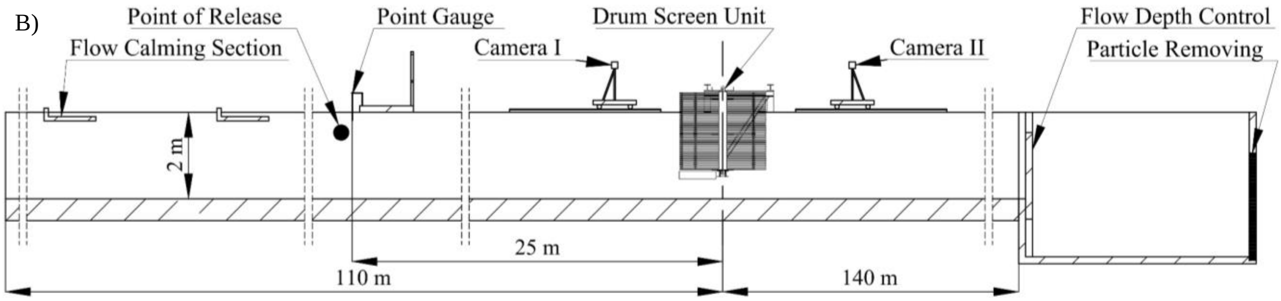


**Fig. 1.** A) Technical sketch of the tested drum screen unit; B) Sketch of the test stand including control and measurement devices

different installation heights of the drum screen unit between 0.37 m and 0.87 m above the channel bottom led to high variations in the blocking ratio. In each test run, 20 identical plastic particles were released 25 m upstream of the drum axis in the upper 30 cm of the water column. We observed the transport path of the particles and documented their vertical flow depth distribution. The installed cameras recorded the interaction of the particles with the horizontal bar rakes. Performing each experiment in triplicate increased the statistical significance of the results and the reproducibility of the experiments.

## 3. Results

The vertical flow depth distribution varied strongly with the particle properties of the tested polymers. The probability of stopping the plastics did not only change with the polymer type and the fragment size but also with the approach flow velocity (see Fig. 2A). The result highlights the influence of the hydraulic conditions on the particle-rake-interaction. While rigid EPS and HDPE fragments wedged between the bar rakes, flexible LDPE and PS fragments wrapped around individual rake bars. According to the larger projected height, almost every base body is stopped by the horizontal bar rakes, with lower stopping ratios for EPS trays. Smaller fragments and the EPS trays passed through the rake due to an unfavorable alignment of the particles caused by the resulting moments of the acting forces. The smaller the bar spacing, the higher the probability of stopping (see Fig. 2 B). This effect arises especially for small fragment sizes.

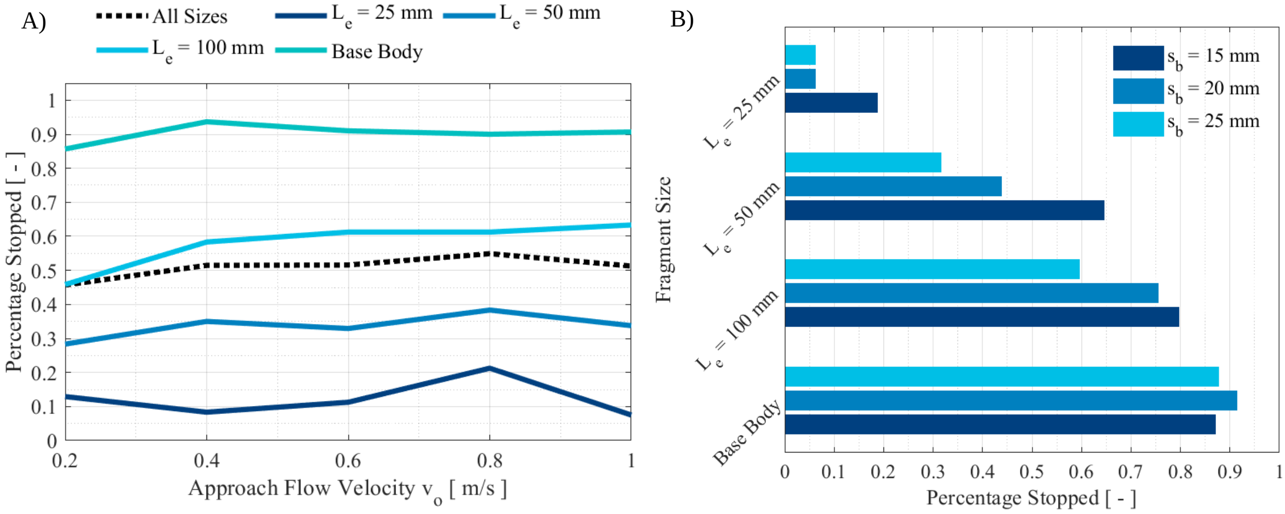


**Fig. 2.** A) Percentage of particles stopped for different approach flow velocities and fragment sizes at a bar spacing of 25 mm B) Percentage of particles stopped for different bar spacing and fragment sizes at an approach flow velocity of 0.4 m/s

## 4. Discussion and Conclusion

The study provides novel findings on the dependencies of transport processes of diverse macroplastics and their interaction with a bar rake system. The results indicate large differences in polymer type and fragment size, confirming the approach of this study that unification approaches or downscaling of macroplastic particles are not possible without losing crucial characteristics of the transport processes.

**Acknowledgements**

The Federal Ministry for Economic Affairs and Energy has supported this study on the basis of a decision by the German Bundestag. We thank the Gesellschaft für Planung, Maschinen- und Mühlenbau Erhard Muhr mbH for the construction of the drum screen unit in the test stand. We would like to thank our colleague Nadja Sappl (TUM) for the support in the technical drawing. We thank the students Moritz Hageneier und Oliver Donsbach for the assistance in the data collection.

**References**

Azevedo-Santos VM, Brito MFG, Manoel PS, Perroca JF, Rodrigues-Filho JL, Paschoal LRP, Gonçalves GRL, Wolf MR, Blettler MCM, Andrade MC, Nobile AB, Lima FP, Ruocco AMC, Silva CV, Perbiche-Neves G, Portinho JL, Giarrizzo T, Arcifa MS, Pelicice FM. 2021. Plastic pollution: A focus on freshwater biodiversity. Ambio:1–12.

Honingh D, van Emmerik T, Uijttewaal W, Kardhana H, Hoes O, van de Giesen N. 2020. Urban River Water Level Increase Through Plastic Waste Accumulation at a Rack Structure. Front. Earth Sci. 8.

Meijer L, van Emmerik T, Ent R. 2021. More than 1000 rivers account for 80% of global riverine plastic emissions into the ocean. Science Advances 7:eaaz5803.

Moore, C.,J., Lattin, G., L., Zellers, A., F. 2011. Quantity and type of plastic debris flowing from two urban rivers to coastal waters and beaches of southern California. Journal of Integrated Coastal Zone Mangement 11(1):65–73.

# Freshwater Macroplastic Transport Based on Global Hydrological Modelling

Alexandra MURRAY[1], Nicola BALBARINI[2], Gregers Helge JØRGENSEN,[3] Kim Wium OLESEN[4]

[1,2,3,4] DHI A/S, Denmark
email: almm@dhigroup.com,
email: niba@dhigroup.com,
email: ghj@dhigroup.com,
email: kwo@dhigroup.com

ABSTRACT

Freshwater is a main transport mechanism for macroplastic and understanding how plastic moves through the global river network is essential to addressing plastic pollution. The UNEP-DHI Centre's macroplastic transport model based on DHI's Global Hydrological Model simulates plastic load in 870,000 points in the world's rivers. The mobilization of plastic is dependent on river discharge and is calculated hourly in real-time and as 9-month forecasts at a daily timestep. Calibration of such global models remains a challenge, especially given the scarcity of waste data. UNEP-DHI's model presents opportunities for linkages with modelling work at different scales to best inform decision-makers working to tackle plastic pollution.

## 1. Introduction

Plastic pollution is a global crisis facing aquatic environments. The resolution adopted by the UN Environment Assembly "End Plastic Pollution: Towards a legally binding instrument" is the starting point for global action to address this threat (UNEA-5, 2022). The treaty produced by the resolution's Intergovernmental Negotiating Committee and National Action Plans produced by individual nations are all founded on plastic data – one must know the problem scope, location, and magnitude and monitor the progress of implemented measures.

Models are essential tools to meet these ends due to the scarcity of plastic waste data. Global, freshwater models are important in the context of national strategic planning and transboundary river cooperation, yet even the most advanced models at this scale produce outputs at yearly or monthly resolution and are based on monthly run-off time series (Meijer et al., 2021). A finer temporal resolution for run-off inputs would allow the connection between water flow and plastic transport to be more explicit, and a finer output resolution would provide decision makers with the most up-to-date information relevant for mitigation activities. The UNEP-DHI Centre has developed a model that addresses these needs and, unlike probability-based models, is easily adaptable as new knowledge about plastic transport dynamics is discovered.

## 2. Model Description and Performance

The UNEP-DHI Centre has developed a global macroplastic transport model that simulates plastic load in over 870,000 points in the global river network. It uses DHI's Global Hydrological Model (GHM) as its underlying engine, which produces daily or hourly run-off time series. The plastic transport model thus produces long-term historical daily time series, real-time hourly time series, short-term (10-day) hourly forecasts, and seasonal (9-month) daily forecasts of plastic load.

DHI's GHM is comprised of distributed rainfall-runoff models in more than 1 million grid cells at 0.1° resolution from 60°S to 60°N. Water is then routed overland and through more than 35 million km of river and approximately 870,000 sub-basins, delineated using the HydroSHEDS data products (Lehner & Grill, 2013). The average basin size is 100-200 km$^2$, and the outlet of each basin is a simulation node. The model uses ERA5 precipitation and IBM meteorological forecasts as inputs, among others (DHI, 2021; Hersbach et al., 2018; IBM, 2018). The model's kinematic router relates the average discharge in the basin to the discharge calculated in the rainfall-runoff models to find the flow velocity based on the Manning formula for open channel flow.

Plastic input is defined by a plastic-escaped-to-the-environment dataset for the world's 85,086 municipalities developed by the University of Leeds and UN Habitat. Of the plastic escaped to the environment, some is modelled to move directly to long-term storage (buried on land), some directly to freshwater aquatic environments, and some transported overland by the calculated run-off. Once in the aquatic environment, some plastic moves to short term storage on the riverbank and some is mobilized by the river. The basic equation governing these transitions from storage to mobilization is:

$$P_{mobile} = SP \times a\left(\frac{Q}{Q_{avg}}\right)^b \quad (1)$$

where $P_{mobile}$ – mobilized plastic [kg $s^{-1}$], $SP$ – plastic storage [kg], $Q$, $Q_{avg}$ – (average) discharge [$m^3$ $s^{-1}$], $a$, $b$ – constants determined during calibration [-]. The internal timestep of DHI's GHM's router is 10 minutes, thus the relationship between $Q$ and $Q_{avg}$ is updated frequently for a simulation spanning days-years. The mass of plastic mobilized by the basin run-off and river discharge are controlled by $a$ and $b$. These were determined during calibration of two rivers, the Seine, France and Ciliwung, Indonesia, based on modelled and field-based calculations for yearly river emissions (Tramoy et al., 2020; van Emmerik et al., 2019). In comparison to hydrological time series, plastic waste time series are short and with coarse resolution; calibration was conducted on yearly emissions from multiple sources. The proportion of plastic that remains on land to the plastic escaped to the environment for the UNEP-DHI and Meijer et al, 2021 models are presented in Fig. 1 for 46 basins of varying size. UNEP-DHI provides a comparatively conservative estimate for smaller basins.

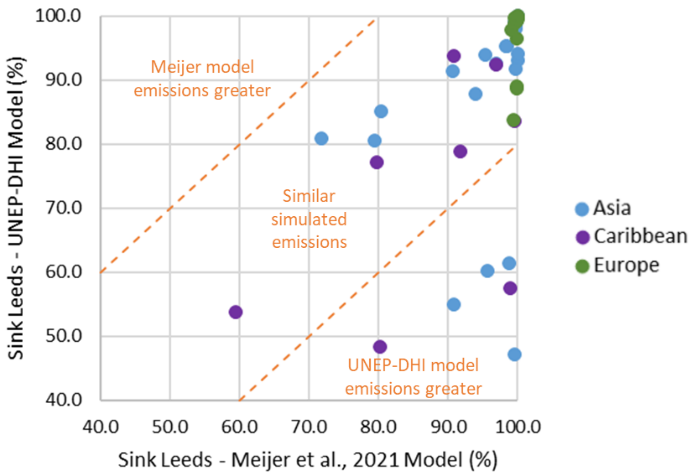


**Fig. 1.** Relative terrestrial sink values for the UNEP-DHI and Meijer et al., 2021 models. Each dot corresponds to a river basin, colours correspond to basin region. Basins in the lower third are those where Meijer et al., 2021 estimates more plastic remains on land than UNEP-DHI (where UNEP-DHI estimates more plastic emitted to the sea). Basins in the middle third are simulated similarly by both models.

## 3. Conclusions and Future Opportunities

The UNEP-DHI Centre's macroplastic transport model describes the movement of plastic once it exits the anthropogenic sphere until it reaches the sea. This movement is described not based on probabilities and monthly run-off time series, but on advanced, operational, hydrological modelling results that support real-time and forecasts plastic load simulation. The model informs the GPML risk and warning system for plastic litter in rivers, available on the GPML Digital Platform (datahub.gpmarinelitter.org), where it informs decision-makers tacking plastic pollution.

As improved monitored datasets and time series of plastic pollution become available, the model can continually be calibrated to best describe plastic freshwater transport. Most critically, the model is easily adaptable as descriptions of plastic dynamics in terrestrial and freshwater aquatic environments are refined and discovered. The work presented here offers opportunities to bridge modelling activities at different scales and foster the current global, political momentum to address pollution.

**References**

DHI A/S (2021) DHI's Global Hydrological Model Documentation
Hersbach H, Bell B, Berrisford P, Biavati G, Horányi A, et al. (2018) ERA5 hourly data on single levels from 1979 to present
IBM (2018) Enhanced Forecast Weather Data, Weather Data Company Packages
Lehner B, Grill G (2013) Global river hydrography and network routing: baseline data and new approaches to study the world's large river systems, Hydrological Processes, 27(15), 2171–2186
Meijer LJJ, van Emmerik T, van der Ent R, Schmidt C, Lebreton L (2021) More than 1000 rivers account for 80% of global riverine plastic emissions in to the ocean, Science Advances, 7, 1-13
Tramoy R, Gasperi J, Colasse L, Tassin B. (2020) Transfer dynamic of macroplastics in estuaries - New insights from the Seine estuary: Part 1. Long term dynamic based on date-prints on stranded debris, Marine Pollution Bulletin, 152
United Nations Environment Assembly of the United Nations Environment Programme, Fifth Session (UNEA-5) (2022) End plastic pollution: Towards an international legally binding instrument, Draft resolution K2200647 L.23 Rev.1
van Emmerik T, Loozen M et al. (2019) Riverine plastic emission from Jakarta into the ocean. Environmental Research Letters, 14

# Estimation of the energy dissipation rate with the Kolmogorov 4/5-law in turbulent flows on gravel beds

Francesco COSCARELLA[1], Nadia PENNA[2], Sergio SERVIDIO[3], Roberto GAUDIO[4]

[1,2,4] Dipartimento di Ingegneria Civile, Università della Calabria, Rende (CS) 87036, Italy
email: francesco.coscarella@unical.it (for author 1)
email: nadia.penna@unical.it (for author 2)
email: gaudio@unical.it (for author 4)

[3] Dipartimento di Fisica, Università della Calabria, Rende (CS) 87036, Italy
email: sergio.servidio@fis.unical.it

ABSTRACT

In this study, turbulent statistics of flow on gravel beds are described by using the laws of turbulence in conjunction with the Double-Averaging Methodology (DAM). For this purpose, an experimental campaign in a laboratory flume was performed. Applying the Taylor frozen-in hypothesis to the Kolmogorov 4/5-law for the spatial increments of the streamwise velocity, it is revealed the existence of the well-known inertial subrange and an accurate Turbulent Kinetic Energy (TKE) dissipation rate $\varepsilon$ assessment is obtained. The present work shows the validity of this statistical methodology (Kolmogorov's 4/5-law) to study the turbulence characteristics at small scales.

## 1. Introduction

The aim of this work is to provide a statistical description of turbulence by applying the laws of turbulence to gravel-bed flows. A similar study on a macro-rough bed (pebbles) was recently carried out by Coscarella et al. (2017) and is now extended to the case of gravel beds. The law of turbulence examined in detail in this study was developed by Kolmogorov (1941) and is well-known as the Kolmogorov 4/5-law:

$$\langle \overline{\Delta u^3} \rangle = -\frac{4}{5}\langle \varepsilon \rangle r, \tag{1}$$

where $\Delta u$ is the streamwise velocity increment at the longitudinal spatial distance $r$. The angle brackets indicate the spatially averaged value of a quantity, whereas the overbar is the time-averaged value. In general, the velocity increment of the three-dimensional velocity vector $\Delta\mathbf{u}$ along the three-dimensional increment vector $\mathbf{r}$ is defined as

$$\Delta\mathbf{u} = [\mathbf{u}(\mathbf{x}+\mathbf{r}) - \mathbf{u}(\mathbf{x})] \cdot \frac{\mathbf{r}}{|\mathbf{r}|}, \tag{2}$$

where $\mathbf{u}$ is the three-dimensional velocity vector and $\mathbf{x}$ is the point of location. The Kolmogorov 4/5-law is strictly valid within the inertial subrange for large Reynolds numbers or when the homogeneous and isotropic conditions are satisfied (Qian, 1997). Furthermore, it represents a direct measurement of the TKE dissipation rate.

## 2. Experimental setup

The laboratory experiments were carried out at the *Laboratorio* "*Grandi Modelli Idraulici*", *Università della Calabria*, Italy, in a recirculating 9.6 m-long tilting flume with a rectangular cross section of width 0.485 m and height 0.5 m. The test section was located at 6.48 m downstream of the flume inlet. Two experimental runs were performed with uniform bed sediments [i.e., with geometric standard deviation of the grain size distribution $\sigma_g = (d_{84}/d_{16})^{0.5} < 1.5$, where $d_{16}$ and $d_{84}$ are the sediment sizes for which 16% and 84% by weight of sediment is finer, respectively]. The bed was prepared by using medium sized gravel with $d_{50}$ =10.54 mm (Run 1) and very fine gravel $d_{50}$ =3.25 mm (Run 2). The longitudinal slope of the flume bottom, $S_0$, was fixed at 1‰ by maneuvering a hydraulic jack. To damp the disturbance of the pump on the turbulence characteristics of the flow, a honeycomb was mounted at the flume inlet. The flow discharge, $Q$ = 19.60 l/s, was measured by a V-notch weir installed in a downstream tank, located upstream of the restitution channel. At the outlet, a tailgate was installed to regulate the water depth, $h$ = 0.13 m, at the test section within the flume. An Acoustic

Doppler Velocimeter (ADV) [Nortek Vectrino] with a four-beam down-looking probe was used to capture the three instantaneous velocity components (streamwise, $u$, spanwise, $v$, and vertical, $w$). The ADV transmitting length was 0.3 mm and the sampling volume was a cylinder with a base diameter of 6 mm and height of 1 mm. The sampling frequency was set to 100 Hz and the duration of a single sampling to 600 s. Three velocity profiles were measured at different abscissae (with streamwise spatial resolution of 2 cm) along the flume centerline, where the side-wall effect was negligible, from 6.48 m to 6.52 m from the inlet.

## 3. Results and discussion

In order to identify whether homogeneity in the inertial subrange is developed in the flow in presence of a gravel bed, the third-order statistics were computed. Furthermore, this detailed statistical analysis was used to estimate the TKE dissipation rate, applying the Kolmogorov 4/5-law for the structure function of the streamwise velocity. The Kolmogorov 4/5-law is considered to be valid for three-dimensional homogeneous, isotropic turbulence at large Reynolds numbers (Kolmogorov, 1941). Nevertheless, according to Iyer et al. (2017), the homogeneity of turbulence is a property of the flow only at a length scale smaller than the inertial length scale of the energy spectrum. Thus, to validate this condition, 2D class frequency histograms for the third-order time-averaged velocity structure function $\overline{\Delta u^3}$ at different vertical distances were computed [specifically at $z = 0.1h$ (inner layer) and $z = 0.5h$ (outer layer) for all runs]. The 2D histograms as a function of the space increment $r$ are shown in Fig. 1, calculated using the Taylor frozen-in hypothesis. Figure 1 shows that the Kolmogorov 4/5-law occurs at a small $r$. In particular, at small scales, $\overline{\Delta u^3}$ increases linearly as $r$ increases, and then, at larger scales, it has a dispersive pattern. Considering that the black solid line in each subplot of Fig. 1 has a slope equal to $4\langle\varepsilon\rangle/5$, it is clearly evident that the homogeneity of turbulence occurs at low vertical distances and at high frequencies in a narrow band. This means that the gravel bed does not much affect the spatial variability of $\overline{\Delta u^3}$ at a given vertical distance for a low $r$, and therefore, the $\overline{\Delta u^3}$ values are considered to be close to their double-averaged value $\langle\overline{\Delta u^3}\rangle$. At the same time, it implies that the statistical homogeneity is preserved in the inertial subrange. As regards the larger scales, $\overline{\Delta u^3}$ shows low frequencies over a wide distribution, implying that out of the inertial subrange the homogeneity is no longer maintained. In addition, examining the Kolmogorov 4/5-law, another important feature can be highlighted: the TKE dissipation rates (i.e., the black solid lines slope multiplied by 5/4) have the highest values in the vicinity of the bed (Fig. 1a,c) and decrease as one moves toward the free surface (Fig. 1b,d). Moreover, the effect of bed roughness is clearly recognizable: in fact, at a fixed elevation, $\langle\varepsilon\rangle$ increases as the bed roughness size increases.

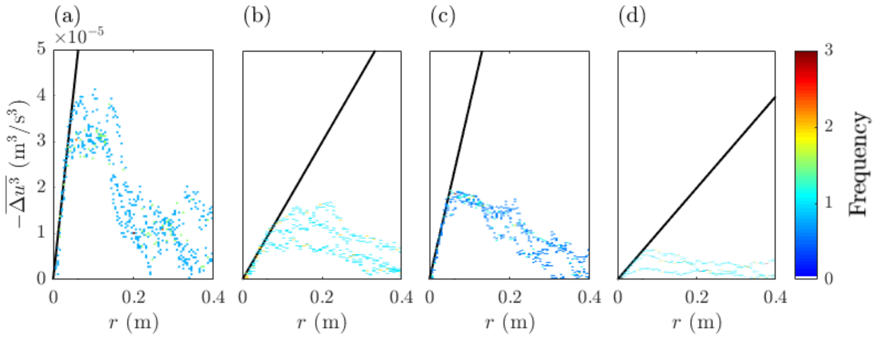


**Fig. 1.** Frequency histogram of $-\overline{\Delta u^3}$ at (a) Run 1 and $z = 0.1h$, (b) Run 1 and $z = 0.5h$, (c) Run 2 and $z = 0.1h$, and (d) Run 2 and $z = 0.5h$. The solid black line in each panel represents the Kolmogorov's 4/5-law.

In Conclusion, our analysis reveals that, at small scales, the distributions of the third-order moments become very narrow, indicating a universal behavior of turbulence and the possibility of estimating the TKE dissipation rate.

**Acknowledgements**

The authors acknowledge the financial support provided by the "*SILA*" PONa3_00341 project, "An Integrated System of Laboratories for the Environment" and "*PAC Calabria 2014-2020 - Asse Prioritario 12, Azione B) 10.5.12*".

**References**

Coscarella F, Servidio S, Ferraro D, Carbone V, Gaudio R (2017) Turbulent energy dissipation rate in a tilting flume with a highly rough bed, Physics of Fluids, 29(8), 085101
Kolmogorov AN (1941) Dissipation of energy in the locally isotropic turbulence, Dokl. Akad. Nauk, SSSR, 32(1), 16–18pp.
Iyer KP, Sreenivasan KR, Yeung PK (2017) Reynolds number scaling of velocity increments in isotropic turbulence, Physical Review E, 95(2), 021101
Qian J (1997) Inertial range and the finite Reynolds number effect of turbulence, Physical Review E, 55(1), 337–342

# Fitting tidal models to cross-sectional ADCP data in estuarine environments

Hendrik JONGBLOED[1], Bart VERMEULEN[1], Antonius J.F. HOITINK[1]

[1] Hydrology and Quantitative Water Management, Wageningen University and Research, The Netherlands
email: henk.jongbloed@wur.nl

ABSTRACT

## 1. Introduction

Flow velocities in river, channel or estuarine environments are often estimated using moving-boat Acoustic Doppler Current Profiler sensors. Usually, obtained raw data are projected and processed on a pre-defined computational mesh. For every ADCP velocity profile, the measured flow velocity is solved from the radial beam velocities to directly obtain Cartesian velocity vector data. This approach suffers from spatial homogeneity assumptions: To estimate flow velocities, the acoustic beams from the transducer diverge. Hence, the larger the distance from the instrument, the larger the assumption of spatial flow homogeneity becomes. For ship-mounted ADCP measurements, the resulting performance is worst near the bed, where the velocity gradients are largest and the spatial homogeneity assumption is least justifiable. An improved method of mesh-based velocity estimation was presented recently (Vermeulen et al., 2014). Rather than solving for flow velocities for each ADCP profile measurement and thereafter projecting them on the computational mesh, flow velocities are solved per mesh cell by collecting all radial velocity measurements in that cell. Thereafter, the flow velocity is solved for per computational cell, based on all radial velocity measurements within that cell performed at different times. This approach however requires assumptions on temporal homogeneity: temporal variations should be small compared to spatial variations (Moradi et al., 2019). Thus, there is a trade-off between assumptions on spatial and temporal homogeneity. The temporal homogeneity assumption holds for inland riverine systems, were temporal variations are typically small. For tidal systems however, temporal variations play a more prominent role. Therefore, the novel method cannot directly be applied to ADCP processing in tidal systems.

In the present work, we present a fitting procedure that to a large degree circumvents both the spatial and temporal homogeneity assumptions in tidal environments. It extends the novel method (Vermeulen et al. 2014) to reduce the dependence on the spatial homogeneity assumption, and uses available information on tidal motion to reduce the problem of temporal homogeneity.

## 2. Method

Following Vermeulen et al. (2014), we relate the Cartesian flow velocity $\boldsymbol{u}$ within a specific computational sigma-layered cell $j$ at time $t_i$ to the measured radial velocities $\boldsymbol{b}$ by a transformation matrix R:

$$\boldsymbol{b}_j^i = \mathrm{R}_j^i \boldsymbol{u}_j(t_i) + \boldsymbol{\varepsilon}_j^i.$$

Herein, the vector $b_j^i$ contains all radial velocity measurements in cell $j$ at a time $t_i$, the matrix $\mathrm{R}_j^i$ transforms from Cartesian coordinates to ADCP beam coordinates and $u_j(t_i)$ is the Cartesian flow velocity. In practice, radial velocity measurements will be affected by measurement noise and uncertainties, parametrized by the random vector $\varepsilon_j^i$. Next, we assume that the flow in cell $j$ and time $t_i$ is homogeneous within the cross-sectional cell (which holds in the small cell limit), and may be written component-wise (with $d = x, y, z$) as a superposition of one subtidal $n_c^d$ and tidal constituents:

$$u_j^d(t_i) = a_{0,j}^d + \sum_{c=1}^{n_c^d} (a_{c,j}^d \cos\omega_c^d t_i + b_{c,j}^d \sin\omega_c^d t_i) = \begin{pmatrix} 1 & \cos\omega_1^d t_i & \sin\omega_1^d t_i & \cdots \end{pmatrix} \begin{pmatrix} a_0^d \\ a_1^d \\ b_c^d \\ \vdots \end{pmatrix} = \mathrm{M}_j^{i,d} \boldsymbol{p}_j^d.$$

In the above line, $\mathrm{M}_j^{i,d}$ denotes the model matrix at time $t_i$, cell $j$ and dimension $d$. Substitution yields

$$\boldsymbol{b}_j^i = \mathrm{R}_j^i \mathrm{M}_j^i \boldsymbol{p}_j + \boldsymbol{\varepsilon}_j^i,$$

which gives a direct relation between cell-based radial velocity measurements $\boldsymbol{b}_j^i$ and tidal constituent and phase parameters $\boldsymbol{p}_j$. By solving the above system of equations using regularized linear least squares, we obtain an estimate of the tidal flow parameter per computational cell element.

## 3. Results

The above method has been successfully applied to two 13-hour measurement campaigns in the Rhine-Meuse delta, the Netherlands. We have fitted the two dominant diurnal and quarterdiurnal tidal constituents to the data (Fig. 1). Besides clearly showing subtidal estuarine circulation (upper plot), the fit also shows large vertical phase differences in the quarterdiurnal tide. The tidal parameter estimation algorithm combines well with the method of Vermeulen et al., 2014), and preliminary results also indicate that terms in the momentum balance may be estimated reliably by extending the approach of the current work.

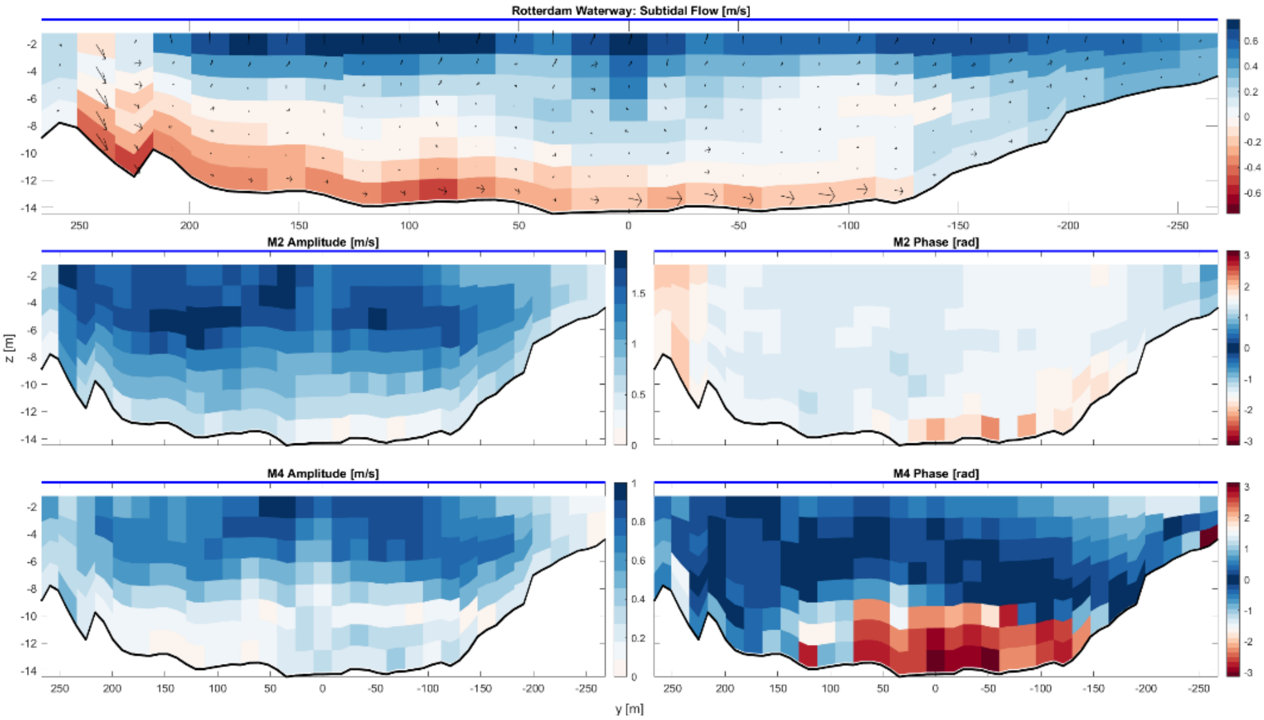


**Fig. 1.** Subtidal flow, M2 and M4 tidal amplitude and phase estimates obtained from a 13-hour measurement campaign in the Rotterdam Waterway, the Netherlands. Note that the M4 constituent shows considerable internal tidal asymmetry.

## 4. Conclusion

The proposed method of estimating tidal parameters without first computing Cartesian flow velocity vectors using regularized linear least squares has been  applied to several field data sets. The present approach avoids stringent assumptions on flow homogeneity in space and time by combining the approach of Vermeulen et al. (2014) with regression with respect to tidal parameters. The method can straightforwardly be extended to estimate spatial gradients, thereby allowing for an efficient and consistent estimating procedure of terms in the momentum balance from raw ADCP data.

**Acknowledgements**

We thank M.C. Verbeek and J.Y. Zomer for their previous work as MSc students contributing to this work. The ADCP Toolbox that was extended in the present work has been introduced in Vermeulen et al. (2014), is open source and can be downloaded from GitHub: https://github.com/bartverm/adcptools.

**References**

Vermeulen B, Sassi MG, Hoitink AJF (2014) Improved flow velocity estimates from moving-boat ADCP measurements, Water Resources Research, 50(5), 4186-4196

Moradi G, Vermeulen B, Rennie CD, Cardot R, Lane SN (2019) Evaluation of aDcp processing options for secondary flow identification at river junctions, Earth Surface Processes and Landforms, 44(14), 2903-2921

# Monitoring Fish Passage Hydrodynamics with Hydroacoustic Measurement Techniques: A Case Study for Çataloluk Small Hydropower Plant in Turkey

Serhat KUCUKALI[1], Ahmet ALP[2], Meliha Gamze EKREN[1]

[1] Hacettepe University, Civil Engineering Department, Turkey
email: kucukali78@gmail.com

[2] K.Maraş Sütçü İmam University, Fisheries Department, Turkey
email: aalp46@gmail.com

ABSTRACT

A pilot study has been carried out at the vertical slot fish passage of Çataloluk Small Hydropower Plant (SHP), which is located in Ceyhan River Basin in Tekir River in Turkey. Accordingly, 3D velocities and turbulence quantities were collected at several points in the pool with Acoustic Doppler Velocimeter (ADV) for various discharges at the Cataloluk fish passage. The pool depth was measured continuously through the year by using Ultrasonic Distance Sensor (UDS). The UDS monitoring data revealed that pool depth is highly variable during operation that can have important implications for fish passage design. The fish movements were recorded continuously in the selected pool with underwater digital video cameras. The prototype measurements showed that by placing brush blocks in the vertical slot pool, the flow energy is effectively dissipated by the vibrations and bending of the bristles leading to an about 17% reduction in the spatially averaged turbulence kinetic energy. The proposed monitoring technique is cost-effective, efficient, and easy to implement in existing pool-type fish passages.

## 1. Introduction

In many existing pool-type fish passes the hydraulic conditions are not favorable for upstream fish migrations due to high turbulence levels and unfavorable flow conditions such as short-circuit currents, wall jets, and unacceptable specific hydraulic power values (Kucukali and Hassinger, 2018). In this context, it is necessary to retrofit existing vertical slot fish passes to allow the passage of such small-bodied and weak swimming capacity fish. In this paper, it has been proposed to place permeable brush blocks in the pools of vertical slots to enhance energy dissipation as an innovative concept.

## 2. Prototype Measurements

The fish passage performance and flow structure of a vertical slot fish pass, with and without brush blocks, were investigated at the Cataloluk Small Hydropower Plant on the Tekir River, located in the Ceyhan River Basin of Turkey. An Acoustic Doppler Velocimeter, ADV (10-MHz Nortek Vectrino) was used to measure the three-dimensional instantaneous velocity fields. The turbulence quantities were collected at 100 Hz frequency during a sampling time of 30 seconds. It would have been better to have a longer sampling duration with ADV; but, in our case, it is risky to sample for a longer duration due to possible variation of headwater level. Hydraulic conditions tend to have repeating patterns. Accordingly, a representative basin is selected for the flow and turbulence measurements. In Figure 4, open circles show the velocity measurement points taken by the acoustic doppler. The position accuracy is approximately 2 mm. The measuring grid was not distributed uniformly over the base area, since it was to be expected that larger velocity gradients occur in the area of the beam and the vicinity of the wall. As shown in Figure 4 a grid with 10 cross sections and 11 longitudinal sections as well as 4 vertical planes were selected. From those measurements, the local power velocity $V_{pm}$ is calculated using Eq. (1)

$$V_{pm} = \sqrt[3]{\frac{\sum |V_i^3|}{n}} \quad \text{in which} \quad V = \sqrt{u^2 + v^2 + w^2} \tag{1}$$

where n is the number of velocity samples. The local power velocity ($V_{pm}$), is thought to be a useful parameter to understand fish migration patterns. Data on instantaneous velocity were filtered with ExploreV software using the Goring and Nikora (2002) phase-space threshold despising method. The signal post-processing included the removal of average signal-to-noise ratio data less than 15 dB and the removal of average correlation values less than 70%. The deleted data was not substituted. The average pool depth (i.e. water level) was continuously monitored throughout the year by using an Ultrasonic Distance Sensor (UDS) which has a sampling rate of 1Hz at the representative pool of the fish passage with Nivus i-series and Nivus GPRS data logger. 30-minutes time-averaged pool depths are recorded.

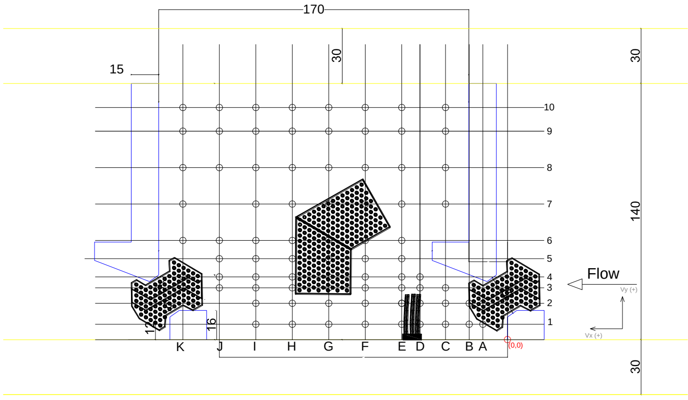

**Fig. 1.** Top view of the vertical slot-brush fishway and the velocity measurement grid (open circles) in a repeating section. Capital letters show the longitudinal measurement sections.

## 3. Results and Discussion

Within the scope of the project, three-dimensional velocity measurements and fish monitoring studies were conducted for different real-time operating conditions (Table 1). After the installation of brush blocks and substrate maximum velocity observed near the bed downstream of the slot was reduced by 50%, (ii) spatially averaged power velocity is reduced by 20%, (iii) turbulent jet region reduced and recirculation regions disappeared (Fig. 1).

**Table 1.** The flow conditions in the pool that ADV measurements were taken

| | | | | |
|---|---|---|---|---|
| $d_p$ (m) | 0.59 | 0.73 | 0.97 | 1.19 |
| Q ($m^3 s^{-1}$) | 0.145 | 0.183 | 0.261 | 0.329 |
| Rej | 6.6E+05 | 8.3E+05 | 1.2E+06 | 1.5E+06 |
| $Fr_j$ | 0.46 | 0.43 | 0.40 | 0.37 |

Notes: $d_p$=average pool depth, Q=discharge, $Re_j$= Jet Reynolds number, $Fr_j$= Jet Froude number

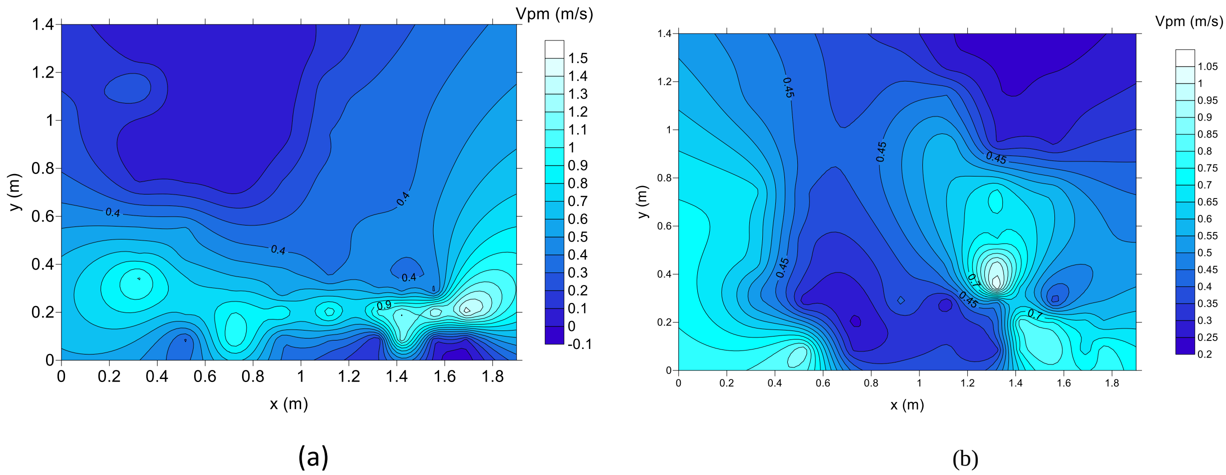


**Fig. 1**. Power velocity distribution in the Cataloluk vertical slot fish pass pool, Q=0.145 $m^3 s^{-1}$, z=0.18 m. (a) Existing structure, (b) after the installation of brush blocks and substrate . Dimensions are in cm. x = (x, y, z) – position vector [m], x – longitudinal coordinate [m], y – transversal coordinate [m], z – vertical coordinate [m]

**Acknowledgments**

This work is supported by the Scientific and Technical Research Council of Turkey under the Scientific and Technological Research Projects Funding Program (1001 TUBITAK) grant with agreement number 117M151.

**References**

Goring, D.G., & Nikora, V.I. (2002). Despiking acoustic Doppler velocimeter data. ASCE Journal of Hydraulic Engineering, 128, 117-126.

# Flow field investigation by means of ADCP for the evaluation of hydropower propellers installed at open channel

Massimo GUERRERO[1], Irene CAVALIERI[2], Slaven CONEVSKI[3], Nils RUTHER[4], Leonardo SCHIPPA[5]

[1] University of Bologna, Italy
email: massimo.guerrero@unibo.it

[2,5] University of Ferrara, Italy
email: schlrd@unife.it
email: irene.cavalieri@unife.it

[3,4] Norwegian University of Science and Technology, Trondheim, Norway
email: slaven.conevski@ntnu.no
email: nils.ruther@ntnu.no

ABSTRACT

The acoustic Doppler current profiler was applied in the Biffis channel that is a regulated concrete irrigation channel in the Adige River plain (Italy). This campaign aimed at evaluating the effects on the hydrodynamic field induced by propellers prototype installed for the hydropower exploitation. The reconstructed velocity maps and the spectral analysis of velocity time series in fixed positions made evident a convective acceleration close to the channel boundaries due to the operating propellers. This gave rise to flow velocities of about 1.6 m/s close to the channel concrete bed. Furthermore, within the wake of installed prototypes, velocity oscillations were observed within the entire investigated frequency range of 0.1-0.3 Hz.

## 1. Introduction

The Biffis open channel continuously diverts 130-135 $m^3/s$ from the Adige River (Fig. 1). In this study, the 1.2 MHz acoustic Doppler current profiler (ADCP) Rio Grande by Teledyne-RDI, mounted on a trimaran, was used to investigate the performance of two arrays of four propellers prototype (Fig. 1) installed at Biffis channel for hydropower exploitation and their possible impacts on channel flow. The investigation of river channel velocity field by means of the ADCP is a well consolidated practice (Guerrero and Lamberti, 2011, Parsapour-Moghaddam and Rennie, 2018).


**Fig. 1.** The Biffis open channel draining water from the Adige River close to Trento, Italy, on the left and the investigated cross-section with the installed array of four prototype propellers out of water (non-productive phase) on the right.

## 2. Methods

The Rio Grande ADCP combines four mono-static piezoelectric transducers, which project and receive coherent pulses along acoustic beams towards the channel bed. The ADCP compass was preliminarily calibrated to reach a 2 degree total error. The DSM232 GPS receiver by Trimble was integrated in the ADCP acquisition software (i.e., WinRiver II by Teledyne RDI) and the NMEA string received in real time, was used to locate the measurement sections. The profile resolution was fixed to 0.25 m whereas profiling time interval was close to 1 s.

### 2.1. *The ADCP campaign*

Two cross sections, equipped with four-propellers array were investigated during two days (i.e., June 17th and 18th, 2021). The flow discharged was measured within 130-135 $m^3/s$ which reflected a small change in the diverted flow during the two days campaign. These sections are trapezoidal and triangular. The former is about 25-m wide and 6.1m deep whereas the triangular one has 22-m and 7.2-m width and height, respectively.

Moving and fixed deployment were conducted for a total of 24 measurements few meters upstream and downstream of the arrays. These measurements differently combined the operational and non-operational phases of the arrays. The moving measurement were aimed at mapping the time averaged velocity field and entailed from 4 to 10 repeated transects, depending on the inspection of profiling quality in the field. Each repetition took 2-3 minutes. The ADCP towing velocity was manually kept as low as possible as it is suggested by the operation manual. In any case it was close to 0.1 m/s which is one order of magnitude lower than the expected flow velocity and entailed negligible bias on velocity profiling (Huang, 2017). Continuous time series of velocity profiles with a duration of 20-30 minutes were aimed at characterizing time oscillations and were measured at fixed positions aligned with selected propellers. No moving condition of the channel concrete bed was preliminarily verified, and consequently the bottom track reference was explicitly used for water velocity assessment.

### 2.2. *Data analysis*

Spatial patterns and oscillation periods were investigated from mapped velocity field and measured time series, respectively. Aiming at a mapping of steady spatial patterns, the velocity magnitude from repeated transects were binned within a 0.5 x 0.25 $m^2$ regular grid and grouped values in the same grid cell were statistically characterized. The power spectral density was assessed for the time series of velocity magnitude at each fixed position and profile bin. The frequency and water depth corresponding to the maximal power were identified for each position.

## 3. Results

Preliminary results revealed a relevant flow spatial-acceleration towards channel boundaries downstream of propellers that is the effect of flow deviation operated by the prototypes while spinning into water during operational phase for hydropower exploitation (Fig. 2). The maximal velocity magnitude reached 1.6 m/s while approaching the channel bed that is larger than the observed maximum value equal to 1.5 m/s for the condition without the propellers spinning into water.

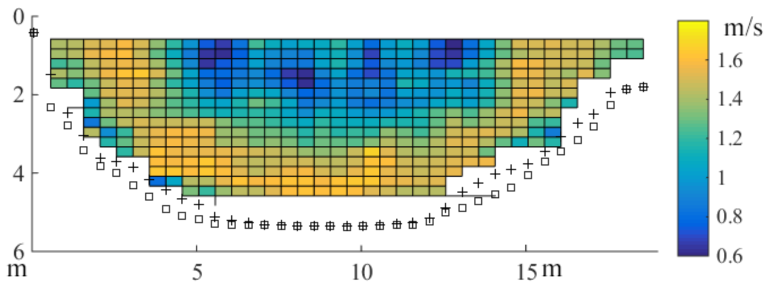


**Fig. 1.** Binned and averaged velocities within 0.5 x 0.25 $m^2$ regular grid; velocity data are from moving ADCP repeated transect downstream of propellers array during operational phase for hydropower exploitation. Channel profile (black marks) is from ADCP signal devoted to locate the bottom; square and plus marks reflect maximal observed deviations in repeated transects.

Maximal spectral powers were observed at frequencies close to 0.06 Hz and 0.1-0.3 Hz. Undisturbed conditions (i.e., apart from the wake produced by spinning propellers into water) where characterized by lower spectral powers and mostly appearing at the highest frequency of 0.3 Hz.

Overall, this preliminary analysis indicates a relevant deformation of the velocity mean field nearby channel margins due to operating propellers. This may result in additional forces at protected banks and propellers reduced performance because of flow bypassing towards margins.

**References**

Guerrero M, Lamberti A (2011) Flow field and morphology mapping using ADCP and multibeam techniques: Survey in the po river, Journal of Hydraulic Engineering, 137 (12), 1576-1587
Huang H (2017) A modified Simpson model for estimating random uncertainty of moving-boat ADCP streamflow measurements, Flow Measurement and Instrumentation, 61, 84-93
Parsapour-Moghaddam P, Rennie CD (2018) Calibration of a 3D hydrodynamic meandering river model using fully spatially distributed 3D ADCP velocity data, Journal of Hydraulic Engineering, 144 (4), 04018010

# A new hyperband acoustic profiler – Suspended particulate matter monitoring in the river in France, example on the Rhône and Isère river

Stéphane FISCHER[1], Gilles PIERREFEU[2], Marie BURCKBUCHLER[1], Thierry FRETAUD[2]

[1]UBERTONE, France
email: info@ubertone.fr

[2] Compagnie Nationale du Rhône, France
email: g.pierrefeu@cnr.tm.fr

ABSTRACT

Suspended Particulate Matter (SPM) measurements are a very important challenge of operational flow monitoring. The ANR project MESURE led to the development of a compact dual-frequency ABS prototype tested on a river. Following this research project, a compact commercial version was developed by Ubertone, composed of a hyperband acoustic module, and of a battery-wifi-logger module. In this paper, we present the deployment of this UB-SediFlow during sediment managing operations. The UB-Sediflow was installed on a floating board. In parallel, another team collected SPM reference samples to qualify UB-SediFlow. Post-processing analysis over a large frequency range gave quality data and this campaign showed an easy deployable instrument allowing real time data visualization.

## 1. Introduction

The ANR project MESURE (ANR-16-ASMA-0005, 2017-2020) proposed to advance further regarding the SPM metrology (sediment concentration, size and flux) using multifrequency hydro-acoustic observations. A dual-frequency ABS (Acoustic Backscattering System) prototype was first developed by Ubertone and tested in laboratory and field campaigns. This prototype was then upgraded to allow a larger range of emission frequencies. In this paper, we present field campaign results of the hyperband ABS UB-SediFlow.

## 2. Method

### *2.1. Hyperband ABS*

The UB-SediFlow is a multi-frequency acoustic profiler (Fig. 1), which measures backscattered echo profiles along 4 acoustic beams. The system is composed of two hardware modules linked by a cable. The waterproof acoustic module (up to 20m) includes 4 wideband transducers (covering the full range 300kHz to 6MHz) and an acoustics electronic board. The splashproof logger (acquisition and communication module) includes a battery (autonomy of 12 hours) and communicates through wifi (signal range between 50 and 100m).

**Fig. 1.** From left to right : the UB-SediFlow on a floating board, the acoustic module and the user interface

The acoustic module UB-Sediflow was installed on a CNR floating board (Fig. 1) which was deployed with a rope from the bridge on the river at a fixed position or moving to get a transect.

### *2.2. Theory*

The acoustic backscattered intensities measured by acoustic profilers can be inverted through different methods to get concentration and grain size information (Hurther, 2011). All the methods derive from the sonar equation (Thorne, 1997), which includes the necessity of a calibration.

*2.3. Field measurements*

During the sediment managing operations APAVER of May 2021 on the Rhône river, France, the UB-SediFlow was set with 6 acoustic configurations: 0.5 ; 1.0 ; 1.5 ; 2.3 ; 4.5 and 5.2 MHz. The inversion of the acoustic data has been compared with pycnometer samples and the CNR's reference measurement over 5 days (May 19 to 21, 25 and 26th, 2021).

## 3. Results and discussion

When analysing the acoustic data, the distinction between fine and coarse particles (<100µm<) is made. The fine sediment concentration estimator was calibrated on May 19th in the morning with a pycnometer near the water surface at the very beginning of the campaign. The coarse sediment concentration estimator is calibrated near the water surface on the 20th, during a peak of concentration.

The acoustic measurement of the concentration of fine sediments has an uncertainty close to the 20% of the reference pycnometer. Figure 2 shows concentration evolutions on May 20th according to different measurement methods, including the reference value computed by the CNR from several methods.

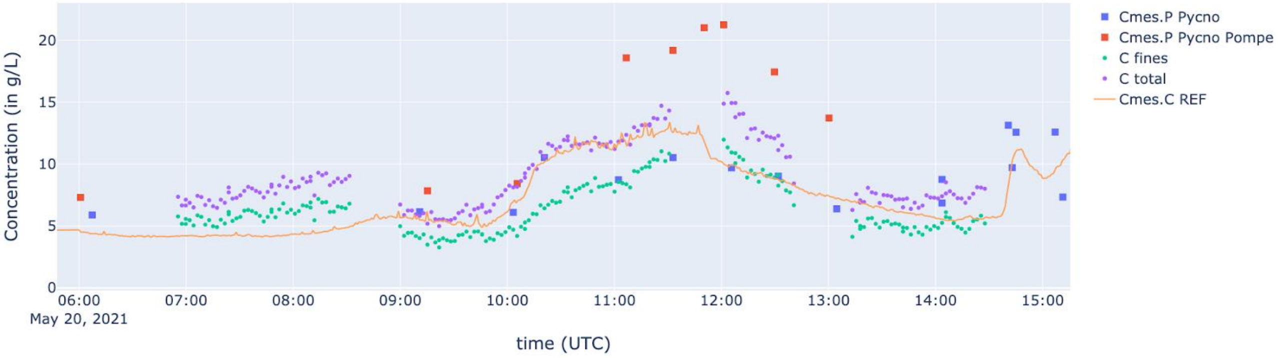


**Fig. 2.** Concentration measurements, in the first meter under the surface, by UB-SediFlow (dots) and pycnometer (squares) compared to reference value (line), on May 20th.

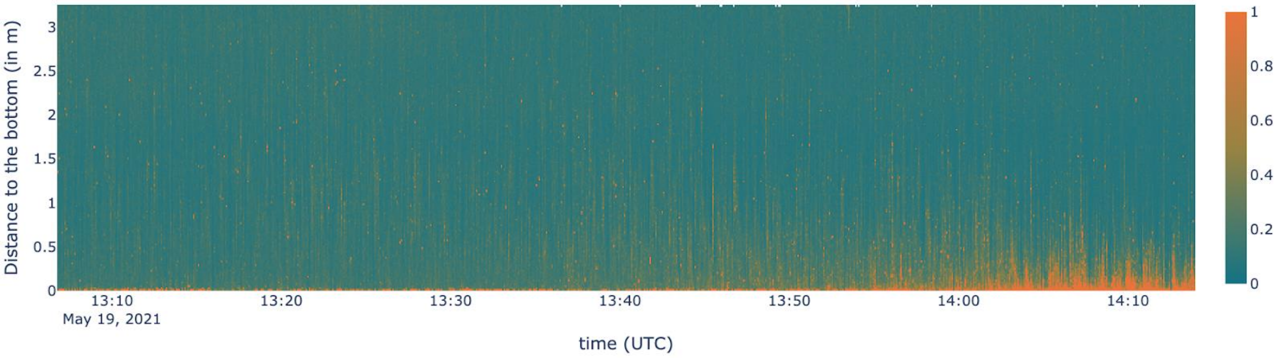


**Fig. 3.** Coarse particles concentration profiles (in g/L) measured by acoustic method, on May 19th in the afternoon.

Coarse particle (>100microns) concentration measurements over the whole vertical allow a quantification of the concentration along the depth (see Fig. 3 on May 19th afternoon). This measurement could be improved with two points of calibration at the surface and near the bottom.

## 4. Conclusion

The UB-SediFlow gave quality data over a large frequency range and showed an easy deployable instrument allowing real time data visualization. The first result led the CNR team to improve the knowledge of sand flux spatially and temporally. The advantage of this sensor is the optimization of the number of samples on site to estimate SPM flux. A laboratory calibration campaign on the DEXMES facility is planned to confirm consistency of the field in-situ calibration. The next step will be to qualify this instrument with more SPM reference values.

**References**

Thorne PD & Hardcastle PJ (1997) Acoustic measurements of suspended sediments in turbulent currents and comparison with in-situ samples, Journal of the Acoustical Society of America, vol. 101, p. 2603–2614.

Hurther, D., Thorne, P. D., Bricault, M., Lemmin, U. & Barnoud, J.-M. (2011). A multifrequency Acoustic Concentration and Velocity Profiler (ACVP) for boundary layer measurements of fine-scale flow and sediment transport processes, Coastal Engineering, vol. 58, p. 594–605

# Measuring near-bed flow field in shallow quasi-uniform flow conditions with the use of an Ultrasonic Velocity Profiler

Arianna VARRANI[1], Łukasz PRZYBOROWSKI[1], Magdalena MROKOWSKA[1], Paweł ROWIŃSKI[1], Massimo GUERRERO[5]

[1] Institute of Geophysics Polish Academy of Sciences, Poland
email: avarrani@igf.edu.pl
email: lprzyborowski@igf.edu.pl
email: m.mrokowska@igf.edu.pl
email: pawelr@igf.edu.pl
[2] University of Bologna, Italy
email: massimo.guerrero@unibo.it

ABSTRACT

Experiments of incipient motion conditions were carried out in a flume bedded with plastic particles with average diameter of 3mm. Such particles can be referred to as microplastics, and their mobility is, like that of natural, clastic sediments, highly linked to the near-bed flow field. Near-bed velocity measurements were performed with a portable ultrasonic velocity profiler (UVP), the UB-Lab P by Ubertone. Transversal velocity profiles were taken at 4-5 increasing distances from the bed surface, to (i) derive information on the near-bed flow field and its distribution in the transversal direction and (ii) investigate the deepest half of the flow depth, where log-law velocity distribution was assumed. This study presents the first results concerning near-bed velocity measurements over a bed made of microplastic particles.

## 1. Introduction

The estimation and measurement of flow velocities and their distribution in the presence of relatively shallow flows (depth below 0.1m), with low Reynolds numbers, can be challenging, even in controlled laboratory conditions. In particular, the near-bed flow field, crucial for the estimate of incipient motion, is the focus of this study, which sees the presence of lightweight ellipsoidal grains composing the bed layer. Threshold conditions are typically investigated by the use either of image-based velocimetry or acoustic devices, i.e. Doppler velocimetry. The latter methods use two types of transducers: (i) mono-static, consisting of single emitter/receiver profiling the velocity projection along the beam direction (i.e. ultrasonic velocimeters and profilers, UVP), used in this study, and (ii) multi-static that usually combines receivers and emitter to converge in the measurement volume. Due to the relatively low density of the used bed material, and the shallow depth of the studied flows, it was critical not to perturb the free surface.

## 2. Methods

The UVP UB-Lab P by Ubertone was used with two mono-static transducers (it can accommodate up to 3) and a portable compact control unit (UBERTONE, 2020). The shallow water depth, in the range of 4-6 cm, required external installation on the polycarbonate wall, with ultrasound gel: an ad-hoc designed holder was used to clamp the transducers from outside the flume at a side wall; this ensured both transducers were set at a constant, fixed angle in all tests, and avoided perturbations on the free surface. Velocity vectors were estimated by measuring two components laying on parallel and horizontal planes at 4-5 increasing distances from the bed surface, to eventually reconstruct the velocity profiles along 140-160 verticals. The transducers' frequency was 3.0 MHz, pulse repetition frequency was fixed at 600 and 1200, depending on the hydraulic conditions, which resulted in a sampling rate of 1.6-1.75 Hz.

### *2.1 Experimental setup*

The experiments were conducted in the Hydrodynamic Models Laboratory (HML) at the Institute of Geophysics, Polish Academy of Sciences. HML is equipped with a 0.25m-wide, 0.3m-deep and 5.2m-long flume, with water recirculation. The tests were carried out with two types of granular beds, composed respectively of PA6 (polyamide 6, density, $\rho = 1.1 g/cm^3$) and POM (polyoxymethylene, $\rho = 1.4 g/cm^3$) grains with 3mm average diameter. Incipient motion conditions were firstly assessed visually and the tested discharges (measured with a flowmeter at the inlet pipe) were in the range $1.9\text{-}2.1 \cdot 10^{-3}\ m^3/s$ for PA6 and 2.3-

2.5·$10^{-3}$ $m^3$/s for POM bed tests. The mean water depth was around 6cm and 4.5cm for PA6 and POM bed respectively, and it was not constant along the flume with an average increase of around 2-3 mm along a 1.5m-long stretch. The bed slope was <0.0001. The bed layer was levelled manually, and the transducers' positioning was manually adjusted, starting from 0.5cm up to 3.5cm and 2cm respectively for the PA6- and POM-bed tests. The transversal profiles of velocity were measured at fixed distances from the bed surface, i.e., at 0.05, 0.08, 0.1, 0.2 and 0.35 m above the bed.

## 3. Results

The measured streamwise velocity in horizontal profiles at different depths was analysed and the resulting time-averaged flow field for a sample test is reported in Figure 1a). The blind region close to the left wall (starting from 0 up to 5cm) is dictated by the type of transducer used, while the quasi-symmetrical lack of values close to the right wall is due to reflection (giving low SNR). Figure 1b) shows, as from Nezu & Rodi (1986), the normalised velocities U+ versus the normalised depth Z+ at which they were measured. U+ and Z+ are calculated as $U+\frac{U}{U_*}$ and $Z+\frac{z}{\nu/U_*}$, where $U$ is the cross-sectional time-averaged velocity, $z$ is the vertical coordinate, ν is the kinematic viscosity of water, and $U_*$ is the shear velocity resulting from the slope parameter derived from the log-fitting of the measured velocities (4 or 5 points depending on the type of bed).

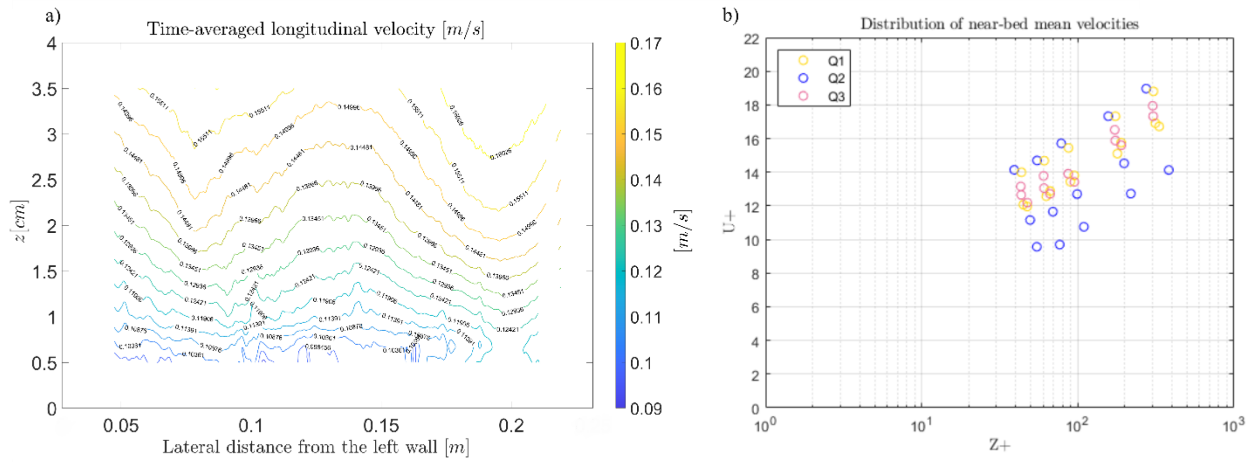


**Fig. 1.** a) Sample streamwise flow velocity isolines at 2.5m from the flume inlet. b) distribution of measured near-bed velocities U+ versus normalised depth Z+ (logarithmic scale is applied to the x-axis) for a sample section for discharges Q1, Q2, Q3.

## 4. Discussion and conclusions

The present application shows that, for shallow depths, the lateral configuration offers the advantage of not disturbing the bed while measuring at less than two times the bed particle's diameter $d_p$. By repeating measurements of transversal profiles over the same vertical plane, by accurately positioning the transducers at progressive distances from the bed, one can obtain enough data to fit the law of the wall (log distribution). Observed patterns in Figure 1a) reflect non-perfect uniform flow conditions, which will be accounted for in future analyses. Our incipient motion experiments on a bed of microplastics saw *Re* ranging in the order of 5-9·$10^3$, which is lower than in the study by Nezu & Rodi (1986), for a smooth immobile bed. The results in Figure 1b) show that the range of both U+ and Z+ in the measured zone (i.e. the lower half of the flow up to ~2$d_p$) is comparable to that expected for a logarithmic profile (i.e. Z+ > 30). This information will be coupled at a second stage with bed particles' movements retrieved from video recordings, to define baseline conditions for the incipient motion of the PA6 and POM particles.

**Acknowledgements**

The work of AV was funded by NCN National Science Centre, Poland, call PRELUDIUM 19, Grant 020/37/N/ST10/01828. The work of AV, ŁP, MM and PR was supported by a subsidy from the Polish Ministry of Education and Science. AV and ŁP were funded by an internal grant for young scientists at IG-PAS, number 500-10-51. AV was also supported by UBERTONE's UVP Innovation Springboard for the use of UB-Lab P. We would like to thank the UBERTONE team for the rental of a UB-Lab P and their technical support.

**References**

Nezu I. and Rodi W. (1986). Open-channel flow measurements with a laser Doppler anemometer. Journal of hydraulic engineering, 112(5), 335-355.
UBERTONE (2020) UB-Lab P Acoustic Profiler User Manual, rev2

# Velocity Distribution Above Different Types of Simulated Vegetation

Aristotelis MAVROMMATIS[1], George CHRISTODOULOU[2]

[1,2] Applied Hydraulics Laboratory, School of Civil Engineering,
National Technical University of Athens, 5 Heroon Polytechniou, Zografou 15780, Greece
email: arismaur@central.ntua.gr
email: christod@hydro.civil.ntua.gr

ABSTRACT

Velocity profiles were obtained experimentally for three types of simulated vegetation elements arranged at a sparse parallel pattern. Above the top of the canopy the data are found to follow closely a logarithmic law, the constants of which depend on the type of element and the proximity to the elements alignment.

## 1. Introduction

In recent years river management and design has shifted to a more ecological approach aiming to protect and restore vegetation, acknowledging its benefits to the natural habitat. Therefore, much research has focused on the interaction between vegetation and water flow. Several studies have concluded that the vertical profile of velocity has a characteristic S-shape and the distribution above the vegetation canopy follows a logarithmic law. Analytical expressions of these distributions have been proposed, among others, by Carollo et al. (2002), Stephan and Gutknecht (2002) and Li et al. (2014). Most of these formulas refer to dense or meadow-like vegetation canopies. Nepf (2012) noticed the difference between sparse and dense canopies and reported that in the first case the velocity distribution is nearly logarithmic throughout the water depth. The present paper attempts to explore the dependence of the velocity profiles above a low density canopy on the geometry of vegetation elements.

## 2. Experiments

Experiments were conducted in a laboratory flume 16 m long and 0.50 m wide, as listed in Table 1.Three types of elements were used, mimicking submerged small plants with rigid stems with or without foliage: (a) simple rods, (b) compound elements consisting of plastic spheres fixed on top of rods and (c) compound elements consisting of flexible needles arranged axisymmetrically on top of the same rods. The elements were placed on a false perforated bottom and arranged on a 10x10 cm mesh, therefore at a density of 100 stems/m$^2$.Velocity and turbulence measurements were obtained by means of a 3-D ADV instrument (ADV Lab Ver. 2.7 Probe N0187 Nortec AS) on vertical lines at nine locations within the vegetation array, shown in Fig.1(a). The instrument operates at a frequency of 25 Hz and each measurement lasted 2 min, yielding a total of 3000 values of instantaneous velocities at each measurement point. For comparison purposes, the discharge Q= 41 l/s and the flow depth in the measurement area H = 25 cm were constant throughout the experiments. More details of the experimental setup and procedure and partial qualitative results were presented in previous papers (Mavrommatis and Christodoulou 2019, 2020), whereas the present paper focuses on the quantitative description of velocity profiles above the canopy.

## 3. Results and Discussion

The upper part of the measured velocity profiles at all locations was compared to a logarithmic equation of the following form:

$$u = \frac{u_*}{k}\ln\left(\frac{z}{h}\right) + C \qquad (z>h) \qquad (1)$$

where u=local temporal-mean longitudinal velocity, $u_*$ =local friction velocity at top of the canopy obtained as the RMS value of the cross-product of velocity fluctuations, $u_*^2$= <-u'w'>, z=distance from bed, h= vegetation height, k=0.4 and C=constant. A satisfactory fitting of the experimental data to Eq. (1) was generally observed, as illustrated for Exp2 in Fig. 1(b). However, considerable differences were noted in fitting the data of individual locations. In particular, in each experiment, three distinct groups could be identified depending on the distance from the elements alignment (axis), i.e. (i) locations A, B, C (on axis), (ii) locations D, E, F

(2.5 cm off-axis), (iii) locations G, H, I (5 cm off-axis, half-distance between adjacent elements lines). The derived values of $u_*$ and C are listed in Table 1. It is seen that generally $u_*$ is much higher for the compound elements compared to the simple ones and decreases in all cases with distance from the axis. The C values are lower for the compound elements and generally increase with distance from the axis. The smallest differences between the three groups are observed for the semi-flexible compound elements, suggesting a relatively more homogeneous flow field above the canopy.

**Table 1.** Experimental characteristics and results

| Exp. | Vegetation type | $u_*$ (cm/s) average | C (cm/s) average | $u_*$ on A-B-C | C on A-B-C | $u_*$ on D-E-F | C on D-E-F | $u_*$ on G-H-I | C on G-H-I |
|---|---|---|---|---|---|---|---|---|---|
| Exp1 | simple rigid | 1.700 | 29.523 | 2.331 | 25.659 | 1.400 | 30.995 | 1.353 | 31.996 |
| Exp2 | compound semiflexible | 4.763 | 26.591 | 5.163 | 23.256 | 5.069 | 25.274 | 4.314 | 29.032 |
| Exp3 | compound rigid | 4.749 | 23.604 | 6.255 | 19.682 | 4.958 | 22.485 | 4.036 | 26.032 |

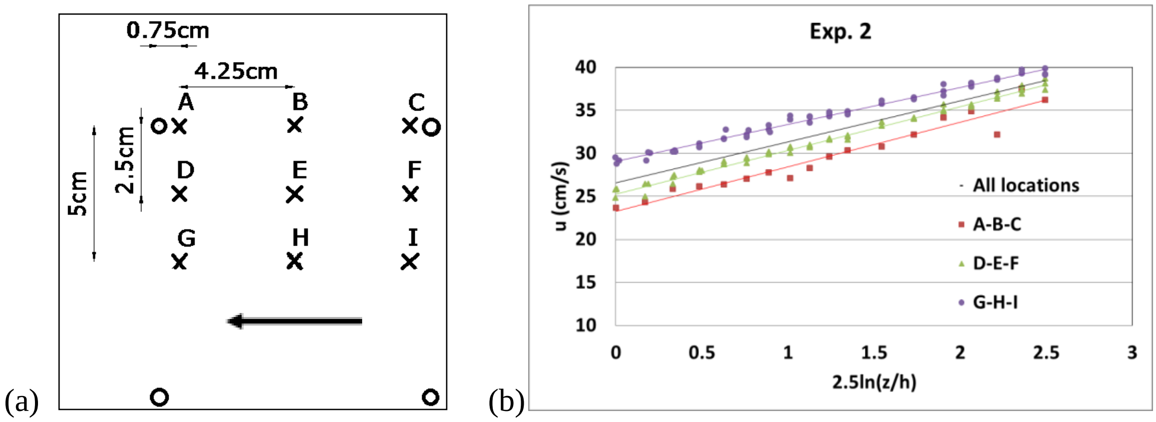


**Fig. 1.** (a) Location of measurements (x) and elements (o) within the vegetation array; arrow denotes the flow direction. (b) Fitting of data of Exp2 to Eq.(1)

## 4. Conclusions

Detailed velocity measurements were obtained above simulated vegetation canopies consisting of three different types of elements arranged on a parallel pattern at a density of 100 stems/$m^2$. Results confirm earlier observations that the velocity distribution closely follows a logarithmic law but reveal significant variations depending on the type of elements and the proximity to the elements alignment. Therefore in sparse canopies, a single mathematical expression for the velocity distribution is not representative. Evaluation of the respective constants of Eq.(1) shows that the flow field tends to be more variable above simple stems without foliage and least variable above compound semi-flexible vegetation.

**References**

Carollo FG, Ferro V and Termini D (2002) Flow velocity measurements in vegetated channels, Journal of Hydraulic Engineering, 128, :664-673
Li Y, Wang Y, Anim DO, Tang C, Du W, Ni L, Yu Z, Acharya K (2014) Flow characteristics in different densities of submerged flexible vegetation from an open-channel flume study of artificial plants, Geomorphology, 204, 314–324
Nepf HM (2012) Hydrodynamics of vegetated channels, Journal of Hydraulic Research, 50, 262-279
Stephan U and Gutknecht D (2002) Hydraulic resistance of submerged flexible vegetation, Journal of Hydrology, 269, 27-43
Mavrommatis A, Christodoulou G (2019) Comparative study of flow through vegetation stems with and without foliage. Proceedings of 16th International Conference on Environmental Science and Technology (CEST2019), Rhodes, Greece
Mavrommatis A, Christodoulou G (2020) Experimental study of flow through vegetation stems with foliage. Proceedings of 15th International Conference on Protection and Restoration of the Environment, Patras, Greece

# Dealing with temporal and spatial variations in specific sediment attenuation for ADCP based suspended sediment estimates

Bart VERMEULEN[1], Toine HEUS[1], Anouk BOON[1], Ton HOITINK[1]

[1] Wageningen University, Hydrology and Quantitative Water Management, the Netherlands
email: bart.vermeulen@wur.nl
email: ton.hotink@wur.nl

ABSTRACT

Estimating sediment concentration from Acoustic Doppler Current Profilers (ADCPs) is often challenging due to the combined effect of backscatter and attenuation caused by sediments. This combined effect can make the relation between backscatter and sediment concentration ambiguous. In this study, an existing method is used to estimate sediment concentrations that assumes the specific attenuation (i.e. per unit of concentration) to be constant over depth. The method is applied to measurements collected in the hyperturbid Ems Estuary. A tidally varying specific attenuation is included in the inversion to account for tidal variation in grain size distribution. This variation is confirmed by in-situ measurements of the grain size distribution. The obtained sediment concentration are validated with samples and show an improvement of the method including temporal variation in specific attenuation. Eventually we explore the possibility to use bottom backscatter to estimate attenuation.

## 1. Introduction

Estimating sediment concentration from Acoustic Doppler Current Profilers (ADCPs) is a widely used method that allows to obtain spatial information on the distribution of sediments. Estimating concentrations from backscatter is, however, a non-trivial task, since the strength of the received signal is affected both by the backscatter strength but also by the attenuation. Both depend on the sediment concentration. Sassi et al. (2021) developed a method that allows to explicitly estimate sediment concentrations accounting for sediment attenuation. In this method specific attenuation is considered constant over depth, which roughly boils down to assuming that grain size distribution does not vary over depth. Also, one value is often used for the specific attenuation, which means that no variation in space or time is accounted for.

## 2. Methods

During 2019 several data were collected during the Ems-Dollart field campaign. This study focuses on the Emder Fahrwasser (Fig. 1). During 14 hours a stationary boat collected ADCP data with a 1200 kHz RioGrande. Every 15 min during slack and every 30 min otherwise a frame was lowered equipped with Conductivity Temperature Depth (CTD), a LISST 200x for grain size distribution measurements, an OBS and a pump to collect in situ samples. Water samples were collected 3 meters below the surface and 1.5 meter above the bed. For depths exceeding 8 m a third sample was collected at mid-depth.

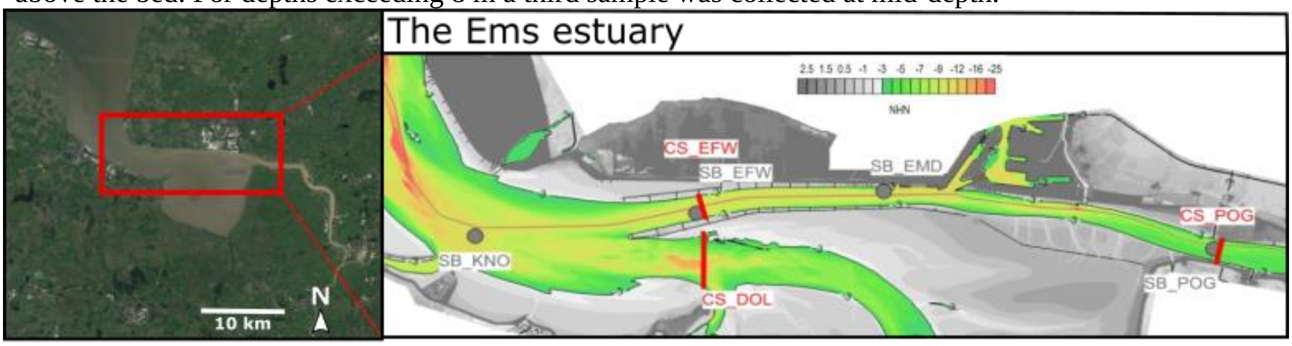


**Fig. 1.** Ems estuary, located at the border between Germany and the Netherlands. This study focuses on the Emder Fahrwasser (CS_EFW and SB_EFW data).

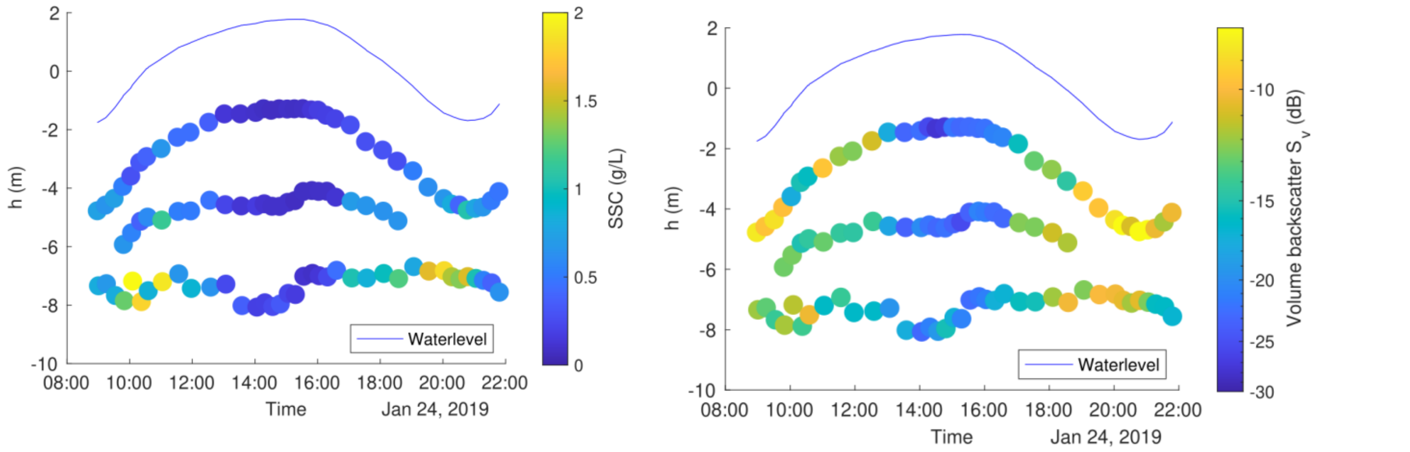


**Fig. 2.** Suspended sediment concentration (left) and Volume backscatter (right) uncorrected for attenuation. Dots indicate the locations where water samples were collected

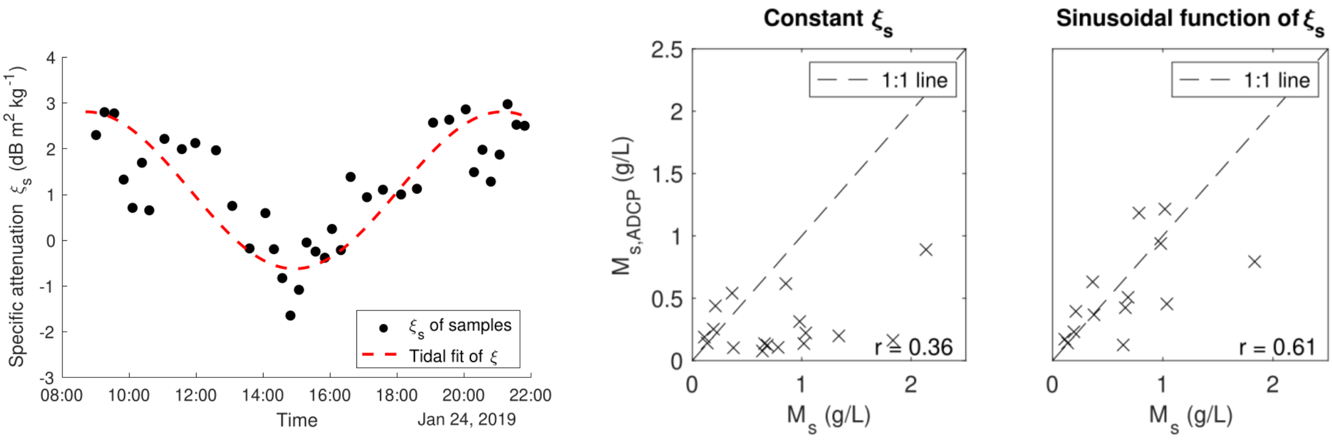


**Fig. 3.** Estimated values for the specific attenuation (left) including a semi-diurnal fit (left panel). Validation of the backscatter inversion assuming a constant specific attenuation (middle panel) and assuming a tidally varying specific attenuation (right panel)

## 3. Results

Comparing the SSC with the backscatter strength, the effect of attenuation can easily be seen with backscatter values being lower than at the surface, while concentration are higher near the bed (Fig. 2, at around 9:00 and 20:00). At around 14:00 the effect of attenuation seems smaller. This effect is confirmed when calibrating specific attenuation from water samples (Fig. 3, left panel). A semi-diurnal variation is observed. Including this time varying specific attenuation improves the validation of the SSC obtained from ADCP data. The negative attenuation observed around 15:00 is compensating for the assumption of constant grain size distribution in depth, which is not the case at that time.

## 4. Discussion and Conclusions

Including temporal variation of specific attenuation improves the quality of the suspended sediment concentrations obtained from ADCP backscatter data. As to the origin of the observed backscatter, based on the grain size distributions ($D_{50}$ ranged between 10 µm and 20 µm) the contribution of viscous attenuation is significant during periods with high attenuation. Including these temporal effects seems a promising method to obtain reliable SSC measurements from ADCPs in hyperturbid areas.

**Acknowledgments**

We thank Rijkswaterstaat and the Bundesanstalt für Wasserbau for collecting and providing the data. We thank Christian Maushake for the provided support in post-processing the data.

**References**

Sassi, M. G., Hoitink, A. J. F., and Vermeulen, B. (2012), Impact of sound attenuation by suspended sediment on ADCP backscatter calibrations, Water Resour. Res., 48, W09520, doi:10.1029/2012WR012008.

# Bedload transport assessment with ADCP in a large gravel bed river

Sándor BARANYA[1], Gergely T. TÖRÖK[1,2]

[1] Department of Structural Engineering, Faculty of Civil Engineering, Budapest University of Technology and Economics, Műegyetem rkp. 3., H-1111 Budapest, Hungary.
email: baranya.sandor@emk.bme.hu

[2] MTA-BME Water Management Research Group, Eötvös Loránd Research Network, Műegyetem rkp. 3., H-1111 Budapest, Hungary
email: torok.gergely@emk.bme.hu

ABSTRACT

Quantification of bedload transport of rivers is of major interest since this mode of sediment transport plays a crucial role in the morphological changes. Direct measurement of bedload transport in large rivers is, however, challenging, sometimes even not feasible. To overcome this issue, surrogate acoustic techniques have been thoroughly tested to quantify bedload transport, but there are still open questions regarding their use in field circumstances, especially in large rivers. In this paper we introduce the results of an intensive bedload measurement campaign, performed in the gravel bed section of the Danube River in Hungary between 2019-2021. A so called BfG type bedload sampler was employed to measure the sediment transport in a direct manner, moreover, parallel with the sampling, acoustic Doppler current profiler (ADCP) was also used from the mounted on the sampling vessel. The bias of the Bottom Tracking signal from the GPS detected real positions was analyzed and compared with the measured bedload transport rates. Furthermore, video camera footages taken from the bedload sampler provided crucial supporting information about the uncertainties of the direct sampling.

## 1. Introduction

The bedload transport in rivers, i.e. the movement of coarse particles at the river bed, plays a crucial role in the morphological changes, thus the quantification of the spatial and temporal variation of this process is of major importance in river engineering. Conventional, i.e. direct physical sampling methods have been used for decades and so their application limits are quite well revealed. It is known that their use in large rivers are very cost and time demanding, moreover, the uncertainty in physical samplings can be significant. Furthermore, applying bedload samplers in flood situations can be unsafe and due to the severe flow conditions it might even be unfeasible. Complementary indirect methods are therefore under development which are using acoustic and imagery methods to quantify the bedload transport. For instance, Ramooz and Rennie (2010) tested the Bottom Tracking signal of an ADCP in laboratory circumstances to measure the so called virtual bedload velocity. They introduced strong relationship between the collected bedload and the measured virtual bedload velocity. Latosinski et al. (2017) assessed the ADCP data to estimate bedload transport rate in the Parana River and compared the results with empirical formula. Conevski et al. (2020) tested the influence of different instrument frequencies for the estimation of bedload transport in the sand bed Elbe and Oder rivers in Germany. They compared the results with physical samplings and found acceptable agreement between the virtual bedload velocity and the measured bedload transport rates. In this study, we make an attempt to further decrease the uncertainties for the ADCP based bedload transport estimation with completing the measurements with direct bedload samplings as well as with assessing underwater videos of the river bed.

## 2. Methods

Intensive measurement campaigns of bedload transport were carried out in the Upper-Hungarian section of the Danube River at rkm 1791, between 2019-2021. The mean flow discharge here is around 2200 m3/s, the river width is ~350 m, the longitudinal slope is around 15 cm/km. The river bed mainly contains gravel of 2-20 mm. The measured flow range was between 1200 and 4300 m3/s, so low and high flows were also analyzed. During one campaign 5 verticals in a cross-section were measured. For sampling the bedload, a BfG-type sampler was employed, lowered from a vessel. In each vertical 15 minutes long samplings were carried out. Parallel with the sampling a 1200 KHz Rio Grande ADCP was continuously measuring fixed to the vessel. A water resistant video camera was mounted on the bedload sampler enabling the recording of the river bed during the samplings. The virtual bedload velocity was calculated following the method introduced by Rennie and Villard (2004), i.e. the differences between the instrument positions detected by an RTK-GPS and the ADCP's Bottom Tracking were processed and divided by the measurement time. This way, a set of measured bedload transport rate and related virtual bedload velocity data pairs was generated.


**Fig. 1.** BfG-type bedload sampler (left), video footage from the camera fixed to the sampler (right).

## 3. Results

For the assessment, we only used those measurements where all the three methods, i.e. the physical sampling, the underwater videos and the ADCP surveys, provided adequate information for the same sample. Unsuccessful samplings, non-visible videos or ADCP data with false positions were excluded therefore. The remaining data, ~20 data pairs, were then further analyzed. Based on the videos, we distinguished two transport modes: continuous and discontinuous movement of the sediment grains. The former represents sheetflow kind of motion, whereas the latter rather indicates the incipient motion range. When relating the physically measured bedload transport rate with the ADCP based virtual bedload velocity, it could be shown that the data for the two transport modes can be well separated indeed. On the one hand, when the grains indicated incipient or intermittent motion, the related velocities strongly varied, leading to weak correlation. On the other hand, when the gravel transport was rather continuous, however only for three cases here, the Bottom Tracking better represented the transport rate. Moreover, the gradient of the fitted regression line is significantly higher, indicating much higher rate at the same virtual velocity when the transport is permanent. Further representative data, preferably covering a wider range, is needed to verify the above presented assumptions.

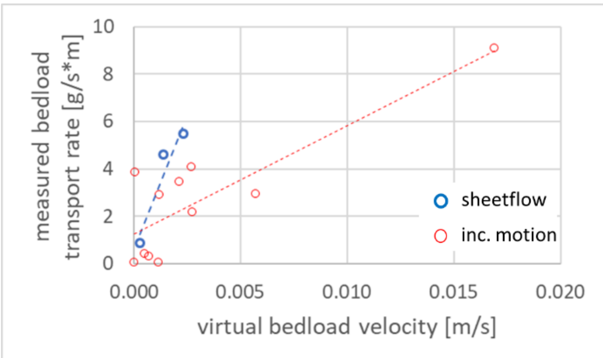


**Fig. 2.** Virtual bedload velocity against measured bedload transport rate.

**Acknowledgments**

The field measurements were carried out within the AT-HU Interreg project SEDDON II.

**References**

Conevski S, Guerrero M, Winterscheid A, Rennie CD, Ruther N (2020) Acoustic sampling effects on bedload quantification using acoustic Doppler current profilers, Journal of Hydraulic Research 58:6, 982-1000
Latosinski FG, Szupiany RN, Guerrero M, Amsler ML, Vionnet C (2017) The ADCP's bottom track capability for bedload prediction: Evidence on method reliability from sandy river applications, Flow Measurement and Instrumentation, 54, 124-135.
Ramooz R, Rennie CD (2010) Laboratory measurements of Bedload with an ADCP. U.S. Geological Survey Scientific Investigation Report 2010-5091.
Rennie CD, Villard PV (2004) Site specificity of bedload measurement using an acoustic Doppler current profiler J. Geophys. Res., 109, F03003.

# Assessment of acoustic features of clay-silt suspended sediment from numerous observed particle size distributions and dual-frequencies

Flóra POMÁZI[1], Massimo GUERRERO[2] and Sándor BARANYA[1]

[1] Department of Hydraulic and Water Resources Engineering, Faculty of Civil Engineering, Budapest University of Technology and Economics, Műegyetem rkp. 3., H-1111 Budapest, Hungary
email: pomazi.flora@emk.bme.hu
baranya.sandor@emk.bme.hu

[2] Department of Civil, Chemical, Environmental and Materials Engineering, University of Bologna, Bologna, Italy
email: massimo.guerrero@unibo.it

ABSTRACT

Acoustic methods are increasingly applied for high resolution mapping of suspended sediment transport. In this study, we assessed the acoustic features (i.e., the backscattering strength, and the normalized scatter- and viscous-attenuation coefficients) of the clay-silt suspended sediment of the Middle-Hungarian Danube River from a high number of observed particle size distributions obtained by laser diffraction. We found that the scattering-viscous attenuation (i.e., the attenuation due to sediment) variation is not relevant when compared to backscattering strength variation. Furthermore, the backscatter coefficient depends on the skewness of the particle size distribution and mean particle size. Analyzing corresponding signals of two acoustic instruments of significantly different operating frequency, we proposed a model for backscatter correction.

## 1. Introduction

Measuring and describing the complex dynamic processes of fluvial suspended sediment transport is a rather challenging task that calls for using advanced measurement techniques, such as indirect methods. Indeed, both acoustic and optical surrogates have been widely used in sediment monitoring. Many studies have been conducted for testing the applications and limitations of indirect methods (e.g., Gray and Gartner, 2009). This assessment is a follow-up of a case study testing different indirect methods (Pomázi and Baranya, 2020), in which, based on a large dataset, high scatter was experienced in Pomázi and Baranya (2020) when calibrating the acoustic instruments. The goal of the present study is to find a suitable approach for backscatter coefficient correction that is required for particles distribution change (e.g., Guerrero et al., 2016).

## 2. Methodology

### *2.1. Acoustic measurements*

In this study, a 1.2 MHz ADCP (Acoustic Doppler Current Profiler) and an 8MHz LISST-ABS (Acoustic Backscatter Sensor) were used to collect nonintrusive suspended sediment samples. The two instruments differ only in their operating frequency, and thus, their range of sampling. They emit, then measure the sound that scattered on the traveled distance (there and back). The acoustic theory, i.e., the theory of sound scattering due to water and sediment particles is well-known (e.g., Urick, 1983). To determine the suspended sediment concentration from the acoustic backscatter, attenuation and scattering due to water and sediment particles must be accounted for. The common acoustic features are the backscatter coefficient and the normalized scatter- and viscous-attenuation coefficients that depend on the sediment characteristics (i.e., concentration and particle size).

### *2.2. Sampling and analysis*

Undisturbed, physical water-sediment samples were collected using a US-P61-A1 isokinetic sampler in 15-45 points of each study cross sections. For the particle size analysis, a laser diffraction instrument, the LISST-Portable|XR (by Sequoia Inc.) was used which analyses low-angle laser scattering. The laser light emitted by the instrument passes through the analyzed sample volume – scattering due to the suspended sediment particles in the sample. From the scattering area of scattered light detected on the 44 detector rings each referring to a given particle size range, the probability density function, and the volumetric particle size distribution (PSD) are determined. Moreover, assuming a specific density for the suspended sediment material, the volume concentration (resulting from the volumetric distribution) can be converted to mass concentration. However, for the assessment of acoustic features, the number PSD had to be produced, to account for the prevailing amounts of clay-silt fractions over sand in the Danube (Guerrero et al., 2016).

## 3. Results, discussion and conclusion

Assessing the backscatter coefficient and the normalized scatter- and viscous-attenuation coefficients, we found that the scattering-attenuation reflects the same variation as the backscatter coefficient, both a $10^{-2}$ magnitude smaller than the viscous-attenuation coefficient. Thus, the attenuation variation due to sediment (i.e., scattering-attenuation) is negligible when compared to the attenuation due to friction (i.e., viscous-attenuation). Moreover, the maximum attenuation variation is 3 dB, while the backscatter variation is 30 dB. Therefore, the attenuation variation due to sediment is not relevant when compared to backscatter variation. So, as a further approximation, a constant sediment attenuation coefficient could be used in this study case. Furthermore, the backscatter coefficient and the concentration appear to be correlated, but with a further differentiation based on the mean particle size.

The backscatter coefficient depends on the skewness and the mean particle size. However, the effect of skewness seems to be diminishing in the coarser particle range. The backscatter coefficient for the 8MHz LISST-ABS shows a smaller variation than the 1.2 MHz ADCP backscatter coefficient. As the applied acoustic instruments are operating on significantly different frequencies, this difference in the variations of the backscatter coefficients can be used to further correct the backscatter measured by the 1.2 MHz ADCP and ultimately, to assess the concentration. Based on the results, we propose a model that relates concentration and backscatter at dual-frequencies, accounting for the driving parameters of the 1.2 MHz backscatter (i.e., concentration and skewness).

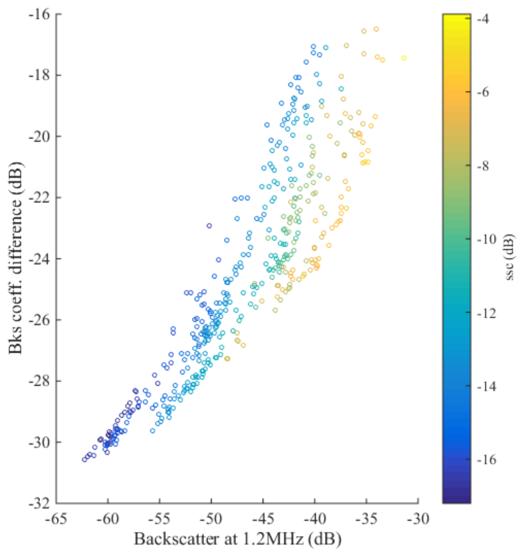


**Fig. 1.** The proposed model for correcting backscatter at 1.2 MHz by using dual frequency.

**Acknowledgements**

This research was partly funded by the project entitled "Drinking water: multidisciplinary assessment of secure supply from the source to the consumers" (project nr. 2018-1.2.1-NKP-2018-00011) supported by the National Research, Development and Innovation Office.

**References**

Gray JR, Gartner JW (2009) Technological advances in suspended-sediment surrogate monitoring, Water Resour Res, 45(4),
Guerrero M, Rüther N, Szupiany R, Haun S, Baranya S, Latosinski F (2016) The Acoustic Properties of Suspended Sediment in Large Rivers: Consequences on ADCP Methods Applicability, Water, 8(1), 13-54.
Pomázi F, Baranya S (2020) Comparative Assessment of Fluvial Suspended Sediment Concentration Analysis Methods, Water, 12(3), 873-891.
Urick, RJ (1983) Principles of Underwater Sound, Peninsula Publishing: Los Altos, CA, USA, 423 pp.

# Disaggregation Phenomena in Mixing Processes During Laminar-Turbulent Acceleration in Pipe Flows

Zhangjie PENG[1], Luan Ho[2], Ian GUYMER[1]

[1] Department of Civil and Structural Engineering, The University of Sheffield, UK
email: zhengjie.peng@sheffield.ac.uk
email: i.guymer@sheffield.ac.uk
[2]Tunley Engineering LTD, UK
email: luanho_uk@hotmail.com

ABSTRACT

Temporal concentration profiles resulting from an injected pulse of fluorescent tracer were recorded at multiple locations along a pipe during controlled unsteady flow conditions for flows that changed from laminar (Re=230) to turbulent (Re=18300) conditions. Disaggregation of the tracer cloud was observed during experiments, and the shape of the concentration profiles was found to be affected by injection times during the flow transitions. Further experimental investigation to elucidate the cause of disaggregation of dye involves developing a 2D LIF system at 4 sites along the pipe and measuring the cross-sectional tracer concentration profiles simultaneously under unsteady flow conditions.

## 1. Introduction

Disaggregation of the tracer cloud in pipe flows during acceleration from laminar to turbulent flows was first reported in Hart *et al.* (2021). In their study, temporal concentration profiles resulting from a tracer injection under different flow conditions (steady-state conditions and during the transition conditions from steady flow to unsteady flow) were measured at 6 locations downstream from the injection point. Disaggregation of a upstream single peak to multiple downstream peaks was observed at all the downstream locations along the pipe when the tracer was injected during the acceleration process. Based on this previously unreported phenomenon, they highlighted the need for further detailed studies, including measurements of temporal variations in the velocity and tracer cloud distributions across the pipe to elucidate and quantify the specific processes. This study was built upon the work of Hart *et al.* (2021), focusing on understanding the physical processes occurring during low Re flow accelerations and using the understanding to make realistic predictions of mixing under these conditions in pipe networks.

## 2. Preliminary Tests

Preliminary tests were conducted at The University of Sheffield in a 6 m long and 24 mm (diameter) pipe. Four fluorometers located at 0.65 m, 1.29 m, 2.27 m and 2.85 m downstream from the tracer injection point were used to measure the tracer concentration profiles. A downstream butterfly valve was used to create acceleration flows from Re=230 to Re=18300 in 30 s, and multiple tracer injections were made during this 30 s period. The flow rate was measured by a flowmeter at the end of the pipe.

## 3. Results

Fig. 1 shows the temporal concentration profiles resulting from a tracer injection that was made at different times during the acceleration. Two-peaks profiles started at the furthest locations to the injection point (i.e. x=2.85 m and x=2.27 m, Fig. 1(a)) and started to develop at all the measurement locations when the injection was made at 5 s after the acceleration started (Fig. 1(b)). For injections made at a late stage of the acceleration (i.e. 12 s after the acceleration), concentration profiles resumed normal distribution profiles, showing only one peak (Fig. 1(d)). The first peak of the concentration profiles showed a higher magnitude than the second one when the injection was made at a very early stage of the acceleration (i.e. 4 s, Fig. 1(a)); the two peaks reached similar magnitude when the injection was made at 5s (Fig. 1(b)); and the second peak showed a higher magnitude than the first peak when the injection was made at 6 s after the start of the acceleration (Fig. 1(c)). The preliminary results in Fig. 1 confirmed that the downstream two-peaks tracer concentration profiles are repeatable, and the magnitude of the two peaks is influenced by the time the injection was made.

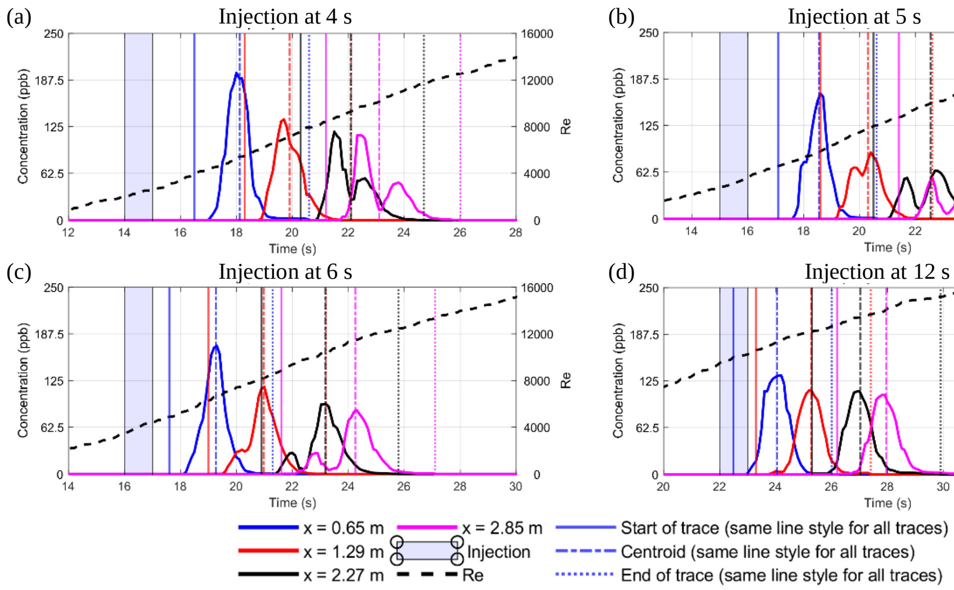


**Fig. 1.** Tracer temporal concentration profiles at four downstream locations from the injection point at different injection times to the start of acceleration; (a) injection at 4s; (b) injection at 5s; (c) injection at 6s; (d) injection at 12s.

## 4. Further Work

Hart *et al.* (2021) hypothesised that the multiple peaks are caused by the tracer in the centre of the pipe being accelerated more rapidly than the tracer near the pipe boundary. The next step of this study involves developing a 2D LIF system (Fig. 2) that uses a laser light sheet generator to illuminate the cross-section of the pipe and capture the concentration profiles at 4 sites along the pipe. This will enable the measurement of radial tracer concentration profiles during accelerations to construct the spatial and temporal development of tracer cloud disaggregation. The results will also provide further information to test the hypothesis of Hart et al. (2021) and will be presented at the conference.

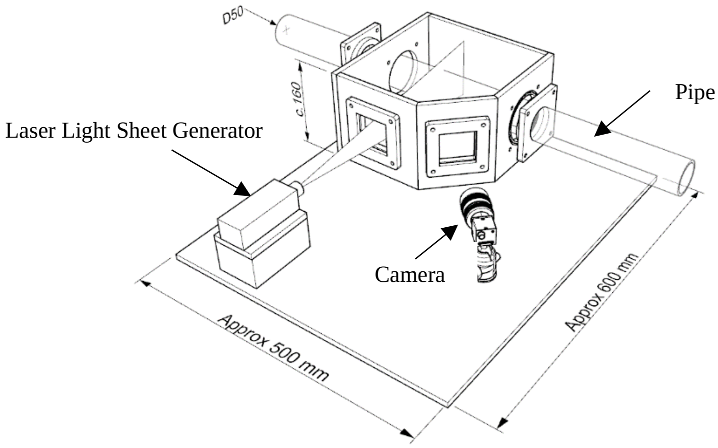


**Fig. 2.** Conceptual drawing for the 2D LIF system measuring the pipe cross-section tracer concentration profiles.

**Acknowledgements**

This work is supported by the EPSRC Grant EP/P012027/1.

**References**

Hart, J. *et al.* (2021) 'Longitudinal Dispersion in Unsteady Pipe Flows', *Journal of Hydraulic Engineering*, 147(9), p. 04021033. doi: 10.1061/(asce)hy.1943-7900.0001918.

# Creative experimental testing of transient tsunami bore impact on a realistic skewed bridge

Denis ISTRATI[1], Ian BUCKLE[2]

[1,2] University of Nevada, Reno, United States
email: distrati@unr.edu
email: igbuckle@unr.edu

ABSTRACT

In response to the catastrophic effects of recent tsunamis on coastal bridges, this study presents a smart experimental setup that enabled the hydraulic testing of the largest skewed superstructure to date. The data demonstrate the importance of the three-dimensional effects and resultant yaw and roll moments, which overload the individual abutments. This in turn suggests the need for a paradigm shift in the assessment of tsunami risk to coastal bridges to include not just the estimation of maximum total forces but also the consideration of multiple load cases with appropriate combination of forces and moments that will represent the most critical instants of the complex 3D tsunami-bridge interaction of skewed superstructures.

## 1. Introduction

Recent major tsunamis caused unprecedented damage to coastal communities and transportation infrastructure. In fact the tsunami waves, damaged 81 on the coast of Sumatra in 2004 (Unjoh, 2007) and 252 in Japan (Maruyama et al., 2013), with most of these witnessing a washout of the superstructure by the tsunami flow. Such events demonstrated the vulnerability of bridges and the need to decipher the hydrodynamic effects in order to develop tsunami-resilient transportation networks. Although several studies have been conducted in the last decade, the majority of them investigated the total applied tsunami loads either via small-scale (1:100$^{th}$ - 1:20$^{th}$) experiments of simplified models or via two-dimensional computational fluid dynamic analyses of rigid models that could not account for the actual dynamic properties of a bridge and could not capture accurately the fluid-structure interaction. Moreover, the majority of the studies were limited to straight bridges and a flow direction normal to thee bridge span, without the consideration of the three-dimensional effects that will occur during the inundation of skewed bridges. To overcome the aforementioned limitations of past studies, this research project conducted hydrodynamic experiments of tsunami bore impact on skewed bridges, which generated new fundamental knowledge related to tsunami-bridge-interaction in realistic environments.

## 2. Experimental setup

In order to achieve the largest possible scale, the hydrodynamic tests were conducted in the flume at Oregon State University, which is 104.24 m long, 3.66 m wide and 4.57 m deep. Moreover, in contrast to past studies that simulated multi-span bridges with piers at small-scale, the novel approach of this project was the representation of a single-span at a large-scale using a smart experimental setup. As shown in Fig. 1, the actual abutments or piers were not constructed, which maximized the available space for the superstructure. Instead, the setup consisted of two black beams and red bent caps that had been originally designed to investigate hurricane waves (Bradner et al, 2011). Leveraging these components, frictionless rails with carriages and load cells that could withstand the tsunami loads were installed between the black beams and red bent caps, allowing the latter to slide on the beams and measure the forces transferred from the bridge to the flume walls..

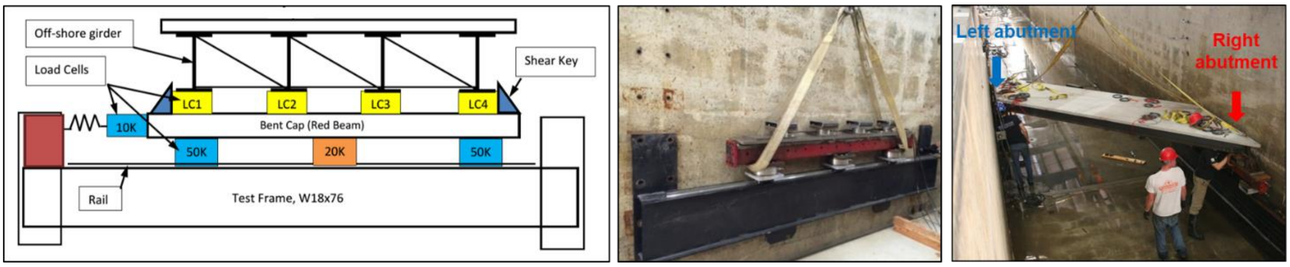


**Fig. 1.** Experimental setup in dry conditions and during the hydrodynamic tests.

With this approach it became feasible to fit a 1:5th scale straight and skewed superstructure with a 45° skew angle, which was made of the same materials and structural components as in current design practice (AASHTO, 2012), i.e. reinforced concrete slab, steel girders, cross-frames and steel/elastomeric bearings. The bent caps were connected in the horizontal direction with rigid links or springs with different stiffness, enabling the quick investigation of different substructure flexibilities. Moreover, other unique aspects of the hydrodynamic tests included: (a) the optimization of the flume bathymetry with a combination of slabs that permitted the generation of both unbroken solitary waves and turbulent bores (see Istrati et al, 2021), (b) the extensive instrumentation that recorded the hydrodynamic properties (free-surface, velocities, water pressures), the impact pressures on the bridge and the structural response (forces, stresses, accelerations, displacements), and (c) the quantification of the demand in individual cross-frames, bearings and bent caps, which is necessary for the design of real-life bridges but had not be available in the literature until now.

## 3. Results and discussion

Figure 2 presents selected time-histories of the total hydrodynamic forces, the individual horizontal forces in each abutment/bent cap (i.e. Fh,l and Fh,r) and the yaw moment (Mz), as well as, the maximum normalized uplift per abutment. The experimental data of bore impact on skewed bridges reveal that:

- The superstructure witnesses significant lateral (Fh) and vertical (Fv) forces, with the latter one consisting of an uplift phase (positive values) followed by a downward one. However, the magnitude of the impulsive components is small relative to the case of straight bridges seen in Istrati et al., 2018.
- The Fh is not equally distributed to the two abutments (i.e. 50%) like in the case of straight bridges, but one of them has to resist about 75% of Fh. This is a result of the yaw moment that is generated during the three-dimensional interaction of the bore with the structure and the gradual application of pressures on the girders.
- The maximum uplift transferred to a single abutment can reach 104% of the total applied tsunami uplift, which seems surprising at first sight and has not been discussed in the past. However, this seems to be justified by the tsunami-induced roll moment (Mx) that switches sign as the bore propagates through the superstructure, overloading a different abutment as the process takes place.

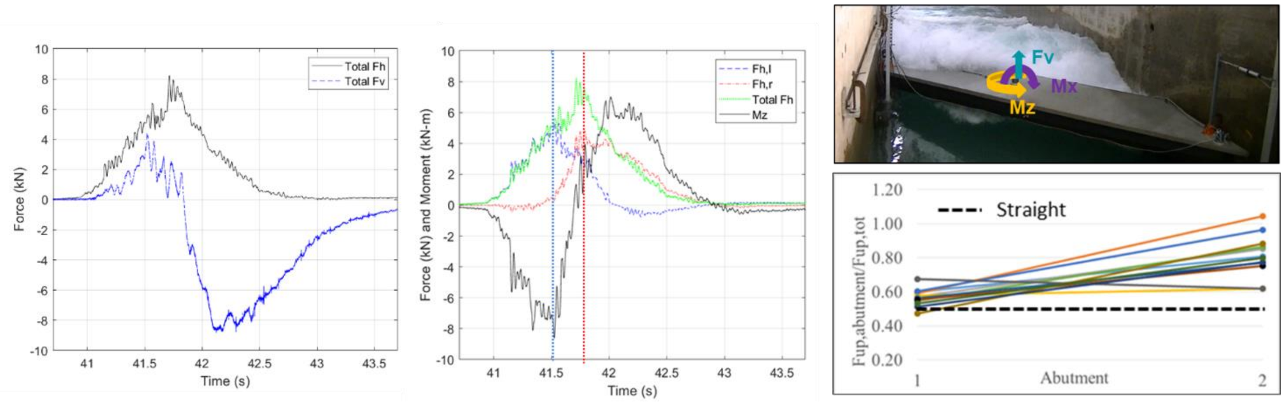


**Fig. 2.** Bore-induced total forces and moments, and distributed demand in individual abutments

**Acknowledgements**

The presented experimental work was funded by the Federal Highway Administration under Contract No. DTFH61-07-C-00031. Authors wish to thank Solomon Yim, Pedro Lomonaco, Tao Xiang, Tim Maddux and the staff of Hinsdale Wave Research Laboratory at OSU for their assistance during the experiments. Any opinions, findings, and conclusions or recommendations expressed herein are those of the authors and do not necessarily reflect the views of the funding agency.

**References**

AASHTO LRFD Bridge Design Specifications (2012). ISBN: 978-1-56051-523-4, Publication Code: LRFDUS-6.
Bradner, C., Schumacher, T., Cox, D., & Higgins, C. (2011). Experimental setup for a large-scale bridge superstructure model subjected to waves. Journal of waterway, port, coastal, and ocean engineering, 137(1), 3-11.
Istrati, D, Buckle, IG (2021) Tsunami Loads on Straight and Skewed Bridges–Part 1: Experimental Investigation and Design Recommendations, No. FHWA-OR-RD-21-12. Oregon. Dept. of Transportation, Research Section.
Istrati D, Buckle, IG, Lomonaco P, Yim, S (2018) Deciphering the tsunami wave impact and associated connection forces in open-girder coastal bridges, Jl Marine Science & Eng, 2018, MDPI,6 (148).
Maruyama K, Tanaka, Y, Kosa, K, Hosoda, A, Arikawa, T, Mizutani, N, Nakamura, T (2013) Evaluation of tsunami force acting on bridge girders, Proc Thirteenth East Asia-Pacific Conference on Structural Engineering and Construction (EASEC-13), 2013
Unjoh S. (2007) Bridge damage caused by tsunami, B Japan Assoc Earthquake Eng 2007, 6: 6–28

# Velocity Measurements in Transient Flow Downstream of a Submerged Vertical Drop

Eugene RETSINIS[1] and Panos PAPANICOLAOU[2]

[1,2] School of Civil Engineering, National Technical University of Athens, 9 Iroon Polytexneiou St., 15780, Athens, Greece
email: retsinis@central.ntua.gr
email: panospap@mail.ntua.gr

ABSTRACT

## 1. Introduction

Hydraulic jumps occur when supercritical flow becomes subcritical under momentum conservation conditions. The hydraulic jump is used as energy dissipation mechanism in the design of stilling basins. In some cases a vertical negative step is constructed at the entrance of a stilling basin in order to stabilize the hydraulic jump under all operating conditions. In laboratory experiments, the flow is controlled by a sluice gate upstream, and a sharp crested overflow downstream of the step. Five different rapidly varying types of flow have been observed around a step under supercritical flow conditions upstream (Moore and Morgan, 1957; Ohtsu and Yasuda, 1991; Mossa et al. 2003): the minimum B-jump is the hydraulic jump at the toe of the step; the B-jump is a submerged jump downstream of the step; the wave-train is a transient, surface jet-type flow without formation of a hydraulic jump; the wave-jump is the flow of an ascending jet forming a standing wave downstream of the step before it dives and results in a submerged hydraulic jump; and the A-jump is the flow where the hydraulic jump is formed upstream of the step. These flow profiles appear with this sequence by increasing the tailwater depth downstream continuously. The transition from supercritical to subcritical flow over a fully submerged negative step has been studied by experiments regarding the measurement of flow depths upstream and downstream of the jump as well as the pressure at the face of the step, but not the internal turbulent flow properties in terms of velocity measurements. The aim of the present work is the measurement of the two-dimensional velocity field in the region of a wave-train using Particle Image Velocimetry (PIV) for three upstream Froude numbers 1.99, 2.55 and 2.99.

## 2. Experimental

The measurements were made in the Laboratory of Applied Hydraulics of the School of Civil Engineering at the National Technical University of Athens, Greece, in a horizontal channel 10.50 m long with rectangular cross section 0.255 wide and 0.50 high. The section of the channel where measurements were taken has been modified to accommodate the experiments by replacement of the steel, nontransparent bottom with Lucite, and the vertical side glass walls with new ones with improved optical properties. The water supply was obtained via a recirculation system that consists of a 3 kW pump with variable speed motor and maximum discharge capacity of 40 L/s connected to a 2.65 $m^3$ water tank at the downstream end of the channel, and PVC pipe of nominal diameter 0.2 m through which water was pumped to the upstream end of the channel. A downstream facing vertical step 10.3 cm high and 1 m long made of Lucite was placed 4.85 m upstream of the channel end. A vertical sluice gate was positioned 0.35 m upstream of the step face, in order to control the supercritical flow. The flowrate was measured with an ultrasonic flow meter of 2-5% accuracy, attached in the horizontal PVC pipe and the flow depths were measured with point gauges.

The two-dimensional velocity field in the vertical mid-plane of the channel downstream of the step was measured with PIV technique under a wave-train. To implement PIV silver coated hollow glass seeding spheres of diameter 10 μm and density 1.04 $g/cm^3$ were illuminated with a dual cavity double pulsed $Nd^{+3}$-YAG laser with maximum energy output 135 mJ, and maximum flashing frequency of 15 Hz at visible green light (532 nm). The images of the particles were captured with a CCD camera with spatial resolution 2048 x 2048 pixels and maximum frequency of 15 Hz. After dividing the images into a dense grid of smaller interrogation windows, cross-correlation was utilized to compute the local average two-dimensional displacement vector in each interrogation window, and hence, the instantaneous two-dimensional velocity field. Three different experiments were implemented for the measurement of the velocity field of the transient wave-train flow type, the hydraulic conditions of which (height of the step d, discharge Q, upstream and downstream depths $y_1$ and $y_2$, the upstream and downstream velocities $V_1$ and $V_2$, and the upstream Froude number) are summarized in Table 1.

**Table 1.** Initial hydraulic conditions of the experiments measured with the PIV technique.

| Experiment | d (cm) | Type of jump | Q (L/s) | $y_1$ (cm) | $y_2$ (cm) | $V_1$ (m/sec) | $V_2$ (m/sec) | $Fr_1$ |
|---|---|---|---|---|---|---|---|---|
| 1 | 10.3 | Wave-train | 14.21 | 4.30 | 21.50 | 1.30 | 0.26 | 1.99 |
| 2 | 10.3 | Wave-train | 18.17 | 4.30 | 22.96 | 1.66 | 0.31 | 2.55 |
| 3 | 10.3 | Wave-train | 21.26 | 4.30 | 24.23 | 1.94 | 0.34 | 2.99 |

## 3. Results

The length scale $y_c$+d contains information regarding the potential energy of the flow in terms of the step height d and the minimum energy (or flow rate) in terms of critical depth $y_c$, and was used to normalize the vertical distance from the bottom. The mean velocity flow field and vorticity field are depicted in Fig. 1 for Experiment 1 of Table 1. The vertical distribution of dimensionless horizontal velocity component $u/V_1$ and turbulence intensity $u_{rms}/V_1$ are shown in Fig. 2 versus the dimensionless vertical distance from the bottom $y/(y_c+d)$ for Froude numbers 1.99, 2.55 and 2.99 at dimensionless horizontal distance from the step $x/(y_c+d)=0.95$. From Figs. 1(left) and 2(left), it is evident that there exists a significant recirculation area below the top of the step. The mean velocity field exhibited its highest value at a level higher than that of the step, while the greatest value of vorticity was observed at the location downstream of the step face, where the supercritical water jet met the subcritical flow. From Fig. 2(right), it can be noted that the turbulence intensity in the horizontal direction can be as high as 24% at $y/(y_c+d)=0.6$ for Froude number $Fr_1=2.99$.

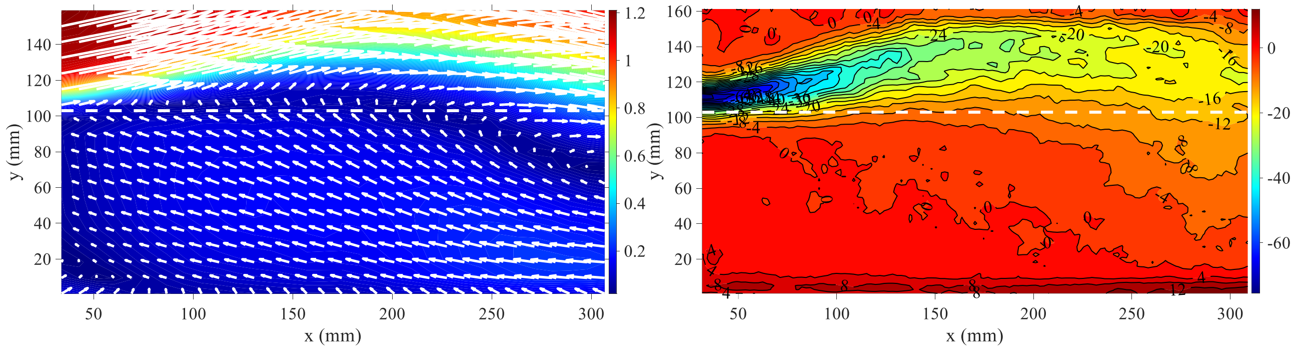


**Fig. 1.** Mean velocity field (m/s) left, and vorticity field ($s^{1}$) right, of a wave-train with Froude number 1.99 (dotted line shows schematically the elevation of the step).

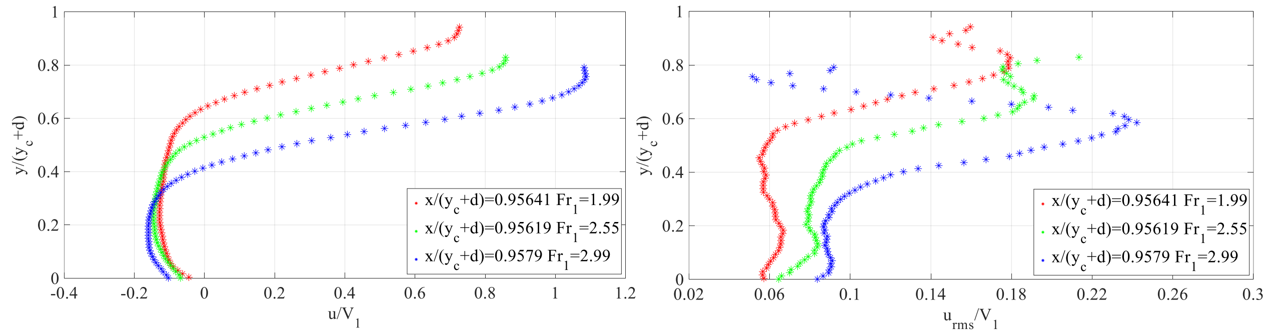


**Fig. 2.** Normalized horizontal velocity $u/V_1$ left, and turbulent intensity of the horizontal velocity $u_{rms}/V_1$ right, versus the dimensionless distance from the bottom $y/(y_c+d)$ for wave-train with Froude numbers 1.99, 2.55 and 2.99, at distance $x/(y_c+d)=0.95$ from the step.

### References

Moore, W.L., and Morgan, C.W., (1957). The Hydraulic Jump at an Abrupt Drop, Journal of the Hydraulics Division, Proceedings of the American Society of Civil Engineers, Vol. 83, Nº HY 6, Paper 1149, December, pp. 1-21.

Mossa, M., Petrillo, A., and Chanson, H., (2003). Tailwater Level Effects on Flow Conditions at an Abrupt Drop, Journal of Hydraulic Research, Vol. 41, Nº 1, pp. 39-51.

Ohtsu, I., and Yasuda, Y., (1991). Transition From Supercritical to Subcritical Flow at an Abrupt Drop, Journal of Hydraulic Research, Vol. 29, Nº 3, pp. 309-328.

# Scaling Issues in Physical Modelling of Spillway Aerators

James YANG[1,2], Shicheng LI[2], Chang LIN[3]

[1] Vattenfall AB, R&D Hydraulic Laboratory, 81426 Älvkarleby, Sweden
email: jamesya@kth.se

[2] Civil and Architectural Engineering, Royal Institute of Technology, 10044 Stockholm, Sweden
email: shicheng@kth.se

[3] Department of Civil Engineering, National Chung Hsing University, Taichung 40227, Taiwan
email: chenglin@nchu.edu.tw

ABSTRACT

Subjected to sub-atmospheric pressure, the two-phase aerator flow does not obey the Froude law of similitude. This paper discusses the air-flow upscaling from model to prototype. If the water flow velocity in the model exceeds 6.5–7.5 m/s, the model results can be directly upscaled to prototype. Otherwise, the prototype air-flow rate is significantly underestimated.

## 1. Introduction

High-velocity flows are the major concern for cavitation in design of both surface spillways and low-level outlets. Installation of an aerator is a common practice to avoid cavitation damages. It is often used in open chutes, but its use in flood tunnels are not either uncommon. The flow at an aerator is a typical two-phase flow affected by such factors as spillway and aerator layout, flow conditions and air cavity characteristics.

## 2. Comparisons between model and prototype

In a Froude model, the water flow should be exposed to the atmospheric pressure in all directions. There are cases where sub-atmospheric air pressure is present in the form of an enclosed air cavity, which is the case in an aerator flow. The Euler law of similarity (pressure to inertial forces ratio) should be satisfied, a condition seldom met in laboratory.

For high dams, aeration tests are sometimes made in several scales, which is the case for the 149.5 m Baishan dam, China (Shi 2007). Fig. 1 shows its layout of the spillway. It has four gated openings, with sill el. is +404.0 m and net width 12.0 m each. The full pool level is between +420–422 m and the design discharge amounts to 11 000 m$^3$/s. The aerator offset is at el. +384.0 m. Model tests were performed in scales 1:λ = 1:20, 1:40 and 1:70. After the commissioning, prototype measurements of air flows were made. Fig. 1 plots both the model and prototype results, in which $X1 = \frac{V}{\sqrt{gD}}\sqrt{\frac{t+s}{D}}\frac{1}{\cos\alpha\cos\theta} = \mathrm{F}\sqrt{\frac{t+s}{D}}\frac{1}{\cos\alpha\cos\theta}$, $\beta$ = ratio of air flow to water flow, $V$ and $D$ = approach flow velocity and depth, $\alpha$ = chute slope with the horizontal, $t$ = chute bottom offset at the aerator, $s$ and $\theta$ = deflector height and angle with the chute bed and $g$ = gravitational acceleration. For a given model scale, $\beta$ is weakly dependent on *X1*. A larger model gives obviously rise to more air flow. In the prototype, the dependence of $\beta$ on *X1* is significant, implying that higher flow velocity leads to more air entrainment. The model-prototype difference is large.

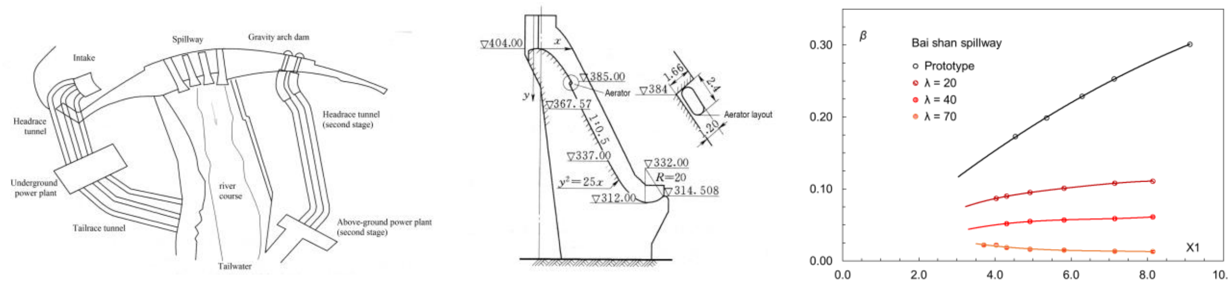


**Fig. 1.** Baishan dam – layout of the facility, longitudinal profile of spillway with aerator and model-prototype air flow comparison.

Another example is the aerators in JinPing-I flood tunnel on Yalong River, China(Lian et al. 2017). The tunnel is ~1400 m long, built with four aerators at varying intervals (Fig. 2). Each of the three upstream aerators is composed of both an offset and a deflector. All the offsets are 1.5 m high and the deflectors are 0.5, 0.4 and 0.2 m high. The fourth one is shaped in a 3D configuration, featuring sudden-narrowed sidewalls and a convex deflector. From up- to downstream, their protection lengths are 81.0, 87.8, 128.6, and 115.6 m. An air shaft is constructed that connects to each aerator.

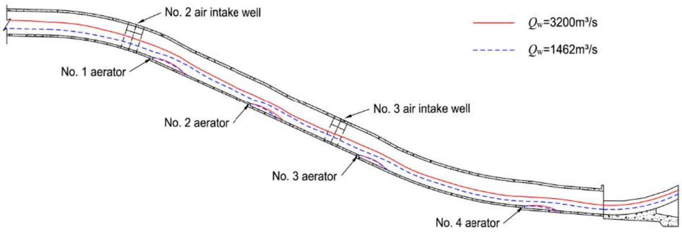


**Fig. 2.** JinPing-I flood tunnel with free-surface flow, longitudinal profile (Lian et al. 2017).

Froude model tests were made in scale $\lambda$ = 30. After the competition, prototype measurements were of air flow rates, cavity pressure and air concentration. The air flow is upscaled from model to the prototype size by $\lambda^{2.5}$. The results show that, at Q = 3200 m$^3$/s, the prototype air flow rates at no. 2 and no. 4 aerators are 3.4 and 2.3 times the model ones. The air demand in the prototype is considerably larger than in the model. Depending on model scale and also flow conditions, the air demand can differ by a factor of up to 4–7 (Lian et al. 2017).

The aerator experiments were performed in a large test rig at Institute of Water Resources and Hydropower Research, Beijing (Shi 2007). $V$ = 6.6–15.4 m/s, $D$ = 0.050–0.251 m, F = 4.34–21.90, R = (0.69–1.41)×10$^6$ and W = 325–490. Together with the field data from two prototypes (Baishan and Fengjiashan) and their scale models (Shi 2007), Fig. 3a presents, as a $\beta_1$-$X1$ relationship, the flume test results, in which $\beta_1 = \beta/\sqrt{\cos\alpha}$. The results demonstrate that, if the model approach velocity $V$ exceeds 7.5 m/s, the conversion from the models coincide with the prototype data; the model velocity within $V$ = 6.6–7.02 m/s gives fairly close results. Fig. 3b compares the model-prototype results for the Foz do Areia spillway aerators (Pinto et al. 1982). For $\lambda$ = 8 and 15, the velocity is larger than 7.5 m/s and the models reproduce correctly the prototype air-flow behaviours.

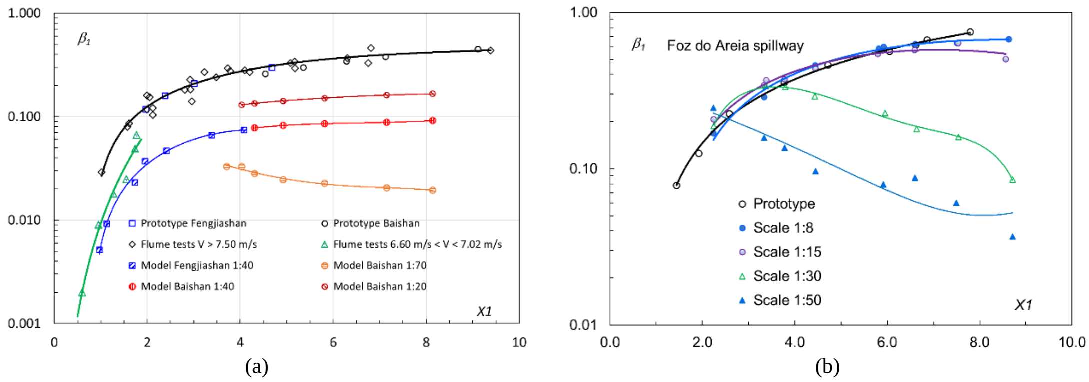


**Fig. 3.** Model-prototype comparison of air flow. (a) Flume tests, including also data of two dams; (b) Foz do Areia spillway tests

## 3. Conclusions

Hydraulic model tests by the Froude law are often performed to evaluate spillway aerator behaviors. The presence of the air cavity subjected to sub-atmospheric pressure requires that the Euler law should also be satisfied, which is seldom the case. The prototype measurements show that that a direct mode-prototype upscaling is possible if the model water flow velocity is above 6.5–7.5 m/s. Below this limit, any attempt to correct the model data is theoretically incorrect and would cause significant errors.

**Acknowledgements**

The study is funded by Vattenfall R&D and Swedish Hydropower Centre (SVC), as part of research project "Two-phase flow modelling: evaluations and simulations for safer spillway discharge" (contract VKU14126).

**References**

Lian, J, Qi, C, Liu, F, Gou, W, Pan, S and Ouyang, Q (2017). Air entrainment and air demand in the spillway tunnel at the Jinping-I dam. Applied Science, 7, 930. doi.org/10.3390/app7090930.
Pinto, NLS, Neidert, SH and Ota, JJ (1982). Aeration at high velocity flows. Water Power and Dam Construction, 34(2), 34–38.
Shi, QS (2007). High-velocity aerated flow. China Water and Power Press, Beijing, China.

# Stereo-PIV measurements within a canopy of spheres in shallow open-channel flows

Michele TREVISSON[1], Olivier EIFF[1], Dieter GROSS[1], Yulia AKUTINA[1]

[1]Institute for Hydromechanics (KIT), Germany
email: michele.trevisson@kit.edu
email: olivier.eiff@ kit.edu
email: dieter.gross@ kit.edu
email: yulia.akutina@ kit.edu

ABSTRACT

To measure the flow field of shallow open-channel flows not just above but inside the canopy composed of spheres, a top-viewing stereo Particle Image Velocimetry (sPIV) system was implemented for vertical longitudinal plane measurements. A glass plate was installed at the water-surface to avoid random image distortions from surface waves and fluorescent particles were used to filter out reflections on the spheres. To validate the use of the glass plate and a necessarily steep viewing angle of the stereo cameras, the instantaneous flow-field above the spheres' crests was measured simultaneously with a third side-looking camera for standard 2D PIV processing. 2D PIV measurements were also performed without a glass plate for comparisons to assess its impact on the flow.

## 1. Introduction

Particle image velocimetry (PIV) has been used increasingly to study turbulent open-channel flows as it is a non-intrusive technique, offering spatially and temporally resolved measurements. With rough beds, both 2D-PIV and stereo-PIV (sPIV) systems have been successfully applied to measure the flow above the roughness elements (e.g., Manes et al., 2007 and Akutina et al., 2019, respectively). However, impaired optical access does not usually allow the investigation of the flow within the interstices of the roughness elements, except for specially designed canopies and optical systems. These include the work of Florens et al. (2013) or Chagot et al. (2020) who used “spy cubes” and telecentric optical arrangements with transparent cuboids and transparent channel bottoms. For non-rectilinear roughness elements, refractive index matching (RIM) of the bed elements and the fluid can be an option (e.g. Rousseau et al., 2020). This solution, while possible in viscous flows when sediments are included (Mouilleron et al., 2009), is out of reach when the flow is also turbulent. Since our long-term goal is to include fine-sediment erosion within the bed of spheres, another solution was sought. It consists in viewing the flow from above with steep viewing angles which implicate image distortions and errors which can only be compensated with stereo vision. The top viewing results in two further issues: (i) random image distortions when viewing through a wavy free-surface, and (ii) laser sheet reflections on the bed. To avoid the random image distortions, the free surface was flush-covered with a glass plate over the measurement region, an intrusive solution also implemented by others (e.g. Cameron et al., 2013). To remove the reflections, fluorescent particles were used which allow the reflections to be filtered out. Since neither the very steep viewing angle in stereo-PIV nor the effect of the glass plate on the flow has to our knowledge been validated directly, the flow field above the sphere's crest was measured simultaneously with a third side-looking camera.

## 2. Set-up and results

The bed is made of a two-layered staggered pattern of spheres ($R$ = 1 cm; Fig. 1a,b) glued on the bottom of a 9 m long tilting flume 30 cm in width $W$. The stereo-PIV system is composed of two high-speed 2 Mpx cameras and of a 4 W continuous blue laser with a 445 nm wavelength. In order to access the bed interstices down to $z = -1.5\,R$, the cameras are installed with a horizontal stereo angle of 26.5° and with a steep vertical viewing angle of 20° (Fig. 1a,b). The flow is seeded with fluorescent particles with a mean diameter of 50 µm and with a density of 1.1 g/cm$^3$, assuring almost neutrally buoyant conditions. By equipping the cameras with 475 nm longpass filters, laser reflections at the bed are filtered out, while the particle emission signal, in the yellow-red spectral region, is retained. The glass plate (25 cm long and 29.5 cm wide) is fixed flush on the water surface. A third camera is installed on the side of the flume (Fig. 1a) with a perpendicular view of the laser sheet allowing 2D PIV measurements. All three cameras are triggered simultaneously to measure the same instantaneous flow above the spheres' crests. A total of three experiments are performed by varying the water depth and the Reynolds number (Table 1). Each experiment is performed with and without the glass plate.

Table 1. Flow parameters: water depth *H*, bulk Reynolds number *Re* = *UH*/ν, flow rate *Q*, slope *i*, bulk velocity *U* = *Q*/(*HW*).

| | *H* [cm] | *Re* | *Q* [l/s] | *i* [%] | *U* [cm/s] |
|---|---|---|---|---|---|
| Exp. 1 | 5.8 | 15000 | 4.5 | 0.11 | 25 |
| Exp. 2 | 5.8 | 30000 | 9.0 | 0.61 | 51 |
| Exp. 3 | 10.8 | 30000 | 9.2 | 0.07 | 28 |

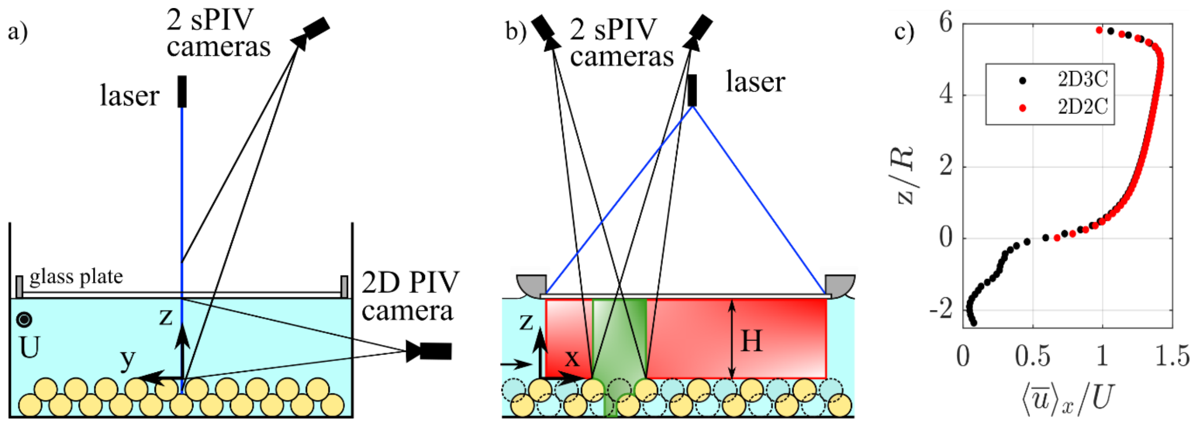


**Fig. 1.** a) Transverse view of the sPIV and 2D-PIV set-up; b) longitudinal view of the sPIV set-up with the green and red measurement areas of the sPIV and 2D PIV, respectively; c) vertical profiles of the longitudinally- and time-averaged streamwise velocity $\langle\overline{u}\rangle_x$ obtained with sPIV (2D3C) and 2D PIV (2D2C) in Exp. 1 (with the glass plate).

Fig. 1c shows the longitudinally- and time- averaged longitudinal velocity profiles using 2D PIV and sPIV for Exp. 1. The profiles match very well. A thin boundary layer below the glass plate can also be identified. The turbulent stresses (not shown) also match well, except for the vertical variance which is overestimated by the sPIV system. As seen in Fig. 1c, the sPIV system yields results down to the second layer of spheres, as desired. Below the crests (z < 0), a direct validation with 2D PIV is not possible since the view is obstructed. However, analysis via topological principles (Foss, 2004) of the mean in-plane vector flow field within the canopy revealed it to be kinematically correct.

The influence of the boundary layer developing under the glass plate was analyzed via the displacement thickness $\delta^*$. It develops with a typical smooth wall law $(x - x_0)^{4/5}$ with the introduction of a virtual origin $x_0$ to account for a non-zero $\delta^*$ at the leading edge of the boat. $\delta^*$ covers approximately 1% *H*, suggesting a quasi-negligible contraction of the effective cross-section of the bulk flow. The bulk flow statistics show slightly accelerated flow conditions with the glass plate present in accordance with the displacement thickness.

## 3. Conclusions

Measurements of the flow in the interstices of a bed of spheres were performed using a top-viewing sPIV system with a steep viewing angle, a glass plate on the water surface and fluorescent seeding particles. The mean flow field is successfully validated with 2D PIV above the canopy and is in accordance with topological principles within the canopy. The boundary layer developing under the glass plate can be treated with traditional scaling laws for turbulent boundary layers developing along a smooth plate and the displacement height is about 1% of the water depth *H*.

### References

Akutina, Y., Eiff, O., Moulin, F., Rouzes, M. (2019) Lateral bed-roughness variation in shallow open-channel flow with very low submergence, Environmental Fluid Mech., 19, 1339-1361.
Cameron S.M., Nikora V.I., Albazrak I., Miler O. Stewart M., Siniscalchi F. (2013) Interactions between aquatic plants and turbulent flow: a field study using stereoscopic PIV, J. Fluid Mech., 732, 345-372.
Chagot, L., Moulin, F., Eiff, O. (2020) Towards converged statistics in three-dimensional canopy-dominated flows, Experiments in Fluids, 61 (24).
Mouilleron H., Charru F., Eiff O. (2009) Inside the moving layer of a sheared granular bed, J. Fluid Mech. 628, 229-239.
Florens, E., Eiff, O., Moulin, F. (2013) Defining the roughness sublayer and its turbulence statistics, Experiments in Fluids., 37.
Foss, J. (2004) Surface selections and topological constraints evaluations for flow field analysis, Experiments in Fluids, 37, 883-898.
Manes C., Pokrajac D., McEwan I. (2007) Double-Averaged Open-Channel Flow with Small Relative Submergence, Journal of Hydraulic Engineering, 133.
Rousseau, G., Ancey, C., (2020) Scanning PIV of turbulent flows over and through rough porous beds using refractive index matching, Experiments in Fluids, 61 (172).

# Refractive-index-matching using salt water

Yulia Akutina[1], Pengning Sun[1], Olivier Eiff[1]

[1] Karlsruhe Institute of Technology, Institute for Hydromechanics, Germany
email: yulia.akutina@kit.edu, olivier.eiff@kit.edu

ABSTRACT

In order to perform optical flow measurements around solid bodies, refractive-index matching (RIM) techniques are often employed: RI of a transparent object is matched with that of the working fluid. The solid becomes ``invisible'' and a full optical access inside or behind the body is made possible free of distortions. In this work, we study the use of polymer THV since it has close RI to water allowing readily available sodium chloride (table salt) to be added to water in order to reach the necessary refractive index. For validation, an experimental flow set-up with a patch of THV tubes was prepared to allow the flow to be measured by two independent particle image velocimetry (PIV) systems. One camera views the flow at the edge of the patch through the patch while the other camera has a free optical path to the same measurement plane. Comparing the results from the two measurement systems gives an estimate of the measurement errors. A mathematical model of light refraction is employed to analyse the PIV errors and their dependence on the tubes' geometry. An optimal PIV box size to the tube thickness ratio is proposed.

## 1. Introduction

In order to gain optical access for flow measurements through objects in the flow, refractive index matching (RIM) has been employed since at least Budwig (1994). In this technique, the RI of the working fluid is matched with that of the transparent material of the objects. As a result, the light rays are not refracted by the fluid-solid interface, but go through in a straight line, resulting in an unperturbed optical access. Many different RIM pairs (fluid-solid) have been used in the past. However, most of them require high-cost materials, special handling and equipment, many of them are toxic or unstable. The ones that bare lower costs are often too viscous for high-Reynolds number experiments. See an extensive review of RIM options in Wright et al. (2017). The easiest solution to this problem is to find a material that has the same RI index as water. This material should also be highly transparent, chemically stable, robust and available or transformable into the desired shape. Leis et al. (2005), Byron and Variano (2013) and Weitzman et al. (2014) proposed manufacturing procedures for different hydrogels having a RI close to water. Fort and Bardet (2021), on the other hand, proposed a technique to produce an impermeable polymer with a RI matching water. The downside of using these materials is a complex manufacturing procedure, and in case of hydrogel, its softness and water absorption.

Here, we propose to use a polymer, tetrafluoroethylene, hexafluoropropylene and vinylidene fluoride (THV hereafter), which has a RI of 1.363 close to water (1.333 for green light at 20 degrees C). It is highly transparent, relatively low-cost and is commercially available at various shapes (cylinders, beats, sheets). In order to match the RI, NaCl (table salt) was added to the water. Since perfect matching is never achieved or maintained, two-camera particle image velocimetry measurements were performed with and without THV obstructions in the optical path. This allowed the estimation of the errors incurred by the differences in the RI between the material and the fluid. A mathematical model was also employed to analyze the error distribution depending on the shape and thickness of the material and optimal PIV resolution.

## 2. Experimental setup

In a shallow square tank, a patch of THV hollow tubes was placed in its middle (Fig. 1a). Ultimately, this arrangement serves as a model for a vegetation patch. A non-stationary dipole flow was generated in the tank using two flaps. After closing the flaps abruptly, two counter-rotating vortices propagated into the patch creating a flow. Two PIV systems, facing each other, were located on opposite sides of the tank. They were arranged in this manner to allow them to take simultaneous images of the same laser-illuminated measurement plane with and without THV tubes in the otherwise equivalent optical path.

Two sets of experiments were performed with two types of THV tubes. One with thinner wall, 0.5 mm, and one with thicker wall, 1.5 mm. The inner diameter was 10 mm and 9 mm, respectively, rendering the outer diameter constant at 10.5 mm.

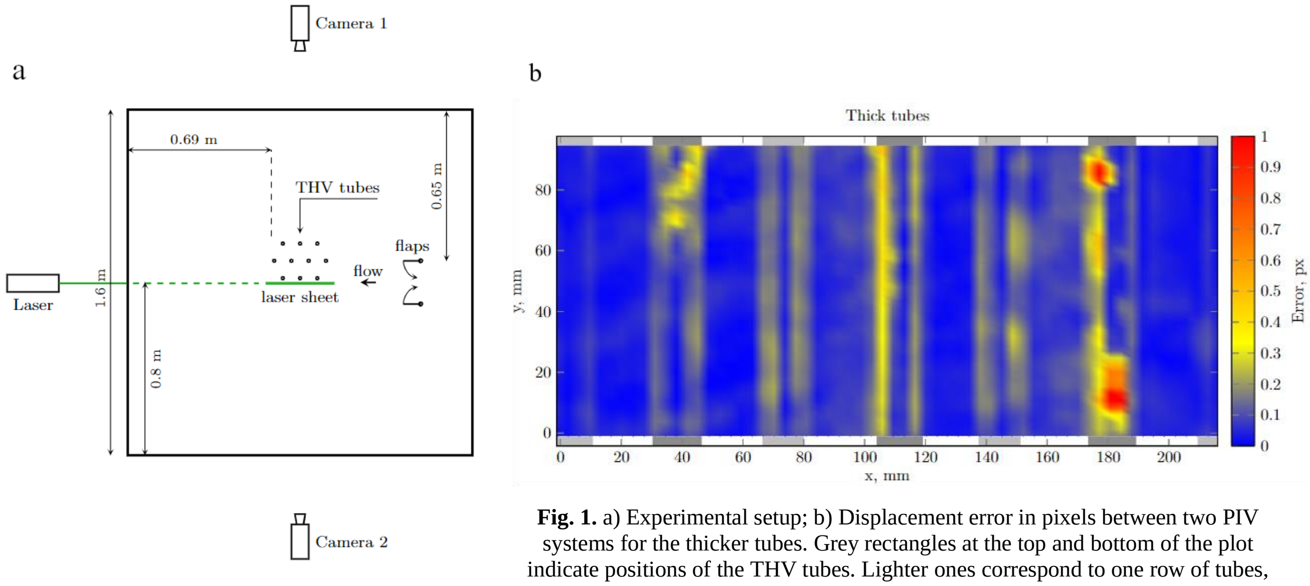


**Fig. 1.** a) Experimental setup; b) Displacement error in pixels between two PIV systems for the thicker tubes. Grey rectangles at the top and bottom of the plot indicate positions of the THV tubes. Lighter ones correspond to one row of tubes, while darker ones signify that at that location two tubes were positioned one behind another.

## 3. Results

Simultaneous PIV data obtained from the two cameras were subtracted from one another resulting in the estimate of the error produced by imperfection of the RIM, in particular differences in RI, here about 0.0005. Fig. 1b shows the time-averaged difference between the two displacement fields in pixels for the thicker tubes. The achievable precision of a PIV algorithm, given high quality of the set-up, is approximately 0.05-0.1 pixels. From the figure, it is evident that this is indeed the error that is observed in between the PIV tubes (e.g. around x = 20, 60 or 200 mm), where both cameras have a completely free optical path. At the locations of the tubes, in particular their edges, where both the thickness of the material and its curvature are high, higher errors are observed. The additional error (above the baseline PIV precision) is then up to 0.15 pixel for one tube in the optical path and up to 0.3 pixel for two tubes. It should be noted that at x = 180 mm errors reach 1 px, but these were found to be caused by bubbles on the inside one of the tube.

A refraction model of light rays passing through a cylindrical tube, based on the model of Lowe and Cutt (1992), was developed. Using this model, analysis were performed on what levels of RI mismatch can produce which level of PIV error in pixels. These results were verified with the experiments. Optimal PIV-resolution versus tube thickness and allowed difference in the RI are given.

It is concluded, that PIV measurements using THV and salt solution can be performed at relatively low cost without compromise on the Reynolds number. While the measured increase in errors is comparable to the bias error of PIV, even including several rows of relatively thick tubes in the optical path.

**References**

Budwig R (1994) Refractive index matching methods for liquid flow investigations, Experiments in Fluids, 17, 350–355
Byron ML, Variano EA (2013) Refractive-index-matched hydrogel materials for measuring flow-structure interactions, Experiments in Fluids 54, 1456
Fort C, Bardet, PM (2021) Refractive-index-matched polymer for experimental fluid dynamics in water, Experiments in Fluids, 62, 249
Leis AP, Schlicher S, Franke H, Strathmann M (2005) Optically transparent porous medium for nondestructive studies of microbial biofilm architecture and transport dynamics, Applied and Environmental Microbiology, 71(8), 4801-4808
Lowe ML, Vafidis C, Whitelaw JH (1992) Refraction through cylindrical tubes, Experiments in Fluids, 10, 50-54
Weitzman JS, Samuel LC, Craig AE et al. (2014) On the use of refractive-index-matched hydrogel for fluid velocity measurement within and around geometrically complex solid obstructions, Experiments in Fluids, 55, 1862
Wright SF, Zadrazil I, Markides, CN (2017) A review of solid–fluid selection options for optical-based measurements in single-phase liquid, two-phase liquid–liquid and multiphase solid–liquid flows, Experiments in Fluids, 58**,** 108

# Model complexity and information content in flood prediction: A view through an algorithmic information theory lens

Steven WEIJS[1]

[1] Dept. of Civil Engineering, University of British Columbia, Canada
email: steven.weijs@civil.ubc.ca

ABSTRACT

Building predictive models is akin to data compression: by describing the patterns found in observations in the most compact way, we can extrapolate to predict unseen observations. Minimizing description length of data is an underlying objective in both physics based and data driven approaches. An emerging perspective from Algorithmic Information Theory is presented, which could contribute to a consistent framework to provide guidance on the strengths and weaknesses of both approaches, and their combination.

## 1. Challenge for flood prediction

"Prediction is very difficult, especially about the future" is a Danish proverb often attributed to Niels Bohr. While in essence, this can be boiled down to the difficulty of extrapolating observations in time, this statement can be generalized to extrapolating in space, or even more generally from the seen to the unseen.

For riverine flood prediction, predicting the unseen involves extrapolations in all these domains. Firstly, usually predictions are most useful for the future, which we can still influence by actions in the present. An exception to this are forensic analyses of past floods, for example to improve models. Secondly, extrapolation in space is needed because locations of interest for flood prediction are not always the ones that are gauged. Thirdly, extrapolations from observed to unobserved variables are necessary. For example, though water level is often both a variable of interest for flood risk and also is the measured variable for river monitoring, streamflow is typically the variable used in models because more large-scale patterns are present that are useful for extrapolation. An example of these large scale patterns is mass conservation within the hydrological cycle, as opposed to momentum conservation in local channel geometry, which is much harder to extrapolate to many sites.

### *1.1. Physically based approaches*

In the physically based approach, known physical laws are applied in the computation of the dynamics hydrological processes and hydraulics. Conservation of mass, energy and momentum are typically applied in both the hydrological and the hydraulic components of the model. In the hydrological part, however, the energy balance is mostly applied on the surface, and momentum balance is often fully empirical, due to lack of measureable boundary conditions. This makes physically based approaches at least partially rely on data driven parameter fitting.

### *1.2. Machine learning approaches*

Machine learning approaches revolve around generic function approximators that describe underlying patterns found in data. Traditional approaches in flood forecasting revolved around local, short-term predictions of flows, based on a number of selected lagged variables, such as past streamflow, precipitation, and temperature. While the approach has in some occasions performed very well for its task, criticism often involved poor performance for extreme events that exceed events in the training period, poor interpretability, and difficulty applying models to new sites.

Recent work partly addresses these criticisms by applying machine learning over much larger and much more diverse data sets, focusing on a large number of sites at the same time. This has two main effects. Firstly, more data allows us to identify patterns of higher complexity. Secondly, the larger diversity of input data changes some prediction problems from extrapolation problems to interpolation problems. Some remarkable successes have been demonstrated in recent literature for out-of-sample prediction see Kratzert et al. (2019) and subsequent work.

## 2. Algorithmic information theory perspective

The general prediction problem can be formulated as the problem of extending a sequence of symbols. And the only thing that allows us to make such extensions with some degree of reliability is structure present in the observations, though uncertainty will typically remain and should be explicitly communicated.

Algorithmic Information Theory (AIT; Solomonoff, 1964, Kolmogorov, 1968, Li and Vitanyi, 2008) revolves around distinguishing patterns in a fixed volume of available data (a sequence of symbols) to allow extrapolation (sequence extension). A particular challenge with all prediction and extrapolation is the distinction between what is pattern and what is random. This is a particular area where AIT provides some unique insights, as it provides a formalization of Occam's Razor and also of the concept of randomness.

### *2.1. Model complexity control*

As Herman Weyl (1932) paraphrased Gottfried Wilhelm Leibniz (1686): *"If arbitrarily complex laws are permitted, then the concept of law becomes vacuous, because there is always a law!"*. This makes clear that in order to successfully predict from past data, the complexity of our models should be limited to make sure we are capturing the general law, and not only the specific instance. A typical approach for complexity control in hydrological prediction is to do cross-validation approaches, in which part of the data is reserved for testing the model and not used in model building or calibration. Alternative approaches use complexity penalization approaches.

### *2.2. Modeling as data compression*

A good model should describe the observations with little error, while not being overly complex, otherwise the model is restating the observations, instead of the generic laws and pattern that can be extrapolated. Both these aspects, prediction error and model complexity, can be measured in terms of description lengths. Algorithmic information theory provides us with a framework to quantify both description lengths in a common unit, the bit. Accordingly, we can identify the theoretically best model with optimal complexity for the data we are trying to explain, by asking the question: *Which model can describe the data with the lowest number of bits?* In this view, model building and data compression are essentially the same problem (Weijs and Ruddell, 2021).

### *2.3. Describing vs. explaining, prediction vs. understanding*

One could argue that models should not only describe the data, but also explain the phenomena, and the goal of models is not only to make useful predictions, but also to increase understanding. I argue that the notion of minimizing description length turns descriptions into explanations, and that understanding is means to get better predictions, not necessarily a goal that should be pursued in any situation.

### *2.4. Role of physically based knowledge*

Prior knowledge, such as knowledge of conservation laws and observations of the landscape, can contribute information to model predictions, without adding complexity to a model, because the added description length consists of statements that are thought the be true independently, and not used solely to explain the date at hand. In the discussion of complex physically based vs data driven models, a consistent way of measuring model description length is needed, that takes into account these sources of "free" model complexity.

## 3. Conclusions

In general, riverine flood forecasting can be seen as a special case of extrapolation of a sequence, which is the one of the core problems treated by AIT. Taking this abstract view based in theoretical computer science can contribute to a consistent framework to provide guidance on the strengths and weaknesses of both data driven and physics based approaches, and their combination.

**References**

Kratzert F, Klotz D, Shalev G, Klambauer G, Hochreiter S, Nearing G (2019) Towards learning universal, regional, and local hydrological behaviors via machine learning applied to large-sample datasets. Hydrology and Earth System Sciences, 23, 5089–5110.
Kolmogorov AN (1968) Three Approaches to the Quantitative Definition of Information." International Journal of Computer Mathematics 2 (1): 157–68.
Li M, Vitanyi PMB. (2008) An Introduction to Kolmogorov Complexity and Its Applications. Springer-Verlag New York Inc.
Solomonoff RJ (1964) A Formal Theory of Inductive Inference. Part I." Information and Control 7 (1): 1–22.
Weijs SV, Ruddell BL (2020) Debates: Does Information Theory Provide a New Paradigm for Earth Science? Sharper Predictions Using Occam's Digital Razor, Water Resources Research 56 (2): e2019WR026471

# Can we use hydraulic handbooks in blind trust? Two examples from a real-world complex hydraulic system

Vasilis BELLOS[1,2], Panagiotis KOSSIERIS[3], Andreas EFSTRATIADIS[4], Ilias PAPAKONSTANTIS[5], Panos PAPANICOLAOU[6], Panagiotis DIMAS[7], Christos MAKROPOULOS[8]

[1] Democritus University of Thrace, Greece
email: vbellos@env.duth.gr

[2,3,4,5,6,7,8] National Technical University of Athens
email: vmpellos@mail.ntua.gr; pkossier@mail.ntua.gr; andreas@hydro.ntua.gr; ipapak@mail.ntua.gr; panospap@hydro.ntua.gr; pdimas@mail.ntua.gr; cmakro@mail.ntua.gr

ABSTRACT

In this work, we investigate whether the parameters of physics-based hydraulic models, omnipresent in every relevant engineering handbook, can be used in blind trust in a real-world complex system. Here, we focus on the discharge coefficient for flows through a sluice gate and the Manning's coefficient for steady flows, and we compare their typical literature values (experimentally derived) against the ones obtained via a "grey-box" calibration approach using real flow data from the complex raw-water conveyance system of Athens, Greece.

## 1. Introduction

In the design and control of hydraulic works, modelling approaches are bounded by two extreme cases: the pure "white-box" and pure "black-box" approach. In the first case, the system is described via physically-based equations, whose parameters are obtained on the basis of hydraulic handbooks. In the second case, data-driven models (such as Machine Learning algorithms) are calibrated against field data, without any prerequisite to obey physical laws and provide physically meaningful parameters. In between these two approaches lies the "grey-box" approach (Bellos et al., 2018) that combines the advantages of these two extreme cases to develop more robust and scientifically sound models. Here, we adopt this approach to investigate the question posed in the title for two widely known hydraulic coefficients: a) the discharge coefficient of sluice gates; b) the Manning's coefficient of a channel. The motivation behind this work is the development of an operational tool to provide advice on the optimal flow control of the complex raw-water conveyance system of Athens, Greece. The control in the lower part of the system, which is our study area, is performed via a series of Λ-type regulation structures, which include a sluice gate and a broad crested weir.

## 2. Real world examples

### 2.1. Sluice gate discharge coefficient

The tool is based on a model that simulates the current situation regarding the flow characteristics in every Λ-type structure and predicts the required opening of the sluice gates for a new desirable discharge. For this reason, the relationships proposed by Wu and Rajaratnam (2015) are used, in which the discharge $Q$ is calculated by:

$$Q = C_d\, a\, B\, \sqrt{2g(H_1 - H_2)} \tag{1}$$

where $C_d$ is the discharge coefficient of the sluice gate, $a$ is the gate opening, $B$ is the width of the channel, $H_1$ is the water depth upstream of the Λ-type structure and $H_2$ is the water depth just downstream of the structure. The latter can be calculated in respect of $y_t$, namely the water depth at some distance downstream of the structure, as follows:

$$H_2 = C_d\, a \left[ 2\left(1 - \frac{C_d\, a}{y_t}\right) + \sqrt{4\left(1 - \frac{C_d\, a}{y_t}\right)^2 + \left(\frac{y_t}{C_d\, a}\right)^2 - 4\left(\frac{H_1}{C_d\, a}\right)\left(1 - \frac{C_d\, a}{y_t}\right)} \right] \tag{2}$$

Due to the discrepancy between the desired accuracy of the flow regulation and the current accuracy of the monitoring system, we adopt a "grey-box" modelling approach, where the discharge coefficient is calibrated in real time. Yet, when these values unreasonable, we apply a global discharge coefficient, as a safety net, which was computed using historical data. In Fig. 1, we give the results of the calibration (in respect to the ratio $a/H_1$) and we compare them with the corresponding theoretical results (Wu and Rajaratnam, 2015).

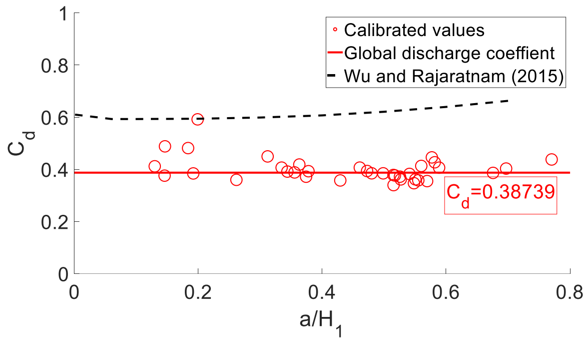


**Fig. 1.** Comparison of the discharge coefficient in respect to the ratio $a/H_1$, as calibrated using historical data, against the theoretical values given by Wu and Rajaratnam (2015).

### *2.2. Manning coefficient*

Furthermore, to indicate the time response between the time instant when a sluice gate is moved (either opening or closing) and the time instant when the latter move is captured by the flow meter, we calibrated a global Manning coefficient of the channel $n$, assuming that flow is steady and uniform. In Fig. 2 we compare this global Manning coefficient against values reported in classic hydraulic handbooks, such as Chanson (2004) and Chaudhry (2008), for several categories of a concrete channel

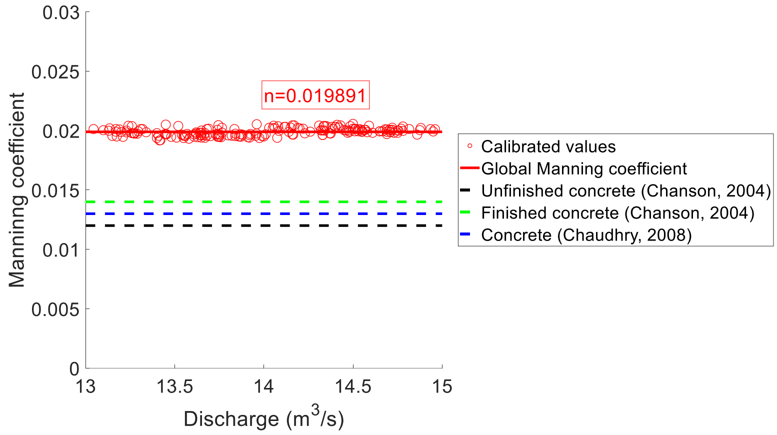


**Fig. 2.** Comparison of the Manning coefficient for several discharges, as calibrated using historical data, against values reported by Chanson (2004) and Chaudhry (2008).

## 3. Discussion and concluding remarks

In this work, we performed a blind test, assuming that two physical parameters have no physical meaning and are calibrated with the absence of any prior knowledge, in a real-world case study. According to our findings, it seems that the calibrated values are on the one hand different from the corresponding values proposed in the literature, which are derived from theory or ideal laboratory conditions. In this respect, this difference should be attributed to the complex reality of field conditions, and lies within the expected range of parametric uncertainty. On the other hand, although we live in the era of big data and artificial intelligence it seems that physics still works, but shifting from theory to practice should be done carefully, by adopting more "grey-box" modelling approaches that account for both physics and real-world data.

**Acknowledgements**
This work was carried out in the framework of Fiware4Water project (2019-2022), receiving funding from the European Union's Horizon 2020 research and innovation programme under grant agreement No. 821036.

**References**

Bellos V, Nalbantis I, Tsakiris G (2018). Friction modeling of flood flow simulations, Journal of Hydraulic Engineering, 144(12), 04018073.
Chaudhry, MH (2008) Open channel flow, Second edition, Springer, 528 pp.
Chanson H (2004) The hydraulics of open channel flow: an introduction, Second edition, Elsevier, 585 pp.
Wu S and Rajaratnam N (2015) Solutions to rectangular sluice gate flow problems, Journal of Irrigation and Drainage Engineering, 118(1), 1113, 56-60.

# Modelling River Ice Breakup and Ice jam Flooding

Hung Tao SHEN[1]

[1] Department of Civil and Environmental Engineering, Clarkson University, USA
email: htshen@clarkson.edu

ABSTRACT

Ice jams following the mechanical breakup of river ice cover can cause severe flooding with rapidly increasing stages and attain higher stages than those associated with ice-free conditions. This paper discusses methods for forecasting the occurrence of breakup and ice jams and the application of a deterministic model to simulate the related flood extent.

## 1. Introduction

A premature breakup is the breakup of a relatively competent ice cover by a river wave (Xia & Shen, 2002) associated with a rapid change in river discharge and water level before the thermal melt out of the cover. These changes in hydraulic conditions often originate from runoff produced by rainfall and snowmelt during a warm spell. However, it is much more challenging to predict since it is a very dynamic process triggered by rapid changes in the weather condition and ice jam releases.

The ice-jam flood level could produce a far higher level than ice-free seasons with the same discharge. The complex mechanisms involved and the usual lack of observed data make it more challenging to determine the timing and severity of ice jam floods than ice-free floods. This paper discusses methods for forecasting breakup and ice jam events and a physical-based numerical model on ice jam floods.

## 2. Forecasting cover breakup and ice jam

Studies on forecasting ice cover breakup and ice jam formation with data-driven and machine learning techniques have been conducted in the last couple of decades, but with limited success (Madaeni et al. 2020). This is partly due to the lack of understanding of the key mechanisms of breakup ice jams. The cover breakup is caused by the river wave produced by a rapid increase of discharge over that during the freezing period before the breakup, $\Delta Q$. The critical $\Delta Q$ for cover breakup varies with the cover strength. A forecast of basin runoff due to snowmelt and rainfall with a hydrological model could be used to estimate the $\Delta Q$. In the U.S., the National Weather Service, https://water.weather.gov/ahps/, can provide the 3-7 days forecast of stage and discharge. The cover strength could be related to the cover thickness obtained from the degree-day method (Shen and Yapa 1985). Whether jam will form after a breakup is governed by the amount of the ice mass (cover thickness) in the ice run, the channel morphology, and the discharge. Wong (2021) presented an example of forecasting breakup and ice jam flooding using runoff and cover thickness models and showed a successful forecast on the occurrence of an ice jam flooding in Feb. 2022 a week in advance. Wong's criteria for cover breakup discharge and related cover thickness for jam formation were determined based on over 60 years of historical data.

The potential for, and severity of, jamming and flooding are strongly related to the suddenness of the onset of the spring freshet, combined with the state of the ice cover at the time that onset occurs. Since the weather condition during the breakup time often changes rapidly, rapid forecasting in a nowcasting mode for possible river ice breakup and ice jam flooding is needed for emergency operations. Figure 1 shows an example of the relationship between jamming potential and the discharge change from pre-breakup to break up and break up cover thickness, based on 81 years of historical data from Grasse River, NY (Shen et al.

2007). Such a relationship could be used to rapid forecast possible ice jam formation. The cover thickness can be determined by a freezing-degree-day method (Shen and Yapa 1985), while the discharge change, ΔQ, could be obtained using the degree-day-melt (DDM) method for forecasting catchment runoff.

## 3. Modeling ice jam flooding

Ice jam formation and release is a highly dynamic process. The resulting flooding from an ice jam event is affected by the basin runoff, channel morphology, thermal-ice condition, and weather conditions at breakup time. Therefore, it is difficult to apply data-driven approaches with limited available satellite images. However, deterministic models have been developed that could be used to model jam-related flooding and potential mitigation schemes (Shen 2010, Huang and Shen 2021). Figure 1b shows an example of the simulated flooding extent validated with satellite images of a breakup ice jam event on the Lower Mohawk River, N.Y. Such a simulation demands a long computing time. However, based on simulations for past ice jam events, a flood risk mapping for flood-prone areas could be developed. Additionally, the model could also be used to develop mitigation schemes for flood management (Huang and Shen 2021).

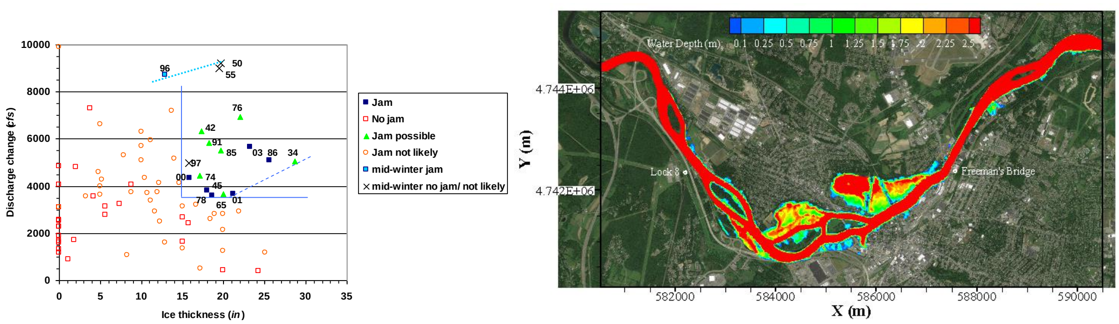


**Fig. 1.** a) Jamming potential with discharge change and cover thickness, Grasse River, NY; b) Simulated water depth - January 2018 Mohawk River breakup jam event.

## 4. Conclusions

This paper discussed methods for forecasting ice cover breakup and jam formation. The cover breakup results from a river wave caused by the increase of discharge over the freezing period discharge, while the formation of ice jam is affected by the ice mass transported after the breakup. The critical values of both of these depend on the cover thickness. The discharge change could be forecasted with a hydrological runoff model or a degree-day-melt method. The cover thickness can be calculated based on the freezing-degree-day method. Criteria on discharge change and cover thickness for breakup and jam formation are discussed. The application of a numerical model for simulating ice jams and related flooding on jam and flood management applications is discussed.

**References**

Huang F and Shen HT (2021) A Numerical Model Study on Ice Jam Flooding in the Lower Mohawk River, Report for Ice Jam Mitigation Panel Reimagine the Canals Task Force, New York Power Authority, Department of Civil and Environmental Engineering, Potsdam, NY 13699-5710, USA, 75 pp.

Madaeni F, Lhissou R, Chokmani K, Raymond S, Gauthier Y. (2000) Ice jam formation, breakup and prediction methods based on hydroclimatic data using artificial intelligence: A review, Cold Regions Science and Technology, 174 (2020) 103032.

Shen, H.T. (2010) Mathematical Modeling of River Ice Processes, Invited review paper, Cold Regions Science and Technology, 62(1), 3-13.

Shen HT, Jayasundara NC, Tuthill A, Mihm J, and Frankenstein G. (2005) Frequency and severity of past ice jams on the Grasse River, Proceedings, 13th Workshop on River Ice, Mount Ascutney, Vermont.

Shen HT, Yapa PD. (1985) A unified degree-day method for river ice cover thickness simulation, Canadian Journal of Civil Engineering, 54-62.

Wang JCW. (2021) Forecasting and management of ice breakups with the inclusion of snowmelt in the degree day method and the use of HEC products, Proceedings, 21st Workshop on the Hydraulics of Ice Covered Rivers, Saskatoon, Saskatchewan, Canada.

# Machine-learning and physics-based numerical modelling for flood level forecasting in rivers: insights from a case study in Italy

Susanna DAZZI[1], Alessia FERRARI[2], Paolo MIGNOSA[3]

[1,2,3] Department of Engineering and Architecture, University of Parma, Italy
email: susanna.dazzi@unipr.it (for author 1)
email: alessia.ferrari@unipr.it (for author 2)
email: paolo.mignosa@unipr.it (for author 3)

ABSTRACT

This paper considers the case study of the Parma River (Italy) to highlight drawbacks in data-driven methods for flood forecasting, in particular their limited flexibility in accounting for possible modifications in the river geometry or roughness, in comparison with physics-based models, which can be updated quite easily.

## 1. Introduction

Early Warning (EW) systems can contribute to preparedness against floods, for example thanks to flood alerts and emergency measures. To forecast flood levels for EW, Machine Learning (ML) methods (i.e. "black-box" models, which are fully data-driven and unaware of any underlying physical relations) are gaining momentum as surrogates for physics-based models, thanks to increasing availability of large datasets.

This work stems from recent analyses concerning flood level forecasting for a case study in Italy, and aims at drawing the attention to some limitations of data-driven models in case some engineering works, such as management of floodplain vegetation, were carried out along the river. To this end, two approaches are here compared: (i) a ML model specifically trained as a surrogate flood routing tool to provide level predictions at a specific section, and (ii) a high-resolution two-dimensional (2D) hydraulic model of the whole river reach.

## 2. Study area, data, and methods

This work focuses on the downstream stretch of the Parma River (northern Italy), from Ponte Verdi gauging station (in Parma city center) to the confluence with the Po River (Fig. 1a). Recorded levels at the intermediate station of Colorno, which is also a "bottleneck" section of particular interest for EW, are available from 2012.

A detailed 2D hydraulic model was available for this river from previous studies (Mignosa et al., 2020), for which the GPU-accelerated shallow-water PARFLOOD code (Vacondio et al., 2017) was used. The high-resolution grid (cell size 2 m × 2 m) was obtained from LiDAR surveys. A detailed roughness calibration was performed by reconstructing two major flood events occurred in Oct-2014 and Dec-2017.

In this area, Dazzi et al. (2021) compared different ML methods for the quick forecasting of flood levels in Colorno, and identified Long Short-Term Memory (LSTM) networks as the most accurate one for peak level prediction. LSTM input data were the hourly values from $t-11$ to $t$ (with $t$ being the current time) of recorded levels at the stations shown in Fig. 1a: Ponte Verdi (upstream), Colorno, and Casalmaggiore (on the Po River downstream). The LSTM output was the level at Colorno at time $t+X$ ($X$ varies from 1 to 9 h). The training dataset included the flood events occurred in 2013-2017, while testing was based on data from 2018-2019.

Both approaches were then applied to two recent flood events, occurred in Dec-2020 and Jan-2021. It is worth mentioning that, during the summers of 2019 and 2020, extraordinary maintenance works for the control of riparian and floodplain vegetation were undertaken along an extended stretch of the river. The implications of these works on the predictive capability of LSTM and 2D models are here shown and discussed.

## 3. Results and discussion

Table 1 reports the error metrics for the evaluation of the LSTM model, in particular the Root Mean Square Error (RMSE) and the Nash-Sutcliffe Efficiency coefficient (NSE), for selected lead times. Results for the testing dataset show that a good predictive accuracy is obtained, though it progressively reduces for longer forecasting horizons (6-9 h). Focusing on single events, it is apparent that the model performance degrades significantly for the most recent floods (Dec-2020, Jan-2021) compared to previous events (e.g. Feb-2019). To analyze this issue, the recorded levels in Colorno are compared with the series of LSTM forecasts for two lead times (3 and 6 h): predicted values are quite close to observations for the Feb-2019 event (Fig. 1b), while the LSTM model overestimates the water levels for the Jan-2021 event (Fig. 1c). Interestingly, the 2D hydraulic model also performs fairly in reproducing the Feb-2019 flood, while levels are largely overestimated for the Jan-2021 event (Figs. 1b-1c). A similar trend was observed for the Dec-2020 event for both approaches.

**Table 1.** Error metrics in the water levels predicted by the LSTM model for selected lead times.

| Dataset | RMSE (m) for different lead times | | | | NSE (-) for different lead times | | | |
|---|---|---|---|---|---|---|---|---|
| | 1 h | 3 h | 6 h | 9 h | 1 h | 3 h | 6 h | 9 h |
| Training (2013-2017) | 0.030 | 0.062 | 0.122 | 0.218 | 0.9996 | 0.9981 | 0.9924 | 0.9757 |
| Testing (2018-2019) | 0.022 | 0.067 | 0.151 | 0.248 | 0.9997 | 0.9973 | 0.9860 | 0.9618 |
| Event Feb 2019 | 0.050 | 0.115 | 0.171 | 0.321 | 0.9993 | 0.9958 | 0.9895 | 0.9525 |
| Event Dec 2020 | 0.076 | 0.240 | 0.416 | 0.595 | 0.9976 | 0.9730 | 0.9044 | 0.7988 |
| Event Jan 2021 | 0.054 | 0.228 | 0.446 | 0.635 | 0.9991 | 0.9831 | 0.9306 | 0.8491 |

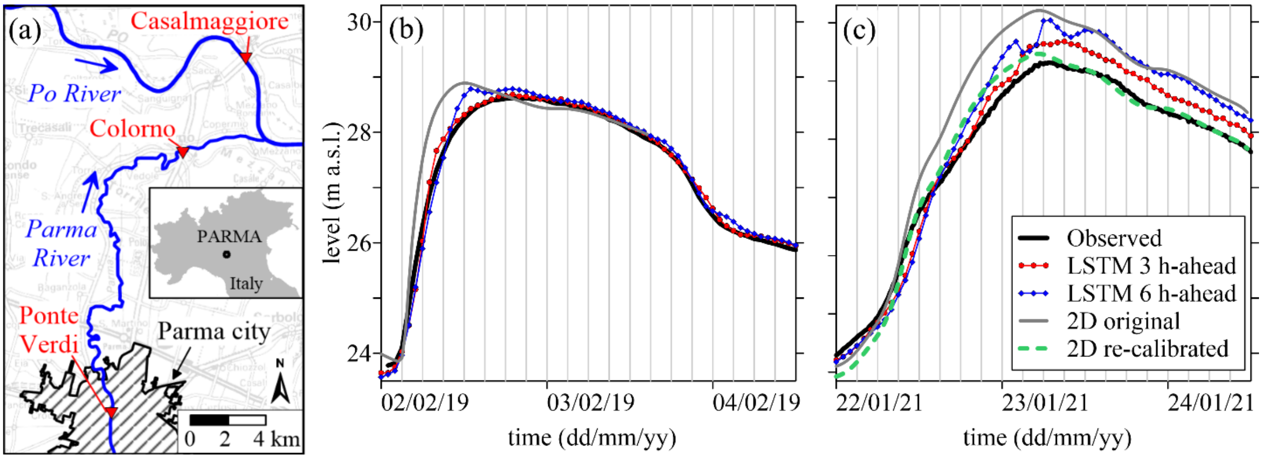


**Fig. 1.** (a) Sketch of the study area. (b) Levels in Colorno for the Feb-2019 event. (c) Levels in Colorno for the Jan-2021 event.

The physical explanation of the over-prediction of flood levels for the recent events is straightforward after recalling that maintenance works on the vegetation were performed in 2019-2020. This entails a significant reduction in the river roughness and a corresponding decrease in the flood levels (discharge being equal). A physics-based model can be updated quite easily to account for such (physical) modification in the river conditions. In this case, for example, the calibration of the 2D hydraulic model was revised by reducing the roughness coefficients until the recorded levels in Colorno were correctly predicted for the Dec-2020 event. Then, when the re-calibrated model was applied to simulate the Jan-2021 event, a good prediction could be obtained again (Fig. 1c). On the other hand, the LSTM model could not be re-trained to consider the new river configuration, since a single flood event does not constitute a large enough dataset to obtain a reliable model.

As regards computational times, the performance is clearly more favorable for the ML model, which requires just a few seconds to provide a prediction for the next 9 h. However, quite competitive runtimes can be obtained using parallelized 2D models. As an example, it is estimated that, thanks to GPU acceleration and latest-generation video cards, the PARFLOOD model would simulate 9 h of physical time in less than 5 min if slightly larger grid resolutions (4-5 m) were adopted for this case study.

## 4. Conclusions

In this work, a drawback of data-driven approaches for flood forecasting was highlighted, i.e. the lack of flexibility in accounting for possible modifications in the river conditions (e.g. river engineering works) until a large enough dataset of flood events is collected, since previous data records become obsolete. Conversely, physics-based models can be easily revised after just one flood event, and have the additional advantage of providing results not only for specific sections, but for the whole river reach (and possibly outside), while parallelization techniques can relieve or overcome the issue of their higher computational demand.

**References**

Dazzi S, Vacondio R, Mignosa P (2021) Flood stage forecasting using machine-learning methods: a case study on the Parma River (Italy), Water, 13(12), 1612.
Mignosa P, Ferrari A, Dazzi S, Vacondio R (2020) Flooding scenarios caused by dam-break/dam-breach at flood control reservoirs, In: Proceedings of the Italian Conference on Integrated River Basin Management (ICIRBM 2020), 41, 55-68, EdiBios (in Italian).
Vacondio R, Dal Palù A, Ferrari A, Mignosa P, Aureli F, Dazzi S (2017) A non-uniform efficient grid type for GPU-parallel Shallow Water Equations models, Environmental modelling & software, 88, 119-137.

# Effects of vegetation on Manning's roughness coefficient in natural streams: a case-study in Attica, Greece

Georgios VAGENAS[1,2], Christos THEODOROPOULOS[1], Anastasios STAMOU[1]

[1]Department of Water Resources and Environmental Engineering, School of Civil Engineering, National Technical University of Athens, Greece (vagenasgiorgos@central.ntua.gr)
[2]Institute of Marine Biological Resources and Inland Waters, Hellenic Centre for Marine Research (HCMR), Athens-Sounion, Greece

ABSTRACT

Ecohydraulic research has recently focused on the effects of streambed and riparian vegetation on the hydraulic properties of river reaches due to the ecological importance of vegetation, since vegetation patches can be used in riverine ecological restoration and flood management strategies. In this study, we measured hydraulic data (flow velocity and water depth) in 98 riverine microhabitats, explored the effect of vegetation on bed roughness and determined the Manning's roughness coefficients for flexible and rigid vegetation in two natural streams of Attica, Greece. The presence of vegetation increased the Manning's roughness coefficients of unvegetated substrates by 44% to 57%. Our results can be used for the proper calibration of hydraulic models in vegetated streams, providing more robust support to relevant restoration or flood management strategies.

## 1. Introduction

Flow resistance is a fundamental component in the investigation of the hydraulic properties in streams. Vegetation patches in perennial, intermittent and ephemeral watercourses can function as: (i) 'ecosystem engineers' by providing habitat components that enhance the presence and conservation of native biota and (ii) geomorphological components that can inhibit unnecessary sediment transport (Theodoropoulos et al., 2021), or cause regional flow and depth elevations (Stamou et al., 2012). We explored the effects of vegetation on river hydraulics (flow velocity and water depth). Instead of using conventional velocity-profile based estimations we applied empirical formulas in order to determine the Manning's roughness coefficients for flexible and rigid vegetation (emergent and submerged), in patches of varying densities, in the Oinoi and Lykorema Streams (Attica, Greece). Our ultimate aim was to contribute to the design and application of proper calibrated hydraulic or ecohydraulic models.

## 2. Materials and methods

We measured flow velocity (V; m/s), water depth (D; m), and the type and density (%) of vegetation patches by using a rectangular frame (0.25 x 0.25 m$^2$) in 98 unpolluted microhabitats of the Oinoi (n=60) and Lykorema (n=38) streams (Attica, Greece), which have similar geo-hydraulic features. Sampling was carried out in spring and summer of 2021. Then, we introduced the field-hydraulic data (V, D) in the two following Manning's roughness equations for emergent rigid vegetation (Eq. a; ERV; $n_{ERV}$) and submerged flexible (Eq. b; SFV; $n_{SFV}$) vegetation:

$$\text{(a)}\quad n_{ERV} = n_o\sqrt{1+\left(\frac{C_d\sum A}{2gAL}\right)\left(\frac{1}{n_o}\right)^2 R^{\frac{4}{3}}}$$

$$\text{(b)}\quad n_{SFV} = K_n 0.183\left(\frac{E_s A_s}{\rho A_i V_*^2}\right)^{0.183}\left(\frac{H}{Y_o}\right)^{0.243}(MA_i)^{0.243}\left(\frac{\nu}{V_* R}\right)^{0.115}\left(\frac{1}{V_*}\right)^{0.243} R^{\frac{2}{3}}S^{\frac{1}{2}}$$

Detailed description of all variables and metrics can be found in Cantisani et al., (2014) and references therein. Finally, we calculated the average Manning's roughness and the average proportional change (PC; Eq. c) of the Manning's boundary coefficient ($n_o$) (the Manning's roughness base for unvegetated substrates) for both streams in total as follows:

$$\text{(c)}\quad PC\ n_o(\%) = \frac{n-n_o}{n}*100$$

by considering that the n value for a clean, unvegetated natural stream is equal to $n_o$=0.03. In case PC was positive, the value indicated a proportional increase in bed roughness compared to the boundary threshold, while negative PC suggested decrease of boundary bed roughness.

## 3. Results and discussion

The average flow velocity in both streams was 0.22 m/s (standard error; SE= ±0.014; min=0.033; max=2.038) and the average water depth was 0.12 m (SE= ±0.004; min=0.01; max=0.64). Vegetation patches had larger n compared to $n_o$, since the PC ranged from 31.7% to 28.44% for the ERV and SFV patches (Table 1). Maximum positive (+) change was calculated for high density (i.e., full) ERV sites (57.07%) and lowest for sparse SFV (13.78%). The n-VR (VR: product of velocity and hydraulic radius) profile demonstrated that higher densities of vegetation had higher Manning's roughness coefficient compared to lower (i.e., sparse) densities for both ERV and SFV (Figure 1A-B), in accordance with previous studies (Errico et al., 2018).

**Table I.** Collective table of the Manning roughness coefficient (n) and the proportional change of the manning's boundary value (PC $n_o$) in varying densities (Full; Sparse; Total | Vegetation patches -VP-) of emergent rigid vegetation (ERV) and submergent flexible vegetation (SFV) in two natural streams of Attica. The parentheses in the Manning's n column indicate the sample size while in the proportional change (PC $n_o$) whether the change was positive (+) or negative (-).

| Vegetation Density | Full (80% ≥ VP ≤ 100%) | | Sparse (0% ≥ VP ≤ 50%) | | Total (0% ≥ VP ≤ 100%) | |
|---|---|---|---|---|---|---|
| Manning (n) | n | PC $n_o$ | n | PC $n_o$ | n | PC $n_o$ |
| ERV | 0.047 (12) | 57.07% (+) | 0.035 (17) | 16.49% (+) | 0.040 (34) | 31.70% (+) |
| SFV | 0.043 (14) | 44.68% (+) | 0.034 (6) | 13.78% (+) | 0.039 (25) | 28.44% (+) |

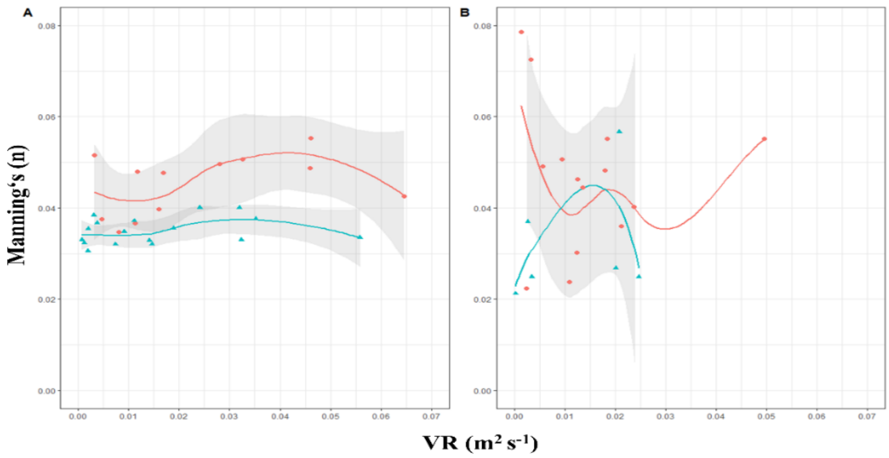


**Figure 1.** Manning's n – VR ($m^2$ $s^{-1}$) profile for the emergent rigid (A) and submergent flexible (B) vegetation. The full vegetated patches (80% ≥ VP ≤ 100%) are coloured with red, while the sparse (0% ≥ VP ≤ 50%) with blue. The regression derived from a local polynomial smoother (span=0.9) while the gray region depicts the standard error.

## 4. Conclusion

Hydro-geomorphological properties in natural streams are affected by vegetation patterns (type and density). We found that rigid and flexible vegetation increased the bed roughness of unvegetated clean substrates up to 57% and 44% in high local densities, respectively. Previous works have efficiently achieved the prediction of Manning's n coefficient through dedicated formulas (Salah Abd Elmoaty and El-Samman, 2000). Subsequently, ad hoc calibrations of the Manning's coefficient derived from local studies can increase the accuracy of regional hydraulic and ecohydraulic models, providing robust support to ecological restoration or flood management strategies. However, spatial and temporal patterns (e.g., seasonality, substrate etc.) should be thoroughly examined since are able to affect the distribution and density of vegetated patches, as well as the hydraulic properties of a natural or artificial stream.

**Acknowledgments**
This work is part of the project 'VEGGIE: Effects of vegetation on river hydraulics and habitat suitability (SARF No. 65228200)', funded by the Basic Research Programme Committee (PEVE 2020) of the National Technical University of Athens, Greece.

**References**
Cantisani, A., Giosa, L., Mancusi, L., Sole, A. (2014) FLORA-2D: a new model to simulate the inundation in areas covered by flexible and rigid vegetation. International Journal of Engineering and Innovative Technology, 3(8), 179-186.
Errico, A., Pasquino, V., Maxwald, M., Chirico, G. B., Solari, L., Preti, F. (2018) The effect of flexible vegetation on flow in drainage channels: Estimation of roughness coefficients at the real scale. Ecological Engineering 120, 411–421.
Salah Abd Elmoaty, M., El-Samman T. A. (2020) Manning roughness coefficient in vegetated open channels. Water Science, 34(1), 124–131.
Stamou, A., Papadonikolaki, G., Gkesouli, A., Nikoletopoulos, A. (2012) Modeling the effect of vegetation on river floodplain hydraulics. Proceedings of the International Conference on Environmental Science and Technology, 14(3), 371-377.
Theodoropoulos, C., Syrmou, E.M., Karaouzas, I., Gritzalis, K., Stamou, A. (2021) Simulated effects of streambed vegetation on river hydraulics and the habitat suitability of freshwater macroinvertebrates. Proceeding of the 17th International Conference on Environmental Science and Technology.

# Application of Machine Learning based surrogate hydrodynamic models in flood simulation uncertainty assessment

Saba MIRZA ALIPOUR[1], Joao LEAL[1]

[1] Department of Engineering and Science, University of Agder, Jon Lilletuns vei 9, 4879 Grimstad, Norway
email: saba.m.alipour@uia.no

email: joao.leal@uia.no

ABSTRACT

Flood modelling process is always incorporated with uncertainty and capturing the uncertainty can be challenging due to the heavy computational requirements. Surrogate models developed based on physical models using machine learning techniques (like Support Vector Regression, SVR) can be used as fast and reliable tools to overcome the computational constrains. Therefore, this study aims to present the uncertainty of 100-year flood water level using intensive Monte Carlo (MC) simulations and to show the applicability and potential of surrogate models for intensive task like uncertainty analysis. The results show that the surrogate model easily reproduces a large number of simulations (more than 25,000) that are required for a converged MC, which would not be feasible using the physical model.

## 1. Introduction

Hydrodynamic models are popular tools for flood modeling purposes. The disadvantage of 2D models is that they require intensive computational efforts, however they provide accurate results. Flood simulation results, are subjected to uncertainty. As a result, a growing body of literature recommends taking the uncertainty into account (e.g., Merwade et al., 2008, Beven et al., 2015). However, this is often hampered by the high computational costs. There are alternative solutions to overcome the computational constrains such as, simplification of the model or using data driven surrogate models. The later mimic physical models, while they demand significantly less computational effort. Therefore, this study seeks to analyze the uncertainty associated with 100-year flood water level using Monte Carlo analysis and to demonstrate the applicability of Machine learning based surrogate models that can tackle the computational demand from uncertainty analysis.

## 2. Methods

### *2.1. Surrogate hydrodynamic model (Emulator)*

In the current study, a surrogate hydrodynamic model (called emulator here after) is trained using Support vector regression (SVR) to mimic a physical 2D model to simulate 100-year floods. The physical model named HiSTAV, is a GPU based 2DH hydrodynamic model (see details in Conde et al. (2020)). The model solves shallow-water equations using a finite volume scheme (unstructured meshes). The model requires inputs such as topo-bathymetric dataset, Strickler roughness coefficient values, runoff coefficient values (in form of raster files) and precipitation intensity and provides water level and flow velocity as outputs. The case of the study is the Tovdal river near Birkeland town area, located in Agder province (Norway). The data of a flood event occurred in 2017 in this region, has been used to calibrate the model. The simulation time for the 1,700 km$^2$ catchment (composed of 401,769 mixed mesh elements) is about 12 GPU hours which is a long run time. Hence, we trained an emulator using Support Vector Regression (SVR) model based on the water level data obtained from the 1,300 simulations performed with the physical 2D model. The details of the model and the process of the emulation can be found in Alipour and Leal (2021). The use of this surrogate 2D hydrodynamic model (with an accuracy of $R^2$ = 0.999, see also the surrogate model performance in Fig. 1-a) allows us to overcome the unaffordable computational resources of running the physical-based model.

### *2.2. Probabilistic approach (Monte Carlo simulations)*

The inputs spaces were randomly sampled, and the flood water level is simulated for each input set until reaching a converged MC. Table 1, presents the input set and their spaces. The roughness and runoff coefficient spaces have uniform distributions, and the precipitation intensity space is an empirical distribution which is modified based on the ensemble of 100-year precipitation values obtained by fitting the GEV distribution to

10 annual maxima precipitation series resulted from 10 different regional climate models using a Bayesian MCMC method (details are presented in Alipour et al., 2021).

**Table 1. Input parameters description and spaces**

| Parameters | | Acronym | Range |
|---|---|---|---|
| Strickler roughness (m1/3/s) | Forests (broad-leaved, coniferous) | Ks_F | 15-40 |
| | River and water courses | Ks_R | 20-50 |
| Runoff coefficient (%) | Forests (broad-leaved, coniferous) | C_F | 50-70 |
| 100 year precipitation (mm/Hour) | | ip | 5-13 |

The use of emulator eases the constraint of the heavy computational demand and enables us to perform 100,000 MC simulations ensuring a stabilized and converged MC. The convergence criteria is defined as the fluctuation in mean and standard deviation (SD) (Ehlers et al., 2019).

## 3. Results

According to the results of 100,000 MC simulations, displayed in Fig. 1-b, the water level values range between 24 m to 32 m, indicating that there is a large degree of uncertainty associated with water level magnitudes.

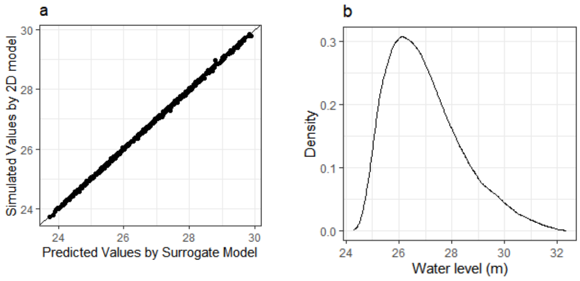


Fig. 1. a. Performance of the emulator and b. 100-year flood water level distribution resulted from 100,000 MC simulations

The MC convergence results are displayed in Fig 2. A full convergence is achieved after about 25,000 simulations, which would not be possible to achieve using a physical model that requires 12 GPU hours for each simulation. Therefore, we suggest flood modelers to use machine learning based surrogate models as a complementary tool to consider the uncertainty and make more safe decisions.

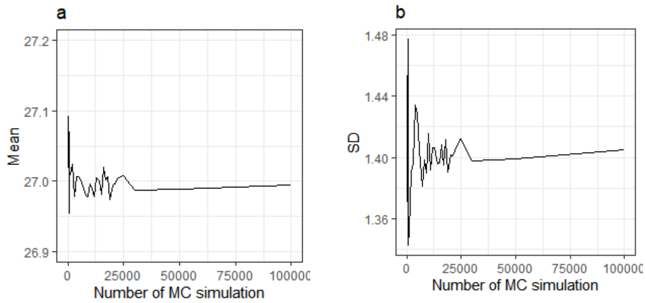


Fig. 2. Convergence of MC simulations through variation in a. Mean and b. Standard deviation (SD)

## 4. Conclusion

Given the large uncertainty found in the flood water level, we highly recommend taking the uncertainty into account. To overcome the computational burdens which is the main obstacle in uncertainty assessment, machine learning based surrogates can be an accurate and fast alternative.

### References

Alipour, S.M., Engeland, K., Leal, J., 2021. Representation of 100-year design rainfall uncertainty in catchment-scale flood modeling: A MCMC bayesian approach. Norsk Vannforening, 04.
Alipour, S.M., Leal, J., 2021. Emulation of 2D Hydrodynamic Flood Simulations at Catchment Scale Using ANN and SVR. Water, 13(20): 2858.
Beven, K., Lamb, R., Leedal, D., Hunter, N., 2015. Communicating uncertainty in flood inundation mapping: a case study. International Journal of River Basin Management, 13(3): 285-295.
Conde, D.A., Canelas, R.B., Ferreira, R.M., 2020. A unified object-oriented framework for CPU+ GPU explicit hyperbolic solvers. Advances in Engineering Software, 148: 102802. DOI:https://doi.org/10.1016/j.advengsoft.2020.102802
Ehlers, L.B., Sonnenborg, T.O., Refsgaard, J.C., 2019. Observational and predictive uncertainties for multiple variables in a spatially distributed hydrological model. Hydrological Processes, 33(5): 833-848.
Merwade, V., Olivera, F., Arabi, M., Edleman, S., 2008. Uncertainty in flood inundation mapping: current issues and future directions. Journal of Hydrologic Engineering, 13(7): 608-620.

# Seasonal dynamic of pharmaceutical and personal care products in rural wastewater treatment plants during COVID-19 pandemic conditions

Kennedy C. CONCEICAO[1], Cristina A. VILLAMAR[2]

[1]Facultad de Ingeniería, Departamento de Ingeniería Civil Química, Universidad de Santiago de Chile, Santiago, Chile
email: kennedy.costa@usach.cl

[2]Facultad de Ingeniería, Departamento de Ingeniería Civil en Obras Civiles, Universidad de Santiago de Chile, Santiago, Chile
email: cristina.villamar@usach.cl

ABSTRACT

Environmental impacts of pharmaceutical and personal care products (PPCPs) are related with potential environmental risk to aquatic ecosystems and effects in the public health. The dynamic of PPCPs generation is influenced by consumption habits, seasonality, and extreme disease situation (e.g., SARS-CoV-2 pandemic). The use of pharmaceutical and personal care products has increased during COVID-19 pandemic. Thus, azithromycin, ciprofloxacin, caffeine, ibuprofen, losartan and triclosan were widely used. The main objective is to evaluate the spatial temporal variability of PPCPs from rural domestic wastewater treatment plants (WWTPs). Samples were collected for PPCPs analysis in influents and effluents from 10 WWTPs during warm and cold seasons. Chromatographic analysis (GC-DAD) using C18 column and solid phase extraction were used. Caffeine, ibuprofen, ciprofloxacin, azithromycin, losartan and triclosan were seasonally monitored. The experimental results showed that PPCP concentrations in the influents and effluents were 11.1–1077.4 µg/L and 0.1–595 µg/L for both seasons, respectively. PPCP removal efficiencies exhibited large variability between 14.7–100% for antibiotics, physic stimulants, NSAIDs, antihypertensives and disinfectants. Therefore, the emerging compounds showed seasonal variation, resulting from the conditions of use, sales, and health such as the COVID-19 pandemic.

## 1. Introduction

Pharmaceuticals and personal care products (PPCPs) are of scientific and public interest. They present a potential threat to the ecosystem and human health, as not completely removed by the WWTPs, and are discharged into the environment, affecting water, soil, and air quality (Pompei et al., 2019). They can generate mutagenic effects, (pandemic COVID-19) health risks, antibiotic resistance and endocrine alteration in organisms exposed to them (Buchan and Quiñones et al., 2016). Consequently, WWTPs generally have primary, secondary and occasionally tertiary treatment phases. Overall, the conventional and non-conventional secondary treatments are capable and found efficient for PPCP removal (Mohapatra and Kirpalani, 2019). Activated sludge is the world's most widely used secondary treatment process, and it has been shown to be one of the better technologies for contaminant removal (Komolafe et al., 2021). This process can remove several PPCP types in WWTPs, such as diclofenac (65%), ibuprofen (92%), naproxen (81%) and bezafibrate (51%) (Lindqvist et al. (2005). Biofiltration technology integrates mechanisms, such as biodegradation, sorption and oxidation. Some removal efficiencies considering biofilters incorporating microorganisms (BM), plants and microorganisms (BPM), earthworms and microorganisms (BEM) and all organisms (hybrid biofilters HB) (Tejedor et al., 2019), reached mean removal efficiencies for pharmaceuticals from <20 to >70% (Class: analgesic/anti-inflammatory, antibiotics, psychiatric and stimulants/psychoactive drugs) (Li et al., 2014). This wide variability evidenced by PPCPs in wastewater is conditioned by seasonal factors, which can also be exacerbated by health crises (COVID-19 pandemic). Indeed, the use of drugs during the pandemic increased by almost 47% (Fortune, 2022). Therefore, this work aims to evaluate the seasonal variation on concentrations and removal efficiencies of PPCPs, in the influent/effluent of rural Chilean WWTPs.

## 2. Methodology

Wastewater samples (influent/effluent) from at least 10 WWTPs from Chilean rural areas, which are located between the regions Valparaíso (UTM: x:317496.4 y:6364765.8), Metropolitan (UTM: x:301908.8 y:6302340.1) and Bernardo O'Higgins (UTM: x:290294.1 y:6196680.5) were monitored. Domestic wastewater samples were of manual and semi-composite type. The monitoring details and campaign protocols are described by Yan et al. (2016). Sampling campaigns during 2021, contemplated two monitoring, one in the warm season (November to March) and another in the cold season (May to September). The wastewater samples were extracted and cleaned by Solid Phase Extraction–Hydrophilic Lipophilic Balance (SPE-HLB) with an Oasis HLB cartridge. PPCPs were separated and quantified by HPLC chromatography. The mobile phase consisted of methanol, formic acid (0.2% v/v) and acetonitrile at 40 °C. The injection volume was 20 µL (Toledo-Neira and Álvarez-Lueje, 2015). The removal efficiency is given by the Eq (1):

$$\text{Removal efficiency (\%)} = \frac{C_i - C_e}{C_i} \tag{1}$$

where $C_i$ and $C_e$ are the influent and effluent PPCP concentrations, respectively.

## 3. Results

The experimental results showed that the concentration of influent/effluent considered in the monitoring were the following. Antibiotics were detected in the influents at concentrations of 66.2-1077.4 µg/L and 25.9-142.9 µg/L, for azithromycin and ciprofloxacin, respectively. Meanwhile, effluent reported values of 25.6–595 µg/L and 15.6–59.9 µg/L were found for azithromycin and ciprofloxacin, respectively. Caffeine was in very prevalent concentrations ranging between 40.1 and 165.8 µg/L in the influents and between 15.2 and 40.8 µg/L in the effluents for the two seasons. Ibuprofen concentration was up to 154.6 µg/L for influents, and up to 42.7 µg/L for effluents in both seasons. Losartan presented concentrations of 50 µg/L in influents and up to 35 µg/L in effluents. Losartan is among the most prescribed drugs in Chile in people with high blood pressure (ISP, 2022). Moreover, the antibacterial agent triclosan was found at average-high (>60 µg/L) levels in influents and low-average in effluents (<40 µg/L). The compounds showed discrepant seasonal variation as their consumption during the year depends on their therapeutic usage, and of the health pandemic Covid-19 (Gwenzi et al., 2021).

**Acknowledgements**

This researcher was supported by the Fondecyt (project grant 11190352). Authors thank the facilities provided to this research by Chilean rural WWTPs. Moreover, authors thank the Interdisciplinary Lab of Water and Sciences Technology (KoYaku Lab), and the Environmental Electrochemistry Lab (LeQMA lab).

**References**

Buchan SJ, Quiñones RA (2016) First insights into the ocean-graphic characteristics of a blue whale feeding ground in Northern Patagonia, Chile, 183–199 pp.

Environmental Protection Agency – EPA (2007) Pharmaceuticals and Personal Care Products in Water, Soil, Sediment, and Biosolids by HPLC/MS/MS, United States, https://www.epa.gov/sites/production/files/201510/documents/method_ 1694_ 2007.pdf (accessed on November 30, 2020).

Fortune (2022) Counterfeit medical products jumped 47% in peak Covid-19, Indian, https://www.fortuneindia.com/macro/counterfeit-medical-products-jumped-47-in-peak-covid-19/107590 (accessed on March 29, 2022).

Gwenzi W, Selvasembian R, Offiong NAO, Mahmoud AED, Sanganyado E, Mal J 2022 COVID-19 drugs in aquatic systems: a review. Environmental Chemistry Letters, 1-20.

Instituto de Salud Pública – ISP (2022) ISP entrega antecedentes de decomiso de más de 10 mil kilos de medicamentos, Chile, https://www.ispch.cl/noticia/isp-entrega-antecedentes-de-decomiso-de-mas-de-10-mil-kilos-de-medicamentos/ (accessed on March 28, 2022).

Komolafe O, Mrozik W, Dolfing J, Acharya K, Vassalle L, Mota CR, Davenport R (2021) Occurrence and removal of micropollutants in full-scale aerobic, anaerobic and facultative wastewater treatment plants in Brazil, Journal Environment Managment, 287, 112286.

Li Y, Zhu G, Ng WJ, Tan SK (2014) A review on removing pharmaceutical contaminants from wastewater by constructed wetlands: design, performance and mechanism. Science Total Environmental, 468, 908-932.

Lindqvist N, Tuhkanen T, Kronberg L (2005) Occurrence of acidic pharmaceuticals in raw and treated sewages and in receiving waters. Water Reseacrh, 39(11), 2219-2228.

Mohapatra DP, Kirpalani DM (2019) Advancement in treatment of wastewater: fate of emerging contaminants. The Canadian Journal Chemical Engineering, 97(10), 2621-2631.

Pompei CME, Campos LC, da Silva BF, Fogo JC, Vieira EM (2019) Occurrence of PPCPs in a Brazilian water reservoir and their removal efficiency by ecological filtration, Chemosphere, 226, 210-219.

Tejedor J, Cóndor V, Almeida-Naranjo CE, Guerrero VH, Villamar CA (2020) Performance of wood chips/peanut shells biofilters used to remove organic matter from domestic wastewater. Science of The Total Environment, 738, 139589.

Toledo-Neira C, Álvarez-Lueje A. (2015) Ionic liquids for improving the extraction of NSAIDs in water samples using dispersive liquid–liquid microextraction by high performance liquid chromatography-diode array–fluorescence detection, Talanta, 134, 619-626.

Yan Q, Feng G, Gao X, Sun C, Guo JS, Zhu Z (2016) Removal of pharmaceutically active compounds (PhACs) and toxicological response of Cyperus alternifolius exposed to PhACs in microcosm constructed wetlands, Journal Hazards Materials, 301, 566-575.

# Is missing knowledge hampering the effectiveness of sustainable water management? The cases of Laspias and Lissos rivers, Thrace, Greece

Nena IOANNIDOU, Dionissis LATINOPOULOS, Anastasia MIRLI, Cate A. BAKALAKOU, Maria KARASANI, Chrysoula NTISLIDOU[1], Ifigenia KAGALOU[1], Christos S. AKRATOS[1]

[1]Civil Engineering Dpt, Democritus University of Thrace,Xanthi, Greece,
email: ikagkalo@civil.duth.gr

ABSTRACT

More than half of the European (EU) water bodies still lag behind the 2000/60/EC directive due to various reasons. A complete, updated, and holistic knowledge base is central in forming a proper monitoring suite, within a tailored management scheme. In Eye4Water project, a series of hierarchical procedures was followed to properly describe and quantify the status quo of two lesser researched river basins and finally assess the knowledge gaps. The aim is to gather the current knowledge through systemic literature review in a hyper-matrix, to organize it through conceptual models, assisting management, embedded with indices, map it and finally assess the actual knowledge gaps to form properly the monitoring targets. The case studies are two heavily modified (partly or entirely) riverine systems, located in Thrace, in rural peri-urban basins, having tributaries with intermittent flow, fragmented habitats, receiving multiple pressures, but being still systems of major economic and environmental importance for the area. The methodology that was followed revealed important lack in our knowledge on four main categories: pressures, environmental quality, monitoring systems and land/resources uses. The identified gaps may hamper the decision making but, in early stages, can describe a "roadmap" to adjust the monitoring scheme and prioritize management goals.

## 1. Introduction

The need to upscale water management' effectiveness across Europe could never be more urgent. Sustainable water management is crucial to ensure the capacity of both natural and human systems to adapt to changing conditions and crises, among other challenges. The 2020 State of the Environment Report confirms that even though more than 20 years have passed since the Water Framework Directive (WFD) adoption, more than half of EU freshwaters fail to achieve "good ecological status" (EEA 2019). WFD introduces a framework for a "basin approach" in line with Integrated Water Resources Management paradigm (Bielsa and Cazcarro 2015). Specifically, in Mediterranean basins, sustainable water management is crucial not only for negating the multiple pressure effects that the water bodies are subject to, but also for ensuring the multiple related ecosystem services. Knowledge synthesis as a procedure is governed by a wide range of methods synthesizing the best available information regarding a topic in a systemic way, to support decision making (Dicks et al., 2018). Indices have the possibility to describe an issue in a simplified and targeted way, to disseminate measurable and comparable information, and determine the distance from a management goal. Many sets of globally accepted indices are designed for specific matters. Conceptual models incorporating indices for management, are fundamental tools for communication strategic planners and decision makers through the logical framework and the information coding they provide. Gap Analysis is a way to visualize the distance from optimal target by identifying practical deficiencies or knowledge lack.

The aim of this research is to introduce a hierarchical approach to gather the current information on a variety of fields, to synthesize knowledge, to group and communicate quantified indices to finally identify the gaps which may hamper the effective decision making. A Second aim is to provide an overview for two lesser researched rivers of primary importance for the local community, located in Thrace, North Greece. Laspias river watershed is a mountainous/agricultural area of 212 km$^2$ that flows into a Ramsar protected coastal zone. It is a Heavily Modified Water Body (HMWB) subject to several pressures as landfill, Wastewater Treatment Plant, intense industrial and agricultural activity and livestock units. Lissos river catchment covers 1486 km$^2$ hosting a wide variety of habitats and a Ramsar protected estuary. It is a HMWB and suffers from similar pressures, along with sand extractions and flow intercepting constructions.

## 2. Applied Methodology

### 2.1. Literature review, knowledge synthesis and SWOT-PEST analysis

A literature review was conducted using Google Scholar to retrieve publications describing the status quo of the basins, without time constraints, using a list of keywords. These were combined with datasets collected by national, regional and local authorities, institutions or international geospatial services. Knowledge Synthesis was applied using the Scoping Review method, to assure objectivity. The data gathered formed the basis for a combined SWOT-PEST analysis model. The two models create a management hyper-matrix that integrates all administratively useful information to define the current state of the study areas. The connection of the SWOT analysis with the PEST model is accomplished by incorporating in each branch of the SWOT the terms of the PEST. Based on the results, four fields were analyzed: *Pressures, Environmental Quality, Monitoring Systems and Land/Resources Uses* where some indicators from the Common International Classification of Ecosystem Services, Sustainable Development Goals and United Nations Statistics Division sets were selected to describe the main characteristics of each field.

### 2.2. GAP analysis

To quantify the deviation from the desired management state (where we are and where we want to be) and prioritize management actions, a Knowledge Gap Analysis was conducted in three steps (Latinopoulos et al. 2018). The first step is to accurately outline and define the objectives. This is the desired knowledge level (100% of the target value). The desired management objective was derived from guidelines, initiatives, as well as national and international standards, such as the WFD. A number of equally distributed questions, based on the indicator sets, were selected to reflect the preferred state in all four categories. In the second step, the questions were "graded" adopting a five-level scale with a percentage return of 20%. The third step was to estimate the gap, which stems from the difference between current and desired level.

## 3. Results and Discussion

The analysis revealed the bigger gaps in *Pressures*, a category related to environmental health and human wellbeing while the *Land and Resources Uses* in the system are better known (Fig 1). The environmental state, as expressed by the *Environmental Quality* category reflects the majority of available scientific information and, as a percentage stands close to the *Monitoring Systems category*.

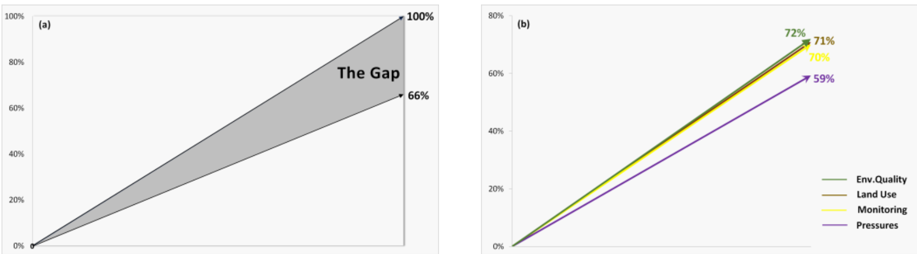


**Fig. 1.** Knowledge Gap plot (a) for the average and (b) for the four pilot categories.

Knowledge Gap Analysis is a useful and effective tool for defining the lack of information, offering a new perspective on environmental management practices for assessing both management and environmental performance. In this research, the two waterbodies revealed an important knowledge gap and this assisted in monitoring prioritization and management design. Eye4Water project, will contribute to improve the current state, support regional development and minimize this "gap" through the development of a monitoring strategy, the provision of predictive tools, innovative technology and collaboration with stakeholders.

**Acknowledgements**

The research was performed under Eye4Water project (MIS 5047246), Co-financed by Greece and the European Union - European Regional-Development Fund

**References**

Bielsa J, Cazcarro I (2015) Implementing integrated water resources management in the Ebro River Basin: from theory to facts. Sustainability, 7(1), 441-46

Dicks LV et al. (2018) Knowledge synthesis for environmental decisions: an evaluation of existing methods, and guidance for their selection, use and development: a report from the EKLIPSE project. 84 pp, http://www.eklipse-mechanism.eu/apps/Eklipse_data/website/EKLIPSE_D3-1-Report_FINAL_WithCovers_V6.pdf. Accessed December 2021

EEA (2019) 'The European environment - state and outlook 2020. Knowledge for transition to a sustainable Europe, Luxembourg: Publications Office of the European Union, 499 pp.

Latinopoulos D, Sidiropoulos P, Kagalou I (2018) Addressing gaps in environmental water policy issues across five Mediterranean freshwater protected areas, Water 10(12), 1853

# Expectations and challenges in smart rice terrace farming systems in remote rural areas for sustainable climate-resilient society

Daisuke NOHARA[1], Yoriyuki YAMADA[1]

[1] Kajima Technical Research Institute, Japan
email: noharad@kajima.com
email: yoriyuki@kajima.com

ABSTRACT

Rice terrace farming is a traditional rice cultivation system that has been developed in mountainous areas since more than hundreds of years ago. It usually consists of multiple small paddy fields cultivated stepwise on steep hills, which forms a unique landscape. In addition to their landscape harmonized with the nature, rice terraces have various functions such as higher quality food production, slope stabilization, flood retardation and diverse ecosystems, all of which can contribute to improve sustainability of the society. On the other hand, some rice terraces have been abandoned recently, due to depopulation and aging in rural communities, as well as low economic efficiency arising from difficulty in introducing large-scale agriculture. This work introduces expectations and challenges in smart rice terrace farming that has been experimentally introduced in rural areas in Japan recently in order to overcome the situation where rice terraces and their multiple functions have been vanishing. The work also depicts the potential advantages of advanced rice terrace farming systems in climate change mitigation and adaptation, which can contribute to development of sustainable climate-resilient society.

## 1. Rice terraces and their multiple functions

Rice terrace farming is a traditional rice cultivation system that is commonly seen in the countries where wet rice agriculture is popular in mountainous areas. Rice terraces usually consist of multiple small paddy fields cultivated stepwise on steep hills, which has developed characteristic landscape and water management systems (**Fig.1**). Considering their excellent cultural values and beautiful landscape harmonized with nature, some of the rice terraces have been registered to the UNESCO World Heritage sites. Such traditional landscapes also become important scenic resources for rural areas, which greatly contribute to rural economy.

In addition to their beautiful traditional landscape, rice terraces have various functions that are important for sustainability of rural communities. They contribute to prevent landslide disasters due to heavy rainfall by stabilizing the slope on which they are located. Irrigation on the rice terraces stabilizes the groundwater level, which also contributes to prevent landslides. In the event of heavy rainfall, rice terraces can provide a flood retarding function by storing rainwater. They are usually irrigated by using groundwater in the mountain slope that contains rich minerals, which enables to produce higher quality of rice that can be traded at a high price. Irrigation systems of rice terraces in various local hydrologic conditions have nurtured unique ecosystems that can enhance biodiversity. These functions are important not only to rural society, but also to whole society including urban areas. Considering their important roles in various aspects described above, studies have been conducted to investigate their multidisciplinary values.

## 2. Challenges in rice terrace farming in remote rural areas in Japan

Rice terraces have been well developed in mountainous areas in Japan since hundreds of years ago. Despite the advantages of rice terraces described above, rice terrace farming in such remote rural areas faces challenges in its sustainability in recent years. Agriculture in flatlands has been successfully modernized and mechanized by introducing large-scale agriculture with centralized water supply systems in Japan. It is, however, difficult for rice terraces in hilly areas to introduce such large-scale agriculture, because paddy fields on the steep slopes are not suitable for firm land readjustment to create a big rectangular unit of firm land which has an advantage in increasing agricultural efficiency by introducing mechanization. Farming in rice terraces therefore requires great care, which degrades farm productivity. Furthermore, remote rural areas in Japan have been suffering from depopulation, aging society, and declining birthrate. Due to this recent social structure, Japanese remote rural areas have also faced a shortage of young farmers. For these reasons, some of rice terraces in those areas have been abandoned, which degrades various functions of rice terrace farming systems.

**Fig. 1.** Rice terraces and new smart farming technologies in remote rural areas in Japan: (a) Overview of Hoshitoge rice terraces, (b) smart surveying of field level using UAVs, and (c) automated water supply system installed into the paddy field.

## 3. Smart farming systems for rice terraces in remote rural areas

As one of the measures to overcome the challenges in rice terrace farming systems in remote rural areas in Japan, smart farming (SF) systems are expected to increase the sustainability of rice terrace farming by improving agricultural efficiency. In Hoshitoge rice terraces (**Fig.1**), which are located in remote rural areas in Tokamachi City, Niigata Prefecture, a heavy snowfall area near the coast of the Japan Sea, experimental introduction of new SF approaches has started to investigate the effectiveness of such technologies in making rice terrace farming more efficient. Those smart technologies include: surveying the difference in elevation in the paddy field by unmanned aerial vehicles (UAVs), semi-automated leveling of the field surface by use of construction machines operated by information and community technology, and smart water management with monitoring of water level and temperature in the paddy fields as well as use of automated water supply system. Sensors used in those smart facilities are equipped with small solar-power panels, which allow them to supply energy by themselves. Although some of these technologies have been applied successfully to large paddy fields in flatlands, it was a challenging attempt to introduce them into farming in the rice terraces that have unfavorable terrain conditions for common SF technologies. The results of experimental introduction showed potential effects of SF on mitigating work burden in rice terrace farming, which can provide increased opportunity not only for experienced elderly farmers to continue agriculture in remote rural areas, but also for less experienced farmers such as young urban citizens or women to participate in farming in these areas.

## 4. Expected role of smart rice terrace farming in climate change mitigation and adaptation

There are growing concerns about impacts of changing climate on resilience and sustainability of society in Japan. Extreme heavy rainfall would occur more frequently in the future, which can bring more chance of large-scale floods and landslides. On the other hand, severe droughts may occur more frequently in the future due to changes in seasonal rainfall patterns, evapotranspiration, and snow process. Food security and healthy ecosystems would be threatened by increase in heat waves and water temperature induced by climate change. Smart farming is expected to become a prospective countermeasure against such challenges posed by climate change through enhanced multidiscipline functions of rice terraces. Rice terraces and distributed farm ponds can be used for flood retention if their water level can be lowered by smart management prior to floods considering real-time forecasts. Preserving rice terraces increases the protection level against landslides. Farming in mountainous terraces has more advantage in resilience against global warming over that in flatlands, because rice terraces are located in a cooler climate and therefore less susceptible to heat waves. Similarly, management of water amount and temperature is easier in terraces as they can use snowmelt water that is more available at high altitudes. A rich amount of water and difference in elevation in the terraces also give a good potential for small hydropower generation, which contributes to carbon neutral and climate change mitigation. Although rice terraces are expected to become an effective green infrastructure for climate-resilient society, there are still major challenges to evaluate the effectiveness of improved rice terrace farming on climate change mitigation and adaptation. Japanese rice terraces usually have very small catchments, often less than 1 $km^2$. Although climate change impacts on hydrological processes have been widely assessed by using results of advanced climate experiments (e.g., Nohara et al., 2018), they are usually based on river basin scale. Impact assessment of climate change on hydrological processes in small catchments is therefore very important. It is also needed to develop an effective method to evaluate multilateral effects and functions of rice terrace farming which contributes to identify the requirements for sustainable and resilient society under changing climate.

**Acknowledgements**

This work was supported by the Demonstration Project of Smart Agriculture (Japan MAFF) and JSPS KAKENHI 19K04616.

**References**

Nohara D, Suzuki S Sato, Y (2018): Impact assessment of climate change on operation of reservoir systems for water use in Japan, Proc. 21st IAHR-APD Congress, Yogyakarta, 755-764.

# Assessing natural clay-based materials to control eutrophication

Ierotheos ZACHARIAS[1], Irene BILIANI[1]

[1] Laboratory of Environmental Engineering, Department of Civil Engineering, University of Patras
email: izachari@upatras.gr
email: biliani.i@g.upatras.gr

ABSTRACT

Sewage discharges, deposition of suspended solids, fertilizer run-offs, and many other anthropogenic activities increase nutrient production of inland and coastal waters, resulting in Eutrophication. Scientists and stakeholders have recognized the urgent need for restoration applications. This work presents chemical restoration methods that aim to reduce the P and N loads within the water column using clay-based materials.

## 1. Introduction

Dynamic balances govern the maintenance of aquatic ecosystems. Eutrophication is an imbalance in function caused by changes in the quantity of nutrients (mainly nitrogen and phosphorus) entering the water bodies. The primary sources of eutrophic pollution are wastewater discharges and agricultural run-offs released into the aquatic environment, coastal population increase, land use, and extensive use of nutrients from agricultural fertilizer use. Eutrophication is observed worldwide in numerous close regions with minimum water renewal, like the Baltic Sea, the Black Sea, the Gulf of Mexico (Le Moal et al., 2019), the Chinese Lake Taihu (Yu et al., 2020), or the Greek Gulf of Amvrakikos (Kountoura and Zacharias, 2011), as well as many others.

Restoring eutrophic water bodies has been identified as a primary goal of the United Nations and European Member-States because they are viewed as crucial to attaining sustainable development. As a result, the European Member States have implemented the Water Framework Directive 2000/60 on 23 October 2000 and acknowledged the need to monitor, protect and restore them (Zacharias et al., 2020). Additionally, two of the UN 17 Sustainable Development Goals for 2030 highlight the need to amend water quality (i.e., Goal 6: "Clean Water and Sewerage" and Goal 14: "Life on Water") (Fehri et al., 2019).

By applying innovative, natural, ecologically friendly clay-based materials, this work aims to identify which materials can chemically restore eutrophic aquatic ecosystems. This study aims to assess the ammonium and orthophosphate adsorbance efficiency of natural clay-based materials.

## 2. Materials and methods

Clay-based materials can be applied for chemical remediation purposes of eutrophic aquatic environments. Scientists, stakeholders, and public authorities disagree with using modified materials. After World War II, many clay-based materials were applied to restore eutrophic water body quality status. This work identifies natural clay-based materials that have been used in aquatic environments and assesses their adsorbance efficiency. This work evaluates the application of zeolite, bentonite, calcite, alum, and perlite as adsorbent materials for eutrophication control.

Ammonium and orthophosphate experiments were performed to observe the behaviour of clay-based materials in time. Ammonium and orthophosphate experiments were also used to investigate the equilibrium adsorbance capacity of the selected natural materials.

## 3. Results and discussion

### *3.1. Zeolite*

Natural zeolite has been investigated in laboratory isotherm and kinetics experiments for phosphorus and ammonium adsorbents. Natural zeolite has a high adsorption capacity, and for this reason, it is widely used as an adsorbent material. Isotherm experiments showed that natural zeolite adsorption capacity increasing with decreasing orthophosphate and ammonium ion concentration. The kinetics experiments performed for natural zeolite concluded that equilibrium is achieved around 8 hours after the introduction of the material. Although the results indicate that the ammonium adsorbance capacity of zeolite is higher than the orthophosphate absorbance capacity, zeolite can be used for both ammonium and orthophosphate control.

*3.2. Bentonite*

Over the past century, Bentonite has been the most widely used eutrophication sorbent material. Removing phosphate that was found in water bodies at low concentrations continues to be a challenging procedure. However, Bentonite is a highly efficient material in orthophosphate reduction, and it is considered to have a high equilibrium capacity and removal at low nutrient concentrations. Bentonite is less effective at removing ammonium ion concentrations from aquatic environments.

*3.3. Calcite*

Another clay-based material that has been evaluated for orthophosphate and ammonium control is calcite. The results indicate that the application of calcite is not able to adsorb ammonium anions. Regarding the applications of calcite in orthophosphate environments, researchers conclude that their application results in alkaline environments, altering the structure of the organisms which dominate in the aquatic environment.

*3.4. Alum*

Alum is another material that has been evaluated in this study. The results indicate that alum has a good adsorbance capacity for orthophosphate control and moderate to inadequate for ammonium ion control. Researchers support that alum can no longer be applied as adsorbent material in its natural form because it significantly alters the pH levels of the water body being examined.

*3.5. Perlite*

The last natural material that has been examined in this study is perlite. Perlite presents moderate to poor adsorbance capacity for both ammonium and orthophosphate ions. Therefore, the researchers believe that natural perlite cannot be used as an adsorbent material in its raw form.

## 4. Conclusions

Developing effective natural water treatment technologies is becoming more critical as the circular economy approach progresses. The research is part of the BLUE-GREENWAY project, whose primary purpose is to achieve maximum reductions in ammonium and orthophosphate compounds without altering the natural aquatic environment. Also, researchers agree that there is no one-size-fits-all strategy for restoration. Each aquatic environment is distinct and is governed by a unique collection of characteristics, environmental circumstances, interconnectedness, and the species that exist or function inside it. As a result, scientific monitoring and consultation are critical for determining the most effective technique and parameterizing the methodological approach for ecosystem long-term ecological and sustainable restoration.

**Acknowledgements**

This work was created as part of the project "BLUEGREENWAY: Innovative solutions for improving the environmental status of eutrophic and anoxic coastal ecosystems," funded by Iceland, Liechtenstein, and Norway through the EEA and Norway Grants Fund for Regional Cooperation.

**References**

Fehri R, Khlifi S, Vanclooster M (2019) Disaggregating SDG-6 water stress indicator at different spatial and temporal scales in Tunisia, Science of the Total Environment, 694, 133766

Kountoura K, Zacharias I (2011) Temporal and spatial distribution of hypoxic/seasonal anoxic zone in Amvrakikos Gulf, Western Greece, Estuarine, Coastal and Shelf Science, 94, 123–128

Le Moal M, Gascuel-Odoux C, Ménesguen A, Souchon Y, Étrillard C. Levain A, Moatar F, Pannard A, Souchu P, Lefebvre A, Pinay G (2019) Eutrophication: A new wine in an old bottle?, Science of the Total Environment, 651, 1–11

Yu C, Li Z, Xu Z, Yang Z (2020) Lake recovery from eutrophication: Quantitative response of trophic states to anthropogenic influences, Ecological Engineering, 143, 105697

Zacharias I, Liakou P, Biliani I (2020) A Review of the Status of Surface European Waters Twenty Years after WFD Introduction, Environmental Processes, 7, 1023-1039

# Water quality in urban rivers: River Fucha Case in Bogota, Colombia

Luisa URIBE[1]

[1] Universidad Nacional Abierta y a Distancia - UNAD, Colombia
email: luisa.uribe@unad.edu.co

ABSTRACT

The largest city in Colombia, Bogota, is crossed from east to west by four rivers. All of them discharge their waters into the Bogota River. One of them, the Fucha River, originates in an exclusive ecosystem, Páramo Cruz Verde. The Fucha river was divided into four sections to evaluate its quality standards. The Instituto de Hidrología, Meteorología y Estudios Ambientales (IDEAM) established the General Quality Index for Surface Waters (ICACOSU), which evaluates quality in a range between Excelent to Very deficient. The Secretaria Distrital de Ambiente (SDA) established quality standards for the Fucha river 8 years ago. However, the measurements of water quality parameters and the indices show that the river does not reach the minimum standards for existence of captive life. We monitored 16 points and calculated ICACOSU for sections 1 to 3 of Fucha River. In particular, we found that Fucha river starts in good range and finishes in very deficient range. In particular, section 2 starts with a Medium range and ends in Bad range due to increase in total coliforms (TC) from 0.00 MPN/100 mL to $9.59 \times 10^7$ MPN/100 mL. On the other hand, section 3 starts with a bad range and ends in very deficient range due to reduction in concentration of dissolved oxygen (DO) from 9.75 mg/L to 0.17 mg/L. The detailed study of the quality of the river allows establishing minimum values of parameters such as DO and TC that enable aquatic life in the water.

## 1. Introduction

The capital of Colombia is Bogota City, which has four rivers that cross the city from east to west. Namely Tunjuelito, Fucha, Salitre, and Torca. All of them discharge their waters into the Bogota River, which ends in the Magdalena River, which finally flows into the Pacific Ocean. Complying with international commitments, such as Millennium Development Goals (MDG) Goal 6, which ensures access to water and sanitation for all, and Organisation for Economic Co-operation and Development (OECD) provision on water governance, Colombia created a National Policy for the Comprehensive Management of Water Resources, which expires in year 2022 and needs a proof analysis. This policy regulates Planning and Management Plans for Hydrographic Basins (POMCAS) and proposes water quality standards (Cerón-Vivas et al., 2019; Romanelli and Massone, 2016; Trujillo-Zapata et al., 2020).

The Fucha River grows up in an exclusive ecosystem: Páramo de Cruz Verde into the Andes Mountain range. This important river is located just five kilometers from the edge of the city. Due to city administration, it is divided into four sections, to establish its water quality and review fulfillment of water quality standards. The SDA has only 5 monitoring points along the Fucha river. We evaluated ICACOSU at sections 1, 2 and 3 with 16 monitoring points, and soon it will be evaluated at section 4. The fulfillment of the urban water quality standards is the way for the achievement of real decontamination of Bogota River (Peña et al., 2016). Therefore, knowing the current state of urban rivers is the added value offered by this research project, which allows stakeholders to make significant decisions.

## 2. Materials and methods

The research project determined ICACOSU using the following physical, chemical, and biological parameters: dissolved oxygen (DO), total suspended solids (TSS), chemical oxygen demand (COD), Electrical conductivity (EC), pH, total coliforms (TC), and biological oxygen demand ($BOD_5$). Compliance with regulatory quality standards was analyzed. The bibliographic sources of environmental authorities were reviewed, including land use and territorial entities involved. Bogotá is divided into 16 localities; each one establishes land use and permissible development activities. The Fucha river crosses five localities: San Cristobal, Antonio Nariño, Puente Aranda, Fontibón and Kennedy.

Reconnaissance tours in the Fucha River were carried out to locate the main domestic and industrial discharges points. Therefore, 16 monitoring points were established according to access to the river, morphology of the river, and the identified discharge points. Water samples were taken in these 16 points during the dry season of April 2018 and September 2020. On site parameters DO, EC and pH were measured. In the laboratory, parameters TSS, COD, TC and $BOD_5$ were analyzed. Samples were analyzed according to Standard Methods and using properly calibrated equipment. Then, the ICACOSU was calculated based on the following equations:

$$ICACOSU = ICACOSU_{fa} * 0.8 + ILAG * 0.2 \quad (1)$$

where: *ICACOSU*: water quality index for surface streams in general. $ICACOSU_{FA}$: the aggregate index of physicochemical quality. *ILAG*: the Environmental Capacity Index.

$$ICACOSU_{FA} = (Si_{DO}*0.2)+(Si_{TC}*0.18)+(Si_{TSS}*0.15)+(Si_{BOD}*0.15)+(Si_{COD}*0.12)+(Si_{EC}*0.12)+(Si_{pH}*0.08) \quad (2)$$

where: $Si_{OD}$: DO saturation percentage sub-index, $Si_{SST}$: TSS subindex, $Si_{DQO}$: COD subindex, $Si_{pH}$: pH subindex, $Si_{C}$: TC subindex, $Si_{DBO}$: BOD subindex, $Si_{COD}$: EC subindex

The result is qualitative in the following ranges: 0.00 to 0.25 is Very Deficient, 0.26 to 0.50 is Bad, 0.51 to 0.70 is Medium, 0.71 to 0.90 is Good and 0,91 to 1 is Excellent.

## 3. Results and concluding remarks

ICACOSU along the sections has the following trend: section 1 started with a Good range ending with Medium range (Mora and García, 2020), section 2 started with a Medium range ending in Bad range (Mora and García, 2020), section 3 started with a Bad range ending in Very deficient range (Reyes and Hernández, 2021).

Fucha river in section 1 has the greatest recovery capacity, because the river is not channeled there, and organizations such as the Vida Corporation has worked together with the Local Mayor's Office of San Cristobal to preserve and take care of the Fucha River's watershed. Fucha river in section 2 enters to location Antonio Nariño, it is channeled and begins to across the commercial area of the Restrepo neighborhood. The main problem here is from street dwellers (Leal, 2019). For this reason, Fucha River's watershed is full of waste. Sites like bays, bases of the pedestrian and vehicular bridges are perfect spaces for the accumulation of domestic waste (Leal, 2019). The homeless citizens living on the street along the river increase TC (0.00 MPN/100 mL at point #1 to $9.59 \times 10^7$ MPN/100 mL at point #16). Fucha river in section 3 meets the industrial location Puente Aranda and Fontibón. It receives industrial effluents with a high content of organic matter (Reyes and Hernández, 2021), resulting in reduction of DO from 9.75 mg/L at point #1 to 0.17 mg/L at point #16. The river looses self-purification capacity within only 6 kilometers. Fucha river EC also increases (from 13.75 µS/cm at point #1 to 547.0 µS/cm at point #16). TSS concentration also increases (20.17 mg/L at point #1 to 69.0 mg/L at point #16) due to the discharge of water from the canals San Blas, Albina, Río Seco and Comuneros. The quality standards are fulfilled at half of the points. For this reason, standards do not allow the fulfillment of the quality objectives to be met by 2020. It is also discouraging that the values proposed as quality objectives do not tend to preserve the river as a river but as a drainage channel.

In conclusion, urban water needs an agenda of good water governance to formulate policies and strategies with real implementation. Stakeholder engagement needs data and information to improve policies, also following international policies like ODS6 and OECD.

**Acknowledgements**

Investigación group Metamofo Cobides from UNAD and the students.

**References**

Cerón-Vivas, A., Gamarra, Y., Villamizar, M., Restrepo, R., & Arenas, R. (2019). Calidad de agua de la quebrada Mamarramos. Santuario de Flora y Fauna Iguaque, Colombia.
Peña Guzmán, Carlos Andrés, Melgarejo Moreno, Joaquín, & Prats Rico, Daniel. (2016). El ciclo urbano del agua en Bogotá, Colombia: estado actual y desafíos para la sostenibilidad. 7(6), 57-71.
Romanelli, Asunción, & Massone, Héctor Enrique. (2016). Desarrollo de indicadores ambientales e índice de calidad de lagos someros pampeanos de Argentina con alta intervención antrópica. 7(6), 123-137.
Trujillo-Zapata, S. A., Cortés-Orozco, C. P., Vinasco-Guzmán, M. C., Ortega-Astudillo, J. D., & Cruz-Ospina, C. A. (2020). Evaluación de la calidad del agua en la fuente abastecedora de Pitalito – Huila: Río Guachicos y sus afluentes principales, utilizando los índices de contaminación e índice de calidad de agua 23(2), 182-192.
Mora, Daniela; García José. (2020). Determinación de calidad del recurso hídrico del Río Fucha en los tramos 1 y 2.
Leal, Laura (2019). Influencia de la población en la gestión de residuos sólidos en el tramo 2 del río Fucha - Bogotá D.C.
Reyes, A. & Hernández, J. L. (2020). Determinar el estado actual de la calidad del agua en el tramo tres (3) del Río Fucha según la Resolución No. 5731 de 2008.

# Integration of small-scale hydropower in water management: A case study from Shakimardan, Uzbekistan

Markus REISENBÜCHLER[1], Beatrice MARTI[2], Tobias SIEGFRIED[3], Oyture ANARBEKOV[4], Bertalan ALAPFY[5], Nils RÜTHER[6]

[1,5,6] Technical University of Munich, Germany
email: markus.reisenbuechler@tum.de
email: bertalan.alapfy@tum.de
email: nils.ruether@tum.de)

[2,3] hydrosolutions GmbH, Switzerland
email: marti@hydrosolutions.ch
email: siegfried@hydrosolutions.ch

[4] International Water Management Institute, Uzbekistan
Email: o.anarbekov@cgiar.org

ABSTRACT

Sustainable water management is one of the major issues of our time, largely driven by climate change. The EU Horizon 2020 project Hydro4U contributes to solve this challenge by showing how decentralized small hydropower can be integrated into a forward-looking water management in remote areas, and how benefits can be created on different levels. The Uzbek Shakimardan enclave in Central Asia serves hereby as a study site.

## 1. Introduction

Hydro4U is an EU funded project to demonstrate sustainable small-scale hydropower (SHPP) in Central Asia (Reisenbüchler et al., 2021). We demonstrate how SHPPs can contribute to solving the current and future challenges posed by the energy transition, but especially by climate change. Central Asia is a particularly challenging region. On one hand, there are already numerous conflicts about water, and on the other hand, studies indicate that climate change will hit this region particularly hard suggesting that air temperature will increase significantly over the next decades. It is obvious that this will have an impact on the water balance, and thus possibly exacerbate the conflicts (Siegfried et al., 2012). The following article introduces a demonstration site in Hydro4U and presents aspects from the Water-Food-Energy-Climate-NEXUS.

## 2. The Shakimardan Demonstration site

### *2.1. Site description*

The remote area of Shakimardan is an Uzbek enclave surrounded by Kyrgyzstan in Central Asia. The enclave is located at an average altitude of 2764 m above sea level and includes the glacier-formed main channel Shakimardan River formed by the tributaries Koksu and Kara Kecheuu. The region is still very close to natural state, although downstream in Kyrgyzstan and Uzbekistan there are numerous weirs in the river and water is diverted and extracted. Together with the local company Uzbekgidroenergo, Hydro4U will build an innovative Francis-container power plant (approx. 2MW) in the Koksu River to supply the remote area with green energy.

### *2.2. Hydrology and Climate Change*

Due to the expected change in temperature and thus hydrology, Hydro4U partner Hydrosolutions performed a detailed hydrological modeling. Thereby, historical data from Uzbek Hydromet archives could be used, which contains a time series of the monthly (mean-max) discharges from 1948 to 1998 of river Koksu. Thereby, clear trends are already recognizable (Fig. 1.a.), which indicate an increase of melt water as well as precipitation in the months May to October at Koksu river. Using data from the Chelsa project (WSL, 2022), for instance, an increase in air temperature (0.23°C to 5.9°C) and precipitation (760 mm/a to 804 mm/a), comparing the periods of 1981-2010 to 2071-2100, was predicted for this area (using SSP585, CMIP6). Incorporating different shared socioeconomic pathways (SSP), changes of the hydrological regimes were predicted and possible flow duration curves were determined – one of the most important design value for the sustainable layout – now and in the future – of the SHPP and the entire water management (Fig. 1.b.).

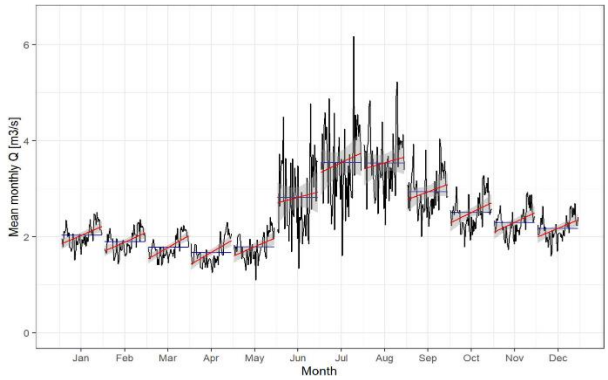


Fig. 1.a. Trends in mean monthly discharges from 1948 to 1998.

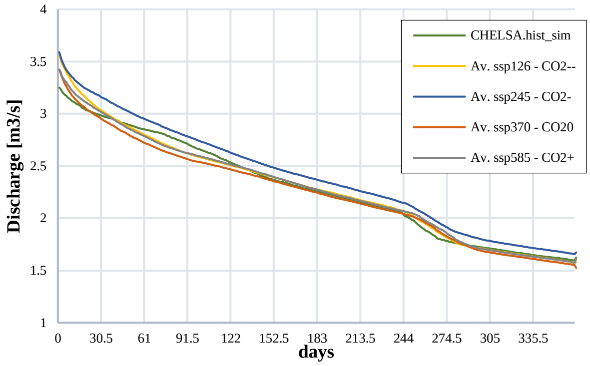


**Fig. 1.b.** Historical and Future Flow duration Curves in Koksu River

### *2.3. Water-Energy-Food-Climate NEXUS*

However, a sustainable impact is not only achieved with the construction of the SHPP. The implementation of the Shakimardan power plant allows the site to be studied with a forward-looking, transnational Water-Food-Energy-Climate NEXUS approach. It is a concern to prevent transnational conflicts through the best possible transparency in water management. The water that is diverted upstream into the power plant, minus the ecological residual flow, is completely returned to the river downstream of the power plant and does not affect downstream sections. This process has already been communicated to the regional population in an extensive stakeholder process, and their concerns and needs have been considered thoroughly. This was especially necessary since many people in the region depend on water directly and indirectly. Figure 2 shows the downstream irrigation system and the irrigated areas. Hydro4U aims to anchor an online based solution for water planning and accounting, named Count4D (https://count4d.pythonanywhere.com/), to link the water consumers, e.g., irrigation sector with water providers.

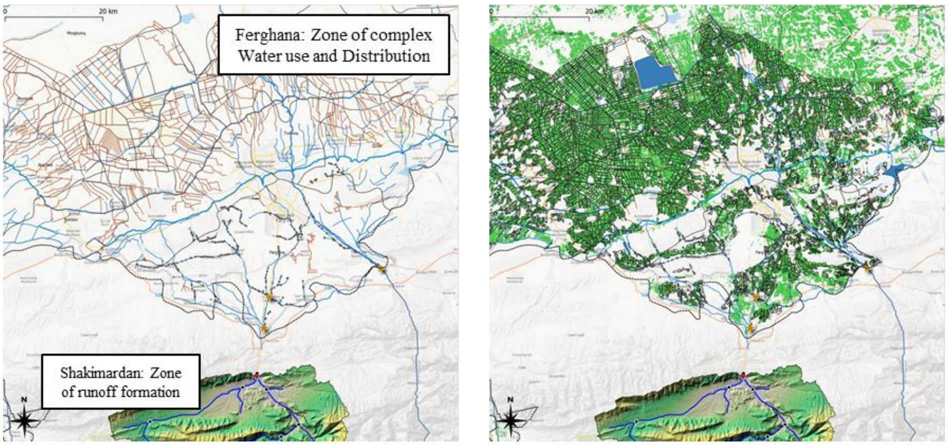


**Fig. 2.** Water Management in Ferghana region downstream of Shakimardan Enclave (left: irrigation network, right: irrigated areas).

## 3. Conclusion

Decentralized small hydropower solutions in remote regions can contribute to the energy transition if they are sustainable. Hydro4U shows with the example of the demonstration site Shakimardan how this is possible. Based on hydrological modeling taking climate change into account, the future water balance could be mapped. The implementation of the hydropower plant is sustainably possible through ecological assessment and management including residual water management. Through stakeholder dialogues, awareness for water is raised and innovative approaches such as the Count4D tool are anchored in the region.

**Acknowledgements**

This project has received funding from the European Union’s Horizon 2020 research and innovation under grant agreement No 101022905. For further details see our homepage: www.hydro4u.eu

**References**

Reisenbüchler, M., Alapfy, B., Rutschmann, P., & Siegfried, T. (2021). Hydro4U - Nachhaltige Kleinwasserkraft in Zentralasien. WASSERWIRTSCHAFT, 12, 10-15.

Siegfried, T., Bernauer, T., Guiennet, R., Sellars, S., Robertson, A. W., Mankin, J., Bauer-Gottwein, P., & Yakovlev, A. (2012). Will climate change exacerbate water stress in Central Asia? Climatic Change, 112(3), 881-899.

WSL. (2022). Climatologies at high resolution for the earth’s land surface. https://www.wsl.ch/de/projekte/chelsa.html

# Digital Twins for Port Facilities Management

Meysam MAJIDI NEZHAD[1], Benedetto NASTASI[2], Giuseppe PIRAS[1], Davide ASTIASO GARCIA[2]

[1] Department of Astronautics, Electrical and Energy Engineering (DIAEE), Sapienza University of Rome, Italy.
[2] Department of Planning, Design, Technology of Architecture, Sapienza University of Rome, Italy.
*Corresponding author: E-mail: meysam.majidinezhad@uniroma1.it

ABSTRACT

This study aims to develop methods and strategies for integrating saving energy generation systems from Renewable Energy Systems (RESs) to manage port facilities. In addition, an infrastructure digitization policy has been implemented to optimize maintenance and energy efficiency processes to achieve ZED (Zero Energy District) in Lazio ports. Finally, a Digital Twin (DT) has been launched using the BIM (Building Information Modelling) and GIS (Geographic Information Systems) software to maximize the energy efficiency measures producing beneficial effects for the investigated area (Lazio port).

## 1. Introduction

Ports can be considered as one of the highly energy-consumed facilities globally. Fossil fuel emissions from ports represent about 3% of the global Greenhouse Gas (GHG) emissions (Lindstad and Eskeland 2016). Recently, ports have begun to use Renewable Energy Systems (RES) to reduce fossil energy demand and GHG emissions (Gibbs et al. 2014). Firstly, the current activities in the port area need to be thoroughly reviewed, which play a crucial role in consumed energy (Woo et al. 2018). Leading to accurate and reliable targeting and planning data types, layers, land and marine parameters analysis can be considered the main bases for informed decision-making in the RESs ports sector. Data from Earth Observation (EO) open-source platforms including their integration with the Internet of Things (IoT) and low-cost sensors along with many software and machine learning methods and deep learning algorithms can be used to develop Digital Twin (DT) intelligent monitoring and design. In this case, DT models can improve the RES efficiency and stability in ports (Cumo 2021,Agostinelli et al. 2021). Furthermore, an intelligent hybrid DT model based on open data and software can be used to manage and predict port facilities (Agostinelli et al. 2022). This is if geographical factors can affect the RES type and amount, and the familiarity level with the technology can be used for DT design and development (Agostinelli et al. 2022). Figure 1 shows the BIM models output in Lazio ports case studies.


**Fig. 1.** Shows BIM models outputs of Lazio ports.

The RESs type concerning local/regional/national industrial activities directly affects the port performance, which can significantly increase their ports efficiency. The geographical location and RESs potential assessment analysis show that solar and wind energy are potentially durable in Lazio ports like other Mediterranean ports. Furthermore, the results show that the Lazio ports have good potential for installing solar PV panels, and also have an excellent ability for micro wind turbines installations. Figure 2 shows the BIM models outputs for PV and macro wind turbines installations in Lazio ports case studies.

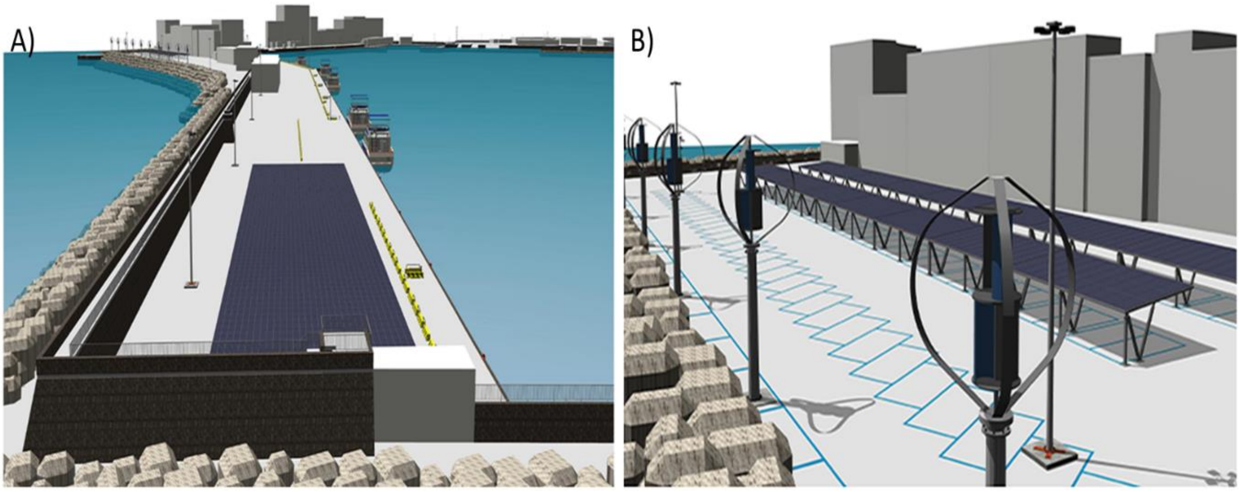


**Fig. 2.** Shows BIM models output of; A) the solar asphalt, and B) the micro wind turbines.

BIM technology enables modelling and processes related to the building models production and analysis in different scenarios. BIM models provide the 3D outputs, and enable shareholders to use low-error data collection and sharing to optimize the process (Dixit et al. 2019). BIM technology also offers a range of easy, practical, operational and versatile tools in the construction industry stakeholders. The technology combines tools to improve BIM acceptance in construction renovation work based on a reciprocal information flow (Daniotti et al. 2020). BIM modelling can be considered an essential step in the DTs delivery journey. Moreover, using BIM models can be considered a process enabling to create and display digital displays in design, construction, and operation (www.buildingsmart.org). Hence, the basic need to update its intelligent evolution to connect information and ideas between all shareholders. BIM models and DT strategies have many similarities. These similarities can be attributed to having common principles such as: improving the user process vision and aligning shareholders and politicians (www.buildingsmart.org).

**Acknowledgements**

This research has been carried out within the project "An integrated multidisciplinary and multiscale digital approach fostering the decarbonisation of port areas" protocol RG12117A8A106E46, funded by the Sapienza University of Rome. Italy.

**References**

Agostinelli S, Cumo F, Majidi Nezhad M, Orsini G, Piras G (2022) Renewable Energy System Controlled by Open-Source Tools and Digital Twin Model: Zero Energy Port Area in Italy. Energies 15(5).
Agostinelli S, Cumo F, Guidi G, Tomazzoli C (2021) Cyber-Physical Systems Improving Building Energy Management: Digital Twin and Artificial Intelligence. Energies 14(8): 1–25.
Cumo F (2021) DIGITAL TWIN for CRITICAL INFRASTRUCTURES: The VENTOTENE ISLAND PORT CASE STUDY, ITALY. WIT Transactions on the Built Environment 205: 217–22.
Dixit MK, Venkatraj V, Ostadalimakhmalbaf M, Pariafsai F, Lavy S (2019) Integration of facility management and building information modeling (BIM): A review of key issues and challenges. Facilities, 37, 455–483
Daniotti B, Masera G, Bolognesi CM, Spagnolo SL, Pavan A, Iannaccone G, Signorini M, Ciuffreda S, Mirarchi C, Lucky M, et al (2020) Workshop: BIM4EEB: A BIM-Based Toolkit for Efficient Renovation in Buildings. Proceedings, 65, 17. https://doi.org/10.3390/proceedings2020065017
Gibbs D, Rigot-Muller P, Mangan J, Lalwani Ch (2014) The Role of Sea Ports in End-to-End Maritime Transport Chain Emissions. Energy Policy 64: 337–48. http://dx.doi.org/10.1016/j.enpol.2013.09.024.
Lindstad HE, Eskeland GS (2016) Environmental Regulations in Shipping: Policies Leaning towards Globalization of Scrubbers Deserve Scrutiny. Transportation Research Part D: Transport and Environment 47(2016): 67–76. http://dx.doi.org/10.1016/j.trd.2016.05.004.
Woo JK, Moon DSH, Lee Lam JS (2018) The Impact of Environmental Policy on Ports and the Associated Economic Opportunities. Transportation Research Part A: Policy and Practice 110(October): 234–42. http://dx.doi.org/10.1016/j.tra.2017.09.001.
Www.Buildingsmart. Org/Take-Bim-Processes-to-the-next-Level-with-Digital-Twins.

# Towards integrated modelling of Watershed-Coast System morphodynamics in a changing climate: A critical review from a coastal engineering perspective

Achilleas G. SAMARAS

Department of Civil Engineering, Democritus University of Thrace, PC 67100, Xanthi, Greece
email: achsamar@civil.duth.gr

ABSTRACT

## 1. Introduction

The term Watershed-Coast Systems (WACS), coined by Samaras and Koutitas (2014a), refers to the entities consisting of watersheds of rivers/natural streams and the areas adjacent to their outlets where sediment delivery from the upstream is critical for the balance of the coastal sediment budget, thus playing a key role in long-term evolution of coastal morphology. The study of such systems in a changing climate emerges as an issue of major concern nowadays, as the shift in climate pressures will affect both watersheds and coastal zones, and implications will extend from morphological to ecological and socio-economic ones, threatening ecosystems, cultural heritage, settlements, infrastructure, as well as human life.

From this standpoint, the physical problem in question can be divided into four basic components: (A) climate change; (B) watershed dynamics; (C) coastal dynamics; and (D) integration of the Watershed-Coast System (Fig. 1). Components (B) and (C) have been studied in detail over the years; the last few decades so are (A) and the impact of (A) on (B) and of (A) on (C). Numerical models have been proven essential in the above, with various models and modelling systems currently available which are able to represent natural processes at different scales in space and time. However, the critical component (D) – which independently of (A) defines the essence of the WACS concept – has not been analysed to the extent one would expect to, considering its importance for coastal evolution modelling.

## 2. Coastal morphodynamics and WACS: Concepts and Modelling

The evolution of coastal morphology has been studied extensively by many researchers, starting from purely theoretical concepts for the systemisation of empirical knowledge and observational understanding, up to entire methodological frameworks for the implementation of modelling tools of varying types and complexity in order to simulate natural and human induced geomorphic processes at different spatial and temporal scales.

Nevertheless, even the works that stand out in literature (e.g. Cowell et al., 2003; Peckham et al., 2013; Payo et al., 2017) do present one or both of the following essential limitations when it comes to the study of WACS: (a) the not-integrated study of the terrestrial and coastal fields as an entity and (b) the scales in space and time at which they have been successfully implemented. The first limitation has its basis in the – admittedly extremely complex – interplay between processes taking place in watersheds, coasts and the coastal zone. The second limitation derives from considering how the aforementioned scales relate to actual case-studies of importance for watershed/coastal management and engineering purposes.

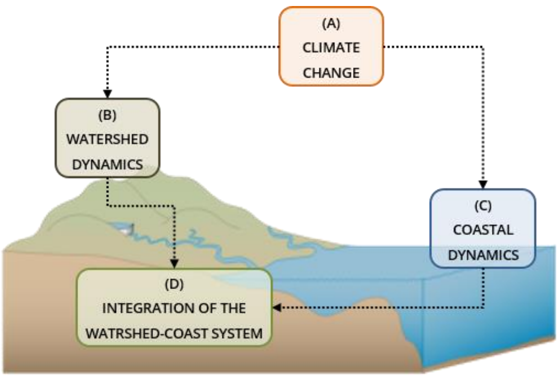


**Fig. 1.** The physical problem in question.

Approaches that have attempted to overcome these limitations have been proposed by two groups: by Samaras and Koutitas (2012, 2014a, 2014b), later adopted by Malara et al. (2020), and by the group led by Prof. Ranasinghe from IHE Delft (works from Ranasinghe, 2016 up to Bamunawala et al., 2021), who also suggested the term Catchment-Estuary-Coastal (CEC) for these systems. Both approaches present certain advantages and disadvantages; at this stage, it can be said that the second approach is better systematized and presented.

## 3. Towards the integrated modelling of WACS for management and engineering purposes

Climate crisis and its observed impacts highlight the need for urgent action in order to mitigate and adapt to climate change in view of a dire future (IPCC, 2022). This action requires bold steps towards translating existing scientific knowledge into policy and practice, a task unlikely to succeed unless a pragmatic approach with focus on real-life applicability is followed. The coastal engineering community must rise to the challenge, as coastal zones – located at the land-sea interface and hosting about two thirds of the world's population – will undoubtedly be at the forefront of all relevant attempts.

In this context, the review presented in this work will first identify the critical issues that need to be addressed moving towards the integrated modelling of WACS for management and engineering purposes in a changing climate, and then evaluate relevant literature on the basis of these aspects. Figure 2 presents a general methodological framework for such an approach. The left part of this flowchart, especially regarding (A), (B), and (C), has been theorised by few other researchers to various extents. However, it is the incorporation of the right part of the flowchart that introduces many of the major challenges ahead.

Accordingly, modelling approaches should be formed and/or evaluated based on the following: (i) inclusion of all four components described in Section 1 and Fig. 1; (ii) consideration of projected climate change-induced changes in management practices and engineering works in both fields (terrestrial, coastal) when defining future scenarios; (iii) applicability to scales suitable for watershed/coastal management and engineering purposes; (iv) adaptability to methods for addressing ecological/socio-economic implications and stakeholders engagement. The model validation aspect in panel (D) of Fig. 2 is also critical from a methodological point of view and will be further analysed.

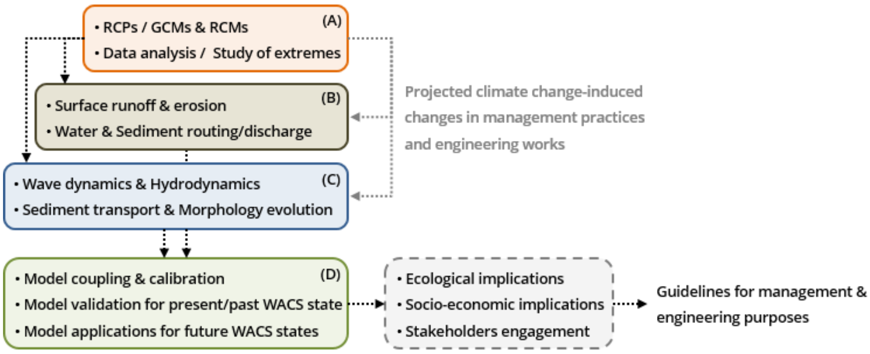


**Fig. 2.** General methodological framework for the integrated modelling of WACS morphodynamics in a changing climate (A, B, C, D with reference to Fig. 1; RCP: Representative Concentration Pathways; GCM/RCM: Global/Regional Climate Models).

**References**

Bamunawala J, Ranasinghe R, Dastgheib A, et al. (2021) Twenty-first-century projections of shoreline change along inlet-interrupted coastlines, Sci. Rep., 11(1), 14038.
Cowell PJ, Stive MJF, Niedoroda AW, et al. (2003) The Coastal-Tract (Part 1): A Conceptual Approach to Aggregated Modeling of Low-Order Coastal Change, J. Coastal Res., 19(4), 812-827.
IPCC (2022) Climate Change 2022: Impacts, Adaptation and Vulnerability, Working Group II Contribution to the Sixth Assessment Report of the Intergovernmental Panel on Climate Change (Final Draft), IPCC, 3676 pp.
Malara G, Zema DA, Arena F, et al. (2020) Coupling watershed - coast systems to study evolutionary trends: A review, Earth-Sci. Rev., 201, 103040.
Payo A, Favis-Mortlock D, Dickson M, et al. (2017) Coastal Modelling Environment version 1.0: a framework for integrating landform-specific component models in order to simulate decadal to centennial morphological changes on complex coasts, Geosci. Model Dev., 10(7), 2715-2740.
Peckham SD, Hutton EWH, Norris B (2013) A component-based approach to integrated modeling in the geosciences: The design of CSDMS, Comput. Geosci., 53, 3-12.
Ranasinghe R (2016) Assessing climate change impacts on open sandy coasts: A review, Earth-Sci. Rev., 160, 320-332.
Samaras AG, Koutitas CG (2012) An integrated approach to quantify the impact of watershed management on coastal morphology, Ocean Coast. Manage., 69, 68-77.
Samaras AG, Koutitas CG (2014a) The impact of watershed management on coastal morphology: A case study using an integrated approach and numerical modeling, Geomorphology, 211, 52-63.
Samaras AG, Koutitas CG (2014b) Modeling the impact of climate change on sediment transport and morphology in coupled watershed-coast systems: A case study using an integrated approach, Int. J. Sediment Res., 29(3), 304-315.

# Operational Oil Spill modeling forced by real-time met-ocean forecasts: A hypothetical scenario for the North Aegean Sea

Panagiota KERAMEA[1], Nikolaos KOKKOS[1], Spyridon NTOUGIAS[1], Paraschos MELIDIS[1], Dionissis LATINOPOULOS, Christos AKRATOS[2], Ifigenia KAGALOU[2], Georgios SYLAIOS[1,*]

[1] Department of Environmental Engineering, Democritus University of Thrace, 67100 Xanthi, Greece.
[2] Department of Civil Engineering, Democritus University of Thrace, 67100 Xanthi, Greece.

*Corresponding author: E-mail: gsylaios@duth.gr, Tel +30 25410 79398, 25410 79743.

ABSTRACT

## 1. Introduction

Oil spills of any size have severe environmental, social, and economical consequences becoming a major hazard to world oceanic health in recent decades. The rise in global oil and gas demand, as well as the corresponding expansion in oil and gas production, particularly from coastal and offshore marine reserves, has greatly raised the potential of inadvertent oil leakage into the sea. In this work, we simulate a hypothetical accidental oil leak release in the North Aegean Sea, in the vicinity of the Dardanelles Strait, the main tanker route connecting the Mediterranean and the Black Sea. The hydrodynamics of the area have been described by Kokkos and Sylaios (2016). An operational oil spill model was used to assess the oil dispersive qualities and disclose the relative magnitude of weathering processes. The OpenOil transport and fate numerical model was used to run numerical simulations. Oil entrainment, vertical mixing, oil resurfacing, and oil emulsification are all part of this study, which combines algorithms with physical processes. The oil dispersion model was coupled to NOAA-GFS and CMEMS real-time met-ocean forecasts. Results focused on the description of oil droplets' movement due to the wind/water circulation, but also on the distribution of oil mass balance and oil mass characteristics, such as oil patchiness.

## 2. Materials and Methods

*The OpenOil Model and Experimental Setup*

OpenOil is a newly-integrated oil spill transit and fate submodule (Röhrs et al., 2019) of OpenDrift, a python-based, open-source code model (Dagestad et al., 2018). The discharged oil is represented by particles with individual parameters such as mass, viscosity and density, also known as Lagrangian elements. Model equations allow the transport of each particle towards its new location due to the established current, wind, and Stokes drift. The model includes algorithms with a variety of physical processes, including oil entrainment by waves (Li et al., 2017), vertical mixing owing to oceanic turbulence (Visser 1997), oil resurfacing due to buoyancy (Tkalich and Chan, 2002) and oil emulsification (Li et al., 2017). The model's physics are very sensitive to the specification of the oil droplet size distribution (Hole et al., 2019), based on the Stokes Law, i.e., sinking velocity is analogous to particle diameter. The oil properties of OpenOil are derived from the ADIOS Oil database (Lehr et al., 2002), an open-source, python-written database including measured parameters of nearly 1,000 different oil kinds.

In this study one scenario was investigated: the release of crude oil to the east of North Aegean Sea and the Dardanelles Strait. The time period for this simulation was 7 days, from 14 March at 00:30 to 21 March at 00:30. The type of oil used was "ODA 2019", with density 802.4 kg $m^{-3}$ and viscosity 10 cPoise. Initially, approximately 1,000 oil particles were released and the initial radius of the spill was set to 2,000 m. The OpenOil model was coupled with real-time winds from NCEP/NCAR (National Centers for Environmental Prediction / National Center for Atmospheric Research) Reanalysis from NOAA GFS (Global Forecasting System). In addition, OpenOil was coupled with hydrodynamic data from CMEMS database (Copernicus Marine Environment Monitoring Service).

## 3. Results

The experiment considers that the oil spill is released near the Dardanelles Strait, and thus, the oil spill will be affected by the Black Sea Water entering the North Aegean Sea with high speeds (Fig. 1a). During the time of the incident, the strong NE-SW surface current jet prevailed, with speeds ranging from 0.2 to 0.5 m/s (Fig. 1d).

Oil particles were moved towards Lemnos, Aghios Efstratios, Sporades and Evia Islands (Fig. 1a). The wind speed in the area ranged from 2 to 11 m/s and was blowing from the ENE (Fig. 1d). At the end of the 7-day simulation, a significant portion of oil particles (~70%) has been beached along the coastline of Imbros, Limnos, Aghios Efstratios and the northern Dardanelles coastline. The remainder (~10%) appears at the sea area near Sporades Islands and Evia Island, and a small portion (~20%) has been beached along their coastline (Fig. 1a). Figure 1b shows that 20 hours after the initial oil release, approximately 40% of the mass was evaporated, 25% of the released oil mass was in the surface, 20% of oil particles were dispersed in the water column, approximately 10% of oil droplets were stranded along the coastline, almost 5% were submerged in the water column, and near-zero levels were biodegraded. Moreover, after 80 hours of simulation only the portion of oil particles being dispersed (~40%) and beached (~20%) increased. Oil properties changed over time as the oil mass balance evolves after oil release, as shown in Fig. 4c. For example, the dynamic oil viscosity remains nearly stable for the first 80 hours of simulation, reaching 100 cPoise, but rises again after the first 100 hours, up to the maximum dynamic viscosity value of 600-700 cPoise (Fig. 4c). Furthermore, the simulation demonstrates that, while the initial oil density was 800 kg m$^{-3}$, it approaches 1,000 kg m$^{-3}$ after the first 20 hours until the end of simulation (Fig. 4c).

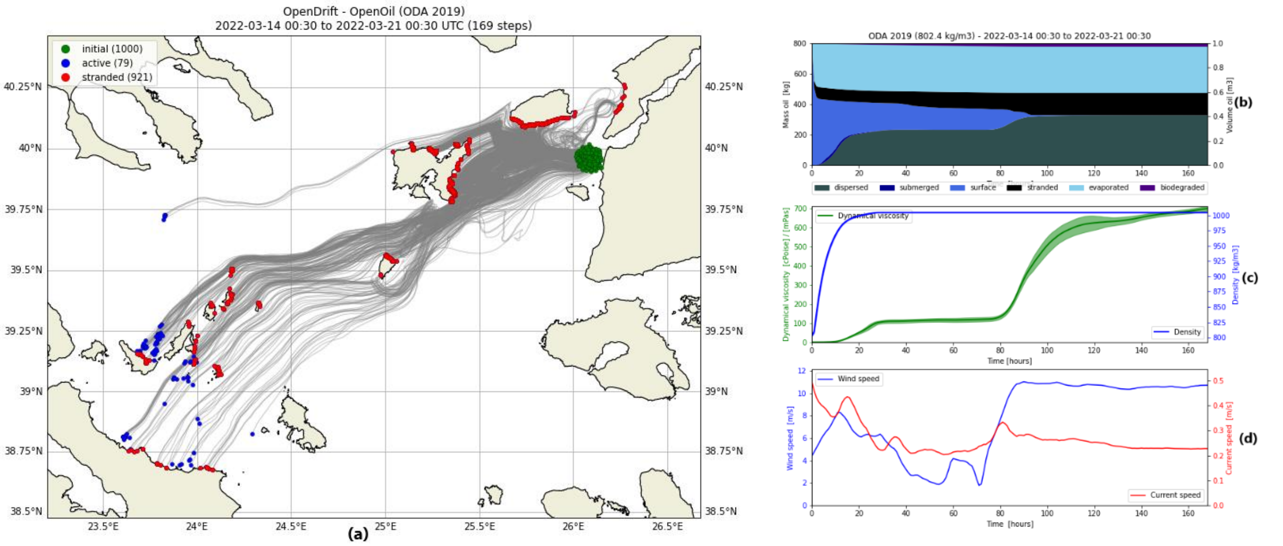


**Fig. 1 (a)** Oil spill simulation close to the Dardanelles Strait and North Aegean Sea at the end of 7-day simulation via OpenOil submodule. Green dots represent the initial positions of the oil elements, grey lines are their trajectories over time, and blue dots are the positions of oil droplets at the end of the simulation. Red dots represent elements which have been stranded, in other words, those that hit the shoreline. Time evolution of OpenOil model results, for **(b)** the oil budget and the relative impact of each physical and biochemical process; **(c)** the oil properties (mean and standard deviation of oil mass density and viscosity); **(d)** the prevailing wind and surface current speed, during the 7-day simulation period.

**Acknowledgements**

This work was funded by the Eye4Water project, MIS 5047246, implemented under the action: “Support for Research Infrastructure and Innovation” by the Operational Program “Competitiveness, Entrepreneurship and Innovation” in the framework of the Co-financed by Greece and the European Union-European Regional Development.

**References**

Dagestad KF, Röhrs J, Breivik O, Ådlandsvik B (2018) OpenDrift v1.0: A generic framework for trajectory modelling. Geoscientific Model Development, 11, 1405-1420, doi:10.5194/gmd-11-1405-2018.
Hole LR, Dagestad KF, Röhrs J, Wettre C, Kourafalou VH, Androulidakis Y, Kang H, Le Hénaff M, Garcia-Pineda O (2019) The DeepWater Horizon Oil Slick: Simulations of River Front Effects and Oil Droplet Size Distribution. Journal of Marine Science and Engineering, 7, doi:10.3390/jmse7100329.
Kokkos N, Sylaios G (2016) Modeling the buoyancy-driven Black Sea Water flow into North Aegean Sea. Oceanologia 58(2), 103-116, doi:10.1016/j.oceano.2015.12.003.
Lehr W, Jones R, Evans M, Simecek-Beatty D, Overstreet R (2002) Revisions of the ADIOS oil spill model. Environmental Modelling and Software, 17, 189-197, doi:10.1016/s1364-8152(01)00064-0.
Li C, Miller J, Wang J, Koley SS, Katz J (2017) Size distribution and dispersion of droplets generated by impingement of breaking waves on oil slicks. Journal of Geophysical Research: Oceans, 122, 7938-7957.
Röhrs J, Dagestad KF, Asbjørnsen H, Nordam T, Skancke J, Jones CE, Brekke C (2018) The effect of vertical mixing on the horizontal drift of oil spills, Ocean Science, 14, 1581-1601, doi:10.5194/os-14-1581-2018.
Tkalich P, Chan ES (2002) Vertical mixing of oil droplets by breaking waves. Marine Pollution Bulletin, 44, 1219-1229, doi:10.1016/S0025-326X(02)00178-9.
Visser, AW (1997) Using random walk models to simulate the vertical distribution of particles in a turbulent water column. Marine Ecology Progress Series, 158, 275-281, doi:10.3354/meps158275.

# Heavy metals monitoring along the Laspias and Lissos Rivers

Anastasia MAKRI[1], Konstantinos AZIS[1], Vassiliki PAPAEVANGELOU[2], Cate A. BAKALAKOU[2], Dionissis LATINOPOULOS[2], Ifigenia KAGALOU[2], Spyridon NTOUGIAS[1], Christos AKRATOS[2], Paraschos MELIDIS[1,*]

[1] Department of Environmental Engineering, Democritus University of Thrace, 67132 Xanthi, Greece
[2] Department of Civil Engineering, Democritus University of Thrace, 67132 Xanthi, Greece

*Corresponding author: E-mail: pmelidis@env.duth.gr

## ABSTRACT

In river water environments, concentrations of heavy metals (HM) are commonly at low range. This could be drastically changed by anthropogenic pressures, which includes industrial, agricultural and municipal sources (Grieshaber et al., 2018). Heavy metals are mobile and non-biodegradable, can be bio-accumulated and can cause harmful effects on animals and human health (Zhang et al., 2021; Xiao et al., 2021). Soil is the foundation of all agricultural activities. An intense agricultural activity belongs to the potential pathways of diffuse heavy metal transportation from soils to surface waters (Bur et al., 2009). According to Zhou et al. (2020) around 40% of the world’s lakes and rivers are polluted by heavy metals, deriving from anthropogenic sources. The upper concentration limits of heavy metals in water are set by regional and national authorities (Karaouzas et al., 2021).
The current work is part of the “Eye4water” research initiative, which seeks to improve water management in Eastern Macedonia and Thrace (EMT) area. The water quality of two EMT rivers, i.e., Lissos and Laspias, are under evaluation in the frame of this research project. Laspias torrent watershed is located in Xanthi Prefecture, Thrace District, North Greece (24°53΄E and 40°59΄N). Lissos torrent watershed is located in Rhodope County, Thrace District, North Greece (25° 31΄E and 41° 01΄N) (Figure 1).

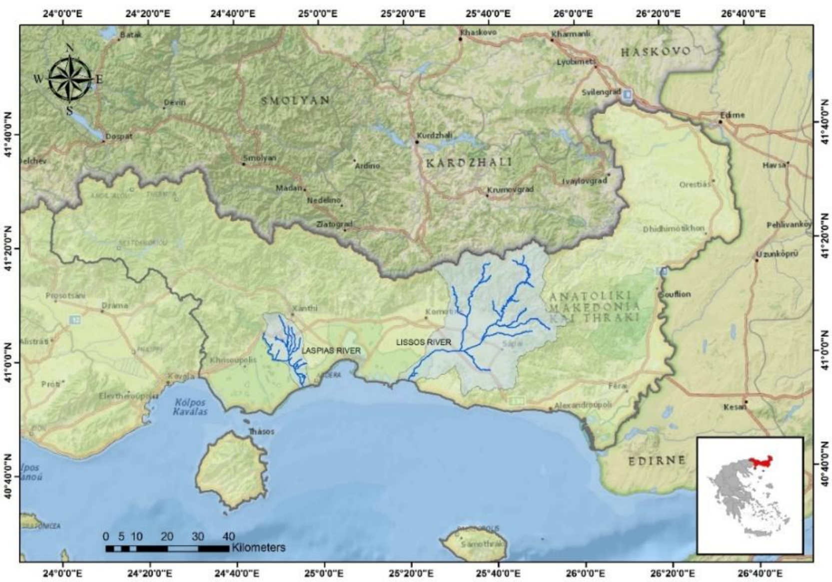


**Figure 1**. Laspias and Lissos torrent, EMT-R.

The study of these rivers was initiated by their vulnerability to pollution from both point and non-point sources. The monitoring of these freshwater ecosystems was based on twelve sampling stations in Lissos river and seven stations in Laspias river, which are both influenced by various pollution sources (Figure 2). An industrial zone, various livestock units and a municipal wastewater treatment plant are the major point sources of pollution in Laspias river.

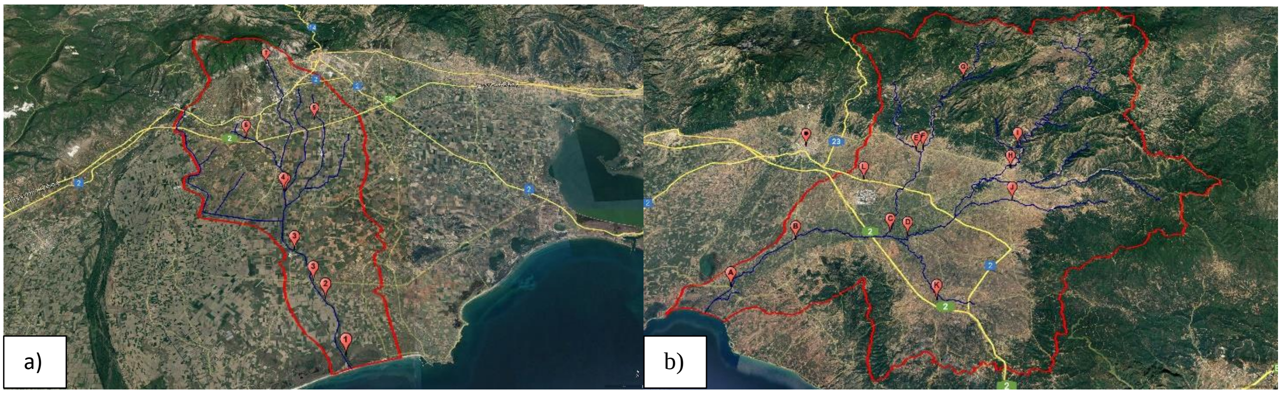


**Figure 2.** Sampling sites of (a) Laspias torrent basin and (b) Lissos torrent basin.

On the other hand, agricultural runoff and discharge of wastewaters in the river are non-point sources of pollution (Gikas, 2017). In the Lissos watershed, the industrial park and the municipal wastewater treatment plant of the city of Komotini are the major point sources of pollution. However, the increasing agricultural activity in the region is the main cause of pollution in the watershed (Gikas et al., 2013).

To evaluate potential heavy metal pollution in these rivers, samples were collected at various periods over the year. The first campaign for monitoring heavy metals in these rivers was conducted in June 2021. Heavy metal analysis was carried out through ICP-OES (Inductively Coupled Plasma - Optical Emission Spectrometry). The determination of heavy metals with ICP-OES is a rapid and accurate method in order to estimate possible heavy metals pollution in these freshwater ecosystems. During monitoring, twenty-two metals (Ag, Al, As, Ba, Be, Ca, Cd, Co, Cr, Cu, Fe, K, Mo, Na, Ni, Pb, Se, U, V, Zn, Mg, Mn) were analysed to assess heavy metal pollution. Interesting results regarding the water quality of these rivers were obtained. A total of nineteen and fourteen metals were detected in Lissos and Laspias river, respectively. Moreover, elements, such as Co, Mo, Pb, Se and V were detected in Lissos, but not in Laspias river. The highest metal concentrations were measured in samples affected by industrial activities.

In Lissos river, Ag, Al, As, Ba, Ca, Co, Cr, Fe, K, Na, Pb, U, Zn, Mg and Mn were the main metals detected, as a consequence of extensive anthropogenic and agricultural activities. In Laspias river, Al, As, Ba, Ca, Co, Cr, Fe, K, Na, Ni, U, V, Zn, Mg and Mn were the major heavy metals identified. However, heavy metal concentrations were greater in Laspias than in Lissos river. For instance, Ba, which usually comes from several industrial activities, had an average concentration of 80 μg/L in Laspias river and was found two-fold that in Lissos river. Zn, which is included in high concentrations in phosphoric fertilisers (Wu et al., 2017) and can leach from agricultural soils to river water, was detected in Lissos at average concentration of 20 μg/L and in Laspias river at 30 μg/L. Cr was found high at one sampling station in both rivers, probably due to the presence of corrosion inhibitors and pigments, thus Cr at 30 μg/L in Laspias and at 10 μg/L in Lissos. Mn, which is abounding in nature in dissolved, colloidal and complex forms, and can cause surface and ground water pollution (Galvin, 1995), was detected in all Laspias stations and in seven out of twelve stations of Lissos river. However, higher Mn concentrations (> 130 μg/L) were determined in Lissos, as compared to Laspias (70 μg/L). Ni, which can be found in pesticide formulations, was measured at only one sampling point in both rivers at concentration of 30 μg/L in Lissos and 50 μg/L in Laspias.

## Acknowledgements

Funded by Eye4Water project, MIS 5047246, implemented under the action: “Support for Research Infrastructure and Innovation” by the Operational Program “Competitiveness, Entrepreneurship and Innovation” in the framework of the Co-financed by Greece and the European Union-European Regional Development Fund.

## References

Bur, T., Probst, J.L., N'guessan,M., Probst, A., 2009. Distribution and origin of lead in stream sediments from small agricultural catchments draining Miocene molassic deposits (SW France). Appl. Geochem. 24 (7), 1324–1338.

Galvin RM, (1995) Occurrence of metals in waters: An overview. Department of Physical Chemistry and Applied Thermodynamics, Faculty of Hygiene, University of Cordoba, Spain.

Gikas GD. (2017) Water quantity and hydrochemical quality monitoring of Laspias River, North Greece Journal of Environmental Science and Health - Part A Toxic/Hazardous Substances and Environmental Engineering, 52 (14), pp. 1312-1321.

Gikas GD, Dimou D, Tsihrintzis VA. (2013) River water quantity and quality monitoring in an agricultural basin in north Greece Fresenius Environmental Bulletin, 22 (7 A), pp. 2006-2016.

Grieshaber, C.A., Penland, T.N., Kwak, T.J., Cope, W.G., Heise, R.J., Mac Law, J., et al., 2018. Relation of contaminants to fish intersex in riverine sport fishes. Sci. Total Environ. 643, 73-89.

Karaouzas I, Kapetanaki N, Mentzafou A, Kanellopoulos TD, Skoulikidis N. (2021) Heavy metal contamination status in Greek surface waters: A review with application and evaluation of pollution indices Chemosphere, 263.

Xiao H, Shahab Asfandyar, Xi Beidou, Chang, Qixin; You, Shaohong; Li, Jieyue; Sun, Xiaojie; Huang, Hongwei; Li, Xiangkui (2021). Heavy metal pollution, ecological risk, spatial distribution, and source identification in sediments of the Lijiang River, China. Environmental Pollution, 269.

Zhang Y, Wang S, Gao Z, Zhang H, Zhu Z, Jiang B, Liu J, Dong H. (2021) Contamination characteristics, source analysis and health risk assessment of heavy metals in the soil in Shi River Basin in China based on high density sampling Ecotoxicology and Environmental Safety, 227, art. no. 112926.

Zhou Q, Yang N, Li Y, Ren B, Ding X, Bian H, Yao X, (2020). Total concentrations and sources of heavy metal pollution in global river and lake water bodies from 1972 to 2017. Glob. Ecol. Conserv. 22.

Wu, Q., Qi, J., Xia, X., 2017. Long-term variations in sediment heavy metals of a reservoir with changing trophic states: implications for the impact of climate change. Sci. Total Environ. 609, 242-250.

# Assessing the Coastal Erosional Processes in Strymonikos Gulf (Northern Greece) by blending satellite imagery with observed and simulated waves

Konstantinos ZACHOPOULOS, Nikolaos KOKKOS, Maria ZOIDOU, Panagiota KERAMEA and Georgios SYLAIOS*

Laboratory of Ecological Engineering and Technology, Department of Environmental Engineering, Democritus University of Thrace, Vas. Sofias 12, 67100 Xanthi, Greece
*Corresponding author: gsylaios@env.duth.gr

ABSTRACT

Coastal zones are experiencing increased natural and human disruptions such as sea level rise, resource over-exploitation and coastal erosion. Waves, tides, winds, storms, sea level change, and human activities such as dams constructed upstream in rivers, all have an impact on coastal sedimentation and the geomorphologic processes of the shore. Satellite-borne coastline extraction and detection of change rates over time are used in coastal zone monitoring of these impacts. The present study focuses in Strymonikos Gulf (North Aegean, Greece) examining and assessing the coastline erosion "hotspots" using historic satellite images from Sentinel 2 sensor, wave data from an in-situ buoy and Copernicus wave products. The erosional processes were interrelated to the incident wave power and the propagating wave direction, in conjunction to the concentration of suspended particulate matter (SPM) in Strymon river plume.

**Keywords:** Coastal processes; Shoreline evolution; Satellite image classification; Copernicus products (CMEMS); GIS analysis.

## 1. Introduction

The coastal zone is a very dynamic geomorphologic system where changes occur at diverse temporal and spatial scales (Mills et al. 2005), mostly related to erosion, as a result of natural and/or anthropogenic activities (Gracia et al. 2018). Natural effects include shoreline interactions with incident waves, tides, storms, tectonic and physical processes and the sediment load transported from the watershed by rivers (Anh et al. 2021). Coastal zone monitoring is an important task for national/regional development and environmental protection, in which the assessment of the state of historic shorelines is important (Rasuly et al., 2010). Coastal authorities are faced with the increasingly complex task of balancing development and managing coastal risks. Integrated Coastal Zone Management (ICZM) provides a framework to resolve conflicts, mitigate impacts of short-/long-term uses and support strategies for sustainable coastal management (Anfuso et al., 2011). The area was selected based on its high economic, archaeologic and aesthetic values and the potential vulnerability to coastal erosion and their exposure to climate change impacts.

## 2. Study area

This study focuses on the shoreline of the Strymonikos Gulf, Northern Greece. The total length of the shoreline is about 42 km, covering the coastal zone from Olympiada to Kariani. The study focuses on two geographical sub-areas: a) the Asprovalta beach (around 12.5 km long); and b) the site of Orfani-Kariani coastal zone (around 9.8 km long). The areas are characterized by fine to very fine sands, separated by rocky peninsulas.

## 3. Methodology

The shoreline movement analysis was carried out from 2016 to 2020 using Sentinel-2 satellite images with 10 m spatial resolution. The methodology employed in this study entailed the process of shoreline delineation from historical satellite images by applying a semi-automatic classification process, allowing the identification of materials in an image according to their spectral signature. The new raster file was classified by applying the minimum distance classification algorithm. Moreover, in-situ collected wave data from an upward-facing ADCP deployed at 20 m depth and historic offshore wave time-series data at five data points, were retrieved from the reanalysis and forecast products of the Copernicus Marine Environmental Monitoring Service (CMEMS) for the same period. Wave data comprised the daily time-series of the spectral significant wave height ($H_{mo}$), the zero up-crossing wave period ($T_{o2}$) and the wave direction relative to the north ($\phi_o$). A simple wave-ray model was used to transform the offshore wave characteristics into the wave characteristics at the breaker zone. All parameters were produced following the equations described by the Coastal Engineering Manual (U.S. Army Corps of Engineers 2008) (Demirbilek and Vincent, 2008). To estimate the SPM concentration, the retrieved images were processed using the Sentinel Toolbox Development Platform (SNAP) v.8.0 software, which was based on the ESA BEAM repository, following the C2RCC algorithm. The C2RCC processor has been developed for visually complex Case 2 waters, based on neural network technology, and has been trained from a large database accounting for extreme sets of scattering and absorption properties.

## 4. Results

According to the methodology described above, identification of beaches vulnerable to coastal erosion was carried out. The Strymonikos Gulf is characterized by elongated beaches having morphology directly influenced by the sediment fluxes of the Strymon River.

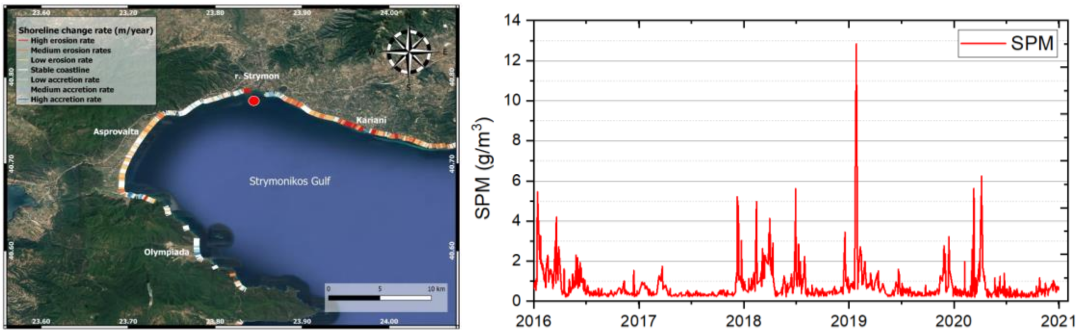


Figure 1. Left: Shoreline change rate (m/year) in Strymonikos Gulf; and Right: Suspended Matter Particles concentration in Strymon River estuaries for the time period 2016-2020.

Several hotspots of coastal erosion are observed along the coastal zone for the time period 2016-2020, with average erosion rate of -1.8 ± 0.4 m/year and average shoreline movement of -3.6 ± 0.6 m. The higher erosion rates are observed in the zone attached on the west side of the port of Kariani (-4.5 ± 0.4 m/year). In Kariani the most frequent incident wave orientation is ESE and SE with wave heights up to 3.6 m and the mean incident wave energy is estimated ~239.93 J $m^{-1}s^{-1}$. Moreover, in Kariani the direction of incident waves affects the sediment transport, moving material from the south-eastern beaches to the north-western coasts. Additionally, the sandy long beach of Asprovalta is gradually eroded through the years. Significant shoreline retreat is observed at the eastern beach (about -0.5 ± 0.2 m/year). The beach is protected from high wave events, but appears exposed to SE waves, with an average height of 0.5 m, maximum height of about 2 m and mean incident wave energy about 100.79 J $m^{-1}s^{-1}$. Since the shoreline position is strongly related to the sediment load from Strymon River, intense shoreline retreat is observed when the annual SPM concentration load is reduced.

## 5. Conclusion

The coastal erosional processes in the study area appear affected from the incident wave energy, the direction of waves propagation and the SPM fluxes exported from the Strymon river. The higher erosion rates correspond to periods of increased incident wave energy from directions favoring the longshore sediment transport and the SPM inflow into the gulf. The present study constitutes a successful effort to correlate coastal erosion rates produced by historic satellite images to the offshore wave data, the incident to the coast wave energy and the concentration of SPM assessed through Sentinel 2 satellite imagery.

### References

Anfuso G, Pranzini E, & Vitale G (2011). An integrated approach to coastal erosion problems in northern Tuscany (Italy): Littoral morphological evolution and cell distribution. Geomorphology, 129(3-4), 204-214, https://doi.org/10.1016/j.geomorph.2011.01.023.

Anh T, Trung B, Nguyen A, Liou A, & Phan T (2021). Human impacts on estuarine erosion-deposition in southern central Vietnam: Observation and hydrodynamic simulation. Sustainability, 13(15), 8303, https://doi.org/10.3390/su13158303.

Demirbilek, Z., & Vincent, C. L. (2008). PART II-Water Wave Mechanics. Costal Engineering Manual. EM 1110-2-1100. US Army Corps of Engineers. Cap, 1.

Gracia A, Rangel-Buitrago N, Oakley A., & Williams T (2018). Use of ecosystems in coastal erosion management. Ocean & Coastal Management, 156, 277-289, https://doi.org/10.1016/j.ocecoaman.2017.07.009.

Mills P, Buckley J, Mitchell L., Clarke J, & Edwards J (2005). A geomatics data integration technique for coastal change monitoring. Earth Surface Processes and Landforms: The Journal of the British Geomorphological Research Group, 30(6), 651-664, https://doi.org/10.1002/esp.1165.

Rasuly A, Naghdifar R, & Rasoli M (2010). Monitoring of Caspian Sea coastline changes using object-oriented techniques. Procedia Environmental Sciences, 2, 416-426, https://doi.org/10.1016/j.proenv.2010.10.046.

# C2RCC algorithm recalibration for the assessment of Chlorophyll-a concentration in shallow coastal lagoons

Maria ZOIDOU, Nikolaos KOKKOS, Konstantinos ZACHOPOULOS, Panagiota KERAMEA and Georgios SYLAIOS*

Laboratory of Ecological Engineering and Technology, Department of Environmental Engineering, Democritus University of Thrace, 67100 Xanthi, Greece
*Corresponding author: gsylaios@env.duth.gr

ABSTRACT

Chlorophyll-a (Chl-a) is one of the main biological parameters measured to assess the ecological status in aquatic systems. Remote sensing has been an effective tool for the systematic monitoring of water quality, recording surface Chl-a levels and gaining knowledge on eutrophication dynamics. In Sentinel 2 image analysis, the SNAP software and the C2RCC processor are being widely used for Chl-a assessment. However, in the highly productive, turbid and shallow coastal lagoons this algorithm fails to produce valid results and recalibration is needed. In-situ Chl-a concentration data sampled from the Nestos coastal lagoons and the respective reflectance values for bands 4-7 were imported in a Takagi-Sugeno neuro-fuzzy model to improve Chl-a assessment. Based on these results, the spatio-temporal variability of Chl-a concentration for Eratino lagoon (Nestos lagoon complex) was assessed to determine the current ecological status from 2015 to 2021.

**Keywords:** chlorophyll-a, eutrophication, remote sensing, Takagi-Sugeno neuro-fuzzy model, Sentinel 2.

## 1. Introduction

Consistent and cost-efficient monitoring in coastal ecosystems is essential, but in situ monitoring (e.g., water sample collection and laboratory analysis) is a time and money consuming method for estimating the quality of water on a regular basis. Satellite remote sensing is a feasible and cost-effective method to monitor water bodies when water quality over large regions has to be monitored with regular frequency. There is also the possibility to estimate water quality in non-accessible water bodies. However, passive satellite remote sensing depends highly on weather, like cloudiness, air mass changes, and sunlight conditions, which directly affect the quality and quantity of data. In parallel, the current algorithms for SPM and Chl-a concentration evaluation based on spectral reflectances, like the C2RCC for Sentinel 2, have been validated in the open sea environment of Case 1 (in which their inherent optical properties are dominated by phytoplankton, e.g., most open ocean waters) and Case 2 waters (containing coloured dissolved organic matter (CDOM) and inorganic mineral particles in addition to phytoplankton (Ansper and Alikas 2019, Soomets et al., 2020). However, the interference of (a) the shallow sea bottom reflection, (b) the sun glint and (c) the presence of non-algal particles on the optical signal (spectral reflectances) measured by satellites has not been adequately evaluated. Yu et al. (2020) developed a semi-empirical algorithm to correct Chl-a concentration observed by SPOT6 at the very shallow parts of Sanya Bay, China. In the present work, we attempt to recalibrate the C2RCC processor using in-situ Chl-a concentration data and the respective spectral reflectance values for the appropriate training of a Takagi-Sugeno neuro-fuzzy algorithm to correct the satellite-derived Chl-a values.

## 2. Methodology

A series of Sentinel 2 historic satellite images were retrieved for the study area (Eratino lagoon, Nestos delta, Northern Greece) to cover the period from early 2015 to late 2021. Eratino Lagoon belongs to the Nestos complex, part of the East Macedonia and Thrace National Park. The area is protected by the Convention on Wetlands of International Importance (Ramsar Convention). It covers an area of 2.9 km$^2$, about 5.9 km long, 0.7 km wide and has a perimeter of 43 km. The mean depth of the lagoon is 0.8 m and the maximum depth is 3.4 m.

All Sentinel 2 images were retrieved from the L1C product containing reflectances with the same atmospheric correction. To derive the Chl-a concentration, retrieved images were processed by Sentinel Toolbox Development Platform (SNAP) v.8.0 software, using the C2RCC processor (Brockman et al., 2020). The C2RCC processor is developed for optically complex Case 2 waters. It is based on neural network technology and has been trained under extreme ranges of scattering and inherent absorption properties (IOPs). The C2RCC results of Chl-a concentration was derived, after the provision of additional background data in parameters such as water surface salinity, elevation, ozone, water surface temperature and air pressure. Salinity and temperature values were used from previous in situ data and values of the surface ozone layer and air pressure data were retrieved from ERA5 model with 30 km spatial resolution.

A database of 122 in-situ Chl-a concentration values, collected from the shallow parts of Nestos lagoons complex were associated with the respective reflectance values from bands 4 to 7 of Sentinel 2. 60% of data from the database were used for training the Takagi-Sugeno neuro-fuzzy model, 20% for model validation and 20% for model testing. The model was implemented in Matlab 2022 utilizing the standard Adaptive Neural Fuzzy Inference System (ANFIS) algorithm. Initially, the fuzzification of input values (4 antecedents: reflectances at each band; 1 output: log(Chl-a)) through the general bell-shaped membership function and the grid partition method, led to the definition of membership values in the three fuzzy set ("low", "medium", "high"). Then, a series of multiple-input–single output fuzzy rules were applied of the form: *if band1 is "LOW" AND band2 is "MEDIUM" AND band3 is "LOW" and band4 is "HIGH" then log(Chl-a) = f(band1, band2, band3, band4)*. Finally, the evaluation and weighting of the basic functions and the final evaluation of the output Chl-a value were followed in the defuzzification step. Model testing error analysis exhibited the following metrics: Mean Squared Error = 0.000018; Root Mean Squared Error = 0.00418; $r^2$ = 0.996. Using this neuro-fuzzy model all Sentinel 2 Chl-a data were corrected for Eratino lagoon.

## 3. Results

Figure 1 illustrates the Chl-a concentration distribution for 19 July 2021, as derived by applying the C2RCC processor (left panel) and the neuro-fuzzy model (right panel). C2RCC processor estimated high Chl-a values ranging from 15-30 μg/l. The highest values were found at the northern and eastern parts of the lagoon. The lowest values (close to zero) were estimated at the freshwater inflow stream, at the northern part of the basin. As this instream supplies nutrients from agricultural runoff, Chl-a values were expected to be high. The Chl-a values adapted after the neuro-fuzzy model application were significantly lower (up to 3 μg/l). The neuro-fuzzy model seems to capture the expected higher values at the instream flow (reaching 30 μg/l).

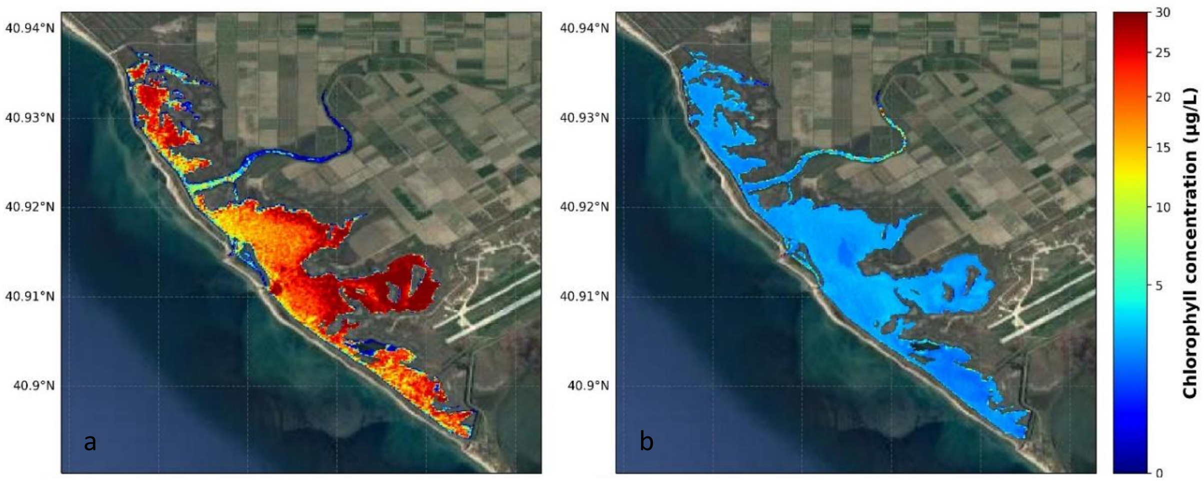


**Fig. 1.** Spatial evolution of Chl-a in Eratino lagoon (19/07/2020) derived using a) the C2RCC processor and b) the neuro-fuzzy model.

## 4. Conclusions

In this work, a neuro-fuzzy model was developed to correct the observed by the Sentinel 2 satellite Chl-a values. The algorithm was implemented at Eratino Lagoon (Northern Greece), giving satisfactory results.

### References

Ansper A, Alikas K (2019) Retrieval of Chlorophyll *a* from Sentinel-2 MSI Data for the European Union Water Framework Directive Reporting Purposes, *Remote Sensing*; 11(1):64. https://doi.org/10.3390/rs11010064
Brockmann C, Doerffer R, Peters M, Kerstin S, Embacher S and Ruescas A (2016) Evolution of the C2RCC Neural Network for Sentinel 2 and 3 for the Retrieval of Ocean Colour Products in Normal and Extreme Optically Complex Waters, ESA Special Publication, Vol 740, 54 pp.
Soomets T, Uudeberg K, Jakovels D, Brauns A, Zagars M, Kutser T (2020) Validation and Comparison of Water Quality Products in Baltic Lakes Using Sentinel-2 MSI and Sentinel-3 OLCI Data, Sensors (Basel), Jan 29; 20(3):742. https://doi.org/10.3390/s20030742
Yu Y, Chen S, Qin W, Lu T, Li J, Cao Y. A (2020) Semi-Empirical Chlorophyll-a Retrieval Algorithm Considering the Effects of Sun Glint, Bottom Reflectance, and Non-Algal Particles in the Optically Shallow Water Zones of Sanya Bay Using SPOT6 Data, Remote Sensing, 12(17):2765. https://doi.org/10.3390/rs12172765

# Modelling Sediment Diffusion during the construction of the EAST-MED POSEIDON Natural Gas Pipeline

Aristeidis BLOUTSOS[1], Elpida PANAGIOTATOU[2], Anastasios STAMOU[3]

[1,2,3] Department of Water Resources and Environmental Engineering, School of Civil Engineering, National Technical University of Athens, Greece
email: abloutsos@mail.ntua.gr (for author 1)
email: epanagiotatou@mail.ntua.gr (for author 2)
email: stamou@mail.ntua.gr (for author 3)

ABSTRACT

We apply the CORMIX model to simulate the behavior of the Suspended Particulate Matter (SPM) plumes that are released into the water column during dredging for the installation of the EAST-MED POSEIDON Natural Gas Pipeline. We performed calculations in 4 investigation areas that included two flow conditions for the minimum and maximum flow velocities and 32 sensitivity analysis scenarios to investigate the effect of current velocity near the bottom and the composition of sediments. Calculations showed that for all scenarios the SPM plumes are characterized by strong buoyancy being classified in CORMIX as flow class NV2. Calculated Suspended Sediment Concentrations (SSC) at distances shorter than 20 m from the discharge location are generally lower than the threshold value of 35 mg/L, while at distances longer than 50 m SSC range from 0.8 to 18.2 mg/L for the maximum current velocity and from 0.0 to 7.6 mg/L for the minimum current velocity.

## 1. Introduction

During dredging operations, sediment particles are removed from the seabed and released into the water column as SPM. The SPM forms a plume that is transported away from the dredging site by water mass circulation following a path that consists of 3 zones: initial mixing, near-field and far-field. The excessive increase of SPM in coastal waters caused by dredging is considered as a pollution event and the most important of the likely effects is the enhanced turbidity and sedimentation; the changes in SSC values is the most important parameter that is determined by sediment diffusion model to quantify the changes in turbidity.

In the present work, we estimate the impacts caused to marine environment during the construction phase of the landfall sites in Crete (LF2), Peloponnese (LF3) and Patraikos Gulf (LF4 and LF5) using the CORMIX model that was developed in part through cooperation with the US EPA, the US Army Corps of Engineers, and the US Bureau of Reclamation (USEPA, 1999).

## 2. Materials and methods

We applied the CORMIX model to estimate the behavior of the SPM plumes and the spatial distribution of SSC. The input data included (1) dredging characteristics (type of dredger; capacity of dredger; cycle time; output of dredger), (2) sediment characteristics (density and classes), (3) ambient characteristics (temperature; salinity; background sediment concentration; density; flow velocity near the bottom and at the surface), and (3) site and discharge characteristics (sediment mass released; sediment plume concentration; sediment plume density; sediment plume discharge; discharge velocity; sediment plume area; shore Location; distance to shoreline; water depth; bottom slope; vertical angle of discharge; horizontal angle of discharge; discharge height above channel bottom; and water depth at the source of the plume). We obtained the data from field surveys, the relevant literature and practical experience. We performed calculations in the 4 investigation areas LF2, LF3, LF4 and LF5 that are shown in Figure 1 for two flow conditions that correspond to the minimum and maximum flow velocities, which were determined based on data obtained from the Copernicus Marine Environment Monitoring Service (CMEMS). Additionally to these 8 scenarios, we performed calculations for 32 sensitivity analysis scenarios to investigate the effect of current velocity near the bottom for values ranging from 0.50 to 0.90 m/s and for various compositions of sediments.

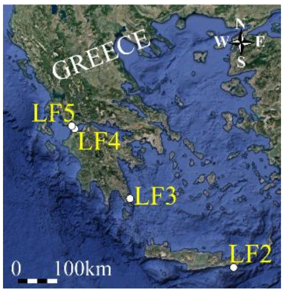


**Fig. 1.** Locations of the 4 investigation areas LF2, LF3, LF4 and LF5 (Source: Google Earth).

## 3. Results and discussion

In all calculation scenarios, the SPM plume is characterized by strong buoyancy and the SPM plume is classified as the flow class NV2 in CORMIX system (Doneker and Jirka, 1991). Initially, the flow of the sediment plume is dominated by the upward plume momentum (jet-like); the axis of the plume rises to a maximum height, being weakly deflected by the ambient current. Then, the plume is strongly affected by gravity and rapidly falls downwards and impinges on the sea bottom; the impingement angle ranges from 20.2$^o$ to 32.5$^o$ for the maximum current velocity, while it is constant (approximately equal to 57$^o$) for the minimum current velocity. The length of the near field region ranges from 6.7 m to 13.5 m for the maximum current velocity and it is almost constant (175.0 m) for the minimum current velocity. After impingement, the flow laterally spreads across the ambient flow in the downstream direction, its half-width (BH) is steadily increasing and its thickness (BV) is decreasing. At the end of the near field region, BH ranges from 12.4 m to 26.0 m for the maximum current velocity, while for the minimum current velocity it is almost constant and approximately equal to 350.0 m; moreover, BV for the maximum current velocity ranges from 0.9 m to 1.4 m and for the minimum current velocity it is approximately equal to 0.28 m. The mixing rate is relatively small in all scenarios; thus, the dilution at 1200 m downstream of the discharge location is also small ranging from 3.3 to 3.9 for the maximum current velocity, while it is constant and equal to 4.7 for the minimum flow velocity. Thus, the worst conditions are those for the maximum current velocity. Table 1 summarizes the values of the SSC in the water column at various distances from the discharge location (x=0).

**Table 1.** Suspended Sediment Concentrations (mg/L) in the water column

| Site | LF2 | | LF3 | | LF4 | | LF5 | |
|---|---|---|---|---|---|---|---|---|
| x(m) | Max | Min | Max | Min | Max | Min | Max | Min |
| 10 | 6.8 | 21.6 | 14.6 | 115.1 | 38.8 | 147.0 | 35.0 | 153.1 |
| 20 | 4.7 | 2.5 | 6.2 | 13.2 | 27.7 | 23.3 | 23.7 | 36.7 |
| 30 | 3.1 | 0.0 | 3.4 | 0.0 | 23.1 | 8.2 | 18.2 | 7.4 |
| 50 | 1.2 | | 0.8 | | 18.2 | 7.6 | 13.1 | 5.4 |
| 100 | 0.1 | | 0.0 | | 15.2 | 5.4 | 10.4 | 3.9 |
| 150 | 0.0 | | | | 13.9 | 4.4 | 9.6 | 3.1 |
| 300 | | | | | 10.7 | 2.0 | 7.8 | 2.3 |

## 4. Conclusions

At distances shorter than 20 m from the discharge location, the SSC values for the maximum current velocity are lower than the threshold value of 35 mg/L for all sites. For the minimum current velocity, the corresponding concentrations are lower than the threshold value of 35 mg/L with the exception of the site LF5 at which the SSC is slightly higher than the threshold value (36.7 mg/L). At distances longer than 50 m from the dredging location, SSC range from 0.8 to 18.2 mg/L for the maximum current velocity, while for the minimum current velocity, the corresponding concentrations range from 0.0 mg/L (at sites LF2 and LF3) to 7.6 mg/L.

**Acknowledgements**

The present work was supported by Asprofos Engineering S.A. within the project "East-Med Poseidon Natural Gas Pipeline: Simulation of oil pollution dispersion, sediment diffusion and underwater noise" (NTUA's ELKE Grant No. 62394400).

**References**

Doneker RL, Jirka GH (1991) Expert Systems for Mixing-Zone Analysis and Design of Pollutant Discharges. Journal of Water Resources Planning and Management, 117(6), 679–697. https://doi.org/10.1061/(ASCE)0733-9496(1991)117:6(679)

USEPA (1999) Review of the D-CORMIX model, Science Advisory Board Report EPA-SAB-EC-99-011, USEPA, Washington, DC, USA, http://www.epa.gov/science1/ec99011.pdf.

# Leakage estimation and optimal sizing of pressure management areas using probabilistic and hydraulic modeling tools: Application to the water distribution network of the Historical Center of Patras.

Athanasios V. SERAFEIM[1], George KOKOSALAKIS[1,2], Roberto DEIDDA[3], Nikolaos Th. FOURNIOTIS[4], Irene KARATHANASI[5] and Andreas LANGOUSIS[1]

[1] Department of Civil Engineering, University of Patras, Patras, Greece
email: A.V.S.: athanseraf@hotmail.com ; G.K.: gkokosalakis@upatras.gr ; A.L.: andlag@upatras.gr
[2] School of Business and Economics Department of Maritime Transport and Logistics, Deree American College of Greece, Athens, Greece
email: gkokosalakis@acg.edu
[3]Dipartimento di Ingegneria Civile, Ambientale ed Architettura Università degli Studi di Cagliari, Cagliari, Italy
email: rdeidda@unica.it
[4]Department of Civil Engineering, University of the Peloponnese, Patras, Greece
email: nfou@uop.gr
[5] Municipal Enterprise of Water Supply and Sewerage of the City of Patras, Patras, Greece
email: i.karathanasi@deyap.gr

ABSTRACT

Reduction of water losses in Water Distribution Networks (WDNs) is a crucial task for all water agencies and experts, as the lost water remains unbilled undermining their environmental footprint and financial viability. This work focuses on the development of an innovative framework that combines statistical clustering approaches and hydraulic modeling principles, for robust estimation of water losses and optimal partitioning of the historical center of the city of Patras into Pressure Management Areas (PMAs), without undermining the overall hydraulic resilience of the network.

## 1. Introduction

The most common approach for water loss estimation in Water Distribution Networks (WDNs) is that of the Minimum Night Flow (MNF). The latter is based on the concept that human activity during late night and early morning hours is minimal and, thus, the volume of water entering the WDN is mainly associated with leakages. Control of water losses can be effectively accomplished by partitioning the WDN into pressure management areas (PMAs), as a means of reducing the inlet pressure to the lowest permissible limit that meets the requirements set by the consumption/demand. In a previous work, Serafeim et al. (2021) developed a probabilistic approach based on statistical metrics, which estimates the MNF as the overall average of the most probable states of the night flow during the low consumption period of the year. Recently, Serafeim et al. (2022b) developed a search algorithm for WDN partitioning into PMAs based on a hierarchical clustering approach (see e.g. Hosking and Wallis, 1997). This work presents an application of the two developed approaches to the historical center of Patras (the most populous city in western Greece) aiming at the optimal partitioning of the existing PMA into smaller ones, without undermining the hydraulic resilience of the region.

## 2. Area and Data

In the analysis that follows, we use consumption (billed and unbilled) and flow-pressure data from PMA Kentro (see Figure 1.a), which includes the historical center of the city of Patras. PMA Kentro consists of more than 62 km of pipeline (mainly HDPE and PVC pipes), covers an area of 1 206 867 m$^2$, and serves approximately 14 000 consumers (based on data from the Hellenic Statistical Authority and the Municipality of Patras), which correspond to more than 16 000 active hydrometers (see Serafeim et al., 2022a).

## 3. Methodology

### *3.1. Minimum Night Flow estimation*

We estimate MNF as the ensemble mean, $\bar{Q}_{lmod}$ , of the lowest modal values $Q_{lmod}^{(j)}$ observed during the night hours of different days $j$ in the low consumption period of the year, using Eq. 1. $Q_{lmod}^{(j)}$ denotes the lowest modal value of the empirical probability density function (PDF) of observed flows within the night hour range of day $j$ ($j$ = 1, 2, …, $n$), and $n$ is the number of days.

$$\mathrm{MNF} := \overline{Q}_{lmod} = \frac{1}{n}\sum_{j=1}^{n} Q_{lmod}^{(j)} \tag{1}$$

After estimating the MNF for a selected PMA, we decompose it to net night flow, which equals the leakage rate during night hours, and users' night consumption, which can be both authorized and unauthorized, using the billed and unbilled consumption data (for more details, see Serafeim et al., 2022a).

### *3.2. Hierarchical Clustering and PMA partitioning*

The developed algorithm: a) groups the computational nodes into homogeneous clusters in terms of calculated pressure heads, b) distributes the total water loss spatially based on the estimated pressures, and c) repeats steps (a) and (b) till convergence to an optimal configuration that does not undermine the hydraulic resilience of the network (for more details see Serafeim et al., 2022b).

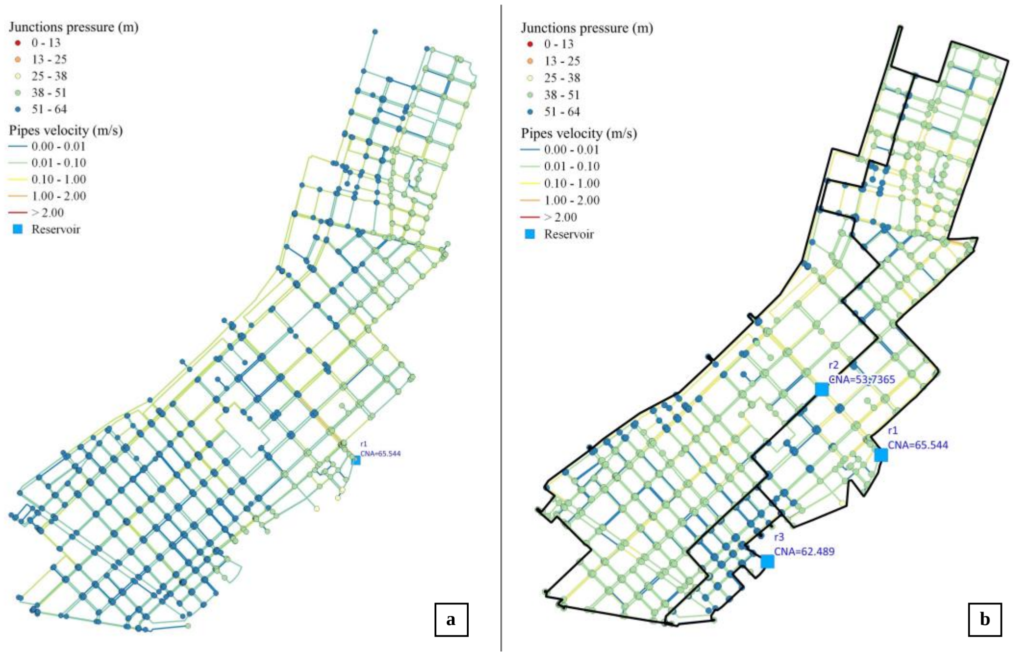


**Fig. 1.** Nodal pressures and water velocity results for PMA Kentro before (a) and after (b) partitioning.

## 4. Results -Discussion

Using the Serafeim et al. (2022a) MNF approach, the leakage rate for the original configuration of PMA Kentro (Figure 1.a) was estimated to be 76.8 l/s, which was reduced by approximately 15% (i.e. to 65.3 l/s) after applying the suggested partitioning (Figure 1.b). This reduction, which corresponds to approximately 67 000 € of annual savings, was achieved without altering the overall hydraulic resilience of the network, and/or the minimum pressures found at critical nodes of the pipeline grid.

**Acknowledgements**

The research project was supported by the Hellenic Foundation for Research and Innovation (H.F.R.I.) under the "1st Call for H.F.R.I. Research Projects to support Faculty Members and Researchers and the procurement of high-cost research equipment grant" (Project Number: 1162).

**References**

Hosking, J.R.M. and R. Wallis (1997) *Regional frequency analysis: An approach based on L-moments*, Cambridge University Press, Cambridge, U.K.

Serafeim, A.V., G. Kokosalakis, R. Deidda, I. Karathanasi and A. Langousis (2021) Probabilistic estimation of minimum night flow in water distribution networks: large-scale application to the city of Patras in western Greece, Stochastic Environmental Research and Risk Assessment, doi: https://doi.org/10.1007/s00477-021-02042-9.

Serafeim, A.V., G. Kokosalakis, R. Deidda, I. Karathanasi and A. Langousis (2022a) Probabilistic Minimum Night Flow Estimation in Water Distribution Networks and Comparison with the Water Balance Approach: Large-Scale Application to the City Center of Patras in Western Greece, Water, 14, 98, https://doi.org/10.3390/w14010098.

Serafeim, A.V., G. Kokosalakis, R. Deidda, N Th. Fourniotis and A. Langousis (2022b) Combining statistical clustering with hydraulic modeling for resilient reduction of water loses in water distribution networks: Large scale application to the city of Patras in Western Greece (in preparation).

# Bayesian hierarchical modelling as a tool to assess lakes suitability for recreational use

Nikos MELLIOS[1], Jannicke MOE[2], Chrysi LASPIDOU[1]

[1] Department of Civil Engineering, University of Thessaly, 38334 Volos, Greece
email: nmellios@uth.gr
email: laspidou@uth.gr

[2] Norwegian Institute for Water Research (NIVA), Gaustadalléen 21, 0349 Oslo, Norway
email: jannicke.moe@niva.no

ABSTRACT

In this work, we model the response of cyanobacteria abundance to variations in lake Total Phosphorus (TP) and Total Nitrogen (TN) concentrations, using a data set from 822 Northern European lakes. We divide lakes in 10 groups based on their physico-chemical characteristics, following a modified lake typology defined for the Water Framework Directive (WFD). This classification is used in a Bayesian hierarchical linear model which employs a probabilistic approach, transforming uncertainty into probability thresholds. The hierarchical model is used to calculate probabilities of cyanobacterial concentrations exceeding risk levels for human health associated with the use of lakes for recreational activities, as defined by the World Health Organization (WHO). Different TN and TP concentration combinations result in variable probabilities to exceed pre-set thresholds. Our objective is to support lake managers in estimating acceptable nutrient concentrations and allow them to identify actions that would achieve compliance of cyanobacterial abundance risk levels with a given confidence level.

## 1. Introduction

Bayesian hierarchical models can combine prior and data-driven knowledge both from multiple groups of lakes and from lakes of the same group to make predictions for a single lake belonging to a specific group. In other words, the hierarchical approach moves one step further from the classical "grouping" approach by considering the effects of the ensemble of lakes on predictions. The Bayesian modelling framework, which is based on probability distributions is very suitable for the analysis of cyanobacteria blooms, as they are rare events with high uncertainty. The method has been used extensively in the past with convincing results; however, the method has not been used for prediction of cyanobacteria abundance**.** Here, we use a multi-lake data set of 822 Northern European lakes and evaluate trends in Cyanobacteria Biomass (CBB) using nutrient concentrations as predictors. Results are implemented for analyzing lake CBB concentrations according to the three risk levels associated to human health for recreational activities (Low—CBB ≤ 2mg/L; Medium—CBB between 2 and 10 mg/L and High—CBB > 10mg/L), as defined by the World Health Organization.

## 2. Materials and Methods

### *2.1. Categorizing lakes into groups*

The chosen lake classification is very similar to the one used by Malve and Qian (2006) and included 10 groups, modifying lake types to fit the availability of data in our dataset. The grouping of lakes was determined by mean depth, humic type, and surface area.

### *2.2. Bayesian hierarchical linear regression model*

The hierarchical modelling approach implemented in this work is shown below:

$$y_{ijk} \sim N(X\beta_{ij}, \tau^2) \tag{1}$$

$$X\beta_{ij} = \beta_{0,ij} + \beta_{1,ij} * TN_{ijk} + \beta_{2,ij} * TP_{ijk} \tag{2}$$

$$\beta_{ij} \sim N(\beta_i, \sigma_i^2) \tag{3}$$

$$\beta_i \sim N(\beta, \sigma^2) \tag{4}$$

$$\beta \sim N(0, 10000) \tag{5}$$

$$\sigma_i, \sigma \sim gamma(0.001, 0.001) \quad (6)$$

$$\tau = unif(0, 100) \quad (7)$$

where, $y_{ijk}$ is the k$^{th}$ observed CBB value from lake j in group i. X is the model matrix consisting of observed TN and TP values from lake j in group i, $\beta_{ij} = [\beta_{0,ij}, \beta_{1,ij}, \beta_{2,ij}]$ is the lake-specific linear regression model parameter vector which includes the intercept ($\beta_{0,ij}$) and the slopes for TN ($\beta_{1,ij}$) and TP ($\beta_{2,ij}$), $\tau^2$ is the model error variance, $\beta_i = [\beta_{0,i}, \beta_{1,i}, \beta_{2,i}]$ is the vector of model parameter means for lake group i, $\sigma_i^2 = [\sigma_{0,i}^2, \sigma_{1,i}^2, \sigma_{2,i}^2]$ is the vector representing the variance of model parameters among lakes belonging to group i, while $\beta = [\beta_0, \beta_1, \beta_2]$ and $\sigma^2 = [\sigma_0^2, \sigma_1^2, \sigma_2^2]$are the means and variance among groups, respectively.

## 3. Results and discussion

The Bayesian hierarchical linear regression model calculates lake-specific probabilities of CBB concentrations to exceed the two health risk levels for recreational use, under different TP and TN concentrations. Enabling lake managers to define combinations of TP and TN concentrations that will result in exceedance risk levels for pre-defined thresholds appropriate for each ecosystem can lead to optimal monitoring schemes and can minimize uncertainty associated with each lake ecosystem. In Fig. 1, we show the contour diagram of the exceedance probability response surface for all percentiles, for the 2 mg/L threshold. For a lake eutrophication management scheme, the lake manager can identify the risk level that (s)he wants to operate under. If a 90% risk level is chosen, then the combination of TN and TP concentrations that correspond to the 90% line in Fig. 8 signify the concentrations that give a 90% probability to exceed the 2 mg/L threshold. For a lower risk level, lower TN and TP concentrations are required. Alternatively, if TN and TP concentrations in the lake are measured under a monitoring scheme, or if criteria for TN and TP are set by the European Water Framework Directive or a relevant authority, the lake manager can have an estimate of what the risk level is to exceed the 2 mg/L threshold. To show how this might work, in Fig. 8, we plot the observed combinations of TN and TP concentrations for lake Engelsholm Sø along with the corresponding CBB concentrations. With red font, we show the CBB concentrations that exceed the preset thresholds, and we see that indeed all high CBB concentrations appear in the area that is above the 97.5% exceedance line. Only a few high CBBs are found on the risk level lines 25% and higher, while there is no "red font" in the "safe" area under the 2.5% risk line.

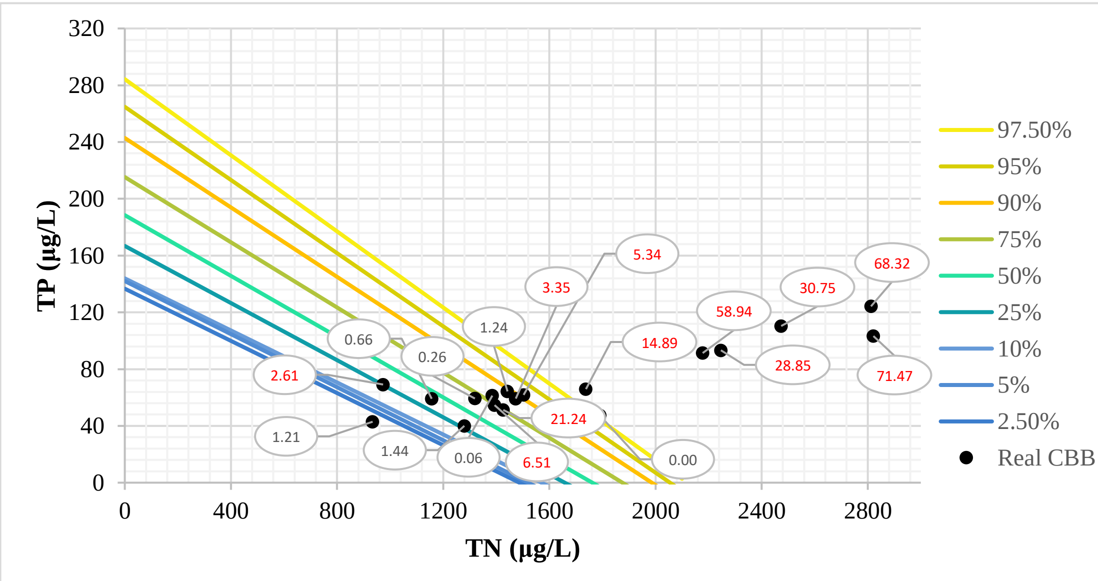


**Fig. 1.** Contour plot showing TN and TP concentrations and associated risk of exceedance for CBB concentrations of 2 mg/L.

### Acknowledgements

The work described in this paper has been conducted within the project WATER4CITIES, which is implemented in the framework of the EU Horizon2020 Program, Grant Agreement Number 734409.

### References

Mellios NK, Moe J, Laspidou C (2020) Using Bayesian hierarchical modelling to capture cyanobacteria dynamics in Northern European lakes, Water research, 186, 116356

Malve O, Qian SS (2006) Estimating nutrients and chlorophyll a relationships in Finnish lakes, Environmental Science & Technology, 40(24), 7848-7853

# Hydraulic Manifold Flow Problem: Analytical and Numerical Solutions

L. Amara[1], R.F. Carvalho[2]

[1]Department of Civil Engineering and Hydraulics, Faculty of Science and Technology, University of Jijel, Algeria
email: lyes.amara@univ-jijel.dz
[2]University of Coimbra, MARE, Department of Civil Engineering, Coimbra, Portugal
email: ritalmfc@dec.uc.pt

ABSTRACT

Hydraulic manifold usually consists of one relatively large pipe, in which there are numerous junctions with small pipes, usually relatively closely spaced, all allowing flow from the main pipe. The flow in dividing manifolds is a spatially varied flow and it is traditional analyzed as steady flow with different considerations of the two opposing forces known as friction and momentum. This work shows current past studies of manifolds based on Bernoulli, continuity and momentum equations and describes different general mathematical model for computing flows in manifold systems considering energy losses in different ways, whether friction is or is not considered and whether junction losses are or are not considered. The non-dimensional parameters affecting the flow distribution are identified, as well as comparison between models in different flow regimes: (1) equilibrium (2) momentum dominant (3) friction dominant and (4) momentum-friction reciprocity. For a special case, it presents an analytical solution and numerical simulations using 3D Finite volume methods, which are compared. Analytical solution is of great interest for most practical cases in hydraulic engineering. However, when kinetic energy is important, it may lead to some deviation. 3D numerical models results are fair.

## 1. Introduction

Manifold flow has several kind of applications as in irrigation systems, ventilation and refrigeration, fire sprinkler systems, submarine diffuser as part of a wastewater dispersal operation or large locks on navigable waterways. The optimal distribution of fluid throughout the equipment and the efficient of manifold system is of paramount importance as the flow mal-distribution can result into increased pressure drop, creation of dead zones or hot spots, back-mixing and in the case of industrial applications reduced heat or mass transfer and thermal induced failures.

Although manifold can be attributed to dividing, combining, parallel and reverse flow, in this work we will focus on a pipe dividing flow. Two opposing forces known as friction and momentum are usually considered, the friction tends to produce a pressure drop whereas loss of momentum due to deceleration of the fluid through branching in the manifold results in a pressure rise.

## 2. Analytical Solution

Consider a manifold pipe of a constant diameter $D$ and length $L$ having an equally-spaced circular exit ports, all of the same diameter $d$ (Fig. 1). The manifold is connected upstream to a tank or a reservoir under a total head $H$ and the downstream end of the main is a dead end. The exit flow from each port of circular section is done by Eq. 1.

$$q = C_d S \sqrt{2gh} \tag{1}$$

where $q = q(x)$ is the flow rate of exit ports along the manifold, $h = h(x)$ the driving head which is the vertical distance from the centreline of port to the local hydraulic grade line above that port (Fig. 1), $S$ the cross-section area of the exit port, $g$ acceleration due to gravity and $C_d$ is the discharge coefficient taking account of different energy losses through the orifices port and eventually lateral small pipes. Here in Eq. (1), the flow from the lateral ports is presumed to exit as a jet into the atmosphere. Considering an infinite number of exit ports spaced of an infinitesimal distance $dx$, the elementary head loss $dJ$ along the manifold can be expressed by Darcy-Weisbach equation. According to Bernoulli's theorem, conservation of the total energy along the manifold requires the following equality:

$$H = h + \frac{Q_x^2}{2gA^2} + J \qquad (2)$$

with $A = \pi D^2/4$ denoting the manifold cross-section area. Differentiating Eq. (2) with respect to the streamwise x-coordinate and neglecting kinetic energy effect (convective acceleration) and combining those concepts and after some simplifications, it can be obtained:

$$\frac{dh}{dx} + C\left[\int_x^L K\sqrt{h}\,dx\right]^2 = 0 \qquad (3)$$

which is a non-linear first-order differential equation due to the varying coefficients $K$ and $C$ that governs the manifold problem.

## 3. Numerical Model

OpenFOAM® is a widely used open source C++ toolbox, which includes different solvers, tools and libraries that can be used to solve any Partial differential equation as Navier-Stokes equations / Reynolds-Averaged Navier-Stokes (RANS) equations governing the motion of the 3D incompressible and isothermal flows in (Eq. (1) to (2)):

$$\nabla \cdot u = 0 \qquad (1)$$

$$\frac{\partial \rho u}{\partial t} + \nabla \cdot (\rho u u) = g - \nabla p * + \rho g + \nabla \cdot \tau \qquad (2)$$

where $u$ is the mean velocity vector, $p*$ is the modified pressure adapted by removing the hydrostatic pressure from the total pressure, $\alpha$ is the VOF function, $t$ is the time, $\rho$ is the fluid density, $g$ is the acceleration due to gravity, $\tau$ is the shear stress tensor. Simulations require a detailed 3D model of the geometry that was constructed by coordinates to define the bottom and the structure using Salome to represent it through a stl ("stereolithography") file, to be used in OpenFOAM® snappyHexMesh tool to built a mesh in a parallelepiped cutted by the stl (Fig 1).

## 4. Example

In order to verify accuracy of the present analytical solution, a comparison is performed on an example taken from Yıldırım (2007). Then characteristics are changed and analytical and numerical solutions are compared. Figure 1 shows the scheme, the numerical results and the superimposed graphs for pressure and flow obtained by analytical and numerical results.

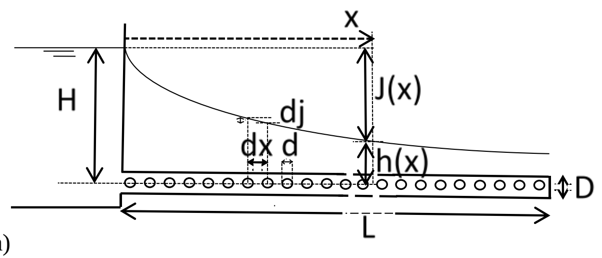

a)

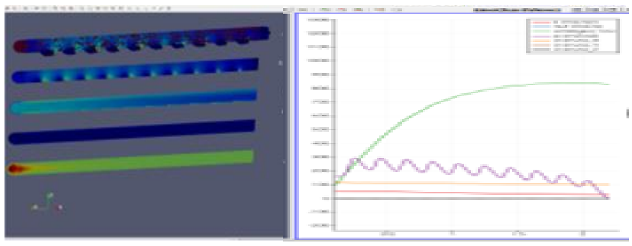
b)

**Fig. 1.** Manifold model: a) Scheme; b) example of numerical solution for 10 holes.

## 5. Conclusions

In the present paper a simplified dividing manifold flow problems is presented and modelled. For seek of verification and validation, a comparison with available data from Yıldırım (2007). was performed. Then, different parameters related with energy dissipation characteristics were changed and differences between analytical and numerical solutions rise when those effects become more important.

**Acknowledgements**

FCT (Portuguese Foundation for Science and Technology) through the Project UID/MAR/04292/2020, financed by MEC (Portuguese Ministry of Education and Science) and FSE (European Social Fund), under the programs POPH/QREN (Human Potential Operational Programme from National Strategic Reference Framework) and POCH (Human Capital Operational Programme) from Portugal2020. The authors also acknowledge the Laboratory for Advanced Computing at University of Coimbra for providing HPC, computing.

**References**

Yıldırım, G. (2007). Analytical relationships for designing multiple outlets pipelines. *Journal of irrigation and drainage engineering*, *133*(2), 140-154.

# FIWARE-enabled smart solution for the optimal management and operation of raw-water supply hydraulic works

Panagiotis Kossieris[1], Christos Pantazis[1], Vasilis Bellos[1,2] and Christos Makropoulos[1]

[1] National Technical University of Athens, School of Civil Engineering, Department of Water Resources & Environmental Engineering, emails: pkossier@mail.ntua.gr, xpanta@outlook.com, vmpellos@mail.ntua.gr, cmakro@mail.ntua.gr

[2] Democritus University of Thrace, Department of Environmental Engineering, Greece
email: vbellos@env.duth.gr

ABSTRACT

Raw-water supply systems are characterised by high complexity and large-scale nature, since they are typically composed of a variety of interconnected hydraulic works. The optimal management and operation of such systems is undoubtedly a key priority, and at the same time, a challenge, for any water utility. In the era of digital transformation, the development of standardized and interoperable solutions that allow seamless integration of tools and models (usually developed by different providers), along with the existing network of sensors (usually installed by different vendors), is of paramount importance towards a holistic and integrated management of such complex systems. In this work, we showcase a first attempt to develop such an interoperable digital solution for the management of the external raw-water system that serves the city of Athens (Greece). Specifically, we build around FIWARE, a standardization framework supported by the European Connecting Europe Facility, to develop a FIWARE-enabled web platform that integrates a great number of flow and quality sensors, and supports system operators in decision making via innovative models and analytics.

## 1. Introduction

To support water utilities in the management and operation of the complex raw-water supply systems, a plethora of models, services and tools are required. Typically, these services are being developed as standalone applications, tied tightly to the peculiarities of the problem and sub-system in focus, built on top of isolated information systems, and without any provision for integration with other, new or existing, tools and data sources. A possible remedy to this fragmentation is data standardization, since it provides the means for the seamless integration of different services and data sources, which will lead eventually to a more integrated and holistic management of the complex and large-scale water systems (Makropoulos & Savić, 2019). An ever-growing development in the realm of data standardization is FIWARE (FIWARE, 2022), a curated framework of open-source platform components and standardization protocols, supported by the European Commission, which aim to accelerate the development of smart solutions. The cornerstone of FIWARE is the *Context Broker* (*CB*) that supports the management of context information, enables context updates and allows access to the context information in a standardised way. This is achieved via a simple yet powerful Application Programming Interface API, currently aligned with the *NGSI-LD* standard (NGSI-LD, 2021), by the European Telecommunications Standards Institute (ETSI).

## 2. A Fiware-enabled smart solution for the raw-water conveyance system of Athens

### *2.1. The external raw-water conveyance system of Athens*

The external conveyance system that serves the metropolitan area of the city of Athens (Attica, Greece) is one of the largest and more complex in Europe and worldwide, composed by an extensive system of aqueducts of total length greater than 495 km. Across the conveyance system, a large number of hydraulic structures exist to regulate flow and store raw-water near Athens, along with stilling basins for energy dissipation and hydro-power stations for energy productions. In this work, we focus on the open-channel aqueduct of “Mornos channel”, which is one of the most important parts of the system with a total length of 131 km, conveying water from the western regions of Greece to the four water treatment plants of Athens. The management of the system is conducted via an extensive network of sensors, which monitor, on real-time basis, water quality parameters (i.e., temperature, turbidity and conductivity), the hydraulic conditions (discharge and water level) and the operation of hydraulic works (e.g., sluice gate openings). The sensors have been installed from different vendors over the years, leading inevitably to the development of independent proprietary information systems that co-exist within the water utility. In this context, the integration of different legacy systems (i.e., sensors, data streams, data management and visualization platforms, algorithms) into a single digital solution with interoperable and portable capabilities is of high practical interest to facilitate the management of the system.

### *2.2. A FIWARE-enabled web platform for optimal raw-water management*

To integrate the different data sources of the system under study into a common information system, a fully operational FIWARE-enabled digital solution has been developed. The cornerstone of the solution is a fully functional and easily extendable *CB* that currently integrates data from more than 50 sensors, along with static information of the conveyance system (e.g., location of sensors, length of aqueducts, characteristics of hydraulic structures). This enables any third-party FIWARE-compliant application, model and tool to obtain access to this data using NGSI-LD standardization protocols in a straightforward and interoperable way.

Taking advantage of the integrated data sources, a new FIWARE-compliant web platform has been developed to support the operators to process, analyse and visualise data from different sensors, allowing the combined monitoring of flow and quality characteristics of raw-water via a single web portal, on real-time basis. The platform has been based on Nessie technology, an information system developed in the National Technical University of Athens, for the collection, process, analysis and visualization of high-resolution data from sensors. The dashboard of the web platform developed is presented in Fig. 1.

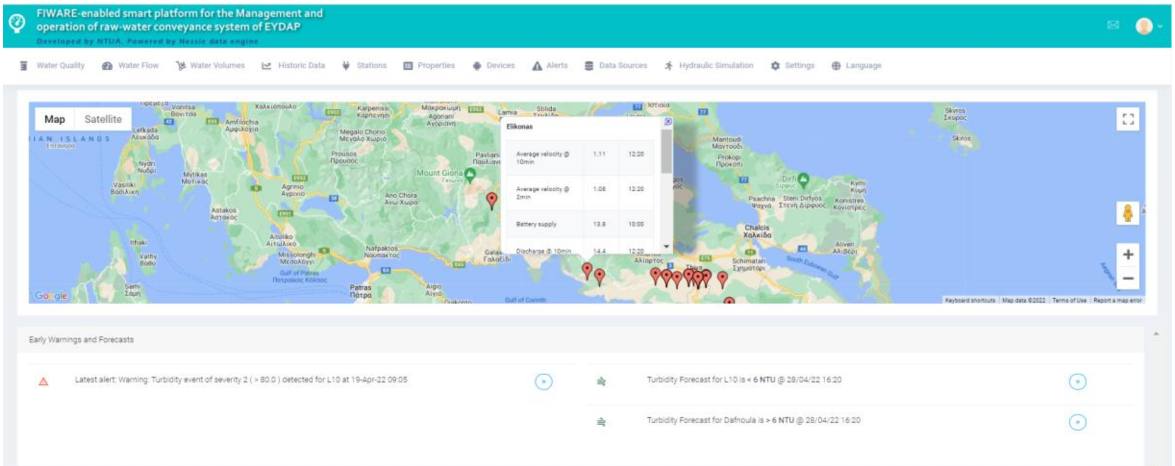


**Fig. 1.** Web platform for the real-time monitoring and management of raw-water system of Athens.

On top of this, a series of analytics have been developed and integrated with the platform to support operators in decision making towards the optimal management of the conveyance system. The first analytic provides advice on the optimal openings of sluice gates to establish specific flow conditions in the conveyance system. It is based on grey-box approach that combines physics-driven equations to model flow through sluice gates and over spillways, along with data-driven techniques for parameter estimation and data reconciliation (Bellos et al., 2022). The second analytic concerns quality aspects of raw-water and provides early-warnings for high turbidity events along with forecasts for the level of turbidity at the downstream parts of the system, given turbidity of raw-water upstream. To accomplish this, a deep neural network was developed to simulate the highly non-linear and noise behaviour of turbidity. The third analytic is a dynamic regression model that provides forecast of the next-day water supply volumes, to enable support operators to regulate the flow in the channel accordingly. The three analytics have been integrated with the FIWARE-enabled solution and are available to the end-users via the dashboard of the web platform.

**Acknowledgements**

This work was carried out in the framework of Fiware4Water project (2019-2022), receiving funding from the European Union's Horizon 2020 research and innovation programme under grant agreement No. 821036.

**References**

Bellos V., Kossieris P., Efstratiadis A., Papakonstantis I., Papanicolaou P., Dimas P., & Makropoulos C. (2022). Fiware-enabled tool for real-time control of the raw-water conveyance system of Athens. Proceedings of the 39th IAHR World Congress,19-24 June 2022, Granada, Spain.
FIWARE. (2022). FIWARE: THE OPEN SOURCE PLATFORM FOR OUR SMART DIGITAL FUTURE. https://www.fiware.org/
Makropoulos, & Savić. (2019). Urban Hydroinformatics: Past, Present and Future. Water, 11(10), 1959.
NGSI-LD. (2021). Context Information Management (CIM), NGSI-LD API. https://www.etsi.org/deliver/etsi_gs/CIM/001_099/009/01.01.01_60/gs_CIM009v010101p.pdf

# Setting the basis of a Smart Platform for the Systematic Monitoring and Control of the Water Supply Network of Tilos Island

Miltiadis GYMNOPOULOS[1], Georgios TZANES[2], Georgios MITSOPOULOS[3], Dimitrios ZAFIRAKIS[4], Ioannis KALDELLIS[5], Anastasios STAMOU[6]

[1,2,3,6] Department of Water Resources and Environmental Engineering, School of Civil Engineering, NTUA
email: mgymnopoulos@mail.ntua.gr
email: gtzanes@mail.ntua.gr
email: gmitsop@mail.ntua.gr
email: stamou@mail.ntua.gr

[2,4,5] Mechanical Engineering Department, School of Engineering, UNIWA
email: g.t.tzanes@uniwa.gr
email: dzaf@uniwa.gr
email: jkald@uniwa.gr

ABSTRACT

We develop optimally the new water supply network of Livadia village in Tilos Island using the EPANET model. This optimal EPANET network, which involves 3 pressure reducing valves, 7 isolating valves, 3 flowmeters and 7 pressure gauges, faces the significant problem of high pressures of the existing network that causes damages and failures, and sets the basis of the Smart Platform for the systematic monitoring and control of the hydraulic and energy behavior of the water supply network of the Municipality of Tilos.

## 1. Introduction

Water supply networks in Greek islands face multiple challenges, such as freshwater seasonal availability, water quality issues, aging of infrastructure and, often, excessive energy demand. Such challenges threaten their economic efficiency, long-term sustainability, and resiliency, given that they become more and more intense due to the effects of climate change. The project DarWEN aims at the development of a Smart Platform to deal with the above-mentioned threats, and furthermore, optimize the efficiency of water and energy systems via a holistic approach that is applied in Tilos Island. This approach involves the development of a Smart Platform for the systematic monitoring and control of the hydraulic and energy behavior of the water supply network of the Municipality of Tilos. In this work, we present the basis of the Smart Platform that is the hydraulic model of the proposed new water supply network of the Livadia village.

## 2. Materials and methods

We used the hydraulic model EPANET (Rossman, 2000) and based on data from the final design of the network and field measurements that we performed within the present study, we developed the model of the existing water supply network of Livadia village that is shown in Figure 1; it consists of 3 wells (Mikro Chorio, Athymies and Fraktis), a spring (Potamos), a small collecting tank, two tanks, a break pressure tank (BPT) and the distribution network.

## 3. Results and discussion

A major problem of the existing network is the very high static pressures that often exceed the permissible maximum value of 60 m causing network damages/failures. To detect the locations of high pressures, we performed calculations of the existing network, which showed that pressure exceeds 60 m in 372 of the totally 373 consumption nodes, it exceeds 110 m in most of the nodes, and its maximum value is equal to 122.5 m. Then, we divided the network in 3 pressure zones based mainly on ground elevations and performed calculations for various scenarios - combinations of isolation and pressure reducing valves - to configure the new optimal distribution network that involves the minimum number of valves. For this optimal new network, which involves 3 pressure reducing valves and 7 isolating valves, calculations showed that the pressure is smaller than 60 m in 363 nodes, while its maximum value is equal to 90.0 m. In this network, we installed 3 additional flow meters and 7 pressure gauges to control discharge and pressure.

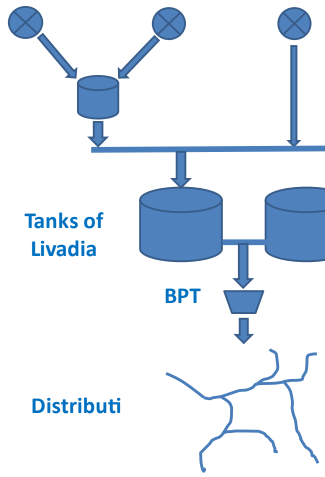


**Fig. 1.** Schematic layout of the water supply network of Livadia.

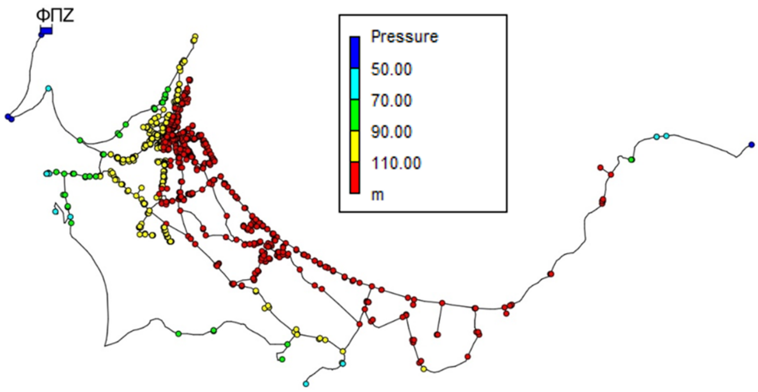


(a)

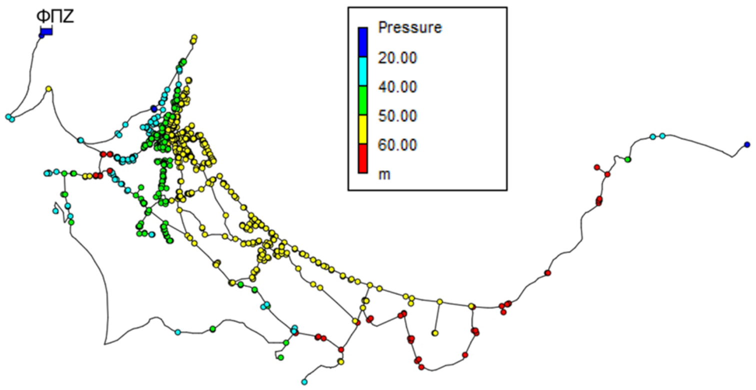


(b)

**Fig. 2.** Calculated pressure values of (a) the existing distribution network and (b) the new optimal distribution network.

## 4. Conclusions

Using the EPANET model, we configured the optimal water supply network of Livadia village in Tilos Island that faces the significant problem of high pressures of the existing network that causes several damages and failures. This EPANET network, which involves 3 pressure reducing valves, 7 isolating valves, 3 flow meters and 7 pressure gauges, sets the basis of the Smart Platform for the systematic monitoring and control of the hydraulic and energy behavior of the water supply network of the Municipality of Tilos.

**Acknowledgements**

This research has been co-financed by the European Union and Greek national funds through the Operational Program Competitiveness, Entrepreneurship, and Innovation, under the call RESEARCH – CREATE – INNOVATE (project code: T2EΔK-01578).

**References**

Rossman LA (2000) EPANET 2, User's Manual. U.S. Environmental Protection Agency, Cincinnati, OH, U.S., 200 pp.

# SWANP 4.0: a novel release of software for water network analysis, partitioning and protection of water distribution networks

Armando DI NARDO[1,3], Enrico CREACO[2,3], Michele IERVOLINO[1,3], Giovanni Francesco SANTONASTASO[1,3]

[1] Department of Engineering Università degli Studi della Campania Luigi Vanvitelli, Italy
email: armando.dinardo@unicampania.it
email: michele.iervolino@unicampania.it
email: giovannifrancesco.santonastaso@unicampania.it

[2] Department of Civil Engineering and Architecture Università di Pavia
email: creaco@unipv.it

[3] Med.Hydro srl, spinoff company, Italy
email: info@medhydro.eu

ABSTRACT

The paper presents SWANP© 4.0 (Smart Water Network Partitioning and Protection), a novel software release developed by the authors with the support of the water utility GORI Spa and the spin-off company Med.Hydro srl. The release 4.0 offers to the operators some innovative tools based on the main results of research activities carried out by the authors on the topics of hydraulic modelling, water network partitioning and water quality protection. The novel approaches have already been tested on real case studies of national and international water utilities. SWANP© 4.0 is available after a free registration at the website www.swanp.net for a limited number of networks, and it allows performing DDA (demand drive approach) and PDA (pressure driven approach) simulations, defining automatically the optimal layout in terms of number, shape and dimension of DMA (district meter area), managing water pressure with pressure PRV (pressure regulation valves), identifying optimal positioning of water quality detection points with or without calibration model and computing resilience of water systems by means of innovative global and local performance indices able to compare original and modified layouts.

## 1. Context

Hydraulic commercial software dedicated to water distribution network simulations contains generally the tools traditionally required by operators to study the behaviour of water networks under both design and service conditions. However, while significant progresses were achieved in Graphical User Interfaces, integration with calibration tools, with GIS (Geographic Information System) framework and with remote control systems to better describe and manage devices, water demands and water losses, no significant improvements were achieved in water network partitioning (Di Nardo et al., 2013), water network protection (Di Nardo et al., 2015), optimization procedures (Santonastaso et al., 2019) and local and global performance indices (Di Nardo et al., 2020). This clashes with the research achievements in the two recent decades, consisting of numerous operational algorithms and tools for these applications.

Based on more than 15 years of research in the field of water network analysis conducted to investigate more accurate numerical methods, to find optimal design procedure to define automatically optimal water network partitioning for the shape and dimension of district meter areas (DMAs), and to investigate innovative approaches to network protection from accidental or intentional contamination, as well as testing novel methodologies on some national and international case studies, the SWANP© (Smart Water Network Partitioning and Protection) software has been updated to the 4.0 release.

The novel release of SWANP© 4.0, funded by GORI Spa and developed by the spin-off company Med.Hydro srl, is freely available on-line on website www.swanp.net for a limited number of networks upon registration.

## 2. Software innovative features

SWANP© was developed in Phyton and integrated in a user-friendly GIS interface, which contains innovative open libraries that are updated automatically. It includes some innovations based on the implementation of advanced optimization approaches essentially regarding: 1) an advanced hydraulic simulation engine in DDA and PDA approach, based on high-order global algorithm (Creaco et al., 2021); 2) a dedicated tool to automatically define the optimal layout of DMAs and provide to water utilities a flexible decision support system to find different solutions in terms of number of districts, performance indices, compliance with the physical constraints, etc. based on some clustering and dividing optimization procedures developed by (Santonastaso et al., 2019); 3) to manage water pressure with pressure PRV (pressure regulation valves); 4) an innovative tool to select the optimal positioning of quality detection devices to protect water system from contamination based on both topological and simulation approaches (Santonastaso et al., 2021).
In Figures 1 and 2, two sample screenshots of SWANP© 4.0 are reported showing the results of the clustering phase with 4 DMAs and of the dividing phase with 4 flow meters and 11 gate valves for a small network.


**Fig. 1.** An example of Clustering phase obtained with SWANP© 4.0


**Fig. 2.** An example of Dividing phase obtained with SWANP© 4.0

**Acknowledgements**
This research was supported by shared resources of the GORI spa (www.goriacqua.com) and Med.Hydro (www.medhydro.eu) that are the 1owners of SWANP© 4.0 available at www.swanp.net

**References**

Di Nardo A, Di Natale M, Santonastaso G.F, Venticinque S (2013) An automated tool for smart water network partitioning. Water Resources Management, 27, 4493–4508.
Di Nardo A, Di Natale M, Musmarra D, Santonastaso GF, Tzatchkov V, Alcocer-Yamanaka VH (2015) Dual-use value of network partitioning for water system management and protection from malicious contamination. Journal of Hydroinformatics, 17, 3, 361-376.
Santonastaso GF, Di Nardo A, Creaco Enrico (2019) Dual topology for partitioning of water distribution networks considering actual valve locations. Urban Water Journal, 16, 7, 469-479.
Di Nardo A, Di Natale M, Di Mauro A, Díaz EM, Blázquez Garcia JA, Santonastaso GF, Tuccinardi FP (2020) An advanced software to design automatically permanent partitioning of a water distribution network. Urban Water Journal,17,3, 259-265.
Creaco E, Di Nardo A, Iervolino M, Santonastaso GF (2022) High-Order Global Algorithm for the Pressure-Driven Modeling of Water Distribution Networks. Journal of Water Resources Planning and Management, 148, 3.
Santonastaso G, Di Nardo A, Creaco E, Musmarra D, Greco R, (2021) Comparison of topological, empirical and optimization-based approaches for locating quality detection points in water distribution networks. Environmental Science and Pollution Research, 28, 33844–33853.

# Stress-testing for water-energy systems by coupling agent-based models

Georgia Konstantina SAKKI[1], Andreas EFSTRATIADIS[1], Christos MAKROPOULOS[1]

[1] Department of Water Resources and Environmental Engineering, School of Civil Engineering, National Technical University of Athens, 15780 Athens, Greece
email: sakkigk@mail.ntua.gr

email: andreas@itia.ntua.gr

email: cmakro@mail.ntua.gr

ABSTRACT

## 1. The water-energy nexus under uncertainty

### *1.1. Setting the scene*

Managing water resources for growing demands of energy and food while sustaining the environment is the greatest challenge of our era, especially when we are dealing with complex adaptive natural–human systems (Machell et al., 2015). The performance of water-energy systems is strongly depending on hydroclimatic processes and human behaviors, while both components are highly uncertain and unpredictable in a long-term perspective. In this vein, the typical engineering approach across the water-energy nexus, in which the role of society is reflected in rather simplified means, e.g., in terms of water and/or energy demands, legal constraints, technical specifications and management rules, is insufficient. Herein, we propose the incorporation of the human factor to the long-term management policy of water-energy systems, since the social and the technical system are inextricably linked (Walker et al., 2015). To assess the management of such systems, we attempt to stress-test them under different disturbances, which are driven by both expected and highly unpredictable changes e.g., socioeconomic and hydrometeorological fluctuations, and black-swan events, respectively. By coupling the two major research fields, namely the water-energy nexus and the social behavior, in an uncertainty-aware framework, we introduce the concept of *stochastic socio-hydrological systems.* In this context, the response and adaptation of society plays the role of music, while the plethora of disturbances the role of the conductor.

### *1.2. The social component and its modelling*

In order to establish a comprehensive approach for representing such complex sociotechnical systems, we first outline and explain all important synergies, complementarities and conflicts induced by the social factor. In addition to the obvious interaction of water and energy demands, also driven by weather conditions, we investigate several other social drivers, including decision-making, management policy and operation, and reaction to external influences and pressures.

An important issue, which deserves further investigation, is the response time of each factor. In particular, media and public awareness campaigns may take longer to create tangible effects, while sharp changes in energy and water prices may induce faster reactions. Furthermore, we also study the effect of crucial, urgent and abnormal circumstances, which are totally unpredictable and may affect both the micro- and macro-behavior of an entire society over the longer term. These include geopolitical changes, economic crises, pandemics, as well as long-term water shortages, causing major changes to spatiotemporal patterns of water and energy consumption. To simulate the human component of sociotechnical systems, we take advantage of recent advances in agent-based modelling (ABM), which integrate complex adaptive system theory and distributed artificial intelligence (Bonabeau, 2002). The key principle of ABMs is to divide a complex system into representative elements, called agents, characterized by their own data, knowledge and behaviors. By adopting a bottom-up approach, as demonstrated in Figure 1, to study the agent interactions both with the technical system and among each other, at the micro level, it will allow us to draw conclusions about the system's (emergent) behavior at the macro level.

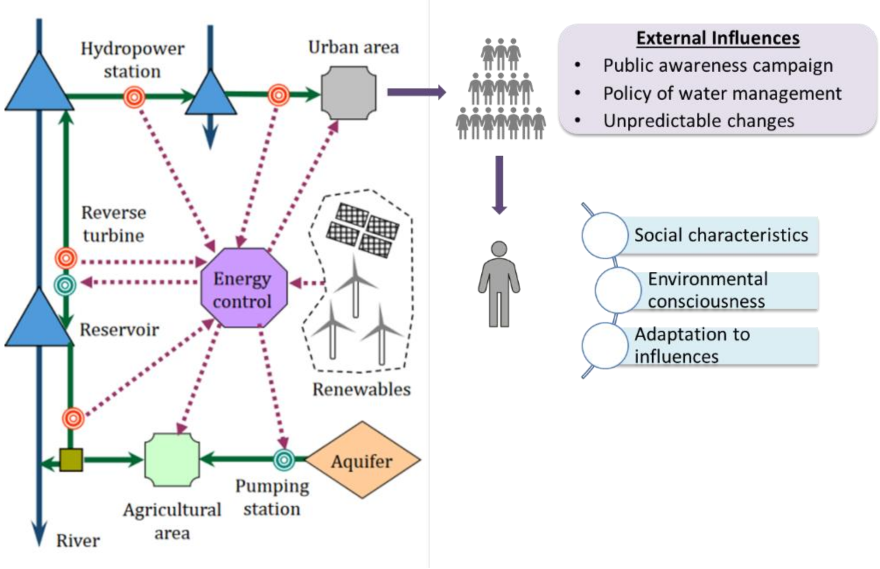


**Fig. 1.** Conceptual demonstration of a water-energy system taking account for the social component.

### *1.3. The hydrometeorological component and its modelling*

In a highly fluctuating and eventually changing climate, the historical data of crucial hydrometeorological drivers, e.g., rainfall, runoff, and evaporation, provide insufficient information for the long-term assessment of water-energy systems under the stress-testing paradigm. To overcome this, we use stochastic models in order to provide synthetically-generated input time series that reproduce the probabilistic regime of the process of interest, as reflected in the historical data, and their long-term changes, that are of key importance in the assessment of reliability, sustainability and resilience of water-energy systems (Koutsoyiannis et al., 2009).

## 2. Revisiting the long-term management of the Athens water-energy system

As a proof of concept of the proposed framework, we analyze the complex and highly extended water-energy system of Athens, Greece, and we push it beyond its standards, in order to determine its turning point of resilience. Specifically, the water-energy system of Athens addresses intrinsically uncertain water supply and irrigation demands that may stress it across all scales, and it is also subject to a number of operational and environmental constraints. This system includes two interconnected reservoirs (Mornos, Evinos), providing water via gravity, as well as the natural lake Hylike, lying in a karstic background, providing water through pumping, with significant cost. In this vein, we investigate whether this system is successful, robust, and resilient under numerous external influences and stresses, by using as a key information the human's behavior.

The core simulation model employs a simplified representation of the main system elements, to estimate the abstractions from the three reservoirs, driven by synthetic inflow data of 2000 years length, and stochastic demands. The inflows are generated a priori, through the anySim stochastic simulation package (Tsoukalas et al., 2020). On the other hand, the demand data are provided by an ABM procedure, which accounts for dynamic information obtained from the simulation model, by means of storage conditions and associated water prices.

**Acknowledgements**

The research of this paper was carried out within the framework of the project "Modernization of the management of the water supply system of Athens – Update", funded by the Water Supply and Sewerage Company of Athens (EYDAP S.A.).

**References**

BonabeauE (2002) Agent-based modeling: Methods and techniques for simulating human systems, Proceedings of the National Academy of Sciences, 99(suppl_3), 7280–7287
Koutsoyiannis D, Makropoulos C, Langousis A, Baki S, Efstratiadis A, Christofides A, Karavokiros G, Mamassis N (2009) HESS Opinions: Climate, hydrology, energy, water: recognizing uncertainty and seeking sustainability, Hydrology and Earth System Sciences, 13(2), 247–257
Machell J, Prior K, Allan R, Andresen JM (2015) The water energy food nexus – challenges and emerging solutions, Environmental Science: Water Research & Technology, 1(1), 15–16. https://doi.org/10.1039/C4EW90001D
TsoukalasI, Kossieris P, MakropoulosC (2020) Simulation of Non-Gaussian Correlated Random Variables, Stochastic Processes and Random Fields: Introducing the anySim R-Package for Environmental Applications and Beyond, Water, 12(6), 1645
Walker WE, Loucks DP, Carr G (2015) Social Responses to Water Management Decisions, Environmental Processes, 2(3), 485–509

# SINERGEA - Energy: Modelling energy consumption in wastewater systems during rainfall events

Luís M DAVID[1], Armando PINTO[2], Anabela OLIVEIRA[3], António MARTINS[4]; Alexandre ATAÍDE[5]; Osvaldo SILVA[6]

[1,2,3] Laboratório Nacional de Engenharia Civil, Portugal
email: ldavid@lnec.pt
email: aoliveira@lnec.pt
email: apinto@lnec.pt

[4,5,6] Águas do Algarve S.A., Portugal
email: antonio.m.martins@adp.pt
email: a.almeida@adp.pt
email: osvaldo.silva@adp.pt

ABSTRACT

## 1. Introduction

The urban water cycle infrastructures are important consumers of electricity. Thus several efforts have been made recently to increase their energy efficiency. During rainfall events, the increase in flows pumped by interceptor sewers and treated in wastewater treatment plants (WWTP) can lead to significant increases in energy consumption. These flow increases occur not only in the combined sewer systems, but also in separate wastewater systems, due to water infiltration into the sewers, the rainfall-derived infiltration and inflow (RDII) component, and illicit misconnections between stormwater and sewage systems. Controlling rainfall-derived inflows into wastewater systems is a difficult challenge that has received increasing attention.

However, in coastal urban areas, it is also a common practice to store and transport stormwater from ephemeral watercourses to the WWTP to protect bathing water quality during small rainfall events. Coastal wastewater systems often require multiple pumping stations (PS) along the coast, each with its own sanitary sewer overflow (SSO). Most PS are designed considering only the dry weather flows and their flow measurement considers only the pumped flows, i.e., it completely ignores the discharged SSO. Thus, increasing the energy efficiency of these systems requires the knowledge on three key issues: the flows pumped and treated during wet weather; the impact on receiving water bodies of the SSO discharged at each pumping station; the potential to improve the energy efficiency of the system as a whole.

Within the SINERGEA Project, an intelligent real-time decision support system was developed, aiming at the management of emergencies of flooding and bathing water contamination, and the efficient use of energy (David et al, 2022). This system is being demonstrated at the city of Albufeira, Portugal, and its coastal neighbourhood. This paper describes the objectives and methodology developed to model energy and its application to the demonstration case.

## 2. Integrated modelling of energy consumption and wet weather discharges

The integrated management of the energy efficiency of waste water systems and the quality of water bodies must include the integrated modelling of both systems. It should also take into account tariffs, potential for improvement in each equipment or station in the system and alternatives for the design and management of the entire sanitation infrastructure. Given that currently few deterministic modelling programs include energy consumption modelling, the well-known SWMM model is used herein to model the hydrodynamic component and a generic, new tool was developed to calculate energy consumption in pumping stations and WWTP using Python.

The calculation of energy consumption in pumps is based on the results of flow rates and water heights provided by SWMM. The calculation of the energy consumption of the remaining drainage and treatment equipment is carried out in a simplified way, taking into account different types of functions: fixed consumption (or consumption that varies depending on the month); consumption as a function of the flow provided by SWMM during a set of previous calculation steps; consumption as a function of flow and external variables such as temperature and previous rainfall. In the mass balances, it also allows for considering the contribution of energy production equipment by alternative energy sources, such as photovoltaic panels (depending on the atmospheric radiation of long and short waves) or the use of biogas in WWTP. The model provides energy consumption, cost and carbon footprint results by equipment, by station and for the overall system. In practical applications, the equipment to be modelled in each pumping station or WWTP will depend on the quantity and quality of the existing information on the operation and energy consumption of each equipment.

An important challenge for the success of these approaches is related to the estimation of flows discharged by sanitary sewer overflows, since these discharges are usually not monitored. An innovative methodology was developed that uses a lumped conceptual model to estimate the useful area of the catchment and the flows discharged by SSO from the flows measured in pumping stations. The parameters obtained for the conceptual model serve as a basis for the SWMM model calibration.

## 3. Demonstration case

The SINERGEA system is being demonstrated on the city of Albufeira, Portugal, and its coastal neighbourhood, where the stormwater separate network, the interceptor sewer system, and coastal bathing waters were modelled in detail (David et al, 2022). Figure 1 shows the SWMM model of the interceptor sewer system, which serves several coastal urban-tourist developments. It has a WWTP, ten pumping stations (some with variable speed drive) and two submarine outfalls.

Figure 2 shows results of the energy consumption model in a pumping station. Figure 3 shows the results of the calibration of the flows pumped in a pumping station, where the estimation of the flows discharged by SSO is also obtained. The model is currently being calibrated and will soon be validated for other rainfall events, providing results on energy consumption, costs and carbon footprint by equipment, by season and for the overall system. The model will then be used to study alternatives that promote energy efficiency.


**Fig. 1**. Map of the interceptor sewer system and WWTP.

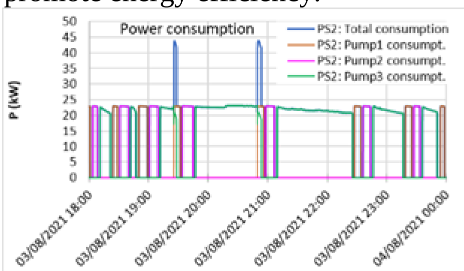


**Fig. 2**. Energy consumption at a pumping station.

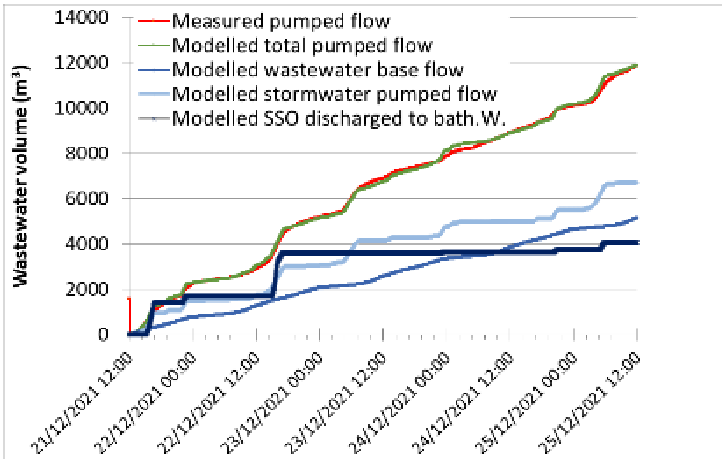


**Fig. 3.** Calibration of flows pumped at a pumping station and estimation of SSO discharges.

**Acknowledgements**

This work was co-funded by the European Regional Development Fund (FEDER), under programs POR Lisboa2020 and CrescAlgarve2020, through Project SINERGEA (ANI 33595).

**References**

David et al. (2022). SINERGEA - Real-time forecasting system for managing floods, bathing water quality and wastewater energy consumption. Submitted to the 7th IAHR Europe Congress.

# Average hyper-annual rainfall as a regional variable in Central Macedonia: use of a geostatistical approach to identify areas with drought trends

Anthimos Spyridis[1], Alexandros Konstantinidis [2], Vasiliki Koutalou[3], Konstantinos Perakis[4] Aris Psilovikos[5]

[1,3] HYETOS SA, GR
email: yetos@otenet.gr
[2] Department of Surveying and Geoinformatics Engineering, IHU, GR
email: akonsta @ihu.gr
[4] Department of Planning and Regional Development, University of Thessaly, Pedion Areos, 38334, Volos, GR
email: kostasperakis1@gmail.com
[5] Department of Ichthyology & Aquatic Environment, University of Thessaly, Fytoko Str., 38446, Volos, GR
email: psiloviko@uth.gr

## ABSTRACT

Natural phenomena, as observed and recorded in nature, can be determined by a spatial distribution of certain characteristic measurable quantities that describe them and are called Regionalized Variables. The geostatistic approach of such physical problems is based on the spatial structure presented by all these regional variables. The correct mathematical study of such variables is difficult and shows significant deviations because spatial variability is usually extremely unstable, with all kinds of discontinuity and anisotropies.

The numeric values of a regional variable z(x) and z($_{xi}$) should not be interpreted as independent realizations of a random function Z(x), because this view does not consider the spatial autocorrelation between two adjacent values z(x+h) and z(x). In the science of geostatistics the two independent aspects, randomness and spatial structure, that characterize peripheral variables, are a random function.

The present paper examines a new regional variable of the average hyper-annual rainfall, of five years for the years 2015-2020 for an area of the Region of Central Macedonia (Fig. 1.), which was approached through geostatistical analysis. For this purpose, rainfall data from 14 Meteorological Stations of the region were used, supported by the National Observatory of Athens (free data from meteo.gr).

These data were utilized as input for the extraction of an experimental semi-variogram (Fig. 2.), referring to the aforementioned regional variables. The output immediately showed the spatial structure of the phenomenon. In this experimental semi-variogram, several theoretical semi-variogram models were adapted, with the Exponential one to prove the most adaptive in our case. By This Model (Power Model), which describes with very good adjustment the corresponding experimental semi-variogram, the characteristic sizes (range, sill, nugget effect) were extracted and the degree of spatial dependency of the examined regional variable was determined and quantified. [xxx1] By studying the behavior of the semi-variogram for various directions ω (directions ω = 0°, 45°, 90° and 135°, with angular tolerance 45°), it was possible to determine the anisotropy of the phenomenon.With the help of the exponential model of adjustment of the semi-variogram and using an appropriate geostatistical interpolation method (Kriging method), the optimal surface was obtained that simulates the new peripheral variable.

From this process, the vector spatial planes that display the iso-curves for the new regional variable (Fig.3) were produced, the perpendicular vectors on the iso-lines (Fig. 4), and which vividly show the mode of manifestation and the spatial distribution of the phenomenon. Also, a corresponding one was produced that shows the flow paths of the phenomenon (Fig. 5) that lead to the emergence of low values, and therefore, in areas that show a tendency for drought.

In conclusion, it appears that this new regional variable, i.e., the average hyper-annual rainfall of five years with a spatial structure, with its corresponding geostatistical treatment, can be used as a basic parameter of drought, since rainfall is the most important component of drought.


**Fig. 1** Area of Interest

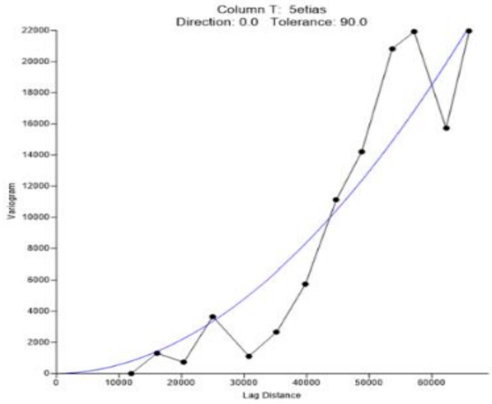


**Fig. 2** Semi-Variogram

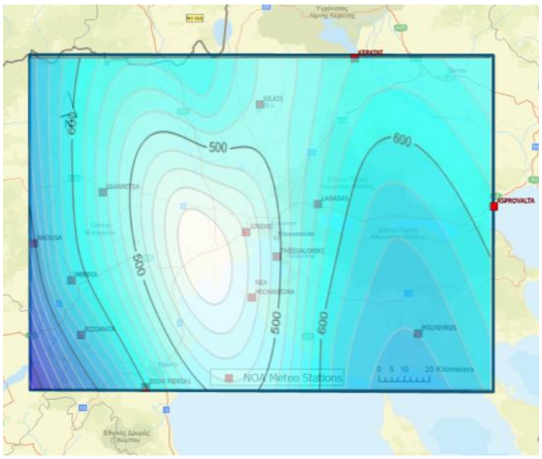


**Fig. 3** iso-lines

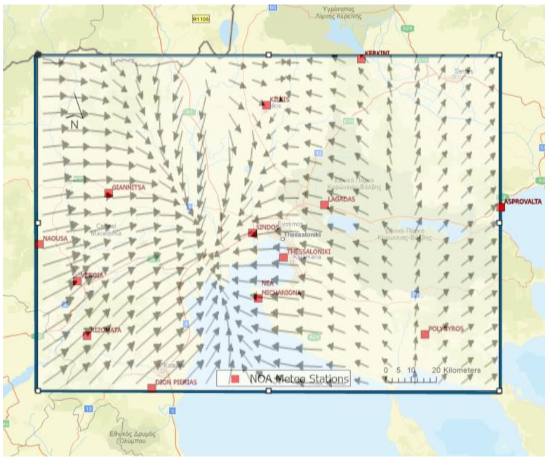


**Fig. 4** Flow Directions

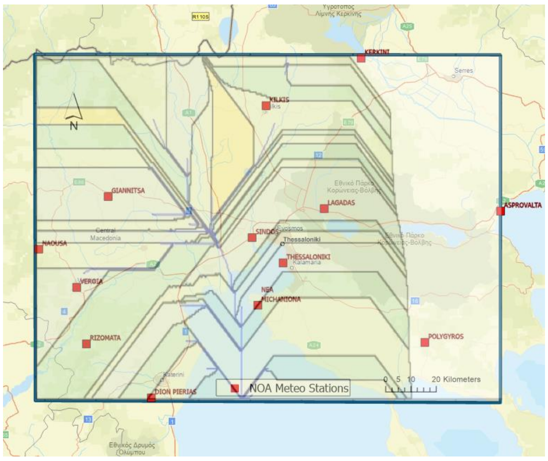


**Fig. 5** Flow paths

## References

Goovaerts P (2000) Geostatistical approaches for incorporating elevation into the spatial interpolation of rainfall. J. Hydrol., 228(1-2), 113-129.

Isaaks EH, Srivastava RM (1989) An introduction to applied geostatistics. Oxford Univ. Press, New York, 561 pp.

Ly S, Charles C, Degré A (2013) Different methods for spatial interpolation of rainfall data for operational hydrology and hydrological modeling at watershed scale: a review. Biotechnologie, Agronomie, Société et Environnement, 17 (2), p. 392-406.

# Optimal management of wedge-shaped aquifers using genetic algorithms

Iraklis Nikoletos[1] and Konstantinos L. Katsifarakis[1*]

[1] Aristotle University of Thessaloniki, Greece
*email: klkats@civil.auth.gr

ABSTRACT

This paper focuses on pumping cost minimization under steady-state conditions in wedge-shaped confined aquifers. The method of images has been used to obtain analytical expressions for the hydraulic head level drawdown functions and, by extension, for the pumping cost function. As application examples, we consider a system of five wells pumping simultaneously in the following cases: semi-infinite confined aquifers bounded by two constant head boundaries, intersecting at angles of a) 90°, b) 60° and c) 30°. Genetic algorithms have been used to determine the optimal distribution of the total required flow rate to the wells. The results indicate that in each case the pumping cost is minimized when the drawdown at the location of the wells are equal to each other.

## 1. Formulation of the optimization problem

The pumping cost function in any type of aquifer is given by the relationship.

$$K = A \cdot \sum_{i=1}^{N} Q_i \cdot (s_i + \delta_i) \tag{1}$$

where K is the pumping cost, $Q_i$ is the flow rate of well i, $s_i$ is the drawdown at point i and $\delta_i$ is the distance between the initial hydraulic head level at well i and a reference level, and A is a cost coefficient. Considering A as constant and that the initial groundwater level is horizontal, namely $\delta_i = \delta$, the objective function that should be minimized is

$$K = \sum_{i=1}^{N} Q_i \cdot s_i \tag{2}$$

Given that the total required flow rate $Q_T$ is constant, the following constraint applies:

$$\sum_{i=1}^{N} Q_i = Q_T \tag{3}$$

In the following paragraphs, we discuss the pumping cost minimization problem, described by Eqs. (2) to (3), in three cases of semi-infinite aquifers, to which the method of images applies. They are bounded by two straight-line constant head boundaries intersected at angles 90°, 60° and 30°, respectively; namely, we concentrate on wedge-shape aquifers (Chuang and Yeh 2018; Madhavi 2021; Yeh et al. 2008). In all application examples the boundaries are intersected at O(0, 1500). We seek the optimal distribution of $Q_T$ = 200 L/s to five wells, with coordinates given in Table 1.

**Table 1.** Coordinates of Wells

| Well | 1 | 2 | 3 | 4 | 5 |
|---|---|---|---|---|---|
| x | 50 | 150 | 250 | 350 | 700 |
| y | 1250 | 400 | 700 | 500 | 200 |

According to the method of images (Nikoletos and Katsifarakis 2022), the $s_i$ values can be calculated by Eqs. (4), (5) and (6), for boundary intersection angles equal to 90°, 60° and 30°, respectively. These equations are based on the substitution of flow boundaries by fictitious wells, as shown schematically in Figure 1.

$$K = \sum_{i=1}^{5} Q_i \cdot \sum_{j=1}^{5} Q_j \cdot \left(-\frac{1}{2\pi K\alpha}\right) ln \frac{r_{ij} \cdot r_{iJ3}}{r_{iJ1} \cdot r_{iJ2}} \tag{4}$$

$$K = \sum_{i=1}^{5} Q_i \cdot \sum_{j=1}^{5} Q_j \cdot \left(-\frac{1}{2\pi K\alpha}\right) ln \frac{r_{ij} \cdot r_{iJ3} \cdot r_{iJ5}}{r_{iJ1} \cdot r_{iJ2} \cdot r_{iJ6}} \quad (5)$$

$$K = \sum_{i=1}^{5} Q_i \cdot \sum_{j=1}^{5} Q_j \cdot \left(-\frac{1}{2\pi K\alpha}\right) ln \frac{r_{ij} \cdot r_{iJ3} \cdot r_{iJ5} r_{ij} \cdot r_{iJ7} \cdot r_{iJ9}}{r_{iJ1} \cdot r_{iJ2} \cdot r_{iJ4} r_{iJ6} \cdot r_{iJ8} \cdot r_{iJ10}} \quad (6)$$

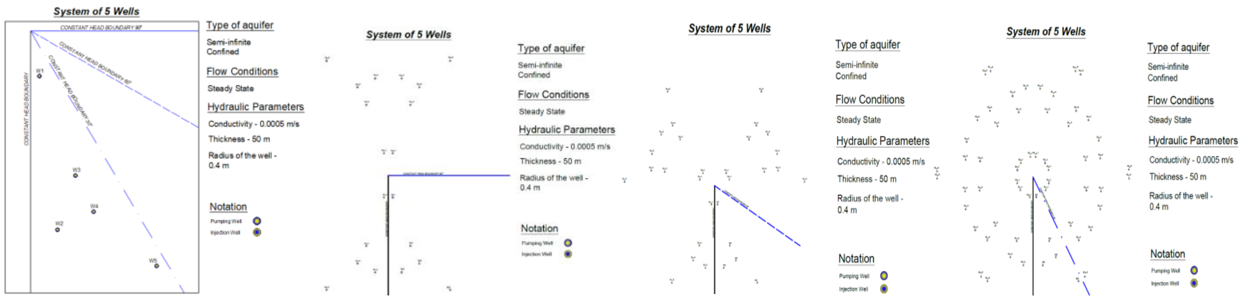


**Fig. 1.** Real and Fictitious wells in each case

To find the optimal distribution of $Q_T$ to the five wells, we have used the method of genetic algorithms, which has been widely applied to water resources problems (Katsifarakis and Karpouzos 2012). We have opted for simple binary genetic algorithms, using the tournament method in the selection process and one-point crossover. The parameters used, are: Population Size: 60; Generations: 400; Crossover Probability: 0.5; Mutation-Antimetathesis Probability: 1/Chromosome length and Tournament Constant: 3.

## 2. Results and Discussion

In this paper, we have studied the minimization of pumping cost under steady groundwater flow conditions in semi-infinite wedge-shaped aquifers where the method of images applies. Table 2 shows the flow rate distribution and the drawdown values at the location of the wells for each case.

**Table 2.** Drawdowns and Flow rate distribution

| Well | 1 | 2 | 3 | 4 | 5 |
|---|---|---|---|---|---|
| Case 1- 90° | | | | | |
| Flow rate (L/s) | 58.22 | 40.98 | 36.65 | 30.72 | 33.43 |
| Drawdown (m) | 20.63 | 20.65 | 20.62 | 20.66 | 20.57 |
| Case 2 – 60° | | | | | |
| Flow rate (L/s) | 57.21 | 40.09 | 36.94 | 31.08 | 34.68 |
| Drawdown (m) | 20.03 | 20.00 | 20.03 | 20.00 | 20.01 |
| Case 3 – 30° | | | | | |
| Flow rate (L/s) | 49.61 | 35.83 | 36.22 | 32.67 | 45.67 |
| Drawdown (m) | 16.74 | 16.74 | 16.77 | 16.77 | 16.78 |

The basic conclusion is that minimizing pumping cost (namely the energy consumption) is achieved when drawdowns at the wells are equal to each other.

### References

Chuang MH and Yeh HD (2018) An Analytical Solution of Groundwater Flow in Wedge-shaped Aquifers with Estuarine Boundary Conditions, 32, 5027-5039

Karpouzos DK and Katsifarakis KL and (2012) Genetic algorithms and water resources management: an established, yet evolving, relationship" in "Hydrology, Hydraulics and Water Resources Management: A Heuristic Optimisation Approach" (ed. K.L. Katsifarakis), pp. 7-37, WITPress, ISBN 978-1-84564-664-6, 2012

Mahdavi A (2021) Response of dual-zone heterogeneous wedge-shaped aquifers under steady-state pumping and regional flow, 147, 103823

Nikoletos IA and Katsifarakis KL (2022) Approximate application of the method of images in fields with two boundaries intersected at angles between 180° and 90°, Journal of Hydrology, 607, 127519

Yeh HD, Chang YC and Zlotnik VA (2008) Stream depletion rate and volume from groundwater pumping in wedge-shape aquifers, 349, 501-511

# Identifying water consumption profiles through unsupervised clustering of household timeseries: the case of Attica, Greece

Nikos PELEKANOS[1], Georgios MORAITIS[1], Panagiotis DIMAS[1], Panagiotis KOSSIERIS[1], Christos MAKROPOULOS[1]

[1] Dept. of Water Resources and Environmental Engineering, National Technical University of Athens
email: npelekanos@mail.ntua.gr; georgemoraitis@mail.ntua.gr; pdimas@mail.ntua.gr; pkossier@central.ntua.gr; cmakro@mail.ntua.gr

ABSTRACT

Urban water systems are complex, socio-technical systems, tasked with meeting water demands, generated through a continuous (socio-technical) interplay between customers and infrastructure, maintaining high reliability levels. Understanding demand patterns at different scales, is thus essential to manage the associated water distribution infrastructure and better serve customers. Here, we analyse water consumption data from 40 municipalities in Attica, Greece, served by the water company of Athens, EYDAP S.A., using machine learning techniques to detect principal patterns in water consumption. The data, which were extracted and provided by EYDAP S.A., are monthly time series of consumption points between 2010 and 2021, a sample which is analysed through an unsupervised data clustering process, to gain insights on dominant consumption patterns and to identify characteristic customer profiles.

## 1. Introduction

Adaptive urban water management, especially within a context of resilient smart cities, prompts utilities to adopt hydro-informatic approaches to understand past, manage present and (to the extent possible) predict future consumption behaviour of their customers (Makropoulos and Savić 2019). Detecting trends, similarities, and differences and grouping customers under homogenous consumption profiles, allows utilities and regulators to design better, more pro-active water demand management strategies. However, geographical or social aggregation criteria may lead to information loss, as inhomogeneous consumptions are blended to form a "characteristic consumption profile" for each criterion of reference. To overcome such biases, this work applies unsupervised data clustering techniques, resulting in an evidence-based, data-driven identification of principal consumption profiles for the examined regions in Attica.

## 2. Methodology

We utilized a dataset comprising of 120,000 consumption point timeseries at monthly step, covering the period from Apr-2010 to Aug-2021. The selection was made by picking 3000 points from 40 different municipalities of Attica, Greece with the sole condition being that in each timestep the consumption should be under 25 $m^3$/month, thus assuming only household level consumers for all timeseries. As a pre-processing step, each sequence of our 120,000 sample dataset was normalized utilizing the Z-score:

$$y'_i = \frac{y_i - \bar{x}}{\sigma} \tag{1}$$

where $\bar{x}$ is the mean and $\sigma$ is the standard deviation of each timeseries $y_i$ (for $i$ = 1:120,000). The purpose of this scaling reflects the need of fitting our dataset in an uninformative range, allowing for an unbiased (from average) water consumption pattern comparison in a width-invariant way.

For the timeseries segmentation, we applied a k-means type unsupervised algorithm in which the default 'Euclidean' distance measure was replaced by the Dynamic Time Warping (DTW) (Petitjean et al. 2011) as more suitable to sequential values distance metrics. Intuitively, DTW expresses a measure of similarity between two temporal sequences (i.e., consumption timeseries), where their shapes 'match', regardless of temporal shifts. The DTW equation can be expressed as follows:

$$DTW(x, y) = \min_{\pi} \sqrt{\sum_{(i,j)\in\pi} d(x_i, y_i)^2} \tag{2}$$

where $\pi = [\pi_o, \ldots, \pi_k]$ is a path that satisfies more complex conditions, the detailed explanation of which is included in the work Berndt and Clifford (1994). The selection of the optimal number $k$ of clusters was estimated through a preliminary assessment, by exploring various $k$ components of Gaussian Mixture

Modelling approaches and scoring each realisation by estimating its corresponding Bayesian Information Criterion (BIC). The lower BIC score resulted for a $k = 30$ cluster segmentation, which is assumed optimal.

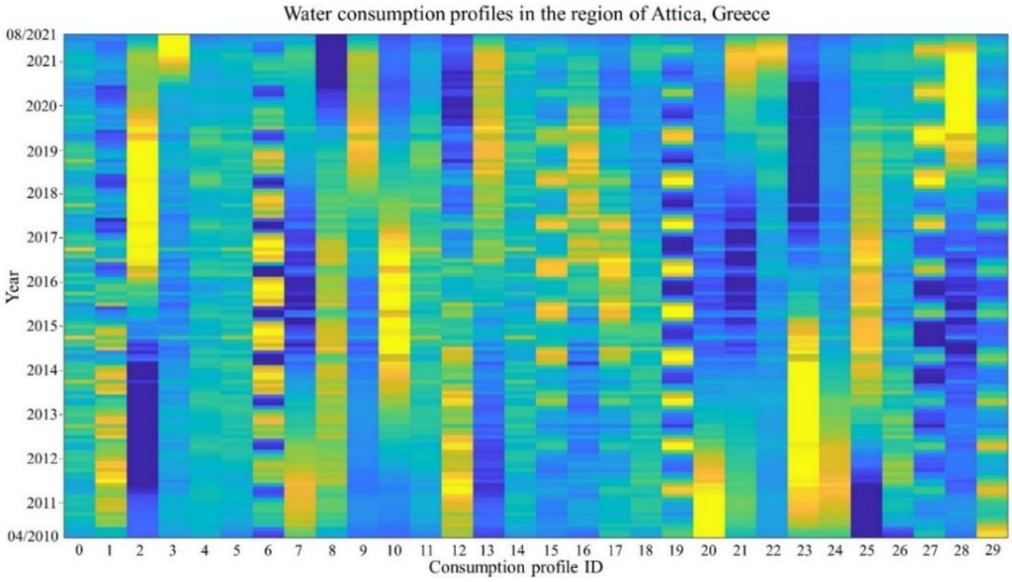


**Fig. 1.** 30 characteristic consumption profiles in the Attica region, derived through unsupervised clustering of 120,000 measurement points. Darker blue areas show lower consumption and lighter yellow areas show consumption peaks per profile.

Finally, for each cluster created, a characteristic timeseries (profile) representing the overall cluster shape was created by averaging the scaled monthly values of each cluster timeseries set. The homogenised cluster behaviour for the derived consumption profiles is presented in Fig. 1. Each characteristic timeseries was decomposed into three components: trend, seasonality, and residual (noise) (Fig. 2). Additionally, for each cluster, the percentage of inclusion of each municipality is calculated, a tactic which enables us to observe dominant patterns in some municipalities.

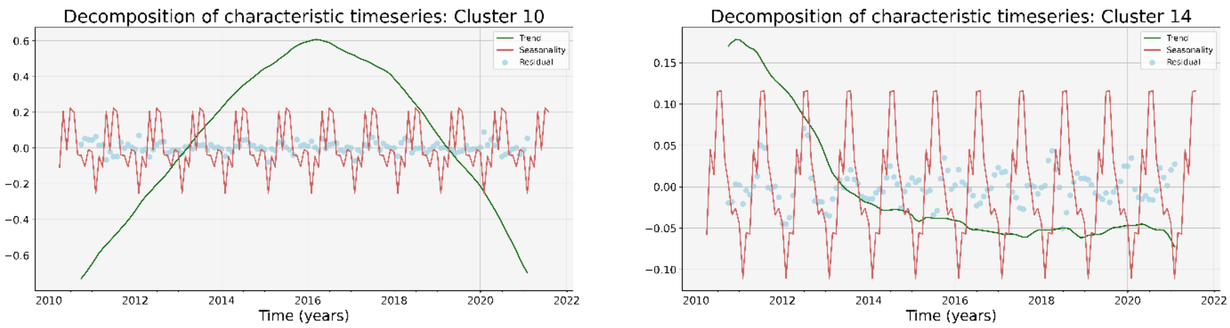


**Fig. 2.** Decomposition of the characteristic timeseries from Cluster 10 and 14.

## 3. Discussion and concluding remarks

We analysed an extensive dataset of point consumption timeseries and produced the characteristic consumption profiles, which summarize the behaviour of 30 distinct clustered customer groups in the water supply system of Attika, Greece. These profiles can be utilized to model the consumption of the region, as a surrogate training dataset for demand forecasting, as well as a template to produce synthetic consumer demands in unmetered regions and/or District Metered Areas (DMAs) for design or optimal control purposes.

**Acknowledgements**
This work was carried out in close cooperation with the General Directorate of Water Supply and the organizational units of EYDAP S.A. in order to make the data available and provide necessary comments on them, in the framework of the Service Contract of the Project entitled *Provision of services for the Investigation, Assessment, and Management of Water Losses in the Internal Water Distribution Network of EYDAP S.A.* Results presented herein are of the authors and cannot be taken to represent the views of EYDAP S.A.

**References**

Berndt, D. J., and Clifford, J. (1994). "Using Dynamic Time Warping to Find Patterns in Time Series." Proceedings of the 3rd International Conference on Knowledge Discovery and Data Mining, AAAIWS'94, AAAI Press, 359–370.
Makropoulos, C., and Savić, D. A. (2019). "Urban hydroinformatics: Past, present and future." Water (Switzerland), 11(10).
Petitjean, F., Ketterlin, A., and Gançarski, P. (2011). "A global averaging method for dynamic time warping, with applications to clustering." Pattern Recognition, 44(3), 678–693.

# Laboratory simulation of transients in looped water distribution network

Silvia MENICONI[1], Filomena MAIETTA[2], Caterina CAPPONI[3], Stefano ALVISI[4]
Valentina MARSILI[5], Marco FRANCHINI[6], and Bruno BRUNONE[7]
[1,2,3,7] Department of Civil and Environmental Engineering, University of Perugia, Italy
silvia.meniconi@unipg.it
filomena.maietta@studenti.unipg.it
caterina.capponi@unipg.it
bruno.brunone@unipg.it
[4,5,6] Department of Engineering, University of Ferrara, Italy
lvssfn@unife.it
mrsvnt@unife.it
marco.franchini@unife.it

ABSTRACT

This paper analyses some tests carried out in a looped water distribution network (WDN) at the Water Engineering Laboratory of the University of Perugia. Specifically, the aim of such tests is to evaluate the effect of transients generated by a water consumption change, i.e., a complete and fast closure of a valve simulating an end-user maneuver. This end-user was located at the downstream end section of a service line placed in three different sections of the WDN. The tests allow examining the effect of the network topology and the location of the transient generation point.

## 1. Introduction

Water distribution networks (WDNs) are complex systems subject to physical and operational loads and requirements. One of these loads is the occurrence of pressure transients caused by, as an example, pump shotdowns and pressure regulating devices. Numerous papers analyse numerically the resulting transient behaviour of WDNs (e.g., Karney and McInnis, 1992; Creaco et al, 2019; Bohorquez et al., 2020). Viceversa, very few papers deal with transient laboratory (e.g., Zeng et al., 2021) and field tests (e.g., Starczewska et al., 2015). In particular, a possible source of transients is the unavoidable water consumption change; such transients are very frequent, one could say "almost continuous", and a narrow set of papers analyze in details their effects experimentally (Marsili et al., 2021, 2022; Lee et al., 2012; Lee 2015). Such papers do not allow drawing general conclusions and do not highlight, for example, the role of the location of the transient source. To fill this gap, an extensive experimental campaign was carried out at the Water Engineering Laboratory (WEL) of the University of Perugia, Italy in a looped WDN with one or more active service lines. To simulate actions initiated in the plumbing system – i.e., the shutting off of valves and shower heads or the automatic off of the solenoid valve on the washing machine – transients were generated by the complete closure of an end valve. Pressure signals were acquired both in the main pipes and service lines, to follow the propagation of pressure waves. In this paper the effect of the location of the transient generation point on the dynamic behavior of the network has been examined.

## 2. The experimental setup

The experimental set-up at WEL is a two 100x100 square meters network simulating a District Metered Area (DMA), supplied by a 42.3 m long pipe with an internal diameter of 93.3 mm (nominal diameter DN110) and a pressurized tank (Fig. 1) in which the head is assured by a pump. All the pipes are high density polyethylene (HDPE) pipes; specifically, in loop I the pipes have an internal diameter of 63.8 mm (DN75), whereas in loop II the other three pipes – excluding the one in common with loop I have an internal diameter of 42.6 mm (DN50). In order to simulate a service line, a 23.6 m long branch of 20 mm internal diameter (DN25) was alternatively installed at sections 5, 6, and 7. A solenoid valve in series with a ball valve was used to simulate an end-user, at the downstream end of the service line (i.e., at nodes 5u, 6u, and 7u of Fig. 1). Such a device allows generating controlled, repeatable, and fast transients, and consequently sharp pressure waves.

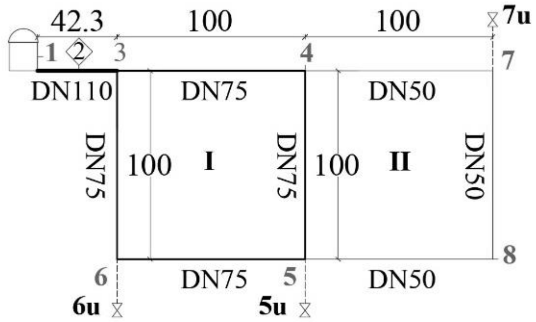


**Fig. 1.** The two-loop network at the WEL: layout with the pipe length, nominal diameter, and location of the measurement sections indicated.

## 3. Simulation of a water consumption change and discussion of results

To point out the mechanism of propagation of pressure waves due to a water consumption change, three fast and complete closure maneuvers were alternatively executed at the end-users 5u (test 1), 6u (test 2) and 7u (test 3). Fig. 2 compares the dimensionless pressure signals, $h$ $(=(H-H_e)/\Delta_u)$, acquired at the end-user (Fig. 2a) for a given steady-state discharge, with $H$ and $\Delta_u$ being the pressure head and the pressure wave generated by the maneuver at a given end-user, respectively, and $e$ indicating the end conditions achieved when the effect of the maneuver fully vanishes. Specifically, Fig. 2a highlights that, even if the maneuver is the same, during the first phases of the transient, the service line is more excited when the maneuver is executed at the end-use 5u, because of the more complex shape of junction 5 (cross junction) with respect to junctions 6 and 7 (tee junctions) that generate larger reflected waves and smaller transmitted ones. The comparison of Fig. 2b, 2c and 2d shows that the most severe transient for the main pipes is the one generated at node 7u (test 3). This difference is mainly due to the already mentioned different shape of the junction connecting the service line. Moreover, it is worthy pointing out the crucial role, for a given pipe material, of the ratio between the main pipe cross sectional areas connected to the service line, and the service line itself: the smaller this ratio, the larger the transmitted pressure wave (Swaffield and Boldy, 1993; Bohorquez et al., 2020).

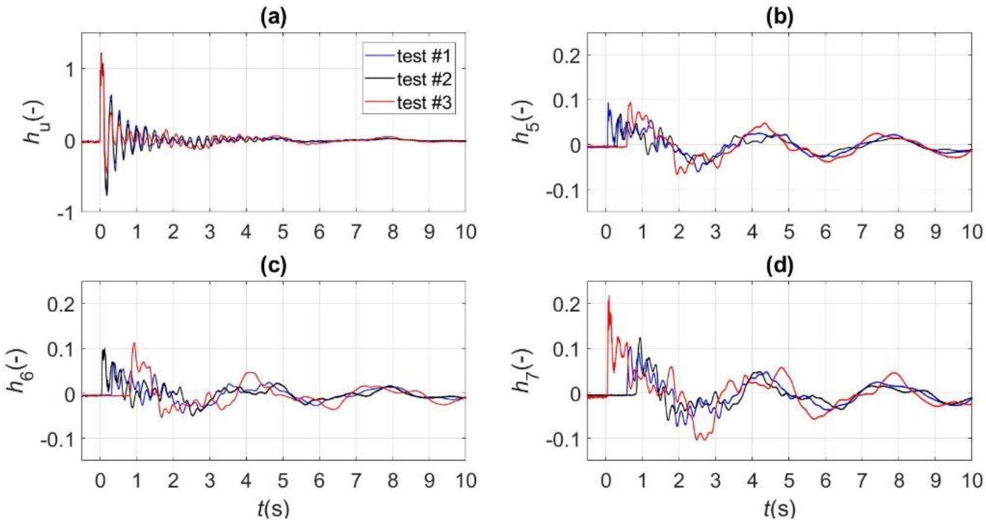


**Fig. 2.** Dimensionless pressure signals acquired at sections: a) end-user; b) 5; c) 6; and d) 7 for tests 1, 2, and 3 for a given initial discharge.

**References**

Bohorquez J, Lambert M, Simpson A (2020) Identifying head accumulation due to transient wave superposition in pipelines. J Hydraul Eng, 146, 04019044.
Karney B, McInnis D (1992) Efficient calculation of transient flow in simple pipe networks. J Hydraul Eng, 118 (7), 1014-1030.
Lee J (2015). Hydraulic transients in service lines. Int J Hydraul Eng, 4, 31–36.
Lee J, Lohani V, Dietrich A, Loganathan G (2012) Hydraulic transients in plumbing systems. Water Sci Technol W.S, 12 619–629.
Creaco E, Campisano A, Fontana N, Marini G, Page P, Walski T (2019) Real time control of water distribution networks: A state-of-the-art review. Water Research, 161, 517–530.
Marsili V, Meniconi S, Alvisi S, Brunone B, Franchini M (2021) Experimental analysis of the water consumption effect on the dynamic behaviour of a real pipe network. J Hydraul Res, 59, 477–487.
Marsili V, Meniconi S, Alvisi S, Brunone B, Franchini M (2022) Stochastic approach for the analysis of demand induced transients in real water distribu-tion systems. J Water Resour Plan Manag, 141, 04021093.
Zeng W, Zecchin A, Cazzolato B, Simpson AR Gong J, Lambert M (2021) Extremely sensitive anomaly detection in pipe networks using higher-order paired-impulse response function with a correlator J Water Resour Plan Manag, 147, 04021068.
Starczewska D, Collins R, Boxall J (2015) Occurrence of transients in water distribution networks. Proc Eng, 119, 1473–1482.
Swaffield J, Boldy A (1993) Pressure surges in pipe and duct systems. Ashgate Publishing Group.

# The sustainable development goals are linked with the improvement of a wastewater treatment plant. A case study in Spain

Modesto PÉREZ-SÁNCHEZ [1], Silvia DOÑATE [2]; Jose SATORRE-AZNAR [3]; P. Amparo LÓPEZ-JIMÉNEZ[4],

[1,3,4] Hydraulic and Environmental Engineering Department, Universitat Politècnica de València, Valencia, Spain
[2,3]DAM. Valencia, Spain
email: mopesan1@upv.es
email: silvia.donate@dam-aguas.es
email:josaaz@dihma.upv.es
email: palopez@upv.es

ABSTRACT

This research project, called ARTEMISA, aims to improve the indicators that allow the assessment of compliance with the Sustainable Development Goals (SDGs) established by the 2030 Agenda. The project will focus on the process of debugging. Specifically, an evaluation and proposal of new indicators will be carried out to characterize the water purification process focused on improving the SDGs (mainly SDG6 and SDG7), to reduce energy consumption in the distribution of the fluid to reduce the cost of purified and/or regenerated water. The reduction of the costs of purification - regeneration has a direct implication on the reduction of the operating costs of irrigation water used to supply the water needs of crops. These crops are subsequently the raw material (e.g., vegetables, citrus fruits, table grapes, among others) of the Valencian agri-food industries. The improvement of energy efficiency not only has an economic implication but also an environmental implication with the reduction of energy consumption and, therefore, $CO_2$ emissions. These implications affect different indicators, which allow measuring the degree of achievement of the different SDGs, where water engineering is involved.

## 1. Method

Increasing efficiency in the water cycle, in any of its phases (catchment-distribution-final use), is a primary objective to achieve the development of sustainable systems (Corominas, 2010). The search for improved efficiency has been developed first, seeking at an increase in hydraulic efficiency, and secondly and directly linked to this, an increase in energy efficiency. The improvement of energy efficiency has become a primary objective in distribution and treatment systems, a direct consequence of the increase in energy costs. Therefore, the energy analysis of wastewater treatment and reclamation systems through the development of audits has become a common technique used by managers of the different wastewater treatment and reclamation systems (Gómez, 2016).

The energy used in purification can account for 50% of the energy consumed in the water cycle from catchment through distribution to regeneration. Within the catchment, the research team has experience in the development of operating models that guarantee the optimization of water and energy resources, minimizing the operating cost of the systems, taking into account the capacities of the facilities and water quality (Pérez-Sánchez et al., 2017). In addition, members of the research team have optimization models for wastewater treatment systems seeking to improve efficiency by reducing energy costs, and propose energy and nutrient recovery in these systems through the quantification of indicators (Seco et al., 2018).

## 2. Method

The particular objectives were: (i) To characterise existing indicators applied to sustainability (IAS) that enable the evaluation of the degree of achievement of the different targets included in the SDGs, where hydraulic engineering can incorporate tools for their achievement. This characterisation will include the definition of new quantifiable indicators that complement the existing ones for their inclusion in the measurement of the scope of the different targets; (ii) Establish a classification of scales of operation of the different IAS to be able to establish a classification of sustainable development (SDC) of the hydraulic system; Identify and characterise the main energy consumption scenarios in a wastewater treatment plant, which are linked to water circulation, focusing on the impulsion systems. Two main activities were developed: (i) Compilation of information on the state of the art in the use of indicators applied to sustainability in hydraulic systems. (ii)

Identification and characterisation of the main energy consumption scenarios in a wastewater treatment plant, which is linked to water circulation.

## 3. Results

In this case, a comprehensive analysis of the relationship between the different targets set by the 17 SDGs has been carried out. Sixty-eight indicators with a direct relationship to wastewater treatment were identified that impact 90 of the 169 targets set by the 2030 Agenda. Figure 1 shows the distribution of these indicators across the different SDGs.

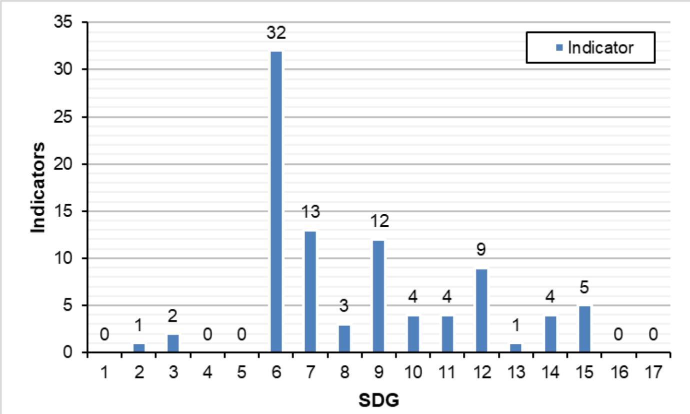


**Fig. 1.** Indicators related to each SDG in a waste-water treatment plant

Figure 1 shows that 35.6% of the indicators fall under SDG6 - Water and Sanitation, and most of them are applied to technical management. Within this technical management, those indicators that have to do with energy efficiency, both in the impulsion systems present in the wastewater treatment plant and the hydraulic recovery capacity of the same, are of special interest within the proposed project. The rest of the indicators can constitute a basis for the company to start compiling information on the different variables that have been established to measure them and to include them in the evaluation of its sustainability and the degree of achievement of the targets of the different SDGs. This will make it possible to carry out an evolution of the degree of achievement of the different indicators within the plant itself. These indicators are focused on four different areas: social (12), technical (26), environmental (16) and economic (14) management, although some of them may have interrelationships between different areas.

## 4. Conclusion

The energy audit showed the elements, which had an installed power lower than 15 kW established 34.42% of the accumulated energy consumption. When the range was between 15 and 50 kW, the energy consumption was 20.50%, while the elements with more than 50 kW represent 45.08% of the annual energy consumption. The energy audit revealed the distribution of consumption, showing the importance of the blower equipment in the biological process, with consumption representing 56% of the plant. The sludge and deodorization process showed an annual energy consumption equal to 14.6%, and the wastewater pumping stations 16.7%. Therefore, these four process groups represent 87.5% of the energy consumption and their optimization is crucial to improve the compliance of the different targets of the SDGs.

**Acknowledgements**

Authors greatly acknowledge financial support from the "Conselleria de Innovación, Universidades, Ciencia y Sociedad Digital, Generalitat Valenciana" in the grant AEST2021/058 called "Energy Optimisation Strategy in the Hydraulic Circuit to Reduce the Energy Footprint in Wastewater Treatment Plants through the Proposal of Indicators for the Fulfilment of the Sustainable Development Goals.[ARTEMISA]" for the first author of this contribution.

**References**

Corominas, J., 2010. Agua y Energía en el riego en la época de la sostenibilidad. Ingeniería del Agua 17 (3), 219–233.

Gómez, E., 2016. Caracterización y mejora de la eficiencia energética del transporte de agua a presión. Universitat Politècnica de Valencia.

Pérez-Sánchez,M.; Díaz-Madroñero, M.; López-Jiménez, P.A.; Mula, J. (2017) "Mathematical Programming Model for Procurement Selection in Water Irrigation Systems. A Case Study," J. Eng. Sci. Technol. Rev., vol. 10, no. 6, pp. 146–153, 2017.

Seco, A., Aparicio, S., Gonzalez-Camejo, J., Jiménez-Benítez, A., Mateo, O., Mora, J. F, Giménez, J. B. (2018)"Resource recovery from sulphate-rich sewage through an innovative anaerobic-based water resource recovery facility (WRRF)," Water Sci. Technol., vol. 78, no. 9, pp. 1925–1936, Dec. 2018.

# Do urban water systems contribute to compliance of the SDGs?: case studies in Eastern Spain

Camila GARCIA[1], Pilar CONEJOS FUERTES [2]; Jaime CASTILLO SORIA [3]; P. Amparo LÓPEZ-JIMÉNEZ[4], Modesto PÉREZ-SÁNCHEZ[5]

[1,2,4,5] Hydraulic and Environmental Engineering Department, Universitat Politècnica de València, Valencia, Spain
[2]Idrica. Valencia, Spain
[3]Global Omnium, Valencia, Spain
email: cgarcia1@posgrado.upv.es
email: Jcastillo@globalommnium.com
email: pilar.conejos@idrica.com
email: palopez@upv.es
email: mopesan1@upv.es

ABSTRACT

Due to the current social development, higher quantities and better water quality are demanded, putting water resources under greater stress. However, if the resources are managed in a sustainable way, it will be possible to satisfy the present needs without compromising its long-term capacity. Nowadays, urban water systems are trying to focus on a sustainable management that improves the performance of the economic, social, technical, and environmental fields of the systems. In this sense, water systems can contribute to the achievement of the SDGs, even though it can be a challenge due to the actual social conditions to operate this way. Therefore, key performance indicators (KPIs) can be a useful tool to audit and evaluate sustainability in hydraulic systems over time. This contribution presents an analysis of the implementation of a set of sustainability indicators that will allow to assess the compliance of all the SDGs that intervenes in different water systems. Based on the results, the study also proposes a classification by levels of sustainability considering a memory of the evolution of the system. The proposed methodology can be applied to all types of hydraulic systems (supply, sanitation, treatment). A set of indicators were established to measured or monitor the sustainability in different processes such as operation, maintenance, management, and infrastructure of hydraulic systems. For the implementation of the KPIs, first a characterization of the system must be carried out considering aspects such as the location, elements of the network and operation mode. A detailed analysis was carried out to establish the relationship between the water systems and each SDGs. Based on that, a set of indicators was defined that could measure the contribution of water systems to the compliance of all SDGs. The analysis was made in the supply network of the Valencian Community, Spain. The result of the analysis allows to establish a benchmarking on the sustainable aspects of the water distribution system that will help to improve sustainability in the systems. In that sense, it can become a design, diagnosis, and management tool. The results shows that water systems are related to some of the targets of each SDGs. Improving the performance and sustainability of urban water systems will not only help to achieve goal 6 but also all the others SDGs will benefit, since the close relationship between water systems and each SDGS, which highlights the relevance of sustainability indicators in hydraulic systems.

## 1. Method

In the present work, a system of KPIs and the methodology for the implementation was proposed. Such system allows the evaluation from a sustainable point of view of different process and types of urban water systems. All the SGDs proposed by the UN (Un-Water, 2021) have a connection with water resources, and some of them are more explicit than others. Therefore, it was possible to associate targets and keywords which were used later to define the indicators.

A total number of 145 indicators were established and characterized with properties such as being quantifiable, auditable, concise in meaning and universal in its use. An outline of the process was also suggested that should be followed to implement the KPIs. Such procedure consists of a system characterization (information of the environment and the network), assessment, diagnosis with the sustainable indicators, and finally, a plan proposal must be made.

## 2. Results

An implementation was carried out in the supply network of the city of Valencia (East Spain). Certain indicators were defined of those already established that allowed the evaluation depending on the data obtained and the characteristics of the system. In Fig. 1, the number of targets is presented, that were related to each SGD. Also, the proportion of company contribution can be seen which represents the percentage of indicators that were measured in the evaluation (since not all the indicators for each SDG were able to be applied).


**Fig. 1.** Targets related to water system and proportion of contribution of the company for each SDGs

## 3. Conclusion

Based on the results of the analysis, solutions can be proposed and actions can be taken to improve network management and lead to a sustainable operation of water resources. With this methodology it is possible to keep an evolutionary memory of the state of the network and follow the improvement of the networks. This will allow to obtain a level of sustainability to measure the degree of achievement of the SDGs based on the tracking records. In addition, the KPIs proposed and the reports allow the comparison with other networks. In this way, more sustainable networks can serve as an example for those that are still in process.

Through sustainable management of water systems, the present demands should be provided without compromising its capacity in the future and leading towards an optimal operation. Based on the results of the methodology proposed in this study, it is possible to monitor and take actions about the managements of water systems. Such actions can be focused on the improvement of the contribution for just one particular SDG, for example to enhance SGD 7 by implementing more the use of clean energy, or creating an energy plan focused on the energy efficiency. In this way, all the strategic plans of a company can be linked to the contribution of sustainability and the compliance with the SDGs. By improving the performance and sustainability of the systems, it is not only possible to achieve the objectives of goal 6, but also other associated goals will benefit, which highlights the relevance of sustainability indicators in any hydraulic system.

**Acknowledgements**

Authors greatly acknowledge financial support from the "Catedra Aguas de Valencia" in the grant "Assessing water distribution systems across indicators based on Sustainable Development Goals" for the first author of this contribution. Grant PID2020-114781RA-I00 funded by MCIN/AEI/ 10.13039/501100011033

**References**

Bagheri, A., Hjorth, P. (2006). A framework for process indicators to monitor sustainable development: practice to an urban water system. Development and Sustainability, 9, 143-161.
Cabrera E., Dane P., Haskins S., Theuretzbacher H. (2011). Benchmarking para servicios de agua. IWA publishing.
Choulot, A., Denis V., Punys, P. (2012). Integration of small hydro turbines into existing water infrastructures. Hydropower-Practice and application.
Guio-Torres, D. (2008). Sustainability Indicators for Assessment of Urban Water Systems: The need for a common ground.
Guppy L., Uyttendale P., Villolth K., Smakhtin V. (2018). Groundwater and Sustainable Development Goals: Analysis of Interlinkages. UNU-INWEH
Hellstrom, D., Jeppson, U., Karman, E. (2000). A framework for systems analysis of sustainable urban water management. Environmental Impact Assessment Review, 20, 311-321.
Hassing, J., Ipsen, N., Clausen, T. (2009). Integrated water resources management in action. DHI Water policy and UNEP-DHI center for water and environment.
INE. (2021). Indicadores de la agenda 2030 para el desarrollo sostenible.
Llacer-Iglesias, R., López-Jiménez, P., Pérez-Sánchez, M. (2021). Energy self-sufficiency aiming for sustainable wastewater systems: are all options being explored?. Sustainability, 13.
Llacer-Iglesias, R., López-Jiménez, P., Pérez-Sánchez, M. (2021). Hydropower technology for sustainable energy generation in wastewater systems: learning from the experience. Water, 13.
Loucks D., Gladwell J. (1999). Sustainability criteria for water resource systems. International Hydrology Series - UNESCO.
Lundin, M. (2011). Indicators for Measuring the Sustainability of Urban Water Systems – a Life Cycle Approach.
Lundin, M., Bengtsson, M., Molander, S. (2000). Life cycle assessment of wastewater systems: influence of system boundaries and scale on calculated environmental loads. Environment Science Tech, 34, 180-186.
Lundin, M., Molander, S. Morrison, G. (1999). A set of indicators for the assessment of temporal variations in the sustainability of sanitary systems. Water Science Tech, 39 (5), 235-242.
Lundin, M., Morrison, G. (2002). A life cycle assessment based procedure for development of environmental sustainability indicators for urban water systems. Urban water, 4. Elsevier, 145-152.
Macías-Ávila, C., Sánchez-Romero,F., López Jiménez, P., Pérez-Sánchez, M. (2021) Leakage Management and Pipe System Efficiency. Its Influence in the Improvement of the Efficiency Indexes. Water, 199 (13)
Maurya, S., Singh, P., Sing, A. (2020). Identification of indicators for sustainable urban water development planning. Ecological indicators, 108.
Mercedes-García, A., Sánchez-Romero, F., Pérez-Sánchez, M., López Jiménez, P. (2021) Objectives, Keys and Results in the Water Networks to Reach the Sustainable Development Goals. Water, 1268 (13).
Morrison, G. Fatoki, O., Zinn, E., Jacobsson, D. (2001). Sustainable development indicators for urban water systems: a case study evaluation of Williams Town, South Africa. Water SA, 27 (2).
Pardo, M., Manzano, J., Cabrera, E., García-Sierra, J. (2002). Energy audit of irrigation networks. Biosystems engineering, 115. Elsevier, 89-101.
Popawala, R., Shah N. (2011). Evaluation of sustainability index for urban water management system. 2nd International Conference on Environmental Science and Development, 4.
Romero, L., Pérez-Sánchez, M., López-Jiménez, P. (2017). Improvement of sustainability indicators when traditional water management changes: a case study in Alicante (Spain). AIMS Environmental science, 4, 502-522.
Short A., Milman A. (2008). Incorporating resilience into sustainability indicators: An example for the urban water sector. Global Enviromental Change, 18 (4), 758-767.
Spiller M. (2016). Adaptive capacity indicators to assess sustainability of urban water systems – Current application. Science of the total environment., 569–570 (1), 751-761.
UN-Water. (2021). The UN water development report 2021, valuing water.
UN-Water. (2021). Summary progress update 2021: SDG6 – water and sanitation for all.
Van der Graaf J., Meester-Broertjes H., Bruggeman W. and Vles E. (1997). Sustainable technological development for urban water cycles. Water Science Tech, 35 (10),213-220.

# Systemic Resilience Analysis through a Water-Energy-Food-Climate Nexus Approach

Alexandra E. IOANNOU, Chrysi S. LASPIDOU

Civil Engineering Department, University of Thessaly, 38334, Volos, Greece
email: alexioannou@uth.gr

email: laspidou@uth.gr

ABSTRACT

Water, energy, and food (WEF) are vital resources for human wellbeing, poverty reduction, and sustainable development. Climate change effects are proved to threaten the WEF security and vice versa. Considering these threats as disturbances to a system, resilience is understood as the system's adaptive ability of maintaining its functionality even when the system is being affected by a disturbance. Resilience helps researchers and policymakers to comprehend how complex systems adapt and transform to withstand changes in the environment and measure a WEF system's capability to either adapt or collapse due to climate change conditions. This research focuses on exploring the resilience of a Water-Energy-Food-Climate (WEFC) system at national level. The case study is based on the structure of a System Dynamics Model (SDM), that maps sector-specific data from major databases for the national case study of Greece. In terms of enhancing environmental security, we measured systemic resilience, using different metrics, in different cases of disturbances and ultimately indicate the most efficient policies to increase system's elasticity.

## 1. System Dynamics Model

System dynamics modeling has broadly been used as a simulator of complex real systems, helping researchers and policymakers to frame and understand the complexities of and interlinkages within the system, while at the same time, it provides information on how the system might evolve over time (Bakhshianlamouki et al., 2020). To conceptualize a complex dynamic system prior to simulation analysis, causal loop diagrams (CLDs) are used to identify the key variables in a system and indicate the causal relationship between them using links (Randers, 1980). As the next step, to quantify the variables in the loop, the stock-and-flow diagram (SFD) is used since SFDs can perfectly capture the stock and flow behavior of a system (Figure 1).

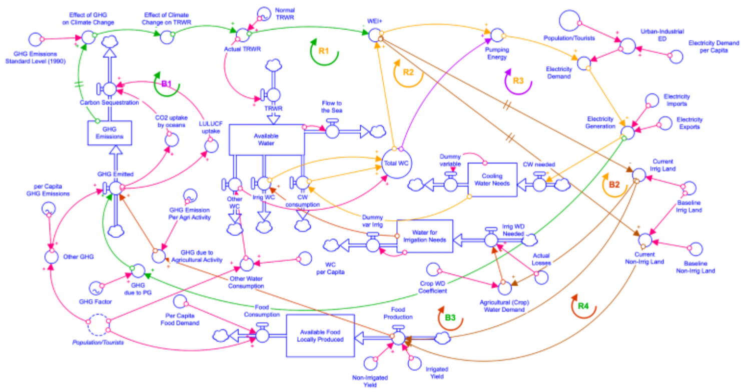

**Fig. 1.** Stock-and-Flow diagram for the nation case study of Greece

## 2. System Resilience Analysis

To assess System Resilience Analysis for our case study, we study the system behavior and quantify its ability to withstand shock under climate change; in this case, an extreme drought scenario is imposed on the system, and its ability to withstand it is investigated. The ecological and engineering measures of resilience were applied to the developed SDM for the baseline scenario (with no interventions) and for two suggested policies aiming to enhance WEF security; the implementation of renewable energy systems (RESs) (policy I) and increased stakeholder awareness and education, followed by increased funding to implement advanced irrigation systems with minimal losses in agriculture (policy II).

In Figure 2a, we show the SFD that includes the implementation of policy I. The outer loop shown with black arrows is reinforcing loop R1, while the balancing loop B1combines black and blue arrows and goes through the available water stock and through total water consumption and pumping energy. For policy I, we add the parameter fraction of RES in total energy generation mix (shown in the box in Figure 2a), and this way, we reduce the GHG emissions due to power generation by 30% as compared to the baseline scenario. For policy II, we add extra variables in the SDM, and a new loop is formed (reinforcing loop R5). Here, awareness and education are designed to lead to stakeholders demanding and obtaining more funding for the implementation of efficient irrigation technologies that will lead to increased irrigation efficiency and reduced actual losses in agriculture (Figure 2b).

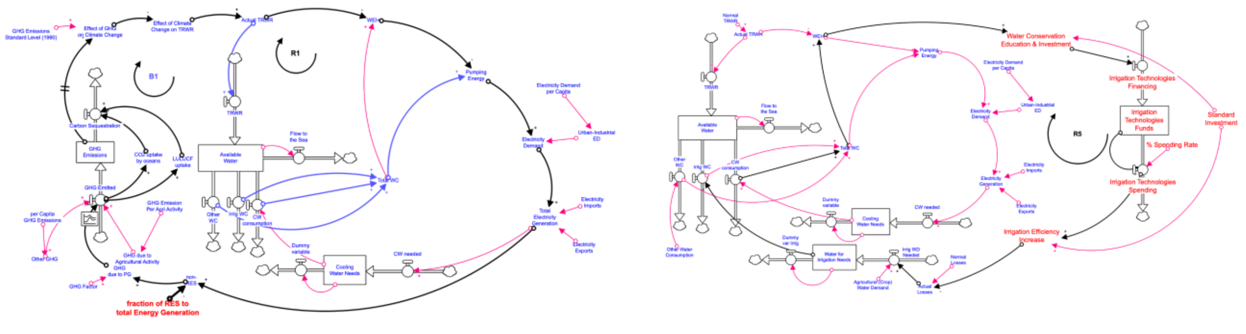


(a) (b)

**Fig. 2.** Stock-and-Flow diagram with the implementation (a) of policy I – RESs, and (b) of policy II –irrigation funding

We follow a methodology as described by Herrera (2017), to quantify five essential metrics of resilient behavior (for three scenarios), thus providing the policymakers with a quantitative basis to enhance the resilience of socio-ecological systems. Engineering ($\sigma_H$, $\bar{R}$, and $\bar{\rho}$) and ecological ($\sigma_E$ and $I_{RES}$) resilience measures are quantified (Table 1), and the respective thresholds are also identified in order to define system hardness ($\sigma_H$) and elasticity ($\sigma_E$). To find system hardness, we keep increasing the magnitude of the system disturbance (TRWR reduction) over a period of 10 years, specifically from 2014 to 2024, and we observe how F(x)—available water—changes. The highest disturbance/change in the TRWR that produces the least noticeable change in F(x) is its hardness ($\sigma_H$), the engineering threshold (shown in Table 1).

**Table 1.** Results of engineering and ecological resilience measures for the three scenarios

| **Scenarios** | **Engineering resilience** | | | **Ecological resilience** | |
|---|---|---|---|---|---|
| | **Hardness ($\sigma_H$)** | $\bar{R}$ | $\bar{\rho}$ | **Elasticity ($\sigma_E$)** | **Index of Resilience ($I_{RES}$)** |
| **Baseline** | $\mathbf{2.54 \cdot 10^9 m^3}$ | $\mathbf{0,80 \cdot 10^9 m^3}$ | 0.107 | $\mathbf{5,08 \cdot 10^9 m^3}$ | 33,4% |
| **Policy I** | $\mathbf{2,54 \cdot 10^9 m^3}$ | $\mathbf{2,38 \cdot 10^9 m^3}$ | 0.108 | $\mathbf{15,24 \cdot 10^9 m^3}$ | 46,6% |
| **Policy II** | $\mathbf{2,54 \cdot 10^9 m^3}$ | $\mathbf{1,34 \cdot 10^9 m^3}$ | 0.108 | $\mathbf{10,16 \cdot 10^9 m^3}$ | 40% |

We observe that when all scenarios are compared, the baseline is the least resilient system, having the lowest hardness, while policy I has the highest. With the implementation of policies, the system can withstand bigger changes (higher hardness) in the TRWR, such as extreme droughts caused by climate change, before available water is affected. $\bar{R}$ variable shows how quickly the system will recover from the disturbance, and it is the highest for policy I, while in terms of robustness, the two policies appear similarly robust and more robust than the baseline. Ecological resilience is assessed. The Greek simulated system can withstand an extreme drought event affected for a 10-year period under the allowing circumstances of engineering and ecological thresholds found for the two policies; the baseline scenario has little tolerance to such disturbance (reduction on TRWR) and easily breaks when it overcomes the ecological threshold without being able to recover. Policy I, seems to be the most promising scenario as its resilience measures have the highest values, so the system can even recover from the shock for a more severe drought.

**References**

Bakhshianlamouki, E., Masia, S., Karimi, P., van der Zaag, P., and Sušnik, J. (2020). A System Dynamics Model to Quantify the Impacts of Restoration Measures on the Water-Energy-Food Nexus in the Urmia Lake Basin, Iran. Sci. Total Environ.708, 134874. doi: 10.1016/j.scitotenv.2019.134874

Herrera, H. (2017). From Metaphor to Practice: Operationalizing the Analysis ofResilience Using System Dynamics Modelling.Syst. Res.34 (4), 444–462. doi:10.1002/sres.2468

Randers, J. (1980). Guidelines for Model Conceptualization. Elem. Syst. Dyn.method117, 139

# A HEC-HMS model for the Aliakmon River digital twin

Dimitra FRISALI[1], Eleni FOTOPOULOY[1], Zisis MALLIOS[1], Charis STAVRIDIS[1], Nikolaos THEODOSIOU[1]

[1] School of Civil Engineering, Aristotle University of Thessaloniki, GR54124 Thessaloniki, Greece
email: frysalid@civil.auth.gr
email: lefoto@civil.auth.gr
email: zmallios@civil.auth.gr
email: cstavrid@outlook.com
email: niktheod@civil.auth.gr

ABSTRACT

In recent years there has been a need for more efficient tools, able to suggest management practices of rivers and watercourses. A digital twin in general is a data-driven digital representation of resources, processes, or systems in the built or the natural environment. A digital twin is able to evaluate current performance and suggest alternative management methods that can lead to more efficient system behavior. The aim of the present work is the development of a hydrological model of Aliakmon River in northern Greece, on which a digital twin will be based. The model is formulated in HEC-HMS using only free access data that are available online. The results are very encouraging, proving that the model is extremely effective in adapting to changes in the flow regime of the river under study and concluding that it can be used as the basis of a digital twin, utilizing the new features of HEC-HMS.

## 1. Introduction

In recent years, the need for more efficient management of water resources has become urgent, due to population growth and other factors. For this reason, water resources management decisions should be based on advanced tools that can reflect the real conditions of the natural environment, like a digital twin that can analyze scenarios of "what would happen if" (Alzamora et. al, 2021). This work presents the structure of a digital twin of Aliakmo River in Greece, based entirely on free software and data, with an emphasis on the structure and the results of the hydrological model. Precisely, the digital twin will be based on the hydrological model that will be created on the HEC-HMS software (Bartles et. al., 2021).

## 2. Methodology

On the main stem of the river there are five large reservoirs that are used for energy production and for meeting the irrigation and water supply needs of the wider region. The main tributary of Aliakmon is the Almopaios River. Almopaios River meets Aliakmon River about 40 km before its estuary, a few kilometres downstream from the last of the large dams (Agia Varvara Dam) -. The outflow of the Asomata reservoir flows into the Agia Varvara regulating reservoir. From there, large quantities of water are diverted through channel A0 to the plains of Thessaloniki, mainly during the summer months, to meet the irrigation needs of the fields in the wider area. In addition, a significant amount of water (about 2-3 $m^3/s$) is diverted throughout the year to the city of Thessaloniki to meet the city's water supply needs. Furthermore, on the irrigation channel A0, the hydroelectric

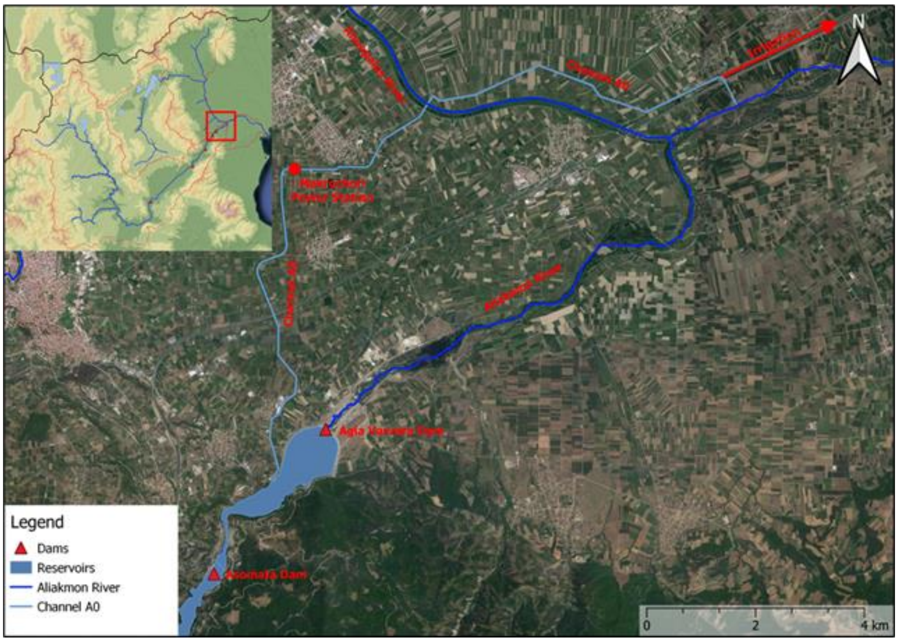


**Fig. 1.** Agia Varvara reservoir and the irrigation channel A0.

power station of Makrokhori is also in operation. The Makrokhori hydroelectric power station operates throughout the year and therefore the quantities of water passing through the irrigation channel A0 are greater than the irrigation needs of the area. The A0 channel is connected at some point to the Aliakmnonas River in order to return to it the surplus water that is not needed to meet irrigation and water supply needs. Downstream of the Agia Varvara dam, a small hydroelectric power station is installed to exploit the ecological flow of the river for energy. It has a constant flow rate of 4.5 $m^3/s$. In cases where the water entering the Agia Varvara reservoir from the Asomata dam is more than the water diverted to the A0 canal and the ecological flow, it is over-flowed by the dam's spillways. The proposed digital twin will have as main objective to evaluate and optimize the management of the water of the Agia Varvara reservoir, i.e., it will be able to evaluate the production of electricity and the corresponding coverage of irrigation water needs and propose better options. The aim of the digital twin will be to be able to propose water management options for a few days ahead of time. The necessary data for the execution of the model, i.e., the water inflows to the dam of Agia Varvara, the irrigation and water supply needs as well as the meteorological data will be automatically retrieved using the scripting language of HEC–DSSvue and stored in the database (dss file) of HEC–HMS. The hydrological model will then receive this data and will be executed. The results of the hydrological model will be evaluated based on economic and environmental criteria and then an optimization algorithm will be executed looking for a better management of the available water in the reservoir. The operation of the digital twin will use weather forecast data that can be obtained from open forecast databases like the Open-Skiron – OpenWRF service (https://openskiron.org/en/openwrf) which offers five days of daily weather forecast data in GRIB format.

## 3. Results

The model was calibrated using data for the entire 2018 and then evaluated using data from 2019 to 2021. Four statistical indicators were used to evaluate its effectiveness. The statistical measures that were used for this purpose are, the Mean Square Root Error Ratio (RSR), Nash Sutcliffe Yield (NSE), Bias Rate (PBIAS) and Determination Rate ($R^2$). Based on all these statistical measures above, the model proved to have a very good fit to the observed data. Figure 2 shows that the model for the year 2018, not only follows the periodicity of the river flow but also presents the peaks on the same days.

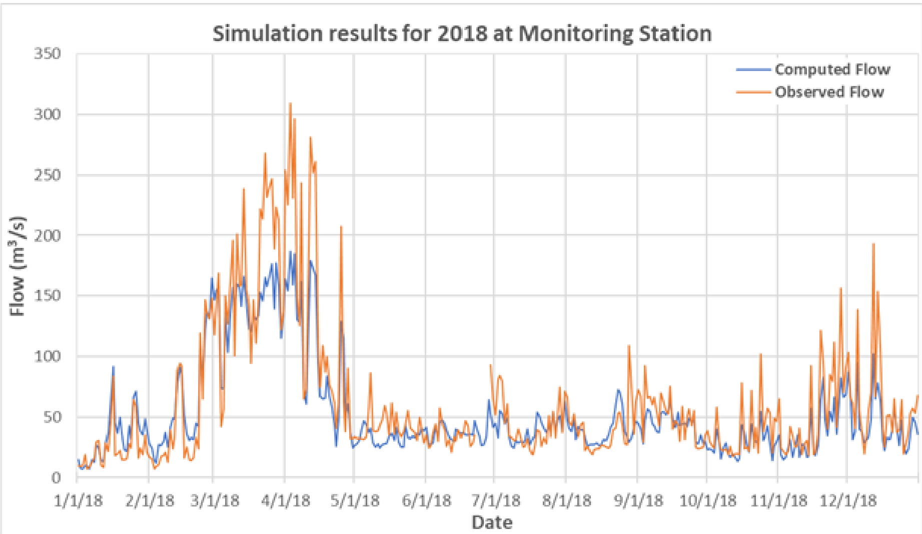

**Fig. 2.** Observed flow versus Computed flow for 2018 (calibration period).

## 4. Conclusions

A necessary condition for the creation of the digital twin is the creation of a well-structured hydrological model, which as it was proved above, it is achieved in the present work. Then it is required the connection of the model with the flow of meteorological data and energy production, so that in the final stage the development of an optimization algorithm will be done, in order to promote alternative strategies for the management of Agia Varvara reservoir. Finally, it could be used to address the effects of climate change and identify adaptation measures.

### References

Alzamora, F.M.; Conejos, P.; Castro-Gama, M.; Vertommen, I. (2021) Digital Twins - A New Paradigm for Water Supply and Distribution Networks. Association for Hydro-Environment Engineering, International hydrolink, 49–54.

Bartles, M.; Brauer, T.; Ho, D.; Fleming, M.; Karlovits, G.; Pak, J.; Van, N.; Willis, J. (2021) Hydrologic Modeling System HEC-HMS User's Manual. U.S. Army Corps of Engineers, Institute for Water Resources, Hydrologic Engineering Center (CEIWR-HEC), Davis, CA.

# Synergies between ecosystem services and land uses: Preliminary assessment results

Despoina CHARCHOUSI, Maria P. PAPADOPOULOU, Athina GOULA

National Technical University of Athens
email: charchousi@mail.ntua.gr; mpapadop@mail.ntua.gr; athina.goula@outlook.com

ABSTRACT

Groundwater Footprint (GF) could be considered as a management tool to help in groundwater management with emphasis on the environmental water needs. The parameters embedded in GF estimation are groundwater abstraction (C), recharge (R), and contribution to the environmental requirements (E), all essentials for the assessment of various Ecosystem Services (ES) such as water provision. The ES provided by C, R, E are closely related with the preservation of specific land uses and in parallel land uses impact C, R, E provisioning. To this framework, the present study focuses on the assessment of a) the significance of C, R, E on different types of land uses and b) the importance of specific land uses for the maintenance of C, R, E provisioning. To proceed with the assessment, a structure questionnaire using a 3-step scale is developed and filled by a pool of experts, aiming to reach consensus for each question. For the questions that consensus is not reached, experts are asked to review their answers based on group's opinion (second round questionnaire). At this stage of the study, the first round of questionnaire has been completed and consensus is reached for 37,5% of the questions, while the second round of the assessment is ongoing.

## 1. Introduction

GF is a groundwater management tool, introduced by Gleeson et al. (2012), that expresses the area required to sustain groundwater use and dependent ecosystems. Therefore, the ratio GF to the real area of an aquifer of interest can express sustainable (GF/A<1) or unsustainable (GF/A>1) groundwater management. GF estimation is based on C, R, and E. GF expresses an aquifer water balance between inflows (R) and outflows (C, E), focusing on environmental needs. C, R and E are essential for the provision of Ecosystems Services (ES) such as water provision (C, E), regulation of water cycling (R, E), nutrient cycling (C, E, R), aesthetic values (E). However, increasing water needs, especially under the pressure of climate change, are raising water conflicts in ES management. GF is a useful tool that can be used to express the potential groundwater stress in an area of interest and in parallel to highlight pressure on ES provision (C, R, E). Provisioning of C, R and E is closely related to the types of the land uses met in an area. In this framework, the scope of the present study is to assess C, R and E importance for the maintenance and protection of different types of land uses and in parallel to evaluate the impact of these land uses on C, R, and E availability. The assessment is based on experts' opinion, so the Delphi method is adopted to gather opinions and build consensus among experts by using a series of questionnaires (Walters et al., 2021). Hereafter, the methodological steps of the assessment process as well as primary results of this study will be presented.

## 2. Materials and methods

In the first step of the assessment, a structured questionnaire is developed to be distributed among the experts that are asked to evaluate: a) the impact of different types of land uses on C, R, E using a 3-point scale (1-negative, 2-neutral, 3-positive impact); and b) the significance of C, R, E for the conservation and protection of the various land uses using also a 3-point scale (1-not at all - low, 2-moderate, 3-very important). A detailed level 3 CORINE land cover classification consisting of 44 land use classes is embedded in the analysis.

The completed questionnaires are processed in order to investigate whether consensus has been reached. In Delphi method, consensus is not clearly defined. Diamond et al. (2014) report that out of 98 consensus-based Delphi studies, the most common definition for consensus was percentage agreement (75% median threshold). Therefore, 75% is set as threshold for consensus in this study also. The results of the analysis of the completed questionnaires indicates the end of the first round of the Delphi method and consist the basis for the second round. Specifically, the questions for which consensus have not been reached are included in the second round of questionnaire that is distributed to a sub-group of the initial experts in the framework of the second round and contains feedback of the outcomes of the first round so as the experts can review their answers taking into consideration other experts' opinion. Additionally, experts' comments on the formulation of the questionnaire are taken into consideration and additional information is included in the second round of the questionnaire, wherever needed. Following second round's statistical analysis and in case that consensus is not reached, a third or even a fourth round should be conducted.

## 3. Preliminary results (1st round) and concluding remarks

In the framework of the 1st round, the questionnaires have been completed by 25 experts. The analysis of the completed questionnaires has indicated that consensus has been reached in 37.5% of the questions. These questions are then excluded from the second round of the questionnaire. Fig. 1 presents the preliminary results of the questionnaire (1st round) for the land cover "vineyards"; the results of the first round highlighted first the negative impact of vineyards on groundwater provision (Figure 1a), and then, no consensus was reached, and therefore, this question will be included in the second round. Also, for the case of R & E, the results do not lead to a reliable conclusion and the question should be included in the second round (Figure 1b). In Fig. 1c and Fig. 1d, the significance of C, R and E for the conservation of vineyards is pointed out.

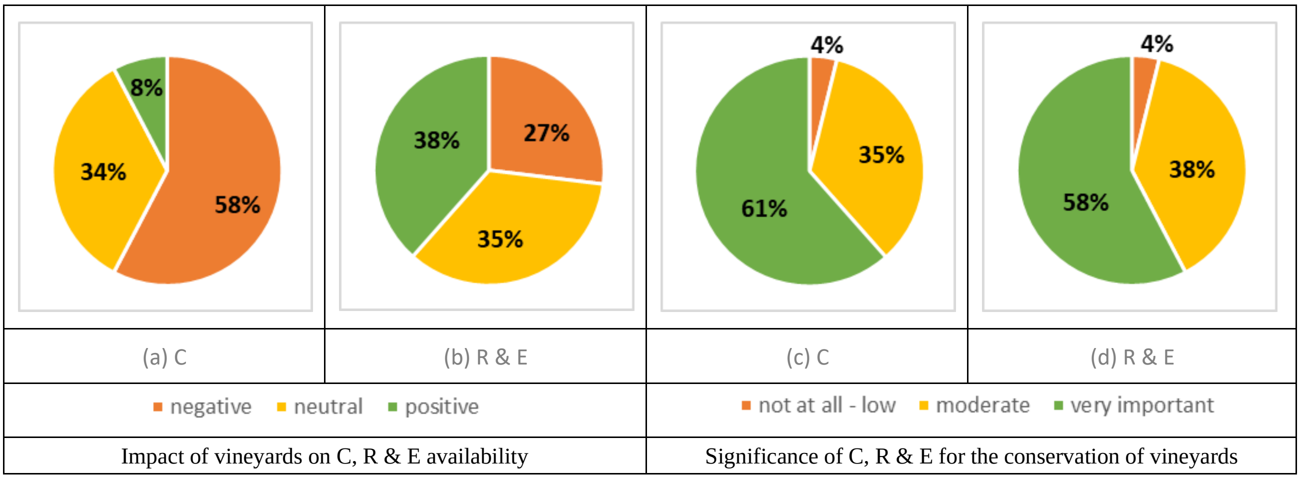


**Fig. 1.** Results of the Delphi Process (1st round): Impact of land cover "vineyards" on (a) C and (b) R & E availability and significance of (c) C and (d) R & E for the conservation of vineyards / Results expressed in agreement percentage

In the framework of the on-going 2nd round, the questionnaire will be distributed again to a sub-set of the initial to experts in order to complete a shorter questionnaire as the questions for which consensus is reached are not included in this round. Statistics of the 1st round will be also included in the questionnaire so as the experts can review their answers based on expert's collective opinion. The analysis of the 2nd round will point out if there is a need to proceed with a 3rd round based on the consensus rate. Reaching consensus for all questions will signify the end of the assessment and the importance of GF parameters for each type of land use will be quantified.

**Acknowledgments**

The present research was conducted within the project "National Network on Climate Change and its Impacts (NNCCI) - CLIMPACT" of the General Secretariat of Research and Technology of Greece.

**References**

Diamond IR, Grant RC, Feldman BM, Pencharz PB, Ling SC, Moore AM, Wales PW (2014) Defining consensus: a systematic review recommends methodologic criteria for reporting of Delphi studies, Journal of Clinical Epidemiology, 67, 401-409

Gleeson T, Wada Y, Bierkens M et al. (2012) Water balance of global aquifers revealed by groundwater footprint, Nature, 488, 197-200, https://doi.org/10.1038/nature11295

Walters D, Kotze DC, Rebelo A, Pretorius L, Job N, Lagesse JV, Riddell E, Cowden C (2021) Validation of a rapid wetland ecosystem services assessment technique using the Delphi method, Ecological Indicators, 125, https://doi.org/10.1016/j.ecolind.2021.107511

# Modelling fish movement trajectories in rivers

George MITSOPOULOS[1], Jon SVENDSEN[2], Anastasios STAMOU[1]

[1]Department of Water Resources and Environmental Engineering, School of Civil Engineering,
National Technical University of Athens, Greece
email: gmitsop@central.ntua.com
email: stamou@mail.ntua.com

[2] Technical University of Denmark, National Institute of Aquatic Resources, Freshwater Fisheries, Denmark
email: jos@aqua.dtu.dk

ABSTRACT

We present an integrated model that consists of a hydrodynamic model and a Fish Movement Model. Firstly, we calibrate the model using measured water velocities and fish trajectories in a part of the Konge River in western Denmark that is confined by 3 river sections: (1) inflow-upstream, (2) outflow towards a fish farm, and (3) outflow-downstream. Secondly, we perform a sensitivity analysis to identify the most significant model parameters. Thirdly, we apply the model to simulate fish trajectories; calculated fish numbers (1) exiting from the two outflows and (2) showing milling or not behaviour, are in satisfactory agreement with measured values.

## 1. Introduction

Generally, we consider fish movement as a two-step process: fish (1) evaluate all agents within the detection range of their sensory ovoid and (2) respond to them by moving. Fish movement is mainly driven by a hydraulic stimulus that we can determine using a hydrodynamic model (HYM), while we can determine fish trajectories using a Fish Movement Model (FMM). In this work (1) we present an integrated model that consists of a HYM and a FMM, (2) we calibrate it (the HYM and FMM using measured water velocities that range from 0 to 2.45 m/s and trajectories of migratory fish, respectively), and (3) we apply it to simulate the fish trajectories in a part of the Konge River in western Denmark that is shown in Fig.1 (Svendsen et al., 2011).

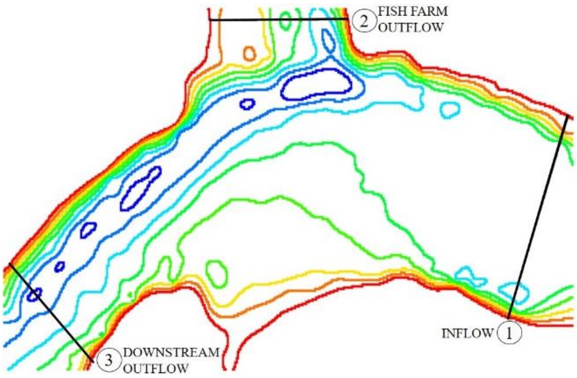


**Fig. 1.** The area of study and its bathymetry (range=0-2.05 m; red color=2.05 m; blue color=0.0 m)

## 2. Materials and methods

The integrated model consists of (1) the HYM TELEMAC-2D (Galland et al., 1991) and (2) a FFM that is based on the Eulerian-Lagrangian-Agent Method ELAM (Goodwin et al., 2006). The output of TELEMAC-2D (steady state hydrodynamic stimulus that is the acceleration magnitude) is the input to the FMM. At each time step and each node of the computational domain the FMM performs the following for each fish: (1) it defines its initial position, (2) it determines its sensory ovoid that is the area in which the fish perceives the hydrodynamic stimulus at 5 sensory, (3) it decides on its fish behaviour (B1: to follow the direction of flow, B2: to move towards higher velocities, and B3: to swim against the flow), based on the magnitude of the Detection Metric, (4) it calculates its velocity, its new position, and checks this position in relation to the boundaries of the computational domain. The cross-sectional boundaries of the area of study that are shown in Fig.2 are (1) inflow-upstream, (2) entrance to the Jedsted Mill Fish Farm, and (3) outflow – downstream.

## 3. Results and discussion

Firstly, we calibrated the hydrodynamic model; we defined the velocity profile at the inflow, as shown in Fig. 2, and we calculated the velocity profiles at the 2 outflows to determine the distribution of Manning values in the computational domain that ranged from 0.01 to 0.30. Figure 2 depicts a very satisfactory agreement between calculated values and measurements (RMSE ranged from 0.005 to 0.016). Secondly, we performed a Sensitivity Analysis to identify the most significant model parameters that are the threshold values th2 and th3 that modify the fish behaviour from B1 (default) to B2 and B3, respectively; the fish trajectories for the values of th2 are shown in Fig. 3. Thirdly, we performed calculations with the calibrated model using 100 fish to determine the fish trajectories and the number of the fish that (1) leave the area from the 2 outflow boundaries and (2) has a milling or non-milling behaviour that are shown in Table 1. Table 1 depicts that calculated fish percentages that (1) exit from the two outflows of the domain and (2) show a milling behaviour are in satisfactory agreement with measured values.

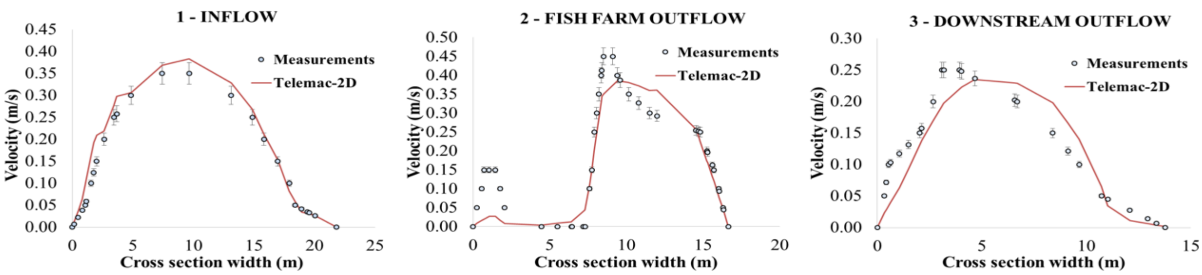


**Fig. 2.** The measured and modeled velocity profiles at the cross-sections

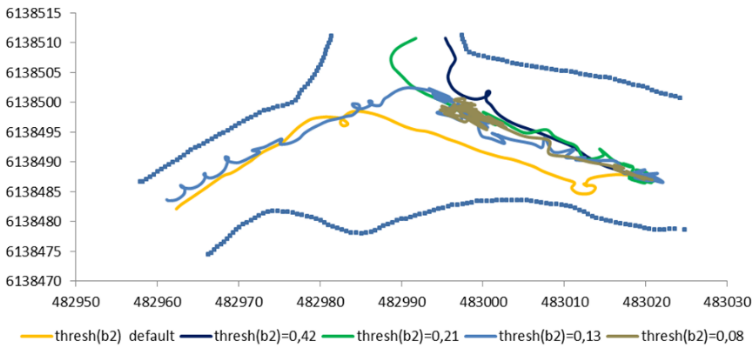


**Fig. 3.** Calculated fish trajectories for various values of th2

**Table 1.** Percentages of fish destination preference and milling or non-milling behavior

| Fish behavior | Exiting from the downstream outflow | Exiting from the fish farm outflow | Number of milling fish |
|---|---|---|---|
| Measurements | 67 % | 33 % | 34 % |
| Model | 60 % | 40 % | 29 % |

## 4. Conclusions

We calibrated and applied an integrated model to calculate the number of fish that (1) exit from the two outflows of the domain and (2) show a milling behaviour are in satisfactory agreement with measured values.

**Acknowledgments**

«This research is co-financed by Greece and the European Union (European Social Fund- ESF) through the Operational Programme «Human Resources Development, Education and Lifelong Learning» in the context of the project "Strengthening Human Resources Research Potential via Doctorate Research" (MIS-5000432), implemented by the State Scholarships Foundation (IKY)».

**References**

Galland JC, Goutal N and Hervouet JM (1991) TELEMAC: A New Numerical Model for Solving Shallow Water Equations, Advances in Water Resources AWREDI, 14 (3), 138–148.

Goodwin RA, Nestler JM, Anderson JJ, Weber LJ, Loucks DP (2006) Forecasting 3-D fish movement behavior using a Eulerian-Lagrangian-agent method (ELAM), Ecological Modelling 192, 197-223.

Svendsen JC, Aarestrup K, Malte H, Thygesen H (2011) Linking individual behaviour and migration success in Salmo salar smolts approaching a water withdrawal site: implications for management, Aquatic Living Resources 24(02):201 – 209.

# Removal of irgasan, ibuprofen, amoxicillin and paracetamol from water using organic residues under a bibliometric-statistical analysis

Paula MADARIAGA[1], Silvana PÁRRAGA[2], Kennedy C. CONCEICAO[1], Cristina VILLAMAR[3]

[1]Universidad de Santiago de Chile, Facultad de Ingeniería, Departamento de Ingeniería Química, Av. L. B. O'Higgins 3363, Estación Central, Santiago, Chile

[2]Escuela Politécnica Nacional, Departamento de Ingeniería Civil y Ambiental, Ladrón de Guevara E11-253, P.O. Box 17-01-2759, Quito, Ecuador

[3]Universidad de Santiago de Chile, Facultad de Ingeniería, Departamento de Ingeniería Civil en Obras Civiles, Av. Ecuador 3659, Estación Central, Santiago, Chile
email: cristina.villamar@usach.cl

ABSTRACT

Irgasan, ibuprofen, amoxicillin, and paracetamol have increased their use due to the pandemic. However, organic residues emerge as a viable treatment for their removal from wastewater. Thus, the aim of this study was to evaluate bibliometric-statistical analysis of scientific publications to stablish this potential use. Bibliometric (keywords co-occurrence) analysis used scientific publications (2010-2022) from Scopus database where keywords with highest occurrence were related to "adsorption" and "activated carbon". Systematic-statistical analysis used articles from different scientific platforms and showed that research on the topic increased, where ibuprofen removal was the most studied (38.6%). The highest adsorption capacity of organic residues according to biomass type is obtained for herbaceous and agricultural biomass. Finally, the correlation analysis established that the main variable influencing the removal is the surface area.

## 1. Introduction

Due to current COVID-19 pandemic, the use of pharmaceuticals and personal care products (PPCPs) has increased considerably. Amoxicillin, ibuprofen and paracetamol are used for general treatment of hospitalized patients. Also, irgasan, a potent antiseptic, is used in various toiletries, such as soap, being one of the main implements recommended to prevent contagion through constant hand washing (WHO, 2020). Several negative effects on the health of humans and animal species are attributed to these contaminants, such as alterations in the endocrine system and resistance to antibacterial pathogens (García-Gómez et al., 2011).

Carbon-based materials have been widely used in the PPCPs removal through adsorption (Krasucka et al., 2021). In general, activated carbon has been used as a high removal efficiency adsorbent, but its use is limited by its high investment cost (Alhashimi & Aktas, 2017). Thus, opportunities have emerged in the use of organic residues as an alternative material, with studies for the removal of irgasan, ibuprofen, amoxicillin and paracetamol through rice husks, cotton seeds, among others (Shin et al., 2020; Villaescusa et al., 2011). There is a lot of information, but there has not been a systematized study that evaluates the data presented in these publications. Therefore, this study seeks to bibliometrically analyze the available information and evaluate the adsorptive properties of various types of organic residues in the removal of the 4 PPCPs mentioned.

## 2. Methodology

Bibliometric analysis was carried out using the scientific journal repository Scopus. The keywords used were "emerging pollutants", "adsorption", "organic waste", "waste water" with at least one of the emerging contaminants (irgasan, ibuprofen, amoxicillin and paracetamol) for the temporality between the years 2010 and 2022. 114 scientific publications were found. Application of a keyword co-occurrence analysis was performed through VOSviewer software. Then, systematic analysis was carried out focusing in the specific temporality between 2010 and 2020 with the search results from various of the most used scientific databases. Information was limited according to language, publication status, type of study, contact system, residue and contaminant status, allowing the collection of comparable information, obtaining 80 scientific publications related.

Statistical analysis (two-way ANOVA test) was carried out in the software InfoStat (2020) to establish significant differences ($p < 0.05$) between the types of organic residue and efficiency parameters (max.

adsorption capacity and removal percentage) for each contaminant. The database was subjected to normality (Shapiro-Wilks's test) and variance homogeneity (F test). Then, parametric (Fisher's parametric test) and nonparametric (Kruskal Wallis test) analysis were used according to homoscedasticity of the database. Finally, a multiple correlation analysis (Spearman test) was performed in order to define the influential conditions in the removal of contaminants: material characteristics, control parameters, performance parameters and process efficiency.

## 3. Results

Bibliometric analysis evidenced the most important concepts in the study. The term "activated carbon" had 58 occurrences. In other categories, "pH" (26), "isotherm" (41), "Scanning electron microscopy" (27), "ibuprofen" (35) and "chemical activation" (12) were highlighted. The largest number of publications related to the subject was found between the years 2018-2022, reaching 76.3% of the total, which shows that the removal of this type of contaminants through organic residues is an emerging topic. Specifically, for the contaminants analyzed, it was shown that ibuprofen was the one that presented the most studies in general with 38.6% of 114 scientific publications. From systematic analysis, herbaceous and agricultural biomass (HAB) represented 70% of the residues analyzed, followed by 26.7% by woody biomass (WB). Specifically, it was reported that the most used subgroup was husks and shells with 26.9%. Also, HAB presented the best results in terms of maximum adsorption capacity with values of 90 mg/g for irgasan, 48.2 mg/g for ibuprofen, 152.5 mg/g for amoxicillin and 74 mg/g for paracetamol. Thus, this determines that these residues stand out with respect to other types due to their structure and availability. WB presented similar adsorption values, due to the similarity in the lignocellulosic composition of the materials and their texture (Crini et al., 2018). Finally, the correlation analysis determined that the surface area is the main factor on which the removal of this compounds depends, being related through a linear regression with the maximum adsorption capacity for the 4 emerging contaminants studied. Thus, the activation, whether physical or chemical, plays a fundamental role in the adsorbent properties, since it increases the surface area and the pores number of the natural residue, thus improving the adsorbent effect (da Silva-Lacerda, 2015).

## 4. Conclusions

The use of organic residues for the removal of emerging contaminants is constantly growing, being an emerging issue motivated by its cost in relation to other technologies. Activated carbon has positioned itself as the most used material, and ibuprofen as the most studied contaminant in this context, with 38.6% of the publications studied. Agricultural organic residues have been the most studied for adsorption issues, reaching the highest adsorption capacity values (152.5 mg/g for amoxicillin). It is also identified that the surface area is the most important parameter to consider, presenting a linear relationship with the maximum adsorption capacity of the compounds.

**Acknowledgements**

This work was supported by FONDECYT under Grant project 11190352 and National Agency for Research and Development (ANID)/Scholarship Program/Doctorado Nacional/2019 under Grant 21192016.

**References**

Alhashimi, H. A., & Aktas, C. B. (2017). Life cycle environmental and economic performance of biochar compared with activated carbon: A meta-analysis. Resources, Conservation and Recycling, 118, 13-26.
Crini, G., Lichtfouse, E., Wilson, L. D., & Morin-Crini, N. (2018). Adsorption-Oriented Processes Using Conventional and Non-conventional Adsorbents for Wastewater Treatment (pp. 23-71). Springer International Publishing.
da Silva-Lacerda, V. (2015). Aprovechamiento de residuos lignocelulósicos para la producción de biocombustibles y bioproductos.
García-Gómez, C., Gortáres-Moroyoqui, P., & Drogui, P. (2011). Contaminantes emergentes: efectos y tratamientos de remoción. Química Viva, 10(2), 96-105.
Krasucka, P., Pan, B., Sik Ok, Y., Mohan, D., Sarkar, B., & Oleszczuk, P. (2021). Engineered biochar – A sustainable solution for the removal of antibiotics from water. Chemical Engineering Journal, 405, 126926.
Oliva, M. P., Corral, C., Jesoro, M., & Barajas, J. R. (2019). Moringa-functionalized rice husk ash adsorbent for the removal of amoxicillin in aqueous solution. Paper presented at the MATEC Web of Conferences, 268 01005.
Shin, J., Lee, Y., Lee, S., Kim, S., Ochir, D., Park, Y., Kim, J., & Chon, K. (2020). Single and competitive adsorptions of micropollutants using pristine and alkali-modified biochars from spent coffee grounds. Journal of Hazardous Materials, 400, 123102.
Villaescusa, I., Fiol, N., Poch, J., Bianchi, A., & Bazzicalupi, C. (2011). Mechanism of paracetamol removal by vegetable wastes: The contribution of $\pi$–$\pi$ interactions, hydrogen bonding and hydrophobic effect. Desalination, 270(1), 135-142.
WHO. (2020). Clinical management of COVID-19: interim guidance.

# Experimental investigations on plunge pool protection measures for Ilarion Dam in Greece

Romain VAN MOL[1], Azin AMINI[2], Kreouza MANGINA[3], Giovanni DE CESARE[4], Anton J. SCHLEISS[5]

[1,2,4,5] Ecole Polytechnique Fédérale de Lausanne (EPFL), Switzerland
email: romain.vanmol@epfl.ch
email: azin.amini@epfl.ch
email: giovanni.decesare@epfl.ch
email: anton.schleiss@epfl.ch

[3] PPC S.A., Greece
email: k.mangina@dei.gr

ABSTRACT

Ilarion Dam is a 130 m high earthfill dam at Aliakmon River in northern Greece. The dam was commissioned in 2010. It has two spillway tunnels with ski jumps at the outlets. The two spillways are designed to release a total discharge of 5'500 $m^3/s$ during the probable maximum flood (PMF). During the flood events in 2013 and 2015, where only one spillway was working, scour holes have formed inside the plunge pool and erosion was observed at its banks and further down the tailrace channel. After a series of preliminary numerical investigations on the hydrodynamic behavior of the plunging jets, a physical model was built to assess the stability of prims protection carpets mitigate further scour of the plunge pool.

## 1. Physical model

The physical model is based on Froude's number similarity and reproduces the last 60 m of the spillway tunnels, the flip buckets, the plunge pool, and some 220 m of the tailrace channel of the Ilarion Dam.

A cost-effective solution to limit scour development is to use coarse riprap (Sá Lopes et al., 2006). It is usually made of rock-filled materials. The resulting non-uniform surface topography increases the roughness. This roughness dissipates to a higher extend the energy of moving water. Recent studies of the effectiveness of a riprap protection layer include case studies at the Poses-Amfreville Dam (Sixdenier et al., 2017) and the Beaumont-Monteux Dam (Derrien et al., 2019). Nevertheless, the block size of riprap is limited to some 5 to 7 tons which may not resist to high-velocity jet flow impact. Thus, a coarse protection layer can also be created using large concrete prisms. Such prisms show a strong resistance against high-velocity flow impact. Concrete prisms, obtained by dividing cubes diagonally, were successfully applied as protection of (i) alluvium downstream of a diversion tunnel (Emami and Schleiss, 2006 a, b), (ii) bank and bed erosion in steep mountain rivers (Schleiss, 1998) and (iii) scour protection downstream of high weirs (Wüthrich et al., 2021). This method also provides the possibility of installation during powerhouse operation without limitations on electricity generation. The prisms are placed in two layers. The lower one in a geometric configuration and the upper one in a random configuration. This results in a higher spatial density of prisms. They are also better interlocked than if they were placed in a more standard geometric configuration. A random configuration prevents them from moving during major floods. However, this arrangement has the disadvantage of being more difficult to implement from a technical point of view. The different size of prisms used in this experimental study are presented in Table 1. Assuming an average density of the concrete of 2500 $kg/m^3$, the prototype protection prisms will have a weight of 13.3 tons (medium size) and 29.3 tons (large size) thus being somewhat heavier than the tested mortar prims in the model.

The model equipment included a 3D scan with a Leica P20 laser scanner to survey the topography. Scans are taken at dry model in order to measure how the mobile bed has evolved. This makes it possible to compare the simulated scour with the measured one on site. The model equipment included also an ultrasonic level probe to follow the water level in the plunge pool and to measure the wave amplitude and frequency. Several scenarios were tested, first the two flood events in 2013 and 2015 recorded at the dam were reproduced to assess the correct behavior of the physical model. Then multiple arrangements of prisms were tested with a 1000-year flood event to find the most resilient one. Scenarios with one vs two spillways operational were also tested to see if the rotational effect observed in the numerical simulation (Van Mol et al., 2022) occurred also on the physical model. Finally, a wide range of flood events have been tested for the optimal configuration determined in the previous step.

**Table 1.** Concrete prisms characteristics as tested in the model

| Type | Cube size [m] | Prism volume [m$^3$] | Average density [kg/m$^3$] | Average weight [tons] |
|---|---|---|---|---|
| Medium (yellow) | 2.20 | 5.32 | 2275 (model) | 12.11 |
| Large (grey) | 2.86 | 11.70 | 2382 (model) | 27.86 |

## 2. Main results, discussion and conclusions

The optimal configuration protects the plunge pool and the tailwater channel fully up to flood events with a return period of 100 years. Scour at the plunge pool bed is reported but this does not represent a safety problem for the dam or the ancillary structures. For bigger flood events with return periods such as 1000 years (Fig. 1) and 10000 years, damage was observed along the right bank of the tailwater channel. However, it remains contained and does not affect the integrity of the plunge pool and the safety of the dam.

**(a)** Before flood **(b)** During flood **(c)** After flood

**Fig. 1.** Aerial view picture sequence of the plunge pool for the 1000-year flood run

The performed tests confirm that it is mandatory to have two layers of prisms, where the lower on is partially buried in the relatively fine substratum as it occurs during the erosion process. Moreover, the more regular pattern of the lower layer allows the second layer to be particularly efficient in terms of energy dissipation due to form friction. As long as possible it is recommended to operate both spillways symmetrically. Indeed, this a simple and cost-effective solution. When both spillways are operating the rotational flow is strongly attenuated and the depth of the scour is considerably reduced because the material which is excavated form one hole with be deposited in the other and vice-versa.

**Acknowledgements**

The authors would like to acknowledge the Public Power Corporation S.A. (PPC) for granting the study.

**References**

Derrien S, Clutier A, Blancher B, and Carraz F (2019). Étude sur modèle réduit des affouillements en aval du barrage de Beaumont-Monteux sur l'Isère. La Houille Blanche, Société Hydrotechnique de France, 1 :48–55
Emami S, Schleiss AJ (2006a). Design of erosion protection at diversion tunnel outlets with concrete prisms. Canadian Journal of Civil Engineering, NRC Research Press Ottawa, Canada, 33(1): 81-92.
Emami S, Schleiss AJ (2006b). Performance of large concrete prisms as erosion protection at Seymareh diversion tunnel outlets during a large flood Commission Internationale des Grands Barrages - Vingt Deuxième Congrès des Grands Barrages, CIGB-ICOLD, Barcelone, C. 12, pp. 799-813, 2006
Sá Lopes A, Proença MF, Maia R (2006). Energy dissipation downstream of dams established in alluvial beds. Proceeding of the International Conference on Fluvial Hydraulics, Lisbon, Portugal
Schleiss, A. J. (1998). “Erosionschutz an Gebirgsflüssen mit eingegrabenen Betonprismen.” Wasser, Energie, Luft – Eau, Energie, Air, 90(Heft 3/4), 45–52.
Sixdenier JP, Shaiek S, Erpicum S, Pirotton M, and Lahaye R (2017). Protection contre l'affouillement du barrage de Poses-Amfreville: études sur modèles réduit et numérique. Symposium *Hydraulique des barrages et des digues*., Société Hydrotechnique de France, Paris
Van Mol R, Mörtl C, Amini A, Siachou S, Schleiss AJ, De Cesare G (2022). Plunge pool scour and bank erosion: Assessment of protection measures for Ilarion Dam by physical and numerical modelling. Hydro 2022, Strasbourg, France
Wüthrich D, Chamoun S, Bollaert EFR, De Cesare G, Schleiss AJ (2021). Experimental and Numerical Study on Scour-Protection Methods in a Stilling Basin: Case Study of Chancy-Pougny Dam. Journal of Hydraulic Engineering, American Society of Civil Engineers, 147(6), 05021002

# Assessment of a Precipitation- Runoff relation based on a new fuzzy adaptive regression

Mike SPILIOTIS[1], Luis GARROTE[2]

[1] Department of Civil Engineering, School of Engineering, Democritus University of Thrace, 671 00 Xanthi, Greece
[2]Department of Civil Engineering: Hydraulics, Energy and Environment, Universidad Politécnica de Madrid, 28040 Madrid, Spain
email: m.spiliotis@gmail.com
email: l.garrote@upm.es

ABSTRACT

In this work, an adaptive fuzzy based regression is proposed to include a non-constant behavior of the runoff as function of the precipitation. For high precipitation, beyond a fuzzy threshold, a conventional (crisp) relation between precipitation and runoff is established, while for low precipitation, a curve with different behavior must be derived. Between these curves and for a runoff range each curve holds to some degree. Therefore, it can be suggested that the proposed method emanates from the physical problem itself. Hence, a simplified Sugeno architecture scheme is established based on only two logical rules. The training process is achieved based on a combination between the Particle Swarm Optimization (PSO) method and the conventional least square method.

## 1. Scope of the article

In this article, an adaptive fuzzy based regression is proposed to represent the non-constant behaviour of the relationship between precipitation and runoff at the annual scale, which may be successfully described by the law presented in Eq. (1):

$$E = k(P - P_0) \tag{1}$$

where $E$ is annual runoff in mm, $P$ is annual precipitation in mm, and $k$ (dimensionless) and $P_0$ (mm) are two parameters that may be estimated through linear regression. $P_0$ may be interpreted as a runoff threshold and $k$ is a runoff coefficient at the annual scale. For humid climates, where annual precipitation is always greater than the runoff threshold, this simple relation is always valid. However, in certain arid or semiarid climates, annual precipitation may be lower than the runoff threshold and this would yield negative runoff, meaning that the relationship may not be valid for low precipitation years. In this work, a solution is proposed for this problem. For high precipitation, beyond a fuzzy threshold, a conventional (crisp) relation between precipitation and runoff is established, while for low precipitation, a curve with lower slope must be derived. Between these curves, and for a precipitation range close to the runoff threshold, each curve holds to some degree.

A simplified Sugeno architecture scheme is established based on only two logical rules. The training process is achieved based on a combination between the Particle Swarm Optimization (PSO) method and the conventional least square method. There are plenty of examples that illustrate the application of the Sugeno Systems to hydrological problems based on the MATLAB toolbox. Even if the errors remain within acceptable range, sometimes the rational and logical basis of the application is erroneous (Sen, 2010; Spiliotis et al., 2017). On the other hand, there are also applications of the if-then systems based on a logical explanation, but these lack a proper training process. The method proposed for the application presented in this work was successfully applied by Spiliotis et al. (2017) to assess the bedload transport in gravel-bed rivers as function of the discharge.

## 2. Proposed simplified architecture of the fuzzy rule-based system

In the proposed model, only one variable has the ability to derive the use of the proper linear relation. This variable (precipitation) takes only two linguistic values (high and low), and thus, only two rules are applied. Hence, there are two regions without uncertainty where only one regression equation is activated. However, between two crisp areas (Fig. 1) there is a grey region where both rules are activated to some degree. The shape of the membership functions $\mu_1$ and $\mu_2$ are presented in Fig.1. Let's assume only one input variable (precipitation) $x$. For the variables $\beta_1$ and $\beta_2$, *(decision varibles)* the final output $y$ for the input $x$ is given as follows:

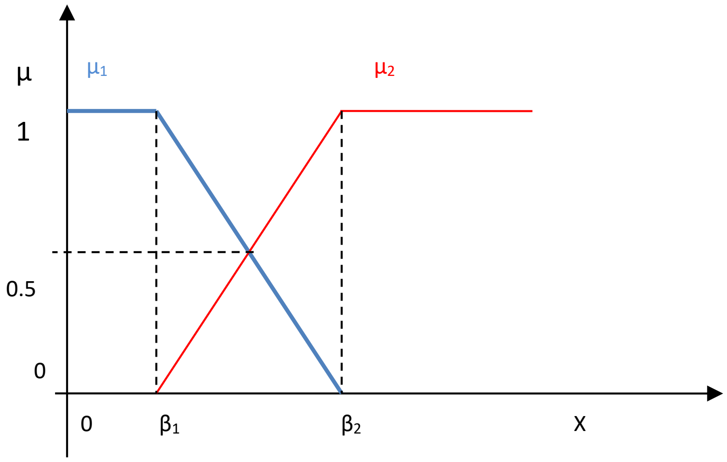


**Fig. 1:** Architecture of the fuzzy rules

$$y=\frac{\mu_1(x)(a_{10}+a_{11}x)+\mu_2(x)(a_{20}+a_{21}x)}{\mu_1(x)+\mu_2(x)}=\frac{\mu_1(x)}{\mu_1(x)+\mu_2(x)}a_{10}+\frac{\mu_2(x)}{\mu_1(x)+\mu_2(x)}a_{20}+\frac{\mu_1(x)x}{\mu_1(x)+\mu_2(x)}a_{11}+\frac{\mu_2(x)x}{\mu_1(x)+\mu_2(x)}a_{21} \quad (2)$$

where $x$ indicates annual precipitation (mm) and $y$ indicates basin annual runoff (mm). In the coefficients $\alpha$ the first index indicates the rule whilst the second index indicates the coefficient either of the constant term (0) or the independent variable (1).

## 3. Results

The proposed method was successfully applied to the basins of two water resource systems in Southern Spain: the Guadiana II and the Sierra Filabres-Estancias basins. The results are presented in Figure 2.

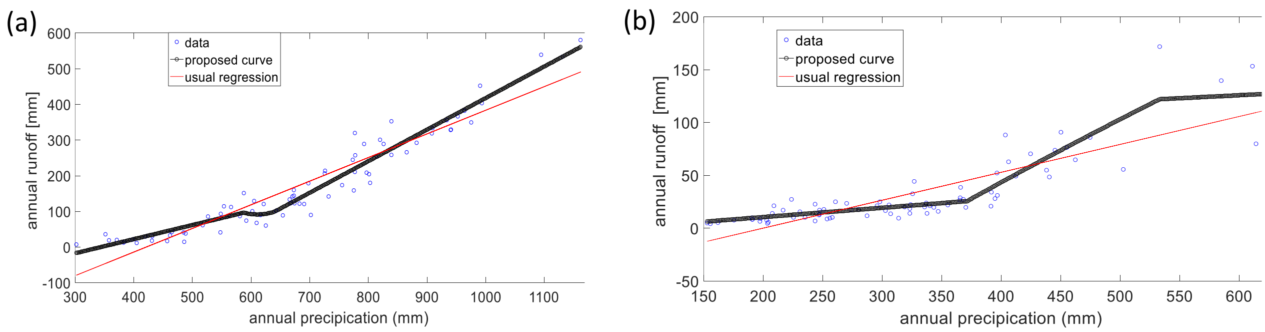


**Fig. 2.** The proposed method and the conventional regression applied in order to assess a relation between annual precipitation and runoff in case of (a) Guadiana II and (b) Sierra Filabres-Estancias basins

The results for the examined cases indicate that the proposed method simulates better the relation between the annual precipitation and the annual runoff compared to the conventional regression. By comparing the two graphs of Fig. 2, the first has a short grey region (the thresholds $\beta_1$ and $\beta_2$ are equal to 587.34 mm and 640.53 mm-below the median) whilst the second grey zone has a larger range (the thresholds $\beta_1$ and $\beta_2$ are equal to 371.3 mm and 533.3 mm-above the median). The proposed method is suitable to estimate the annual water wield, but it is not intended to assess the peak flow under a significant rainfall.

**References**

Sen Z (2010) Fuzzy logic and Hydrological Modelling. CRC Press, Taylor and Francis Group.

Spiliotis M, Mediero L and Garrote L (2016). Optimization of Hedging Rules for Reservoir Operation During Droughts Based on Particle Swarm Optimization. Water Resources Management, 30(15), 5759–5778.

Spiliotis M, Kitsikoudis V, Hrissanthou V (2017) Assessment of bedload transport in gravel-bed rivers with a new fuzzy adaptive regression, European Water, 57, 237-244.

# Future water availability in the Iberian Peninsula according to the CMIP6 projections: How to teach water engineers to make the calculations?

Gabriel Ibarra-Berastegui
Bilbao's Faculty of Engineering, Energy Engineering Department
Plaza Ingeniero Torres Quevedo, 1. 48013 Bilbao, Spain

Phone: (+34)946014274
email: gabriel.ibarra@ehu.eus
https://www.ehu.eus/en/web/eolo/

The recent compromise of the European Union towards a climate-neutral economy by 2050 represents a major challenge for Higher Education institutions that must also incorporate climate-related contents in the syllabus of a number of subjects.

The University of the Basque Country (http://www.ehu.es) is the most important University in the Autonomous Region of the Basque Country, Spain. The students of the Faculty of Engineering (Bilbao) in the last year of their studies, before becoming engineers, can select a block of subjects intended to enhance their knowledge on Hydraulics and Fluid Mechanics.

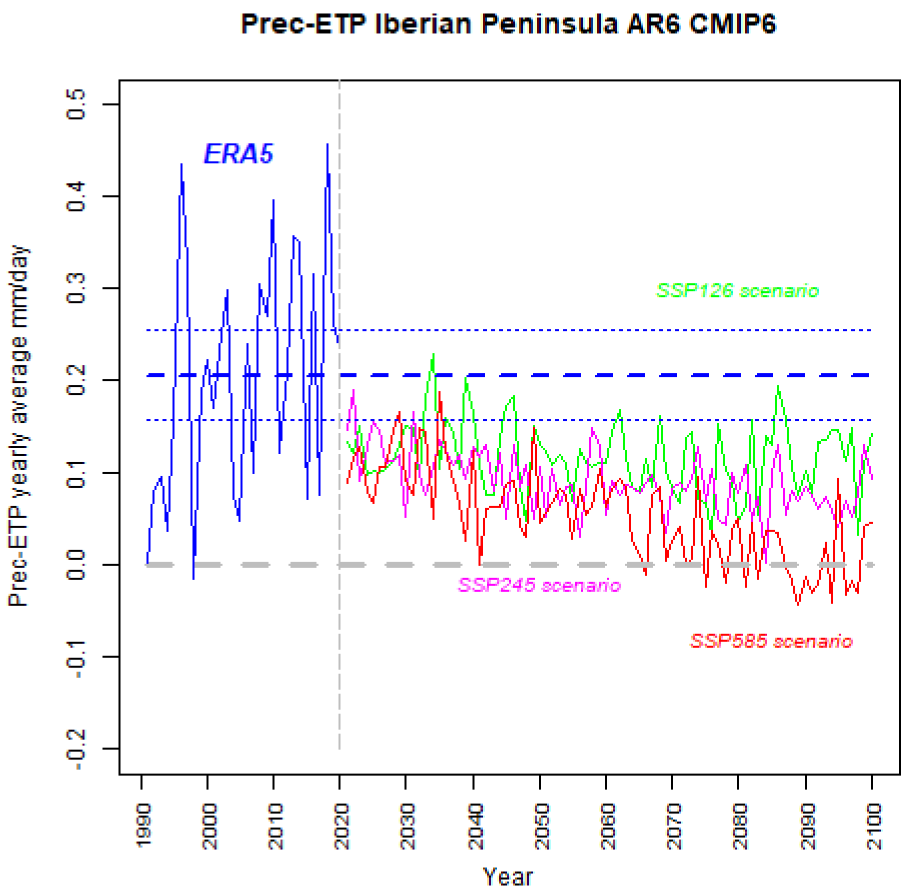

More particularly, in one of these subjects called "Management and Maintenance of Hydraulic Systems" students learn to solve a set of practical exercises linked to the urban water management. The methodology followed during the classes is Problem-Based Learning (PBL) and due to the rather small number of students (<15), peer-to-peer methodology is also encouraged. This means that students focus in learning in a hands-on way instead of memorizing facts related to water management.

In urban water management, three hydraulic systems are connected: water supply, stormwater and wastewater systems. Water supply is an issue of major concern in the context of a rapidly evolving economy with important changes in industry needs and population numbers. Long-term changes driven by climate oscillations in precipitation and evapotranspiration have an impact on water availability for all kind of human uses.

For this reason, if water shortage is to be avoided, information on future projections must be incorporated by decision makers and stakeholders into the long-term hydraulic planning of any region or country. Recently, the International Panel of Climate Change (IPCC) has released the AR6 report with updated climate projections that can be used to estimate future projections for a region like the Iberian Peninsula (figure 1)

In the subject "Management and Maintenance of Hydraulic Systems" in the framework of the PBL methodology, a specific problem has been incorporated to teach students how to understand what climatic models are and how to extract sensible information on future projections of water availability. The last step includes how to include this information into the long-term planning of water supply in several regions of Spain

Incorporating climate change contents in a completely practical way, has been most welcomed by students. To that purpose, the PBL methodology has proven an appropriate tool, thus exhibiting again all its potential as an educational tool in engineering studies. PBL can provide an easy adaptation to a continuously changing professional environment where new challenges –like climate change impacts- must be addressed from both, a technical and economical point of view.

For this reason, the PBL methodology contributes to minimizing the gap between theoretical education and real-life problems for future engineers dealing with future water availability planning in a context of climate-driven changes that they must know how to deal with.

*Keywords—Climate change. Water management. PBL.*

# Macro Meets Meso: Evaluation of Fish Mesohabitat in Rivers in the Context of Macrohabitat Regions

Hannah SCHWEDHELM[1], James BARRY[2], Brian COGHLAN[2], Ciara FLEMING[2], César RODRÍGUEZ[3], Sara GARRIDO[3], Katarzyna SUSKA[4], Janusz LIGIĘZA[4], Piotr PARASIEWICZ[4]

[1] Chair of Hydraulic and Water Resources Engineering, Technical University Munich, Germany
email: hannah.schwedhelm@tum.de

[2] Inland Fisheries Ireland, Ireland
email: ciara.fleming@fisheriesireland.ie, brian.coghlan@fisheriesireland.ie, james.barry@fisheriesireland.ie
[3] General Secretary, AEMS-Ríos con Vida, Spain
email: cesar.rodriguez@riosconvida.es, sara.garrido@riosconvida.es
[4] S. Sakowicz Inland Fisheries Institute, Poland
email: k.suska@infish.com.pl, j.ligieza@infish.com.pl, p.parasiewicz@infish.com.pl

ABSTRACT

A recent approach to cluster rivers into macrohabitat types according to their expected fish community offers a reference benchmark in form of expected quantitative habitat structure for European rivers. For two alpine rivers in Austria, mountain river in Ireland, lowland river in Poland, and Mediterranean river in Spain, habitat distributions have been assessed using the MesoHABSIM model. High similarity between the observed habitat structure and the habitat structure defined for these macrohabitat regions could be observed.

## 1. Introduction

Habitat models are powerful tools for planning and assessment in river management. However, it can be difficult to identify or define target fish species for which such models should be developed. Regional approaches to cluster rivers according to their similarities have been proposed and gained attention in recent studies in order to facilitate river management on a continental scale (river clustering: Arthington et al. (2006), ELOHA approach: Poff et al. (2010), e-flow definition: Parasiewicz et al. (2018)). Such an approach was established within the H2020-project AMBER, where European rivers have been clustered into macrohabitat types representing regions with similar composition of fish habitat-use guilds (Fish Community Macrohabitat Types (FCMacHT)). The determinants of the classification are macroscale geographical attributes such as slope, watershed area and gradient (Parasiewicz et al. in review, Coghlan et al 2020). It can be assumed that the composition of fish guilds corelates with the habitat structure, which means that the most common species also inhabit the most common habitats or expressed differently, the natural habitat structure supports the predominant fish assemblage (Parasiewicz 2007b). The hypothesis of this study is therefore, that the fish habitat distribution observed in the river should correspond with those predicted by FCMacHT model.

## 2. Material and Methods

The MesoHABSIM model (Parasiewicz 2001, 2007a) was applied at two Austrian rivers, Leutascher Ache and upper Inn. Within the AMBER project also the Munster Blackwater River in Ireland, Vistula River in Poland and the River Guadalhorce in Spain have been analysed the same way. The FCMacHT regions to which the five rivers belong are shown in Table 1 (Parasiewicz et al. in review, Coghlan et al 2020). Hydromorphologically all analysed river stretches are not heavily modified or were subject of restoration measures in the past. It was evaluated for each site, if and to which proportion the observed habitat features present suitable habitats for the fish community as defined by FCMacHT. For this evaluation the affinity index model was used (Novak und Bode 1992).

## 3. Results

Table 1 shows the range of the affinity index observed for the five different rivers. Figure 1 shows the proportions of the observed habitats which provides suitable habitats for the three individual fish habitat-use guilds for a range of flow conditions of 5-60 l/(s·km²) for the Inn River and the Leutascher Ache River. The composition of the expected habitat-use fish guilds for this FCMacHT region is shown in the first column of Fig. 1. In addition, Fig. 1 includes affinity indices, which show how strong the compositions of the proportions correspond to those defined by FCMacHT for each specific flow condition. In particular for these two rivers, high correlations of 77.1-86.4% for Leutascher Ache and even 80.4-98.7% for Inn River could be observed.

**Table 1.** Affinity Index and FCMacHT classification ranges for the four rivers

| River | FCMacHT | Affinity Index [%] |
|---|---|---|
| Leutascher Ache (Austria) | Mountain, Alpine Rivers | 77-86 |
| Inn (Austria) | Mountain, Alpine Rivers | 80-99 |
| Munster Blackwater (Ireland) | Pan-European calcareous headwaters | 73 |
| Vistula (Poland) | Central European submountain and highland | 66-72 |
| Guadalhorce (Spain) | Mediterranean mountain and upland | 75-76 |

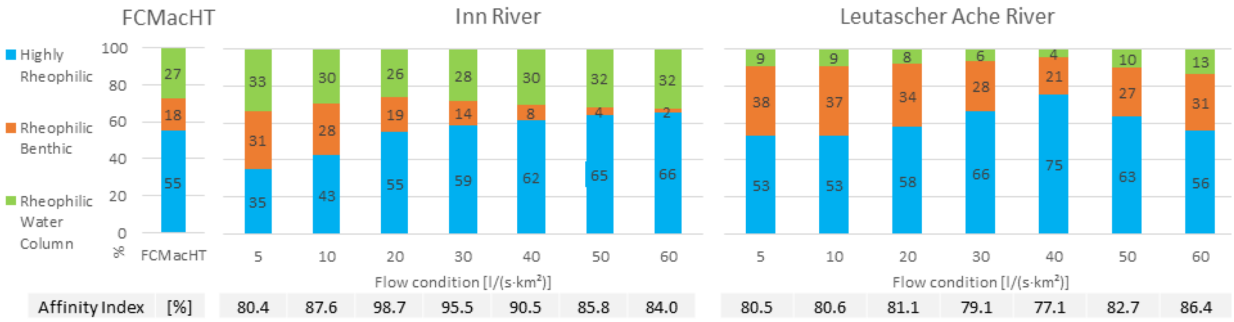


**Fig. 1.** Observed habitat compositions and defined habitat compositions in FCMacHT for the Inn River and the Leutascher Ache River for different flow conditions of 5-60 l/(s·km²)

## 4. Discussion and Conclusion

For the five rivers, the proportions of the suitable habitats for each guild are similar to the proportions of these guilds within the defined fish assemblage. This is shown by the high affinity indices. Therefore, the five river stretches provide suitable habitat for habitat-use guilds, which are expected in these rivers. As all river stretches are not heavily altered, the observed high affinity indices show the validity of the definition of such macrohabitat regions together with the definition of the assemblage of the fish habitat-use guilds for these regions. This is especially significant as, for example the two alpine rivers, have different characteristics in regards to catchment size, flow values, fish species and hydrological regimes. In addition, even for the anthropogenically restored stretch such as the at the upper Inn River or Munster Blackwater suitable habitat occurs for the defined guilds which highlights the importance and effectiveness of restoration measures even in spatially limited areas. Within the AMBER project, several anthropogenically impacted rivers have been analysed as well and showed much lower affinity indices. This FCMacHT has therefore the potential to facilitate river management in regions where specific data on fish species is missing and provides reference conditions for anthropogenically altered rivers. It can be used as a benchmark in the design process of restoration measures or the determination of environmental flows.

**Acknowledgements**

The study is based on data obtained within the two projects AMBER and FIThydro which have received funding from the European Union's Horizon 2020 research and innovation programme under grant agreement No 689682 and 727830, respectively. We thank all project partners for their support and expertise.

**References**

Arthington AH, Bunn SE, Poff NL, Naiman RJ (2006) The challenge of providing environmental flow rules to sustain river ecosystems, Ecological Applications, 16 (4), 1311–1318

Coghlan B, Morrissey B, Rodriguez Ruiz C, Fleming C, Bubb D, Oliveira E. de, et al. (2020) D4.2 Report of Case Studies Demonstrating the Effects of Barrier Removal, Mitigation and Installation, AMBER Project Deliverable 4.2

Novak MA, Bode RW (1992) Percent Model Affinity: A New Measure of Macroinvertebrate Community Composition, Journal of the North American Benthological Society, 11 (1), 80–85

Parasiewicz P (2001) MesoHABSIM: A concept for application of instream flow models in river restoration planning, Fisheries, 26 (9), 6–13

Parasiewicz P (2007a) The MesoHABSIM model revisited, River Research and Applications, 23 (8), 893–903

Parasiewicz, P (2007b) Using MesoHABSIM to develop reference habitat template and ecological management scenarios, River Research and Applications, 23 (8), 924–932

Parasiewicz P, Prus P, Suska K, Marcinkowski P (2018) "E = mc2" of Environmental Flows: A Conceptual Framework for Establishing a Fish-Biological Foundation for a Regionally Applicable Environmental Low-Flow Formula, Water, 10 (11), 1501

Poff NL, Richter BD, Arthington AH, Bunn SE, Naiman RJ, Kendy E, et al. (2010) The ecological limits of hydrologic alteration (ELOHA): a new framework for developing regional environmental flow standards, Freshwater Biology, 55 (1), 147–170

Parasiewicz P, Belka K, Łapińska M, Ławniczak K, Prus P, Adamczyk M, Buras, et al. (in review). Over 200,000 kilometers of river-fish habitat is lost to impoundments in Europe. Nature

# Identification of the kind of sorption isotherm and its parameters by a Bayesian formulation of the Ensemble Kalman Filter

Alicia SANZ-PRAT[1], J. Jaime GÓMEZ-HERNÁNDEZ[1]

[1] Research Institute of Water and Environmental Engineering, Universitat Politècnica de València, Valencia, Spain
email: asanpra@iiama.upv.es

ABSTRACT

## 1. Motivation

The effects on human health and environmental systems resulting from anthropogenic contamination (e.g., emerging organic contaminants, heavy metals, microplastics) in soil and aquifers are still unknown, especially when their presence in nature may last up to decades due to complex reactive processes along their transport in groundwater as solved-precipitated compounds. Under uncertain scenarios driven by Climate Change, such mechanisms may be affected by forecasted lower water table levels and higher temperature ranges in the groundwater. Current official estimations establish in over 2500 million of potentially contaminated sites distributed throughout Europe, wherein source identification and delineation of the affected area may have socio-economic and legal implications. In this context, the protection of the environmental, social, and economic services of the natural resources is identified as of vital importance in the Sustainable Development Goals SDG6- Clean water and sanitation, and SDG15- Life on land.

However, when a contaminant event is detected, consequent decisions rely on commonly sparse databases to define the status of soil and aquatic ecosystems. Despite constrained model assumptions and demanding computational time, hydrogeology stochastic inverse models (SIM) are considered excellent methodologies to extract consistent and valued input parameter information from non-sampled areas by analyzing predictive responses of the system in comparison with actual observed responses. The Forensic Hydrogeology project (FORENSHYD) attempts to contribute with a next step toward pioneer technologies yielding reliable reactive compound simulations will enhance the efficiency of water management administrations.

## 2. Objective

The main objective of FORENSHYD is to answer where, when, and how much contaminant has been discharged into an aquifer using the ensemble Kalman Filter (EnKF) for reactive transport inverse modeling. In this study, we focus on the sorption processes, as those are commonly relevant at field scale. We propose merging the EnKF with Bayesian Probability Theory (Evensen, 2009) to estimate both the sort of isotherm sorption processes, as well as the magnitude of their parameters. The application of such achievement may clarify preliminary conceptual models and simplify the calibration processes in the site studies of the InTheMED project.

## 3. Methodology

The EnKF starts with initializing the model parameters, followed by iterated steps of (i) **prediction** of the state variables by direct modeling from time $k = 0$ and (ii) **updating** the estimated values of the parameters from the deviations between observations and predictions. Parameters and corrected variables serve as input data in the next iteration at time $k + 1$. The novelty of this work lies in using Bayesian statistics, as the maximum likelihood estimator, to optimize the fitting between observed and simulated concentrations. The method assumes that for each sorption isotherm type: lineal, Freundlich and Langmuir, there is a probability density functions defined by statistical parameters. Such parameters are included in the parameter vector to update during the iteration of the EnKF. The method is demonstrated in numerical scenarios of isotherm sorption systems in two dimensions of increasing complexity subject to coupled nonlinear physicochemical processes, heterogeneous media, and dynamic environmental conditions.

**Acknowledgements**

This project has received funding from the European Union's Horizon 2020 Research and Innovation Programme under the Marie Sklodowska-Curie grant agreement Nº 895526.

**References**

Evensen G (2009) Data assimilation, The Ensemble Kalman Filter, Springer, 314 pp.

# Performance evaluation of urban storm drainage systems under rare rainfall events: The example of the city of Argos, Argolis region, Greece

Alexandros Kotsovos, Ioannis Nalbantis

National Technical University of Athens, Greece
email: alexstorm100@gmail.com
email: nalbant@central.ntua.gr

ABSTRACT

The aim of this work is the performance evaluation, under rare rainfall events, of the stormwater drainage system of the city of Argos, Argolis region, Peloponnese, Greece. For this purpose, the system is modelled using the software package SWMM. Synthetic storm hyetographs for return periods from 5 to 100 years are constructed based on the generalized Intensity-Duration-Frequency (IDF) curve that is available for the city, as well as limited information and assumptions regarding the system itself. System performance is evaluated using four indices based on statistics of both peak flow velocity in underground conduits and flood duration at system manholes. These indices revealed serious deficiencies of the system, which appear even for low return periods (e.g. 5 years).

## 1. Methodology

### *1.1. Design hyetographs and flood simulation*

Flow simulations in the studied system are performed using the Storm Water Management Model (SWMM) of EPA (2015). Synthetic storm hyetographs are constructed using the Alternating Block method and the official Intensity-Duration-Frequency (IDF) curve (Ministry of the Environment and Energy, 2018) for storm durations of 1, 3, 6 and 12 h and return periods of 5, 10, 25, 50 and 100 years. The hyetograph time step is 10 min, while the dual system option is selected to allow floodwaters at manholes to be routed through the urban street network. The latter is necessary since, even for flood events of low return period, many conduits are surcharged, causing manhole overflow (as covers are blown out of the ground) and overflowing . As a result, it is more realistic to consider two parallel networks, one for the underground pipes and another for the street network of open channels.

### *1.2. Performance indices*

In this study elementary indices are used, which directly reflect the compliance of the studied system with typical performance requirements. By adopting the maximum permissible and minimum required flow velocity of 6.0 m/s and 0.6 m/s respectively (Presidential Decree 696/74, 1974), the exceedance frequency of peak flow velocity over 6.0 m/s, PU, indicates pipe erosion risk, while the exceedance frequency of peak flow velocity below 0.6 m/s, PL, can inform us about sewers with acute self-cleansing problem. In addition, the median flooding duration of manholes, FDm, is employed with the purpose to assess the level of disturbance in the studied urban environment. Moreover, flood duration is employed for the assessment of the percentage of manholes that are flooded, PF. More advanced performance indices are given by Kourtis (2021) and Kourtis and Tsihrintzis (2021).

### *1.3. Study area*

The study area covers the city of Argos bounded from southeast by the Torrent Xerias. It has a total extent of 440 ha and is drained to the above torrent through three distinct outlets (Kotsovos, 2022). The area includes an urban part of 288 ha and a peri-urban one (152 ha). The total length of sewers is 31.6 km. A map from the Municipal Water Supply and Sewerage Company of Argos and Mycenae formed the basis for drafting the system layout. This information was later completed using assumptions about the depth of manholes, the length of conduits and various other features of the system. Since no information on urban watersheds was available, these are extracted from the Digital Elevation Model of the Hellenic Mapping and Cadastral Organization. Part of the entire model of the study area is shown in Fig. 1.

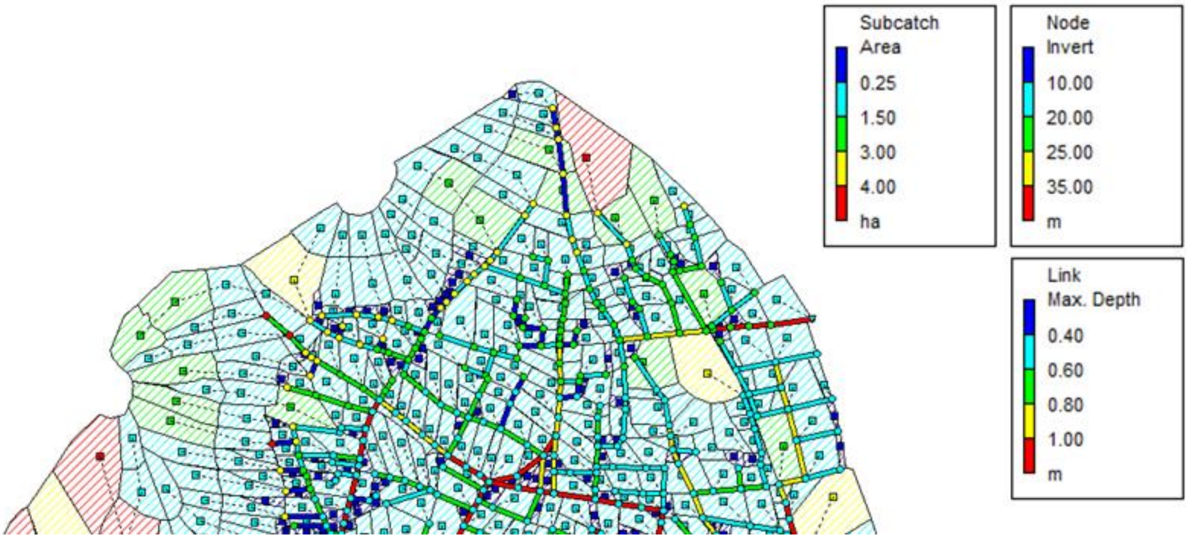


**Fig. 1.** Part of the model of the study area within SWMM; basins (subcatchments) are coloured according to their area, manholes (nodes) according to their elevation of invert and conduits (links) according to their maximum depth of cross section.

## 2. Results

Simulations allowed obtaining discharge hydrographs and water volumes for all system outfalls, the maximum flow at each outfall, the flow velocity and flow depth in the conduits and the flood duration at manholes. Model results were undergone post-processing to assess performance indices defined in subsection 1.2 and depicted in Table 1.

**Table 1.** Performance indices for the studied system

| Index of subsection 1.2 | Return period (years) | | | | |
|---|---|---|---|---|---|
| | 5 | 10 | 25 | 50 | 100 |
| PU | <0.002 | <0.002 | 0.006 | 0.006 | 0.008 |
| PL | 0.096 | 0.086 | 0.070 | 0.062 | 0.060 |
| FDm (h) | 0.01 | 0.10 | 0.17 | 0.30 | 0.35 |
| PF (%) | 66 | 74 | 89 | 95 | 100 |

## 3. Concluding remarks

Results presented in Section 2 indicate that the studied drainage system is incapable of conveying storm water safely to the system outfalls even for events of low return period. Peak flow velocity exceedances over the safe limit are very rare unlike the frequency of insufficient flow velocities for conduit self-cleansing which is significant. Manholes are inundated to a high percentage even for the low return period of 5 years and progressively the whole sewer network is flooded up to the 100-year period storm event. This deficiency is due to insufficient dimensions of pipes and manhole depths for most of pipes. As a result, streets are flooded even for low return period events.

**Acknowledgements**

The Hellenic Mapping and Cadastral Organization is warmly thanked for providing geospatial data.

**References**

EPA (2015) Storm Water Management Model User's Manual Version 5.1, EPA/600/R-14/413b, United States Environmental Protection Agency, pp. 353

Kotsovos A (2022) Flood hazard assessment in the city of Argos, Argolis region, Greece, Diploma Thesis, School of Rural, Surveying and Geoinformatics Engineering, National Technical University of Athens, pp. 203

Kourtis I (2021) Adaptation of storm sewer systems to climate change, PhD Thesis, School of Rural, Surveying and Geoinformatics Engineering, National Technical University of Athens, pp. 214

Kourtis IM, Tsihrintzis VA (2021) Adaptation of urban drainage networks to climate change: A review, Science of the Total Environment, 771: 145431

Ministry of the Environment and Energy (2018) Flood hazard management plan for Water District of Eastern Peloponnese (EL 03), Government Gazette 2692 B / 6.07.2018, pp. 352

Presidential Decree 696/74 (1974) On the remuneration of engineers for the study, supervision and project receipt of Transportation, Hydraulic and Structural works, as well as of Topographical, Cadastral and Cartographic studies and related requirements, Government Gazette 301/A/8-10-1974, pp. 30

# A simple method for the enhancement of river bathymetry in LIDAR DEM

Gabriele FARINA[1], Marco PILOTTI[2], Luca MILANESI[3]

[1,2,3] University of Brescia, DICATAM, Italy
email: g.farina008@unibs.it
email: marco.pilotti@unibs.it
email: luca.milanesi@unibs.it

ABSTRACT

The preparation of an accurate bathymetry is of paramount importance for flood modeling. A recurrent flaw of LIDAR-derived Digital Elevation Models (DEM) is a wrong representation of bed bathymetry due to the presence of water along rivers, that prevents a careful reproduction of the actual bed morphology and consequently an incorrect estimation of the conveyance. This contribution provides a simple algorithm designed to tackle this problem that can be applied when land surveyed cross sections are available to complement DEM data. The proposed algorithm, that requires the coupled use of both a 2D Shallow Water Equations solver and a GIS software, is successfully applied to a 37 km long stretch of the Mella river (Northern Italy).

## 1. Introduction

The European legislation 2007/60/EC prescribes the review of the hazard maps and flood risk maps every six years in order to take into account the impact of climate change, availability of new data and the increasing knowledge on hazard computation and flooding risk. There is a fundamental agreement on the procedure to compute hazard maps using suitable mathematical models (typically, the Shallow Water Equations, SWE) and the quality level that can be obtained is potentially very good provided that the description of the floodplain, watercourse and hydraulic structures present along the area of interest is accurate. Accordingly, DEM produced with LIDAR survey provides a detailed description of the floodplain topography but, on the other hand, the description of the river bathymetry could be unrealistic, mostly as consequence of the use of lasers based on red light, unable to penetrate water bodies. The consequence of the poor description of the riverbed is an unrealistically low conveyance that can be measured in correspondence of the surveyed cross sections where the riverbed elevation is known, thus suggesting the need of the correction of the bathymetry. In the literature, several methods are proposed to tackle this problem as a function of the data available; for instance, when only the DEM is available, typical procedures are based on the estimation of the water normal depth using Manning equation with simplified cross sections and a reasonable guess on the discharge value (e.g., Roub et al., 2012; Bhuyan et al., 2015). When both surveyed cross section and DEM are available, a different kind of interpolation can be done in order to reconstruct the bathymetry of the river to be substituted into the original DEM (Dysarz, 2018; Merwade et al., 2008; Caviedes et al., 2014). In this contribution we provide a simple method to improve the description of the river bathymetry in a DEM, that can be used when the data is properly filtered from vegetation and a set of topographically-surveyed $CS_{sur}$ are available. The method uses the information obtained by a low-flow simulation with a 2D SWE solver.

## 2. The Algorithm

The proposed algorithm for the improvement of a river bathymetry within a raster DEM ($DEM_{ori}$, in the following) requires the use of a GIS software and of a 2D SWE solver along with a set of $n$ rectilinear cross section ($CS_{sur}$ in the following) of the watercourse. The steps that compound the algorithm can be summarized in the following points:

1. In order to identify the subset of cells of $DEM_{ori}$ representing the bed of the river a 2D simulation is performed with a suitably chosen low flow Q, such that the riverbed only is flooded by water. Using the results of this simulation, the shapefile of the outline of the flooded domain ($SHP_{fld}$) is obtained.
2. A set of $n$ cross sections ($CS_{DEM}$) is extracted from $DEM_{ori}$ in correspondence of the available $CS_{sur}$, limiting their transversal extent $l_j$ (where $j$ is the index of the CS) to the outline of the previously identified flooded domain. Then, for each cross section, the average vertical offset $\Delta z_j$ is computed.

3. A fictious channel is built, made up of rectangular cross sections of depth $\Delta z_j$ with the same width $L_j$ and position of the $CS_{sur}$ set. Then, the geometry of the fictitious channel is converted to a raster file, called $DEM_{offset}$.
4. $DEM_{offset}$ is clipped using the polygon $SHP_{fld}$. Then the final corrected DEM ($DEM_{corr}$, in the following) is built as the difference of elevations between $DEM_{ori}$ and the clipped $DEM_{offset}$.

## 3. Application to the Mella river

The Mella river is a pre-alpine Italian watercourse in the province of Brescia, one of the most strongly urbanized areas of northern Italy. This area is covered by a 0.8 m grid LIDAR DEM surveyed in 2009. In our test, a 37 km long stretch of the river was considered. Along the same stretch of the river, 120 CSs were surveyed in 2002, with a lateral extension that typically covers the floodplain for a width 4 times larger than the river bed. The proposed algorithm was applied with a positive result, as shown by the comparison of the cross sections extracted from $DEM_{ori}$ and $DEM_{corr}$ ($CS_{DEM}$ and $CS_{corr}$, respectively) in correspondence of $CS_{sur}$ (see Fig. 1). The geometry of $CS_{corr}$ is very close to the corresponding $CS_{sur}$, leading to stage-conveyance curves that are in very good agreement.

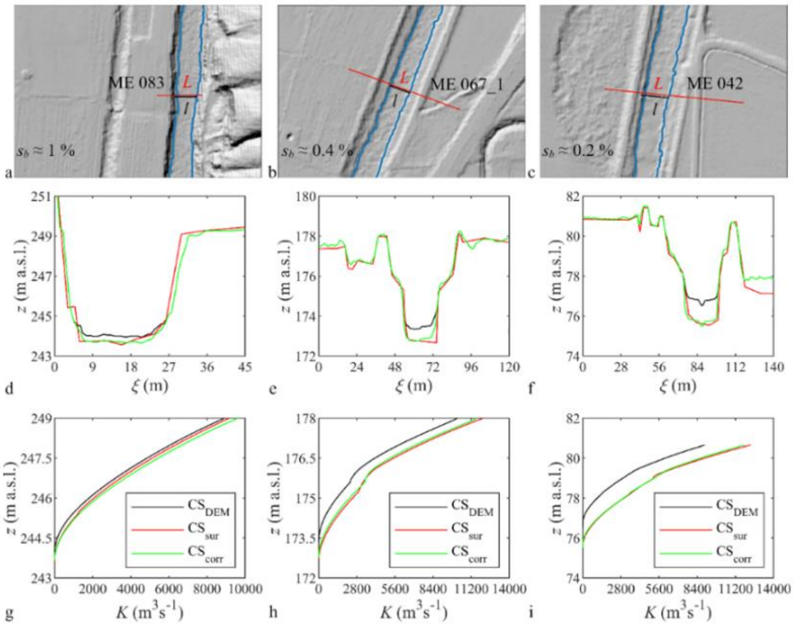


**Fig. 1**. Plan view of CSs ME 083 (a), ME 067_1 (b), and ME 042 (c) from the Mella river test case with indication of the flooded area and of the part of the CS representing the river bed. The CSs geometry extracted from $DEM_{ori}$ and $DEM_{corr}$ and the stage-conveyance curves are compared to the data from $CS_{sur}$ (d, g: CS ME 083; e, f: CS ME 067_1; f, i: CS ME 042).

## 4. Conclusions

The proposed simple methodology relies on the availability of surveyed CSs and of a DEM filtered from vegetation. In particular, the methodology takes advantage of the information obtained by a 2D flood simulation that is also the final goal of the DEM improvement activities. Accordingly, this step is not to be considered as an overburden but as a preliminary activity (to be possibly performed with a simple parabolic model) that anticipates a necessary step of the overall workflow. On the contrary, the 2D simulation gives a physical basis to the methodology and captures automatically the possible river planimetric width variability or the presence of islands between two consecutive $CS_{sur}$, providing a careful reconstruction of the river bed. On the other hand, a 1D reconstruction of the watercourse, based on the interpolation of the $CS_{sur}$ set only, could miss this aspect.

**References**

Bhuyian MNM, Kalyanapu AJ, Nardi F (2015) Approach to digital elevation model correction by improving channel conveyance, J. Hydrol. Eng., 20(5)
Caviedes-Voullième D, Morales-Hernández M, López-Marijuan I, García-Navarro P (2014) Reconstruction of 2D river beds by appropriate interpolation of 1D cross-sectional information for flood simulation, Environ. Modell. Softw., 61 (0), 206-228
Dysarz T (2018) Development of RiverBox - an ArcGIS toolbox for river bathymetry reconstruction, Water, 10(9), 1266
Merwade V, Cook A, Coonrod J (2008) GIS techniques for creating river terrain models for hydrodynamic modeling and flood inundation mapping, Environ. Modell. Softw., 23, 1300–1311
Roub R, Hejduk T, Novák P (2012) Automating the creation of channel cross section data from aerial laser scanning and hydrological surveying for modeling flood events, J. Hydrol. Hydromech., 60(4), 227– 241

# Hydrological modeling in experimental catchment in urban and peri-urban environments

Evgenia Koltsida[1] and Andreas Kallioras[1]

[1] Laboratory of Engineering Geology and Hydrogeology, School of Mining and Metallurgical Engineering, National Technical University of Athens, Athens, Greece
email: ekoltsida@metal.ntua.gr; kallioras@metal.ntua.gr

ABSTRACT

In this study, the SWAT model was used to simulate the hydrological components of an experimental catchment with urban and peri-urban characteristics. Daily and hourly precipitation inputs were used for discharge simulation. Sensitivity analysis, model calibration and validation were performed using the SUFI-2 algorithm in the SWAT-CUP program. Both models showed satisfactory perfromance, however, the daily model outperformed the hourly model (e.g., daily model: $NSE_{calibration} = 0.65$ and $NSE_{validation} = 0.78$; hourly model: $NSE_{calibration} = 0.49$ and $NSE_{validation} = 0.6$). The water balance results indicated that the total water yield of the hourly model was higher than the total water yield of the daily model. Actual evapotranspiration contributed a large amount of water loss from the catchment, about 60% for the daily model and 53% for the hourly model. The simulated hydrological components provide knowledge to understand the catchment characteristics. The satisfactory outcomes of this study suggest that the SWAT model is an appropriate tool to predict water balance components to support future urban development planning and strategies in the region.

## 1. Introduction

SWAT (Soil and Water Assessment Tool) is a physically based, continuous time river basin model which has been developed to predict the influence of management practices on water resources (Arnold et al., 2012). In the SWAT model, the catchment is delineated in sub-basins, which are further divided into hydrologic response units (HRUs) according to elevation, slope, land use and soil attributes (Neitsch et al., 2011). The water balance is simulated separately for every hydrologic response unit (HRU). In this study, the SWAT model was applied to simulate the hydrological components of an experimental catchment with urban and peri-urban characteristics located in Athens, Greece. The main objectives were: to (i) evaluate the performances of the daily and hourly models for discharge simulation; and (ii) investigate the suitability of the SWAT model for the estimation of the major hydrological components.

## 2. Materials and Methods

The experimental study site is a sub-basin (140 km$^2$) of the Kifissos River basin (380 km$^2$) and the elevation ranges from 94 m to 1399 m (south to north). The mean annual rainfall is 643 mm and the mean annual evapotranspiration is 483 mm. The urban areas, shrubland and agriculture account for 34.1, 15.9 and 12.4 % of its land cover, respectively. The input data include a digital elevation model (30 m × 30 m, US Geological Survey, USGS), a land use map (100 m × 100 m, Corine Land Cover, CLC, 2018) a soil map (30 arc seconds, Food and Agriculture Organization, FAO) meteorological data and discharge data.

The study site was delineated into 25 sub-basins and into 175 hydrologic response units. The Penman-Monteith method was used for the estimation of the potential evapotranspiration, the Curve Number (CN) method for the daily model and the Green and Ampt Mein Larson (GAML) method for the hourly model were used for the surface runoff estimation, and the variable storage coefficient method was used to calculate the channel routing. The models were calibrated for 2018 and validated for 2019 for streamflow, with the SUFI-2 algorithm in the SWAT-CUP program (Abbaspour et al., 2007). In SUFI-2 the uncertainties of the parameters are calculated at the 2.5% and 97.5% levels of the cumulative distribution of all output variables, which is referred to as the 95% prediction uncertainty (95PPU).

## 3. Results and Discussion

The daily model showed better performance than the hourly model (e.g., daily model: $NSE_{calibration} = 0.65$ and $NSE_{validation} = 0.78$, hourly model: $NSE_{calibration} = 0.49$ and $NSE_{validation} = 0.6$). Figure 1 presents hydrographs of the two models at the outlet of the study area. The daily model simulated with more accuracy the discharge peaks, although both models captured the patterns, seasonality and the trend of the observed data. According to guidelines ($R^2 > 0.60$, NSE > 0.50, and PBIAS ≤ ±15%) by Moriasi et al. (2015), the models presented satisfactory performance for both calibration and validation periods.

The sensitivity analysis processes showed that the most sensitive parameters for the daily model were connected to groundwater, channel routing and surface runoff, and for the hourly model, they were all related to channel routing. The differences in the sensitivity of the parameters reflect the different surface runoff estimation method used by the two models (Boithias et al., 2017). The mean annual water yield of the hourly model (254 mm) was higher than the mean annueal water yield of the daily model (207 mm) which resulted in a higher total simulated discharge for the hourly model. In addition, the largest amount of water loss from the study area was due to actual evapotranspiration. The mean annual actual evapotranspiration for the daily model was 439 mm (about 60%) and for the hourly model was 389 mm (about 53%). The soil water content and percolation components were estimated at 131 mm and 86 mm for the daily model, and 91 mm and 165 mm for the hourly model, respectively. The different values of the hydrological components of the two models could be attributed to the different calibrated ranges of the parameters controlling the water balance (Jin and Jin, 2020).

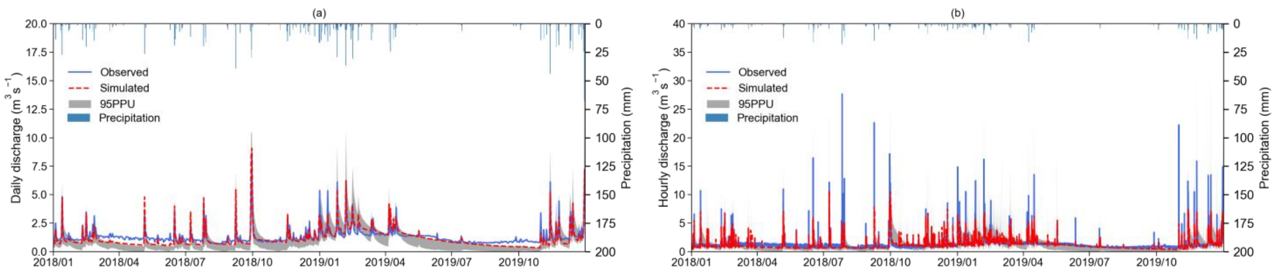


**Fig. 1.** Observed and simulated daily (a) and hourly (b) discharge during calibration and validation periods.

## 4. Conclusions

In this study, the SWAT model was applied for discharge estimation of an experimental catchment using daily and hourly rainfall inputs. The findings of the sensitivity analysis process indicate that the operational time step affects the sensitivities of the parameters to the model outputs and demonstrate the need for different management strategies for the simulation of hourly models. The water balance estimation provided essential knowledge and contributed to the understanding of the earth-surface processes and the mechanisms controlling discharge. The satisfactory performances of the two models suggest that the SWAT model is a reliable and promising tool to predict hydrological components in an urban/peri-urban environment.

**Acknowledgements**

The research work was supported by the Hellenic Foundation for Research and Innovation (HFRI) under the HFRI PhD Fellowship grant (Fellowship Number: 1586).

**References**

Abbaspour, K.C., Yang, J., Maximov, I., Siber, R., Bogner, K., Mieleitner, J., Zobrist, J., Srinivasan, R., 2007. Modelling hydrology and water quality in the pre-alpine/alpine Thur watershed using SWAT. Journal of Hydrology 333, 413–430. https://doi.org/10.1016/j.jhydrol.2006.09.014

Arnold, J.G., Moriasi, D.N., Gassman, P.W., Abbaspour, K.C., White, M.J., Srinivasan, R., Santhi, C., Harmel, R.D., Van Griensven, A., Van Liew, M.W., Kannan, N., Jha, M.K., 2012. SWAT: Model Use, Calibration, and Validation. Transactions of the ASABE 55, 1491–1508. https://doi.org/10.13031/2013.42256

Boithias, L., Sauvage, S., Lenica, A., Roux, H., Abbaspour, K., Larnier, K., Dartus, D., Sánchez-Pérez, J., 2017. Simulating Flash Floods at Hourly Time-Step Using the SWAT Model. Water 9, 929. https://doi.org/10.3390/w9120929

Jin, X., Jin, Y., 2020. Calibration of a Distributed Hydrological Model in a Data-Scarce Basin Based on GLEAM Datasets. Water 12, 897. https://doi.org/10.3390/w12030897

Neitsch, S.L., Arnold, J.G., Kiniry, J.R., Williams, J.R., 2011. Soil & Water Assessment Tool Theoretical Documentation Version 2009, Texas Water Resources Institute. Texas Water Resources Institute Technical Report No. 406, Texas, USA. https://doi.org/10.1016/j.scitotenv.2015.11.063

# Floods of Dinaric karst fields: case studies from Dalmatia (Croatia)

Igor LJUBENKOV[1]

[1] WATER DEVELOPMENT Ltd. Split, Croatia
email: info@waterdevelopment.hr

ABSTRACT

In the area of Dalmatia, southern Croatian region, there are at least 100 karst fields (poljes), whose areas vary from 10 ha to 9,500 ha. Eleven fields have an area of more than 1,000 ha. The largest field in Dalmatia is Imotsko-Bekijsko polje with an area of 9,500 ha, located on the territory of two countries - Croatia and Bosnia and Herzegovina. The fields in the Dinaric karst represent the areas with the most favourable living conditions. Therefore, settlements have been formed along the edges of the fields since ancient times. They are usually elongated in one direction (NW - SE), surrounded by bare and sometimes inaccessible rocky terrain, and covered with fertile soil, so they have a huge social and economic role. Almost all fields in the Dinaric karst are occasionally exposed to flooding in the colder and wetter part of the year (from October to April), although significant water management works have been carried out on some of them so far. This has significantly improved the situation in some fields, by significantly increasing the security of flood protection, reducing damage to agriculture and water management, and in some places significant water reserves for water supply and irrigation. However, Dalmatian fields are still exposed to occasional flooding in winter and drought in summer.

## 1. Karst poljes in Dalmatia

A karst field can be defined as a depression in a carbonate massif, with fertile soil and a relatively slight slope. Numerous hydrological and hydrogeological forms are present in karst fields, such as permanent and occasional springs, permanent and occasional watercourses, ponors, estavelas, etc. with very complex and variable hydrological relations (Bonacci, 1987).

Karst fields exist in many parts of the world, including the Mediterranean countries, among which the largest number of classic karst fields occur in the Dinaric area. The Dinaric karst covers almost half of the territory of the Republic of Croatia, including the whole of Dalmatia, the southern Croatian region. In the Dinaric karst, the fields represent the areas with the most favorable living conditions. In the area of Dalmatia there are at least 100 karst fields with an area of more than 10 ha. Eleven fields are larger than 1000 ha (Table 1). Almost all fields in the Dinaric karst are occasionally exposed to flooding in the colder and wetter part of the year (from October to April), although significant reclamation works have been carried out on some of them so far. The only exception is Sinjsko polje, where the protection against external waters and the drainage system have been completely completed.

Floods cause great material damage, especially in agriculture. Therefore, man has always performed numerous interventions in the fields with the aim of improving the hydrological regime, in order to reduce the spatial coverage and duration of floods. At first, these were some minor interventions, such as increasing the capacity of the ponors, regulation of watercourses, etc. With technological development, interventions and facilities become larger and more complex. From the middle of the 20th century until today, numerous hydro-technical facilities have been built, which has significantly improved the general situation in the Dalmatian karst fields. In terms of flood protection, these are: reservoirs, retentions, tunnels, embankments, channels, etc. In addition, the flood protection program includes works such as: regulation of watercourses as well as cleaning and arranging natural ponors.

## 2. Case studies

Several large hydraulic facilities have been built for flood protection in the Imotsko-Bekijsko polje. The first such facility was the Petnjik tunnel from 1951, which was constructed to drain the southeastern lowest part of the field, with a capacity of 40 $m^3/s$. After that (in 1950s), two retentions of Rastovaca and Prolosko blato for receiving large waters were completed. The works were continued after a long time, so three reservoirs were made in the upper part of the catchment area, in the period from 1989 to 1994, namely: Ricice (Volume V = 35.2 $Mm^3$, year of construction 1989), Tribistovo (V = 5 $Mm^3$, 1990) and IGM (V = 0.13 $Mm^3$, 1994). The construction of major facilities in this water management system ending in 2004 when HEPP Pec Mlini started to work, whose supply tunnel (capacity 30 $m^3/s$) set parallel to the tunnel Petnjik.

Before the construction of the tunnel Petnjik (1951) field was flooded almost every year. Thus, the largest recorded flood before the construction of the tunnel was in winter 1934/35 when the maximum coverage of the flood was 5,333 ha (56% of the field), and the total duration of approximately 6.5 months (Ljubenkov, 2015). In the following period (from 1951 to 1989), after construction the tunnel Petnjik and before construction the Ricice retention, the largest flood recorded in winter 1959/60. The maximum coverage of the floods was 4,097 ha (43% of the field), and total duration was 89 days. In the next period (1989 -2004, after the construction of the reservoir Ricica and before HEPP Pec Mlini) the maximum flood was registered in January 1996, with area of 2,035 ha. In the present conditions, after HEPP construction the largest flood was in January 2010 which included 2,676 hectares (28% of the field), and the corresponding amount of water was 57 $Mm^3$. The duration of the flood, there was only 23 days (Ljubenkov, 2015).

In December 2020 and December 2021 many fields were flooded in Dalmatia. The large floods of the Vrgorsko polje and the Rastok were recorded in December 2020, as well as flooding of many small fields in the middle and south Dalmatia. Dicmanjsko polje near Split was flooded both time in 2020 and 2021. The largest historical flood of Dicmanjsko polje was in December 2021, with a flooded area of about 230 ha (14% of the field).

## 3. Conclusion

Almost all fields in Dalmatia are exposed to occasional floods. Since this is a karst area, it is a very complex process of surface and underground runoff. Many facilities have been built so far, which have increased the level of flood protection in some fields. On the other hand, some fields have remained almost intact so far with natural runoff conditions.

**Table 1.** The largest karst fields in Dalmatia

| Field (polje) | Area (ha) | Elevation (m a.s.l.) |
|---|---|---|
| Imotsko-Bekijsko | 9,500 | 250-270 |
| Sinjsko | 7,290 | 290-295 |
| Vransko | 3,580 | 0-20 |
| Lišansko | 3,510 | 100-150 |
| Petrovo | 3,490 | 250-280 |
| Vrgorsko | 3,010 | 20-28 |
| Kosovo | 2,340 | 220-250 |
| Konavosko | 2,120 | 50-70 |
| Hrvatačko | 2,000 | 300-310 |
| Rastok | 1,700 | 60-70 |
| Dicmanjsko | 1,700 | 310-350 |

**References**

Bonacci O (1987) Karst Hydrology, Springer-Verlag, 184 pp.
Ljubenkov I (2015) Multicriteria flood mitigation in the Imotsko-Bekijsko polje (Croatia, Bosnia and Herzegovina), Journal of water and land development, 26, 73-81.

# Towards a methodical approach for modelling runoff during extreme rainfall events on large catchment using 2D Shallow Water Equations

Jean-Paul TRAVERT[1], Florent TACCONE[1], Vito BACCHI[1]

[1] National Laboratory for Hydraulics and Environment, EDF R&D, France
email: jean-paul.travert@edf.fr
email: florent.taccone@edf.fr
email: vito.bacchi@edf.fr

ABSTRACT

## 1. Introduction

Extreme floods have become more frequent and severe in the recent years exacerbated by climate change. There are numerous recent examples of major floods such as the July 2021 catastrophic flooding events in Germany, Belgium and in China, or the April 2022 floods in South Africa. These extreme events caused human casualties, high economical costs and damages in sensitive areas. To design appropriate mitigation measures, especially with increasing urbanization and decreasing infiltration rates, numerical models are proactive tools widely used.

This study investigates the September 8th and 9th France flooding event in France. During this extreme event, historical records of more than 130 mm of rainfall in two hours were locally measured at Agen, causing exceptional runoff. The main objective of this study is to propose an approach to test the ability of the TELEMAC-2D depth-averaged computation code, (www.opentelemac.org) to simulate runoff on a large catchment with a good accuracy both for discharges and water depths and evaluate the computation cost, necessary for practical applications. A physically based model allows using water depths and spatialized velocities data in the catchment with a better accuracy than the widely spread conceptual rainfall-discharge models. Some rainfall-discharge models using the Shallow Water Equations (SWE) in 2D, using finite volume schemes with hydrostatic reconstruction (Chen et al., 2017) have already been used successfully for extreme events on rather small catchments up to 100 km² (Taccone et al., 2020; Brigode et al., 2021; Yassine et al., 2021), but there is still a need to test and extend the methodology for larger catchment cases.

In this study a global methodology is proposed to model runoff on a large catchment. It will be described the process of cutting the catchment in sub-catchments for implementing a physically based model of this scale.

## 2. Material and method

### *2.1. Description of the study domain*

Agen is located in the South-West of France within a large catchment being rather downstream of the Garonne River. The discharge data are not available at the hydrometric station of Agen, so the outlet of the catchment has been placed downstream of Agen which represents a catchment of 50 558 km². Waterways' discharge and water depths are recorded by hydrometric stations that are freely available on a national database (hydro.eaufrance.fr).

### *2.2. Available data*

One of the main issues is to treat and retrieve the data on such a large scale. For the topography, which is a key parameter when it comes to runoff with SWE, Digital Elevation Map is available at 1 m resolution for France through lidar produced by the National Institute of Geographic and Forest Information (www.ign.fr). Rainfall data can be extracted from radar products by "Météo France" at 1 km resolution every 5 min or from satellites products with the Global Precipitation Measurement Program from the NASA at a resolution of 10 km every 30 min. The land use is extracted from the Corine Land Cover (CLC) 2018 product provided by Copernicus Mission at a resolution of 100 m and the soil hydrological groups from the Food and Agriculture Organization at a resolution of 250 m.

## 3. Preliminary results

The preliminary analysis shows that on rather small catchment of around 1 000 km², a mesh with a resolution of 25 m is needed to obtain the convergence of the discharge at the outlet of the catchment. It could be expected, to have convergence on larger catchment with a coarser mesh because of phenomenon of compensation between the different areas, but it was not the case, thus the use of 25 m resolution mesh at least is needed for larger catchment to model the appropriate discharge at the outlet. For the bottom friction, using Manning-Strickler law is not suited for this type of model because of the resolution of the mesh which is larger than the width of most rivers and the resolution of the CLC map that is not fine enough. Thus, other friction laws such as Lawrence model have been evaluated in this study.

Directly simulating runoff over a catchment of 50 558 km² is not recommended. Indeed, with more than 170 million elements in the mesh, the computational cost is too important even with the use of High-Performance Cluster (HPC) leading to days of simulation with thousands of processors.

Moreover, it has been underlined that for representing with a good accuracy the runoff, the mesh needs to be constraint by the hydrographic network. However, GIS software such as QGIS (www.qgis.org) is unable to extract this network and cannot apply some pretreatments with rasters that have too many cells.

In view of these difficulties, it is proposed to delineate the catchment in smaller sub-catchments as shown on Fig. 1. This methodology allows extracting much more easily the data and the hydrographic network while using less processors, and more importantly calibrating the models by sub-catchments with intermediate hydrometric stations. The simulation can be launched on HPC in parallel from the upstream of the catchment to the downstream by retrieving the discharge at the outlet of the sub-catchments and by placing source discharge boundaries at the inlet of the downstream sub-catchments.

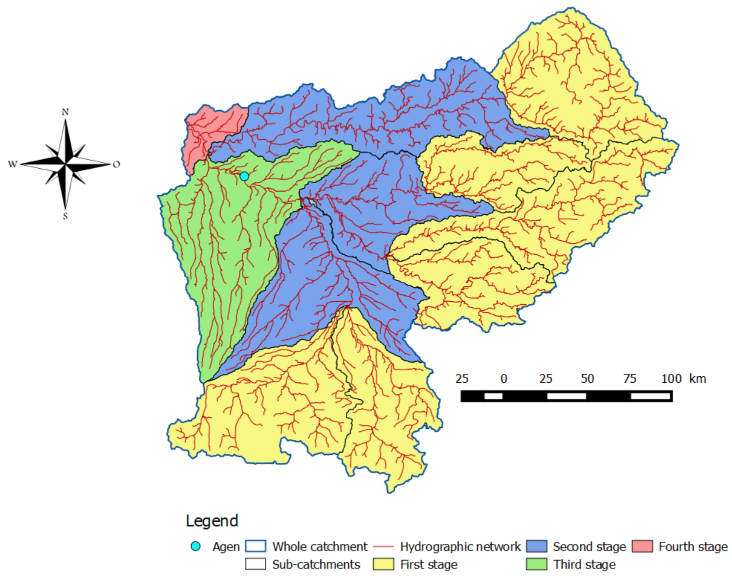


**Fig. 1.** Sub-catchments delineation from whole catchment with different zones to be simulated

## 4. Conclusion

Simulating rain induced runoff on a large catchment scale is source of major problems for preparing the data, calibrating the model and computational cost. However, the approach proposed in this work already enables the practitioner to extract more easily the data on a large catchment and the calibration can be done in parallel on the different sub-catchments without simulating the whole domain directly.

### References

Brigode P, Bourgin F, Yassine R, Delestre O, Lagrée P (2021) Are hydrologic-hydraulic coupling approaches able to reproduce Alex flash-flood dynamics and impacts on southeastern French headwaters?, SimHydro2021

Chen G, Noelle S (2017) A new hydrostatic reconstruction scheme based on subcell reconstructions, SIAM Journal on Numerical Analysis, 55(2), 758-784

Taccone F, Germain A, Delestre O, Goutal N (2020) A new criterion for the evaluation of the velocity field for rainfall-runoff modelling using a shallow-water model, Advances in Water Resources, 140, 103581

Yassine R, Lastes M, Argence A, Gandouin A, Imperatrice C, Michel P, Zhang R, Brigode P, Delestre O, Taccone F (2021) Simulation of the Alex storm flash-flood in the Vésubie catchment (south eastern France) using TELEMAC-2D Hydraulic Code, SymHydro 2021

# A Multi-Criteria Analysis Framework for Assessment of Nature-Based Solutions (NbS)

Ioannis M. KOURTIS[1], Chrysaida-Aliki PAPADOPOULOU[1], Maria P. PAPADOPOULOU[1], Chrysi S. LASPIDOU[2], Vassilios A. TSIHRINTZIS[1]

[1]National Technical University of Athens, [2]University of Thessaly
email: xpap@survey.ntua.gr; gkourtis@mail.ntua.gr; mpapadop@mail.ntua.gr; laspidou@uth.gr; tsihrin@otenet.gr

ABSTRACT

In the present work, a Multi-Criteria Decision Analysis (MCDA) framework is proposed, aiming at the preliminary assessment of different Nature-based Solutions (NbS) for flood risk management. The alternative NbS, i.e., afforestation, basin restoration and creation of intermittently flooding wetlands were assessed on the basis of five evaluation criteria, including: flood mitigation, economic, social and environmental benefits as well as associated benefits offered by ecosystem services. Criteria weights were calculated by employing the Analytical Hierarchy Process (AHP) method. In addition, a ranking system was introduced for assessing the impacts of different alternatives. The suggested assessment approach was tested in a small sub-basin of the transboundary Nestos river, shared by Greece and Bulgaria. Results revealed that the most efficient alternative is afforestation. Moreover, it can be noted that the approach adopted in this analysis may effectively support pre-feasibility studies supporting the holistic assessment of different NbS for flood risk management.

## 1. Introduction

In recent years, it has become clear that flood mitigation via conventional techniques (e.g., dikes) are not able to fully protect people assets and lives, existing infrastructure and different sectors (e.g., agriculture) against different types of floods (e.g., fluvial, flash, coastal etc.), although they still have an important role to play (Kourtis et al. 2020). Despite being a relatively new concept as flood mitigation measures, Nature-based Solutions (NbS) such as wetlands, forests and flood plains, have come to the fore as they can complement and/or act as a sustainable alternative of conventional flood mitigation measures. NbS can have a wide range of effects mainly associated with flood risk mitigation, enhancement of water security, and resilience to climate change in a sustainable way (Kourtis et al. 2021). Moreover, NbS can deliver a variety of co-benefits through the enhancement of ecosystems and the related ecosystem services. As a result, they are globally acknowledged as one of the key tools to deliver on climate change adaptation and mitigation objectives.

The aim of the present work is to provide a simplified and reliable framework for the assessment of different NbS (scenarios) for flood risk mitigation, based on Multi-Criteria Decision Analysis (MCDA) and a proposed ranking system (Table 1). The first scenario is associated with a business-as-usual (BAU) approach where no flood mitigation scenarios are taken into consideration. Three different NbS are also assessed, namely afforestation (Scenario 2; creating a forest via plantation of trees), basin restoration (Scenario 3; infiltration improvement via engineering techniques), and seasonal wetland (Scenario 4; temporary storage of flood excess volumes). All examined scenarios are ranked based on five evaluation criteria. The proposed assessment approach was tested in a small sub-basin of the transboundary Nestos river basin shared by Greece and Bulgaria.

## 2. Materials and methods

The methodology proposed herein constitutes a simplified methodology for assessing the effects of NbS on mitigating flood risk, taking into account the associated benefits and co-benefits (i.e., ecosystem services) offered by those solutions. Fig. 1 presents the proposed methodological framework. The first step is associated with the determination of the type of hazard to be alleviated. In our case, floods have been indicated by local stakeholders (decision makers at local scale, Civil Protection representatives, farmer associations, etc.) as the most important hazard in the study area during a workshop that took place in the Municipality of Nestos. The second step is associated with the identification of the most appropriate NbS. In the third step, the sustainable flood mitigation alternatives are screened based on their effectiveness with respect to addressing local needs.

Finally, all scenarios are assessed on the basis of five criteria: (i) flood mitigation; (ii) economic benefits; (iii) social benefits; (iv) environmental benefits; and (v) ecosystem services benefits.


**Fig. 1.** Methodological steps of the proposed framework

The AHP method (Saaty 1987) was used for assigning weights in the five criteria, while the ranking of the alternative NbS was estimated by applying the Weighted Summation MCDA (WS-MCDA) method. The proposed ranking system is presented in Table 1. Values on the different criteria for the different scenarios (effects of each alternative on each criterion) were assigned based on engineering judgment.

**Table 1.** Proposed ranking system

| Index | Description | Index | Description |
|---|---|---|---|
| 5 | Very high positive impact | -5 | Very high negative impact |
| 4 | High positive impact | -1 | Negligible negative impact |
| 3 | Moderate positive impact | -2 | Low negative impact |
| 2 | Low positive impact | -3 | Moderate negative impact |
| 1 | Negligible positive impact | -4 | High negative impact |
| 0 | No positive or negative impact | 0 | No positive or negative impact |

## 3. Results and concluding remarks

The weights of evaluation criteria were elicited by employing the AHP and calculated equal to: 0.396, 0.099, 0.072, 0.207 and 0.226, for criteria (i) to (v), respectively. The results of MCDA regarding the four NbS flood mitigation scenarios analyzed herein are in accordance with previous works (e.g., Ferreira et al. 2020). Table 2 presents the results of the proposed assessment approach. Overall, the most effective strategy for mitigating flood risk, taking into account the associated co-benefits was found to be Scenario 2 (i.e., afforestation). The respective classification of the NbS, based on the proposed approach was: Scenario 1 > Scenario 3 > Scenario 4 > Scenario 2. Such kind of classification can support a preliminary selection of different alternatives for the design of NbS for alleviating flood risk.

**Table 2.** Weighted Summation Effects Table - Ranking of NbS

| Criteria | Weights AHP method | Scenario 1 BAU | Scenario 2 Afforestation | Scenario 3 Basin restoration | Scenario 4 Seasonal wetland |
|---|---|---|---|---|---|
| (i) Flood mitigation | 0.396 | -3 | 2 | 3 | 3 |
| (ii) Economic benefits | 0.099 | -2 | -1 | -3 | -2 |
| (iii) Social benefits | 0.072 | -5 | 3 | 1 | -2 |
| (iv) Environmental benefits | 0.207 | -1 | 3 | 1 | 3 |
| (v) Ecosystem services | 0.226 | -1 | 4 | 1 | 4 |
| Final Score | - | 0.05 | 0.93 | 0.61 | 0.91 |

*The final score was calculated employing the Weighted Summation MCDA (WS-MCDA) approach

**Acknowledgments**

Part of the work described in this paper has been conducted within the project NEXOGENESIS. This project has received funding from the European Union's Horizon 2020 research and innovation programme under Grant Agreement No. 101003881.

**References**

Ferreira CSS, Mourato S, Kasanin-Grubin M, Ferreira AJD, Destouni, G, Kalantari Z (2020) Effectiveness of nature-based solutions in mitigating flood hazard in a Mediterranean peri-urban catchment, Water, 12(10), 2893.
Kourtis IM, Tsihrintzis VA, Baltas E (2020) A robust approach for comparing conventional and sustainable flood mitigation measures in urban basins, Journal of Environmental Management, 269, 110822.
Kourtis IM, Bellos V, Kopsiaftis G, Psiloglou B, Tsihrintzis VA (2021). Methodology for holistic assessment of grey-green flood mitigation measures for climate change adaptation in urban basins, Journal of Hydrology, 603, 126885.
Saaty RW (1987) The analytic hierarchy process-what it is and how it is used. Mathematical Modelling, 9(3-5), 161-176.

# Influence of urban pattern on rainfall-runoff processes

Dongfang LIANG[1], Zhiwei HE[1], Bowen CHE[1], Nichenggong ZHU[1], Yiming LI[1], Yuhao CEN[1]

[1] Department of Engineering, University of Cambridge, UK
email: dl359@cam.ac.uk, zh278@cam.ac.uk, bc540@cam.ac.uk, nz284@cam.ac.uk, yl842@cam.ac.uk, yc515@cam.ac.uk

ABSTRACT

Real urban environments are highly complex, and it is likely that there are numerous parameters that influence the rainfall-runoff processes, *e.g*. urban characteristics such as road width, orientation and building coverage. The main objective of this study is to perform a parametric study on rainfall-runoff processes in urban environments, in order to gain a better understanding of the impact urban pattern geometry has on the flow of surface runoff. A shock-capturing shallow water equations solver is used to undertake a large number of computational simulations to unveil the dominating urban parameters that influence flooding in urban systems. A sensitivity analysis is performed on the simulation results to quantify the influence of each parameter. The outcome of this research provides useful guidelines for the design of future flood-resilient urban environments and the improvement of existing drainage systems in cities.

## 1. Urban pattern representation

Bruwier et al. (2017) are among the first to perform a parametric study on realistic urban configurations. Using an anisotropic porous model, they investigated the influence of several urban pattern characteristics on inundation depths along the upstream boundaries. A steady inflow of water was prescribed at the inlet of the catchment, representing a flood front. Bruwier's research group examined hydraulic computations on 2,290 urban configurations, which were generated by means of a self-developed urban generator tool, based on the procedural modelling technique. This was followed by a parametrised study using 11 urban parameters controlling the building geometries and locations. Each of the parameters was randomly selected from a range of variation, representative of real-world information of built environments. Directly contacting the author of the paper and signing a written agreement enabled direct access to all of the 2,290 urban configurations, developed at Purdue University by the team of Prof. Daniel G. Aliaga.

The urban layouts, consisting of irregular arrays of buildings, are provided in a shapefile format, comprising of polygons, polylines and points defining each grid point in the domain. In order to enable their use for this study, the methodology shown in Fig. 1 has been followed.

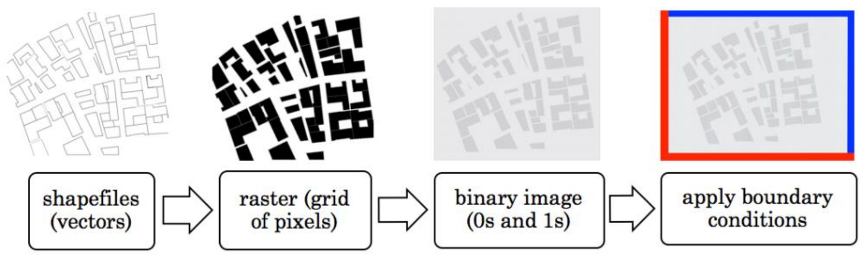


**Fig. 1.** Methodology of converting urban pattern shape files to computational domain description files.

Firstly, the shapefiles are converted into raster format, comprising of pixels. This is achieved through a workflow generated using FME, a data processing software. This enables batch conversion of the shapefiles and the ability to specify the desired resolution and attributes of the resulting image.

## 2. Overland flow solver

The two-dimensional non-linear Shallow Water Equations (SWEs) make use of a depth-averaged dynamic wave approximation, which is particularly suitable for predicting rainfall-runoff in urban environments. The general form of the SWEs can be described using the three equations, describing the principles of mass conservation and momentum conservation in the horizontal directions. A Total Variation Diminishing (TVD) MacCormack finite difference numerical scheme is applied to solve the SWEs at a high accuracy and efficiency, which has been extensively validated against published experimental and analytical results. Detailed implementation of the numerical scheme and details of the numerous validation tests can be found in Liang et al. (2006).

In order to represent buildings in the simulations, the building-hole (BH) method is used, where the grid cells representing buildings are excluded from the computation. The rainfall intensity over the whole domain is increased to compensate for the ‘loss’ of rainfall falling over these ‘holes’.

## 3. Results

Uniform rainfall intensity is applied over the entire computational domain, and the hydrograph, *i.e*. S-curve, at the end of the catchment is calculated from the numerical simulation results. The dimensionless S-curve is constructed using the following normalised flow rate $Q^*$and normalised time $t^*$, as detailed in Liang *et al*. (2015).

$$Q^* = \frac{Q}{A \times i} \tag{1}$$

$$t^* = \frac{t \times \sqrt{S \times g}}{A^{0.25}} \tag{2}$$

where $Q$ is the flow rate, $A$ is the domain area, $i$ is the rainfall intensity, $t$ is time, $S$ is the domain slope and $g$ is gravitational acceleration. According to the S-curve, the time of concentration can be obtained, which is an important parameter to quantify the speed of the rainwater accumulation at the end of the catchment. Estimation of the full time of concentration is prone to large errors and is not desired. In this study, the time to reach 70% of the dimensionless equilibrium flow rate, $t^{*70}$, is used to characterise the rainfall-runoff response.

The final stage of the project involved carrying out a sensitivity analysis to identify the influence of various urban parameters on rainfall-runoff processes. The sensitivity of $t^{*70}$ to a number of urban characteristics is then quantified using a multiple linear regression (MLR), allowing the identification of the most influential urban parameters. The coefficients $\beta_i$ characterises the sensitivity of the non-dimensional time of concentration to each one of the 12 non-dimensional urban characteristics. Table 1 shows that the most influential parameter is roughness, followed by building coverage.

**Table 1.** MLR coefficients for 12 urban pattern parameters

| Order | Parameter | $\beta_i$ |
|---|---|---|
| P1 | Street length | 0.0623 |
| P2 | Street orientation | 0.0127 |
| P3 | Street curvature | 0.0123 |
| P4 | Street width (major) | -0.0064 |
| P5 | Street width (minor) | -0.0029 |
| P6 | Park coverage | -0.0111 |
| P7 | Parcel area | -0.0471 |
| P8 | Front setback | -0.0117 |
| P9 | Rear setback | 0.0165 |
| P10 | Side setback | -0.0427 |
| P11 | Building coverage | 0.3160 |
| P12 | Roughness *n* | 0.9346 |

**Acknowledgements**

This work was funded by EPSRC grant numbers EP/I019308/1, EP/K000314/1, EP/L010917/1 and EP/N021614/1. For the purpose of open access, the authors have applied a Creative Commons Attribution (CC BY) license to any Author Accepted Manuscript version arising. The underlying data can be accessed by emailing the authors.

**References**

Bruwier M, Mustafa A, Aliaga D, Erpicum S, Archambeau P, Nishida G, Zhang X, Pirotton M, Teller J, Dewals, B (2017). Influence of urban patterns on flooding. Proceedings of the 37th IAHR World Congress, 2039-2047
Liang D, Lin B, Falconer R (2007). Simulation of rapidly varying flow using an efficient TVD–MacCormack scheme, International Journal for Numerical Methods in Fluids, 53, 811-826
Liang D, Özgen I, Hinkelmann R, Xiao Y, Chen JM (2015). Shallow water simulation of overland flows in idealised catchments, Environmental Earth Sciences, 74(11), 7307-7318

# Traditional Nature-based Solutions for rural drought resilience in the Cuvelai basin, Angola. How surface water monitoring can support better decision-making and management.

Natalia LIMONES[1], Marcus WIJNEN[2], Aleix SERRAT-CAPDEVILA[3]

[1] University of Seville, Spain
email: natalialr@us.es
[2] Independent Consultant, the Netherlands
email: mwijnen@verizon.net
[3] The World Bank, Angola
email: aserratcapdevila@worldbank.org

ABSTRACT

The Angolan part of the Cuvelai basin is suffering a severe drought from 2013 to the time of writing of this document (2022), which has also affected the remaining part of the basin in Namibia (Liu et al., 2021) and the rest of the South of Angola (Limones et al, 2020). Throughout these years, some episodes of abundant rain brought some occasional relief, but were not enough to initiate a recovery. In March 2022, the SPEI global drought monitor (https://spei.csic.es/map/) marked the southern half of Angola, with the upper Cuvelai basin as its core, as the current major hotspot of extreme long-term drought (SPEI48 drought index < -4) in the world, with some states of the center of Brazil and the western half of South Africa.

Recent research reveals that climate change has already modified rainfall intra-annual and inter-annual variability and seasonality, and has increased the frequency of droughts in the region (Limones et al, 2020; Makondo and Thomas, 2020).

According to the Angola Drought Post Disaster Needs Assessment (PDNA) prepared by the United Nations Development Programme Post-Disaster (UNDP) in 2017, the Cunene province- containing the Cuvelai upper basin- was the most impacted one in the country by then. Subsequent analyses by the World Bank confirm that the situation has only worsened afterwards in the area (Serrat-Capdevila et al., 2022). The livelihoods of the growing population of the Cuvelai rely increasingly on cattle herding and subsistence agriculture (Mendelsohn et al. 2013), which were the most affected sectors (Angola PDNA, 2017).

This study focuses on a part of the Angolan southern province of Cunene: the chanas (also called oshana, or ishanas) drainage area at the western section of the Cuvelai river basin, in the border with Namibia (see Figure 1).

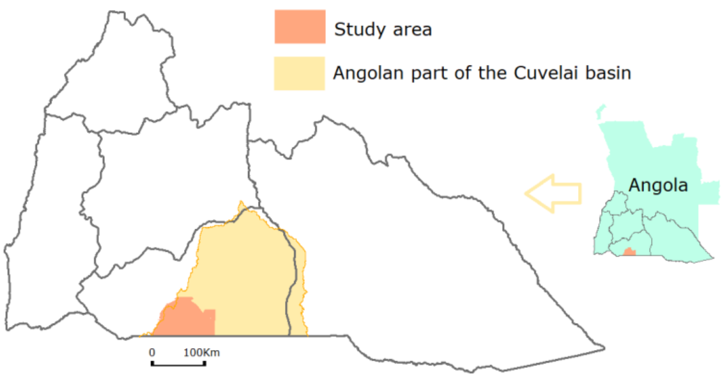


**Figure 1.** Study area in the context of the southern Angolan provinces and the Cuvelai Basin

The chanas drainage area is an unusual hydrological feature that continues in Namibia, as a network of hundreds of shallow, braided, non-permanent channels of variable width that drain a very flat area from the north to the south. The soils in the chanas get saturated in the wet season and some flow is generated almost every year, especially in the western channels, experiencing occasional flooding too (Mendelsohn et al. 2013). In fact, rains in the region are variable and unpredictable, and exceptionally high and low flows alternate.

Despite of the absence of secure and safe water points, this is also the most populated part of the basin in Angola, as the central and east drainage areas of the Cuvelai are almost uninhabited (according to the WorldPop Open Population Repository datasets). Livestock water supply relies almost entirely on the harvesting of surface water in "*chimpacas*", tanks constructed in the downstream parts of the chanas by excavating the clayey infill of the channels over a depth of a few meters, till the top of the limestone substratum (Serrat-Capdevila et al., 2022). This is the building-with-nature approach that the Cuvelai inhabitants adopt to store the seasonal abundance of surface water.

These straightforward infrastructures, when well designed and maintained, can last for the entire year. In some cases, they contain water also in dry years although, in general, this solution does not provide adequate water security in the variable climatic conditions of the Cuvelai region and its use should be limited to livestock, as a complement to other safe drinking supply options.

Apart from very limited exceptions, the local population and members of administration do not keep systematic track-record of when each *chimpaca* was constructed, when it has been operational, when it filled- up with water and when it dried or experienced another issue.

## 1. Rationale, objectives and approach

This study has several thematic and methodological objectives, and it is meant to support the current efforts to create water and food security in the Cuvelai basin.

First, it aims to test the ability of a remote sensing product, the European Commission's Joint Research Centre Global Surface Water Explorer (GSWE) monthly water history, to reveal the historical dynamics of *chimpaca* surface water presence. GSWE is a Landsat-based product that maps the location and temporal distribution of water surfaces at the global scale and monthly time step from 1985 (https://global-surface-water.appspot.com). The *chimpacas* are detected with GSWE because it has pixels of 30 meters and these pans are typically at least double in length and width. The study discusses the possibility of the establishment of remotely- sensed monitoring of water shortage in these infrastructures, incorporating additional imagery products, and of performing short-term prediction of their status using other hydrological indicators connected to its functioning.

Also, the study analyzed closely the 2013- 2020 hydrological drought in the area, measuring the resistance of the surface water presence in the *chimpacas* during this period too, in order to consider their capacity to provide drought resilience to the transhumant communities of the Cuvelai. Additionally, the authors reflect on the feedback received from the community and the government about the local operation, ownership, conflics, issues and maintenance habits of these Nature-based infrastructures, and on the aspects to be considered in *chimpaca* design or rehabilitation to avoid creating negative incentives or deepening water insecurity and vulnerability. It is discussed how this work can inform and support investments and interventions in governance, in planning new water harvesting structures optimally, or in rehabilitation of the pans that did not perform efficiently, following the example of those that did because are regularly desilted or have not filled up with sediments.

**Acknowledgements**

The study here presented was funded as part of an Advisory Services and Analytics activity by the World Bank Water Global Practice and the Korean Green Growth Trust-fund, aimed at prioritizing water resources mobilization responses to the drought in the south of Angola.

**References**

Limones, Marzo-Artigas, Wijnen, Serrat-Capdevila (2020) Evaluating drought risk in data-scarce contexts. The case of southern Angola, Journal of Water and Climate Change, 11 (S1).
Liu, Xuan, and Jie Zhou (2021) Assessment of the Continuous Extreme Drought Events in Namibia during the Last Decade, Water 13, no. 20: 2942.
Makondo, C.C., Thomas, D.S.G (2020) Seasonal and intra-seasonal rainfall and drought characteristics as indicators of climate change and variability in Southern Africa: a focus on Kabwe and Livingstone in Zambia, Theor Appl Climatol 140, 271–284.
Mendelsohn, J.; Jarvis, A.; Robertson, T. A (2013) Profile and Atlas of the Cuvelai-Etosha Basin; Research and Information Services of Namibia (RAISON) & Gondwana Collection: Windhoek, Namibia.
Serrat-Capdevila, A., Limones, N., Marzo-Artigas, J., Marcus, W., & Petrucci, B. (2022) Water Security and Drought Resilience in the South of Angola. World Bank Publications.

# Rainfall intensity-duration patterns for flood occurrence in Attica region

Elissavet FELONI[1], Evangelos BALTAS[1], Kostas LAGOUVARDOS[2], Anastasios STAMOU[1]

School of Civil Engineering, National Technical University of Athens, Iroon Polytechniou 5, 15780 Athens, Greece
National Observatory of Athens, Institute for Environmental Research and Sustainable Development, P. Penteli, Greece
emails: feloni@chi.civil.ntua.gr; baltas@chi.civil.ntua.gr; lagouvar@meteo.noa.gr; stamou@central.ntua.gr

ABSTRACT

Attica region suffers from heavy rainfall that triggers flood events causing significant damages, mainly in the urbanized areas. This analysis presents indicative thresholds regarding maximum rainfall intensity (I)-duration (D), which separate events in three categories: (i) events that are not associated with floods and usually correspond to low intensities, (ii) events that are linked to the highest intensities and thus with flood occurrence, and (iii) events experience a range of intensities that correspond to mixed conditions concerning flood occurrence. The analysis is performed using the available precipitation records from 14 stations located in the Attica region (Central Greece) for the period 2005-2016. A dataset regarding Fire Service operations in flooded properties in the area during the same period is also used in order to classify each event as flood-related or not, in case flooded properties recorded or not, respectively. The I-D thresholds are expressed using power low equations that describe two limits: the first one ('lower limit') defines the area below which floods are absent and above which flood occur or not, while the second ('upper limit') defines the minimum limit of maximum intensities above which only events linked to flooding are observed. The corresponding equations are determined per station with the aim to cover a significant part of t region, however the reliability of the estimated thresholds is affected by the spatial distribution and the varying length of records.

## 1. Introduction

The intensity - duration (I-D) threshold is a typical meteorological-threshold approach that initially adopted for rainfall events induced landslides and debris flow, especially in areas that suffer from wildfires and deep erosion. Indicatively, Guzzetti et al. (2007) determine I-D thresholds for the initiation of landslides in the CADSES, central and southern Europe, while Cannon et al. (2008) present thresholds for debris flows and floods occurrence in southern California. Regarding floods, research interest focuses on the determination of the conditions that increase the possibility of flood occurrence and on their continuous monitoring for issuing warnings. In many areas where networks of sensors continuously record the characteristics of storms, local thresholds have been determined and serve as flash-flood guidance, in the frame of flood early warning systems operation, based on the concept of comparing the rainfall features with recordings of storms that caused flooding in the past, as a rational way to predict flooding (e.g., Amadio et al., 2003; Bracken et al., 2008; Norbiato et al., 2008; Golian et al., 2010) and they mainly examine rainfall intensities in two groups; events related and not related to floods. In Greece, Papagiannaki et al. (2015) estimated rain thresholds related to flood triggering after taking into account flash flood events in Attica region between 2005 and 2014, while the study of Georganta et al. (2022) provides updated thresholds for the same region.

## 2. Methodology

The I-D curves are estimated for 14 stations located in the entire Attica region, using the available 10-min rainfall measurements for the period 2005-2016. Maximum rainfall intensities for various durations are calculated per event, while each event is classified as 'flood-related' or 'not flood-related', based on the entire database of citizens' calls for water pumping to the Integrated Emergency Coordination Centre of the Hellenic Fire Service within the same period. Critical thresholds are introduced in the entire analysis, both for the minimum rainfall inter-event time to separate rainfall events and for the minimum number of emergency calls per day above which we assume the occurrence of flood, as described in detail by Georganta et al. (2022). The final step of the determination of power law equation parameters per station was accomplished by applying optimization techniques.

## 3. Results and Discussion

Two power law equations are determined per station (Table 1), which correspond to the two thresholds; the lower limit, below which only events not inducing floods are observed, and the upper limit, above which only events inducing floods are observed. The area between these two thresholds denotes I-D values that correspond to mixed conditions; i.e., either flood occurrence or not.

**Table 1.** Values of I-D curves' parameters per station

| Station | m.a.s.l. | Station Network | Lower limit | | Upper limit | |
|---|---|---|---|---|---|---|
| | | | *a* | *b* | *a* | *b* |
| Lavrio | 3 | NOANN (METEO.GR) | 5.13 | -0.65 | 16.39 | -0.60 |
| Markopoulo | 104 | NOANN (METEO.GR) | 5.44 | -0.66 | 19.33 | -0.64 |
| Nea Smyrni | 51 | NOANN (METEO.GR) | 5.63 | -0.70 | 19.37 | -0.64 |
| Pikermi | 133 | HOA (METEONET) | 6.10 | -0.72 | 20.35 | -0.65 |
| Menidi | 210 | HOA (METEONET) | 5.39 | -0.67 | 27.56 | -0.66 |
| Ano Liosia | 184 | HOA (METEONET) | 5.17 | -0.65 | 22.24 | -0.73 |
| Galatsi | 176 | HOA (METEONET) | 5.44 | -0.68 | 18.71 | -0.66 |
| Penteli | 729 | HOA (METEONET) | 6.71 | -0.76 | 20.81 | -0.66 |
| Zografou | 181 | HOA (METEONET) | 5.68 | -0.70 | 23.08 | -0.68 |
| Ilioupoli | 206 | HOA (METEONET) | 5.66 | -0.68 | 22.48 | -0.60 |
| Glyfada | 185 | HOA (METEONET) | 5.82 | -0.69 | 22.33 | -0.64 |
| Agios Kosmas | 6 | HOA (METEONET) | 5.49 | -0.68 | 25.17 | -0.72 |
| Psyttalia | 20 | HOA (METEONET) | 5.53 | -0.68 | 18.45 | -0.64 |
| Mandra | 258 | HOA (METEONET) | 6.61 | -0.56 | 21.25 | -0.58 |

The analysis revealed that the values of these thresholds significantly differ among the 14 stations, especially regarding constant, *a*. The highest coefficient of variation of parameter *a* is observed among stations located in Athens basin and especially concerning the upper limit. For Athens basin and East Attica, the average *b* (law's exponent) ranges between -0.6 and -0.7 for both limits, with a low standard deviation; lower than 0.04 in both cases. In Mandra station (West Attica) *b* is equal to -0.56 and -0.58 for the lower and upper limit, respectively. Indicatively, the average 1-h maximum rainfall intensity for flood occurrence is defined at 22.0 mm/h, 18.7 mm/h and 21.25 mm/h for Athens basin, East and West Attica, respectively, however in the western part only one available station is taken into consideration.

The I-D patterns described in this section resulted from fitting power law distributions to the I-D pairs. Comparing the values with similar thresholds presented in previous relevant research for the study area, we observe variations, mainly due to the different approached performed. For instance, the critical thresholds that adopted for events separation and classification are decisive for the determination of particular I-D pairs, on which the two limits are defined. Station network density, availability of rainfall measurements and historical evidence to detect floods are among factors controlling uncertainties of this analysis and this fact should be taken into account, especially when the establishment of alert systems to warn communities of impending floods is based on similar approaches.

### References

Guzzetti F, Peruccacci S, Rossi M, Stark CP (2007) Rainfall thresholds for the initiation of landslides in central and southern Europe, Meteorology and atmospheric physics, 98(3), 239-267.
Cannon SH, Gartner JE, Wilson RC, Bowers JC, Laber JL (2008) Storm rainfall conditions for floods and debris flows from recently burned areas in southwestern Colorado and southern California, Geomorphology, 96(3-4), 250-269.
Amadio P, Mancini M, Menduni G, Rabuffetti D, Ravazzani G (2003) A real-time flood forecasting system based on rainfall thresholds working on the Arno Watershed: definition and reliability analysis, In Proceedings of the 5th EGS Plinius Conference, Corsica, France.
Golian S, Saghafian B, Maknoon R (2010) Derivation of probabilistic thresholds of spatially distributed rainfall for flood forecasting, Water Resources Management, 24(13), 3547-3559.
Norbiato D, Borga M, Degli Esposti S, Gaume E, Anquetin S (2008) Flash flood warning based on rainfall thresholds and soil moisture conditions: An assessment for gauged and ungauged basins, Journal of Hydrology, 362(3-4), 274-290.
Bracken LJ, Cox NJ, Shannon J (2008) The relationship between rainfall inputs and flood generation in south–east Spain, Hydrological Processes: An International Journal, 22(5), 683-696.
Papagiannaki K, Lagouvardos K, Kotroni V, Bezes A, (2015) Flash flood occurrence and relation to the rainfall hazard in a highly urbanized area, Natural Hazards and Earth System Sciences, 15(8), 1859-1871.
Georganta C, Feloni E, Nastos P, Baltas E (2022) Critical Rainfall Thresholds as a Tool for Urban Flood Identification in Attica Region, Greece, Atmosphere, 13(5):698.

# Implementation of the Gridded Flash Flood Guidance Method in the Mandra Basin in west Attica, Greece

Apollon BOURNAS[1], Evangelos BALTAS[1], Anastasios STAMOU[1]

[1] Department of Water Resources and Environmental Engineering, School of Civil Engineering, National Technical University of Athens, 5 Iroon Polytechniou, 157 80, Athens, Greece
email: abournas@chi.civil.ntua.gr
email: baltas@chi.civil.ntua.gr
email: stamou@central.ntua.gr

ABSTRACT

The implementation of a Flash Flood Forecasting system (FFFs) is considered the first and most cost-effective way to mitigate the social-economic impacts of flooding. The Flash Flood Guidance system (FFGs) is a well-established FFFs, developed in the U.S., but currently applied in multiple regions across the globe. The heart of the system is the derivation of the Flash Flood Guidance (FFG), defined as the rainfall threshold above which minor flooding is expected over a specified region. The FFG is a function of the threshold runoff, i.e. the maximum runoff which can be safely routed through the studied region, and the soil moisture conditions. In this research work, the derivation of the FFG values for predefined soil moisture conditions is performed, for the Mandra subbasin, located within the western part of Attica region in Greece. A methodology is applied for deriving the threshold runoff, and establishing the rainfall-runoff model based on the Unit Hydrograph theory and the Soil Conservation Service, Curve Number method to perform the needed FFG computations. The result is the generation of threshold rainfall maps, for a predetermined accumulation period and different soil moisture conditions, which highlight the flood prone areas, as well as, showcasing the impact of soil moisture conditions in flood generation.

## 1. Introduction

Flash floods have gained increased attention over the years, since not only they are among the deadliest weather-related hazards worldwide, but they have been associated with the effects of climate change and therefore new policy measures are sought after. In Greece, a large number of areas have suffered from flash flooding, with the 15th of November 2017 event in Mandra being the most recent devastating event, with huge social-economic impacts and the cost of human lives. A contributing factor, apart from the unplanned urbanization of the area, was the near non-existent flood warnings which could have assisted into targeted decision making and mitigation measures. In this research work, we assess the use of the Flash Flood Guidance system (FFGs) (Georgakakos 2006), and specifically the Gridded FFGs (Schmidt et al. 2007; Bournas and Baltas 2022). The FFGs is a rainfall-based warning system which incorporates the three key elements of flash flood generation, a) the rainfall forecast input, b) the basin geomorphological characteristics and c) the soil moisture conditions, in order to trigger flash flood warnings. While the system is easy to comprehend, its implementation in a data scarce area is a challenging task and increased attention should be taken (Georgakakos et al. 2022).

## 2. Methods and data used

The FFG system is based upon the comparison of forecasted rainfall of pre-defined accumulation period with the calculated Flash Flood Guidance (FFG) of the same period, defined as the rainfall threshold above which minor flooding is expected over a specified region. The methodology applied consists of, a) the delineation of the study area in smaller subunits, e.g. grids, b) the derivation the runoff threshold of each subunit i.e. the maximum runoff which can be safely routed, and c) the derivation of the FFG values by performing inverse engineering and computing the needed rainfall value that will cause the threshold runoff, under specified soil moisture conditions. In this implementation, we use the gridded FFG methodology, where the calculations are performed in 500m x 500m grids. The runoff threshold is calculated through rainfall-runoff modelling using a design storm of a five-year rainfall return period. The FFG computations are then performed using a rainfall-runoff model based on Unit Hydrograph theory where the parameters are estimated through the geomorphological characteristics of the basin, e.g. grid slope and area. Finally, the soil moisture conditions are incorporated with the use of an adjustment factor of the Soil Conservation Service Curve Number (SCS-CN) method, and specifically by utilizing the Antecedent Moisture Conditions (AMC) -I -II and -III values of each grid. The study area is the greater Mandra area, which is consisted of two main subbasins, the Ag. Aikaterini and Soures subbasins, as well as the urban part of the Mandra city.

## 3. Results

The methodology applied and the results generated can be summed up in Figures 1 and 2. In Figure 1, the main parameters of the rainfall-runoff model applied are presented, the SCS-CN AMC-II, and the mean slope of each grid. In Figure 2, the FFG values are presented for a 3-hour accumulation rainfall period and for three predefined soil moisture conditions, defined from the use of the CN AMC-I, -II and -III, values which are referred to dry, half saturated and completely wet conditions. It is evident that when wet conditions are met, the FFG values are much lower, which indicate that it is much easier to flood. The mean value in the AMC-I and AMC-II conditions is 75 mm and 38 mm, respectively, while for the AMC III the FFG is low at only 20mm. Finally, another interesting factor is the identification of grids which are more prominent to flood, highlighted by the small FFG values, which are located on the bottom left of each figure, mainly where the urban part of basin is found, that features high CN values and low slopes. The method, also produces a good estimate of flood risk, where the areas with small FFG values can be identified as high flood risk areas.

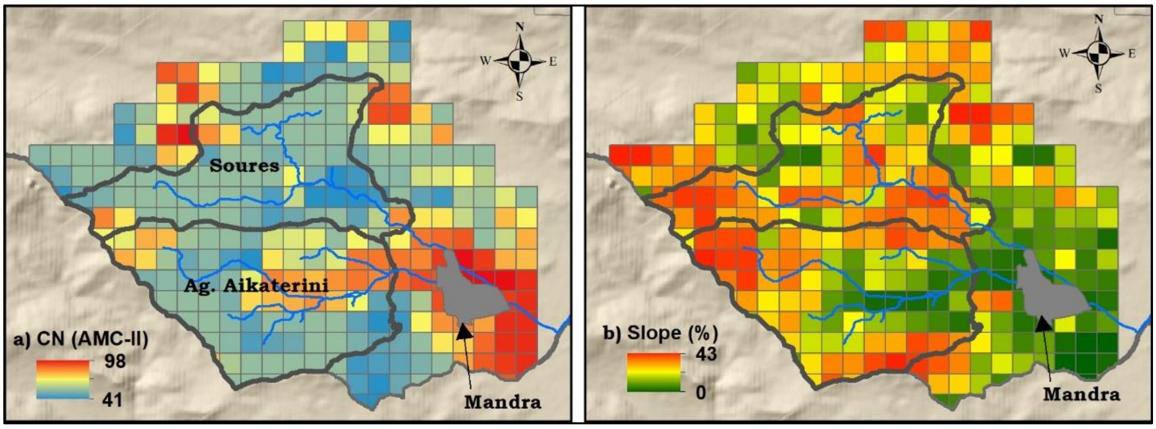


**Fig. 1.** The Mandra subbasin characteristics: a) CN AMC-II, b) Slope percentage

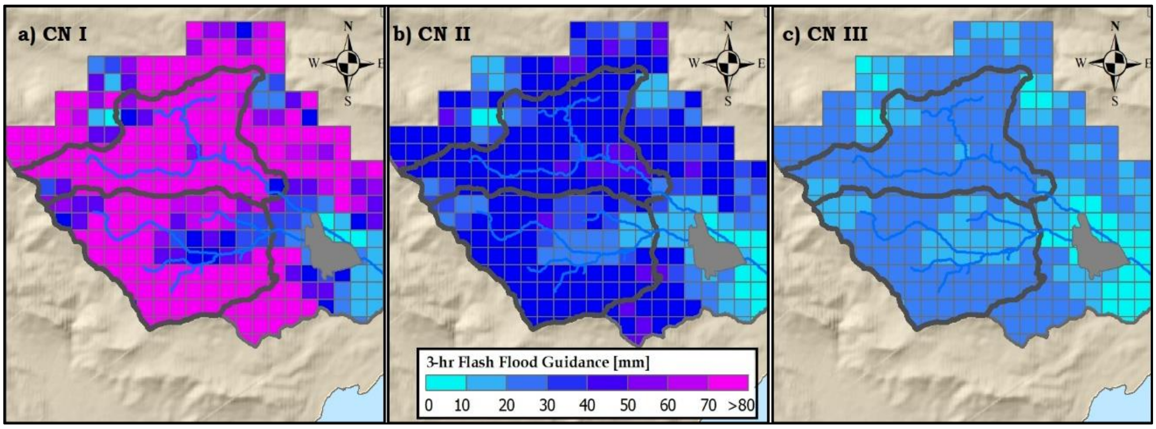


**Fig. 2.** FFG values for a 3-hour rainfall accumulation period and for three soil moisture conditions a) dry (AMC-I), b) half-saturated (AMC-II) and c) wet conditions AMC-III)

### References

Bournas A, Baltas E (2022) Investigation of the gridded flash flood Guidance in a Peri-Urban basin in greater Athens area, Greece. Journal of Hydrology 610:127820. https://doi.org/10.1016/j.jhydrol.2022.127820

Georgakakos KP (2006) Analytical results for operational flash flood guidance. Journal of Hydrology 317:81–103. https://doi.org/10.1016/j.jhydrol.2005.05.009

Georgakakos KP, Modrick TM, Shamir E, Campbell R, Cheng Z, Jubach R, Sperfslage JA, Spencer CR, Banks R (2022) The Flash Flood Guidance System Implementation Worldwide: A Successful Multidecadal Research-to-Operations Effort. Bulletin of the American Meteorological Society 103:E665–E679. https://doi.org/10.1175/BAMS-D-20-0241.1

Schmidt JA, Anderson AJ, Paul JH (2007) Spatially-variable, physically-derived flash flood guidance. In: Preprints, 21st Conf. on Hydrology, San Antonio, TX, Amer. Meteor. Soc. B

# Investigating velocity fluctuation by means of ADV at compound channel with installed hydropower propeller turbines

Slaven CONEVSKI[3], Massimo GUERRERO[1], Irene CAVALIERI[2], Nils RUTHER[4], Leonardo SCHIPPA[5]

[1] University of Bologna, Italy
email: massimo.guerrero@unibo.it

[2,5] University of Ferrara, Italy
email: schlrd@unife.it
email: irene.cavalieri@unife.it

[3,4] Norwegian University of Science and Technology, Trondheim, Norway
email: slaven.conevski@ntnu.no
email: nils.ruther@ntnu.no
[3] Norwegian Geotechnical Institute, Oslo, Norway

ABSTRACT

An acoustic Doppler velocimeter (ADV-FlowTracker 2) was used to measure the velocity field in three different positions in the Biffis channel. The channel is a regulated compound concrete channel continuously diverting 130-135 $m^3/s$ from the Adige River (Italy) for irrigation. Three different experiments were conducted with three different hydraulic conditions (turbines in production or off). Turbulent fluctuations are key factors in entrainment of the sediments from the bank surface. This campaign aimed to evaluate capability of the ADV to examine the influence of the of propellers turbines (prototypes) on the free surface channel flow, the velocity fluctuations and to identify presence of coherent structures. The results showed that the velocity fluctuations related to the channel geometry are present in all measurements regardless of the active turbines. However, the turbulent kinetic energy, the length and the number of the turbulent events are larger for the cases when the turbines were in production. The turbulent events are shorter for the case in which both turbine-arrays worked.

## 1. Introduction

The Biffis compound channel continuously drains 130-135 $m^3/s$ flow discharge from the Adige River for irrigation (Fig. 1). Two cross sections, equipped with four-propellers array were investigated in two days (i.e., June 17th and 18th, 2021). These sections are trapezoidal and triangular. The former is about 25-m wide and 6.1 m deep whereas the triangle has 22-m and 7.2-m width and height, respectively. In this study, FlowTracker2 (FT2, Handheld ADV) by Sontek-Xylem, was applied to investigate the influence on the surface velocity flow, of the two arrays propeller turbines, installed at Biffis compound channel (Fig. 1). Turbulent fluctuations are key factors in entrainment of the sediments from the bank surface. Thus, this work aims to evaluate the capability of the ADV to examine the presence of turbulence events and coherent structures in and out of operation of the turbine's operation.

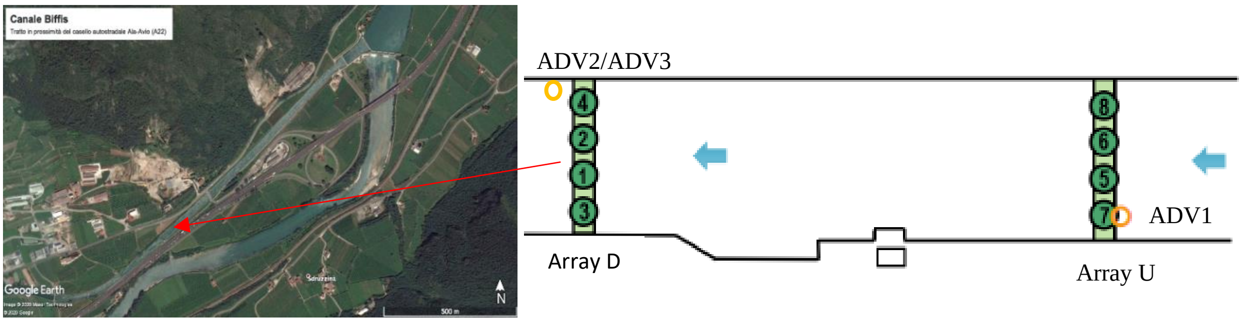


**Fig. 1.** The Biffis compound channel draining water from the Adige River close to Trento, Italy, on the left and the performed experiments with the FT2 (ADV).

## 2. Methods

The FlowTracker2 (FT2, Handheld ADV) is a single-point Doppler current meter designed for field velocity measurements. The FT2 is a bistatic Doppler current meter with a side-looking probe able to measure the point velocity in 3 directions. The FT2 uses pulse-coherent signal processing delivering 3D point velocities at 10 Hz sampling frequency (SonTek 2019).

### *2.1. The ADV-FT2 experiments*

To investigate the velocity fluctuations three experiments were performed (see Fig. 1): i.) ADV1- Both turbine arrays are turned off, and the ADV is placed in the position corresponding to the turbine 7 in the upstream array; ii.) ADV2- Array U is in production mode, the ADV is placed as close as possible to the right bank, namely about 100 cm distance from the wall; ii) ADV3- this time Array D is in production mode, the ADV is placed in the same position as for ADV2. The ADV was installed on a fixed structure and measurements were performed as shown in Fig.1. Three series of 20 minutes were conducted for each experiment.

### *2.2. Data analysis*

The raw velocity data obtained by the ADV is usually noisy and needs to be de-spiked and filtered (Goring 2002). To extract useful information related to the velocity fluctuations a power spectra analysis was performed in all 3 directions, aligning with the flow of the channel (i.e., X- flow direction, Y- perpendicular to the flow and Z- upwards). The identification of eventual large-scale coherent structures was carried out using a recently developed method based on the filtering phase-space algorithm (fPSA) (WU, et al. 2022). In addition, the turbulent kinetic energy was calculated for each experiment and the Reynolds parameters were examined.

## 3. Results and discussion

Preliminary results demonstrated that the ADV1 follows the slope of energy dissipation (-5/3). While ADV2 and ADV3 deviate from the slope due to the lack of time and space to dissipate the energy (i.e., turbines in productions).

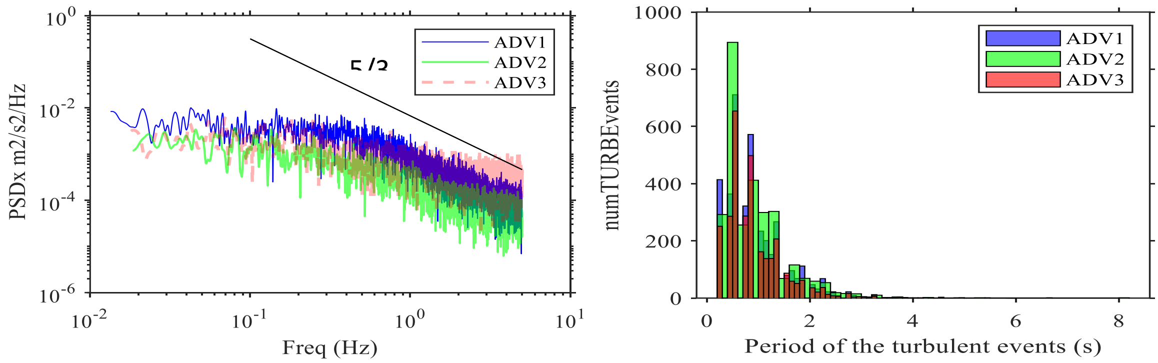


**Fig. 1.** Power Spectra Analysis of the velocity fluctuations only in the flow direction (left); Distribution of the period of the turbulent events detected by the fPSA only in the flow direction (right).

Although not very distinct, the maximal spectral powers were observed at frequencies close to 0.03-0.06 Hz and 0.1-0.2 Hz for all experiments. These frequencies are associated to the fluctuations due to the geometry/morphological changes of the channel. Whereas the higher frequencies (larger than 0.5 Hz) are most likely related with the wake spined by the turbines. ADV2 and ADV3 did not show significant differences in the velocity fluctuations (e.g., maximal frequencies Fig.1, left) except the higher TKE of the ADV3 and flatter dissipation slope (left Fig. 1). Deeper analysis should be performed on the spectral leakage and identification of the dominant frequencies.

The fPSE method detected turbulent events with shorter periods (Fig.1 right) corresponding to frequencies of 1-3 Hz. It is visible that the ADV3 exhibit shorter turbulent periods (turbine working right next to the ADV probe), while ADV1 and ADV2 show slightly skewed distribution giving longer mean average period (also longer maximum and median of the lengths of the total periods). It is assumed that the fPSA was unable to detect the lower frequencies and the fluctuation due to the channel geometry and it effectively identified the turbulent events associated with the turbine propellers. A further investigation should be performed to clarify the effect of the turbulent events on the bank erosion in addition to a detailed analyses on their origins and characteristics.

**References**

Goring, D. G. and Nikora, V. I. 2002. "Despiking Acoustic Doppler Velocimeter Data." *Journal of Hydraulic Engineering* 117–126. doi:doi.org/10.1061/(ASCE)0733-9429(2002).

SonTek. 2019. *FlowTracker2 User's Manual 1.6.* User's Manual, SonTek – a Xylem brand.

WU, JIAYI, Andrew Nichols, Anton Krynkin, and Martin Croft. 2022. "Objective phase-space identification of coherent turbulent structures in 1D time series data." *Journal of Hydraulic Research.*

# Modelling of plastic waste accumulation at hydraulic structures

Chit YAN TOE[1], Wim UIJTTEWAAL[1], Davide WÜTHRICH[1]

[1] Faculty of Civil Engineering and Geosciences, Delft University of Technology, the Netherlands
email: c.yantoe-1@tudelft.nl

ABSTRACT

Plastic debris items are collected in the riverine and marine waters using a variety of techniques and devices. Understanding the interaction between plastic items and their ambient environment is therefore essential for effective waste-removal systems. This research will investigate the motions of large plastic items in the disturbed flow conditions due to the presence of two different capturing devices, i.e. booms (floating barrier) and gates. Using a CFD approach combined with a finite-particle technique for particle representation, different interactions between the structure and plastic debris under various hydrodynamic conditions are studied. In addition, new insights are expected to implement parameterization for larger-scale hydraulic models.

## 1. Introduction

The large amount of plastic debris released in the aquatic environments raises a serious environmental concern, hence non-profit organizations and entrepreneurs are developing new and innovative techniques to capture and remove plastic waste from rivers and oceans, recycling them for further uses. However, the lack of complete understanding of plastic debris motion in open channel flows, as well the complexity of physical interactions between the capturing devices and plastic debris, limits efficient removal system.

The boom-type capturing device is the most frequently used tool for collecting and guiding plastic debris towards the receptacle or other storage structures. It is noted that hydraulic structures (e.g. gate, culverts, bridge) can also function as a boom-type capturing device, however, with significantly different hydraulic response (Fig. 1). For the case of a hydraulic structure, the plastic debris accumulated at the structure may lead to an increase in water level upstream, and/or a modified hydraulic performance.

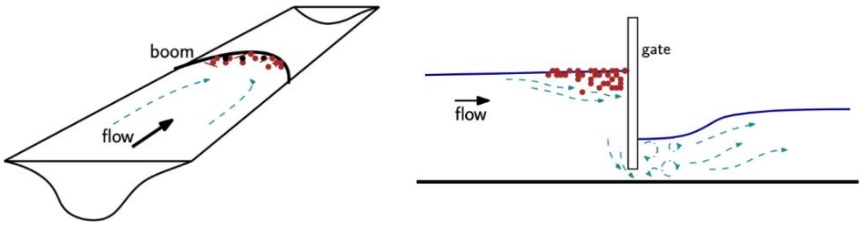


**Fig. 1.** Boom-type capturing device and hydraulic gate for plastic waste collection.

The disturbed flow induced by these capturing devices enhances turbulence processes and further complicates the trajectory of plastic debris items. The flow disturbances are expected to occur in both horizontal and vertical directions, causing major difficulties in providing accurate prediction of debris motion. The wake downstream of these devices was shown to potentially affect the retention of plastic items (Schouten, 2021). In addition, because of the presence of a hydraulic structure, vertical distribution of plastic items may deviate from theoretical distribution profile (Zaat, 2020). Therefore, an efficient capturing system necessitates a better understanding of the coupling between flow hydrodynamics and plastic items, as well as their mutual interactions.

### *1.1. Types of interactions*

Different interaction mechanisms arising from the disturbed flow can be grouped in four categories: (1) flow and structure, (2) flow and particles, (3) particles and structures, and (4) particles themselves. Unsteady and non-uniform flow conditions may change the orientation and position of a flexible structure, whereas fast-moving flows can induce structural vibration in case of rigid structure, which can affect the flow properties. The resulting flow condition will determine the kinematics of plastic items and assess how the presence of particles can change the flow condition. It is also envisaged that the interaction of particles and capturing devices, as well as particle-particle interaction, will also play an important role for the formation patches and carpets of debris possibly clogging the water system.

### *1.2. Considerations for modelling of plastic items*

The above-mentioned interactions cannot be realized through a simple numerical model that considers the particles as a pure Eulerian continuum or even as a point-particle, without having the finite-size and mass. Particles with significant size and mass may deviate from the fluid flow path (Cartwright et al. 2010) because the drag, lift, Basset history force, and buoyant force are non-negligible terms in the equation of particle motion. These forcing terms depend not only on physical properties of plastic items but also on kinematic conditions such as rotation and preferential orientation (DiBenedetto et al., 2018). Generally, large plastic items with significant inertia, have a longer response time to the flow and behave as a body rather than a passive-tracer.

Drag force occurs on the surface of the moving body relative to the fluid, that is usually parametrized by drag coefficient in the Maxey-Riley equation (DiBenedetto et al., 2018). Drag coefficients for simple geometry can be derived using analytical expressions, whereas the coefficients for complex geometry must be obtained from experiments or particle-resolving models. For plastic items of arbitrary shape, theoretical drag coefficients are unavailable to be included in the particle equation, therefore requiring an explicit representation technique of plastic items in the numerical model, or conducting laboratory experiments.

Added-mass also plays an important role for the case of an accelerating body in the flow, that is parametrized as a forcing term in the Maxey-Riley equation. Besides, entrapment of water or air can occur inside the plastic items such as plastic bag or water bottle. This mass-entrapment property has direct consequences on the effective mass, buoyancy and lift force of plastic items. Therefore, modelling these physical processes is a rather complicated task and requires an accurate particle representation technique.

When a barrier hinders the motion of plastic debris in the channel, a carpet develops just upstream of the structure, visually looking like a sheet. Carpet formation results in an additional boundary layer development below the plastic items, including friction and possible flow separation affecting the transport of plastic items. Incorporating this phenomenon in the numerical model may be accomplished by the explicit consideration of the shape of the particle.

## 2. Future implementations

To address the above-mentioned issues, kinematics of plastic debris in the disturbed flow and their dynamic interaction with the structure will be investigated using both laboratory experiments and numerical simulations. Different classes of plastic debris items will be defined in relation to their behavior in the proximity of boom-type devices and gated structures in open channel flow. Compared to previous studies, the present research will focus on plastic items with larger size > 5 cm, since they are responsible for significant interaction with structures.

Numerical modelling of detailed physical mechanisms will be emphasized here, requiring a Computational Fluid Dynamics (CFD) approach implemented with particle modelling technique. OpenFOAM will be used for CFD computations because of its versatility for multiphase flow modelling and its large user community. In this research, different representations for the particle will be applied and their accuracy in trajectory prediction will be compared with experimental results. Finally a parametrization of these small-scale hydrodynamic processes for large-scale hydraulic models will be derived and discussed.

**Acknowledgements**

This research is supported financially by NUFFIC (The Dutch organisation for internationalisation in education) and Rijkswaterstaat, in collaboration with HKV and Deltares.

**References**

Cartwright, J. H., Feudel, U., Károlyi, G., Moura, A. D., Piro, O., & Tél, T. (2010). Dynamics of finite-size particles in chaotic fluid flows. In Nonlinear dynamics and chaos: advances and perspectives (pp. 51-87). Springer, Berlin, Heidelberg.
DiBenedetto, M. H., Ouellette, N. T., & Koseff, J. R. (2018). Transport of anisotropic particles under waves. Journal of Fluid Mechanics, 837, 320-340
Loth, E. (2010). Particles, Drops and Bubbles: Fluid Dynamics and Numerical Methods, Draft for Cambridge University Press.
Schouten, D. (2021). Simulation of the interception of plastic fluxes in rivers, Master Thesis, TUDelft.
Zaat, L. (2020). Below the surface: A laboratorial research to the vertical distribution of buoyant plastics in rivers, Master Thesis, TUDelft.

# Effects of microplastic particles on cohesive sediment erosion

Maria PONCE[1], Claudia SOTO[1], Yomer CISNEROS[1], Silke WIEPRECHT[1], Stefan HAUN[1]

[1] Institute for Modelling Hydraulic and Environmental Systems, University of Stuttgart, Stuttgart, Germany
email: maria.ponce-guzman@iws.uni-stuttgart.de

ABSTRACT

The occurrence of microplastic particles (MPs) in freshwater ecosystems results in an increasing scientific attention in studying interactions of MPs with the aquatic environment. Reservoirs and lakes act due to the small flow velocities as sinks for MPs. As a result of their low density, MPs deposited in bed sediments may change the resuspension behavior of these sediment accumulations. This research aims at gaining knowledge on the influence of MPs on the erosion threshold and the resulting erosion rates of cohesive sediments. Experimental erosion tests are performed to determine the erosion evolution of artificial sediment mixtures with and without MPs. The first results indicate that the presence of MPs increases the temporal and spatial variability of erosion, provoking a more remarkable stochastic behavior of the erosion processes. In addition, it can be seen that resuspension is biased by the occurrence of polymer with lower density, but also the number of particles.

## 1. Introduction

Reservoirs and lakes are eminent sites for MP accumulations. This is first, because of low flow velocities and turbulences that enhance settling and deposition, and, second, the presence of clay and silt that bind particles, as a result of the high surface loading and high absorption potential. However, MPs in bed sediments change the properties of the sediment matrix and may influence its erosion behavior by promoting the resuspension of fine sediment. These circumstances may cause a high concentration of fine sediments in the water phase during high discharge rates, which may favor eutrophic conditions, especially in shallow water bodies. To scale the potential risk and to determine a remedial design, it is necessary to quantify and predict the ongoing processes of cohesive sediment erosion, influenced by MPs. This study analyzes the effect of MPs on the erosion threshold and on erosion rates, based on a set of erosion experiments where the number of particles and the density of the MPs are varied.

## 2. Materials and Methods

Six homogenized and saturated sediment mixtures are artificially produced for the experiments, consisting of 15 % kaolinite ($d_{50}$ = 0.047 mm) and 85 % fine sand ($d_{50}$ = 0.193 mm). The first two sediment mixtures (control group) does not contain any MPs, whereas the remaining four mixtures are spiked with a specific polymer type and a unique number of particles per dry weight of the sediment. The four MP-sediment combinations are the following: 500 particles of polystyrene (PS, $d_{50}$=2.5 mm, $\rho$=0.96-1.05 g cm$^{-3}$), 500 particles of polyamide (PA, $d_{50}$ =2.5 mm, $\rho$=1.01-1.04 g cm$^{-3}$), 1000 particles of PA and 1000 particles of polylactide (PLA, $d_{50}$=3 mm, $\rho$=1.38 g cm$^{-3}$), respectively. The polymers selected are colorless pellets without additives. The erosion tests are performed in the SETEG erosion flume at the University of Stuttgart. Details on the experimental setup can be found in Noack et al. (2018). During the erosion tests, the flow velocities within the flume are increased in a sequence of 12 steps of 600 seconds each. The increasing flow discharges reach from 1 to 12 ls$^{-1}$, resulting in a mean bed shear stress between 0.04 and 1.6 Pa. The spatial and temporal erosion evolution was captured by the photogrammetric sediment erosion detection method PHOTOSED (Noack et al., 2018), following the approach suggested by Beckers et al. (2020), allowing a pixel-based topographic change detection (minimum detectable change one mm$^3$) from consecutive images obtained with 1 Hz. A comparison of the temporal erosion rates and the erosion threshold is performed to quantify the effect of MPs on the erosion stability. The erosion rates are derived from the volumetric erosion for a representative time step and a defined rectangular Region Of Interest (ROI). The temporal evolution of the eroded volume is used to distinguish between floc and surface erosion, based on the erosion modes described by Winterwerp et al. (2010). An advantage of this approach is that both, the hydrodynamics and the characteristics of the sediment mixture, are taken into account. While the floc erosion shows spatial and temporal variation, mainly related to the turbulent flow, the surface erosion is linked to the sediment characteristics. Hence, the erosion threshold of the MP-sediment mixture is estimated from the surface erosion, following the approach of Jacobs et al. (2011).

## 3. Results and Discussion

Over time, the evolution of the eroded volume for the sediment mixtures without MPs (Fig. 1a) shows the clear transition between floc and surface erosion at τ=1.39 Pa. Furthermore, erosion measurements with high spatial resolution show and confirm the difference between these two modes. While only individual flocs are disrupted in floc erosion, large sediment layers are eroded in surface erosion. As for erosion rates, the artificial cohesive sediment mixtures without MPs show small temporal variations, whereas the overall trend of sediment mixtures with MPs show an increase in temporal and spatial variation, especially during the floc erosion phase (Fig. 1b). It is also noticed that peak values occur randomly even at low shear stress, indicating that some particles or flocs have a critical shear stress for initiation of motion lower than the imposed shear stress. The stochastic nature of erosion due to the spatial inhomogeneity of the sediment properties is already mentioned in Winterwerp et. al. (2010). Here, it is related to the inclusion of MPs. Analysing the spatial measurements, it becomes evident that sediment erodes mainly around the MPs, which erode easier due to the lesser cohesion between the flocs and the lower bulk density of the mixture. Hence, the results indicate that the presence of MPs weakens the bed strength and triggers a dominant stochastic erosion behaviour. Comparing the erosion threshold for surface erosion, mixtures with MPs achieve an earlier uniformity trend at τ=1.18 Pa against mixtures without MPs. By evaluating the results of the mixtures with MPs, it can be seen that low-density polymers (PS and PA) show higher erosion rates than PLA, with a higher density. Although it is observed that erosion is limited by the occurrence of erodible sediment spiked with MPs, there is no linear increase in erosion rates as the number of polymer particles increases. On the other hand, the number of particles affects the cumulative volume eroded. For example, below shear stress of 1.18 Pa, the sediment mixture with 1,000 PA particles erodes 80% more sediment volume than the mixture with half as many particles.

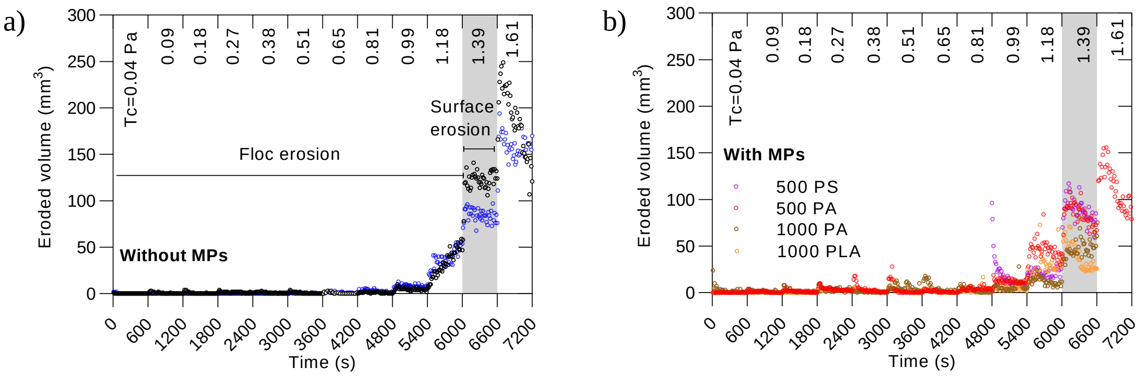


**Fig. 1.** Comparison of the measured eroded volume from homogeneous cohesive sediment mixtures (a) without MPs and (b) with MPs, as a function of time.

## 4. Conclusions and Outlook

The conducted experiments show an increase in the temporal and spatial variability of erosion rates when adding MPs to the cohesive sediment mixture. An explanation for this stochastic behaviour is the non-uniformity of the bed strength (critical shear stress) as a result of the lower density of MPs in the sample. Even though the critical erosion threshold for surface erosion of the mixture has a slight change and more experimental erosion tests are required for a more quantitative analysis. The study results highlight the potential change in resuspension behaviour of cohesive sediments when MPs occur in the bed sediment. While the polymer density affects the erosion peaks, the cumulative eroded volume is affected by the number of particles. To quantify the effect of each MP-sediment combination, the results suggest the necessity to develop a methodology to describe the stochastic behaviour caused by the heterogeneity of the sediment mixture, which is part of future research.

**References**

Beckers, F., Inskeep, C., Haun, S., Schmid, G., Wieprecht, S., Noack, M. (2020) High spatio-temporal resolution measurements of cohesive sediment erosion. Earth Surf. Process. Landf. esp.4889. https://doi.org/10.1002/esp.4889

Jacobs, W., Le Hir, P., Van Kesteren, W., Cann, P. (2011) Erosion threshold of sand–mud mixtures. Cont. Shelf Res. 31, S14–S25. https://doi.org/10.1016/j.csr.2010.05.012

Noack, M., Schmid, G., Beckers, F., Haun, S., Wieprecht, S. (2018) PHOTOSED-PHOTOgrammetric sediment erosion detection. Geosci. Switz. 8.

Winterwerp, J.C., Van Prooijen, B.C. (2010) A stochastic formulation for erosion of cohesive sediments. J. Geophys. Res. 115. https://doi.org/10.1029/2008JC005189

# Gauging suspended sediment concentration in coastal waters by means of proxy acoustical methods

Rui ALEIXO[1,3], Massimo GUERRERO[2], Evelien BRAND[3], Margaret CHEN[3]

[1]CERIS, Instituto Superior Técnico, Universidade de Lisboa, Portugal
email: rui.aleixo@tecnico.ulisboa.pt

[2]University of Bologna, DICAM, Italia
email: massimo.guerrero@unibo.it

[3]Vrije Universiteit Brussel, België
email: eveliend.brand@vub.be
email: margaret.chen@vub.be

ABSTRACT

The need for acoustic proxy methods to determine the suspended sediment concentration (SSC) in water bodies stems from two main reasons: the availability of acoustic measurement devices such as acoustic Doppler current profilers (ADCP) and the need to provide accurate and regular measurements of the SSC. Different methods exist that have been proved to provide reliable results under different conditions, these methods often relate SSC with the acoustic attenuation or backscatter. Another acoustic proxy method is based on the attenuation to backscatter ratio (ABR). This method has been successfully used in fluvial environments with good results. The goal of this paper is to propose the application of the ABR method to several data bases of field data measured in a coastal area of Belgium, to determine the SSC and compare the calculated values with the ones obtained by means of calibrated optical backscatter point sensor (OBS). Different issues related with the ABR method application were identified and are discussed.

## 1. Introduction

Environmental monitoring is crucial to assess the condition of environments such as rivers, coastal areas, etc. Monitoring allows to measure and register different variables that play a critical role in ecological processes (Aleixo et al. 2020). A common instrument found in such monitoring stations are ADCPs that are used to measure velocity profiles and estimate the flowrate. Besides the information regarding the velocity profile, ADCPs also generate an echo profile along its axis. The echo is a function of different variables, namely SSC but also of temperature, salinity, particle size distribution, organic content, etc.

The goal of this paper is to analyse the ability of the ABR method, applied to the ADCP's echo profiles, to determine the SSC in coastal environments and identify its possibles drawbacks and data requirements.

### *1.1. Mathematical model*

The basis of the acoustic methods is the sonar equation that can be written as (Thorne and Hanes, 2002, Guerrero et al. 2017):

$$I_{dB} - C + 20\log(r\psi) + 40r\alpha_w \log(e) = -40\,\zeta_s M_s \log(e) r + 10\log\left({k_s}^2 M_s\right) \qquad (1)$$

where $I_{dB}$ is the echo intensity level in dB, $C$ is the instrument constant (dB), $k_s$ is the backscatter coefficient, $M_s$ is the concentration, $r\psi$ is the geometric spreading, $r$ is the distance to the source (m), $\alpha_w$ is the water attenuation and $\zeta_s$ is the attenuation coefficient. Equation (1) can be seen as an equation of the type (Guerrero et al. 2017):

$$y = mr + b \qquad (2)$$

where the slope $m$ is related with the attenuation that in turn gives the SSC for a given particle size distribution (PSD) and $b$ is related to the backscatter. In a sense, the determination of the attenuation and backscatter is a regression problem. From here, one can define the attenuation to backscatter ratio, ABR as (Guerrero and di Federico, 2018):

$$ABR = \frac{\zeta_s}{{k_s}^2} \qquad (3)$$

The ABR at a given frequency and for homogeneous concentration depends on the actual PSD only and can be estimated from echo profiling (Guerrero et al., 2017; Guerrero and di Federico, 2018). We therefore look for a model to relate the SSC to the attenuation and to the ABR as a parameter which fixes the actual PSD. This has been succesfully achieved in fluvial environments (Aleixo et al., 2020), however, extending this method to coastal environments has proven challenging.

While in the fluvial environment the processes (e.g., sediment yield and transport) are mostly controlled by the hydrology and flow rate/water depth, showing a strong seasonal dependence, e.g., floods in Autumn/Spring versus dry periods in Summer, which relate to acoustic features of scattering suspended particles, in coastal environments, the observed variations are strongly tide depending: for example the attenuation term prevails during tide peaks whereas it is evanescent during falling and rising phases.

## 2. Monitoring field station and data

The monitoring station was placed in Ostende, Belgium at Mariakerke and consisted of a metallic frame where the following instruments were assembled: 3 ADCPs, 3 OBS, an electromagnetic current meter, and a water level meter (Brand, 2019).

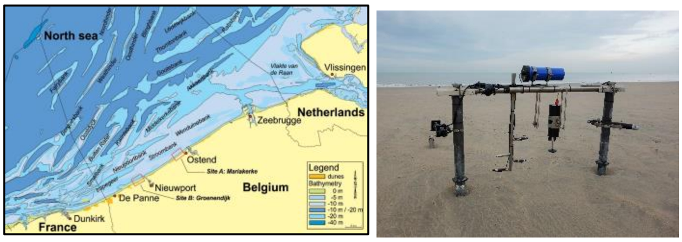


**Fig. 1.** Map with the location of the monitoring station and monitoring station.

Application of the mathematical model and determination of the ABR proved non-trivial and it showed a grouping of the data points into two main clusters: peaking level and changing level tide phases. In the former case the ABR method for SSC assessment appears reliable that is based on sound attenuation cumulated by the acoustic wave traveling through a water-sediment mixture with homogenous concentration. On the contrary during raising and falling phases of the tide, the backscatter distribution along the profiled water column shows that the ABR method hypotheses are not satisfied and call for further analysis.

.

## 3. Conclusions

Meaningful evidence regarding the SSC arises from ADCP echo intensity profiling during tide cycles in coastal environments. During peaking levels, which are characterized with high flow velocity the sound attenuation maximizes that enables the application of the ABR method previously applied in riverine environment. In this case a homogenous, well mixed SSC is expected. Variations phases of the water level, i.e., the falling and rising tide phases exhibit negligible sound attenuation, on the contrary the echo intensity level is reinforced towards the sea floor that most likely means increasing SSC at bottom. This gives a distribution of the backscattering strength that hinders the application of the ABR method.

**Acknowledgements**

The measurements were part of the CREST project, funded by the Strategic Basic Research (SBO) program of Instituut voor Innovatie door Wetenschap en Technologie (IWT).

**References**

Aleixo R, Guerrero M, Nones M, Rüther N (2020) Applying ADCPs for long term monitoring of SSC in rivers. Water Resources Research, vol 56, 1. https://doi.org/10.1029/2019WR026087
Brand, E (2019) Intertidal beach morphodynamics of a macro-tidal sandy coast (Belgium). PhD Thesis.VUB. Belgium
Guerrero M, Rüther N, Haun S, Baranya S (2017) A combined use of acoustic and optical devices to investigate suspended sedimentin rivers.Advances in Water Resources,102, 1–12. https://doi.org/10.1016/j.advwatres.2017.01.008
Guerrero M, DiFederico V (2018) Suspended sediment assessment by combining sound attenuation and backscatter measurements analytical method and experimental validation, Advances in Water Resources,113, 167–179. https://doi.org/10.1016/j.advwatres.2018.01.020
Medwin H, Clay C (1998) Fundamentals of Acoustical Oceanography, Academic Press, London, UK, 1998.
Thorne, PD, Hanes DM (2002) A review of acoustic measurement of small-scale sediment processes.Continental Shelf Research, 22(4), 603–632. https://doi.org/10.1016/S0278-4343(01)00101-7

# River-Sea System Connectivity: Analysis of River Plume Dispersal in the Northern Adriatic Sea

Rossella BELLONI[1], Claudia ADDUCE[2], Federico FALCINI[3], Vittorio Ernesto BRANDO[4]

[1,2] Roma Tre University, Italy
email: rossella.belloni@uniroma3.it

email: claudia.adduce@uniroma3.it

[1,2,3,4] National Research Council – Research Institute of Marine Science, Italy
email: federico.falcini@cnr.it
email: vittorio.brando@cnr.it

ABSTRACT

Connectivity describes the efficiency of material transfer between the components of a system. In this study, high-resolution multispectral satellite data from the Copernicus Sentinel-2 mission were used to investigate the degree of sediment connectivity of the Po river-sea system (northern Adriatic Sea, Italy) in its final section, the coastal area. The analysis was performed investigating the spatio-temporal variability of Po River plume morphologies captured by the satellite images and evaluating the influence of the main environmental forcings affecting sediment dynamics in the study area (wind and river discharge) and therefore river-sea system connectivity. Although with some intrinsic limitations, the analysis showed the good potential of high-resolution remotely sensed data to capture the main features of sediment dynamics, and therefore their relevance for a better understanding of the processes that govern sediment connectivity in coastal area.

## 1. Introduction

In fluvial and coastal geomorphology, connectivity is a measure of how efficiently the transport of sediment through the river-sea system is. The river-sea system includes the whole river basin and the surrounding coastal area which extension is determine by river plume dynamics.

In recent years, many techniques have been developed to quantify sediment connectivity (Najafi et al., 2021). However, because of the challenges involved in monitoring the sediment transport in coastal areas there are limited applications in coastal environments despite the huge impact on the ecology and morphology of coastal areas. Rivers are indeed the major way through which nutrients, sediments and pollutants are transported up to the coastal waters.

The analysis of phenomena occurring in complex environments requires monitoring techniques that provide data with a spatiotemporal resolution consistent with the scales of interest. The most direct method of deriving such information involves satellite imagery. The main objective of this work was therefore to investigate the potential of high-resolution remote sensing data from the Copernicus Sentinel-2 mission to investigate the degree of sediment connectivity of a river-sea system in its final section (coastal area), using as a case study the area of the Po River prodelta in Italy.

## 2. Materials and methods

A time series of Level-1C Sentinel-2 images for the area of the northern Adriatic Sea was collected and processed for the period 2015 - 2018 selecting those without any source of disturbance (clouds and sun glint effect) and showing visible river plumes. The images were later processed using a processor developed for the atmospheric correction and processing of satellite images for coastal and inland water applications, ACOLITE (Vanhellemont and Ruddick, 2014, 2015 and 2016). The processor can also output several parameters derived from the water reflectance. In this study, it was used to obtain high-resolution turbidity maps, a key parameter both in water quality and sediment transport monitoring of coastal and inland waters, using the algorithm developed by Dogliotti et al. (2015).

River-sea system sediment connectivity was then investigated analyzing the spatio-temporal variability of river plume dispersal in the study area (Falcini et al., 2012; Brando et al., 2015; Braga et al., 2017). On this aim, for each satellite image, the overall coastal area affected by the river plume dispersal was identified comparing the turbidity values with a threshold equal to the Adriatic Sea background turbidity. In the end, the degree of sediment connectivity of the system in the coastal area was evaluated considering the frequency of the suspended sediments dispersal in the alongshore direction. Turbidity maps were also coupled with in situ measurements of the main environmental forcings affecting sediment transport in the study area (wind and river discharge) to evaluate their role in affecting river plume morphologies. Considering that the dynamic captured by the satellite image depends on the evolution of the forcings in the antecedent period, discharge and wind data referred to a temporal window of 72 hours before the satellite acquisition were considered for the analysis (Braga et al., 2017).

## 3. Results and conclusions

The analysis showed plume patterns with a moderate spatio-temporal variability (Fig. 1) and confirmed the major role of wind and river discharge in affecting their overall structure, and therefore their major role in affecting the sediment connectivity of the Po river-sea system.

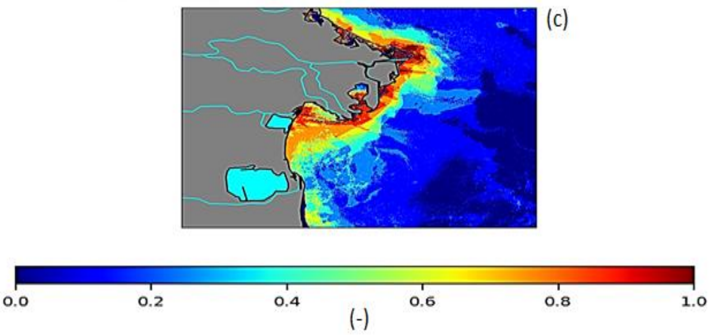


**Fig. 1.** Map of frequency of occurrence of Po river plume.

Long-lasting northerly winds tend to compress the plume against the coast, hampering the bulge formation and therefore promoting the sediment supply along the surrounding coastal areas, increasing the system sediment connectivity. Southerly winds, in contrast, causing the detachment of the geostrophic current of the plume from the coast, determine an offshore sediment transport. The highest river discharge events seem instead to limit the influence of the wind on river plume morphology, which tends to show a more prototypical morphology (Horner-Devine et al.,2015).

**References**

Braga F, Zaggia L, Bellafiore D, Bresciani M, Giardino C, Lorenzetti G., ... & Brando VE (2017) Mapping turbidity patterns in the Po river prodelta using multi-temporal Landsat 8 imagery, Estuarine, Coastal and Shelf Science, 198, 555-567.
Brando VE, Braga F, Zaggia ., Giardino C, Bresciani M, Matta E, ... & Carniel S (2015) High-resolution satellite turbidity and sea surface temperature observations of river plume interactions during a significant flood event, Ocean Science, 11(6), 909-920.
Dogliotti AI, Ruddick KG, Nechad B, Doxaran D, & Knaeps E (2015) A single algorithm to retrieve turbidity from remotely-sensed data in all coastal and estuarine waters, Remote Sensing of Environment, 156, 157-168.
Falcini F, Khan NS, Macelloni L, Horton BP, Lutken CB, McKee KL, ... & Jerolmack DJ (2012) Linking the historic 2011 Mississippi River flood to coastal wetland sedimentation, Nature Geoscience, 5(11), 803-807.
Horner-Devine AR, Hetland RD, MacDonald DG (2015) Mixing and transport in coastal river plumes, Annual Review of Fluid Mechanics, 47, 569–594.
Najafi S, Dragovich D, Heckmann T, & Sadeghi SH (2021) Sediment connectivity concepts and approaches, Catena, 196, 104880.
Nechad B, Ruddick KG, Park Y (2010) Calibration and validation of a generic multisensor algorithm for mapping of total suspended matter in turbid waters, Remote Sens. Environ., 114 (4), 854-866.
Vanhellemont Q, Ruddick K (2014) Turbid wakes associated with offshore wind turbines observed with Landsat 8, Remote Sensing of Environment, 145, 105–115.
Vanhellemont Q, Ruddick K (2015) Advantages of high quality swir bands for ocean colour processing: examples from Landsat-8, Remote Sensing of Environment, 161, 89–106.
Vanhellemont Q, & Ruddick K (2016) Acolite for Sentinel-2: Aquatic applications of MSI imagery, In Proceedings of the 2016 ESA Living Planet Symposium, Prague, Czech Republic (pp. 9-13).

# Low-cost turbidimeter: from the washing machine to the research field

Maria F. S. GISI[1,2,3], Oldrich NAVRATIL [3], Frédéric CHERQUI [1,2], Etienne COSSART [3], Tim FLETCHER [2], Kathryn RUSSELL [2], Paulo V. R. M. DA SILVA [1,2,3], Bastien BOURJAILLAT [3],
Lucas MAURER [3], Pascal KRIEG [3], Benoit ANQUEZ [3], Philippe NAMOUR [4]
1 Univ. Lyon, INSA Lyon, DEEP, EA7429, 69621 Villeurbanne, France
2 The University of Melbourne, SEFS, Burnley, VIC 3121, Australia
3 Univ. Lyon, CNRS UMR 5600 Environnement Ville et Société, Lyon, France
4 Unité de recherche RiverLy INRAE Lyon-Grenoble Auvergne-Rhône-Alpes, CS 20244, 69625 Villeurbanne Cedex
email: maria.gisi@insa-lyon.com

ABSTRACT

Turbidity is a key water quality parameter, used to indicate the level of suspended solids in aquatic systems. The cost of data collection, however, often hinders high temporal and spatial measurement resolution of turbidity measurement. These last years have seen the (r)evolution of monitoring, where technological advances can support the development of innovative monitoring systems, offering lower costs, miniaturization, real-time access to data, modularity, connectedness (Internet of Things) and open-source programming. This innovative monitoring needs, however, to be compatible with the research goals and provide valid and reliable data. Thispaper focuses on the adaptation of a very low-cost sensor used in industry for sediment monitoring in rivers. The aim is to shed light on the problems encountered by researchers while developing these sensors and propose solutions to these problems.

## Why does turbidity matter?

Total Suspended Solids (TSS) is a key parameter to understand and control the quality in many water-related systems (Sampedro & Salgueiro, 2015). This parameter, although very easily identifiable, is hard to quantify. Turbidity can be used as a surrogate to understand not only the amount but also the size, shape and even composition of the particles present in the water. It characterizes how the particles suspended in the water scatter and absorb light, rather than transmitting it (Zhu et al., 2020). Turbidity is either acquired by laboratorial analysis of samples or by deploying sensors into environments such as streams, lakes and sewer pipes. These sensors need to be robust enough to endure harsh weather conditions without compromising the data. Currently, many commercial sensors exist in the market but, with costs reaching five to ten thousand euros per sensor, high spatial resolution cannot be expected. Recently a trend has been growing to develop low-cost internet of things (IoT) connected technology. This technology is now reaching the scientific community, providing lower costs and real-time access to data. A key challenge in this process is to optimize the use of new technologies, rather than simply replacing the functionality of existing monitoring systems. The goal is to create a monitoring chain where all stakeholders have access to relevant information and alerts. This idea is explained in Figure 1.

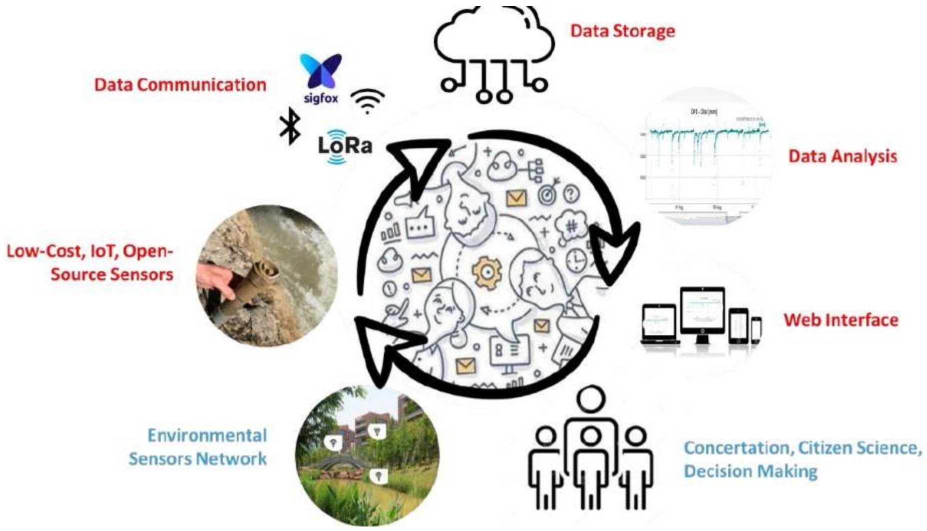


**Fig. 1.** Monitoring chain: from the elaboration of the low-cost monitoring system to the use of data. The text in red corresponds to the steps currently being developed by the authors.

**From the washing machine to the river**

We propose to develop an autonomous energy field turbidimeter with real-time data transmission. The entire system is constructed using Arduino components, and its main component, the sensor SEN0189 (DFRobot, 2022) was first developed to be used in washing machines. To our knowledge, this is currently the only low-cost commercially available sensor suitable for this type of measurements. The head consists of a printed circuit protected by a transparent plastic cap, on which two LEDs separated by about 1cm allow the measurement of the turbidity by operating in the near infrared light spectrum. The sensor measures how much of the emitted light is attenuated when going through the water until reaching the receiver. This principle is not new, and has already been put into application by many authors (Rymszewicz et al., 2017; Parra et al., 2018). What changes in this research in comparison to previous studies is the approach made to rectify inconsistencies in the measured data, which are constantly present.

Several challenging issues need to be solved before the deployment of low-cost turbidity sensors in the field: the key challenges are presented below in Table 1.

**Table 1:** Issues with deploying low-cost turbidimeter

| Issues | Description | How to identify it | Possible solution |
|---|---|---|---|
| Ambient solar noise | Sun light causes overestimation of measured values because it increases the amount of light on the receiver LED. | Using control measurements with varying solar influence (in the light, shadow and completely dark) | • Use LED with lower sensitivity<br>• Develop sun protection casing for sensor<br>• Measure sunlight influence before any measurement |
| Fouling | Accumulation of dirt/algae/calcareous materials blocks the passage of light between the LEDs | • Identify trend of increase in measured values.<br>• Do measurements before and after cleaning the probe | • Develop way to keep sensors clean (acid, ultrasonic, mechanical)<br>• Implement alert system when trend of increase is identified |
| Accuracy | Turbidity measurement accuracy can be affected by voltage measurement | Direct voltage measurement from the Arduino board is questionable | Use a dedicate component to accurately monitor the voltage: ADS1115 |
| Calibration | Without sensor calibration the acquired data is not valid | Before the deployment of any sensor calibration is needed | Develop fast standard calibration procedure |

Our preliminary lab experiments (in controlled environment) showed promising results in comparison with well-established commercial sensors. The next stage was to implement some of the solutions presented in Table 1. To counter the influence of solar light, the emitters and receivers were substituted with LEDs less sensitive to ambient lighting. According to our experiments, solar noise tends to increase measured voltage by circa 60%; the LEDs substitution limits the increase to circa 10%.

Experiments to assess the influence of the water temperature in turbidity measurement have shown that it is possible to compensate for temperature changes and obtain results very close to reference scientific-grade sensors. Another encouraging preliminary result is the apparent better performance of the low-cost sensors than the wide turbidity range commercial sensors for concentration above 2g/L of sediments in water.

The preliminary results encourage us to further pursue the directions taken for addressing the impacts of solar noise and of temperature. The SEN0189 has proven its applicability for turbidity measurement in water-related systems. Fouling problems will also need to be investigated to reduce field maintenance interventions. The issues we encountered and the problem-solving approach we followed can be of inspiration for other researchers aiming to use and adapt low-cost technology. Another important step is to consider the whole monitoring chain, from the measurement to the data visualisation.

**References**

DFRobot (2022) https://wiki.dfrobot.com/Turbidity_sensor_SKU__SEN0189 (last access 08.03.2022)
Parra, L., Rocher, J., Escrivá, J., & Lloret, J. (2018). Design and development of low-cost smart turbidity sensor for water quality monitoring in fish farms. Aquacultural Engineering, 81, 10-18.
Rymszewicz, A, O'sullivan, JJ, Bruen, M, Turner, JN, Lawler, DM, Conroy, E, & Kelly-Quinn, M (2017). Measurement differences between turbidity instruments, and their implications for suspended sediment concentration and load calculations: A sensor inter-comparison study. Journal of Environmental Management, 199, 99-108.
Sampedro, Ó, & Salgueiro, JR (2015). Turbidimeter and RGB sensor for remote measurements in an aquatic medium. Measurement, 68, 128-134
Zhu, Y, Cao, P, Liu, S. Zheng, Y, & Huang, C (2020). Development of a new method for turbidity measurement using two NIR digital cameras. Acs Omega, 5, 5421-5428

# Using Participatory System Dynamics Modelling for analyzing Water-Energy-Food Nexus resilience: the Lower Danube case study

Raffaele GIORDANO[1], Albert SCRIECIU[2] and Alessandro PAGANO[1]

[1] Istituto di Ricerca sulle Acque - CNR, Italy
email: alessandro.pagano@ba.irsa.cnr.it

[2] GeoEcoMar, Romania
email:albert.scrieciu@geoecomar.ro

ABSTRACT

Nexus thinking is based on the development of holistic approaches to water, energy and food systems, and oriented to reach the security of resources. System-thinking techniques and System Dynamics Modelling tools have shown a huge potential in Nexus studies, as they can be used to to map the complex and non-linear connections among the different elements - i.e. ecological resources, ecological processes, human processes and activities, and infrastructures – which affect the production and mobilization of Ecosystem Services that contribute to the Nexus resilience. The present work, which has been performed within the H2020 REXUS project proposes some preliminary results of the use of Particupatory System Dynamics Modelling for the analysis of a Nexus system in the Lower Danube (Romania) area.

## 1. Introduction

Both the concepts of 'Nexus' and 'resilience' are not new. Nexus is about interconnections among different sectors (water, energy, food, ecosystems, climate), whereas resilience is about the capacity of a system to respond to threats and retain its ability to deliver benefits (Lawford et al. 2013). The interplay between Nexus and resilience has recently received increasing attention (e.g. Hogeboom et al. 2021) and is connected to the concept of resource security, which is expected to worsen in the near future, driven e.g. by disruptive shocks including climate change (Hoekstra and Wiedmann, 2014; Steffen et al., 2018). Nexus thinking advocates that water, energy and food systems should be viewed holistically in order to reach water, energy and food (WEF) security (WEF, 2011). A Nexus system is considered resilient if, under internal and external stressors resources security is guaranteed by the capability of ecosystems to produce the required Ecosystem Services (ES).

In this framework, the present work proposes an ES-based approach to better capture and model the existing connections between Nexus and resilience. Participatory System Dynamics Modelling (PSDM) techniques allow to identify and analyse in an integrated way all the factors and processes related to the production of the needed ES, including non-linear feedbacks, trade-offs, and interactions related to Nexus management. Stakeholders' knowledge and scientific information are integrated for the purpose in the form of a Causal Loop Diagram (CLD). The results of the implementation of the methodological approach in one of the REXUS pilot cases, namely the Lower Danube area, are summarized in the present work.

## 2. Methodological approach

SDM is a methodology and mathematical modeling technique to frame, understand and discuss complex systems. It is widely used for policy analysis and design, and represents a holistic and cost-effective modelling approach. For the purpose of the present work, it is used as an integrated modelling tool, for representing Nexus systems as complex socio-ecological systems, i.e. based on the strong interaction among networks of agents and natural resources. The use of Participatory approaches in SDM (PSDM) helps integrating local knowledge and stakeholders' perceptions on the investigated problem. Specifically, Causal Loop Diagrams (CLDs) are identified as a suitable modelling approach to provide an improved understanding of the system under investigation, focusing on the relationships among different variables. In the REXUS project, semi-structured interviews were used to feed the CLD mainly referring to: i) the most important ES to be produced for the Nexus security and the local development; ii) the key ecological resources and processes needed for the ES production; iii) the key actors interested/involved in the ES production; iv) the infrastructures needed for the actual use of the ES, and v) the main barriers hampering the ES production processes.

## 3. Preliminary results and way forward

The Lower Danube case study (Romania) is characterized by a key ecological resource - i.e. the Danube river – which has the potential to produce a wide range of ESs. Most of the stakeholders consider the provisioning ESs as key for guaranteeing the Nexus security and resilience, particularly with respect to food and ecosystem domains. Although water resources are rather abundant in the area, their potential to produce and mobilize ESs is hampered by the lack of effective policies and infrastructures. The results of the interviews were structured in Causal Loop Diagrams to describe the cause-effects web of non-linear connections affecting the production of ESs, according to the stakeholders' problem understandings. The following Figure 1 shows one of the CLDs, referring to the role of riparian wetlands.

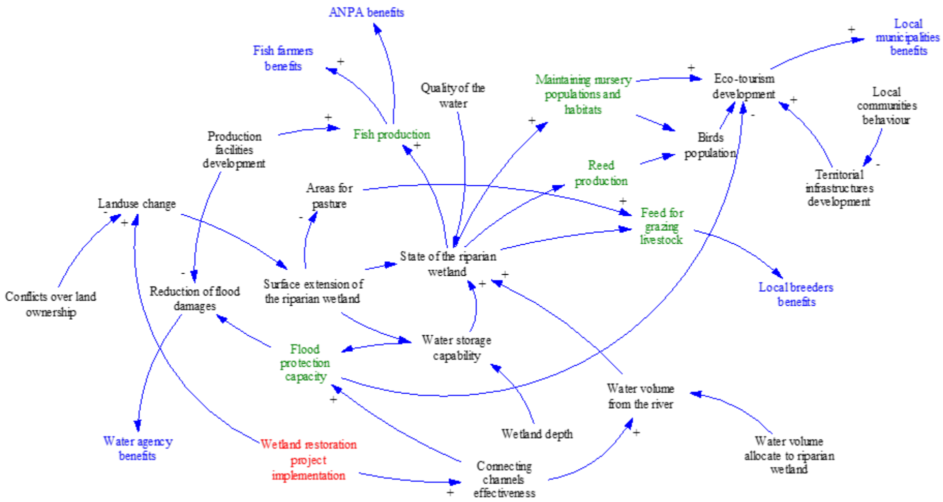


**Figure 1.** Sub-model focusing on the role of the riparian wetland to produce ESs in the Lower Danube pilot area

Specifically, wetlands contribute to food security by increasing aquaculture production, which in turn, would contribute to the community's well-being. Moreover, wetlands are expected to play a key role in enhancing biodiversity and, thus, attracting eco-tourists. Finally, the wetlands produce regulating ES, contributing e.g. to flood risk reduction. However, currently, most of the former riparian wetlands are used either as pasture areas or as agricultural land, being in a fairly bad status from the ecological point of view. A project for restoring riparian wetlands is currently under discussion and is supposed to improve the connection between the river and the former wetlands, through the realization of new - or renovation of existing - channels. The high level of conflict among different institutional actors is also hampering this transition.

The whole model will be used to better understand how Nexus security and resilience in the pilot area could be achieved, ultimately identifying the multi-dimensional impacts that different policies may have on the system as a whole and on different stakeholders.

**Acknowledgements**

The present work has been carried out within the Project REXUS (Horizon 2020 Research and Innovation Programme, Grant Agreement No 101003632, https://rexusproject.squarespace.com/). The authors would like to thank all project partners for their useful feedbacks, and all stakeholders from the pilot area for their invaluable contribution to modelling activities.

**References**

Hoekstra, A. Y., & Wiedmann, T. O. (2014). Humanity's unsustainable environmental footprint. Science, 344(6188), 1114–1117.
Hogeboom RJ, Borsje BW, Deribe MM, van der Meer FD., Mehvar S, Meyer MA, Özerol G, Hoekstra AY, Nelson AD (2021). Resilience Meets the Water–Energy–Food Nexus: Mapping the Research Landscape. Frontiers in Environmental Science, 9, 1–18.
Lawford R, Bogardi J, Marx S, Jain S, Wostl CP, Knüppe K, Ringler C, Lansigan F, Meza F (2013). Basin perspectives on the Water–Energy–Food Security Nexus. Current Opinion in Environmental Sustainability, 5(6), 607–616.
Steffen W, Rockström J, Richardson K, Lenton T M, Folke C, Liverman D, Summerhayes CP, Barnosky AD, Cornell SE., Crucifix M, Donges JF, Fetzer I, Lade SJ, Scheffer M, Winkelmann R, Schellnhuber HJ (2018). Trajectories of the Earth System in the Anthropocene. Proceedings of the National Academy of Sciences, 115(33), 8252–8259.
WEF. (2011). Water security: the water–food–energy–climate nexus. Washington DC: World Economic Forum

# Detection of pressure regulation malfunctions and issuance of alerts in water distribution networks

Anastasios PERDIOS[1], George KOKOSALAKIS[1,2], Nikolaos Th. FOURNIOTIS[3], Irene KARATHANASI[4] and Andreas LANGOUSIS[1]

[1] Department of Civil Engineering, University of Patras, Patras, Greece
email: A.P.: tassosper13@hotmail.com ; G.K.: gkokosalakis@upatras.gr ; A.L.: andlag@upatras.gr
[2] School of Business and Economics Department of Maritime Transport and Logistics, Deree American College of Greece, Athens, Greece
email: gkokosalakis@acg.edu
[3]Department of Civil Engineering, University of the Peloponnese, Patras, Greece
email: nfou@uop.gr
[4] Municipal Enterprise of Water Supply and Sewerage of the City of Patras, Patras, Greece
email: i.karathanasi@deyap.gr

ABSTRACT

Pressure reducing valves (PRVs) are widely used to regulate pressures in the supply and distribution parts of water networks, by reducing the upstream pressure to a set outlet pressure (i.e., downstream of the PRV), usually referred to as set point. As all types of mechanical equipment, PRVs may exhibit malfunctions affecting pressure regulation, such as high frequency fluctuations around the set point and/or prolonged systematic deviations from the set point, allowing their detection to be approached in a statistical context. This work focuses on the implementation of a novel statistical framework (see Perdios et al., 2022) to an existing pressure management area (PMA) of the city of Patras in western Greece, aiming at early detection of PRV malfunctions. The implemented framework uses: a) the cumulative distribution function (CDF) of the root mean squared error (RMSE) to monitor the performance of PRVs by detecting individual malfunctions, and b) the hazard function concept to identify a proper duration of sequential events from (a) to issue alerts.

## 1. Introduction

Installation of PRVs has been essential in managing water losses in Water Distribution Networks (WDNs) (see e.g., Prescott and Ulanicki, 2008). While novel methods for hydraulic modeling and improvement of PRV functionality under a wide range of network configurations have attracted significant attention, including real time control (RTC) and optimal selection of sensor locations (see e.g., Farley et al., 2010; Galuppini et al., 2020), no rigorous statistical framework currently exists to monitor their operation level. This work presents the implementation of a recently developed statistical framework to an existing pressure management area (PMA) of Patras WDN (the most populous city in western Greece), aiming at early detection of PRV major malfunctions that lead to pressure fluctuations and may significantly influence the network's lifetime.

## 2. Area and Data

We use pressure data at 1-min temporal resolution from PMA Diagora, which is part of the WDN of the city of Patras, for the 3-year period from 01/Jan./2017 to 31/Dec./2019. PMA Diagora consists of 12.8 km of pipeline (mainly PE and PVC pipes), covers an area of 352.5 m$^2$, and serves approximately 4000 consumers; see Serafeim et al. (2021).

## 3. Methodology

### *3.1. CDF of RMSE*

As a first step, we use the root mean squared error (RMSE) in Eq. (1) to describe both systematic and random deviations from the pressure set point, calculated within a window of constant duration *D*:

$$\mathrm{RMSE}(t) = \sqrt{\frac{\sum_{i=0}^{n}\left[y(t-idt) - y_{set}(t-idt)\right]^2}{n+1}} \tag{1}$$

where $y(t)$ and $y_{set}(t)$ denote the observed downstream pressure and the pressure set point at time $t$, respectively, $dt$ is the temporal resolution of the data (in our case $dt$ =1 min), and $n = D/dt$.

After estimating the RMSEs, we use their empirical cumulative distribution function (CDF) to detect individual malfunctions based on their frequency of occurrence.

### *3.2. Hazard function and issuance of alerts*

In the second and last step of the implemented methodology, we utilize the hazard function concept described in Eq. (2) (see e.g., Benjamin and Cornell, 1970) to identify a proper scale of continuous individual malfunctions to issue alerts:

$$h_T(t_0) = \frac{f_T(t_0)}{1 - F_T(t_0)} = \frac{f_T(t_0)}{S_T(t_0)} \tag{2}$$

where $T$ is a non-negative random variable denoting the waiting time until a status change occurs, $f_T$ is the probability density function (PDF) of $T$, $F_T$ is the CDF of $T$, and $S_T$ is the survival function of $T$ defined as 1-$F_T$.

## 4. Results - Discussion

The obtained results show that the suggested methodological framework allows timely and reliable detection and alerting of major PRV malfunctions (see Figure 1), as indicated by the repair dates reported by the Municipal Enterprise of Water Supply and Sewerage of the City of Patras (DEYAP), substantially reducing its response time with significant financial and operational benefits.

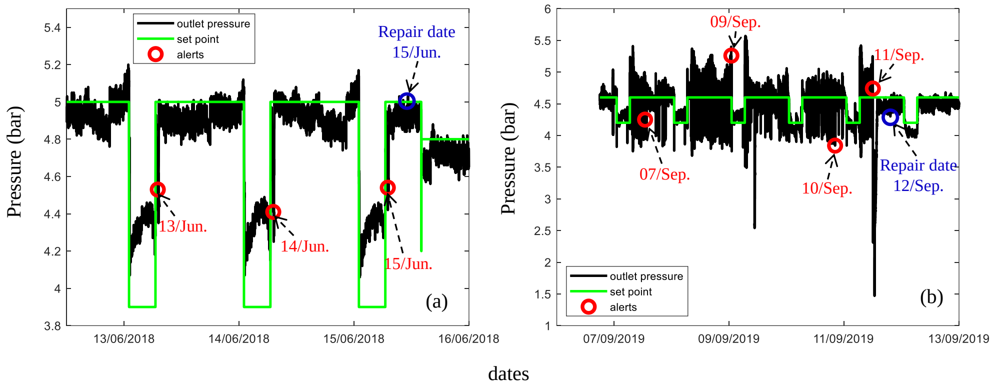


**Fig. 1.** Illustration of PRV outlet pressure (black line) and set point (green line) for PMA Diagora: a) in June 2018, and b) in September 2019. Red circles denote the dates of the alerts issued by the developed framework, whereas blue circles denote the reported repair dates.

**Acknowledgements**

The research work has been conducted within the project PerManeNt, which has been co-financed by the European Regional Development Fund of the European Union and Greek national funds through the Operational Program Competitiveness, Entrepreneurship and Innovation under the call RESEARCH – CREATE – INNOVATE (project code: T2EDK-04177).

**References**

Benjamin, J.R. and C. A. Cornell (1970) *Probability, Statistics and Decision for Civil Engineers*, McGraw-Hill, New York, ISBN: 07004594
Farley, B., S. Mounce and J. Boxall (2010) Field testing of an optimal sensor placement methodology for event detection in an urban water distribution network, *Urban Water Journal*, 7(6), 345-356.
Galuppini, G., L. Magni and E. Creaco (2020) Stability and Robustness of Real Time Pressure Control in Water Distribution Systems, *J. Hydraul. Eng.*, 146(4), Article 04020023.
Prescott, S. and B. Ulanicki (2008) Improved control of pressure reducing valves in water distribution networks, *J. Hydraul. Eng.*, 134(1), 56–65.
Perdios, A., G. Kokosalakis, N. Th. Fourniotis, I. Karathanasi and A. Langousis (2022) Statistical framework for the detection of pressure regulation malfunctions and issuance of alerts in water distribution networks, *Stoch. Env. Res. Risk Asses.* (submitted).
Serafeim, A.V., G. Kokosalakis, R. Deidda, I. Karathanasi and A. Langousis (2021) Probabilistic estimation of minimum night flow in water distribution networks: large-scale application to the city of Patras in western Greece, Stochastic Environmental Research and Risk Assessment, doi: https://doi.org/10.1007/s00477-021-02042-9.

# Groundwater Modelling of Managed Aquifer Recharge facilities for the optimal management of coastal aquifer systems

Angeliki VLASSOPOULOU[1], Martha PERDIKAKI[1], Efthymios CHRYSANTHOPOULOS[1], Christoph SCHUTH[2], Laura FOGLIA[3], Andreas KALLIORAS[1]

[1] National Technical University of Athens, School of Mining & Metallurgical Engineering, Greece
email: avlass@metal.ntua.gr

[2] Technical University of Darmstadt, Institute of Applied Geosciences, Germany
[3] UC Davis University of California, Department of Land, Air and Water Resources, USA

ABSTRACT

Optimal management of coastal aquifers usually involves the operation of artificial recharge facilities as a key measure to address some of their most typical problems, such as depletion of groundwater resources and seawater intrusion. At the same time, a sound strategic plan for monitoring and modelling of all relevant hydrological processes is required so that both the effectiveness of these hydraulic works is evaluated as well as a reliable prediction of the future quantitative and qualitative condition of the aquifer is achieved.

In particular, with regard to the simulation of the above, one of the important challenges that arise is the different spatial and temporal scales with which the hydrological processes are associated within the model domain. Managed Aquifer Recharge (MAR) facilities are considered boundary conditions that have a point effect on a model domain which usually involves a coarse and widely extended grid. The construction of a different model which will be developed based on the appropriate MAR scale is neither a desirable nor a cost and time effective solution to the above. However, the existence of different codes and/or packages in order to provide sufficient grid refinement option is thought to be an appropriate solution to the above problem.

The scope of this ongoing research is to simulate the hydrological processes associated with the injection of recharge-water into an aquifer through a long-term and systematic MAR scheme, using the well-known public domain and open-source USGS MODFLOW-2005 code (finite difference method) and the use grid refinement tools.

It is envisaged that the aforementioned modelling approach will enable the more precise and reliable simulation of injection wells, within a larger model domain of a coastal aquifer system.

## 1. Introduction

It is common that simulations of ground-water flow and transport often need highly refined grids in local areas of interest in order to improve simulation accuracy. Areas where there is need of grid refinement usually are where hydraulic gradients change significantly over short distances, such as near pumping or injection wells. Moreover, areas where there is need of mass transport simulation of site-scale contamination within a regional aquifer, as well as areas where detailed representation of heterogeneity is needed.

Refinement of the finite-difference grid used by MODFLOW-2005 for modular three-dimensional, ground-water flow model, can be achieved by using different approaches; from globally refined grids, to variable spaced and locally refined grids as discussed by Mehl and Hill (2007).

Telescopic Mesh Refinement (TMR) is a grid refinement method provided by MODFLOW-2005 that combines two or more different-sized finite-difference grids—usually a coarse grid, which incorporates regional boundary conditions, and a locally refined grid, which focuses on the area of interest. The link between the coarse and local grids is most commonly accomplished by first simulating the coarse grid and using its results to interpolate heads and fluxes, or a combination of both, onto the boundaries of the local grid (Mehl and Hill, 2013).

## 2. Modelling of Argolis aquifer system

The coastal aquifer system of Argolis in Peloponnese, Greece, is being modelled in an effort to optimise the irrigation water use through the understanding, description and predictions of the water demand and supply of the system. For decades, the main economic activity in the region of Argos is agriculture and it is considered one of the most irrigated areas in the country. As a consequence, contamination of groundwater due to seawater intrusion and nitrate pollution have occurred over the years of exploitation. For this reason, MAR has been applied to the area by the local authorities since 1990, using a variety of different methods: from surface basins to shallow wells or deep boreholes.

Monitoring of the groundwater levels in the area, combined with hydrochemical analysis in water samples is an ongoing process that feeds the model being developed with data that depict the current quantitative and qualitative state of the groundwater aquifer system. In Figure 1, the digital elevation and the electrical conductivity measured at the end of the irrigation period in 2021 is shown.

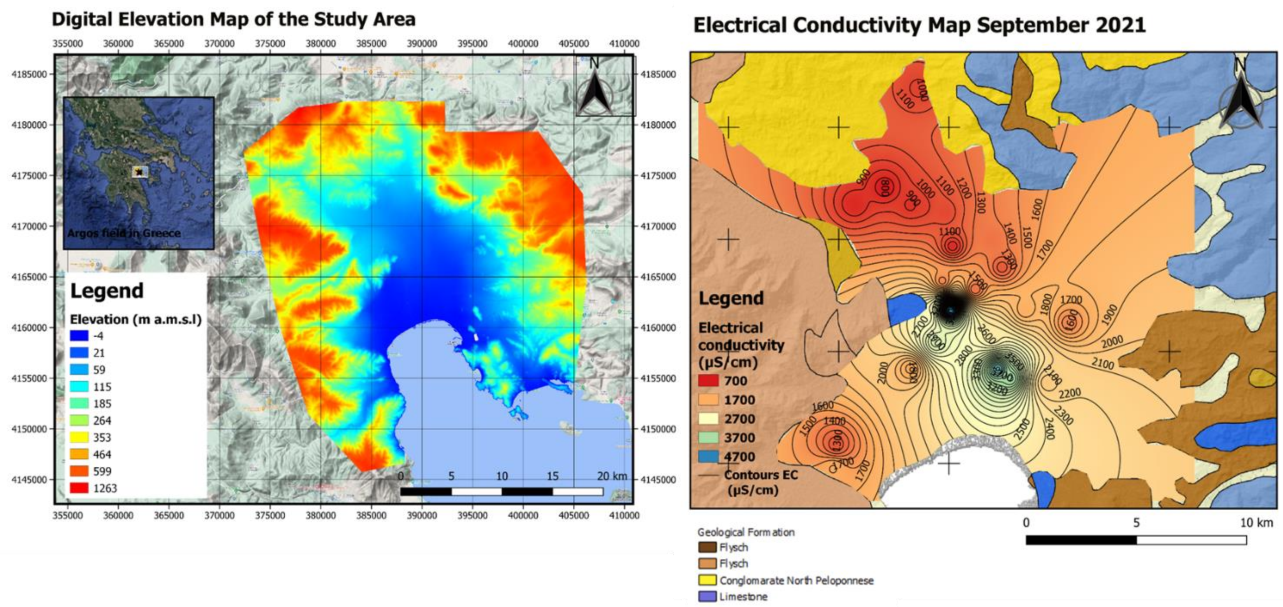


**Fig. 1.** Map of the digital elevation of the area of study which is the Argos field in Peloponnese, Greece (on the left) and map of the electical conductivity measured on water samples being collected in September 2021 (on the right)

**Acknowledgements**
This research is part of the MARSoluT ITN project, which receives funding from the European Union’s Horizon 2020 research and innovation programme under the Marie Skłodowska-Curie grant agreement no. 814066.

**References**

Mehl, S., Hill, M. C., & Leake, S. A. (2006). Comparison of local grid refinement methods for MODFLOW. Groundwater, 44(6), 792-796
Mehl, S.W., and Hill, M.C., 2007, MODFLOW-2005, The U.S. Geological Survey modular ground-water model—Documentation of the multiple-refined-areas capability of local grid refinement (LGR) and the boundary flow and head (BFH) package: U.S. Geological Survey Techniques and Methods 6-A21, 13 p.
Mehl, S.W., and Hill, M.C., 2013, MODFLOW–LGR—Documentation of ghost node local grid refinement (LGR2) for multiple areas and the boundary flow and head (BFH2) package: U.S. Geological Survey Techniques and Methods
book 6, chap. A44, 43 p., http://pubs.usgs.gov/tm/6A44/.

# Evaluation of an HRES using pumped-storage or hydrogen storage for water and energy demands in Skyros island

Athanasios-Foivos PAPATHANASIOU[1], Maria Margarita BERTSIOU[1], Evangelos BALTAS[1]

[1] National Technical University of Athens, Greece
email: n_papathan@hotmail.com; mbertsiou@chi.civil.ntua.gr; baltas@chi.civil.ntua.gr

ABSTRACT

As in most islands of the Greek Territory, in Skyros, the electricity needs of the residents are mainly covered by autonomous energy stations. Electricity is produced by consuming fossil fuels. Moreover, the water in the network is not potable, so it is necessary to use bottled water. The solution is given through desalination. This paper examines the potential construction of a Hybrid Renewable Energy System (HRES) for drinking water and electrical needs without emitting any pollutants into the atmosphere. Wind turbines electrify the system while pumped storage hydropower and hydrogen are used to store excess energy. These two methods are a solution to the issue of storage and controlled distribution of the clean wind energy produced by the wind turbines.

## 1. Introduction

In Skyros, as in most Greek islands, the energy needs are covered by autonomous power stations (APS), which produce energy through fossil-fuel consumption, a non-environmentally-friendly choice. The main disadvantages of APS are that in case of damage to the station, there will be a total blackout; moreover, during the summer, APS are sometimes unable to cover the electricity demand. The solution is to take advantage of the potential of Renewable Energy Sources (RES) and to use energy storage methods like pumped storage and hydrogen for better energy management (Katsaprakakis, 2016). The combination of different RES coupling with a storage system constitutes a Hybrid Renewable Energy System (HRES).

In recent years, the research in the desalination industry has focused on the combination of desalination plants with RES, in order to reduce both energy costs and also the cost of the produced desalinated water. Of all desalination processes, Reverse Osmosis (RO) is the most suitable method because of its low energy consumption, the suitability for connection with RES and the production of high quantities of desalinated water (Al-Karaghouli and Kazmerski, 2013).

## 2. Study area

Skyros is an island in the Aegean Sea. It is the southernmost and the largest island of the Sporades archipelago. The island has a total area of 220 $km^2$ and a coastline length of 134 km. Based on the last census of 2011, there are 2.994 inhabitants, a number that reaches 12.000 during summer months due to tourism (Hellenic Statistical Authority, 2011). Due to its geographical position and the influence of the sea, the climate of the island is described as the Mediterranean. The average annual temperature during the years 2011–2020 is 18,5°C, the total annual rainfall is 491 mm and the prevailing winds are mainly northerly, around 3 – 4 Beaufort (Lagouvardos et al., 2017).

Skyros has a water supply that is not suitable for human consumption, as it comes from brackish water sources, mainly from the source “Anavallousa”. For this reason, residents have to use bottled water. For electricity needs, the island has a local autonomous power station.

## 3. Methodology

The installation of an HRES, coupled with a desalination unit, on the island of Skyros, is evaluated for meeting water and electricity demands. This system provides a solution to the non-potable water that reaches the households and, also, to the instability of the local power grid.

Hydrogen is produced based on the method of Polymer Electrolyte Membrane (PEM) electrolysis (Zeng and Zhang, 2010). To produce 1 kg of hydrogen, 0,06 MWh of electrical energy and 9 kg of clean water are required (Rievaj et al., 2019).

In order to evaluate the response of the HRES, two scenarios have been examined. In both scenarios, wind turbines electrify the system, providing 30% of the energy directly to the power grid to cover electrical needs, while the remaining 70% is available for desalination, pumping and hydrogen production, with priority given to desalination. If there is excess energy after meeting water needs, it is used for the remaining electricity demands. The difference between the two scenarios has to do with the methods of how the excess energy is stored, after meeting electrical needs. The 1st scenario depends on the method of pumped-storage hydroelectricity. If there is a lack of energy, the turbine produces hydroelectric energy. If there is an excess in energy, it is used to pump water into the reservoir. The 2nd scenario examines the use of hydrogen technology. If there is a lack of energy, electrical energy is produced from hydrogen. If there is an excess, it is used to produce hydrogen.

## 4. Results and concluding remarks

The usage of the produced wind energy for the two scenarios throughout the year is shown in Figure 1. In both scenarios, 30% of the produced wind energy is being provided to the power grid, 9% is used for desalination and 7% is used directly to cover electricity demands. The rest 54% of the produced wind energy is treated differently in each of the two scenarios. In the 1st scenario, 18% is used for pumping and 36% is not usable, either because the reservoir is full, or because there is not enough energy for the water pumps to function. In the second scenario, 54% is used for hydrogen production.

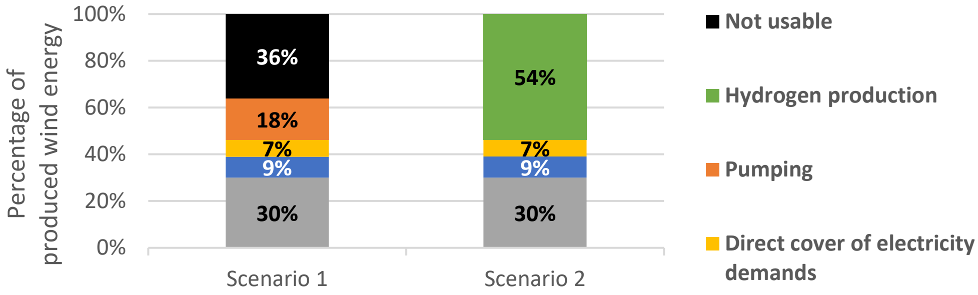


**Fig. 1** Distribution of energy produced by the HRES.

A water reservoir is used to store the desalinated water, so in both scenarios, there is total coverage of the water demands.

Figure 2 presents a comparison of the two scenarios, depicting the mean monthly demand for electrical energy, the coverage of the two scenarios and the coverage of the wind turbines. In the 2nd scenario, there is the highest coverage of the demands at the percentage of 90% throughout the year. The lowest coverage of electricity demands occurs in the 1st scenario, where the electricity needs are covered at 86%.

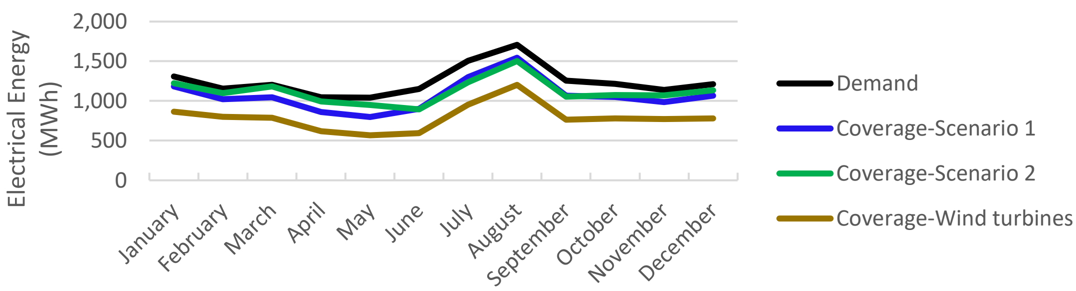


**Fig. 2** Mean monthly demand of electricity energy, coverage from the three scenarios and coverage from the wind turbines.

**References**

Al-Karaghouli A, Kazmerski L (2013) Energy consumption and water production cost of conventional and renewable-energy-powered desalination processes, Renewable and Sustainable Energy Reviews, 24, 343-356, ISSN 1364-0321
Hellenic Statistical Authority, Available at: https://www.statistics.gr/ (Accessed 15 April 2022)
Katsaprakakis D (2016) Hybrid power plants in non-interconnected insular systems, Applied Energy, 164, 268-283
Lagouvardos K, Kotroni V, Bezes A, Koletsis I, Kopania T, Lykoudis S, Mazarakis N, Papagiannaki K, Vougioukas S (2017) The automatic weather stations NOANN network of the National Observatory of Athens: Operation and database, Geoscience Data Journal, 4(1), 4-16
Rievaj V, Gaňa J, Synák F (2019) Is hydrogen the fuel of the future?, Transportation Research Procedia, 40, 469-474, ISSN 2352-1465
Zeng K, Zhang D (2010) Recent progress in alkaline water electrolysis for hydrogen production and applications, Progress in Energy and Combustion Science, Issue 3, 36, 307-326, ISSN 0360-1285

# An Integrated Climate Change Assessment of Water Resources of Coastal Agricultural Watersheds: The case of Almyros Basin, Greece

Aikaterini LYRA[1], Athanasios LOUKAS[2], Dimitrios MALAMATARIS[3], Lampros VASILIADES[1], Pantelis SIDIROPOULOS[1,2], Nikitas MYLOPOULOS[1]

[1] Department of Civil Engineering, School of Engineering, University of Thessaly, 38334 Volos, Greece
email: klyra@uth.gr; lvassil@civ.uth.gr; psidirop@civ.uth.gr; nikitas@civ.uth.gr
[2] School of Rural and Surveying Engineering, Aristotle University of Thessaloniki, 54124 Thessaloniki, Greece
email: agloukas@topo.auth.gr
[3] Soil and Water Resources Institute-Land Reclamation Department, Hellenic Agricultural Organization "DEMETER", 57400 Sindos, Greece
email: dimalamataris@gmail.com

ABSTRACT

This study studies the historical and future evolution of the degraded quantity and quality of water resources in the coastal and agricultural Almyros Basin, in Greece. Multi-model ensembles of RCP4.5 and RCP8.5 projections from the Med-CORDEX database for precipitation and temperature have been corrected for bias and used in the analysis. The simulation of surface water and groundwater has been performed using an Integrated Modelling System that contains coupled models of surface hydrology (UTHBAL), groundwater hydrology (MODFLOW), nitrate leaching/crop growth (REPIC), nitrate pollution (MT3DMS) and seawater intrusion (SEAWAT). The results indicate that the water deficit will become larger, the nitrate pollution will be reduced, in general, although local prohibiting concentrations will be present, and the seawater intrusion will advance inland.

## 1. Historical Water Quantity/Quality Status of the Study Area

Intensive groundwater abstractions for irrigation and nitrogen fertilization for crop production maximization, have caused a large water deficit, nitrate pollution and seawater intrusion in the Almyros aquifer. Alfalfa, cereals, cotton, maize, olives trees and orchards, vegetables, vineyards, and wheat are cultivated in the study area. The climate of the region is semi-arid, Mediterranean, the existence of ephemeral streams and the absence of surface water storages contribute to the basin water deficit (Lyra et al., 2021a; 2021b).

## 2. Future Water Quantity/Quality Status

### *2.1. Quantile Empirical Mapping Bias Correction*

Quantile Empirical Mapping (Eq. 1) has been applied on timeseries of areal monthly precipitation and temperature. F is the distribution of the variable (Lee and Singh, 2018), on the centroids of Almyros sub-basins, for multi-model ensembles of medium (RCP4.5) and extreme (RCP8.5) enforcing emissions (Fig. 1). The method performed very well, compared with the observed data, as it is indicated by Nash-Sutcliffe Efficiency (Eff, Eq. 2) where Y, F represent the simulated and the observed values, both for 1971-2000 and 2001-2018. The values of Eff were equal to 0.90 and 0.93 for precipitation under RCP4.5 and RCP8.5, respectively. The respective values of Eff for temperature range from 0.85 to 0.88 under RCP4.5, and from 0.96 to 0.90 for RCP8.5, respectively.

$$\hat{y}=F^{-1}_{RCP}\left(F_{Observed}(x)\right) \tag{1}$$

$$Eff=1-\frac{\sum_{i=1}^{n}(y_i-f_i)^2}{\sum_{i=1}^{n}(y_i-\bar{y})^2} \tag{2}$$

### *2.2. Climate Change and Integrated Modelling System*

The agriculture in the basin relies only on groundwater irrigation abstractions. The assessment of climate change impacts on surface water and groundwater resources is critical to sustainable water resources management of the basin.

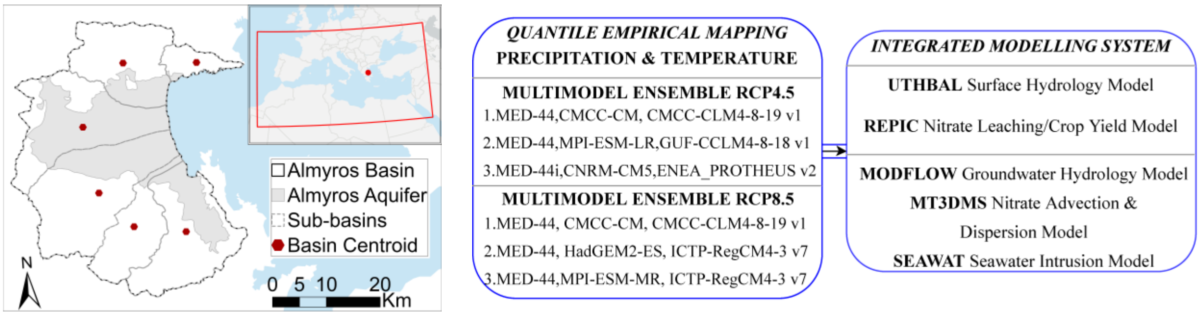


**Fig. 1.** Graphical abstract of Integrated Climate Change Simulation for Almyros Basin

The simulated results of water balance and water quality indicators are presented in

Table **1**.

**Table 1.** Mean annual values of precipitation (P) [mm], temperature (T) [°C], surface runoff (Q) [mm], groundwater recharge (Rg) [mm], groundwater water balance (GWB) [$hm^3$], nitrates leaching (NL) [mg/L], groundwater nitrates ($NO_3$) and groundwater chlorides (Cl) concentrations [mg/L] for historical and future periods.

| Model Variable Averages per Time Period | 1970-2000 | 2001-2018 | 2019-2050 | 2051-2080 | 2081-2100 |
|---|---|---|---|---|---|
| P Observed | 551.3 | 584.3 | – | – | – |
| P RCP4.5 (QEM) | 566 | 606.1 | 558.6 | 565.9 | 553.2 |
| P RCP8.5 (QEM) | 560.5 | 590.6 | 556.4 | 562.1 | 565.7 |
| T Observed | 14.8 | 15.6 | – | – | – |
| T RCP4.5 (QEM) | 14.8 | 15 | 15.4 | 16.2 | 16.4 |
| T RCP8.5 (QEM) | 14.8 | 15.6 | 16.5 | 18.3 | 22.5 |
| Q Obs. (UTHBAL) | 114.5 | 107.3 | – | – | – |
| Q RCP4.5 (UTHBAL) | 123.9 | 107 | 103.5 | 101.8 | 93 |
| Q RCP8.5 (UTHBAL) | 131.5 | 108.7 | 101.4 | 89.9 | 77.5 |
| Rg Obs. (UTHBAL) | 551.3 | 584.3 | – | – | – |
| Rg RCP4.5 (UTHBAL) | 566 | 606.1 | 558.6 | 565.9 | 553.2 |
| Rg RCP8.5 (UTHBAL) | 560.5 | 590.6 | 556.4 | 562.1 | 565.7 |
| GWB Obs. (MODFLOW) | -11.8 | -12.2 | – | – | – |
| GWB RCP4.5(MODFLOW) | -15.7 | -13.5 | -17.2 | -10.35 | -7.73 |
| GWB RCP8.5 (MODFLOW) | -14.6 | -12.4 | -18.1 | -10.30 | -6.10 |
| NL Obs. $NO_3$ (REPIC) | 36 | 47 | – | – | – |
| NL $NO_3$ RCP4.5 (REPIC) | 31 | 70 | 34 | 35 | 41 |
| NL $NO_3$ RCP8.5 (REPIC) | 35 | 80 | 48 | 47 | 50 |
| $NO_3$ Obs. (MT3DMS) *Max | 32/ 139* | 29/ 135* | – | – | – |
| $NO_3$ RCP4.5 (MT3DMS) | 32/ 139* | 30/ 133* | 24/ 112* | 17/ 90* | 17/ 81* |
| $NO_3$ RCP8.5 (MT3DMS) | 33/ 139* | 30/ 133* | 28/ 139* | 20/ 667* | 19/ 95* |
| Cl Obs. (SEAWAT) *Max | 139/ 6808* | 148/ 19824* | – | – | – |
| Cl RCP4.5 (SEAWAT) | 138/ 5788* | 127/ 11378* | 182/ 20284* | 570/ 20290* | 798/ 20182* |
| Cl RCP8.5 (SEAWAT) | 137/ 4927* | 122/ 11936* | 178/ 20282* | 517/ 20280* | 703/ 20182* |

## 3. Conclusion

The results indicate that the quantity and quality status of surface water and groundwater would deteriorate under the climate change scenarios. The water deficit and quality degradation are milder under RCP4.5 scenario compared to RCP8.5.

**Acknowledgements**

“This research is co-financed by Greece and the European Union (European Social Fund- ESF) through the Operational Programme «Human Resources Development, Education and Lifelong Learning» in the context of the project “Strengthening Human Resources Research Potential via Doctorate Research” (MIS-5000432), implemented by the State Scholarships Foundation (IKY)”. "The simulations used in this work were downloaded from the Med-CORDEX database (www.medcordex.eu)".

**References**

Lee T, Singh VP (2018) Statistical downscaling for hydrological and environmental applications, CRC Press, 161 pp.
Lyra A, Loukas A, Sidiropoulos P, Tziatzios G, Mylopoulos N (2021a) An Integrated Modeling System for the Evaluation of Water Resources in Coastal Agricultural Watersheds: Application in Almyros Basin, Thessaly, Greece, Water, 13(3), 268.

Lyra A, Loukas A, Sidiropoulos P (2021b) Impacts of irrigation and nitrate fertilization scenarios on groundwater resources quantity and quality of the Almyros Basin, Greece, Water Supply, 21(6), 2748-2759.

7th IAHR EUROPE CONGRESS

SEPTEMBER 7-9, 2022

ATHENS, GREECE

Divani Caravel Hotel

www.iahreuropecongress.org